IAU Commissions G1 and G4

INFORMATION BULLETIN ON VARIABLE STARS
Vol. 63

Nos. 6201-6271, 6299, 6300

2017 March - 2019 June

Konkoly Observatory
Budapest

Contents 6201

6214 Discovery of a New delta Scuti Variable in the Field of RW UMi
Alis, S.; Saygac, A. T.; Fisek, S.; Esenoglu, H. H.
05 September 2017

6215 Variability of the object M1-15 = SS73 6 during 45 years
Kondratyeva, L.; Denissyuk, E.; Rspaev, F.; Krugov, A.
12 September 2017

6216 NY Her: possible discovery of negative superhumps
Sosnovskij, A.; Pavlenko, E.; Pit, N.; Antoniuk, K.
14 September 2017

6217 110 Minima timings of ultra-short orbital period eclipsing binaries
Gazeas, K.; Loukaidou, G.; Tzouganatos, L.; Karampotsiou, E.; Petropoulou, M.
20 September 2017

6218 120 Minima timings of eclipsing binaries
Palafouta, S.; Gazeas, K.; Christopoulou, E.; Bakogianni, V.; Dervou, M.; Loukaidou, G.
20 September 2017

6219 Times of Minima of Some Eclipsing Binary Stars with Eccentric Orbit in the Kepler Field
Bulut, I.
11 October 2017

6220 OAN-TNT Results of Observations - Photoelectric Maxima of Pulsating Stars
Pena, J. H.; Renteria, A.; Pina, D. S.; Villarreal, C.; Calderon, J.; Pani, A.; Huepa, H.; students from the Latin American School of Observational Astronomy (ESAOBELA) 16 and 17 as well as the students from the Advanced Observational Courses (AOA) 15, and 16 at Facultad de Ciencias, UNAM and students of the workshop in Observational Astronomy (TAO)
27 October 2017

6221 Detection of short-periodic oscillations in UW Vir
Mkrtichian, D. E.; Gunsriwiwat, K.; Awiphan, S.; Komonjinda, S., Reichart, D. E.; Haislip, J. B.; Kouprianov, V. V.; Ivarsen, K. M.; Crain, J. A.; Foster, A. C.; Poshyachinda, S.; Rujopakarn W.
14 November 2017

6222 14 years of photometric monitoring of MM Dra and a suspected variable in the field of blazar 1ES 1959+650
Hicks, S.; Laney, C.D.; Carini, M.T.; Richardson, W.N.; Antoniuk, K.; Pit, N.
14 November 2017

6223 Direct Distance Estimation and Absolute Parameters of Z Draconis
Terrell, D.; Nelson, Robert H.
23 November 2017

6224 V500 Cyg - A Classical Algol
Nelson, Robert H.
11 December 2017

6225 New CCD Minima Times for Selected Eclipsing Binaries
Soydugan, F.; Alicavus, F.; Senyuz, T.; Kahraman Alicavus, F.; Puskullu, C.; Kanvermez, C.; Soydugan, E.
24 November 2017

6226 V736 Cephei - An A-Type Overcontact Binary
Nelson, Robert H.
11 December 2017

6227 New Light-Time Curve of Eclipsing Binary AM Leo
Gorda, S. Yu.; Matveeva, E. A.
11 December 2017

6228 O-C diagrams for 33 RR Lyrae-type stars
Dagne, T.M.; Berdnikov, L.N.; Kniazev, A.Y.; Dambis, A.K.
12 December 2017

6229 Discovery of the Blazhko effect in V1065 Aql, CzeV980, FI Sge, and CzeV1242
Skarka, M.; Cagas, P.
21 December 2017

6230 Times of Minima of 116 Eclipsing Binary Systems (2010-2015)
Lampens, P.; Van Cauteren, P.; Ayiomamitis, A.; Kleidis, S.; Panagiotopoulos, K.; Vanleenhove, M.; Hambsch, J.; Hautecler, H.; Van Wassenhove, J.; Vermeylen, L.
17 December 2017

6231 Secular Variation and Physical Characteristics Determination of the HADS Star EH Lib
Pena, J.H.; Villarreal, C.; Pina, D.S.; Renteria, A.; Soni, A., Guillen, J. Calderon, J.
13 December 2017

6232 CCD Times of Minima of Eclipsing Binaries
Kubicki, D.
19 December 2017

6233 Spectroscopy of bright Algol-type semi-detached close binary system HU Tauri (HR 1471)
M. Parthasarathy
23 January 2018

6234 CCD Minima for Selected Eclipsing Binaries in 2017
Nelson, Robert H.
23 January 2018

6235 Timing of AR CrB eclipses
Kozyreva, V. S.; Irsmambetova, T. R.; Ibrahimov, M. A.; Krushevska, V. N.; Kuznyetsova, Yu. G.; Khalikova, A. V.; Parmonov, O. U.; Karimov, R. G.; Bogomazov, A. I., Satovskii, B. L.; Tutukov, A. V.
23 January 2018

6236 Revised coordinates of variable stars in Cassiopeia
NESCI, R.
7 February 2018

6237 114 Minima timings of ultra-short orbital period eclipsing binaries
Loukaidou, G.; Gazeas, K.
13 February 2018

6238 Discovery of short-period oscillations in the mass-accreting component of TT Vel
Mkrtichian, D. E.; Gunsriwiwat, K.; Reichart, D. E.; Haislip, J. B.; Kouprianov, V. V.; Poshyachinda, S.
7 March 2018

6239 Precession of the Disk in Pleione - Study of the Halpha Line Profile
Ernst Pollmann
16 March 2018

6240 2MASS J06422218-0226285 - a new Outburst Source
Blex, Susanne; Hackstein, Moritz; Haas, Martin; Kimeswenger, Stefan; Chini, Rolf; Hodapp, Klaus
05 April 2018

6241 Multicolor light curves and Period Analysis of IL Cnc
Alton, K.B.
17 May 2018

6242 Revised coordinates of 3 variable stars in Cygnus
Nesci, R.
6 June 2018

6243 New transit timing observations for GJ 436 b, HAT-P-3 b, HAT-P-19 b, WASP-3 b, and XO-2 b
MACIEJEWSKI, G.; STANGRET, M.; OHLERT, J.; BASARAN, C.S.; MACIEJCZAK, J.; PUCIATA-MROCZYNSKA, M.; BOULANGER, E.
13 July 2018

6244 BAV-Results of observations - Photoelectric Minima of Selected Eclipsing Binaries and Maxima of Pulsating Stars
Pagel, Lienhard
13 July 2018

6245 The Period Evolution of V473 Tau
OZUYAR, D.; STEVENS, I. R.
20 July 2018

6246 Photometry of GS UMa: a suspected delta Scuti variable
Kahraman Alicavus, F.; Raheem, A.; Coban G. C.; Tambulut, E. M.; Gogulter, U.;BAS, L.; Cevirici, B.
20 July 2018

6247 The Status of GSC 3870-01172 as a Member of a Triple or Quadruple System
Terrell, D.; Nelson, Robert H.
20 July 2018
Terrell, D.; Nelson, Robert H.
20 July 2018

6248 TYC 5353-1137-1: an enigmatic Doubly Periodic Variable of semiregular amplitude
ROSALES, J. A., MENNICKENT, R. E.
27 July 2018

6249 Periodic Halpha Emission in the Eclipsing Binary VV Cephei
POLLMANN, E.; BENNETT, P. D.; VOLLMANN, W.; SOMOGYI, P.
27 July 2018

6250 Times of minima of some eclipsing binary stars with eccentric minima in the Kepler field II.
Bulut, I.
12 August 2018

6251 Photometry of OV Bootis at the 2017 Outburst
Tanabe, Kenji; Akazawa, Hidehiko; Fukuda, Naoya
16 August 2018

6252 The Period Analysis of the Hierarchical System DI Peg
OZUYAR, D.; ELMASLI, A.; CALISKAN, S.
24 August 2018

6253 SU Aur: A deep fading event in Visible and near-infrared bands
Grankin, K.N.; Shenavrin, V.I.; Irsmambetova, T.R.; Petrov, P.P.
12 September 2018

6254 The variable carbon star CGCS 6107
Nesci, R.; Calabresi, M.; Rossi, C.; Ochner, P.
14 September 2018

6255 Revised coordinates of variables in the field of M16-M17
Nesci, R.
15 September 2018

6256 Period Analysis, Roche Modeling and Absolute Parameters for AU Ser, an Overcontact Binary System
Alton, K.B.; Nelson, R.H.; Terrell, D.
10 December 2018

6257 UU Aqr - No superhumps but variations on the time scale of days
Bruch, Albert
19 January 2019

6258 Distance, Luminosity and evolutionary status of epsilon Aurigae (F0Iaep) from Gaia DR2 parallax
Parthasarathy, M.; Muneer, S.
8 January 2019

6259 Detection of a delta Scuti-type pulsating component in the detached eclipsing binary system TU CMa
MKRTICHIAN, D.E.
29 January 2019

6260 HD220735 and HD30110, new short period variable stars
Pena, J. H.; Soni, A.; Renteria, A.; Pina, D. S.
30 January 2019

6261 The 82nd Name-List of Variable Stars. Part I - RA 0hr to 18hr, Novae and Globular-cluster Variables
Kazarovets, E.V.; Samus, N.N.; Durlevich, O.V.; Khruslov, A.V.; Kireeva, N.N.; Pastukhova, E.N.
21 February 2019

6262 CCD Minima for Selected Eclipsing Binaries in 2018
Nelson, Robert H.
12 August 2019

6263 On the Period and Light Curve of the A-Type W UMa binary GSC 3208~1986
EATON, JOEL A.; ODELL, ANDREW P.; POLAKIS, THOMAS A.
27 March 2019

COMMISSIONS G1 AND G4 OF THE IAU
INFORMATION BULLETIN ON VARIABLE STARS

Volume 63 Number 6201 DOI: 10.22444/IBVS.6201

Konkoly Observatory
Budapest
17 March 2017

HU ISSN 0374 – 0676

BN PEGASI – A SEMIDETACHED ECLIPSING BINARY

NELSON, ROBERT H.[1,2]

[1] 1393 Garvin Street, Prince George, BC, Canada, V2M 3Z1, email: bob.nelson@shaw.ca

[2] Guest investigator, Dominion Astrophysical Observatory, Herzberg Institute of Astrophysics, National Research Council of Canada

The variability of BN Peg (AN 145.1935; NSVS 14426159; TYC 537-44-1), amongst many others, was discovered photographically by Hoffmeister (1935) who gave coordinates, a magnitude range, and a finder chart, and described the system as an Algol. Jensch (1935) supplied elements (epoch, period) and 15 photographic eclipse timings. Mallama (1980) and Kreiner (2004) presented up-to-date elements. Over the years, there have been a number of eclipse timings, but no light curve analysis.

Light curve and radial velocity data have been acquired, but before any analysis, the first task was to examine the period variation. An eclipse timing difference (O-C) plot using all available data is reproduced in Figs. 1 and 2.

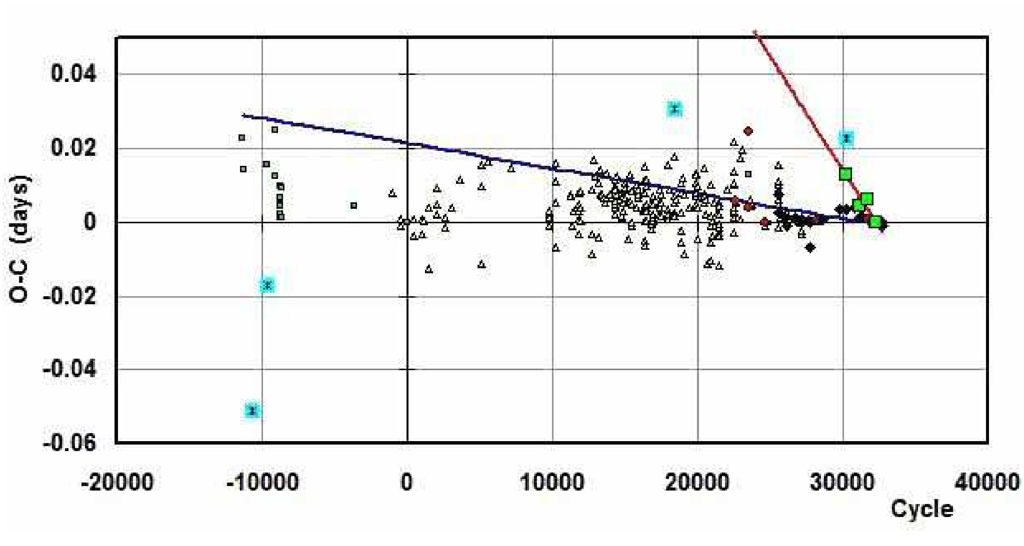

Figure 1. BN Peg – eclipse timing (O-C) diagram with fits to primary and secondary eclipse timings. Legend: small squares – photographic; triangles – visual; filled circles – photoelectric; filled diamonds – CCD. The four large squares are secondary minima (PE and CCD). The asterisk symbols are rejected readings.

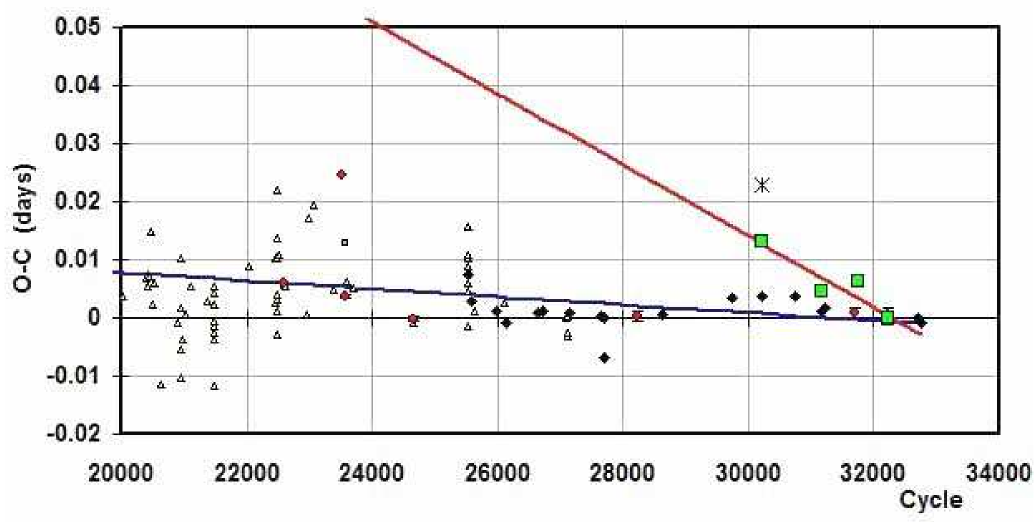

Figure 2. BN Peg – eclipse timing (O-C) diagram, identical to Fig. 9 but in more detail.

It will be seen that the many points since the first (in 1929) display considerable scatter. While the scatter is understandable for the photographic and visual points display, it is not clear why the photoelectric (PE) and CCD points are not more consistent. One possibility is that the system is undergoing an elliptical orbit with apsidal motion due to a third body. If that is the case, some of the supposedly deviant points would fit together with the other secondary minima to obey a different relation – that depicted in more detail in Fig. 10. (The first secondary minimum may still be deviant, however, and was not included in the fit of Fig. 10.) Also, the period may be changing over the long term, and there may even be a short-term cyclic component. However, all this is very speculative; future eclipse timings will be required to settle the matter. The eclipse timing (O–C) Excel file may be found online at Nelson (2016).

Although both the spectroscopic and photometric data were taken at about cycle 32 000, it seemed the safest procedure (in view of the scatter) to take the best-fit for the primary eclipse data from cycle 25,500 to the present. Small errors in the slope should not affect the phasing significantly. The result, equation (1) was used for all phasing.

$$\mathrm{JD(Hel)\,MinI} = 2457254.7346 + 0.7132973\mathrm{E} \tag{1}$$

In July-August of 2015, the author took 145 frames in V, 146 in R_C (Cousins) and 161 in the I_C (Cousins) band at his private observatory in Prince George, BC, Canada. The telescope was a 33 cm f/4.5 Newtonian on a Paramount ME mount; the camera was a SBIG ST-10XME. Standard reductions were then applied. The variable, comparison and check stars are listed in Table 1. The coordinates and magnitudes for all three stars are from the Tycho Catalogue (Hog et al. 2000).

In October of 2015 and again in September of 2016, the author then took a total of 9 medium resolution (R$\sim$10000 on average) spectra of BN Peg at the Dominion Astrophysical Observatory (DAO) in Victoria, British Columbia, Canada using the Cassegrain spectrograph attached to the 1.85 m Plaskett Telescope. He used the 21181 grating with 1800 lines/mm, blazed at 5000 Å giving a reciprocal linear dispersion of 10 Å/mm in the first order. The wavelengths ranged from 5000 to 5260 Å, approximately. A log of observations is given in Table 2. The following elements were used for both RV and

Table 1: Details of variable, comparison and check stars.

Object	GSC	RA (J2000)	Dec (J2000)	V (mag)	$B-V$ (mag)
Variable	0537-0044	$21^h28^m04\overset{s}{.}27$	$04°59'01''.97$	10.84(7)	+0.43(10)
Comparison	0537-1042	$21^h28^m32\overset{s}{.}20$	$04°57'53''.99$	10.55(6)	+0.97(11)
Check	0537-0899	$21^h29^m00\overset{s}{.}79$	$05°00'57''.50$	10.59(6)	+0.70(10)

Table 2: Log of DAO observations.

DAO Image #	Mid Time (HJD−2400000)	Exposure (sec)	Phase at Mid-exp	V_1 (km/s)	V_2 (km/s)
13241	57298.7895	3600	0.762	+75.3	–242.1
13280	57299.8133	2400	0.198	–114.7	+168.1
13318	57300.6283	2400	0.340	–99.4	+157.9
9241	57644.7374	1800	0.760	+75.4	–222.7
9308	57645.8432	360	0.311	–117.5	—
9362	57646.8286	1800	0.692	+67.7	–213.0
9445	57650.7527	1384	0.194	–118.0	+179.7
9557	57653.6707	1200	0.284	–126.4	+169.3
9559	57653.6860	1200	0.306	–109.3	+181.0

photometric phasing:

Frame reduction was performed by software 'RaVeRe' (Nelson 2009). See Nelson et al. (2014) for further details.

Radial velocities were determined using the Rucinski broadening functions (Rucinski 2004; Nelson 2010b; Nelson et al. 2014). An Excel worksheet with built-in macros (written by him) was used to do the necessary radial velocity conversions to geocentric and back to heliocentric values (Nelson 2010a). The resulting RV determinations are also presented in Table 2. For the 2015 data, the results were corrected 2.2% and 1.0% up, respectively, to allow for the small phase smearing. (Because of the shorter exposure times possible with the newly-coated optics, no correction was necessary for the 2016 data.) Correction was achieved by dividing the RVs by the factor f = (sinX)/X; where $X = 2\pi t/P$, where t denotes exposure time and P denotes the orbital period. For spherical stars, this correction is exact; in other cases, it can be shown to be close enough for any deviation to fall below observational errors. The mean rms errors for RV_1 and RV_2 were 4.2 and 7.7 km/s, respectively, and the overall rms deviation from the (sinusoidal) curves of best fit was 6.5 km/s. The best fit yielded the values $K_1 = 98.7(3)$ km/s, $K_2 = 208.6(7)$ km/s and $V_\gamma = –22.6(4)$ km/s, and thus a mass ratio $q_{sp} = K_1/K_2 = M_2/M_1$ =.0.473(2).

The author used the 2003 version of the Wilson-Devinney (WD) light curve and radial velocity analysis program with Kurucz atmospheres (Wilson and Devinney 1971; Wilson 1990; Kallrath et al. 1999) as implemented in the Windows front-end software WDwint (Nelson 2009) to analyze the data. To get started, the spectral type F5 (taken from SIMBAD, no reference given; main sequence assumed) was adopted. Interpolated tables from Cox (2000) gave a temperature $T_1 = 6650 \pm 300$ K and $\log g = 4.355 \pm 0.020$. (The quoted errors refer to two and one half spectral sub-classes.) An interpolation program by Terrell (1994, available from Nelson 2009) gave the Van Hamme (1993) limb darkening values; and finally, a logarithmic (LD=2) law for the limb darkening coefficients was se-

Table 3: Limb darkening values from Van Hamme (1993) for $T_1 = 6650$ K and $T_2 = 4221$ K.

Band	x_1	x_2	y_1	y_2
Bol	0.640	0.548	0.243	0.266
V	0.705	0.781	0.280	0.260
R_C	0.632	0.749	0.287	0.297
I_C	0.548	0.664	0.275	0.309

lected, appropriate for temperatures < 8500 K (ibid.). The limb darkening coefficients are listed below in Table 3. (The values for the second star are based on the later-determined temperature of 4248 K and assumed spectral type of K6.) Convective envelopes for both stars were used, appropriate for cooler stars (hence values gravity exponent $g = 0.32$ and albedo $A = 0.500$ were used for each).

From the GCVS 4 designation (EW) and from the shape of the light curve, mode 2 (detached) was used. Early on, it was noted that the maxima between eclipses were unequal. This is the O'Connell effect (Davidge & Milone 1984, and references therein) and is usually explained by the presence of one or more star spots. Because Max II (phase 0.75) was lower than Max I (phase 0.25), a solution was first obtained with a spot added to star 1. (Later on, a solution was sought with the spot on star 2 but it gave poorer residuals than the one for star 1, so the former was adopted.)

Convergence by the method of multiple subsets was reached after a considerable number of iterations. (The subsets were: (a, e, L_1), (ω, T_2, q), (V_γ, Ω_2). and (e, i, Ω_1). The spots were handled separately.)

Detailed reflections were tried, with nref = 2, but there was little–if any–difference in the fit from the simple treatment. There are certain uncertainties in the process (see Csizmadia et al. 2013; Kurucz 2002). On the other hand, the solution is very weakly dependent on the exact values used.

In the first set of iterations when the fit was near, the sigmas for each dataset were adjusted, based on the output of WD (viz. computed from the sum of residuals for each dataset plus number of points). To aid in comparison between different solutions, the same sigmas were then used throughout the different trails.

Despite multiple trials, no completely satisfactory solution could be reached in mode 2 with $T_1 = 6650$ K. (The fit for the secondary eclipse in the I band was poor.) A better solution was achieved by assuming an earlier spectral type, that of F2, with a temperature of $T_1 = 7000$ K (Cox 2000). Designate these as solutions A and B, respectively. Additional considerations (see later discussion) suggested that mode 5 (Algol) should be investigated. Trials therefore were made with mode 5 at the same two temperatures. Solution D with $T_1 = 7000$ K was unsatisfactory, but solution C with $T_1 = 6650$ K stood out from all the rest for a number of reasons to be discussed later.

All four models are presented in Table 4. Note that estimating the uncertainties in temperatures T_1 and T_2 is somewhat problematic. A common practice is to quote the temperature difference over–say–1.5 spectral sub-classes (assuming that the classification is good to one spectral sub-classes, the precision being unknown). In addition, various different calibrations have been made (Cox 2000, pages 388-390 and references therein, and Flower 1996), and the variations between the various calibrations can be significant. (Flower gives $T_1 = 6542$ K for F5 for example.) However, there is an additional uncertainty here because a spectral type (for star 1) is assumed to be F2. Therefore, a larger uncertainty, that of two and one half spectral sub-classes is adopted here, giving an uncertainty of ± 300 K to the absolute temperatures of each. The modelling error in temperature T_2, relative to T_1, is indicated by the WD output to be much smaller, around 20 K.

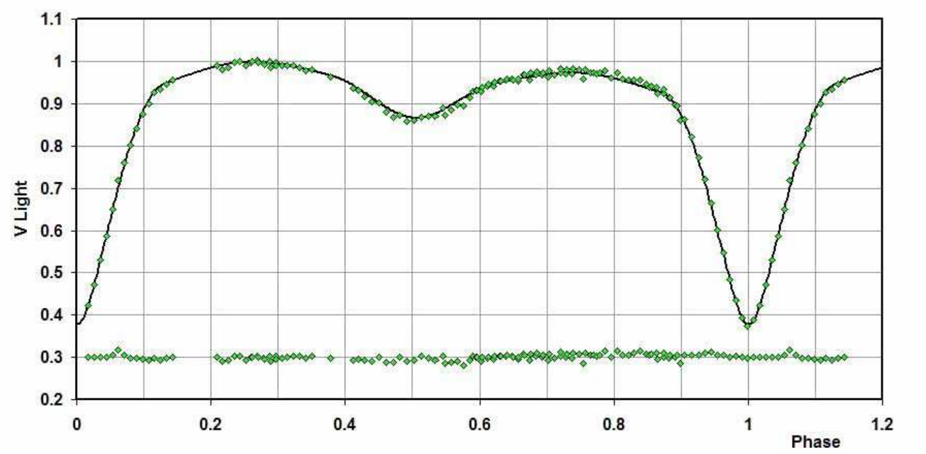

Figure 3. *V* light curves for BN Peg (solution C) – data, WD fit, and residuals.

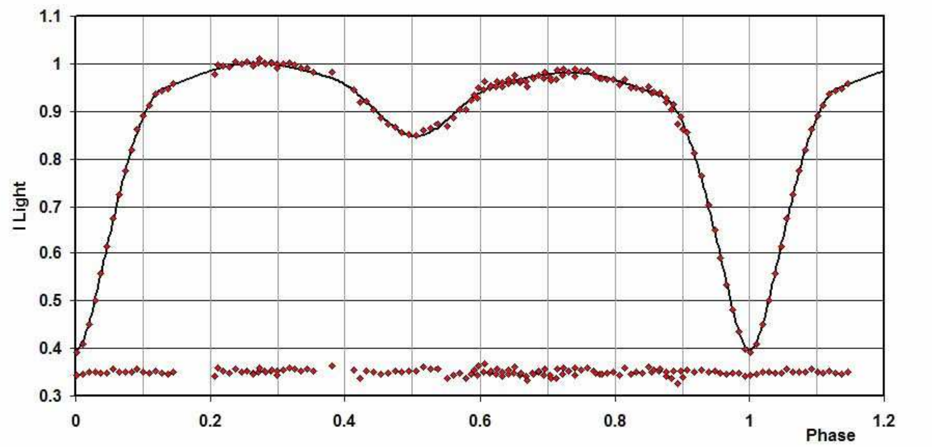

Figure 4. *R* light curves for BN Peg (solution C) – data, WD fit, and residuals.

The light curve data and the fitted curves for solution C are depicted in Figures 3–5. The residuals (in the sense observed-calculated) are also plotted, shifted upwards by 0.30, 0.35, and 0.35 units, respectively.

The radial velocities and the fit of solution C are shown in Fig. 6. A three-dimensional representation from Binary Maker 3 (Bradstreet 1993) is shown in Fig. 7.

The WD output fundamental parameters and errors are listed in Table 5. Most of the errors are output or derived estimates from the WD routines. From Kallrath & Milone (1999), the fill-out factor is $f = (\Omega_I - \Omega)/(\Omega_I - \Omega_O)$, where Ω is the modified Kopal potential of the system, Ω_I is that of the inner Lagrangian surface, and Ω_O, that of the outer Lagrangian surface, was also calculated.

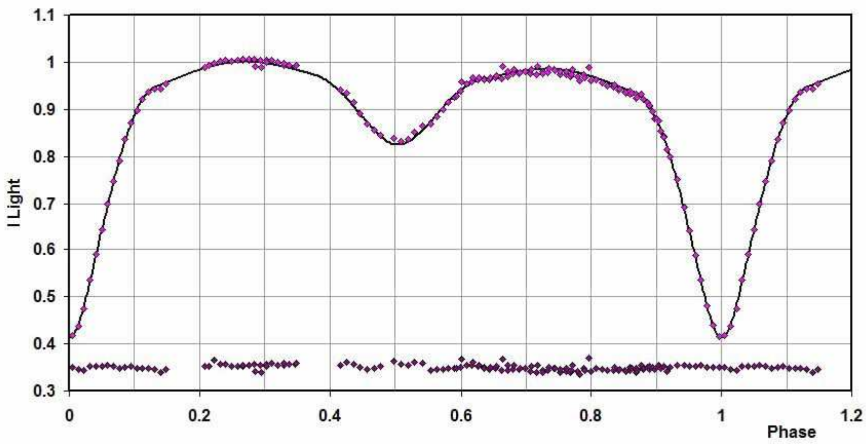

Figure 5. *I* light curves for BN Peg (solution C) – data, WD fit, and residuals.

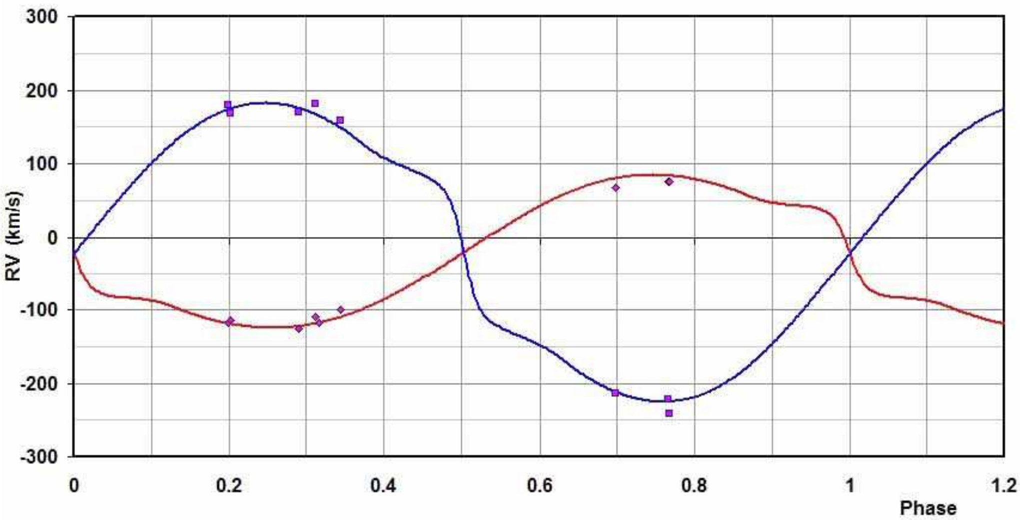

Figure 6. Radial velocity curves for BN Peg – data and WD fit.

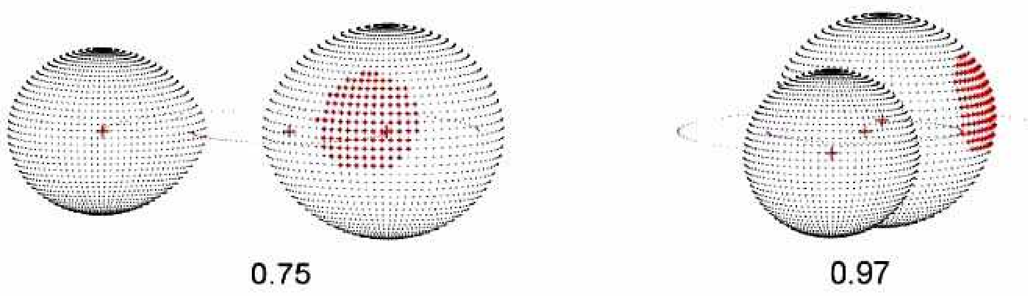

Figure 7. Binary Maker 3 representation of the system – at phases 0.75 and 0.97.

Table 4: Wilson-Devinney parameters.

Solution >>	A	B	C	D		
WD Quantity	value	value	value	value	error	unit
Mode	2	2	5	5	—	—
Spectral type	F5	F2	F5	F2	—	—
Temperature T_1	6650	7000	6650	7000	[fixed]	K
Temperature T_2	4248	4388	4221	4389	20	K
$q = m_2/m_1$	0.490	0.505	0.486	0.505	0.004	—
Potential Ω_1	3.108	3.133	3.159	3.175	0.008	—
Potential $\Omega_2 2$	2.901	2.944	2.881	2.903	0.008	
Inclination, i	83.4	83.5	82.6	82.2	0.1	deg
Semi-maj. axis, a	4.59	4.61	4.59	4.61	0.06	sol. rad.
Syst. velocity, V_γ	−22.0	−20.8	−20.8	−20.8	1.8	km/s
Eccentricity, e	0.006	0.006	0.014	0.008	0.001	—
Phase shift	0.0028	0.0028	0.0023	0.0025	0.0003	—
Arg. periastron, ω	19.2	19.1	17.6	19.8	0.1	deg
Spot co-latitude	81	75	79	75	10	deg
Spot longitude	74	78	81	78	5	deg
Spot radius	27.4	27.4	34.9	27.4	4	deg
Spot temp. factor	0.9659	0.9650	0.9793	0.9650	0.0020	—
$L_1/(L_1 + L_2)$ (V)	0.9475	0.9472	0.9460	0.9417	0.0002	—
$L_1/(L_1 + L_2)$ (R_C)	0.9222	0.9243	0.9195	0.9169	0.0003	—
$L_1/(L_1 + L_2)$ (I_C)	0.8952	0.8991	0.8911	0.8897	0.0004	—
r_1 (pole)	0.3777	0.3762	0.3707	0.3707	0.0004	orb. rad.
r_1 (point)	0.4329	0.4320	0.4205	0.4216	0.0008	orb. rad
r_1 (side)	0.3946	0.3930	0.3862	0.3864	0.0005	orb. rad.
r_1 (back)	0.4116	0.4103	0.4020	0.4026	0.0006	orb. rad.
r_2 (pole)	0.2914	0.2917	0.2944	0.2987	0.0003	orb. rad.
r_2 (point)	0.3756	0.3695	0.4216	0.4274	0.0017	orb. rad
r_2 (side)	0.3032	0.3033	0.3068	0.3115	0.0003	orb. rad.
r_2 (back)	0.3324	0.3313	0.3389	0.3438	0.0005	orb. rad.
$\sum \omega_{res}^2$	0.01801	0.01745	0.01737	0.01845	—	—

Table 5: Fundamental parameters.

Solution >>>	A	B	C	D		
Quantity	value	value	value	value	Error	unit
mode	2	2	5	5	—	—
Temperature, T_1	6650	7000	6650	7000	300	K
Temperature, T_2	4248	4338	4221	4389	300	K
Mass, m_1	1.717	1.723	1.725	1.723	0.05	$M_\odot$
Mass, m_2	0.841	0.870	0.839	0.870	0.004	$M_\odot$
Radius, R_1	1.81	1.82	1.78	1.78	0.02	$R_\odot$
Radius, R_2	1.42	1.43	1.45	1.47	0.02	$R_\odot$
$M_{bol,1}$	2.88	2.66	2.93	2.70	0.1	mag
$M_{bol,2}$	5.36	5.21	5.35	5.14	0.1	mag
Log g_1	4.16	4.16	4.18	4.17	0.01	cgs
Log g_2	4.06	4.07	4.04	4.04	0.02	cgs
Luminosity, L_1	5.8	7.1	5.5	6.9	0.5	$L_\odot$
Luminosity, L_2	0.59	0.68	0.60	0.72	0.05	$L_\odot$
Fill-out factor 1	−0.86	−0.822	−1.06	−0.96	0.10	—
Fill-out factor 2	−0.15	−0.20	0	0	0.10	—
Distance, r	354	394	345	389	35	pc

To determine the distance r, the analysis (using solution C) proceeded as follows: First the WD routine gave the absolute bolometric magnitudes of each component; these were then converted to the absolute visual (V) magnitudes of both, $M_{V,1}$ and $M_{V,2}$, using the bolometric corrections BC = −0.140 and −0.984 for stars 1 and 2 respectively. The latter were taken from interpolated tables constructed from Cox (2000). The absolute V magnitude was then computed in the usual way, getting $M_V = 3.02 \pm 0.20$ magnitudes. The apparent magnitude in the V passband was $V = 10.84 \pm 0.07$, taken from the Tycho values (Hog et al. 2000) and converted to a Johnson magnitude using relations due to Henden (2001). The colour excess (in $B-V$) was obtained in the usual way, by subtracting the tabular value of $B - V$ (for that spectral class) from the observed (converted Tycho) value. This gave $\mathrm{E}[B-V] = -0.07$ magnitudes which is not physically possible. However, reference to the dust tables of Schlegel et al. (1998) revealed a value of $\mathrm{E}[B - V] = 0.063$ for those galactic coordinates. Since the $\mathrm{E}[B - V]$ values have been derived from full-sky far-infrared measurements, they therefore apply to objects outside of the Galaxy; this value of $\mathrm{E}[B - V]$ so derived then represents an upper limit for closer objects within the Galaxy. Hence the lower value of half that, 0.032 is reasonable, and was adopted. (An uncertainty of–say–half this amount was used in the error calculation for distance.)

Galactic extinction was obtained from the usual relation $A_V = R\,\mathrm{E}[B - V]$, using R = 3.1 for the reddening coefficient. Hence, for solution C, a distance r = 345 pc was calculated from the standard relation:

$$r = 10^{0.2(V - M_V - A_V + 5)}\ \mathrm{pc} \qquad (2)$$

The errors were assigned as follows: $\delta M_{bol,1} = \delta M_{bol,2} = 0.01$, $\delta \mathrm{BC}_1 = 0.020$, $\delta \mathrm{BC}_2 = 0.330$ (the variation of 2.5 spectral sub-classes), $\delta V = 0.07$, $\delta \mathrm{E(B-V)} = 0.10$, all in magnitudes, and $\delta R = 0.1$. Combining the errors rigorously (i.e., by adding the variances) yielded an estimated error in r of 35 pc.

The evolutionary status of this system is interesting. Solution A (detached, F5, T_1

= 6650 K) gives a primary mass, radius and luminosity that are too large for the zero age main sequence (ZAMS) values listed in column 3 (Cox, 2000). Reference to the evolutionary tables of Schaller et al. (1992, solar type, mass 1.7 solar masses, their table 16) reveals that the temperature of $T_1 = 6650$ K is too low to fit the terminal age main sequence (TAMS) or any evolved state. Solution A is therefore rejected.

Turning to solution B (detached, F2, $T_1 = 7000$ K), one might believe that star 1 started with a higher temperature on the TAMS but cooled as it evolved. However, reference to the same evolutionary tables (ibid) reveals that, for an age of 1.3 Gy, the temperature would fit, but then the actual luminosity at 7.1 $L_\odot$ would be too small for their computed value of 11.3 $L_\odot$. For this reason, we reject solution B.

Solution C (Algol, F5, $T_1 = 6650$ K) fits better because temperature T_1 matches the assumed spectral type, the mass ratio matches the spectrographic value, and the sum of residuals squared is the lowest of the four solutions. Also, most importantly, Solution C makes sense because Algols are known to have experienced mass flow from the secondary (but originally more massive star) to its companion. That would explain the excess mass for the F5 star. Its larger radius would then account for the higher luminosity. Therefore we adopt solution C (mode 5, Algol) as the correct one.

In conclusion, the fundamental parameters of this system have been determined, albeit to a somewhat lower level of precision than one would like. It is to be hoped that higher precision data from a planned remote site with routine photometric skies plus a renewed classification will confirm the exact nature of this system.

Acknowledgements: It is a pleasure to thank the staff members at the DAO (especially Dmitry Monin and David Bohlender) for their usual splendid help and assistance.

References:

Bradstreet, D.H., 1993, "Binary Maker 2.0 - An Interactive Graphical Tool for Preliminary Light Curve Analysis", in Milone, E.F. (ed.) Light Curve Modelling of Eclipsing Binary Stars, pp 151-166 (Springer, New York, N.Y.)

Cox, A.N. 2000, Allen's Astrophysical Quantities, 4th ed., (Springer, New York, NY)

Csizmadia, S., Pasternacki, T., Dreyer, C., Cabrera, A., Erikson, A., Rauer, H., 2013, *A&A*, **549**, A9 DOI

Davidge, T.J., Milone, E.F., 1984, *ApJS*, **55**, 571 DOI

Flower, P.J., 1996, *ApJ*, **469**, 355 DOI

Henden, A., 2001, http://www.tass-survey.org/tass/catalogs/tycho.old.html

Hoffmeister, C. von, 1935, *AN*, **255**, 401 DOI

Høg, E., et al., 2000, *A&A*, **355**, L27

Jensch, A. von, 1935, *AN*, **255**, 417 DOI

Kallrath, J., Milone, E.F., 1999, Eclipsing Binary Stars–Modeling and Analysis (Springer-Verlag)

Kallrath, J., Milone, E.F., Terrell, D., Young, A.T., 1998, *ApJ*, **508**, 308 DOI

Kreiner, J.M., 2004, *AcA*, **54**, 207

Kurucz, R.L., 2002, *Baltic Astron.*, **11**, 101

Mallama, A.D., 1980, *ApJS*, **44**, 241 DOI

Nelson, R.H., 2009, Software, http://www.variablestarssouth.org/profilegrid_blogs/software-by-bob-nelson/

Nelson, R.H., 2010a, Spreadsheets, http://www.variablestarssouth.org/profilegrid_blogs/spreadsheets-by-bob-nelson/
Nelson, R.H., 2010b, "Spectroscopy for Eclipsing Binary Analysis" in The Alt-Az Initiative, Telescope Mirror & Instrument Developments (Collins Foundation Press, Santa Margarita, CA), R.M. Genet, J.M. Johnson and V. Wallen (eds)
Nelson, R.H., 2016, Bob Nelson's *O-C* Files, http://www.aavso.org/bob-nelsons-o-c-files
Nelson, R. H., Şenavcı, H.V. Baştürk, Ö., Bahar, E., 2014, *New Astron.*, **29**, 57 DOI
Rucinski, S. M., 2004, *IAUS*, **215**, 17
Schaller, G., Schaerer, D., Meynet, G., Maeder, A., 1992, *A&AS*, **96**, 269
Schlegel, D.J., Finkbeiner, D.P., Davis, M., 1998, *ApJ*, **500**, 525 DOI
Terrell, D., 1994, Van Hamme Limb Darkening Tables, vers. 1.1.
Van Hamme, W., 1993, *AJ*, **106**, 2096 DOI
Wilson, R.E., Devinney, E.J., 1971, *ApJ*, **166**, 605 DOI
Wilson, R.E., 1990, *ApJ*, **356**, 613 DOI

COMMISSIONS G1 AND G4 OF THE IAU
INFORMATION BULLETIN ON VARIABLE STARS

Volume 63 Number 6202 DOI: 10.22444/IBVS.6202

Konkoly Observatory
Budapest
17 March 2017

HU ISSN 0374 – 0676

NEW CCD TIMES OF MINIMA OF 17 ECCENTRIC ECLIPSING BINARY SYSTEMS

KIM, CHUN-HWEY[1]; KIM, HYUN-WOO[1,2]; PARK, JANG-HO[1,2]; SONG, MI-HWA[1]; JEONG, MIN-JI[1]; KIM, HYE-YOUNG[1]

[1] Department of Astronomy and Space Sciences, Chungbuk National University, Cheongju 361-763, Republic of Korea; e-mail: kimch@chungbuk.ac.kr

[2] Korea Astronomy and Space Science Institute, Daejeon 305-348, Republic of Korea

Observatory and telescope:
Sobaeksan Optical Astronomical Observatory (SOAO): 61cm Boller and Chivens reflecting telescope on an equatorial mount.

Detector:	A PIXIS 2K CCD for the observing seasons of 2009-2011 and a FLI 4K CCD for those of 2015-2017 were used and the fields of view for the CCD systems are $17.6' \times 17.6'$and $15.2' \times 15.2'$, respectively.

Method of data reduction:
Reduction of all CCD frames was made with the IRAF/DIPHO[1] software package.

Method of minimum determination:
Times of minimum light were computed with the method of Kwee & van Woerden (1956).

Explanation of the remarks in the table:
C1 and C2 denote the PIXIS 2K and FLI 4K CCD cameras, respectively. C3 = TYC 3570-1573-1 = 2MASS J19554410+5213346 = KIC 12903449 = [DCO2008] T-CYG1-1373. The '*d*' denotes the total eclipse duration times of seven binary stars having a flat-bottom at primary or secondary eclipses.

[1]IRAF is distributed by the National Optical Astronomical Observatories, operated by the Association of the Universities for Research in Astronomy, inc., under cooperative agreement with the National Science Foundation.

Times of minima:					
Star name	Time of min. HJD 2400000+	Error	Type	Filter	Rem.
AG Ari	57717.0978	0.0002	II	*R*	C2, $d \simeq 49^{\rm m}$
AL Ari	57357.9840	0.0002	II	*R*	C2, $d \simeq 65^{\rm m}$
CG Aur	57409.1039	0.0002	I	*R*	C2
V645 Aur	57768.15414	0.00008	II	*R*	C2, $d \simeq 12^{\rm m}$
WW Cam	57363.05325	0.00006	II	*V*	C2, $d \simeq 12^{\rm m}$
	57769.04056	0.00004	I	*R*	C2
AS Cam	57475.98222	0.00005	I	*V*	C2, $d \simeq 53^{\rm m}$
AV CMi	57770.1307	0.0003	II	*R*	C2
OX Cas	57330.9347	0.0002	I	*R*	C2
PV Cas	55100.2708	0.0002	II	*BVRI*	C1
	55480.1232	0.0004	II	*BVRI*	C1
	55494.9672	0.0002	I	*BVRI*	C1
	55550.9830	0.0002	I	*BVRI*	C1
	55836.3097	0.0003	I	*BV*	C1
	55837.2198	0.0002	II	*BVRI*	C1
	55838.05977	0.00007	I	*BVRI*	C1
	55866.0682	0.0002	I	*BVRI*	C1
	55922.0810	0.0002	I	*BVRI*	C1
	57332.11993	0.00006	II	*R*	C2
V381 Cas	57330.0947	0.0001	I	*R*	C2
V821 Cas	57332.2172	0.0003	II	*R*	C2
CO Lac	57688.0732	0.0002	II	*BVR*	C2
MZ Lac	57319.9878	0.0005	II	*R*	C2
V401 Lac	57553.1778	0.0001	II	*R*	C2
	57718.05706	0.00005	I	*R*	C2, $d \simeq 32^{\rm m}$
V498 Mon	57718.2093	0.0006	II	*R*	C2
FT Ori	57320.27040	0.00007	II	*R*	C2, $d \simeq 40^{\rm m}$
TYC 3570-1573-1	57238.2590	0.0001	I	*R*	C2, C3

Remarks:

In order to obtain the eclipse timings of some eccentric eclipsing binary stars (EEB) the CCD photometric observations of the systems were made during the observing seasons of 2009–2017. All the raw CCD images obtained were pre-processed by compensating for bias, dark, and flat using the IRAF/CCDPRO package and post-processed using IRAF/DAOPHOT. Further details of raw data processing were described in Kim et al. (2014). A total of 28 timings for 17 EEBs were obtained from the observations. Type I and II labels in the fourth column of the table denote primary and secondary eclipses, respectively. Individual filtered timings determined from the multi-bandpass observations of PV Cas and CO Lac were calculated to be the weighted mean timings which are listed in the table. All the timings were archived into the database of Kreiner et al. (2001).

Acknowledgements:
We thank the staff of the Sobaeksan Optical Astronomical Observatory for assistance with our observations. We have frequently used the SIMBAD and VizieR databases operated by the Centre de Donnees Astronomiques (Strasbourg). This work was supported by the Basic Science Research Program through the National Research Foundation of Korea (NRF) funded by the Ministry of Education (2015R1D1A1A01058924).

References:

Kim, C.-H., Song, M.-H., Yoon, J.-N., Han, W. & Jeong, M.-J., 2014, *ApJ*, **788**, 134 DOI
Kreiner, J. M., Kim, C.-H., & Nha, I.-S., 2001, *An Atlas of (O-C) Diagrams of Eclipsing Binary Stars* (Krakow: Wydawn. Nauk. Akad. Pedagogicznej) DOI
Kwee, K. K., & van Woerden, H., 1956, *Bull. Astron. Inst. Neth.*, **12**, 327

COMMISSIONS G1 AND G4 OF THE IAU
INFORMATION BULLETIN ON VARIABLE STARS
Volume 63 Number 6203 DOI: 10.22444/IBVS.6203

Konkoly Observatory
Budapest
06 April 2017
HU ISSN 0374 – 0676

V2197 Cyg – A SEMI-DETACHED ECLIPSING BINARY?

NELSON, ROBERT H.[1,2]; ROBB, RUSSELL M.[2,3]

[1] 1393 Garvin Street, Prince George, BC, Canada, V2M 3Z1, email: bob.nelson@shaw.ca

[2] Guest investigator, Dominion Astrophysical Observatory, Herzberg Institute of Astrophysics, National Research Council of Canada

[3] Department of Physics and Astronomy, University of Victoria, Victoria, B.C., Canada, V8P 2W7

The variability of V2197 Cyg (NSVS 5761314, TYC 3167-1279-1), amongst many others, was discovered photographically by Margoni & Stagni (1984, hereafter M&S) who gave coordinates, magnitude ranges in B and V, finder charts for all 99 stars, elements (epoch, period), and preliminary light curves for about half the stars (but not for V2176 Cyg, their #58). Andronov et al. (1993) performed U, B, V, R, and I photometry of this and three other M&S stars; they went on in Andronov et al. (1994) to identify the system as an eclipsing variable, also giving the elements (including period = 0.46771 d) and eclipse duration. Skiff (1997) identified the M&S variables with those in the IRAS and GSC catalogues. Hoffman et al. (2008) provided an updated period, quoted 2MASS colours, and classified the system as β Lyrae. Since then, there have been a number of eclipse timings but no light curve analysis.

Light curve and radial velocity data have been acquired, but before any analysis could be performed, the first task was to examine the period variation. An eclipse timing difference (O–C) plot using all available data and the elements of Kreiner (2004) is reproduced in Fig. 1.

It will be seen that, even though all data are electronic (PE or CCD), there is a fair amount of scatter–larger than most of the error ranges. Clearly there must be unexplained physical reason for this discrepancy; future accurate data are required to sort out true relationship. In the meantime, the line of best fit must suffice. In view of the fact that all data were taken between cycles 7000 and 9000 (approximately), any errors due to uncertainties in the period are likely to be small.

A slightly different set of elements, specified in equation (1) was used in all phasing.

$$\mathrm{JD\,(Hel)\,Min\,I} = 2457514.9187(5) + 0.4657489(1)E \qquad (1)$$

In August of 2012, the lead author took 82 frames in V, 79 in R_C (Cousins) and 77 in the I_C (Cousins) band at his private observatory in Prince George, BC, Canada. The telescope was a 33 cm f/4.5 Newtonian on a Paramount ME mount; the camera was an SBIG ST-10XME. Standard reductions were then applied. The variable, comparison and check stars are listed in Table 1. The coordinates and magnitudes for all three stars are

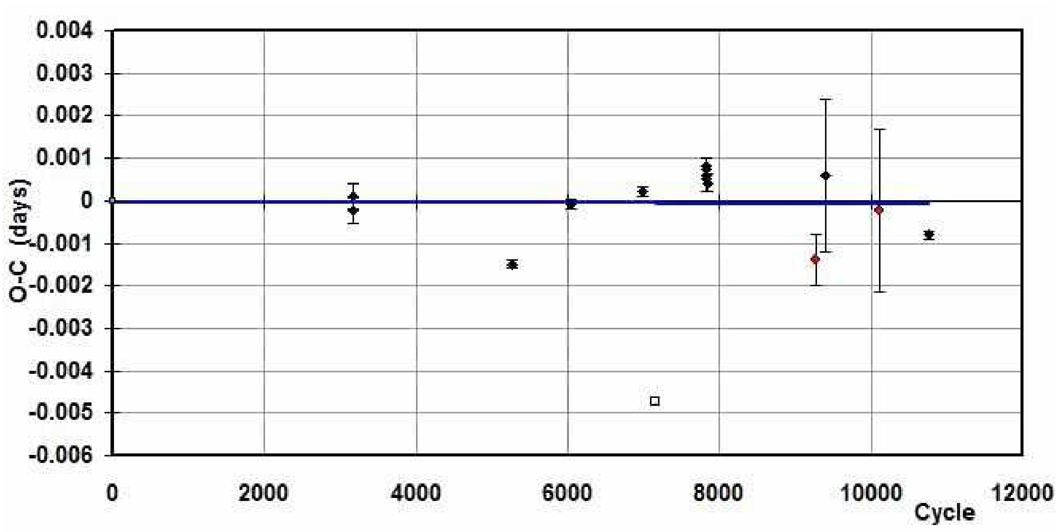

Figure 1. V2197 Cyg – eclipse timing (O–C) diagram. Legend: filled circles – photoelectric; black diamonds – CCD. The open square represents a rejected reading.

Table 1: Details of variable, comparison and check stars.

Object	GSC	RA (J2000)	Dec (J2000)	V (mag)	$B-V$ (mag)
Variable	3167-1279	$20^h50^m16\overset{s}{.}321$	$37°56'45\overset{''}{.}29$	12.04(17)	+0.17(22)
Comparison	3167-0649	$20^h50^m32\overset{s}{.}961$	$37°57'48\overset{''}{.}77$	10.47(4)	+0.30(6)
Check	3167-1451	$20^h50^m13\overset{s}{.}62$	$37°55'54\overset{''}{.}3$	11.66(na)	1.28(na)

from the Tycho Catalogue (Hog et al. 2000) and the 2MASS catalogue, (Cutri et al. 2003), except for the magnitudes of the check star, for which there was no reference in SIMBAD.

In September of 2011, 2013, and 2014, the lead author then took a total of 7 medium resolution (R $\sim$ 10000 on average) spectra of V2197 Cyg at the Dominion Astrophysical Observatory (DAO) in Victoria, British Columbia, Canada using the Cassegrain spectrograph attached to the 1.85 m Plaskett Telescope. He used the 21181 grating with 1800 lines/mm, blazed at 5000 Å giving a reciprocal linear dispersion of 10 Å/mm in the first order. The wavelengths ranged from 5000 to 5260 Å, approximately. A log of observations is given in Table 2. (The last value for V2 listed in the table, –270.7 km/s, was not used in the modelling on the grounds that it was deviant by more than 3σ from the curve of best fit; however, it is plotted in Fig. 6 for reference.)

Frame reduction was performed by software 'RaVeRe' (Nelson 2009). See Nelson et al. (2014) for further details.

Radial velocities were determined using the Rucinski broadening functions (Rucinski 2004; Nelson 2010b; Nelson et al. 2014). An Excel worksheet with built-in macros (written by him) was used to do the necessary radial velocity conversions to geocentric and back to heliocentric values (Nelson 2010a). The resulting RV determinations are also presented in Table 2. For all the data, the results were corrected typically 5 % up to allow for the small phase smearing. Correction was achieved by dividing the RVs by the factor $f = (\sin X)/X$; where$X = 2\pi\, t/P$, and where t denotes exposure time and P denotes the orbital period. For spherical stars, this correction is exact; in other cases, it can be shown to be close enough for any deviation to fall below observational errors. The mean

Table 2: Log of DAO observations.

DAO Image #	Mid Time (HJD−2400000)	Exposure (sec)	Phase at Mid-exp	V_1 (km/s)	V_2 (km/s)
7849	55808.9875	3561	0.229	–148.0	+159.8
8141	55820.6522	3600	0.274	–142.0	+172.0
8153	55820.9065	3600	0.820	+89.4	–217.9
8217	55825.8105	2876	0.350	–134.4	+140.5
9629	56544.6973	3600	0.857	+77.8	–205.6
9638	56544.8504	3600	0.186	–131.0	+174.0
24359	56906.9975	3600	0.745	+97.9	–270.7

rms errors for RV_1 and RV_2 were 9.1 and 14.0 km/s, respectively, and the overall rms deviation from the (sinusoidal) curves of best fit was 12.3 km/s. The best fit yielded the values $K_1 = 123.0(8)$ km/s, $K_2 = 214.3(1.1)$ km/s and $V_\gamma = -30.8(6)$ km/s, and thus a mass ratio $q_{sp} = K_1/K_2 = M_2/M_1 = 0.574(5)$.

One of the authors (R.M.R.) obtained a spectrum of V2197 Cyg at the Dominion Astrophysical Observatory (DAO) with the 1.85 m telescope and the 2131 Cassegrain spectrograph, operating at a reciprocal dispersion of about 60 Å/mm and 0.9 Å/px. The start time of the exposure was 2013 June 22 at UT+09:25:33 and lasted 666 s (JD 2456465.8927), corresponding to phase 0.66. The strength of the G-Band and Hydrogen lines indicate F3(±1)V. A comparison spectrum of 48 Boo (F3V) observed with the same configuration is plotted for comparison in Fig. 2, where the spectra have been scaled and offset an arbitrary amount. The spectrum of V2197 Cyg has been smoothed with a 3 point running average. The lines are (left to right) Ca II K-line, Ca II H-line blended with Hϵ, Hδ, and Hγ.

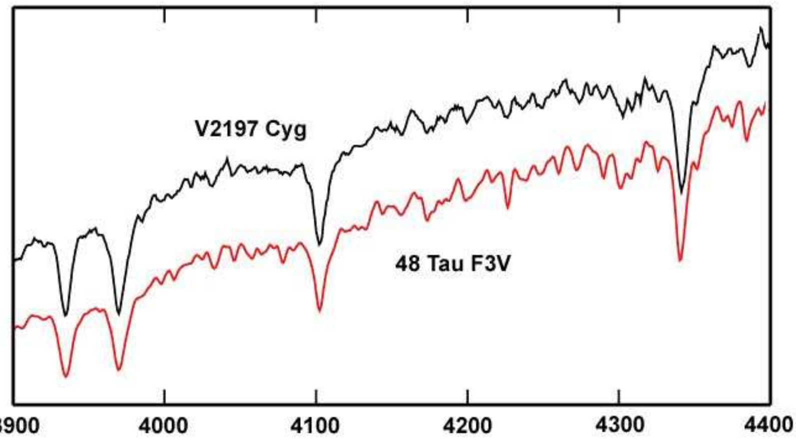

Figure 2. Classification spectra.

Next, the lead author (R.H.N.) used the 2003 version of the Wilson-Devinney (WD) light curve and radial velocity analysis program with Kurucz atmospheres (Wilson and Devinney 1971; Wilson 1990; Kallrath et al. 1998) as implemented in the Windows front-end software WDwint (Nelson 2009) to analyze the data. Using the spectral type of F3V,

Table 3: Limb darkening values from Van Hamme (1993) for $T_1 = 6820$ K and $T_2 = 5037$ K.

Band	x_1	x_2	y_1	y_2
Bol	0.639	0.643	0.249	0.160
V	0.696	0.797	0.284	0.107
R_C	0.622	0.735	0.291	0.165
I_C	0.537	0.647	0.280	0.183

the tables of Cox (2000), and those of Flower (1996) gave a temperature $T_1 = 6820 \pm 200$ K and $\log g_1 = 4.328 \pm 0.012$. (The quoted errors refer to one and one half spectral subclasses.) An interpolation program by Terrell (1994, available from Nelson 2009) gave the Van Hamme (1993) limb darkening values; and finally, a logarithmic (LD = 2) law for the limb darkening coefficients was selected, appropriate for temperatures < 8500 K (ibid.). The limb darkening coefficients are listed below in Table 3. (The values for the second star are based on the later-determined temperature of 5037 K and assumed spectral type of K2.) Convective envelopes for both stars were used, appropriate for cool stars (hence values gravity exponent $g = 0.32$ and albedo $A = 0.500$ were used for each).

From the shape of the light curve, it was clear that the system was in near contact but the difference in the depths of the two minima indicate that the stars are not in thermal contact. Various modes were tried: mode 3 (contact), mode 2 (detached), mode 5 (Algol) and, finally mode 6 (double contact). Convergence was obtained by the method of multiple subsets: (a, V_γ, L_1), (T_2, q), (i, T_2) and (T_2, Ω_1). The net result was residuals (or, more correctly, sums of residuals squared) that were nearly identical, making it difficult to choose between the scenarios. A useful procedure was to proceed with mode 6 (because the potentials were fixed from the mass ratio, thereby reducing the number of free parameters), find the optimum using differential corrections, then switch to another mode, making slight adjustments in potentials Ω_1 and Ω_2 as necessary to satisfy the conditions for that mode, then proceeding with differential corrections once again. This led to the best minimum. Mode 3 failed because differential corrections wanted increases in potential Ω_1 that would force star 1 inside the Roche lobe (i.e., $\Omega_1 > \Omega_i$ where the latter is the inner critical potential), and in any case, the unequal depths of minima precluded this mode. Mode 2 (detached) also failed for the same reason, except that this time, differential corrections wanted potential $\Omega_2 > \Omega_i$, that is for the secondary to be at or inside the Roche lobe. Therefore only mode 5 (semi-detached) and mode 6 (double contact) remained.

In the first set of iterations when the fit was near, the sigmas for each dataset were adjusted, based on the output of WD (viz. computed from the sum of residuals for each dataset plus number of points). The same values were then used throughout in order that results from the different iterations could be compared.

It would seem that mode 5 (semi-detached) gave the best solution, but only by a very small margin. Also, in view of the errors in the data, it seems clear that another data set might well favour a different mode. Therefore one cannot in confidence differentiate between the two modes. On the other hand, all produce virtually identical fundamental parameters—certainly well within the estimated errors.

Detailed reflections were tried, with $n_{ref} = 2$, but there was little—if any—difference in the fit from the simple treatment. There are certain uncertainties in the process (see Csizmadia et al. 2013; Kurucz 2002). On the other hand, the solution is very weakly dependent on the exact values used.

Solutions were tested for third light; suggested corrections were smaller than estimated

Table 4: Wilson-Devinney parameters.

WD Quantity	Mode 5	Mode 6	error	unit
Temperature T_1	6820	6820	[fixed]	K
Temperature T_2	5037	5037	12	K
$q = m_2/m_1$	0.595	0.595	0.018	—
Potential Ω_1	3.0551	3.0542	0.063	—
Potential Ω_2	3.0542	3.0542	—	
Inclination, i	80.20	80.20	0.07	deg
Semi-maj. axis a	3.182	3.182	0.056	$R_\odot$
Syst. velocity, V_γ	–25.2	–25.2	0.6	km/s
Phase shift	0.0011	0.0011	0.0001	—
$L_1/(L_1 + L_2)\,(V)$	0.8743	0.8744	0.0002	—
$L_1/(L_1 + L_2)\,(R_C)$	0.8455	0.8456	0.0002	—
$L_1/(L_1 + L_2)\,(I_C)$	0.8195	0.8197	0.0002	—
r_1 (pole)	0.3996	0.3997	0.0023	orb. rad.
r_1 (point)	0.5253	0.5532	0.1387	orb. rad
r_1 (side)	0.4229	0.4231	0.0032	orb. rad.
r_1 (back)	0.4517	0.4519	0.0052	orb. rad.
r_2 (pole)	0.3136	0.3136	0.0022	orb. rad.
r_2 (point)	0.4468	0.4468	0.0085	orb. rad
r_2 (side)	0.3277	0.3277	0.0024	orb. rad.
r_2 (back)	0.3599	0.3599	0.0023	orb. rad.
$\sum \omega_{res}^2$	0.02513	0.02519	—	—

errors. Therefore third light was eliminated. In spite of the fact that spots might be expected on one or other stars, no attempt was made to include them, as there was no need. It seems likely that any indication of a spot occurring on the secondary would be overwhelmed by the light of the primary.

The two acceptable solutions are presented in Table 4. For the most part, the error estimates are the formal errors provided by the WD routines and are known to be low; the actual errors may be several times the quoted ones. However, it is a common practice to quote these estimates, and we do so now. Also, estimating the uncertainties in temperatures T_1 and T_2 is somewhat problematic. A common practice is to quote the temperature difference over—say—1.5 spectral sub-classes (assuming that the classification is good to one spectral sub-class). In addition, various different calibrations have been made (Cox 2000, page 388–390 and references therein; and Flower 1996), and the variations between the various calibrations can be significant. Here a spectral type (for star 1) was determined to be F3($\pm$1) sub-classes. Then the uncertainty over one and one half spectral sub-classes gives an uncertainty of $\pm$200 K to the absolute temperatures of each. The modelling error in temperature T_2, relative to T_1, is indicated by the WD output to be much smaller, around 12 K.

The light curve data and the fitted curves are plotted in Figures 3–5. The residuals (in the sense observed-calculated) are also plotted, shifted upwards by 0.40 units.

The radial velocities and the fit are plotted in Fig. 6. A three-dimensional representation from Binary Maker 3 (Bradstreet, 1993) is depicted in Fig. 7.

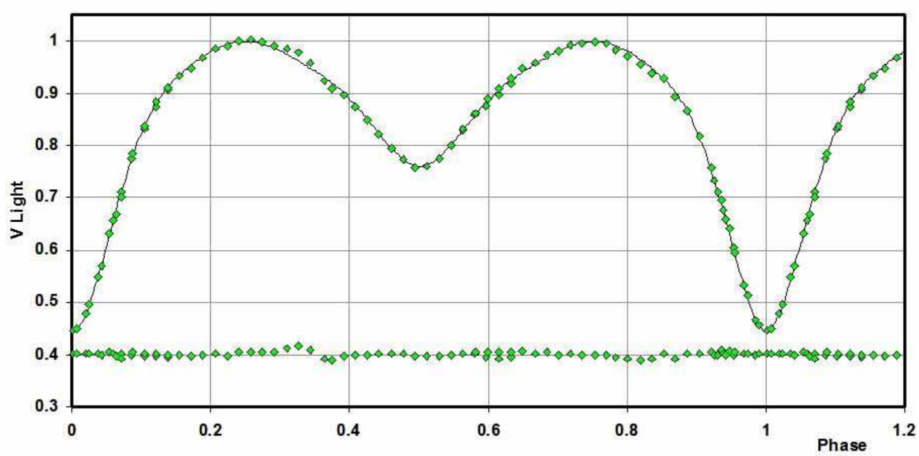

Figure 3. V light curves for V2197 Cyg – data, WD fit, and residuals.

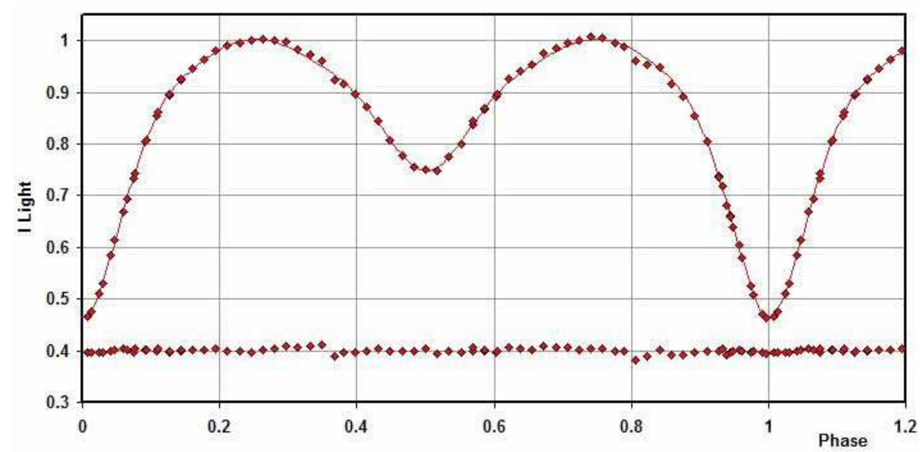

Figure 4. R_C light curves for V2197 Cyg – data, WD fit, and residuals.

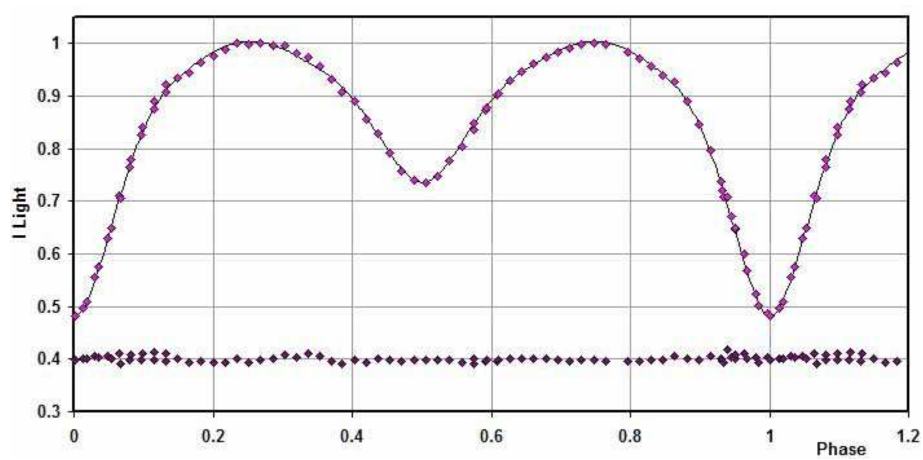

Figure 5. I_C light curves for V2197 Cyg – data, WD fit, and residuals.

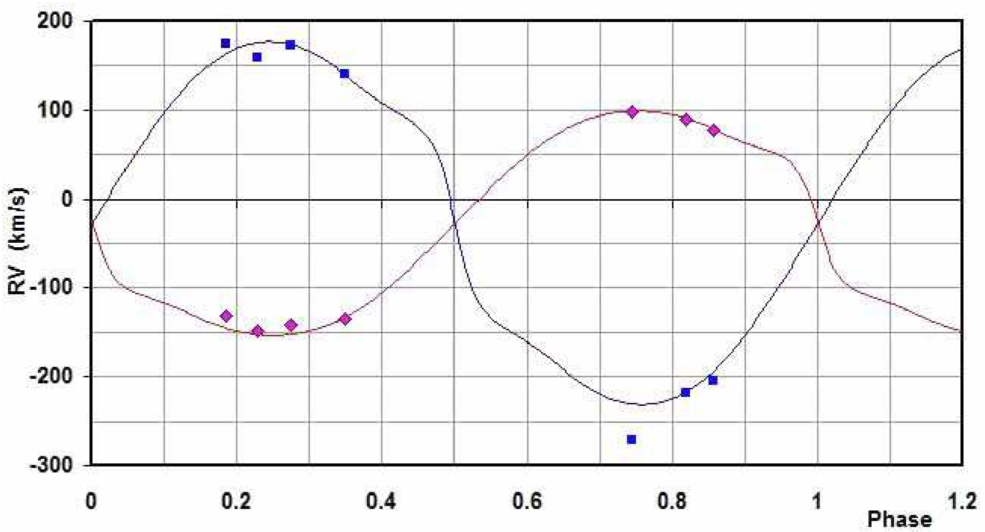

Figure 6. Radial velocity curves for V2197 Cyg – data and WD fit.

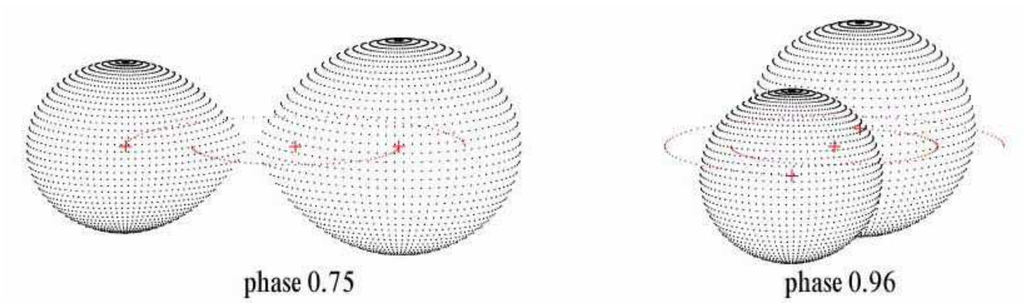

Figure 7. Binary Maker 7 representation of the system – at phases 0.75 and 0.97.

The WD output fundamental parameters and errors are listed in Table 5 using the data from the mode 5 solution (and are virtually identical with those from mode 6). From its temperature, star 2 was assumed to be spectral class K2. Most of the errors are output or derived estimates from the WD routines. From Kallrath & Milone (1999), the fill-out factor is $f = (\Omega_I - \Omega)/(\Omega_I - \Omega_O)$, where Ω is the modified Kopal potential of the system, Ω_I is that of the inner Lagrangian surface, and Ω_O, that of the outer Lagrangian surface, was also calculated.

To determine the distance r, the analysis proceeded as follows: first the WD routine gave the absolute bolometric magnitudes of each component; these were then converted to the absolute visual (V) magnitudes of both, $M_{V,1}$ and $M_{V,2}$, using the bolometric corrections BC = –0.120 and –0.420 for stars 1 and 2 respectively. The latter were taken from interpolated tables constructed from Cox (2000). The absolute V magnitude was then computed in the usual way, getting $M_V = 3.39 \pm 0.12$ magnitudes. The apparent magnitudes in the B and V passbands were $B = 12.10 \pm 0.01$ mag and $V = 11.65 \pm 0.01$ mag (presumed errors), taken from the Andronov et al. (1993). The colour excess (in B–V) was obtained in the usual way, by subtracting the tabular value of B–V (for that spectral class) from the observed value. This gave $E[B\text{–}V] = +0.07 \pm 0.08$ magnitudes.

Hence, for the mode 5 solution, a distance $r = 407$ pc was calculated from the standard

Table 5: Fundamental parameters.

Quantity	Observed	Tables	error	unit
Temperature, T_1	6820	6820	200	K
Temperature, T_2	5037	5026	200	K
Mass, m_1	1.25	1.48	0.02	$M_\odot$
Mass, m_2	0.75	0.74	0.01	$M_\odot$
Radius, R_1	1.36	1.38	0.02	$R_\odot$
Radius, R_2	1.07	0.80	0.02	$R_\odot$
$M_{bol,1}$	3.41	3.45	0.02	mag
$M_{bol,2}$	5.24	5.98	0.02	mag
$\log g_1$	4.27	4.33	0.01	cgs
$\log g_2$	4.25	4.51	0.03	cgs
Luminosity, L_1	3.57	4.54	0.07	$L_\odot$
Luminosity, L_2	0.66	0.36	0.01	$L_\odot$
Fill-out factor 1	–0.0003	—	—	—
Fill-out factor 2	0	—	—	—
Distance, r	407	—	50	pc

relation:

$$r = 10^{0.2(V-M_V-A_V+5)}\ \mathrm{pc} \qquad (2)$$

The errors were assigned as follows: $\delta M_{bol,1} = \delta M_{bol,2} = 0.02$, $\delta BC_1 = 0.015$, $\delta BC_2 = 0.120$ (the variation over 1.5 spectral sub-classes), $\delta V = 0.02$, all in magnitudes. Combining the errors rigorously (i.e., by adding the variances) yielded an estimated error in r of 51 pc.

The distance estimate is in statistical agreement with the value of 320 ± 50 pc from the Gaia Catalogue[1] (Gaia Collaboration 2016, Lindegren et al. 2016).

For comparison, the tabular values for the fundamental parameters, taken from Cox (2000) for F3 and K2 main sequence stars, are given in Table 5. Of course, these apply to detached stars, which these are not; however, comparisons are useful. Star 1 is seen to be undermassive and underluminous for F3 (and the same for F4 which has a tabulated mass of 1.44 $M_\odot$ and a luminosity of 4.04 $L_\odot$) while star 2 has a larger radius (which is to be expected for one that fills its Roche lobe) and a higher luminosity (a function of its larger radius). The luminosities are fairly close but display differences, as one would expect for interacting stars.

In conclusion, the fundamental parameters of this system have been determined, albeit to a somewhat lower level of precision than one would like, mostly due to the uncertainty in the spectral class and the degree of interstellar absorption. Also, more accurate photometric data might enable one to distinguish definitively between the various modes.

Acknowledgements: It is a pleasure to thank the staff members at the DAO (especially Dmitry Monin, David Bohlender, and the late Les Saddlmyer) for their usual splendid help and assistance.

This work has made use of data from the European Space Agency (ESA) mission Gaia

[1] https://www.cosmos.esa.int/web/gaia/gaia-data

(https://www.cosmos.esa.int/gaia), processed by the Gaia Data Processing and Analysis Consortium (DPAC, https://www.cosmos.esa.int/web/gaia/dpac/consortium). Funding for the DPAC has been provided by national institutions, in particular the institutions participating in the Gaia Multilateral Agreement.

The eclipse timing (O–C) Excel file may be found online at Nelson (2016).

References:

Andronov, I. L., Chinarova, L. L., Kolesnikov, S. V., Shakhovskoy, N. M.. Shvechkova, N. A., 1993, *IBVS*, No. 3933

Andronov, I. L., Chikrigin, A. V., Kimeridze, G. N, 1994, *Odessa Astron. Pub.*, **7**, 89

Bradstreet, D.H., 1993, "Binary Maker 2.0 – An Interactive Graphical Tool for Preliminary Light Curve Analysis", in Milone, E.F. (ed.) Light Curve Modelling of Eclipsing Binary Stars, pp 151-166 (Springer, New York, N.Y.)

Cox, A. N., ed, 2000, Allen's Astrophysical Quantities, 4th ed., (Springer, New York, NY)

Csizmadia, S., Pasternacki, T., Dreyer, C., Cabrera, A., Erikson, A., Rauer, H., 2013, *A&A*, **549**, A9 DOI

Cutri, R.M., et al., 2003, VizieR On-line Data Catalog: II/246

Flower, P. J., 1996, *AJ*, **469**, 355 DOI

Gaia Collaboration, Prusti, T. et al. 2016, *A&A*, **595**, A1 DOI

Hoffman, D. I., Harrison, T. E., Coughlin, J. L., McNamara, B. J., Holtzman, J. A, Taylor G. E., and. Vestrand, W. T., 2008, *AJ*, **136**, 1067 DOI

Høg, E., et al., 2000, *A&A*, **355**, L27

Kallrath, J., Milone, E. F., 1999, Eclipsing Binary Stars–Modeling and Analysis (Springer-Verlag)

Kallrath, J., Milone, E.F., Terrell, D., and Young, A.T., 1998, *ApJ*, **508**, 308 DOI

Kreiner, J.M., 2004, *AcA*, **54**, 207

Kurucz, R.L., 2002, *Baltic Astron.*, **11**, 101

Lindegren, L. et al., 2016, *A&A*, **595**, A4 DOI

Margoni, R., Stagni, R., 1984, *A&AS*, **56**, 87

Nelson, R.H., 2009, Software, http://www.variablestarssouth.org/profilegrid_blogs/software-by-bob-nelson/

Nelson, R.H., 2010a, Spreadsheets, http://www.variablestarssouth.org/profilegrid_blogs/spreadsheets-by-bob-nelson/

Nelson, R.H., 2010b,"Spectroscopy for Eclipsing Binary Analysis" in The Alt-Az Initiative, Telescope Mirror & Instrument Developments (Collins Foundation Press, Santa Margarita, CA), R.M. Genet, J.M. Johnson and V. Wallen (eds)

Nelson, R.H., 2016, Bob Nelson's O–C Files, http://www.aavso.org/bob-nelsons-o-c-files

Nelson, R. H., Şenavcı, H.V. Baştürk, Ö., Bahar, E., 2014, *New Astron.*, **29**, 57 DOI

Rucinski, S. M., 2004, *IAUS*, **215**, 17

Skiff, B.A., 1997, *IBVS*, No. 4431

Terrell, D., 1994, Van Hamme Limb Darkening Tables, vers. 1.1.

Van Hamme, W., 1993, *AJ*, **106**, 2096 DOI

Wilson, R.E., Devinney, E.J., 1971, *ApJ*, **166**, 605 DOI

Wilson, R.E., 1990, *ApJ*, **356**, 613 DOI

COMMISSIONS G1 AND G4 OF THE IAU
INFORMATION BULLETIN ON VARIABLE STARS
Volume 63 Number 6204 DOI: 10.22444/IBVS.6204

Konkoly Observatory
Budapest
13 April 2017

HU ISSN 0374 – 0676

COLLECTION OF MINIMA OF ECLIPSING BINARIES, PART III.

ZASCHE, P.[1]; UHLAŘ, R.[2]; SVOBODA, P.[3]; KUČÁKOVÁ, H.[1,6]; MAŠEK, M.[4,5]; JURYŠEK, J.[4,5]

[1] Institute of Astronomy, Charles University, V Holešovičkách 2, Prague 8, CZ-18000 Czech Republic; e-mail: zasche@sirrah.troja.mff.cuni.cz

[2] Private Observatory, Pohoří 71, Jílové u Prahy, CZ-25401 Czech Republic

[3] Private observatory, Výpustky 5, Brno, CZ-614 00 Czech Republic

[4] Variable Star and Exoplanet Section of Czech Astronomical Society, Czech Republic

[5] Institute of Physics, Czech Academy of Sciences, Na Slovance 1999/2, CZ-182 21 Praha 8, Czech Republic

[6] Institute of Physics, Faculty of Philosophy and Science, Silesian University in Opava, Bezručovo nám. 13, CZ-746 01 Opava, Czech Republic

Observatory and telescope:
CCD photometry with various ground-based and automatic survey telescopes were used for the times of minima determination.

Method of data reduction:
The reduction of the CCD frames using the C-Munipack and IRAF routines.

Method of minimum determination:
The minima times were mostly computed with the Kwee - van Woerden method (Kwee & van Woerden, 1956), some of them with the polynomial fitting method, and the minima from the survey telescopes by the AFP method (Zasche et al. 2014).

Table 1: Times of minima of eclipsing binaries

Star Name	HJD 24.....	Error	Type	Filter	Instrument/Source	Observer
WZ And	56955.61616	0.00279	Sec	C	BOOTES-1	MM
BX And	56940.41838	0.00028	Sec	R	N200/1000	RU
BX And	56963.29642	0.00024	Prim	C	N150/750	RU
BX And	57387.31853	0.00027	Prim	C	RF34/135	RU
BX And	57646.61120	0.00025	Prim	C	RF34/135	RU
BX And	57754.29518	0.00059	Sec	C	RF34/135	RU
GZ And	56940.40108	0.00021	Sec	C	N150/750	RU
GZ And	56964.34424	0.00078	Prim	R	N200/1000	RU
V342 And	57234.42718	0.00069	Prim	C	RF34/135	RU
V389 And	57260.49447	0.00039	Prim	R	RF34/135	RU
V389 And	57660.39841	0.00068	Sec	C	RF34/135	RU

Table 1 – continued from previous page

Star Name	HJD 24.....	Error	Type	Filter	Instrument/Source	Observer
V392 And	56900.49329	0.00132	Prim	C	N150/750	RU
V392 And	57248.47125	0.00036	Prim	C	N150/750	RU
V392 And	57319.28003	0.00027	Sec	R	RF34/135	RU
V392 And	57600.49858	0.00069	Prim	R	N200/1000	RU
RY Aqr	57233.54659	0.00025	Prim	C	RF34/135	RU
RY Aqr	57238.42719	0.00152	Sec	C	RF34/135	RU
RY Aqr	57594.41826	0.00097	Sec	R	N200/1000	RU
RY Aqr	57723.22140	0.00031	Prim	C	RF34/135	RU
SU Aqr	57241.55137	0.00032	Prim	C	RF34/135	RU
SU Aqr	57614.50750	0.00093	Prim	C	RF34/135	RU
DX Aqr	57327.33408	0.00160	Sec	C	RF34/135	RU
DX Aqr	57625.48445	0.00075	Prim	I	RF34/135	RU
V342 Aql	57198.51390	0.00375	Prim	R	RF34/135	RU
V346 Aql	57189.50099	0.00015	Prim	C	RF34/135	RU
V346 Aql	57199.45773	0.00012	Prim	C	N150/750	RU
V346 Aql	57215.49924	0.00065	Sec	C	N150/750	RU
V346 Aql	57574.51488	0.00011	Prim	C	RF34/135	RU
V346 Aql	57640.34740	0.00159	Sec	C	RF34/135	RU
V418 Aql	57639.32520	0.00065	Prim	R	N200/1000	RU
V418 Aql	57640.43773	0.00605	Sec	R	N200/1000	RU
V803 Aql	57191.48532	0.00009	Sec	R	BOOTES 2	MM
V889 Aql	54856.75681	0.01157	Prim	C	Pi of the sky	
V889 Aql	54860.69863	0.02356	Sec	C	Pi of the sky	
V889 Aql	53010.74475	0.02675	Prim	V	ASAS	
V889 Aql	53359.40826	0.05255	Sec	V	ASAS	
V889 Aql	54656.59989	0.02132	Prim	V	ASAS	
V889 Aql	54660.52492	0.09115	Sec	V	ASAS	
V1461 Aql	57213.48870	0.00038	Prim	C	RF34/135	RU
V1461 Aql	57608.41422	0.00039	Prim	R	N200/1000	RU
V1470 Aql	57209.43086	0.00154	Sec	C	RF34/135	RU
V1470 Aql	57535.49961	0.00176	Prim	C	RF34/135	RU
V1470 Aql	57614.40805	0.00067	Sec	C	RF34/135	RU
σ Aql	56937.35850	0.00132	Sec	I	RF34/135	RU
σ Aql	56940.28000	0.00055	Prim	I	RF34/135	RU
σ Aql	57164.56308	0.00179	Prim	I	RF34/135	RU
σ Aql	57204.54466	0.00063	Sec	I	RF34/135	RU
σ Aql	57205.52001	0.00046	Prim	I	RF34/135	RU
σ Aql	57517.56909	0.00095	Prim	I	RF34/135	RU
σ Aql	57518.54978	0.00073	Sec	I	RF34/135	RU
AL Ari	57335.49906	0.00063	Sec	C	RF34/135	RU
AL Ari	57337.33158	0.00026	Prim	C	RF34/135	RU
AL Ari	57708.32864	0.00039	Prim	C	RF34/135	RU
BQ Ari	56932.47474	0.00049	Prim	R	N200/1000	RU
BQ Ari	56959.43321	0.00055	Sec	R	N200/1000	RU
BQ Ari	57277.48728	0.00066	Prim	C	N150/750	RU
AK Aur	57431.41003	0.00066	Prim	R	N200/1000	RU
AK Aur	57774.35085	0.00484	Prim	C	RF34/135	RU
IU Aur	56933.59657	0.00142	Sec	R	N200/1000	RU

Table 1 – continued from previous page

Star Name	HJD 24.....	Error	Type	Filter	Instrument/Source	Observer
IU Aur	57099.35360	0.00103	Prim	C	RF34/135	RU
IU Aur	57396.43407	0.00060	Prim	C	RF34/135	RU
IU Aur	57772.31789	0.00084	Sec	C	RF34/135	RU
IU Aur	57780.47946	0.00159	Prim	C	RF34/135	RU
LY Aur	56930.58641	0.00028	Sec	I	N150/750	RU
V424 Aur	57414.28174	0.00089	Sec	C	RF34/135	RU
V424 Aur	57760.52832	0.00230	Prim	C	RF34/135	RU
V424 Aur	57773.38076	0.00045	Prim	C	RF34/135	RU
V424 Aur	57818.38244	0.00087	Sec	C	RF34/135	RU
V462 Aur	57279.58040	0.00132	Prim	C	RF34/135	RU
V462 Aur	57338.43518	0.00077	Sec	C	RF34/135	RU
V462 Aur	57712.61980	0.00188	Sec	C	RF34/135	RU
V462 Aur	57815.41068	0.00145	Prim	C	RF34/135	RU
V560 Aur	56905.50727	0.00112	Prim	C	N150/750	RU
V560 Aur	57297.52461	0.00086	Sec	C	N150/750	RU
V560 Aur	57333.44107	0.00228	Prim	C	RF34/135	RU
V560 Aur	57431.25216	0.00049	Prim	R	N200/1000	RU
V560 Aur	57758.29868	0.00135	Prim	C	RF34/135	RU
V560 Aur	57774.33696	0.00349	Sec	C	RF34/135	RU
CK Boo	57543.49680	0.00059	Prim	C	RF34/135	RU
CK Boo	57776.64353	0.00038	Sec	R	N200/1000	RU
CK Boo	57799.54315	0.00055	Prim	C	RF34/135	RU
EM Boo	57153.44395	0.00128	Sec	C	RF34/135	RU
EM Boo	57466.56699	0.00154	Prim	C	RF34/135	RU
EM Boo	57482.46810	0.00060	Sec	C	RF34/135	RU
EM Boo	57493.47589	0.00145	Prim	C	RF34/135	RU
EQ Boo	57079.49993	0.00037	Prim	R	RF34/135	RU
EQ Boo	57081.67258	0.00059	Sec	R	RF34/135	RU
EQ Boo	57128.41590	0.00018	Prim	R	N200/1000	RU
EQ Boo	57141.46122	0.00046	Sec	C	RF34/135	RU
EQ Boo	57478.45235	0.00056	Sec	C	RF34/135	RU
EQ Boo	57503.45388	0.00065	Prim	C	RF34/135	RU
EQ Boo	57780.65762	0.00027	Prim	C	RF34/135	RU
EQ Boo	57804.57056	0.00029	Sec	C	RF34/135	RU
ET Boo	57099.47098	0.00032	Prim	R	RF34/135	RU
ET Boo	57125.59422	0.00052	Sec	R	RF34/135	RU
ET Boo	57383.61114	0.00029	Sec	R	N200/1000	RU
ET Boo	57800.62925	0.00066	Prim	C	RF34/135	RU
GK Boo	57042.61228	0.00009	Prim	R	BOOTES 2	MM
GK Boo	57058.61755	0.00007	Sec	R	BOOTES 2	MM
GK Boo	57091.58439	0.00009	Sec	R	N200/1000	RU
GK Boo	57182.60027	0.00009	Prim	R	BOOTES 2	MM
GS Boo	57812.56375	0.00053	Prim	R	WHOO	HK
i Boo	57089.52009	0.00045	Prim	I	RF34/135	RU
i Boo	57483.47858	0.00026	Prim	I	RF34/135	RU
i Boo	57483.61210	0.00057	Sec	I	RF34/135	RU
SZ Cam	56930.48684	0.00239	Prim	C	RF34/135	RU
SZ Cam	57297.47359	0.00137	Prim	I	RF34/135	RU

Table 1 – continued from previous page

Star Name	HJD 24.....	Error	Type	Filter	Instrument/Source	Observer
SZ Cam	57745.43284	0.00109	Prim	C	RF34/135	RU
SZ Cam	57776.45158	0.00229	Sec	C	RF34/135	RU
CV Cam	57396.28010	0.00037	Sec	C	RF34/135	RU
CV Cam	57414.28411	0.00089	Prim	C	RF34/135	RU
CV Cam	57736.43122	0.00065	Prim	C	RF34/135	RU
DT Cam	56281.31626	0.00019	Prim	C	RF34/135	RU
DT Cam	56292.47172	0.00058	Sec	R	RF34/135	RU
DT Cam	57691.58808	0.00066	Sec	C	RF34/135	RU
S Cnc	57125.34136	0.00436	Sec	R	N200/1000	RU
S Cnc	57746.58285	0.00042	Prim	C	RF34/135	RU
CX CVn	57491.52442	0.00169	Sec	C	RF34/135	RU
CX CVn	57519.40728	0.00017	Prim	R	N200/1000	RU
CX CVn	57778.65292	0.00042	Prim	C	RF34/135	RU
CX CVn	57783.59782	0.00519	Sec	C	RF34/135	RU
CX CVn	57829.51763	0.00265	Sec	C	RF34/135	RU
FZ CMa	57719.58252	0.00166	Prim	C	RF34/135	RU
GU CMa	57385.40972	0.00069	Prim	C	RF34/135	RU
GU CMa	57410.36896	0.00049	Sec		RF34/135	RU
GU CMa	57719.52996	0.00129	Sec	C	RF34/135	RU
GU CMa	57723.55253	0.00128	Prim	C	RF34/135	RU
KL CMa	56981.48154	0.00113	Prim	C	RF34/135	RU
KL CMa	57101.31649	0.00059	Prim	C	RF34/135	RU
KL CMa	57334.58940	0.00076	Sec	C	RF34/135	RU
KL CMa	57492.54049	0.00096	Prim	C	FRAM Nikkor	MM
KL CMa	57720.52364	0.00047	Sec	C	RF34/135	RU
KL CMa	57790.36087	0.00069	Prim	C	RF34/135	RU
MP CMa	57775.39545	0.00167	Prim	C	RF34/135	RU
AR Cas	57328.39456	0.00107	Prim	C	RF34/135	RU
YZ Cas	56930.53220	0.00031	Prim	I	RF34/135	RU
YZ Cas	57359.38502	0.00352	Prim	C	RF34/135	RU
YZ Cas	57627.41920	0.00050	Prim	I	RF34/135	RU
CC Cas	56928.37710	0.00148	Sec	C	RF34/135	RU
CC Cas	57315.47827	0.00308	Sec	C	RF34/135	RU
CR Cas	57019.35147	0.00017	Prim	R	BOOTES 2	MM
CR Cas	57046.33173	0.00049	Sec	R	BOOTES 2	MM
V649 Cas	56897.43889	0.00142	Sec	C	RF34/135	RU
V649 Cas	57319.49920	0.00021	Prim	V	RF34/135	RU
V649 Cas	57349.35357	0.00366	Sec	V	RF34/135	RU
V649 Cas	57594.48070	0.00094	Prim	C	RF34/135	RU
V649 Cas	57600.44068	0.00438	Sec	V	RF34/135	RU
V745 Cas	56932.48742	0.00219	Sec	R	RF34/135	RU
V745 Cas	56937.41702	0.00213	Prim	C	RF34/135	RU
V745 Cas	56963.51877	0.00228	Sec	C	RF34/135	RU
V745 Cas	56978.34873	0.00178	Prim	C	RF34/135	RU
V745 Cas	57021.37427	0.00595	Sec	C	RF34/135	RU
V745 Cas	57248.47677	0.00285	Sec	R	N200/1000	RU
V745 Cas	57260.45208	0.00079	Prim	R	N200/1000	RU
V745 Cas	57595.45386	0.00188	Sec	C	RF34/135	RU

Table 1 – continued from previous page

Star Name	HJD 24.....	Error	Type	Filter	Instrument/Source	Observer
V745 Cas	57643.44207	0.00106	Sec	C	RF34/135	RU
V745 Cas	57645.55849	0.00085	Prim	C	RF34/135	RU
V776 Cas	56924.37305	0.00082	Prim	C	RF34/135	RU
V776 Cas	56930.31908	0.00145	Sec	C	RF34/135	RU
V776 Cas	57329.55795	0.00289	Prim	C	RF34/135	RU
V776 Cas	57333.30118	0.00150	Sec	C	RF34/135	RU
V776 Cas	57615.38517	0.00039	Prim	C	RF34/135	RU
V776 Cas	57751.25147	0.00072	Sec	C	RF34/135	RU
V779 Cas	57271.32359	0.00026	Prim	R	RF34/135	RU
V779 Cas	57722.42202	0.00022	Prim	C	RF34/135	RU
V791 Cas	56929.45181	0.00091	Prim	C	RF34/135	RU
V791 Cas	57297.50070	0.00307	Sec	C	RF34/135	RU
V791 Cas	57365.34497	0.00066	Prim	C	RF34/135	RU
V791 Cas	57707.43465	0.00342	Sec	C	RF34/135	RU
V793 Cas	57706.28343	0.00079	Sec	C	RF34/135	RU
V793 Cas	57753.36000	0.00035	Prim	C	RF34/135	RU
U Cep	56928.48825	0.00182	Sec	C	RF34/135	RU
U Cep	57226.42750	0.00160	Prim	C	RF34/135	RU
U Cep	57580.45131	0.00018	Prim	C	RF34/135	RU
VW Cep	57266.35347	0.00093	Prim	C	RF34/135	RU
VW Cep	57266.49507	0.00038	Sec	C	RF34/135	RU
VW Cep	57504.30706	0.00024	Prim	R	RF34/135	PS
VW Cep	57504.44832	0.00017	Sec	R	RF34/135	PS
VW Cep	57504.58571	0.00015	Prim	R	RF34/135	PS
ZZ Cep	57275.37789	0.00027	Prim	C	RF34/135	RU
ZZ Cep	57519.54539	0.00014	Prim	C	RF34/135	RU
CW Cep	57640.52325	0.00099	Prim	BVR	RF34/135	PS
CW Cep	57644.56422	0.00151	Sec	BVR	RF34/135	PS
NN Cep	57640.42498	0.00142	Sec	BVR	RF34/135	PS
NN Cep	57644.54341	0.00145	Sec	BVR	RF34/135	PS
V383 Cep	57142.52748	0.00127	Sec	C	RF34/135	RU
V442 Cep	56898.48506	0.00160	Sec	R	RF34/135	RU
V442 Cep	56963.41550	0.00235	Prim	V	RF34/135	RU
V442 Cep	57261.51094	0.00089	Prim	V	RF34/135	RU
V442 Cep	57275.34980	0.00153	Sec	R	RF34/135	RU
V442 Cep	57277.46716	0.00065	Sec	R	RF34/135	RU
V442 Cep	57590.43758	0.00379	Sec	R	RF34/135	RU
V453 Cep	57626.39066	0.00047	Prim	R	RF34/135	RU
V453 Cep	57629.34930	0.00049	Sec	R	RF34/135	RU
V839 Cep	56963.46425	0.00255	Sec	R	N200/1000	RU
V839 Cep	56978.31412	0.00035	Prim	R	N200/1000	RU
V839 Cep	57262.40168	0.00057	Sec	R	N200/1000	RU
RW Com	57828.46856	0.00009	Sec	R	WHOO	HK
KK Com	57116.37305	0.00046	Prim	R	N200/1000	RU
KK Com	57425.51909	0.00194	Sec	C	RF34/135	RU
KK Com	57465.56964	0.00099	Prim	C	RF34/135	RU
KK Com	57772.58611	0.00102	Sec	C	RF34/135	RU
KK Com	57811.56060	0.00080	Prim	C	RF34/135	RU

Table 1 – continued from previous page

Star Name	HJD 24.....	Error	Type	Filter	Instrument/Source	Observer
KR Com	57070.63406	0.00165	Sec	I	N200/1000	RU
KR Com	57123.46766	0.00149	Prim	C	RF34/135	RU
KR Com	57385.59971	0.00039	Sec	C	RF34/135	RU
KR Com	57435.56923	0.00060	Prim	B	N150/600	MM
KR Com	57442.50524	0.00228	Prim	C	RF34/135	RU
KR Com	57757.65105	0.00375	Sec	C	RF34/135	RU
KR Com	57798.65387	0.00022	Prim	B	N150/600	MM
VV Crv	54930.95021	0.00897	Sec	BVRI	RF34/135	RU
VV Crv	54932.60208	0.00834	Prim	VRI	RF34/135	RU
VV Crv	55275.33222	0.00491	Prim	I	RF34/135	RU
VV Crv	55276.85347	0.00264	Sec	I	RF34/135	RU
VV Crv	55619.61631	0.00297	Sec	BVRI	RF34/135	RU
VV Crv	55649.52548	0.00398	Prim	BVRI	RF34/135	RU
VV Crv	55680.96073	0.00852	Prim	BVRI	RF34/135	RU
VV Crv	56012.67849	0.00117	Sec	C	RF34/135	RU
VV Crv	56048.88192	0.00209	Prim	C	RF34/135	RU
VV Crv	56061.46023	0.00309	Prim	C	RF34/135	RU
VV Crv	56355.47092	0.00090	Sec	C	RF34/135	RU
VV Crv	56388.48566	0.00404	Prim	C	RF34/135	RU
VV Crv	56737.52416	0.00409	Prim	I	RF34/135	RU
VV Crv	56761.06633	0.00209	Sec	I	RF34/135	RU
VV Crv	57086.56072	0.00375	Prim	I	RF34/135	RU
VV Crv	57127.44313	0.00185	Prim	C	RF34/135	RU
VV Crv	57465.45411	0.00093	Sec	I	RF34/135	RU
VV Crv	57498.47110	0.00222	Prim	I	RF34/135	RU
VV Crv	57773.63260	0.00162	Sec	C	RF34/135	RU
VV Crv	57825.53062	0.00186	Prim	C	RF34/135	RU
RV Crt	57423.55434	0.00059	Sec	C	RF34/135	RU
RV Crt	57800.46045	0.00126	Sec	C	RF34/135	RU
RV Crt	57824.45351	0.00205	Prim	C	RF34/135	RU
CG Cyg	56932.41467	0.00018	Prim	R	N200/1000	RU
CG Cyg	57214.53610	0.00018	Prim	R	N200/1000	RU
CG Cyg	57241.35862	0.00032	Sec	R	N200/1000	RU
CG Cyg	57631.40555	0.00025	Sec	R	N200/1000	RU
CG Cyg	57632.35286	0.00005	Prim	R	N200/1000	RU
V367 Cyg	57262.47641	0.00239	Sec	C	RF34/135	RU
V729 Cyg	57261.50676	0.00587	Sec	R	N200/1000	RU
V1191 Cyg	57199.52758	0.00019	Prim	R	N200/1000	RU
V1191 Cyg	57207.52166	0.00021	Sec	C	N150/750	RU
V1191 Cyg	57615.40201	0.00027	Prim	R	N200/1000	RU
V1191 Cyg	57666.33313	0.00037	Sec	R	N200/1000	RU
V2083 Cyg	56924.44975	0.00054	Sec	C	RF34/135	RU
V2083 Cyg	57105.59956	0.00024	Sec	R	RF34/135	RU
V2083 Cyg	57178.43170	0.00026	Sec	I	N200/1000	RU
V2083 Cyg	57205.50692	0.00075	Prim	C	RF34/135	RU
V2083 Cyg	57500.57312	0.00037	Prim	R	RF34/135	RU
V2154 Cyg	56933.35313	0.00018	Prim	C	RF34/135	RU
V2154 Cyg	57296.38078	0.00017	Prim	R	RF34/135	RU

Table 1 – continued from previous page

Star Name	HJD 24.....	Error	Type	Filter	Instrument/Source	Observer
V2165 Cyg	57678.30243	0.00119	Sec	C	RF34/135	RU
V2169 Cyg	57206.44491	0.00064	Prim	C	RF34/135	RU
V2169 Cyg	57531.51851	0.00052	Sec	R	N200/1000	RU
V2247 Cyg	56919.48919	0.00076	Sec	R	N200/1000	RU
V2247 Cyg	57158.54218	0.00019	Prim	R	N200/1000	RU
V2247 Cyg	57214.38377	0.00065	Sec	R	N200/1000	RU
V2247 Cyg	57586.44568	0.00029	Prim	R	N200/1000	RU
V2247 Cyg	57628.48250	0.00079	Sec	R	N200/1000	RU
V2486 Cyg	56898.38881	0.00025	Prim	R	N200/1000	RU
V2486 Cyg	56905.38814	0.00089	Sec	C	N150/750	RU
V2486 Cyg	57225.47495	0.00055	Prim	C	RF34/135	RU
V2486 Cyg	57547.46912	0.00100	Prim	C	RF34/135	RU
TY Del	57240.52201	0.00272	Sec	C	RF80/400	MM
MR Del	56905.45758	0.00014	Prim	R	N200/1000	RU
MR Del	57166.82372	0.00068	Prim	BVRI	FRAM Nikkor	MM
MR Del	57186.90850	0.00160	Sec	BVRI	FRAM Nikkor	MM
MR Del	57206.47200	0.00024	Prim	R	RF34/135	RU
MR Del	57242.46835	0.00090	Prim	C	RF80/400	MM
MR Del	57291.50774	0.00101	Prim	BVRI	FRAM 0.3m	MM
MR Del	57579.48061	0.00019	Prim	C	RF34/135	RU
RR Dra	57173.38354	0.00013	Prim	R	OND65	HK
RR Dra	57824.57730	0.00008	Prim	R	OND65	HK
TW Dra	57102.51481	0.00059	Sec	I	N200/1000	RU
TW Dra	57154.44061	0.00108	Prim	C	RF34/135	RU
TW Dra	57474.41226	0.00042	Prim	C	RF34/135	RU
TW Dra	57481.43742	0.00287	Sec	C	RF34/135	RU
WW Dra	57106.60865	0.00249	Sec	R	RF34/135	RU
WW Dra	57576.52784	0.00257	Prim	C	RF34/135	RU
WW Dra	57775.61272	0.00046	Prim	C	RF34/135	RU
BH Dra	57125.46070	0.00028	Prim	R	N200/1000	RU
BH Dra	57326.26050	0.00077	Sec	C	RF34/135	RU
BH Dra	57482.53412	0.00239	Sec	C	RF34/135	RU
BV Dra	57464.44922	0.00023	Sec	R	RF34/135	RU
BV Dra	57465.32536	0.00016	Prim	R	RF34/135	PS
CM Dra	57464.56100	0.00009	Sec	R	N200/1000	RU
GQ Dra	57128.45915	0.00072	Prim	C	N150/750	RU
GQ Dra	57453.58250	0.00110	Sec	C	RF34/135	RU
GQ Dra	57481.54032	0.00027	Prim	C	RF34/135	RU
GQ Dra	57775.64630	0.00021	Prim	R	N200/1000	RU
GZ Dra	57520.42326	0.00073	Prim	C	RF34/135	RU
GZ Dra	57600.41500	0.00400	Sec	C	RF34/135	RU
HI Dra	57099.58018	0.00035	Prim	R	RF34/135	RU
HI Dra	57207.41378	0.00325	Sec	C	RF34/135	RU
HI Dra	57329.28775	0.00089	Sec	C	RF34/135	RU
HI Dra	57531.50138	0.00157	Prim	C	RF34/135	RU
HI Dra	57563.47626	0.00075	Sec	C	RF34/135	RU
KP Eri	56934.63049	0.00042	Prim	C	N150/750	RU
KP Eri	57340.49702	0.00099	Sec	C	RF34/135	RU

Table 1 – continued from previous page

Star Name	HJD 24.....	Error	Type	Filter	Instrument/Source	Observer
KP Eri	57396.35240	0.00039	Prim	R	N200/1000	RU
KP Eri	57690.51367	0.00105	Sec	C	RF34/135	RU
KP Eri	57731.47282	0.00065	Prim	C	RF34/135	RU
FT Gem	57476.36579	0.00027	Prim	R	OND65	PZ
V335 Gem	56949.53643	0.00069	Prim	R	N150/750	RU
V335 Gem	57338.44660	0.00045	Prim	C	RF34/135	RU
V335 Gem	57773.32575	0.00099	Prim	C	RF34/135	RU
AD Her	57616.39552	0.00409	Prim	C	RF34/135	RU
AK Her	57122.47748	0.00039	Sec	C	RF34/135	RU
AK Her	57145.44971	0.00023	Prim	C	RF34/135	RU
AK Her	57580.46220	0.00053	Prim	R	N200/1000	RU
V624 Her	57137.58638	0.00082	Prim	C	RF34/135	RU
V624 Her	57215.49509	0.00270	Prim	C	RF34/135	RU
V624 Her	57589.41545	0.00049	Prim	V	RF34/135	RU
V819 Her	56923.33716	0.00216	Prim	C	RF34/135	RU
V819 Her	57090.55324	0.00179	Prim	I	RF34/135	RU
V819 Her	57128.44886	0.00409	Prim	C	RF34/135	RU
V819 Her	57158.55358	0.00067	Sec	I	RF34/135	RU
V822 Her	57137.53655	0.00059	Sec	R	RF34/135	RU
V822 Her	57153.53908	0.00135	Prim	R	RF34/135	RU
V822 Her	57498.53873	0.00063	Prim	I	N200/1000	RU
V822 Her	57514.53672	0.00046	Sec	C	RF34/135	RU
V994 Her A	57470.65283	0.00173	Sec	C	RF34/135	RU
V994 Her A	57494.58898	0.00041	Prim	C	RF34/135	RU
V994 Her A	57589.41355	0.00032	Sec	I	N200/1000	RU
V994 Her A	57590.41983	0.00029	Prim	I	N200/1000	RU
V994 Her B	57473.60366	0.00113	Sec	C	RF34/135	RU
V994 Her B	57547.44882	0.00115	Sec	R	RF34/135	RU
V994 Her B	57576.45406	0.00110	Prim	R	RF34/135	RU
RX Hya	57379.53239	0.00089	Prim	C	RF34/135	RU
RX Hya	57387.51115	0.00289	Sec	R	RF34/135	RU
RX Hya	57760.57873	0.00019	Prim	C	RF34/135	RU
OZ Hya	57464.41241	0.00074	Prim	R	N200/1000	RU
OZ Hya	57800.40859	0.00122	Prim	C	RF34/135	RU
OZ Hya	57805.49411	0.00199	Sec	C	RF34/135	RU
OW Hya	57772.51112	0.00228	Prim	I	RF34/135	RU
V394 Lac	57235.44596	0.00196	Sec	R	RF34/135	RU
V394 Lac	56905.45185	0.00759	Sec	C	RF34/135	RU
V394 Lac	57335.30521	0.00121	Prim	C	RF34/135	RU
V401 Lac	57190.46729	0.00064	Sec	C	RF34/135	RU
V401 Lac	57234.42453	0.00028	Prim	R	N150/750	RU
V401 Lac	57701.37930	0.00047	Sec	C	RF34/135	RU
V402 Lac	57179.48098	0.00085	Sec	I	N150/750	RU
V402 Lac	57203.50507	0.00106	Prim	C	RF34/135	RU
TX Leo	57057.58417	0.00130	Prim	I	RF34/135	RU
TX Leo	57722.63791	0.00209	Prim	C	RF34/135	RU
XY Leo	57828.33069	0.00039	Sec	R	WHOO	HK
AM Leo	57380.62412	0.00029	Prim	C	RF34/135	RU

Table 1 – continued from previous page

Star Name	HJD 24.....	Error	Type	Filter	Instrument/Source	Observer
AM Leo	57799.46145	0.00039	Prim	C	RF34/135	RU
AM Leo	57799.64437	0.00056	Sec	C	RF34/135	RU
VW LMi	57499.41168	0.00021	Sec	R	CTA FRAM	MM
IV Lib	57518.55237	0.00485	Prim	R	N200/1000	RU
δ Lib	57100.49054	0.00039	Sec	I	RF34/135	RU
δ Lib	57178.45985	0.00079	Prim	I	RF34/135	RU
δ Lib	57519.41274	0.00132	Sec	I	RF34/135	RU
TZ Lyr	57199.41659	0.00040	Sec	R	N200/1000	RU
TZ Lyr	57204.44226	0.00049	Prim	R	N200/1000	RU
TZ Lyr	57571.44607	0.00006	Prim	R	N200/1000	RU
TZ Lyr	57576.47118	0.00035	Sec	R	N200/1000	RU
RR Men	51947.10248	0.00096	Prim	V	ASAS	
RR Men	52178.46478	0.00166	Prim	V	ASAS	
RR Men	52609.99319	0.00218	Prim	V	ASAS	
RR Men	52986.93739	0.00325	Prim	V	ASAS	
RR Men	53670.62160	0.00238	Prim	V	ASAS	
RR Men	54341.30542	0.00137	Prim	V	ASAS	
RR Men	54884.60647	0.00095	Prim	V	ASAS	
V498 Mon	57410.42173	0.00032	Prim	C	N150/600	MM
V684 Mon	57021.40412	0.00069	Prim	R	N200/1000	RU
V684 Mon	57057.48184	0.00224	Sec	R	RF34/135	RU
V684 Mon	57329.63000	0.00136	Sec	C	N150/750	RU
V684 Mon	57367.62760	0.00176	Prim	C	RF34/135	RU
V684 Mon	57380.57738	0.00179	Prim	R	RF34/135	RU
V684 Mon	57396.29085	0.00109	Sec	R	RF34/135	RU
V684 Mon	57419.45872	0.00169	Prim	C	RF34/135	RU
V684 Mon	57420.35420	0.00085	Sec	C	RF34/135	RU
V684 Mon	57666.59620	0.00045	Sec	C	RF34/135	RU
V684 Mon	57704.57798	0.00198	Prim	C	RF34/135	RU
V684 Mon	57755.46345	0.00075	Sec	C	RF34/135	RU
V684 Mon	57806.40716	0.00099	Prim	C	RF34/135	RU
V727 Mon	57364.52452	0.00306	Sec	C	RF34/135	RU
V727 Mon	57750.58751	0.00215	Prim	C	RF34/135	RU
V730 Mon	57319.55860	0.00075	Sec	R	N200/1000	RU
V730 Mon	57326.55368	0.00069	Prim	C	RF34/135	RU
V730 Mon	57753.51845	0.00268	Sec	C	RF34/135	RU
V730 Mon	57772.39066	0.00109	Sec	R	N200/1000	RU
V879 Mon	57328.60023	0.00052	Sec	C	N150/750	RU
V879 Mon	57443.41264	0.00055	Prim	C	RF34/135	RU
V879 Mon	57725.51438	0.00018	Prim	C	RF34/135	RU
V879 Mon	57783.47199	0.00046	Sec	C	RF34/135	RU
V920 Mon	56963.58526	0.00109	Prim	R	N150/750	RU
V931 Mon	57070.34770	0.00015	Prim	R	N200/1000	RU
V931 Mon	57701.64121	0.00205	Prim	C	RF34/135	RU
V931 Mon	57783.37771	0.00099	Prim	C	RF34/135	RU
V931 Mon	57803.37596	0.00229	Sec	C	RF34/135	RU
U Oph	57178.46744	0.00019	Sec	C	RF34/135	RU
U Oph	57563.41530	0.00019	Prim	R	RF34/135	RU

Table 1 – continued from previous page

Star Name	HJD 24.....	Error	Type	Filter	Instrument/Source	Observer
U Oph	57589.41646	0.00021	Sec	C	RF34/135	RU
V2388 Oph	56897.37594	0.00089	Sec	I	RF34/135	RU
V2388 Oph	57101.55935	0.00040	Prim	I	RF34/135	RU
V2388 Oph	57154.50843	0.00062	Prim	I	RF34/135	RU
V2388 Oph	57248.37630	0.00029	Prim	R	RF34/135	RU
V2388 Oph	57295.30810	0.00082	Sec	I	N200/1000	RU
V2388 Oph	57499.49379	0.00152	Prim	R	RF34/135	RU
V2610 Oph	57100.60414	0.00086	Sec	C	RF34/135	RU
V2610 Oph	57116.59558	0.00053	Prim	R	N200/1000	RU
V2610 Oph	57197.41717	0.00089	Sec	C	RF34/135	RU
V2610 Oph	57198.48345	0.00058	Prim	C	RF34/135	RU
V2610 Oph	57483.60300	0.00079	Sec	C	RF34/135	RU
V2610 Oph	57499.59241	0.00252	Prim	C	RF34/135	RU
V2610 Oph	57514.52155	0.00219	Prim	R	N200/1000	RU
ER Ori	57383.32499	0.00046	Prim	C	RF34/135	RU
ER Ori	57383.53526	0.00042	Sec	C	RF34/135	RU
ER Ori	57440.27325	0.00039	Sec	C	RF34/135	RU
ER Ori	57701.51282	0.00016	Sec	C	RF34/135	RU
ER Ori	57708.49935	0.00062	Prim	C	RF34/135	RU
V1031 Ori	57060.33323	0.00173	Prim	R	RF34/135	RU
V1031 Ori	57327.68783	0.00539	Sec	C	RF34/135	RU
V1031 Ori	57438.35058	0.00268	Prim	C	RF34/135	RU
V1031 Ori	57700.58008	0.00085	Prim	C	RF34/135	RU
V1031 Ori	57799.34091	0.00043	Prim	C	RF34/135	RU
V1804 Ori	56963.64495	0.00142	Prim	R	RF34/135	RU
V1804 Ori	57323.58178	0.00129	Sec	R	N200/1000	RU
V1834 Ori	56959.62807	0.00066	Prim	I	N150/750	RU
V1834 Ori	57414.31059	0.00079	Prim	I	N200/1000	RU
V1834 Ori	57750.42345	0.00109	Sec	C	RF34/135	RU
V1834 Ori	57772.32098	0.00148	Prim	C	RF34/135	RU
δ Ori	57730.53455	0.00349	Sec	C	RF34/135	RU
η Ori	56978.40949	0.00159	Sec	I	RF34/135	RU
η Ori	57030.29569	0.00172	Prim	C	RF34/135	RU
η Ori	57713.42116	0.00219	Sec	I	RF34/135	RU
η Ori	57749.36805	0.00349	Prim	C	RF34/135	RU
η Ori	57801.32601	0.00127	Sec	C	RF34/135	RU
η Ori	57805.32354	0.00204	Prim	C	RF34/135	RU
η Ori	57825.31116	0.00119	Sec	C	RF34/135	RU
KP Peg	57334.28120	0.00069	Prim	C	RF34/135	RU
PU Peg	57240.50518	0.00165	Sec	C	RF34/135	RU
PU Peg	57625.37803	0.00055	Prim	R	N200/1000	RU
V415 Peg	57631.47240	0.00360	Prim	C	RF34/135	RU
V416 Peg	56898.45190	0.00095	Prim	C	N150/750	RU
V416 Peg	56930.50872	0.00087	Sec	C	RF34/135	RU
V416 Peg	57210.48062	0.00056	Prim	C	N150/750	RU
V416 Peg	57215.46260	0.00039	Sec	R	N200/1000	RU
V416 Peg	57235.40686	0.00069	Sec	R	N200/1000	RU
V416 Peg	57237.56027	0.00029	Prim	R	N200/1000	RU

Table 1 – continued from previous page

Star Name	HJD 24.....	Error	Type	Filter	Instrument/Source	Observer
V416 Peg	57242.54139	0.00159	Sec	C	RF34/135	RU
V416 Peg	57245.37920	0.00273	Sec	R	RF34/135	RU
V416 Peg	57262.47201	0.00148	Sec	R	RF34/135	RU
V416 Peg	57272.45614	0.00152	Sec	C	RF34/135	RU
V416 Peg	57277.44871	0.00035	Prim	R	N200/1000	RU
V416 Peg	57279.58258	0.00186	Sec	R	RF34/135	RU
V416 Peg	57282.42824	0.00089	Sec	R	RF34/135	RU
V416 Peg	57287.41705	0.00050	Prim	R	N200/1000	RU
V416 Peg	57574.51519	0.00192	Sec	C	RF34/135	RU
V416 Peg	57626.52319	0.00032	Prim	C	RF34/135	RU
ST Per	56928.39653	0.00059	Prim	R	N200/1000	RU
ST Per	57320.35001	0.00045	Prim	R	N200/1000	RU
ST Per	57627.55673	0.00055	Prim	R	N200/1000	RU
AG Per	56930.43280	0.00044	Sec	I	N200/1000	RU
AG Per	56933.51403	0.00037	Prim	C	RF34/135	RU
AG Per	57287.48746	0.00127	Sec	I	N150/750	RU
AG Per	57345.34642	0.00125	Prim	R	RF34/135	RU
AG Per	57643.57490	0.00020	Prim	R	RF34/135	RU
AG Per	57646.56982	0.00075	Sec	V	RF34/135	RU
EX Per	56937.58542	0.00355	Prim	C	N150/750	RU
EX Per	57666.49223	0.00065	Prim	R	N200/1000	RU
IQ Per	56928.53916	0.00013	Sec	R	N200/1000	RU
IQ Per	56950.40749	0.00011	Prim	R	N200/1000	RU
IQ Per	57248.54925	0.00047	Prim	C	RF34/135	RU
IQ Per	57275.51001	0.00165	Sec	C	RF34/135	RU
IQ Per	57712.34283	0.00092	Prim	C	RF34/135	RU
IQ Per	57746.26745	0.00029	Sec	C	RF34/135	RU
V482 Per	57812.36409	0.00065	Sec	C	RF34/135	RU
V593 Per	57296.49581	0.00389	Sec	C	RF34/135	RU
V593 Per	57721.48158	0.00106	Sec	C	RF34/135	RU
V736 Per	57276.54158	0.00149	Sec	R	N200/1000	RU
V736 Per	57632.49618	0.00189	Prim	C	RF34/135	RU
V871 Per	56950.57815	0.00039	Sec	C	BOOTES-1	MM
β Per	56927.33940	0.00046	Prim	C	RF34/135	RU
SZ Psc	57723.35242	0.00109	Prim	C	RF34/135	RU
AQ Psc	56933.48646	0.00021	Prim	C	N150/750	RU
AQ Psc	56950.36976	0.00014	Sec	C	RF34/135	RU
AQ Psc	57260.45972	0.00042	Sec	C	RF34/135	RU
AQ Psc	57355.34642	0.00029	Prim	C	RF34/135	RU
AQ Psc	57700.39735	0.00089	Sec	C	RF34/135	RU
AQ Psc	57714.42755	0.00029	Prim	C	RF34/135	RU
ET Psc	56924.37692	0.00046	Prim	C	N150/750	RU
ET Psc	56924.59795	0.00039	Sec	C	N150/750	RU
ET Psc	57275.59438	0.00078	Sec	R	N200/1000	RU
ET Psc	57318.42746	0.00055	Prim	C	RF34/135	RU
ET Psc	57644.38305	0.00045	Prim	C	RF34/135	RU
ET Psc	57644.60808	0.00040	Sec	C	RF34/135	RU
EU Psc	56958.54699	0.00350	Sec	C	RF34/135	RU

Table 1 – continued from previous page

Star Name	HJD 24.....	Error	Type	Filter	Instrument/Source	Observer
EU Psc	57261.50830	0.00056	Sec	C	RF34/135	RU
EU Psc	57367.30837	0.00089	Prim	C	RF34/135	RU
EU Psc	57736.29842	0.00049	Prim	C	RF34/135	RU
PV Pup	57359.58988	0.00051	Sec	C	RF34/135	RU
PV Pup	57731.59474	0.00159	Sec	C	RF34/135	RU
PV Pup	57751.52412	0.00085	Sec	C	RF34/135	RU
PV Pup	57830.45504	0.00165	Prim	C	RF34/135	RU
U Sge	57126.52026	0.00032	Prim	C	RF34/135	RU
U Sge	57623.47720	0.00019	Prim	C	RF34/135	RU
UZ Sge	57190.53396	0.00005	Prim	R	BOOTES 2	MM
V338 Sge	57202.46430	0.00165		C	RF34/135	RU
V505 Sgr	57167.90453	0.00026	Prim	N	FRAM Nikkor	MM
V505 Sgr	57197.47642	0.00015	Prim	R	RF34/135	RU
V505 Sgr	57242.42389	0.00027	Prim	R	N150/750	RU
V505 Sgr	57579.53596	0.00032	Prim	V	N200/1000	RU
V505 Sgr	57611.47330	0.00023	Prim	R	RF34/135	RU
PS Ser	57516.44694	0.00234	Sec	C	RF34/135	RU
V413 Ser	57204.44837	0.00455	Sec	C	RF34/135	RU
V413 Ser	57213.47345	0.00068	Sec	C	N150/750	RU
V413 Ser	57518.53900	0.00032	Sec	C	RF34/135	RU
V413 Ser	57569.45115	0.00085	Prim	C	RF34/135	RU
CD Tau	57338.60148	0.00019	Prim	C	RF34/135	RU
CD Tau	57364.36593	0.00012	Sec	C	RF34/135	RU
CD Tau	57783.45115	0.00052	Sec	C	RF34/135	RU
V1128 Tau	56934.44458	0.00025	Prim	C	RF34/135	RU
V1128 Tau	57329.44275	0.00019	Sec	R	RF34/135	RU
V1128 Tau	57329.59476	0.00023	Prim	R	RF34/135	RU
V1128 Tau	57713.29580	0.00029	Sec	C	RF34/135	RU
V1128 Tau	57713.44696	0.00066	Prim	C	RF34/135	RU
V1154 Tau	56922.57218	0.00090	Sec	C	RF34/135	RU
V1154 Tau	57333.60704	0.00043	Prim	C	RF34/135	RU
V1154 Tau	57366.32372	0.00055	Sec	C	RF34/135	RU
V1154 Tau	57722.54568	0.00030	Prim	R	N200/1000	RU
V1154 Tau	57755.26860	0.00029	Sec	C	RF34/135	RU
ξ Tau	57332.40573	0.00328	Sec	C	RF34/135	RU
ξ Tau	57632.58156	0.00262	Prim	I	RF34/135	RU
ξ Tau	57700.49745	0.00166	Sec	I	RF34/135	RU
ξ Tau	57725.50262	0.00137	Prim	C	RF34/135	RU
λ Tau	57332.45941	0.00158	Prim	I	RF34/135	RU
λ Tau	57755.42912	0.00175	Prim	V	RF34/135	RU
λ Tau	57757.42626	0.00115	Sec	C	RF34/135	RU
RS Tri	57018.21795	0.00038	Prim	R	N200/1000	RU
RS Tri	57329.37038	0.00015	Prim	C	N150/750	RU
RS Tri	57640.52303	0.00015	Prim	R	N200/1000	RU
W UMa	57105.31954	0.00030	Prim	C	RF34/135	RU
W UMa	57105.48814	0.00075	Sec	C	RF34/135	RU
W UMa	57425.44007	0.00014	Sec	C	RF34/135	RU
W UMa	57439.28452	0.00032	Prim	C	RF34/135	RU

Table 1 – continued from previous page

Star Name	HJD 24.....	Error	Type	Filter	Instrument/Source	Observer
W UMa	57774.41891	0.00015	Sec	C	RF34/135	RU
W UMa	57774.58562	0.00025	Prim	C	RF34/135	RU
AC UMa	56978.54040	0.00195	Prim	R	N200/1000	RU
AC UMa	57122.48553	0.00039	Prim	R	N200/1000	RU
AC UMa	57410.39441	0.00296	Prim	R	N200/1000	RU
AW UMa	57102.47289	0.00032	Sec	C	RF34/135	RU
AW UMa	57439.40772	0.00042	Sec	C	RF34/135	RU
AW UMa	57470.33081	0.00055	Prim	C	RF34/135	RU
AW UMa	57756.60570	0.00025	Sec	C	RF34/135	RU
AW UMa	57772.61842	0.00038	Prim	R	N200/1000	RU
DN UMa	57037.54014	0.00197	Prim	V	RF34/135	RU
DN UMa	57128.36887	0.00097	Sec	V	RF34/135	RU
DN UMa	57383.60612	0.00119	Prim	C	RF34/135	RU
DN UMa	57461.48686	0.00056	Prim	R	RF34/135	PS
DN UMa	57481.37791	0.00059	Sec	C	RF34/135	RU
DN UMa	57499.55696	0.00068	Prim	R	RF34/135	PS
DN UMa	57749.59087	0.00135	Sec	C	RF34/135	RU
DN UMa	57762.56913	0.00172	Prim	C	RF34/135	RU
DN UMa	57775.55669	0.00093	Sec	V	RF34/135	RU
DN UMa	57828.32514	0.00099	Prim	R	RF34/135	PS
GT UMa	57037.53767	0.00094	Prim	C	RF34/135	RU
GT UMa	57132.45950	0.00123	Sec	R	RF34/135	RU
GT UMa	57383.45435	0.00022	Prim	R	RF34/135	RU
GT UMa	57499.34359	0.00042	Sec	C	RF34/135	RU
GT UMa	57776.54454	0.00035	Sec	C	RF34/135	RU
GT UMa	57814.39262	0.00049	Prim	C	RF34/135	RU
HR UMa	57070.62708	0.00049	Sec	R	RF34/135	RU
HR UMa	57090.52777	0.00028	Prim	R	N200/1000	RU
HR UMa	57102.32206	0.00048	Prim	C	RF34/135	RU
HR UMa	57387.56550	0.00019	Sec	C	RF34/135	RU
HR UMa	57410.41898	0.00062	Prim	C	RF34/135	RU
HR UMa	57760.51764	0.00085	Sec	C	RF34/135	RU
HR UMa	57783.36537	0.00044	Prim	C	RF34/135	RU
II UMa	57091.49087	0.00034	Prim	R	N200/1000	RU
II UMa	57417.45543	0.00065	Prim	C	RF34/135	RU
II UMa	57438.49983	0.00146	Sec	C	RF34/135	RU
II UMa	57773.54640	0.00065	Sec	C	RF34/135	RU
II UMa	57775.60753	0.00029	Prim	C	RF34/135	RU
NU UMa	57060.53093	0.00044	Sec	R	RF34/135	RU
NU UMa	57151.39700	0.00022	Prim	C	RF34/135	RU
NU UMa	57396.49705	0.00049	Sec	R	RF34/135	RU
NU UMa	57476.34028	0.00049	Prim	C	RF34/135	RU
NU UMa	57531.42022	0.00037	Prim	R	RF34/135	PS
NU UMa	57798.55638	0.00032	Sec	C	RF34/135	RU
NU UMa	57823.32660	0.00059	Prim	C	RF34/135	RU
AH Vir	57124.38348	0.00042	Sec	C	RF34/135	RU
AH Vir	57465.48688	0.00046	Sec	C	RF34/135	RU
AH Vir	57480.36048	0.00031	Prim	R	N200/1000	RU

Table 1 – continued from previous page

Star Name	HJD 24.....	Error	Type	Filter	Instrument/Source	Observer
AH Vir	57773.57815	0.00049	Sec	C	RF34/135	RU
AH Vir	57821.46227	0.00125	Prim	C	RF34/135	RU
AH Vir	57823.50042	0.00018	Prim	C	RF34/135	RU
DL Vir	57101.56776	0.00125	Prim	C	RF34/135	RU
DL Vir	57134.45601	0.00042	Prim	R	RF34/135	RU
DL Vir	57505.41186	0.00198	Prim	C	RF34/135	RU
DL Vir	57814.54777	0.00070	Prim	C	RF34/135	RU
HT Vir	57073.52224	0.00037	Prim	R	RF34/135	RU
HT Vir	57080.65773	0.00016	Sec	I	N200/1000	RU
HT Vir	57442.67113	0.00017	Sec	C	RF34/135	RU
HT Vir	57480.38048	0.00015	Prim	C	RF34/135	RU
HT Vir	57480.58373	0.00016	Prim	C	RF34/135	RU
HT Vir	57799.58809	0.00025	Prim	C	RF34/135	RU
HT Vir	57820.58475	0.00015	Sec	C	RF34/135	RU
HY Vir	57122.46306	0.00105	Sec	R	RF34/135	RU
HY Vir	57480.39414	0.00067	Sec	C	RF34/135	RU
HY Vir	57536.41250	0.00045	Prim	C	RF34/135	RU
HY Vir	57820.57377	0.00048	Prim	C	RF34/135	RU
LV Vir	57099.51998	0.00046	Sec	C	RF34/135	RU
LV Vir	57480.50713	0.00034	Prim	R	N200/1000	RU
LV Vir	57518.37982	0.00018	Sec	C	RF34/135	RU
LV Vir	57811.54035	0.00179	Sec	C	RF34/135	RU
Z Vul	57220.45186	0.00010	Prim	C	RF34/135	RU
Z Vul	57560.46379	0.00155	Sec	C	RF34/135	RU
Z Vul	57576.41603	0.00017	Prim	C	RF34/135	RU
PS Vul	57628.44440	0.00215	Prim	I	RF34/135	RU
V402 Vul	56898.35984	0.00120	Prim	R	RF34/135	RU
V402 Vul	57179.48989	0.00136	Sec	R	RF34/135	RU
V402 Vul	57206.49162	0.00179	Sec	R	N150/750	RU
BD+03 2482	57751.58187	0.00039	Prim	C	RF34/135	RU
BD+03 2482	57774.49967	0.00059	Sec	C	RF34/135	RU
BD+42 2782	57106.57710	0.00032	Prim	C	RF34/135	RU
BD+42 2782	57153.39965	0.00015	Sec	C	N150/750	RU
BD+42 2782	57498.38010	0.00068	Sec	C	RF34/135	RU
BD+42 2782	57498.56691	0.00038	Prim	C	RF34/135	RU
GSC 01742-01524	56932.40796	0.00022	Sec	C	N150/750	RU
GSC 01742-01524	56945.36540	0.00013	Prim	C	N150/750	RU
GSC 01742-01524	57275.38085	0.00019	Prim	C	N150/750	RU
GSC 01742-01524	57275.55444	0.00042	Sec	C	N150/750	RU
GSC 01742-01524	57722.37025	0.00045	Sec	C	N200/1000	RU
EPIC 202073186	57442.32578	0.00212	Prim	C	RF34/135	RU
EPIC 202073186	57775.46620	0.00055	Prim	R	N200/1000	RU
EPIC 202073186	57829.35812	0.00076	Prim	R	N200/1000	RU
HD 6421	56919.49579	0.00036	Prim	C	N150/750	RU
HD 6421	57282.50515	0.00139	Prim	C	RF34/135	RU
HD 6421	57287.38968	0.00117	Prim	R	RF34/135	RU
HD 6421	57632.48575	0.00152	Prim	R	N200/1000	RU
HD 24105	56932.53974	0.00018	Prim	C	N150/750	RU

Table 1 – continued from previous page

Star Name	HJD 24.....	Error	Type	Filter	Instrument/Source	Observer
HD 24105	57345.51264	0.00063	Prim	R	RF34/135	RU
HD 24105	57626.51032	0.00038	Sec	C	RF34/135	RU
HD 24105	57719.33445	0.00040	Prim	C	RF34/135	RU
HD 24105	57760.37801	0.00039	Sec	C	RF34/135	RU
HD 47934	57755.38801	0.00191		C	RF34/135	RU
HD 47934	57764.43911	0.00105		C	RF34/135	RU
HD 55338	56958.58457	0.00038	Prim	C	N150/750	RU
HD 55338	57018.55587	0.00033	Sec	R	N200/1000	RU
HD 55338	57089.42484	0.00032	Prim	R	RF34/135	RU
HD 55338	57387.44084	0.00036	Prim	R	N200/1000	RU
HD 55338	57396.53266	0.00232	Sec	R	N200/1000	RU
HD 55338	57441.35622	0.00045	Sec	R	N200/1000	RU
HD 55338	57714.53652	0.00099	Prim	C	RF34/135	RU
HD 55338	57734.52540	0.00159	Sec	C	RF34/135	RU
HD 55338	57754.51255	0.00192	Prim	C	RF34/135	RU
HD 63238	56963.62196	0.00142	Prim	R	N200/1000	RU
HD 63238	57070.48210	0.00099	Sec	R	N200/1000	RU
HD 63238	57342.66403	0.00069	Prim	C	RF34/135	RU
HD 63238	57751.63409	0.00129	Sec	C	RF34/135	RU
HD 63238	57804.35702	0.00075	Prim	C	RF34/135	RU
HD 73710	57408.52435	0.00387		C	RF34/135	RU
HD 73710	57419.51808	0.00156	Sec	C	RF34/135	RU
HD 73710	57751.59742	0.00537	Sec	C	RF34/135	RU
HD 73710	57798.42790	0.00220	Prim	C	RF34/135	RU
HD 86222	57018.60914	0.00028	Prim	C	RF34/135	RU
HD 86222	57057.59769	0.00052	Sec	R	N200/1000	RU
HD 86222	57102.50930	0.00039	Prim	R	RF34/135	RU
HD 86222	57360.62051	0.00032	Sec	R	RF34/135	RU
HD 86222	57406.51746	0.00040	Prim	C	RF34/135	RU
HD 86222	57749.51557	0.00032	Sec	C	RF34/135	RU
HD 86222	57783.56935	0.00153	Prim	C	RF34/135	RU
HD 86222	57825.51883	0.00096	Sec	R	N200/1000	RU
HD 99666	57037.58886	0.00366	Sec	R	N200/1000	RU
HD 99666	57069.53772	0.00055	Prim	R	RF34/135	RU
HD 99666	57425.57845	0.00053	Prim	C	RF34/135	RU
HD 99666	57749.67580	0.00098	Sec	C	RF34/135	RU
HD 99666	57774.52230	0.00055	Prim	C	RF34/135	RU
HD 178661	56924.37973	0.00059	Prim	C	RF34/135	RU
HD 178661	57141.57980	0.00214	Prim	C	RF34/135	RU
HD 178661	57158.51988	0.00049	Prim	R	N150/750	RU
HD 178661	57205.49676	0.00189	Sec	R	N150/750	RU
HD 178661	57594.45015	0.00022	Prim	C	RF34/135	RU
HD 178661	57692.27027	0.00123	Sec	C	RF34/135	RU
HD 179923	57240.44819	0.00054	Prim	R	N200/1000	RU
HD 179923	57189.51594	0.00039	Prim	C	N150/750	RU
HD 179923	57277.32757	0.00052	Prim	R	N200/1000	RU
HD 179923	57564.46885	0.00089	Prim	C	RF34/135	RU
HD 179923	57626.37406	0.00145	Sec	R	N200/1000	RU

Table 1 – continued from previous page

Star Name	HJD 24.....	Error	Type	Filter	Instrument/Source	Observer
HD 180848	56898.36214	0.00062	Prim	C	N150/750	RU
HD 180848	56904.35399	0.00166	Sec	C	N150/750	RU
HD 180848	56934.28830	0.00040	Prim	R	N200/1000	RU
HD 180848	56934.29587	0.00095	Prim	C	RF34/135	RU
HD 180848	56935.32989	0.00088	Prim	C	RF34/135	RU
HD 180848	56940.27841	0.00095	Sec	R	N200/1000	RU
HD 180848	56959.28244	0.00051	Prim	R	N200/1000	RU
HD 180848	56964.22799	0.00042	Sec	R	N200/1000	RU
HD 180848	57100.64115	0.00089	Sec	R	N200/1000	RU
HD 180848	57105.59207	0.00145	Prim	R	N200/1000	RU
HD 180848	57106.63080	0.00046	Prim	R	N200/1000	RU
HD 180848	57118.60848	0.00098	Prim	R	N200/1000	RU
HD 180848	57119.64412	0.00116	Prim	R	N200/1000	RU
HD 180848	57130.58366	0.00045	Prim	R	N200/1000	RU
HD 180848	57135.53240	0.00150	Sec	C	RF34/135	RU
HD 180848	57141.51755	0.00092	Prim	R	N200/1000	RU
HD 180848	57153.49355	0.00032	Prim	R	N200/1000	RU
HD 180848	57154.53584	0.00058	Prim	R	N200/1000	RU
HD 180848	57159.48090	0.00059	Sec	C	RF34/135	RU
HD 180848	57171.46076	0.00115	Sec	C	RF34/135	RU
HD 180848	57519.52970	0.00024	Prim	R	N200/1000	RU
HD 180848	57576.54340	0.00037	Sec	C	RF34/135	RU
HD 180848	57628.35006	0.00018	Prim	R	N200/1000	RU
HD 180848	57707.23495	0.00036	Sec	C	RF34/135	RU
HD 180848	57713.22293	0.00055	Prim	C	RF34/135	RU
HD 181469	57141.58282	0.00097	Prim	R	N150/750	RU
HD 181469	57297.34139	0.00063	Prim	R	N200/1000	RU
HIP 247	57643.35340	0.00022		R	N200/1000	RU
HIP 247	57661.43653	0.00089		R	N200/1000	RU
HIP 41322	57800.50502	0.00045	Sec	R	N200/1000	RU
HIP 41322	57830.31078	0.00032	Prim	C	RF34/135	RU
KIC 6187893	56955.42094	0.00163	Prim	C	BOOTES-1	MM
KIC 10686876	56954.40782	0.00179	Prim	C	BOOTES-2	MM
TYC 2364-2327-1	57275.46254	0.00049	Sec	R	N200/1000	RU
TYC 2364-2327-1	57297.64044	0.00049	Prim	R	N200/1000	RU
TYC 2364-2327-1	57328.50055	0.00187	Prim	C	N150/750	RU
TYC 2364-2327-1	57329.46691	0.00079	Sec	C	N150/750	RU
TYC 2364-2327-1	57625.52694	0.00039	Prim	R	N200/1000	RU
TYC 2364-2327-1	57713.28526	0.00031	Sec	R	N200/1000	RU
TYC 2364-2327-1	57790.43397	0.00079	Sec	R	N200/1000	RU
TYC 2364-2327-1	57820.33283	0.00275	Prim	C	RF34/135	RU

Explanation of the remarks in the table:
BVRI filters by the specification by Bessell (1990), *C* - unfiltered. Observers: PZ - Petr Zasche, RU - Robert Uhlař, HK - Hana Kučáková, PS - Petr Svoboda, MM - Martin Mašek. Instruments: OND65 - 65 cm telescope in Ondřejov observatory; RF34/135 - 34 mm refractor; N150/750 - 150 mm Newton reflector; N200/1000 - 200 mm Newton reflector; BOOTES-1 - Spain, Nikkor lens 400 mm f/2.8 + CCD G4 16000, BOOTES-2 - Spain, 0.6-m RC f/8 + CCD Andor iXon3 888; WHOO - White Hole Observatory Opava, Meade LX200GPS + CCD ATIK 383L; FRAM Nikkor - Nikkor 300mm G4-16000; N150/600 - Newton 150/600 mm + CCD MII G2-1600; RF80/400 - RF80/400 mm + CCD Meade DSI; FRAM 0.3 m - 0.3 m G2-1600; CTA FRAM - 135 mm lens + G4-16000. The telescope FRAM is part of the Pierre Auger Observatory, located in Malargüe, see e.g. Ebr et al. (2014).

Remarks:
The ephemerides (hence also primary/secondary distinction) were taken from the online "$O - C$ gateway" (Paschke & Brát 2006). For the double eclipsing systems their A/B pairs were designated according to the published ephemerides for both pairs. For some of the systems not included in the "$O - C$ gateway" the following ephemerides were used: BD+03 2482: HJD $= 2454318.8550 + 9.178400 \cdot E$ GSC 01742-01524: HJD $= 2456564.5490 + 0.345567 \cdot E$ EPIC 202073186: HJD $= 2457829.3581 + 1.224790 \cdot E$ HD 6421: HJD $= 2454520.0760 + 1.627830 \cdot E$ HD 24105: HJD $= 2454214.7257 + 1.262923 \cdot E$ HD 47934: HJD $= 2457764.4300 + 4.530500 \cdot E$ HD 55338: HJD $= 2453023.7644 + 1.211460 \cdot E$ HD 63238: HJD $= 2456758.4240 + 2.849950 \cdot E$ HD 73710: HJD $= 2448296.5500 + 7.220300 \cdot E$ HD 86222: HJD $= 2451234.5236 + 0.987045 \cdot E$ HD 99666: HJD $= 2451999.7190 + 1.014370 \cdot E$ HD 178661: HJD $= 2454954.2120 + 1.540395 \cdot E$ HD 179923: HJD $= 2457564.4695 + 0.878114 \cdot E$ HD 180848: HJD $= 2456486.5038 + 0.520679 \cdot E$ HD 181469: HJD $= 2454961.2200 + 8.652220 \cdot E$ HIP 247: HJD $= 2454160.0700 + 2.260400 \cdot E$ HIP 41322: HJD $= 2451869.2050 + 1.528488 \cdot E$ KIC 6187893: HJD $= 2454954.0762 + 0.789178 \cdot E$ KIC 10686876: HJD $= 2454953.9505 + 2.618412 \cdot E$ TYC 2364-2327-1: HJD $= 2454267.6050 + 1.928731 \cdot E$.

Acknowledgements:
We would like to thank the "ASAS", and "PI of the sky" teams for making all of the observations easily public available. We would like to thank the Pierre Auger Collaboration for the use of its facilities. The operation of the robotic telescope FRAM is supported by the EU grant GLORIA (No. 283783 in FP7-Capacities program) and by the grant of the Ministry of Education of the Czech Republic (MSMT-CR LM2015038). The data calibration and analysis related to FRAM telescope is supported by the Ministry of Education of the Czech Republic MSMT-CR (LG15014 and CZ.02.1.01/0.0/0.0/16_013/0001402). This work was also supported by the Czech Science Foundation grant no. GA15-02112S. The use of "O-C gateway" (Paschke & Brát 2006) is also acknowledged.

References:

Bessell, M. S. 1990, *PASP*, **102**, 1181 DOI
Ebr, J., Janeček, P., Prouza, M., et al. 2014, Revista Mexicana de Astronomia y Astrofisica Conference Series, **45**, 114
Kwee, K. K., van Woerden, H., 1956, *BAN*, **12**, 327
Paschke, A., Brát, L., 2006, *OEJV*, **23**, 13
Zasche, P., Wolf, M., Vraštil, J., et al. 2014, *A&A*, **572**, A71 DOI

ERRATUM FOR IBVS 6204

HD 73710 should be HD 73709
Minimum 57480.58373 for HT Vir - should be secondary instead of primary

Zasche, P.

COMMISSIONS G1 AND G4 OF THE IAU
INFORMATION BULLETIN ON VARIABLE STARS
Volume 63 Number 6205 DOI: 10.22444/IBVS.6205

Konkoly Observatory
Budapest
13 April 2017

HU ISSN 0374 – 0676

GSC 02505-00411: A NEW δ Sct STAR IN THE FIELD OF RZ LMi

ISHIOKA, R.[1]; KOKUMBAEVA, R. [2]

[1] Academia Sinica Institute of Astronomy and Astrophysics, 11F of AS/NTU-AM Building, No.1, Sec. 4, Roosevelt Rd, Taipei 10617, R.O.C., e-mail: ishioka@asiaa.sinica.edu.tw

[2] Fesenkov Astrophysical Institute, Street Observatory 23, Almaty 050020, Kazakhstan, e-mail:kokumbaeva@aphi.kz

GSC 02505-00411 ($RA_{2000}=09^h51^m27.^s4$; $DEC_{2000}=+34°13'08.''0$) is a moderately bright star ($B=14.^m32$, $V=14.^m16$; Henden et al. 2015, $R=14.^m17$; Ofek et al. 2012), located nearby RZ LMi, a cataclysmic variable known with extremely frequent outbursts. Gontcharov et al. (2011) selected this star as an evolved subdwarf at a distance of 1512 pc with an absolute Ks magnitude of 2.65, based on its proper motion and photometric information taken from several all-sky survey catalogs. A low-resolution spectrum was taken by LAMOST project and this star is classified as an A1IV star (Luo et al. 2016). Owing to its location, this star has been observed coincidentally with RZ LMi, and its variability with small amplitude and short period was detected by one of the authors (RK). In this paper, we present out results of time-series observations and discuss its properties.

Observations were done by "East" Zeiss-1000 telescope equipped with Apogee U16M D9 CCD at Tien-Shan Astronomical Observatory in 2017. Exposure time was 90 sec except for a night with the exposure time of 30 sec. Images were reduced in the standard way, and we measured differential magnitude against a comparison star, GSC 02505-00363 ($B=14.^m68$, $V=13.^m95$; Henden et al. 2015, $R=13.^m60$; Ofek et al. 2012), whose constancy was examined with a check star, GSC 02505-00469. Figure 1 shows the light curves of GSC 02505-00411 (black lines). The data are available electronically through the IBVS website as `6205-t2.txt`.

The light curves clearly show variability with a period of $\sim$30 min and amplitude changing with the range from $<$0.01 mag to $\sim$0.03 mag. Using the discrete Fourier transform analysis program against the data removed nightly average magnitudes and long term variabilities, we detected the strongest peak at 43.8422 c/d ($0.^d022809$), the secondary peak at 27.8976 c/d ($0.^d035845$), and a possible third peak at 44.5365 c/d ($0.^d022453$), which are listed in Table 1. The power spectrum is shown in Figure 2. Figure 3 shows phase folded light curves with the detected periods, after prewhitening for the other periods. We show the 3-frequency model generated from our Fourier solution overlaid in Figure 1 (red lines). It is clear that additional frequencies exist, however, the quality of our data sets is not enough to detect them.

Based on the amplitude and period of its variations in addition to its spectral type of A1IV, we concluded that GSC 02505-00411 is a δ Sct star. δ Sct stars are pulsating variables of spectral types A to early F with luminosity classes V to III. The pair of short

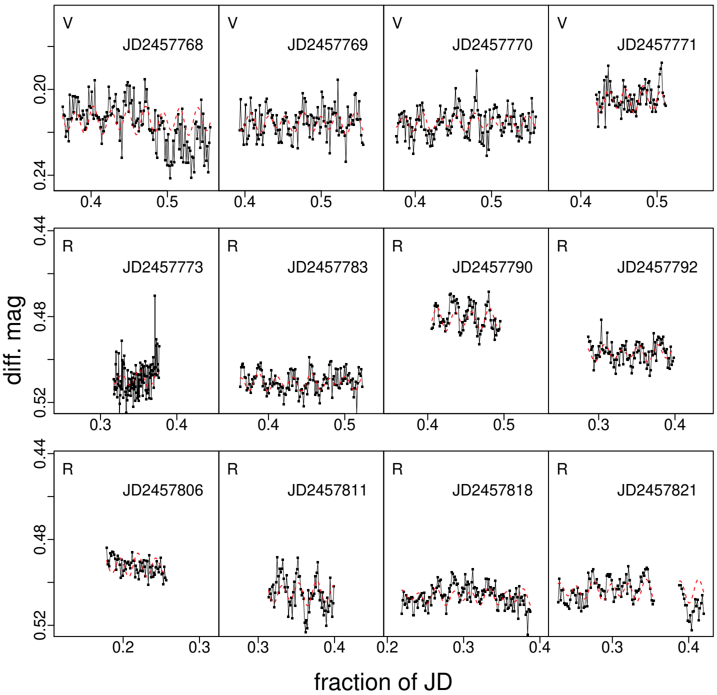

Figure 1. Light curves of GSC 02505-00411 (black line). Two frequency model generated from our Fourier solution is overlaid (red line).

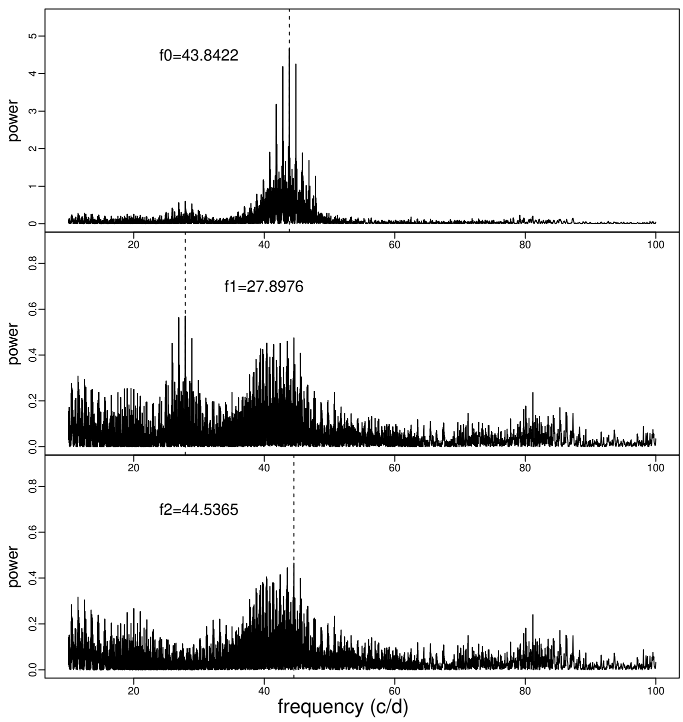

Figure 2. Power spectra of GSC 02505-00411.

Table 1: Frequencies detected in GSC 02505-00411

Mode	Freq. (c/d)	Ampl. (mmag)
f_0	43.8422±0.0025	41
f_1	27.8976±0.0028	15
f_2	44.5365±0.0063	14

pulsation period of 33 min and early spectral type of A1IV is consistent with the relation between spectral type and period for the δ Sct stars (eg. see Figure 6 in Chang et al. 2013). The 2MASS colors of GSC 02505-00411 ($J-H = 0.15$ $H-K = 0.01$; Cutri et al. 2003 & Skrutskie et al. 2006) fall within the region for the class of δ Sct stars in 2MASS colour space (Debosscher et al. 2011).

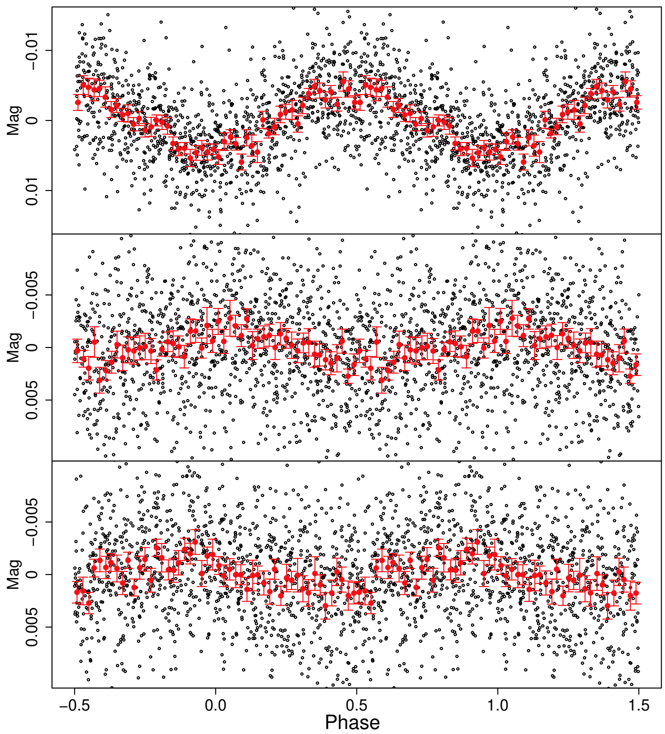

Figure 3. Phase folded light curves of GSC 02505-00411. From top to bottom, for the primary period of 0.022809 d, the secondary period of 0.035845 d, and the possible third period of 0.022453 d after prewhitening for the other periods, respectively.

GSC 02505-00411 is a δ Sct star with multiple frequencies with the primary frequency of 43.84 c/d. This star is in the field of RZ LMi, which means further data will be provided from the observations for this famous cataclysmic variable star.

Acknowledgements: This research was supported by Committee of Science, Ministry of Education and Science of the Republic of Kazakhstan (grant No.0075/GF4). This research has made use of the VizieR database operated at the Centre de Données Astronomiques (Strasbourg) in France. The authors are grateful to Dr. Kusakin, A., Reva, I., and Krugov, M. for the observation at TShAO. The DFT program used for our

analysis was written by Dr. T. Kato.

References:

Chang, S.-W., Protopapas, P., Kim, D.-W., Byun, Y.-I. 2013, *AJ*, **145**, 132 DOI
Cutri, R. M., Skrutskie, M. F., van Dyk, S., et al. 2003, *yCat* **2246**
Debosscher, J., Blomme, J., Aerts, C., De Ridder, J. 2011, *A&A*, **529**, A89 DOI
Gontcharov, G. A., Bajkova, A. T., Fedorov, P. N., Akhmetov, V. S. 2011, *MNRAS*, **413**, 1581 DOI
Henden, A. A., Levine, S., Terrell, D., Welch, D. L. 2015, *AAS*, **225**, 336.16
Luo, A- L., Zhao, Y.-H., Zhao, G., et al. 2016, *yCat*, **5149**
Ofek, E. O., Laher, R., Surace, J., et al. 2012, *PASP*, **124**, 854 DOI
Skrutskie, M. F., Cutri, R. M., Stiening, R., et al. 2006, *AJ*, **131**, 1163 DOI

COMMISSIONS G1 AND G4 OF THE IAU
INFORMATION BULLETIN ON VARIABLE STARS
Volume 63 Number 6206 DOI: 10.22444/IBVS.6206

Konkoly Observatory
Budapest
3 May 2017

HU ISSN 0374 – 0676

MINIMA TIMES OF THREE SELECTED SYSTEMS IN CANCER

GÖKAY, G.; DERMAN, E.; GÜROL, B.

Ankara University, Faculty of Science, Dept. of Astronomy and Space Sciences, Ankara, TÜRKİYE;
e-mail: ggokay@science.ankara.edu.tr

Observatory and telescope:
37" Kepler Space Telescope

Detector:	42 e2v CCD90s cameras, total 105 square degree FOV, 2200 × 1024 pixels for each CCD

Method of data reduction:
Data used here are pre-search data conditioning simple aperture photometry flux values and downloaded from Kepler[1] archive.

Method of minimum determination:
All minima times are weighted average BJD of the values obtained with parabolic and sine function fitting and Kwee & van Woerden (1956) method.

[1] https://archive.stsci.edu/k2/

Times of minima:					
Star name	Time of min. HJD 2400000+	Error	Type	Filter	Rem.
ES Cnc	57140.19210	0.00016	II	*Kepler*	
	57140.72375	0.00025	I	*Kepler*	
	57141.25920	0.00027	II	*Kepler*	
	57141.79312	0.00714	I	*Kepler*	
	57142.32820	0.00023	II	*Kepler*	
	57142.86174	0.00023	I	*Kepler*	
	57143.39817	0.00029	II	*Kepler*	
	57143.92864	0.00113	I	*Kepler*	
	57144.46591	0.00019	II	*Kepler*	
	57144.99722	0.00028	I	*Kepler*	
	57145.53485	0.00031	II	*Kepler*	
	57146.06515	0.00029	I	*Kepler*	
	57146.60330	0.00018	II	*Kepler*	
	57147.13166	0.00026	I	*Kepler*	
	57147.67304	0.00022	II	*Kepler*	
	57148.20084	0.00048	I	*Kepler*	
	57148.74229	0.00041	II	*Kepler*	
	57149.26815	0.00030	I	*Kepler*	
	57149.80610	0.00098	II	*Kepler*	
	57150.33772	0.00029	I	*Kepler*	
	57150.87567	0.00028	II	*Kepler*	
	57151.40554	0.00602	I	*Kepler*	
	57151.94642	0.00073	II	*Kepler*	
	57152.47549	0.00646	I	*Kepler*	
	57153.01687	0.00057	II	*Kepler*	
	57153.54085	0.00020	I	*Kepler*	
	57154.08282	0.00049	II	*Kepler*	
	57154.60948	0.00766	I	*Kepler*	
	57155.14936	0.00050	II	*Kepler*	
	57155.67797	0.00453	I	*Kepler*	
	57156.21496	0.00038	II	*Kepler*	
	57156.74506	0.00026	I	*Kepler*	
	57157.28206	0.00020	II	*Kepler*	
	57157.81205	0.00016	I	*Kepler*	
	57158.35135	0.00034	II	*Kepler*	
	57158.87954	0.00216	I	*Kepler*	
	57159.42186	0.00050	II	*Kepler*	
	57159.94770	0.00552	I	*Kepler*	
	57160.48549	0.00015	II	*Kepler*	
	57161.01506	0.00063	I	*Kepler*	
	57161.55666	0.00097	II	*Kepler*	
	57162.08280	0.00011	I	*Kepler*	
	57162.62475	0.00046	II	*Kepler*	
	57163.15032	0.00034	I	*Kepler*	
	57163.69094	0.00029	II	*Kepler*	
	57164.21934	0.00189	I	*Kepler*	
	57164.75272	0.00022	II	*Kepler*	

Times of minima:					
Star name	Time of min. HJD 2400000+	Error	Type	Filter	Rem.
ES Cnc	57165.28665	0.00435	I	*Kepler*	
	57165.82562	0.00027	II	*Kepler*	
	57166.35503	0.00032	I	*Kepler*	
	57166.89236	0.00057	II	*Kepler*	
	57167.42170	0.00032	I	*Kepler*	
	57167.95407	0.00010	II	*Kepler*	
	57168.48991	0.00030	I	*Kepler*	
	57169.02107	0.00033	II	*Kepler*	
	57169.55777	0.00420	I	*Kepler*	
	57170.09457	0.00029	II	*Kepler*	
	57170.62625	0.00050	I	*Kepler*	
	57171.16488	0.00036	II	*Kepler*	
	57171.69359	0.00027	I	*Kepler*	
	57172.22657	0.00006	II	*Kepler*	
	57172.75957	0.00045	I	*Kepler*	
	57173.29561	0.00032	II	*Kepler*	
	57173.82863	0.00022	I	*Kepler*	
	57174.36198	0.00026	II	*Kepler*	
	57174.89761	0.00031	I	*Kepler*	
	57175.42997	0.00055	II	*Kepler*	
	57175.96378	0.00017	I	*Kepler*	
	57176.49622	0.00050	II	*Kepler*	
	57177.03168	0.00022	I	*Kepler*	
	57177.56336	0.00057	II	*Kepler*	
	57178.09863	0.00024	I	*Kepler*	
	57178.62873	0.00063	II	*Kepler*	
	57179.16728	0.00021	I	*Kepler*	
	57179.69860	0.00055	II	*Kepler*	
	57180.23340	0.00018	I	*Kepler*	
	57180.76379	0.00069	II	*Kepler*	
	57181.29939	0.00030	I	*Kepler*	
	57181.83277	0.00024	II	*Kepler*	
	57182.36647	0.00019	I	*Kepler*	
	57182.90359	0.00023	II	*Kepler*	
	57183.43470	0.00018	I	*Kepler*	
	57183.97141	0.00054	II	*Kepler*	
	57184.50271	0.00037	I	*Kepler*	
	57185.03389	0.00080	II	*Kepler*	
	57185.57243	0.00037	I	*Kepler*	
	57186.09937	0.00046	II	*Kepler*	
	57186.64222	0.00073	I	*Kepler*	
	57187.16963	0.00058	II	*Kepler*	
	57187.70618	0.00029	I	*Kepler*	
	57188.23707	0.00098	II	*Kepler*	
	57188.77556	0.00025	I	*Kepler*	
	57189.30662	0.00167	II	*Kepler*	
	57189.84304	0.00035	I	*Kepler*	

Times of minima:					
Star name	Time of min. HJD 2400000+	Error	Type	Filter	Rem.
ES Cnc	57190.37177	0.00026	II	*Kepler*	
	57190.91064	0.00079	I	*Kepler*	
	57191.44585	0.00052	II	*Kepler*	
	57191.97891	0.00023	I	*Kepler*	
	57192.52141	0.00095	II	*Kepler*	
	57193.57799	0.00056	II	*Kepler*	
	57194.11157	0.00071	I	*Kepler*	
	57194.65228	0.00030	II	*Kepler*	
	57195.17933	0.00148	I	*Kepler*	
	57195.72360	0.00088	II	*Kepler*	
	57196.24820	0.00039	I	*Kepler*	
	57196.78810	0.00073	II	*Kepler*	
	57197.31624	0.00071	I	*Kepler*	
	57197.85499	0.00026	II	*Kepler*	
	57198.38547	0.00036	I	*Kepler*	
	57198.92577	0.00048	II	*Kepler*	
	57199.45250	0.00040	I	*Kepler*	
	57199.98996	0.00040	II	*Kepler*	
	57200.52199	0.00060	I	*Kepler*	
	57201.06137	0.00034	II	*Kepler*	
	57201.59063	0.00038	I	*Kepler*	
	57202.12900	0.00073	II	*Kepler*	
	57202.65799	0.00034	I	*Kepler*	
	57203.19854	0.00088	II	*Kepler*	
	57203.72754	0.00011	I	*Kepler*	
	57204.26789	0.00094	II	*Kepler*	
	57204.79494	0.00250	I	*Kepler*	
	57205.33497	0.00046	II	*Kepler*	
	57205.86145	0.00032	I	*Kepler*	
	57206.39606	0.00074	II	*Kepler*	
	57206.92953	0.00084	I	*Kepler*	
	57207.47214	0.00042	II	*Kepler*	
	57207.99790	0.00046	I	*Kepler*	
	57208.54200	0.00058	II	*Kepler*	
	57209.06401	0.00104	I	*Kepler*	
	57209.60887	0.00079	II	*Kepler*	
	57210.13328	0.00029	I	*Kepler*	
	57210.68092	0.00077	II	*Kepler*	
	57211.20089	0.00113	I	*Kepler*	
	57211.74893	0.00034	II	*Kepler*	
	57212.26886	0.00045	I	*Kepler*	
	57212.81547	0.00086	II	*Kepler*	
	57213.33577	0.00031	I	*Kepler*	
	57213.88478	0.00046	II	*Kepler*	

Times of minima:					
Star name	Time of min. HJD 2400000+	Error	Type	Filter	Rem.
HV Cnc	57144.49617	0.00647	II	*Kepler*	
	57149.70916	0.00469	I	*Kepler*	
	57154.87854	0.02173	II	*Kepler*	
	57160.05590	0.00071	I	*Kepler*	
	57165.22350	0.00170	II	*Kepler*	
	57170.39350	0.00023	I	*Kepler*	
	57175.56557	0.00444	II	*Kepler*	
	57180.73304	0.00239	I	*Kepler*	
	57191.07121	0.00061	I	*Kepler*	
	57201.41008	0.00033	I	*Kepler*	
	57206.57681	0.00119	II	*Kepler*	
	57211.74497	0.00304	I	*Kepler*	
HD 75638	57141.93059	0.00050	I	*Kepler*	
	57153.56623	0.00082	I	*Kepler*	
	57159.38222	0.00100	I	*Kepler*	
	57165.20106	0.00032	I	*Kepler*	
	57171.01750	0.00945	I	*Kepler*	
	57194.28592	0.01062	I	*Kepler*	
	57205.92409	0.00060	I	*Kepler*	

Acknowledgements:

This paper includes data collected by the Kepler/K2 mission. Funding for the Kepler/K2 mission is provided by the NASA Science Mission directorate.

Reference:

Kwee, K. K., van Woerden, H., 1956, *Bull. Astron. Inst. Neth.*, **12**, 327

COMMISSIONS G1 AND G4 OF THE IAU
INFORMATION BULLETIN ON VARIABLE STARS
Volume 63 Number 6207 DOI: 10.22444/IBVS.6207

Konkoly Observatory
Budapest
4 May 2017

HU ISSN 0374 – 0676

DD CMa: A NEW GALACTIC DPV OF EXTREME SHORT PERIOD

ROSALES G., J.; MENNICKENT, R. E.

Astronomy Department, University of Concepción, Concepción, Chile. e-mail: jrosales@astro-udec.cl

We have performed a new search for interacting binaries of the type Double Periodic Variables (DPVs) in ASAS[1] (Pojmanski, 1997). We have considered Eclipsing Algols Semi-detached and Detached (EA/SD and EA/ED respectively) within the minimum orbital period of a clasical DPV. The DPVs are intermediate binary stars that show closely linked photometric variations being the long period roughly 33 times longer than the orbital period (Mennickent et al. 2003, 2016a, Poleski et al. 2010). The nature of the second period is unknown but suspected to reflect the strength variations of a wind generated in the stream-disc impact region (Mennickent et al. 2012, 2016b, van Rensbergen et al. 2008). DPVs are considered as one specific evolutionary step for more massive Algols, one posssibly involving mild mass transfer and systemic mass loss (Mennickent et al. 2008). But an interesting property of these objects is the surprising constancy of their orbital periods, which is not expected in Algols undergoing RLOF mass transfer (Garrido et al. 2013). Also the DPVs seem to be hotter and more massive than classical Algols and seem to have always a B-type component; their orbital periods typically run between 3 and 100 days. DPVs have been found in the Galaxy (MW), the Large Magellanic Cloud (LMC) and the Small Magellanic Cloud (SMC).

We carried out a visual inspection in ASAS for orbital period less than 3 but longer than 2 days. At this opportunity we have found only one new candidate to DPVs from 821 objects and determined the orbital and long period by using the PDM IRAF [2] software (Stellingwerf 1978). Also we have estimated the errors for the orbital period and long cycle by visual inspection of the light curves phased with trial periods near the minimum of the periodogram given by PDM. We disentangled the two main photometric frequencies using a code specially designed for this purpose by Zbigniew Kołaczkowski. The code adjusts the orbital signal with a Fourier series, this code is able to disentangle both frequencies if we give us the fundamental frequency plus their harmonics. Then it removes this signal from the original time series letting the long periodicity present in a residual light curve. As result we obtain both isolated light curves without additional frequencies. The results of the search is presented in Table 1, and the disentangled light curves are shown in Figures 1 and 2. DD CMa was confirmed as the DPV that shows the shortest long-period found until moment, which makes it very peculiar. It is possible that under certain circumstances this short orbital period might let small room for the existence of an accretion disc and this fact makes this system particularly important to test models for the long-cycle based on disc winds. We believe that DD CMa is an optimal target for

[1] `http://www.astrouw.edu.pl/asas/`
[2] IRAF is distributed by the National Optical Astronomy Observatories, which are operated by the Association of Universities for Research in Astronomy, Inc., under cooperative agreement with the National Science Foundation.

photometric monitoring and spectroscopic studies to help understand the mass loss process and evolutionary stage of the Algols and specifically the DPVs. Also we have searched for the presence of close nebulosity around this system with the WISE image service[3] (Wright et al. 2010) especially in the band in W4 (22 mm), and we have confirmed the absence of nebulosity, which is relevant when discussing systemic mass loss and evolutionary stage in close binary stars with mass loss process.

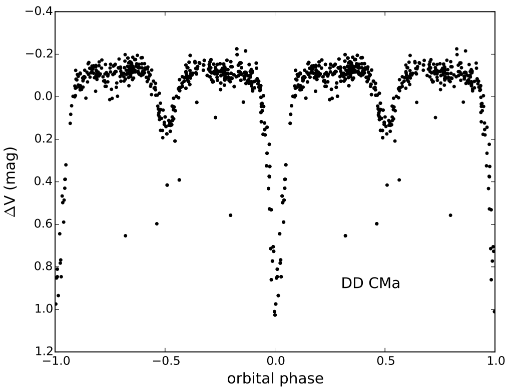

Figure 1. Disentangled ASAS V-band light curve of the new confirmed Double Periodic Variable.

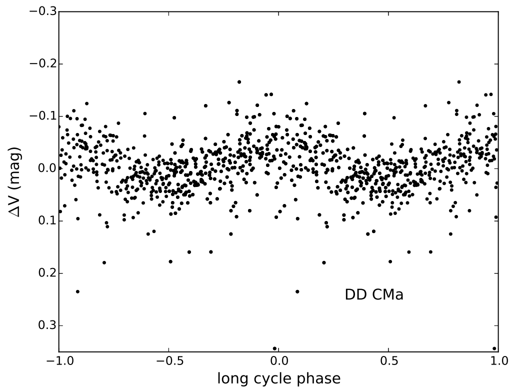

Figure 2. Disentangled ASAS V-band light curve of the new confirmed Double Periodic Variable.

Table 1: New confirmed Double Periodic Variable and their orbital (P_o) and long period (P_l). Both epoch for the minimum brightness of the orbital light curve and the maximum brightness of the long-cycle light curve are given.

ASAS-ID	Other ID	RA (2000)	DEC (2000)	P_o (days)	P_l (days)	$T_0(min_o)$ 2450000+	$T_0(max_l)$ 2450000+	V (ASAS) (mag)
072409-1910.8	DD CMa	07:24:09	−19:10:48	2.0084(1)	89.18(16)	2763.46515	4207.411	11.41

References:

Garrido, H. E., Mennickent, R. E., Djurašević, G., et al. 2013, *MNRAS*, **428**, 1594 DOI
Mennickent, R. E., Pietrzyński G., Diaz M., Gieren W., 2003, *A&A*, **399**, L47 DOI
Mennickent, R. E., Kołaczkowski, Z., Michalska, G., et al. 2008, *MNRAS*, **389**, 1605 DOI
Mennickent, R. E., Kołaczkowski, Z., Djurašević, G., et al. 2012, *MNRAS*, **427**, 607 DOI
Mennickent, R. E., Otero, S., Kołaczkowski, Z. 2016a, *MNRAS*, **455**, 1728 DOI
Mennickent, R. E., Zharikov, S., Cabezas, M., et al. 2016b, *MNRAS*, **461**, 1674 DOI
Pojmanski, G. 1997, *AcA*, **47**, 467
Poleski R., Soszyński I., Udalski A., et al. 2010, *AcA*, **60**, 179
Stellingwerf, R. F. 1978, *ApJ*, **224**, 953 DOI
van Rensbergen W., De Greve J. P., De Loore C., et al. 2008, *yCat*, **348**, 71129
Wright, E. L., Eisenhardt, P. R. M., Mainzer, A.K et al. 2010, *AJ*, **140**, 1868 DOI

[3] http://irsa.ipac.caltech.edu/applications/wise/

COMMISSIONS G1 AND G4 OF THE IAU
INFORMATION BULLETIN ON VARIABLE STARS
Volume 63 Number 6208 DOI: 10.22444/IBVS.6208

Konkoly Observatory
Budapest
13 May 2017

HU ISSN 0374 – 0676

MASS AND PRECESSION OF THE DISK IN ζ Tau

POLLMANN, ERNST

Emil-Nolde Straße 12, 51375 Leverkusen, Germany

Observatory of the Vereinigung der Sternfreunde Köln, Germany

1 Introduction

ζ Tauri (HD 37202, HR 1910) is a well known classical Be binary star with a gaseous circumstellar disk. Observations of the Hα emission line of that star reach back many decades. Since ζ Tau is a binary, any tilt of the disk will be modulated by the tidal force of the companion. This can manifest itself as nodding. During the observing period from approximately JD 2455500 to JD 2457500 the equivalent width of the Hα emission of ζ Tau decreased significantly what led to a depletion of the circumstellar disk. The depletion of the circumstellar disk led to a significant decrease of the equivalent width of the Hα emission of ζ Tau (Ruzdjak et al. 2009). The disk matter reached its minimum at JD 2456359, but afterwards new material was supplied into the disk, and the emission strength increased. The study presented here investigates how the minimum of the disk mass affects the precession period. In addition to monitoring the Hα equivalent width of ζ Tau, studying the time behavior of the central absorption (CA) core of that emission profile is also of interest. The depth of CA is defined as the difference between the local continuum level (equal to unity) and the minimum value at the line minimum intensity (Fig. 1). While the Hα emission line samples the disk as a whole, the region probed by the shell lines (CA) is restricted to the line of sight. The diagnostics they provide should not be neglected, as their properties (absorption depth) reflect the structure and dynamics of the disk in the observers direction (Escolano et al. 2015).

In the literature it is assumed (Schaefer et al. 2010) that the CA is caused by a different angle of the disk plane related to the observer's line of sight, as a consequence of the disk precession around the primary star. It is also known that the precession of the disk depends on its size (radius) and its mass due to gravitational effects (Katz et al. 1982, Larwood et al. 1996, Lubow & Ogilvie 2001).

2 Observation and Results

The Hα spectra were obtained with 0.2 m to 0.4 m telescopes with a long-slit (in most cases) and echelle spectrographs with resolutions of R = 10000–20000. All spectra included the 6400–6700 Å region, with a S/N of ~ 100 for the continuum near 6600 Å. The

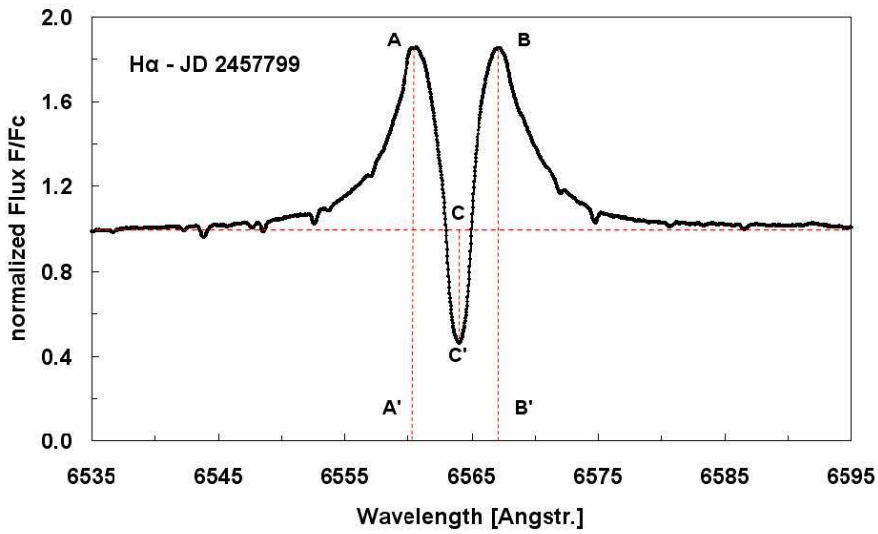

Figure 1. Measured quantities illustrated on a Hα line profile: (AA) and (BB) emission peaks, depth of the central absorption (CC). The horizontal line marks the normalized continuum.

spectra have been reduced with standard professional procedures (instrumental response, normalisation, wavelength calibration) by using of the program VSpec and the spectral classification software package MK32. The EWs reported here included the entire Hα emission profile (including both red and blue components) from 6540 to 6590 Å. Figure 2 shows the long-term monitoring of the Hα equivalent width (EW) as a result of collaboration between amateurs (mostly members of the ARAS spectroscopy group) astronomers. Figure 2 represents the time interval which includes the EW historical minimum on JD 2456359.

The higher disk mass (top-left-frame) in Fig. 3 corresponds to a precession period of (approximately) 1430 days (Schaefer et al. 2010).

3 PDM analysis and discussion

The bottom-right red frame in Fig. 3 also shows that within the time window highlighted in Fig. 2 the disk mass minimum coincides with the EW minimum. High-resolution spectra of ζ Tau were taken during the time window from JD 2455640 (March 2011) to JD 2457799 (February 2017) in collaboration with the ARAS group. This time window contains the time interval where the mass of the disc of ζ Tau reached its lowest value within the whole time this star has been observed. From those spectra the depth of the CA within the Hα emission profile was measured and the resulting time series is shown in Fig. 4.

In other words, the CA investigation presented here was performed within a time window when the disk mass of ζ Tau was the lowest for the entire time of the star studies. Therefore a logical question is: How does the disk mass minimum depend on the precession period during that time section?

Figure 4 shows the Hα CA time series (the time window shown in red in Figs. 2 & 3) of the normalized high-resolution spectra from JD 2455640 to JD 2457799. Phase

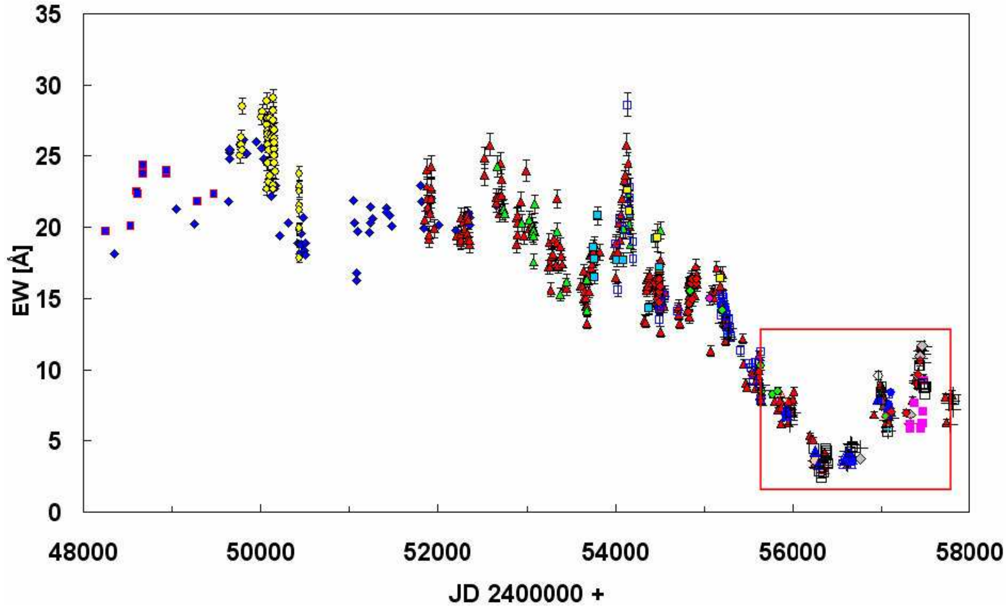

Figure 2. Long-term monitoring of the Hα equivalent width (EW). The red frame represents the time window of the historical EW minimum at JD 2456359. The time of the minimum around JD 2456300 corresponds to ∼JD 2456650 in time scale of Fig. 3.

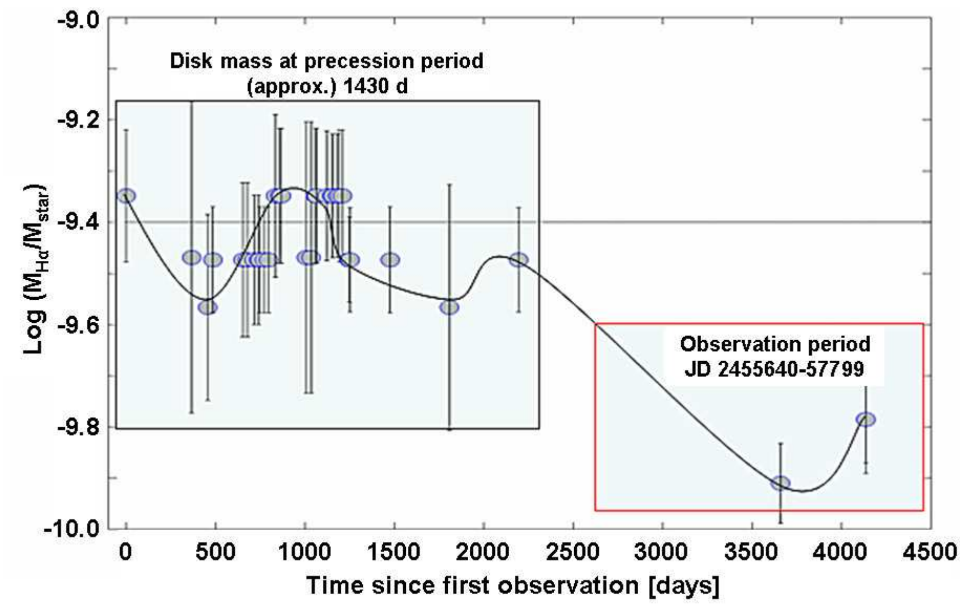

Figure 3. Disk mass versus time since the first observation, taken from Tycner & Sigut, 2015. The zero-time corresponds to JD 2452977 (2003/12/03). The red frame corresponds to the same time window highlighted in Fig. 2.

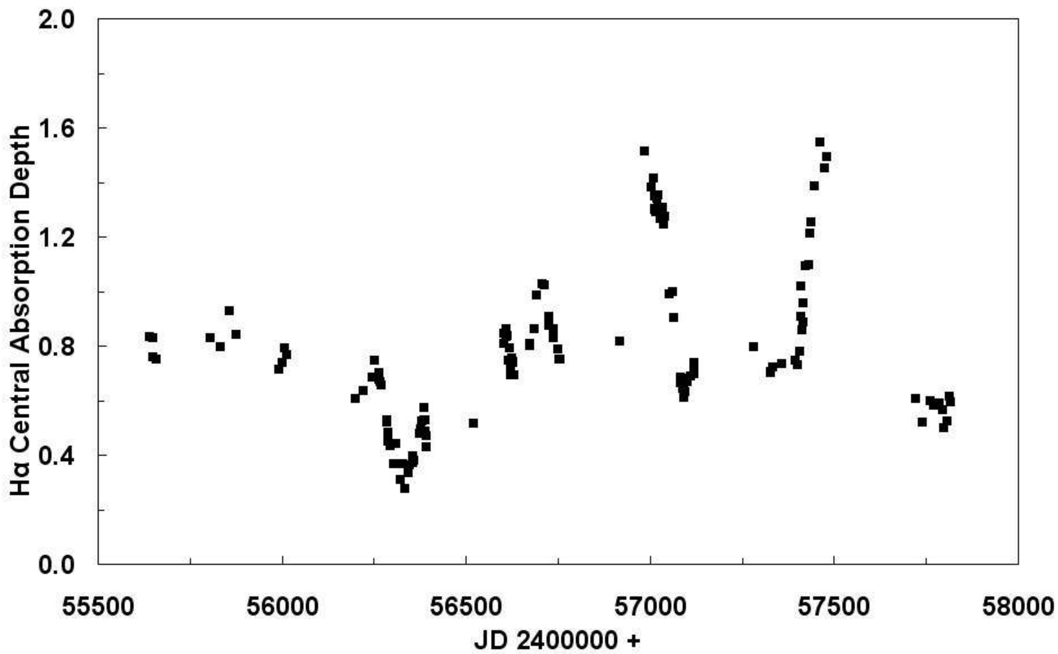

Figure 4. The CA in Hα of ζ Tau is a function of time from JD 2455640 to JD 2457799 (red frame in Figs. 2 & 3).

dispersion minimization (PDM) analysis on the time series was performed with the use of the program AVE (Barbera 1998), and produced the phase plot of Fig. 5 with the discriminant factor plotted in Fig. 6.

In contrast to Escolano et al. (2015), who found only marginal CA variations of the shell lines between approximately JD 2449000 and JD 2455000, the CA, as measured in this work, covered a considerable range of F/F_c from 0.28 to 1.55. The PDM analysis led to a CA period of 442 ± 5 d. But the question is, what are the mechanisms responsible for that periodic behavior? The periodic tilt of the disc as an effect of the precession could be manifested as a nodding, and could subsequently affect the variability in CA. Also, it is well known that the precession is, among other factors, a function of mass. Nevertheless it remains unclear whether the Hα CA period of ζ Tau found herewith can be understood as a consequence of changed precession period and changed disk mass, as shown in the plot from Tycner & Sigut (2015) in Fig. 2. But if we attribute the CA variability to a nodding caused by disk tilting, then this is the precession period. This investigation will continue during the coming years.

Acknowledgements: The spectra used for the evaluation of the CA of Hα were taken by the following observers of the ARAS spectroscopy group: J. Guarro, C. Sawicki, O. Garde, T. Lester, M. Leonardi, B. Mauclaire, N. Montigiani, A. Miroshnichenko, B. Koch, Ch. Buil, St. Ubaud, P. Fosanelli, H. Kalbermatten, St. Charbonnel, E. Pollmann. I am grateful for the ARAS collaboration. I am also grateful to Sara and Carl Sawicki (Alpine, Texas, USA) for their helpful improvements and suggestions in language; and to Prof. Dr. Anatoly Miroshnichenko (University of North Carolina at Greensboro) for his comprehensive support improving this work in several aspects.

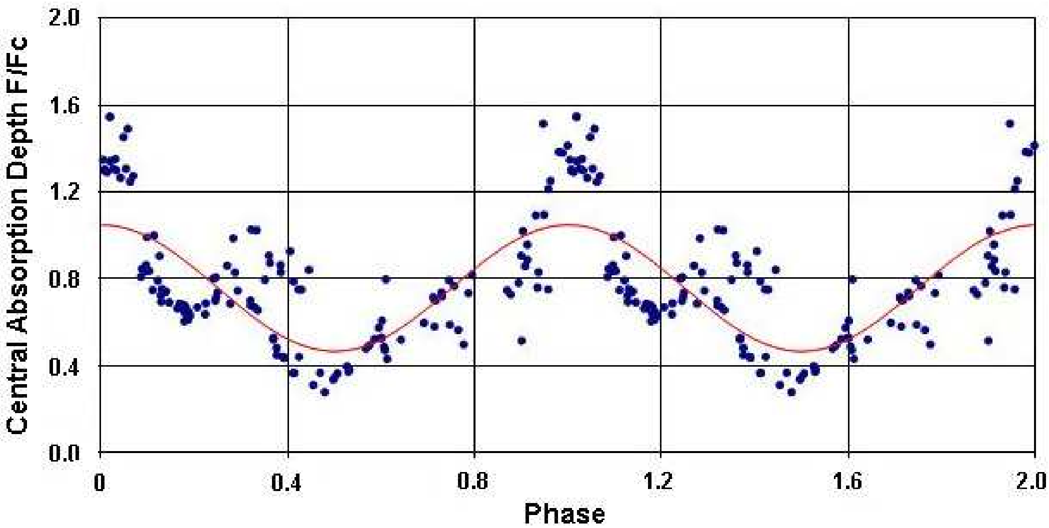

Figure 5. Phase plot of the PDM analysis in Fig. 6; period = 442 d (±5), Epoch = JD 2455571 (±16).

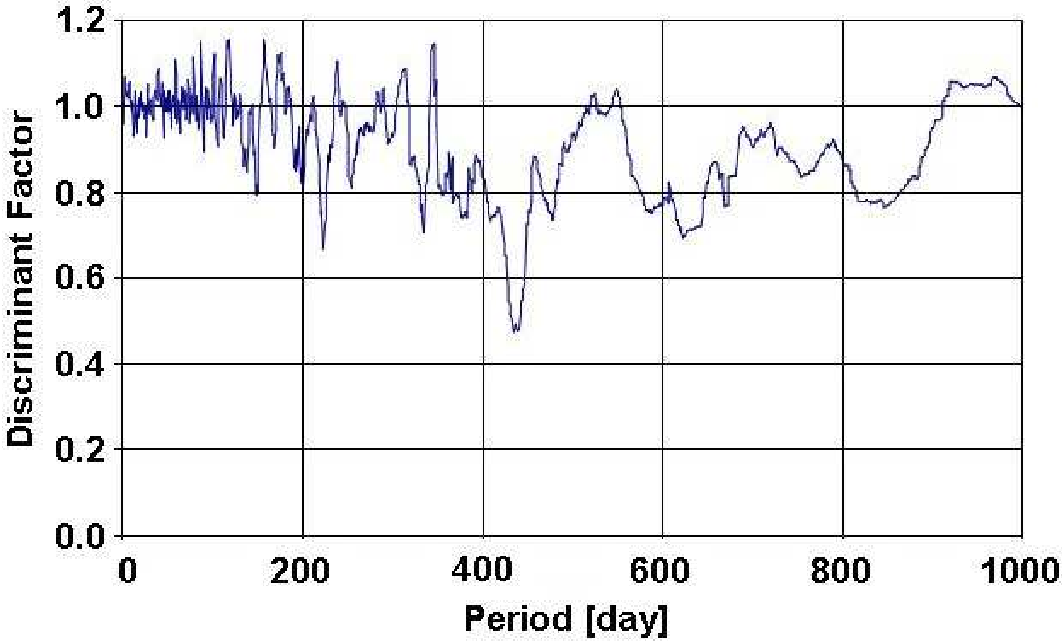

Figure 6. PDM analysis of the time series in Fig. 4.

References:

Barbera, R., 1998, AVE code, version 2.51, http://astrogea.org/soft/ave/aveint.htm
Escolano, C., Carciofi, A. C., Okazaki, A. T., Rivinius, Th., Baade, D., and Štefl, S., 2015, *A&A*, **576**, A112, DOI
Katz, J. I., Anderson, S. F., Grandi, S. A., Margon, B., 1982, *ApJ*, **260**, 780, DOI
Larwood, J. D., Nelson, R. P. , Papaloizou, J. C. B., Terquem, C. , 1996, *MNRAS*, **282**, 597, DOI
Lubow, S. H., Ogilvie, G. I., 2001, *ApJ*, **560**, 997, DOI
Rudjak, D., et al., 2009, *A&A*, **506**, 1319, DOI
Schaefer, G. et al. 2010, *AJ*, **140**, 1838, DOI
Tycner, Ch., Sigut, A., 2015, "The Variable and Asymmetric Disk of ζ Tau", poster, IAU General Assembly, Meeting 29, 08/2015, id. 2255073

COMMISSIONS G1 AND G4 OF THE IAU
INFORMATION BULLETIN ON VARIABLE STARS
Volume 63 Number 6209 DOI: 10.22444/IBVS.6209

Konkoly Observatory
Budapest
23 May 2017

HU ISSN 0374 – 0676

TIMES OF MINIMA OF SOME ECLIPSING BINARIES

BAHAR, E.[1,2]; YÖRÜKOĞLU, O.[1,2]; ESMER, E.M.[1,2]; KILIÇOĞLU, T.[1,2]; ÖZTÜRK, D.[1,2]; DOĞRUEL, M.B.[1,2]; ÖZUYAR, D.[1,2]; GÜMÜŞ, D.[1,2]; İZCİ, D.D.[1,2]; KETEN, B.[1,2]; TEZCAN, C.T.[1,2]; ŞENAVCI, H.V.[1,2]; YILMAZ, M.[1,2]; BAŞTÜRK, Ö.[1,2]; SELAM, S.O.[1,2]; EKMEKÇİ, F.[1,2]; ALBAYRAK, B.[1,2]; ÇALIŞKAN, Ş.[1,2]; AKÇAR, A.E.[1,2]

[1] Ankara University, Faculty of Science, Department of Astronomy and Space Sciences, TR-06100, Tandoğan, Ankara, Turkey; e-mail: enbahar@ankara.edu.tr

[2] Ankara University Kreiken Observatory, TR-06873, Ahlatlıbel, Ankara, Turkey

Observatory and telescope:
14" Schmidt-Cassegrain telescope of the Ankara University Kreiken Observatory

Detector:	Apogee ALTA U47+ CCD camera. 1024 x 1024 pixels.

Method of data reduction:
Reduction of the CCD frames and differential photometry were performed with the standard tasks of IRAF[1]package

Method of minimum determination:
The minima times of eclipsing binaries were calculated using Kwee & van Woerden's (1956) method.

[†]Based on the observations performed at Ankara University Kreiken Observatory
[1]IRAF is distributed by the National Optical Astronomical Observatories, operated by the Association of the Universities for Research in Astronomy, inc., under cooperative agreement with the National Science Foundation

Times of minima:					
Star name	Time of min. HJD 2400000+	Error	Type	Filter	Rem.
AB And	57205.43594	0.00005	II	*R*	MY
AD And	57685.40230	0.00010	I	*VRI*	OK
CN And	57693.32582	0.00011	II	*VRI*	FT
LO And	57676.34309	0.00010	II	*VRI*	OY
BF Aur	57354.33181	0.00032	II	*BVRI*	SU, ST
IM Aur	57316.49553	0.00006	I	*BVRI*	HVS
SS Ari	57618.47954	0.00013	I	*BVRI*	DO
TY Boo	57552.35813	0.00004	I	*BVRI*	EME
AQ Boo	57084.35677	0.00039	I	*BVRI*	AO
EF Boo	57565.34457	0.00006	I	*BVRI*	EY
GR Boo	57519.49783	0.00015	II	*BVR*	DDI, BA
TX Cnc	57427.36069	0.00006	I	*BVRI*	FM, GG
BI CVn	57136.53486	0.00012	II	*BVRI*	MBD
	57137.49497	0.00008	I	*BVRI*	EB
DF CVn	57107.47573	0.00006	I	*BVRI*	SC
GM CVn	57115.49932	0.00008	II	*BVRI*	TA
V445 Cas	57676.43290	0.00010	I	*R*	ZA
V523 Cas	57715.24015	0.00004	I	*BVRI*	SOS
SU Cep	57546.39957	0.00019	I	*BVRI*	TK
RW Com	57084.26725	0.00012	I	*BVRI*	HC, PT
RZ Com	57130.29145	0.00005	II	*R*	YK
	57200.36261	0.00014	II	*R*	MHT
CC Com	57115.41505	0.00007	I	*BVRI*	OBR
TW CrB	57091.56687	0.00005	I	*R*	ES
AW CrB	57556.40438	0.00010	I	*BVRI*	CTT
CG Cyg	57600.48063	0.00010	II	*VRI*	ED
V382 Cyg	57556.48570	0.00025	II	*BVRI*	HD
HL Dra	57509.52496	0.00013	I	*BVRI*	HKA
DM Del	57595.43717	0.00008	I	*VRI*	IC
RZ Dra	57581.48322	0.00007	I	*VRC*	MNB
V345 Gem	57696.52207	0.00019	I	*BVRI*	ME
SZ Her	57164.35186	0.00003	I	*R*	BSA
SW Lac	57618.36841	0.00006	II	*BVRI*	MYN
	57676.26014	0.00004	I	*BVRI*	MU
AW Lac	57233.37074	0.00026	I	*BVRI*	BS, SL
SW Lyn	57715.59651	0.00027	II	*BVRI*	YE
FI Lyn	57448.34290	0.00005	I	*BVRI*	OT
V868 Mon	57031.54513	0.00010	II	*BVRI*	SO
	57087.34725	0.00007	I	*BVRI*	DG
UX Peg	57677.30173	0.00018	I	*VRI*	MB
BX Peg	57214.49830	0.00009	I	*BVRI*	MD
	57602.45522	0.00008	II	*VR*	ZNA
DI Peg	57267.48225	0.00006	I	*BVRI*	IO
IU Per	57427.24633	0.00013	I	*BVRI*	KC
	57672.35866	0.00011	I	*VRI*	MO
KW Per	57643.46847	0.00004	I	*VRI*	MK, US
DZ Psc	57720.25992	0.00010	II	*R*	SB
DK Sge	57211.41677	0.00013	I	*BVRI*	MTY
	57287.27934	0.00021	I	*R*	BR
RZ Tau	57715.49654	0.00005	I	*BVRI*	BB
AH Tau	57715.31396	0.00007	I	*BVRI*	AUU
GR Tau	57696.45224	0.00017	I	*VRI*	BK
HH UMa	57526.35810	0.00035	II	*VRI*	ZFY
AX Vir	57134.52523	0.00029	II	*BVRI*	YN
	57140.49666	0.00011	I	*BVRI*	DOR
	57485.43767	0.00005	I	*BVRI*	SCN
NN Vir	57564.34965	0.00015	I	*BVRI*	OB
AW Vul	57564.46965	0.00004	I	*BVRI*	OV
BE Vul	57227.42021	0.00008	I	*BVRI*	NS
TYC 1174-344-1	57316.24981	0.00026	I	*BVRI*	MA

Explanation of the remarks in the table:

Observers:

AUU:	A. Ulus Uludağ	MK:	Merve Keskin
AO:	Anıl Özkeleş	MY:	Mesut Yılmaz
BR:	Bahire Reçber	MTY:	Muhammed T. Yıldız
BSA:	Berhan S. Azizoğlu	ME:	Murat Esendemir
BB:	Bükem Belen	MU:	Murat Uzundağ
BK:	Burak Keten	MYN:	Murat Yazgan
BS:	Buse Sayar	MHT:	M. Hayri Türkyılmaz
BA:	Büşra Akerdem	NS:	Nebahat Sürüoğlu
CTT:	C. Tuğrul Tezcan	OK:	Oğuzhan Karadeniz
DG:	Damla Gümüş	OT:	Okay Tercan
DO:	Derya Öztürk	OBR:	Ömer Bayraktar
DDI:	D. Dilan İzci	OY:	Onur Yörükoğlu
DOR:	Doğuş Özuyar	OV:	Özge Varol
EME:	E. Murat Esmer	OB:	Özgür Baştürk
EY:	Emincan Yıldız	US:	Uğur Şenaslan
ED:	Emre Demirbağ	PT:	Pınar Tunç
EB:	Engin Bahar	SL:	Seher Lal
ES:	Ezgi Sertkan	SU:	Sefacan Uzun
FM:	Fatih Mazlum	SB:	Selda Başar
FT:	Furkan Tomak	SOS:	Selim O. Selam
GG:	Gamze Gök	SO:	Sercan Öz
HVS:	H. Volkan Şenavcı	SC:	Şeyma Çalışkan
HC:	Hediye Çelik	ST:	Sibel Taş
HD:	Hüseyin Deniz	SCN:	Şule Çeken
IO:	İbrahim Özavcı	TA:	Tarık Akkaya
IC:	Işıl Çetinkaya	TK:	Tolgahan Kılıçoğlu
KC:	Kadem Çelik	YE:	Yağız Eraslan
HKA:	H. Kübra Aygören	YN:	Yahya Nasolo
MNB:	M. Naim Bağıran	YK:	Yasemin Karademirci
MA:	Melisa Alçakır	ZA:	Zeynep Avcı
MB:	Meltem Baydar	ZFY:	Z. Fatma Yıldırım
MO:	Mert Özküm	ZNA:	Z. Nur Acar
MD:	Merve Dağgün		

Acknowledgements:

We would like to thank all the observers and the staff at the Ankara University Kreiken Observatory. Authors from Ankara University acknowledge the support by the research fund of Ankara University (BAP) through the project 15A0759001.

Reference:

Kwee, K.K., van Woerden, H., 1956, *BAN*, **12**, 327

COMMISSIONS G1 AND G4 OF THE IAU
INFORMATION BULLETIN ON VARIABLE STARS
Volume 63 Number 6210 DOI: 10.22444/IBVS.6210

Konkoly Observatory
Budapest
13 July 2017

HU ISSN 0374 – 0676

DISCOVERY OF SHORT-PERIOD OSCILLATIONS IN THE MASS-ACCRETING COMPONENT OF BD Vir

MKRTICHIAN, D.E.; A-THANO, N.; AWIPHAN, S

National Astronomical Research Institute of Thailand, 191 Siriphanich Bldg., Huay Kaew Rd., Suthep, Muang, 50200 Chiang Mai, Thailand.

The "**Tha**i **S**ky **S**urvey for **o**EA **S**tars" (THASSOS) project is focused on searching for and studies of new mass-accreting pulsating components of a semi-detached Algol-type systems, so called class of oEA stars suggested by Mkrtichian et al. (2002, 2004). oEA components of binaries have been evolved into the instability strip after the first high- mass transfer stage and show δ Sct-like oscillations like classical δ Sct-type stars in well detached eclipsing binary systems, without any history of mass transfer. BD Vir is a 2.548572-day semi-detached Algol type eclipsing binary system with an A8 V primary component, showing long-term orbital period variation (Kreiner, 2004).

The new CCD photometric observations for BD Vir were obtained during 4 nights (February 13, March 13, 31 and April 20, 2017) using the 0.5m telescope of Thai National Observatory in Thailand. All observations were made at the orbital phase interval 0.45-0.72. Johnson B-filter was used, exposures varied from 20 to 80 seconds depending on seeing and the weather conditions. All stars in the field of view were reduced by SExtractor and the Python written codes for differential photometry. Exposures were binned by 4 points to get a better accuracy. The comparison star TYC 6120-50-1 (RA = $13^{\rm h}27^{\rm m}16\overset{\rm s}{.}245$ DEC= $-16^\circ07'45\overset{''}{.}85$) was used.

Pulsational variations were searched for in the out-of-eclipse parts of the light curve after removal of slow orbital light variations using the low order polynomial fits. Residual light curves are shown in Figure 1. We searched for periodic variations in the residual data by using the Period04 software (Lenz & Breger, 2005).

We applied the Discrete Fourier Transforms (DFT) and the signal pre-whitening techniques for consecutive detection of signals in the data. Steps of DFT analyses and consecutive pre-whitenings of found frequencies are shown in Figure 2 from top to bottom. We detected two pulsation frequencies at 34.159 c/d and 29.735 c/d. Frequencies, amplitudes of oscillations and their accuracies are listed in Table 1.

Conclusion: We discovered short-period pulsational light oscillations in a primary mass-accreting component of the semi-detached eclipsing binary system BD Vir. We conclude, that BD Vir is a new member of oEA group of pulsators suggested by Mkrtichian et al. (2002, 2004).

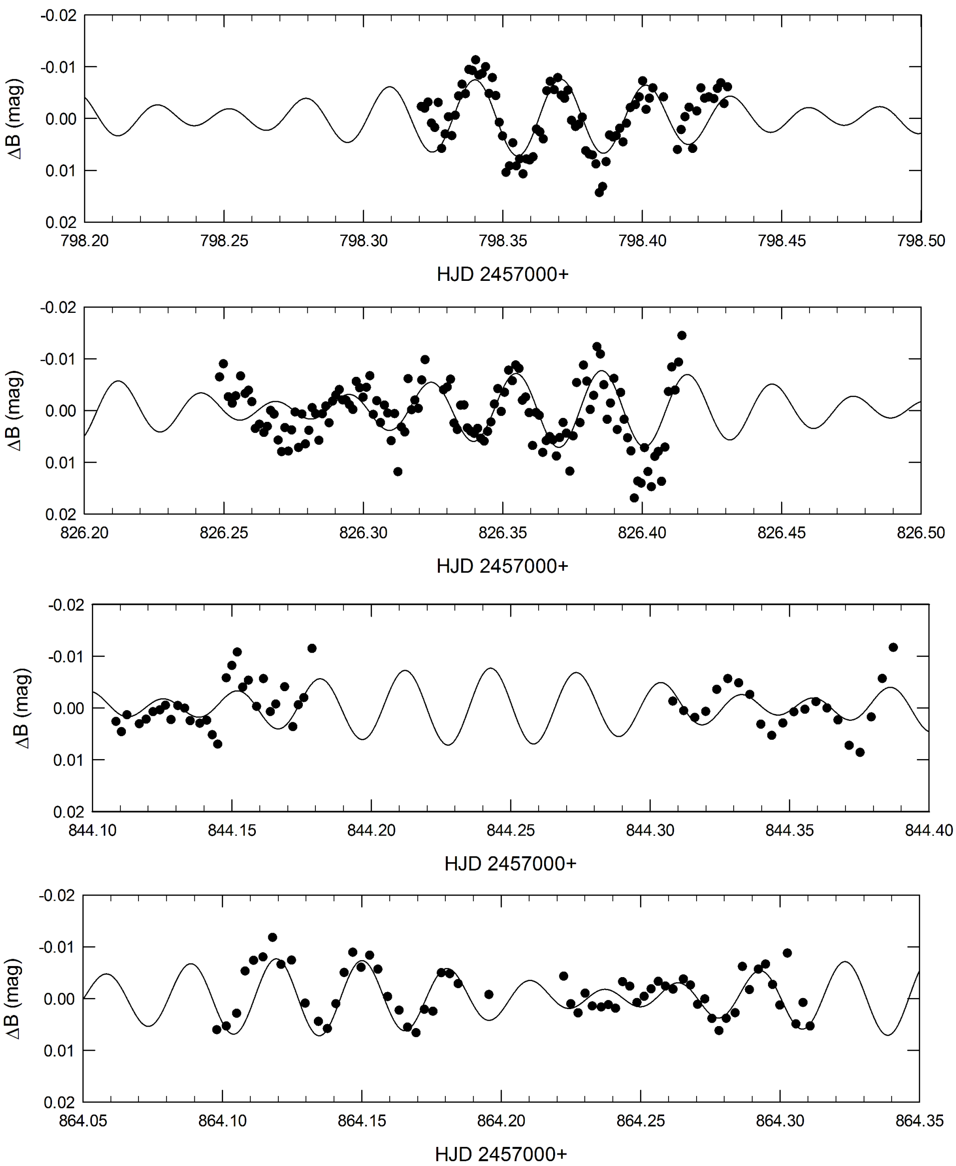

Figure 1. The nightly residual light variations of BD Vir (dots). Solid line is a two frequency fit to the data.

Table 1: Pulsation frequencies and amplitudes.

Frequency (c/d)/(σ)	Amplitude (mag)/(σ)
f_1=34.1599(4)	0.0045(2)
f_2=29.7353(6)	0.0030(2)

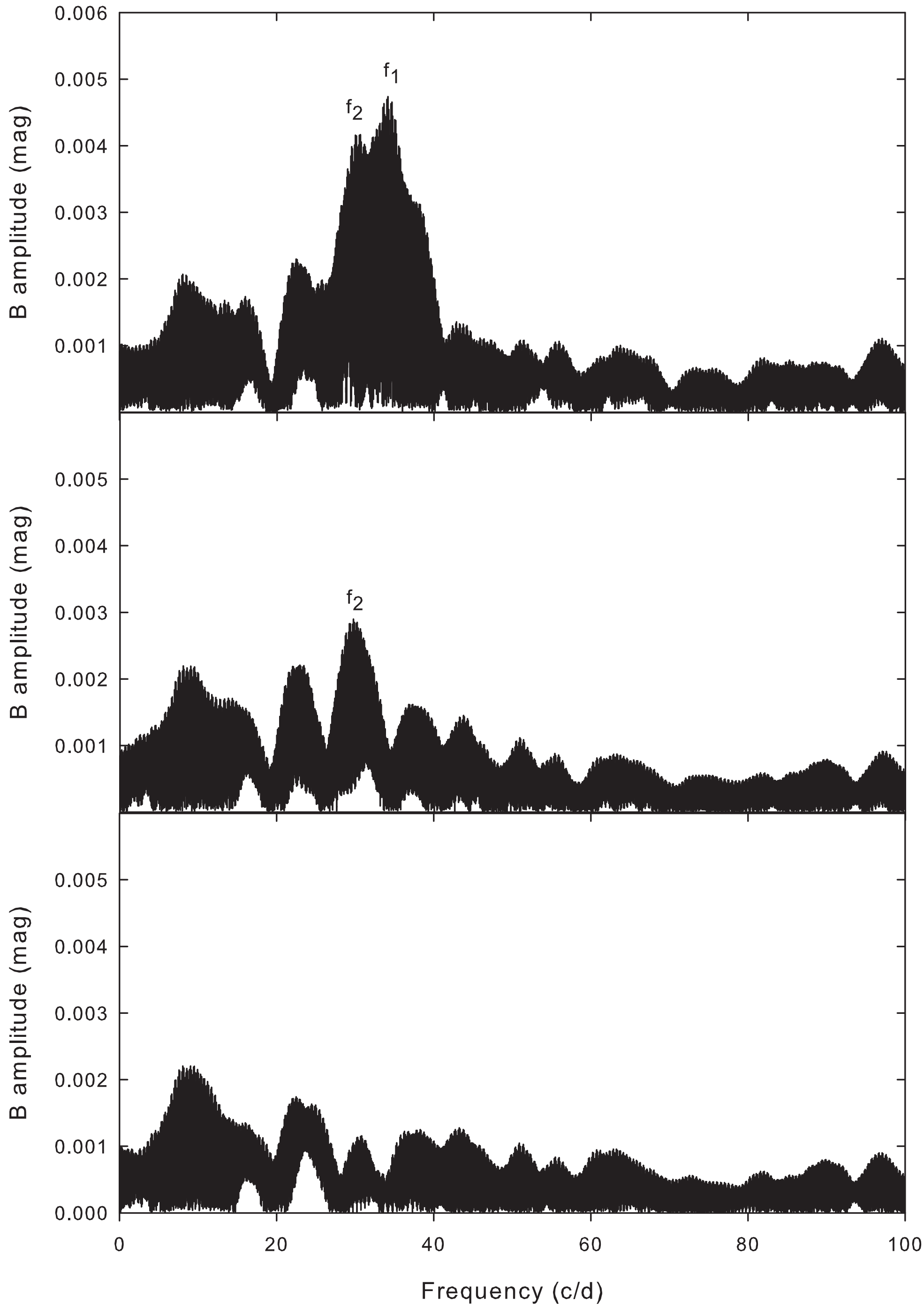

Figure 2. The DFT amplitude spectra of the primary component. Top panel - the DFT of the residual light curve, highest peak is at 34.16 c/d. Middle panel - the DFT of residuals after removal of 34.16 c/d, highest peak at 29.73 c/d. Bottom panel - the DFT after removal of 34.16 and 29.73 c/d.

Acknowledgements:

We acknowledge this work as part of the research activity supported by the National Astronomical Research Institute of Thailand (NARIT), Ministry of Science and Technology of Thailand.

References:

Kreiner J.M., 2004, *AcA*, **54**, 207
Lenz P., Breger M., 2005, *Communications in Asteroseismology*, **146**, 53 DOI
Mkrtichian D. et al., 2002, *ASP Conf. Ser.*, **259**, 96
Mkrtichian, D.E., Kusakin, A.V., Rodriguez, E., et al., 2004, *A&A*, **419**, 1015 DOI

COMMISSIONS G1 AND G4 OF THE IAU
INFORMATION BULLETIN ON VARIABLE STARS
Volume 63 Number 6211 DOI: 10.22444/IBVS.6211

Konkoly Observatory
Budapest
16 July 2017

HU ISSN 0374 – 0676

DISCOVERY OF δ SCT TYPE PULSATIONS IN THE ECLIPSING BINARY IK Vir

OHSHIMA, OSAMU[1,2]; AKAZAWA, HIDEHIKO[1,3]

[1] Department of Biosphere-Geosphere Science, Okayama University of Science, Ridai-cho 1-1, Kita-ku, Okayama, 700-0005, Japan

[2] Ohshima Tamashima Observatory, Tamashima 3-10-15, Kurashiki, Okayama, Japan, e-mail: o2@otobs.org

[3] Akazawa Funao Observatory, Funao 107, Kurashiki, Okayama, Japan, e-mail: akazawa_hide@mx1.tamatele.ne.jp

We report the detection of δ Sct type variations in the eclipsing binary system, IK Vir (V=11.54 mag, A6, $P_{\rm orb}$ = 0.72 d, Velichko et al. 1991 and Kazarovets et al. 1993), in our V-band photometry. The observations were carried out with Moravian G2–1600 CCD camera attached to 28 cm Schmidt-Cassegrain telescope at Akazawa Funao Observatory. Total observational runs are twenty one nights from March 26 to May 26 in 2015. IK Vir is measured differentially to BD+02 2522 = GSC 0281–0223 as the comparison star. BD+02 2522 is measured to GSC 0281–0255 as the check star. All the data in this observational season are shown in the lower light curve in Figure 1. To highlight short period (about 30 minutes) variations, data from only five observing runs, chosen so that there is no overlap in the same phase range, are plotted in the upper light curve in Figure 1. All the V-band photometric data obtained for this study are available as electronic tables(`6211-t3.txt`) from IBVS website.

The light curves in Fig. 2 for three individual nights show beat phenomena, which suggests that the variations are multiply periodic. In order to extract short period variations, third-order polynomials are fitted and subtracted from data for eight nights runs which covered out-of-eclipse phases.The residuals are analysed by the Period4 program (Lenz and Breger, 2005). The first six dominant frequencies are listed in Table 1 and their power spectra at each subtraction phase are shown in Fig. 3. The over-plotted solid line in Fig. 2 shows the light curve synthesized from the detected multiple periods.

When we tried to subtract the synthesized light curve from observational data, the short period variations were naturally cancelled in the residuals out-of-eclipse. However, in the period between the phase of about -0.15 to 0.15 covering the primary eclipse, the short period variations could not well cancelled (Fig. 4). This indicates that the pulsating component is the primary and it might indicates that nonradial oscillations of a specific low order mode are emphasized by the eclipse and that some phase shift has occurred (Unno et al. 1989). The new times of minima obtained in 2015 are listed in Table 2. Together with the times of minima listed in the O–C Gateway[1] since 1999, a new ephemeris for primary minimum could be calculated as follows:

$$HJD_{\rm Min} = 2451275.3649312(1) + 0.7236021(2) \times E$$

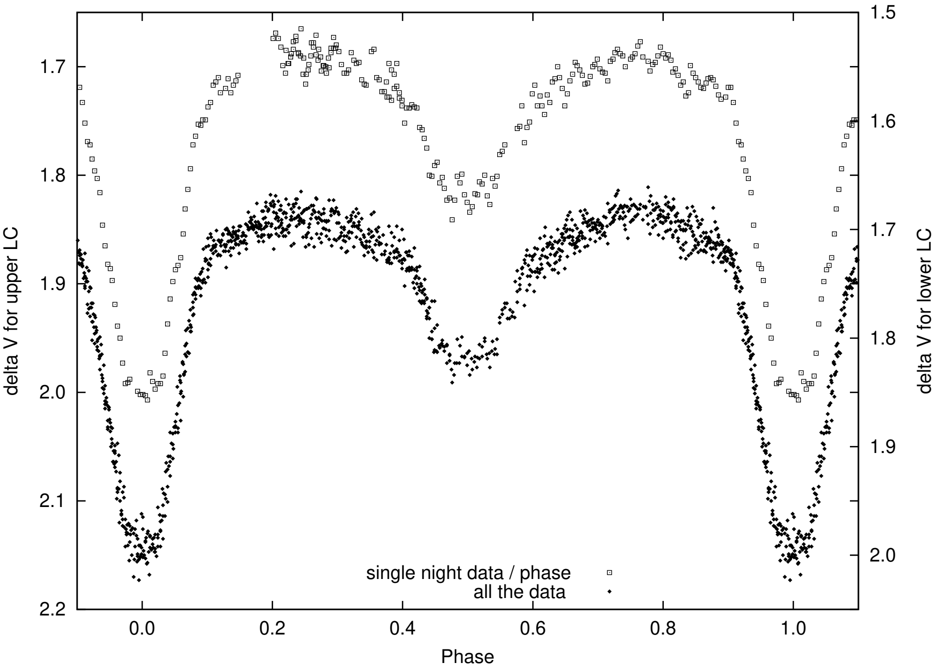

Figure 1. Light curve of IK Vir. Upper one consists of five night runs with no overlap. In the lower one we plotted all the data we obtained.

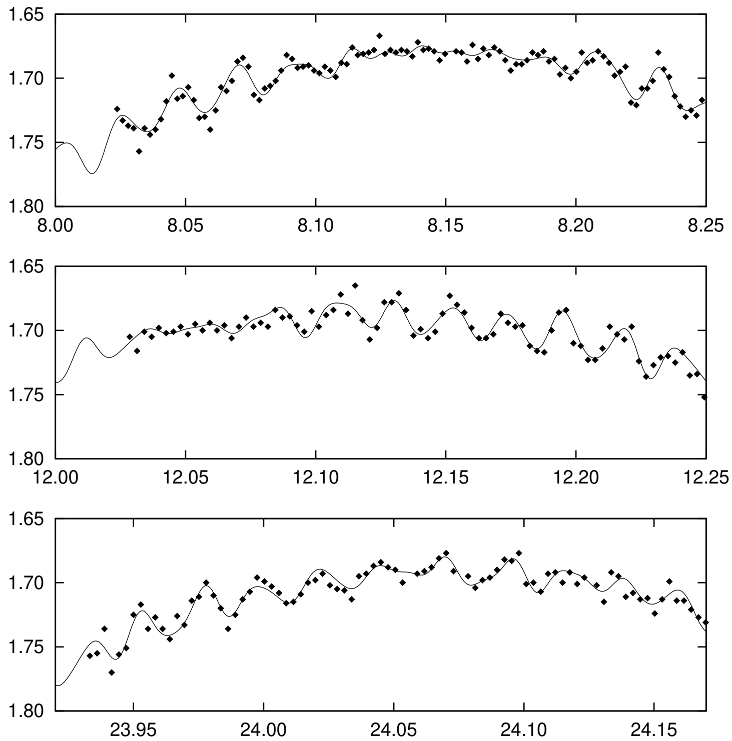

Figure 2. The beat phenomenon in V band light curve. The line indicates the light curve calculated from the six frequencies in Table 2.

Table 1: Most dominant six frequencies and the corresponding amplitudes.

	Frequency(c/d)	amplitude
F1	43.87960	0.00167
F2	48.22544	0.00074
F3	46.69045	0.00049
F4	38.87607	0.00041
F5	75.70104	0.00037
F6	29.40399	0.00044

Table 2: New times of minima of IK Vir.

HJD−2450000	Uncertainty	Type	$O-C$
7127.13421	0.00039	I	−0.00090
7130.02980	0.00010	I	0.00028
7134.00844	0.00010	II	−0.00089
7135.09531	0.00009	I	0.00057
7139.07266	0.00010	II	−0.00189
7164.03957	0.00009	I	0.00075

References:

Kazarovets, E. V., Samus N. N. and Goranskij V. P., 1993, *IBVS*, **3840**
Lentz, P. and Breger, M., 2005, *Communications in Astroseismology*, **146**, 53 DOI
Unno W., Osaki Y., Ando H., Saio, H. and Shibahashi H., 1989, *Nonradial Oscillations of Stars*, 2nd edition, Tokyo: University of Tokyo Press, p.22
Velichko, F.P. , Kwiatkowski, T. and Krugly, Yu.N., 1991, *Astr Tsirk*, **1548**, 27

[1] http://var.astro.cz/ocgate/

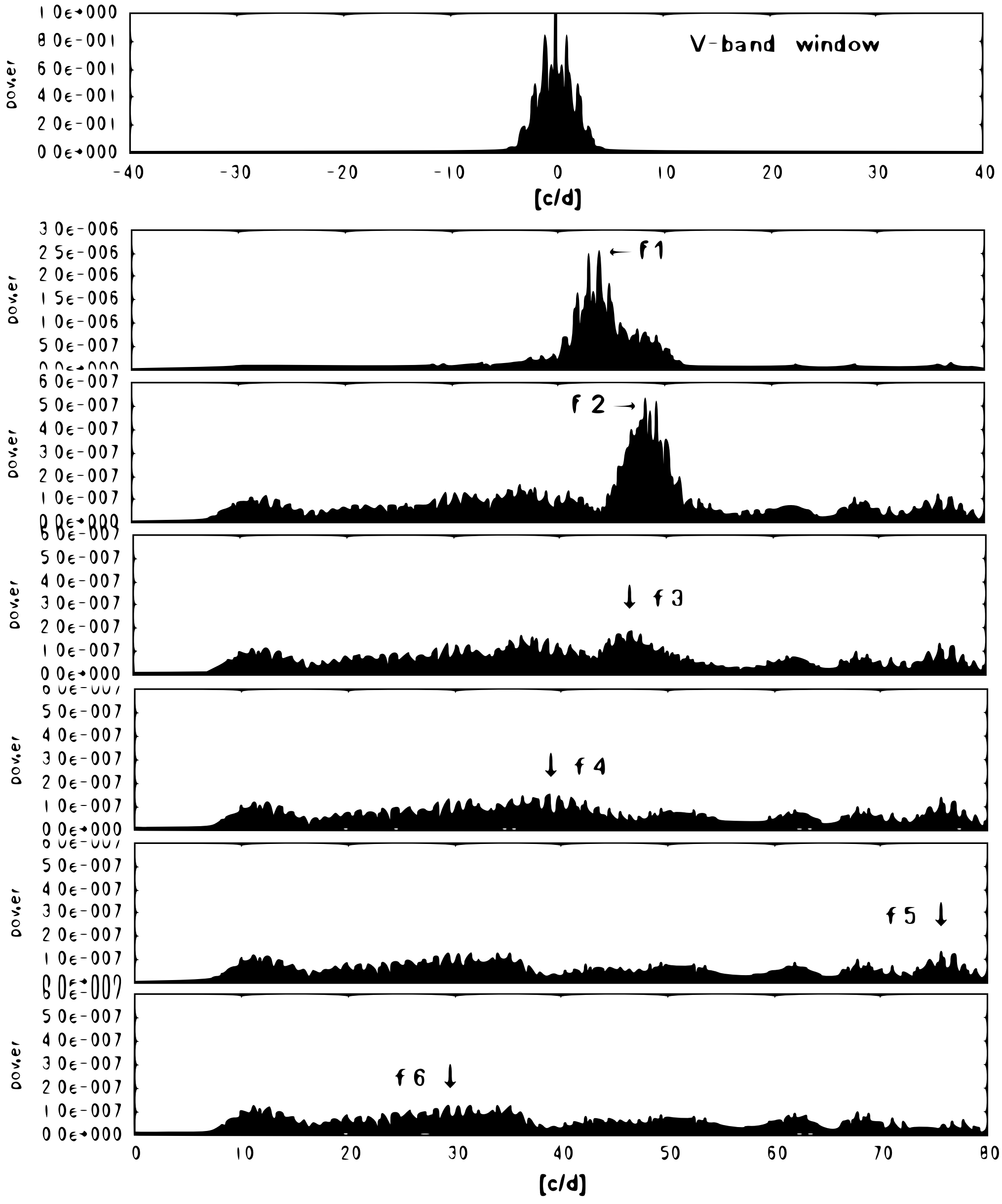

Figure 3. Power spectra of short period variations out-of-eclipse of IK Vir.

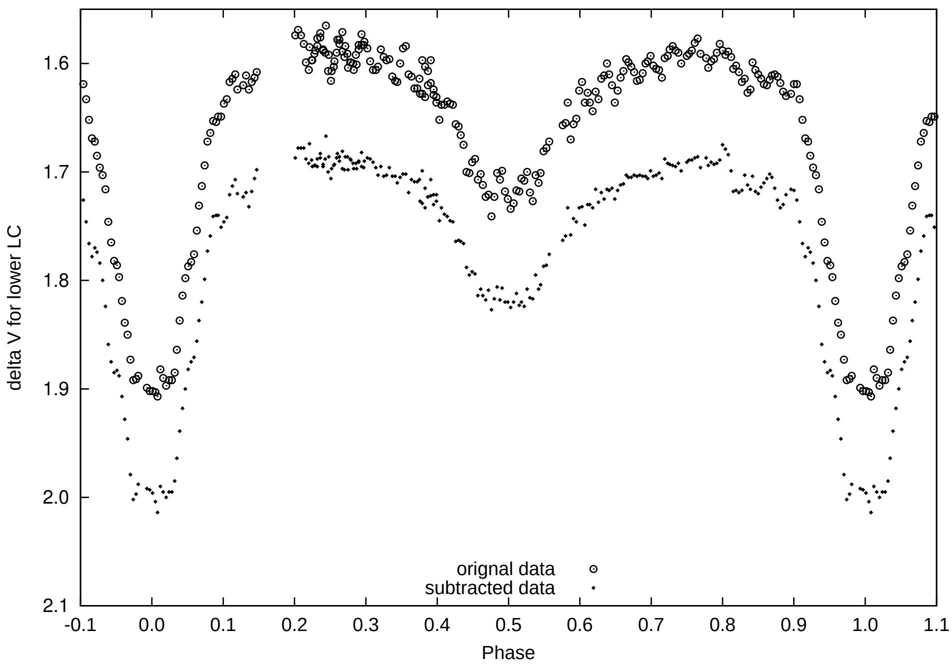

Figure 4. The light curves of IK Vir. Upper one is the plot of the original data which is the same as in Fig. 1. Lower one is a light curve in which the synthesized short period variations are subtracted from the upper one.

COMMISSIONS G1 AND G4 OF THE IAU
INFORMATION BULLETIN ON VARIABLE STARS
Volume 63 Number 6212 DOI: 10.22444/IBVS.6212

Konkoly Observatory
Budapest
3 August 2017

HU ISSN 0374 – 0676

SHORT TIME SCALE PERIOD VARIATIONS OF THE RRc STAR V468 Hya

BERDNIKOV, L.N.[1,2]; DAGNE, T.[1]; KNIAZEV, A.Y.[2,3,4]; DAMBIS, A.K.[2]

[1] Astronomy and Astrophysics Research division, Entoto Observatory and Research Center, P.O.Box 8412, Addis Ababa, Ethiopia, lberdnikov@yandex.ru

[2] Sternberg Astronomical Institute, Lomonosov Moscow State University, Universitetskii pr. 13, Moscow, 119992 Russia

[3] South African Astronomical Observatory, P.O. Box 9, Observatory, Cape Town, 7935 South Africa

[4] Southern African Large Telescope, P.O. Box 9, Observatory, Cape Town, 7935 South Africa

Introduction

The high luminosity and large age of RR Lyrae type variables make them ideal distance indicators and tracers for the study of the structure and kinematics of old Galactic subsystems – the halo and the thick disk. However, the number of RR Lyrae variables in the extended solar neighbourhood with both precise photometry and bona fide radial velocities is rather limited – a total of about 400 stars (Dambis et al. 2013). That is why we started a program aimed at obtaining photometric observations and radial-velocity measurements for the greatest possible number of RR Lyraes.

To ensure very efficient use of limited spectroscopic resources, for radial-velocity measurements of each star we use single-epoch spectra obtained with the Southern African Large Telescope (SALT). Ideally, the spectroscopic observation of every object should be accompanied by photometric observations carried out at the same time to construct the current light curve of the star and calculate the phase of the spectroscopic observation. This phase is needed to determine the systemic radial velocity using an appropriate template radial velocity curve. Alternatively, we have to study period variations for every object and determine the phases of spectroscopic observations using $O - C$ diagram or use some recently published light elements (ephemeris).

In this paper we give the results of a study of period changes for RRc star V468 Hya. To construct its $O - C$ diagram, we used Hertzsprung's (1919) method (whose computer implementation is described by Berdnikov (1992)) to reduce our own CCD observations obtained with the 76-cm and 1-m telescopes of the South African Astronomical Observatory (SAAO) as well as the data from NSVS (Wils et al. 2006), ASAS-3 (Pojmanski 2002), and CATALINA (Drake et al. 2013) surveys.

Table 1 lists the inferred $O - C$ values. The first and second columns give the inferred time of maximum brightness and its standard error, respectively; the third column gives the type of observations used; the fourth and fifth columns give the number of epoch, E,

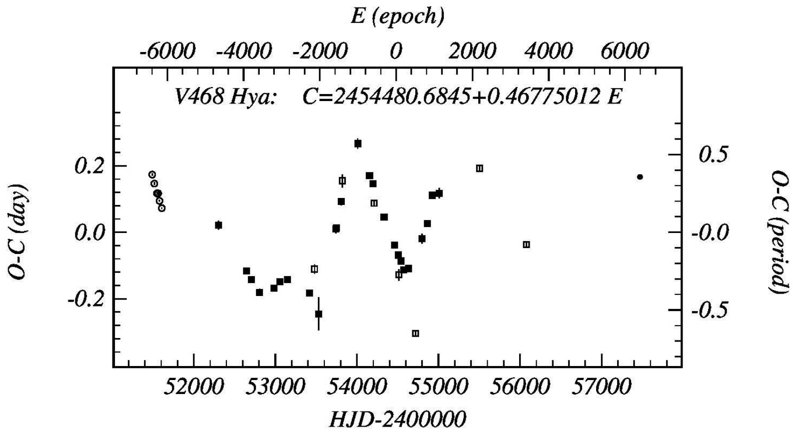

Figure 1. $O - C$ diagram of V468 Hya.

and the $O - C$ residual (in days), and the sixth and seventh columns give the number of observations, N, and the data source.

The data from Table 1 are shown in the $O - C$ diagram (Fig. 1) by different symbols with vertical error bars (which are usually smaller than symbols): open and filled circles for NSVS and our observations respectively, and open and filled squares for CATALINA and ASAS-3 data respectively. We used the following mean light elements (ephemeris):

$$HJDMax = 2454480.6845 + 0\overset{d}{.}46775012\ E. \tag{1}$$

The resulting $O - C$ diagram can be represented as a sequence of many straight-line fragments, and this behaviour is indicative of many abrupt period changes. It is worth noting that only the central part of the diagram is reliable because epoch miscalculations are possible in big gaps at its ends.

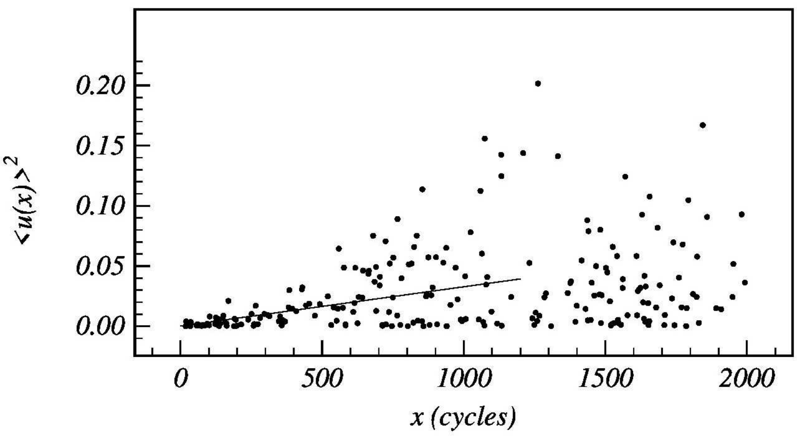

Figure 2. Relation between the square of the mean accumulated delay $\langle u(x)\rangle$, and the difference in the cycle number x, for V468 Hya. The line shows the fit of relation(2) for $x < 500$, giving the random period fluctuation $\varepsilon = 0\overset{d}{.}0057 \pm 0\overset{d}{.}0022$.

Table 1: Times of maximum brightness of V468 Hya

Max HJD	Error, *days*	Band	E	$O-C$, *days*	N	Data source
2451490.0636	0.0037	V	−6394	0.1734	25	Wils et al. (2006)
2451516.2306	0.0041	V	−6338	0.1464	25	Wils et al. (2006)
2451547.5404	0.0030	V	−6271	0.1169	25	Wils et al. (2006)
2451563.4439	0.0054	V	−6237	0.1169	25	Wils et al. (2006)
2451579.3250	0.0026	V	−6203	0.0945	25	Wils et al. (2006)
2451607.3681	0.0028	V	−6143	0.0726	33	Wils et al. (2006)
2452301.4583	0.0131	V	−4659	0.0216	24	Pojmanski (2002)
2452645.5838	0.0046	V	−3923	−0.1169	26	Pojmanski (2002)
2452707.7694	0.0032	V	−3790	−0.1422	25	Pojmanski (2002)
2452807.8295	0.0106	V	−3576	−0.1805	25	Pojmanski (2002)
2452980.4412	0.0070	V	−3207	−0.1687	25	Pojmanski (2002)
2453056.7036	0.0076	V	−3044	−0.1495	25	Pojmanski (2002)
2453147.4548	0.0091	V	−2850	−0.1419	25	Pojmanski (2002)
2453419.6450	0.0044	V	−2268	−0.1823	25	Pojmanski (2002)
2453480.5240	0.0132	V	−2138	−0.1107	12	Drake et al. (2013)
2453530.4385	0.0492	V	−2031	−0.2455	25	Pojmanski (2002)
2453740.2460	0.0126	V	−1583	0.0099	25	Pojmanski (2002)
2453748.6685	0.0102	V	−1565	0.0129	35	Drake et al. (2013)
2453810.0227	0.0103	V	−1434	0.0919	25	Pojmanski (2002)
2453819.4407	0.0195	V	−1414	0.1549	17	Drake et al. (2013)
2454010.3947	0.0153	V	−1006	0.2668	21	Pojmanski (2002)
2454154.3652	0.0052	V	−698	0.1703	25	Pojmanski (2002)
2454194.5675	0.0057	V	−612	0.1461	25	Pojmanski (2002)
2454211.3475	0.0088	V	−576	0.0870	12	Drake et al. (2013)
2454332.9205	0.0058	V	−316	0.0450	25	Pojmanski (2002)
2454464.2749	0.0049	V	−35	−0.0383	25	Pojmanski (2002)
2454505.4068	0.0043	V	53	−0.0685	25	Pojmanski (2002)
2454512.3634	0.0170	V	68	−0.1281	24	Drake et al. (2013)
2454540.0024	0.0043	V	127	−0.0864	25	Pojmanski (2002)
2454575.9930	0.0052	V	204	−0.1125	25	Pojmanski (2002)
2454633.0620	0.0094	V	326	−0.1091	15	Pojmanski (2002)
2454718.9331	0.0079	V	510	−0.3039	70	Drake et al. (2013)
2454797.7999	0.0149	V	678	−0.0192	26	Pojmanski (2002)
2454863.3304	0.0100	V	818	0.0264	25	Pojmanski (2002)
2454921.8840	0.0092	V	943	0.1112	25	Pojmanski (2002)
2455010.2951	0.0157	V	1132	0.1174	25	Pojmanski (2002)
2455502.9108	0.0066	V	2185	0.1923	25	Drake et al. (2013)
2456078.9497	0.0089	V	3417	−0.0370	33	Drake et al. (2013)
2457471.6452	0.0037	V	6394	0.1664	11	This paper

We analyzed the $O-C$ residuals for each maximum r, which we denoted as $z(r)$, for the presence of random fluctuations of the pulsation period using the method described by Eddington and Plakidis (1929). For this purpose, we calculated the delays $u(x) =\mid z(r+x)-z(r)\mid$ for maxima separated by x cycles. According to Eddington and Plakidis (1929), the mean value, $\langle u(x)\rangle$, is related to the random fluctuation of the period, ε, by the formula

$$\langle u(x)\rangle^2 = 2\alpha^2 + x\varepsilon^2, \qquad (2)$$

where α characterizes the amount of random error in the measured epochs of maximum brightness.

Figure 2 shows the results of our calculations, which indicate the presence of a linear trend of $\langle u(x)\rangle^2$ for cycle number differences $x < 500$, where formal fit of formula (1) gives the solution

$$\langle u(x)\rangle^2 = 0.154\ 10^{-3}\ (\pm 0.279\ 10^{-2}) + 0.326\ 10^{-4}\ (\pm 0.49\ 10^{-5})\ x,$$

so that $\alpha = 0\overset{\mathrm{d}}{.}009 \pm 0\overset{\mathrm{d}}{.}037$, which is close to the mean uncertainty of the epochs of maximum brightness (second column of Table 1). The derived mean period fluctuation,

$\varepsilon = 0\overset{d}{.}0057 \pm 0\overset{d}{.}0022$ satisfies the combined dependence of ε on the period for all pulsating variables (Turner et al. 2009).

Thus, our data are indicative of the presence of big random period fluctuations $\varepsilon/P \approx 0.012$ dominating the $O - C$ diagram, which demonstrates no signs of periodicity. This diagram demonstrates how unsafe it is to use the published ephemeris to calculate the phase of spectroscopic observations.

Acknowledgements: This study was supported by the Russian Foundation for Basic Research (grant no. 14-02-00472). This work makes use of observations from the South African Astronomical Observatory(SAAO), supported by the National Research Foundation of South Africa, and data from the CATALINA, ASAS and NSVS projects. The data reduction of all data was supported by the Russian Science Foundation (project no. 14-50-00043), and the light-curve analysis was supported by the Russian Science Foundation (project no. 14-22-00041).

References:

Berdnikov, L.N. 1992, *Soviet Astronomy Letters*, **18**, 207
Dambis, A.K., Berdnikov, L.N., Kniazev, A.Yu., et al. 2013, *MNRAS*, **435**, 3206 DOI
Drake, A.J., Catelan, M., Djorgovski, S.G., et al. 2013, *ApJ*, **765**, 154 DOI
Eddington, A.S., Plakidis, S. 1929, *MNRAS*, **90**, 65 DOI
Hertzsprung, E. 1919, *AN*, **210**, 17 DOI
Pojmanski, G. 2002, *AcA*, **52**, 397
Turner, D.G, Percy, J.R., Colivas, T., et al. 2009, *AIP Conf. Ser.*, **1170**, 167 DOI
Wils, P., Lloyd, C., Bernhard, K. 2006, *MNRAS*, **368**, 1757 DOI

COMMISSIONS G1 AND G4 OF THE IAU
INFORMATION BULLETIN ON VARIABLE STARS
Volume 63 Number 6213 DOI: 10.22444/IBVS.6213

Konkoly Observatory
Budapest
10 August 2017
HU ISSN 0374 – 0676

SS CANCRI: THE SHORTEST MODULATION-PERIOD BLAZHKO RR LYRAE

CAFOLLA, C.[1]; MATHEW, R.S.[1]; EDGE, A.C.[1]; SWINBANK, A.M.[1]; LANSBURY, G.B.[1]; WILSON, R.W.[1]; BUTTERLEY, T.[1]; LUCEY, J.R.[1]; HARDY, L.K.[2]; LITTLEFAIR, S.P.[2]; DHILLON, V.S.[2]

[1] Department of Physics, Durham University, South Road, Durham DH1 3LE, United Kingdom.

[2] The Department of Physics and Astronomy, Hounsfield Road, Sheffield S3 7RH United Kingdom.

Corresponding author: clodomiro.cafolla@durham.ac.uk

1 Introduction

RR Lyrae stars play a crucial role in our understanding of astrophysics, providing both standard candles and tests for stellar evolution (Jurcsik et al. 2006). Some aspects of the physics governing their pulsation behaviour are still under investigation and discussion, in particular, the Blazhko effect. The Blazhko effect is a periodic modulation in the pulsation amplitude of light curves (Jurcsik et al. 2009, Kovács 2009).

This paper aims to contribute to a better understanding of the Blazhko effect by studying SS Cancri (SS Cnc). SS Cnc ($\alpha_{2000} = 08^{\rm h}06^{\rm m}25\overset{\rm s}{.}56$, $\delta_{2000} = +23°15'05\overset{\prime}{.}8$) is a pulsating variable star belonging to the RRab-type star Lyrae, with a pulsation period of 0.367337 d and a metallicity corresponding to [Fe/H] $= -0.03$ (Elmasli et al. 2006, Jurcsik et al. 2006).

SS Cnc is characterised by the shortest known Blazhko period (Jurcsik et al. 2006), and hence may provide fundamental constraint for theoretical models of the Blazhko effect (Gillet 2013).

Models have been proposed to explain the Blazkho effect. They include resonance between a radial mode and a non-radial mode (Dziembowski and Cassisi 1999, Nowakowski and Dziembowski 2001) and the influence of a magnetic oblique rotator on the stellar pulsations (Cousens 1983, Shibahashi 2000). However, these require a regular variation in the light and radial velocity curves, yet the observations show more irregular variations (Smolec et al. 2011, Gillet 2013). Also, the magnetic oblique rotator model is not supported by any clear evidence of a strong magnetic field in RR Lyrae stars (Chadid et al. 2004, Kolenberg and Bagnulo 2009). Two other models have been recently proposed to explain short period Blazhko effect. Stothers (2010) suggested that the Blazhko modulation would be mainly caused by irregular changes of the magnetic field determining structural variations in the outer convective zone. In order to confirm this model, a quantitative model capable of reproducing the light modulation must be produced, in particular for the case of a very short modulation Blazhko period (Gillet 2013). Alternatively, Buchler and Kolláth (2011) suggested that the modulation can be caused by resonance coupling between a low order (typically fundamental) radial mode and a high order radial (the so-called strange) mode (Benkő et al. 2014). Having the shortest Blazhko period so far reported (Jurcsik et al.2006), SS Cnc represents an ideal object to investigate the validity of these two models.

In this paper, we report a study of the light curve modulation of SS Cnc in the B, V and R bands. We use the data to study the periodic modulation of the light curve, the variation in the maxima and search for periodic changes in the other regions of the light curve.

2 Observations

The observations were carried out with 14" telescopes, located in Durham, UK (Durham Astrolab 2015), and a 0.5 m in La Palma, Canary Islands (Hardy et al. 2015). Images are processed using standard correction and optimization techniques (Durham Astrolab 2015). Photometric measurements are made relative to two reference stars whose magnitude is reported by the AAVSO Photometric All-Sky Survey[1] (APASS, Henden and Munari 2014) and by VizieR catalogue (Ochsenbein et al. 2000, Zacharias et al. 2012). The two stars are: UCAC4 567-041675, located at $\alpha_{2000} = 08^h06^m24^s$, $\delta_{2000} = 23°16'54''$; and UCAC4 567-041673, located at $\alpha_{2000} = 08^h06^m21^s$, $\delta_{2000} = 23°12'16''$.

The observation interval is between 2015 January 04 and 2015 March 04 in 31 separate runs, each lasting 1–9 hours. Individual exposures are 30 s. In total 10,250 frames have been obtained. After correcting images, the observational data are discarded if they are affected by an instrumental magnitude error twice larger than the average (± 0.015 mag), or if they are collected under poor observing conditions (FWHM > 5″). Fig. 1 shows the portion of the greatest interest of the light curve in the B, V and R pass-bands within approximately the same observation time. Each of these light curves represents data taken during a single observational session. In order to improve readability, an offset of −0.5 and −1.5 mag has been applied to the V and B band data, respectively.

3 Results

3.1 Light Curve Minima and Maxima

Table 1 shows the values for maximum, minimum and average magnitude in the B, V and R bands; the last column shows the average magnitude values from the Simbad database (Wenger et al. 2000).

	Min Mag	Max Mag	Avg Mag	Avg Mag (Simbad)
B	13.35 ± 0.02	11.56 ± 0.03	12.48 ± 0.02	12.40 ± 0.16
V	12.76 ± 0.02	11.42 ± 0.01	12.21 ± 0.01	12.11 ± 0.15
R	12.64 ± 0.01	11.51 ± 0.02	12.15 ± 0.01	n.a.

Table 1: The values of maximum, minimum and average magnitude for each of the three band filters used, compared with the literature data from the Simbad database for the average magnitude.

[1] https://www.aavso.org/apass

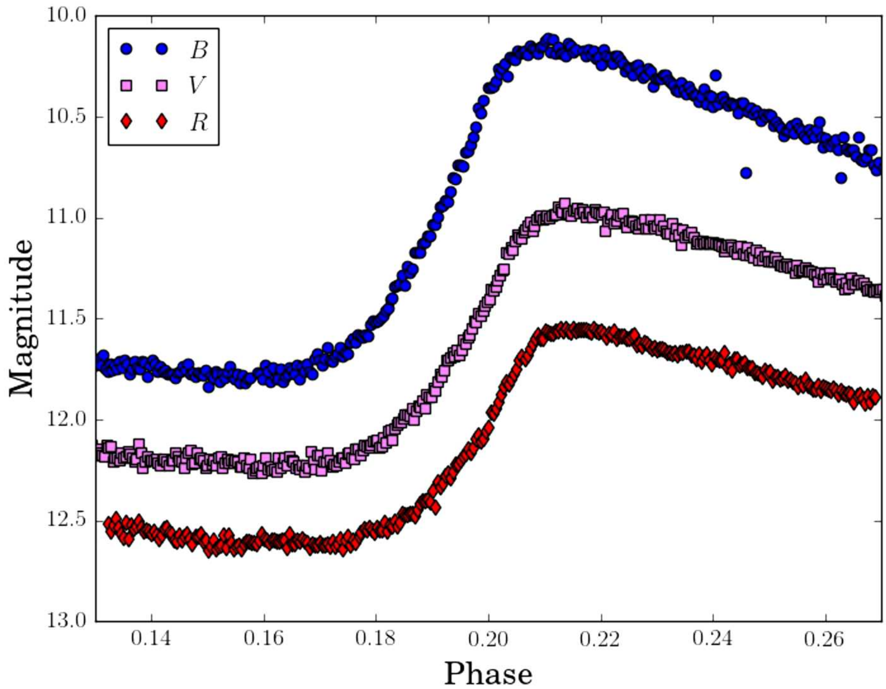

Figure 1. Light curves observed in the B, V and R bands. In order to improve readability, an offset of -0.5 and -1.5 has been applied to the V and B data, respectively. V and B band observational data were taken on 2015 February 07 using Draco-2 telescope and East-14 telescope, respectively. R-band observational data were taken on 2015 February 08 using West-12 telescope. All telescopes are in Durham, UK.

3.2 Period

The period is obtained using *VSTAR* software which uses Date Compensated Discrete Fourier Transform (DCDFT)[2]. The error on the period is computed using the jackknife method (Efron 1982). *VSTAR* software returns a period of 0.367405 ± 0.000002 d, which is within 0.02% of that of 0.367337 d reported by Jurcsik et al. (2006).

The period is also determined using *Period04* software which performs multiple-frequency fits with a combination of least-squares fitting and the Discrete Fourier Transform algorithm. The uncertainty is calculated using a Monte Carlo simulation (Lenz and Breger 2005, Hughes and Hase 2010). The algorithm returns the error on the frequency, α_f, and that on the amplitude; the error on the period, α_P, is calculated using the functional approach (Hughes and Hase 2010). *Period04* algorithm returns a value of 0.36731 ± 0.00004 d, which is in good agreement with that of 0.367337 d reported by Jurcsik et al. (2006), the difference between the former and the latter being smaller than 0.01%. It also confirms the value obtained from the *VSTAR* algorithm.

Using *Period04* algorithm, 9 harmonics of the pulsation frequency are detected, as shown in Table 2.

Harmonics	Frequency (cycles/d)	Period (d)	Amplitude (mag)
f_0	2.7225 ± 0.0003	0.36731 ± 0.00004	0.420 ± 0.010
$2f_0$	5.4443 ± 0.0002	0.18368 ± 0.00001	0.242 ± 0.002
$3f_0$	8.1700 ± 0.0200	0.12250 ± 0.00030	0.140 ± 0.010
$4f_0$	10.8870 ± 0.0010	0.09185 ± 0.00001	0.096 ± 0.008
$5f_0$	13.6090 ± 0.0090	0.07348 ± 0.00005	0.060 ± 0.004
$6f_0$	16.3000 ± 0.2000	0.06120 ± 0.00080	0.043 ± 0.009
$7f_0$	19.0560 ± 0.0030	0.05248 ± 0.00001	0.035 ± 0.003
$8f_0$	21.7800 ± 0.0200	0.04592 ± 0.00004	0.026 ± 0.003
$9f_0$	24.4970 ± 0.0030	0.04080 ± 0.00001	0.021 ± 0.003

Table 2: 9 harmonics of the pulsation frequency are detected. The table shows the frequency components and corresponding periods and amplitudes for each harmonic.

The period is compared with the available literature data to search any long-term change in the times of the light curve maxima. This is done using an observed-minus-calculated (O–C) diagram. The observed maximum peak times, $t_{maxpeak}$, are obtained from the GEOS RR Lyr database[3] (Boninsegna et al. 2002) and the calculated ones are given by:

$$t_{max\_calc} = t_0 + nP, \tag{1}$$

where t_0 is the time of a chosen reference observed maximum, n is an integer and P is the period, which is taken to be value of 0.367337 d reported by Jurcsik (2006). No change in period is discernible over the last 80 years (Fig. 8 in Appendix A). There is a significant scatter, probably due the Blazhko effect: an O–C variation of 0.011 ± 0.003 d is, indeed, observed over the Blazhko period of 5.313 d (Fig. 9 in Appendix A). Further pieces of information are available in the Appendix.

[2]https://www.aavso.org/vstar-overview
[3]http://www.ast.obs-mip.fr/users/leborgne/dbRR/

3.3 The Blazhko effect

For each V-band light curve, the maximum and the minimum are calculated by fitting a 3^{rd} degree polynomial curve to the region around the peak ± 0.5 hours. The fitting procedure is performed at least 5 times, and shifting the area of interest. Amplitude and time values are calculated as the mean of the repeated measurements. The standard errors are taken to be the associated uncertainties (Hughes and Hase 2010).

Table 3 shows the V-band maxima and the relative times when they are observed. Time is expressed as Modified Julian Date (MJD = JD − 2400000.5).

Time (day)	Amplitude (mag)
57051.035 ± 0.005	11.482 ± 0.020
57052.867 ± 0.001	11.462 ± 0.008
57053.970 ± 0.080	11.444 ± 0.007
57055.072 ± 0.003	11.436 ± 0.008
57058.010 ± 0.004	11.466 ± 0.007
57062.055 ± 0.004	11.461 ± 0.009
57070.132 ± 0.004	11.430 ± 0.008
57073.072 ± 0.003	11.466 ± 0.010
57074.909 ± 0.002	11.444 ± 0.006
57077.844 ± 0.004	11.454 ± 0.020
57080.045 ± 0.002	11.459 ± 0.008
57082.991 ± 0.003	11.436 ± 0.009
57084.824 ± 0.002	11.465 ± 0.020
57085.927 ± 0.002	11.445 ± 0.009

Table 3: Observed V-band peaks and relative times. Time is expressed as Modified Julian Date (MJD = JD − 2400000.5).

The model, which describes the maximum brightness variation, is given by:

$$P_{var}(t) = A\sin(\frac{2\pi t}{T} + \phi) + A_0, \quad (2)$$

where A is the amplitude, t is the time, T is the period and ϕ is the phase. A_0 is a fixed offset given by the mean of the peaks, which is not varied; hence, it is not a free parameter. The errors on the free parameters of the model, that are, amplitude, period and phase, are obtained minimising χ^2 (Hughes and Hase 2010).

Figure 2 shows the change of the V-band maximum magnitude over time. This confirms Jurcsik's study (2006), according to which SS Cnc exhibits Blazhko modulation period. In Fig. 2, the fitting model used to characterise the peak variation is given by Eq. 2. The numerical values of the free parameters in the model are: $A = 0.019 \pm 0.014$ mag, $T = 5.41 \pm 0.06$ d, and $\phi = 1400 \pm 700$. Our Blazhko period of 5.41 ± 0.06 d is in good agreement with the value calculated by Jurcsik et al. (2006) of 5.309 d, the difference being about 2 standard errors. The amplitude is also in agreement with that reported by Jurcsik (2006); considering the peak to peak variation, our amplitude differs, by about 2 standard deviations, from the value of about 0.1 mag found by Jurcsik. The discrepancy may depend on the very extreme values of the Blazhko cycle not taking place during the times of observation.

The fitting model is tested using χ^2 as a hypothesis test, the error bars on the data being heteroscedastic (Hughes and Hase 2010). χ^2_{min}, that is, the minimised sum of the

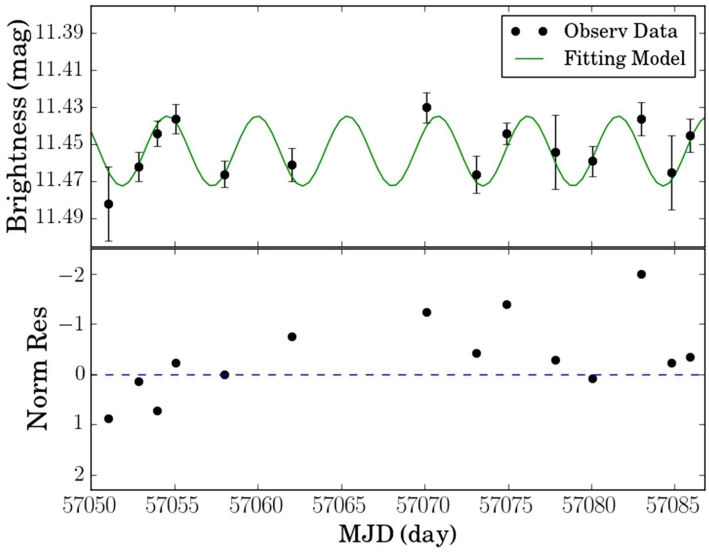

Figure 2. Blazhko modulation period is calculated to be 5.41 ± 0.06 d. Observational data correspond to the V-band light curve peaks. Errors on the time are too small to be clearly seen. In the bottom subplot, the normalised residuals are shown. MJD stands for Modified Julian Date. Given the convention of a decreasing scale for increasing brightness, normalised residuals are plotted on an inverse y-scale, in order to improve readability and visual comparison between the two subplots.

squared normalised residuals, is 9.86; ν, that is, the number of degrees of freedom of the system, is 11 (14 data points minus the 3 free parameters, A, T, and ϕ in Eq. 2); dividing the former by the latter, χ^2_ν is calculated to be 0.90, which is very close to the ideal value of 1, suggesting that the null hypothesis, which is that the model holds true, should not be rejected. The associated probability density function, $P(\chi^2_{min}; \nu)$, is calculated to remove any ambiguity in whether or not to reject the null hypothesis. P(9.86; 11) is 0.54, which is slightly greater than the ideal value of 0.5; hence, it is confirmed that the null hypothesis should not be rejected (Hughes and Hase 2010).

The difference in the peaks being small, the data are also fitted using a flat line model. This returns a value of χ^2_ν of 2.29 and $P(\chi^2_{min}; \nu)$ of 0.005. Both these two values indicate a poor fit. Furthermore, the Bayesian information criterion (BIC) for model selection is applied to confirm the hypothesis that the sinusoidal model is a better fit in comparison with a flat line model. BIC is defined as

$$BIC = \chi^2 + k \ln(n), \tag{3}$$

where k and n are the model free parameters and the data points, respectively (Kass and Raftery 1995). For the flat line model, BIC is 32.37, whereas the sinusoidal model is characterised by a BIC of 17.78. The difference between the two BICs being larger than 10, there is a very strong evidence against the model with the highest BIC, that is, the flat line model (Kass and Raftery 1995).

It should be noted that, both here and in the data analysis presented in the following sections, the errors on the brightness are taken into account, as they have a significantly larger influence on the corresponding variable in comparison with the errors on time; this assumption is also tested comparing ordinary least-squares algorithms and orthogonal

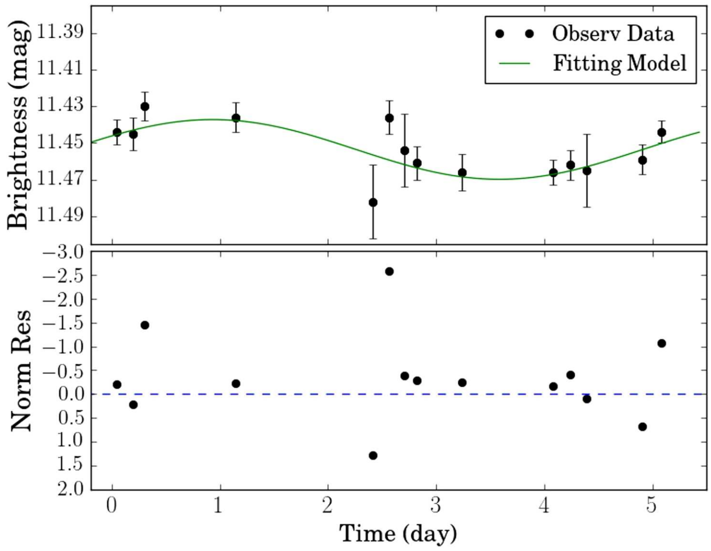

Figure 3. Blazhko modulation period: phase folded data. V-band light curve peaks are phase-folded. In the bottom subplot, the normalised residuals are shown. The phase-folded plot confirms the sinusoidal nature of the Blazhko effect, and returns a value for the Blazhko period of 5.313 ± 0.018 d.

distance regression ones (Hughes and Hase 2010). The differences between the outputs of the two fitting procedures tend to be small, if not negligible.

Figure 3 shows the Blazhko effect in the phase-folded plot: the data points are folded, and after a period the next peak is plotted at day zero. The phase-folded plot confirms the sinusoidal nature of the Blazhko effect, and returns a more precise value for the Blazhko period, that is, 5.313 ± 0.018 d ($\chi^2_\nu = 1.15$ and P(12.63; 11) = 0.32). The amplitude of the modulation is 0.016 ± 0.003 mag. Furthermore, the phase-folded data analysis shows no clear structure in the distribution of the normalised residuals, which fluctuate randomly around the zero. This suggests that even if the normalised residuals in Fig. 2 do not appear to be completely randomly distributed, this could be due to chance rather than any actual structure. The period used to phase-fold the data is taken to be 5.3 d, as it allows obtaining the most precise period and a value for χ^2_ν very close to the ideal one of 1.

An analysis is performed to assess whether V-band minimum magnitude exhibits any significant change over time and any correlation with the maximum variation. No clear evolution is found in the modulation of the minima, and no correlation seems to be present between the maxima and the minima variations (see Appendix B).

3.4 Periodic modulation in the ascending and descending gradients

As shown in Fig. 1, the light curve exhibits two almost linear gradients, where particular features, such as humps, bumps or changing slope tend to be absent. The first gradient is ascending and starts after the quadratic like curve following the minimum, and finishes before the inflection point leading to the maximum region. The second gradient is descending and follows the straight line after the maximum region. The two gradients are fitted with a straight line. The values of the gradients for each light curve, and the associated standard errors are computed using the same procedure described in the previous section with regards to the maxima and minima. The light curves, where the ascending gradient is calculated, have to meet the condition that both the maximum and the minimum are present in the same observation.

The time evolution of the two gradients is analysed, as shown in Fig. 4 and Fig. 5. The model, used to describe the observational data, is represented by Eq. 2. The ascending gradient varies with a periodicity of 3.80 $\pm$ 0.01 d, an amplitude of 0.09 $\pm$ 0.03 mag h^{-1} and a phase ϕ = 3.5 $\pm$ 0.1. Statistical analysis of the model is performed. P(10.98; 4) returns a value of about 0.03, suggesting that the model should not be rejected. Furthermore, χ^2_ν is 2.75, which is smaller than the largest acceptable value for a system with $\nu \leq 5$, that is, 2.9 (Hughes and Hase 2010).

The descending gradient shows a periodicity of 4.01 $\pm$ 0.07 d and an amplitude of 0.01 $\pm$ 0.08 mag h^{-1}, with ϕ = 7000 $\pm$ 2000. In this case, Eq. 2 is a good model to fit the data, as χ^2_ν is 1.60 and P($\chi^2_\nu;\nu$) 0.11 (Hughes and Hase 2010). The residuals, however, are not completely randomly distributed with respect to the zero line (bottom subplot of Fig. 5), but there is a slight tendency to have negative values for the values relative to the last observations.

Further studies performed on a larger data set and with more sensitive instruments are needed to confirm the behaviour of the gradients.

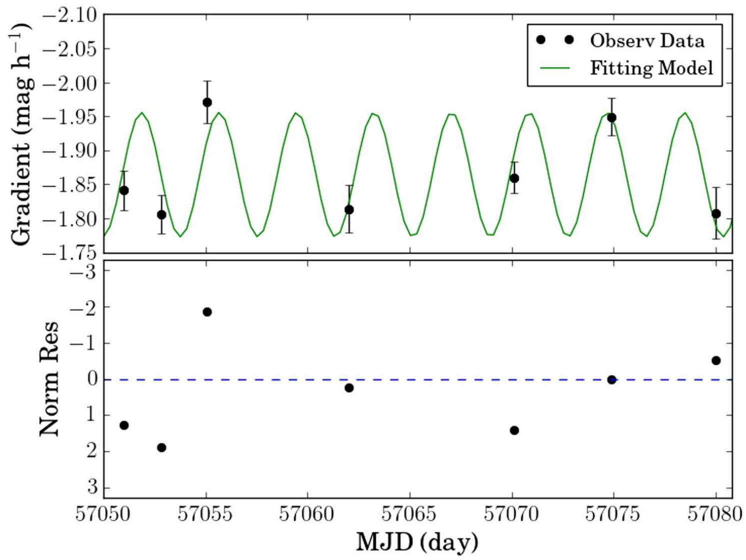

Figure 4. Modulation period of the V-band light curve ascending gradient: 3.80 $\pm$ 0.01 d. In the bottom subplot, the normalised residuals are shown. MJD stands for Modified Julian Date.

To assess whether there is any relationship between the descending and ascending gradients, only the light curves, where both the gradients are observed within the same night, are studied. Even if the analysis is based on a small number of points, the two gradients do not seem to be proportional, as shown in Fig. 6. When the descending gradient has low values, the ascending gradient may have high or low values. Similarly, when the ascending gradient has low values, the descending gradient may have high or low values. The magnitude variations of the two gradients being ambiguously related to

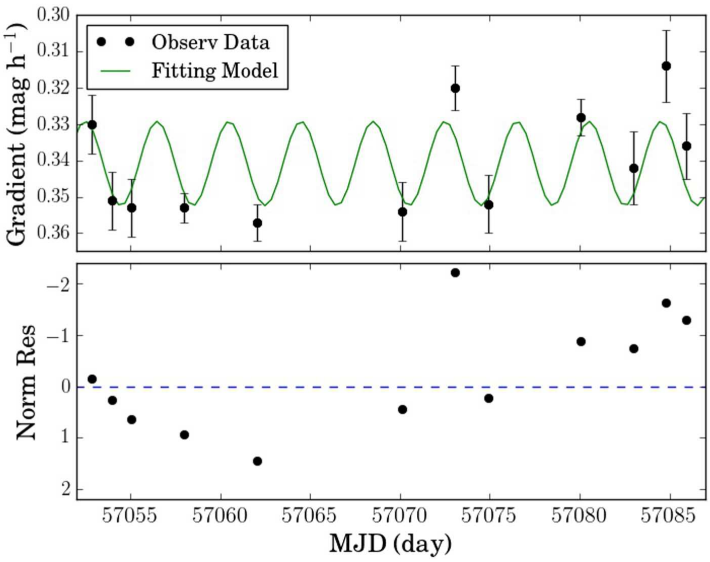

Figure 5. Modulation period of the V-band light curve descending gradient: 4.01 ± 0.07 d. In the bottom subplot, the normalised residuals are shown. MJD stands for Modified Julian Date.

each other, a hysteresis mechanism may be present. If this were the case, they would change in different points on the Blazhko phase.

To assess the validity of this hypothesis, the two gradients are analysed with respect to the maxima in the Blazhko curve (Fig. 8). The ascending gradient seems to be greater when closer to the peak in the Blazhko maxima curve. The minimum values for the ascending gradient are, instead, reached close to the mimimum value in the Blazhko maxima curve. The descending gradient increases its value only after the minimum in the Blazhko maxima sine curve. The descending gradient tends to remain the same when considering the other parts of the Blazhko maxima curve. A hysteresis behaviour may characterise the modulation of the two gradients. As the data set is limited, this investigation should be, however, considered only as a pilot study and hence further analyses are needed to validate the pattern presented here.

4 Discussion

As mentioned in the Introduction, physical models for the Blazhko effect have been under intense discussion in the literature.

With the main period being observed to be stable over time, the pulsating mechanism in SS Cnc is unlikely to be produced by the light travel time effect of a binary, or by tides generated by the binary system, as proposed by Elmasli et al. (2006). Alternatively, models explaining the Blazhko effect as due to the resonance between radial and non-radial modes predict that the light curve would have specific features in the frequency spectra (a triplet structure). These features, however, have not been detected in satellite data. In addition, observations have found higher order components than those predicted by this model (Smolec et al. 2011). New advances in explaining the phenomenon have been proposed by Buchler & Kolláth (2011) using the amplitude equation formalism.

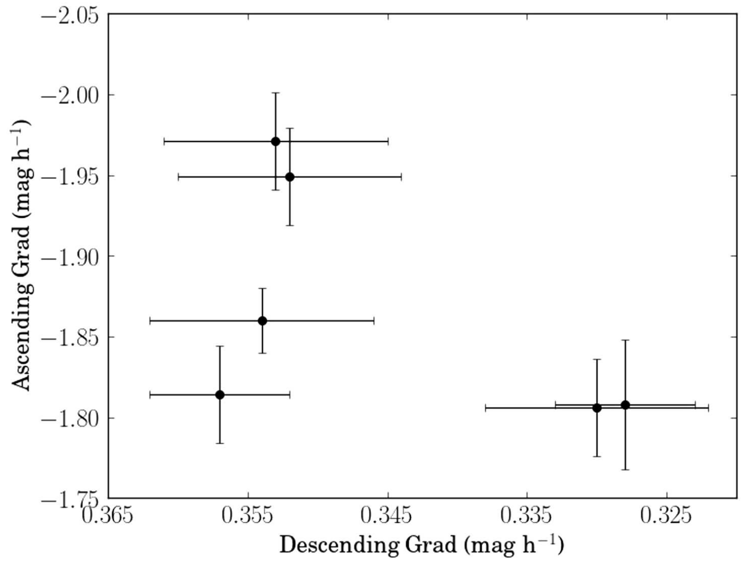

Figure 6. The V-band light curves, where both the gradients are observed within the same night, are studied. No linear relationship seems to be present between the ascending and the descending gradients. For low values of the descending gradient, the ascending gradient may take both high and low values. The ascending gradient is unambiguously characterised by low values only for high values of the descending gradient.

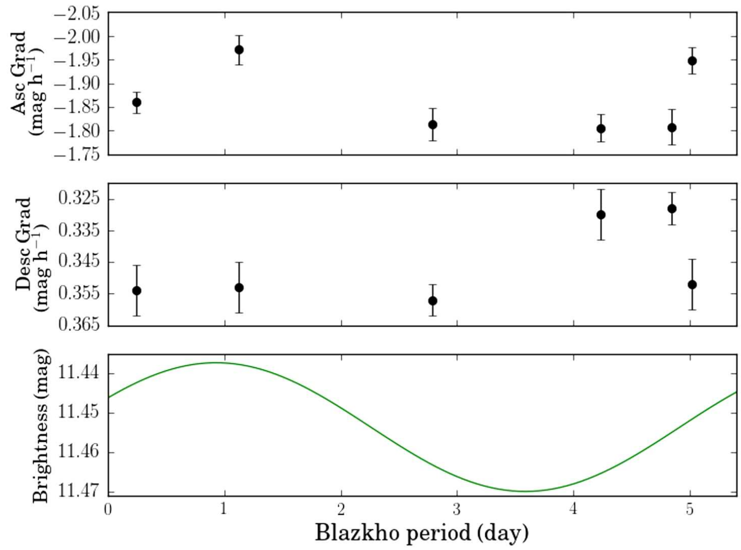

Figure 7. Phase folded observational data of the V-band light curve ascending and descending gradients, taken during the same day, are compared to the Blazhko modulation period of the V-band light curve maxima. The ascending gradient seems to mirror the behaviour of the maxima. The descending gradient period may be characterised by a hysteresis pattern with respect to the maxima modulation.

According to this model, the mechanism responsible for the modulation period would be a resonance coupling between a low order and a high order radial mode. This model has been also supported by Kepler space telescope data for 15 Blazhko RR Lyrae stars (Benkő et al. 2014). On the other hand, it has been suggested that the Blazhko effect is connected to the cyclic strengthening and weakening of turbulent convection in the outer stellar layers, caused by a transient magnetic field, which would have an irregular amplitude. When the magnetic field decays, the turbulent convection would become more vigorous. The magnetic field would decay cyclically and be substituted by a new one, produced by the turbulent-rotational dynamo (Smolec et al. 2011, Gillet 2013). However, this theory is unlikely to be the sole mechanism behind the Blazhko effect as it would be only effective for long modulation periods, typically for more than 100 d, in agreement with the thermal time-scales of the pulsation in RR Lyrae stars (Molnár et al. 2012). Therefore, it does not adequately describe the observed short-period Blazhko modulation such as that found in SS Cnc. Indeed, using hydrodynamic simulations, it was not possible to reproduce the Blazhko phenomenon through changes in convection unless implausible variations in the convective parameters on short time-scales take place (Molnár et al. 2012). Instead, numerical hydrodynamical simulations (Szabó et al. 2010, Kolláth et al. 2011) point to the Blazhko effect being associated with the half-integer (9:2) resonance between the fundamental pulsation mode and a destabilizing overtone. Further studies have also pointed out that irregular amplitude modulations can occur as a result of the nonlinear, resonant mode coupling between the 9th overtone and the fundamental mode. Hence, some of the irregular features observed in this paper may be due to irregular destabilization of the fundamental pulsation (Buchler & Kolláth 2011, Benkő et al. 2014). Furthermore, Buchler & Kolláth model presents some advantages in comparison with other resonance coupling models, such as the one proposed by Gillet (2013). The latter model is based on the interaction between the shocks generated by the fundamental mode and the first overtone. The first overtone is, however, observed only in a minority of RR-ab type star Lyrae, even with the precision of Kepler (Benkő et al. 2014, Molnár et al. 2017). Our observations highlighting the hysteresis-like variation in the ascending and descending gradients and the lack of any significant variation in the magnitude of the minima over the Blazhko period provide an additional test of the competing models for the mechanisms driving the Blazhko effect. Further observations are needed to confirm the results presented in this paper and investigate if a resonance between the fundamental pulsation mode and a destabilizing overtone is present.

5 Conclusions

The characteristics of SS Cnc have been studied in order to better understand the Blazhko effect. The Blazhko effect has been studied in the V-band. The Blazhko period is found to be 5.313 ± 0.018 d; the amplitude of the Blazhko effect is 0.016 ± 0.003 mag. The peak variation exhibits a sinusoidal pattern. The ascending and descending gradients show a sinusoidal periodic modulation. The variation in the maxima, within some limitations, seems to be associated with a corresponding variation in the ascending and descending gradient behaviour. The minimum magnitude seems to be constant over time. The findings may support the theory of resonance coupling between a low order radial mode and a high order radial mode, which would give rise to a regular, either single or multiperiodic, variation.

6 Acknowledgements

The authors are very grateful to Dr. R. Szabó for carefully reading the manuscript and for his helpful suggestions. This research was made possible through the use of the AAVSO Photometric All-Sky Survey (APASS), funded by the Robert Martin Ayers Sciences Fund. This research has made use of the SIMBAD database and of the VizieR catalogue access tool, operated at CDS, Strasbourg, France. The research has also made use of the GEOS RR Lyr database. ACE, AMS, RWW, TB and JRL acknowledge support from STFC grant ST/L00075X/1.

References:

Benkő, J.M., Plachy, E., Szabó, R., Molnár, L. and Kolláth, Z., 2014, *ApJS*, **213**, 31 DOI
Boninsegna, R., Vandenbroere, J. and Le Borgne, J.F., 2002, *IAU Coll.*, **185**, 166
Buchler, J.R. and Kolláth, Z., 2011, *ApJ*, **731**, 24 DOI
Chadid, M., Wade, G.A., Shorlin, S.L.S. and Landstreet, J.D., 2004, *A&A*, **413**, 1087 DOI
Cousens, A., 1983, *MNRAS*, **203**, 1171 DOI
Dziembowski, W.A. and Cassisi, S., 1999, *AcA*, **49**, 371
Durham Astrolab, Durham Univ. Phys. Dep., 2015, `http://community.dur.ac.uk/physics.astrolab`
Efron, B., 1982, *SIAM*, **38**
Elmasli, A., Aksu, O., Albayrak, B. and Selam, S.O., 2006, *ASPC*, **349**, 233
Gillet, D., 2013, *A&A*, **554**, A46 DOI
Hardy, L.K., Butterley, T., Dhillon, V.S., et al., 2015, *MNRAS*, **454**, 4316 DOI
Henden, A. and Munari, U., 2014, *Contrib. Astron. Obs. Skalnaté Pleso*, **43**, 518
Hughes, I. and Hase, T., 2010, Measurements and their Uncertainties, *Oxford University Press*
Jurcsik, J., Szeidl, B., Sódor, Á. et al., 2006, *AJ*, **132**, 61 DOI
Jurcsik, J., Sódor, Á., Szeidl, B. et al., 2009, *MNRAS*, **400**, 1006 DOI
Kass, R.E. and Raftery, A. E., 1995, *JASA*, **90**, 773
Kolenberg, K. and Bagnulo, S., 2009, *A&A*, **498**, 543 DOI
Kolláth, Z., Molnár, L. and Szabó, R., 2011, *MNRAS*, **414**, 1111 DOI
Kovács, G., 2009, *AIPC*, **1170**, 261 DOI
Lenz, P. and Breger, M., 2005, *CoAst*, **146**, 53 DOI
Molnár, L., Kolláth, Z. and Szabó, R., 2012, *MNRAS*, **424**, 31 DOI
Molnár, L., Plachy, E., Klagyivik, P. et al., 2017, `arXiv:1703.02420`
Nowakowski, R.M., and Dziembowski, W.A., 2001, *AcA*, **51**, 5
Ochsenbein, F., Bauer, P. and Marcout, J., 2000, *A&AS*, **143**, 23 DOI
Shibahashi, H., 2000, *IAU Colloq.,* **7**, 299
Smolec, R., Moskalik, P., Kolenberg, K., Bryson, S., Cote, M.T. and Morris, R.L., 2011, *MNRAS*, **414**, 2950 DOI
Stothers, R.B., 2010, *PASP*, **122**, 536 DOI
Szabó, R., Kolláth, Z., Molnár, L. et al., 2010, *MNRAS*, **409**, 1244 DOI
Wenger, M., Ochsenbein, F., Egret, D. et al., 2000, *A&AS*, **143**, 9 DOI
Zacharias, N., Finch, C.T., Girard, T.M. et al., 2012, *yCat*, **1322**

A Appendix. O–C

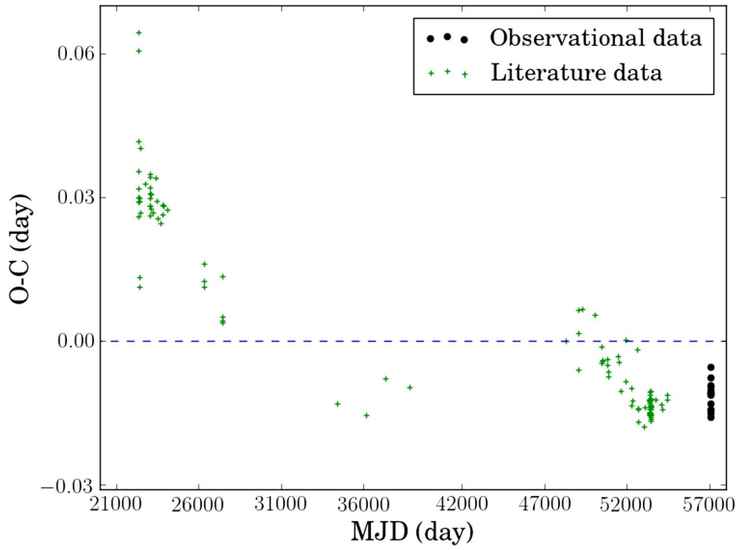

Figure 8. Observed minus calculated (O–C) diagram. Black points correspond to the observational data collected by the authors. Excluding the data before MJD 27000, no significant change overt time would be clearly observable.

The O–C diagram (Fig. 8) shows a change of the pulsation period over time. When constructing the O–C diagram, t_0 is taken to be MJD 48289.40200 (i.e. 1991 A.D). The choice is based on the fact that the observed maxima, available in the literature immediately before MJD 48289.40200, were recorded in 1966 A.D. CCD devices being invented in 1969, instruments before this date were, probably, not so sensitive as the ones developed in the last 30 years.

It should be noted that the data taken before MJD 15000 (i.e. pre-1900 A.D.) are excluded due to the timing uncertainties of maxima from visual observations. The analysis of the reduced data set seems apparently to confirm Elmasli's hypothesis: the pulsation period shows a variation, which could be due to the light travel time variation expected in a binary system (Elmasli et al. 2006). However, given the large gaps in the O–C data, the analysis does not lead to completely reliable conclusions.

In addition, if the data before MJD 27000, that is, before $\approx$ 1934 A.D., were not considered, no change over time would be clearly observable. The decision not to include data from the beginning of the last century could be justified given the limited accuracy and precision of the detecting systems available at that time. Within this further reduced data set, the difference between the lowest and highest value of the O–C would give a variation of 0.031 d, that is, a negligible gradient in comparison with SS Cnc period. The measurement of this gradient has no corresponding error, as the two values used to compute it are retrieved from the GEOS RR Lyr database, where no errors appear available. The data after MJD 27000 are, however, not on a straight gradient, but seem to fluctuate with no definite structure. Fluctuations could be due to imprecision in the measurements. Hence, further studies of the pulsation period, alongside with radial velocity measurements, are needed to definitely reject the hypothesis of a companion star for SS Cnc. Further observations are needed also to assess whether the tendency of the values to lie below the zero is due to chance, or whether there is any sinusoidal structure, whose minima values the literature has so far highlighted.

Figure 9 shows a change of the pulsation period over time, considering the phase folded V-band maxima observed in the present study. The period of 5.313 d is used to phase fold the data. A sinusoidal modulation (Fitting model 1) may seem to be present. This hypothesis should not be rejected as χ^2_ν is 0.76, which is close to the ideal value of 1. $P(\chi^2_\nu;\nu)$ is, however, 0.68, that is, slightly higher than the ideal value of 0.5; hence, the null hypothesis may be questioned (Hughes and Hase 2010). It should be, also, noted that the O–C variation (-0.011 ± 0.003 d) is close to the average error on the observed peak times, that is, $\pm$ 0.003 d. In light of this and of the aforementioned value of $P(\chi^2_\nu;\nu)$ for the sinusoidal model, a flat line model is tested (Fitting model 2). χ^2_ν and $P(\chi^2_\nu;\nu)$ for this flat line model are 1.78 and 0.04, respectively. These values may suggest that the null hypothesis should not be rejected and the flat line model fits the data (Hughes and Hase 2010). Bayesian information criterion (BIC) is, then, used to compare the two fitting models. BIC is 25.81 for the flat line model and 16.29 for the sinusoidal one. The difference between the two BICs being 9.52, there is a strong evidence against the model with the highest BIC, that is, the flat line model (Kass and Raftery 1995).

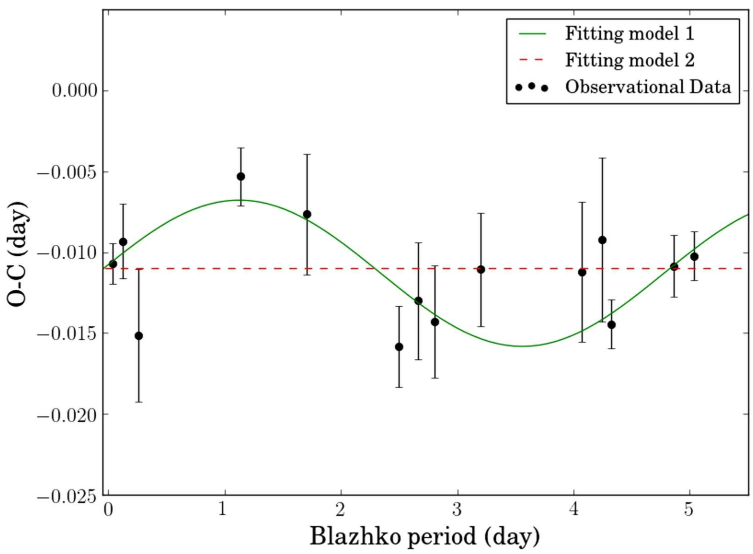

Figure 9. Observed minus calculated (O–C) diagram for the phase folded V-band maxima observed in the present study.

B Appendix. Minima

The fitting model, given by Eq. 2 and represented by the green curve in Fig. 10, is used to fit the data. The periodicity, T, is 5.40 $\pm$ 0.09 d. Statistical analysis of the model is performed. ν is 4, the data points being 7 and the free parameters 3, χ^2_ν is 0.17 and $P(\chi^2_\nu;\nu)$ returns a value bigger than 0.5, that is 0.95, suggesting that the null hypothesis should be, at least, questioned (Hughes and Hase 2010). The reason for this is mainly due to the fact that the magnitude variation is of the same order of magnitude as the errors on the data points. This is caused by the observations not being sensitive enough. Another limitation is represented by the analysis being based on a very small data set, which resulted in a low value of ν; this was due to long periods of bad weather. The two limitations can also explain the minima period being different from the maxima one. Further investigations appear necessary to assess whether also the light curve minima exhibit a modulation period. A flat line model is also tested (Fitting model 2). In this case, χ^2_ν is 0.74 and $P(\chi^2_\nu;\nu)$ is 0.62. These values suggest that the null hypothesis should be questioned, that is, the flat model does not fit the data perfectly. The lower value of P suggests, however, that the linear fit may be slightly better than the sinusoidal one (Hughes and Hase 2010).

An analysis of the phase folded data is performed, confirming, for the flat line model, a value for $P(\chi^2_\nu;\nu)$ of 0.62, which is close to the ideal threshold of 0.5 (Hughes and Hase 2010). The $P(\chi^2_\nu;\nu)$ of 0.95 for the sinusoidal model is, also, confirmed, suggesting that this model should be rejected. The value of $P(\chi^2_\nu;\nu)$ for the sinusoidal model is, probably, due to the fact that the amplitude variation is of the same order of magnitude as the errors on the data points.

The analysis is suggestive of no significant change of the minima over time.

The modulation period of the minima seems independent from that of the maxima, as shown in Fig. 11 and in Fig. 12.

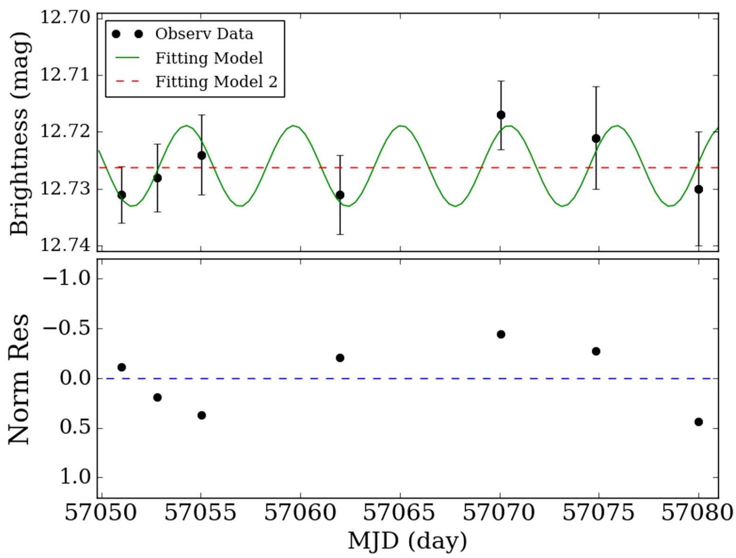

Figure 10. The modulation period of the V-band light curve minima. In the bottom subplot, the normalised residuals, with respecft to the sinusoidal fitting model, are shown. The minima do not seem to show any periodic modulation. The flat line model (Fitting model 2), with $P(0.74; 6) = 0.62$, seems to be slightly better than the sinusoidal one (Fitting model), characterised by $P(0.17; 4) = 0.95$ and with respect to which the normalised residuals are plotted in the bottom suplot.

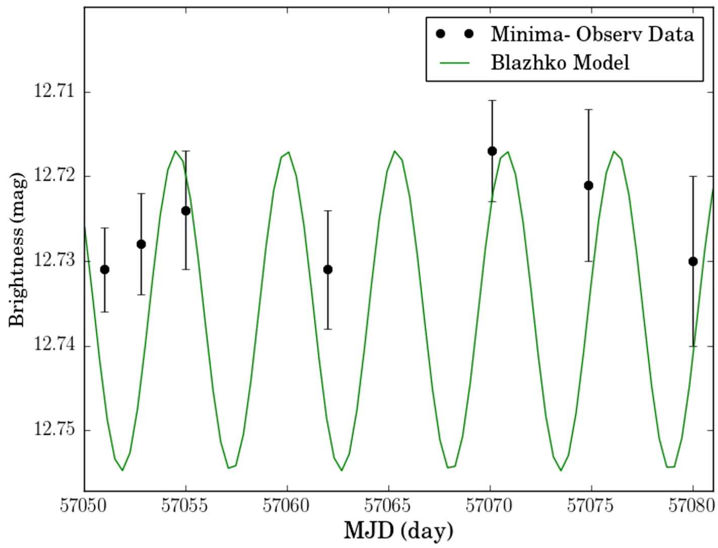

Figure 11. The V-band light curve minima are shown as dots and do not show any clear correlation with the modulation period of the maxima. The modulation period of the V-band light curve maxima (Blazhko Model) is plotted as a continuous green line. An offset of 1.28 mag has been applied to the Blazhko Model in order to improve readability.

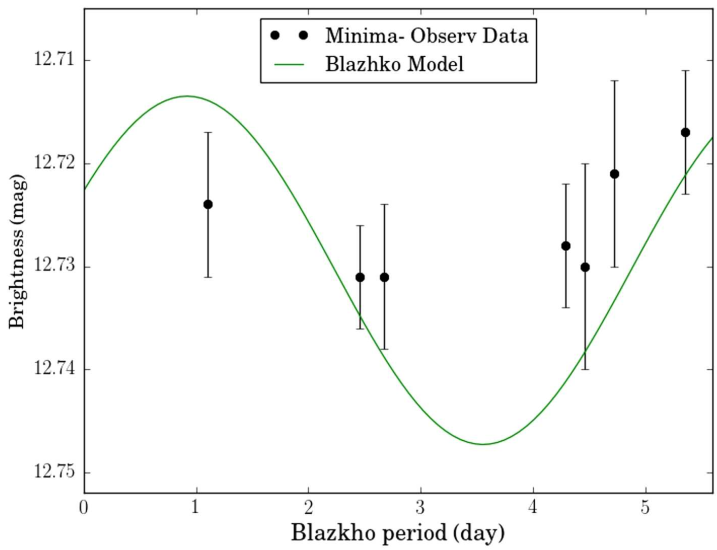

Figure 12. Phase folded data points of the V-band light curve minima are shown as dots. The period of 5.40 d is used to phase fold the minima. Phase folded modulation period of the V-band light curve maxima is the continuous green curve, labelled as Blazhko Model. No clear correlation seems to be present between the minima and the sinusoidal model obtained by fitting the maxima. An offset of 1.28 mag has been applied to the Blazhko Model in order to improve readability.

COMMISSIONS G1 AND G4 OF THE IAU
INFORMATION BULLETIN ON VARIABLE STARS
Volume 63 Number 6214 DOI: 10.22444/IBVS.6214

Konkoly Observatory
Budapest
05 September 2017

HU ISSN 0374 – 0676

DISCOVERY OF A NEW δ SCUTI VARIABLE IN THE FIELD OF RW UMi

ALIS, S.[1,2]; SAYGAC, A. T.[1,2]; FISEK, S.[1]; ESENOGLU, H. H.[1,2]

[1] Istanbul University, Department of Astronomy and Space Sciences, 34119 Beyazit, Istanbul, Turkey
e-mail: salis@istanbul.edu.tr

[2] Istanbul University Observatory Research and Application Centre, 34119 Beyazit, Istanbul, Turkey

During observations of the old nova RW UMi a new variable has been identified in the same field. RW UMi, new variable, and comparison stars are marked in the finding chart given in Fig. 1. Variability of this star noticed as it was being used as a comparison star of RW UMi. Light curves that can be seen in Fig. 2, reveal that the new star is a short-period pulsator, likely a δ Scuti star.

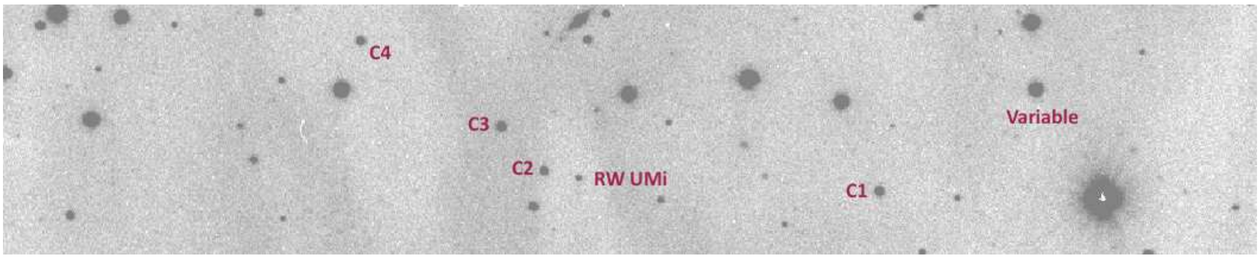

Figure 1. Identification chart of the field. New variable, RW UMi and comparison stars are marked.

RW UMi has been observed several nights since August 2015 with the 1.5 m RTT150 telescope of the TUBITAK National Observatory (aka. TUG) (Antalya, Turkey) and TFOSC imaging spectrograph attached to the telescope's Cassegrainian focus. TFOSC has a 2k×2k Fairchild 447 back-illuminated chip with a pixel size of 15 microns. In order to increase temporal resolution, the field was observed in the sub-frame mode which yields an effective area of 1040×200 pixels. Processing of frames led to an identification of a new variable. Five out of 13 nights observations could be used to construct the light curves of the new variable. This is due to overexposure for the variable as the program object RW UMi is very faint ($i \simeq 19$ mag). All the data were reduced in standard way using appropriate IRAF[1] packages. Photometry of objects was performed with aperture photometry. Differential magnitudes of the new variable were computed

[1]Image Reduction and Analysis Facility, http://iraf.noao.edu

against the comparison star C1. Other comparison stars were used to check C1 and were not found any variability for all observing runs. Light curves of the variable are given in Fig. 2.

Table 1. Log of observations.

Date	JD Interval 2457000+	Duration (hours)	Number of Frames	Filter	Exposure Time (seconds)
07.08.2015	242.2814 – 242.5742	7.02	245	Clear	40
18.09.2015	284.3248 – 284.4500	3.00	235	Clear	30
19.09.2015	285.3157 – 285.3818	1.59	82	Clear	60
10.09.2016	642.3663 – 642.5736	4.98	64	Clear	45
02.06.2017	907.3219 – 907.4308	2.61	155	Clear	45

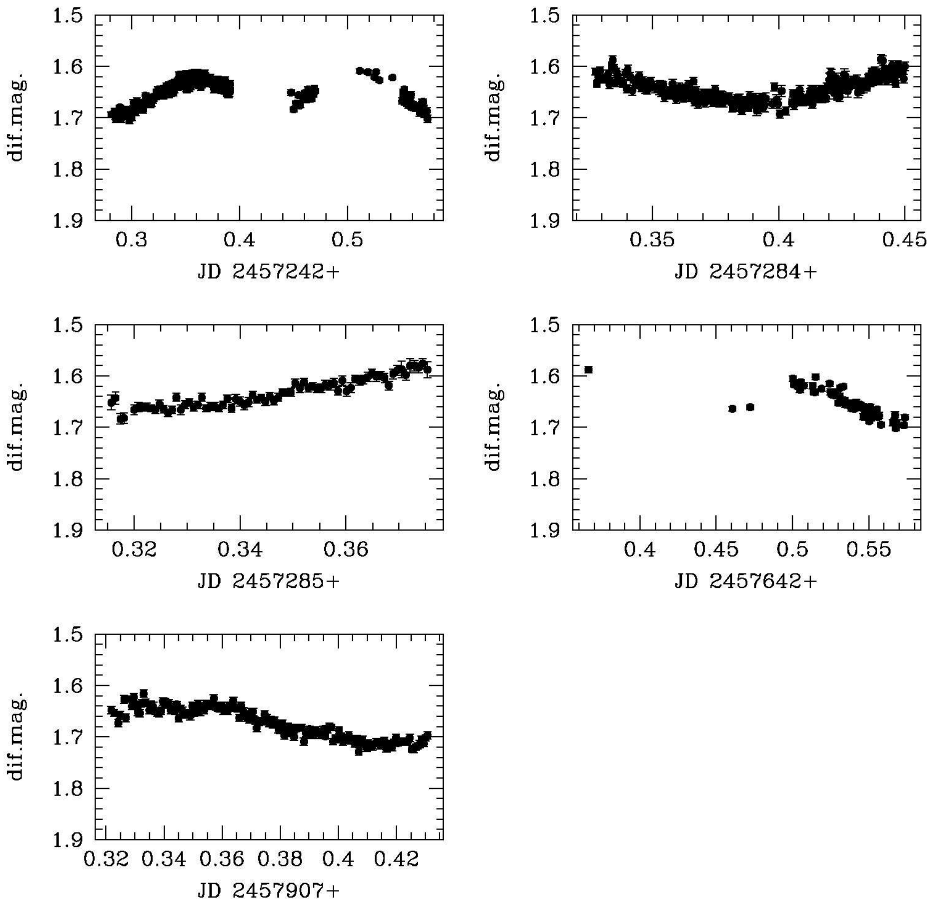

Figure 2. Light curves of the new variable. Differential magnitudes are computed using comparison star C1.

New variable has no record in the SIMBAD Astronomical Database or in General Catalogue of Variable Stars, either. However, the object is detected in the Sloan Digital Sky Survey with i-band magnitude $i = 14.55$. Coordinates of the new variable taken from SDSS are $\alpha = 16^{\text{h}}48^{m}8^{\text{s}}.23$ (J2000) and $\delta = +76^{\circ}58'02''.53$ (J2000) (SDSS J164808.23+765802.5).

In order to perform a Fourier analysis, all available data given in Table 1 are combined. Fourier analysis performed with Period04 (Lenz & Breger, 2005) revealed a frequency of 7.62731 c/d which corresponds a period of 0.131 d (3.147 h). Power spectrum of the Fourier transformation is given in Figure 3. Light curves of the first two runs are plotted with the resulting model in Figure 4.

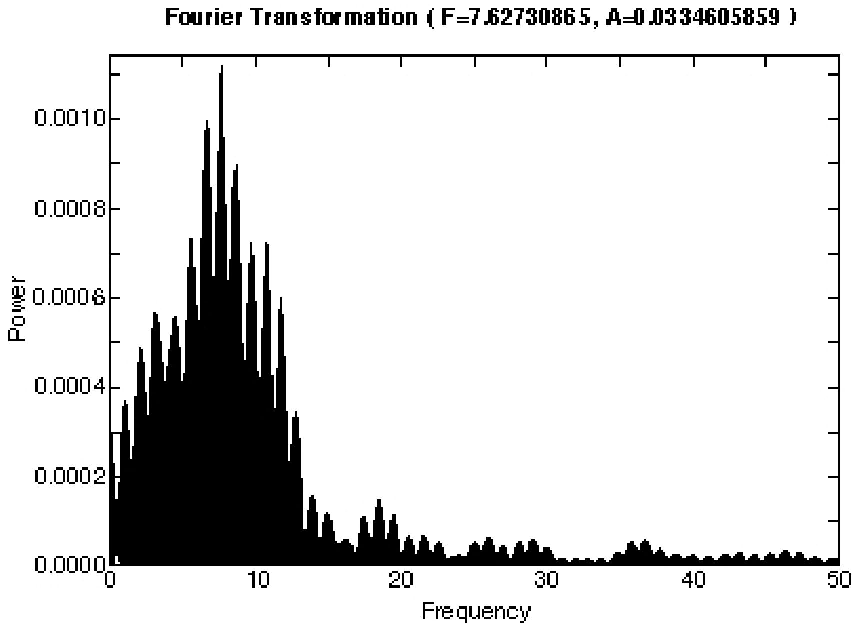

Figure 3. Power spectrum of the Fourier transformation.

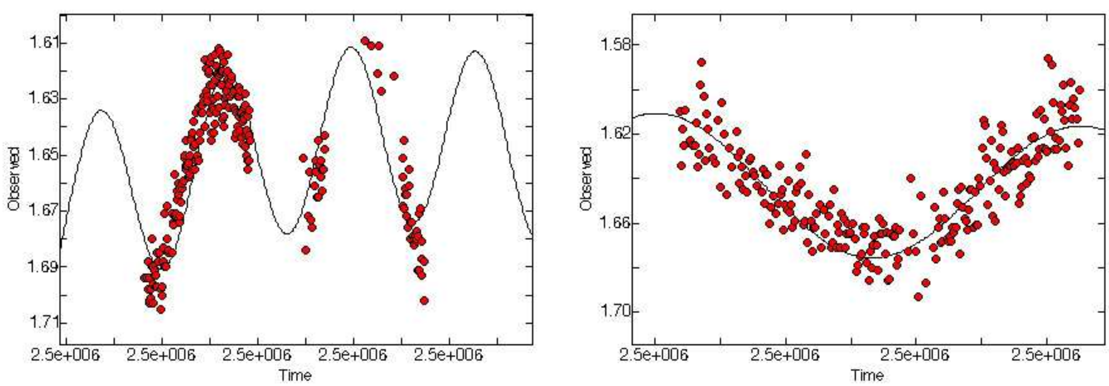

Figure 4. Model curves overplotted on light curves of the 07.08.2015 (left) and 18.09.2015 (right) runs.

Based on the SDSS *ugriz* magnitudes, $B-V$ colour of the new variable is computed using Karaali, Bilir and Tuncel (2005) transformation equations which then yielded a colour index of $B-V=0.62$. This colour index implies an effective temperature of $T_{\rm eff}$ = 5800 K (Ramirez & Melendez, 2005). Thus, period determined from Fourier analysis and effective temperature indicate that this new variable is most probably a δ Scuti-type pulsating star.

Acknowledgements: We thank to TUBITAK for a partial support in using RTT150 (Russian-Turkish 1.5 m telescope in Antalya) with project numbers 15BRTT150-864 and 17AT100-1174.

References:

Karaali, S., Bilir, S., Tuncel, S., 2005, *PASA*, **22**, 24 DOI
Lenz, P. and Breger M., 2005, *CoAst*, **146**, 53 DOI
Ramirez, I. and Melendez, J., 2005, *ApJ*, **626**, 446 DOI

COMMISSIONS G1 AND G4 OF THE IAU
INFORMATION BULLETIN ON VARIABLE STARS
Volume 63 Number 6215 DOI: 10.22444/IBVS.6215

Konkoly Observatory
Budapest
12 September 2017

HU ISSN 0374 – 0676

VARIABILITY OF THE OBJECT M1–15 = SS73 6 DURING 45 YEARS

KONDRATYEVA, L.; DENISSYUK, E.; RSPAEV, F.; KRUGOV, A.

Fesenkov Astrophysical Institute, Almaty, Kazakhstan. e-mail: lu_kondr@mail.ru

Initially the object M1–15 was included in the Catalogue of Galactic Planetary Nebulae by Perek & Kohoutek (1967), later it was classified as a Be star by Sanduleak & Stephenson (1973) and received a new designation: SS73 6. Shaw & Kaler (1989) discovered some high excitation lines of He II, 4686 Å, [OIII], 5007 Å, [NII], 6583 Å in its spectrum and suspected that this could be a symbiotic star. However later only HI, [OI] and [NII] lines were observed in the spectrum of M1–15, and no trace of a cool component was detected.

All available photometric data for this object are compiled in Table 1. Our observations were carried out in 2012 with the 1-meter Carl-Zeiss Jena reflector, located at Assy-Turgen Observatory of Fesenkov Astrophysical Institute (FAPHI). It was equipped with the CCD camera SBIG ST-7 (765 × 510, 9μ) and samples of BVR filters. HD 69901 and HD 71099 were used as standards. Increase of brightness of M1–15 by $0.^{m}2$ in all filters was registered during 1984–2012.

The main volume of spectral data was obtained with the original slit spectrograph, attached to the 0.7-m Cassegrain reflector AZT-8, located at Observatory of FAPHI. In 1971–1995 the spectrograph was equipped with the three-cascade image-tube, and the special astronomical film was used as a detector. A sample of gratings and objective lenses provided a spectral range from 3700 to 8200 Å. Since 2005 the spectrograph has been equipped with the CCD camera SBIG ST-8 (1530 × 1210, 9μ) with available spectral range 4000–7500 Å. The entrance slit width equals to $3''$ - $4''$ and $10''$- $15''$. Spectrograms, obtained with the broad slit are used for emission fluxes and EW determination, and those, with narrow slit for the study of emission profiles. Some spectra of M1–15 were obtained with a Shelyak eShel spectrograph and a slit spectrograph, attached to the 1-meter Carl-Zeiss Jena reflector (Tyan–Shan Observatory of FAPHI). Table 2 gives the log of observations.

All spectrograms were corrected for atmospheric extinction. There are emission lines of HI, [OI] and [NII], 6583 Å in the spectrum of M1–15. The object is observed on a background of an HII region, and an appropriate extended Hα emission is present on our spectrograms, obtained with the maximal expose time. This line together with the sky spectrum was measured on both sides of the stellar continuum and was subtracted from the observable spectrum of the object. The absolute fluxes and equivalent widths for the Hα and Hβ are listed in Table 3. It is noticeable that the flux of Hα increased more than twice up to 2010–2013 and then began to decrease. Behaviour of the F(Hβ) and EW values is quite similar.

Table 1: Photometric BVR observations of M1-15

Date	B mag	V mag	R mag	References
1984–1985	13.77±0.02	13.03±0.02		Shaw & Kaler, 1989
1990–1998	13.66±0.02	13.02±0.02	12.37±0.02	Vieira et al., 2003
2012	13.56±0.01	12.94±0.02	13.05±0.06	Zacharias et al., 2012
29.02.2012	13.57±0.01	12.86±0.03	12.12±0.02	FAPHI

Table 2: List of spectral observations

Date	Range (Å)	R=$\lambda/\Delta\lambda$	Telescope	Spectrograph
28.12.1973	6400-6700	7000	AZT-8 (0.7m)	Slit Spectrograph + image-tube
10.11.1991	6400-6700	7000	AZT-8 (0.7m)	Slit Spectrograph + image-tube
03.03.2005	4700-5100 6100-7100	7000 8700	AZT-8 (0.7m)	Slit Spectrograph + CCD ST-8
13.11.2010	6200-7000	13000	1-m (Assy-Turgen)	Slit Spectrograph UAGS+ CCD ST-8
05.12.2010	4700-5100	7000	AZT-8 (0.7m)	Slit Spectrograph + CCD ST-8
29.02.2012	4700-5100	7000	AZT-8 (0.7m)	Slit Spectrograph + CCD ST-8
14.02.2013	6400-6700	26000	AZT-8 (0.7m)	Slit Spectrograph + CCD ST-8
06.03.2015	6400-6700	40000	1-m (TShAO)	eShel Spectrograph +CCD STT 3200
06.03.2016	4400-5100	10000	1-m (TShAO)	Slit spectrograph +CCD ATIK 16200

This is the case when the profiles of HI emission lines consist of two peaks with the variable V/R ratio. The main parameters of Hα profiles are presented in Table 4: 1 – date of observations; 2 – width of Hα profile for $I = 0.5 \times I_{\rm max}$, 3 – distance between "blue" and "red" peaks; 4 – ratio of the maximal intensities of these peaks (V/R); 5 – heliocentric radial velocity of absorption; 6 – width of wings of the profile. All these parameters show strong variability.

Emission profiles of Hα, obtained with resolution of 0.2– 0.5 Å/px, are presented in Fig. 1. In 1973 the profile of Hα was broad and the ratio of maximal intensity to the level of continuum was low. Then, the profile became quite narrow and its dominance over the level of the continuum has increased. The last observations show that the profile of Hα became the same as in the '70s. The heliocentric radial velocities of an absorption component were always close to a zero within the limits of measurement errors. We don't present data on the profiles of Hβ in this paper as this line is about 20 times weaker than the Hα line and its structure is not defined.

Profiles of Hα were especially broad in 1970 and 2016. Here we consider possible mechanisms of line broadening. First of all, rotation of the circumstellar disk contributes

Table 3: Characteristics of Hβ and Hα lines

Date	HJD– 2400000	F(Hβ) 10^{-13}	EW(Hβ) Å	F(Hα) 10^{-12}	EW(Hα) Å
28.12.1973	42045.242			2.60±0.09	160±10
10.11.1991	48571.271			3.10±0.11	205±12
03.03.2005	53433.125	2.82±0.12	20±1	5.05±0.11	230±10
13.11.2010	55514.279			6.02±0.09	250±10
05.12.2010	55536.217	2.60±0.12	28±2		
29.02.2012	55987.242	3.20±0.22	29±10		
14.02.2013	56338.145			5.42±0.04	265±10
06.03.2016	57454.092	1.65±0.11	20±2	3.44±0.12	210±10

Table 4: Properties of Hα profiles

Date	FWHM km/s	Δ_r km/s	V/R	v_r km/s	Wing km/s
28.12.1973	600±40	200±40	0.78	52±35	1300±60
13.11.2010	250±30	130±30	1.12	34±35	850±40
14.02.2013	240±15	100±15	1.37	40±10	650±25
23.03.2015	250±15	120±15	0.92	-13±10	600±25
06.03.2016	650±25	320±25	0.83	-25±23	1300±40

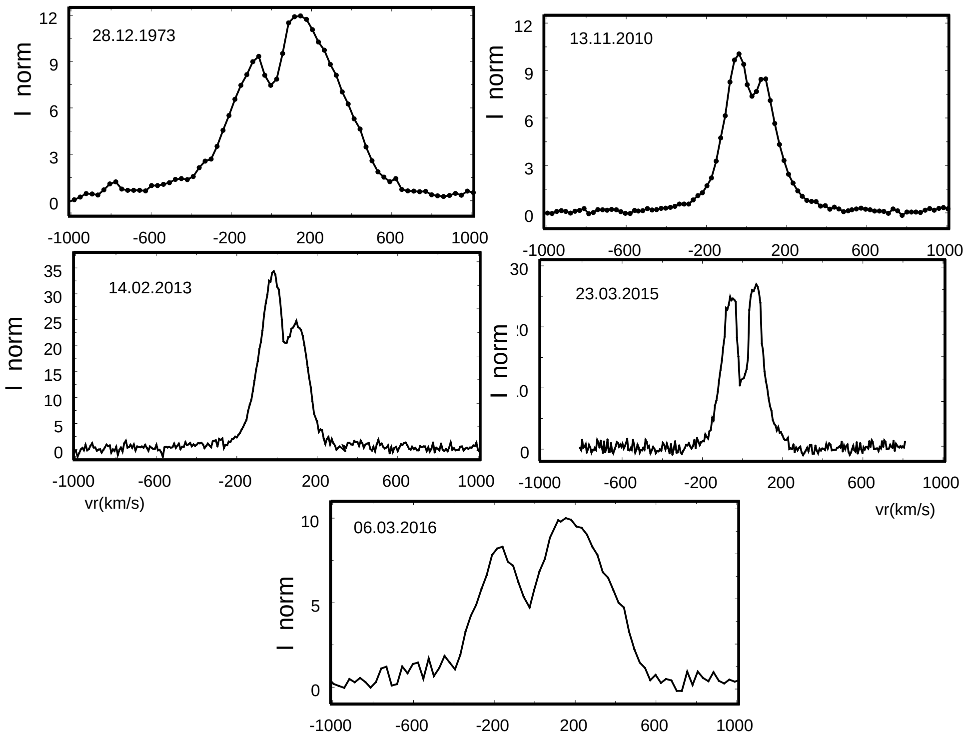

•

Figure 1. Variation of the Hα profiles in 1973 - 2016. X-axis shows heliocentric radial velocity (km/s), Y-axis gives the ratio(I_λ-I_{cont})/I_{cont}

to the width of profile, but this is not enough.

It is possible that line wings are formed in the region dominated by stellar winds. There is no information about UV spectrum of M1–15, and in optical no P Cyg features were observed. Most likely this mechanism can be excluded.

Very wide Hα emission lines may be produced by Rayleigh-Raman scattering, whereby Ly photons are converted to optical photons and fill the Hα broad region (Arrieta & Torres-Peimbert, 2003). In the case of M1–15, the wider profiles correspond to the smaller radiation fluxes, which contradicts the results of the influence of this mechanism.

Electron scattering has been intensively studied, as the line broadening mechanism in QSOs and in WR stars. The cross section of electron scattering is independent of wavelength, thus it is expected that other intense emission lines formed in the same region as Hα have to be similarly broad. Forbidden lines of [NII] and [OI] in the spectrum of M1–15 are seem to be sharp, but they may be formed in the more external envelope not in the central zone. Therefore, this mechanism can not be excluded.

In case of enhanced opacity, self-absorption can in principle decrease emission fluxes and cause widening of lines. The contribution of this mechanism can be significant.

Increasing of the emission fluxes may be associated with the expansion of the region of ionized gas. Accordingly, the zone of neutral gas is shifted to the outer boundaries of the circumstellar disk. With the Keplerian rotation, this leads to a decrease of rotation velocity of neutral layers and to a decrease in the distance between the profile components. Dilution of ionizing radiation will cause the opposite effect.

A period of V/R variations was not yet determined because our data points are ranged rather randomly. If the V/R ratios vary cyclically, that effect may arise from rotation of a circumstellar disk with a non-axisymmetric density distribution. Otherwise, changes of V/R ratio may be caused by incidental density perturbations of the disk.

Acknowledgements: This work has been supported by the Ministry of Education and Science of Republic Kazakhstan - Project No 0073/TFP “Astrophysical studies of stellar and planetary systems”.

References:

Arrieta, A., Torres-Peimbert, S., 2003, *ApJS*, **147**, 97 DOI
Pereira, C., Franco, C., de Araujo, F., 2003, *A&A*, **397**, 927 DOI
Sanduleak, N., Stephenson, C., 1973, *ApJ*, **185**, 899 DOI
Shao, R., Kaler, J., 1989, *ApJS*, **69**, 495 DOI
Vieira, S., Corradi, S., de Alencar, D., et al., 2003, *AJ*, **126**, 2971 DOI
Zacharias, N. Finch, C., Girard, T., et al., 2012, VizieR On-line Data Catalog: I/322A

COMMISSIONS G1 AND G4 OF THE IAU
INFORMATION BULLETIN ON VARIABLE STARS
Volume 63 Number 6216 DOI: 10.22444/IBVS.6216

Konkoly Observatory
Budapest
14 September 2017

HU ISSN 0374 – 0676

NY Her: POSSIBLE DISCOVERY OF NEGATIVE SUPERHUMPS

SOSNOVSKIJ, A.; PAVLENKO, E.; PIT, N.; ANTONIUK, K.

Crimean Astrophysical Observatory, Nauchniy, Crimea, Russian Federation, 298409. †demartin@ukr.net, eppavlenko@gmail.com

1 Introduction

Cataclysmic variables (CVs) are composed of a white dwarf (WD) as the primary star and a Roche-lobe filling red (or brown) dwarf as the secondary star which supplies matter from the inner Lagrangian point. This matter forms an accretion disc around the primary star in the case of a non-magnetic white dwarf. The accretion disc is the main source of variability on large time intervals from minutes to hundreds of days. SU UMa-type dwarf novae are a class of CVs showing two types of outbursts: superoutbursts and normal outbursts with amplitudes of $2\overset{\mathrm{m}}{.}0$-$8\overset{\mathrm{m}}{.}0$ (Warner, 1995).

During superoutburst these objects exhibit light variations called "positive superhumps" (Osaki, 1996). The observed period of the superhumps is a few percent longer than the orbital period of the system. On the other hand, some SU UMa stars show variations shorter than the orbital period, that are called "negative superhumps" (Hellier, 2001), visible mostly in quiescence and in some occasions in the normal outbursts and superoutbursts (Harvey and Patterson, 1995; Pavlenko et al., 2010; Oshima et al., 2014).

NY Her (α =17:52:52.60 δ =+29:22:18.8) was discovered by Hoffmeister (1949) as a Mira-type variable. Kato et al. (2013a) identified this object as an SU UMa-type dwarf nova with a short supercycle. Using superoutburst data taken by the ASASSN team, Poiner's observations and results of follow-up international campaign, Kato et. al. (2017) revealed an updated positive superhump profile with a period of 0.075525 d and much smaller amplitude ($0\overset{\mathrm{m}}{.}10$ mag) than most of SU UMa-type dwarf novae with similar periods of superhumps (or orbital) have. They identified a possible supercycle of $\sim$ 63.5 d and that the duration of the superoutbursts was 10 d. The supercycle length of $\sim$ 63.5 d is between that of the ER UMa-type DN novae subclass (Hellier, 2001; Kato et al., 2013b) that is distinguished by the shortest (20-50d) supercycles and ordinary SU UMa stars which have supercycles longer than 100d. The superoutburst duration of 10 d is much shorter than the duration of superoutbursts seen in the ER UMa-type dwarf novae. Kato et al. (2017) noticed that NY Her may be classified as a unique object with a short supercycle and a small superhump amplitude despite the relatively long P_{sh} and could have the negative superhumps because of infrequent normal outbursts during relatively short supercycle. This motivated us to examine this prediction by photometric investigation of NY Her during quiescence in June 2017.

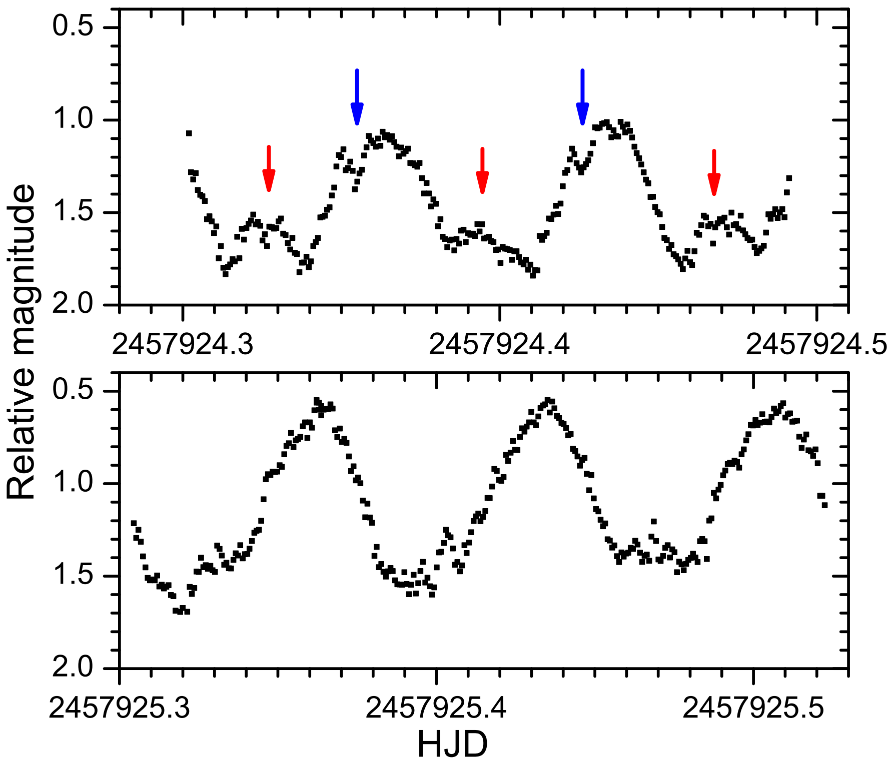

Figure 1. Unfiltered photometry for NY Her for two nights: 19-20 June, 2017. The smaller humps and small dips are marked by red and blue colors respectively.

2 Observations

The photometric CCD observations of NY Her were carried out during 6 nights in June 2017 at the Crimean Astrophysical Observatory (CrAO) in unfiltered light, giving a system close to the R_c band in our case, at two telescopes: 2.6–m ZTSh with APOGEE Alta E-47 and 1.25–m AZT-11 with ProLine PL230. Our priority was time series analysis with high time resolution while performing the multicolor observations. The standard aperture photometry (de-biasing, dark subtraction and flat-fielding) was used for measuring of the variable and comparison star USNO B1 1193-0272323 (R=17.97) (Monet et al., 2003). The accuracy of a single brightness measurement strongly depended on the telescope, exposure time, weather condition and brightness of NY Her, and reached $0^{m}_{.}01$-$0^{m}_{.}03$ for 60 s exposure (ZTSH) and $0^{m}_{.}08$-$0^{m}_{.}15$ for 180 s exposure (AZT-11).

3 Data analysis and discussion

During the quiescent state the brightness of NY Her varied between $18^{m}_{.}5$ and $19^{m}_{.}8$. The example of two original light curves is shown in Fig. 1. As seen in these light curves, the profile changes from night to night. The light curves clearly show variability with a period ~ 1.7 h and strong amplitude variations in a range of $0^{m}_{.}7$-$1^{m}_{.}1$. At first night (Fig. 1, upper pale) one could see the two humped profile with different height and small dip in bigger hump. At the second night (Fig. 1, lower panel) the light curve profiles become more smooth, the smaller hump is no longer visible. To search for precise periodicity we have done the periodogram analysis using the Stellingwerf method (Stellingwerf, 1978)

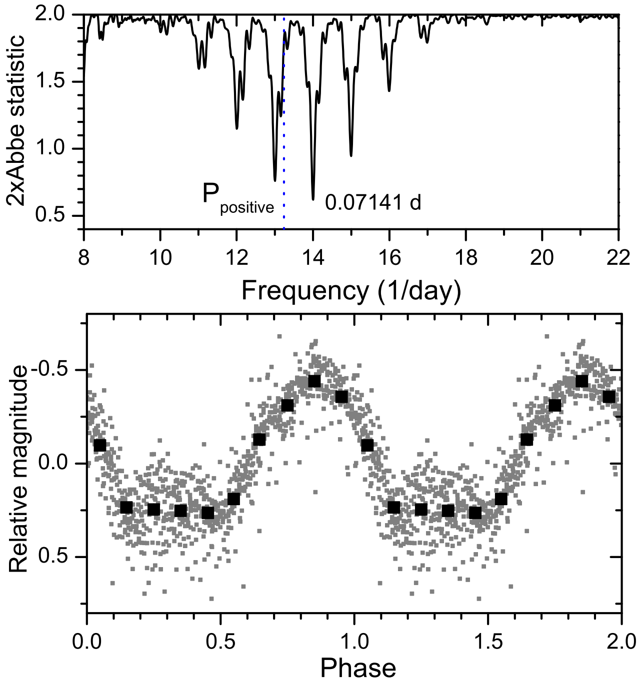

Figure 2. Upper: periodogram for combined data from 6 different nights. Position of the positive superhump period (Kato et al., 2017) is shown by blue dotted line. Lower: data folded on the 0.07141 d period. Original data are shown by gray circles. Black squares denote the mean points.

implemented in ISDA package (Pel't, 1980). The accuracy of trial periods as well as Abbe statistic, also known as Lafler-Kinman statistic (Lafler and Kinman, 1965) was calculated using ISDA package (Pel't, 1980). Before starting the analysis, we subtracted the long term trend. The strongest peak points to the period 0.07141(5) d, surrounded by daily aliased peaks. The periodogram and phase diagram for the most significant period are shown in Fig. 2. Original data show larger scattering in minimum caused by both larger errors and intrinsic variability and smaller one in maximum. The mean light curve displays a flat minimum lasting 0.4 period and amplitude of about $0\overset{\mathrm{m}}{.}7$.

As empirically established relation shows, all known SU UMa stars with related P_{orb} and P_{sh} are located around equation line: $\epsilon{=}P_{\mathrm{sh}}/P_{\mathrm{orb}} - 1 = 0.001(4) + 0.44(6)P_{\mathrm{orb}}$ (Kato et al., 2009). The measured period (of NY Her in quiescence) cannot be an orbital one, because in this case ϵ=0.057 is situated higher this line (taking into account a scatter of observation around this line). According to this relation, the corresponding orbital period should be slightly larger, and be located in that scattering strip between 0.0722-0.0736 d, with ϵ=0.025-0.045.

We suggest that 0.07141(5) d period is the period of negative superhumps of NY Her according to Kato's prediction. However a small probability that this period could be interpreted as the orbital one also cannot be neglected since the eclipsing SU UMa dwarf nova HT Cas has near the same large epsilon (Kato et al., 2009). Further observations of NY Her aimed at finding the orbital period are necessary for the final identification of the brightness modulation during its quiescence in June 2017.

Acknowledgement: We are grateful to Sklyanov A.S. from Kazan Federal University for reading and discussion the paper and to an anonymous referee for valuable comments.

References:

Harvey, D., Patterson, J., 1995, *PASP*, **107**, 1055 DOI
Hellier, C., 2001, *Cataclysmic Variable Stars: How and Why They Vary*, Springer-Verlag London
Hoffmeister, C., 1949, *Erg. Astron. Nachr.*, **12**, 12
Kato, T. et al., 2009, *PASJ*, **61**, S395 DOI
Kato, T. et al., 2013a, *PASJ*, **65**, 23 DOI
Kato, T., Nogami, D., Baba, H., et al. 2013b, arXiv 1301.3202
Kato, T. et al., 2017, arXiv 1706.3870 (accepted to PASJ)
Lafler, J. and Kinman, T.D., 1965, *ApJ Suppl.,* **11**, 216 DOI
Monet, D. et al., 2003, *AJ*, **125**, 984 DOI
Ohshima, T. et al., 2014, *PASJ*, **66**, 67 DOI
Osaki, Y. 1996, *PASP*, **108**, 39 DOI
Pavlenko, E. P. et al., 2010, *AIPC*, **1273**, 320 DOI
Pel't, Ya., 1980 *Frequency Analysis of Astronomical Time Series* Tallinn: Valgus
Stellingwerf, R.F., 1978, ApJ, 224, 953 DOI
Warner, B. 1995, *Cataclysmic Variable Stars* (Cambridge: Cambridge University Press)

COMMISSIONS G1 AND G4 OF THE IAU
INFORMATION BULLETIN ON VARIABLE STARS

Volume 63 Number 6217 DOI: 10.22444/IBVS.6217

Konkoly Observatory
Budapest
20 September 2017

HU ISSN 0374 – 0676

110 MINIMA TIMINGS OF ULTRA-SHORT ORBITAL PERIOD ECLIPSING BINARIES

GAZEAS, K.; LOUKAIDOU, G.; TZOUGANATOS, L.; KARAMPOTSIOU, E.; PETROPOULOU, M.

Section of Astrophysics, Astronomy and Mechanics, Department of Physics, National & Kapodistrian University of Athens, Zografos GR- 15784, Athens, Greece; e-mail: kgaze@phys.uoa.gr

Observatory and telescope:
T1: 0.4m, f/8 Cassegrain telescope, located at the University of Athens Observatory, at Zografos, Athens, Greece. **T2**: 1.2m, f/13 Cassegrain telescope of the National Observatory of Athens, located at the Kryoneri Astronomical Station, at Korinth, Greece.

Detector:	**C1**: ST-10XME CCD camera, KAF-3200ME chip, $16'\times11'$and $25'\times17'$ (using an f/6.3 focal reducer) field of view (FoV) with T1. **C2**: AP47p CCD camera, Marconi 47-10 chip, $2.5'\times2.5'$and $5'\times5'$ (using an f/6.3 focal reducer) FoV with T2. All CCDs have a Peltier-type cooling system and are equipped with a set of *UBVRI* filters (Bessell specifications).

Method of data reduction:
Differential photometry

Method of minimum determination:
Kwee & van Woerden (1956).

Table 1: Times of minima of eclipsing binaries

System	HJD	Error	Type	Filters	Remark
1SWASP J004050.63+071613.9	2456562.3011	0.0010	I	BVRI	T2+C2
	2456562.4156	0.0010	II	BVRI	T2+C2
	2456562.5283	0.0009	I	BVRI	T2+C2
	2456563.3340	0.0006	I	VRI	T2+C2
	2456563.4471	0.0004	I	VRI	T2+C2
	2456563.5602	0.0006	I	VRI	T2+C2
	2456564.3627	0.0009	I	VRI	T2+C2

Table 1: cont.

System	HJD	Error	Type	Filters	Remark
1SWASP J004050.63+071613.9	2456564.4794	0.0008	I	VRI	T2+C2
	2456564.5954	0.0007	I	VRI	T2+C2
1SWASP J052036.84+030402.1	2456343.2294	0.0005	I	BVRI	T1+C1
	2456343.3429	0.0023	II	VR	T1+C1
	2456347.2777	0.0017	II	BVRI	T1+C1
	2456575.5610	0.0002	I	VRI	T2+C2
	2456576.4871	0.0003	I	VRI	T2+C2
	2456576.6022	0.0003	II	BVRI	T2+C2
	2456577.5277	0.0007	II	VI	T2+C2
	2456577.6400	0.0007	I	VI	T2+C2
	2456578.4540	0.0003	II	VR	T2+C2
	2456578.5695	0.0006	I	BVR	T2+C2
	2456679.4611	0.0006	I	BVRI	T1+C1
	2456680.3864	0.0006	I	BVRI	T1+C1
	2456687.3292	0.0004	I	BVRI	T1+C1
	2456687.4440	0.0005	II	BVRI	T1+C1
	2456689.4113	0.0008	I	VRI	T1+C1
	2456699.2449	0.0005	II	BVRI	T1+C1
	2456699.3619	0.0004	I	BVRI	T1+C1
	2456700.2878	0.0006	I	BVRI	T1+C1
	2456700.4015	0.0007	II	BVRI	T1+C1
	2456702.2528	0.0007	II	BVRI	T1+C1
	2456702.3700	0.0009	I	BVRI	T1+C1
	2456703.2921	0.0096	I	BR	T1+C1
	2456703.4023	0.0040	II	VI	T1+C1
	2456705.2613	0.0006	II	BVRI	T1+C1
	2456705.3787	0.0004	I	BVRI	T1+C1
	2456706.3047	0.0004	I	BVRI	T1+C1
	2456707.2296	0.0004	I	BVRI	T1+C1
	2456707.3438	0.0005	II	BVRI	T1+C1
1SWASP J055418.43+442549.8	2456348.3579	0.0007	I	BVRI	T1+C1
	2456352.4002	0.0005	I	BVRI	T1+C1
	2456353.3832	0.0004	II	BVRI	T1+C1
	2456355.3502	0.0005	II	BVRI	T1+C1
	2456355.4582	0.0006	I	BVRI	T1+C1
	2456364.4171	0.0005	I	BVRI	T1+C1
	2456371.3001	0.0004	II	BVRI	T1+C1
	2456375.3423	0.0004	I	BVRI	T1+C1
1SWASP J093012.84+533859.6 (EW)	2456305.6174	0.0002	II	BVRI	T1+C1
	2456306.2982	0.0003	II	BVRI	T1+C1
	2456306.4124	0.0002	I	BVRI	T1+C1
	2456307.4382	0.0002	II	BVRI	T1+C1
	2456307.5512	0.0002	I	BVRI	T1+C1
	2456307.6654	0.0004	II	BVRI	T1+C1
	2456313.4721	0.0003	I	BVRI	T1+C1
	2456313.5870	0.0003	II	BVRI	T1+C1
	2456314.6099	0.0002	I	BVRI	T1+C1

Table 1: cont.

System	HJD	Error	Type	Filters	Remark
1SWASP J093012.84+533859.6 (EW)	2456317.4571	0.0003	II	BVRI	T1+C1
	2456317.5703	0.0004	I	BVRI	T1+C1
	2456317.6854	0.0003	II	BVRI	T1+C1
	2456322.4674	0.0003	II	BVRI	T1+C1
	2456322.5811	0.0003	I	BVRI	T1+C1
	2456322.6936	0.0005	II	BVRI	T1+C1
	2456323.6062	0.0003	II	BVRI	T1+C1
	2456324.4020	0.0003	I	BVRI	T1+C1
	2456324.5173	0.0004	II	BVRI	T1+C1
	2456324.6290	0.0003	I	BVRI	T1+C1
	2456325.3124	0.0002	I	BVRI	T1+C1
	2456325.4277	0.0002	II	BVRI	T1+C1
	2456325.5399	0.0002	I	BVRI	T1+C1
	2456329.5265	0.0002	II	BVRI	T1+C1
	2456329.6393	0.0002	I	BVRI	T1+C1
	2456330.5502	0.0002	I	BVRI	T1+C1
1SWASP J093012.84+533859.6 (EA)	2456305.6603	0.0003	II	BRVI	T1+C1
	2456313.4923	0.0005	II	BVRI	T1+C1
	2456322.6328	0.0004	II	BVRI	T1+C1
	2456324.5903	0.0002	I	BVRI	T1+C1
1SWASP J133105.91+121538.0	2456332.6199	0.0002	II	BVRI	T1+C1
	2456333.6008	0.0002	I	BVRI	T1+C1
	2456335.5632	0.0002	I	BVRI	T1+C1
	2456335.6720	0.0002	II	BVRI	T1+C1
	2456347.4454	0.0002	II	BVRI	T1+C1
	2456347.5542	0.0002	I	BVRI	T1+C1
	2456347.6626	0.0003	II	BVRI	T1+C1
	2456348.5354	0.0006	II	BVRI	T1+C1
	2456348.6439	0.0003	I	BVRI	T1+C1
	2456350.4978	0.0005	II	BVRI	T1+C1
	2456350.6060	0.0010	I	BVRI	T1+C1
	2456353.5497	0.0003	II	BVRI	T1+C1
	2456353.6581	0.0004	I	BVRI	T1+C1
1SWASP J150822.80-054236.9	2456352.4977	0.0007	II	BVRI	T1+C1
	2456352.6285	0.0004	I	BVRI	T1+C1
	2456355.4907	0.0003	I	B	T1+C1
	2456355.6192	0.0003	II	BVRI	T1+C1
	2456356.5296	0.0004	I	BVRI	T1+C1
	2456356.6594	0.0005	II	VRI	T1+C1
	2456357.5699	0.0002	I	BVRI	T1+C1
	2456362.5109	0.0003	I	BVRI	T1+C1
	2456362.6406	0.0007	II	BVRI	T1+C1
	2456364.5913	0.0009	I	BVRI	T1+C1
	2456368.5089	0.0007	I	R	T1+C1
	2456374.4738	0.0004	I	BVRI	T1+C1
	2456374.6034	0.0003	II	BVRI	T1+C1
	2456375.5143	0.0002	I	BVRI	T1+C1

Table 1: cont.

System	HJD	Error	Type	Filters	Remark
1SWASP J150822.80-054236.9	2456375.6436	0.0004	II	BVRI	T1+C1
1SWASP J173003.21+344509.4	2456832.3657	0.0004	I	BRI	T2+C2
	2456832.4780	0.0009	II	BVRI	T2+C2
	2456833.3720	0.0006	II	BVRI	T2+C2
	2456833.4849	0.0007	I	BVRI	T2+C2
	2456834.3814	0.0008	I	B	T2+C2
	2456834.4915	0.0013	II	BVRI	T2+C2
	2456836.3934	0.0009	I	B	T2+C2
	2456836.5035	0.0005	II	B	T2+C2

Explanation of the remarks in the table:

T1, T2, C1, and C2 refer to the instrumentation (telescope and CCD camera) used for each case.

Remarks:

The majority of the above observations were performed utilizing the robotic and remotely controlled telescope at the University of Athens: (http://observatory.phys.uoa.gr) (Gazeas 2016). Note that the system 1SWASP J093012.84+533859.6 is a double-eclipsing quintuple or a quintuple system (Lohr et al. 2013 and Koo et al. 2014), showing eclipses in both contact binary member (EW) and Algol-type member (EA), both included in the above list.

Acknowledgements:

Times of minima of contact binaries presented in this work are by-product of the the *Contact Binaries Towards Merging (CoBiToM) Project*, initiated and still undergoing at the National and Kapodistrian University of Athens since 2012 (PI: K. Gazeas).

References:

Gazeas, K., 2016, *RMxAC*, **48**, 22

Koo, J.-R., Lee, J.W., Lee, B.-C., Kim, S.-L., Lee, C.-U., Hong, K., Lee, D.-J., Rey, S.-C., 2014, *AJ*, **147**, 104 DOI

Kwee, K., van Woerden, H., 1956, *Bulletin of the Astronomical Institutes of the Netherlands*, **12**, 327

Lohr, M.E., Norton, A.J., Kolb, U.C., Maxted, P.F.L., Todd, I., and West, R. G., 2013, *A&A*, **549**, A86 DOI

COMMISSIONS G1 AND G4 OF THE IAU
INFORMATION BULLETIN ON VARIABLE STARS
Volume 63 Number 6218 DOI: 10.22444/IBVS.6218

Konkoly Observatory
Budapest
20 September 2017
HU ISSN 0374 – 0676

120 MINIMA TIMINGS OF ECLIPSING BINARIES

PALAFOUTA, S.; GAZEAS, K.; CHRISTOPOULOU, E.; BAKOGIANNI, V.; DERVOU, M.; LOUKAIDOU, G.

Section of Astrophysics, Astronomy and Mechanics, Department of Physics, National & Kapodistrian University of Athens, Zografos GR-15784, Athens, Greece; e-mail: spalafouta@gmail.com, kgaze@phys.uoa.gr

Observatory and telescope:
T1: 0.4m, f/8 Cassegrain telescope, located at the University of Athens Observatory, at Zografos, Athens, Greece. **T2**: 1.2m, f/13 Cassegrain telescope of the National Observatory of Athens, located at the Kryoneri Astronomical Station, at Korinth, Greece.

Detector:	**C1**: ST-10XME CCD camera, KAF-3200ME chip, $16' \times 11'$ and $25' \times 17'$ (using an f/6.3 focal reducer) field of view (FoV) with T1. **C2**: ST-8XMEI CCD camera, KAF-1603ME chip, $15' \times 10'$ FoV with T1. **C3**: ST-8 CCD camera, KAF-1600 chip, $15' \times 10'$ FoV with T1. **C4**: Photometrics CH250 CCD camera, SI502 chip, $2.5' \times 2.5'$ FoV with T2. **C5**: AP47p CCD camera, Marconi 47-10 chip, $2.5' \times 2.5'$ and $5' \times 5'$ (using an f/6.3 focal reducer) FoV with T2. All CCDs have a Peltier-type cooling system and are equipped with a set of *UBVRI* filters (Bessell specifications).

Method of data reduction:
Differential photometry

Method of minimum determination:
Kwee & van Woerden (1956).

Table 1: Times of minima of eclipsing binaries

System	HJD	Error	Type	Filters	Remark
SV Cam	2456585.4889	0.0003	II	BVRI	T1+C1
	2456586.3782	0.0002	I	BVRI	T1+C1
	2456587.2697	0.0003	II	BVRI	T1+C1
	2456587.5638	0.0001	I	BVRI	T1+C1
	2456588.4759	0.0005	II	BVRI	T1+C1
	2456589.3434	0.0003	I	BVRI	T1+C1
	2456590.2368	0.0004	II	BVRI	T1+C1
	2456590.5290	0.0001	I	BVRI	T1+C1
	2456591.4231	0.0003	II	BVRI	T1+C1
	2456592.3081	0.0002	I	BVRI	T1+C1
	2456593.2038	0.0005	II	BVRI	T1+C1
	2456593.4941	0.0001	I	BVRI	T1+C1
V563 Lyr	2456200.3607	0.0004	II	BVRI	T1+C1
	2456202.3827	0.0008	I	BVRI	T1+C1
	2456205.2711	0.0005	I	BVRI	T1+C1
	2456207.2924	0.0004	II	BVRI	T1+C1
GSC 3122-2426 (Lyr)	2456199.3444	0.0005	I	BVRI	T1+C1
	2456200.2460	0.0006	I	BVRI	T1+C1
	2456200.3960	0.0012	II	BVRI	T1+C1
	2456202.3499	0.0004	I	VRI	T1+C1
	2456203.4024	0.0014	II	VRI	T1+C1
	2456204.3010	0.0014	II	BVRI	T1+C1
	2456205.3557	0.0006	I	VRI	T1+C1
	2456207.3082	0.0008	II	BVRI	T1+C1
V566 Oph	2454980.5158	0.0001	II	BVRI	T1+C2
	2454982.3590	0.0005	I	BVRI	T1+C2
DV Psc	2453617.4871	0.0004	I	BVRI	T2+C4
	2453618.4138	0.0008	II	BVRI	T2+C4
	2453618.5656	0.0001	I	BVRI	T2+C4
	2453696.3168	0.0003	I	BVRI	T1+C3
	2453708.1962	0.0005	II	BVRI	T1+C3
	2453708.3497	0.0003	I	BVRI	T1+C3
	2453709.2756	0.0004	I	BVRI	T1+C3
	2453710.2007	0.0006	I	BVRI	T1+C3
	2453710.3550	0.0022	II	BVRI	T1+C3
	2453712.3612	0.0004	I	BVRI	T1+C3
	2453721.3084	0.0005	I	BVRI	T1+C3
	2453724.2402	0.0007	II	BVRI	T1+C3
	2453736.2712	0.0009	II	BVRI	T1+C3
	2456209.3453	0.0004	I	BVRI	T2+C4
	2456209.5029	0.0006	II	BVRI	T2+C4
	2456212.4315	0.0004	I	BVRI	T1+C1
	2456243.2854	0.0002	I	BVRI	T1+C1
	2456243.4424	0.0006	II	BVRI	T1+C1
	2456245.2932	0.0003	II	BVRI	T1+C1
	2456245.4451	0.0001	I	BVRI	T1+C1

Table 1: cont.

System	HJD	Error	Type	Filters	Remark
DV Psc	2456246.2201	0.0009	II	BVRI	T1+C1
	2456246.3706	0.0001	I	BVRI	T1+C1
	2456559.3820	0.0004	II	BRI	T2+C5
	2456559.5312	0.0002	I	BVRI	T2+C5
	2456560.3082	0.0003	II	VRI	T2+C5
	2456560.4569	0.0002	I	BVRI	T2+C5
	2456560.6163	0.0005	II	BVRI	T2+C5
	2456561.3830	0.0001	I	BVRI	T2+C5
	2456561.5427	0.0003	II	BVRI	T2+C5
	2457674.4238	0.0003	II	I	T1+C1
	2457675.5046	0.0001	I	I	T1+C1
	2457677.3561	0.0004	I	I	T1+C1
	2457679.3604	0.0002	II	I	T1+C1
	2457680.2863	0.0002	II	I	T1+C1
	2457680.4408	0.0001	I	I	T1+C1
	2457681.2145	0.0003	II	I	T1+C1
	2457681.3673	0.0001	I	I	T1+C1
	2457681.5197	0.0001	II	I	T1+C1
	2457685.2213	0.0002	II	I	T1+C1
	2457685.3776	0.0002	I	I	T1+C1
	2457686.3036	0.0001	I	I	T1+C1
	2457687.2296	0.0001	I	R	T1+C1
	2457687.3816	0.0002	II	R	T1+C1
	2457693.4004	0.0002	I	R	T1+C1
	2457694.3258	0.0001	I	R	T1+C1
	2457694.4789	0.0001	II	R	T1+C1
	2457695.4042	0.0002	II	R	T1+C1
	2457696.3298	0.0002	II	R	T1+C1
	2457696.4858	0.0002	I	R	T1+C1
	2457697.2551	0.0002	II	V	T1+C1
	2457698.1814	0.0007	II	V	T1+C1
	2457698.3369	0.0001	I	V	T1+C1
	2457698.4885	0.0004	II	V	T1+C1
	2457699.4149	0.0002	II	V	T1+C1
	2457702.3482	0.0001	I	V	T1+C1
	2457703.4255	0.0003	II	V	T1+C1
	2457706.1986	0.0006	II	B	T1+C1
	2457706.3595	0.0002	I	B	T1+C1
	2457709.2856	0.0005	II	B	T1+C1
	2457709.4448	0.0002	I	B	T1+C1
	2457710.2123	0.0004	II	B	T1+C1
	2457710.3707	0.0002	I	B	T1+C1
	2457711.2961	0.0001	I	B	T1+C1
	2457711.4464	0.0005	II	B	T1+C1
	2457712.3730	0.0005	II	B	T1+C1
	2457713.2984	0.0006	II	B	T1+C1
	2457714.2249	0.0005	II	B	T1+C1

Table 1: cont.

System	HJD	Error	Type	Filters	Remark
DV Psc	2457715.3072	0.0001	I	B	T1+C1
	2457715.4533	0.0010	II	B	T1+C1
	2457716.2327	0.0011	I	B	T1+C1
	2457716.3843	0.0004	II	B	T1+C1
FT UMa	2456605.6571	0.0005	II	BVRI	T1+C1
	2456606.6405	0.0008	I	BVRI	T1+C1
	2456614.4992	0.0005	I	BVRI	T1+C1
	2456631.5205	0.0004	I	BVRI	T1+C1
	2456632.4969	0.0005	II	BVRI	T1+C1
	2456633.4820	0.0003	I	BVRI	T1+C1
	2456646.5813	0.0003	I	BVRI	T1+C1
	2456649.5195	0.0004	II	BVRI	T1+C1
	2456662.6252	0.0004	II	BVRI	T1+C1
	2456675.3882	0.0004	I	BVRI	T1+C1
	2456700.5841	0.0003	II	BVRI	T1+C1
	2456704.5164	0.0003	II	BVRI	T1+C1
AG Vir	2456798.3319	0.0005	I	BVRI	T1+C1
	2456825.3228	0.0004	I	BVRI	T1+C1
NN Vir	2452725.5075	0.0003	II	BVRI	T1+C3
	2452727.4294	0.0003	II	BVR	T1+C3
	2452732.4766	0.0003	I	BVRI	T1+C3
	2452738.4843	0.0004	II	BVRI	T1+C3
	2452739.4465	0.0006	II	BVRI	T1+C3
	2452767.3272	0.0004	II	BVRI	T1+C3
	2452793.2847	0.0007	II	BVRI	T1+C3
	2452793.5231	0.0003	I	VR	T1+C3
	2452795.4456	0.0006	I	BVR	T1+C3

Explanation of the remarks in the table:

T1, T2, C1, C2, C3, C4 and C5 refer to the instrumentation (telescope and CCD camera) used for each case.

Remarks:

A large number of the above observations were performed utilizing the robotic and remotely controlled telescope at the University of Athens: (http://observatory.phys.uoa.gr) (Gazeas 2016).

Acknowledgements:

Times of minima of contact binaries presented in this work are by-product of the *W UMa Project* (Papers I - VII) (Kreiner et al. 2003; Baran et al. 2004; Zola et al. 2004; Gazeas et al. 2005; Zola et al. 2005; Gazeas et al. 2006; Zola et al. 2010.), which aims in performing accurate photometric and spectroscopic study of eclipsing binaries of W UMa type. In addition, part of this work is a result of the *Contact Binaries Towards Merging (CoBiToM) Project*, initiated and still undergoing at the National and Kapodistrian University of Athens since 2012 (PI: K.Gazeas).

References:

Baran, A., Zola, S., Rucinski, S. M., Kreiner, J. M., Siwak, M., Drozdz, M., 2004, *AcA*, **54**, 195 (Paper II)

Gazeas, K., Baran, A., Niarchos, P., Zola, S., Kreiner, J.M., et al., 2005, *AcA*, **55**, 123 (Paper IV)

Gazeas, K., Niarchos, P., Zola, S., Kreiner, J.M., Rucinski, S.M., 2006, *AcA*, **56**, 127 (Paper VI)

Gazeas, K., 2016, *RMxAC*, **48**, 22

Kreiner, J. M., Rucinski, S. M., Zola, S., Niarchos, P., Ogloza, W., Stachowski, G., Baran, A., Gazeas, K., Drozdz, M., Zakrzewski, B., Pokrzywka, B., Kjurkchieva, D., Marchev, D., 2003, *A&A*, **412**, 465 (Paper I) DOI

Kwee, K., van Woerden, H., 1956, *Bulletin of the Astronomical Institutes of the Netherlands*, **12**, 327

Zola, S., Rucinski, S.M., Baran, A., Ogloza, W., Pych, W., Kreiner, J.M., Stachowski, G., Gazeas, K., Niarchos, P., Siwak, M., 2004, *AcA*, **54**, 299 (Paper III)

Zola, S., Kreiner, J.M., Zakrzewski, B., Kjurkchieva, D.P., Marchev, D.V., Baran, A., Rucinski, S.M., Ogloza, W., Siwak, M., Koziel, D., Drozdz, M., Pokrzywka, B., 2005, *AcA*, **55**, 389 (Paper V)

Zola, S., Gazeas, K., Kreiner, J. M., Ogloza, W., Siwak, M., Koziel-Wierzbowska, D., Winiarski, M., 2010, *MNRAS*, **408**, 464 (Paper VII) DOI

COMMISSIONS G1 AND G4 OF THE IAU
INFORMATION BULLETIN ON VARIABLE STARS
Volume 63 Number 6219 DOI: 10.22444/IBVS.6219

Konkoly Observatory
Budapest
11 October 2017
HU ISSN 0374 – 0676

TIMES OF MINIMA OF SOME ECLIPSING BINARY STARS WITH ECCENTRIC ORBIT IN THE KEPLER FIELD

BULUT, İ.

Department of Space Sciences and Technologies, Faculty of Arts and Sciences, Çanakkale Onsekiz Mart University, Terzioğlu Kampüsü, TR-17020, Çanakkale, Turkey; e-mail: ibulut@comu.edu.tr

Observatory and telescope:
The Kepler photometer is a Schmidt telescope design with a 0.95-meter aperture and a 105 square deg (about 12 degree diameter) FOV.

Detector:	The photometer camera contains 42 CCDs with 2200×1024 pixels, where each pixel covers 4 arcsec.

Method of data reduction:
Photometry flux values were taken from the Kepler Database (http://keplerebs.villanova.edu)

Method of minimum determination:
The minima times were computed with the Kwee-van Woerden method (Kwee & van Woerden, 1956).

Remarks:
We present 517 minima times of 6 eclipsing binaries with eccentric orbit. The O−C diagrams are shown in Figs. 1 and 2.

Acknowledgements:
This paper includes data collected by the Kepler mission. Funding for the Kepler mission is provided by the NASA Science Mission directorate.

Reference:

Kwee, K. K., van Woerden, H., 1956, Bull. Astron. Inst. Netherlands, **12**, 327

Times of minima:					
Star name	Time of min. HJD 2400000+	Error	Type	Filter	Rem.
KIC 4932691	54967.70418	0.00299	I	*Kepler*	
	54972.50630	0.01486	II	*Kepler*	
	54985.83524	0.00524	I	*Kepler*	
	54990.47957	0.01034	II	*Kepler*	
	55003.94523	0.00328	I	*Kepler*	
	55022.05529	0.00454	I	*Kepler*	
	55026.68879	0.00806	II	*Kepler*	
	55040.16346	0.00549	I	*Kepler*	
	55045.01905	0.00993	II	*Kepler*	
	55058.27043	0.00400	I	*Kepler*	
	55063.18681	0.01446	II	*Kepler*	
	55076.39419	0.00323	I	*Kepler*	
	55081.19915	0.01471	II	*Kepler*	
	55094.49652	0.00504	I	*Kepler*	
	55099.45777	0.01025	II	*Kepler*	
	55112.60843	0.00424	I	*Kepler*	
	55117.60643	0.02323	II	*Kepler*	
	55130.71894	0.00427	I	*Kepler*	
	55135.39270	0.00551	II	*Kepler*	
	55148.84864	0.00595	I	*Kepler*	
	55153.62809	0.01108	II	*Kepler*	
	55166.94809	0.00349	I	*Kepler*	
	55171.67254	0.01557	II	*Kepler*	
	55189.85773	0.00559	II	*Kepler*	
	55203.16352	0.00605	I	*Kepler*	
	55207.99029	0.00639	II	*Kepler*	
	55221.28102	0.00293	I	*Kepler*	
	55226.06370	0.00618	II	*Kepler*	
	55239.38710	0.00558	I	*Kepler*	
	55244.10342	0.00597	II	*Kepler*	
	55257.49469	0.00599	I	*Kepler*	
	55262.31028	0.02012	II	*Kepler*	
	55280.43424	0.00866	II	*Kepler*	
	55293.72957	0.00471	I	*Kepler*	
	55298.72648	0.00948	II	*Kepler*	
	55311.84560	0.00334	I	*Kepler*	
	55316.80536	0.00950	II	*Kepler*	
	55329.94437	0.00366	I	*Kepler*	
	55334.87176	0.01468	II	*Kepler*	
	55348.05019	0.00516	I	*Kepler*	
	55352.87147	0.00717	II	*Kepler*	
	55366.18314	0.00461	I	*Kepler*	
	55370.97493	0.00031	II	*Kepler*	

Times of minima:					
Star name	Time of min. HJD 2400000+	Error	Type	Filter	Rem.
KIC 4932691	55474.85393	0.00359	I	*Kepler*	
	55492.96744	0.00488	I	*Kepler*	
	55511.07491	0.00368	I	*Kepler*	
	55515.69518	0.02536	II	*Kepler*	
	55529.18751	0.00416	I	*Kepler*	
	55534.01506	0.01239	II	*Kepler*	
	55547.30372	0.00432	I	*Kepler*	
	55552.09953	0.00136	II	*Kepler*	
	55583.51992	0.00457	I	*Kepler*	
	55588.30124	0.00774	II	*Kepler*	
	55601.62815	0.00555	I	*Kepler*	
	55606.45068	0.01115	II	*Kepler*	
	55619.74491	0.00372	I	*Kepler*	
	55624.54875	0.02524	II	*Kepler*	
	55642.68012	0.01251	II	*Kepler*	
	55655.97070	0.00422	I	*Kepler*	
	55660.77593	0.00613	II	*Kepler*	
	55674.07624	0.00336	I	*Kepler*	
	55678.92482	0.01446	II	*Kepler*	
	55692.20751	0.00368	I	*Kepler*	
	55696.83902	0.00769	II	*Kepler*	
	55710.31997	0.00518	I	*Kepler*	
	55715.11061	0.00864	II	*Kepler*	
	55728.40921	0.00580	I	*Kepler*	
	55733.10453	0.00870	II	*Kepler*	
	55837.09629	0.00336	I	*Kepler*	
	55841.73208	0.00782	II	*Kepler*	
	55855.20150	0.00505	I	*Kepler*	
	55873.30815	0.00616	I	*Kepler*	
	55878.10419	0.01676	II	*Kepler*	
	55891.43983	0.00356	I	*Kepler*	
	55896.13096	0.02619	II	*Kepler*	
	55909.55387	0.00607	I	*Kepler*	
	55914.34397	0.01942	II	*Kepler*	
	55927.65944	0.00313	I	*Kepler*	
	55932.41110	0.01621	II	*Kepler*	
	55945.75909	0.00347	I	*Kepler*	
	55963.87715	0.00344	I	*Kepler*	
	55968.71817	0.01174	II	*Kepler*	
	55981.99129	0.00260	I	*Kepler*	
	55986.79681	0.00897	II	*Kepler*	
	56000.10818	0.00399	I	*Kepler*	
	56004.93168	0.00792	II	*Kepler*	

Times of minima:					
Star name	Time of min. HJD 2400000+	Error	Type	Filter	Rem.
KIC 4932691	56018.21168	0.00531	I	*Kepler*	
	56023.10999	0.00719	II	*Kepler*	
	56036.33259	0.00312	I	*Kepler*	
	56054.43580	0.00485	I	*Kepler*	
	56059.19200	0.00648	II	*Kepler*	
	56072.54284	0.00304	I	*Kepler*	
	56077.39264	0.02352	II	*Kepler*	
	56090.66130	0.00502	I	*Kepler*	
	56217.43251	0.00638	I	*Kepler*	
	56222.10179	0.01635	II	*Kepler*	
	56235.54363	0.00497	I	*Kepler*	
	56240.20381	0.00983	II	*Kepler*	
	56253.68256	0.00493	I	*Kepler*	
	56258.30120	0.01005	II	*Kepler*	
	56271.78818	0.00361	I	*Kepler*	
	56276.60675	0.01129	II	*Kepler*	
	56289.89729	0.00528	I	*Kepler*	
	56308.01162	0.00326	I	*Kepler*	
	56326.11999	0.00354	I	*Kepler*	
	56330.77953	0.01279	II	*Kepler*	
	56344.23598	0.00281	I	*Kepler*	
	56349.00703	0.00778	II	*Kepler*	
	56362.34323	0.00628	I	*Kepler*	
	56367.23512	0.00901	II	*Kepler*	
	56380.45960	0.00431	I	*Kepler*	
	56385.17812	0.00408	II	*Kepler*	
	56398.57000	0.00383	I	*Kepler*	
	56403.50721	0.01102	II	*Kepler*	
	56421.35880	0.00662	I	*Kepler*	
	56421.35880	0.00662	II	*Kepler*	
KIC 5986209	55193.64842	0.00072	II	*Kepler*	
	55202.42103	0.00023	I	*Kepler*	
	55217.18138	0.01519	II	*Kepler*	
	55226.15876	0.00028	I	*Kepler*	
	55241.12402	0.00038	II	*Kepler*	
	55249.89820	0.00045	I	*Kepler*	
	55264.86249	0.00036	II	*Kepler*	
	55273.63445	0.00046	I	*Kepler*	
	55288.60083	0.00038	II	*Kepler*	
	55297.37304	0.00054	I	*Kepler*	
	55312.33872	0.00033	II	*Kepler*	
	55321.11099	0.00019	I	*Kepler*	
	55336.07588	0.00042	II	*Kepler*	

Times of minima:					
Star name	Time of min. HJD 2400000+	Error	Type	Filter	Rem.
KIC 5986209	55344.84860	0.00038	I	*Kepler*	
	55359.81417	0.00025	II	*Kepler*	
	55368.58758	0.00028	I	*Kepler*	
	55383.55213	0.00024	II	*Kepler*	
	55392.32588	0.00044	I	*Kepler*	
	55407.29028	0.00022	II	*Kepler*	
	55416.06252	0.00042	I	*Kepler*	
	55431.02708	0.00051	II	*Kepler*	
	55439.80156	0.00052	I	*Kepler*	
	55454.76593	0.00030	II	*Kepler*	
	55463.53828	0.00039	I	*Kepler*	
	55478.50369	0.00035	II	*Kepler*	
	55487.27696	0.00007	I	*Kepler*	
	55502.24210	0.00026	II	*Kepler*	
	55511.01443	0.00038	I	*Kepler*	
	55525.97983	0.00031	II	*Kepler*	
	55534.75278	0.00010	I	*Kepler*	
	55549.71805	0.00027	II	*Kepler*	
	55573.45558	0.00022	II	*Kepler*	
	55582.22885	0.00015	I	*Kepler*	
	55597.19444	0.00087	II	*Kepler*	
	55605.96609	0.00039	I	*Kepler*	
	55620.93123	0.00091	II	*Kepler*	
	55629.70525	0.00011	I	*Kepler*	
	55644.66989	0.00033	II	*Kepler*	
	55653.44196	0.00024	I	*Kepler*	
	55668.40751	0.00035	II	*Kepler*	
	55677.18123	0.00027	I	*Kepler*	
	55692.14564	0.00030	II	*Kepler*	
	55700.91868	0.00007	I	*Kepler*	
	55715.88389	0.00042	II	*Kepler*	
	55724.65616	0.00023	I	*Kepler*	
	55748.39506	0.00020	I	*Kepler*	
	55763.35897	0.00026	II	*Kepler*	
	55772.13268	0.00009	I	*Kepler*	
	55787.09711	0.00038	II	*Kepler*	
	55795.87040	0.00031	I	*Kepler*	
	55810.83502	0.00039	II	*Kepler*	
	55819.60878	0.00010	I	*Kepler*	
	55834.57295	0.00042	II	*Kepler*	
	55843.34611	0.00026	I	*Kepler*	
	55858.31047	0.00040	II	*Kepler*	
	55867.08432	0.00061	I	*Kepler*	

Times of minima:					
Star name	Time of min. HJD 2400000+	Error	Type	Filter	Rem.
KIC 5986209	55882.04886	0.00033	II	*Kepler*	
	55890.82177	0.00010	I	*Kepler*	
	55905.78780	0.00056	II	*Kepler*	
	55914.56047	0.00006	I	*Kepler*	
	55929.52421	0.00032	II	*Kepler*	
	55938.29767	0.00033	I	*Kepler*	
	55953.26292	0.00067	II	*Kepler*	
	55962.03550	0.00053	I	*Kepler*	
	55977.00037	0.00031	II	*Kepler*	
	55985.77614	0.00049	I	*Kepler*	
	56000.73887	0.00022	II	*Kepler*	
	56009.51276	0.00029	I	*Kepler*	
	56024.47691	0.00028	II	*Kepler*	
	56033.25087	0.00051	I	*Kepler*	
	56056.98894	0.00031	I	*Kepler*	
	56071.95244	0.00029	II	*Kepler*	
	56080.72664	0.00026	I	*Kepler*	
	56095.69001	0.00025	II	*Kepler*	
	56104.46506	0.00063	I	*Kepler*	
	56119.42874	0.00023	II	*Kepler*	
	56143.16609	0.00032	II	*Kepler*	
	56151.93970	0.00053	I	*Kepler*	
	56166.90401	0.00038	II	*Kepler*	
	56175.67870	0.00030	I	*Kepler*	
	56190.64219	0.00041	II	*Kepler*	
	56199.41685	0.00041	I	*Kepler*	
	56214.37976	0.00031	II	*Kepler*	
	56223.15481	0.00048	I	*Kepler*	
	56261.85591	0.00030	II	*Kepler*	
	56270.63023	0.00060	I	*Kepler*	
	56285.59425	0.00049	II	*Kepler*	
	56294.36815	0.00013	I	*Kepler*	
	56309.33150	0.00039	II	*Kepler*	
	56333.06980	0.00023	II	*Kepler*	
	56341.84415	0.00015	I	*Kepler*	
	56356.80821	0.00036	II	*Kepler*	
	56365.58226	0.00048	I	*Kepler*	
	56380.54538	0.00045	II	*Kepler*	
	56389.32060	0.00030	I	*Kepler*	
	56404.28350	0.00026	II	*Kepler*	
	56413.05801	0.00019	I	*Kepler*	
KIC 6841577	54973.27350	0.00026	I	*Kepler*	
	54979.87424	0.00091	II	*Kepler*	

Times of minima:					
Star name	Time of min. HJD 2400000+	Error	Type	Filter	Rem.
KIC 6841577	54988.81127	0.00043	I	*Kepler*	
	54995.41256	0.00086	II	*Kepler*	
	55004.34869	0.00052	I	*Kepler*	
	55010.94840	0.00116	II	*Kepler*	
	55019.88608	0.00010	I	*Kepler*	
	55026.48648	0.00093	II	*Kepler*	
	55035.42383	0.00031	I	*Kepler*	
	55042.02373	0.00105	II	*Kepler*	
	55050.96124	0.00043	I	*Kepler*	
	55057.56337	0.00103	II	*Kepler*	
	55066.49848	0.00009	I	*Kepler*	
	55073.09922	0.00110	II	*Kepler*	
	55082.03628	0.00012	I	*Kepler*	
	55097.57373	0.00021	I	*Kepler*	
	55104.17270	0.00092	II	*Kepler*	
	55113.11094	0.00049	I	*Kepler*	
	55119.71237	0.00097	II	*Kepler*	
	55128.64919	0.00033	I	*Kepler*	
	55135.25101	0.00110	II	*Kepler*	
	55144.18666	0.00038	I	*Kepler*	
	55150.78804	0.00103	II	*Kepler*	
	55159.72407	0.00030	I	*Kepler*	
	55166.32461	0.00104	II	*Kepler*	
	55175.26170	0.00008	I	*Kepler*	
	55181.86028	0.00339	II	*Kepler*	
	55190.79861	0.00040	I	*Kepler*	
	55197.39878	0.00088	II	*Kepler*	
	55206.33649	0.00030	I	*Kepler*	
	55212.93796	0.00103	II	*Kepler*	
	55221.87432	0.00034	I	*Kepler*	
	55228.47462	0.00112	II	*Kepler*	
	55237.41173	0.00036	I	*Kepler*	
	55244.01205	0.00075	II	*Kepler*	
	55252.94924	0.00009	I	*Kepler*	
	55259.54996	0.00090	II	*Kepler*	
	55268.48621	0.00033	I	*Kepler*	
	55377.24962	0.00017	I	*Kepler*	
	55383.84985	0.00128	II	*Kepler*	
	55392.78717	0.00029	I	*Kepler*	
	55399.38414	0.00188	II	*Kepler*	
	55408.32464	0.00019	I	*Kepler*	
	55414.92481	0.00097	II	*Kepler*	
	55423.86193	0.00008	I	*Kepler*	

Times of minima:					
Star name	Time of min. HJD 2400000+	Error	Type	Filter	Rem.
KIC 6841577	55430.46256	0.00254	II	*Kepler*	
	55439.39929	0.00046	I	*Kepler*	
	55446.00168	0.00112	II	*Kepler*	
	55454.93651	0.00035	I	*Kepler*	
	55461.53810	0.00226	II	*Kepler*	
	55470.47490	0.00027	I	*Kepler*	
	55477.07542	0.00147	II	*Kepler*	
	55486.01292	0.00038	I	*Kepler*	
	55492.61333	0.00298	II	*Kepler*	
	55501.54945	0.00018	I	*Kepler*	
	55508.15193	0.00262	II	*Kepler*	
	55517.08701	0.00011	I	*Kepler*	
	55532.62455	0.00045	I	*Kepler*	
	55539.22506	0.00094	II	*Kepler*	
	55548.16199	0.00043	I	*Kepler*	
	55570.30184	0.00101	II	*Kepler*	
	55579.23756	0.00034	I	*Kepler*	
	55585.83899	0.00086	II	*Kepler*	
	55601.37630	0.00078	II	*Kepler*	
	55610.31234	0.00013	I	*Kepler*	
	55616.91384	0.00180	II	*Kepler*	
	55625.84973	0.00027	I	*Kepler*	
	55632.45125	0.00122	II	*Kepler*	
	55741.21313	0.00096	II	*Kepler*	
	55750.15053	0.00027	I	*Kepler*	
	55756.75042	0.00101	II	*Kepler*	
	55765.68815	0.00045	I	*Kepler*	
	55772.28940	0.00317	II	*Kepler*	
	55781.22526	0.00050	I	*Kepler*	
	55787.82610	0.00167	II	*Kepler*	
	55796.76263	0.00044	I	*Kepler*	
	55803.36537	0.00194	II	*Kepler*	
	55812.30057	0.00021	I	*Kepler*	
	55818.90180	0.00095	II	*Kepler*	
	55827.83814	0.00029	I	*Kepler*	
	55834.44114	0.00155	II	*Kepler*	
	55843.37558	0.00038	I	*Kepler*	
	55849.97538	0.00096	II	*Kepler*	
	55858.91270	0.00012	I	*Kepler*	
	55874.45044	0.00012	I	*Kepler*	
	55881.05156	0.00176	II	*Kepler*	
	55889.98807	0.00011	I	*Kepler*	
	55912.12557	0.00104	II	*Kepler*	

Times of minima:					
Star name	Time of min. HJD 2400000+	Error	Type	Filter	Rem.
KIC 6841577	55921.06331	0.00028	I	*Kepler*	
	55927.66399	0.00173	II	*Kepler*	
	56107.51330	0.00016	I	*Kepler*	
	56114.11380	0.00105	II	*Kepler*	
	56129.65574	0.00090	II	*Kepler*	
	56145.18845	0.00091	II	*Kepler*	
	56154.12569	0.00043	I	*Kepler*	
	56160.72642	0.00099	II	*Kepler*	
	56176.26457	0.00102	II	*Kepler*	
	56185.20132	0.00031	I	*Kepler*	
	56191.80164	0.00099	II	*Kepler*	
	56200.73849	0.00010	I	*Kepler*	
	56207.34096	0.00178	II	*Kepler*	
	56216.27584	0.00016	I	*Kepler*	
	56222.87201	0.00113	II	*Kepler*	
	56231.81354	0.00048	I	*Kepler*	
	56238.42053	0.00155	II	*Kepler*	
	56253.95181	0.00104	II	*Kepler*	
	56262.88836	0.00035	I	*Kepler*	
	56269.49274	0.00270	II	*Kepler*	
	56278.42657	0.00030	I	*Kepler*	
	56285.02669	0.00081	II	*Kepler*	
	56293.96400	0.00036	I	*Kepler*	
	56300.56403	0.00163	II	*Kepler*	
	56309.50621	0.00081	I	*Kepler*	
	56325.03913	0.00044	I	*Kepler*	
	56331.63855	0.00120	II	*Kepler*	
	56340.57660	0.00041	I	*Kepler*	
	56347.17610	0.00098	II	*Kepler*	
	56356.11448	0.00036	I	*Kepler*	
	56362.71391	0.00093	II	*Kepler*	
	56371.65167	0.00040	I	*Kepler*	
	56378.25150	0.00085	II	*Kepler*	
	56387.18835	0.00043	I	*Kepler*	
KIC 8378922	54983.37810	0.00011	I	*Kepler*	
	54996.86620	0.01383	II	*Kepler*	
	55026.64130	0.00008	I	*Kepler*	
	55045.02337	0.00014	II	*Kepler*	
	55069.90481	0.00014	I	*Kepler*	
	55088.28656	0.00024	II	*Kepler*	
	55113.16786	0.00020	I	*Kepler*	
	55131.55009	0.00009	II	*Kepler*	
	55174.81324	0.00009	II	*Kepler*	

Times of minima:					
Star name	Time of min. HJD 2400000+	Error	Type	Filter	Rem.
KIC 8378922	55199.69468	0.00013	I	*Kepler*	
	55218.07668	0.00019	II	*Kepler*	
	55242.95779	0.00007	I	*Kepler*	
	55261.33969	0.00009	II	*Kepler*	
	55286.22128	0.00006	I	*Kepler*	
	55304.60317	0.00012	II	*Kepler*	
	55329.48446	0.00015	I	*Kepler*	
	55347.86640	0.00010	II	*Kepler*	
	55372.74784	0.00017	I	*Kepler*	
	55391.12985	0.00016	II	*Kepler*	
	55416.01096	0.00012	I	*Kepler*	
	55434.39315	0.00020	II	*Kepler*	
	55459.27439	0.00007	I	*Kepler*	
	55477.65611	0.00011	II	*Kepler*	
	55502.53771	0.00009	I	*Kepler*	
	55520.91965	0.00010	II	*Kepler*	
	55545.80089	0.00012	I	*Kepler*	
	55589.06433	0.00027	I	*Kepler*	
	55607.44614	0.00014	II	*Kepler*	
	55632.32786	0.00032	I	*Kepler*	
	55650.70945	0.00012	II	*Kepler*	
	55675.59088	0.00005	I	*Kepler*	
	55693.97278	0.00011	II	*Kepler*	
	55718.85429	0.00011	I	*Kepler*	
	55737.23593	0.00013	II	*Kepler*	
	55762.11735	0.00016	I	*Kepler*	
	55780.49930	0.00018	II	*Kepler*	
	55805.38079	0.00012	I	*Kepler*	
	55823.76251	0.00015	II	*Kepler*	
	55848.64406	0.00017	I	*Kepler*	
	55867.02620	0.00018	II	*Kepler*	
	55891.90753	0.00008	I	*Kepler*	
	55910.28934	0.00011	II	*Kepler*	
	55935.17062	0.00009	I	*Kepler*	
	55953.55217	0.00038	II	*Kepler*	
	55978.43406	0.00006	I	*Kepler*	
	56021.69718	0.00011	I	*Kepler*	
	56040.07918	0.00011	II	*Kepler*	
	56064.96051	0.00014	I	*Kepler*	
	56083.34247	0.00009	II	*Kepler*	
	56108.22411	0.00021	I	*Kepler*	
	56151.48712	0.00014	I	*Kepler*	
	56169.86905	0.00937	II	*Kepler*	

Times of minima:					
Star name	Time of min. HJD 2400000+	Error	Type	Filter	Rem.
KIC 8378922	56194.75053	0.00011	I	*Kepler*	
	56213.13228	0.00012	II	*Kepler*	
	56256.39533	0.00016	II	*Kepler*	
	56281.27725	0.00011	I	*Kepler*	
	56299.65863	0.00010	II	*Kepler*	
	56324.54045	0.00020	I	*Kepler*	
	56342.92203	0.00011	II	*Kepler*	
	56367.80360	0.00014	I	*Kepler*	
	56386.18541	0.00013	II	*Kepler*	
	56411.06697	0.00029	I	*Kepler*	
KIC 8610483	54979.11435	0.00018	II	*Kepler*	
	54993.19590	0.00012	I	*Kepler*	
	55027.91397	0.00017	II	*Kepler*	
	55041.99582	0.00007	I	*Kepler*	
	55076.71334	0.00021	II	*Kepler*	
	55090.79515	0.00014	I	*Kepler*	
	55125.51268	0.00020	II	*Kepler*	
	55139.59424	0.00015	I	*Kepler*	
	55174.31172	0.00020	II	*Kepler*	
	55188.39387	0.00012	I	*Kepler*	
	55223.11134	0.00027	II	*Kepler*	
	55237.19288	0.00019	I	*Kepler*	
	55271.91040	0.00018	II	*Kepler*	
	55285.99261	0.00020	I	*Kepler*	
	55320.70922	0.00018	II	*Kepler*	
	55334.79185	0.00016	I	*Kepler*	
	55369.50901	0.00019	II	*Kepler*	
	55383.59097	0.00006	I	*Kepler*	
	55418.30833	0.00018	II	*Kepler*	
	55432.39064	0.00026	I	*Kepler*	
	55467.10674	0.00026	II	*Kepler*	
	55481.19033	0.00014	I	*Kepler*	
	55515.90680	0.00019	II	*Kepler*	
	55529.98911	0.00018	I	*Kepler*	
	55578.78863	0.00014	I	*Kepler*	
	55613.50558	0.00017	II	*Kepler*	
	55627.58824	0.00009	I	*Kepler*	
	55662.30479	0.00018	II	*Kepler*	
	55676.38754	0.00019	I	*Kepler*	
	55711.10417	0.00018	II	*Kepler*	
	55725.18684	0.00015	I	*Kepler*	
	55759.90356	0.00019	II	*Kepler*	
	55773.98581	0.00012	I	*Kepler*	

Times of minima:					
Star name	Time of min. HJD 2400000+	Error	Type	Filter	Rem.
KIC 8610483	55808.70286	0.00018	II	*Kepler*	
	55822.78575	0.00006	I	*Kepler*	
	55857.50199	0.00021	II	*Kepler*	
	55871.58490	0.00012	I	*Kepler*	
	55906.30173	0.00026	II	*Kepler*	
	55920.38415	0.00020	I	*Kepler*	
	55955.10031	0.00731	II	*Kepler*	
	55969.18329	0.00011	I	*Kepler*	
	56003.90024	0.00023	II	*Kepler*	
	56017.98293	0.00016	I	*Kepler*	
	56052.69900	0.00028	II	*Kepler*	
	56066.78247	0.00006	I	*Kepler*	
	56101.49863	0.00216	II	*Kepler*	
	56115.58146	0.00007	I	*Kepler*	
	56150.29732	0.00022	II	*Kepler*	
	56164.38107	0.00012	I	*Kepler*	
	56199.09692	0.00020	II	*Kepler*	
	56213.18063	0.00007	I	*Kepler*	
	56261.97970	0.00008	I	*Kepler*	
	56296.69567	0.00016	II	*Kepler*	
	56345.49529	0.00019	II	*Kepler*	
	56359.57875	0.00015	I	*Kepler*	
	56394.29463	0.00028	II	*Kepler*	
	56408.37779	0.00024	I	*Kepler*	
KIC 12217907	54979.59790	0.00011	I	*Kepler*	
	54993.91307	0.00032	II	*Kepler*	
	55022.80262	0.00010	I	*Kepler*	
	55037.11743	0.00030	II	*Kepler*	
	55066.00721	0.00017	I	*Kepler*	
	55080.32264	0.00036	II	*Kepler*	
	55109.21177	0.00014	I	*Kepler*	
	55123.52771	0.00078	II	*Kepler*	
	55152.41615	0.00018	I	*Kepler*	
	55166.73097	0.00021	II	*Kepler*	
	55195.62084	0.00019	I	*Kepler*	
	55209.93493	0.00053	II	*Kepler*	
	55238.82545	0.00014	I	*Kepler*	
	55253.14006	0.00025	II	*Kepler*	
	55282.03019	0.00017	I	*Kepler*	
	55296.34485	0.00031	II	*Kepler*	
	55325.23491	0.00014	I	*Kepler*	
	55339.54953	0.00037	II	*Kepler*	
	55368.43919	0.00011	I	*Kepler*	

Times of minima:					
Star name	Time of min. HJD 2400000+	Error	Type	Filter	Rem.
KIC 12217907	55382.75336	0.00030	II	*Kepler*	
	55411.64384	0.00013	I	*Kepler*	
	55425.95842	0.00039	II	*Kepler*	
	55454.84862	0.00017	I	*Kepler*	
	55469.16325	0.00037	II	*Kepler*	
	55498.05309	0.00009	I	*Kepler*	
	55512.36771	0.00038	II	*Kepler*	
	55541.25793	0.00015	I	*Kepler*	
	55584.46223	0.00008	I	*Kepler*	
	55598.77757	0.00059	II	*Kepler*	
	55627.66700	0.00013	I	*Kepler*	
	55641.98109	0.00039	II	*Kepler*	
	55670.87142	0.00012	I	*Kepler*	
	55685.18621	0.00026	II	*Kepler*	
	55714.07598	0.00015	I	*Kepler*	
	55728.39061	0.00024	II	*Kepler*	
	55757.28066	0.00011	I	*Kepler*	
	55771.59552	0.00023	II	*Kepler*	
	55800.48521	0.00014	I	*Kepler*	
	55814.80019	0.00030	II	*Kepler*	
	55843.68972	0.00018	I	*Kepler*	
	55858.00434	0.00039	II	*Kepler*	
	55886.89424	0.00016	I	*Kepler*	
	55901.20841	0.00039	II	*Kepler*	
	55930.09913	0.00013	I	*Kepler*	
	55944.41260	0.00028	II	*Kepler*	
	55973.30362	0.00010	I	*Kepler*	
	56016.50769	0.00021	I	*Kepler*	
	56030.82287	0.00024	II	*Kepler*	
	56059.71278	0.00016	I	*Kepler*	
	56074.02721	0.00038	II	*Kepler*	
	56102.91721	0.00011	I	*Kepler*	
	56117.23182	0.00018	II	*Kepler*	
	56146.12179	0.00010	I	*Kepler*	
	56160.43603	0.00026	II	*Kepler*	
	56189.32643	0.00009	I	*Kepler*	
	56203.64252	0.00042	II	*Kepler*	
	56232.53102	0.00013	I	*Kepler*	
	56275.73561	0.00016	I	*Kepler*	
	56290.05030	0.00019	II	*Kepler*	
	56333.25518	0.00096	II	*Kepler*	
	56362.14470	0.00018	I	*Kepler*	
	56376.45947	0.00021	II	*Kepler*	
	56405.34955	0.00008	I	*Kepler*	

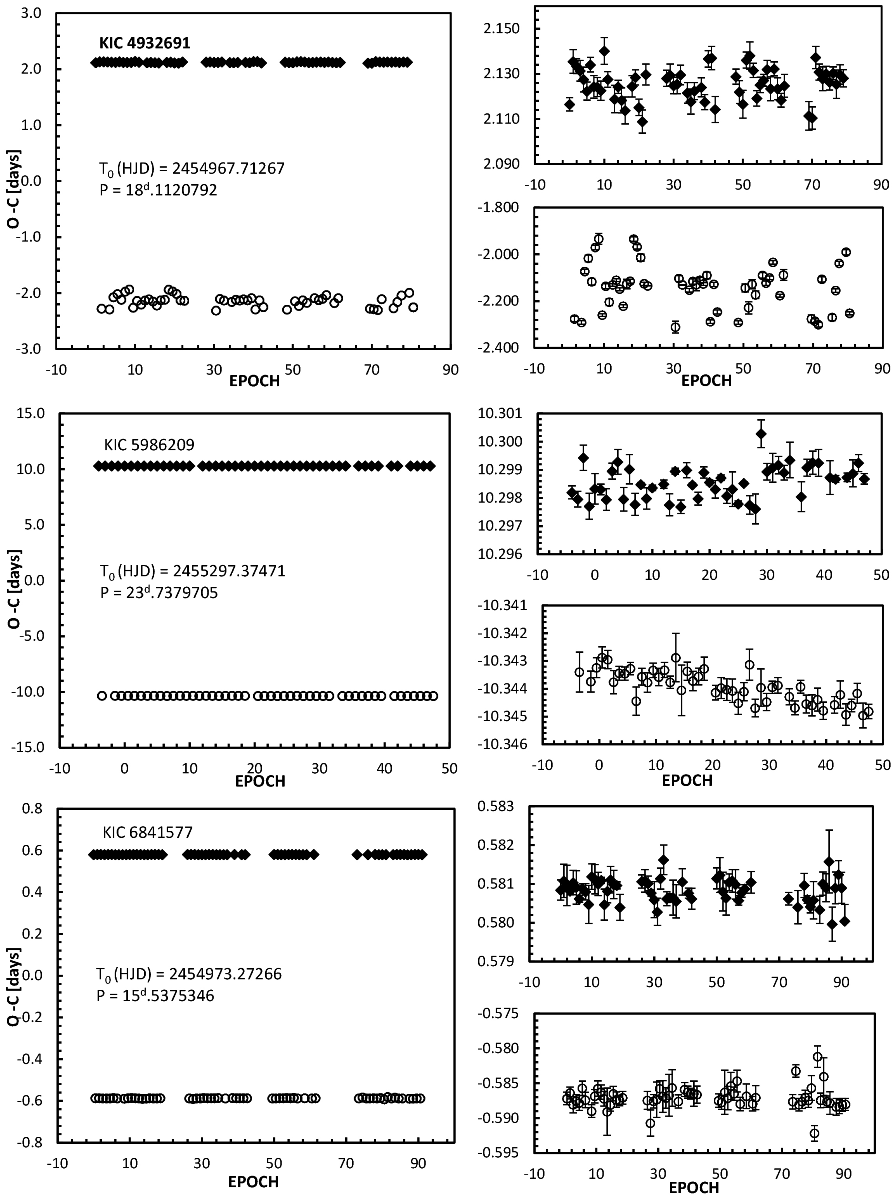

Figure 1. O−C diagrams for KIC 4932691, KIC 5986209, KIC 6841577 determined for primary and secondary minima separately (right) and together (left). The primary minima are denoted by filled symbols, the secondary minima by the symbols.

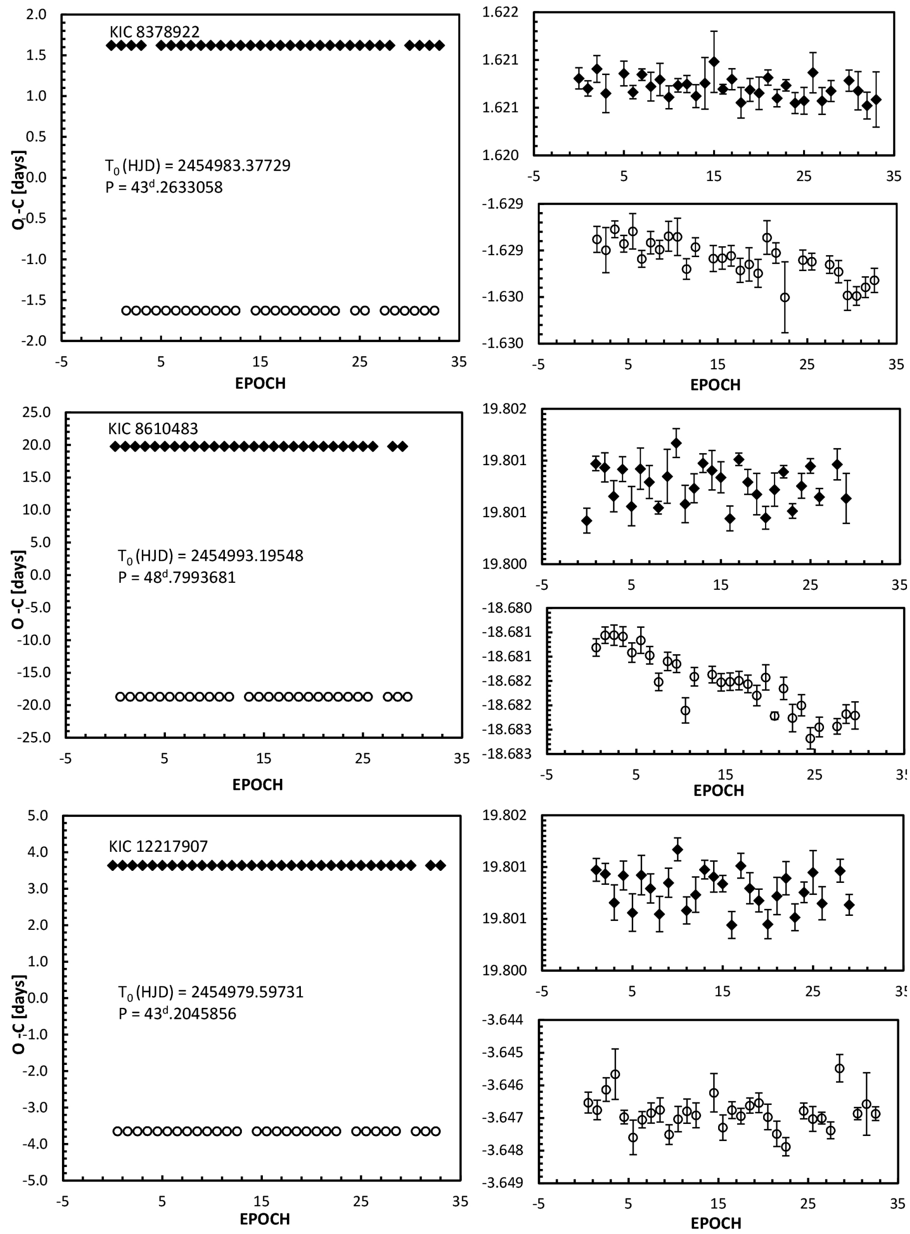

Figure 2. O−C diagrams for KIC 8378922, KIC 8610483, KIC 12217907.

COMMISSIONS G1 AND G4 OF THE IAU
INFORMATION BULLETIN ON VARIABLE STARS
Volume 63 Number 6220 DOI: 10.22444/IBVS.6220

Konkoly Observatory
Budapest
27 October 2017

HU ISSN 0374 – 0676

OAN-TNT RESULTS OF OBSERVATIONS - PHOTOELECTRIC MAXIMA OF PULSATING STARS

PEÑA, J. H.[1,2,3]; RENTERIA, A.[1,2]; PIÑA, D. S.[1,2]; VILLARREAL, C.[1,2]; CALDERON, J.[1,2]; PANI, A.[3]; HUEPA, H.[3]; STUDENTS FROM THE LATIN AMERICAN SCHOOL OF OBSERVATIONAL ASTRONOMY (ESAOBELA) 16 AND 17 AS WELL AS THE STUDENTS FROM THE ADVANCED OBSERVATIONAL COURSES (AOA) 15, AND 16 AT FACULTAD DE CIENCIAS, UNAM AND STUDENTS OF THE WORKSHOP IN OBSERVATIONAL ASTRONOMY (TAO)

[1] Instituto de Astronomía, Apartado Postal 70-264, México D.F. 04510, México, jhpena@astro.unam.mx

[2] Facultad de Ciencias, Universidad Nacional Autónoma de México, México D.F., México.

[3] Observatorio Astronómico Nacional, Tonantzintla, México.

In this second compilation of OAN-TNT results, photoelectric and CCD observations of 10 variable stars obtained from 2016 to January 2017, are presented giving 72 maxima of pulsating stars. The observations were made at both the Observatorio Astronómico Nacional at Tonantzintla (TNT) and San Pedro Mártir (SPM), both belonging to Universidad Nacional Autónoma de México (UNAM). The CCD reduction was done with AstroImageJ (Collins & Kielkopf 2012) and the photoelectric observations were reduced using a classical procedure (see Peña et al., 2016 for details). All times of maxima are heliocentric and were determined with a fifth grade polynomial fitting to the light curve. The epoch values and period to determine the O-C were taken from GCVS (Samus et al., 2017) and are given in days. The star BO Lyn was not listed in this source so its values were taken from Peña et al. (2016). The values in column O-C are determined without incorporation of nonlinear terms. The errors were determined from the RMS error of the residuals evaluated for the times of maxima and are about 0.016 day. The accuracy of each point is given by the exposure time and varies between 3 min for the 1-meter telescope and 1 min for the smaller telescopes. It may seem contradictory to give a longer integration time to the larger aperture telescope. However, this is done since the mounting of the smaller telescopes is of an altazimuth type, which does not allow long integration times. For the 1-meter telescope there were around 40,000 counts, and for the 10-inch telescope there were 11,000 counts, enough to secure high precision. The photoelectric measurements and all the light curves can be requested for inspection.

In Table 1, the stellar coordinates refer to epoch 2000 and the V values are given in magnitudes. All information about telescopes, photometers and filters is specified in the Table remarks. In Table 2 the following quantities are listed: Column 1 is the ID, column 2 the time in HJD, in column 3, N gives the number of data points in each run, column 4 Δt is the time span in days of the run, column 5 the telescope, column 6 the filter used, column 7 detector, column 8 the O-C value, and finally column 9 gives the observers and reducers. Observers and reducers are specified in the remarks at the end of the Table.

Table 1: Characteristics of the observed stars

Star	RA (2000)	DEC (2000)	V (mag)	SpTyp	T_0 (d)	P (d)	Observatory
GP And	00 55 18	+23 09 49.36	10.79	A3	2433861.438	0.07868270	TNT & SPM
RV Ari	02 15 07	+18 04 27.90	11.61	A	2435017.5124	0.093128264	TNT
V367 Cam	04 40 55	+53 38 06.45	10.80	F3VI			TNT
AD CMi	07 52 47	+01 35 50.50	9.38	F3III	2442429.458	0.12297443	TNT & SPM
RR Gem	07 21 33	+30 52 59.46	11.92	A8	2441357.205	0.03973106	TNT
KZ Hya	10 50 54	−25 21 14.00	10.06	B9III	2442516.158	0.059510421	TNT & SPM
EH Lib	14 58 55	−00 56 53.05	9.38	F0	2433438.608	0.088413245	TNT
SZ Lyn	08 09 35	+44 28 17.61	9.43	F2	2438124.398	0.120534920	TNT
BO Lyn	08 43 01	+40 59 51.78	11.49	A5-A8	2457412.8196	0.093357995	TNT & SPM
AE UMa	09 36 53	+44 04 00.39	11.35	A9	2435604.338	0.086017055	TNT

Table 2: Times of maxima of pulsating stars

ID	HJD−2450000	N	Δt (d)	Telescope	Fil	Detector	O−C	Observers/Reducers
GP And	7713.7160	145	0.2074	1M	V	1001	0.0070	DSP/DSP
	7713.7949						0.0072	
	7731.2073	35	0.072	84	y	phot	0.0307	DSP/DSP
	7731.7343	31	0.0701	1M	G	8300	0.0069	TAO/CVR
	7732.6793	59	0.1096	1M	G	8300	0.0077	TAO/CVR
RV Ari	7732.7919	100	0.1059	m1	V	1001		TAO/JHP,ARL
	7733.8260	116	0.1290	m1	V	1001		TAO/JHP,ARL
	7736.7160	160	0.1519	m1	V	1001		TAO/JHP,ARL
	7736.8068							
V367 Cam	7732.7775	185	0.165	m2	G	ST8		TAO/JCC
	7768.7170	155	0.1355	m2	V	1001		TAO/JCC
	7776.7329	170	0.176	1M	V	1001		ESAOBELA17/JCC
	7776.8535							
	7772.7204	169	0.136	m1	V	1001		ESAOBELA17/JCC
	7773.7927	61	0.0839	m1	V	1001		ESAOBELA17/JCC
	7767.7426	164	0.1695	me	V	1001		ESAOBELA17/ARL,JCC
	7768.8225	115	0.09132	me	V	1001		ESAOBELA17/ARL,JCC
AD CMi	7400.8690	48	0.01	84	y	phot	−0.0002	AAS,JGT/JHP
	7409.8501	179	0.14	m2	V	1001	0.0037	ESAOBELA16/DSP
	7430.7541	130	0.13	m2	V	1001	0.0020	ESAOBELA16/DSP
RR Gem	7772.6941	182	0.2460	m2	G	ST8	−0.1929	ESAOBELA17/JHP
	7777.8590	53	0.0640	m2	G	ST8	−0.1931	ESAOBELA17/JHP
KZ Hya	7399.9693	41	0.08	84	y	phot	0.0166	ASS,JGT/DSP
	7411.8755	87	0.09	m1	G	ST8	0.0207	ESAOBELA16/DSP
	7412.8265	113	0.07	m2	V	1001	0.0195	ESAOBELA16/DSP
	7459.8400	82	0.10	m2	V	1001	0.0198	AOA16/DSP
	7459.8989						0.0192	
	7460.7921	52	0.06	m2	V	1001	0.0197	AOA16/DSP
	7470.7894	154	0.13	m1	V	1001	0.0193	DSP/DSP
	7470.8491						0.0194	
	7471.7419	192	0.17	m1	V	1001	0.0196	DSP/DSP
	7471.8013						0.0195	
	7471.8611						0.0198	
	7770.9547	75	0.07	m2	G	ST8	0.0140	ESAOBELA17/DSP
	7772.8602	212	0.16	m1	V	1001	0.0152	ESAOBELA17/DSP
	7772.9198						0.0152	
	7772.9791						0.0150	
	7774.8247	150	0.147	m1	V	1001	0.0158	ESAOBELA17/DSP
	7774.8858						0.0174	
	7774.9449						0.0170	
	7778.8709	89	0.09	m1	V	1001	0.0153	ESAOBELA17/DSP
	7778.9311						0.0159	
EH Lib	6753.9800	280	0.1552	m1	wo	8300	0.0035	DSP/DSP
	7459.8721	103	0.0878	m1	V	1001	0.0043	AOA16/CVR

Table 2: cont.

ID	HJD−2450000	N	Δt (d)	Telescope	Fil	Detector	O−C	Observers/Reducers
EH Lib	7460.8441	103	0.0803	m1	V	1001	0.0037	AOA16/CVR
	7481.8879	90	0.1339	m1	G	8300	0.0052	AOA16/CVR
	7481.9756						0.0045	
SZ Lyn	7730.8865	56	0.06	m1	V	1001	0.0371	TAO/ARL
	7764.8761	166	0.14	m1	G	ST8	0.0359	ESAOBELA17/ARL
	7765.8415	161	0.13	m1	G	ST8	0.0370	ESAOBELA17/ARL
	7766.8055	155	0.13	m1	V	1001	0.0367	ESAOBELA17/ARL
	7777.7738	90	0.06	me	G	ST8	0.0363	ESAOBELA17/ARL
BO Lyn	7399.9256	37	0.0790	84	v	phot		AAS,JG/JHP
	7401.9861	41	0.086	84	v	phot		AAS,JG/JHP
	7409.8305	297	0.228	m14	G	8300		ESAOBELA16/JCC
	7409.9249							
	7411.8816	266	0.123	m14	G	8300		ESAOBELA16/JCC
	7412.7273	356	0.165	m14	G	8300		ESAOBELA16/JCC
	7412.8212							
	7425.7953	469	0.227	m2				AAS,JG/
	7425.8890							
	7770.8271	161	0.1268	m1	V	1001		ESAOBELA17/CVR
	7774.8653	148	0.1424	m2	G	ST8		ESAOBELA17/CVR
	7776.8271	130	0.1367	m2	G	ST8		ESAOBELA17/CVR
	7775.7983	106	0.1081	me	G	8300		ESAOBELA17/JCC
AE UMa	7480.7170			1M	G	8300	0.0055	JG/ARL
	7480.7995						0.0020	
	7776.7838	290	0.23	m1	V	1001	0.0015	ESAOBELA17/DSP
	7776.8661						−0.0021	
	7776.9566						0.0023	
	7778.8489			me	G	8300	0.0023	ESAOBELA17/DSP

Remarks:

1. Telescope	2. Detector	3. Filter
1M - 1m telescope	ST8 - CCD camera ST-8	V - V-filter in UBV system
me - 10" Meade telescope equatorial		
m1 - 10" Meade telescope	1001 - CCD camera ST-1001	G - green in RGB set
m2 - 10" Meade telescope	8300 - CCD camera ST-8300	y - y-filter in *uvby* system
c11 - 11" Celestron telescope	phot - *uvby* photometer	wo - without filter
84 - 0.84m telescope	e2v2 - CCD camera e2v-4290	

AAS: A. A. Soni
OTA: O. Trejo
ARL: A. Rentería
JHP: J. H. Peña
CVR: C. Villarreal
AP: A. Pani
DSP: D. S. Piña
JGT: J. Guillen

ESAOBELA16: Rojas, Cesar; Chacón, Melissa; Osorio, Mabel; Escobar, Amalia; Osorto, Ramón; Rodríguez, Andrea; Gómez, Jorge; Valera, Víctor; Rodríguez, Alexis; Aguilar, Jamie; Arango, Rafael; Agudelo, Malory.
ESAOBELA17: Ramirez, Vanesa; Rodríguez, Mariana; Vargas, Stephany; Castellón, Cindy; Salgado, Ricardo; Mata, Joaquin; Santa Cruz, Raúl; Chipana, Karol; Gonzales, Lisseth; Rodríguez, Reina; De la Fuente, Diana.
TAO: Lenis, Yessica; Palacio, Karla; Montes, Daniela; Rojas, Carolina; Cutiva, Alejandra; Deras, Dan; Miriam, Rojas; Sanchez, Javier; Hernández, Érika.
AOA16: Juarez, Karen; Lozano, Karen; Padilla, Artemio; Velázquez, Roberto; Santillan, Priscila.
AO17: Calderón, Jossette; García, Diego; González, Erik; Paredes, Jesús.

Acknowledgments: We would like to thank the staff of the observatories for their assistance in securing the observations, A. Díaz, C. Guzmán, F. Ruíz, E. Colorado and F. Angeles for technical support. This work was partially supported by IAU and DGAPA through PE113016 and IN106615. Typing and proofreading were done by J. Orta and J. Miller, respectively.

References:

Collins, K., Kielkopf, J., 2012, `http://ascl.net/1309.001`

Peña, J. H., Villarreal, C., Piña, D. S., et al., 2016, *RevMexAA*, **52**, 385

Samus N. N., Kazarovets E. V., Durlevich O.V., Kireeva N. N., Pastukhova E. N., 2017, *Astronomy Reports*, **61**, 80 DOI

COMMISSIONS G1 AND G4 OF THE IAU
INFORMATION BULLETIN ON VARIABLE STARS
Volume 63 Number 6221 DOI: 10.22444/IBVS.6221

Konkoly Observatory
Budapest
14 November 2017

HU ISSN 0374 – 0676

DETECTION OF SHORT-PERIODIC OSCILLATIONS IN UW Vir

MKRTICHIAN, D. E.[1]; GUNSRIWIWAT, K.[2]; AWIPHAN, S[1]; KOMONJINDA, S.[2]; REICHART, D. E.[3]; HAISLIP, J. B.[3]; KOUPRIANOV, V. V.[3]; IVARSEN, K. M.[3]; CRAIN, J. A.[3]; FOSTER, A. C.[3]; POSHYACHINDA, S.[1]

[1] National Astronomical Research Institute of Thailand (NARIT) 260 Moo 4, T. Donkaew, A. Maerim, Chiangmai, 50180 Thailand

[2] Department of Physics and Materials Science, Faculty of Science, Chiang Mai University, Muang, 50200 Chiang Mai, Thailand.

[3] University of North Carolina 269 Phillips Hall, CB 3255 Chapel Hill, NC 27599

Mkrtichian et al. (2002, 2004) introduced a new class of semi-detached Algol-type systems which has mass-accreting pulsating primary components, so called oEA stars. The oEA stars generally lie inside the instability strip after the first high-mass transfer stage and the pulsational characteristics of primary components are similar to characteristics of classical δ Scuti type stars, while the evolutionary status of pulsating components is different. These stars are promising targets for asteroseismic studies as their pulsation properties can be changed by the mass-accretion. Our report is a part of the "**Thai Sky Survey for oEA Stars**" (THASSOS) project initiated at the National Astronomical Institute of Thailand (NARIT) for detection of new oEA stars and studying their oscillation spectra.

UW Vir is a semi-detached Algol-type eclipsing binary systems with P = 1.8107646 d orbital period. The coordinates are RA = $13^{h}15^{m}20\overset{s}{.}7355$, DEC= $-17°28'16\overset{''}{.}924$. The general properties of physical parameters in the binary system were determined by Brancewicz and Dworak (1980). Qian (2000) studied the changes in orbital periods of UW Vir by O–C observations. The O–C curves represented the periodic variations superimposed on upward parabolic segments with periods of 45.9 years. The components of upward curving parabolic variations in UW Vir showed secular period increase with rates of $+1.73 \times 10^{-6}$ d/yr respectively. The secular period increase in UW Vir indicated that the mass transfer occurs from the less to the more massive component which is consistent with their semi-detached configurations. In addition, the periodic changes of the orbital periods of UW Vir also caused by the light-time effects due to the existence of the third body. 12 nights of new photometric observation for UW Vir were acquired from 13 May

Table 1: Pulsation frequencies and amplitudes.

Frequency (c/d)	Amplitude (mag)
$f_1 = 28.78482 \pm 0.00006$	0.0054 ± 0.0006
$f_2 = 46.9010 \pm 0.0001$	0.0030 ± 0.0006

2014 to 14 March 2017. During the first season of observation of this target, 11 night were taken with the 0.6-meter Thai Southern Hemisphere Telescope (TST) PROMPT8 at Cerro Tololo Inter-American Observatory (CTIO) equipped with an Apogee Alta E42 CCD camera. 6 s exposure times through Johnson B filter were used. For the last night, 15 s exposure through Johnson B filter were obtained from the 0.7 m telescope at Gao Mei Gu Observatory (GMO) in China.

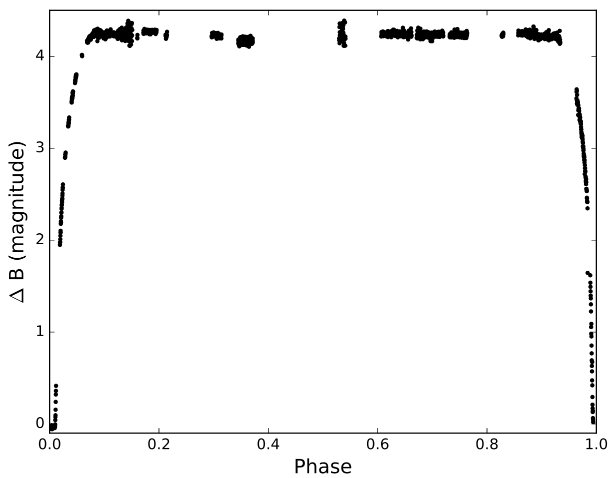

Figure 1. The light curve of UW Vir with the period of 1.8107646 days.

All stars in the field of view were reduced by SExtractor code (Bertin & Arnouts, 1996) and with Python codes written for differential photometry. These pipeline codes were developed for reduction of CCD data coming from the Thai Robotic Telescope (TRT) network. USNOA2 0675-12506346 (TYC 6120-50-1; RA = $13^h14^m47^s.27$, DEC= $-17°30'56''.4$ V=13.2) was used as a comparison star. Phased differential light curve folded according to $HJD = 2452501.1080 + (E \cdot 1.8107646)$ is plotted in Figure 1.

To extract the pulsation variation in the primary component, we omitted all data at primary minimum within phase interval of 0.93–1.07. The oscillation frequencies were analysed after removal of slow orbital variations in out-of-eclipse parts of light curves, using low-order polynomial fits. Residual light curves are shown in Figure 2. After subtracting the orbital variations, the residual data were analysed for the frequencies of pulsation using the Discrete Fourier Transforms (DFT) algorithm realized in the PERIOD04 software (Lenz and Breger, 2005). The signal pre-whitening technique was also used for consecutive detection of signals in the data.

As a result, we detached two pulsational frequencies, amplitudes and phases periodic signals. The periodograms of two the consecutive steps of the DFT analysis are illustrated in Figure 3 from top to bottom in the order as they were performed. The frequencies and amplitude in Table 1 are numbered in the order of successive pre-whitening. The second frequency at 46.9010 c/d is questionable, it has a S/N = 3.75 compared to mean noise in the frequency domain of interest 20-70 c/d and should be checked by further observations.

In summary, we discovered a short-period pulsational oscillations in a primary component of a semi-detached Algol-type binary system, UW Vir. We conclude that UW

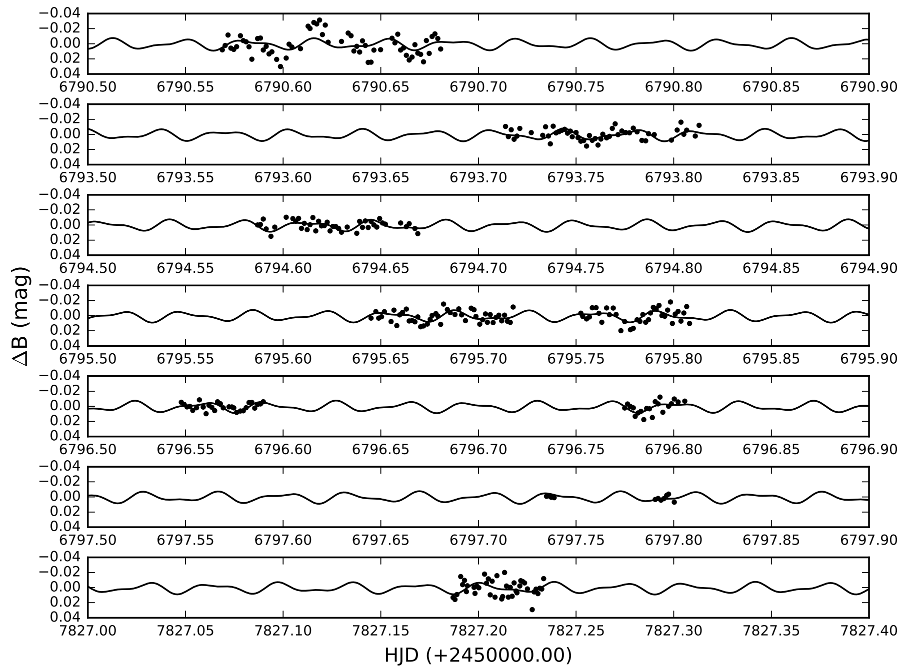

Figure 2. The nightly residual light variations of UW Vir (dots). Solid line is a two-frequency fit to the data.

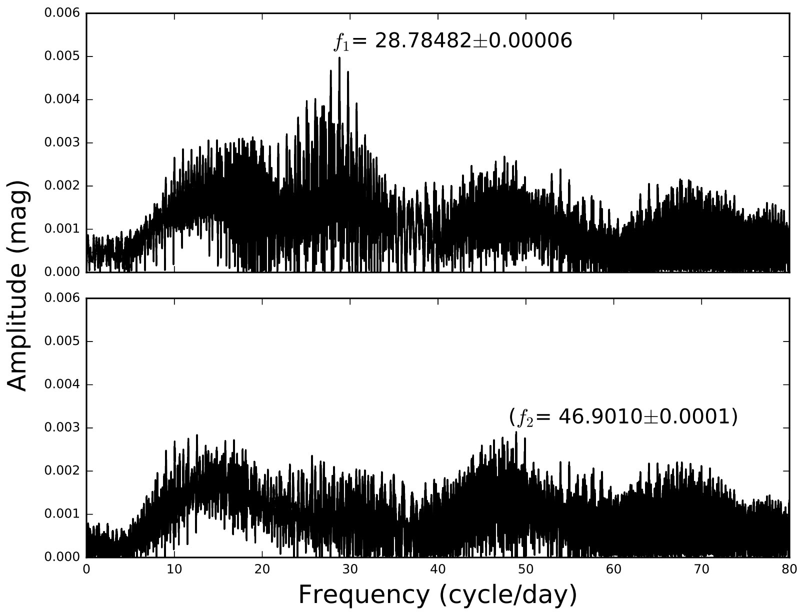

Figure 3. The consecutive steps of DFT analysis of the residual light curve of UW Vir. The top panel shows the DFT of original residual data, bottom panel shows DFT spectrum after removing the dominant frequency of 28.78 c/d.

Vir is a new member of oEA group exhibiting the low-amplitude pulsations of primary component at the dominant frequency $f_1 = 28.78482 c/d$. We would like to mention, that with an ecliptic latitude of –8.8 degrees UW Vir will be potentially observable with the TESS mission, so more pulsation components could be resolved with a short-cadence observations.

Acknowledgements: We acknowledge this work as part of the research activity supported by Graduate School at Chiang Mai University and the National Astronomical Research Institute of Thailand (NARIT), Ministry of Science and Technology of Thailand.

References:

Bertin, E. & Arnouts, S. 1996, *A&AS*, **117**, 393 DOI
Brancewicz, H.K., Dworak, T.Z., 1980, *Acta Astronomica*, **30**, 501
Qian, S., 2000, *A&AS*, **146**, 377 DOI
Lenz, P., Breger M., 2005, Communications in Asteroseismology, 146, 53 DOI
Mkrtichian, D. et al., 2002, *ASP Conf. Ser.*, **259**, 96
Mkrtichian, D.E., Kusakin, A.V., Rodriguez, E., et al., 2004, *A&A*, **419**, 1015 DOI

COMMISSIONS G1 AND G4 OF THE IAU
INFORMATION BULLETIN ON VARIABLE STARS
Volume 63 Number 6222 DOI: 10.22444/IBVS.6222

Konkoly Observatory
Budapest
14 November 2017

HU ISSN 0374 – 0676

14 YEARS OF PHOTOMETRIC MONITORING OF MM Dra AND A SUSPECTED VARIABLE IN THE FIELD OF BLAZAR 1ES 1959+650

HICKS, S.[1]; LANEY, C.D.[1]; CARINI, M.T.[1]; RICHARDSON, W.N.[1,2]; ANTONIUK, K.[3]; PIT, N.[3]

[1] Department of Physics and Astronomy, Western Kentucky University, 1906 College St., USA, email: mike.carini@wku.edu

[2] University of Virginia

[3] Crimean Astrophysical Observatory

1 Introduction

Photometric monitoring of blazars is almost always carried out using the techniques of CCD differential photometry. This requires the availability of several stable, calibrated comparison stars in the same field of view as the blazar. During the course of our long term monitoring program of selected blazars, we have found that two previously published comparison stars for the blazar 1ES 1959+650, identified as star 3 and star 5 in the sequence of Villata et al. (1998), are variable.

Lee et al. (2000) identified star 5 (RA2000=$19^{h}59^{m}44\overset{s}{.}84$, DEC2000=$+65^{\circ}10'7\overset{''}{.}4$) as an W UMa-type eclipsing binary known as MM Dra and initially estimated its period at 0.2644 days. A subsequent study by Bachev et al. (2011) refined the period of MM Dra to 0.26548±0.00001 days and noted the presence of the O'Connell effect. Star 3 (RA2000=$19^{h}59^{m}34\overset{s}{.}5$, DEC2000=$65^{\circ}06'19\overset{''}{.}5$) was first identified as possibly variable by Doroshenko et al. (2007). Pace et al. (2013) also noted the possibility that his source was variable, though the nature of variability remained undetermined. In this paper, we present the results of 14 years of photometric monitoring of both stars with the telescopes of the WKU (Western Kentucky University) BCK (Bell, Crimea, Kitt Peak) network (McGruder, et al. 2015). Observations were obtained primarily in the R_C band, with intensive intra-night monitoring in the V and I_C bands also undertaken on several occasions.

2 Data

Observations were obtained using Western Kentucky University's BCK telescope network, which includes the 0.6 meter telescope at the Bell Observatory, located 12 miles SW of Bowling Green, Kentucky; the 1.3m Robotically Controlled Telescope (RCT) at Kitt Peak National Observatory (KPNO), and the 1.3m AZT-11 telescope at the Crimean Astrophysical Observatory (CRAO). The 0.6 meter Bell Observatory telescope was equipped with a thermoelectrically cooled 1024 × 1024 KAF 1000 CCD with Apogee Ap6ep electronics and a 10' × 10' field of view. The 1.3 meter Robotically Controlled Telescope

(RCT) at Kitt Peak, Arizona was equipped with a 2048 × 2048 pixel SITe CCD with a 9.6' × 9.6' field of view and cooled using a Cryotiger (cryogenic) compressor. The 1.3 meter AZT 11 telescope at the Crimean Astrophysical Observatory in Crimea, Ukraine was equipped with a thermoelectrically cooled FLI IMG1001E camera with 1024 × 1024 CCD with a 10' × 10' field of view. Observations fall into two categories: long-term nightly observations spanning 14 years for each target and short-term continuous observations spanning a few hours on select nights to detect and characterize any short term, intra-night variability.

2.1 Long Term Monitoring

Long term monitoring of both stars was undertaken at all three observatories of the BCK network. An observation log is shown in Tables 1 and 2. A finder chart showing the location of MM Dra, star 3 and the photometric comparisons stars used is displayed in Figure 1.

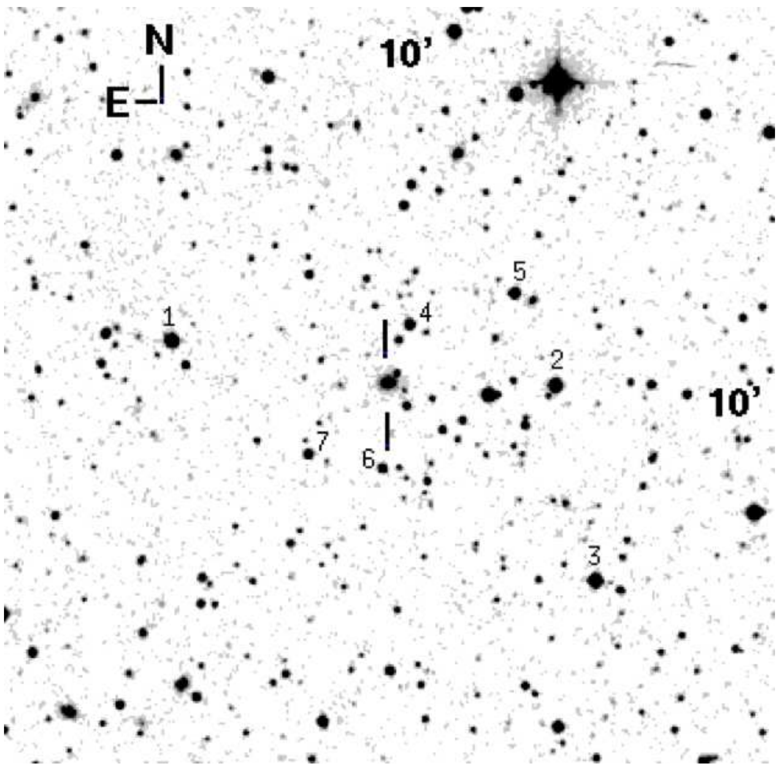

Figure 1. Finding chart for 1ES 1959+650, showing MM Dra (star 5) and star 3 from https://www.lsw.uni-heidelberg.de/projects/extragalactic/charts/1959+650.html

2.2 RCT Observations

The RCT observations were obtained in the R band with three consecutive exposures taken each night the source was observed from 2007 through 2014. Exposure times ranged from 90 seconds to 180 seconds; the exposure time was based upon the brightness level of the blazar since the original intent of the observations was to monitor the blazar. Each of the three exposures was flat fielded and bias corrected using IRAF. Differential aperture

Table 1: Table1. Observing log for MM Dra.

Year	Observatory	Filter	Number of observations
2001	Bell	R	21
2002	Bell	R	3
2003	Bell	R	18
2004	Bell	R	39
2005	Bell	R	57
2006	Bell	R	87
2007	Bell	R	36
2007	RCT	R	12
2008	Bell	R	3
2008	RCT	R	3
2009	Bell	R	24
2010	RCT	R	57
2010	CRAO	R	138
2011	RCT	R	192
2011	CRAO	R	42
2012	Bell	R	6
2012	RCT	R	96
2012	CRAO	R	93
2013	Bell	R	33
2013	RCT	R	153
2013	CRAO	R	24
2014	RCT	R	78

Table 2: Observing log for star 3.

Year	Observatory	Filter	Number of observations
2001	Bell	R	6
2003	Bell	R	3
2004	Bell	R	12
2005	Bell	R	9
2006	Bell	R	63
2007	Bell	R	39
2007	RCT	R	12
2008	RCT	R	3
2009	Bell	R	15
2010	RCT	R	57
2010	CRAO	R	141
2011	RCT	R	162
2011	CRAO	R	51
2012	Bell	R	6
2012	RCT	R	96
2012	CRAO	R	105
2013	Bell	R	84
2013	RCT	R	153
2013	CRAO	R	24
2014	RCT	R	78

photometry with a 5" aperture was performed on each exposure with respect to stars 1, 2, and 4 (Villata et al. 1998) to determine the R band magnitudes for MM Dra and Star 3 using the IRAF apphot package. The average of the magnitudes obtained from each of the three exposures was taken to determine final magnitudes for star 3 and MM Dra for each nightly observation.

2.3 Bell and CRAO Observations

The R band observations obtained at the Bell Observatory had exposure times ranging from 180 to 300 seconds, with three consecutive exposures obtained each night the blazar field was observed from 2001 through 2014. Three consecutive 180-second R band exposures were obtained using the Crimean telescope on each night it was observed. All exposures were flat fielded, dark subtracted and bias corrected using IRAF. Aperture photometry was used to extract magnitudes for MM Dra and Star 3 as described above for RCT observations.

2.4 Intranight observations

Continuous R, V, and/or I band exposures were obtained on several nights at the Bell Observatory. Each observing sequence lasted three to five hours. A log of these observations is presented in Table 3. Exposures were bias, dark, and flat field corrected and aperture photometry was used to extract magnitudes for MM Dra and star 3 as described above.

Table 3: Observing log for Bell Observatory sequences

UT Date	Filter	Exposure length (sec)	Duration (hours)
2003-09-16	V & I	180	4
2003-11-04	V & I	240	4
2003-11-14	V & I	240	3
2003-11-22	R	240	3
2004-09-22	R	180	7
2005-09-07	R	240	6
2005-09-10	R	240	4

3 Results

3.1 MM Dra

The light curve of MM Dra is presented in Figure 2. Data from the Bell Observatory are in blue, data from the RCT in orange and data from CRAO in purple. The total variability amplitude is 0.53 magnitudes. The phase curve, based on the period of 0.26547863d derived as described below, is shown in Figure 3.

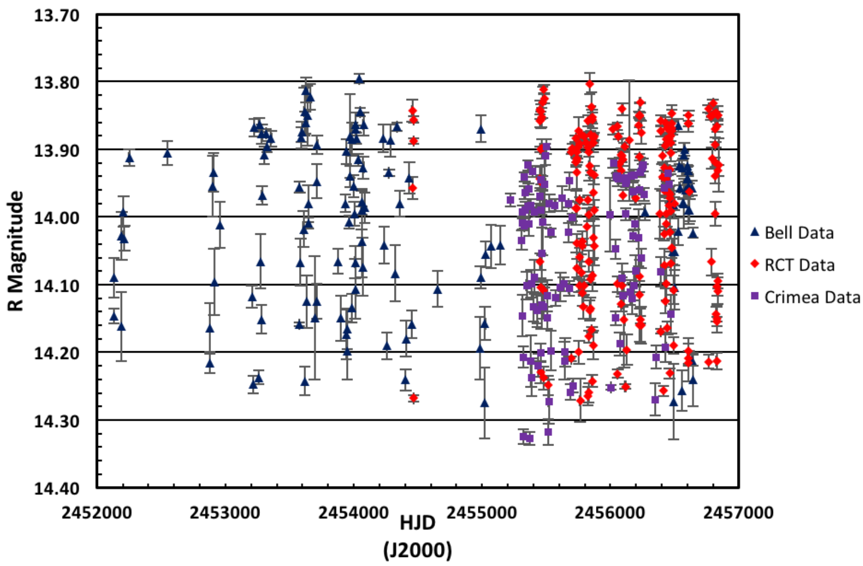

Figure 2. The long term light curve of MM Dra from 2000-2014.

A systematic analysis of the available data gives a period of 0.26547863± 0.0000003 days. Approximate determinations were made using full and quick Fourier methods together with phase binning, but the final value was refined by breaking the data into 1000-day blocks and minimizing phase shifts between blocks. Fourier fitting to the resulting light curve showed that a 6th order fit included only highly significant terms – higher order terms were not significant (less than 2 sigma). Systematic shifts were found in the R data from the three telescopes, with RCT data 0.011± 0.002 brighter and Crimea data 0.029 ± 0.008 fainter than Bell data. It was readily apparent that spurious points remained in the data, and in the end a 0.1 mag error cutoff was employed after phase shifting to a common zero point. This resulted in the elimination of 9 Bell data points, 9 from Crimea and 2 from the RCT. The eliminated points from Crimea in particular deviated significantly from the mean curve. Zero point shifts were then re-determined without the deleted data. This last correction was only about 0.001 mag, and did not affect the choice of 'outliers' to be deleted.

No spectroscopy is available for MM Dra. Given the colors from Huang et al. (2015) and the mean values for nearby stars given on the HST website[1], the VRI color indices for MM Dra suggest a spectral type of approximately K4V at primary minimum, allowing for a reddening of E(B−V) = 0.06 from Burstein and Heiles (1982). The dereddened VRI color indices at primary maximum suggest a type of K2V (Fig. 4). The $V-R_C$ and $R-I_C$ intensity means are 0.646 and 0.520, respectively, while the V, R_C and I_C intensity means are 14.649, 14.003, and 13.483. The dereddened V magnitude is 14.49, which suggests a distance modulus (Mateo and Rucinski 2017) of roughly 8.9 ± 0.3 or a distance of roughly 600 pc, implying a plausible M_V for the system of 5.5.

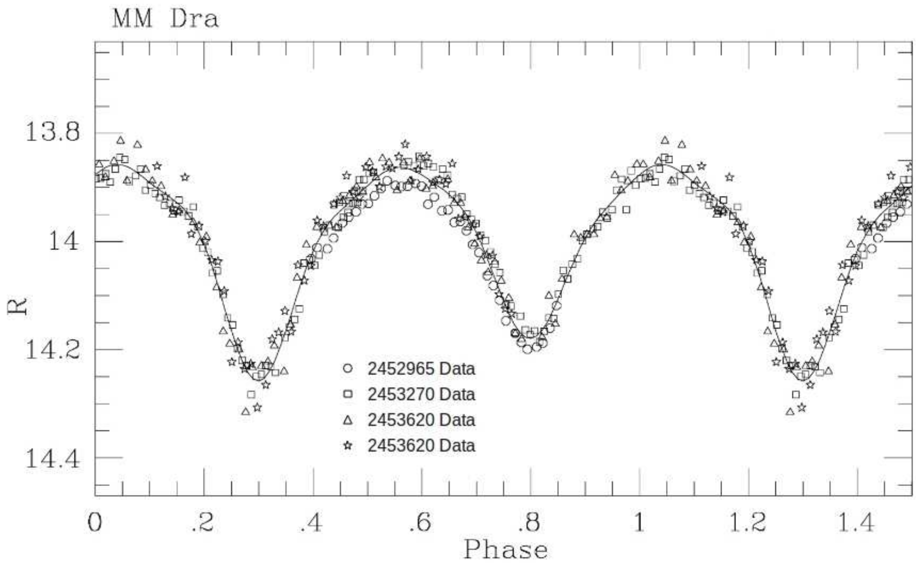

Figure 3. MM Dra data from the four nights of time series data from Bell Observatory, with different symbols for each Julian Date, showing the O'Connell effect.

MM Dra exhibits the O'Connell effect (O'Connell 1951), the phenomenon of variations in the maxima in eclipsing binary systems. Proposed theories for the explanation of asymmetrical maxima include the presence of star spots, interstellar dust and gas, and hot spots from the impact of mass transferring gas streams. (A discussion of the various models, with references, can be found in Wilsey & Beaky 2009). The MM Dra maxima vary by a range of 0.02 to 0.08 magnitude in R band, 0.02 to 0.04 magnitude in I band, and 0.06 to 0.14 magnitude in V band. Figure 3 displays the phase diagram for MM Dra plotted from continuous monitoring on three separate nights from Bell Observatory. The various marker shapes correspond to data obtained on different nights. The phase diagram shows that the observed minima converge for the four nights while a substantial

[1] http://www.stsci.edu/~inr/intrins.html

spread is observed at and near the maxima, confirming the presence of the O'Connell effect.

3.2 Star 3

The light curve for star 3 is presented in Figure 5. Data from the Bell Observatory are in blue, data from the RCT in red and data from CRAO in green. The total variability amplitude is 0.25 magnitudes. There is a noticeable dip from HJD 2455000 to HJD 2456000 of 0.2 magnitudes. The data are not sufficient to determine if this is a signature of a second object or a large star spot. A period analysis of star 3 with this 'dip interval' excluded reveals no evidence of any significant periodic components at any periods adequately sampled by our data. As with MM Dra, no spectroscopy is available for this object. VRI color indices were compared with colors given in Huang et al. (2015) and the HST compilation referred to above (Figure 4). The VRI_C color indices for star 3 most closely resemble typical values for a K7-M0 dwarf, but the separation between dwarfs and giants is not large enough to be definitive, especially given that our standards do not include any objects nearly as red as star 3. Its mean dereddened $V-R_C$ and R_C-I_C colors as determined here (0.924 and 0.904) are also very similar to those of HD146051 (0.92 and 0.92) as given for this M0.5III star in Huang et al. (2015).

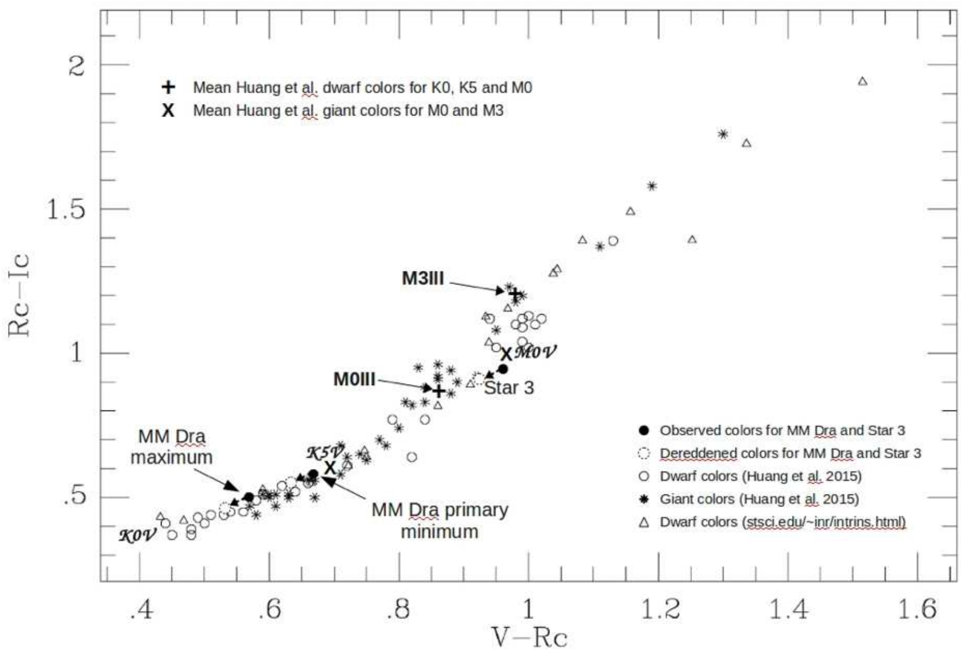

Figure 4. $V-R_C$ vs.$R-I_C$ color-color diagram showing dwarf and giant colors from Huang et al. (2015) and dwarf colors from the HST website (`http://www.stsci.edu/inr/intrins.html`), together with reddened and dereddened colors for MM Dra and star 3.

4 Conclusions

The results of 14 years of photometric monitoring of two variable stars in the field of the TeV blazar 1ES 1959+650 can be briefly summarized. For MM Dra, we confirm the eclipsing binary nature of this object and we refine the period to be 0.26547863$\pm$ 0.0000003 days. A color analysis yields an approximate spectral type of K2 (primary maximum) to K4 (primary minimum), after a small reddening correction. The presence of the O'Connell effect is also confirmed in the phase curve for this source. For star 3, a total variability amplitude of 0.23 magnitudes was found. A period analysis does not reveal the presence of any periodic modulation in its light curve and color analysis yields an approximate spectral type of very late K or early M. Further spectroscopic observations of both of these stars are needed to refine the spectral type and (for star 3) luminosity class.

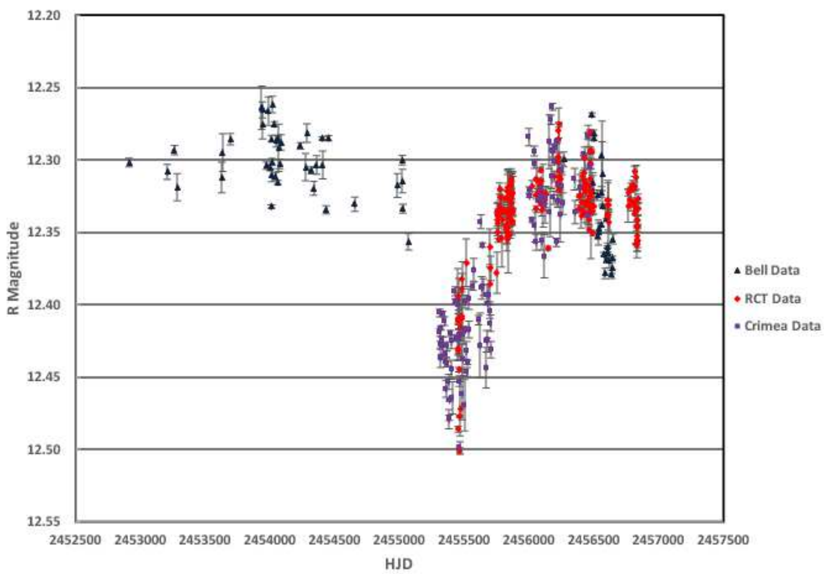

Figure 5. Long term light curve of star 3.

Acknowledgements: The authors wish to thank Kentucky NSF EPSCoR, Kentucky NASA Space Grant, Kentucky NASA EPSCoR, the department of Physics and Astronomy and the Institute for Astrophysics and Space Science at Western Kentucky University for providing support for this project. The authors gratefully acknowledge the numerous observers at WKU's Bell Observatory who gathered the observations used in this paper.

References:

Bachev, R., Semkov, E., Kacharov, N., Gupta, A. C., Ovcharov, E., Strigachev, A., 2011, *Bulgarian Astronomical Journal*, **15**, 93

Burstein, D., Heiles, C., 1982, *AJ*, **87**, 1165 DOI
Doroshenko, V. T., Sergeev, S. G. Efimov, Y. S., et al. 2007, *Astrophysics*, **50**, 40 DOI
Huang, Y., Liu, X.-W., Yuan, H.-B., Xiang, M.-S., Chen, B.-Q., 2015, *MNRAS*, **454**, 2863 DOI
Lee, H. J., Lee, M. G., Kim, S.-L., 2000, *IBVS* **4848**, 1
Mateo, N. M., Rucinski, S. R., 2017, arXiv:1708.01097v1
McGruder, C. H., Antoniuk, K., Carini, M. T., Gelderman, R., Hammond, B., Hicks, S., Laney, D., Shakhovskoy, D., Strolger, L.-G., Williams, J., 2015, *AAS*, **225**, 337.11
O'Connell, D.J.K., 1951, *Pub. Riverview College Obs.* **2**, 85
Pace, C. J., Pearson, R. L., Moody, J. W., Joner, M. D., Little B., 2013, *PASP*, **125**, 344 DOI
Villata, M., Raiteri, C. M., Lanteri, L., Sobrito, G., Cavallone, M. 1998, *A&AS*, **130**, 305 DOI
Wilsey, N. J., Beaky, M. M., 2009, *The Society for Astronomical Sciences*, **28**, 107

COMMISSIONS G1 AND G4 OF THE IAU
INFORMATION BULLETIN ON VARIABLE STARS
Volume 63 Number 6223 DOI: 10.22444/IBVS.6223

Konkoly Observatory
Budapest
23 November 2017

HU ISSN 0374 – 0676

DIRECT DISTANCE ESTIMATION AND ABSOLUTE PARAMETERS OF Z DRACONIS

TERRELL, D.[1]; NELSON, ROBERT H.[2,3]

[1] Dept. of Space Studies, Southwest Research Institute, 1050 Walnut St., Suite 300, Boulder, CO 80302, USA, e-mail: terrell@boulder.swri.edu

[2] 1393 Garvin Street, Prince George, BC, Canada, V2M 3Z1 email: bob.nelson@shaw.ca

[3] Guest investigator, Dominion Astrophysical Observatory, Herzberg Institute of Astrophysics, National Research Council of Canada

Terrell (2006) briefly discussed the early observational efforts on the Algol-type binary Z Draconis and presented differential BVR_CI_C light curves, the first published light curves obtained on a modern photometric system. Since then, the availability of the AAVSO Photometric All-Sky Survey (APASS; Henden, et al. 2012) has made it possible to place the observations on the standard (absolute) system by using APASS standards in the field of Z Dra. We present a re-reduction of the BV images of Terrell (2006) that place the data on the standard system. We also present new spectroscopic observations that yield radial velocities of the primary star and, for the first time, the secondary star, thus enabling us to measure the mass ratio accurately. The combination of standard photometry (with flux calibrations, *viz.* Wilson, et al. 2010) and radial velocities allows for the inclusion of the distance to the binary as a solution parameter, yielding a distance estimate and corresponding error that includes the correlations with other adjusted model parameters directly, rather than being an after-the-fact estimate with simplifying assumptions (*e.g.* spherical stars). This Direct Distance Estimation (DDE) approach is described in Wilson (2008) and application examples are found in Wilson & Van Hamme (2009), Vaccaro, et al. (2010), Wilson & Raichur (2011) and Vaccaro, et al. (2015).

The equipment used to make the photometric observations is described in Terrell (2006). The BV images were bias/dark subtracted and flatfielded using the ccdproc routine in IRAF (Tody, 1993), and instrumental magnitudes were measured using PSF fitting with SExtractor (Bertin & Arnouts, 1996) and PSFEx (Bertin, 2011). The instrumental magnitudes were then transformed onto the standard system using the method described in Terrell, et al. (2016). The resulting BV magnitudes are available from the IBVS web site as file 6223-t3.txt. We chose to use the BV images and not the R_CI_C images for two reasons. First APASS does not provide R_CI_C magnitudes for standards directly, and transformations from the APASS passbands ($BVg'r'i'$) to R_CI_C are still preliminary. Secondly, the DDE approach is best suited to the analysis of light curves in two passbands when solving for the surface temperatures of both stars, as we do here (*viz.* Wilson, 2008). The addition of a light curve in a third passband would allow us to add the interstellar extinction as an adjustable parameter, but the extinction towards Z

Table 1: Radial velocity observations of Z Dra.

DAO image #	Mid time (HJD–2400000)	Exposure (sec)	Phase at mid-exposure†	V_1 ($km\ s^{-1}$)	V_2 ($km\ s^{-1}$)
11-02487	55666.7962	3600	0.275	–82.9 ± 2.3	140.8 ± 5.4
11-02532	55668.8275	1097	0.772	25.6 ± 2.7	–203.3 ± 3.2
11-02569	55670.7885	3600	0.216	–82.0 ± 2.3	143.0 ± 5.9
11-02710	55676.7913	3600	0.639	14.4 ± 2.3	–189.7 ± 7.6
11-02719	55676.9429	3600	0.750	25.9 ± 2.5	–205.4 ± 3.0
11-02752	55678.8829	3600	0.180	–75.8 ± 2.4	117.9± 5.6

† Phases computed using the ephemeris parameters in Table 2.

Dra appears to be very small (Terrell, 2006), as expected for its high galactic latitude and close distance. We did perform some solutions with BVI_C light curves, both adjusting the extinction directly and by doing solutions on a grid of fixed values for the extinction, but the results were not encouraging. The likely small value of the extinction combined with the uncertainties in the I_C calibration probably play a role in the inability to measure the extinction with our data.

In April of 2011, RHN secured a total of six medium resolution (R≈10,000) spectra of Z Dra at the Dominion Astrophysical Observatory (DAO) in Victoria, British Columbia, Canada using the Cassegrain spectrograph attached to the 1.85 m Plaskett Telescope. The 21181 configuration was employed using a grating with 1800 lines/mm, blazed at 5000 Å, and giving a reciprocal linear dispersion of 10 Å/mm in the first order. The wavelengths ranged from 5000 to 5260 Å, approximately. Frame reduction was performed by software RaVeRe (Nelson 2013). See Nelson (2010) and Nelson et al. (2014) for further details. Radial velocities were determined using the Rucinski broadening functions (Rucinski, 2004, Nelson, 2010) as implemented in software Broad (Nelson, 2013; Nelson et al. 2014). A log of the spectroscopic observations is given in Table 1.

The BV light curves and the new radial velocities were analyzed simultaneously with the 2013 version of the Wilson–Devinney program (WD; Wilson & Devinney, 1971; Wilson, 1979; Wilson, 2008). Since Z Dra is a semi-detached system with the lower mass secondary filling its Roche lobe (confirmed by initial experiments with the model using a detached configuration), we employed WD mode 5 in all of our solutions. We performed fitting experiments assuming both convective and radiative envelopes for the primary star, but found that models assuming a convective envelope gave superior fits in all cases, thus our best-fit model assumes a value of 0.32 for the gravity darkening exponents of both stars and a value of 0.5 for the bolometric albedoes. Limb darkening coefficients were automatically computed at each iteration from the Van Hamme (1993) tables. Weights for the various light and velocity curves were determined automatically by WD at each iteration.

In contrast to the traditional way of analyzing photometry using independently and arbitrarily scaled light curves in several passbands, the DDE approach uses standard magnitudes and preserves the color information found in the differences between the light curves in each passband at each point in the binary orbit. With two light curves in different passbands, it is therefore possible to allow the surface temperatures of both stars to adjust in the solution, as opposed to the traditional approach where the temperature of one star is fixed at a value derived from other sources such as spectral types or colors

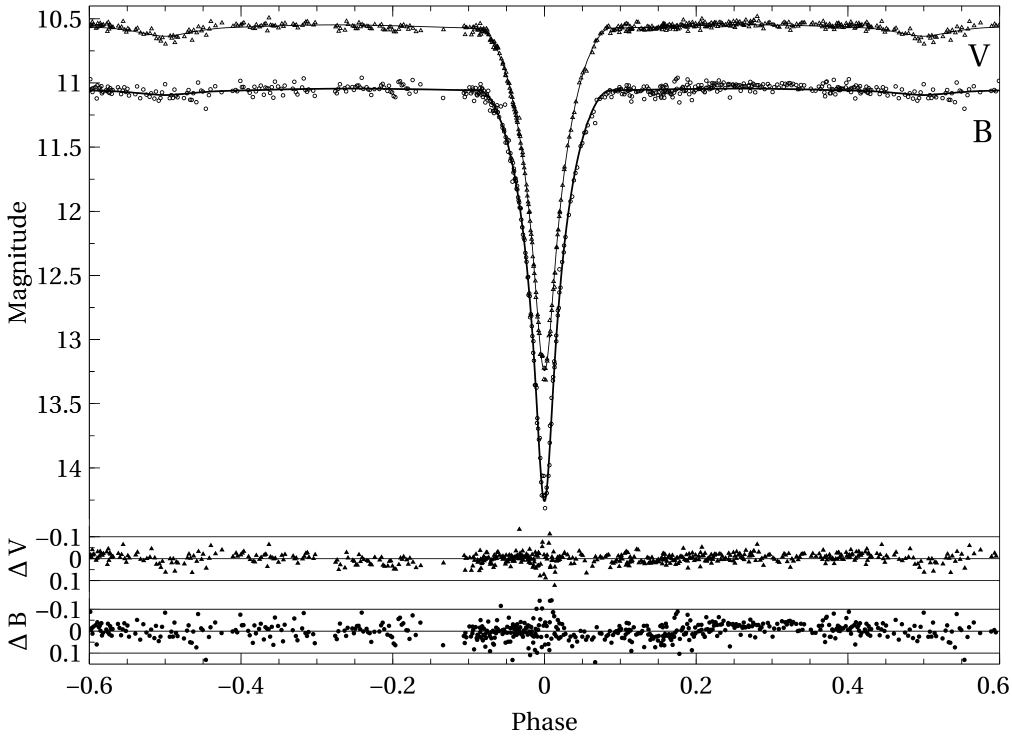

Figure 1. The fits to the B and V light curves of Z Dra. The residuals (observed - computed) from the fits are shown at the bottom.

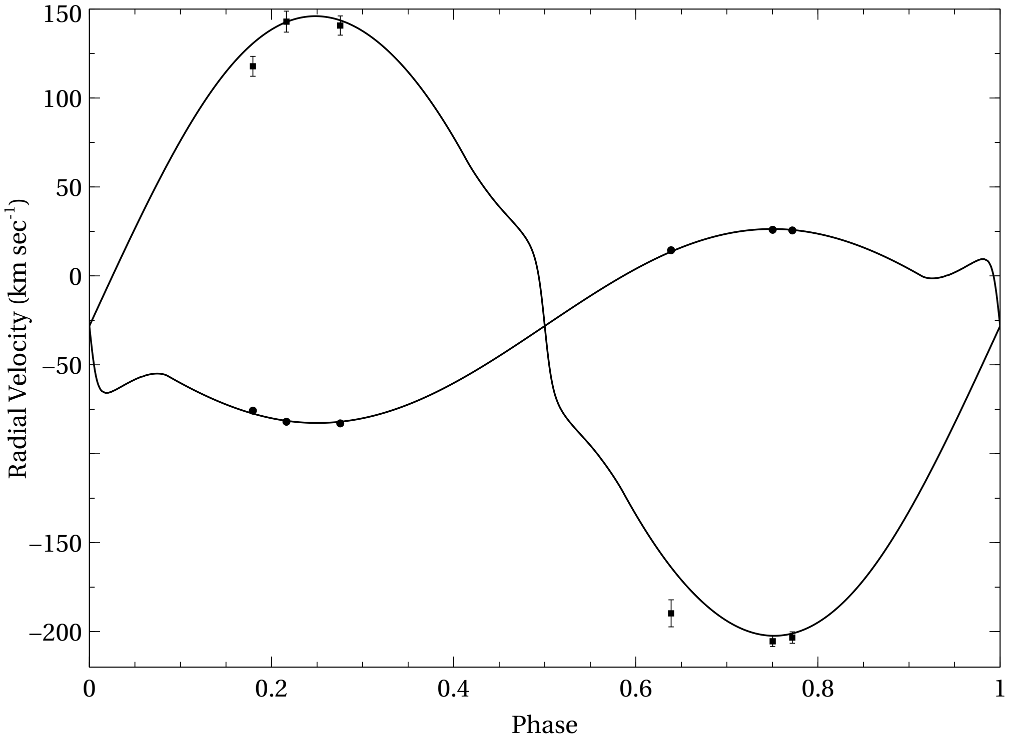

Figure 2. The fits to the radial velocity curves curves of Z Dra. The sizes of the error bars on the primary star velocities are approximately the same size as the points.

Table 2: Parameters from the light/velocity curve solution.

Parameter	Value	Std. error
a	$6.29\ R_\odot$	$0.08\ R_\odot$
V_γ	-28.2 km sec^{-1}	0.5 km sec^{-1}
i	$86\overset{\circ}{.}94$	$0\overset{\circ}{.}06$
T_1	6446 K	11 K
T_2	3936 K	14 K
q	0.304	0.002
Ω_1	4.56	0.02
Ω_2	2.475	(lobe filling constraint)
HJD_0	2453430.71668	0.00006
P	$1\overset{d}{.}3574226$	$0\overset{d}{.}00001$
$\dot{P}$	2.0×10^{-8}	1.1×10^{-8}
$log(d)^\dagger$	2.441	0.005
M_1	$1.39\ M_\odot$	$0.05\ M_\odot$
M_2	$0.42\ M_\odot$	$0.02\ M_\odot$
R_1	$1.48\ R_\odot$	$0.02\ R_\odot$
R_2	$1.77\ R_\odot$	$0.02\ R_\odot$
$L_{V,1}$	$4.0\ L_\odot$	$0.1\ L_\odot$
$L_{V,2}$	$0.134\ L_\odot$	$0.004\ L_\odot$

† Distance d to the binary in parsecs.

as, for example, in the solution for Z Dra of Terrell (2006).

Table 2 shows the adjusted parameters which includes the distance to the system in addition to the expected parameters for a semi-detached solution with light and radial velocity curves. Figure 1 shows the fits to the light curves, and Figure 2 the radial velocity fits. There are clearly small asymmetries present in the light curves, probably due to spots, and we did attempt a few fits with a single cool spot on the primary, but the improvement in the fit was marginal and the question of the uniqueness of such solutions with modest-precision light curves led us to abandon the spot fits. As noted in Terrell (2006), the derived value of $\dot{P}$ is not particularly informative given the complex period changes in the system, but it was included to allow for the change in period between the epochs of the photometric and spectroscopic observations so that they could be analyzed simultaneously. Previous studies of the eclipse timings (*viz.* Khaliullina, 2016 and references therein) conclude that a third star may be present in the system and we included third light as an adjustable parameter in our solutions, but this led to physically unrealistic (negative) values.The estimated distance to the system is 276 ± 3 pc and that compares well to the value of 283^{+19}_{-17} pc from Gaia Data Release 1 (Gaia Collaboration, et al. 2016). If there were third light in the system that was unaccounted for in the model, the distance to the system would be understimated because the system would be too bright for its actual distance. The good agreement with the distance from Gaia supports the argument that any third light in Z Dra must be negligible.

With a mass of $0.42\ M_\odot$ and a radius of $1.77\ R_\odot$, the secondary component is clearly evolved, making Z Dra a short-period Algol. Still unresolved is the nature of the period changes in the system. A period increase due to mass transfer from the lobe-filling secondary seems to be a reasonable conclusion but the somewhat periodic changes on top of that are still debated. The light time effect, the Applegate (1992) mechanism, or a combination of both, are plausible explanations at this point. Further observations, standardized photometry in particular to measure luminosity changes predicted by the Applegate mechanism, will be needed to decide between the various possibilities.

Acknowledgements: This research was made possible through the use of the AAVSO Photometric All-Sky Survey (APASS), funded by the Robert Martin Ayers Sciences Fund and U.S. National Science Foundation grant 1412587. It is a pleasure to thank the staff members at the DAO (David Bohlender, Dmitry Monin, and the late Les Saddlemyer) for their usual splendid help and assistance. Much use was made of the SIMBAD database during this research.

References:

Applegate, J.H., 1992, *ApJ*, **385**, 621 DOI
Bertin, E., 2011, *ASP Conf. Ser.* **442**, 435
Bertin, E., Arnouts, S., 1996, *A&A Suppl. Ser.*, **117**, 393 DOI
Gaia Collaboration, et al., 2016, *A&A*, **595**, A1 DOI
Henden, A. A., Levine, S. E., Terrell, D., Smith, T. C., Welch, D., 2012, *JAAVSO*, **40**, 430
Khaliullina, A.I., 2016, *Astronomy Reports*, **60**, 517 DOI
Nelson, R.H., 2010, "Spectroscopy for Eclipsing Binary Analysis" in The Alt-Az Initiative, Telescope Mirror & Instrument Developments (Collins Foundation Press, Santa Margarita, CA), R.M. Genet, J.M. Johnson and V. Wallen (eds)
Nelson, R.H., 2013, Software by Bob Nelson, `https://www.variablestarssouth.org/bob-nelson/`
Nelson, R. H., Şenavcı, H.V. Baştürk, Ö., Bahar, E., 2014, *New Astr.*, **29**, 57 DOI
Rucinski, S. M., 2004, *IAU Symp.*, **215**, 17
Terrell, D. 2006, *IBVS*, **5742**
Terrell, D. 2016, *IBVS*, **6166**
Tody, D., 1993, *ASP Conf. Ser.*, **52**, 173
Vaccaro, T.R., Terrell, D., Wilson, R.E., 2010, *ASP Conf. Ser.* **435**, 89
Van Hamme, W., 1993, *AJ*, **106**, 2096 DOI
Wilson, R.E., 1979, *ApJ*, **234**, 1054 DOI
Wilson, R.E., 2008, *ApJ*, **672**, 575 DOI
Wilson, R.E., Devinney, E.J., 1971, *ApJ*, **166**, 605 DOI
Wilson, R.E., Raichur, H., 2011, *MNRAS*, **415**, 596 DOI
Wilson, R.E., Van Hamme, W., 2009, *ApJ*, **699**, 118 DOI
Wilson, R.E., Van Hamme, W., Terrell, D., 2010, *ApJ*, **723**, 1469 DOI

COMMISSIONS G1 AND G4 OF THE IAU
INFORMATION BULLETIN ON VARIABLE STARS
Volume 63 Number 6224 DOI: 10.22444/IBVS.6224

Konkoly Observatory
Budapest
11 December 2017

HU ISSN 0374 – 0676

V500 Cyg – A CLASSICAL ALGOL

NELSON, ROBERT H.[1,2,3]

[1] Mountain Ash Observatory, 1393 Garvin Street, Prince George, BC, Canada, V2M 3Z1, bob.nelson@shaw.ca

[2] Guest investigator, Dominion Astrophysical Observatory, Herzberg Institute of Astrophysics, National Research Council of Canada

[3] Desert Blooms Observatory, Benson AZ, 31°56.454′N, 110°15.450′W

The discoverer of the variability of V500 Cyg (AN 1939.0081; TYC 2693–139–1) appears to be undocumented. The first available reference (in the GCVS and SIMBAD) is Whitney (1959) who provided revised elements, three new eclipse timings, and notes regarding a companion separated by 0.3′. Since then, there have been numerous eclipse timings published, but no light curve or analysis.

In order to rectify this lack, the author first secured, in the autumns of 2010, 2013, 2014, and 2015, a total of eight medium resolution (R ∼ 10000 on average) spectra of V500 Cyg at the Dominion Astrophysical Observatory (DAO) in Victoria, British Columbia, Canada using the Cassegrain spectrograph attached to the 1.85 m Plaskett Telescope. He used the 21181 configuration and a grating with 1800 lines/mm, blazed at 5000 Å, and giving a reciprocal linear dispersion of 10 Å/mm in the first order. The wavelengths ranged from 5000 to 5260 Å, approximately. A log of observations is given in Table 1 and an eclipse timing diagram, in Figure 9 later in the paper. The latter was used to derive the following elements, used for both radial velocity (RV) and photometric phasing:

$$\text{JD (Hel) Min I} = 2457914.8640(49) + 0.9242233(2)E \quad (1)$$

where the quantities in brackets are the standard errors of the preceding quantities in units of the last digit.

Frame reduction was performed by software RaVeRe (Nelson 2013). See Nelson (2010) and Nelson et al. (2014) for further details. The normalized spectra are reproduced in Fig. 1, sorted by phase (the vertical scale is arbitrary). Note towards the right the strong neutral iron lines (at 5167.487 and 5171.595 Å) and the strong neutral magnesium triplet (at 5167.33, 5172.68, and 5183.61 Å).

Radial velocities were determined using the Rucinski broadening functions (Rucinski, 2004, Nelson, 2010) as implemented in software Broad25 (Nelson, 2013). See Nelson et al. (2014) for further details. An Excel worksheet with built-in macros (written by him) was used to do the necessary radial velocity conversions to geocentric and back to heliocentric values (Nelson 2014). The resulting RV determinations are also presented in Table 1 (along with standard errors in units of the last digits, enclosed in brackets). The mean rms errors for RV_1 and RV_2 are 3.8 and 11.3 km/s, respectively, and the overall

Table 1: Log of DAO observations

DAO Image #	Mid Time (HJD−2400000)	Exposure (sec)	Phase at Mid−exp	V1 (km/s)	V2 (km/s)
10-17392	55474.7097	3600	0.778	77.4 (2.8)	−215.3 (14.8)
13-09641	56544.8987	3600	0.712	74.1 (4.2)	−225.2 (10.8)
12-24533	56912.6665	3600	0.633	42.3 (1.3)	−196.3 (0.9)
15-13142	57295.8492	3600	0.232	−123.5 (4.8)	159.9 (10.7)
15-13144	57295.8926	3600	0.279	−126.1 (5.0)	174.0 (16.5)
15-13176	57296.8290	3600	0.292	−120.4 (4.6)	163.3 (13.5)
15-13238	57298.7427	3600	0.363	−94.6 (2.6)	104.2 (7.0)
15-13265	57299.6278	3600	0.321	−113.8 (4.8)	134.6 (16.3)

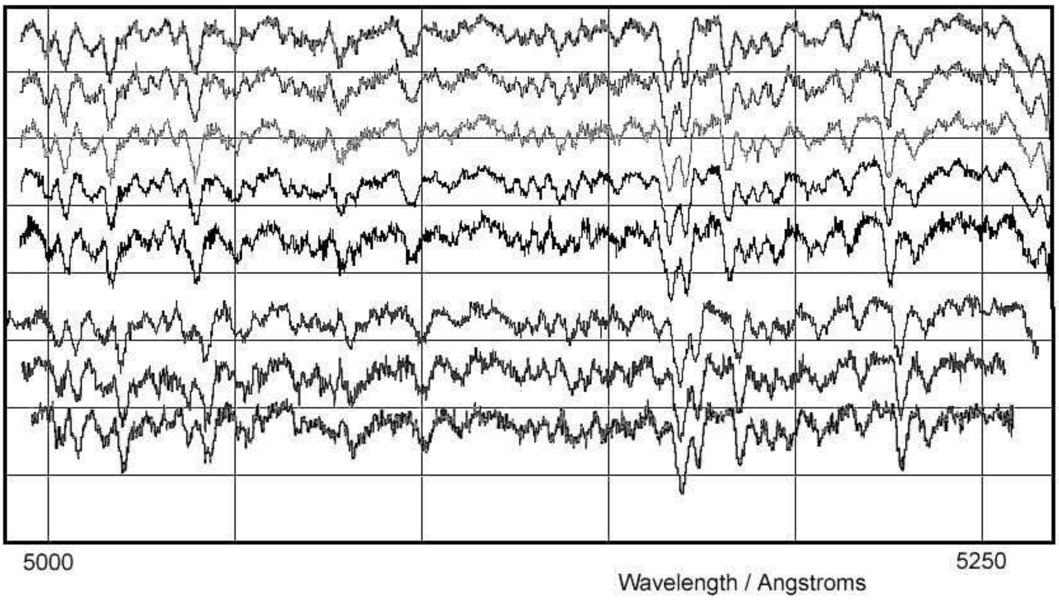

Figure 1. V500 Cyg spectra at phases 0.232, 0.279, 0.292, 0.321, 0.363, 0.633, 0.712, 0.778 (from top to bottom). Each has been shifted vertically for clarity. The vertical scale is arbitrary.

rms deviation from the (sinusoidal) curves of best fit is 9.7 km/s. The best fit yielded the values $K_1 = 98.6(2.7)$ km/s, $K_2 = 196.8(4.9)$ km/s and $V_\gamma = -129.1(2.2)$ km/s, and thus a mass ratio $q_{\rm sp} = K_1/K_2 = M_2/M_1 = 0.50(1)$.

Representative broadening functions, at phases 0.232 and 0.778 are depicted in Figs. 2 and 3, respectively (the vertical scale is arbitrary). Smoothing by a Gaussian filter is routinely done in order to centroid the peak values for determining the radial velocities.

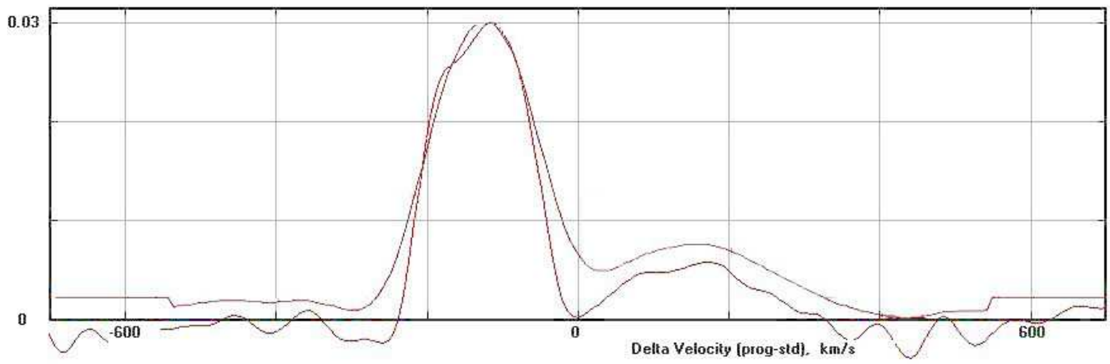

Figure 2. Broadening functions at phase 0.232–smoothed and unsmoothed.

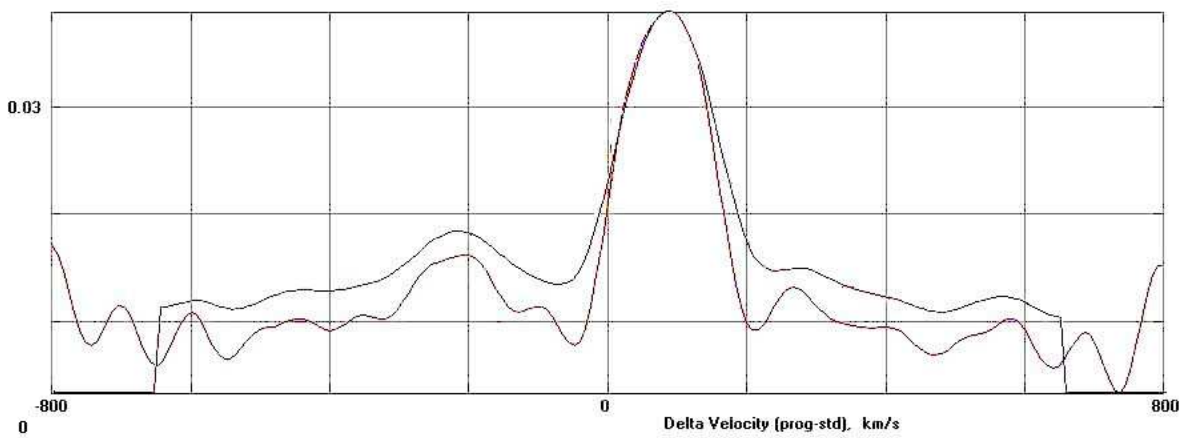

Figure 3. Broadening functions at phase 0.778–smoothed and unsmoothed.

During twelve nights in 2017, May 24 -June 14, the author took a total of 198 frames in V, 197 in $R_{\rm C}$ (Cousins) and 199 in the $I_{\rm C}$ (Cousins) band at the newly-opened Desert Blooms Observatory, jointly owned by the author and Dr. Kevin B. Alton. Hosted at the San Pedro Observatory complex located near Benson, Arizona, the telescope is operated remotely. It consists of a Software Bisque Taurus 400 equatorial fork mount, a Meade LX-200 40 cm Schmidt-Cassegrain optical assembly operating at f/7, a SBIG STT-1603 XME CCD camera (with a field of view $11' \times 18'$), and a filter wheel with the usual B, V, $R_{\rm C}$, and $I_{\rm C}$ filters. For unattended operation, automatic focusing is required owing to the large temperature changes throughout the night (typically +35 °C to +10 °C in late spring).

Table 2: Details of variable, comparison and check stars.

Object	GSC	RA (J2000)	Dec (J2000)	V (mag)	$B-V$ (mag)
Variable	2693-0139	$20^h24^m40^s.379$	$+34°57'05''.40$	11.91 (16)	+0.25 (21)
Comparison	2693-0828	$20^h24^m39^s$	$+34°56'59''$	11.20 (7)	0.22 (9)
Check 1	2693-1630	$20^h24^m28^s$	$+34°55'45''$	12.1	0.34
Check 2	2693-1230	$20^h24^m16^s.9528$	$+34°58'39''.642$	10.91 (7)	+0.73 (14)

Table 3: Limb darkening values from Van Hamme (1993).

Band	x_1	x_2	y_1	y_2
Bol	0.640	0.628	0.242	0.150
V	0.707	0.797	0.278	0.015
R_C	0.634	0.753	0.286	0.104
I_C	0.550	0.667	0.276	0.150

Standard reductions were then applied (see Nelson et al. 2014 for more details). The variable, comparison, and check stars are listed in Table 2. The coordinates and magnitudes for V500 Cyg, the comparison, and check 2 are from the Tycho Catalogue, Hog et al. (2000), with magnitudes converted to standard Johnson values using relations due to Henden (2001). For check 1, the V magnitude is from the GSC catalogue and the approximate $B-V$ value is from our photometry. Quantities in brackets are standard errors, in units of the last digit.

The author used the 2003 version of the Wilson-Devinney (WD) light curve and radial velocity analysis program with Kurucz atmospheres (Wilson & Devinney, 1971, Kurucz, 1979, Wilson, 1990, Kallrath & Milone, 1998, Wilson, 1998) as implemented in the Windows front-end software WDwint (Nelson, 2013) to analyze the data. To get started, the spectral type F4–5 (taken from SIMBAD, no reference given; main sequence assumed) was adopted. Interpolated tables from Flower (1996) gave a temperature $T_1 = 6610 \pm 134$ K (T_1 is the mean of the two sub-classes) and $\log g = 4.348 \pm 0.014$. (The quoted errors refer to one spectral sub-class.) An interpolation program by Terrell (1994, available from Nelson 2013) gave the Van Hamme (1993) limb darkening values; and finally, a logarithmic (LD = 2) law for the limb darkening coefficients was selected, appropriate for temperatures < 8500 K (ibid.). The limb darkening coefficients are listed in Table 3. (The values for the second star are based on the later-determined temperature of 4584 K and assumed spectral type of K5.) Convective envelopes for both stars were used, appropriate for cooler stars (hence values gravity exponent $g = 0.32$ and albedo $A = 0.500$ were used for each).

From the GCVS 4 designation (EA/SD) and from the shape of the light curve, mode 5 (classical Algol) mode was used. Later on, mode 2 (detached) was tried but DC adjustments required decreases in potential 2 below the critical value; consequently mode 2 was abandoned.

Convergence using differential corrections (DC) and the method of multiple subsets was reached in a small number of iterations. (See Wilson & Devinney, 1971 and Kallrath & Milone 1998 for an explanation of the method.) The subsets were: (a, V_γ, i, L_1), (T_2, q), and (T_2, Ω_1). However, the visual fit was poor in that the calculated depth of the secondary minimum was too deep. Therefore, in LC mode temperature T_2 was lowered until the fit was satisfactory. Then, switching back to DC mode, temperature T_2 was held constant while all other parameters allowed to vary. Once convergence was obtained, T_2 was again allowed to vary with only small changes indicated.

Table 4: Wilson–Devinney parameters.

WD Quantity	Value	Revised values	error	Unit
Temperature, T_1	6610	6610	[fixed]	K
Temperature, T_2	4584	4594	200	K
$q = m_2/m_1$	0.557	0.554	0.005	—
Potential, Ω_1	3.703	3.690	0.015	—
Potential, Ω_2	2.984	2.978	[fixed]	
Inclination, i	83.06	83.38	0.10	degrees
Semi-major axis a	5.38	5.38	0.12	solar radii
V_γ	−25.3	−25.3	2.6	km/s
Fill-out, f_1	−2.186	−2.177	0.001	
$L_1/(L_1 + L_2)$ (V)	0.8664	0.8664	0.0003	—
$L_1/(L_1 + L_2)$ (R_C	0.8245	0.8245	0.0004	—
$L_1/(L_1 + L_2)$ (I_C)	0.7866	0.7866	0.0006	—
r_1 (pole)	0.3153	0.3153	0.0015	orbital radii
r_1 (point)	0.3377	0.3377	0.0022	orbital radii
r_1 (side)	0.3234	0.3234	0.0017	orbital radii
r_1 (back)	0.3317	0.3317	0.0019	orbital radii
r_2 (pole)	0.3083	0.3083	0.0007	orbital radii
r_2 (point)	0.4402	0.4402	0.0027	orbital radii
r_2 (side)	0.3220	0.3220	0.0007	orbital radii
r_2 (back)	0.3544	0.3544	0.0007	orbital radii
Phase shift	0.0011	0.0016	0.0001	—
$\Sigma\omega^2_{\rm res}$	0.06012	0.03943	—	—

Detailed reflections were tried, with the number of reflections, $n_{\rm ref} = 3$, but there was little–if any–difference in the fit from the simple treatment.

The model is presented in Table 4 (for an explanation of column 3, see below). For the most part, the error estimates are those provided by the WD routines and are known to be under-estimated; however, it is a common practice to quote these values and we do so here. Also, estimating the uncertainties in temperatures T_1 and T_2 is somewhat problematic. A common practice is to quote the temperature difference over–say–one spectral sub-class (assuming that the classification is good to one spectral sub-class, the precision being unknown in this case). In addition, various different calibrations have been made (Cox, 2000, page 388–390 and references therein, and Flower, 1996), and the variations between the various calibrations can be significant. If the classification is ± one sub-class, an uncertainty of ± 200 K to the absolute temperatures of each, would be reasonable. The modelling error in temperature T_2, relative to T_1, is indicated by the WD output to be much smaller, around 9 K.)

The light curve data and the fitted curves are depicted in Figures 4–6. The residuals (in the sense observed-calculated) are also plotted, shifted upwards by 0.25 units.

It is not clear why, in all three light curves, a few points near phase 0.03 (and all from the same night) are deviant, other than possibly due to a passing cloud which could have differentially affected the flux from one of the stars (variable, comparison) compared to the other. In response to a referee's concerns about these errant points, new modelling trials were undertaken with these points deleted. The result was slight differences in the resultant parameters at convergence; these are reported in column 3. The reader will note that, for the most part, these lie inside the estimated (one sigma) confidence intervals and are therefore not significantly different.

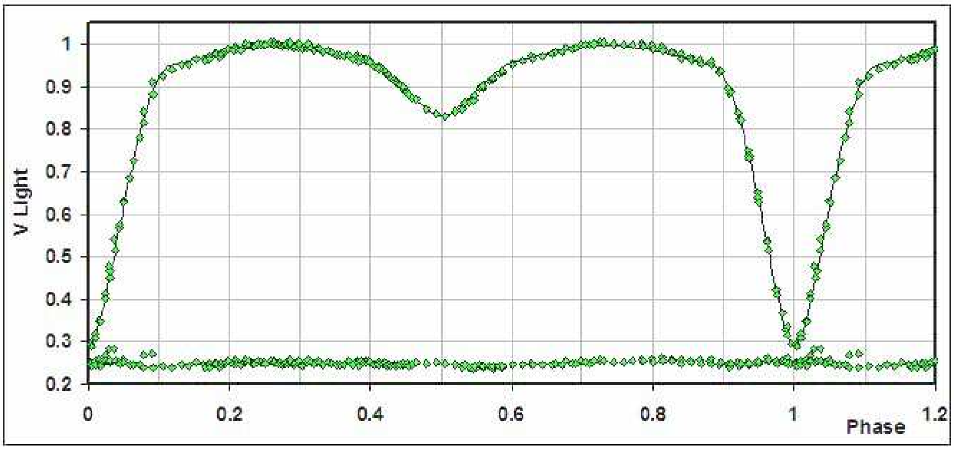

Figure 4. *V* light curves for V500 Cyg – data, WD fit, and residuals.

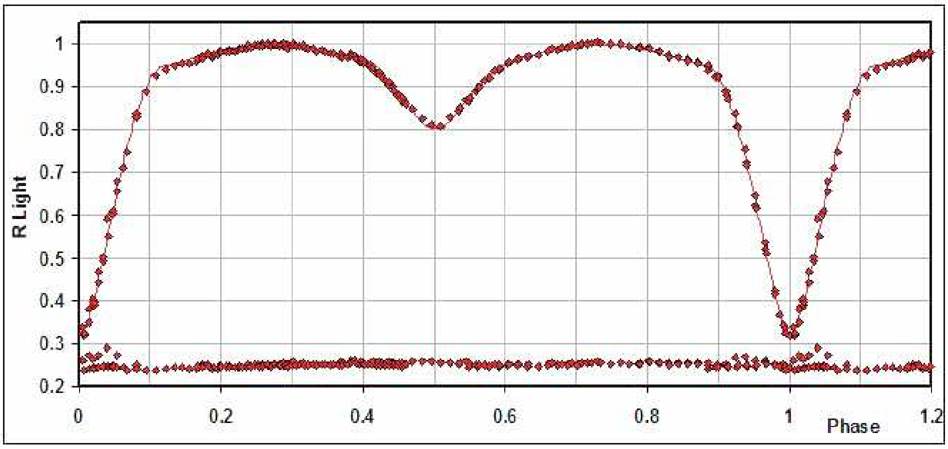

Figure 5. *R* light curves for V500 Cyg – data, WD fit, and residuals.

The radial velocities are shown in Fig. 7. A three-dimensional representation from Binary Maker 3 (Bradstreet, 1993) is shown in Fig. 8. (The crosses are the centres of mass of the individual stars and of the system as a whole. The ellipses are of the respective centres of mass.)

The WD output fundamental parameters and errors are listed in Table 5. Most of the errors are output or derived estimates from the WD routines. From Kallrath & Milone (1998), the fill-out factor is $f = (\Omega_I - \Omega)/(\Omega_I - \Omega_O)$, where Ω is the modified Kopal potential of the system, Ω_I is that of the inner Lagrangian surface, and Ω_O, that of the outer Lagrangian surface, was also calculated.

To determine the distance, the analysis proceeded as follows: first the WD routine gave the absolute bolometric magnitudes of each component; these were then converted to the absolute visual (V) magnitudes of both, $M_{V,1}$ and $M_{V,2}$, using the bolometric

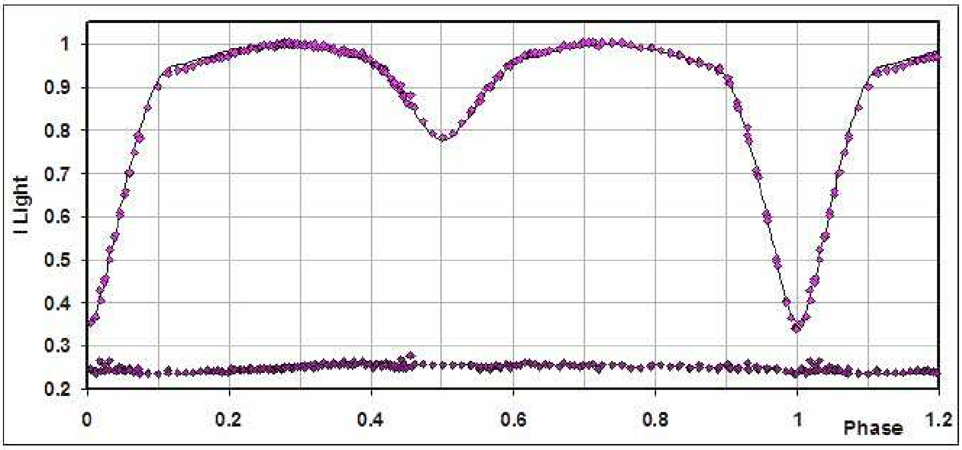

Figure 6. *I* light curves for V500 Cyg – data, WD fit, and residuals.

Table 5: Fundamental parameters.

Quantity	Value	Error	unit
Temperature, T_1	6610	200	K
Temperature, T_2	4584	200	K
Mass, m_1	1.58	0.10	M0
Mass, m_2	0.88	0.04	M0
Radius, R_1	1.74	0.01	R0
Radius, R_2	1.77	0.01	R0
$M_{\rm bol,1}$	3.00	0.02	mag
$M_{\rm bol,2}$	4.55	0.02	mag
$\log g_1$	4.15	0.01	cgs
$\log g_2$	3.88	0.01	cgs
Luminosity, L_1	5.20	0.10	L0
Luminosity, L_2	1.25	0.02	L0
Fill-out factor 1	-2.219	0.010	—
Fill-out factor 2	0	[fixed]	
Distance, r	602	27	pc

corrections BC $= -0.135$ and -0.72 for stars 1 and 2 respectively. The latter were taken from interpolated tables constructed from Cox (2000). The absolute V magnitude was then computed in the usual way, getting $M_V = 2.63 \pm 0.06$ magnitudes. The apparent magnitude in the V passband was $V = 11.93 \pm 0.02$, taken from the Tycho values (Hog et al. 2000) and converted to the Johnson magnitude 11.91 ± 0.02 using relations due to Henden (2001).

Ignoring interstellar absorption, we calculated a preliminary value for the distance $r = 717$ pc from the standard relation:

$$r = 10^{0.2(V - M_V - A_V + 5)} \text{ parsecs} \tag{2}$$

Galactic extinction was obtained from a model by Amôres & Lépine (2005). The code (available in IDL and converted by the author to a Visual Basic routine) assumes that the interstellar dust is well mixed with the gas, that the Galaxy is axisymmetric, that the gas density in the disk is a function of the Galactic radius and of the distance from the Galactic plane, and that extinction is proportional to the column density of the gas, Using Galactic coordinates of $l = 74.0787°$ and $b = -1.5709°$ (SIMBAD), and the initial distance estimate of $d = 0.717$ kpc, a value of $A_V = 0.451$ mag was determined, Further iteration of several steps resulted in final values of $A_V = 0.382$ mag and $r = 602$ pc.

The errors were assigned as follows: $\delta M_{\rm bol,1} = \delta M_{\rm bol,2} = 0.02$, $\delta \rm BC_1 = \delta BC_2 = 0.09$ (the variation of 1 spectral sub-class), $\delta V = 0.02$, $\delta A_V = 0.02$, all in magnitudes. Combining the errors rigorously (i.e., by adding the variances) yielded an estimated error in r of 27 pc.

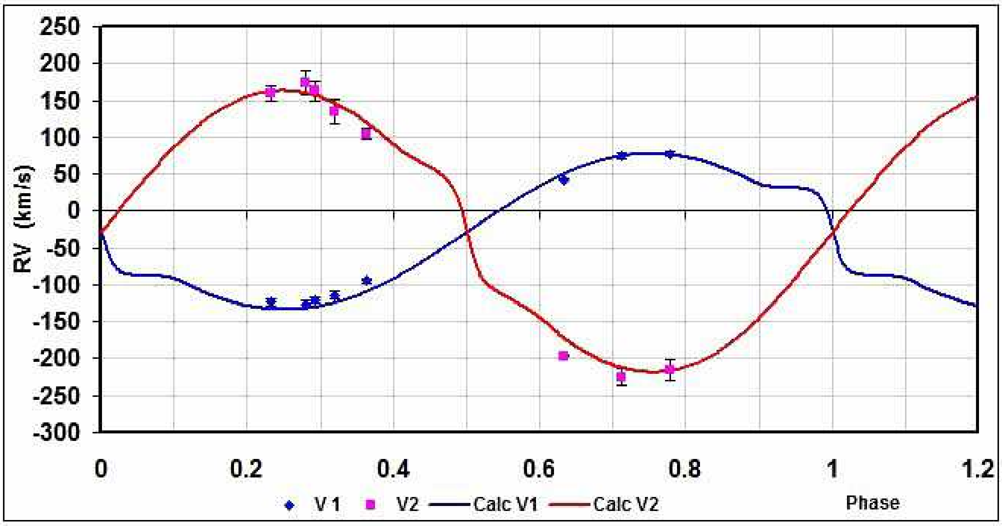

Figure 7. Radial velocity curves for V500 Cyg – data and WD fit.

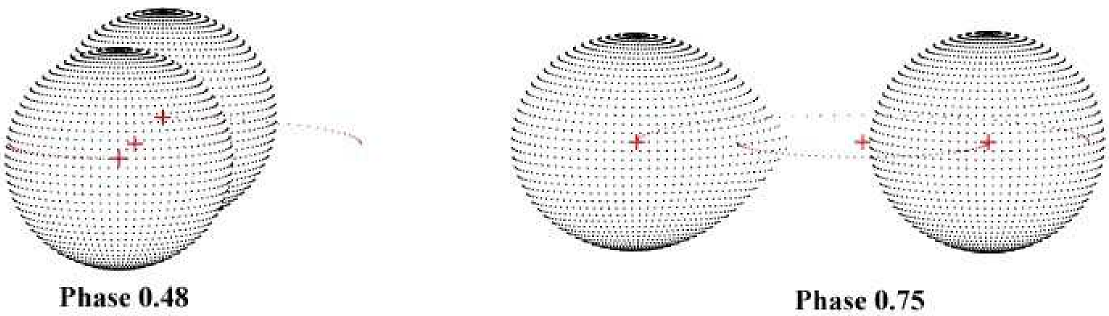

Figure 8. Binary Maker 3 representation of the system – at phases 0.48 and 0.75.

Four new times of minima emerged from the observations; these are reported in Table 6. Each is the mean of three values (one for each filter). Four methods of minimum determination, as implemented in software Minima23 (Nelson 2013), were used: the digital tracing paper method, sliding integrations (Ghedini 1982), curve fitting using five Fourier terms, and Kwee and van Woerden (Kwee & Woerden 1956, Ghedini 1982). Because, in the literature, many (or perhaps most) error estimates can be shown to be low (sometimes unrealistically so), the estimated errors were taken as double the standard deviations of the various determinations.

Table 6: New times of minima for V500 Cyg obtained in this study.

Min (Hel)−2400000	Type	Error (days)
57901.9264	I	0.0002
57908.8590	II	0.0006
57913.9397	I	0.0004
57914.8639	I	0.0009

Some comments regarding the period variation are in order. An eclipse timing difference (O–C) plot using timings from 1988 is depicted in Fig. 9. Although there is considerable scatter, a linear relation over the data collection interval (cycles 28800 to 30770 for the RVs and cycles 31420 to 31440 for the light curve data) is assumed. This yielded a weighted best-fit linear solution and ephemeris of Equation (1) above. (Standard weighting was used: pg = 0.2, vis = 0.1, and PE = CCD = 1. Two nearly identical points lying more than three standard deviations from the curve of best fit were rejected.)

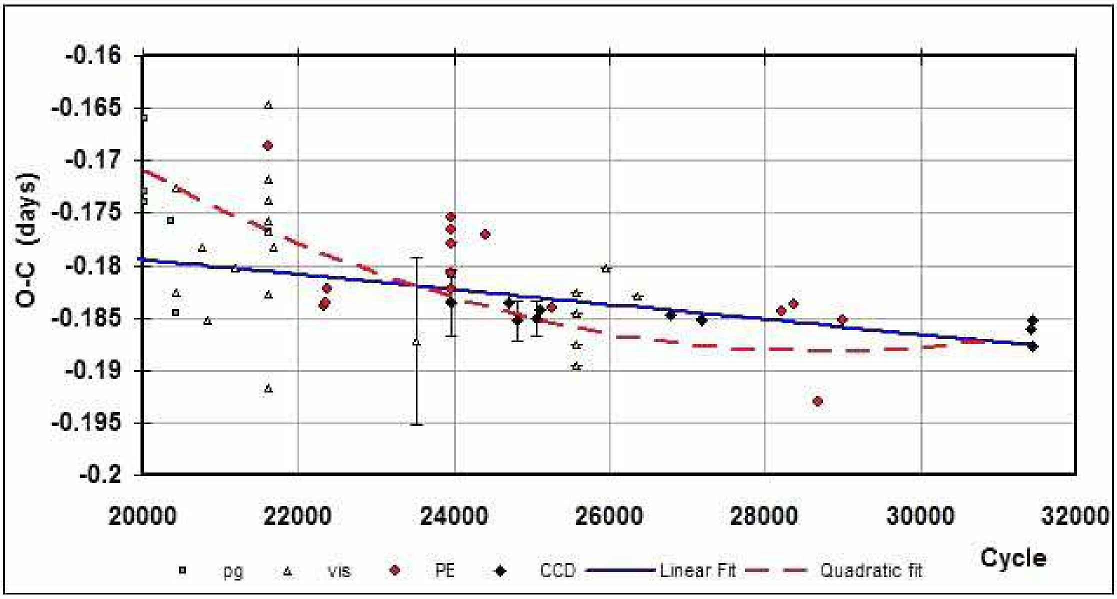

Figure 9. V500 Cyg – eclipse timing (O–C) diagram with linear (solid blue) and quadratic (dashed red) fits for points after cycle 20000 (see equation 1). (Note: pg = photographic; vis = visual; PE = photoelectric; and CCD = charge coupled device.

Also, all the available timing data since the earliest in 1935 (available online at Nelson 2016) are plotted in Fig. 10. There may well be a quadratic relation; the relevant parameters for which are given in Equation 3.

$$\text{JD (Hel) Min I} = 2457914.8651(29) + 0.9242105(5) + 2.1(2) \times 10^{-10} E^2 \qquad (3)$$

However, the quadratic relation does not fit the data since cycle 20000 particularly well (see Fig. 9) and was not used in the analysis. The period behaviour might perhaps be better explained by the light time effect (LiTE; Irwin 1952, 1959) due to a third star. However, due to the obvious scatter in the early photographic data near cycle 0, (due to Wachmann, cited in the O–C Gateway with only the ambiguous reference of AAAN

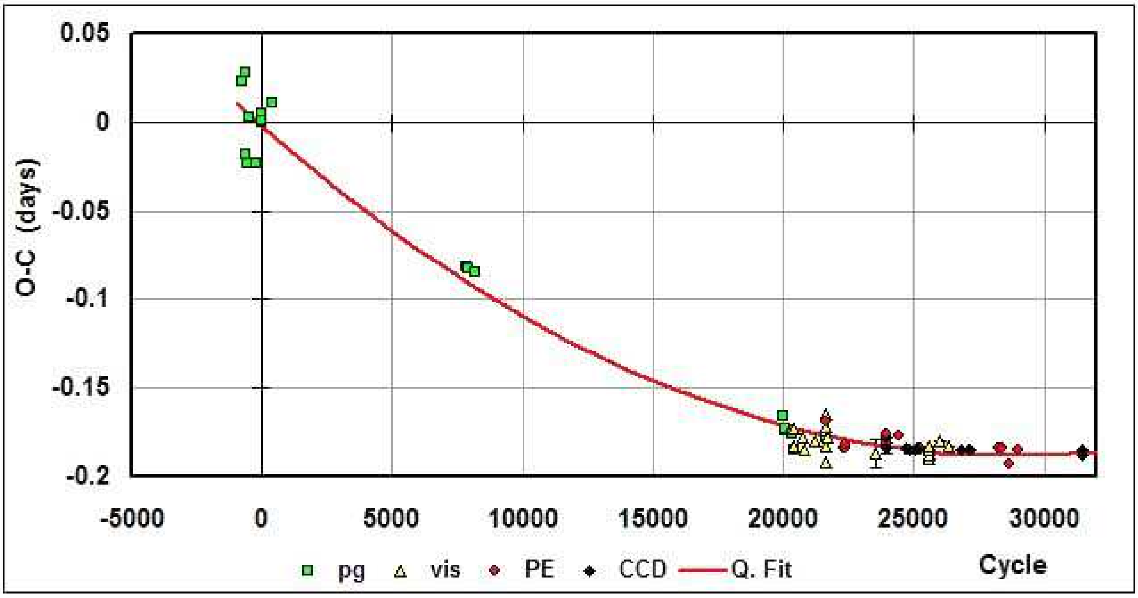

Figure 10. V500 Cyg – eclipse timing (O–C) diagram with a quadratic fit for all available points.

11.5.43), a LiTE analysis does not appear to be justified at this time. High quality data over the coming decades will be required to settle the matter. The reader is referred to Nelson et al. (2014, 2015, 2016) for further discussions on this difficulties encountered in period analysis.

Acknowledgements: It is a pleasure to thank the staff members at the DAO (Dmitry Monin, David Bohlender, and the late Les Saddlmyer) for their usual splendid help and assistance. Many thanks are also due to the San Pedro Observatory resident astronomer/technician Dean Salman for his tireless help. Much use was made of the SIMBAD database during this research.

References:

Amôres, E.B., Lépine, J.R.D., 2005, *AJ*, **130**, 659 DOI

Bradstreet, D.H., 1993, *IAUCB*, **21**, 151 DOI

Cox, A.N., ed, 2000, Allen's Astrophysical Quantities, 4th ed., (Springer, New York, NY) DOI

Flower, P.J., 1996, *ApJ*, **469**, 355 DOI

Ghedini, S., 1982, Software for Photometric Astronomy (Willmann-Bell, Inc.)

Henden, A., 2001, `http://www.tass-survey.org/tass/catalogs/tycho.old.html`

Hog, E., et al., 2000, *A&A*, **355**, L27

Irwin, J.B., 1952, *ApJ*, **116**, 211 DOI

Irwin, J.B., 1959, *AJ*, **64**, 149 DOI

Kallrath, J., Milone, E.F., 1998, Eclipsing Binary Stars–Modeling and Analysis (Springer-Verlag). DOI

Kurucz, R.L., 1979, *ApJS*, **40**, 1 DOI

Kwee, K.K. and Woerden, H., 1956, *BAN*, **12**, 327

Nelson, R.H., 2010, "Spectroscopy for Eclipsing Binary Analysis" in The Alt-Az Initiative, Telescope Mirror & Instrument Developments (Collins Foundation Press, Santa Margarita, CA), R.M. Genet, J.M. Johnson and V. Wallen (eds)

Nelson, R.H., 2013, Software by Bob Nelson,
https://www.variablestarssouth.org/bob-nelson/
Nelson, R.H., 2014, Spreadsheets, by Bob Nelson,
https://www.variablestarssouth.org/bob-nelson/
Nelson, R.H., Şenavci, H.V., Baştürk, Ö, and Bahar, E., 2014, *NewA*, **29**, 57 DOI
Nelson, R.H., Terrell, D., Milone, E.F., 2014, *NewAR*, **59**, 1 DOI
Nelson, R.H., Terrell, D., Milone, E.F., 2015, *NewAR*, **69**, 1 DOI
Nelson, R.H., Terrell, D., Milone, E.F., 2016, *NewAR*, **70**, 1 DOI
Nelson, R.H., 2016, Bob Nelson's O–C Files,
http://www.aavso.org/bob-nelsons-o-c-files
O–C Gateway, Paschke, A., http://var2.astro.cz/ocgate/
Rucinski, S. M., 2004, *IAUS*, **215**, 17
Terrell, D., 1994, Van Hamme Limb Darkening Tables, vers. 1.1.
Van Hamme, W., 1993, *AJ*, **106**, 2096 DOI
Whitney, B.S., 1959, *AJ*, **64**, 258 DOI
Wilson, R.E., and Devinney, E.J., 1971, *ApJ*, **166**, 605 DOI
Wilson, R.E., 1990, *ApJ*, **356**, 613 DOI
Wilson, R.E., 1998, Documentation of Eclipsing Binary Computer Model (available from the author)

COMMISSIONS G1 AND G4 OF THE IAU
INFORMATION BULLETIN ON VARIABLE STARS
Volume 63 Number 6225 DOI: 10.22444/IBVS.6225

Konkoly Observatory
Budapest
24 November 2017

HU ISSN 0374 – 0676

NEW CCD MINIMA TIMES FOR SELECTED ECLIPSING BINARIES

SOYDUGAN, F.; ALİÇAVUŞ, F.; ŞENYÜZ, T.; KAHRAMAN ALİÇAVUŞ, F.; PÜSKÜLLÜ, Ç.; KANVERMEZ, Ç.; SOYDUGAN, E.

Department of Physics, Faculty of Arts and Sciences, Çanakkale Onsekiz Mart University, Terzioğlu Kampüsü, TR-17020, Çanakkale, Turkey

Astrophysics Research Centre and Observatory, Çanakkale Onsekiz Mart University, Terzioğlu Kampüsü, TR-17020, Çanakkale, Turkey

Observatory and telescope:
T30: 0.3 m Cassegrain-Schmidt, T40: 0.4 m Cassegrain-Schmidt, T60: 0.6 m Ritchey-Chrétien, and T122: 1.22 m Cassegrain-Nasmyth telescopes of Çanakkale Onsekiz Mart University Observatory, Çanakkale.

Detector:	C1: STL1001E CCD camera, Peltier cooling, KAF–1001E chip, 1024×1024 pixels. C2: ST10MXE CCD camera, Peltier cooling, KAF–3200ME chip, 2174×1536 pixels. C3: Apogee ALTA U42 CCD camera, Peltier cooling, E2V CCD47–10 chip, 2048×2048 pixels. C4: Apogee ALTA U47 CCD camera, Peltier cooling, E2V CCD47–10 chip, 1024×1024 pixels.

Method of data reduction:
C-MUNIPACK software was used for the reduction process of CCD images and differantial photometry (`http://c-munipack.sourceforge.net/`).

Method of minimum determination:
The minima times of selected eclipsing binaries were computed with the Kwee–van Woerden method (Kwee & van Woerden, 1956).

Times of minima:

Star name	Time of min. HJD 2400000+	Error	Type	Filter	Rem.
EL Aqr	55831.4900	0.0003	I	*BVRI*	T122+C1
	55834.3773	0.0003	I	*BVRI*	T122+C1
	55835.3415	0.0007	II	*BVRI*	T122+C1
	55840.3969	0.0002	II	*BVRI*	T122+C1
	55853.3950	0.0002	II	*BVRI*	T122+C1
	55854.3577	0.0002	II	*BVRI*	T122+C1
HS Aqr	55780.3389	0.0004	I	*BVR*	T30+C2
	55782.4691	0.0002	I	*BVR*	T30+C2
FN Cam	56086.3767	0.0002	I	*BVR*	T60+C3
	56089.4154	0.0002	II	*BVR*	T60+C3
YY CMi	56010.3738	0.0002	I	*BVR*	T40+C4
V401 Cyg	55758.4087	0.0003	I	*BVR*	T40+C3
	55765.4025	0.0003	I	*VR*	T40+C3
	55767.4432	0.0005	II	*BVR*	T40+C3
	55779.3852	0.0003	I	*BVR*	T40+C3
	55795.4126	0.0002	II	*BVR*	T40+C3
	55809.3982	0.0002	II	*BVR*	T122+C1
	55814.3486	0.0002	I	*BVR*	T122+C1
	55816.3894	0.0002	II	*BVR*	T40+C3
V488 Cyg	56092.5163	0.0001	II	*VR*	T30+C1
V700 Cyg	56091.3313	0.0001	I	*VR*	T30+C1
V704 Cyg	56091.5368	0.0001	II	*R*	T30+C1
V726 Cyg	56092.3113	0.0002	I	*R*	T30+C1
V1073 Cyg	55792.3922	0.0002	I	*BVR*	T30+C2
	55814.3982	0.0003	I	*BV*	T30+C2
	55818.3286	0.0004	I	*BVR*	T30+C2
EF Dra	56126.4258	0.0004	II	*BVR*	T122+C1
	56130.4536	0.0003	I	*BVR*	T122+C1
	56131.5155	0.0005	II	*BVR*	T122+C1
V502 Her	56090.3298	0.0001	I	*R*	T30+C1
V728 Her	56091.4689	0.0003	I	*VR*	T30+C1
V829 Her	56092.4579	0.0002	I	*VR*	T30+C1

Times of minima:					
Star name	Time of min. HJD 2400000+	Error	Type	Filter	Rem.
RW Leo	56004.3471	0.0001	I	*VR*	T40+C4
XY Leo	56007.5011	0.0002	II	*V*	T40+C4
XZ Leo	56007.5007	0.0002	II	*VR*	T30+C1
V1010 Oph	56092.3686	0.0003	I	*BV*	T30+C1
BB Peg	56116.4928	0.0001	I	*V*	T30+C1
V357 Peg	55758.4279	0.0005	II	*BVR*	T30+C2
	55760.4521	0.0002	I	*BVR*	T30+C2
	55837.3872	0.0002	I	*BVR*	T30+C2
V407 Peg	55795.4530	0.0006	I	*BVR*	T30+C2
	55796.4143	0.0006	II	*BVR*	T30+C2
	55802.4576	0.0009	I	*BVR*	T30+C2
	55855.3165	0.0006	I	*BVR*	T30+C2
AO Ser	56004.5788	0.0001	I	*VR*	T40+C4
HH UMa	56730.4903	0.0004	I	*BVRI*	T60+C1
	56731.2428	0.0006	I	*BVRI*	T60+C1
	56738.3729	0.0005	I	*BVRI*	T60+C1
HN UMa	56010.5528	0.0002	I	*V*	T40+C4
HR UMa	56053.4795	0.0002	I	*BVR*	T40+C4
TU UMi	55765.3657	0.0003	I	*BVR*	T60+C1
	55774.4160	0.0002	I	*BVR*	T60+C1
PY Vir	56037.3744	0.0002	II	*BVR*	T60+C3
	56038.3084	0.0001	II	*BVR*	T60+C3
	56044.3776	0.0001	I	*BVR*	T60+C3
	56049.3573	0.0001	I	*BVR*	T60+C3
	56050.2933	0.0001	I	*BVR*	T60+C3
	56052.3157	0.0001	II	*BVR*	T60+C3
	56737.3815	0.0002	II	*BVRI*	T60+C3
	56737.5358	0.0003	I	*BVRI*	T60+C3
	56738.4700	0.0001	I	*BVR*	T60+C3
	56738.6281	0.0008	II	*BVR*	T60+C3
GSC 3133-1847	56112.3865	0.0003	II	*BVR*	T30+C1
	56119.4247	0.0005	I	*BVR*	T30+C1

Times of minima:					
Star name	Time of min. HJD 2400000+	Error	Type	Filter	Rem.
SAO 48275	56091.3940	0.0007	I	*BVR*	T40+C4
	56094.3805	0.0004	I	*BVR*	T40+C4
	56100.3438	0.0004	I	*BVR*	T40+C4

Explanation of the remarks in the table:

In the remarks column of the table, telescopes and CCD detectors used in the observations are indicated.

Remarks:

In this study, we present 67 minima times of 29 eclipsing binaries.

Acknowledgements:

This study has been partly supported by the Scientific and Technological Research Council of Turkey (TÜBİTAK, under the Grant No. 111T224). The authors would like to thank the staff at Astrophysics Research Centre and Ulupnar Observatory, Çanakkale Onsekiz Mart University. The project was supported partly by National Planning Agency (DPT) of Turkey (project DPT-2007K120660 carried out at Çanakkale Onsekiz Mart University) and the Scientific Research Projects Coordination Unit of Istanbul University (project no. 3685).

Reference:

Kwee, K. K., van Woerden, H., 1956, *Bull. Astron. Inst. Netherlands*, **12**, 327

COMMISSIONS G1 AND G4 OF THE IAU
INFORMATION BULLETIN ON VARIABLE STARS
Volume 63 Number 6226 DOI: 10.22444/IBVS.6226

Konkoly Observatory
Budapest
11 December 2017
HU ISSN 0374 – 0676

V736 CEPHEI – AN A-TYPE OVERCONTACT BINARY

NELSON, ROBERT H.[1,2]

[1] Mountain Ash Observatory, 1393 Garvin Street, Prince George, BC, Canada, V2M 3Z1
email: bob.nelson@shaw.ca

[2] Guest investigator, Dominion Astrophysical Observatory, Herzberg Institute of Astrophysics, National Research Council of Canada

The discoverer of the variability of V736 Cep (NSV 13635, NSVS 3275157, HD 235475. SAO 33275, TYC 3957-12-1) appears to be undocumented. As part of the HD catalogue, it was classified presumably by Cannon and Pickering (1993) as F8. The first relevant reference is to Otero et al. (2005) who provided coordinates, elements (epoch and period), apparent reference to the above classification, and an eclipse type (EA). Since then, there have been numerous eclipse timings published, but no light curve or analysis.

In order to rectify this lack, the author first secured, in September of 2011, 2013, 2014, and 2015, a total of 14 medium resolution ($R \sim 10000$ on average) spectra of V736 Cep at the Dominion Astrophysical Observatory (DAO) in Victoria, British Columbia, Canada using the Cassegrain spectrograph attached to the 1.85 m Plaskett Telescope. He used the 21181 configuration and a grating with 1800 lines/mm, blazed at 5000 Å, and giving a reciprocal linear dispersion of 10 Å/mm in the first order. The wavelengths ranged from 5000 to 5260 Å, approximately. A log of observations is given in Table 1 and an eclipse timing diagram, in Figure 9 later in the paper. The following elements were used for both radial velocity (RV) and photometric phasing:

$$\text{JD (Hel) Min I} = 2457619.7380 + 0.8578464E \quad (1)$$

Frame reduction was performed by software RaVeRe (Nelson 2013). See Nelson (2010) and Nelson et al. (2014) for further details. The normalized spectra are reproduced in Fig. 1, sorted by phase. Note towards the right the strong neutral iron lines (at 5167.487 and 5171.595 Å) and the strong neutral magnesium triplet (at 5167.33, 5172.68, and 5183.61 Å).

Radial velocities were determined using the Rucinski broadening functions (Rucinski, 2004, Nelson, 2010) as implemented in software Broad25 (Nelson, 2013). See Nelson et al. (2014) for further details. An Excel worksheet with built-in macros (written by him) was used to do the necessary radial velocity conversions to geocentric and back to heliocentric values (Nelson 2014). The resulting RV determinations are also presented in Table 1. The mean rms errors for RV_1 and RV_2 are 5.9 and 6.9 km/s, respectively, and the overall rms deviation from the (sinusoidal) curves of best fit is 9.1 km/s. The best fit yielded the values $K_1 = 49.8$ (1.7) km/s, $K_2 = 251.1$ (2.3) km/s and $V_\gamma = -12.4$ (1.4) km/s, and thus a mass ratio $q_{\rm sp} = K_1/K_2 = M_2/M_1 = 0.198$ (7).

Table 1: Log of DAO observations.

DAO Image#	Mid Time (HJD−2400000)	Exposure (sec)	Phase at Mid-exp	V_1 (km/s)	V_2 (km/s)
11-08068	55815.9293	3600	0.282	−71.5 (5.8)	224.5 (5.8)
11-08086	55816.7831	3600	0.278	−57.1 (7.3)	236.9 (13.4)
11-08169	55823.9181	3600	0.595	13.1 (5.0)	—
11-08200	55824.9408	3600	0.787	38.8 (5.7)	−239.6 (4.0)
11-08211	55825.7162	3600	0.691	29.3 (4.3)	−242.3 (4.1)
11-08214	55825.7657	3600	0.749	11.7 (4.8)	−268.6 (3.8)
13-09667	56545.9245	3600	0.245	−60.2 (5.2)	249.2 (10.7)
14-24341	56906.7363	1200	0.847	26.5 (5.8)	−224.1 (5.4)
14-24403	56908.7899	1200	0.241	−70.5 (4.1)	—
14-24415	56908.8968	1200	0.365	−43.7 (9.1)	176.2 (12.6)
15-13014	57291.8559	1200	0.785	39.7 (5.6)	−247.1 (3.5)
15-13015	57291.8736	1800	0.805	43.2 (8.0)	−250.9 (4.8)
15-13128	57295.6376	3600	0.193	−68.8 (6.1)	238.4 (7.0)
15-12130	57295.6697	1800	0.230	−64.3 (6.0)	237.2 (8.2)

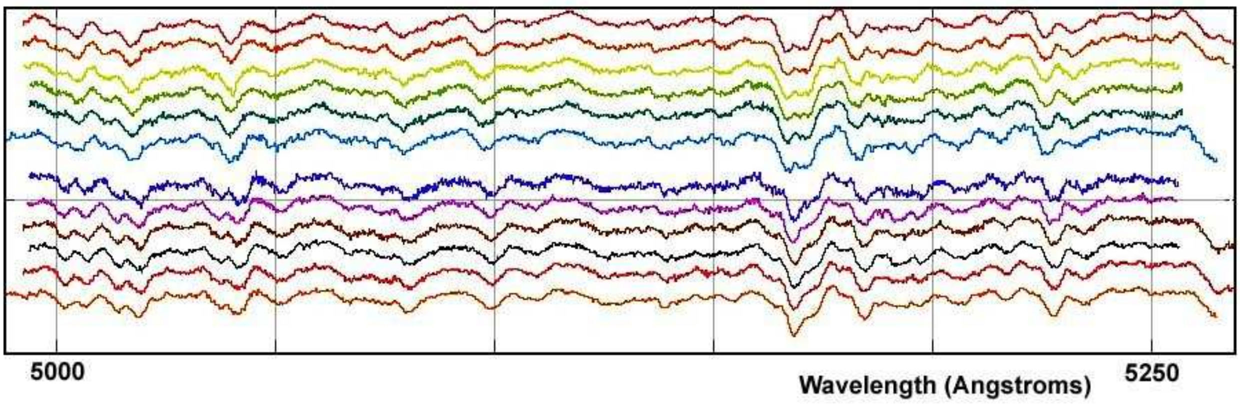

Figure 1. V736 Cep spectra at phases 0.193, 0.230, 0.245, 0.278, 0.282, 0.365, 0.691, 0.749, 0.785, 0.787, 0.805, 0.847 (from top to bottom).

Representative broadening functions, at phases 0.232 and 0.778 are depicted in Figs. 2 and 3, respectively. Smoothing by a Gaussian filter is routinely done in order to centroid the peak values for determining the radial velocities.

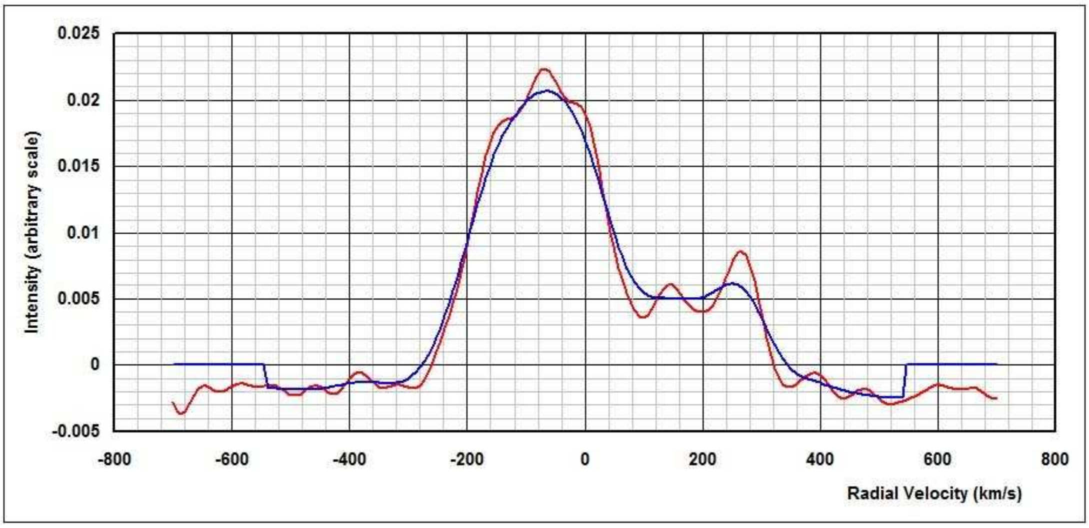

Figure 2. Broadening functions at phase 0.230–smoothed and unsmoothed.

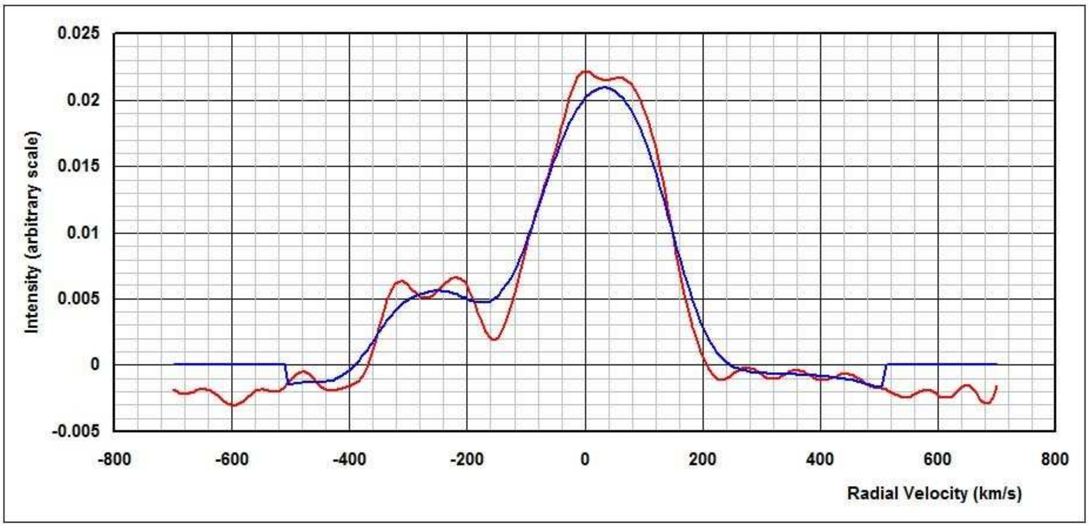

Figure 3. Broadening functions at phase 0.785–smoothed and unsmoothed.

In the autumn months of 2015 and 2016 the author took a total of 269 frames in V, 277 in R_C (Cousins) and 277 in the I_C (Cousins) band at his private observatory in Prince George, B.C., Canada. Renamed Mountain Ash Observatory, it is the former Sylvester Robotic Observatory described in Nelson (2009). A finder chart is included as Fig. 10 at the end of the paper.

Standard reductions were then applied (see Nelson et al., 2014 for more details). The variable, comparison and check stars are listed in Table 2. The coordinates and magnitudes for V736 Cep, the comparison, and check stars are from the Tycho Catalogue, Hog,

Table 2: Details of variable, comparison and check stars.

Object	GSC	RA (J2000)	Dec (J2000)	V (mag)	$B-V$ (mag)
Variable	3957-0012	$21^h16^m29\overset{s}{.}1133$	$+55°23'10\overset{''}{.}236$	9.82 (3)	+0.40 (4)
Comparison	3957-0898	$21^h17^m29\overset{s}{.}8881$	$+55°33'32\overset{''}{.}048$	10.10 (3)	+0.87 (7)
Check	3957-0310	$21^h17^m07\overset{s}{.}2846$	$+55°23'03\overset{''}{.}045$	10.66 (5)	+0.34 (7)

Table 3: Limb darkening values from Van Hamme (1993).

Band	x_1	x_2	y_1	y_2
Bol	0.645	0.644	0.227	0.226
V	0.735	0.739	0.263	0.259
R_C	0.662	0.667	0.274	0.272
I_C	0.579	0.583	0.265	0.264

et al., (2000), and converted to standard Johnson values using relations due to Henden (2001).

The author used the 2003 version of the Wilson-Devinney (WD) light curve and radial velocity analysis program with the Kurucz atmospheres (Wilson and Devinney, 1971, Wilson, 1990, Kallrath and Milone, 1998, Wilson, 1998) as implemented in the Windows front-end software WDwint (Nelson, 2013) to analyse the data. To get started, the spectral type F8 (taken from SIMBAD, no reference given; but there is an implied reference to Cannon and Pickering (1993) in Otero et al. (2005). Interpolated tables from Flower (1996) gave a temperature $T_1 = 6199 \pm 120$ K and $\log g = 4.367 \pm 0.004$. (The quoted errors refer to one spectral sub-class.) An interpolation program by Terrell (1994, available from Nelson 2013) gave the Van Hamme (1993) limb darkening values; and finally, a logarithmic (LD=2) law for the limb darkening coefficients was selected, appropriate for temperatures < 8500 K (ibid.). The limb darkening coefficients are listed in Table 3. (The values for the second star are based on the later-determined temperature of 6101 K and assumed spectral type of F8-9.) Convective envelopes for both stars were used, appropriate for cooler stars (hence values gravity exponent $g = 0.32$ and albedo $A = 0.500$ were used for each).

From the GCVS 4 designation (EW) and from the shape of the light curve, mode 3 (overcontact binary) mode was used.

Convergence was attempted by the method of multiple subsets. The subsets were: (a, V_γ, i, L_1), (T_2, Ω_1), and (q, L_1). However, no reasonable fit could be obtained until a spot was placed on the back side of star 1 (visible during secondary minimum). Thereafter, the fitting proceeded smoothly.

Detailed reflections were tried, with $n_{\rm ref} = 3$, but there was little–if any–difference in the fit from the simple treatment. There are certain uncertainties in the process (see Csizmadia et al., 2013, Kurucz, 2000). On the other hand, the solution is very weakly dependent on the exact values used.

The model is presented in Table 4. For the most part, the error estimates are those provided by the WD routines and are known to be low; however, it is a common practice to quote these values and we do so here. Also, estimating the uncertainties in temperatures T_1 and T_2 is somewhat problematic. A common practice is to quote the temperature difference over–say–one spectral sub-class (assuming that the classification is good to one spectral sub-class, the precision being unknown in this case). In addition, various different calibrations have been made (Cox, 2000, page 388-390 and references therein, and Flower, 1996), and the variations between the various calibrations can be significant. If the classification is ± one sub-class, an uncertainty of ±120 K to the absolute temperatures of each, would be reasonable. The modelling error in temperature T_2, relative to T_1, is indicated by the WD output to be much smaller, around 7 K.

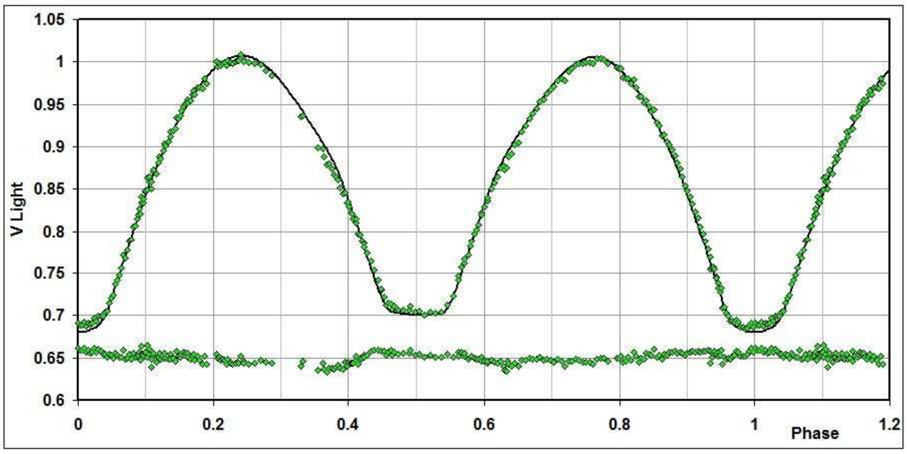

Figure 4. *V* light curves for V736 Cep – data, WD fit, and residuals.

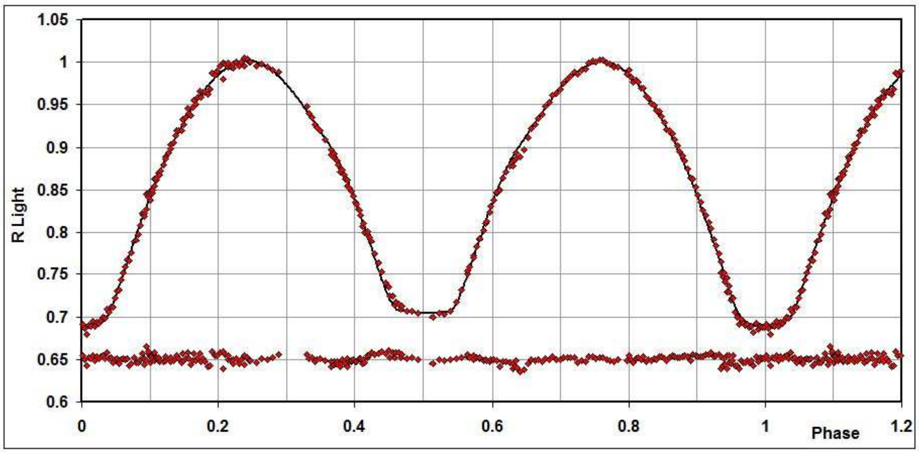

Figure 5. *R* light curves for V736 Cep – data, WD fit, and residuals.

The light curve data and the fitted curves are depicted in Figures 4-6. The residuals (in the sense observed-calculated) are also plotted, shifted upwards by 0.65 units.

The radial velocities are shown in Fig. 7. A three-dimensional representation from Binary Maker 3 (Bradstreet, 1993) is shown in Fig. 8.

The WD output fundamental parameters and errors are listed in Table 5. Most of the errors are output or derived estimates from the WD routines. From Kallrath & Milone (1998), the fill-out factor is $f = (\Omega_{\rm I} - \Omega)/(\Omega_{\rm I} - \Omega_{\rm O})$, where Ω is the modified Kopal potential of the system, $\Omega_{\rm I}$ is that of the inner Lagrangian surface, and $\Omega_{\rm O}$, that of the outer Lagrangian surface, was also calculated.

To determine the distance, the analysis proceeded as follows: First the WD routine gave the absolute bolometric magnitudes of each component; these were then converted

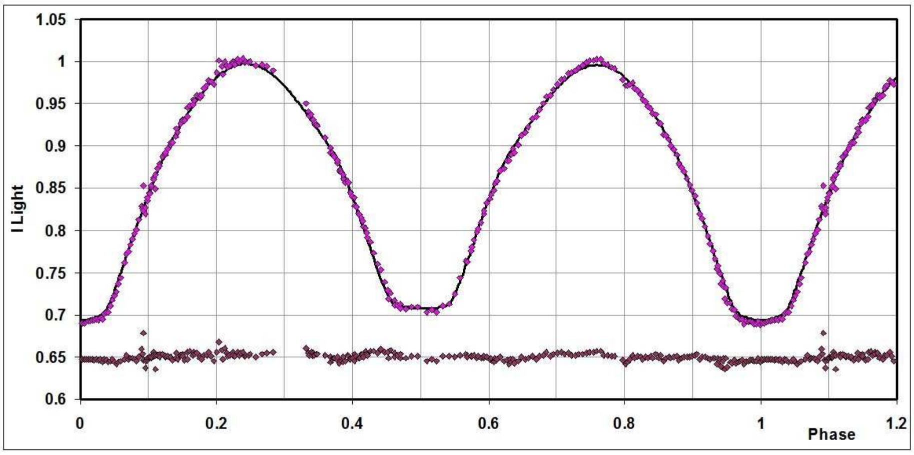

Figure 6. *I* light curves for V736 Cep – data, WD fit, and residuals.

Table 4: Wilson-Devinney parameters.

WD Quantity	Value	error	Unit
Temperature, T_1	6199	[fixed]	K
Temperature, T_2	6101	120	K
$q = m_2/m_1$	0.189	0.001	—
Potential, $\Omega_1 = \Omega_2$	2.152	0.002	—
Inclination, i	80.68	0.17	degrees
Semi-maj. axis, a	5.23	0.06	solar radii.
V_γ	-13.4	1.8	km/s
Fill-out, f_1	0.431	0.024	
Spot co-latitude	70	5	degrees
Spot longitude	171	2	degrees
Spot radius	17.2	0.5	degrees
Spot temp. factor	0.948	0.004	
$L_1/(L_1 + L_2)$ (V)	0.8203	0.0002	—
$L_1/(L_1 + L_2)$ ($R_C c$)	0.8188	0.0001	—
$L_1/(L_1 + L_2)$ ($I_C c$)	0.8174	0.0001	—
r_1 (pole)	0.5041	0.0004	orbital radii
r_1 (side)	0.5541	0.0007	orbital radii.
r_1 (back)	0.5803	0.0009	orbital radii
r_2 (pole)	0.2434	0.0011	orbital radii
r_2 (side)	0.2553	0.0014	orbital radii
r_2 (back)	0.3038	0.0033	orbital radii.
Phase shift	0.0004	0.0001	—
$\Sigma\omega^2_{\rm res}$	0.07958	—	—

Table 5: Fundamental parameters.

Quantity	Value	Error	unit
Temperature, T_1	6199	120	K
Temperature, T_2	6101	120	K
Mass, m_1	2.20	0.06	M0
Mass, m_2	0.41	0.02	M0
Radius, R_1	2.86	0.01	R0
Radius, R_2	1.40	0.01	R0
$M_{\mathrm{bol},1}$	2.20	0.02	mag
$M_{\mathrm{bol},2}$	3.82	0.02	mag
$\log g_1$	3.87	0.01	cgs
$\log g_2$	3.76	0.01	cgs
Luminosity, L_1	10.9	0.2	L0
Luminosity, L_2	2.44	0.05	L0
Fill-out factor 1,2	0.43	0.02	—
Distance, r	316	6	pc

to the absolute visual (V) magnitudes of both, $M_{V,1}$ and $M_{V,2}$, using the bolometric corrections BC $= -0.160$ and -0.17 for stars 1 and 2 respectively. The latter were taken from interpolated tables constructed from Cox (2000). The absolute V magnitude was then computed in the usual way, getting $M_V = 2.14 \pm 0.02$ magnitudes. The apparent magnitude in the V passband was $V = 9.854 \pm 0.03$, taken from the Tycho values (Hog et al. 2000) and converted to the Johnson magnitude 9.816 ± 0.03 using relations due to Henden (2001).

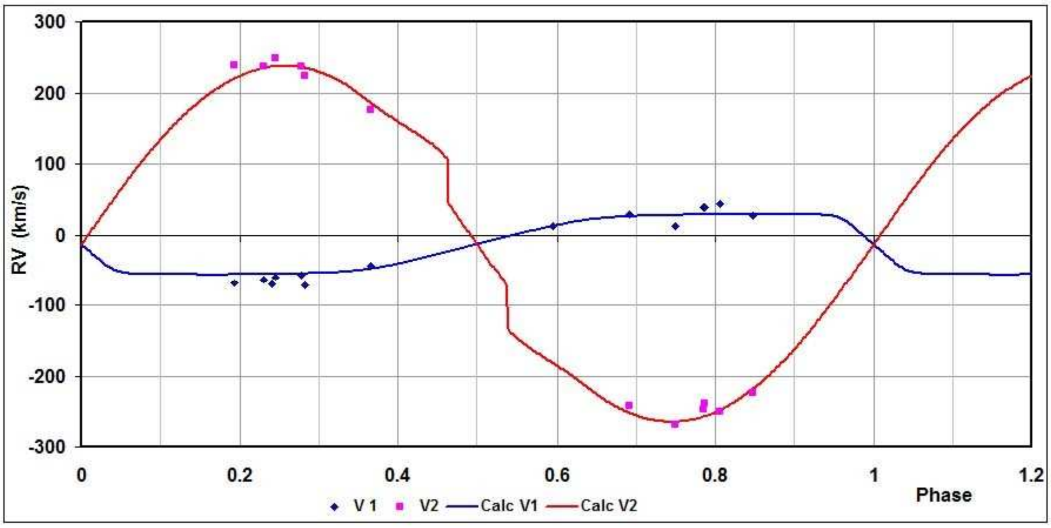

Figure 7. Radial velocity curves for V736 Cep – data and WD fit.

Ignoring interstellar absorption (setting $A_V = 0$), we calculated a preliminary value for the distance $r = 343$ pc from the standard relation:

$$r = 10^{0.2(V - M_V - A_V + 5)} \text{ parsecs} \tag{2}$$

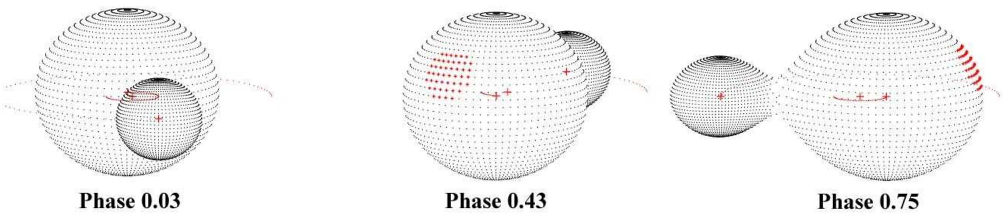

Figure 8. Binary Maker 3 representation of the system – at phases 0.03, 0.43 and 0.75.

Galactic extinction was obtained from a model by Amôres & Lépine (2005). The code (available in IDL and converted by the author to a Visual Basic routine) assumes that the interstellar dust is well mixed with the dust, that the galaxy is axi-symmetric, that the gas density in the disk is a function of the Galactic radius and of the distance from the Galactic plane, and that extinction is proportional to the column density of the gas, Using Galactic coordinates of $l = 95^{\circ}\!.5859$ and $b = +4^{\circ}\!.3732$ (SIMBAD), and the initial distance estimate of $d = 0.343$ kpc, a value of $A_V = 0.175$ magnitude was determined, A further iteration revealed little change in A_V. Substitution into (2) gave $r = 316$ pc.

The errors were assigned as follows: $\delta M_{\rm bol,1} = \delta M_{\rm bol,2} = 0.02$, $\delta \rm BC_1 = \delta BC_2 = 0.009$ (the variation of 1 spectral sub-class), δV = 0.03, $\delta A_V = 0.01$, all in magnitudes. Combining the errors rigorously (i.e., by adding the variances) yielded an estimated error in r of 6 pc which is probably far too low.

Some comments regarding the period variation are in order. An eclipse timing difference (O–C) plot using timings from 1999 is depicted in Fig. 9. Although there is considerable scatter, a linear relation over the interval, cycle 4400 (in 2009) to cycle 7380 (in 2016) was determined. This yielded a best-fit linear solution and ephemeris of Equation (1) above.

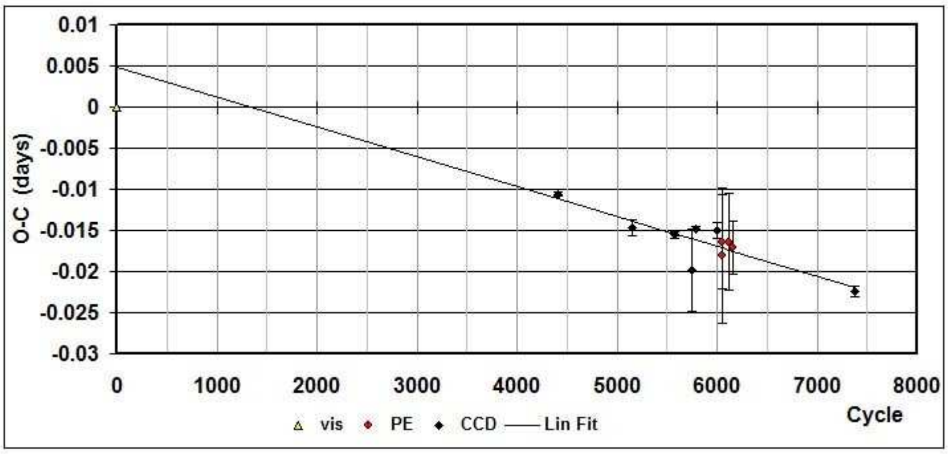

Figure 9. V736 Cep – eclipse timing (O–C) diagram with a linear fit for points after cycle 4000.

In conclusion, all the fundamental parameters for V736 Cephei have been determined. It will be interesting to monitor this system photometrically in the coming years to observe the evolution of the spot.

The Excel file (and many others) are available at Nelson (2016). The 8000+ files are updated annually.

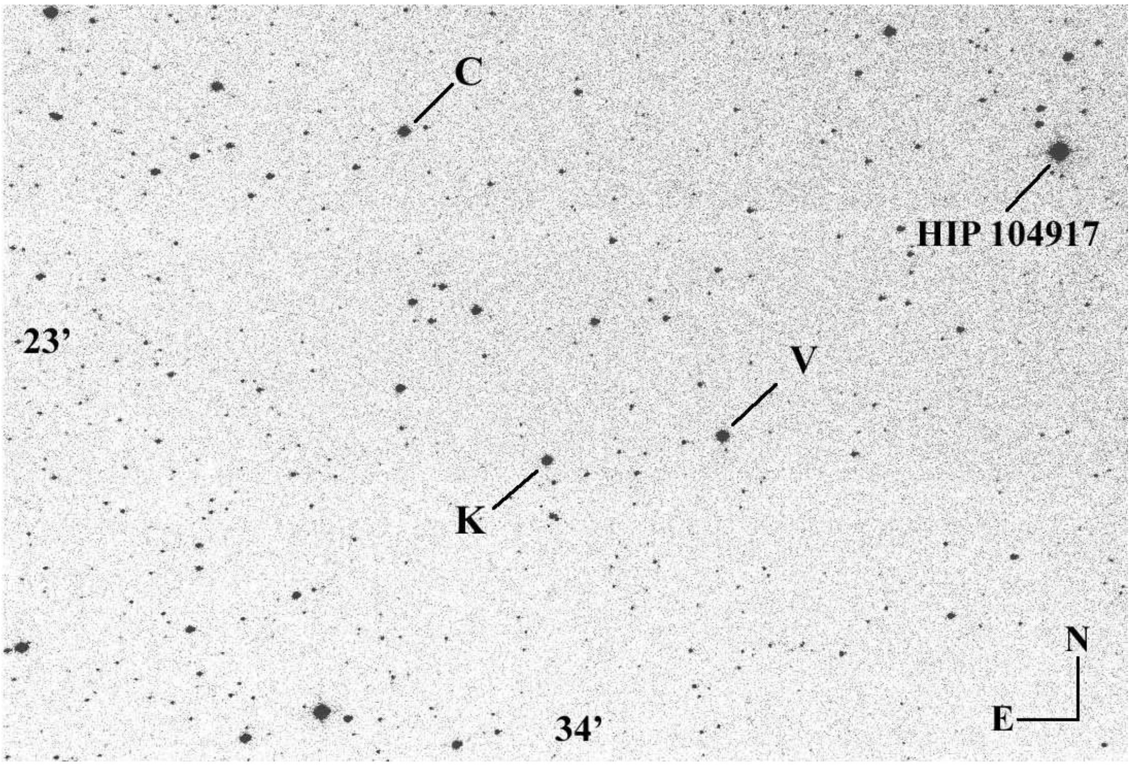

Figure 10. Sample CCD frame of the field of view showing the stars of interest.

Acknowledgements: It is a pleasure to thank the staff members at the DAO (Dmitry Monin, David Bohlender, and the late Les Saddlmyer) for their usual splendid help and assistance. Much use was made of the SIMBAD database during this research.

References:

Amôres, E.B., Lépine, J.R.D., 2005, *AJ*, **130**, 659 DOI

Bradstreet, D.H., 1993, "Binary Maker 2.0 - An Interactive Graphical Tool for Preliminary Light Curve Analysis", in Milone, E.F. (ed.) Light Curve Modelling of Eclipsing Binary Stars, pp 151-166 (Springer, New York, N.Y.) DOI

Cannon, A.J., Pickering, E.C., 1993, Harv. Ann., 91-100 (1918-1924; ADC 1989), Henry Draper Catalogue and Extension 1 (HD, HDE)

Cox, A.N., ed, 2000, Allen's Astrophysical Quantities, 4th ed., (Springer, New York, NY) DOI

Csizmadia, S., Pasternacki, T., Dreyer, C., Cabrera, A., Erikson, A., Rauer, H., 2013, *A&A*, **549**, A9 DOI

Flower, P.J., 1996, *ApJ*, **469**, 355 DOI

Henden, A., 2001, `http://www.tass-survey.org/tass/catalogs/tycho.old.html`

Hog, E., et al., 2000, *A&A*, **355**, L27

Kallrath, J., Milone, E.F., 1998, Eclipsing Binary Stars–Modeling and Analysis (Springer-Verlag). DOI
Kurucz, R.L., 2000, *BaltA*, **11**, 101
Nelson, R.H., 2009, *IBVS*, **5884**
Nelson, R.H., 2010, "Spectroscopy for Eclipsing Binary Analysis" in The Alt-Az Initiative, Telescope Mirror & Instrument Developments (Collins Foundation Press, Santa Margarita, CA), R.M. Genet, J.M. Johnson and V. Wallen (eds) [available on ResearchGate]
Nelson, R.H., 2013, Software by Bob Nelson, `https://www.variablestarssouth.org/bob-nelson/`
Nelson, R.H., 2014, Spreadsheets, by Bob Nelson, `https://www.variablestarssouth.org/bob-nelson/`
Nelson, R.H., 2016, Bob Nelson's $O-C$ Files, `http://www.aavso.org/bob-nelsons-o-c-files`
Nelson, R.H., Şenavci, H.V., Baştürk, Ö, and Bahar, E., 2014, *NewA*, **29**, 57 DOI
Otero, S.A., Wils, P, and Dubovsky, P.A., 2005, *IBVS*, **5586**
Rucinski, S. M., 2004, "Advantages of the Broadening Function (BF) over the Cross-Correlation Function (CCF)", in Stellar Rotation, *Proc. IAU Symp.*, **215**, 17
Terrell, D., 1994, Van Hamme Limb Darkening Tables, vers. 1.1.
Van Hamme, W., 1993, *AJ*, **106**, 2096 DOI
Wilson, R.E., 1990, *ApJ*, **356**, 613 DOI
Wilson, R.E., 1998, Documentation of Eclipsing Binary Computer Model (available from the author)
Wilson, R.E., and Devinney, E.J., 1971, *ApJ*, **166**, 605 DOI

COMMISSIONS G1 AND G4 OF THE IAU
INFORMATION BULLETIN ON VARIABLE STARS
Volume 63 Number 6227 DOI: 10.22444/IBVS.6227

Konkoly Observatory
Budapest
11 December 2017

HU ISSN 0374 – 0676

NEW LIGHT-TIME CURVE OF ECLIPSING BINARY AM Leo

GORDA, S. YU.[1]; MATVEEVA, E. A.[2]

[1] Kourovka Astronomical Observatory of the Ural Federal University; e-mail: stanislav.gorda@urfu.ru

[2] Ural Federal University, 51, Lenin av., Ekaterinburg, Russia, 620000

The eclipsing variable star AM Leo (BD +10°2234 A) is a bright component ($V = 9.1$–9.7 mag) of the visual binary system ADS 8024 ($\rho = 11''.4$, $\theta = 270°$)(Hiller et al. 2004). The most comprehensive survey of the photometric observations of AM Leo were given in the studies of Hiller et al. (2004) and Albayrak et al. (2005a). Many authors noted temporal variations in the light curve of AM Leo. Along with the light curve variations, orbital variations have been observed too. Various hypotheses were proposed to explain this phenomenon. The most likely reason for the period change in AM Leo is now considered to be the presence of a third body in the system. This hypothesis was first suggested by Demircan & Derman (1992). Later Albayrak et al. (2005a) and Qian et al. (2005) have determined the parameters of the light-time curve based on the analysis of the moments of minima from data obtained using photomultiplier and CCD detectors only.

Albayrak et al. (2005a) obtained the mutual orbital period of AM Leo and the third body by the very eccentric orbit to be about 45 years, they also estimated the mass of the third body to be $M_3 = 0.18M_\odot$. These results have been obtained on the basis of the data collected from $JD_\odot = 2435570$ to $JD_\odot = 2453106$. In the paper of Qian et al. (2005) the values of the period 51.8 years and $M_3 = 0.20M_\odot$ were listed. But these values were obtained with less data compared to the paper of Albayrak et al. (2005a).

Since this research a number of new values of the moments of minima of AM Leo have been received. In the paper of Albayrak et al. (2005a) the moments of minima were used which have been distributed on an interval of time, corresponding only to ~ 1.1 of the 45-year period. Now this interval comprises ~ 1.4 times of the period, and the moments of minima are distributed regularly enough throughout. Differences O–C calculated with the new moments of minima, already do not correspond to the light-time curve received by Albayrak et al. (2005a). Thus, now it is the time to define again the parameters of a light-time curve of AM Leo.

We have obtained 72 photoelectric and CCD moments of minima of the eclipsing binary AM Leo generally between 1996–2017 at Kourovka Astronomical Observatory of the Ural Federal University in Russia, which have not been published earlier. Data were obtained by one of the authors with a reflector telescope ($D = 0.45$ m), equipped with a photoelectric photometer, placed in the Cassegrainian focus ($F = 11.0$ m), and by a CCD-camera, placed in the Newtonian focus ($F = 2.0$ m).

The CCD observations data were reduced using the $MaxImDL$ and *Muniwin* (http://c-munipack.sourceforge.net) packages. The minima time were computed by a parabola fitting method and averaged from all filters used during the night. Values of the moments of minima of AM Leo, obtained from our observations, are listed in Table 1. Abbreviation in the column named "Rem." corresponds to the detector used for observations:

- PE — scanning photoelectric photometer (it is not used now);
- CCD1 — CCD camera Apogee Alta-U6 (Kodak KAF-1001E, 1048×1048, 24-micron chip);
- CCD2 — CCD camera FLI PL230 (e2v CCD230-42-1-143, 2048×2048, 15-micron chip).

Additional seven moments of minima obtained by one of the authors in 2015 have been published by Gorda (2016).

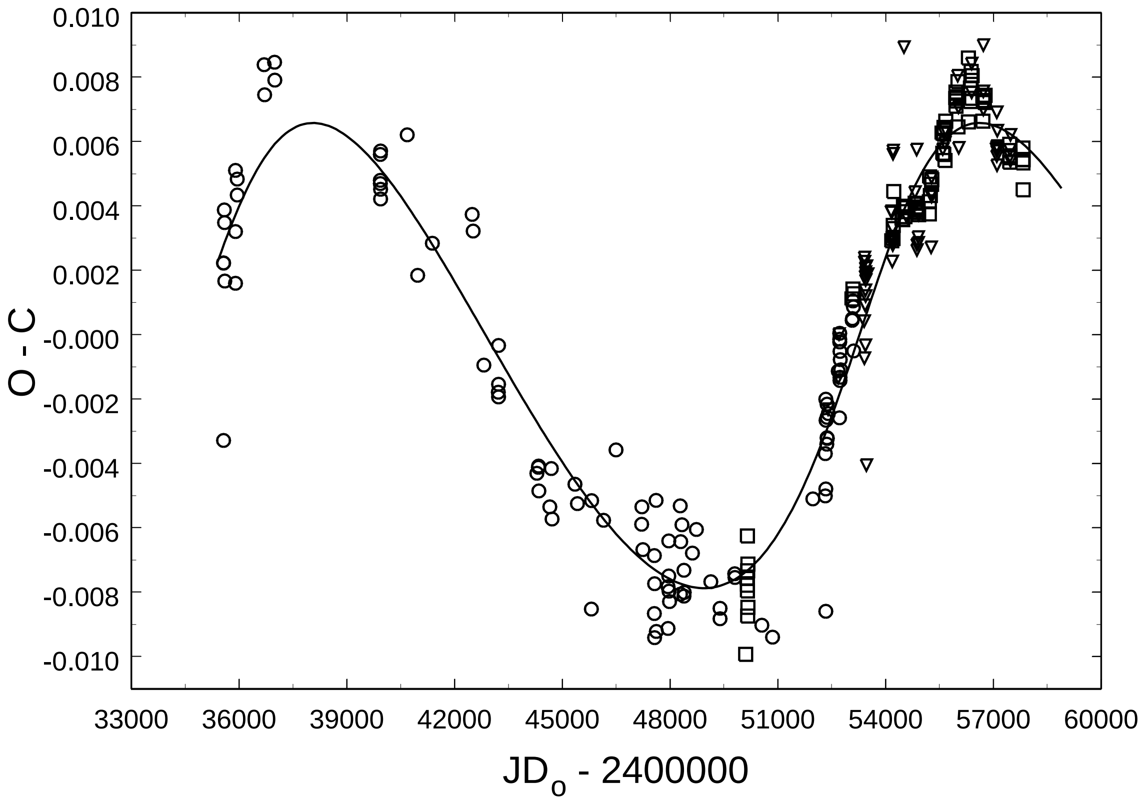

Figure 1. The light-time curve of the variable star AM Leo (solid line); open circles denote values of the O–C calculated from the times of minima from Albayrak et al. (2005a); open triangles represent ones from IBVS (see page 3); open squares denote O–C calculated from our data (see Table 1).

For calculating the O–C differences and the parameters of the light-time curve we used our data (see Table 1), data from the paper of Albayrak et al. (2005a), and also the moments of minima published in *IBVS* from 2002 to 2017 (Pribulla et al. 2002, Gürol et al. 2003, Dvorak 2004, Hübscher 2005, Albayrak et al. 2005b, Hübscher et al. 2005, Kotková & Wolf 2006, Şenavci et al. 2007, Kiliçoğlu et al. 2007,Hübscher 2007, Ogłoza et al. 2007, Hübscher et al. 2008, Nelson 2009, Diethelm 2009, Parimucha 2009, Hübscher et al. 2010, Diethelm 2010, Hübscher & Monninger 2011, Diethelm 2011, Hübscher et al. 2012, Diethelm 2012, Parimucha 2013, Hübscher et al. 2013, Nelson 2013, Hübscher 2013, Zasche 2014, Hübscher & Lehmann 2015, Hübscher 2016a, Hübscher 2016b, Zasche et al. 2017).

Values of parameters of the light-time curve were obtained by a fitting method described by Gorda et al. (2007). Our fit is plotted in Fig. 1 along with the observed values. The parameters of light-time curves obtained by Qian et al. (2005), Albayrak et al. (2005a) and obtained by us are given in Table 2. Designations in the first column of Table 2 correspond to following parameters: N is the total number of the moments of minima under consideration, $\sum(O - C_{LTC})^2$ is the value of the minimum sum of the squares of the residuals of O–C differences from the light-time curve, $JD_{\odot}I_{min}$ and P_{orb} are reference epochs for the primary minimum and the true period of the AM Leo respectively, $a \sin i$, e, w, T_0 and P_{12} are the semi-major axis, inclination, eccentricity, longitude and epoch of the periastron passage and the period of the orbit of the eclipsing pair around the mass center of the AM Leo system with the third body, respectively. A is the semi-amplitude of the light-time curve and $f(m_3)$ is the mass function of the third body.

As it can be seen, the new values of only three parameters of the AM Leo orbit with the third body, namely e, T_0 and P_{12} differ considerably from the ones received by Albayrak et al. (2005a). Our values can be considered as more reliable at the present time because they were obtained by the use of more data, compared to the paper of Albayrak et al. (2005a) and because our moments of minima are distributed on the time interval exceeding the value of P_{12} nearly one and a half times.

The obtained values of $P_{12} = 50.5 \pm 0.5$ and $a \sin i = 1.30 \pm 0.05$ lead to a very small mass function of $f(m_3) = 0.00086 \pm 0.00023 M_{\odot}$ for the third body. The mass of the third body was computed for different values of the orbital inclination of the third body orbit and the derived values are given in Table 3. In this computation, the masses of the components of the eclipsing pair $M_1 = 1.23 M_{\odot}$, $M_2 = 0.54 M_{\odot}$ (Gorda 2016) were applied.

Below we list the light elements that can be used to compute the period of AM Leo for the nearest epoch of observation. We have determined them by analyzing the moments of minima for the last 5 years. These data can be approximated quite accurately by the following parabolic dependence:

$$\begin{array}{cccccccc} JD_{\odot\, min\, I} & = & 2452397.34402 & + & 0.36580143 \cdot E & - & 1.76 \cdot 10^{-10} \cdot E^2. \\ & & \pm 30 & & \pm 44 & & \pm 32 \end{array}$$

We derive from that the following light elements suitable for computing the times of minima of AM Leo at present time:

$$JD_{\odot\, min\, I} = 24577835.30926 + 0.36579882 \cdot E.$$

Acknowledgements: This work was supported in part by the Ministry of Education and Science (the basic part of the State assignment, RK no. AAAA-A17-117030310283-7) and by the Act no. 211 of the Government of the Russian Federation, agreement 02.A03.21.0006.

References:

Albayrak, B., Selam, S. O., Ak, T., Elmasli, A., Özavci İ. 2005a, *AN*, **326**, 122 DOI
Albayrak, B., Yüce, K., Selam, S. O., et al., 2005b, *IBVS*, **5649**
Demircan, O. , Derman E. 1992, *AJ*, **103**, 593 DOI
Diethelm, R. 2009, *IBVS*, **5894**

Diethelm, R. 2010, *IBVS*, **5945**
Diethelm, R. 2011, *IBVS*, **5992**
Diethelm, R. 2012, *IBVS*, **6029**
Dvorak, S.W. 2004, *IBVS*, **5502**
Gorda, S. Yu., Balega, Yu. Yu., Pluzhnik E. A., Shkhagosheva Z. U. 2007, *AstBu*, **62**, 352 DOI
Gorda, S. Yu. 2016, *AstBu.*, **71**, 64 DOI
Gürol, B., Gürdemir, L., Çaglar, A., Kirca, M., Akçay, U., Tunç, A., Elmas, T. 2003, *IBVS*, **5443**
Hiller, M. E., Osborn, W., Terrell, D., 2004, *PASP*, **116**, 337 DOI
Hübscher, J. 2005, *IBVS*, **5643**
Hübscher, J., Paschke, A., Walter, F, 2005, *IBVS*, **5657**
Hübscher, J. 2007, *IBVS*, **5802**
Hübscher, J., Steinbach, Hans-Mereyntje, Walter, F. 2009, *IBVS*, **5874**
Hübscher, J., Lehmann, P. B., Monninger, G., Steinbach, Hans-Mereyntje, Walter, F. 2010, *IBVS*, **5918**
Hübscher, J., Monninger, G. 2011, *IBVS*, **5959**
Hübscher, J., Lehmann, P. B., Walter, F. 2012, *IBVS*, **6010** e Hübscher, J., Braune, W., Lehmann, P. B. 2013, *IBVS*, **6048**
Hübscher, J. 2013, *IBVS*, **6084**
Hübscher, J., Lehmann, P. B. 2015, *IBVS*, **6149**
Hübscher, J. 2016a, *IBVS*, **6156**
Hübscher, J. 2016b, *IBVS*, **6196**
Kiliçoğlu, T., Baştürk, Ö., Şenavci, H., et al., 2007, *IBVS*, **5801**
Kotková, L., Wolf, M. 2006, *IBVS*, **5676**
Nelson, R. H. 2009, *IBVS*, **5875**
Nelson, R. H. 2013, *IBVS*, **6050**
Ogłoza, W., Niewiadomski, W., Barnacka, A., Biskup, M., Małek, K., Sokołowski, M. 2008, *IBVS*, **5843**
Parimucha, Š., Dubovský, P., Baludanský, D., Pribulla, T., Hambálek, Ľ., Vaňko, M., Ogloza, W. 2009, *IBVS*, **5898**
Parimucha, Š., Dubovský, P., Vaňko, M. 2013, *IBVS*, **6044**
Pribulla, T., Vaňko, M., Parimucha, Š., Chochol, D. 2002, *IBVS*, **5341**
Qian, Sh-B., He, J., Xiang, F., Ding, X., Boonrucksar, S. 2005, *AJ*, **129**, 1686 DOI
Şenavci, H.V., Tanriverdi, T., Törün, et al., 2007, *IBVS*, **5754**
Zasche, P., Uhlař, R., Kučáková, H., Svoboda, P., Mašek, M. 2014, *IBVS*, **6114**
Zasche, P., Uhlař, R., Svoboda, P., Kučáková, H., Mašek, M., Juryšek, J. 2017, *IBVS*, **6204**

Table 1: Moments of minima of AM Leo.

Time of min. HJD 2400000+	Error	Type	Filter	Rem.	Time of min. HJD 2400000+	Error	Type	Filter	Rem.
50106.54068	0.00061	II	BV	PE	55594.43435	0.00031	I	BVR	CCD1
50142.39120	0.00205	II	BV	PE	55617.48019	0.00005	I	BVR	CCD1
50156.29112	0.00041	II	BV	PE	55623.33233	0.00084	I	BVR	CCD1
50156.47572	0.00061	I	BV	PE	55625.34501	0.00033	II	BVR	CCD1
50157.38869	0.00054	II	BV	PE	55630.46622	0.00040	II	BVR	CCD1
50159.21672	0.00085	II	BV	PE	55659.36320	0.00114	II	BVR	CCD1
50159.40102	0.00050	I	BV	PE	55679.30038	0.00026	I	BVR	CCD1
50168.36193	0.00025	II	BV	PE	55953.46636	0.00011	II	BVR	CCD1
50169.27776	0.00015	I	BV	PE	55958.40439	0.00029	I	BVR	CCD1
53066.40291	0.00052	I	BV	PE	55960.41672	0.00017	II	BVR	CCD1
53090.36297	0.00013	II	BV	PE	55973.40238	0.00014	I	BVR	CCD1
53123.28460	0.00075	II	BV	PE	55978.34052	0.00041	II	BVR	CCD1
54172.39374	0.00010	II	BVR	CCD1	56016.20116	0.00025	I	BVR	CCD1
54208.24196	0.00011	II	BVR	CCD1	56016.38267	0.00038	II	BVR	CCD1
54214.27804	0.00021	I	BVR	CCD1	56309.38667	0.00037	II	BVR	CCD1
54459.54551	0.00016	II	BVR	CCD1	56309.57155	0.00010	I	BVR	CCD1
54475.45769	0.00021	I	BVR	CCD1	56365.35475	0.00035	II	BVR	CCD1
54497.40597	0.00012	I	BVR	CCD1	56366.26882	0.00012	I	BVR	CCD1
54537.46047	0.00005	II	BVR	CCD1	56385.29096	0.00026	I	BVR	CCD1
54552.27559	0.00043	I	BVR	CCD1	56386.38863	0.00093	I	BVR	CCD1
54571.29691	0.00025	I	BVR	CCD1	56400.28810	0.00008	I	BVR	CCD1
54578.24718	0.00033	I	BVR	CCD1	56412.36013	0.00015	I	BVR	CCD1
54586.29474	0.00027	I	BVR	CCD1	56710.30083	0.00005	II	BVR	CCD1
54825.52650	0.00015	I	BVR	CCD1	56710.48448	0.00030	I	BVR	CCD1
54882.40781	0.00027	II	BVR	CCD1	56770.29242	0.00032	II	BVR	CCD1
54887.52890	0.00031	II	BVR	CCD1	56742.30875	0.00016	I	BVR	CCD1
54888.44357	0.00011	I	BVR	CCD1	56751.27073	0.00046	II	BVR	CCD1
54909.29397	0.00041	I	BVR	CCD1	57458.35613	0.00020	II	BVR	CCD2
54923.19396	0.00026	I	BVR	CCD1	57459.27007	0.00009	I	BVR	CCD2
55217.47827	0.00013	II	BVR	CCD1	57463.29403	0.00008	I	BVR	CCD2
55218.57605	0.00023	II	BVR	CCD1	57463.47687	0.00018	II	BVR	CCD2
55223.51509	0.00016	I	BVR	CCD1	57822.32412	0.00014	II	BVR	CCD2
55246.37686	0.00021	II	BVR	CCD1	57827.26249	0.00008	I	BVR	CCD2
55281.31090	0.00013	II	BVR	CCD1	57828.36025	0.00015	I	BVR	CCD2
55288.26110	0.00034	II	BVR	CCD1	57829.27344	0.00010	II	BVR	CCD2
55570.47523	0.00105	II	BVR	CCD1	57835.31003	0.00015	I	BVR	CCD2

Table 2: Parameters of the light-time curve.

	Qian et al., 2005		Albayrak et al., 2005a		This paper	
Parameter	Value	Error	Value	Error	Value	Error
N	74		103		243	
$\sum(O-C_{LTC})^2$	0.00016		0.00020		0.00045	
$JD_{\odot\,min\,I}$	2439936.8260		2452397.35411	0.00006	2452397.35801	0.00009
P_{orb} (day)	0.36579770		0.365797425	0.000000007	0.365797590	0.000000008
$a\sin i$ (AU)	1.69	0.10	1.36	0.10	1.30	0.05
e	0.58	0.07	0.73	0.04	0.28	0.03
ω (°)	54.0	16.6	22.0	3.0	20.6	2.8
T_0 (HJD)	2436021	859	2436346	70	2435320	50
P_{12} (year)	51.4		44.82	0.34	50.5	0.5
A (day)	0.0097	0.0006	0.0058	0.0003	0.0072	0.0008
$f(m_3)$ ($M_\odot$)	0.00182	0.00033	0.00125	0.00028	0.00086	0.00023

Table 3: Mass and semi-major axis of the third body orbit depending on the orbital inclination.

$i(°)$	$m_3(M_\odot)$	a_3(AU)
10.0	1.12 ± 0.13	12.0 ± 1.1
20.0	0.48 ± 0.04	14.2 ± 1.2
30.0	0.31 ± 0.03	15.0 ± 1.3
40.0	0.24 ± 0.03	15.3 ± 1.4
50.0	0.20 ± 0.02	15.5 ± 1.5
60.0	0.17 ± 0.02	15.6 ± 1.5
70.0	0.16 ± 0.01	15.7 ± 1.5
80.0	0.15 ± 0.01	15.8 ± 1.6
90.0	0.15 ± 0.01	15.8 ± 1.5

COMMISSIONS G1 AND G4 OF THE IAU
INFORMATION BULLETIN ON VARIABLE STARS
Volume 63 Number 6228 DOI: 10.22444/IBVS.6228

Konkoly Observatory
Budapest
12 December 2017
HU ISSN 0374 – 0676

O–C DIAGRAMS FOR 33 RR LYRAE-TYPE STARS

DAGNE, T.M.[1]; BERDNIKOV, L.N.[1,2]; KNIAZEV, A.Y.[2,3,4]; DAMBIS, A.K.[2]

[1] Astronomy and Astrophysics Research division, Entoto Observatory and Research Center, P.O.Box 8412, Addis Ababa, Ethiopia. e-mail:lberdnikov@gmail.com,tesfayedagne7@gmail.com

[2] Sternberg Astronomical Institute, Lomonosov Moscow State University, Universitetskii pr. 13, Moscow, 119992 Russia

[3] South African Astronomical Observatory, P.O. Box 9, Observatory, Cape Town, 7935 South Africa

[4] Southern African Large Telescope, P.O. Box 9, Observatory, Cape Town, 7935 South Africa

In this paper we report O−C diagrams for 33 RR Lyr type variables. The diagrams are based on (1) our observations (light curve data and plots are available in the online version), obtained in 2012 to 2016 with the 0.76-m and 1.0-m telescopes of the South African Astronomical Observatory (SAAO) equipped with CCDs with B, V, and I_C filters of the Kron-Cousins photometric system (Cousins 1976), (2) the data published by Berdnikov et al. (2012) and Le Borgne et al. (2007ab, 2008ab, 2009, 2012, 2013), and (3) the data from NSVS (Wils et al. 2006), ASAS-3 (Pojmanski 2002), Catalina (Drake et al. 2013) , HIPPARCOS (1997), and AAVSO databases. To calculate the O−C residuals we used the Hertzsprung (1919) method as it was computerized by Berdnikov (1992).

Table 2 lists the O−C values computed with the the mean light elements from Table 1. Figs. 1−5 show the corresponding O−C diagrams, where we use different symbols and colors with vertical error bars (which are usually smaller than symbols) for different data: green filled circles and black open circles for NSVS and HIPPARCOS, respectively; blue and red open squares for Catalina and ASAS-3, respectively; pluses for Le Borgne and AAVSO, and red filled squares for Berdnikov et al. (2012) and our observations.

From these O−C diagrams one can infer the following. The time interval covered by our study is too short for investigating any evolutionary period changes. The O−C diagrams of AP Cnc, TV Lib, PS Lup, and BT Sco indicate abrupt period change before the last data point. Some waves are visible in the O−C diagrams for V1184 Cen, V1354 Cen, V559 Hya, QR Lib, V354 Vir and V348 Vir, but we cannot identify them as periodic variations, because this would require observing several waves at least. The lack of data in some time intervals may lead to a miscalculation of the epoch. Examples are the O−C diagrams of RT Equ, IK Hya, V558 Oph, V1041 Oph, and AF Sex. The O−C diagram of V1017 Oph shows a systematic shift between the ASAS and Catalina data, which can be explained by the fact that the brightness of this star is close to the limiting magnitude of ASAS.

Table 1: Mean light element for 33 RR Lyrae stars.

Star Name	Initial epoch	Period	Type
AP Cnc	54546.214032	0.53291468	RRAB
V1179 Cen	54777.082409	0.27421762	RRC
V1184 Cen	53947.822244	0.33966910	RRC
V1354 Cen	54223.176146	0.34628436	RRC
V1360 Cen	54222.583970	0.34425780	RRC
RS Crv	54411.414734	0.53685599	RRAB
AG Crt	54506.758913	0.37684461	RRC
AP Crt	54390.357629	0.54378565	RRAB
RT Equ	53926.975698	0.44481338	RRAB
XY Eri	54660.469076	0.55425154	RRAB
SZ Hya	54521.232137	0.53722276	RRAB
CF Hya	54486.192951	0.59120615	RRC
IK Hya	52780.127072	0.65031872	RRAB
V425 Hya	54491.297178	0.55085320	RRAB
V516 Hya	53913.375194	0.34661720	RRAB:
V559 Hya	54396.214450	0.44794990	RRAB
TV Lib	54410.807510	0.26962370	RRAB
XX Lib	54462.226769	0.69847051	RRAB
QR Lib	53857.026961	0.37547759	RRC
PS Lup	54777.930950	0.47185029	RRAB
V558 Oph	53153.121869	0.42589032	RRC
V1017 Oph	54796.380117	0.30613960	RRC
V1041 Oph	54432.210221	0.35263166	RRC
UU Sco	54436.718392	0.57649333	RRC
BT Sco	54421.761496	0.54873084	RRAB
T Sex	52770.130472	0.32469759	RRC
AF Sex	54383.744749	0.53106543	RRAB
GH Vir	54440.440499	0.60530993	RRAB
V348 Vir	54460.446421	0.56523109	RRAB
V354 Vir	54395.742996	0.59504207	RRAB
V419 Vir	54418.032303	0.51051921	RRAB
V433 Vir	55075.810168	0.58859716	RRAB
V494 Vir	54451.349933	0.54722094	RRAB

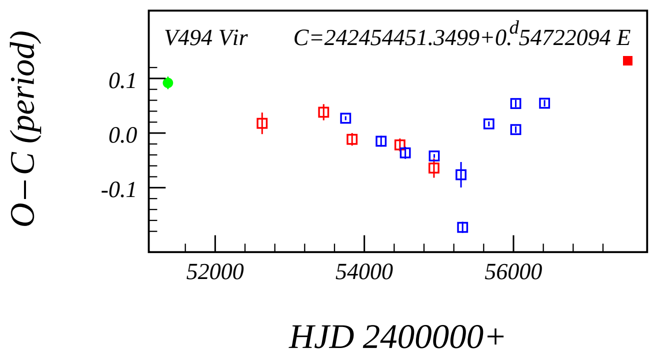

Figure 1. O−C diagram for V494 Vir.

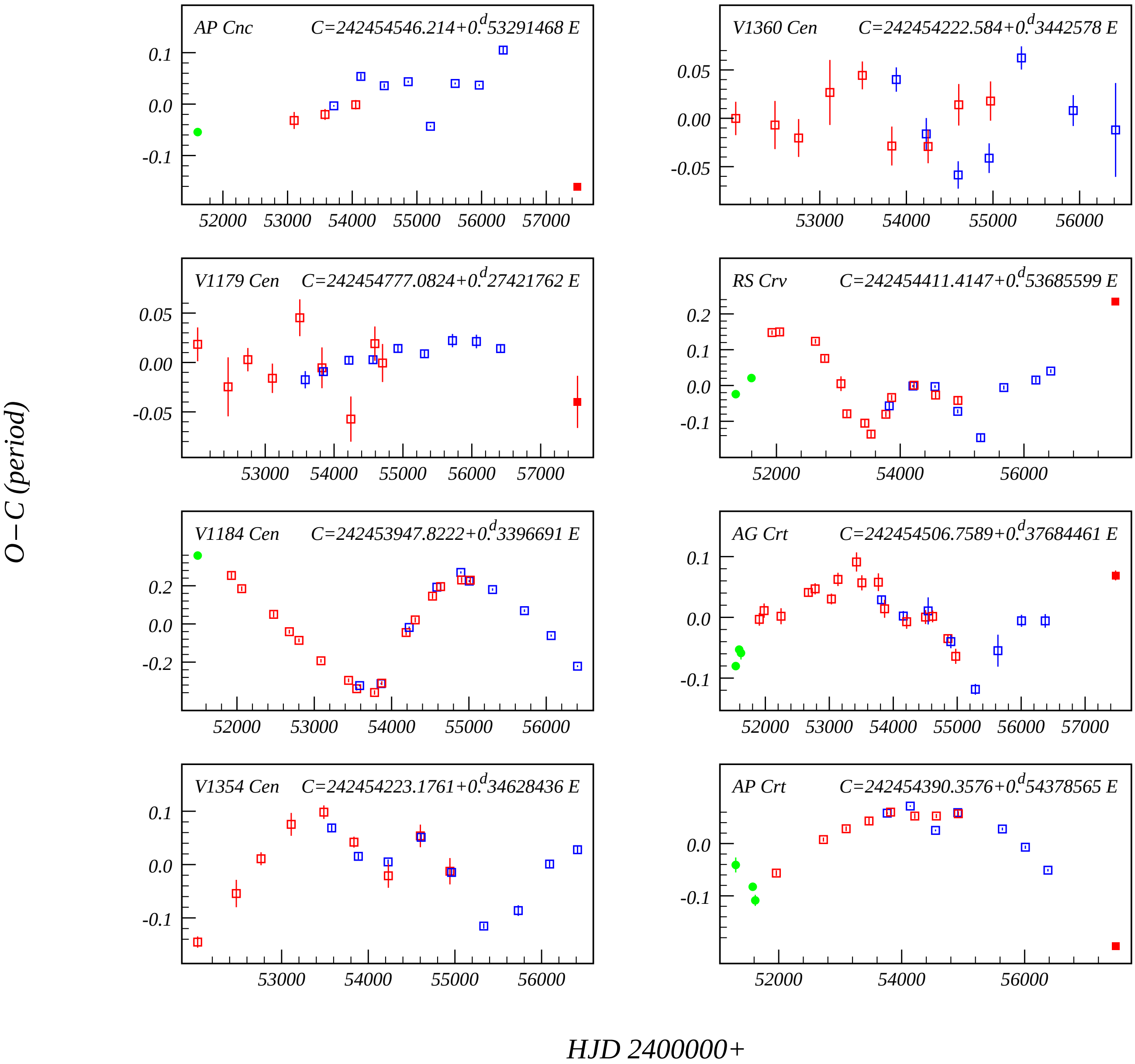

Figure 2. O−C diagrams for AP Cnc, V1179 Cen, V1184 Cen, V1354 Cen, V1360 Cen, RS Crv, AG Crt, and AP Crt.

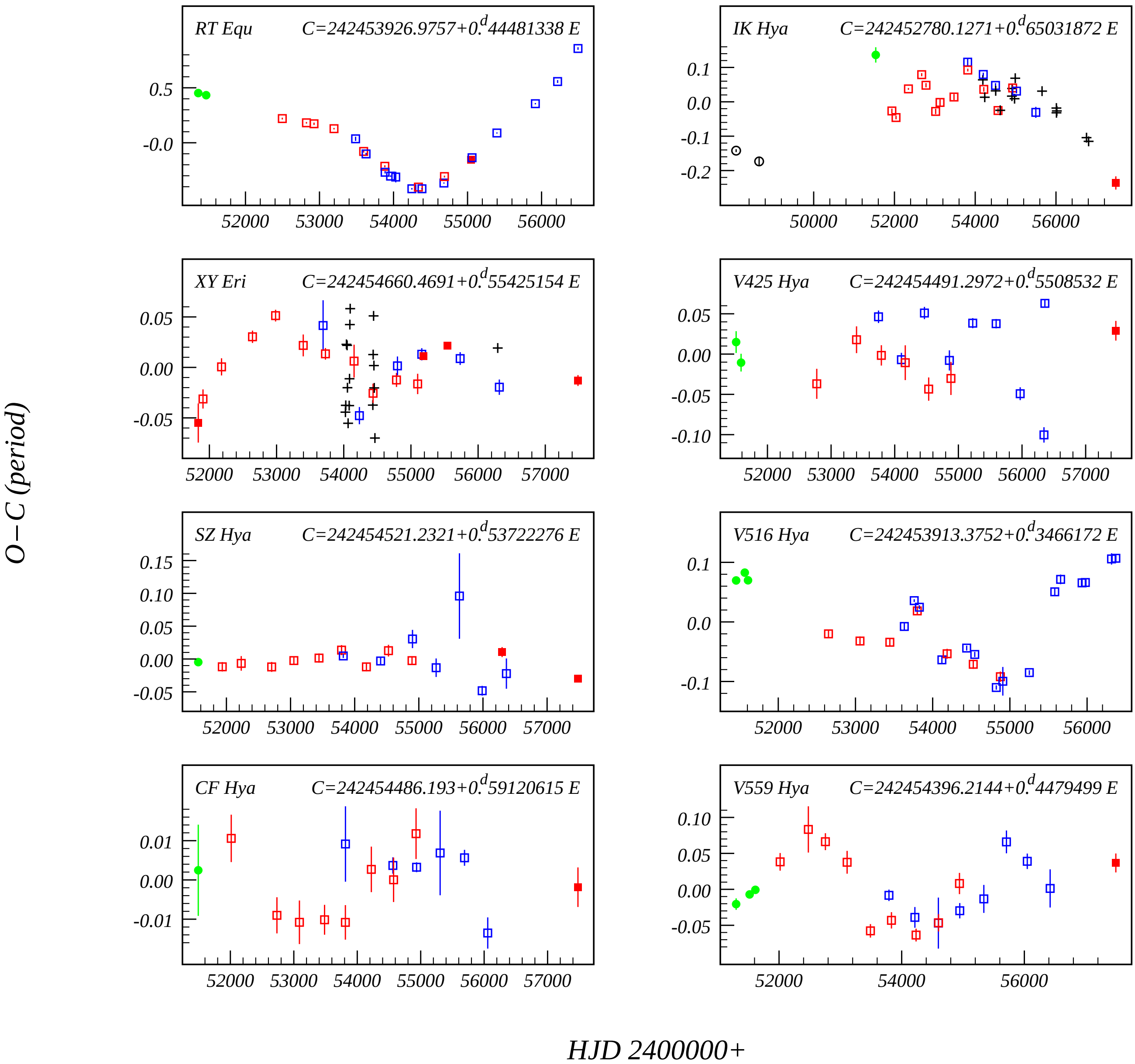

Figure 3. O−C diagrams for RT Equ, XY Eri, SZ Hya, CF Hya, IK Hya, V425 Hya, V516 Hya, and V559 Hya.

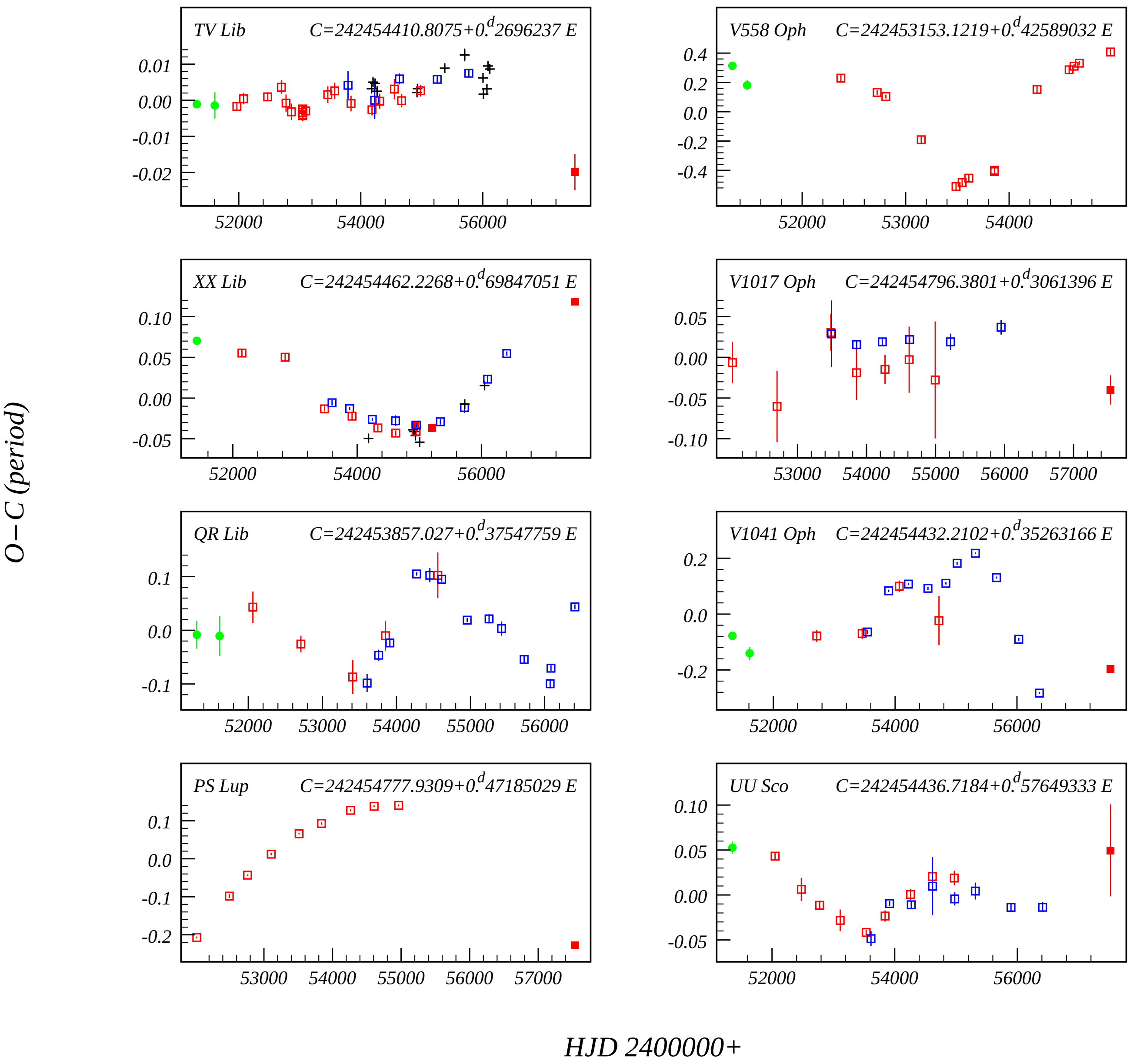

Figure 4. O−C diagrams for TV Lib, XX Lib, QR Lib, PS Lup, V558 Oph, V1017 Oph, V1041 Oph, and UU Sco.

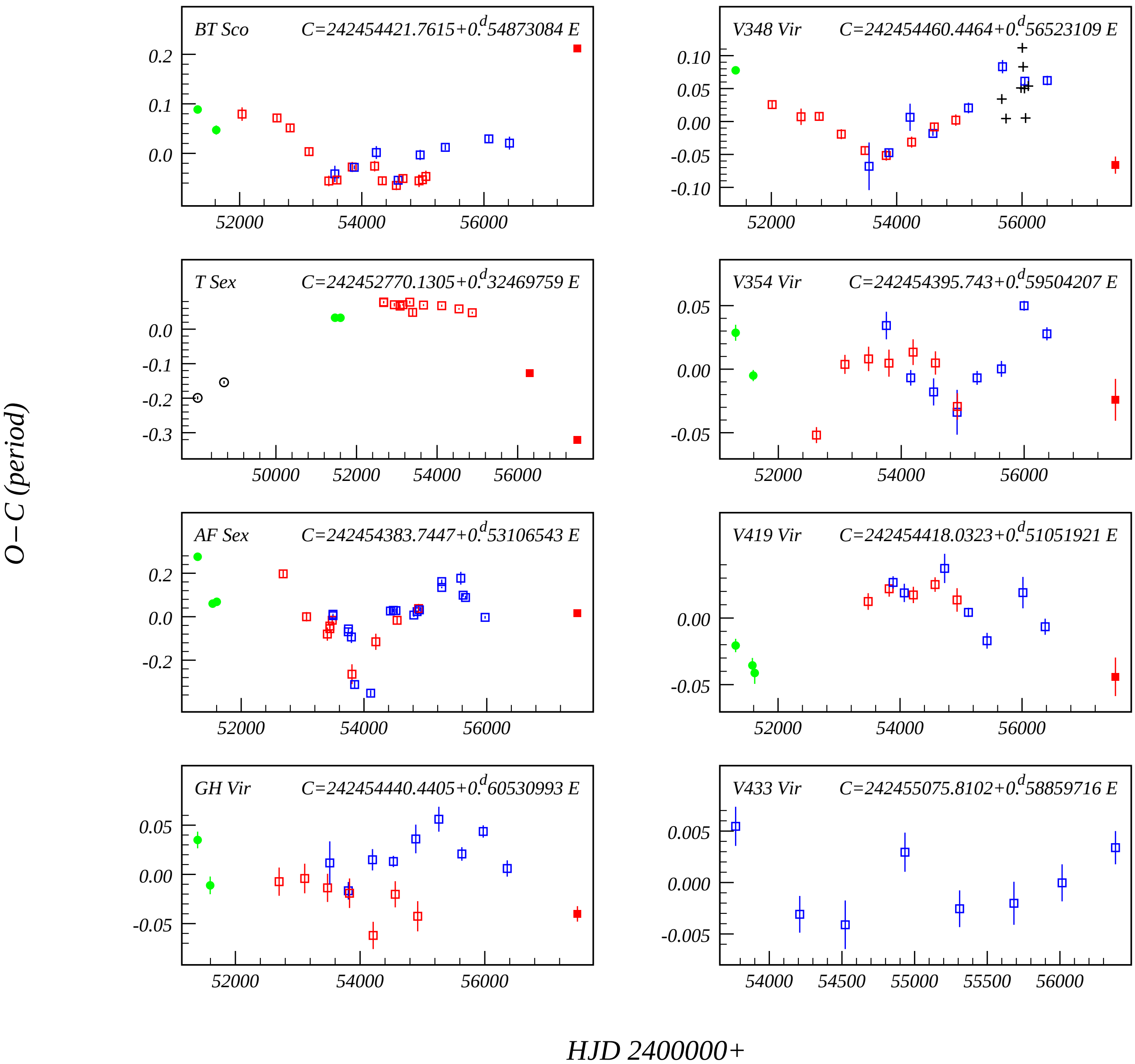

Figure 5. O−C diagrams for BT Sco, T Sex, AF Sex, GH Vir, V348 Vir, V354 Vir, V419 Vir, and V433 Vir.

Table 2: Times of maximum light for 33 RR Lyr type stars.

Max HJD	*Uncertainty*	*Filter*	*E*	O−C	*N*	*Reference*
			AP Cnc			
2451609.82516	0.00428	*V*	−5510	−0.02899	44	Wils et al. (2006)
2453101.99828	0.00878	*V*	−2710	−0.01697	29	Pojmanski (2002)
2453578.96312	0.00564	*V*	−1815	−0.01077	54	Pojmanski (2002)
2453715.39824	0.00080	*V*	−1559	−0.00181	53	Drake et al. (2006)
2454053.80022	0.00481	*V*	−924	−0.00065	27	Pojmanski (2002)
2454133.23382	0.00296	*V*	−775	0.02866	44	Drake et al. (2013)
2454495.07326	0.00220	*V*	−96	0.01904	72	Drake et al. (2013)
2454865.45314	0.00107	*V*	599	0.02321	36	Drake et al. (2013)
2455209.13687	0.00083	*V*	1244	−0.02302	36	Drake et al. (2013)
2455591.28108	0.00103	*V*	1961	0.02136	59	Drake et al. (2013)
2455963.25381	0.00103	*V*	2659	0.01964	48	Drake et al. (2013)
2456334.19874	0.00390	*V*	3355	0.05596	47	Drake et al. (2013)
2457483.02115	0.00195	*V*	5511	−0.08568	9	This paper
			V1179 Cen			
2452019.28084	0.00469	*V*	−10057	0.00504	52	Pojmanski (2002)
2452461.03363	0.00819	*V*	−8446	−0.00676	10	Pojmanski (2002)
2452748.14702	0.00324	*V*	−7399	0.00078	67	Pojmanski (2002)
2453104.35054	0.00408	*V*	−6100	−0.00439	36	Pojmanski (2002)
2453502.25710	0.00511	*V*	−4649	0.01241	47	Pojmanski (2002)
2453581.48880	0.00240	*V*	−4360	−0.00479	12	Drake et al. (2013)
2453823.90048	0.00566	*V*	−3476	−0.00148	48	Pojmanski (2002)
2453845.01418	0.00126	*V*	−3399	−0.00254	56	Drake et al. (2013)
2454215.48533	0.00109	*V*	−2048	0.00061	63	Drake et al. (2013)
2454243.71343	0.00627	*V*	−1945	−0.01571	26	Pojmanski (2002)
2454565.11295	0.00104	*V*	−773	0.00076	28	Drake et al. (2013)
2454592.26496	0.00476	*V*	−674	0.00523	39	Pojmanski (2002)
2454703.59194	0.00528	*V*	−268	−0.00015	60	Pojmanski (2002)
2454927.35755	0.00091	*V*	548	0.00389	36	Drake et al. (2013)
2455312.35761	0.00109	*V*	1952	0.00241	21	Drake et al. (2013)
2455719.30022	0.00185	*V*	3436	0.00607	16	Drake et al. (2013)
2456066.73370	0.00190	*V*	4703	0.00582	27	Drake et al. (2013)
2456417.45607	0.00122	*V*	5982	0.00386	32	Drake et al. (2013)
2457534.60386	0.00724	*V*	10056	−0.01094	7	This paper
			V1184 Cen			
2451491.79664	0.00568	*V*	−7231	0.12166	46	Wils et al. (2006)
2451928.57568	0.00547	*V*	−5945	0.08624	53	Pojmanski (2002)
2452061.36277	0.00418	*V*	−5554	0.06271	49	Pojmanski (2002)
2452474.35475	0.00519	*V*	−4338	0.01706	27	Pojmanski (2002)
2452677.44603	0.00344	*V*	−3740	−0.01378	52	Pojmanski (2002)
2452802.08914	0.00329	*V*	−3373	−0.02923	53	Pojmanski (2002)
2453086.35586	0.00311	*V*	−2536	−0.06555	68	Pojmanski (2002)
2453443.31324	0.00343	*V*	−1485	−0.10039	60	Pojmanski (2002)
2453548.25615	0.00343	*V*	−1176	−0.11523	62	Pojmanski (2002)
2453586.64433	0.00131	*V*	−1063	−0.10966	16	Drake et al. (2013)
2453779.22440	0.00389	*V*	−496	−0.12197	56	Pojmanski (2002)
2453863.81777	0.00134	*V*	−247	−0.10621	57	Drake et al. (2013)
2453872.65004	0.00352	*V*	−221	−0.10533	57	Pojmanski (2002)
2454187.61332	0.00497	*V*	706	−0.01531	53	Pojmanski (2002)
2454227.36367	0.00165	*V*	823	−0.00624	57	Drake et al. (2013)
2454305.50098	0.00458	*V*	1053	0.00717	53	Pojmanski (2002)
2454529.04548	0.00504	*V*	1711	0.04941	52	Pojmanski (2002)
2454585.10691	0.00434	*V*	1876	0.06543	46	Drake et al. (2013)

Table 2: cont.

Max HJD	*Uncertainty*	*Filter*	*E*	O−C	*N*	*Reference*
			V1184 Cen			
2454633.34092	0.00557	*V*	2018	0.06643	52	Pojmanski (2002)
2454895.25101	0.00190	*V*	2789	0.09165	24	Drake et al. (2013)
2454905.42764	0.00499	*V*	2819	0.07820	38	Pojmanski (2002)
2455004.26936	0.00183	*V*	3110	0.07621	20	Drake et al. (2013)
2455017.17843	0.00556	*V*	3148	0.07786	36	Pojmanski (2002)
2455305.54081	0.00218	*V*	3997	0.06117	28	Drake et al. (2013)
2455717.86150	0.00234	*V*	5211	0.02358	24	Drake et al. (2013)
2456063.26067	0.00192	*V*	6228	−0.02073	32	Drake et al. (2013)
2456404.23400	0.00156	*V*	7232	−0.07518	36	Drake et al. (2013)
			V1354 Cen			
2452031.14582	0.00365	*V*	−6330	−0.05033	56	Pojmanski (2002)
2452476.84532	0.00889	*V*	−5043	−0.01880	14	Pojmanski (2002)
2452762.55249	0.00420	*V*	−4218	0.00377	74	Pojmanski (2002)
2453110.59061	0.00744	*V*	−3213	0.02611	40	Pojmanski (2002)
2453487.35592	0.00440	*V*	−2125	0.03404	65	Pojmanski (2002)
2453577.72589	0.00226	*V*	−1864	0.02379	19	Drake et al. (2013)
2453834.65965	0.00354	*V*	−1122	0.01456	49	Pojmanski (2002)
2453885.20795	0.00193	*V*	−976	0.00534	53	Drake et al. (2013)
2454228.71843	0.00158	*V*	16	0.00173	62	Drake et al. (2013)
2454231.47968	0.00779	*V*	24	−0.00729	38	Pojmanski (2002)
2454600.99099	0.00734	*V*	1091	0.01861	43	Pojmanski (2002)
2454609.99348	0.00202	*V*	1117	0.01770	27	Drake et al. (2013)
2454942.05815	0.00856	*V*	2076	−0.00433	26	Pojmanski (2002)
2454961.10302	0.00201	*V*	2131	−0.00510	49	Drake et al. (2013)
2455332.63130	0.00171	*V*	3204	−0.03994	26	Drake et al. (2013)
2455730.86838	0.00347	*V*	4354	−0.02987	26	Drake et al. (2013)
2456092.41945	0.00279	*V*	5398	0.00033	34	Drake et al. (2013)
2456414.47323	0.00269	*V*	6328	0.00965	33	Drake et al. (2013)
2452482.70265	0.00857	*V*	−5054	−0.00240	14	Pojmanski (2002)
2452755.69447	0.00674	*V*	−4261	−0.00701	79	Pojmanski (2002)
2453116.49285	0.01157	*V*	−3213	0.00919	37	Pojmanski (2002)
2453491.39567	0.00496	*V*	−2124	0.01527	150	Pojmanski (2002)
2453831.49724	0.00693	*V*	−1136	−0.00987	84	Pojmanski (2002)
2453883.15957	0.00433	*V*	−986	0.01379	64	Drake et al. (2013)
2454229.46357	0.00565	*V*	20	−0.00556	64	Drake et al. (2013)
2454250.45881	0.00596	*V*	81	−0.01004	95	Pojmanski (2002)
2454597.80481	0.00488	*V*	1090	−0.02016	32	Drake et al. (2013)
2454604.37068	0.00739	*V*	1109	0.00481	105	Pojmanski (2002)
2454955.15038	0.00528	*V*	2128	−0.01419	40	Drake et al. (2013)
2454971.35082	0.00699	*V*	2175	0.00613	84	Pojmanski (2002)
2455328.01724	0.00413	*V*	3211	0.02147	32	Drake et al. (2013)
2455925.97432	0.00550	*V*	4948	0.00276	55	Drake et al. (2013)
2456415.15775	0.01670	*V*	6369	−0.00415	28	Drake et al. (2013)
			RS Crv			
2451342.19601	0.00544	*V*	−5717	−0.01303	23	Wils et al. (2006)
2451596.15307	0.00459	*V*	−5244	0.01115	65	Wils et al. (2006)
2451928.53520	0.00337	*V*	−4625	0.07942	70	Pojmanski (2002)
2452051.47618	0.00417	*V*	−4396	0.08038	69	Pojmanski (2002)
2452630.19283	0.00342	*V*	−3318	0.06627	72	Pojmanski (2002)
2452780.48679	0.00445	*V*	−3038	0.04055	71	Pojmanski (2002)
2453042.97148	0.01107	*V*	−2549	0.00266	39	Pojmanski (2002)
2453137.94987	0.00450	*V*	−2372	−0.04246	38	Pojmanski (2002)
2453428.37488	0.00504	*V*	−1831	−0.05654	60	Pojmanski (2002)

Table 2: cont.

Max HJD	*Uncertainty*	*Filter*	*E*	O−C	*N*	*Reference*
			RS Crv			
2453528.75051	0.00486	*V*	−1644	−0.07298	59	Pojmanski (2002)
2453768.21807	0.00412	*V*	−1198	−0.04319	51	Pojmanski (2002)
2453822.99003	0.00530	*V*	−1096	−0.03054	52	Drake et al. (2013)
2453861.65612	0.00406	*V*	−1024	−0.01808	51	Pojmanski (2002)
2454206.33494	0.00177	*V*	−382	−0.00081	40	Drake et al. (2013)
2454223.51549	0.00447	*V*	−350	0.00035	58	Pojmanski (2002)
2454562.26963	0.00201	*V*	281	−0.00164	43	Drake et al. (2013)
2454571.92026	0.00580	*V*	299	−0.01442	71	Pojmanski (2002)
2454929.44196	0.00300	*V*	965	−0.03880	39	Drake et al. (2013)
2454932.14260	0.00649	*V*	970	−0.02244	43	Pojmanski (2002)
2455299.83311	0.00600	*V*	1655	−0.07829	35	Drake et al. (2013)
2455674.63375	0.00302	*V*	2353	−0.00313	32	Drake et al. (2013)
2456192.17421	0.00431	*V*	3317	0.00816	30	Drake et al. (2013)
2456433.23603	0.00266	*V*	3766	0.02164	26	Drake et al. (2013)
2457480.20932	0.00346	*V*	5716	0.12575	12	This paper
2451590.71532	0.00221	*V*	−7738	−0.02000	33	Wils et al. (2006)
2451618.97653	0.00401	*V*	−7663	−0.02214	25	Wils et al. (2006)
2451906.15301	0.00394	*V*	−6901	−0.00125	26	Pojmanski (2002)
2451980.77367	0.00444	*V*	−6703	0.00418	27	Pojmanski (2002)
2452245.31510	0.00498	*V*	−6001	0.00069	23	Pojmanski (2002)
2452672.67164	0.00256	*V*	−4867	0.01544	38	Pojmanski (2002)
2452778.19038	0.00346	*V*	−4587	0.01769	37	Pojmanski (2002)
2453032.93102	0.00336	*V*	−3911	0.01138	36	Pojmanski (2002)
2453135.44491	0.00414	*V*	−3639	0.02353	35	Pojmanski (2002)
2453425.24924	0.00595	*V*	−2870	0.03436	28	Pojmanski (2002)
2453508.89580	0.00470	*V*	−2648	0.02141	28	Pojmanski (2002)
2453767.03474	0.00552	*V*	−1963	0.02180	30	Pojmanski (2002)
2453816.39048	0.00196	*V*	−1832	0.01089	43	Drake et al. (2013)
2453864.62101	0.00559	*V*	−1704	0.00531	28	Pojmanski (2002)
2454156.67108	0.00310	*V*	−929	0.00081	38	Drake et al. (2013)
2454209.04896	0.00439	*V*	−790	−0.00271	50	Pojmanski (2002)
2454504.12116	0.00432	*V*	−7	0.00016	35	Pojmanski (2002)
2454545.20106	0.00841	*V*	102	0.00400	35	Drake et al. (2013)
2454614.91391	0.00368	*V*	287	0.00059	34	Pojmanski (2002)
2454854.19647	0.00265	*V*	922	−0.01317	27	Pojmanski (2002)
2454899.79280	0.00411	*V*	1043	−0.01504	40	Drake et al. (2013)
2454976.28313	0.00467	*V*	1246	−0.02417	30	Pojmanski (2002)
2455283.39102	0.00333	*V*	2061	−0.04463	33	Drake et al. (2013)
2455636.14154	0.00992	*V*	2997	−0.02067	47	Drake et al. (2013)
2456004.71410	0.00373	*V*	3975	−0.00214	33	Drake et al. (2013)
2456375.52914	0.00424	*V*	4959	−0.00219	35	Drake et al. (2013)
2457475.94360	0.00306	*V*	7879	0.02600	9	This paper
			AP Crt			
2451301.08910	0.00779	*V*	−5680	−0.56604	32	Wils et al. (2006)
2451577.30952	0.00260	*V*	−5172	−0.58873	50	Wils et al. (2006)
2451618.62307	0.00579	*V*	−5096	−0.60289	39	Wils et al. (2006)
2451961.23642	0.00283	*V*	−4466	−0.57450	39	Pojmanski (2002)
2452726.92147	0.00215	*V*	−3059	0.00414	44	Pojmanski (2002)
2453096.70696	0.00248	*V*	−2379	0.01539	31	Pojmanski (2002)
2453468.66440	0.00364	*V*	−1695	0.02345	48	Pojmanski (2002)
2453764.49196	0.00085	*V*	−1151	0.03161	45	Drake et al. (2013)
2453819.41537	0.00280	*V*	−1050	0.03267	48	Pojmanski (2002)
2454139.16762	0.00073	*V*	−462	0.03896	32	Drake et al. (2013)

Table 2: cont.

Max HJD	*Uncertainty*	*Filter*	*E*	O−C	*N*	*Reference*
			AP Crt			
2454213.11210	0.00283	*V*	−326	0.02859	66	Pojmanski (2002)
2454550.24430	0.00093	*V*	294	0.01369	36	Drake et al. (2013)
2454563.31008	0.00218	*V*	318	0.02861	77	Pojmanski (2002)
2454911.88023	0.00369	*V*	959	0.03216	31	Drake et al. (2013)
2454921.12340	0.00249	*V*	976	0.03098	66	Pojmanski (2002)
2455637.27325	0.00148	*V*	2293	0.01513	47	Drake et al. (2013)
2456011.37885	0.00170	*V*	2981	−0.00380	32	Drake et al. (2013)
2456378.41026	0.00128	*V*	3656	−0.02771	28	Drake et al. (2013)
2457478.95327	0.00143	*V*	5680	−0.10685	8	This paper
			RT Equ			
2451362.38274	0.00275	*V*	−5770	1.98024	76	Wils et al. (2006)
2451469.12941	0.00428	*V*	−5530	1.97170	77	Wils et al. (2006)
2452497.44333	0.00359	*V*	−3217	1.43228	20	Pojmanski (2002)
2452823.47445	0.00318	*V*	−2484	1.41519	54	Pojmanski (2002)
2452925.77760	0.00477	*V*	−2253	0.96645	52	Pojmanski (2002)
2453195.75949	0.00300	*V*	−1646	0.94662	35	Pojmanski (2002)
2453487.51611	0.00856	*V*	−990	0.90566	8	Drake et al. (2013)
2453595.99941	0.00458	*V*	−746	0.85449	53	Pojmanski (2002)
2453628.90552	0.00421	*V*	−672	0.84441	44	Drake et al. (2013)
2453882.39921	0.00423	*V*	−101	0.34966	34	Pojmanski (2002)
2453885.93351	0.00484	*V*	−93	0.32546	33	Drake et al. (2013)
2453959.75697	0.00286	*V*	73	0.30990	68	Drake et al. (2013)
2454029.58890	0.02153	*V*	230	0.30612	35	Drake et al. (2013)
2454247.49996	0.00318	*V*	720	0.25863	30	Drake et al. (2013)
2454335.57981	0.00340	*V*	918	0.26543	51	Pojmanski (2002)
2454383.61286	0.00245	*V*	1026	0.25863	28	Drake et al. (2013)
2454680.32667	0.00232	*V*	1694	−0.16289	48	Drake et al. (2013)
2454687.46979	0.00364	*V*	1710	−0.13679	58	Pojmanski (2002)
2455046.05821	0.00238	*V*	2516	−0.06795	39	Berdnikov et al. (2012)
2455060.29956	0.00131	*V*	2548	−0.06063	36	Drake et al. (2013)
2455396.23380	0.00231	*V*	3303	0.03951	40	Drake et al. (2013)
2455915.44955	0.00272	*V*	4470	0.15804	44	Drake et al. (2013)
2456215.78824	0.00590	*V*	5146	−0.19711	24	Drake et al. (2013)
2456491.26135	0.00507	*V*	5765	−0.06348	36	Drake et al. (2013)
			XY Eri			
2451834.30995	0.01074	*V*	−5099	−0.03052	8	Berdnikov et al. (2012)
2451904.71309	0.00526	*V*	−4972	−0.01733	47	Pojmanski (2002)
2452180.74798	0.00471	*V*	−4474	0.00029	51	Pojmanski (2002)
2452641.34752	0.00339	*V*	−3643	0.01680	70	Pojmanski (2002)
2452984.99510	0.00322	*V*	−3023	0.02843	75	Pojmanski (2002)
2453396.78763	0.00600	*V*	−2280	0.01207	43	Pojmanski (2002)
2453692.21463	0.01386	*V*	−1747	0.02299	44	Drake et al. (2013)
2453727.11693	0.00316	*V*	−1684	0.00745	72	Pojmanski (2002)
2454024.71800	0.00000	—	−1147	−0.02456	—	Le Borgne et al. (2007)
2454029.71000	0.00000	—	−1138	−0.02082	—	Le Borgne et al. (2007)
2454039.72000	0.00000	—	−1120	0.01265	—	Le Borgne et al. (2007)
2454049.69600	0.00000	—	−1102	0.01212	—	Le Borgne et al. (2007)
2454054.66100	0.00000	—	−1093	−0.01114	—	Le Borgne et al. (2007)
2454064.61800	0.00000	—	−1075	−0.03067	—	Le Borgne et al. (2007)
2454080.70100	0.00000	—	−1046	−0.02097	—	Le Borgne et al. (2007)
2454085.70400	0.00000	—	−1037	−0.00623	—	Le Borgne et al. (2007)
2454090.72200	0.00000	—	−1028	0.02351	—	Le Borgne et al. (2007)
2454095.71900	0.00000	—	−1019	0.03224	—	Le Borgne et al. (2007)

Table 2: cont.

Max HJD	*Uncertainty*	*Filter*	*E*	O−C	*N*	*Reference*
			XY Eri			
2454153.33237	0.00902	*V*	−915	0.00345	29	Pojmanski (2002)
2454232.56041	0.00473	*V*	−772	−0.02648	58	Drake et al. (2013)
2454432.65100	0.00000	—	−411	−0.02069	—	Le Borgne et al. (2008)
2454435.98300	0.00531	*V*	−405	−0.01420	74	Pojmanski (2002)
2454437.66700	0.00000	—	−402	0.00704	—	Le Borgne et al. (2008)
2454443.78500	0.00000	—	−391	0.02828	—	Le Borgne et al. (2008)
2454448.74600	0.00000	—	−382	0.00101	—	Le Borgne et al. (2008)
2454453.72200	0.00000	—	−373	−0.01125	—	Le Borgne et al. (2008)
2454463.67100	0.00000	—	−355	−0.03878	—	Le Borgne et al. (2008)
2454784.61453	0.00384	*V*	224	−0.00689	70	Pojmanski (2002)
2454799.03281	0.00515	*V*	250	0.00085	34	Drake et al. (2013)
2455099.98147	0.00559	*V*	793	−0.00908	25	Pojmanski (2002)
2455160.96542	0.00335	*V*	903	0.00720	21	Drake et al. (2013)
2455184.79722	0.00200	*V*	946	0.00619	89	Berdnikov et al. (2012)
2455542.84958	0.00197	*V*	1592	0.01205	132	Berdnikov et al. (2012)
2455732.39640	0.00350	*V*	1934	0.00485	39	Drake et al. (2013)
2456291.64200	0.00000	—	2943	0.01064	—	Le Borgne et al. (2008)
2456315.45332	0.00421	*V*	2986	−0.01085	32	Drake et al. (2013)
2457486.03622	0.00298	*V*	5098	−0.00721	13	This paper
			SZ Hya			
2451561.13217	0.00204	*V*	−5510	−0.00256	166	Wils et al. (2006)
2451935.57261	0.00382	*V*	−4813	−0.00638	52	Pojmanski (2002)
2452231.04792	0.00598	*V*	−4263	−0.00359	31	Pojmanski (2002)
2452705.41272	0.00406	*V*	−3380	−0.00649	79	Pojmanski (2002)
2453051.38938	0.00295	*V*	−2736	−0.00129	87	Pojmanski (2002)
2453443.56404	0.00375	*V*	−2006	0.00076	69	Pojmanski (2002)
2453794.91424	0.00412	*V*	−1352	0.00727	78	Pojmanski (2002)
2453821.77060	0.00168	*V*	−1302	0.00250	48	Drake et al. (2013)
2454182.23814	0.00363	*V*	−631	−0.00644	51	Pojmanski (2002)
2454404.11595	0.00269	*V*	−218	−0.00163	60	Drake et al. (2013)
2454526.61119	0.00480	*V*	10	0.00683	71	Pojmanski (2002)
2454893.52618	0.00357	*V*	693	−0.00133	68	Pojmanski (2002)
2454901.06500	0.00748	*V*	707	0.01637	31	Drake et al. (2013)
2455269.57631	0.00758	*V*	1393	−0.00713	37	Drake et al. (2013)
			SZ Hya			
2455632.79757	0.03499	*V*	2069	0.05154	26	Drake et al. (2013)
2455987.28707	0.00397	*V*	2729	−0.02598	28	Drake et al. (2013)
2456297.83347	0.00408	*V*	3307	0.00567	29	This paper
2456364.96870	0.01238	*V*	3432	−0.01195	17	Drake et al. (2013)
2457480.77613	0.00194	*V*	5509	−0.01619	9	This paper
			CF Hya			
2451494.10008	0.00687	*V*	−5061	0.00145	51	Wils et al. (2006)
2452013.77509	0.00357	*V*	−4182	0.00626	63	Pojmanski (2002)
2452733.85259	0.00272	*V*	−2964	−0.00533	74	Pojmanski (2002)
2453088.57523	0.00328	*V*	−2364	−0.00638	52	Pojmanski (2002)
2453484.68373	0.00225	*V*	−1694	−0.00600	78	Pojmanski (2002)
2453812.80275	0.00260	*V*	−1139	−0.00640	80	Pojmanski (2002)
2453813.99697	0.00568	*V*	−1137	0.00541	59	Drake et al. (2013)
2454221.92539	0.00343	*V*	−447	0.00159	65	Pojmanski (2002)
2454561.27831	0.00123	*V*	127	0.00218	37	Drake et al. (2013)
2454572.50907	0.00335	*V*	146	0.00002	83	Pojmanski (2002)
2454926.64850	0.00382	*V*	745	0.00697	45	Pojmanski (2002)

Table 2: cont.

Max HJD	*Uncertainty*	*Filter*	*E*	O−C	*N*	*Reference*
			CF Hya			
2454934.92033	0.00074	*V*	759	0.00191	60	Drake et al. (2013)
2455306.19994	0.00637	*V*	1387	0.00406	46	Drake et al. (2013)
2455690.48321	0.00120	*V*	2037	0.00333	26	Drake et al. (2013)
2456056.42849	0.00235	*V*	2656	−0.00800	16	Drake et al. (2013)
2457478.28618	0.00298	*V*	5061	−0.00110	11	This paper
			IK Hya			
2448079.53094	0.00270	*V*	−7226	−1.39306	51	HIPPARCOS (1997)
2448649.18981	0.00850	*V*	−6350	−1.41339	51	HIPPARCOS (1997)
2451536.80638	0.01450	*V*	−1911	−0.56162	17	Wils et al. (2006)
2451935.99607	0.00446	*V*	−1297	−0.66762	61	Pojmanski (2002)
2452038.73395	0.00329	*V*	−1139	−0.68010	62	Pojmanski (2002)
2452345.73858	0.00175	*V*	−667	−0.62591	34	Pojmanski (2002)
2452674.17646	0.00294	*V*	−162	−0.59898	60	Pojmanski (2002)
2452780.80871	0.00403	*V*	2	−0.61900	58	Pojmanski (2002)
2453020.07647	0.00511	*V*	370	−0.66853	42	Pojmanski (2002)
2453128.69672	0.00601	*V*	537	−0.65150	42	Pojmanski (2002)
2453474.02621	0.00575	*V*	1067	0.00906	67	Pojmanski (2002)
2453812.90822	0.00677	*V*	1588	0.07502	28	Drake et al. (2013)
2453815.49456	0.00262	*V*	1592	0.06009	56	Pojmanski (2002)
2454188.75900	0.00000	—	2166	0.04158	—	Le Borgne et al. (2007)
2454199.17424	0.00337	*V*	2182	0.05172	36	Drake et al. (2013)
2454212.15242	0.00428	*V*	2202	0.02353	54	Pojmanski (2002)
2454235.54900	0.00000	—	2238	0.00863	—	Le Borgne et al. (2007)
2454502.20204	0.00429	*V*	2648	0.03100	21	Drake et al. (2013)
2454506.74400	0.00000	—	2655	0.02073	—	Le Borgne et al. (2008)
2454564.58515	0.00447	*V*	2744	−0.01649	66	Pojmanski (2002)
2454618.56200	0.00000	—	2827	−0.01609	—	Le Borgne et al. (2008)
2454908.63100	0.00000	—	3273	0.01076	—	Le Borgne et al. (2009)
2454913.84800	0.00000	—	3281	0.02521	—	Le Borgne et al. (2009)
2454926.85531	0.00463	*V*	3301	0.02614	51	Pojmanski (2002)
2454973.65800	0.00000	—	3373	0.00589	—	Le Borgne et al. (2009)
2454990.60500	0.00000	—	3399	0.04460	—	Le Borgne et al. (2009)
2455021.14556	0.00424	*V*	3446	0.02018	22	Drake et al. (2013)
2455500.39032	0.01040	*V*	4183	−0.01996	18	Drake et al. (2013)
2455654.55600	0.00000	—	4420	0.02019	—	Le Borgne et al. (2012)
2456009.59800	0.00000	—	4966	−0.01184	—	Le Borgne et al. (2008)
2456011.54000	0.00000	—	4969	−0.02079	—	Le Borgne et al. (2008)
2456020.64800	0.00000	—	4983	−0.01725	—	Le Borgne et al. (2008)
2456755.45760	0.00020	*V*	6113	−0.06781	4600	AAVSO
2456807.47610	0.00025	*V*	6193	−0.07480	4588	AAVSO
2457481.12758	0.01250	*V*	7229	−0.15352	6	This paper
			V425 Hya			
2451507.88445	0.00745	*V*	−5416	0.00820	60	Wils et al. (2006)
2451585.54069	0.00607	*V*	−5275	−0.00586	60	Wils et al. (2006)
2452774.81828	0.01028	*V*	−3116	−0.02033	23	Pojmanski (2002)
2453399.51594	0.00916	*V*	−1982	0.00980	36	Pojmanski (2002)
2453744.91659	0.00427	*V*	−1355	0.02550	84	Drake et al. (2013)
2453789.50930	0.00695	*V*	−1274	−0.00090	38	Pojmanski (2002)
2454104.59439	0.00470	*V*	−702	−0.00384	44	Drake et al. (2013)
2454165.18619	0.01189	*V*	−592	−0.00589	27	Pojmanski (2002)
2454466.53686	0.00419	*V*	−45	0.02808	62	Drake et al. (2013)
2454533.13808	0.00796	*V*	76	−0.02394	40	Pojmanski (2002)
2454858.71193	0.00690	*V*	667	−0.00433	55	Drake et al. (2013)

Table 2: cont.

Max HJD	*Uncertainty*	*Filter*	*E*	O−C	*N*	*Reference*
			V425 Hya			
2454882.93714	0.01131	*V*	711	−0.01666	32	Pojmanski (2002)
2455225.05478	0.00345	*V*	1332	0.02114	47	Drake et al. (2013)
2455593.02435	0.00320	*V*	2000	0.02077	65	Drake et al. (2013)
2455970.86178	0.00440	*V*	2686	−0.02709	52	Drake et al. (2013)
2456344.31208	0.00525	*V*	3364	−0.05526	40	Drake et al. (2013)
2456358.72420	0.00212	*V*	3390	0.03467	36	Drake et al. (2013)
2457473.63235	0.00673	*V*	5414	0.01595	11	This paper
			V516 Hya			
2451454.15029	0.00135	*V*	−7095	0.02413	63	Wils et al. (2006)
2451566.11219	0.00123	*V*	−6772	0.02867	63	Wils et al. (2006)
2451608.04841	0.00108	*V*	−6651	0.02421	62	Wils et al. (2006)
2452650.29517	0.00191	*V*	−3644	−0.00695	71	Pojmanski (2002)
2453058.25944	0.00263	*V*	−2467	−0.01112	63	Pojmanski (2002)
2453444.73691	0.00230	*V*	−1352	−0.01183	48	Pojmanski (2002)
2453632.26599	0.00195	*V*	−811	−0.00265	22	Drake et al. (2013)
2453760.52939	0.00080	*V*	−441	0.01238	23	Drake et al. (2013)
2453800.03777	0.00237	*V*	−327	0.00640	63	Pojmanski (2002)
2453827.07606	0.00114	*V*	−249	0.00855	25	Drake et al. (2013)
2454118.89713	0.00237	*V*	593	−0.02206	41	Drake et al. (2013)
2454186.49102	0.00288	*V*	788	−0.01853	35	Pojmanski (2002)
2454439.87150	0.00144	*V*	1519	−0.01522	29	Drake et al. (2013)
2454525.12990	0.00263	*V*	1765	−0.02465	57	Pojmanski (2002)
2454544.54618	0.00151	*V*	1821	−0.01894	27	Drake et al. (2013)
2454823.20717	0.00125	*V*	2625	−0.03817	20	Drake et al. (2013)
2454876.24589	0.00300	*V*	2778	−0.03189	47	Pojmanski (2002)
2454907.78540	0.00833	*V*	2869	−0.03454	20	Drake et al. (2013)
2455251.28810	0.00141	*V*	3860	−0.02949	29	Drake et al. (2013)
2455580.62145	0.00215	*V*	4810	0.01752	30	Drake et al. (2013)
2455656.53785	0.00280	*V*	5029	0.02476	20	Drake et al. (2013)
2455934.52281	0.00181	*V*	5831	0.02272	25	Drake et al. (2013)
2455976.81032	0.00219	*V*	5953	0.02293	48	Drake et al. (2013)
2456315.81566	0.00329	*V*	6931	0.03665	16	Drake et al. (2013)
2456371.96803	0.00249	*V*	7093	0.03704	16	Drake et al. (2013)
			V559 Hya			
2451299.97554	0.00359	*V*	−6912	−0.00920	32	Wils et al. (2006)
2451519.92497	0.00194	*V*	−6421	−0.00317	107	Wils et al. (2006)
2451613.54936	0.00219	*V*	−6212	−0.00031	75	Wils et al. (2006)
2452017.61761	0.00549	*V*	−5310	0.01713	76	Pojmanski (2002)
2452477.68235	0.01441	*V*	−4283	0.03732	16	Pojmanski (2002)
2452755.85160	0.00527	*V*	−3662	0.02968	70	Pojmanski (2002)
2453109.71920	0.00710	*V*	−2872	0.01686	43	Pojmanski (2002)
2453489.98595	0.00421	*V*	−2023	−0.02585	68	Pojmanski (2002)
2453791.92631	0.00355	*V*	−1349	−0.00372	62	Drake et al. (2013)
2453832.67417	0.00509	*V*	−1258	−0.01931	49	Pojmanski (2002)
2454214.77727	0.00645	*V*	−405	−0.01747	60	Drake et al. (2013)
2454234.02810	0.00399	*V*	−362	−0.02849	57	Pojmanski (2002)
2454597.77088	0.01589	*V*	450	−0.02102	40	Drake et al. (2013)
2454600.45877	0.00540	*V*	456	−0.02083	61	Pojmanski (2002)
2454941.82106	0.00661	*V*	1218	0.00363	43	Pojmanski (2002)
2454946.73155	0.00477	*V*	1229	−0.01333	52	Drake et al. (2013)
2455339.14303	0.00871	*V*	2105	−0.00596	32	Drake et al. (2013)
2455707.84131	0.00711	*V*	2928	0.02955	30	Drake et al. (2013)
2456047.37525	0.00482	*V*	3686	0.01747	33	Drake et al. (2013)

Table 2: cont.

Max HJD	*Uncertainty*	*Filter*	*E*	O−C	*N*	*Reference*
			V559 Hya			
2456420.50061	0.01188	*V*	4519	0.00056	32	Drake et al. (2013)
2457491.56469	0.00590	*V*	6910	0.01643	17	This paper
			TV Lib			
2451311.48278	0.00020	*V*	−11495	−0.00030	71	Wils et al. (2006)
2451606.45102	0.00098	*V*	−10401	−0.00039	36	Wils et al. (2006)
2451968.55557	0.00033	*V*	−9058	−0.00047	27	Pojmanski (2002)
2452078.29299	0.00042	*V*	−8651	0.00011	29	Pojmanski (2002)
2452473.02223	0.00034	*V*	−7187	0.00025	9	Pojmanski (2002)
2452698.96761	0.00053	*V*	−6349	0.00097	24	Pojmanski (2002)
2452775.00031	0.00064	*V*	−6067	−0.00021	24	Pojmanski (2002)
2452862.89698	0.00062	*V*	−5741	−0.00087	23	Pojmanski (2002)
2453040.30933	0.00021	*V*	−5083	−0.00091	21	Pojmanski (2002)
2453045.16276	0.00034	*V*	−5065	−0.00071	89	Pojmanski (2002)
2453046.78014	0.00049	*V*	−5059	−0.00107	45	Pojmanski (2002)
2453047.85855	0.00040	*V*	−5055	−0.00116	50	Pojmanski (2002)
2453049.74642	0.00030	*V*	−5048	−0.00065	101	Pojmanski (2002)
2453096.93042	0.00042	*V*	−4873	−0.00080	71	Pojmanski (2002)
2453458.76664	0.00063	*V*	−3531	0.00041	35	Pojmanski (2002)
2453571.73926	0.00062	*V*	−3112	0.00070	34	Pojmanski (2002)
2453790.94374	0.00106	*V*	−2299	0.00112	31	Drake et al. (2013)
2453840.01389	0.00059	*V*	−2117	−0.00025	40	Pojmanski (2002)
2454176.77500	0.00000	—	−868	0.00086	—	Le Borgne et al. (2007)
2454183.78364	0.00042	*V*	−842	−0.00071	30	Pojmanski (2002)
2454200.77200	0.00000	—	−779	0.00135	—	Le Borgne et al. (2007)
2454227.73302	0.00140	*V*	−679	0.00000	21	Drake et al. (2013)
2454233.66600	0.00000	—	−657	0.00126	—	Le Borgne et al. (2007)
2454267.63800	0.00000	—	−531	0.00067	—	Le Borgne et al. (2007)
2454309.15930	0.00057	*V*	−377	−0.00008	29	Pojmanski (2002)
2454551.28229	0.00077	*V*	521	0.00083	34	Pojmanski (2002)
2454632.97903	0.00041	*V*	824	0.00159	31	Drake et al. (2013)
2454668.56773	0.00050	*V*	956	−0.00004	34	Pojmanski (2002)
2454921.74500	0.00000	—	1895	0.00058	—	Le Borgne et al. (2009)
2454929.83400	0.00000	—	1925	0.00087	—	Le Borgne et al. (2009)
2454979.98385	0.00044	*V*	2111	0.00071	50	Pojmanski (2002)
2455252.84389	0.00028	*V*	3123	0.00156	26	Drake et al. (2013)
2455376.60200	0.00000	—	3582	0.00240	—	Le Borgne et al. (2009)
2455703.11729	0.00048	*V*	4793	0.00339	90	AAVSO
2455771.33072	0.00029	*V*	5046	0.00202	49	Drake et al. (2013)
2456003.74600	0.00000	—	5908	0.00167	—	Le Borgne et al. (2008)
2456010.75500	0.00000	—	5934	0.00045	—	Le Borgne et al. (2008)
2456067.64600	0.00000	—	6145	0.00085	—	Le Borgne et al. (2008)
2456084.63400	0.00000	—	6208	0.00256	—	Le Borgne et al. (2008)
2456114.56200	0.00000	—	6319	0.00233	—	Le Borgne et al. (2008)
2457509.85695	0.00136	*V*	11494	−0.00537	14	This paper
			XX Lib			
2451419.73834	0.00271	*V*	−4356	0.04911	45	Wils et al. (2006)
2452146.13718	0.00253	*V*	−3316	0.03862	92	Pojmanski (2002)
2452841.81022	0.00261	*V*	−2320	0.03503	93	Pojmanski (2002)
2453475.27865	0.00221	*V*	−1413	−0.00929	98	Pojmanski (2002)
2453596.11929	0.00222	*V*	−1240	−0.00405	20	Drake et al. (2013)
2453878.29639	0.00140	*V*	−836	−0.00903	64	Drake et al. (2013)
2453918.10275	0.00288	*V*	−779	−0.01549	90	Pojmanski (2002)
2454182.80400	0.00000	—	−400	−0.03456	–	Le Borgne et al. (2007)

Table 2: cont.

Max HJD	*Uncertainty*	*Filter*	*E*	O−C	*N*	*Reference*
			XX Lib			
2454243.58717	0.00133	*V*	−313	−0.01833	57	Drake et al. (2013)
2454332.28562	0.00277	*V*	−186	−0.02563	95	Pojmanski (2002)
2454617.26780	0.00458	*V*	222	−0.01942	33	Drake et al. (2013)
2454620.74957	0.00223	*V*	227	−0.03000	99	Pojmanski (2002)
2454900.83900	0.00000	—	628	−0.02725	—	Le Borgne et al. (2009)
2454914.80700	0.00000	—	648	−0.02866	—	Le Borgne et al. (2009)
2454934.36996	0.00115	*V*	676	−0.02287	18	Berdnikov et al. (2012)
2454937.85300	0.00000	—	681	−0.03219	—	Le Borgne et al. (2009)
2454948.33375	0.00331	*V*	696	−0.02849	107	Pojmanski (2002)
2454952.52987	0.00185	*V*	702	−0.02320	47	Drake et al. (2013)
2455005.59900	0.00000	—	778	−0.03783	—	Le Borgne et al. (2009)
2455209.56438	0.00059	*V*	1070	−0.02583	24	Berdnikov et al.(2012)
2455339.48539	0.00239	*V*	1256	−0.02034	41	Drake et al. (2013)
2455727.84726	0.00461	*V*	1812	−0.00807	20	Drake et al. (2013)
2455730.64400	0.00000	—	1816	−0.00522	—	Le Borgne et al. (2012)
2456049.86100	0.00000	—	2273	0.01076	—	Le Borgne et al. (2012)
2456098.75942	0.00328	*V*	2343	0.01625	20	Drake et al. (2013)
2456407.50532	0.00181	*V*	2785	0.03818	29	Drake et al. (2013)
2457503.45023	0.00086	*V*	4354	0.08286	10	This paper
			QR Lib			
2451304.52718	0.00980	*V*	−6800	0.74783	24	Wils et al. (2006)
2451612.79337	0.01397	*V*	−5979	0.74692	14	Wils et al. (2006)
2452061.88477	0.01097	*V*	−4783	0.76712	39	Pojmanski (2002)
2452709.55779	0.00584	*V*	−3057	0.36582	47	Pojmanski (2002)
2453409.80047	0.01198	*V*	−1192	0.34280	60	Pojmanski (2002)
2453603.91814	0.00628	*V*	−675	0.33855	15	Drake et al. (2013)
2453759.38537	0.00387	*V*	−261	0.35806	12	Drake et al. (2013)
2453851.76647	0.01046	*V*	−15	0.37167	27	Pojmanski (2002)
2453911.08689	0.00208	*V*	143	0.36663	52	Drake et al. (2013)
2454273.09552	0.00118	*V*	1107	0.41487	38	Drake et al. (2013)
2454450.69553	0.00492	*V*	1580	0.41398	11	Drake et al. (2013)
2454557.70659	0.01602	*V*	1865	0.41392	38	Pojmanski (2002)
2454609.89518	0.00163	*V*	2004	0.41113	34	Drake et al. (2013)
2454954.55504	0.00148	*V*	2922	0.38256	55	Drake et al. (2013)
2455250.43227	0.00316	*V*	3711	0.00797	20	Drake et al. (2013)
2455419.01491	0.00498	*V*	4160	0.00117	16	Drake et al. (2013)
2455723.50564	0.00246	*V*	4971	−0.02042	16	Drake et al. (2013)
2456074.56022	0.00325	*V*	5906	−0.03739	12	Drake et al. (2013)
2456085.83544	0.00202	*V*	5936	−0.02650	24	Drake et al. (2013)
2456408.78901	0.00176	*V*	6796	0.01635	36	Drake et al. (2013)
			PS Lup			
2452020.81197	0.00122	*V*	−5843	−0.09774	83	Pojmanski (2002)
2452495.07287	0.00236	*V*	−4838	−0.04638	23	Pojmanski (2002)
2452761.22248	0.00090	*V*	−4274	−0.02033	95	Pojmanski (2002)
2453106.17109	0.00151	*V*	−3543	0.00572	57	Pojmanski (2002)
2453512.93136	0.00088	*V*	−2681	0.03104	115	Pojmanski (2002)
2453839.46451	0.00167	*V*	−1989	0.04379	73	Pojmanski (2002)
2454263.67427	0.00128	*V*	−1090	0.06014	84	Pojmanski (2002)
2454606.71438	0.00104	*V*	−363	0.06509	96	Pojmanski (2002)
2454963.90620	0.00130	*V*	394	0.06624	79	Pojmanski (2002)
2457534.37276	0.00083	*V*	5842	−0.10758	9	This paper

Table 2: cont.

Max HJD	*Uncertainty*	*Filter*	*E*	O−C	*N*	*Reference*
			V558 Oph			
2451325.75995	0.01001	*V*	−4292	0.55933	107	Wils et al. (2006)
2451467.95087	0.01463	*V*	−3958	0.50289	107	Wils et al. (2006)
2452373.84014	0.00906	*V*	−1831	0.52345	17	Pojmanski (2002)
2452724.30640	0.00716	*V*	−1008	0.48197	88	Pojmanski (2002)
2452808.62069	0.00550	*V*	−809	0.04409	68	Pojmanski (2002)
2453150.91088	0.00976	*V*	−5	−0.08154	38	Pojmanski (2002)
2453486.80238	0.01062	*V*	783	0.20839	34	Pojmanski (2002)
2453546.01295	0.00923	*V*	923	−0.20568	65	Pojmanski (2002)
2453610.76095	0.01234	*V*	1075	−0.19301	31	Pojmanski (2002)
2453858.64838	0.00816	*V*	1657	−0.17375	41	Pojmanski (2002)
2453859.07774	0.00660	*V*	1658	−0.17028	41	Pojmanski (2002)
2454269.44528	0.01012	*V*	2621	0.06488	63	Pojmanski (2002)
2454579.97615	0.01026	*V*	3350	0.12171	45	Pojmanski (2002)
2454627.68647	0.00579	*V*	3462	0.13231	87	Pojmanski (2002)
2454678.37624	0.00634	*V*	3581	0.14114	42	Pojmanski (2002)
2454979.93900	0.01014	*V*	4289	0.17355	35	Pojmanski (2002)
			V1017 Oph			
2452057.04098	0.00781	*V*	−8948	−0.00200	21	Pojmanski (2002)
2452703.59130	0.01341	*V*	−6836	−0.01851	35	Pojmanski (2002)
2453483.66290	0.00702	*V*	−4288	0.00939	57	Pojmanski (2002)
2453493.15266	0.01257	*V*	−4257	0.00882	7	Drake et al. (2013)
2453855.30117	0.01022	*V*	−3074	−0.00582	20	Pojmanski (2002)
2453856.23020	0.00158	*V*	−3071	0.00479	47	Drake et al. (2013)
2454229.10925	0.00117	*V*	−1853	0.00581	28	Drake et al. (2013)
2454267.97866	0.00552	*V*	−1726	−0.00451	39	Pojmanski (2002)
2454617.89983	0.01244	*V*	−583	−0.00090	38	Pojmanski (2002)
2454624.33631	0.00111	*V*	−562	0.00665	16	Drake et al. (2013)
2454995.66848	0.02200	*V*	651	−0.00852	18	Pojmanski (2002)
2455217.63403	0.00308	*V*	1376	0.00582	20	Drake et al. (2013)
2455949.92543	0.00274	*V*	3768	0.01130	22	Drake et al. (2013)
2457535.39886	0.00550	*V*	8947	−0.01226	6	This paper
			V1041 Oph			
2451329.02416	0.00510	*V*	−8797	−1.08535	93	Wils et al. (2006)
2451611.46002	0.00808	*V*	−7996	−1.10745	25	Wils et al. (2006)
2452713.80855	0.00761	*V*	−4871	−0.73286	24	Pojmanski (2002)
2453459.27491	0.00707	*V*	−2757	−0.72982	51	Pojmanski (2002)
2453547.43479	0.00265	*V*	−2507	−0.72786	52	Drake et al. (2013)
2453893.41840	0.00151	*V*	−1527	−0.32328	41	Drake et al. (2013)
2454067.62423	0.00722	*V*	−1033	−0.31749	55	Pojmanski (2002)
2454218.55330	0.00116	*V*	−605	−0.31477	44	Drake et al. (2013)
2454538.38489	0.00191	*V*	302	−0.32009	40	Drake et al. (2013)
2454719.24414	0.03101	*V*	815	−0.36088	34	Pojmanski (2002)
2454833.19123	0.00150	*V*	1138	−0.31382	12	Drake et al. (2013)
2455016.93760	0.00184	*V*	1658	0.06409	31	Drake et al. (2013)
2455317.39240	0.00114	*V*	2510	0.07671	48	Drake et al. (2013)
2455663.99869	0.00131	*V*	3493	0.04608	44	Drake et al. (2013)
2456029.24721	0.00174	*V*	4529	−0.03180	32	Drake et al. (2013)
2456367.35304	0.00131	*V*	5488	−0.09973	40	Drake et al. (2013)
2457535.65240	0.00147	*V*	8801	−0.06906	7	This paper
			UU Sco			
2451354.23893	0.00394	*V*	−5347	0.03037	59	Wils et al. (2006)
2452050.06092	0.00236	*V*	−4140	0.02491	63	Pojmanski (2002)

Table 2: cont.

Max HJD	*Uncertainty*	*Filter*	*E*	O−C	*N*	*Reference*
			UU Sco			
2452478.37414	0.00743	*V*	−3397	0.00359	26	Pojmanski (2002)
2452775.83449	0.00303	*V*	−2881	−0.00662	63	Pojmanski (2002)
2453111.34395	0.00695	*V*	−2299	−0.01628	41	Pojmanski (2002)
2453535.05881	0.00173	*V*	−1564	−0.02401	93	Pojmanski (2002)
2453613.45789	0.00474	*V*	−1428	−0.02803	16	Drake et al. (2013)
2453843.49325	0.00358	*V*	−1029	−0.01351	43	Pojmanski (2002)
2453916.71591	0.00161	*V*	−902	−0.00550	59	Drake et al. (2013)
2454258.58224	0.00348	*V*	−309	0.00029	58	Pojmanski (2002)
2454270.10552	0.00262	*V*	−289	−0.00630	39	Drake et al. (2013)
2454614.29020	0.00321	*V*	308	0.01186	57	Pojmanski (2002)
2454616.01341	0.01865	*V*	311	0.00559	25	Drake et al. (2013)
2454972.29156	0.00472	*V*	929	0.01086	36	Pojmanski (2002)
2454978.04311	0.00422	*V*	939	−0.00252	60	Drake et al. (2013)
2455314.72025	0.00544	*V*	1523	0.00252	28	Drake et al. (2013)
2455895.81508	0.00241	*V*	2531	−0.00793	39	Drake et al. (2013)
2456410.62367	0.00318	*V*	3424	−0.00788	23	Drake et al. (2013)
2457518.68033	0.02951	*V*	5346	0.02860	11	This paper
			BT Sco			
2451312.15243	0.00236	*V*	−5668	0.59734	65	Wils et al. (2006)
2451616.67529	0.00511	*V*	−5113	0.57458	18	Wils et al. (2006)
2452039.21568	0.00749	*V*	−4343	0.59222	44	Pojmanski (2002)
2452610.98895	0.00477	*V*	−3301	0.58796	44	Pojmanski (2002)
2452826.62915	0.00361	*V*	−2907	0.02821	42	Pojmanski (2002)
2453136.08706	0.00379	*V*	−2343	0.00192	35	Pojmanski (2002)
2453459.80572	0.00587	*V*	−1753	−0.03061	36	Pojmanski (2002)
2453558.58515	0.00903	*V*	−1573	−0.02273	14	Drake et al. (2013)
2453592.59965	0.00437	*V*	−1511	−0.02955	45	Pojmanski (2002)
2453842.83532	0.00557	*V*	−1055	−0.01514	51	Pojmanski (2002)
2453876.30756	0.00229	*V*	−994	−0.01548	58	Drake et al. (2013)
2454209.93722	0.00585	*V*	−386	−0.01417	45	Pojmanski (2002)
2454237.93759	0.00713	*V*	−335	0.00093	39	Drake et al. (2013)
2454335.58037	0.00456	*V*	−157	−0.03038	44	Pojmanski (2002)
2454565.49342	0.00518	*V*	262	−0.03556	44	Pojmanski (2002)
2454595.13065	0.00444	*V*	316	−0.02979	34	Drake et al. (2013)
2454674.14979	0.00443	*V*	460	−0.02789	51	Pojmanski (2002)
2454936.98930	0.00692	*V*	939	−0.03045	35	Pojmanski (2002)
2454955.67486	0.00567	*V*	973	−0.00174	27	Drake et al. (2013)
2454992.96108	0.00464	*V*	1041	−0.02922	70	Pojmanski (2002)
2455048.93525	0.00645	*V*	1143	−0.02560	35	Pojmanski (2002)
2455367.23140	0.00318	*V*	1723	0.00667	34	Drake et al. (2013)
2456080.04215	0.00399	*V*	3022	0.01606	35	Drake et al. (2013)
2456418.05564	0.00718	*V*	3638	0.01135	14	Drake et al. (2013)
2457530.43773	0.00091	*V*	5665	0.11603	5	This paper
			T Sex			
2448057.08028	0.00150	*V*	−14514	−0.38937	37	HIPPARCOS (1997)
2448712.00996	0.00134	*V*	−12497	−0.37473	43	HIPPARCOS (1997)
2451467.12979	0.00096	*V*	−4012	−0.31395	89	Wils et al. (2006)
2451601.55455	0.00082	*V*	−3598	−0.31399	89	Wils et al. (2006)
2452673.07092	0.00083	*V*	−299	0.02503	70	Pojmanski (2002)
2452675.66902	0.00103	*V*	−291	0.02555	25	Pojmanski (2002)
2452938.99620	0.00166	*V*	520	0.02298	25	Pojmanski (2002)
2453081.53716	0.00150	*V*	959	0.02170	25	Pojmanski (2002)
2453151.99785	0.00086	*V*	1176	0.02301	70	Pojmanski (2002)

Table 2: cont.

Max HJD	*Uncertainty*	*Filter*	*E*	O−C	*N*	*Reference*
			T Sex			
2453321.81707	0.00128	*V*	1699	0.02539	26	Pojmanski (2002)
2453392.91621	0.00377	*V*	1918	0.01576	8	Pojmanski (2002)
2453662.42210	0.00094	*V*	2748	0.02265	69	Pojmanski (2002)
2454114.72525	0.00097	*V*	4141	0.02206	59	Pojmanski (2002)
2454543.64777	0.00081	*V*	5462	0.01906	52	Pojmanski (2002)
2454872.23814	0.00099	*V*	6474	0.01547	61	Pojmanski (2002)
2456296.62961	0.00240	*V*	10861	−0.04139	16	This paper
2457483.01196	0.00317	*V*	14515	−0.10403	9	This paper
			AF Sex			
2451290.96614	0.00727	*V*	−5824	0.14646	27	Wils et al. (2006)
2451535.14171	0.00429	*V*	−5364	0.03193	80	Wils et al. (2006)
2451602.06041	0.00309	*V*	−5238	0.03638	94	Wils et al. (2006)
2452683.90902	0.00751	*V*	−3201	0.10471	34	Pojmanski (2002)
2453064.57815	0.01139	*V*	−2484	−0.00007	24	Pojmanski (2002)
2453403.35553	0.01625	*V*	−1846	−0.04244	26	Pojmanski (2002)
2453443.72963	0.00861	*V*	−1770	−0.02931	53	Pojmanski (2002)
2453444.26716	0.00535	*V*	−1769	−0.02284	53	Pojmanski (2002)
2453483.04915	0.01150	*V*	−1696	−0.00863	27	Pojmanski (2002)
2453495.27475	0.00179	*V*	−1673	0.00247	12	Drake et al. (2013)
2453495.27833	0.00128	*V*	−1673	0.00605	12	Drake et al. (2013)
2453744.30515	0.00374	*V*	−1204	−0.03682	23	Drake et al. (2013)
2453746.96741	0.00352	*V*	−1199	−0.02989	25	Drake et al. (2013)
2453795.27474	0.01471	*V*	−1108	−0.04951	48	Drake et al. (2013)
2453804.21191	0.02422	*V*	−1091	−0.14045	42	Pojmanski (2002)
2453847.73402	0.00868	*V*	−1009	−0.16571	23	Drake et al. (2013)
2454108.99713	0.00713	*V*	−517	−0.18679	37	Drake et al. (2013)
2454193.03103	0.01980	*V*	−359	−0.06123	30	Pojmanski (2002)
2454430.49245	0.00836	*V*	88	0.01394	23	Drake et al. (2013)
2454477.75887	0.00439	*V*	177	0.01554	48	Drake et al. (2013)
2454520.77447	0.00587	*V*	258	0.01484	25	Drake et al. (2013)
2454539.33814	0.00970	*V*	293	−0.00878	50	Pojmanski (2002)
2454811.78752	0.00427	*V*	806	0.00403	15	Drake et al. (2013)
2454864.90239	0.00220	*V*	906	0.01236	36	Drake et al. (2013)
2454889.33884	0.01151	*V*	952	0.01980	31	Pojmanski (2002)
2454902.61239	0.00289	*V*	977	0.01672	21	Drake et al. (2013)
2455266.44695	0.00199	*V*	1662	0.07146	29	Drake et al. (2013)
2455266.46134	0.00506	*V*	1662	0.08585	29	Drake et al. (2013)
2455576.61172	0.01566	*V*	2246	0.09402	27	Drake et al. (2013)
2455614.80699	0.00406	*V*	2318	0.05257	54	Drake et al. (2013)
2455653.56908	0.00440	*V*	2391	0.04689	27	Drake et al. (2013)
2455972.69094	0.00327	*V*	2992	−0.00158	40	Drake et al. (2013)
2457476.14686	0.00071	*V*	5823	0.00811	8	This paper
			GH Vir			
2451394.54210	0.00513	*V*	−5032	0.02117	91	Wils et al. (2006)
2451595.47707	0.00545	*V*	−4700	−0.00676	89	Wils et al. (2006)
2452701.38060	0.00869	*V*	−2873	−0.00447	28	Pojmanski (2002)
2453111.78268	0.00911	*V*	−2195	−0.00252	16	Pojmanski (2002)
2453477.98943	0.00868	*V*	−1590	−0.00828	39	Pojmanski (2002)
2453513.71805	0.01327	*V*	−1531	0.00705	20	Drake et al. (2013)
2453811.51341	0.00540	*V*	−1039	−0.01007	67	Drake et al. (2013)
2453830.27651	0.00909	*V*	−1008	−0.01158	40	Pojmanski (2002)
2454198.93084	0.00656	*V*	−399	0.00900	36	Drake et al. (2013)
2454209.77987	0.00839	*V*	−381	−0.03755	42	Pojmanski (2002)

Table 2: cont.

Max HJD	*Uncertainty*	*Filter*	*E*	O−C	*N*	*Reference*
			GH Vir			
2454534.27148	0.00347	*V*	155	0.00794	48	Drake et al. (2013)
2454563.91148	0.00805	*V*	204	−0.01224	43	Pojmanski (2002)
2454893.23412	0.00882	*V*	748	0.02179	33	Drake et al. (2013)
2454924.05738	0.00929	*V*	799	−0.02575	34	Pojmanski (2002)
2455263.09063	0.00766	*V*	1359	0.03394	32	Drake et al. (2013)
2455632.30832	0.00418	*V*	1969	0.01257	51	Drake et al. (2013)
2455974.92757	0.00378	*V*	2535	0.02640	44	Drake et al. (2013)
2456359.88192	0.00501	*V*	3171	0.00363	48	Drake et al. (2013)
2457485.73047	0.00476	*V*	5031	−0.02429	8	This paper
			V348 Vir			
2451430.85171	0.00261	*V*	−5359	−0.52130	120	Wils et al. (2006)
2452013.01031	0.00303	*V*	−4329	−0.55072	75	Pojmanski (2002)
2452474.22844	0.00704	*V*	−3513	−0.56116	18	Pojmanski (2002)
2452763.62707	0.00341	*V*	−3002	0.00438	74	Pojmanski (2002)
2453116.31601	0.00427	*V*	−2378	−0.01088	41	Pojmanski (2002)
2453495.57203	0.00373	*V*	−1707	−0.02492	64	Pojmanski (2002)
2453559.42962	0.02045	*V*	−1594	−0.03844	20	Drake et al. (2013)
2453833.57598	0.00441	*V*	−1109	−0.02916	54	Pojmanski (2002)
2453875.97071	0.00271	*V*	−1034	−0.02676	39	Drake et al. (2013)
2454213.44407	0.01167	*V*	−437	0.00364	42	Drake et al. (2013)
2454238.29290	0.00472	*V*	−393	−0.01770	59	Pojmanski (2002)
2454578.00423	0.00211	*V*	208	−0.01026	40	Drake et al. (2013)
2454600.61907	0.00380	*V*	248	−0.00466	67	Pojmanski (2002)
2454943.72019	0.00487	*V*	855	0.00119	49	Pojmanski (2002)
2455145.51814	0.00458	*V*	1212	0.01164	60	Drake et al. (2013)
2455676.84300	0.00000	—	2152	0.01927	—	Le Borgne et al. (2012)
2455688.74063	0.00572	*V*	2173	0.04705	40	Drake et al. (2013)
2455744.65400	0.00000	—	2272	0.00254	—	Le Borgne et al. (2012)
2455983.77300	0.00000	—	2695	0.02879	—	Le Borgne et al. (2008)
2456004.72100	0.00000	—	2732	0.06324	—	Le Borgne et al. (2008)
2456017.70500	0.00000	—	2755	0.04693	—	Le Borgne et al. (2008)
2456038.60000	0.00000	—	2792	0.02838	—	Le Borgne et al. (2008)
2456044.25854	0.00346	*V*	2802	0.03460	32	Drake et al. (2013)
2456056.66200	0.00000	—	2824	0.00298	—	Le Borgne et al. (2008)
2456099.64700	0.00000	—	2900	0.03042	—	Le Borgne et al. (2008)
2456402.61563	0.00408	*V*	3436	0.03518	45	Drake et al. (2013)
2457490.04763	0.00738	*V*	5360	−0.03743	8	This paper
			V354 Vir			
2451305.70657	0.00375	*V*	−5193	0.01704	59	Wils et al. (2006)
2451591.90177	0.00262	*V*	−4712	−0.00299	141	Wils et al. (2006)
2452620.70164	0.00375	*V*	−2983	−0.03086	78	Pojmanski (2002)
2453083.67748	0.00446	*V*	−2205	0.00225	52	Pojmanski (2002)
2453468.67226	0.00572	*V*	−1558	0.00481	56	Pojmanski (2002)
2453757.87833	0.00646	*V*	−1072	0.02043	66	Drake et al. (2013)
2453800.10870	0.00634	*V*	−1001	0.00282	55	Pojmanski (2002)
2454154.15187	0.00365	*V*	−406	−0.00405	51	Drake et al. (2013)
2454192.84162	0.00603	*V*	−341	0.00797	55	Pojmanski (2002)
2454526.64160	0.00635	*V*	220	−0.01065	49	Drake et al. (2013)
2454556.40725	0.00546	*V*	270	0.00290	75	Pojmanski (2002)
2454908.64909	0.01049	*V*	862	−0.02017	46	Drake et al. (2013)
2454912.81710	0.00620	*V*	869	−0.01745	56	Pojmanski (2002)
2455234.15320	0.00326	*V*	1409	−0.00407	36	Drake et al. (2013)
2455629.86038	0.00373	*V*	2074	0.00013	53	Drake et al. (2013)

Table 2: cont.

Max HJD	*Uncertainty*	*Filter*	*E*	O−C	*N*	*Reference*
			V354 Vir			
2455998.81602	0.00232	*V*	2694	0.02969	67	Drake et al. (2013)
2456370.10913	0.00307	*V*	3318	0.01655	91	Drake et al. (2013)
2457485.18709	0.00980	*V*	5192	−0.01433	11	This paper
			V419 Vir			
2451304.87564	0.00256	*V*	−6098	−0.01052	55	Wils et al. (2006)
2451579.52735	0.00285	*V*	−5560	−0.01815	95	Wils et al. (2006)
2451617.30285	0.00416	*V*	−5486	−0.02107	96	Wils et al. (2006)
2453477.66226	0.00319	*V*	−1842	0.00634	57	Pojmanski (2002)
2453821.75709	0.00304	*V*	−1168	0.01122	53	Pojmanski (2002)
2453886.08494	0.00237	*V*	−1042	0.01365	65	Drake et al. (2013)
2454069.86784	0.00351	*V*	−682	0.00964	35	Drake et al. (2013)
2454217.91763	0.00314	*V*	−392	0.00886	47	Pojmanski (2002)
2454574.26402	0.00279	*V*	306	0.01284	63	Pojmanski (2002)
2454730.99960	0.00561	*V*	613	0.01902	39	Drake et al. (2013)
2454934.68468	0.00451	*V*	1012	0.00694	54	Pojmanski (2002)
2455121.01942	0.00177	*V*	1377	0.00216	24	Drake et al. (2013)
2455426.29904	0.00304	*V*	1975	−0.00870	38	Drake et al. (2013)
2456014.43562	0.00602	*V*	3127	0.00975	38	Drake et al. (2013)
2456378.93326	0.00309	*V*	3841	−0.00333	36	Drake et al. (2013)
2457531.15592	0.00739	*V*	6098	−0.02253	9	This paper
			V433 Vir			
2453768.53909	0.00112	*V*	−2221	0.00321	71	Drake et al. (2013)
2454209.39333	0.00105	*V*	−1472	−0.00182	32	Drake et al. (2013)
2454522.52642	0.00139	*V*	−940	−0.00242	36	Drake et al. (2013)
2454933.37139	0.00112	*V*	−242	0.00173	66	Drake et al. (2013)
2455309.48174	0.00105	*V*	397	−0.00150	48	Drake et al. (2013)
2455683.24125	0.00123	*V*	1032	−0.00119	40	Drake et al. (2013)
2456014.62262	0.00106	*V*	1595	−0.00002	59	Drake et al. (2013)
2456381.90926	0.00095	*V*	2219	0.00199	51	Drake et al. (2013)
			V494 Vir			
2451366.71576	0.00628	*V*	−5637	0.05027	112	Wils et al. (2006)
2452629.66116	0.01079	*V*	−3329	0.00974	23	Pojmanski (2002)
2453454.33426	0.00810	*V*	−1822	0.02088	46	Pojmanski (2002)
2453749.28032	0.00198	*V*	−1283	0.01485	61	Drake et al. (2013)
2453835.72008	0.00630	*V*	−1125	−0.00630	32	Pojmanski (2002)
2454224.79228	0.00542	*V*	−414	−0.00818	43	Drake et al. (2013)
2454477.05746	0.00641	*V*	47	−0.01186	42	Pojmanski (2002)
2454549.28263	0.00603	*V*	179	−0.01985	41	Drake et al. (2013)
2454933.41651	0.00970	*V*	881	−0.03507	21	Pojmanski (2002)
2454937.25918	0.00185	*V*	888	−0.02295	27	Drake et al. (2013)
2455296.21730	0.01276	*V*	1544	−0.04176	38	Drake et al. (2013)
2455317.50618	0.00560	*V*	1583	−0.09450	25	Drake et al. (2013)
2455670.02017	0.00238	*V*	2227	0.00920	48	Drake et al. (2013)
2456030.08583	0.00322	*V*	2885	0.00349	48	Drake et al. (2013)
2456030.11193	0.00370	*V*	2885	0.02959	56	Drake et al. (2013)
2456416.45020	0.00318	*V*	3591	0.02987	48	Drake et al. (2013)
2457535.01256	0.00011	*V*	5635	0.07263	7	This paper

Acknowledgements: This work makes use of observations from the South African Astronomical Observatory(SAAO), supported by the National Research Foundation of South Africa, and data from the Catalina, ASAS, GEOS, NSVS, and HIPPARCOS databases. We acknowledge with thanks the variable star observations from the AAVSO International Database contributed by observers worldwide and used in this research. The data reduction of all data was supported by the Russian Science Foundation (project no. 14-50-00043), and the light-curve analysis was supported by the Russian Science Foundation (project no. 14-22-00041). We would also like to thank Entoto Observatory and Bahir Dar University for supporting this research.

References:

Berdnikov, L. N., 1992, *Soviet Astronomy Letters*, **18**, 207
Berdnikov, L. N., et al. 2012, *Astron. Rep.*, **56**, 290 DOI
Cousins A. W. J., 1976, *MmRAS*, **81**, 25
Drake, A. J., Catelan, M., Djorgovski, S. G., et al. 2013, *ApJ*, **765**, 154 DOI
HIPPARCOS 1997, ESA SP-1200: The Hipparcos and Tycho Catalogues
Hertzsprung, E., 1919, *AN*, **210**, 17 DOI
Le Borgne, J. F., et al., 2007a, *IBVS*, **5767**
Le Borgne, J. F., et al., 2007b, *IBVS*, **5790**
Le Borgne, J. F., et al., 2008a, *IBVS*, **5823**
Le Borgne, J. F., et al., 2008b, *IBVS*, **5853**
Le Borgne, J. F., et al., 2009, *IBVS*, **5895**
Le Borgne, J. F., et al. 2012, *IBVS*, **6009**
Le Borgne, J. F., et al., 2013, *IBVS*, **6043**
Pojmanski, G., 2002, *AcA*, **52**, 397
Wils P., Lloyd C., Bernhard K., 2006, *MNRAS*, **368**, 1757 DOI

COMMISSIONS G1 AND G4 OF THE IAU
INFORMATION BULLETIN ON VARIABLE STARS
Volume 63 Number 6229 DOI: 10.22444/IBVS.6229

Konkoly Observatory
Budapest
21 December 2017

HU ISSN 0374 – 0676

DISCOVERY OF THE BLAZHKO EFFECT IN V1065 Aql, CzeV980, FI Sge, AND CzeV1242

SKARKA, M.[1,2,3]; CAGAŠ, P.[3,4]

[1] Astronomical Institute ASCR, Fričova 298, CZ-251 65 Ondřejov, Czech Republic, e-mail: marek.skarka@asu.cas.cz

[2] Konkoly Observatory, MTA CSFK, Konkoly Thege M. út 15-17, 1121 Budapest, Hungary

[3] BSObservatory, Modrá 587, CZ-760 01 Zlín, Czech Republic, e-mail: pavel.cagas@gmail.com

[4] Variable Star and Exoplanet Section of the Czech Astronomical Society, Vsetínská 941/78, CZ-757 01 Valašské Meziříčí, Czech Republic

1 Introduction

The Blazhko (BL) effect (Blazhko, 1907) is a common feature present in almost half of RR Lyrae (RRL) stars pulsating in the fundamental mode (Jurcsik et al., 2009; Benkő et al., 2010). Although it is known for more than a century, not much is known about what stands behind this phenomenon and the explanation of the modulation is still missing (for a review about the Blazhko effect see e.g. Kovács (2016) and Smolec (2016)). About 400 RRLs with the BL effect are catalogued in the Galactic field (Skarka, 2013)[1] and more than 3000 in the Galactic bulge (Prudil & Skarka, 2017). Due to relatively high incidence rate it is not much difficult to discover modulation in RRL stars that were previously considered to show stable pulsation. This is also the case of V1065 Aql, FI Sge, CzeV980, and CzeV1242, the latter two being a newly discovered RRL type stars.

2 Observations

All the stars were observed in the scope of survey dedicated to searching for new variable stars (e.g. Cagaš 2017). The strategy is similar as the one of the space telescope *Kepler* – long-term monitoring of one field.

The photometric unfiltered observations were carried out at BSO[2], Zlín, Czech Republic, using 0.3m Newtonian telescope with coma-corrector (f/4.7) equipped with Moravian instruments CCD G4-16000 (KAF-16803, 4096 × 4096 px) with field of view (FOV) of 90×90 arcmin. The full FOVs are shown in Fig. 1 and Fig. 2 together with the identification of comparison stars. For the reduction (dark frame and flat field corrections) and

[1] http://physics.muni.cz/~blasgalf/
[2] http://www.bsobservatory.org/

aperture photometry we used SIPS software[3]. For more details about the data reduction see Cagaš (2017).

The full journal of observations with number of seasons, nights and points is listed in Table 1. Dates of start and end of the observations are given in Table 1 too. Comparison stars used are listed in Table 2.

Table 1. Journal of observations.

Star	Start JD	End JD	Seasons	Nights	Points
V1065 Aql	2456210	2457662	4	23	2534
CzeV980	2457241	2457662	2	19	2218
FI Sge	2457989	2458046	1	14	1963
CzeV1242	2457989	2458046	1	14	1955

Table 2. Comparison stars.

Star	Comp ID	RA [$^{\rm h\ m\ s}$]	DEC [$^{\circ}\ '\ ''$]	V [mag]
V1065 Aql	UCAC4 520-117983	19 57 27.21	+13 50 38.3	13.129
CzeV980	UCAC4 518-117617	19 54 16.83	+13 33 59.1	13.160
FI Sge	UCAC4 538-127230	20 13 16.21	+17 30 37.0	13.940
CzeV1242	UCAC4 532-123593	20 16 06.33	+16 18 11.5	12.590

3 Analysis

Because all our data sets have only short extent (one to four seasons) we searched for additional data in large sky surveys. Usable data were found only in the ASAS–SN survey (Kochanek et al., 2017; Shapee et al., 2017). Unfortunately, the data cannot be easily stitched together because of different amplitudes. Thus we analysed the data separately.

For the initial pulsation period estimation we used Period04 (Lenz & Breger, 2005). When the rough period was known, we used LCfit routine (Sódor, 2012) for more precise period determination and for prewhitening the frequency spectra and searching for peaks close to the main pulsation components (the consequence of the BL effect).

We also estimated times of maximum light using polynomial fitting routine described in Skarka et al. (2015) that we applied to our data. As the zero epoch we used the most-bright well-defined maximum. The light ephemerides and rough estimation of the modulation period are shown in Table 3. Only in V1065 Aql our data give more precise period estimation than ASAS–SN data. BL period was always estimated on the basis of ASAS–SN data, because our data are not appropriate for that purpose.

[3] `http://www.tcmt.org/software.html`

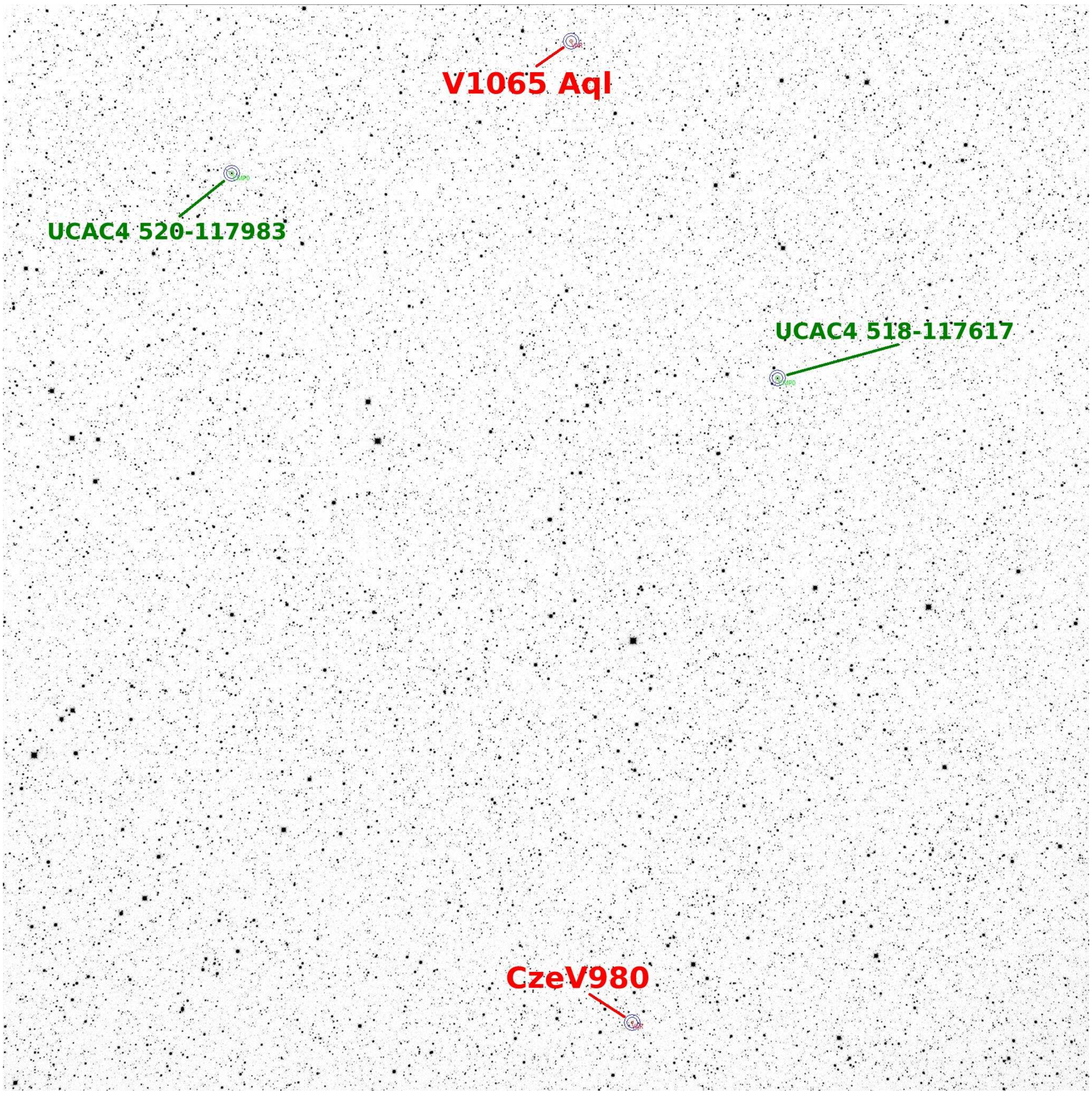

Figure 1. The full observed FOV with V1065 Aql and CzeV980 with identification of stars.

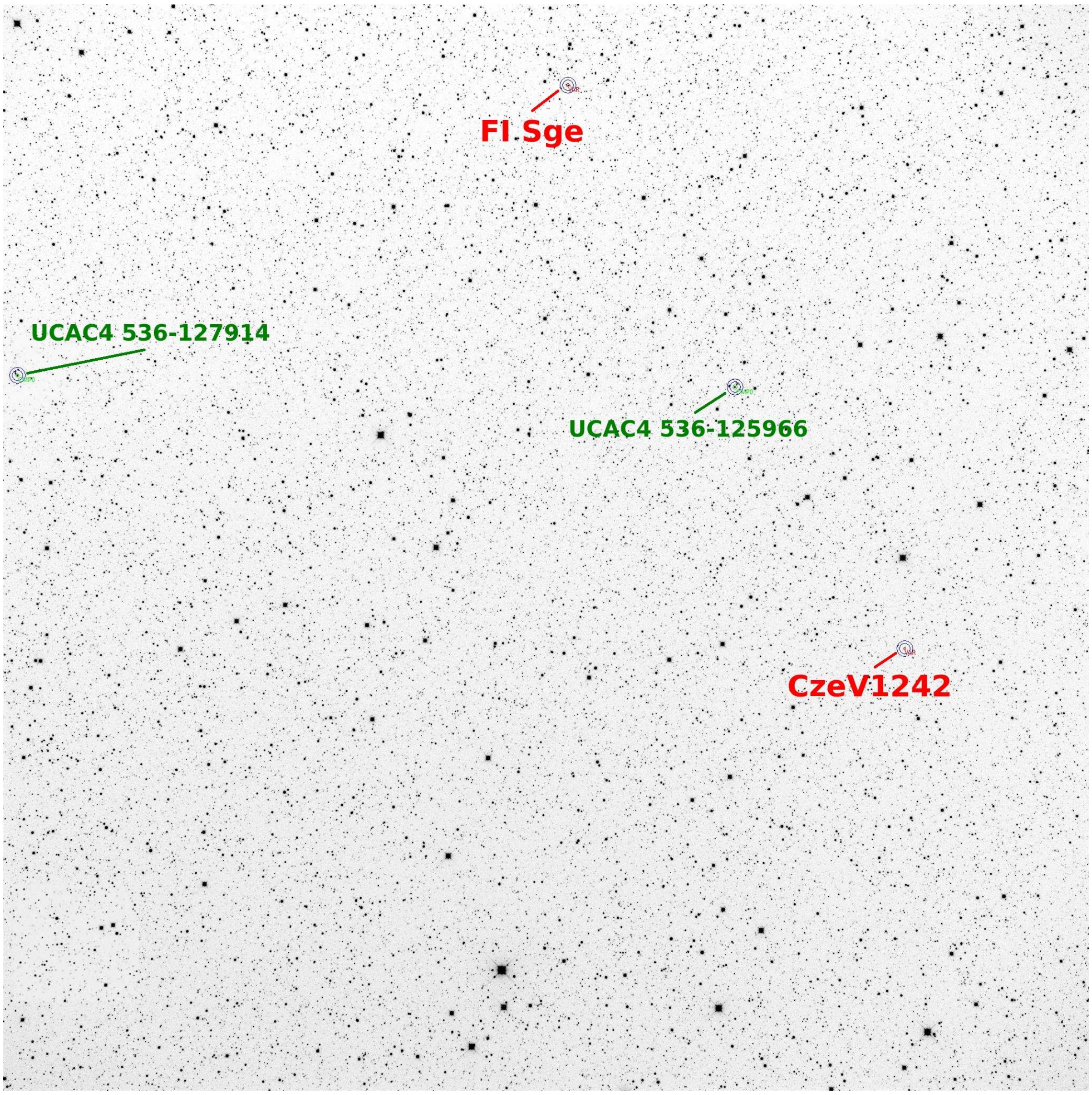

Figure 2. The full observed FOV with FI Sge and CzeV1242 with identification of stars.

Table 3. Light ephemerides and Blazhko period estimation. The upper index 'a' in pulsation period means that it is based on the ASAS–SN data.

Star	Zero epoch [HJD]	Pulsation period [d]	Blazhko period [d]
V1065 Aql	2456212.3690(4)	0.5089976(3)	∼650
CzeV980	2457629.4404(2)	0.529675(3)[a]	∼32.8
FI Sge	2458026.2833(2)	0.504783(2)[a]	∼22.4
CzeV1242	2458043.2929(4)	0.415552(7)[a]	-

4 Remarks on individual stars

4.1 V1065 Aql

The variability of V1065 Aql (J2000 19:55:29.89 +14:02:07.5, photographic magnitude 15.5–16.5) was discovered by C. Hoffmeister (1964) on Sonneberg plates. The modulation is well apparent in variation of the amplitude of light changes in both from our and ASAS–SN data (see the two upper panels of Fig. 3). After removing 8 basic pulsation harmonics from the frequency spectra we identified a peak at 1.9632 c/d (see the detail in the bottom panel of Fig. 3), which suggests the modulation period about 650 d. From the envelope of the ASAS–SN data shown in the upper panel of Fig. 3 it is apparent that this period could be close to the correct one. However, the identified peak has signal-to-noise ratio (SNR) only about 3.8 and the data contain only one modulation cycle. Thus, the period is only the first, rough estimate.

From the phased light curve in the middle panel of Fig. 3 it is clear that the real modulation amplitude in magnitude is very likely significantly larger than we were able to estimate from our data (~ 0.34 mag).

4.2 CzeV980

CzeV980[4] (=UCAC4 514-114877, J2000 19:55:04.99 +12:39:29.26, $J = 14.463$ mag, $J - K = 0.402$ mag) lies in the same field as V1065 Aql (see Fig. 1). This star was found to be a new variable of RRab type.

The coverage of our data is very poor since we observed the star only in two consecutive seasons, in the first season having only one night (the original FOV was somewhat shifted in the first two seasons). However, even from these data the modulation is clearly recognizable (see Fig. 4). The star has the full amplitude of the light changes in maximum BL phase about 1 mag and the amplitude of the modulation is at least 0.23 mag in clear filter. Similarly as in V1065 Aql, our data are not appropriate for modulation period determination (see the detail in Fig. 4), but data from ASAS–SN survey suggest modulation period of 32.9 d (the peak to the left from the basic pulsation frequency in the detail of Fig. 4).

4.3 FI Sge

The variability of FI Sge (J2000 20:13:16.21 +17 30 37.0, V=13.94 mag) was discovered by Hoffmeister (1936). The star was observed only in 14 nights during the summer season 2017 (see Table 1). Side peak at 2.0303 c/d (SNR∼4.4) suggests relatively well defined modulation period of the length of 22.4 d.

[4]Designation gives the identification in the Czech Variable star catalogue (Brát, 2005, Skarka et al., 2017).

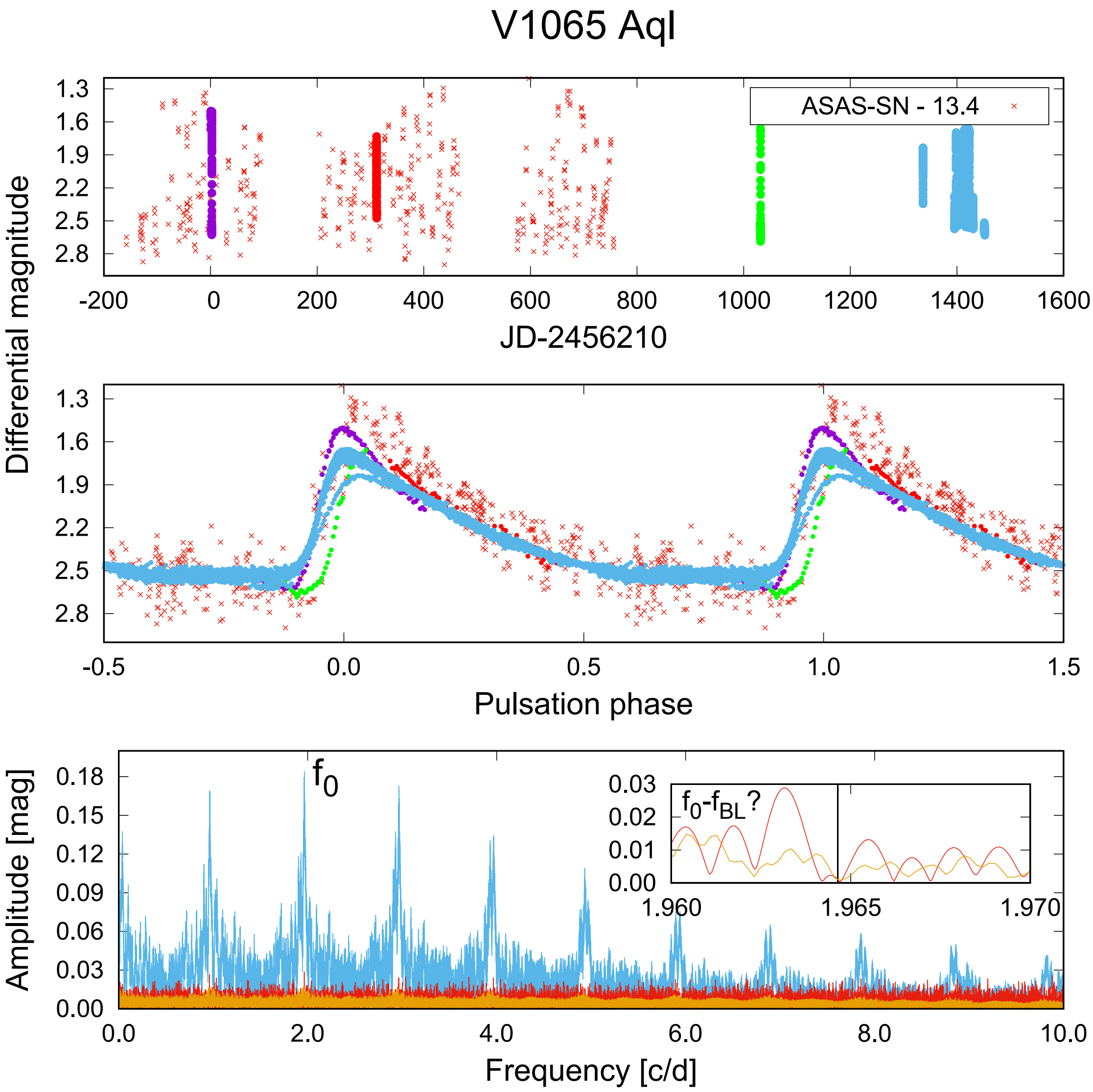

Figure 3. Distribution of V1065 Aql data (top panel), data phased according to ephemerides in Table 3 (middle panel), and corresponding frequency spectra (bottom panel). Different colours in our data (two upper panels) show different seasons, while red asterisks show ASAS–SN data. The light-blue line in the bottom panel shows the frequency spectra based on our data, yellow line shows the residuals after removing 8 pulsation harmonics. The red line shows the residual spectrum based on ASAS–SN data. The detail shows the vicinity of the main pulsation frequency (its position is shown by the black solid line).

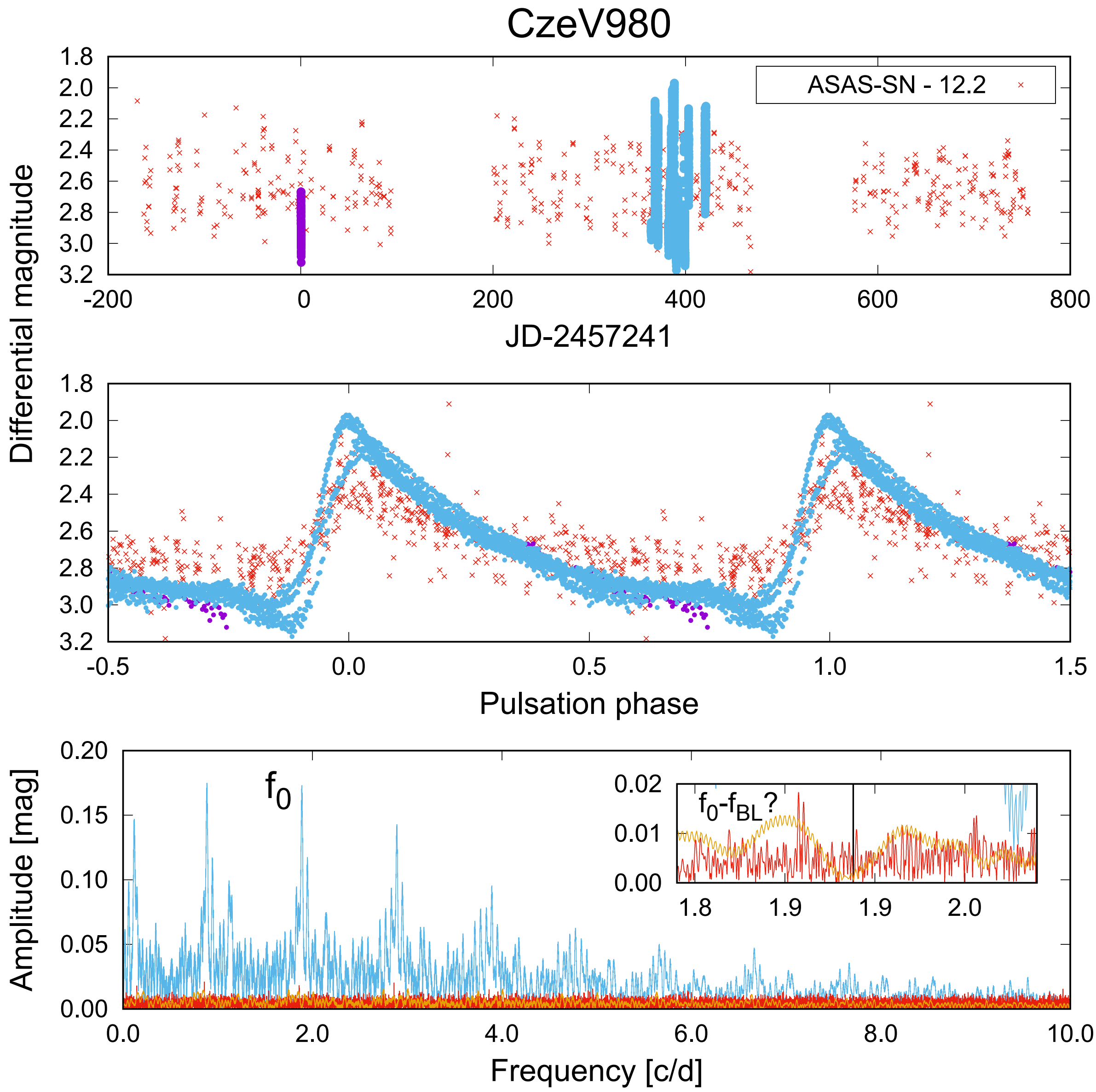

Figure 4. The same as in Fig. 3, but for CzeV980.

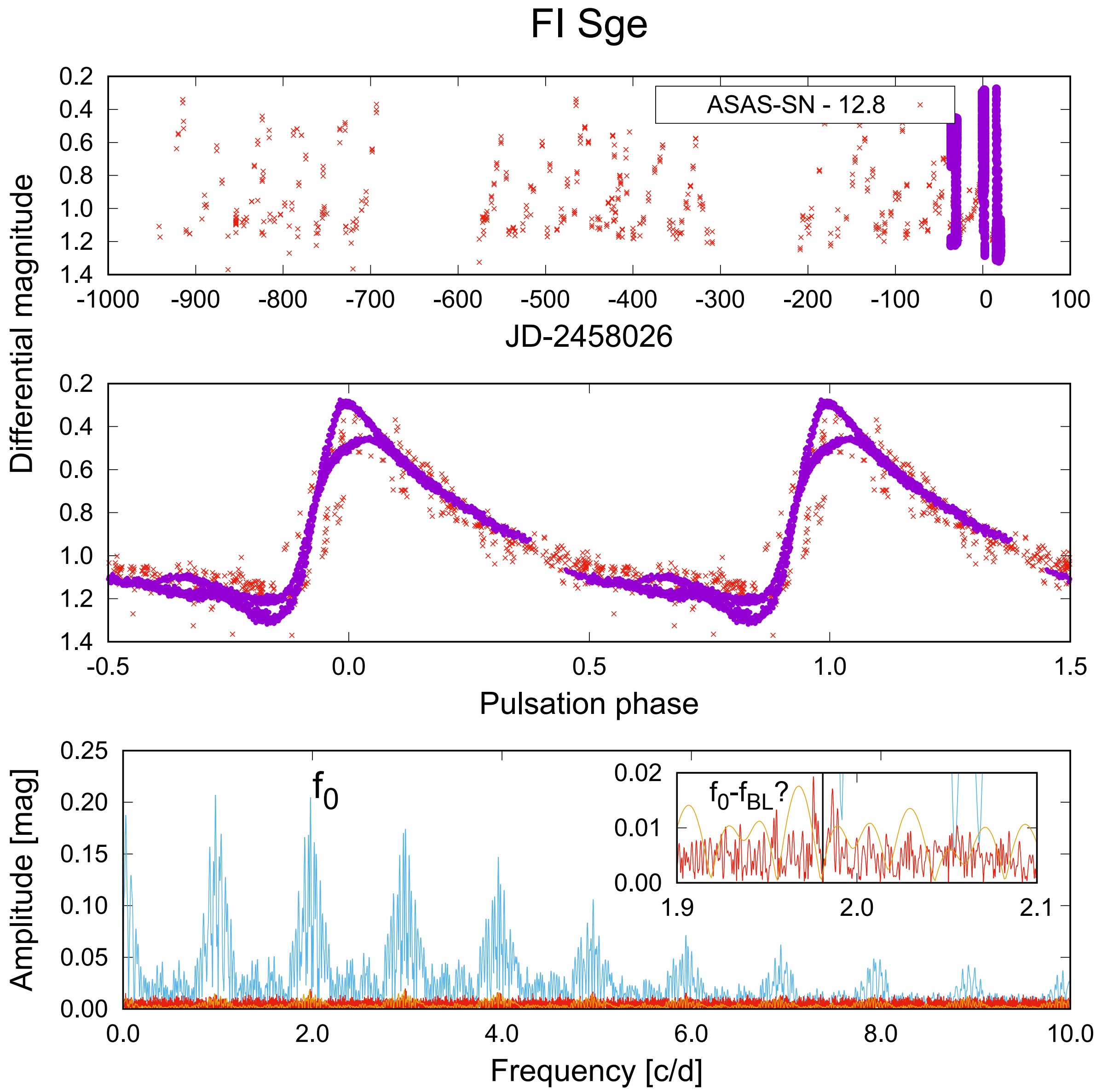

Figure 5. The same as in Fig. 3, but for FI Sge.

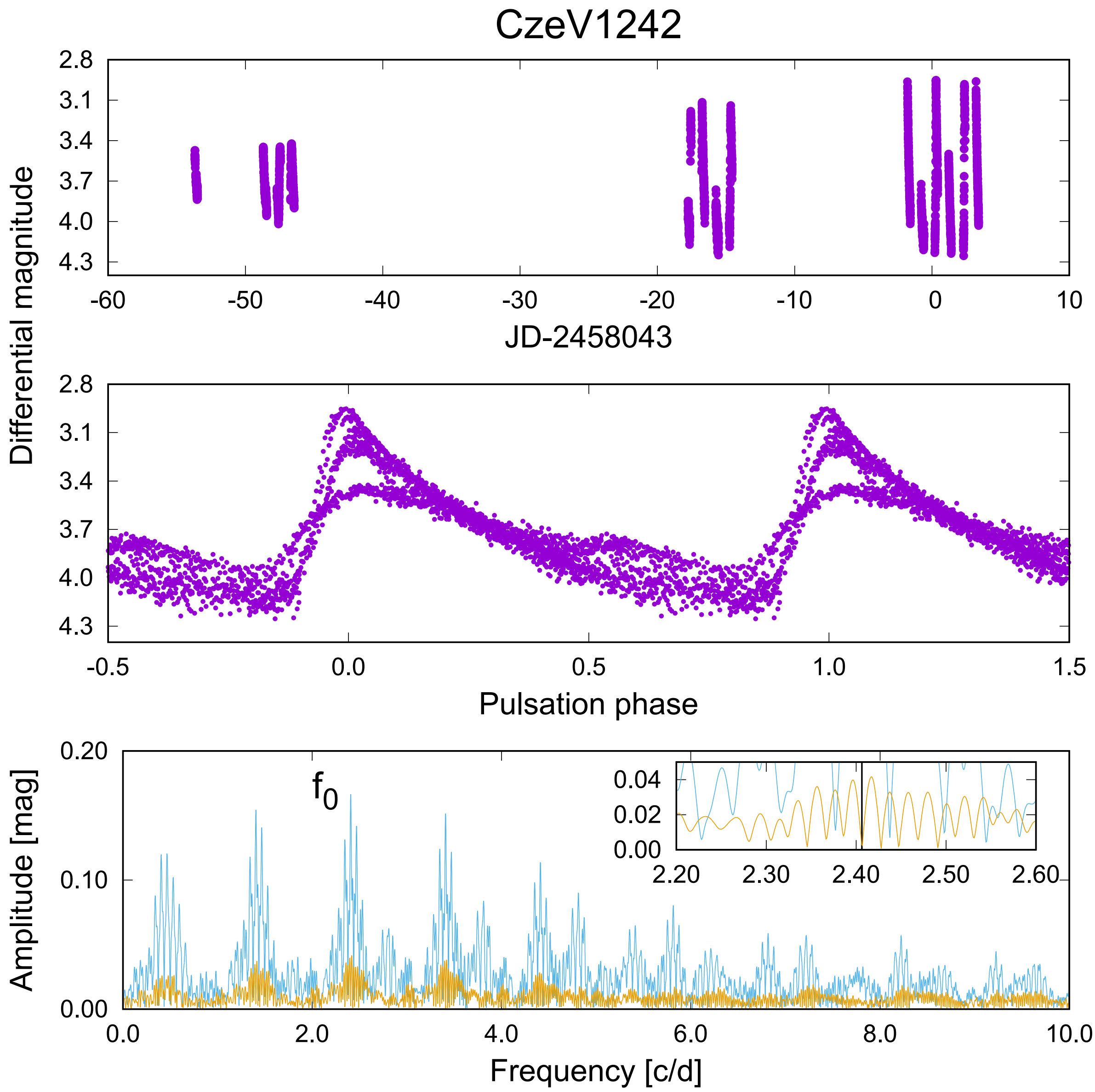

Figure 6. The same as in Fig. 3, but for CzeV1242.

4.4 CzeV1242

For CzeV1242 (USNO-A2.0 1050-16748412, J2000 20:11:14.38 +16:43:30.5, $J = 15.075$ mag, $J - K = 0.227$ mag) the ASAS–SN data were of very bad quality. However, there is no doubt about the presence of the BL effect from the middle panel of Fig. 6. Our data were also of insufficient quality for modulation period determination (the detail in the bottom panel of Fig. 6), thus, we are unable to give the rough estimate.

5 Conclusions

We report a discovery of the modulation in four RRab stars (V1065 Aql, CzeV980, FI Sge, and CzeV1242). The stars with 'CzeV' designation are newly discovered RRab stars. Pulsation periods were estimated from our and ASAS–SN data. We also determined maximum times based on our data. All stars show unambiguous signs of modulation especially in our data (except for V1065 the modulation is not apparent in ASAS–SN data set). In V1065 Aql, CzeV980, and FI Sge we give also first, rough estimates of their modulation periods. More data are needed for a better estimation of the modulation periods and better description of the modulation.

Acknowledgements: The financial support of the Hungarian NKFIH Grant K-115709 and Czech Grant GA ČR 17-01752J are acknowledged (MS).

References:

Benkő, J. M., Kolenberg, K., Szabó, R., et al., 2010, *MNRAS*, **409**, 1585 DOI
Blažko, S., 1907, *AN*, **175**, 325 DOI
Brát, L., 2005, *Perseus Bulletin*, **2**, 26, http://var2.astro.cz/perseus_pdf/2005-2.pdf
Cagaš, P., 2017, *Open European Journal on Variable Stars*, **180**, 8
Hoffmeister, C., 1936, *AN*, **259**, 37
Hoffmeister, C., 1964, *AN*, **288**, 49 DOI
Kochanek, C. S., Shappee, B. J., Stanek, K. Z., et al. 2017, *PASP*, **129**, 104502 DOI
Kovács, G., 2016, *Commmunications of the Konkoly Observatory*, **105**, 61
Lenz, P., Breger, M., 2005, *CoAst*, **146**, 53 DOI
Jurcsik, J., Sódor, Á., Szeidl, B., et al., 2009, *MNRAS*, **400**, 1006 DOI
Prudil, Z., & Skarka, M., 2017, *MNRAS*, **466**, 2602 DOI
Shappee, B. J., Prieto, J. L., Grupe, D., et al., 2014, *ApJ*, **788**, 48 DOI
Skarka, M., 2013, *A&A*, **549**, A101 DOI
Skarka, M., Mašek, M., Brát L., et al., 2017, *Open European Journal on Variable Stars*, **185**, 1
Skarka, M., Dřevěný, R., Auer, R. F., Liška, J., et al. 2015, *Open European Journal on Variable Stars*, **174**, 1
Smolec, R., 2016, *Proceedings of the Polish Astronomical Society*, **3**, 22
Sódor, Á., 2012, *Konkoly Obs. Occ. Tech. Notes*, **15**, 1

Appendix

Table 3. Maximum times with their formal errors.

T_{max}	Err(T_{max})	T_{max}	Err(T_{max})	T_{max}	Err(T_{max})
V1065 Aql		2457633.4919	0.0005	2458026.2833	0.0002
2456210.3307	0.0015	CzeV980		2458027.2927	0.0003
2456212.369	0.0004	2457609.3308	0.0009	2458028.3046	0.0002
2457546.4698	0.0007	2457612.5079	0.0007	CzeV1242	
2457608.5551	0.0004	2457627.3204	0.0003	2457995.519	0.0016
2457609.5734	0.0006	2457628.3809	0.0003	2457996.3518	0.0031
2457624.3337	0.0004	2457629.4404	0.0002	2458025.4274	0.0008
2457625.3507	0.0003	2457644.2881	0.0011	2458026.2594	0.0008
2457626.3685	0.0003	FI Sge		2458028.3408	0.0008
2457627.3866	0.0004	2457989.4358	0.0003	2458043.2929	0.0004
2457628.4043	0.0004	2457994.4832	0.0005	2458043.2929	0.0004
2457629.422	0.0004	2457995.4902	0.0004	2458045.3628	0.0005
2457631.4582	0.0003	2457996.5007	0.0004		
2457632.4755	0.0002	2458025.2723	0.0003		

COMMISSIONS G1 AND G4 OF THE IAU
INFORMATION BULLETIN ON VARIABLE STARS
Volume 63 Number 6230 DOI: 10.22444/IBVS.6230

Konkoly Observatory
Budapest
17 December 2017

HU ISSN 0374 – 0676

TIMES OF MINIMA OF 116 ECLIPSING BINARY SYSTEMS (2010-2015)

LAMPENS, P.[1]; VAN CAUTEREN, P.[2]; AYIOMAMITIS, A.[3]; KLEIDIS, S.[4,6]; PANAGIOTOPOULOS, K.[5,6]; VANLEENHOVE, M.[7,8]; HAMBSCH, J.[8]; HAUTECLER, H.[8]; VAN WASSENHOVE, J.[8]; VERMEYLEN, L.[1]

[1]Koninklijke Sterrenwacht van België, Brussels, Belgium; e-mail: patricia.lampens@oma.be
[2]Koninklijke Sterrenwacht van België, Radio-astronomy Station, Humain, Belgium
[3]Perseus Observatory, Athens, Greece
[4]Zagori Observatory, Epirus, Greece
[5]Pounta Observatory, Laconia, Greece
[6]Elliniki Astronomiki Enosi, Athens, Greece
[7]Leest Observatory, Vereniging Voor Sterrenkunde, Belgium
[8]Vereniging Voor Sterrenkunde, Belgium

Observatory and telescope:
0.305m Riccardi-Honders with SBIG-ST10XME (AA30)
0.25m Newtonian with SBIG-ST10XME (BHO25)
0.20m Schmidt-Cassegrain with SBIG-ST7ME (Hau20)
0.20m refractor with SBIG-STL6303e (HMB20)
0.28m Schmidt-Cassegrain with SBIG-ST10XME (HMB28)
0.30m Schmidt-Cassegrain with SBIG-ST9XE (HMB30)
0.40m Newtonian with SBIG-STL11000 (HMB40)
0.40m Hypergraph with SBIG-STL11000 (HMB40H)
0.13m refractor with SBIG-STL6303E or ST10XME (Hum13)
0.18m refractor with SBIG-ST10XME (Hum18)
0.40m Newtonian with SBIG-ST10XME (Hum40)
0.41m Schmidt-Cassegrain with SBIG-ST10XME (Hum41)
0.15m refractor with SBIG-ST7XME (JVW15)
0.30m Schmidt-Cassegrain with SBIG-ST7XME (Kle30)
0.11m refractor with SBIG-ST10XME, Roque de los Muchachos, La Palma (LPa11)
0.25m Newtonian with SBIG-ST10XME (MVL25)
0.26m Schmidt-Cassegrain with SBIG-ST10XME (Pan26)

Detector:	SBIG-ST7XME, Peltier, KAF-402, 9 μ, 765 × 510 pixels^2
	SBIG-ST9XE, Peltier, KAF-261E, 20 μ, 512 × 512 pixels^2
	SBIG-ST10XME, Peltier, KAF-3200ME, 6.8 μ, 2184 × 1472 pixels^2
	SBIG-STL6303E, Peltier, KAF-6303E, 9 μ, 3072 × 2048 pixels^2
	SBIG-STL11000, Peltier, KAI-11000, 9 μ, 4008 × 2672 pixels^2

Method of data reduction:
The CCD frames were reduced in a standard way with AIP4WIN, Mira-AP7[1] and MaximDL4 respectively used by Kle30, BHO/Hum and all other observers.

Method of minimum determination:
The times of minima were usually computed using a technique of parabolic fitting, in some cases complemented by other methods from the software package *Minima* (e.g. Kle30) (cf. `http://members.shaw.ca/bob.nelson/software1.htm`). Ephemerides were obtained from The Kepler Eclipsing Binary Catalog, 3rd version (Kirk et al. 2016), the O–C Gateway: database of times of minima (E) and maxima (Paschke & Brát, `http://var2.astro.cz/ocgate/`), and Bob Nelson's Database of Eclipsing Binary O–C Files (`http://www.aavso.org/bob-nelsons-o-c-files`).

Times of minima:

Star name	Time of min. HJD 2400000+	Error	Type	Filter	Rem.
XZ And	55850.3240	0.0005	1	C	Hau20
DS And	55838.4291	0.0003	1	V	MVL25
V725 And	56614.3815	0.0002	1	C	AA30
HP Aur	55813.5645	0.0001	1	V	Kle30
HP Aur	55855.5380	0.0001	2	V	Kle30
IU Aur	55600.3501	0.0001	2	V	Kle30
IU Aur	55601.2544	0.0003	1	V	Kle30
UW Boo	55247.9238	0.0002	1	V	HMB30
WW Cam	55244.4980	0.0003	1	V	HMB20
AL Cam	55244.2953	0.0001	1	V	HMB40H
AS Cam	55470.4065	0.0001	2	V	Pan26
AS Cam	55496.3201	0.0006	1	V	Pan26
OO Cam	55930.4304	0.0002	1	V	Kle30
V422 Cam	55587.3501	0.0001	1	V	Pan26
RZ Cas	55609.4230	0.0002	1	C	Hau20
TW Cas	55590.3123	0.0001	1	C	Hau20
AB Cas	55452.4646	0.0002	1	C	Hau20
CV Cas	55204.4082	0.002	1	C	HMB28
CW Cas	56194.3178	0.0002	1	C	AA30
CW Cas	56194.4788	0.0003	2	C	AA30
DN Cas	55834.3265	0.0007	1	V	MVL25
HT Cas	57307.3752	0.0001	1	C	Hum41

[1] Mira-AP7 is distributed by Mirametrics Inc.

Times of minima:					
Star name	Time of min. HJD 2400000+	Error	Type	Filter	Rem.
IT Cas	55507.2707	0.0001	2	V	Pan26
IT Cas	55536.2959	0.0001	1	V	Pan26
IT Cas	55571.3665	0.0002	1	V	MVL25
IV Cas	55211.3024	0.0013	1	V	HMB40
IV Cas	55233.2701	0.0012	1	V	HMB40
IV Cas	55240.2588	0.0018	1	V	HMB40
IV Cas	55832.3729	0.0003	1	V	MVL25
IV Cas	55837.3660	0.0003	1	V	MVL25
IV Cas	55848.3496	0.0001	1	C	Hau20
IV Cas	55851.3449	0.0002	1	V	MVL25
IV Cas	55858.3346	0.0005	1	V	MVL25
MU Cas	55554.3620	0.0003	1	V	Pan26
NU Cas	56179.3757	0.0009	1	C	AA30
OX Cas	55390.4748	0.0001	2	V	Kle30
PV Cas	55428.4499	0.0003	1	V	JVW15
PV Cas	55605.2476	0.0001	1	B	Pan26
PV Cas	55836.3090	0.0001	1	V	MVL25
V471 Cas	56173.3973	0.0005	2	C	AA30
V473 Cas	56175.3776	0.0006	1	C	AA30
V523 Cas	54437.3404	0.0001	2	C	AA30
V821 Cas	55588.2921	0.0001	1	V	Pan26
V1031 Cas	56195.3611	0.0004	1	C	AA30
V1107 Cas	56168.2899	0.0003	1	C	AA30
V1107 Cas	56168.4262	0.0003	2	C	AA30
V1107 Cas	56168.5639	0.0001	1	C	AA30
V1115 Cas	56173.2878	0.0004	2	C	AA30
V1115 Cas	56173.4485	0.0003	1	C	AA30
V1138 Cas	56175.4294	0.0006	1	C	AA30
V1139 Cas	56180.3563	0.0006	1	C	AA30
V1139 Cas	56180.5075	0.0006	2	C	AA30
VZ Cep	55543.4080	0.0001	1	V	MVL25
DV Cep	55673.3714	0.0003	1	V	JVW15
V357 Cep	55499.2885	0.0001	1	C	Pan26
V357 Cep	55501.2505	0.0010	2	C	Pan26
V357 Cep	55836.4169	0.0026	2	V	MVL25
V881 Cep	55198.3532	0.0041	1	C	HMB28
V898 Cep	55820.5807	0.0001	1	V	Kle30
V919 Cep	55480.3045	0.0002	2	C	Hau20
V922 Cep	55771.4493	0.0001	1	V	Kle30
V944 Cep	55506.4540	0.0001	1	V	Pan26
V957 Cep	55813.3955	0.0001	2	V	Kle30
V957 Cep	56499.5103	0.0001	1	V	Kle30
AV CrB	56427.3585	0.0005	1	C	AA30
AV CrB	56427.5124	0.0002	2	C	AA30
BR Cyg	55479.4200	0.0003	1	C	Hau20
BR Cyg	56461.5186	0.0001	1	V	Kle30
DO Cyg	56469.3841	0.0001	1	V	Kle30

Times of minima:					
Star name	Time of min. HJD 2400000+	Error	Type	Filter	Rem.
PV Cyg	55481.3990	0.0004	1	C	MVL25
V442 Cyg	55415.3294	0.0002	1	V	Kle30
V442 Cyg	55817.3620	0.0001	2	V	Kle30
V469 Cyg	56928.3450	0.0002	1	C	Hum40
V526 Cyg	57131.5937	0.0005	1	C	Hum41
V700 Cyg	56165.2958	0.0002	2	C	AA30
V700 Cyg	56165.4423	0.0004	1	C	AA30
V961 Cyg	55320.4697	0.0001	1	V	Pan26
V961 Cyg	55325.5643	0.0001	2	V	Pan26
V961 Cyg	55482.4753	0.0004	2	V	MVL25
V961 Cyg	56503.4109	0.0002	2	V	Kle30
V1136 Cyg	55343.4472	0.0002	1	V	Pan26
V1136 Cyg	55762.4438	0.0001	1	V	Kle30
V1191 Cyg	56176.3082	0.0002	1	C	AA30
V1191 Cyg	56176.4643	0.0002	2	C	AA30
V1193 Cyg	56510.4298	0.0002	2	C	AA30
TZ Dra	55528.2845	0.0002	1	V	JVW15
OO Dra	56794.5101	0.0003	1	V	Hum40
OO Dra	57131.3534	0.0003	1	V	Hum41
AS Eri	56972.5482	0.0002	1	V	LPa11
U Gem	55264.3466	0.0003	1	C	Hum40
V410 Gem	55581.3279	0.0002	1	V	Kle30
TU Her	56917.3919	0.0003	1	V	Hum40
CT Her	55304.4451	0.0002	1	C	Hum18
CT Her	57135.4897	0.0001	1	C	Hum41
RX Her	55493.2605	0.0001	1	B	Pan26
HS Her	55741.5177	0.0003	1	B	Kle30
V1360 Her	56539.3721	0.0001	2	V	Kle30
AU Lac	55415.5200	0.0003	2	V	Kle30
AU Lac	55505.3300	0.0001	1	V	Pan26
AU Lac	57180.4315	0.0001	1	C	Hum41
CO Lac	55456.5114	0.0001	2	V	Kle30
CO Lac	55531.3040	0.0001	1	V	Pan26
IU Lac	56192.2793	0.0002	1	C	AA30
MZ Lac	55770.5241	0.0001	1	V	Kle30
V441 Lac	56192.4044	0.0002	1	C	AA30
Y Leo	55571.5926	0.0002	1	C	Hau20
UU Leo	55625.5713	0.0002	1	V	MVL25
VZ Leo	55265.3424	0.0002	1	V	Hum40
WY Leo	57121.3829	0.0005	1	V	Hum41
XY Leo	55301.3205	0.0001	1	V	Pan26
UW LMi	55581.4406	0.0004	1	V	Pan26
UU Lyn	54883.6615	0.0003	1	B,V	HMB20
UU Lyn	54887.6440	0.0004	2	B	HMB20
UU Lyn	54889.7503	0.0003	1	B,V	HMB20
UU Lyn	54890.6878	0.0003	1	B,V	HMB20
UZ Lyr	55858.3642	0.0004	1	C	Hau20

Times of minima:

Star name	Time of min. HJD 2400000+	Error	Type	Filter	Rem.
FL Lyr	55482.3340	0.0003	2	V	MVL25
FL Lyr	56461.4138	0.0001	1	V	Kle30
V400 Lyr	56516.3527	0.0003	1	C	AA30
V400 Lyr	56516.4832	0.0001	2	C	AA30
V401 Lyr	56516.4128	0.0005	1	C	AA30
V507 Lyr	56529.3122	0.0004	2	C	AA30
V507 Lyr	56551.3291	0.0003	2	C	AA30
V574 Lyr	56524.3104	0.0002	2	C	AA30
V574 Lyr	56524.4480	0.0002	1	C	AA30
V579 Lyr	56506.4361	0.0003	2	C	AA30
V580 Lyr	56517.3282	0.0003	2	C	AA30
V580 Lyr	56517.4724	0.0005	1	C	AA30
V582 Lyr	56501.3337	0.0004	1	C	AA30
V582 Lyr	56501.4629	0.0004	2	C	AA30
V591 Lyr	56519.3118	0.0003	2	C	AA30
V591 Lyr	56519.4628	0.0001	1	C	AA30
V591 Lyr	56544.3955	0.0003	1	C	AA30
V591 Lyr	56546.3467	0.0005	2	C	AA30
V596 Lyr	56528.3138	0.0002	1	C	AA30
V596 Lyr	56528.4627	0.0003	2	C	AA30
FT Ori	55603.3236	0.0002	2	B	Pan26
FT Ori	55604.3271	0.0001	1	B	Pan26
V392 Ori	57296.6310	0.0001	1	V	Hum40
BX Peg	56196.2987	0.0002	2	C	AA30
BX Peg	56196.4381	0.0001	1	C	AA30
IP Peg	55396.5083	0.0001	1	C	Hum40
KW Peg	56196.4516	0.0003	2	C	AA30
V498 Peg	56518.4281	0.0004	1	C	AA30
AG Per	55590.4845	0.0006	1	V	MVL25
IU Per	55850.3223	0.0003	1	V	JVW15
IU Per	56928.4590	0.0001	1	V	Hum40
IU Per	57257.5591	0.0001	1	V	Hum41
IU Per	57276.4135	0.0001	1	V	Hum40
IU Per	57293.5539	0.0002	1	V	Hum41
IU Per	57294.4091	0.0001	1	V	Hum40
DL Sge	55462.3525	0.0002	1	V	MVL25
AO Ser	57127.5074	0.0001	1	C	Hum41
AO Ser	57134.5425	0.0001	1	V	Hum41
AO Ser	57135.4217	0.0001	1	V	Hum41
AO Ser	57178.5103	0.0001	1	C	Hum41
SV Tau	55204.3500	0.0025	1	V	HMB35
RS Tri	55817.5165	0.0001	1	V	Kle30
VV UMa	55223.4579	0.0001	1	V	Hum18
VV UMa	55244.4217	0.0008	2	V	BHO25
VV UMa	55263.3257	0.0001	1	V	Hum18
VV UMa	57094.4948	0.0002	1	V	Hum13
VV UMa	57127.4877	0.0007	1	V	Hum13

Times of minima:					
Star name	Time of min. HJD 2400000+	Error	Type	Filter	Rem.
VV UMa	57134.3618	0.0001	1	V	Hum41
XZ UMa	55247.7165	0.0015	1	V	HMB30
BS UMa	56355.4466	0.0012	1	V	Hum40
BS UMa	56356.3205	0.0005	2	V	Hum40
BS UMa	56356.4943	0.0009	1	V	Hum40
BS UMa	56745.4952	0.0011	1	B	Hum40
BS UMa	56746.3702	0.0002	2	V	Hum40
BS UMa	56746.5444	0.0002	1	V	Hum40
BS UMa	57089.4174	0.0004	1	V	Hum40
BS UMa	57094.4871	0.0003	2	V	Hum40
BS UMa	57133.4566	0.0004	1	V	Hum40
BS UMa	57135.3795	0.0002	1	C	Hum40
DN UMa	56730.3778	0.0008	2	B	Hum13
RU UMi	57128.3626	0.0001	1	V	Hum41
RU UMi	57131.5125	0.0001	1	V	Hum41
AG Vir	55308.3487	0.0001	2	V,Ic	Pan26
AG Vir	55309.3097	0.0003	1	V,Ic	Pan26
DR Vul	56159.3471	0.0003	2	C	AA30
KN Vul	56162.2992	0.0001	1	C	AA30
KN Vul	56162.4768	0.0002	2	C	AA30
GSC 4237 636	56464.4081	0.0004	2	C	AA30
GSC 4237 636	56465.3964	0.0004	2	C	AA30
GSC 4237 636	56468.3614	0.0004	2	C	AA30
GSC 4237 636	56468.5252	0.0005	1	C	AA30
GSC 4237 636	56585.3091	0.0004	2	C	AA30
GSC 4237 636	56592.2274	0.0003	2	C	AA30
GSC 2049 1164	56440.3349	0.0006	1	C	AA30
GSC 2049 1164	56444.5386	0.0002	1	C	AA30
GSC 2996 0677	56361.4618	0.0004	2	C	AA30
GSC 2996 0677	56375.3574	0.0007	1	C	AA30
GSC 2996 0677	56388.3489	0.0004	1	C	AA30
HIP 7666	55446.5057	0.0002	1	B,V	Kle30
KIC 5310387	57181.4443	0.0003	1	C	Hum41
KIC 5376552	57178.4443	0.0002	1	C	Hum40
NSVS 777749	55601.2420	0.0001	1	V	Pan26
NSVS 777749	55601.4436	0.0002	2	V	Pan26
NSVS 828322	55962.3406	0.0007	1		MVL25
NSVS 3842733	56587.3275	0.0004	1	C	AA30

Explanation of the remarks in the table:

Observers: AA = Ayiomamitis, A.; BHO/Hum/LPa = Van Cauteren, P.; HMB = Hambsch, J.; Hau = Hautecler, H.; JVW = Van Wassenhove, J.; Kle = Kleidis, S.; MVL = Vanleenhove, M.; Pan = Panagiotopoulos, K.

Remarks:

We used the filters B and V following the specifications from Bessell (1995). Occasionally, the filter Ic (Cousins) was also used.

Acknowledgements:
The authors thank P. Wils for providing essential software for the predictions and computations. This work has made use of the SIMBAD database, operated at CDS, Strasbourg, France. PVC is grateful for support from Baader Planetarium (`www.baader-planetarium.de`). PL acknowledges the support of the directors of the Royal Observatory of Belgium (ROB) for running the project HOACS ('Humain Optical Observatory for Astrophysics of Coeval Stars') at the radio-astronomy site of Humain.

References:

Bessell, M., 1995, *CCD Astronomy*, **2**, No. 4, 20
Kirk, B., Conroy, K., Prša, A., et al., 2016, *AJ*, **151**, 68 DOI

COMMISSIONS G1 AND G4 OF THE IAU
INFORMATION BULLETIN ON VARIABLE STARS
Volume 63 Number 6231 DOI: 10.22444/IBVS.6231

Konkoly Observatory
Budapest
13 December 2017

HU ISSN 0374 – 0676

SECULAR VARIATION AND PHYSICAL CHARACTERISTICS DETERMINATION OF THE HADS STAR EH Lib

PEÑA, J.H.[1,2,3]; VILLARREAL, C.[1,3]; PIÑA, D.S.[1,3]; RENTERÍA, A.[1,3]; SONI, A.[3], GUILLÉN, J.[3] & CALDERÓN, J.[1,3]

[1] Instituto de Astronomía, Universidad Nacional Autónoma de México, Cd. México
e-mail: jhpena@astro.unam.mx

[2] Observatorio Astronómico Nacional, Tonantzintla

[3] Facultad de Ciencias, Universidad Nacional Autónoma de México

1 Motivation

It has been known for quite a while that some high-amplitude δ Scuti (HADS) stars show long-term variations. In a few cases, after correcting for these long-term variations, the O–C residuals show either sinusoidal variation that can be considered to be due to light-time travel effect provoked by the existence of an unseen companion or, at times, show quadratic behavior that is interpreted as secular period variation. With this in mind a search to determine times of maximum light for several HADS stars is being carried out (see Peña et al., 2015) at the Observatorio Astronómico Nacional de Tonantzintla, México (TNT), an observatory especially suitable for observational teaching practices with small telescopes equipped with modern CCD cameras.

After collecting times of maximum for the HADS stars, a detailed analysis on a star-by-star basis is done. Some results have been published (Peña et al., 2015) and this has stimulated us to study additional stars. These secular variation studies are supplemented with $uvby-\beta$ photoelectric photometry taken at the Observatorio Astronómico Nacional de San Pedro Mártir, México (SPM), since the determination of physical parameters of stars can be done through a comparison with theoretical models.

Previous studies on the nature of EH Lib have been extensive. Mahdy & Szeidl (1980) found that this star has a slightly stable, constant period. Jiang & Yang (1981, 1982) obtained six times of maximum that, together with the photoelectric times of maximum compiled over the past 30 years, permitted them to determine the fit with the formula:

$$T_{max} = T_0 + P_0E + \frac{1}{2}\beta E^2 + A\sin 2\pi\left(\frac{EP_0}{E_0}\right)$$

In their article they specified the initial maximum epoch and the pulsation period as $T_0 = \text{HJD}\,2433438.6088$ and $P_0 = 0.0884132445$ d, the semi-amplitude and the period of the sine curve $\beta = -2.8 \times 10^{-8}$ 1/yr; $A = 0.0015$ d, $P_0 = 6251$ d $= 17.1$ yr. E is the

Table 1: Log of observing seasons and new times of maxima of EH Lib.

Date yr/mo/day	Observers/reducers	Npoints	Time span (day)	Tmax 2400000+	Tel.	Filters	Camera	Obs.
13/03/0203	CVR,DZR/CVR	58	0.10	56354.9736	1 m	G	1001	TNT
13/03/2425	CVR/CVR	120	0.11	56376.8984	1 m	G	1001	TNT
14/04/0506	AOA14/CVR	281	0.15	56753.8916	M10	wo	8300	TNT
14/04/0506	AOA14/DSP	281	0.15	56753.9800	M10	wo	8300	TNT
15/03/0607	AOA15/DSP	114	0.06	57088.8023	C11	wo	8300	TNT
15/04/0102	KV, JG/DSP	52	0.05	57114.7947	M10	V	1001	TNT
15/05/2930	JG,AAS/AAS,JHP	55	0.07	57172.7920	0.84 m	$uvby-\beta$	phot	SPM
15/06/0102	JG,AAS/AAS,JHP	32	0.05	57175.7990	0.84 m	$uvby-\beta$	phot	SPM
15/06/0304	JG,AAS/JHP	43	0.09	57177.8310	0.84 m	$uvby-\beta$	phot	SPM
16/03/1112	KL/CVR	103	0.09	57459.8721	M10	V	1001	TNT
16/03/1213	KL/CVR	103	0.08	57460.8441	M10	V	1001	TNT
16/04/0304	AOA16/CVR	97	0.13	57481.8879	1 m	G	8300	TNT
16/04/0304	AOA16/CVR	97	0.13	57481.9756	1 m	G	8300	TNT

NOTES: CVR, C. Villarreal; DZR, D. Zuñiga; KV, K. Vargas); DSP, D. S. Piña; JHP, J.H. Peña; AAS, A.A. Soni; JG, J. Guillén; KL, K. Lozano; AOA14: J. Camargo, O. Díaz, J. Flores, D. Galicia, C. García, J. Guillén, A. Muñoz, M. Paniagua, E. Pérez, J. Ramírez, D. S. Piña, M. Serratos, R. Yslas, J. Zamarrón; AOA15: U. Arellano, J. Diaz, I. Fuentes, A. Mata, I. Mora, X. Moreno,F. Ruiz, K. Valencia, K. Várgas; AOA16: K. Juárez, K. Lozano, A. Padilla, R. Velázquez, P. Santillán. C11: 11" Celestron, M10: 10" Meade telescopes.

number of periods elapsed since T_0, and $E_0 = 70700$, which can be interpreted as a 17.1 year periodicity as a modulation of the phase of maximum by binary motion.

More recently, Joner (1986), with $uvby-\beta$ photometry determined a reddening value of $\mathrm{E}(b-y) = 0.041$, a mean effective temperature of $T_{\rm eff} = 7840$ K and a mean surface gravity, $\log g = 4.08$. The metal abundance, [Fe/H] $= -0.015$ was also determined. Using a Wesselink method they derived a mean radius of 2.4 $R_\odot$, a mean absolute bolometric magnitude of $M_{\rm bol} = +1.5$ mag, and a mass of 2.0 $M_\odot$.

In their study devoted to EH Lib, Wison et al. (1993) stated that it was a large-amplitude δ Sct variable star and that it had a range of $9.35 - 10.08$ mag in V and a spectral class range A5–F3 according to the General Catalogue of Variable Stars (Baker, 1985).

McNamara and Feltz (1976) obtained a Wesselink radius of 2.1 $R_\odot$, but did not discuss the uncertainty in the result. Later, McNamara and Feltz (1978) used the observed effective gravities of 15 dwarf Cepheids, as they were known at that time, including EH Lib, to derive an empirical equation relating radius R to period P. They proposed the relation: $\log R = 0.80 \log P + 1.17$. They also commented that according to Joner (1986), a mean value of 2.4 $R_\odot$ for the Wesselink radius was found from the values derived for the effective temperature ($T_{\rm eff}$) as a phase function from $uvby-\beta$ photometry. The radial-velocity measurements were taken from photographic spectrograms.

2 Observations

Although our times of maximum light for this star have been published elsewhere (Peña et al., 2016), here we present the detailed procedure for acquiring the data. These were all taken at TNT and SPM, México. In TNT the 1.0 m telescope and a 10- and a 11-inch telescope were used. These telescopes were equipped with CCD cameras: SBIG STL–1001E and STT–8300. In SPM a spectrophotometer in the $uvby-\beta$ system was attached to the 0.84 m telescope. Table 1 presents the newly determined times of maximum light.

2.1 Data acquisition and reduction in TNT

During all the observational nights the following procedure was utilized. Sequence strings were obtained: the integration time for the 1 m telescope (in the G filter) was 3 min and that of the smaller telescopes (in the V filter) was shorter (1 min). It may seem contradictory to give a longer integration time to the larger aperture telescope, however, this was done since the mounting of the smaller telescopes is alt/az which does not allow long integration times. Nevertheless, for the 1 m telescope there were around 40,000 counts and for the 10" and 11" telescopes there were 11,000 counts, enough to secure high precision. The reduction work was done with AstroImageJ (Collins, 2012), a software that is relatively easy to use and has the advantage that it is free and works satisfactorily on the most common computing platforms. With the CCD photometry two reference stars were utilized whenever possible in a differential photometry mode. The results were obtained from the difference $V_{\rm var} - V_{\rm ref}$ and the scatter calculated from the difference $V_{\rm ref1} - V_{\rm ref2}$. This scatter is 0.03941 mag. The times of maxima were easily determined by fitting a fifth-degree polynomial.

2.2 Data acquisition and reduction in SPM

The 0.84 m telescope to which a spectrophotometer was attached was utilized at all times. The observing season lasted six nights from May–June 2015 but only three were devoted to the observation of EH Lib (which were done by A. A. Soni & J. Guillen). The observation and reduction procedures have been extensively utilized. See for example Peña et al. (2016).

The coefficients defined by the following equations with the data adjusted to the standard system are:

$$\begin{aligned}
V_{\rm std} &= 17.6893 + 0.0340(b-y)_{\rm inst} + y_{\rm inst} \\
(b-y)_{\rm std} &= 1.4055 + 0.9692(b-y)_{\rm inst} \\
m_{1_{\rm std}} &= -1.3713 + 1.0928(m_1)_{\rm inst} + 0.0134(b-y)_{\rm inst} \\
c_{1_{\rm std}} &= 0.0419 + 1.0341(c_1)_{\rm inst} + 0.1392(b-y)_{\rm inst} \\
H\beta_{\rm std} &= 2.3513 + -1.3565(H\beta)_{\rm inst}
\end{aligned}$$

The averaged transformation coefficients of each night are listed in Table 2 along with their standard deviations. In these equations the coefficients D, F, H and L are the slope coefficients for $(b-y)$, m_1, c_1 and β. The coefficients B, J and I are the color terms of V, m_1, and c_1. Season errors were evaluated using the standard stars observed. These uncertainties were calculated through the differences in magnitude and colors, for (V, $b-y$, m_1, c_1 and β) as (0.0361, 0.0119, 0.0150, 0.0197, 0.0213), respectively, providing a numerical evaluation of our uncertainties. Emphasis is made on the large range of the standard stars in the magnitude and color values: V:(5.2, 8.8); $(b-y)$:(-0.01, 0.79); m_1:(0.09, 0.70); c_1:(0.23, 1.39) and β:(2.52, 2.90).

Photometric values of the observed star are available as an online table. In this table, column 1 reports the HJD of the observation, columns 2 to 5 the Strömgren values V, $(b-y)$, m_1 and c_1, respectively; column 6, the β.

Table 2: Transformation coefficients obtained for the observed season.

season	B	D	F	J	H	I	L
2015	0.034	0.969	1.093	0.0134	1.034	0.139	−1.3565
σ	0.059	0.0125	0.016	0.015	0.045	0.054	0.0591

3 Period determination

3.1 Time series analysis

As in the case of AE UMa (Peña et al., 2016), we were lucky to have previously reported observations of EH Lib in Strömgren photometry. There are three samples: the data presented by Epstein (1969) in *ubvy* only, that of Joner (1986) and that of the present paper with data from 2015 in $uvby-\beta$ photometry. The question that immediately arises relates to the concordance of these three samples. A phase diagram was built considering all $uvby-\beta$ data with the latest period analysis and the ephemerides elements of Boonyarak et al. (2011), it is shown in Figure 1. What is immediately seen from this figure is that: i) the phase concordance of the three samples implies a constant period for at least the time span of 47 years and ii) there is a large dispersion in the m_1 and β indexes.

To determine the period, at this stage, we will consider only the V magnitude which has a remarkable good behavior given the long time separation of the sets, with only very few discordant points that were discarded. We were left with a set of 264 data points in this V filter.

With such a long time basis in the $uvby-\beta$ time series, a period can be determined through Fourier transforms. As with the short period variable community we utilized Period04 (Lenz & Breger, 2005) with a frequency interval between 0 and 50 c/d. The window pattern is complex due to the scarce and separated data sets. Figure 2 schematically shows the obtained results. The frequency spectrum of the original data presents a peak at $12.3132578 \pm 0.5 \times 10^{-6}$ c/d with an amplitude of $0.212 \pm 5 \times 10^{-3}$ mag and a phase of $0.241 \pm 4 \times 10^{-3}$. The uncertainty was evaluated by the method included in Period04.

The second highest point is at 11.3106898 c/d which corresponds to the period proposed by Boonyarak et al. (2011) of 0.08841326 d. However, when this maximum is enlarged it unfolds into two close maxima at 11.3106898 c/d and 11.3108600 c/d of amplitude of the same order. If the first case is analysed for the residuals, a peak at $23.6246307 \pm 2 \times 10^{-6}$ c/d is obtained which is merely a $2f$ value of the determined frequency. The amplitude which corresponds to this is $0.083 \pm 6 \times 10^{-3}$ mag with a phase of $0.55 \pm 1 \times 10^{-2}$. The analysis of the residuals of these two frequencies yields a peak at $32.9192025 \pm 3 \times 10^{-6}$ c/d with an amplitude of $0.040 \pm 4 \times 10^{-3}$ mag and a phase of $0.22 \pm 1 \times 10^{-2}$. Again, the predictions versus the observations show a remarkable fit.

As can be seen, Period04 gives as output the same numerical values within the errors due to the window function as those proposed by Boonyarak et al. (2011) deduced with a completely different approach (the more canonical O–C method).

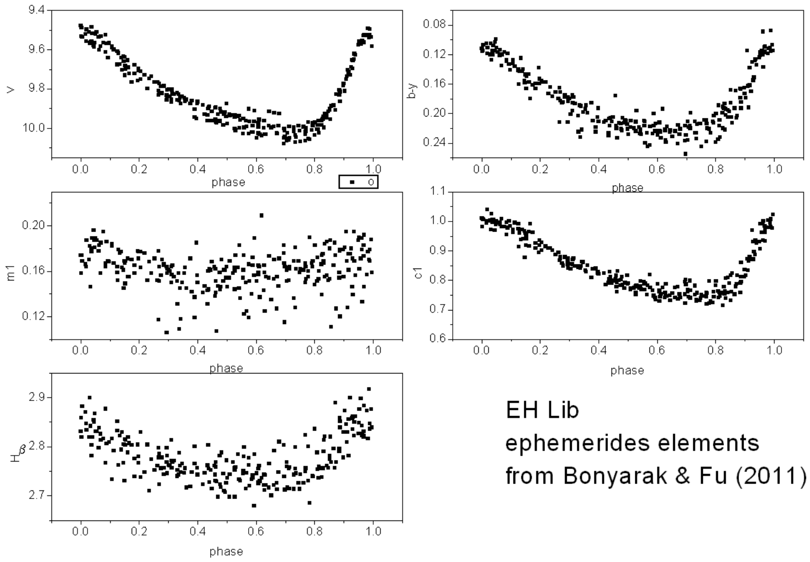

Figure 1. Phase plot of the $uvby-\beta$ photometry of Epstein (1969), Joner (1986) and the present paper. The time span between these sets is 49 years. The period considered is that proposed by Boonyarak (2011).

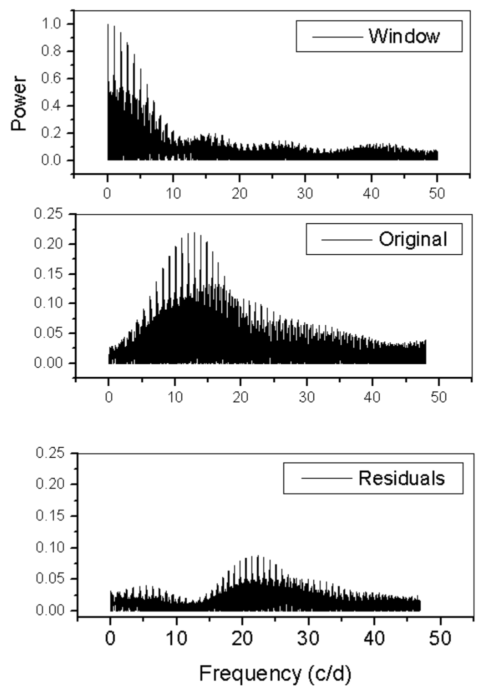

Figure 2. Frequency spectrum of V data of photometry of Epstein (1969), Joner (1986) and the present paper in Period04. Top, Window function; middle original data; bottom, residuals.

Table 3: EH Lib ephemeris equations.

Author	T_0	P	β	Mean (d)	σ (d)
Code, 1950		0.0884	0		
Ashbrook, 1952	2433673.1688	0.08841381	0	0.0014	0.0258
Fitch, 1957	2433438.6078	0.08841325	0	0.0012	0.0023
Sanwal & Panda, 1961	2433438.6079	0.08841324	0	0.0022	0.0026
Oosterhoff & Walraven, 1966	2433438.6090	0.088413216	0	0.0037	0.0042
Epstein, 1969	2433438.610	0.088413	0	0.0054	0.0212
Karetnikov & Medvedev, 1977	2433438.6082	0.0884132445	0	0.0014	0.0024
Mahdy & Szeidl, 1980	2433438.6078	0.088413243	0	0.0020	0.0025
Jiang & Yang, 1982	2433438.6088	0.0884132445	0	0.0008	0.0024
Boonyarak et al., 2011	2433438.6067	0.08841326	0	0.0012	0.0022
Boonyarak et al., 2011	2433438.6064	0.08841324	1.01×10^{-13}	0.0027	0.0026

3.2 O–C analysis

As a first step in carrying out an analysis of the secular variation, an O–C vs. epoch a diagram was constructed with all the compiled times of maximum light. Taking the most recent reported analysis (Boonyarak et al., 2011) we obtained the O–C residuals shown in Figure 3. Only a very few points (five) were outside the standard deviation limits. Hence these points were discarded in the subsequent analyses. Numerically, this is equivalent to adjusting a Gaussian to the O–C residuals and discarding those points beyond one sigma. The limit in this case is 0.0054.

The whole sample of 237 times of maximum covering a time span of 66 years was employed as a first step to determine the behavior of EH Lib. New times of maximum considered after the analysis of Boonyarak et al. (2011) were reported in Hübscher et al. (2009, 2013), Wils et al. (2011, 2012) and this paper all gathered from 2013 to 2016. In two of the papers utilized in our compilation (Pohl 1955, Hübscher et al. 2013), several of the maximum times were observed simultaneously by different observers and included independently in the same paper, so we made an average of these apparently repeated data. Since the times of maximum in the paper by Karetnikov (1977) had no heliocentric correction, we added it and these points are included in our compilation, but not in the analysis. After these procedures there were 226 times of maximum left.

Table 3 summarizes all the previous proposed ephemerides. The main source was Mahdy & Szeidl (1980) and the references within. Other references, with reported, but not analysed observations, were compiled. The large scatter shown by the times of maximum in the O–C vs. epoch diagram became immediately obvious. Visual examination of each point was carried out to discard the inaccurately determined points from those with smaller uncertainties. Hence, following Mahdy & Szeidl (1980) for the analysis, we discarded all observed visual and photographic points. The remaining sample was constituted of 135 times of maximum covering a time span of almost 61 years. As can be seen in Table 3, a mean value and the standard deviation of the O–C values were calculated for each case in which no clear distinction could be made.

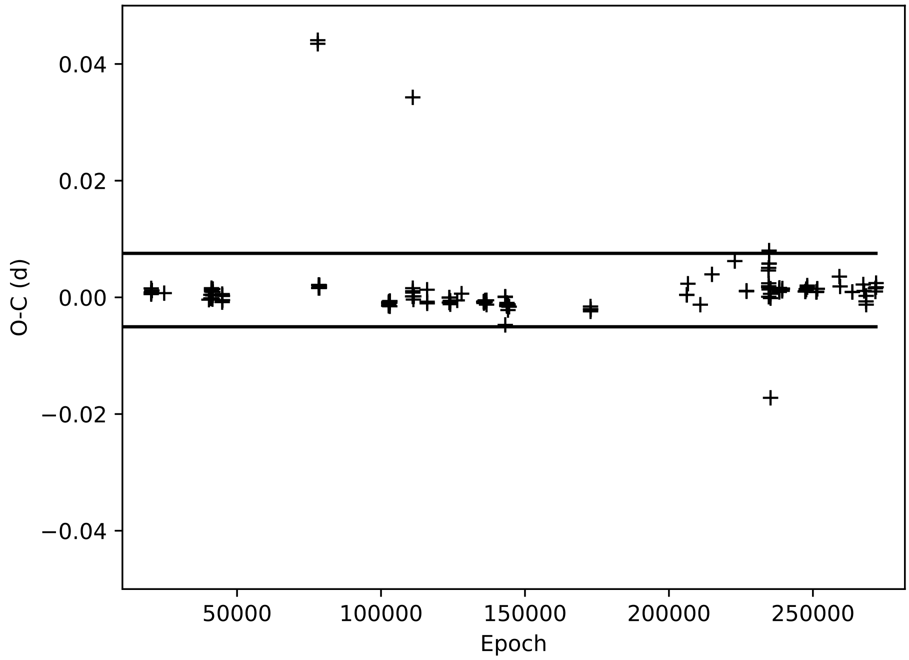

Figure 3. O–C diagram with all the measured times of maximum light.

3.3 Minimization of the standard deviation of the O–C residuals (MSDR)

To determine the ephemerides equation of the variability of EH Lib we, as was previously mentioned, omitted the visual and photographic points and made use of only the photoelectrical ones.

To calculate the ephemerides equation, a standard deviation minimization of the O–C diagram was built. The standard deviation of several O–C diagrams for this same star was calculated. In all cases, as a first step in constructing these O–C diagrams, T_0 and the period P were used as the first time of maximum with each one of the points between 0.087251454 and 0.089596791 with a precision of 1×10^{-9}. This range is the one provided by the average of the difference of consecutive times of maximum light and the standard deviation of the same. With all of the 2345336 periods, the cycle number E of all the times of maximum was calculated. The second step was to make a linear fit of the times of maximum with the cycle number (HJD vs. E) for each different period in the range. The new period P and initial epoch T_0 were obtained and are the parameters of the ephemerides equation needed to construct the O–C diagrams. These linear fits were carried out 2345336 times. Finally, the period and initial epoch with the smallest standard deviation of its O–C diagram was selected as the best equation. The result of these calculations is shown graphically in Figure 4. The O–C diagram obtained with this method is presented in Figure 5 and its equation is:

$$T_{max} = 2435223.7584 + 0.088413266\,E$$
$$(\pm 2 \times 10^{-4}) \qquad (\pm 2 \times 10^{-9})$$

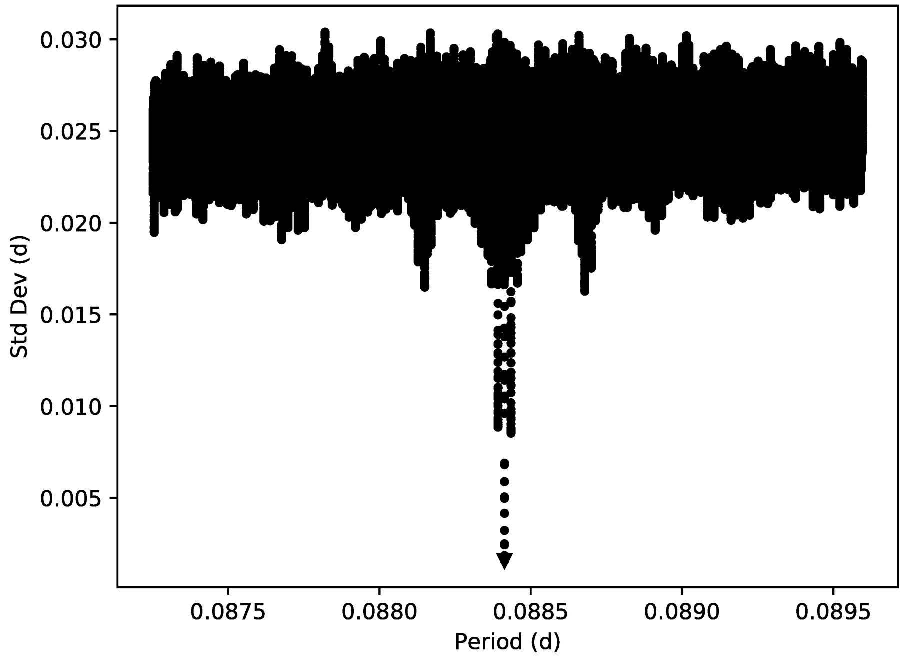

Figure 4. Standard deviation vs. Period of the standard deviation minimization of the O–C residuals method in the linear case.

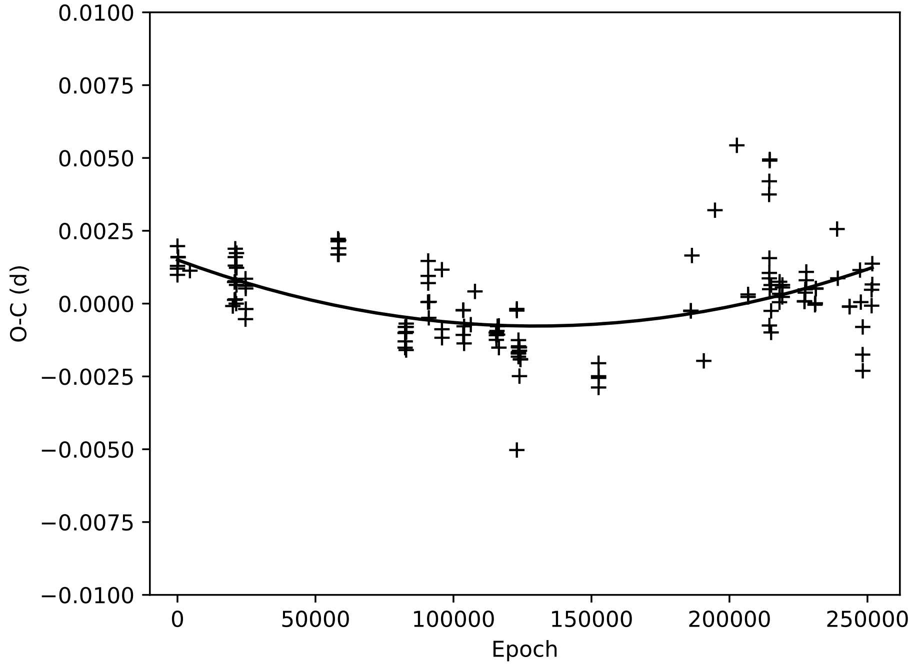

Figure 5. O–C Diagram of EH Lib calculated with the ephemerides equation obtained with the MSDR method in the linear case.

A parabolic trend is present in the O–C diagram as can be seen in Figure 5. To be able to get the parameters of that second order changing period, we followed the same method but instead of fitting the data to a straight line, it was fitted to a parabola. The standard deviation vs. period diagram using the parabolic fit is shown in the Figure 6. The result of subtracting this parabolic trend from the data is shown in the Figure 7. The parabolic equation is:

$$T_{max} = 2435223.7599 + 0.088413231\,E + 1.34 \times 10^{-13}\,E^2$$
$$(\pm 4 \times 10^{-4}) \quad (\pm 6 \times 10^{-9}) \quad (\pm 0.2 \times 10^{-13})$$

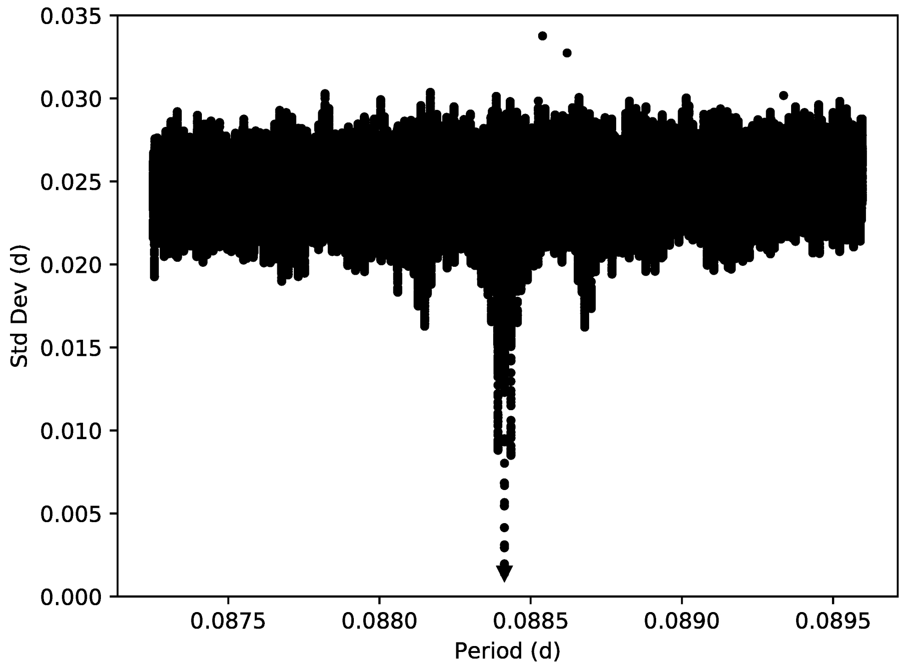

Figure 6. Standard deviation vs. period of the standard deviation minimization of the O–C residuals method in the quadratic case.

4 Determination of physical parameters

To determine the physical characteristics of the star, we first evaluated the reddening through Strömgren photometry and the appropriate unreddening calibrations. As was mentioned before, there are three samples of data with $uvby - \beta$ photometry: that of Epstein (1969) in *ubvy* only; that of Joner (1986), and that present in the online data table which was taken in 2015. A phase diagram was built considering all $uvby - \beta$ data with the ephemerides elements of Boonyarak et al. (2011) and it is shown in Figure 1. A phase concordance within the three samples implies a constant period for at least 47 years although there is a large dispersion in the m_1 and β indexes. The physical parameter determination is done through the calibrations of Nissen (1988), developed to determine

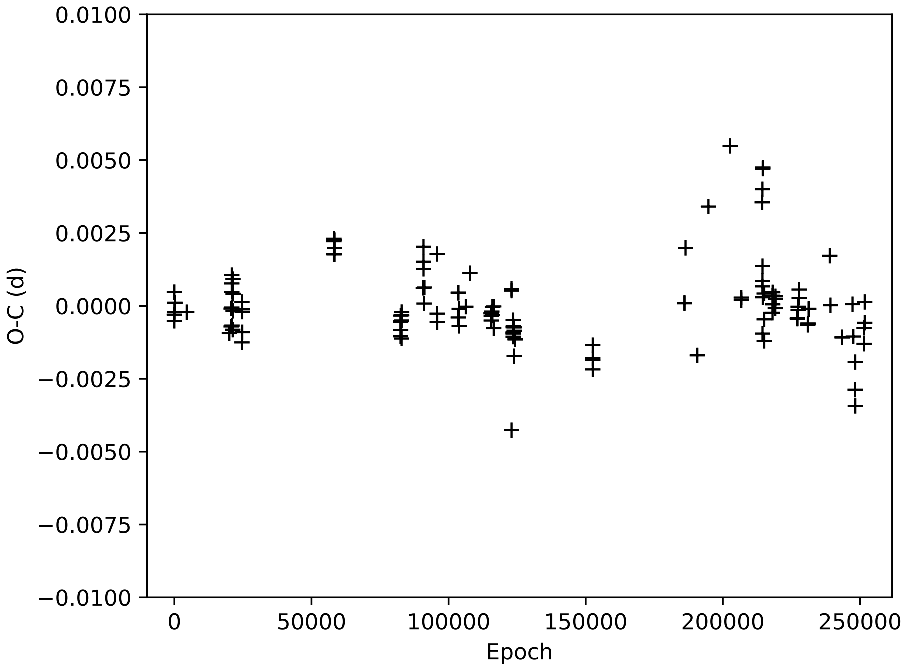

Figure 7. O–C Diagram of EH Lib calculated with the ephemerides equation obtained with the MSDR method in the quadratic case.

reddening, and hence the unrreddened color indexes for the late A and F stars to which EH Lib belongs. Values of reddening, unreddened indexes, absolute magnitude, distance modulus, distance and metallicity were determined through the mathematical expressions proposed by Nissen (1988, his equations 3, 4, and 10), which can be used to calculate the intrinsic color index $(b-y)_0$. The absolute magnitude was then calculated for A and F type stars whereas the metallicity (Nissen 1988, his equations 6, 7, and 8) is determined only when the star is in its F stage.

To avoid large dispersion in the output values due to the large scatter of the m_1 values caused by a noisy u filter, mean values for each index and physical parameter were calculated in phase bins of 0.05. The results of using the above mentioned prescriptions are listed in Table 4 in increasing phase values column 1 lists the mean bin values, and the following columns list the reddening E$(b-y)$, the values for the unreddened $(b-y)_0$, the m_0, the c_0, the β, the M_v indexes.

To determine the physical characteristics of the star, these phase averaged, unreddened values were plotted in a $(b-y)_0$ vs c_0 grid and overlapped with those values calculated by Lester et al.(1986, hereinafter LGK86) for theoretical $uvby-\beta$ indices. The comparison is presented in Figure 8 from which we find the limits of variation of EH Lib in both T_{eff} between 7400 and 8000 K and log g varying around 4.0. Table 5 compares the findings of the previous studies with the new ones determined both from $uvby-\beta$ photometry.

Table 4: Reddening and unreddened values of $uvby-\beta$ photometry for EH Lib.

Phase	$E(b-y)$	$\langle(b-y)_0\rangle$	$\langle m_0\rangle$	$\langle c_0\rangle$	β	M_v
0.05	0.006	0.157	0.177	0.851	2.778	1.7
0.15	0.002	0.122	0.179	0.953	2.809	1.3
0.25	0.001	0.127	0.175	0.968	2.801	1.1
0.35	0.005	0.145	0.171	0.920	2.784	1.3
0.45	0.007	0.159	0.169	0.871	2.772	1.5
0.55	0.002	0.180	0.166	0.833	2.751	1.5
0.65	0.002	0.197	0.167	0.788	2.734	1.6
0.75	0.005	0.201	0.165	0.768	2.732	1.8
0.85	0.006	0.199	0.163	0.763	2.735	1.9
0.95	0.004	0.184	0.170	0.776	2.752	2.1

Table 5: Physical parameters determination through $uvby-\beta$ photometry for EH Lib.

Parameter	Joner(1986)	Present Paper
$\langle E(b-y)\rangle$	0.041	0.021
$T_{\rm eff}$	7840 K	7500 ± 300 K
$\log(g)$	4.08	4.0
$\langle$[Fe/H]$\rangle$	−0.015	−0.133±0.145
$\langle M_{\rm bol}\rangle$	+1.5	
$\langle d\rangle$		372 ± 39 pc

5 Discussion

In previous research, Boonyarak et al. (2011) reported 0.0033 days as the RMS of the residuals of linear and quadratic fits and a period variation rate of (9.44×10^{-9}) per year. Jiang & Yang (1982) used yearly averaged times of maximum light to study the period variations and found a light time effect. They stated that 29 years later the phenomenon was not shown clearly in the direct (O–C) distribution but the light time effect was still visible if the yearly average was used again.

Wilson et al. (1993) calculated the phase using Jiang and Yang's (1982) elements $E_0 = 2433438.6082$ and $E_0 = 2433438.6082$, but they reported that they didn't have enough high precision data to test the hypotheses of either a possible binary orbital motion or a Blazhko effect (Karetnikov & Medvedev, 1979) due to the low amplitude of the effects.

In the present analysis, with a time span 5 years longer, we found that the O–C diagram shows a parabolic behavior (Figure 5) with a RMS of the residuals of 0.00033 and a standard deviation 0.0015. This is consistent with the result reported by Boonyarak et al. (2011) who proposed a linear and a quadratic model but could not discriminate between the two of them because the RMS of the residuals were the same in both cases. With a longer extended time basis, 5 more years of observations, we were able to discriminate between them. Our analysis gave a RMS of the residuals of 0.00033 for the linear case and 0.00026 for the quadratic. This effect is clearly noticeable when fitting a parabola,

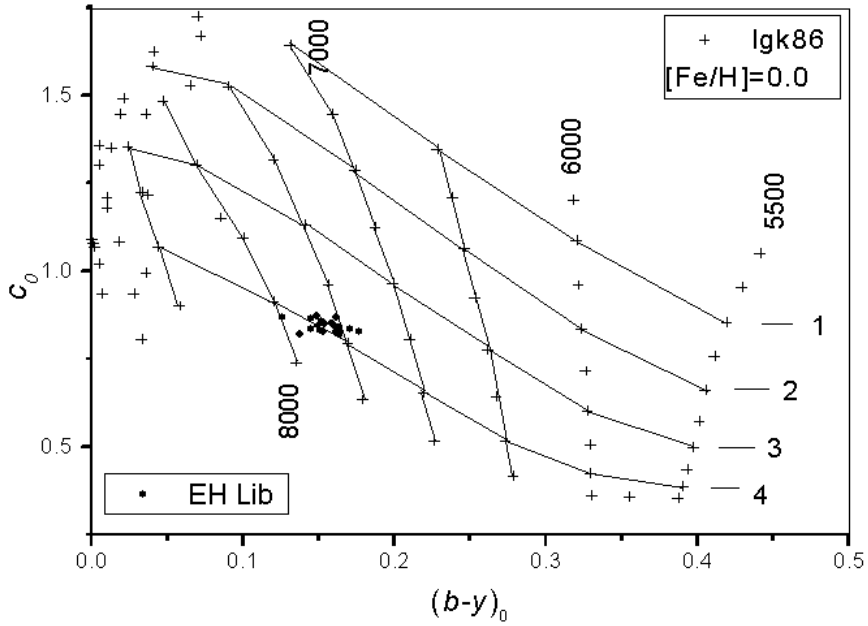

Figure 8. Cycle variation of EH Lib in the theoretical grids of LGK86.

obtaining a flattened O–C diagram in the residuals.

Mahdy and Szeidl (1980) affirmed a constant period, which was correct at that time; but after 36 years of further observations we can see a more complete behavior. Even with the 5 additional years to the Boonyarak et al. (2011) data base, the parabolic behavior is clearly discernable.

For the physical parameters the following is stated: $uvby-\beta$ photoelectric photometry was previously obtained for EH Lib by Epstein (1969) and by Joner (1986). From analogous considerations as those taken in the present paper they derived their own physical parameters. These are presented in Table 4.

6 Conclusions

Thirteen new times of maximum have been gathered for the HADS star EH Lib from two observatories with CCD and $uvby-\beta$ photometry. From the $uvby-\beta$ data, physical parameters were determined and were utilized to obtain the period of the star. The use of two more samples of $uvby-\beta$ photometry previously obtained allowed us to extend the time basis to a time span of 49 years. A minimization of the standard deviation of the O–C residuals was performed to determine the best parameters for the ephemerides equations of EH Lib and a long-term secular variation was found. The physical parameters provided by the present paper are in agreement with those of Joner (1986).

Acknowledgements: We would like to thank the staff of the OAN for their assistance in securing the observations. This work was partially supported by PAPIIT IN104917 and PAPIME PE113016. All authors thank the IA-UNAM for the opportunity to carry out the observations. Typing and proofreading were done by J. Orta, and J. Miller, respectively. C. Guzmán, F. Salas and A. Diaz assisted us in the computing. This research has made use of the Simbad databases operated at CDS, Strasbourg, France and NASA ADS Astronomy Query Form.

References:

Ashbrook, J., 1952, *AJ*, **57**, Q64 DOI
Baker, N. H., 1985, *IBVS*, 2709
Boonyarak, C., Fu, J. N., Khokhuntod, P., & Jian, S., 2011, *ApSS*, **333**, 125 DOI
Code, A. D., 1950, *PASP*, **62**, 166 DOI
Collins, K., 2012, Astronomy Source Code Library, 1309.001
Epstein, I., 1969, *AJ*, **74**, 1131 DOI
Fitch, W. S., 1957, *AJ*, **62**, 108 DOI
Hübscher, J. et al., 2009, *IBVS*, 5889
Hübscher, J. et al., 2013, *IBVS*, 6048
Jiang, S. Y. & Yang, Z. Z., 1981, *Acta Astronomica Sinica*, **22**, 279
Jiang, S. Y. & Yang, Z. Z., 1982, *Chinese Astron. & Astrophys.*, **6**, 24 DOI
Joner, M. D., 1986, *PASP*, **98**, 651 DOI
Karetnikov, V. G. & Medvedev Yu., 1977, *IBVS*, 1310
Karetnikov, V. G. & Medvedev, Yu. A., 1979, *IBVS*, 1537
Lenz, P. & Breger, M., 2005, *CoAst*, **146**, 53 DOI
Lester, J. B., Gray, R. O. & Kurucz, R. I., 1986, *ApJS*, **61**, 509 DOI
Mahdy, H. A. & Szeidl, B., 1980, *CoKon*, **74**, 1
McNamara, D. & Feltz, K. A., 1976, *PASP*, **88**, 164 DOI
McNamara, D. & Feltz, K. A., 1978, *PASP*, **90**, 275 DOI
Nissen, P., 1988, *A&A*, **199**, 146
Oosterhoff, P.Th. & Walraven, Th., 1966, *BAN*, **18**, 387
Peña, J. H., Renteria, A., Villarreal, C. et al., 2015, *IBVS*, 6154
Peña, J. H., Villarreal, C. Piña, D. S. et al., 2016, *RevMexAA*, **52**, 385
Pohl, E. 1955, *AN*, **282**, 235 DOI
Sanwal, N. B. & Pande, M. C., 1961, *Observatory*, **81**, 199
Wils, P. et al. 2011, *IBVS*, 5977
Wils, P. et al. 2012, *IBVS*, 6015
Wilson, W., Milone, E., Fry, D., 1993, *PASP*, **105**, 809 DOI

COMMISSIONS G1 AND G4 OF THE IAU
INFORMATION BULLETIN ON VARIABLE STARS
Volume 63 Number 6232 DOI: 10.22444/IBVS.6232

Konkoly Observatory
Budapest
19 December 2017

HU ISSN 0374 – 0676

CCD TIMES OF MINIMA OF ECLIPSING BINARIES

KUBICKI, D.

Torun Centre for Astronomy, Faculty of Physics, Astronomy and Applied Informatics, N. Copernicus University, Grudziadzka 5, 87-100 Toruń, Poland; e-mail: kubicki@ca.umk.pl

Abstract
We present 7 times of minima of 3 eclipsing binaries.

Observatory and telescope:
T1: 60cm Cassegrain telescope (f/12.5) at the Nicolaus Copernicus University Observatory (53.0943 °N, 18.5532 °E).

Detector:	STL-1001E CCD camera, Peltier cooling, KAF-1001E chip, $11.4' \times 11.4'$ 1024×1024 pixels.

Method of data reduction:
Differential photometry with the software AstroimageJ.

Method of minimum determination:
Marquardt-Levenberg

Times of maxima of eclipsing binaries:

Star name	Time of min. HJD	Error	Type	Filter	$O-C$ [day]	Eph. ref.
SZ Her	2457100.540359	0.000259	I	clear	−0.0005	1
XY Leo	2457070.470608	0.000178	I	*R*	0.0168	1
	2457099.450280	0.000193	I	clear	0.0179	1
	2457100.440553	0.000830	II	clear	0.0139	1
HW Vir	2457070.558122	0.000194	I	clear	−0.0005	1
	2457100.496769	0.000159	II	clear	−0.0001	1
	2457099.504577	0.000119	I	clear	−0.0005	1

Acknowledgements:
These minima times made use of the paper by Kreiner (2004). Special thanks to Krzysztof Goździewski for his invaluable help.

References:

$O-C$ gateway, an on-line database of all known eclipsing binaries (`http://var.astro.cz/ocgate`).

Kreiner, J.M., 2004, *Acta Astronomica*, **54**, 207

COMMISSIONS G1 AND G4 OF THE IAU
INFORMATION BULLETIN ON VARIABLE STARS
Volume 63 Number 6233 DOI: 10.22444/IBVS.6233

Konkoly Observatory
Budapest
23 January 2018

HU ISSN 0374 – 0676

SPECTROSCOPY OF BRIGHT ALGOL-TYPE SEMI-DETACHED CLOSE BINARY SYSTEM HU TAURI (HR 1471)

M. PARTHASARATHY

Indian Institute of Astrophysics, Bangalore – 560034, India
e-mail: m-partha@hotmail.com

Abstract

Radial velocities of the primary component (B8V) of HU Tauri derived from the photographic spectra obtained during January 1974 to December 1974 and spectroscopic orbital elements from the analysis of the radial velocity curve of the B8V primary are given. The Hα line of the late type secondary component is clearly detected on the photographic spectra taken around the quadratures and radial velocities of the secondary component are derived. The radial velocity semi amplitudes of the primary (K_1) and secondary (K_2) are found to be 60 km/sec and 234 km/sec respectively. The mass ratio $M_2/M_1 = K_1/K_2$ is found to be 0.2564. The detection of the Hα line of the secondary is confirmed from the high resolution spectra that I obtained during 1981 and 1983 at quadratures using the 2.1-m McDonald observatory Otto Struve reflector telescope and high resolution coudé Reticon spectrograph.

1 Introduction

The light variability of HU Tauri (HR 1471 = HD 29365, V = 5.92, Sp: B8V) was discovered by Strohmeier (1960). Strohmeier & Knigge (1960) found it to be an eclipsing binary with an orbital period of 2.056 days. Mammano & Margoni (1967) found the system to be a single-lined spectroscopic binary. I made photometric and spectroscopic observations of this system and derived the photometric and spectroscopic elements and absolute dimensions of the components. The observational data and the results of the analysis were included in my PhD thesis (Parthasarathy 1979).

I found that the primary minimum to be an occultation eclipse wherein the B8V primary is eclipsed by the larger cool secondary component which has filled its Roche lobe. I have detected the Hα line of the secondary component and from the radial velocities of the primary and secondary components the mass ratio is found to be 0.2564 (Parthasarathy 1979). Parthasarathy & Sarma (1980) published the B and V light curves of the system. Parthasarathy et al. (1993, 1995) derived the photometric elements using the Wilson & Devinney (1971) light curve synthesis method and confirmed the results obtained by Parthasarathy (1979). Tumer & Kurutac (1979), Dumitrescu & Dinescu (1980) and Dumitrescu & Suran (1993) also obtained the light curves of HU Tauri. Giuricin & Mardirossian (1981) analyzed the B and V light curves of HU Tauri published by Parthasarathy and Sarma (1980). However their results were wrong because they assumed the primary minimum to be a transit. Ito (1988) has obtained complete B and

V light curves; a solution to these light curves was presented by Nakamura et al. (1994). Maxted et al. (1995) obtained spectroscopic orbit and absolute parameters of HU Tauri which are in agreement with those obtained by Parthasarathy et al. (1993, 1995) and Parthasarathy (1979). In this paper I present the radial velocities, spectroscopic orbital elements and Hα profiles of HU Tauri.

Table 1: Radial velocities of HU Tauri.

Plate No	Emulsion	JD(Hel) d	Phase	Radial Velocity km/sec
1	2	3	4	5
		2442000+		
3142	IIa-0	404.238	0.0042	−17
3026	″	363.309	0.1054	−41
3027	″	363.359	0.1295	−62
3006	103a-0	361.312	0.1341	−78
3111	IIa-0	384.131	0.2313	−67
3112	IIa-0	348.157	0.2439	−59
2953	″	353.327	0.2512	−54
2520	103a-0	088.097	0.2668	−63
3092	IIa-0	382.233	0.3083	−63
3093	″	382.268	0.3252	−58
3053	103a-0	378.206	0.3502	−73
3164	IIa-0	411.258	0.4186	−24
3034	″	364.243	0.5598	−04
3016	″	362.228	0.5795	+00
2991	103a-0	360.242	0.6141	+06
2992	″	360.275	0.6298	+16
3019	IIa-0	362.441	0.6831	+30
3137	″	389.298	0.7441	+54
3100	″	383.143	0.7512	+66
3138	″	389.321	0.7552	+51
3101	II-a-O	383.173	0.7656	+62
3126	″	387.323	0.7838	+62
3062	″	379.202	0.8342	+40
3063	″	379.241	0.8528	+42
3143	″	408.086	0.8759	+43
3153	″	410.413	0.8762	+21

2 Observations

Spectroscopic observations of HU Tauri in the blue and in the Hα region were made using the 102-cm telescope and Cassegrain spectrograph of the Kavalur Observatory during the period January 1974 to December 1974.

All the spectra were obtained on photographic plates and were widened to 400 μm with a projected slit width of 20 μm. A few spectra in the Hα region were widened to 800 μm. The blue spectra were obtained on Eastman Kodak 103a-O and IIa-O (baked and unbaked) photographic plates. The spectra in the Hα region were obtained on Eastman Kodak 098-02, 103a-E and 103a-F photographic plates. Typical exposure times were thirty to sixty minutes for spectra in the blue and 90 minutes for spectra in the Hα region.

Table 2: Radial velocities (RV) of B8V primary of HU Tau derived from the Hα line.

Plate No	Emulsion	JD(Hel) d	Phase	RV km/sec
1	2	3	4	5
		2442000+		
3005	103a-E	361.251	0.1044	−30
3113	″	384.199	0.2642	−67
2971	098.02	355.490	0.3030	−63
2382	″	051.164	0.3056	−60
2396	″	053.225	0.3081	−64
2494	″	086.413	0.3165	−68
3122	103a-E	387.132	0.6909	+45
2995	″	360.426	0.7035	+70
2431	098.02	060.272	0.7349	+52
2926	″	350.319	0.7884	+68
2403	″	054.268	0.8153	+46
3105	103a-E	383.315	0.8346	+56

Table 3: Radial velocities derived from the Hα line of the secondary.

Plate No	Emulsion	JD(Hel) d	Phase	RV km/sec
		2442000+		
3008	098-02	361.437	0.1949	-
3113	103-aE	384.199	0.2642	+273
2935	098-02	351.324	0.2769	+243
2382	″	051.164	0.3056	+219
2396	″	053.225	0.3081	+240
2494	″	086.143	0.3165	+223
3017	103-aF	362.306	0.6177	-
2431	098-02	060.272	0.7349	-
2926	″	350.319	0.7884	-
2403	″	054.268	0.8153	−208

Fifty spectrograms in the blue region (25 Å/mm at Hγ) and twenty spectrograms in the Hα region (17 Å/mm) of HU Tauri were obtained. All spectra were measured with

Zeiss Abbe comparator. The spectra in the blue cover a wavelength range from 3700 Å to 4500 Å. The spectral lines used for radial velocity measurement were all the Balmer lines. The HeI 4026.2 Å and SiII 4128 Å lines were found to be very weak and were not used. Several radial velocity standard stars were observed. Radial velocities given in Tables 1, 2 and 3 are on the standard system.

The method of deriving radial velocities from the spectra obtained on photographic plates was described by Petrie (1964).

High resolution coudé Reticon spectra in the Hα region were obtained with the McDonald observatory 2.1 m Otto Struve telescope and coudé spectrograph with Reticon diode array detector. The details of the Reticon diode array and coudé spectrograph can be found in the paper of Vogt, Tull and Kelton (1978). The high resolution spectra in the Hα region were obtained with the above mentioned telescope during 1981 December 18th (phase: 0.2402), 1983 February 28th (phase: 0.7579) and 1982 February 17th (phase: 0.9833). The Hα line of the secondary which was detected by me earlier on the photographic plates (see Figure 1) is clearly present at quadratures in the above mentioned high resolution spectra (see also Figure 4 in Section 3.2).

The radial velocities given in Table 1 are based on the measurements of Hγ, Hδ, Hϵ and H8 absorption lines on the blue plates in the spectra of B8V primary. In the Balmer lines in the blue spectra there is no signature of the secondary component of HU Tau.

Since the blue spectra have a dispersion of 25 Å/mm and Hα region spectra have a dispersion of 17 Å/mm therefore the radial velocities of the B8V primary derived from its Hα line are given in Table 2.

The Hα line of the secondary is clearly resolved only around the quadratures and the radial velocities of the secondary of HU Tau are given in Table 3.

I have considered only the radial velocity curve of the B8V primary. The radial velocities of the secondary are very few in number and they are mostly around the quadratures. The preliminary elements were obtained from the analysis of the radial velocity curve of the B8V primary by using the Lehmann-Filhes (1894) method. The orbit is circular ($e = 0$). Mammano et al. (1967) also found that the orbit is circular. Therefore, using $e = 0$ and using Sterne's (1941) method for improving the elements of an approximate orbit successive least squares solutions were obtained until the corrections become smaller than mean errors of the various unknowns. Solution obtained from the analysis of the radial velocity curve of the B8V primary of HU Tau using the above described method is given in Table 4 (see Figure 2).

I have not attempted the fit of both components radial velocity curves simultaneously as the measured radial velocities of the secondary are very few and secondly they are mostly around the quadatures. I have not attempted to fit simultaneously the photometric and spectroscopic data as our coverage of the B and V light curves and radial velocity curve of the secondary are largely incomplete.

3 Analysis

The columns in Tables 1 and 2 give the plate number, the emulsion, the Heliocentric Julian day of the observation at mid-exposure, the phase, the measured radial velocity reduced to the Sun (ref. Parthasarathy, 1979, Tables 9 and 10) the results of the analysis are given in Tables 1, 2, 3 and 4 in this paper.

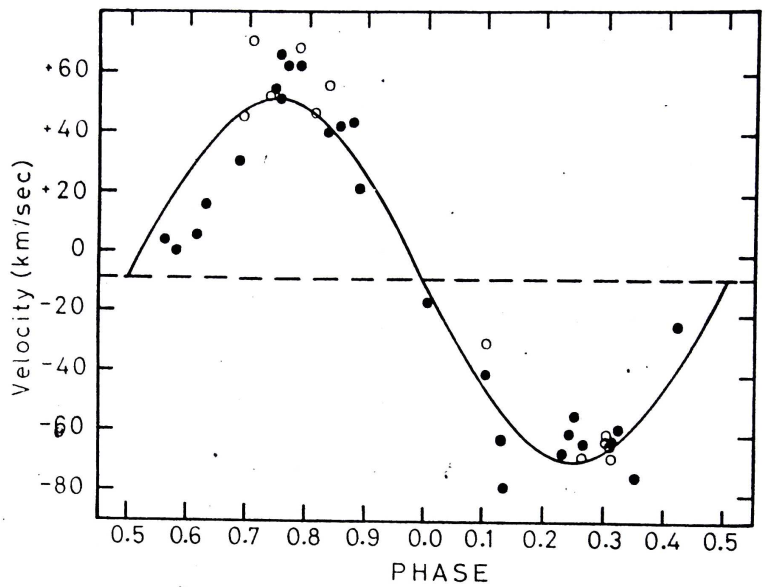

Figure 1. The Hα profiles of HU Tauri at different phases, based on microphotometer tracings. The zero of the velocity scale is the rest position of the line. The Hα absorption line of the secondary is marked in the figure. Plate numbers and phases are given in the figure.

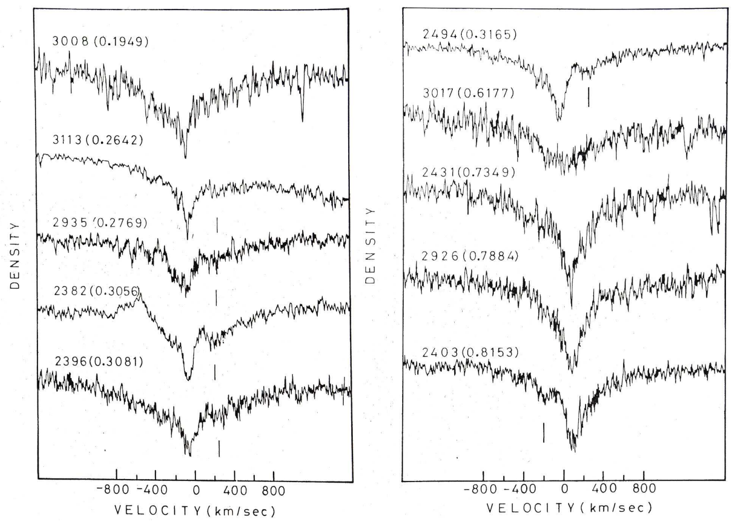

Figure 2. Radial velocity curve of HU Tauri. Open circles denote velocities determined from the Hα line. Filled circles denote the velocities determined from lines shortward of 4400 Å.

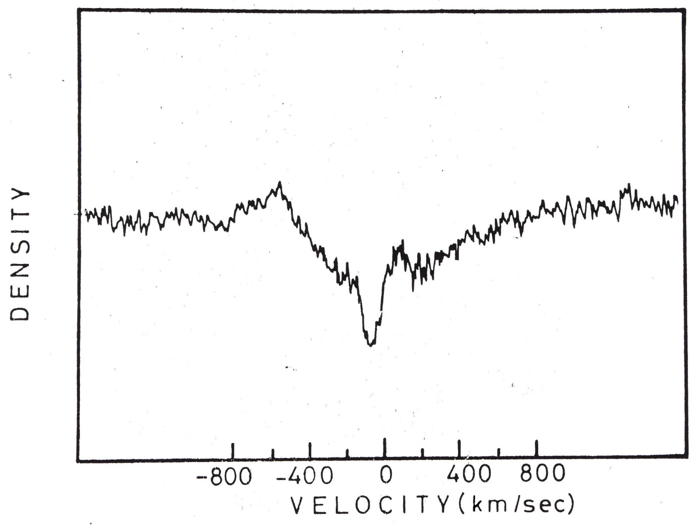

Figure 3. A spectrogram (No. 2382) obtained on 3 January 1974 (phase: 0.3056) shows a violet shifted broad emission feature. The peak velocity of the emission feature is found to be −600 km/sec.

3.1 The Hα line

The radial velocities of the primary component derived from the Hα absorption line are given in Table 2 and they were also used in the orbit computation. A spectrogram (No. 2382) obtained on 3rd January 1974 shows a violet-shifted broad emission feature (Figures 2 & 3). The peak velocity of the emission feature is found to be −600 km/sec (Figures 2 & 3). This spectrogram was obtained on Eastman Kodak 098-02 emulsion like rest of the Hα plates. A few spectra in the Hα region were obtained on 103a-E and 103a-F plates. The spectrogram of 3rd January is well exposed and it is widened to 800 microns and the exposure time was 89 minutes. The violet-shifted emission feature extends very much in to the violet wing of the Hα line. This emission feature is absent on a plate taken immediately after one orbital period. This indicates that this emission is a transient event. The same spectrogram shows absorption feature of the secondary towards the red side of the Hα absorption core of the primary (Figure 3). The spectrum obtained on 6th January 1974 (plate No. 2403, phase: 0.8153) shows clearly that this absorption feature is violet-shifted with respect to the Hα absorption core of the primary. This indicates that we are seeing the Hα absorption line of the secondary.

3.2 The Hα line of the secondary

The radial velocities of the secondary component derived from its Hα line are given Table 2 (ref. Parthasarathy, 1979, table 10). The Hα line of the secondary of HU Tauri is clearly seen in the high resolution coudé Reticon spectra of HU Tauri obtained with the 2.1 m Otto Struve telescope of the McDonald observatory (Figure 4).

From the radial velocities of the Hα line of the secondary (Table 2) K_2 is found to be +234 km/sec. The mass ratio $m_2/m_1 = K_1/K_2$ is found to be 60/234 = 0.2564. Figure 4 shows the high resolution Hα region spectra obtained on 1981 December 18th (phase: 0.2402), on 1983 February 28th (phase: 0.7579) and at phase 0.9833 on 1982 February 17th. The Hα lines of the primary and secondary are relatively broad, indicating that

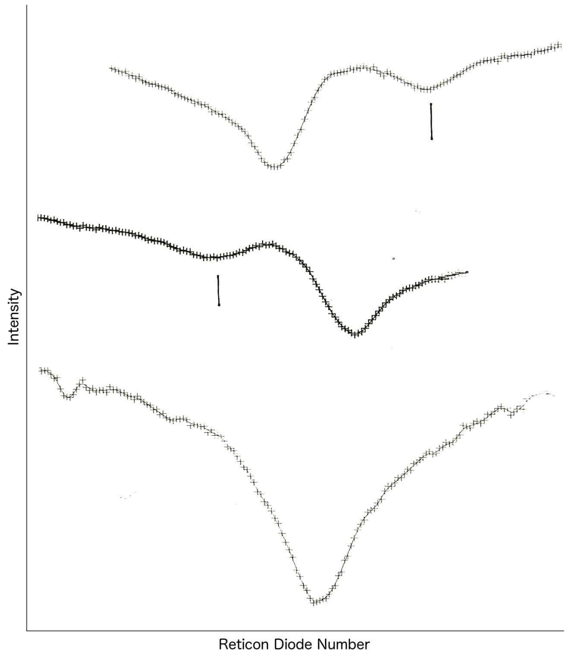

Figure 4. Coudé Reticon high resolution spectra of HU Tauri in the Hα region obtained with the 2.1-m Otto Struve telescope of the McDonald observatory. The Hα line of the secondary is marked. The Hα absorption lines of the primary and secondary at phase 0.2402 are clearly seen. *Top*: phase 0.2402 (1981 December 18), *middle*: phase 0.7579 (1983 February 28), *bottom*: phase 0.9833 (1982 February 17).

they are rotating rapidly.

The probable errors in V_0, K_1 and K_2 are found to be 2 km/sec, 2.5 km/sec and 3.5 km/sec, respectively.

Table 4: Spectroscopic orbital elements of HU Tauri.

V_0	-6.5 km/sec
K_1	60.0 km/sec
K_2	234.0 km/sec
K_1/K_2	0.26
e	0.0
$a_1 \sin i$	1.781×10^6 km
$a_2 \sin i$	6.622×10^6 km
$m_1 \sin^3 i$	4.42 $M_\odot$
$m_2 \sin^3 i$	1.19 $M_\odot$

4 Conclusions

The photometric, spectroscopic elements and absolute dimensions derived by Parthasarathy (1979) are in good agreement with those derived by Parthasarathy et al. (1993, 1995), Ito (1988), Nakamura et al. (1994) and Maxted et al. (1995).

The Hα line of the secondary detected on photographic plates is confirmed with the high resolution coudé Reticon spectra of HU Tauri obtained with the 2.1 meter Otto Struve telescope of the McDonald Observatory (Figure 4). The strength of the Hα line of the secondary (Figures 1, 2 and 4) indicates that it may be a late F–early G III-IV type star.

HU Tauri is a semi-detached Algol-type close binary system. The primary minimum in the light curve is due to an occultation eclipse. The secondary has filled its Roche lobe and mass-transfer and gaseous streams seem to be present in the system, the phase interval 0.56 to 0.68 seems to be affected. Maxted et al. (1995) also mention that around phase 0.15 there is some scatter. In the *IUE* UV high resolution spectrum of HU Tauri outside the eclipse SiIV (1393.755 Å, 1402.770 Å) absorption feature is found, which indicates the presence of high temperature plasma between the components or close to the B8V primary.

Further study of the system based on high resolution and high signal to noise ratio spectra is needed.

Acknowledgements: I am very much thankful to late Prof. M. K. V Bappu for generously allotting observing time on the 1 m telescope of the Kavalur observatory. I am also very much thankful to late Prof. Harlan J. Smith for generously allotting observing time on the 2.1 m Otto Struve telescope of the McDonald observatory. I am thankful to the referee and Dr. László Molnár for helpful comments. I am thankful to Dr. László Molnár for improving the figures in the paper. I am thankful to Dr. S. Muneer, for his help in preparing the IBVS–style manuscript. I am also thankful to Ms Evelin Bányai.

References:

Dumitrescu, A., Dinescu, R., 1980, *IBVS*, No. 1740
Dumitrescu, A., Suran, M.D., 1992, *RoAJ*, **2**, 105
Giuricin, G., Mardirossian, F., 1981, *A&A*, **97**, 410
Ito, Y., 1988, *IBVS*, No. 3212
Mammano, A., Mannino, G., Margoni, R., 1967, *Mem. Soc. Astron. Italiana*, **38**, 459
Maxted, P.F.L., Hill, G., Hilditch, R.W., 1995, *A&A*, **301**, 141
Nakamura, Y., Yamasaki, A., Ito, Y., 1994, *PASJ*, **46**, 267
Parthasarathy, M., 1979, PhD Thesis, Madurai University, Madurai, Tamilnadu, India
Parthasarathy, M., Sarma, M.B.K., 1980, *Ap&SS*, **72**, 477 DOI
Parthasarathy, M., Sarma, M.B.K., Vivekananda Rao, P., 1993, *Bull. Astr. Soc. India*, **21**, 601
Parthasarathy, M., Sarma, M.B.K., Vivekananda Rao, P., 1995, *A&A*, **297**, 359
Strohmeier, W., 1960, *IAU* Cir. No. 1706
Strohmeier, W., Knigge, R., 1960, *Veröff. Remeis-Sternw. Bamberg.* V. 5
Tumer, O., Kurutac, M., 1979, *IBVS*, No. 1547
Wilson, R.E., Devinney, E.J., 1971, *ApJ*, **166**, 605

COMMISSIONS G1 AND G4 OF THE IAU
INFORMATION BULLETIN ON VARIABLE STARS
Volume 63 Number 6234 DOI: 10.22444/IBVS.6234

Konkoly Observatory
Budapest
23 January 2018

HU ISSN 0374 – 0676

CCD MINIMA FOR SELECTED ECLIPSING BINARIES IN 2017

NELSON, ROBERT H.

1393 Garvin Street, Prince George, BC, Canada, V2M 3Z1 e-mail: bob.nelson@shaw.ca

Observatory and telescope:
Mountain Ash Observatory (MAO): 33 cm f/4.5 Newtonian on a Paramount ME Desert Blooms Observatory (DBO): 40 cm f/6.8 SCT on a Paramount Taurus 400

Detector:	MAO: SBIG ST-10XME, 6.8 μm pixels, FOV: $34.4'' \times 23.2''$, $-10° > T > -30°$C DBO: SBIB STT-1603, 9.0 μm pixels, FOV: $18.3'' \times 11.5''$, $-10° > T > -30°$C

Method of data reduction:
Bias and dark subtraction, flat-fielding using light-box flats; aperture photometry–all using MIRA, by Mirametrics. Check stars were used throughout.

Method of minimum determination:
Digital tracing paper method, bisection of chords, curve fitting, and (occasionally) Kwee and van Woerden (1956)

Times of minima:

Star name	Time of min. HJD 2400000+	Error	Type	Filter	$O-C$ [day]	Rem.
V0404 And	58054.6137	0.0002	I	BVI	−0.0005	DBO
V0404 And	58059.6841	0.0003	II	BVI	−0.0004	DBO
V0404 And	58077.5973	0.0004	I	BVI	−0.0021	DBO
V0404 And	58112.7531	0.0003	I	BVI	−0.0001	MAO
V0523 And	58060.663	0.003	I	c	0.0004	MAO
BO Ari	58098.586	0.0003	I	R	0.0015	MAO
ZZ Aur	57757.62	0.001	II	c	0.0031	MAO
AH Aur	57798.6405	0.0003	II	R	−0.0026	MAO
AP Aur	57763.7197	0.0003	II	c	0.0022	MAO
GX Aur	58109.8143	0.0002	I	c	−0.0014	MAO
HL Aur	58059.8735	0.0002	I	c	0.0029	MAO
V0410 Aur	58056.7662	0.0003	II	c	−0.0031	MAO
V0534 Aur	57798.705	0.002	I	R	0.0008	MAO
V0599 Aur	58066.7971	0.0003	II	c	−0.0017	MAO
AC Boo	57809.966	0.0001	I	R	0.0074	MAO

Times of minima:

Star name	Time of min. HJD 2400000+	Error	Type	Filter	$O-C$ [day]	Rem.
GM Boo	57817.9666	0.0002	I	c	0.003	MAO
GR Boo	57812.9215	0.0002	I	c	−0.0013	MAO
QT Boo	57807.906	0.003	II	c	−0.0071	MAO
V0339 Boo	57913.69	0.0004	I	c	0.0051	DBO
G0912-0792 Boo	57914.7199	0.0003	I	c	0.0011	DBO
AO Cam	58002.86	0.0004	I	V	−0.0034	DBO
LR Cam	58077.8802	0.0004	I	R	−0.0001	MAO
OQ Cam	58090.7602	0.0002	I	c	0.003	MAO
V0335 Cam	58112.6508	0.0004	I	c	−0.0012	MAO
V0366 Cam	58107.7308	0.0003	I	R	−0.0004	MAO
V0405 Cam	58077.7718	0.0004	I	R	−0.0074	MAO
V0409 Cam	58060.8647	0.0002	I	c	0.0018	MAO
V0473 Cam	58063.8748	0.0002	I	c	−0.0013	MAO
TX Cnc	58110.8031	0.0003	I	R	−0.0047	MAO
IN Cnc	57832.6819	0.0001	I	c	−0.0005	MAO
IR Cnc	58062.9655	0.0004	I	c	−0.0036	MAO
G1928-0943 Cnc	57812.685	0.0001	II	R	−0.0017	MAO
BI CVn	57899.7702	0.0005	I	R	0.0002	DBO
BO CVn	57868.761	0.0008	I	V	−0.0007	MAO
EY CVn	57817.7542	0.0003	I	c	−0.0007	MAO
GN CVn	57836.8082	0.0001	I	c	−0.0015	MAO
BF CMi	58103.8761	0.0003	I	c	0.0063	MAO
CZ CMi	58073.9944	0.0003	I	R	0.0009	DBO
ZZ Cas	57959.869	0.0002	I	c	0.001	MAO
CW Cas	57963.8178	0.0002	II	c	−0.0027	MAO
DZ Cas	58063.6226	0.0006	II	c	0.0016	MAO
V0776 Cas	57966.8398	0.0004	I	V	0.0003	MAO
V0776 Cas	58090.5923	0.0005	I	R	−0.004	MAO
V0961 Cas	58054.6489	0.0002	I	c	0.0005	MAO
G4046-0154 Cas	57756.5942	0.0001	II	c	0.0003	MAO
XX Cep	57928.8497	0.0002	I	R	−0.0008	MAO
V0870 Cep	57909.879	0.0003	I	c	0.0002	MAO
G4500-0730 Cep	58066.6524	0.0002	II	R	0.0006	MAO
G0054-0373 Cet	58113.6432	0.0005	I	c	−0.0015	MAO
V0500 Cyg	57901.9264	0.0002	I	VRI	0.0014	DBO
V0500 Cyg	57908.859	0.0006	II	VRI	0.0024	DBO
V0500 Cyg	57913.9397	0.0004	I	VRI	−0.0002	DBO
V0500 Cyg	57914.8639	0.0009	I	VRI	−0.0002	DBO
V0836 Cyg	57902.8065	0.0005	I	c	−0.0009	MAO
V0859 Cyg	57875.924	0.0001	II	c	0.002	MAO
V0959 Cyg	58056.6486	0.0004	II	c	−0.0048	MAO
V2197 Cyg	57916.8592	0.0002	I	c	−0.001	MAO
V2282 Cyg	57890.7917	0.0002	II	c	−0.0019	MAO
V2477 Cyg	57912.8369	0.0004	II	c	−0.0009	MAO
V2552 Cyg	58050.6835	0.0003	II	BVI	0.0011	DBO
V2552 Cyg	58052.6329	0.0003	I	BVI	0.0009	DBO

Times of minima:

Star name	Time of min. HJD 2400000+	Error	Type	Filter	$O-C$ [day]	Rem.
V2552 Cyg	58052.7699	0.0005	II	BVI	−0.0014	DBO
V2552 Cyg	58056.6692	0.0002	I	BVI	−0.0012	DBO
Z Dra	57809.8334	0.0003	I	VRI	−0.0045	MAO
RZ Dra	57901.8182	0.0003	II	R	0.0002	MAO
BL Dra	57908.8368	0.0001	I	c	0.0007	MAO
EF Dra	57880.8962	0.0003	I	c	0.0006	MAO
V0349 Dra	57864.7811	0.0001	I	c	−0.0002	MAO
V0388 Dra	57872.8286	0.0002	II	c	0.002	MAO
V0422 Dra	57893.8208	0.0002	I	c	0.0002	MAO
G3897-1017 Dra	57869.7796	0.0002	I	c	−0.0009	MAO
QW Gem	57755.6495	0.0003	I	R	−0.0003	MAO
G1886-1869 Gem	58052.8674	0.0002	II	c	−0.0005	MAO
V0728 Her	57918.6865	0.0002	I	c	−0.0004	MAO
V0829 Her	57876.7968	0.0003	I	c	−0.0029	DBO
V0857 Her	57876.9297	0.0002	II	c	0.0021	DBO
V0921 Her	57900.8203	0.0004	II	V	0.0033	MAO
V1036 Her	57813.0178	0.0001	I	c	0.0003	MAO
V1042 Her	57901.7742	0.0005	II	c	−0.0024	DBO
V1066 Her	57896.9209	0.0005	II	c	0.0013	DBO
V1094 Her	57875.819	0.0008	I	c	0.0003	MAO
V1097 Her	57920.6983	0.0002	II	BVRI	0.0011	DBO
V1097 Her	57920.8779	0.0003	I	BVRI	0.0003	DBO
V1097 Her	57922.6822	0.0002	I	BVRI	0.0003	DBO
V1097 Her	57922.8639	0.0003	II	BVRI	0.0016	DBO
V1100 Her	57826.8836	0.0003	I	c	−0.0005	MAO
V1101 Her	57894.8247	0.0002	I	c	−0.0001	MAO
V1103 Her	57847.7377	0.0004	I	c	−0.033	MAO
V1355 Her	57921.8343	0.0003	I	c	0.0027	MAO
AV Hya	58109.998	0.004	II	BVI	0.0056	DBO
G3621-0711 Lac	57927.8343	0.0004	I	R	0.0051	MAO
AP Leo	57807.8065	0.0003	I	R	0.0009	MAO
CE Leo	57812.8276	0.0001	II	c	−0.0017	MAO
DU Leo	58103.9956	0.0002	I	BVI	0	MAO
XY LMi	58061.0464	0.0002	II	c	−0.0043	MAO
UU Lyn	58064.0352	0.0001	I	c	−0.0004	MAO
BG Lyn	58056.9023	0.0008	I	c	−0.0024	MAO
PV Lyr	57875.8497	0.0005	I	c	−0.0204	DBO
V0591 Lyr	57832.9391	0.0002	II	c	−0.0012	MAO
V0591 Lyr	57895.8722	0.0001	I	c	−0.0009	DBO
G3104-1085 Lyr	57832.9695	0.0005	?	c	0	MAO
G3104-1085 Lyr	57893.8939	0.0007	??	c	0.0014	DBO
G3104-1085 Lyr	57894.758	0.002	??	c	−0.0017	DBO
G3104-1085 Lyr	57895.844	0.0002	??	c	0.0003	DBO
BB Peg	57960.8555	0.0003	I	c	0.0001	MAO
V0534 Peg	57990.7632	0.0003	I	V	0	MAO
IK Per	58111.648	0.0002	I	c	0.0001	MAO

Times of minima:						
Star name	Time of min. HJD 2400000+	Error	Type	Filter	$O-C$ [day]	Rem.
V0882 Per	58053.7838	0.0004	I	c	−0.0001	MAO
CP Psc	58077.6164	0.0003	II	R	0.0003	MAO
G0008-0448 Psc	58099.6042	0.0002	I	c	0	MAO
V0382 Sge	57903.846	0.002	I	c	−0.0014	MAO
G0242-2191 Sex	57806.7662	0.0003	I	c	−0.0002	MAO
CU Tau	58107.638	0.002	I	c	0.0177	MAO
GW Tau	58109.6763	0.0003	I	c	−0.0011	MAO
V1121 Tau	58063.8323	0.003	I	BVI	−0.0009	DBO
V1241 Tau	58073.7999	0.0007	II	BVI	−0.0002	DBO
V1241 Tau	58101.7905	0.0004	II	BVI	−0.0008	DBO
V1241 Tau	58109.6081	0.0003	I	BVI	−0.0043	DBO
X Tri	58062.7342	0.0001	I	R	−0.0016	MAO
CL Tri	58063.7791	0.0002	I	c	0.0013	MAO
XY UMa	58077.9975	0.0001	I	V	−0.0013	MAO
MQ UMa	58083.9512	0.0003	I		0.0035	DBO
V0342 UMa	57806.8894	0.0003	I	c	−0.0104	MAO
V0354 UMa	57847.7377	0.0002	II	c	0.005	MAO
G3807-0759 UMa	57817.6387	0.0004	II	V	−0.0009	MAO
RU UMi	57832.8136	0.0001	I	R	0.0011	MAO
V0496 Vul	57864.9113	0.0002	I	c	−0.0016	MAO

Remarks:

To save space, GSC star names have been shortened to a leading "G" only; times of minimum are heliocentric Julian dates with the leading 24 removed.

$O-C$ values were computed using elements computed from the $O-C$ database listed in the references (Nelson, 2016).

The newly-opened observatory, Desert Blooms in Benson AZ, is described in Nelson (2017).

Acknowledgements:

Thanks are due to Environment Canada for the website satellite views (see reference below) that were essential in predicting clear times for observing runs in this cloudy locale. Thanks are also due to Attilla Danko for his Clear Sky Charts, (see below). This research has made use of the SIMBAD database, operated at CDS, Strasbourg, France.

References:

Kwee, K.K., van Woerden, H., 1956, *BAN*, **12**, 327
Nelson, R.H. 2016, Bob Nelson's $O-C$ Files, `http://www.aavso.org/bob-nelsons-o-c-files`
Nelson, R.H. 2017, *IBVS*, **5224**
Satellite Images for North America, `http://weather.gc.ca/`

COMMISSIONS G1 AND G4 OF THE IAU
INFORMATION BULLETIN ON VARIABLE STARS
Volume 63 Number 6235 DOI: 10.22444/IBVS.6235

Konkoly Observatory
Budapest
23 January 2018

HU ISSN 0374 – 0676

TIMING OF AR CrB ECLIPSES

KOZYREVA, V. S.[1]; IRSMAMBETOVA, T. R.[1]; IBRAHIMOV, M. A.[2]; KRUSHEVSKA, V. N.[3]; KUZNYETSOVA, YU. G.[3]; KHALIKOVA, A. V.[4]; PARMONOV, O. U.[4]; KARIMOV, R. G.[4]; BOGOMAZOV, A. I.[1], SATOVSKII, B. L.[5]; TUTUKOV, A. V.[2]

[1] M. V. Lomonosov Moscow State University, P. K. Sternberg Astronomical Institute, 13, Universitetskij prospect, Moscow, 119991, Russia

[2] Institute of Astronomy, Russian Academy of Sciences, 48 Pyatnitskaya st., 119017, Moscow, Russia

[3] Main Astronomical Observatory, National Academy of Sciences of Ukraine, 27, Akademika Zabolotnoho ulitsa, Kyiv, 03143, Ukraine

[4] Ulugh Beg Astronomical Institute, Uzbek Academy of Sciences, 33, Astronomicheskaya ulitsa, Tashkent, 100052, Uzbekistan

[5] AstroTel Ltd., 1A, Nizhegorodskaya ulitsa, Moscow, 109147, Russia

Abstract

AR CrB is a short-period low-mass eclipsing binary. We conducted photometric observations of the system in 2013, 2014, 2016, 2017, and obtained times of its light curves minima. The timing of eclipses (our times of minima combined with data from the literature) shows that the orbital period of AR CrB could possess periodical variations that can be explained by the gravitational influence of a third companion in a highly eccentric orbit around the central binary.

AR CrB is a short-period low-mass eclipsing binary star, its orbital period is 0.397352 days according to the General Catalogue of Variable Stars (Samus et al., 2017), its type of variability is EW. We conducted a timing of its eclipses using times of minima obtained from our observations (see Table 1) combined with times of minima from the B.R.N.O. database[1], we also calculated (see Tables 2 and 3) and used times of minima from SuperWASP light curves[2,3] (Butters et al., 2010, Paunzen et al., 2014). Our calculations show that the AR CrB orbital period can possess periodical variations that can be explained by the gravitational influence of a third companion in a highly eccentric orbit around the central binary.

The AR CrB eclipsing binary was observed from two observatories: (1) Maidanak observatory of Ulugh Beg Astronomical Institute of Uzbek Academy of Sciences, 60 cm Zeiss telescope (in 2013, 2014), (2) South Station of M. V. Lomonosov Moscow State University, Nauchnij, Crimea, 60 cm Zeiss telescope (2014, 2016, 2017). We used Bessel R (Maidanak) and Cousins R (Crimea) filters, and following CCD cameras: FLI PL 1K×1K (Maidanak), Apogee Ap47p (Crimea, 2014), FLI PL 4022 (Crimea, 2016), Apogee Aspen (Crimea, 2017). Dates of the observations are: 09, 10, 12, 13, 15, 16, 25, 26, 27, 28, 29, 30 May 2013, 15, 24 May, 01, 07, 19, 26, June, 04 July 2014 (Maidanak), 26, 27, April, 06, 21 May 2014, 28, April, 19 May 2016, 19, 30 April 2017 (Crimea). As comparison star

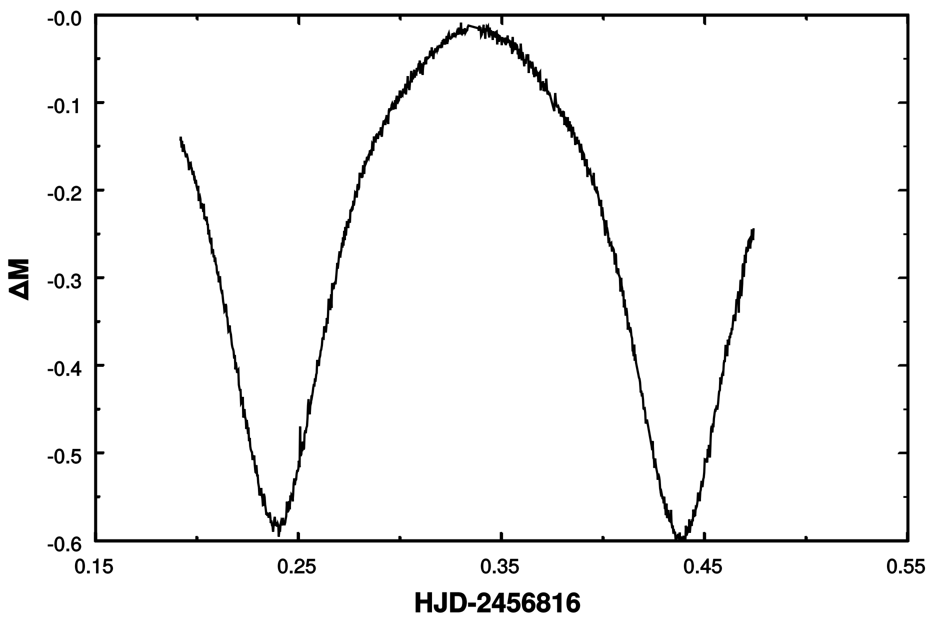

Figure 1. A sample light curve of AR CrB, Bessel *R* filter.

we chose IRAS 15569+2754. Our light curves are available online as supplementary files to the paper (Tables 4–29).

For data processing we used the aperture photometry method with the program C-Munipack[4] for data from the Maidanak observatory and Maxim DL for data from Crimea. For the SuperWASP data we used the "Mag2" column (this column had 1-4 points with the same HJD, so we averaged their magnitude with the same HJD), only symmetric light curves around minima were used to find times of minima. To estimate parameters of the binary a computer code by Kozyreva & Zakharov (2001) was used. Due to the code features we cannot estimate precisely all geometrical quantities of an EW type system, so we present here only several of them: the orbital eccentricity of the central binary is $e = 0.0014 \pm 0.0005$ (the existence of such eccentricity also can be confirmed by the differences in the initial epochs of primary and secondary minima of 0.0003 days), the inclination of this orbit is $i = 82.0 \pm 4°$.

We obtained following ephemerides:

$$\mathrm{Min\ I} = \mathrm{T_1} + \mathrm{P_{orb}} \times \mathrm{E}, \quad (1)$$

$$\mathrm{Min\ II} = \mathrm{T_2} + \mathrm{P_{orb}} \times (\mathrm{E} + 0.5), \quad (2)$$

where $T_1 = \mathrm{HJD}\,2452365.5031 \pm 0.003$ and $T_2 = \mathrm{HJD}\,2452365.5032 \pm 0.003$ are the initial epochs for primary and secondary minima respectively, E is the number of orbital cycles since the initial epoch, $P_{orb} = 0.397351625 \pm 0.000000050$ d is the orbital period of AR CrB. We calculated O–C values for times of minima and fitted them by a light equation and by a parabolic curve. We estimate the significance of our results using a statistical method by Stellingwerf (1978) and calculate the value

[1] http://var2.astro.cz/ocgate/?lang=en
[2] https://exoplanetarchive.ipac.caltech.edu/docs/SuperWASPMission.html
[3] http://wasp.cerit-sc.cz/
[4] http://c-munipack.sourceforge.net

$$\theta = \frac{\sigma^2}{\sigma_0^2}, \quad (3)$$

where σ_0 is the standard deviation that corresponds to the values of O–C calculated using Equations (1) and (2), σ is the standard deviation that is corrected with the theoretical curve. The smaller value of θ corresponds to the better coincidence between observational data and the theoretical fit.

The results of our calculations are presented in Figures 2 and 3. For the parabolic fit we used an expression

$$(O - C) = a + b \cdot \mathrm{HJD} + \mathrm{c} \cdot \mathrm{HJD}^2, \quad (4)$$

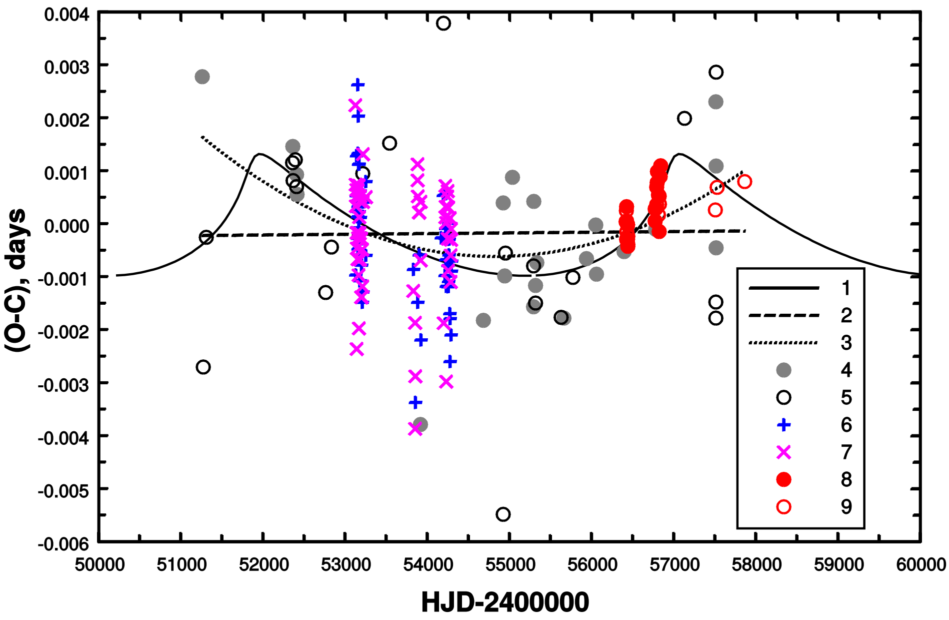

Figure 2. O–C diagram for times of minima of AR CrB from the literature (B.R.N.O. database), from our observations (Table 1), and from the SuperWASP project (Tables 2 and 3, available online). The indications in the Figure are following: (1) is the light equation curve, (2) is the straight line, (3) is the parabolic curve, (4) Min I, B.R.N.O. database, (5) Min II, B.R.N.O. database, (6) Min I, SuperWASP, (7) Min II, SuperWASP, (8) Min I, this work, (9) Min II, this work.

see below for values of parameters in this formula. For the light equation we estimated following parameters: its amplitude A_3, the orbital period of the third companion P_3 days, its orbital eccentricity e, its ascending node longitude ω_3. The time of the periastron passage T_P for the new body is:

$$T_P = T_3 + E_3 \times P_3, \quad (5)$$

where T_3 is the initial epoch, E_3 is the number of the third body orbital cycles since its initial epoch.

For Figure 2 we took into account all available times of minima (from the B.R.N.O. database, SuperWASP times of minima, and our times of minima). The linear curve is parallel to the x axis. Values of parameters in Equation (4) are: $a = 0.53089$, $b =$

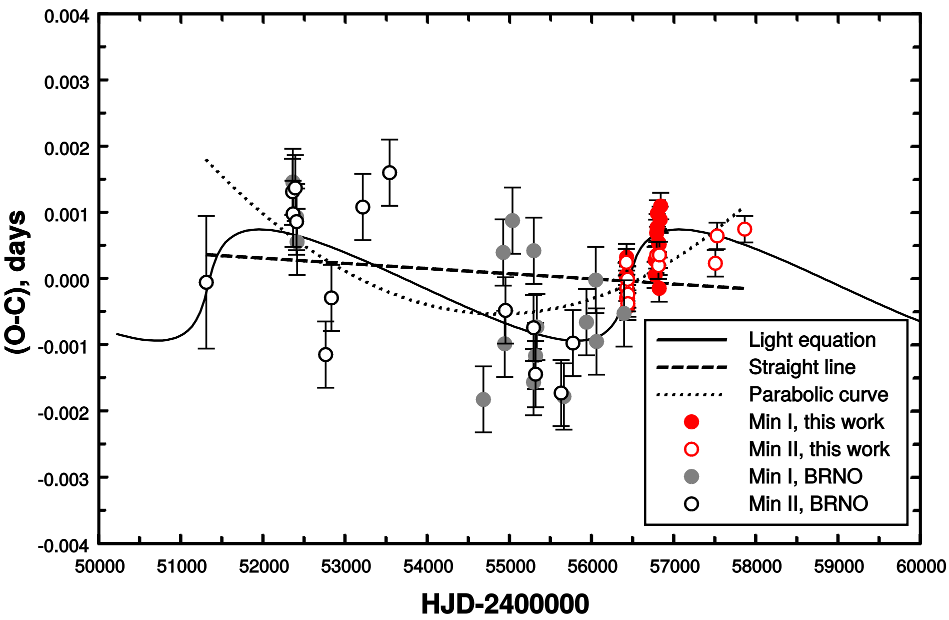

Figure 3. The same as Figure 2 for the best observational points.

-0.000019, $c = 1.78 \cdot 10^{-10}$. The orbital period change in this case corresponds to $8.2 \cdot 10^{-8}$ days per year. For this (parabolic) curve: $\sigma_0 = 0.00120$, $\sigma = 0.00114$, $\theta = 0.90$. For the light equation: $A_3 = 0.0014 \pm 0.0001$, $P_3 = 5108 \pm 50$ days, $e = 0.8$, $\omega_3 = 44°$, $T_3 =$ HJD2455321 $\pm$ 150, $\sigma_0 = 0.00120$, $\sigma = 0.00110$, $\theta = 0.84$. For the linear approximation $\sigma = \sigma_0$ and $\theta = 1$.

For Figure 3 we used only "good" points, i.e., where the deviation is less than $2.5\sigma_0$. For the linear approximation $\sigma = 0.00083$, $\sigma_0 = 0.00084$, and $\theta = 0.98$. Values of parameters in Equation (4) are: $a = 0.55035$, $b = -0.000020$, $c = 1.88 \cdot 10^{-10}$. The orbital period change in this case corresponds to $8.6 \cdot 10^{-8}$ days per year. For the parabolic curve: $\sigma_0 = 0.00084$, $\sigma = 0.00071$, $\theta = 0.71$. For the light equation: $A_3 = 0.0014 \pm 0.0001$, $P_3 = 5360 \pm 50$ days, $e = 0.7$, $\omega_3 = 26°$, $T_3 =$ HJD2455544 $\pm$ 150, $\sigma_0 = 0.00084$, $\sigma = 0.00061$, $\theta = 0.53$.

In both cases (all times of minima and "good" times of minima) the hypothesis of the third companion is more preferable than linear or parabolic curves. So, the possible presence of a third body in AR CrB can be a common feature of binaries. The observed initial distribution of components of binary stars over separations was described as follows (Equation (22), Masevich & Tutukov, 1988, page 110):

$$dN = 0.2 d \log(a/R_\odot),\ 1 \leq \log(a/R_\odot) \leq 6, \tag{6}$$

To estimate the possible multiplicity we can take this function as a probability to find a new companion in a multiple system. Due to selection effects one can miss of component of very close binaries or binaries with faint companions, therefore binaries can be triples/multiples.

There are no spectral data for AR CrB, therefore the masses of components are unknown, so the lower limit of the suggested third body mass can be estimated to be several percent of total mass of the system according to its mass function, its value is ≈ 0.05.

Less favourable explanations (according to θ values) of the orbital period change (in case of the parabolic curve) in AR CrB are the mass transfer between components (that

Table 1: Times of minima of AR CrB obtained from our observations.

HJD–2400000 (d)	O–C (d)	Min
56422.4633	0.00003	I
56426.4368	0.00005	I
56425.4441	0.00025	II
56428.2250	−0.00029	II
56428.4238	0.00032	I
56429.4172	−0.00014	II
56438.3573	−0.00002	I
56439.3512	−0.00001	II
56440.3438	−0.00030	I
56441.3377	−0.00023	II
56442.3304	−0.00043	I
56443.3243	−0.00037	II
56774.5171	0.00028	I
56775.3115	0.00005	I
56784.4509	0.00029	I
56793.1930	0.00069	I
56793.3918	0.00035	II
56799.5507	0.00077	I
56802.3324	0.00098	I
56816.2392	0.00055	I
56816.4380	0.00016	II
56825.3783	0.00051	I
56828.3588	0.00036	II
56835.3125	0.00088	I
56843.2597	0.00109	I
57507.4326	0.00023	II
57528.4927	0.00065	II
57863.4602	0.00075	II

can also cause a long period variation of the orbital period, Liu, Quian and Xiong, 2018) and the Applegate's (1992) magnetic mechanism that changes the quadrupole gravitational momentum of one of the components (or both of them).

References:

Applegate J. H., 1992, *ApJ*, **385**, 621 DOI
Butters O. W., West R. G., Anderson D. R., et al., 2010, *A&A*, **520**, L10 DOI
Kozyreva V. S., Zakharov A. I., 2001, *Astronomy Letters*, **27**, 712 DOI
Liu L., Qian S.-B., Xiong X., 2018, *MNRAS*, **474**, 5199 DOI
Masevich A. G., Tutukov A. V., 1988, Evolution of Stars: Theory and Observations, Moscow, Nauka (in Russian)
Paunzen E., Kuba M., West R. G., Zejda M., 2014, *IBVS*, No. 6090
Samus N. N., Kazarovets E. V., Durlevich O. V., Kireeva N. N., Pastukhova E. N., 2017, *Astronomy Reports*, **61**, 80 DOI
Stellingwerf R. F., 1978, *ApJ*, **224**, 953 DOI

COMMISSIONS G1 AND G4 OF THE IAU
INFORMATION BULLETIN ON VARIABLE STARS
Volume 63 Number 6236 DOI: 10.22444/IBVS.6236

Konkoly Observatory
Budapest
7 February 2018

HU ISSN 0374 – 0676

REVISED COORDINATES OF VARIABLE STARS IN CASSIOPEIA

NESCI, R.

INAF/IAPS, via Fosso del Cavaliere 100, 00133 Roma, Italy, e-mail: roberto.nesci@iaps.inaf.it

Abstract

The identification of the variable stars published on IBVS #3573 has ben revised on the basis of the original (unpublished) finding charts. Cross check with the 2MASS catalog has been made to get more accurate coordinates and to confirm their nature from their $J-H$, $H-K$ colors. The Mira stars, given their known periods, could be used with the astrometric parallaxes of the forthcoming Gaia catalog to improve the Period-Luminosity relation.

1 Introduction

Mira stars are among the brightest star in a stellar population, and their absolute luminosity is fairly related to their pulsation period, so that are useful as standard candles to derive the distances of nearby galaxies.

A list of red variables, including a number of Miras, in a field centered on IC 1805, was published by Gasperoni, Maffei and Tosti (1991, IBVS #3573), giving a measure of their periods on the basis of 7 years of observations using infrared (I-N + RG5) and blue (103aO) Schmidt plates of the Asiago Observatory.

This variable stars sample is statistically well defined, being magnitude limited and followed with 75 plates along 7 years. Gasperoni et al. (1991) did not publish finding charts but only coordinates at B1950, with arcmin approximation, rather poor for a safe identification near the galactic plane. Based on that paper, the stars were imported in the General Catalog of Variable Stars (Samus et al. 2017) by Samus et al. (2003). The individual stars can be searched in SIMBAD by their original provisional name (SV* Mxxx) or by coordinates. They can also be searched in the VSX database, but only with the variable name or the coordinates, and the historic link to Gasperoni et al. (1991) is generally not present.

In the course of a larger on-going research on the Mira stars in Cassiopeia, I found for some of these stars strong inconsistencies between the optical and near infrared (JHK) magnitudes available from cross correlation of the GCVS and 2MASS (Cutri et al. 2003) catalogs, suggesting that some misidentifications have occurred. As a matter of fact, most of these stars are not referred by any paper (besides the discovery one) in the SIMBAD or ADS databases.

2 Identification

In the family archive of the late prof. Paolo Maffei (http://www.archiviomaffei.org) I was able to recover the original paper enlargements of the Asiago plates, with pencil annotations by Maffei of the detected variables and comparison sequences, so it was possible to check for all the stars their actual positions. I also found the two original thesis works (unpublished) of the two Maffei's students V. Gasperoni and G. Tosti on the stars of this field. Comparison of the finding charts with the Digitized Sky Survey infrared plates, available on-line from the Space Telescope Science Institute (http://archive.stsci.edu/cgi-bin/dss_plate_finder), and with the 2MASS catalog and images, available from SIMBAD (http://simbad.u-strasbg.fr/simbad/), and IRSA database (http://irsa.ipac.caltech.edu/) allowed to perform a satisfactory identification for all the variables listed in Gasperoni et al. (1991) with a 2MASS counterpart.

In some cases the coordinates differences between Gasperoni et al. (1991) (precession corrected) and the actual coordinates were small, compatible with the quoted accuracy, but often they were rather large, several arcmin! Two stars have outstanding errors: M279 (presently identified in the GCVS as V0687 Cas) and M289 (identified in the GCVS as V0685 Cas).

In the case of the SR variable M279 the published coordinates are 187 arcmin (3 degrees !) off from the position in the finding chart: the finding chart says that it must be associated to IRAS 02205+6014, a bright and very red star. At the coordinates of M279 published in Gasperoni et al. (1991) the CGVS reports V0676 Cas, but nothing similar to a red star is nearby. In Maffei's finding charts no variable star is reported near the published coordinates.

Similarly dramatic is the situation of the SR variable M289, which is 169 arcmin (again about 3 degrees) off from the published position: at the finding chart position there is a bright and red source in 2MASS, as should be for a SR variable. At this position the VSX catalog reports a low amplitude variable, NSVS 1890163. On his thesis, G. Tosti reports large irregularities in the light curve of this star, which prevented to define a time scale for its variability: the variability amplitude, 0.8 mag, is similar to that reported in the NSVS. The associated name in GCVS is V0685 Cas, but its position corresponds to a rather bright and blue star (B = 13.188, V = 12.697, $B - V$ = 0.49 in the UCAC4 catalog) clearly inconsistent with the Maffei's variable because it is reported to be always below the detection limit ($B \sim 18$ mag) in the Asiago blue plates. Clearly NSVS 1890163 is the actual identification of M289.

I tried to understand from the documents in Maffei's archive how such large errors for these two stars could arise. In Tosti's thesis no coordinates are given, while in Gasperoni's one the coordinates are given as published in Gasperoni et al. (1991): the most likely explanation is therefore that the misprints in the thesis were carried on in the article.

3 Results

Table 1 lists for each star the Maffei's provisional name and the B1950 coordinates as reported in Gasperoni et al. (1991), the J2000 coordinates of the actual 2MASS counterpart as derived from Maffei's original finding charts, the present designation in SIMBAD, the distance between the old (precessed to J2000) and the new position in arcmin. Only in 9 cases the coordinates difference is less than 1 arcmin, that is their formal accuracy:

Table 1: Revised coordinates and identifications of variable stars in the field of IC 1805.

Maffei name	RA1950 orig.	DEC1950 orig.	RAJ2000 corrected	DECJ2000 corrected	GCVS name	offset arcmin	VSX ident.
M278	02:41:51	+62:53:00	02:45:31.33	+63:02:19.6	V0690 Cas	4.07	–
M279	02:37:26	+62:31:00	02:24:16.45	+60:27:56.8	V0687 Cas*	186.83	–
M280	02:31:29	+59:45:00	02:35:09.68	+59:55:28.6	V0678 Cas	2.67	–
M281	02:47:50	+59:14:00	02:51:40.21	+59:26:40.8	V0696 Cas*	0.36	Dauban V268
M282	02:43:40	+57:56:00	02:47:29.08	+58:07:32.3	V0692 Cas	1.14	–
M283	02:25:25	+60:17:00	02:28:55.44	+60:23:26.6	V0675 Cas*	7.13	Dauban V264
M284	02:46:57	+58:16:00	02:50:45.86	+58:37:59.4	V0694 Cas*	9.62	Dauban V258
M285	02:17:54	+60:20:00	02:21:12.48	+60:20:11.8	V0725 Cas*	13.78	NSVS 1837975
M286	02:19:42	+59:24:00	02:23:22.56	+59:38:00.9	V0671 Cas	0.42	V0671 Cas
M287	02:27:11	+62:32:00	02:30:27.53	+62:31:45.6	V0647 Cas	14.23	V0647 Cas
M288	02:32:42	+59:10:00	02:36:24.47	+59:21:34.6	V0679 Cas*	1.48	–
M289	02:36:33	+63:14:00	02:56:00.73	+61:24:04.5	V0685 Cas*	169.00	NSVS 1890163
M290	02:24:19	+61:56:00	02:27:34.59	+61:55:57.1	V0674 Cas*	14.08	–
M291	02:56:41	+61:25:00	03:00:39.86	+61:39:50.6	V0699 Cas	2.96	–
M292	02:22:15	+59:24:00	02:25:42.73	+59:31:14.8	V0673 Cas*	6.45	–
M293	02:56:54	+59:31:00	03:00:45.13	+59:43:05.6	V0700 Cas	0.41	V0700 Cas
M294	02:32:46	+63:24:00	02:36:06.77	+63:25:11.1	V0680 Cas*	12.70	–
M295	02:33:38	+61:48:00	02:37:09.94	+61:55:22.9	V0726 Cas*	6.16	NSVS 1846691
M296	02:47:05	+61:27:00	02:50:57.00	+61:40:41.9	V0695 Cas	1.46	V0695 Cas
M297	02:35:28	+61:51:00	02:39:04.08	+61:59:16.4	V0684 Cas*	5.11	–
M298	02:35:09	+58:50:00	02:38:55.63	+59:02:08.8	V0682 Cas	0.84	V0682 Cas
M299	02:20:50	+59:11:00	02:24:29.93	+59:24:31.3	V0672 Cas	0.08	V0672 Cas
M300	02:50:59	+60:16:00	02:55:02.21	+60:31:09.5	V0697 Cas	3.19	V0697 Cas
M301	02:24:01	+60:37:00	02:27:24.01	+60:40:47.7	V0703 Cas*	9.99	NSV 824
M302	02:37:21	+62:22:00	02:40:51.84	+62:29:41.3	V0686 Cas*	6.01	–
M303	02:35:17	+59:31:00	02:39:00.88	+59:42:55.0	V0683 Cas	1.05	NSVS 1925038
M304	02:43:51	+62:30:00	02:47:31.09	+62:41:02.7	V0693 Cas*	2.79	–
M305	02:55:16	+61:02:00	02:59:20.49	+61:18:01.1	V0698 Cas*	4.14	–
M306	02:31:27	+62:59:00	02:34:40.22	+63:00:03.8	V0677 Cas*	13.15	V0943 Cas
M307	02:41:00	+61:52:00	02:44:38.87	+62:02:59.8	V0688 Cas	2.66	NSVS J0244383+620258
M308	02:42:07	+58:10:00	02:45:58.48	+58:22:14.9	V0691 Cas*	0.89	V0691 Cas
M309	02:41:50	+60:26:00	02:45:44.75	+60:39:28.7	V0689 Cas*	0.96	V0689 Cas
M310	02:29:22	+58:12:00	02:33:01.12	+58:25:37.3	V0508 Per	0.44	V0508 Per
M311	02:18:29	+60:57:00	02:21:40.87	+60:54:41.6	V0670 Cas*	16.45	DE Cas
M312	02:34:51	+58:37:00	02:38:31.49	+58:50:19.1	V0681 Cas*	0.50	V0681 Cas

the median difference for the whole set is 3 arcmin and for 14 stars it is larger than 6 arcmin, 2 of them being about 3 degrees off as discussed above.

After having found the actual positions of the Maffei's variables, I looked if they were present in the VSX catalog with another name, adopting a coordinates tolerance of 1 arcmin: these names are reported in column 8 of Table 1.

For 11 stars the name in VSX is the same as in SIMBAD: generally this happens because the old coordinates were near to the actual ones. For 11 cases a different variable name is listed in VSX, meaning that the variable was 'rediscovered' and not recognized as already known because the old coordinates were significantly different from the actual ones: for these stars the two names should be merged in a single identification in variable star catalogues like VSX or GCVS. For 13 stars no counterpart is present in VSX, indicating that they have not been 'rediscovered': for these stars the GCVS variable name can be retained.

To help the reader, and the keepers of variable stars catalogs, I have marked with an asterisk the GCVS star names which, in the last version of the GCVS (Samus et al. 2017),

Table 2: Table 2. NIR colors, periods and distances for Mira stars.

Maffei ID	name GCVS	Period days	$I-$mean mag	K mag	$I-K$ mag	$J-H$ mag	$H-K$ mag	Dist kpc
M278	V0690 Cas	311	13.85	7.47	6.39	1.12	0.59	8.6
M281	V0696 Cas	189.5	13.85	6.95	6.90	1.33	0.73	4.7
M282	V0692 Cas	420	14.05	4.86	9.19	1.37	0.80	3.3
M283	V0675 Cas	273	12.95	5.93	7.02	1.38	0.75	3.9
M284	V0694 Cas	359	14.5	6.90	7.60	1.30	0.83	7.4
M285	V0725 Cas	228	14.1	6.57	7.53	1.34	0.69	4.5
M287	V0647 Cas	552	8.9	3.60	5.30	1.06	0.55	2.2
M296	V0695 Cas	166.5	11.1	6.35	4.75	1.03	0.49	3.3

have coordinates different by more than 1 arcsec from my determination and therefore must be updated.

I remark that the alignment of VSX and CGVS is not always updated to the last version: this is a source of confusion.

In Table 2, I report for each Mira star the period in days and the apparent average I magnitude from Gasperoni et al. 1991, the K magnitude, the $I-K$, $J-H$ and $H-K$ colors form 2MASS, and a distance estimate. The distances were computed assuming the absolute K magnitude from the Period-Magnitude relation by Whitelock 2012 ($M_K = -3.69(\log P - 2.38) - 7.3$), and a common foreground K absorption of 0.3 mag. These distances are rather indicative because the K magnitude in the 2MASS catalog is taken at an unknown phase in the light curve so may be off up to half magnitude from the average value: a likely error is 0.2 dex in $\log 10(\text{Dist})$. Apparently these Mira stars belong to two broad groups, the main one (6 stars) clustered around 3.5 kpc, likely associated to the Perseus arm, while two stars are much farther, around 8 kpc, likely associated to the Outer arm.

There is no clear correlation between the estimated distance of each Mira star and its $J-H$ (or $H-K$) color, so it is unlikely that a different reddening is the main reason for the spread in distances found.

The $J-H$,$H-K$ color-color plot in Fig. 1 shows the positions of all the Maffei variables with respect to the regions defined by Bessell and Brett (1988). Three groups of stars can be identified in this plot: the first group comprises rather hot stars located on or near the Main Sequence and are generally irregular or eclipse variables; the second group has the Mira and Semiregular variables, with colors typical for this class of stars; the third group has the 4 reddest stars located in the typical area of the carbon stars with dusty envelopes, all classified in Gasperoni et al. (1991) as Semiregular or Irregular: one of them (M280) is already known as carbon star (CGCS 6035, Alksnis et al. 2001), the others (M 279, M286, M294) are most likely carbon stars too. Also M307 (V688 Cas, CGCS 0396) classified as SR, is a carbon stars, but its colors are not extreme so it is located among the Mira stars in this diagram.

4 Conclusions

Given that modern catalogs give coordinates more accurate than one arcsec, and that cross-identifications are now based on automatic coordinates matches rather than on visual comparison of finding charts, an update of the coordinates of these variables in the GCVS and VSX catalogs is necessary to allow recovering the variability history of these stars and to allow cross-identifications with present and future galactic plane surveys.

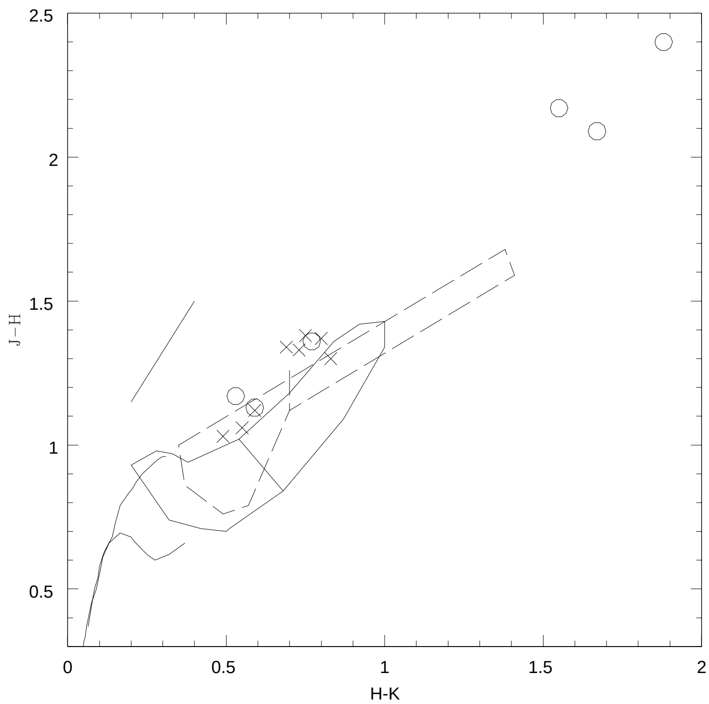

Figure 1. The $J-H, H-K$ diagram with the different areas according to Bessel and Brett (1988). Continuous lines are the Main Sequence and the Giant Branch. The star positions are indicatd by letters: M=Miras, S=Semiregulars, I=Irregulars, E=eclipsing stars. The reddening vector is indicated for E$(B-V)$=1 mag (A$_K \sim 0.3$ mag). All the stars in our sample fall nicely in this diagram, indicating a small absorption; the carbon stars with dusty envelopes are located in the upper right corner .

Thanks to the new more accurate coordinates all these Mira stars can be safely recognized in the forthcoming Gaia catalog of astrometric parallaxes and used to increase the database for studies of the Mira Period-Luminosity relation.

Acknowledgements: This work has made use of the SIMBAD, IRSA, VSX and STScI databases.

References:

Alksnis, A., Balklavs, A., Dzervitis, U., et al., 2001, *Baltic Astronomy*, **10**, 1
Bessell, M.S., and Brett, J.M., 1988, *PASP*, **100**, 1134 DOI
Cutri, R.M., Skrutskie, M.F., vanDyk, S., et al., 2003, *CDS on-line catalog*, II/246
Gasperoni, V., Maffei, P., Tosti, G., 1991, *IBVS*, **3573**
Samus, N.N., et al., 2003, *Astron. Lett.*, **29**, 468 DOI
Samus, N.N., et al., 2017, *CDS Vizier catalog*, B/gcvs
Whitelock, P.A., 2012, *Ap&SS*, **341**, 123 DOI

COMMISSIONS G1 AND G4 OF THE IAU
INFORMATION BULLETIN ON VARIABLE STARS
Volume 63 Number 6237 DOI: 10.22444/IBVS.6237

Konkoly Observatory
Budapest
13 February 2018

HU ISSN 0374 – 0676

114 MINIMA TIMINGS OF ULTRA-SHORT ORBITAL PERIOD ECLIPSING BINARIES

LOUKAIDOU, G.; GAZEAS, K.

Section of Astrophysics, Astronomy and Mechanics, Department of Physics, National & Kapodistrian University of Athens, Zografos GR- 15784, Athens, Greece; e-mail: kgaze@phys.uoa.gr

Abstract

We present 114 times of minima of 6 ultra-short orbital period eclipsing binaries.

Observatory and telescope:
T1: 0.4m, f/8 Cassegrain telescope, located at the University of Athens Observatory, at Zografos, Athens, Greece. **T2**: 1.2m, f/13 Cassegrain telescope of the National Observatory of Athens, located at the Kryoneri Astronomical Station, at Korinth, Greece. **T3**: 2.3m, f/8 Ritchey-Chrétien telescope "Aristarchos" of the National Observatory of Athens, located at Helmos Astronomical Station, Kalavryta, Greece

Detector:	**C1**: ST-10XME CCD camera, KAF-3200ME chip, $16' \times 11'$ and $25' \times 17'$ (using an f/6.3 focal reducer) field of view (FoV) with T1. **C2**: AP47p CCD camera, Marconi 47-10 chip, $2.5' \times 2.5'$ and $5' \times 5'$ (using an f/6.3 focal reducer) FoV with T2. **C3**: LN $1k \times 1k$ CCD camera, SITeAB chip, $4.8' \times 4.8'$ FoV with T3. All CCDs have a Peltier-type cooling system and are equipped with a set of UBVRI filters (Bessell specifications).

Method of data reduction:
Differential photometry

Method of minimum determination:
Kwee & van Woerden (1956).

Times of minima:					
Star name	Time of min. HJD 2400000+	Error	Type	Filter	Rem.
1SWASP J003033.05+574347.6	56934.6364	0.0001	II	BVRI	T3+C3
	57258.3632	0.0001	I	BVRI	T3+C3
	57258.4767	0.0001	II	BVRI	T3+C3
1SWASP J080150.03+471433.8	56778.3594	0.0008	II	BVRI	T2+C2
	56780.3148	0.0014	II	BVRI	T2+C2
	56804.3564	0.0007	I	B	T2+C2
	56805.3312	0.0006	II	BVRI	T2+C2
1SWASP J122224.73+334614.5	56773.5654	0.0013	II	BVRI	T1+C1
	56775.3749	0.0006	II	BVRI	T1+C1
	56776.4311	0.0015	II	B	T1+C1
	56777.3511	0.0009	I	BVRI	T1+C1
	56777.5286	0.0012	II	BVRI	T1+C1
	56778.4305	0.0008	I	BVRI	T1+C1
	56779.3222	0.0009	II	BVRI	T1+C1
	56779.4984	0.0011	I	BVRI	T1+C1
1SWASP J174310.98+432709.6	56778.5054	0.0009	I	VRI	T2+C2
	56779.5421	0.0019	I	BV	T2+C2
	56780.4404	0.0005	II	BVRI	T2+C2
	56780.5685	0.0011	I	BVRI	T2+C2
	56804.4391	0.0022	II	BVRI	T2+C2
	56804.5740	0.0003	I	BVRI	T2+C2
	56805.4780	0.0008	II	BVRI	T2+C2
	56807.4068	0.0016	I	BV	T2+C2
	56808.4433	0.0018	I	BV	T2+C2
1SWASP J220734.47+265528.6	56902.4454	0.0001	I	BVI	T3+C3
	57257.3707	0.0011	I	R	T1+C1
	57257.3829	0.0001	I	BVRI	T3+C3
	57257.4984	0.0001	II	BVRI	T3+C3
	57257.5087	0.0013	II	R	T1+C1
	57257.6145	0.0001	I	BVRI	T3+C3
	57257.6148	0.0004	I	R	T1+C1
	57262.3532	0.0003	II	R	T1+C1
	57262.4705	0.0004	I	R	T1+C1
	57262.5886	0.0005	II	R	T1+C1
	57263.3967	0.0004	I	R	T1+C1
	57263.5093	0.0008	II	R	T1+C1
	57264.3193	0.0004	I	R	T1+C1
	57264.4378	0.0005	II	R	T1+C1
	57264.5496	0.0025	I	R	T1+C1
	57265.3602	0.0004	II	I	T1+C1
	57265.4779	0.0012	I	I	T1+C1
	57265.5937	0.0005	II	I	T1+C1
	57266.4014	0.0003	I	I	T1+C1
	57266.5173	0.0010	II	I	T1+C1
	57267.3245	0.0003	I	I	T1+C1
	57267.4430	0.0003	II	I	T1+C1
	57267.5598	0.0012	I	I	T1+C1

Times of minima:					
Star name	Time of min. HJD 2400000+	Error	Type	Filter	Rem.
1SWASP J220734.47+265528.6	57268.3674	0.0010	II	V	T1+C1
	57268.4832	0.0005	I	V	T1+C1
	57268.6014	0.0009	II	V	T1+C1
	57269.2890	0.0004	II	V	T1+C1
	57269.4071	0.0008	I	V	T1+C1
	57269.5240	0.0005	II	V	T1+C1
	57270.3318	0.0005	I	V	T1+C1
	57270.4485	0.0009	II	V	T1+C1
	57270.5675	0.0010	I	V	T1+C1
	57271.3722	0.0008	II	V	T1+C1
	57271.4888	0.0007	I	V	T1+C1
	57271.6076	0.0014	II	V	T1+C1
	57272.2939	0.0002	II	B	T1+C1
	57272.4136	0.0017	I	B	T1+C1
	57277.3847	0.0009	II	B	T1+C1
	57277.5039	0.0009	I	B	T1+C1
	57278.3055	0.0012	II	B	T1+C1
	57278.4242	0.0004	I	B	T1+C1
	57278.5470	0.0008	II	B	T1+C1
	57279.3502	0.0004	I	B	T1+C1
	57279.4668	0.0007	II	B	T1+C1
	57280.3922	0.0008	II	B	T1+C1
1SWASP J234401.81-212229.1	56893.5798	0.0007	II	BVR	T1+C1
	56894.5447	0.0004	I	I	T1+C1
	56895.5050	0.0005	II	I	T1+C1
	56896.5748	0.0004	II	I	T1+C1
	56897.5355	0.0002	I	I	T1+C1
	56898.4989	0.0005	II	R	T1+C1
	56898.6030	0.0007	I	R	T1+C1
	56899.5661	0.0012	II	R	T1+C1
	56900.5279	0.0004	I	R	T1+C1
	56901.4876	0.0004	II	R	T1+C1
	56903.5188	0.0006	I	V	T1+C1
	56904.4806	0.0007	II	V	T1+C1
	56911.5260	0.0009	II	V	T1+C1
	56914.5242	0.0009	II	V	T1+C1
	56915.4828	0.0013	I	V	T1+C1
	56917.5131	0.0007	II	V	T1+C1
	56920.5057	0.0009	II	V	T1+C1
	56924.4607	0.0013	I	B	T1+C1
	56933.4377	0.0011	I	B	T1+C1
	56941.3475	0.0026	I	B	T1+C1
	56942.3029	0.0015	II	B	T1+C1
	56942.4087	0.0010	I	B	T1+C1
	56943.3718	0.0023	II	B	T1+C1
	56946.2566	0.0006	I	I	T1+C1
	56946.3630	0.0010	II	I	T1+C1
	56948.3900	0.0006	I	I	T1+C1

Times of minima:					
Star name	Time of min. HJD 2400000+	Error	Type	Filter	Rem.
1SWASP J234401.81-212229.1	56949.2476	0.0003	I	I	T1+C1
	56949.3542	0.0012	II	I	T1+C1
	56950.3150	0.0003	I	I	T1+C1
	56950.4209	0.0004	II	I	T1+C1
	56951.2760	0.0007	II	R	T1+C1
	56951.3827	0.0007	I	R	T1+C1
	56952.2412	0.0003	I	R	T1+C1
	56954.2668	0.0007	II	R	T1+C1
	56954.3736	0.0013	I	R	T1+C1
	56956.2967	0.0003	I	R	T1+C1
	56961.3202	0.0005	II	V	T1+C1
	56963.3483	0.0008	I	V	T1+C1
	56964.3103	0.0006	II	V	T1+C1
	56977.2434	0.0017	I	B	T1+C1
	56977.3465	0.0011	II	B	T1+C1
	56982.2590	0.0008	II	B	T1+C1
	56983.2247	0.0021	I	B	T1+C1
	56983.3320	0.0004	II	B	T1+C1
	56984.2990	0.0013	I	B	T1+C1

Explanation of the remarks in the table:

T1, T2, T3, C1, C2 and C3 refer to the instrumentation (telescope and CCD camera) used for each case.

Remarks:

The majority of the above observations were performed utilizing the robotic and remotely controlled telescope at the University of Athens: (http://observatory.phys.uoa.gr) (Gazeas 2016). The "Aristarchos" telescope is operated on Helmos Observatory by the Institute for Astronomy, Astrophysics, Space Applications and Remote Sensing of the National Observatory of Athens.

Acknowledgements:

Times of minima of contact binaries presented in this work are by-product of the the *Contact Binaries Towards Merging (CoBiToM) Project*, initiated and still undergoing at the National and Kapodistrian University of Athens since 2012 (PI: K. Gazeas).

References:

Gazeas, K., 2016, *RMxAC*, **48**, 22

Kwee, K., van Woerden, H., 1956, *Bulletin of the Astronomical Institutes of the Netherlands*, **12**, 327

COMMISSIONS G1 AND G4 OF THE IAU
INFORMATION BULLETIN ON VARIABLE STARS
Volume 63 Number 6238 DOI: 10.22444/IBVS.6238

Konkoly Observatory
Budapest
7 March 2018

HU ISSN 0374 – 0676

DISCOVERY OF SHORT-PERIOD OSCILLATIONS IN THE MASS-ACCRETING COMPONENT OF TT Vel

MKRTICHIAN, D. E.[1]; GUNSRIWIWAT, K.[1]; REICHART, D. E. [2]; HAISLIP, J. B. [2]; KOUPRIANOV, V. V. [2]; POSHYACHINDA, S.[1]

[1] National Astronomical Research Institute of Thailand (NARIT) 260 Moo 4, T. Donkaew, A. Maerim, Chiangmai, 50180 Thailand

[2] University of North Carolina 269 Phillips Hall, CB 3255 Chapel Hill, NC 27599

The "Thai Sky Survey for oEA Stars" (THASSOS) project is focused on searching for and studying new mass-accreting pulsating components of semi-detached Algol-type systems, the class of pulsators called oEA stars (Mkrtichian et al., 2002, 2004). Up to now, within the frame of the THASSOS project, four new oEA stars, VY Hya (Gunsriwiwat & Mkrtichian, 2016), GQ TrA (Mkrtichian et al., 2016), BD Vir (Mkrtichian et al., 2017a), and UW Vir (Mkrtichian et al., 2017b) were discovered.

TT Vel is a semi-detached Algol-type eclipsing binary system with a 2.1084 day orbital period. The system is photometrically-neglected and there is no accurate photometric light curve of the system. The A5 V primary component of the system can be pulsating as it is within in the instability strip. For these reasons it was included to the THASSOS oEA candidate list.

12 nights of photometric observations for TT Vel were acquired from March 28 to April 16, 2014 using the 0.6-meter Thai Southern Hemisphere Telescope (TST) PROMPT8 at Cerro Tololo Inter-American Observatory (CTIO). The telescope is equipped with an Apogee Alta E42 CCD camera. Three second exposure times through Johnson B filter were used. All stars in the field of view were reduced with the MaxIm DL 5 software using aperture photometry. HD 89623 (V = 8.09 mag, $B - V$ = 0.00 mag) was used as a comparison star. The phased differential light curve, folded according to HJD = 2456751.320 + 2.1083805×E, is shown in Figure 1.

During the search for pulsational variations in the primary component, we omitted all data at primary minima. The slow orbital variations in out-of-eclipse parts of light curves were removed using low-order polynomial fits. The residual light curves are shown in Figure 2.

Table 1: Pulsation frequencies and amplitudes.

Frequency (c/d)	Amplitude (mag)
f_1=16.455±0.002	0.0046± 0.0003
f_2=15.485±0.003	0.0023± 0.0003

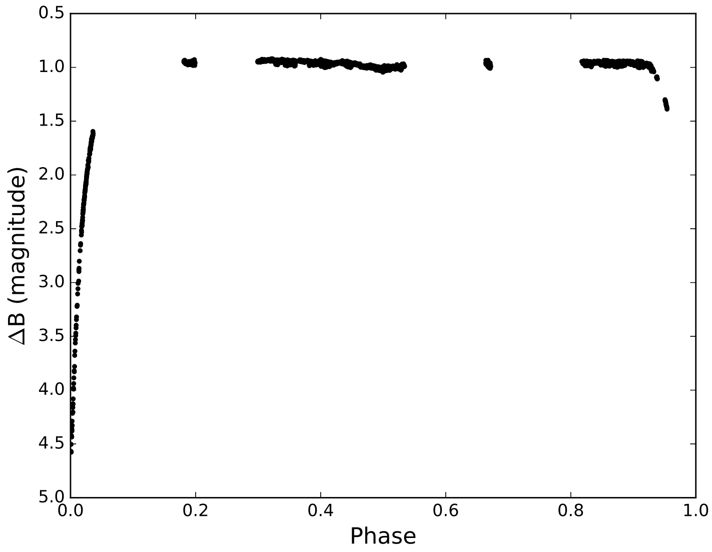

Figure 1. The phased orbital light curve of TT Vel (dots).

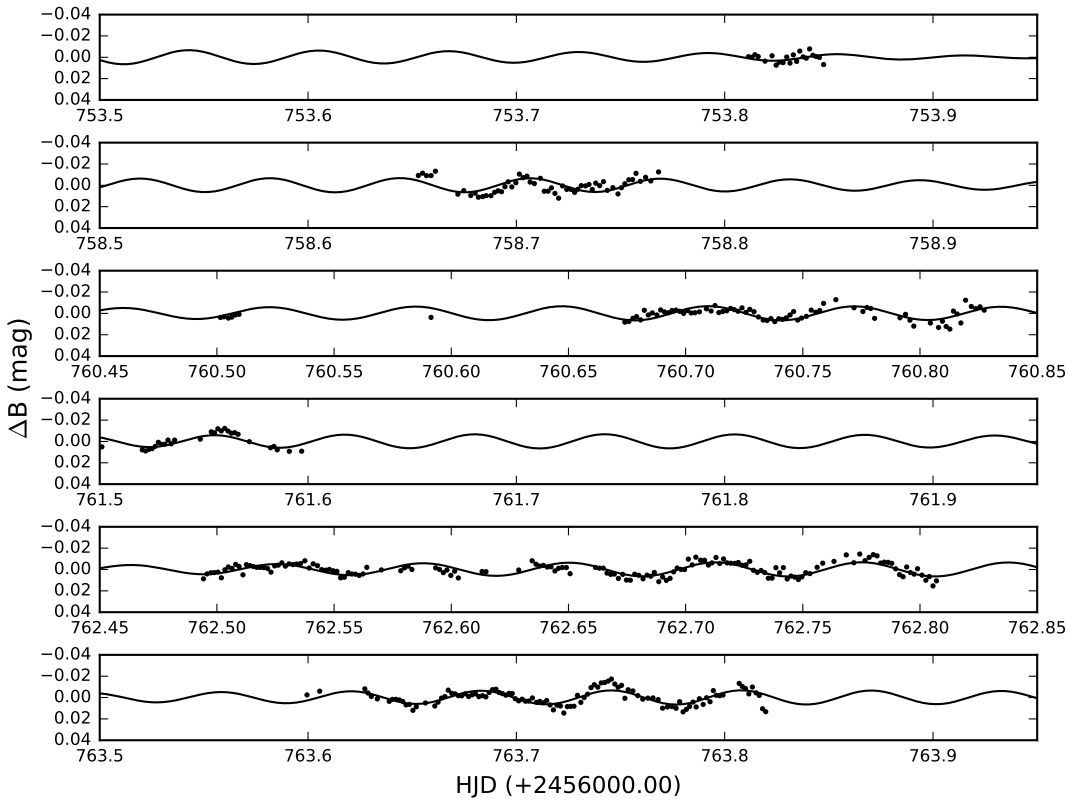

Figure 2. The nightly residual light variations of TT Vel (dots). The solid line is a two-frequency fit to the data.

The periodic signals in the residual data were analysed using the Period04 software (Lenz & Breger, 2005), designed for the Discrete Fourier Transform (DFT) analysis and the pre-whitening technique for consecutive detection of signals in the data. The frequency spectra of consecutive steps of the DFT analysis are shown in Figure 3, from top to bottom. As a result, we detected two periodic signals at frequencies 16.455 c/d and 15.485 c/d. The frequencies and amplitudes of signals are given in Table 1.

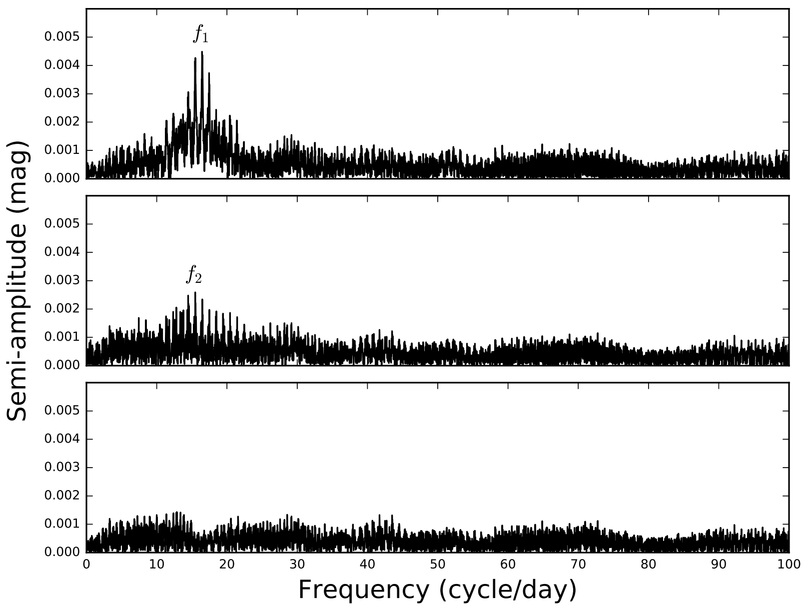

Figure 3. The DFT frequency spectra of the primary component. Top panel - the DFT of the residual light curve, highest peak is at 16.455 c/d. Middle panel - the DFT of the residuals after removal of 16.455 c/d, the highest peak is at 15.485 c/d. Bottom panel - the DFT after removal of 16.455 and 15.485 c/d.

Conclusion: We discovered short-period, δ Scuti-type multiperiodic pulsations in the primary component of the semi-detached, Algol-type binary system TT Vel. We conclude that TT Vel is a new member of the oEA group of pulsators.

Acknowledgements: We acknowledge this work as part of the research activity supported by the National Astronomical Research Institute of Thailand (NARIT), Ministry of Science and Technology of Thailand.

References:

Gunsriwiwat K., Mkrtichian D. E., 2016, *IBVS*, **6178**
Lenz P., Breger M., 2005, *Communications in Asteroseismology*, **146**, 53 DOI
Mkrtichian D. et al., 2002, *ASP Conf. Ser*, **259**, 96
Mkrtichian, D.E., Kusakin, A.V., Rodriguez, E., et al., 2004, *A&A*, **419**, 1015 DOI
Mkrtichian D. E., Gunsriwiwat K., Komonjinda S., 2016, *IBVS*, **6182**
Mkrtichian D. E., A-thano N., Awiphan S., 2017a, *IBVS*, **6210** DOI
Mkrtichian D. E., et al., 2017b, *IBVS*, **6221** DOI

COMMISSIONS G1 AND G4 OF THE IAU
INFORMATION BULLETIN ON VARIABLE STARS
Volume 63 Number 6239 DOI: 10.22444/IBVS.6239

Konkoly Observatory
Budapest
16 March 2018

HU ISSN 0374 – 0676

PRECESSION OF THE DISK IN PLEIONE
STUDY OF THE Hα LINE PROFILE

ERNST POLLMANN

Emil-Nolde Straße 12, 51375 Leverkusen, Germany
Observatory of the Vereinigung der Sternfreunde Köln, Germany

Abstract

Medium-resolution spectroscopy of the binary system Pleione (28 Tau), obtained over the time period October 2004 (JD 2453300) to March 2018 (JD 2458185) by the ARAS Spectroscopy Group, has been used to determine the central absorption depth (CA), V/R ratio, radial velocity (RV) and equivalent width of the Hα emission, in order to study the disk precession as a consequence of the periastron passages of the companion. We found an exact coincidence of the CA maxima with the minima of V/R and RV as a result of the disk precession. This has never before been observed during the maximum shell phase in the years around 1980, or during the initial shell phase around August/October 1974.

1 Introduction

Pleione (28 Tau, HD 23862) is a B8Vpe star (Hoffleit & Jaschek 1982) and a member of the Pleiades cluster. Hα emission was first detected in 28 Tau by E. C. Pickering in 1890. It is known to exhibit prominent long-term spectroscopic variations and cyclic changes in its spectrum from a Be phase to a Be-shell phase since the 19th century. Since 1938, an alternation of Be-shell and Be phases has been reported with a 35-36 years cycle. A comprehensive summary of observations of this star is given by Hirata (1995) and Hirata et al. (2000). The variations of the spectrum of 28 Tau from 1938 to 1975 have been described in detail by Gulliver (1977) who give a well documented bibliography of the star. Because of the periodic changes of the spectral characteristics of a Be phase to a Be-shell phase (and back), and because the disk is not in the equatorial plane "for some reason" (probably caused by the companion star in the periastron) but slanted to the equator and precesses around the central star, corresponding variations of the Hα line profile are observable (Hummel, 1998).

The observation and study of the Hα emission line and its profile of this binary system reveals at least five types of variability:

1. the equivalent width (EW)
2. the red and blue line wings
3. the intensity ratio of the V to R component of the Hα line profile (V/R)
4. the radial velocity (RV)

5. the central absorption depth (CA).

Figure 1 shows the variation of the Hα line profile at some typical epochs:

1974: the early shell phase

1981: the shell maximum phase

1999: the Be phase with maximum emission

2004: the Be phase.

One can readily see that the profiles changed from the edge-on type (shell-line profile) to the surface-on type (wine-bottle type), implying that the disk inclination angle changed significantly.

Katahira et al. (1996) analysed shell RV's from the two consecutive shell phases separated by some 34 years, and concluded that 28 Tau is a spectroscopic binary with an orbital period of 218 days. The forming of a new disk and its observation of the Hα EW and the line wings between November 2005 and May 2007 have been impressively documented by Katahira et al. (2006), Tanaka et al. (2007) and Iliev (2000). The ARAS spectroscopy community (http://www.astrosurf.com/aras/) has been investigating the change of the V/R ratio and the radial velocity of the Hα double peak profile since 2012 (Pollmann 2015). The RV results in that investigation were very well in agreement with that of Katahira et al. (1996) and Nemravova et al. (2010).

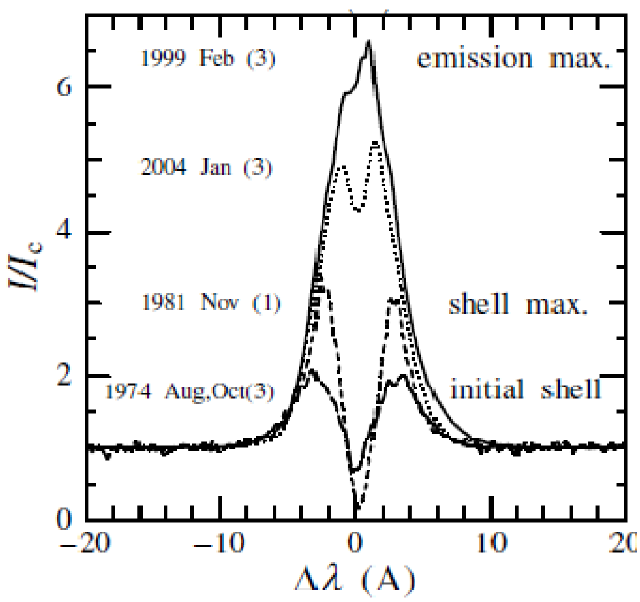

Figure 1. Variation of the Hα line profile at some typical epochs (with friendly permission of R. Hirata, 2007)

But the question regarding point 5 is, how can we understand the causes of the variability of the Hα CA?

The depth of the Hα CA is defined as the difference between the local continuum level (equal to unity) and the minimum value at the line minimum intensity (Fig. 2). While the Hα emission line samples the disk as a whole, the region probed by the shell lines, represented by the depth of the central absorption CC', is restricted to the line of sight.

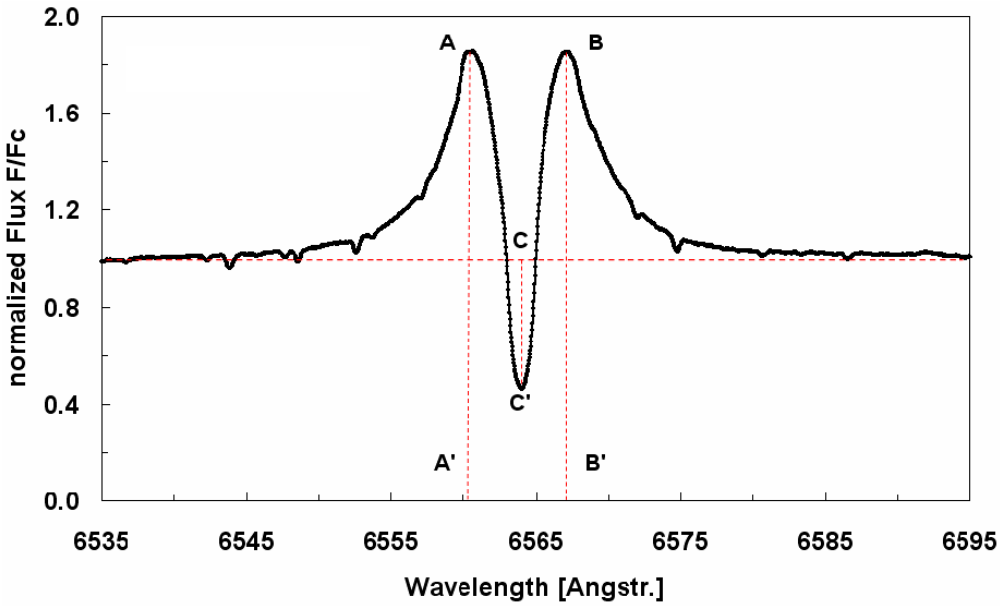

Figure 2. Measured quantities illustrated on an Hα line profile: (AA') and (BB') emission peaks, depth of the central absorption (CC'). The horizontal line marks the normalized continuum.

The diagnostics they provide should not be ignored, as their properties (absorption depth) reflect the structure and dynamics of the disk in the observer's direction.

In the literature it is assumed (Schaefer et al. 2010) that the changes in CA is caused by a different angle or density distribution of the disk plane with respect to the observer's line of sight, as a consequence of the disk precession around the primary star. Since 28 Tau is a binary, any tilt or change in the projected position angle of the disk may be modulated by the tidal force of the companion.

2 Observation and results

For the investigation presented here, 272 representative spectra of the time span October 2004 (JD 2453300) to March 2018 (JD 2458185; end of this investigation period) were taken from the BeSS database. The Hα spectra were obtained with 0.2 m to 0.4 m telescopes with a long-slit (in most cases) and echelle spectrographs with resolutions of R = 10000-20000. All spectra included the 6400-6700 region, with a S/N of 100 for the continuum near 6600 Å. The spectra have been reduced with standard professional procedures (instrumental response, normalisation, wavelength calibration) using the program VSpec and the spectral classification software package MK32. Figure 3 shows the CA time behaviour from October 2004 to March 2018.

The time span from October 2004 (approx. JD 2453300) until August 2011 (JD 2455800) was dominated by the behavior after the formation of a new disk and the corresponding decrease of the EW and the CA. Noteworthy in Fig. 3 is that the periodic CA variability seen from JD 2455900 until today (March 2018) was not observed in the period prior to at least October 2004.

Activity phases of the star, in which the disk precession as a consequence of the periastron passages of the companion, causes pronounced changes in the RV and the V/R ratio

(Pollmann, 2015), as well as the central absorption depth CA. These are called "maximum shell phase" (Hirata, 2007).

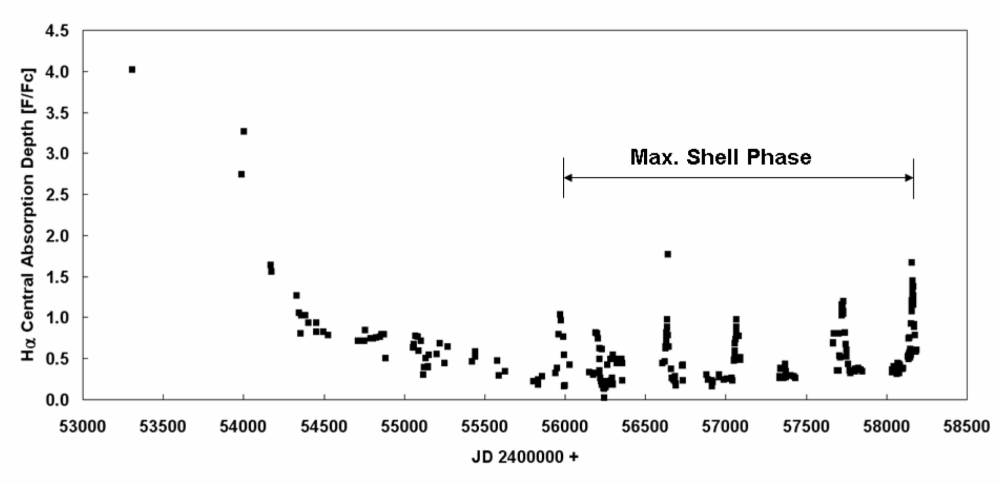

Figure 3. Central absorption depth of the Hα emission in 28 Tau. Amateur spectra of the BeSS Database since October 2004 (JD 2453300) after the Hα EW maximum to March 2018 (JD 2458185) (CA measurement accuracy ± 5%).

Figure 4 shows the CA variability during the maximum shell phase since approx. JD 2455900 to JD 2458185 (March 2018). Next we complete a period analysis and these results are shown in Figures 5 and 6.

The period analysis of the CA time series data in Fig. 4 was performed with the use of the program AVE (Barbera 1998), and produced the Scargle periodogram with the discriminant factor plotted in Fig. 5 and the phase diagram in Fig. 6. This period of 218.6 days is exactly in agreement with the period of the V/R ratio and the radial velocity found by Pollmann (2015). The exact coincidence of the CA maxima with the minima of V/R and RV (shown in Fig. 7) as a result of disk precession has never before been observed during the maximum shell phase in the years around 1980, or during the initial shell phase around August/October 1974. It is known that the precession of the disk depends on its size (radius) and its mass due to gravitational effects (Katz et al. 1982, Larwood et al. 1996, Lubow & Ogilvie 2001).

It is interesting to locate the time section of the periodic CA variability in Fig. 4 in the long-term monitoring of the Hα EW in Fig. 8. Here we adopt the convention that positive Hα EW is the flux above the continuum. It is noticeable that this time section coincides approximately with an EW range, in which the disk has largely minimal mass

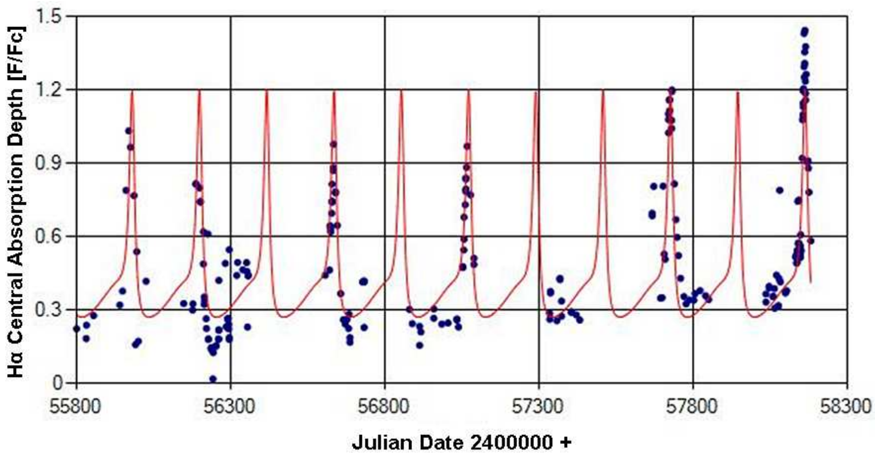

Figure 4. Central absorption depth of the Hα emission in 28 Tau. Max. shell phase since approx. JD 2455900 to JD 2458164 (February 2018)

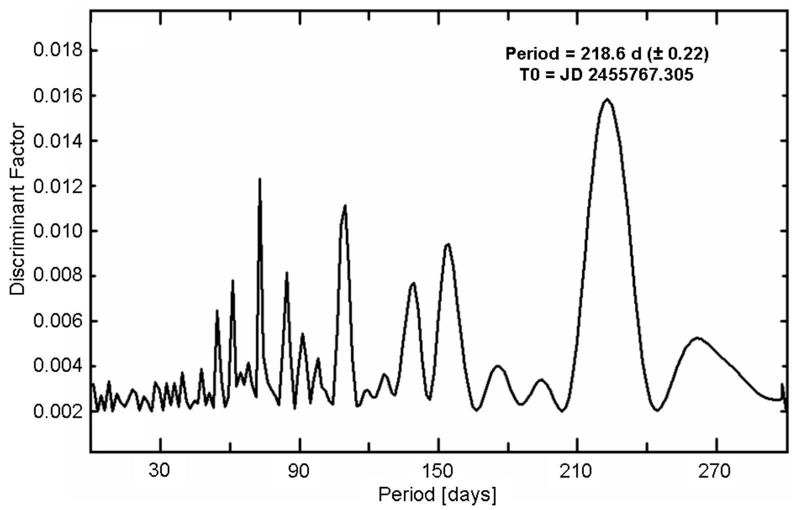

Figure 5. Periodogram of the CA time series data in Fig. 4

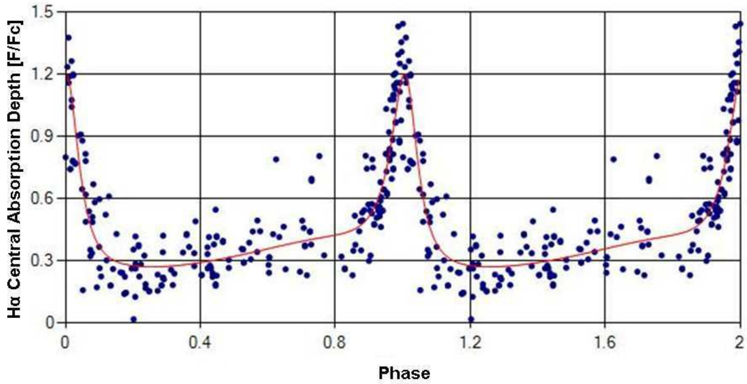

Figure 6. Phase diagram for the 218.6 day period shown in Fig. 5

and/or minimum density, volume or size. The relatively strong and rapid EW variation during this time may be due to the frequency of observations which were able to capture these changes.

Because of the well-known relationship between mass and precession in a spinning top, it might be interesting to see if the disk's expected increase in size and volume over the next few years will change the precession period of 218.6 days.

We plan to continue this interesting project as collaboration with professional experts. The more ARAS observers that are willing to take part in this project the larger the database we will have to find out a possible link between the CA period to the typically disk parameters (size, volume, mass, density). Also the monitoring of the periodic V/R variability, which reflects the libration of the disk rotational axis — as it has been found at the Be binary zeta Tau (Pollmann, 2017), will be part of further studies.

Acknowledgements: I am grateful for the ARAS spectroscopy group collaboration. I am also grateful to the referee Prof. Carol Evelyn Jones for her helpful suggestions as well Sara and Carl Sawicki (Alpine, Texas) for their improvements in language. The following observers of the ARAS group contributed with their spectra in the BeSS database:

Th. Garrel, C. Sawicki, J. Montier, J. S. Devaux, M. Pujol, M. Leonardi, V. Desnaux,P. Berardi, Ch. Buil, K. Graham, St. Ubaud, B. Mauclaire, H. Kalbermatten, F. Houpert,E. Pollmann, N. Montigiani, M. Mannucci, J. N. Terry, J. Guarro, J. Martin, Th. Lemoult, O. Garde, St. Charbonnel, T. Lester, A. Favaro, Dong Li, P. Fosanelli, A. de Bruin, B. Hanisch, A. Heidemann, E. Bertrand, E. Barbotin, J. Foster, J. Ribeiro, O. Thizy, E. Bryssinck, A. Halsey.

References:

Barbera, R., 1998, AVE code, version 2.51, `http://www.gea.cesca.es`
Gulliver, A. F., 1977, *ApJS*, **35**, 441 DOI

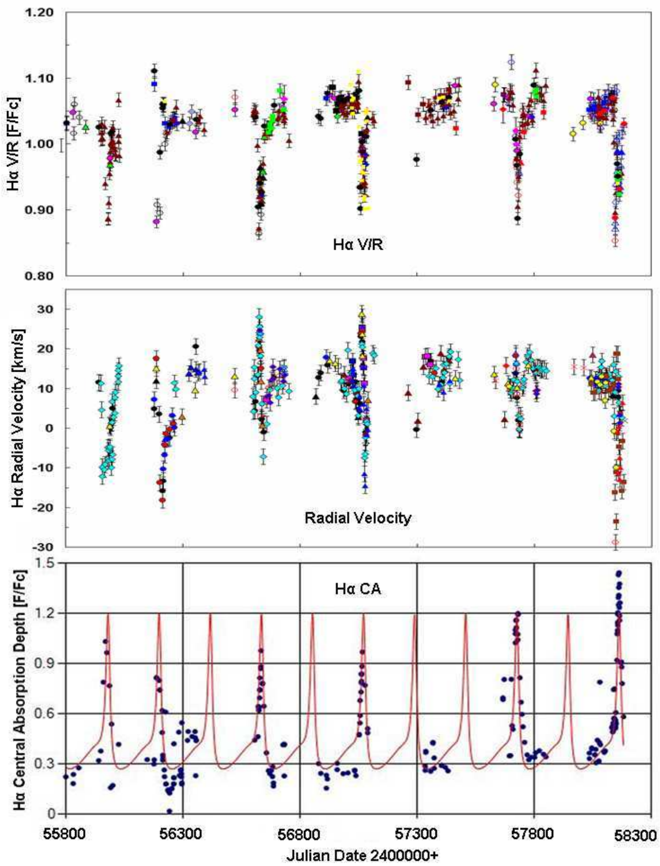

Figure 7. Illustration of the exact temporal coincidence of the Hα V/R ratio (top), the radial velocity, (middle) and the central absorption depth, (bottom) in the time period JD 2455900 to 2458185

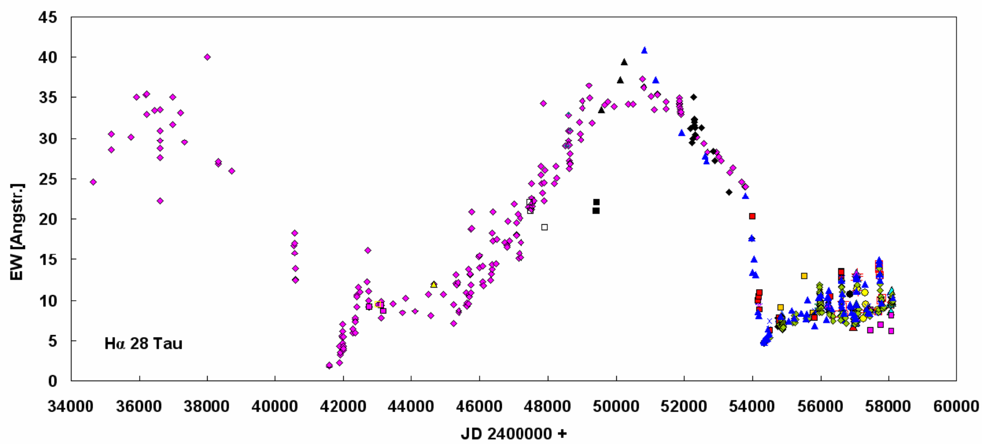

Figure 8. Long-term monitoring of the Hα EW in 28 Tau since October 1953 by the following observers (the measurements accuracy of the EW determination of the amateur observations since JD 2450840, January 1998 is ± 5%)

Hirata, R., 1995, *PASJ*, **47**, 195
Hirata, R., Shimada, M. R., Masuda, S., 2000, *ASP Conference Series*, **214**, 558
Hirata, R., 2007, *ASP Conference Series*, **361**, 267
Hoffleit, D., Jaschek, C., 1982, The Bright Star Catalogue, 4th ed. (New Haven: Yale University Observatory)
Hummel, W., 1998, *A&A*, **330**, 243
Iliev, L., 2000, *ASP Conference Series*, **214**, 566
Katahira, J., I., Hirata, R., Katoh, M., Ballereau, D., Chauville, J., 1996, *PASJ*, **48**, 317 DOI
Katahira, J., Narusawa, S., Okazaki, S., Inoue, K., Kawabata, Y., Sadakane, K., Hirata, R., 2006, *Be Star Newsletter*, **38**
Katz, J. I., Anderson, S. F., Grandi, S. A., Margon, B., 1982, *ApJ*, **260**, 780, DOI
Larwood, J. D., Nelson, R. P. , Papaloizou, J. C. B., Terquem, C. , 1996, *MNRAS*, **282**, 597 DOI
Lubow, S. H., Ogilvie, G. I., 2001, *ApJ*, **560**, 997 DOI
Pollmann, E., 2015, *IBVS*, **6199** DOI
Pollmann, E., 2017, *IBVS*, **6208** DOI
Nemravova, J., Harmanec, P., Kubat, J., Koubsky, P., Iliev, L., Yang, S., Ribeiro, J., Slechta, M., Kotovka, L., Wolf, M., Skoda, P., 2010, *A&A*, **516**, A80 DOI
Schaefer, G. et al., 2010, *AJ*, **140**, 1838, DOI
Tanaka, K., Sadakane, K., Narusawa, S., Y., 2007, *PASJ*, **59**, L35 DOI

COMMISSIONS G1 AND G4 OF THE IAU
INFORMATION BULLETIN ON VARIABLE STARS
Volume 63 Number 6240 DOI: 10.22444/IBVS.6240

Konkoly Observatory
Budapest
05 April 2018
HU ISSN 0374 – 0676

2MASS J06422218-0226285 - A NEW OUTBURST SOURCE†

BLEX, SUSANNE[1]; HACKSTEIN, MORITZ[1]; HAAS, MARTIN[1]; KIMESWENGER, STEFAN[2,3]; CHINI, ROLF[1,2]; HODAPP, KLAUS[4]

[1] Astronomisches Institut, Ruhr-Universität Bochum, Germany; e-mail: sublex@astro.rub.de
[2] Instituto de Astronomía, Universidad Católica del Norte, Chile
[3] Institute for Astro- and Particle Physics, University of Innsbruck, Austria
[4] Institute for Astronomy, University of Hawaii, USA

Abstract

We discovered the outburst of 2MASS J06422218–0226285. Between end 2012 and early 2014, this object brightened by 3 mag in r and i, and by 3.7 mag in J. Since then, it has stayed at high brightness of about 16 mag in r and 15 mag in i. Possible explanations for this kind of light curve might be a Catalysmic Variable, a Symbiotic Binary or a FUor or EXor type Young Stellar Object. The color properties favor an outbursting Young Stellar Object.

2MASS J06422218–0226285 brightened between the end of 2012 and early 2014 by about 3 mag in r and i, and by 3.7 mag in J, and has stayed at high brightness since then.

This object has been photometrically surveyed by several missions at optical and infrared wavelengths. Among these surveys are GSC II in 1991 (Lasker et al. 2008), 2MASS in 1998 (Skrutskie et al. 2006), DENIS in 2000 (Epchtein et al. 1994), IPHAS in 2006 (Barentsen et al. 2014), and WISE in 2010 (Wright et al. 2010). Viironen et al. (2009) described J06422218–0226285 as a planetary nebula (PN) and also have found that Hα probably has been in emission before the outburst. There is no prominent star forming region close to the object.

While analyzing exceedingly red and variable objects among the Galactic Disc Survey (GDS, Haas et al. 2012, Hackstein et al. 2015), Blex (2017) discovered the brightening of 2MASS J06422218–0226285 (or GDS J064221-022628). The discovery of the outburst motivated further measurements at the Universitätssternwarte Bochum (USB) near Cerro Armazones, Chile. Between November 23$^{\rm rd}$ and December 12$^{\rm th}$ in 2017, the latest optical data in the B, V, r, and i filters have been collected. During three nights in February to March 2018, we were able to obtain narrow-band spectro-photometry of HeI, H_2 (1-0) S1, Brγ, CO, and K_c, as wll as JHK_s broadband photometry. Our search for Hα emission after the outburst using narrow bands at 6450, 6563 and 6721 Å has failed due to a too low object brightness and poor S/N at these wavelengths.

Figure 1 shows the r- and i-band light curves from the GDS together with previous photometry of GSC II, DENIS, and IPHAS (Barentsen et al. 2014) data points. The light

†Based on data collected under the ESO/RUB — USB agreement at the Paranal Observatory

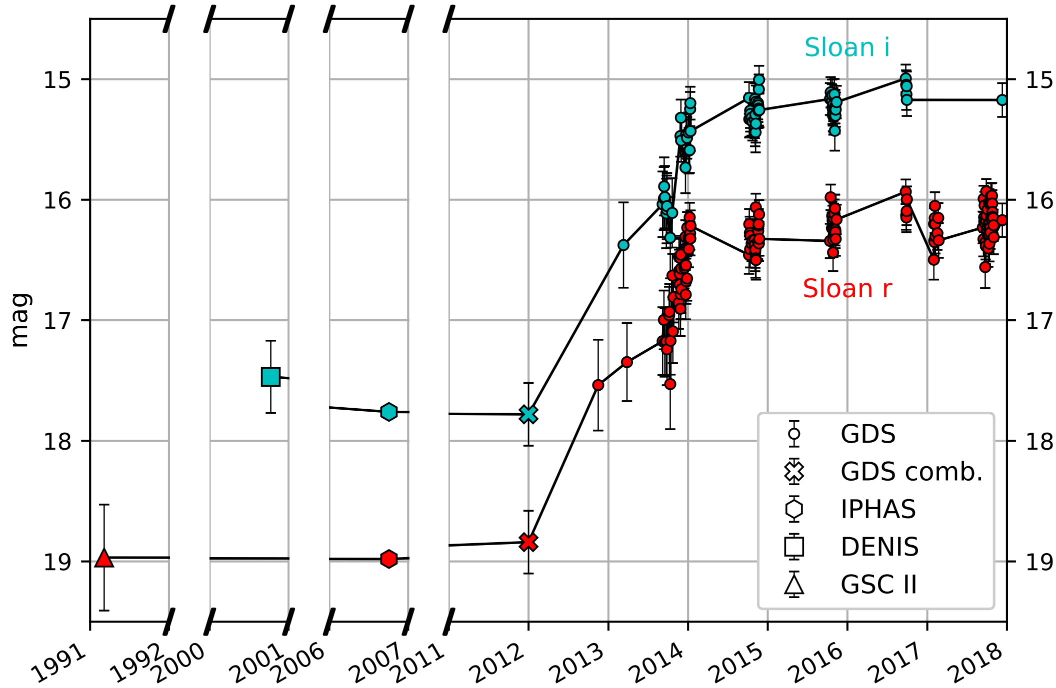

Figure 1. GDS light curve in r and i with additional IPHAS, DENIS, and GSC II data points; the IPHAS error is smaller than the symbol size.

curve values are listed in Tables 2 and 3 (at the end of the paper). The latest measurement in December 2017 yielded an r magnitude of 16.170 ± 0.139 and an i magnitude of 15.173 ± 0.140. A check of the single segments of the GDS light curve showed no short-term periodicity. The GSC II, IPHAS, and GDS measurements suggest a constant brightness of about $r = 19$ mag between 1991 and 2012. A constant faint state lasting back from 1991 to 1955 is further supported by the sequence of past DSS1, DSS2, and present GDS image cutouts (Fig. 2).

The optical to mid-infrared spectral energy distribution (SED) is depicted in Fig. 3, separated for both faint and bright states. Already before 2012, J06422218–0226285 has shown an infrared excess in the 2MASS and WISE color-color diagrams, consistent with a classical T Tauri star surrounded by circumstellar dust. After the outburst, the star has become much redder, suggesting dispersed dust. Although Hα does not appear in emission after the outburst, a strong P Cygni-type absorption could balance out potential emission.

Our near-infrared JHK_s and narrow-band spectro-photometry reveals a potential Brackett–gamma (Brγ) emission (Fig. 4, Tab. 1). The resulting Brγ flux would be about $5.1 \cdot 10^{-17}$ W/m^2, comparable to the range found by Carr et al. (1990) for Young Stellar Objects (YSOs). The large Brγ equivalent width of about 19 Å would place J06422218–0226285 among strongly accreting YSOs. In this scenario, the increase in brightness can be explained as a FUor- or EXor-type outburst.

Furthermore, matching with 2MASS allowed for searching the environment of J06422218–0226285 for K-excess objects in the JHK_s color-color diagram, which lie at least 2σ right-hand of the slope $(J - H) = 1.7\,(H - K) - 0.12$. We considered only

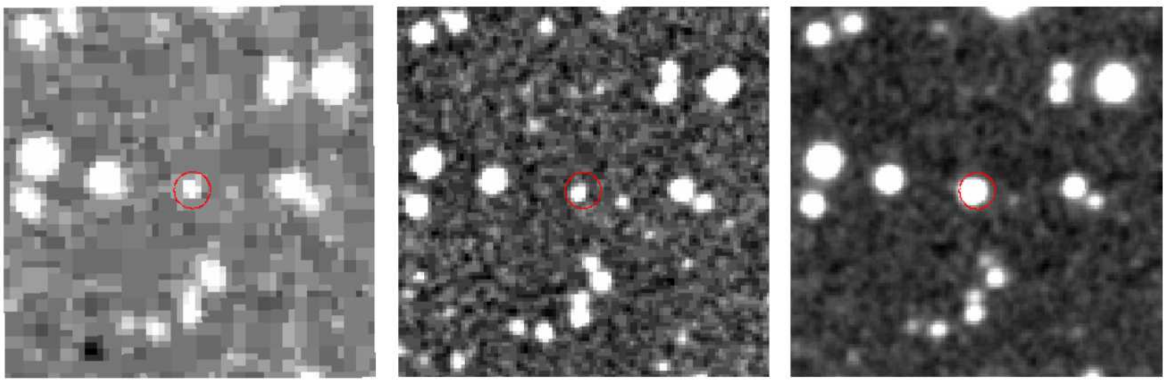

(a) *DSS1 1955* **(b)** *DSS2 1991* **(c)** *GDS 2012-2017*

Figure 2. Comparison of the cutouts from the red filter of the DSS and the Sloan r filter of the GDS; angular size: approximately $100{\times}100''$.

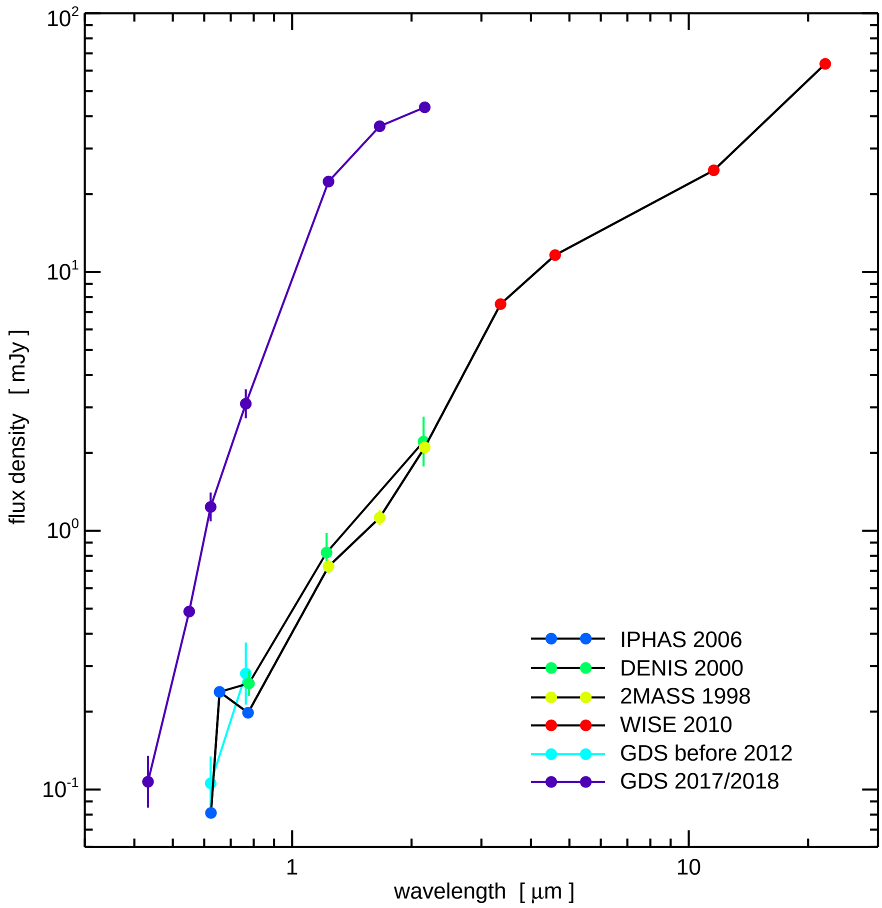

Figure 3. Spectral energy distribution; depicted GDS filters: B, V, r, i, J, H, K_s; error bars (if not seen) are smaller than the symbol size.

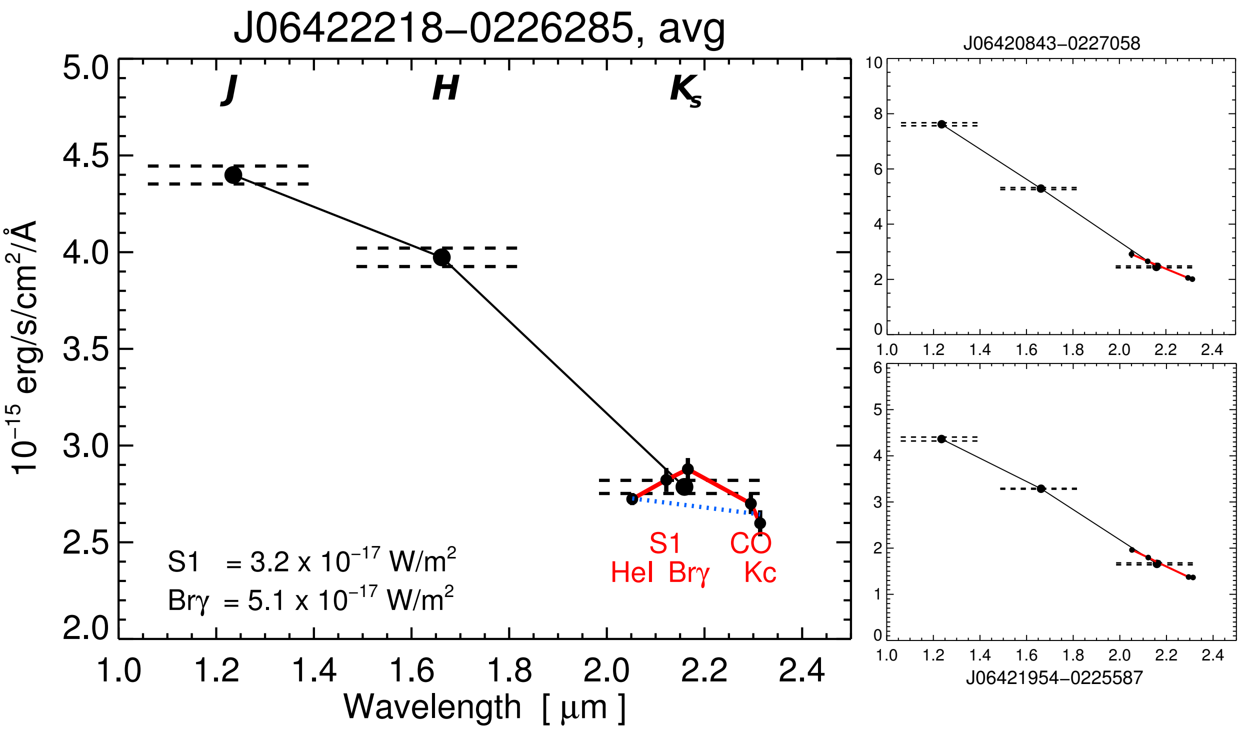

Figure 4. Average near infrared photometry of 2MASS J06422218–0226285 (left large panel) and two nearby stars of similar brightness (right, two small panels). The photometry was obtained in three nights in Feb–Mar 2018 with the IRIS telescope at USB in the broadband filters JHK_s and five narrow bands (FWHM = 275 Å) centered at 2.05, 2.121, 2.167, 2.29 and 2.314 μm (HeI, H_2 (1-0) S1, Brγ, CO, K_c, black filled circles connected with a red line). The horizontal dashed lines indicate the bandwidth and error range of the broadband J, H, K_s. For 2MASS J06422218-0226285 the error range in all bands is ∼2%, thus significantly larger than for other nearby stars of similar brightness (< 0.5%); this indicates a remaining small variability of 2MASS J06422218–0226285. For 2MASS J06422218–0226285 the flux in the Brγ filter lies above both the K_s broadband flux and the continuum as interpolated between HeI and CO and K_c (blue dotted line). While HeI and CO absorption cannot be ruled out yet, for an outbursting object it appears more likely that Br$_\gamma$ and hydrogen S1 are in emission.

Table 1: Near-infrared photometry obtained in three nights in Feb–Mar. 2018 with IRIS.

Filter	λ	f_ν	f_ν error	flux	flux error
	μm	mJy	mJy	10^{-15} erg/s/cm^2/Å	10^{-15} erg/s/cm^2/Å
J	1.235	22.3641	0.235612	4.3988384	0.0463431
H	1.662	36.5833	0.438685	3.9732172	0.0476444
K_s	2.159	43.2917	0.527097	2.7862547	0.0339240
HeI	2.052	38.1709	0.437991	2.7232539	0.0312480
H_2 (1-0) S1	2.121	42.2975	0.928504	2.8223840	0.0619564
Brγ	2.166	44.9465	0.899277	2.8779934	0.0575820
CO	2.295	47.3339	0.944012	2.6997119	0.0538422
K_c	2.314	46.3109	1.20148	2.5981670	0.0674066

precisely measured stars with 2MASS quality flag A or B in all three filters. We searched a 1200″ box around the target to maintain a balance between the consideration of only the close environment of the star and sufficient statistics. This yields a rate of 1.49 % (16 out of 1077) K_s excess stars near J06422218–0226285. The resulting rate needs to be compared with the expected frequency of K_s excess stars near the galactic plane. For this purpose, we used the center coordinates of 15 randomly selected GDS fields with 6h < RA < 11h and investigated the 2MASS stars in a 1200″ box around these coordinates. In total, 26588 2MASS stars (with flag A, B) are covered by these boxes with 151 of them (0.57 %) being K-excess stars. To estimate the field-to-field fluctuation, the fraction of K-excess stars is calculated individually for each field and then averaged, resulting in a mean of 0.62 % and standard deviation of 0.31 %. Thus, the rate of K_s excess stars near J06422218–0226285 is almost 3σ above that of the mean. Note that only in one of the 15 boxes the rate of K-excess stars is as high as in the case of J06422218–0226285. Hence, one might speculate that J06422218–0226285 is located in a region of thin star formation or a star forming region at the end of its lifespan. Additionally, IRAS-IRIS and AKARI images indicate a nebulous surrounding. These findings, Hα emission before and Brγ emission after the outburst, and the present and past infrared excess support the claim of a YSO; albeit it is not close to a known star-forming region and there are no emission or reflection nebulae nor a high number of Hα objects near J06422218–0226285 and the amplitude is rather low for a FUor. Accordingly, these indications require further confirmation by spectroscopy.

Alternatively to a YSO, J06422218–0226285 could be a cataclysmic variable (CV). As already noted in Warner (1995a), some subclasses of CVs show stable high states after an outburst for several years up to decades (see, e.g., MV Lyr in Warner, 1995b, and RX And and TZ Per in Simonsen et al., 2014). It is believed that this is caused by a mass transfer feedback heating the secondary star. In this case, the Hα and Brγ emission can be explained by the surrounding accretion disk. Also, the irregular $r - i$ color variations of up to 0.8 mag fit this scenario.

Several features of J06422218–0226285 in the light curve and the SED are reminiscent of a symbiotic binary. Among them are the signs of circumstellar gas and dust and different variability effects on the time scales of days to months. These could explain the shape of the SED and the minor variations of the light curve after the outburst. Since the novae of symbiotic binaries rise up to 3 mag in the optical in a couple of years at most and last for up to a century (see Skopal, 2015 and Munari, 2012), the characteristics of the outburst of J06422218–0226285 fit this scenario as well.

Viironen et al. (2009) identified J06422218-0226285 as a planetary nebula candidate due to its position in IPHAS and 2MASS color-color diagrams. However, in a DENIS IJK_s color-color diagram (Fig. 5), the object lies outside of the area of PNs; instead it exhibits symbiotic Mira colors (see Schmeja & Kimeswenger, 2001 and Schmeja & Kimeswenger, 2003). Furthermore, the light curve does not fit a pulsating star, and the increase in brightness certainly is too vast and rapid for Post-AGB evolution. After the outburst, J06422218–0226285 still resides outside the area of PNs. Here, the I magnitude has been estimated from a black-body fit to the SED (Fig. 3).

To summarize, based on the Bochum Galactic Disk Survey, we detected a remarkable 3–4 mag outburst of J06422218–0226285 in 2013. The nature of the star is still puzzling. The multi-band photometry is consistent with a FUor- or EXor-type YSO, albeit the star is located in a thin star forming region. Also, the alternatives of a cataclysmic variable or a symbiotic binary or a PN/post-AGB are possible. In any case, the system shows

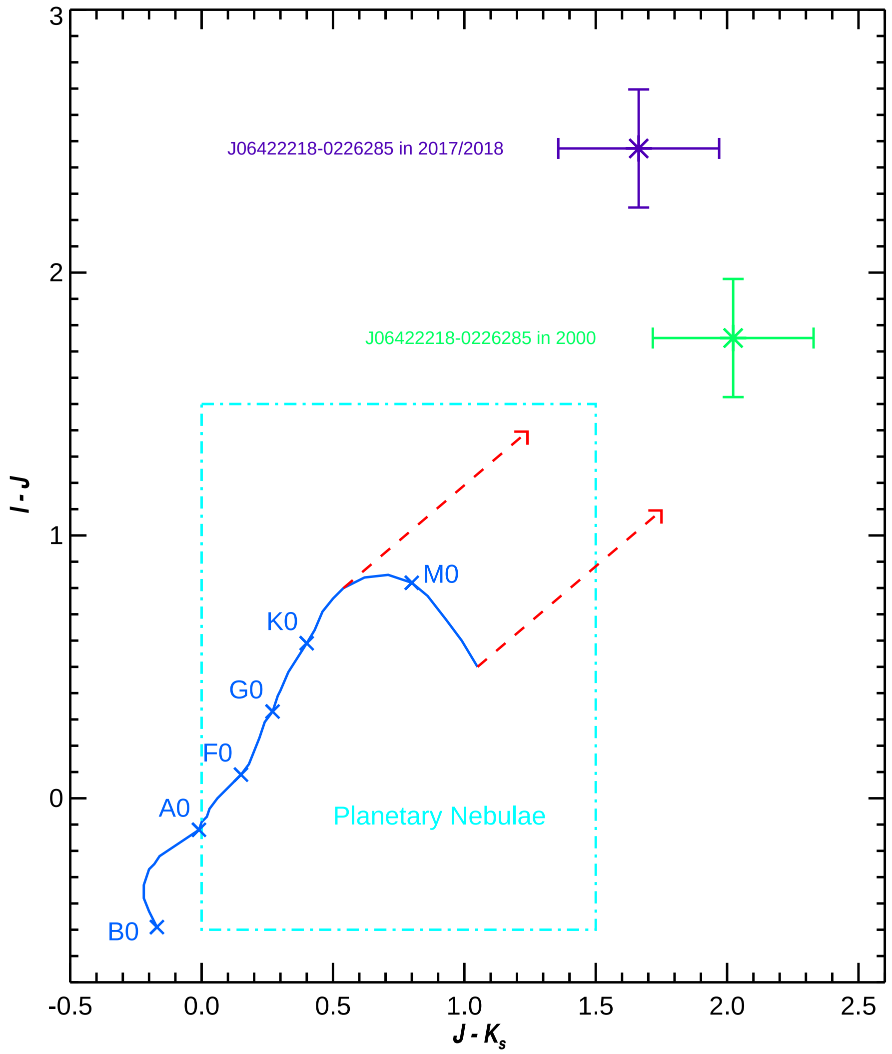

Figure 5. IJK_s color-color diagram: blue curve – main sequence stars; blue crosses – position of B0, A0, F0, G0, K0, M0 stars; red dashed-dotted lines – reddening paths for $A_V = 3.5$; cyan area – expected colors for planetary nebulae; green and purple cross – 2MASS J06422218–0226285.

exceptionally rare features, worth to clarify with future observations (e. g. spectroscopic or X-ray or radio).

Acknowledgements: We thank the referee for the instructive comments.

References:

Barentsen, G., Farnhill, H. J., Drew, J. E., et al., 2014, *MNRAS*, **444**, 3230 DOI
Blex, S., 2017, Variable Infrared Excess Objects from the Bochum Galactic Disk Survey, Master Thesis, Ruhr-Universität Bochum
Carr, J. S. & Tokunaga, A. T., 1992, *ApJL*, **393**, L67 DOI
Epchtein, N., de Batz, B., Copet, E., et al., 1994, *ApSS*, **217**, 3 DOI
Haas, M., Hackstein, M., Ramolla, M., Drass, H., Watermann, R., Lemke, R., & Chini, R., 2012, *AN*, **333**, 706 DOI
Hackstein, M., Fein, C., Haas, M., et al., 2015, *AN*, **336**, 590 DOI
Lasker, B. M., Lattanzi, M. G., McLean, B. J., et al., 2008, *AJ*, **136**, 735 DOI
Munari, U., 2012, *JAAVSO*, **40**, 572
Schmeja, S. & Kimeswenger, S., 2001, *A&A*, **377**, L18 DOI
Schmeja, S. & Kimeswenger, S., 2003, *ASPC Series*, **303**, 446
Simonsen, M., Boyd, D., Goff, W., et al., 2014, *JAAVSO*, **42**, 177
Skopal, A., 2015, *ASPC Series*, **496**, 226
Skrutskie, M. F., Cutri, R. M., Stiening, R., et al., 2006, *AJ*, **131**, 1163 DOI
Viironen, K., Mampaso, A., Corradi, R. L. M., et al., 2009, *A&A*, **502**, 113 DOI
Warner, B., 1995a, Cataclysmic Variable Stars, *Cambridge Astrophysics Series* 28, Cambridge University Press
Warner, B., 1995b, *ApSS*, **230**, 83 DOI
Wright, E. L., Eisenhardt, P. R. M., Mainzer, A. K., et al., 2010, *AJ*, **140**, 1868 DOI

Table 2: GDS r magnitudes; the first line gives the magnitude of co-added images between 2010 and 2012.

MJD	mag	err	MJD	mag	err	MJD	mag	err
55197-55927	18.840	0.260	56949.270	16.364	0.145	57791.030	16.306	0.140
56246.235	17.538	0.377	56953.250	16.338	0.142	57800.043	16.278	0.137
56377.999	17.347	0.324	56963.259	16.333	0.141	57804.022	16.151	0.124
56541.379	17.173	0.281	56964.242	16.375	0.146	57806.020	16.337	0.144
56547.376	16.997	0.244	56965.229	16.439	0.154	58008.386	16.230	0.132
56551.386	17.184	0.284	56966.229	16.414	0.151	58011.375	16.327	0.143
56558.372	17.176	0.282	56967.218	16.487	0.160	58012.381	15.992	0.108
56561.326	17.241	0.297	56968.217	16.063	0.113	58014.379	16.146	0.123
56571.313	16.958	0.236	56969.216	16.501	0.162	58015.372	16.175	0.126
56572.368	16.929	0.231	56978.220	16.349	0.143	58016.374	16.047	0.113
56576.293	17.529	0.374	56979.217	16.260	0.133	58018.364	16.195	0.128
56577.290	17.170	0.281	56980.215	16.214	0.128	58019.363	16.559	0.173
56586.329	16.629	0.180	56981.211	16.203	0.127	58021.356	16.350	0.146
56588.334	17.092	0.263	56982.209	16.363	0.145	58022.353	16.385	0.150
56591.360	16.809	0.209	56983.205	16.121	0.118	58023.350	16.176	0.126
56615.275	16.854	0.217	56984.202	16.324	0.140	58024.349	15.931	0.103
56616.287	16.473	0.159	57308.297	16.342	0.142	58025.345	16.132	0.122
56617.226	16.589	0.174	57311.297	15.980	0.105	58027.347	16.244	0.133
56619.207	16.703	0.192	57317.256	16.236	0.130	58028.337	16.270	0.136
56620.208	16.616	0.178	57318.256	16.134	0.120	58030.336	16.081	0.117
56622.199	16.484	0.160	57320.256	16.173	0.124	58032.327	16.298	0.140
56623.176	16.904	0.226	57321.256	16.232	0.130	58033.324	16.404	0.152
56624.176	16.785	0.205	57322.256	16.438	0.154	58034.322	16.297	0.140
56625.176	16.455	0.156	57323.256	16.334	0.141	58035.309	16.196	0.128
56626.177	16.571	0.172	57324.312	16.246	0.131	58036.316	16.283	0.138
56627.179	16.743	0.198	57325.299	16.154	0.122	58037.312	16.023	0.111
56641.126	16.565	0.171	57328.256	16.116	0.118	58038.314	16.365	0.148
56642.129	16.546	0.168	57330.266	16.071	0.114	58039.338	16.252	0.134
56646.116	16.308	0.138	57331.224	16.072	0.114	58040.298	16.188	0.127
56647.117	16.787	0.205	57332.224	16.248	0.132	58041.295	16.037	0.112
56648.119	16.544	0.168	57333.224	16.268	0.134	58042.292	16.231	0.132
56649.105	16.676	0.187	57334.224	16.325	0.140	58043.289	16.271	0.137
56653.106	16.653	0.184	57338.224	16.164	0.123	58044.331	16.037	0.112
56654.107	16.232	0.130	57655.340	15.934	0.101	58045.352	15.971	0.107
56660.305	16.313	0.139	57657.335	16.130	0.119	58046.341	16.155	0.124
56661.304	16.410	0.150	57658.336	16.147	0.121	58047.363	16.135	0.122
56665.267	16.146	0.121	57659.367	16.094	0.116	58049.310	16.166	0.125
56667.275	16.279	0.135	57660.322	15.997	0.107	58050.356	15.967	0.106
56668.266	16.322	0.140	57784.034	16.498	0.165	58051.342	16.032	0.112
56669.263	16.217	0.128	57785.034	16.201	0.129	58052.364	16.102	0.119
56937.286	16.458	0.157	57786.033	16.340	0.145	58053.359	16.141	0.123
56938.348	16.203	0.127	57787.033	16.351	0.146	58056.293	16.151	0.124
56941.291	16.275	0.135	57788.032	16.152	0.124	58057.350	16.212	0.130
56942.291	16.411	0.151	57789.032	16.051	0.114	58058.360	16.311	0.141
56943.285	16.298	0.137	57790.032	16.202	0.129	58097.696	16.170	0.139

Table 3: GDS i magnitudes; the first line gives the magnitude of co-added images between 2010 and 2012.

MJD	mag	err	MJD	mag	err
55197-55927	17.780	0.300	56967.218	15.441	0.167
56362.121	16.376	0.354	56968.217	15.369	0.157
56541.379	16.037	0.271	56969.216	15.187	0.135
56547.376	15.989	0.261	56978.220	15.198	0.136
56548.378	15.890	0.241	56979.217	15.217	0.138
56551.386	15.979	0.259	56980.215	15.262	0.143
56558.372	16.114	0.288	56981.211	15.244	0.141
56560.341	16.081	0.281	56982.209	15.085	0.124
56561.326	16.053	0.275	56983.205	15.005	0.116
56576.293	16.315	0.337	56984.202	15.256	0.143
56585.271	16.109	0.287	57308.297	15.164	0.132
56623.176	15.472	0.171	57311.297	15.109	0.126
56625.176	15.320	0.151	57317.256	15.175	0.133
56626.177	15.509	0.176	57318.256	15.132	0.129
56646.116	15.733	0.212	57320.256	15.232	0.140
56649.105	15.458	0.169	57321.256	15.244	0.141
56653.106	15.487	0.173	57322.256	15.285	0.146
56660.305	15.443	0.167	57323.256	15.212	0.138
56661.304	15.593	0.189	57324.312	15.311	0.150
56665.267	15.589	0.188	57325.299	15.296	0.148
56667.275	15.248	0.142	57328.256	15.126	0.128
56668.266	15.199	0.136	57330.266	15.428	0.165
56669.263	15.431	0.165	57331.224	15.229	0.140
56937.286	15.155	0.131	57332.224	15.228	0.140
56938.348	15.332	0.152	57333.224	15.303	0.149
56941.291	15.326	0.151	57334.224	15.253	0.142
56942.291	15.261	0.143	57338.224	15.190	0.135
56943.285	15.288	0.147	57655.340	14.994	0.115
56949.270	15.318	0.150	57657.335	15.046	0.120
56953.250	15.354	0.155	57658.336	15.127	0.128
56963.259	15.336	0.153	57659.367	15.058	0.121
56964.242	15.165	0.132	57660.322	15.172	0.133
56965.229	15.396	0.161	58097.696	15.173	0.140
56966.229	15.294	0.147			

COMMISSIONS G1 AND G4 OF THE IAU
INFORMATION BULLETIN ON VARIABLE STARS
Volume 63 Number 6241 DOI: 10.22444/IBVS.6241

Konkoly Observatory
Budapest
17 May 2018

HU ISSN 0374 – 0676

MULTICOLOR LIGHT CURVES AND PERIOD ANALYSIS OF IL Cnc

ALTON, K.B.

70 Summit Ave, Cedar Knolls, NJ, USA, email: kbalton@optonline.net

Abstract

The spectral type and orbital period were estimated from multicolor (B, V and I_c) ccd-based photometric observations acquired in 2014 and 2018. Period analysis from eclipse timing differences indicate that no significant change in the orbital period 0.267656 d has occurred since 2003.

IL Cnc (V=$12^{m}_{.}6$; $08^{h}55^{m}51^{s}_{.}507$ $+20°03'38''_{.}56$ (epoch=J2000)) was first reported to be a W UMa-type variable star by Rinner et al. (2003) based on unfiltered ccd data. Photometric data were also collected from this system during the ROTSE-I survey (NSVS; Woźniak et al. 2004) and later captured by the ASAS Survey (Pojmański et al. 2005). Sparsely sampled light curve data acquired over the time span between 1999 and 2005 were folded by period analysis. This report describes the results from the first multicolor (BVI_C) ccd-based photometric study conducted on this variable target. The analysis of eclipse time differences (ETD) calculated from times-of-minima published in the literature and new data presented herein has resulted in an improved ephemeris for IL Cnc.

Time-series images were taken (90-sec) in 2014 with an SBIG ST-8XME CCD camera mounted at the Cassegrain focus of a 0.28-m catadioptric telescope. This f/6.4 instrument located in UnderOak Observatory (UO; NJ, USA) produces an image scale of 2.06″/px (bin=2×2) and a field-of-view (FOV) of 17.5′×26.3′. Image acquisition (raw lights, darks, and flats) at UO was performed as described elsewhere (Alton 2016) and produced at least 282 values in each bandpass (B,V and I_C). Similarly at Desert Bloom Observatory (DBO; AZ, USA), an SBIG STT-1603ME CCD camera mounted at the Cassegrain focus of a 0.4-m catadioptric telescope was used for imaging IL Cnc in 2018. This f/6.8 instrument produces an image scale of 1.36″/px (bin=2×2) and a FOV of 11.5′×17.2′. At DBO, image acquisition (75-sec) was performed using MaxIm DL Version 6.13 (Diffraction Limited) or TheSkyX Pro Version 10.5.0 (Software Bisque). This most recent imaging campaign produced at least 235 individual photometric values in each bandpass. Both ccd cameras were equipped with B, V and I_C filters manufactured to match the Johnson-Cousins-Bessell prescription. Calibration and registration of all images collected at UO and DBO were performed with AIP4Win v2.4.0 (Berry and Burnell 2005). Instrumental readings were reduced to catalog-based magnitudes using the reference MPOSC3 star fields (Warner 2007) built into MPO Canopus v10.7.1.3 (Minor Planet Observer). The 2014 and 2018 light curves (LC) used an identical ensemble of five non-varying comparison stars in the same FOV. The identity, J2000 coordinates and color index ($B - V$) of these stars are listed in Table 1. Only data from images taken above 30° altitude (airmass <2.0) were accepted in order to minimize error due to differential refraction and color extinction.

Table 1. FOV identity, name, coordinates and color index $(B-V)$ for the target (T) and comparison stars (1-5) used for ensemble aperture photometry.

FOV Identity	Name	$\alpha_{2000.0}$ hh:mm:ss	$\delta_{2000.0}$ ° ′ ″	MPOSC3 $(B-V)$
1	GSC 01400-0523	08 56 04.26	+20 00 08.2	0.560
2	GSC 01400-0279	08 56 04.97	+20 01 06.8	0.711
3	GSC 01400-0330	08 56 11.63	+20 09 37.5	0.652
4	GSC 01400-0161	08 55 35.04	+20 05 05.6	0.588
5	GSC 01400-0406	08 55 34.19	+20 08 21.6	0.557
T	IL Cnc	08 55 51.51	+20 03 38.6	0.983

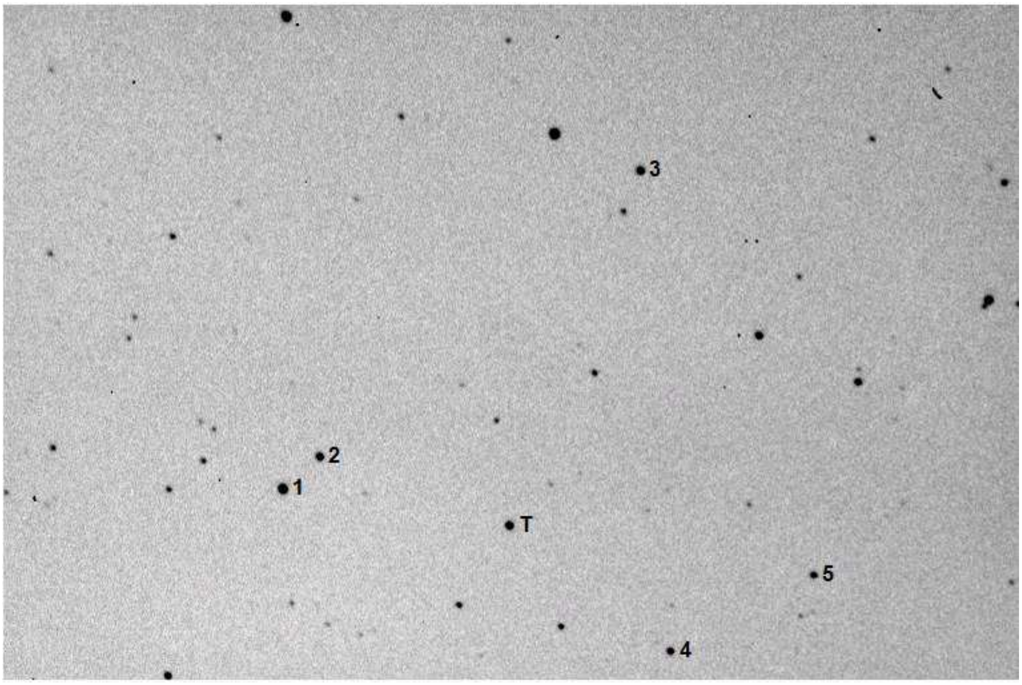

Figure 1. Observed field-of-view for IL Cnc (T) obtained at UO. The comparison stars are marked according to the numbers (1-5) assigned in Table 1.

Sparsely sampled LC data from the ROTSE–I (1999–2000) and ASAS surveys (2002–2005) were adjusted to the same average magnitude and subjected to period analysis using the ANOVA routine proposed by Schwarzenberg-Czerny (1996) and implemented within Peranso v2.5 (Vanmunster 2006). The period-folded ($P = 0.267656 \pm 0.000009$ d) results (Fig. 2) indicate that significant differences in the brightness at maximum and minimum light can occur.

Photometric data from 2014 (Fig. 3) and 2018 (Fig. 4) could be folded using an identical period solution (0.267656 ± 0.000001 d) derived by Fourier analysis (FALC; Harris et al. 1989). This period was independently verified using ANOVA (Schwarzenberg-Czerny 1996). Nine new times-of-minima (ToM) were calculated using the method of Kwee and van Woerden (1956). A mean ToM value was calculated for each night time session since no obvious color dependency (BVI_C) was observed. These are summarized in Table 2 along with other published ToM values dating back to 2003. Cycle number and ETD values were calculated from the reference ephemeris (Rinner et al. 2003) where:

$$HJD_0 = 2452721.5705 + 0\overset{d}{.}26765 \times E.$$

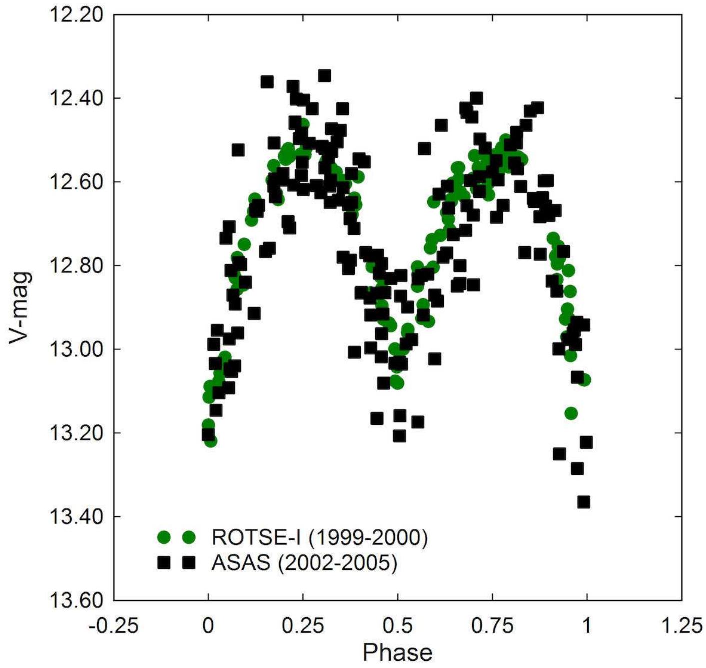

Figure 2. Folded ($P = 0.267656 \pm 0.000009$ d) light curves (V-mag) for IL Cnc produced from the ROTSE–I and ASAS Surveys.

Regression analysis of the ETD values calculated from all the observed and predicted minimum times versus the period cycle number produced a straight-line relationship indicating that the orbital period for this system does not appear to have substantially changed since 2003 (Fig. 5). These data lead to an improved linear ephemeris:

$$HJD = 2458131.9657(9) + 0.2676559(1) \times E.$$

It is clear from the steep slope of the ETD vs. epoch plot represented in Fig. 5, that the initial estimate for the orbital period (P=0.26765 d) was not sufficiently accurate, otherwise the data would have fallen on a line nearly parallel to the x-axis. If one were to substitute the improved value (P=0.2676559 d) for the original value reported by Rinner et al. 2003, then the resulting linear fit would illustrate this effect (Fig. 6). Since all but the first value represents data collected over a relative short time span ($\approx$ 10 y), it is far too early to establish whether some underlying periodicity may remain hidden in the data. Additional ToMs will be necessary to more thoroughly examine the secular behavior of this system.

The multicolor LCs (BVI_C) for IL Cnc shown in Fig. 3 (2014) and Fig. 4 (2018) exhibit a shape characteristic of an eclipsing W UMa-type binary system. Peak asymmetry is observed in the 2018 LCs during maximum light such that Max II>Max I whereas not as much difference was observed at quadrature in 2014. This behavior, also called the O'Connell effect (O'Connell 1951), is generally attributed to hot or cold spots which can be large enough to affect the brightness in localized regions of either star. W UMa-type overcontact systems are well known to be photospherically active and from year-to-year can show large differences in maximum and minimum light. LC data collected from IL Cnc during the ASAS Survey dramatically illustrate this effect particularly during Min I and Max II (Fig. 2). No high resolution classification spectrum is available for IL Cnc, however an estimate from (B–V) and (V–I_C) color indices generated from the new LCs herein

Table 2. Eclipse time differences (ETD) calculated from published times-of-minima for IL Cnc along with eight new values reported for the first time in this study.

HJD (ToM) -2400000	Error	ETD	Cycle Number	Minimum type	Reference
52721.5705	-	0.000	0	primary	Rinner et al. (2003)
54500.4124	0.0004	0.04000	6646	primary	Hübscher et al. (2010)
54831.9068	0.0009	0.04987	7884.5	secondary	Diethelm (2009)
54866.4299	0.0003	0.04613	8013.5	secondary	Hübscher and Monninger (2011)
55245.8286	0.0009	0.05095	9431	primary	Diethelm (2010)
55275.4110	0.0013	0.05802	9541.5	secondary	Hübscher and Monninger (2011)
55295.3479	0.0010	0.05500	9616	primary	Hübscher and Monninger (2011)
55295.4840	0.0009	0.05727	9616.5	secondary	Hübscher and Monninger (2011)
55523.9260	0.0002	0.06000	10470	primary	Nelson (2011)
55571.8365	0.0003	0.06115	10649	primary	Diethelm (2011)
55571.9700	0.0003	0.06083	10649.5	secondary	Diethelm (2011)
55627.3762	0.0002	0.06347	10856.5	secondary	Hübscher and Lehmann (2012)
55667.6576	0.0004	0.06355	11007	primary	Diethelm (2011)
56000.6190	0.0040	0.06835	12251	primary	Diethelm (2012)
56000.7575	0.0007	0.07302	12251.5	secondary	Diethelm (2012)
56355.6678	0.0002	0.07943	13577.5	secondary	Nelson (2014)
56643.5313	0.0001	0.08585	14653	primary	Hübscher (2014)
56677.7910	0.0002	0.08585	14781	primary	Nelson (2015)
56711.6489	0.0003	0.08602	14907.5	secondary	This study
56714.5936	0.0003	0.08656	14918.5	secondary	This study
56719.1427	0.0002	0.08601	14935.5	secondary	This study
56720.6151	0.0006	0.08568	14941	primary	This study
56732.5252	0.0005	0.08562	14985.5	secondary	This study
56743.3679	0.0011	0.08850	15026	primary	Hübscher and Lehmann (2015)
56743.5003	0.0011	0.08707	15026.5	secondary	Hübscher and Lehmann (2015)
57414.3818	0.0005	0.10385	17533	primary	Hübscher (2017)
57414.5167	0.0007	0.10492	17533.5	secondary	Hübscher (2017)
58129.8257	0.0002	0.11824	20206	primary	This study
58130.8961	0.0002	0.11913	20210	primary	This study
58131.8318	0.0001	0.11801	20213.5	secondary	This study
58131.9667	0.0002	0.11910	20214	primary	This study

and those reported by four other surveys (USNO-B1, 2MASS, SDSS-DR9 and UCAC4) cataloged in VizieR (Lasker et al. 1996) suggests that it is an early K type system. This assignment is supported by a recent publication (Qian et al. 2017) in which low resolution (R $\approx$ 1800) spectra were obtained from over 7900 stars; therein IL Cnc is classified as a main sequence K3 system. Nonetheless, additional high resolution spectroscopic data may be required to unequivocally classify this system. Attempts to model these data with PHOEBE 0.31a (Prša and Zwitter 2005), a GUI front-end to the Wilson-Devinney code (Wilson and Devinney 1971), failed to produce a unique solution for the mass-ratio since IL Cnc only exhibits a partial eclipse ($i \approx 74°$). As such any photometric solution will suffer from degeneracy while trying to simultaneously optimize orbital inclination (i) and mass-ratio (q_{ph}) unless there is a total eclipse (Terrell and Wilson 2005). This behavior is manifestly confirmed (Fig. 7) during a procedure called "q-search" or "grid-search" to find a best value for the mass-ratio. Essentially q is incrementally changed within a fixed interval during Roche modeling while the orbital inclination (i), surface potential of the primary (Ω_1) and effective temperature of the secondary (T_2) were allowed to vary during optimization by differential corrections to minimize χ^2. As can be seen (Fig. 7) there is essentially no meaningful difference in the curve fits when q_{ph} varies between 1.5 and 2. In this case it is evident that radial velocity data will be necessary to produce an accurate mass-ratio and Roche model for IL Cnc.

In summary, LC and eclipse timing data for IL Cnc has revealed a W UMa-type system in which the orbital period has not meaningfully changed since 1999. A preliminary classification of IL Cnc based on color index $(B–V)$ and $(V–I_C)$ and low resolution spectroscopic data suggests that the primary component is an early K-type star. A comparison of LCs produced from photometric data collected during the ROTSE-I and ASAS surveys along with those new data reported herein suggest that IL Cnc has an active photosphere like most other overcontact binary systems possessing a strong magnetic dynamo. Due to limitations imposed by a partial eclipse, it is not possible to derive a reliable value for the mass-ratio for this system without supporting radial velocity data.

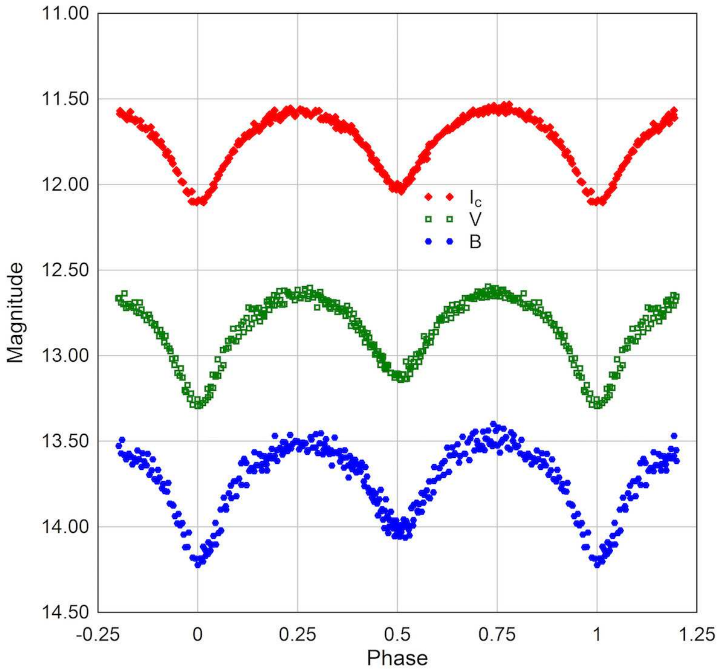

Figure 3. Folded ($P = 0.267656 \pm 0.000001$ d) light curves (BVI_C) for IL Cnc produced at UnderOak Observatory in 2014

Acknowledgments: This research has made use of the SIMBAD and VizieR databases, operated at Centre de Données astronomiques de Strasbourg, France. In addition, the International Variable Star Index maintained by the AAVSO, the ASAS Catalogue of Variable Stars and the Northern Sky Variability Survey were mined for valuable information. The diligence and dedication of all associated with these organizations is greatly appreciated. Many thanks to the anonymous referee who provided valuable feedback on this report.

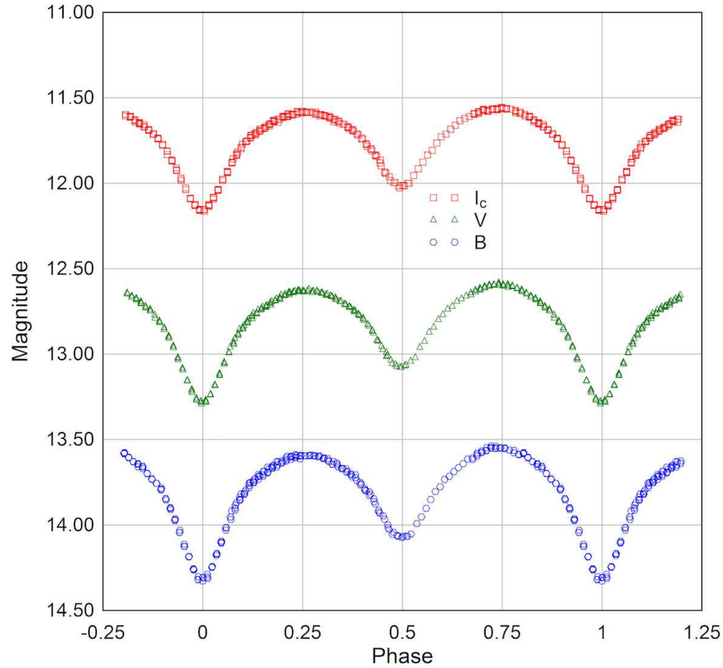

Figure 4. Folded ($P = 0.267656 \pm 0.000001$ d) light curves (BVI_C) for IL Cnc produced at Desert Bloom Observatory in 2018

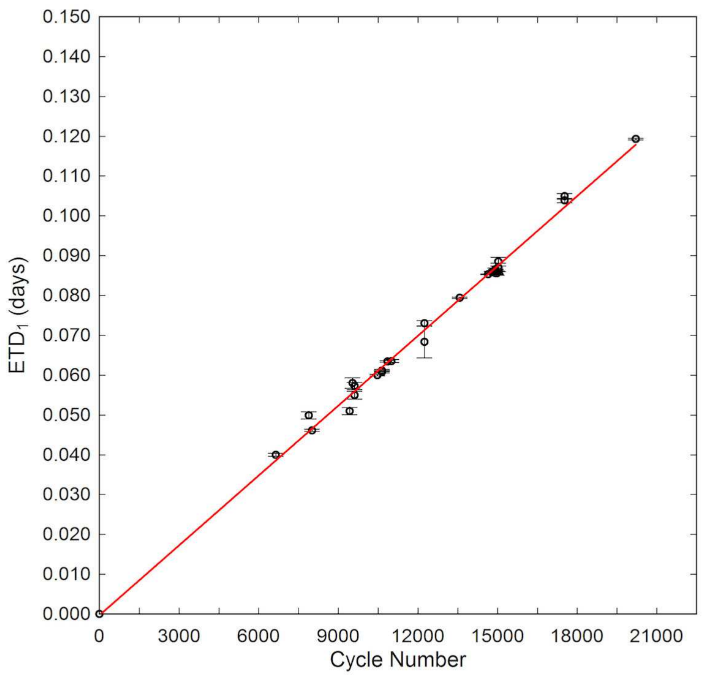

Figure 5. Linear ephemeris for IL Cnc determined from eclipse timing differences observed between 2003 and 2018 using the period ($P = 0.26765\ d$) defined by Rinner et al. 2003

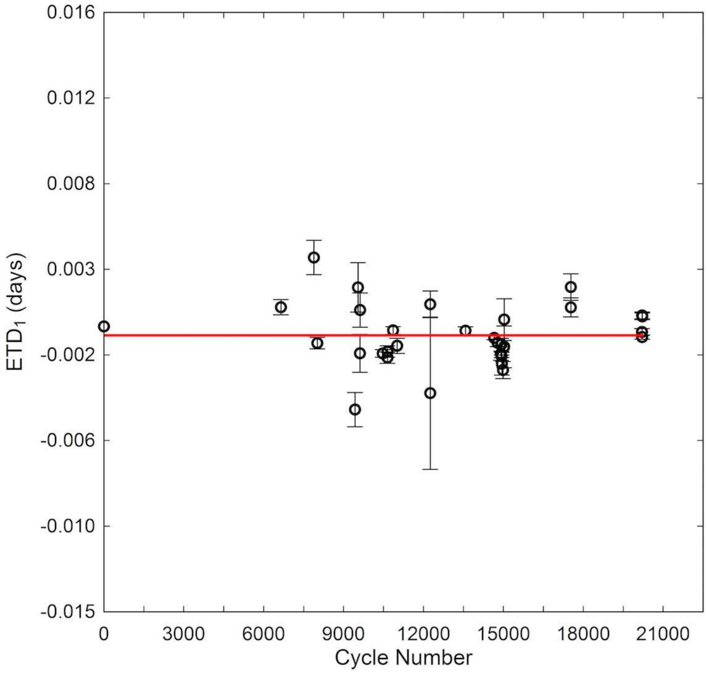

Figure 6. Linear ephemeris for IL Cnc determined from eclipse timing differences observed between 2003 and 2018 using the improved value for orbital period ($P = 0.2676559 \pm 0.0000001$d)

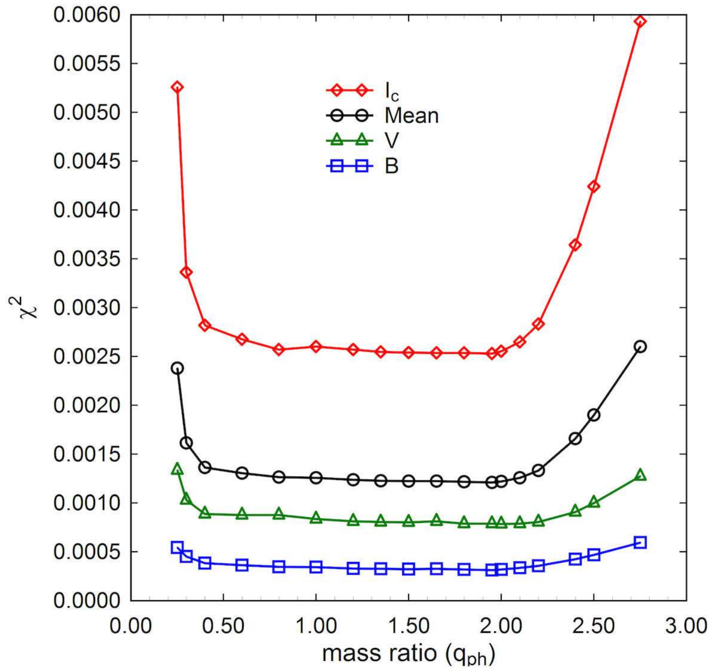

Figure 7. Results from q-search illustrating failure to find a unique value for the photometric mass-ratio (q_{ph}) where the best LC model fit reaches a distinct minimum error (χ^2)

References:

Alton, K.B., 2016, *JAAVSO*, **44**, 87
Berry, R. and Burnell, J., 2005, *The Handbook of Astronomical Image Processing*, 2nd Ed, Richmond VA, Willmann-Bell
Diethelm, R., 2009, *IBVS*, **5959**
Diethelm, R., 2010, *IBVS*, **5945**
Diethelm, R., 2011, *IBVS*, **5992**
Diethelm, R., 2012, *IBVS*, **6029**
Harris, A.W., Young, J.W., Bowell, E., et al., 1989, *Icarus*, **77**, 171 DOI
Hübscher, J., 2014, *IBVS*, **6118**
Hübscher, J., 2017, *IBVS*, **6196** DOI
Hübscher, J. and Lehmann, P.B., 2012, *IBVS*, **6026**
Hübscher, J. and Lehmann, P.B., 2015, *IBVS*, **6149**
Hübscher, J., Lehmann, P.B., Monninger, G., et al., 2010, *IBVS*, **5918**
Hübscher, J. and Monninger, G., 2011, *IBVS*, **5871**
Kwee, K.K. and Woerden, H. van, 1956, *BAN*, **12**, 327
Lasker, B.M., Sturch, C.R., Lopez, C., et al., 1996, *VizieR Online Data Catalog, Version 1.1*
Nelson, R.H., 2011, *IBVS*, **5966**
Nelson, R.H., 2014, *IBVS*, **6092**
Nelson, R.H., 2015, *IBVS*, **6131**
O'Connell D.J.K., 1951, *Pub. Riverview College Obs.*, **2**, 85
Qian, S.-B., He, J.-J., Zhang, J., et al., 2017, *Research in Astron. Astrophys.*, **17**, 087 DOI
Pojmański, G., Pilecki, B., Szczygiel, D., 2005, *AcA*, **55**, 275
Prša, A., and Zwitter, T., 2005, *ApJ*, **628**, 426 DOI
Rinner, C., Starkey, D. Demeautis, Ch., et al., 2003, *IBVS*, **5428**
Schwarzenberg-Czerny, A., 1996, *ApJ*, **460**, L107 DOI
Terrell, D. and Wilson, R.E., 2005, *ApSS*, **296**, 221 DOI
Vanmunster, T., 2006, *Peranso v2.5, Perios Analysis Software*, CBA Belgium Observatory
Warner, B. 2007, *Minor Planet Bulletin*, **34**, 113
Wilson, R. E. and Devinney, E. J., 1971, *ApJ*, **166**, 605 DOI
Woźniak, P.R., Vestrand, W.T. Akerlof, C.W., et al., 2004, *AJ*, **127**, 2436 DOI

COMMISSIONS G1 AND G4 OF THE IAU
INFORMATION BULLETIN ON VARIABLE STARS

Volume 63 Number 6242 DOI: 10.22444/IBVS.6242

Konkoly Observatory
Budapest
6 June 2018

HU ISSN 0374 – 0676

REVISED COORDINATES OF 3 VARIABLE STARS IN CYGNUS

NESCI, R.

INAF/IAPS, via Fosso del Cavaliere 100, 00133 Roma, Italy, e-mail: roberto.nesci@iaps.inaf.it

Abstract

The identification of the variable stars published on IBVS #1302 has ben checked on the basis of the original (unpublished) finding charts. For 3 stars significant differences were found and are reported here to allow an easier recovery by automatic cross-check procedures using digital catalogs. Some data from the recent Gaia DR2 catalog are also given.

A search for late type variable stars was made by P. Maffei (1977) using infrared plates (Kodak 103 I-N + RG5 filter) covering a 5 degrees wide field centered on γ Cyg. The aim was to discover Mira variables in a magnitude limited sample. In that paper, published in IBVS, only coordinates for the year 1950 were given for the stars, without finding charts: because the present practice of making cross-identification of astronomical sources is based only on coordinates coincidences between different catalogs, some stars may be misidentified simply due to misprints: this is most likely in the galactic plane, given the large density of stars. Having found the original finding charts in the library of the late prof. Maffei, I made a systematic check of all the 62 variables found by him in that field. The large majority of the stars have coordinates nearly coincident with those given in the 2MASS catalog (Cutri et al. 2003): only in 3 cases the differences are remarkable.

For these stars I report in Table 1 the Maffei's provisional name, the B1950 coordinates as reported in Maffei (1977), the J2000 coordinates of the actual 2MASS counterpart as derived from Maffei's original finding charts, the offset in arcsec from the present SIMBAD position, the present star designation in SIMBAD.

Table 1. Revised coordinates of variable stars in the field of γ Cyg.

Maffei name	RA1950 orig.	DEC1950 orig.	RAJ2000 2MASS	DECJ2000 2MASS	dist arcsec	GCVS name
M247	20:13:21.8	+41:08:25	20:15:07.07	+41:17:47.5	8.9	NSV25072
M251	20:19:29.7	+38:53:19	20:21:18.81	+39:03:05.4	10.9	NSV25113
M254	20:17:15.1	+38:45:10	20:19:03.95	+38:54:45.7	9.9	NSV13006

In Table 2, I report some relevant data (ID, parallax, G magnitude, $G_{\rm BP}$, $G_{\rm RP}$ color index, proper motion in RA and DEC) of these stars in the Gaia DR2 (Gaia Collaboration et al. 2018) catalog: for none of them is reported the variability status.

Table 2. Gaia DR2 most relevant data.

Maffei name	GaiaDR2 id.	G mag	G_{BP}, G_{RP} mag	paral. mas	RA p.m. mas/yr	DEC p.m. mas/yr
M247	2062620870978142592	13.81	0.98	1.98±0.03	4.76±0.04	6.60±0.05
M251	2061392957003016704	16.85	5.02	−0.29±0.16	−2.94±0.27	−3.56±0.26
M254	2061308294621233536	16.09	2.49	0.16±0.05	−2.01±0.08	−3.19±0.07

Below are some remarks on the individual stars.

M247: it is located between two much brighter stars. It is listed in the GSC2.3.2 catalog with magnitude N=13.94 mag. Maffei reports an amplitude of 1.0 mag without variability type, suggesting it may be a Carbon star. The 2MASS colors (J−H=0.346 mag, H−K=0.005 mag) are quite blue.

M251: the GSC2.3.2 catalog reports N=16.00 mag and no Red magnitude, but it is a bright source in 2MASS. Maffei reports an amplitude of 0.9 mag without a variability type. The 2MASS colors (J−H=1.645 mag, H−K=0.848 mag) are typical of the Mira and SR stars in the field. The Gaia DR2 parallax is of low quality and formally negative.

M254: the GSC2.3.2 catalog reports N=14.85. Maffei reports an amplitude of 0.9 mag, without a variability type. The 2MASS colors (J−H=0.853 mag, H−K=0.261 mag) are rather blue.

Acknowledgement This work has made use of the on line service at the Heidelberg University (`http://gaia.ari.uni-heidelberg.de/index.html`) to explore the Gaia DR2 catalog.

References:

Cutri, R.M., Skrutskie, M.F., vanDyk, S., et al., 2003, *CDS Vizier catalog*, II/246
Maffei, P., 1977, *IBVS*, **1302**
Gaia Collaboration et al., 2018, arXiv 1804.09365

COMMISSIONS G1 AND G4 OF THE IAU
INFORMATION BULLETIN ON VARIABLE STARS
Volume 63 Number 6243 DOI: 10.22444/IBVS.6243

Konkoly Observatory
Budapest
13 July 2018

HU ISSN 0374 – 0676

NEW TRANSIT TIMING OBSERVATIONS FOR GJ 436 b, HAT-P-3 b, HAT-P-19 b, WASP-3 b, AND XO-2 b

MACIEJEWSKI, G.[1]; STANGRET, M.[1]; OHLERT, J.[2,3]; BASARAN, Ç.S.[4]; MACIEJCZAK, J.[5]; PUCIATA-MROCZYNSKA, M.[5]; BOULANGER, E.[5]

[1] Centre for Astronomy, Faculty of Physics, Astronomy and Informatics, Nicolaus Copernicus University, Grudziadzka 5, 87-100 Toruń, Poland, e-mail: gmac@umk.pl

[2] Michael Adrian Observatorium, Astronomie Stiftung Trebur, 65468 Trebur, Germany

[3] University of Applied Sciences, Technische Hochschule Mittelhessen, 61169 Friedberg, Germany

[4] Astronomy and Space Sciences Department, Istanbul University, 34116 Fatih Istanbul, Turkey

[5] Zespół Szkół Uniwersytetu Mikołaja Kopernika, Gimnazjum i Liceum Akademickie, Szosa Chełmińska 83, 87-100 Toruń, Poland

Abstract

We present new transit observations acquired between 2014 and 2018 for the hot exoplanets GJ 436 b, HAT-P-3 b, HAT-P-19 b, WASP-3 b, and XO-2 b. New mid-transit times extend the timespan covered by observations of these exoplanets and allow us to refine their transit ephemerides. All new transits are consistent with linear ephemerides.

Precise transit timing for an exoplanet may lead to discovering deviations from a linear ephemeris that can be interpreted as a departure from a simple Keplerian model of the planetary orbital motion. Those so called transit timing variations (TTVs) could be induced by unseen planetary companions, such as in the Kepler-19 system (Ballard et al. 2011, Malavolta et al. 2017), or by nearby low-mass planets in compact planetary systems, such as WASP-47 (Becker et al. 2015). Transit timing is also a great tool for studying star-planet interactions (e.g. Birkby et al. 2014, Ragozzine & Wolf 2009). For the exoplanet WASP-12 b, a decrease of the orbital period, that can be interpreted as the result of orbital decay due to tidal dissipation inside the star, has been detected (Maciejewski et al. 2016). In this research note, we present new transit observations for hot exoplanets in the systems GJ 436 (Butler et al. 2004, Gillon et al. 2007), HAT-P-3 (Torres et al. 2007), HAT-P-19 (Hartman et al. 2011), WASP-3 (Pollacco et al. 2008), and XO-2 (Burke et al. 2007). The photometric time series were used to determine mid-transit times a number of epochs after previous observations available in the literature, and to refine transit ephemerides. We find no deviations from the Keplerian solutions for any investigated exoplanets.

The bulk of observations was acquired with the 0.6 m Cassegrain telescope at the Centre for Astronomy of the Nicolaus Copernicus University (Toruń, Poland). An SBIG STL-1001 CCD camera was used as detector. The instrumental setup offered a field of view of $11\farcm8 \times 11\farcm8$. In order to increase the signal-to-noise ratio for transit timing purposes, observations were acquired ether without any filter (clear mode) or through a blue blocking ($\lambda < 500$ nm) long-pass filter (LP500). The maximum of the spectral response in the LP500 filter was found to be close to the middle of the R band, and for white light the maximum was found to fall between the V and R bands. The transit of XO-2 b on 2014 Mar 20 was observed with the 1.2 m Trebur telescope at the Michael Adrian Observatory (Trebur, Germany). The instrument was equipped with an SBIG STL-6303 CCD camera and provided a $10\overset{\prime}{.}0 \times 6\overset{\prime}{.}7$ field of view. For that run, photometric measurements were acquired alternately in a Bessel R filter and in white light. To suppress flat-field errors, telescopes were guided manually with an accuracy of a few arc seconds. The timestamps were synchronised to UTC with at least sub-second accuracy via Network Time Protocol. Basic information on the observations are listed in Table 1.

Table 1. List of observed transits.

Date	Telescope	Filter	$t_{\rm exp}$ (s)	$N_{\rm exp}$	$N_{\rm fin}$	pnr	Epoch	$T_{\rm mid}$ (BJD$_{\rm TDB}$) +2450000
				GJ 436 b				
2017 Mar 26	0.6 m Toruń	LP500	15	525	177	1.14	1259	$7839.47013^{+0.00052}_{-0.00051}$
2018 Feb 22	0.6 m Toruń	LP500	15	570	189	1.12	1385	$8172.60146^{+0.00067}_{-0.00064}$
				HAT-P-3 b				
2017 Mar 28	0.6 m Toruń	LP500	25	506	257	1.01	1249	$7840.53170^{+0.00024}_{-0.00022}$
2018 May 07	0.6 m Toruń	LP500	25	598	301	1.10	1389	$8246.49585^{+0.00027}_{-0.00028}$
				HAT-P-19 b				
2015 Oct 04	0.6 m Toruń	clear	40	354	271	1.84	551	$7300.37489^{+0.00042}_{-0.00038}$
2015 Oct 08	0.6 m Toruń	clear	50	343	315	1.83	552	$7304.38284^{+0.00039}_{-0.00039}$
				WASP-3 b				
2017 Apr 30	0.6 m Toruń	LP500	15	550	190	1.39	2020	$7874.4583^{+0.0011}_{-0.0011}$
2018 Apr 15	0.6 m Toruń	LP500	15	637	211	1.85	2209	$8223.50975^{+0.00072}_{-0.00078}$
				XO-2 b				
2014 Mar 20	1.2 m Trebur	R	60	146	146	1.34	990	$6737.45198^{+0.00038}_{-0.00041}$
		clear	20	146	146	1.85		
2018 Jan 07	0.6 m Toruń	LP500	25	641	326	1.03	1396	$7799.49032^{+0.00032}_{-0.00032}$
2018 Apr 06	0.6 m Toruń	LP500	15	930	318	1.57	1555	$8215.41123^{+0.00044}_{-0.00043}$

Dates are given in UTC for mid-transit times. $t_{\rm exp}$ is the exposure time used. $N_{\rm exp}$ is the number of scientific exposures recorded. $N_{\rm fin}$ is the number of data points in the final light curve after resampling. pnr is the photometric scatter in parts per thousand of the normalised flux per minute of observation. Epoch is the transit number from the initial time T_0. $T_{\rm mid}$ is the best-fitting mid-transit time.

The observations were subjected to a standard reduction procedure which included dark correction and flat-fielding with sky flats. The magnitudes were obtained with the AstroImageJ package (Collins et al. 2017) employing the differential aperture photometry method. Both the aperture size and the set of comparison stars were optimised for individual light curves to achieve the smallest photometric scatter for the target star. Simultaneous detrending against the airmass, position on the matrix, time, and seeing was used if justified. The light curves were normalised to unity outside transits and the timestamps were converted to barycentric Julian dates in barycentric dynamical time (BJD$_{\rm TDB}$). The photometric noise rate (pnr), defined as the rms per minute of exposure (Fulton et al. 2011), was calculated to quantify the quality of each light curve. The final light curves were resampled into 1 minute intervals.

The Transit Analysis Package (TAP, Gazak et al. 2012) was used to derive mid-transit times. The software employs the approach of Mandel & Agol (2002) to generate transit models and the wavelet-based technique of Carter and Winn (2009) to account for the time-correlated noise. For the individual systems, their transit parameters such as the inclination and semi-major axis in stellar radii were taken from the literature and allowed to vary under Gaussian penalties determined by parameters' uncertainties. Transit depths, coded by the ratio of planetary and stellar radii, were kept free for the individual light curves in order to account for imperfect de-trending and possible third-light contamination. Tables of Claret & Bloemen (2011) were explored with the `EXOFAST` applet[1] (Eastman et al. 2013) to estimate the limb darkening (LD) coefficients of the quadratic law for the LP500 and R bands, as well as the white light. Stellar parameters were taken from von Braun et al. (2012) for GJ 436 and from Torres et al. (2012) for HAT-P-3, HAT-P-19, WASP-3, and XO-2. To account for possible inaccuracies in predictions of the LD law (e.g. Müller et al. 2013), the LD coefficients were allowed to vary around the theoretical predictions under the Gaussian penalties equal to 0.1. Since multi-parameter de-trending is not implemented in TAP, we applied a simplified approach in which the intercept and slope of the out-of-transit brightness were allowed to float to account for any remaining trends in the total error budget. The fitting procedure was based on 10 Markov chain Monte Carlo walks with 10^6 steps each. Median and the 15.9 and 85.1 percentile values of marginalised posteriori probability distributions were taken as the best-fitting values and their 1-σ uncertainties. No correlations between the determined mid-transit times, $T_{\rm mid}$, and other fitted parameters were found. The results are given in Table 1, and the light curves[2] with the best-fitting models are plotted in Fig. 1.

The new mid-transit times were combined with those available in the literature to refine the transit ephemerides in a form

$$T_{\rm mid} = T_0 + P \times E, \quad (1)$$

where E is the transit number starting from the initial epoch T_0, which is usually adopted from the discovery paper, and P is the orbital period. The results for the individual exoplanets, together with the goodness of the fit represented by the reduced chi square $\chi^2_{\rm red}$, are given in Table 2. The timing residuals from the linear ephemerides are plotted in Fig. 2. The new transits are consistent with the refined linear ephemerides for all investigated exoplanets.

Table 2. Refined transit ephemerides.

Planet	T_0 (BJD$_{\rm TDB}$)	P (d)	$\chi^2_{\rm red}$
GJ 436 b	2454510.801640 ± 0.000076	2.64389797 ± 0.00000040	5.6
HAT-P-3 b	2454218.75960 ± 0.00016	2.89973764 ± 0.00000026	2.2
HAT-P-19 b	2455091.53501 ± 0.00015	4.00878332 ± 0.00000059	0.73
WASP-3 b	2454143.85112 ± 0.00022	1.84683510 ± 0.00000032	3.2
XO-2 b	2454147.75066 ± 0.00012	2.61585937 ± 0.00000024	2.0

Acknowledgements: We are grateful to the anonymous referee for comments that helped to clarify some steps of the presented analysis. GM and MS acknowledge the financial support from the National Science Centre, Poland through grant no. 2016/23/B/ST9/00579.

References:

Ballard, S., Fabrycky, D., Fressin, F., et al., 2011, *ApJ*, **743**, 200 DOI
Becker, J.C., Vanderburg, A., Adams, F.A., et al., 2015, *ApJ*, **812**, L18 DOI
Birkby, J.L., Cappetta, M., Cruz, P., et al., 2014, *MNRAS*, **440**, 1470 DOI
Burke, Ch.J., McCullough, P.R., Valenti, J.A., et al., 2007, *ApJ*, **671**, 2115 DOI

[1] http://astroutils.astronomy.ohio-state.edu/exofast/limbdark.shtml
[2] The photometric time series are available online in Tables 3–7

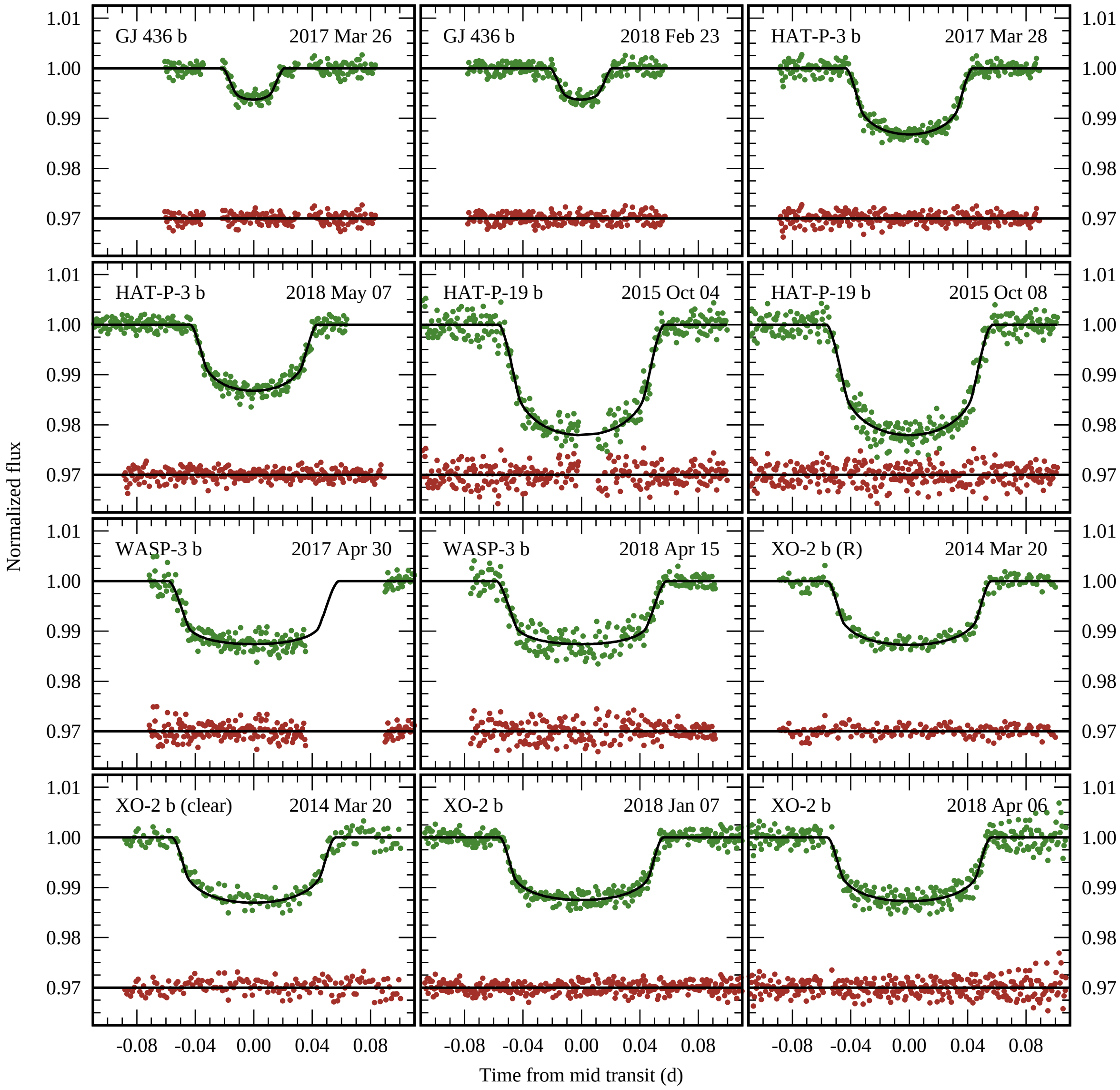

Figure 1. New transit light curves for GJ 436 b, HAT-P-3 b, HAT-P-19 b, WASP-3 b, and XO-2 b. The continuous lines show the best-fitting transit models. The residuals are plotted below.

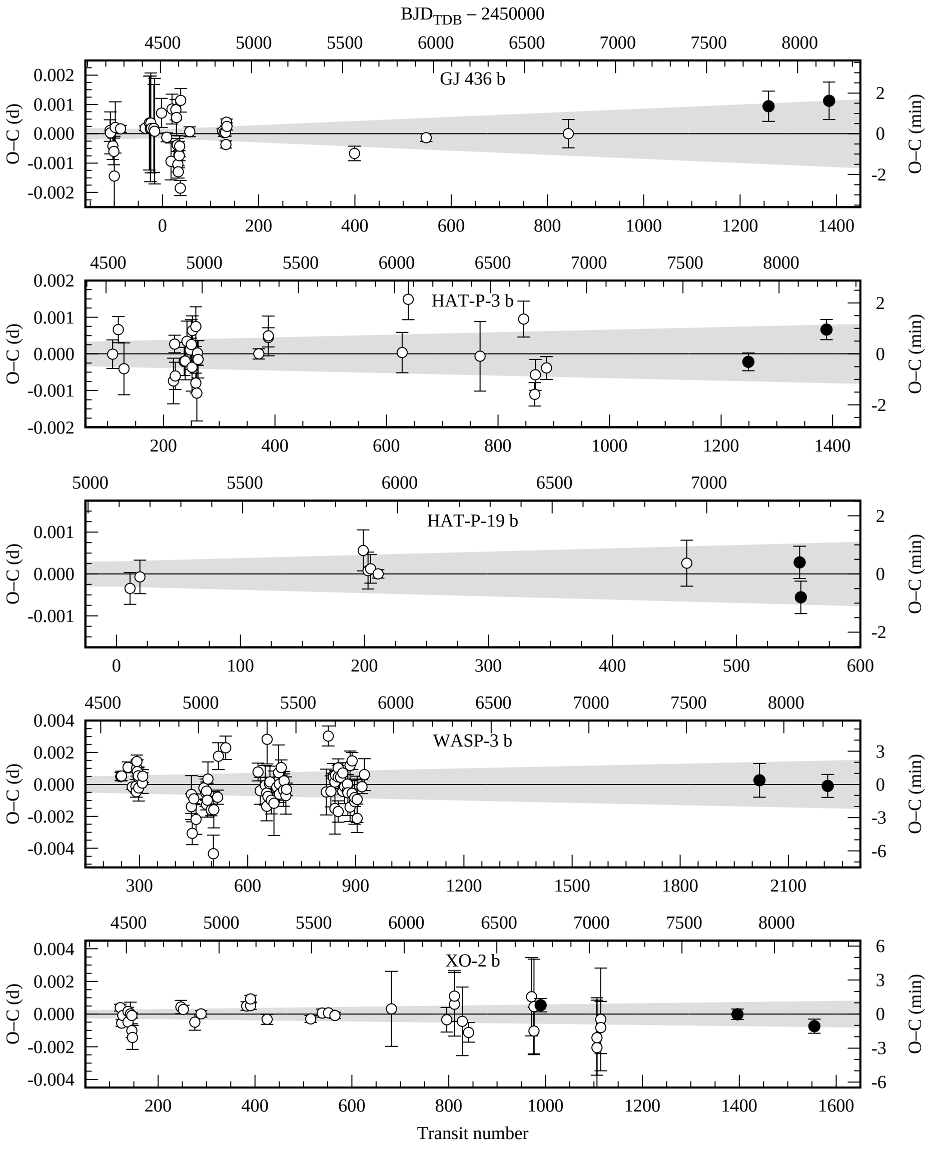

Figure 2. Transit timing residuals from the linear ephemerides for GJ 436 b, HAT-P-3 b, HAT-P-19 b, WASP-3 b, and XO-2 b. Open circles show literature data, and the filled dots place mid-transit times reported in this research note. The propagation of the ephemerides' uncertainties at the 95.5% confidence level are marked by grey areas.

Butler, R.P., Vogt, S.S., Marcy, G.W., et al., 2004, *ApJ*, **617**, 580 DOI
Carter, J.A., & Winn, J.N., 2009, *ApJ*, **704**, 51 DOI
Claret, A., & Bloemen, S., 2011, *A&A*, **529**, A75 DOI
Collins, K.A., Kielkopf, J.F., Stassun, K.G., et al., 2017, *AJ*, **153**, 77 DOI
Eastman, J., Gaudi, B. S., & Agol, E., 2013, *PASP*, **125**, 83 DOI
Fulton, B.J., Shporer, A., Winn, J.N., et al., 2011, *AJ*, **142**, 84 DOI
Gazak, J.Z., Johnson, J.A., Tonry, J., et al., 2012, *Advances in Astronomy* , **2012**, 697967 DOI
Gillon, M., Pont, F., Demory, B.-O., et al., 2007, *A&A*, **472**, L13 DOI
Hartman, J.D., Bakos, G.Á., Sato, B., et al., 2011, *ApJ*, **726**, 52 DOI
Maciejewski, G., Dimitrov, D., Fernández, M., et al., 2016, *A&A*, **588**, L6 DOI
Malavolta, L., Borsato, L., Granata, V., et al., 2017, *AJ*, **153**, 224 DOI
Mandel, K., & Agol, E., 2002, *ApJ*, **580**, L171 DOI
Pollacco, D., Skillen, I., Collier Cameron, A., et al., 2008, *MNRAS*, **385**, 1576 DOI
Müller, H.M., Huber, K.F., Czesla, S., et al., 2013, *A&A*, **560**, A112 DOI
Ragozzine, D., Wolf, A.S., 2009, *ApJ*, **698**, 1778 DOI
Torres, G., Bakos, G.Á., Kovacs, G., et al., 2007, *ApJ*, **666**, L121 DOI
Torres, G., Fischer, D.A., Sozzetti, A., et al., 2012, *ApJ*, **757**, 161 DOI
von Braun, K., Boyajian, T.S., Kane, S.R., et al., 2012, *ApJ*, **753**, 171 DOI

COMMISSIONS G1 AND G4 OF THE IAU
INFORMATION BULLETIN ON VARIABLE STARS
Volume 63 Number 6244 DOI: 10.22444/IBVS.6244

Konkoly Observatory
Budapest
13 July 2018

HU ISSN 0374 – 0676

BAV-RESULTS OF OBSERVATIONS - PHOTOELECTRIC MINIMA OF SELECTED ECLIPSING BINARIES AND MAXIMA OF PULSATING STARS

(BAV MITTEILUNGEN NO. 247)

PAGEL, LIENHARD

Bundesdeutsche Arbeitsgemeinschaft für Veränderliche Sterne e.V. (BAV), Munsterdamm 90, 12169 Berlin, Germany, www.bav-astro.de, publikat@bav-astro.de

In this 89th compilation of BAV results, photoelectric observations obtained mostly in the year 2017 are presented giving 1894 minima and 456 maxima. All moments of minima and maxima are heliocentric UTC. The errors are tabulated in column "±" All information about photometers and filters are specified in the columns "Cam" and "Fil".

The photometric measurements and all the light curves with evaluations can be obtained from the offices of the BAV for inspection.

Please use the BAV-Website (`http://www.bav-astro.de/sfs/index.php/`) for an easy access to all the publications of the BAV including the "Lichtenknecker Database of the BAV" (`http://www.bav-astro.de/LkDB/index.php/`).

Table 1: Times of minima and maxima

Variable	Ext	HJD 24.....	±	Obs	Type	Cam	Fil	n
RT And	min	57964.4832	0.0002	AG	EA/RS	1603	-Ir	40
RT And	min	57980.5217	0.0006	AG	EA/RS	1603	-Ir	33
WZ And	min	57781.3674	0.0001	SCI	EB	ST7	o	119
WZ And	min	58023.4616	0.0007	AG	EB	1603	-Ir	60
XX And	max	58058.3870	0.0015	ALH	RRAB	3200M	V	496
AA And	min	57964.4959	0.0008	AG	EB	1603	-Ir	40
AB And	min	57987.3693	0.0003	AG	EW	1603	-Ir	44
AB And	min	57987.5351	0.0009	AG	EW	1603	-Ir	44
AB And	min	58043.2928	0.0012	DIE	EW	314LC		26
AB And	min	58045.2814	0.0029	DIE	EW	314LC		24
AB And	min	58041.3056	0.0002	DIE	EW	314LC		23
AB And	min	58042.2927	0.0009	DIE	EW	314LC		23
AC And	max	57966.4560	0.0010	AG	*	1603	-Ir	32
CC And	max	57973.4890	0.0010	AG	DSCT	1603	-Ir	32
CI And	max	58023.4060	0.0010	AG	RRAB	1603	-Ir	57
CN And	min	57973.5404	0.0005	AG	EB	1603	-Ir	36
CP And	min	58019.4700	0.0010	AG	EA	1603	-Ir	30
GK And	min	58011.3968	0.0011	AG	EA	1603	-Ir	29
GP And	min	58044.3055	0.0011	ALH	DSCT	3200M	V	450
GP And	max	58044.3326	0.0005	ALH	DSCT	3200M	V	450
GP And	min	58044.3858	0.0009	ALH	DSCT	3200M	V	450
GP And	max	58044.4105	0.0005	ALH	DSCT	3200M	V	450
GP And	min	58044.4640	0.0007	ALH	DSCT	3200M	V	450
GP And	max	58044.4901	0.0008	ALH	DSCT	3200M	V	450
GP And	min	58044.5425	0.0014	ALH	DSCT	3200M	V	450
OV And	max	57973.4440	0.0010	AG	RRAB	1603	-Ir	36

Table 1: cont.

Variable	Ext	HJD 24.....	±	Obs	Type	Cam	Fil	n
QW And	min	58018.5128	0.0023	AG	EW	1603	-Ir	55
V0355 And	min	57992.5155	0.0015	AG	EA	1603	-Ir	44
V0382 And	min	57987.4031	0.0024	AG	EB	1603	-Ir	44
V0392 And	min	58023.3323	0.0015	AG	EA	1603	-Ir	58
V0404 And	min	58018.4451	0.0004	AG	EA/RS	1603	-Ir	57
V0441 And	min	57987.5137	0.0031	AG	EW	1603	-Ir	35
V0460 And	min	58079.3405	0.0010	ALH	DSCT	3200M	V	442
V0460 And	max	58079.3640	0.0004	ALH	DSCT	3200M	V	442
V0460 And	min	58079.4145	0.0010	ALH	DSCT	3200M	V	442
V0460 And	max	58079.4391	0.0005	ALH	DSCT	3200M	V	442
V0460 And	min	58079.4900	0.0010	ALH	DSCT	3200M	V	442
V0460 And	max	58079.5146	0.0005	ALH	DSCT	3200M	V	442
V0460 And	min	58079.5640	0.0015	ALH	DSCT	3200M	V	442
V0460 And	max	58079.5900	0.0008	ALH	DSCT	3200M	V	442
V0483 And	min	57973.5171	0.0022	AG	EW	1603	-Ir	36
V0488 And	min	57973.5426	0.0025	AG	EB	1603	-Ir	35
V0524 And	min	58040.3348	0.0011	ALH	SXPHE	3200M	V	506
V0524 And	max	58040.3703	0.0007	ALH	SXPHE	3200M	V	506
V0524 And	min	58040.4292	0.0011	ALH	SXPHE	3200M	V	506
V0524 And	max	58040.4647	0.0006	ALH	SXPHE	3200M	V	506
V0524 And	min	58040.5229	0.0012	ALH	SXPHE	3200M	V	506
V0524 And	max	58040.5592	0.0008	ALH	SXPHE	3200M	V	506
V0524 And	min	58040.6172	0.0019	ALH	SXPHE	3200M	V	506
V0525 And	min	58018.3246	0.0015	AG	EA/RS	1603	-Ir	56
V0527 And	min	58018.4364	0.0014	AG	EW	1603	-Ir	56
V0530 And	min	58023.5066	0.0014	AG	EB	1603	-Ir	57
V0531 And	min	58019.3390	0.0022	AG	EW	1603	-Ir	29
V0531 And	min	58023.4055	0.0025	AG	EW	1603	-Ir	57
V0538 And	min	58019.3729	0.0040	AG	EB	1603	-Ir	24
V0544 And	max	58019.3430	0.0010	AG	SXPHE	1603	-Ir	30
V0544 And	max	58019.4490	0.0010	AG	SXPHE	1603	-Ir	30
V0546 And	min	58023.3417	0.0008	AG	EW	1603	-Ir	56
V0546 And	min	58023.5361	0.0008	AG	EW	1603	-Ir	56
V0595 And	min	57964.4759	0.0009	AG	RRC	1603	-Ir	39
V0600 And	min	57964.5268	0.0020	AG	EW	1603	-Ir	39
V0611 And	min	57964.4822	0.0031	AG	EB	1603	-Ir	39
V0613 And	min	57939.4786	0.0009	AG	EA	1603	-Ir	26
V0613 And	min	57940.4140	0.0022	AG	EA	1603	-Ir	26
V0629 And	min	58011.3712	0.0058	AG	EA	1603	-Ir	24
V0638 And	min	58011.3980	0.0011	AG	EW	1603	-Ir	24
V0664 And	min	58011.4380	0.0033	AG	EW	1603	-Ir	28
V0666 And	min	57966.5182	0.0009	AG	EW	1603	-Ir	31
V0670 And	max	57966.4760	0.0010	AG	DSCT	1603	-Ir	31
V0670 And	max	57966.5790	0.0010	AG	DSCT	1603	-Ir	31
V0670 And	max	57989.4040	0.0010	AG	DSCT	1603	-Ir	37
V0670 And	max	57989.5000	0.0010	AG	DSCT	1603	-Ir	37
V0670 And	max	57989.6000	0.0020	AG	DSCT	1603	-Ir	37
V0670 And	max	58019.3020	0.0010	AG	DSCT	1603	-Ir	37
V0670 And	max	58019.3970	0.0010	AG	DSCT	1603	-Ir	37
V0674 And	min	57989.4077	0.0011	AG	EA	1603	-Ir	38
V0674 And	min	58019.4824	0.0115	AG	EA	1603	-Ir	38
V0683 And	min	57968.3707	0.0004	AG	EA	1603	-Ir	40
V0705 And	min	58011.3658	0.0009	AG	EW	1603	-Ir	32
V0706 And	min	58011.4575	0.0001	AG	EA	1603	-Ir	23
V0707 And	min	57987.3449	0.0057	AG	EA	1603	-Ir	44
V0712 And	min	57973.4268	0.0008	AG	EW	1603	-Ir	38
V0712 And	min	57987.3768	0.0011	AG	EW	1603	-Ir	43
V0712 And	min	57987.5578	0.0018	AG	EW	1603	-Ir	43
V0714 And	min	57973.4758	0.0034	AG	EA	1603	-Ir	38
V0726 And	min	57973.5615	0.0031	AG	EW	1603	-Ir	32
V0736 And	min	58023.4266	0.0010	AG	EW	1603	-Ir	60
V0736 And	min	58023.6072	0.0015	AG	EW	1603	-Ir	60
V0743 And	min	58023.4963	0.0012	AG	EW	1603	-Ir	45
CY Aqr	max	58043.3224	0.0007	WLH	SXPHE	ST10	-IR	120
CY Aqr	max	58043.3832	0.0007	WLH	SXPHE	ST10	-IR	120
HS Aqr	min	57995.4074	0.0006	AG	EA	1603	-Ir	36
V0351 Aqr	min	57643.3243	0.0020	RATRCR	EW	1600	V	77
V0351 Aqr	min	58023.3627	0.0020	AG	EW	1603	-Ir	41
XZ Aql	min	57992.4224	0.0007	AG	EA	1603	-Ir	28
AA Aql	max	57994.3418	0.0007	WLH	RRAB	ST10	V-IR-UV	75
KO Aql	min	57900.5072	0.0009	AG	EA	1603	-Ir	25

Table 1: cont.

Variable	Ext	HJD 24.....	±	Obs	Type	Cam	Fil	n
KP Aql	min	57917.4709	0.0018	AG	EA	1603	-Ir	27
V0343 Aql	min	57940.4287	0.0014	AG	EA	1603	-Ir	26
V0415 Aql	min	57563.4700	0.0003	RATRCR	EA	1600	V	127
V0417 Aql	min	57939.4642	0.0007	AG	EW	1603	-Ir	24
V0417 Aql	min	58001.4908	0.0025	AG	EW	1603	-Ir	38
V0609 Aql	min	57940.4389	0.0065	AG	EB	1603	-Ir	26
V0699 Aql	min	57987.3390	0.0025	AG	EW	1603	-Ir	34
V1070 Aql	max	57952.4430	0.0010	AG	RRAB	1603	-Ir	30
V1331 Aql	min	57939.5082	0.0020	AG	EB	1603	-Ir	26
V1353 Aql	min	57973.4151	0.0023	AG	EB	1603	-Ir	38
V1426 Aql	min	58001.4356	0.0042	AG	EA	1603	-Ir	34
V1430 Aql	min	57952.4263	0.0006	AG	EA/RS	1603	-Ir	33
V1455 Aql	min	57992.3966	0.0045	AG	EA	1603	-Ir	29
V1461 Aql	min	57995.4055	0.0015	AG	EA	1603	-Ir	27
V1747 Aql	min	57919.4844	0.0011	AG	EA	1603	-Ir	24
V1796 Aql	min	57939.4949	0.0015	AG	EW	1603	-Ir	23
V1796 Aql	min	57940.5339	0.0018	AG	EW	1603	-Ir	25
V1796 Aql	min	58001.4061	0.0019	AG	EW	1603	-Ir	34
V1808 Aql	min	57940.4515	0.0006	AG	EW	1603	-Ir	26
V1814 Aql	min	57987.4743	0.0006	AG	EA	1603	-Ir	39
V1817 Aql	min	57952.4668	0.0010	AG	EA	1603	-Ir	34
V1825 Aql	min	57988.5158	0.0008	AG	EA	1603	-Ir	41
V1826 Aql	min	57992.5111	0.0019	AG	EA	1603	-Ir	37
BQ Ari	min	57657.5126	0.0001	RATRCR	EW	1600	V	173
TZ Aur	max	57824.3851	0.0010	BRW	RRAB	383L+	C	172
WW Aur	min	57800.5711	0.0026	AG	EA	1603	-Ir	44
AP Aur	min2	57829.4865	0.0011	JU	EB	ST7	o	94
AR Aur	min	57810.3146	0.0007	AG	EA	1603	-Ir	32
EP Aur	min2	57800.3744	0.0019	JU	EB	ST7	o	105
V0459 Aur	min	57800.4967	0.0030	AG	EB	1603	-Ir	44
V0574 Aur	max	57822.3589	0.0014	MZ	RRAB	ST7	-Ir	59
V0574 Aur	max	57829.3170	0.0013	MZ	RRAB	ST7	-Ir	44
V0574 Aur	max	57840.3282	0.0009	MZ	RRAB	ST7	-Ir	114
V0574 Aur	max	54394.6930	0.0060	MZ	RRAB	SWASP		44
V0574 Aur	max	54405.7030	0.0060	MZ	RRAB	SWASP		60
V0574 Aur	max	54419.6170	0.0060	MZ	RRAB	SWASP		57
V0574 Aur	max	54437.5990	0.0060	MZ	RRAB	SWASP		39
V0574 Aur	max	54516.4450	0.0080	MZ	RRAB	SWASP		113
V0574 Aur	max	57704.6604	0.0010	MS	RRAB	16803	V	90
RS Boo	max	57842.4800	0.0010	AG	RRAB	1603	-Ir	44
ST Boo	max	57852.5760	0.0030	AG	RRAB	1603	-Ir	51
TU Boo	min	57855.3814	0.0000	AG	EW	1603	-Ir	40
TU Boo	min	57855.5422	0.0027	AG	EW	1603	-Ir	40
TU Boo	min	57874.3519	0.0003	AG	EW	1603	-Ir	84
TU Boo	min	57874.5135	0.0002	AG	EW	1603	-Ir	84
TV Boo	max	57829.3630	0.0020	AG	RRC	1603	-Ir	49
TV Boo	max	57836.5480	0.0010	AG	RRC	1603	-Ir	34
TW Boo	max	57843.3900	0.0010	AG	RRAB	1603	-Ir	44
TZ Boo	min	57838.3847	0.0015	AG	EW	1603	-Ir	47
TZ Boo	min	57838.5327	0.0021	AG	EW	1603	-Ir	47
UW Boo	min	57825.5241	0.0072	AG	EA	1603	-Ir	51
VW Boo	min	57867.4962	0.0004	AG	EW	1603	-Ir	44
XY Boo	min	57843.3748	0.0012	AG	EW	1603	-Ir	41
XY Boo	min	57843.5593	0.0009	AG	EW	1603	-Ir	41
XY Boo	min	57846.5250	0.0006	AG	EW	1603	-Ir	43
YZ Boo	max	57846.3860	0.0020	AG	DSCT	1603	-Ir	42
YZ Boo	max	57846.4900	0.0020	AG	DSCT	1603	-Ir	42
YZ Boo	max	57846.5940	0.0020	AG	DSCT	1603	-Ir	42
YZ Boo	max	57853.3580	0.0010	AG	DSCT	1603	-Ir	40
YZ Boo	max	57853.4650	0.0010	AG	DSCT	1603	-Ir	40
YZ Boo	max	57853.5690	0.0010	AG	DSCT	1603	-Ir	40
ZZ Boo	min	57841.6160	0.0011	AG	EA	1603	-Ir	42
AC Boo	min	57798.6857	0.0001	SCI	EW	ST7	o	75
AC Boo	min	57838.3393	0.0001	AG	EW	1603	-Ir	49
AC Boo	min	57838.5152	0.0007	AG	EW	1603	-Ir	49
AC Boo	min	57840.4544	0.0024	AG	EW	1603	-Ir	46
AC Boo	min	57840.6292	0.0005	AG	EW	1603	-Ir	46
AC Boo	min	57852.4408	0.0003	NWR	EW	16IC	o	352
AC Boo	min	57852.4389	0.0002	FR	EW	1603	-Ir	195
AC Boo	min2	57852.6132	0.0001	FR	EW	1603	-Ir	195
AC Boo	min2	57853.3187	0.0001	FR	EW	1603	-Ir	257

Table 1: cont.

Variable	Ext	HJD 24.....	±	Obs	Type	Cam	Fil	n
AC Boo	min	57853.4960	0.0002	FR	EW	1603	-Ir	257
AD Boo	min	57852.5021	0.0011	AG	EA	1603	-Ir	51
AD Boo	min	57853.5374	0.0003	AG	EA	1603	-Ir	42
AE Boo	max	57867.3580	0.0010	AG	RRC	1603	-Ir	44
AN Boo	max	57839.4580	0.0010	AG	RRAB	1603	-Ir	41
AN Boo	max	57846.3820	0.0010	AG	RRAB	1603	-Ir	38
AQ Boo	min	57839.4122	0.0006	AG	EW	1603	-Ir	41
AQ Boo	min	57839.5795	0.0019	AG	EW	1603	-Ir	41
AQ Boo	min	57846.4082	0.0012	AG	EW	1603	-Ir	44
AQ Boo	min	57846.5777	0.0004	AG	EW	1603	-Ir	44
AR Boo	min	57825.4201	0.0016	AG	EW	1603	-Ir	48
AR Boo	min	57825.5928	0.0004	AG	EW	1603	-Ir	48
AS Boo	max	57825.5090	0.0010	AG	RRAB	1603	-Ir	47
AW Boo	max	57839.5430	0.0010	AG	RRAB	1603	-Ir	40
AW Boo	max	57846.3970	0.0010	AG	RRAB	1603	-Ir	43
AX Boo	max	57846.3760	0.0020	AG	RRAB	1603	-Ir	42
AY Boo	max	57839.5990	0.0010	AG	RRAB	1603	-Ir	41
AZ Boo	max	57846.3840	0.0010	AG	RRAB	1603	-Ir	42
BD Boo	max	57855.3980	0.0010	AG	RRAB	1603	-Ir	33
BE Boo	max	57839.4710	0.0010	AG	RRAB	1603	-Ir	41
BE Boo	max	57846.6090	0.0020	AG	RRAB	1603	-Ir	37
BO Boo	max	57874.4370	0.0010	AG	RRAB	1603	-Ir	84
BQ Boo	max	57846.5410	0.0010	AG	RRAB	1603	-Ir	44
BR Boo	max	57839.4030	0.0010	AG	RRC	1603	-Ir	41
BR Boo	max	57846.4070	0.0010	AG	RRC	1603	-Ir	42
BW Boo	min	57853.5348	0.0014	AG	EA	1603	-Ir	43
CK Boo	min	57874.4798	0.0017	AG	EW	1603	-Ir	38
CV Boo	min	57846.3592	0.0037	AG	EA	1603	-Ir	42
CV Boo	min	57853.5613	0.0007	AG	EA	1603	-Ir	40
DU Boo	min	57836.5032	0.0032	AG	EB	1603	-Ir	36
DV Boo	min	57874.4289	0.0025	AG	EA	1603	-Ir	39
EF Boo	min	57829.4279	0.0009	AG	EW/RS	1603	-Ir	51
EF Boo	min	57829.6384	0.0011	AG	EW/RS	1603	-Ir	51
EL Boo	min	57867.3787	0.0021	AG	EW	1603	-Ir	44
EL Boo	min	57867.5835	0.0021	AG	EW	1603	-Ir	44
EM Boo	min	57855.5200	0.0019	AG	EA	1603	-Ir	41
ET Boo	min	57838.3639	0.0020	AG	EB	1603	-Ir	49
ET Boo	min	57840.6208	0.0010	AG	EB	1603	-Ir	46
ET Boo	min2	57852.5552	0.0002	FR	EB	1603	-Ir	97
ET Boo	min	57853.5214	0.0001	FR	EB	1603	-Ir	103
EW Boo	min	57838.6278	0.0019	AG	EA	1603	-Ir	46
FP Boo	min	57843.5841	0.0015	AG	EW	1603	-Ir	40
GG Boo	min	57839.4574	0.0028	AG	EB	1603	-Ir	53
GH Boo	min	57825.6160	0.0011	AG	EW	1603	-Ir	48
GK Boo	min	57838.3415	0.0004	AG	EA	1603	-Ir	49
GK Boo	min	57838.5789	0.0015	AG	EA	1603	-Ir	49
GK Boo	min	57846.4637	0.0016	AG	EA	1603	-Ir	44
GK Boo	min	57853.3904	0.0020	AG	EA	1603	-Ir	43
GK Boo	min	57853.6315	0.0005	AG	EA	1603	-Ir	43
GN Boo	min	57843.4359	0.0026	AG	EW	1603	-Ir	42
GN Boo	min	57843.5858	0.0014	AG	EW	1603	-Ir	42
GN Boo	min	57844.3408	0.0014	AG	EW	1603	-Ir	40
GN Boo	min	57844.4926	0.0030	AG	EW	1603	-Ir	40
GN Boo	min	57844.6417	0.0003	AG	EW	1603	-Ir	40
GP Boo	min	57852.4022	0.0025	AG	EB	1603	-Ir	48
GT Boo	min	57840.4271	0.0032	AG	EB	1603	-Ir	42
GV Boo	min	57825.5494	0.0013	AG	EW	1603	-Ir	48
GW Boo	min	57843.4126	0.0011	AG	EW	1603	-Ir	41
GW Boo	min	57846.6044	0.0016	AG	EW	1603	-Ir	37
HH Boo	min	57825.4092	0.0023	AG	EW	1603	-Ir	51
HH Boo	min	57825.5651	0.0010	AG	EW	1603	-Ir	51
IK Boo	min	57825.4104	0.0008	AG	EW	1603	-Ir	48
IK Boo	min	57825.5616	0.0006	AG	EW	1603	-Ir	48
IN Boo	min	57855.4433	0.0015	AG	EW	1603	-Ir	38
IN Boo	min	57855.5862	0.0002	AG	EW	1603	-Ir	38
IN Boo	min	57874.4457	0.0000	AG	EW	1603	-Ir	84
IN Boo	min	57874.5888	0.0005	AG	EW	1603	-Ir	84
KP Boo	min	57879.4459	0.0025	AG	EB	1603	-Ir	41
MN Boo	min	57838.3729	0.0014	AG	EW	1603	-Ir	48
MN Boo	min	57838.5740	0.0032	AG	EW	1603	-Ir	48
MQ Boo	min	57879.5790	0.0003	AG	EB	1603	-Ir	41

Table 1: cont.

Variable	Ext	HJD 24.....	±	Obs	Type	Cam	Fil	n
MT Boo	min	57879.5281	0.0007	AG	EW	1603	-Ir	41
MV Boo	min	57843.4470	0.0047	AG	EA/RS	1603	-Ir	43
MV Boo	min	57852.3582	0.0041	AG	EA/RS	1603	-Ir	51
MW Boo	min	57879.4169	0.0004	AG	EW	1603	-Ir	41
NY Boo	min	57879.5185	0.0007	AG	EW	1603	-Ir	39
OS Boo	min	57879.4672	0.0007	AG	EW	1603	-Ir	40
PU Boo	min	57838.5311	0.0008	AG	EW	1603	-Ir	49
QQ Boo	min	57831.6964	0.0003	MS	EW	16803	V	104
QQ Boo	min	57848.5598	0.0003	MS	EW	16803	V	143
QQ Boo	min	57848.6992	0.0006	MS	EW	16803	V	143
QQ Boo	min	57858.5131	0.0016	MS	EW	16803	V	108
QQ Boo	min	57858.6524	0.0009	MS	EW	16803	V	108
QQ Boo	min	57862.5228	0.0002	MS	EW	16803	V	200
QQ Boo	min	57862.6599	0.0006	MS	EW	16803	V	200
QQ Boo	min	57510.4315	0.0002	RATRCR	EW	1600	V	147
QW Boo	min	57831.6630	0.0004	MS	EW	16803	V	99
QW Boo	min	57848.5346	0.0003	MS	EW	16803	V	144
QW Boo	min	57848.6792	0.0002	MS	EW	16803	V	144
QW Boo	min	57858.5683	0.0003	MS	EW	16803	V	108
QW Boo	min	57862.4956	0.0002	MS	EW	16803	V	182
QW Boo	min	57862.6408	0.0006	MS	EW	16803	V	182
V0339 Boo	min	57843.4789	0.0020	AG	EW	1603	-Ir	40
SV Cam	min	57815.5150	0.0034	AG	EA/RS	1603	-Ir	43
AK Cam	min	57853.4540	0.0014	AG	EA	1603	-Ir	41
AL Cam	min	57815.2917	0.0051	AG	EA	1603	-Ir	39
AY Cam	min	57846.5405	0.0011	AG	EA	1603	-Ir	44
AY Cam	min	57853.3790	0.0019	AG	EA	1603	-Ir	42
AZ Cam	min	57836.4404	0.0016	AG	EA	1603	-Ir	40
DI Cam	min	57853.5698	0.0034	AG	EA	1603	-Ir	43
DI Cam	min	57901.4704	0.0079	AG	EA	1603	-Ir	32
DI Cam	min	57926.4886	0.0027	AG	EA	1603	-Ir	21
FN Cam	min	57839.4779	0.0008	AG	EW	1603	-Ir	54
NR Cam	min	57839.3758	0.0022	AG	EW	1603	-Ir	55
NR Cam	min	57839.5047	0.0013	AG	EW	1603	-Ir	55
NR Cam	min	57839.6302	0.0009	AG	EW	1603	-Ir	55
NR Cam	min	57840.3981	0.0009	AG	EW	1603	-Ir	46
NR Cam	min	57840.5283	0.0028	AG	EW	1603	-Ir	46
NU Cam	min	57836.4079	0.0016	AG	EB	1603	-Ir	39
NU Cam	min	57840.5492	0.0024	AG	EB	1603	-Ir	47
NX Cam	min	57727.5221	0.0004	RATRCR	EW:	1600	V	224
V0456 Cam	min	57409.4770	0.0006	RATRCR	EW	1600	V	142
V0489 Cam	min	57839.5662	0.0001	AG	EA/RS	1603	-Ir	45
V0499 Cam	min	57841.5374	0.0013	AG	EA	1603	-Ir	50
V0514 Cam	min	57815.2919	0.0042	AG	EW	1603	-Ir	39
V0514 Cam	min	57815.4727	0.0009	AG	EW	1603	-Ir	39
V0516 Cam	min	57840.4931	0.0009	AG	EA	1603	-Ir	47
V0517 Cam	min	57810.3229	0.0015	AG	EA	1603	-Ir	33
V0572 Cam	max	56731.3820	0.0010	AG	DSCT	1603	-Ir	39
V0572 Cam	max	56731.4660	0.0010	AG	DSCT	1603	-Ir	39
V0572 Cam	max	56731.5540	0.0010	AG	DSCT	1603	-Ir	39
V0572 Cam	max	57815.3330	0.0010	AG	DSCT	1603	-Ir	39
V0572 Cam	max	57815.4170	0.0010	AG	DSCT	1603	-Ir	39
V0572 Cam	max	57815.5050	0.0010	AG	DSCT	1603	-Ir	39
RW Cnc	min	57827.4452	0.0016	ALH	RRAB	ST8XM	V	374
RW Cnc	max	57827.5092	0.0010	ALH	RRAB	ST8XM	V	374
RY Cnc	min	57843.4391	0.0016	AG	EA	1603	-Ir	43
SS Cnc	max	57843.5180	0.0010	AG	RRAB	1603	-Ir	43
TT Cnc	max	57798.5090	0.0030	AG	RRAB	1603	-Ir	60
TX Cnc	min	57799.3320	0.0013	AG	EW	1603	-Ir	59
TX Cnc	min	57799.5186	0.0011	AG	EW	1603	-Ir	59
VZ Cnc	max	57815.3190	0.0010	AG	DSCT	1603	-Ir	40
VZ Cnc	max	57815.4990	0.0010	AG	DSCT	1603	-Ir	40
WW Cnc	min	57798.4531	0.0030	AG	EA	1603	-Ir	137
WW Cnc	min	57446.3616	0.0001	RATRCR	EA	1600	V	131
WW Cnc	min2	57775.4306	0.0006	RATRCR	EA	1600	V	74
WW Cnc	min2	57823.5575	0.0003	RATRCR	EA	1600	V	95
WX Cnc	min	57812.3827	0.0006	AG	EA	1603	-Ir	73
WY Cnc	min	57799.6151	0.0004	AG	EA/RS	1603	-Ir	65
XZ Cnc	min	57798.4546	0.0009	AG	EB	1603	-Ir	60
XZ Cnc	min	57725.5589	0.0001	RATRCR	EB	1600	V	165
YY Cnc	min	57812.3894	0.0009	AG	EB	1603	-Ir	68

Table 1: cont.

Variable	Ext	HJD 24.....	±	Obs	Type	Cam	Fil	n
YY Cnc	min	57833.3468	0.0010	AG	EB	1603	-Ir	75
AS Cnc	max	57844.3700	0.0010	AG	RRAB	1603	-Ir	44
EF Cnc	max	57798.3420	0.0020	AG	RRC	1603	-Ir	72
EH Cnc	min	57843.3654	0.0002	AG	EW	1603	-Ir	45
EH Cnc	min	57844.4123	0.0004	AG	EW	1603	-Ir	44
FF Cnc	min	57799.3201	0.0022	AG	EA	1603	-Ir	55
IR Cnc	min	57843.3296	0.0018	AG	EB	1603	-Ir	43
IR Cnc	min	57844.4084	0.0012	AG	EB	1603	-Ir	44
IT Cnc	min	57843.4160	0.0005	AG	EW	1603	-Ir	43
IT Cnc	min	57844.3275	0.0011	AG	EW	1603	-Ir	39
IW Cnc	max	57833.4514	0.0010	MS	RRAB	16803	V	72
KM Cnc	min	57843.3462	0.0004	AG	EW	1603	-Ir	43
KM Cnc	min	57844.4190	0.0008	AG	EW	1603	-Ir	44
KQ Cnc	max	57776.4180	0.0013	MZ	RRAB	ST7	-Ir	110
KQ Cnc	max	57844.4930	0.0010	AG	RRAB	1603	-Ir	42
KS Cnc	max	57812.4770	0.0010	AG	RRAB	1603	-Ir	76
KS Cnc	max	57854.3844	0.0010	MS	RRAB	16803	V	108
KY Cnc	min	57815.3701	0.0009	AG	EA	1603	-Ir	40
LQ Cnc	max	57462.3695	0.0040	MZ	RRC	ST7	-Ir	152
LQ Cnc	max	57464.3992	0.0040	MZ	RRC	ST7	-Ir	179
LU Cnc	min	57775.4306	0.0003	RATRCR	EW	1600	V	74
LU Cnc	min	57823.5575	0.0003	RATRCR	EW	1600	V	95
MN Cnc	min	57812.3393	0.0003	AG	EW	1603	-Ir	72
MN Cnc	min	57812.4752	0.0008	AG	EW	1603	-Ir	72
W CVn	max	57839.3490	0.0010	AG	RRAB	1603	-Ir	54
RR CVn	max	57836.3710	0.0010	AG	RRAB	1603	-Ir	30
RU CVn	max	57855.4970	0.0010	AG	RRAB	1603	-Ir	25
RV CVn	min	57855.4339	0.0009	AG	EW	1603	-Ir	39
RZ CVn	max	57840.4120	0.0010	AG	RRAB	1603	-Ir	45
ST CVn	max	57840.3300	0.0010	AG	RRC	1603	-Ir	44
ST CVn	max	57855.4610	0.0020	AG	RRC	1603	-Ir	39
UV CVn	max	57825.4960	0.0010	AG	RRAB	1603	-Ir	47
UW CVn	min	57825.4731	0.0015	AG	EW	1603	-Ir	48
UW CVn	min	57825.6161	0.0023	AG	EW	1603	-Ir	48
VZ CVn	min	57838.4917	0.0007	AG	EA	1603	-Ir	49
XZ CVn	max	57855.4670	0.0020	AG	RRC	1603	-Ir	35
YZ CVn	min	57874.4518	0.0018	AG	EA	1603	-Ir	84
AT CVn	max	57800.5110	0.0050	AG	RRC	1603	-Ir	82
AT CVn	max	57836.3420	0.0020	AG	RRC	1603	-Ir	48
AT CVn	max	57853.5240	0.0020	AG	RRC	1603	-Ir	55
BI CVn	min	57825.4265	0.0010	AG	EW	1603	-Ir	54
BI CVn	min	57825.6156	0.0022	AG	EW	1603	-Ir	54
BI CVn	min	57829.4586	0.0008	AG	EW	1603	-Ir	53
BI CVn	min	57829.6504	0.0019	AG	EW	1603	-Ir	53
BO CVn	min	57836.4188	0.0009	AG	EW	1603	-Ir	38
BO CVn	min	57838.4892	0.0009	AG	EW	1603	-Ir	49
CI CVn	min	57825.5548	0.0018	AG	EA	1603	-Ir	56
CI CVn	min	57829.6344	0.0013	AG	EA	1603	-Ir	55
DF CVn	min	57815.3716	0.0013	AG	EW	1603	-Ir	37
DF CVn	min	57815.5299	0.0035	AG	EW	1603	-Ir	37
DF CVn	min	57842.3347	0.0000	AG	EW	1603	-Ir	40
DF CVn	min	57842.5011	0.0015	AG	EW	1603	-Ir	40
DF CVn	min	57853.4502	0.0005	AG	EW	1603	-Ir	56
DF CVn	min	57853.6165	0.0004	AG	EW	1603	-Ir	56
DH CVn	min	57836.4799	0.0007	AG	EW	1603	-Ir	29
DI CVn	min	57836.3955	0.0030	AG	EW	1603	-Ir	29
DI CVn	min	57836.5484	0.0079	AG	EW	1603	-Ir	29
DK CVn	min	57842.5162	0.0025	AG	EA	1603	-Ir	40
DK CVn	min	57853.4049	0.0004	AG	EA	1603	-Ir	56
DL CVn	min	57842.5454	0.0020	AG	EB	1603	-Ir	41
DN CVn	max	57800.4210	0.0050	AG	RRC	1603	-Ir	82
DN CVn	max	57836.3450	0.0010	AG	RRC	1603	-Ir	30
DN CVn	max	57853.3330	0.0020	AG	RRC	1603	-Ir	49
DQ CVn	min	57842.4977	0.0032	AG	EW	1603	-Ir	40
DQ CVn	min	57853.5475	0.0022	AG	EW	1603	-Ir	56
DR CVn	min	57842.3486	0.0006	AG	EW	1603	-Ir	41
DR CVn	min	57842.5248	0.0010	AG	EW	1603	-Ir	41
DR CVn	min	57853.3835	0.0015	AG	EW	1603	-Ir	56
DR CVn	min	57853.5401	0.0012	AG	EW	1603	-Ir	56
DR CVn	min	57782.6285	0.0003	RATRCR	EW	1600	V	164
DS CVn	max	57842.4210	0.0010	AG	RRAB	1603	-Ir	38

Table 1: cont.

Variable	Ext	HJD 24.....	±	Obs	Type	Cam	Fil	n
DS CVn	max	57853.5510	0.0010	AG	RRAB	1603	-Ir	56
DX CVn	min	57842.3955	0.0006	AG	EW	1603	-Ir	40
DX CVn	min	57842.5733	0.0009	AG	EW	1603	-Ir	40
DY CVn	min	57842.3567	0.0008	AG	EW	1603	-Ir	43
DY CVn	min	57842.4800	0.0016	AG	EW	1603	-Ir	43
DY CVn	min	57842.6027	0.0010	AG	EW	1603	-Ir	43
EF CVn	min	57825.3902	0.0006	AG	EW	1603	-Ir	48
EF CVn	min	57825.5262	0.0010	AG	EW	1603	-Ir	48
EF CVn	min	57825.6612	0.0017	AG	EW	1603	-Ir	48
EH CVn	min	57825.4339	0.0011	AG	EW	1603	-Ir	48
EH CVn	min	57825.5673	0.0016	AG	EW	1603	-Ir	48
EH CVn	min	57840.5910	0.0041	AG	EW	1603	-Ir	45
EH CVn	min	57855.3529	0.0020	AG	EW	1603	-Ir	40
EH CVn	min	57855.4817	0.0029	AG	EW	1603	-Ir	40
EI CVn	min	57855.4649	0.0029	AG	EW	1603	-Ir	35
EN CVn	min	57825.3766	0.0016	AG	EA	1603	-Ir	54
EO CVn	min	57810.4088	0.0002	AG	EW	1603	-Ir	46
EO CVn	min	57780.6252	0.0005	RATRCR	EW	1600	V	168
EX CVn	min	57842.4406	0.0003	AG	EW	1603	-Ir	41
EX CVn	min	57842.5799	0.0014	AG	EW	1603	-Ir	41
EY CVn	min	57842.4269	0.0010	AG	EW	1603	-Ir	41
EY CVn	min	57842.6064	0.0017	AG	EW	1603	-Ir	41
FO CVn	max	57842.3620	0.0010	AG	RRC	1603	-Ir	50
FO CVn	max	57844.3680	0.0030	AG	RRC	1603	-Ir	42
FO CVn	max	57846.3620	0.0030	AG	RRC	1603	-Ir	44
FQ CVn	min	57825.4531	0.0008	AG	EW	1603	-Ir	48
FQ CVn	min	57825.6395	0.0015	AG	EW	1603	-Ir	48
FQ CVn	min	57840.4831	0.0029	AG	EW	1603	-Ir	45
FQ CVn	min	57855.5047	0.0016	AG	EW	1603	-Ir	40
FU CVn	min	57844.4779	0.0003	RATRCR	EW	1600	V	127
FV CVn	min	57825.4518	0.0009	AG	EW	1603	-Ir	48
FV CVn	min	57825.6108	0.0009	AG	EW	1603	-Ir	48
GG CVn	min	57825.3573	0.0004	AG	EW	1603	-Ir	48
GG CVn	min	57825.5494	0.0010	AG	EW	1603	-Ir	48
GM CVn	min	57825.4286	0.0010	AG	EW	1603	-Ir	48
GM CVn	min	57825.6115	0.0007	AG	EW	1603	-Ir	48
UZ CMi	min	57800.4756	0.0031	AG	EW	1603	-Ir	44
UZ CMi	min	57811.5004	0.0017	AG	EW	1603	-Ir	40
XZ CMi	min	57800.5071	0.0016	AG	EB	1603	-Ir	45
XZ CMi	min	57811.5041	0.0051	AG	EB	1603	-Ir	40
YY CMi	min	57798.5512	0.0019	AG	EB	1603	-Ir	47
AD CMi	max	57811.3580	0.0010	AG	DSCT	1603	-Ir	37
AD CMi	max	57811.4830	0.0020	AG	DSCT	1603	-Ir	37
AK CMi	min	57800.5485	0.0025	AG	EA	1603	-Ir	41
AM CMi	min	57782.3941	0.0008	RATRCR	EB	1600	V	107
BB CMi	min	57800.3015	0.0005	AG	EB	1603	-Ir	44
BB CMi	min	57811.3968	0.0014	AG	EB	1603	-Ir	40
BF CMi	min	57800.4321	0.0019	AG	EA	1603	-Ir	40
BH CMi	min	57798.4112	0.0016	AG	EW	1603	-Ir	47
BX CMi	min	57773.3864	0.0001	RATRCR	EA	1600	V	84
CW CMi	min	57798.2811	0.0020	AG	EW	1603	-Ir	45
CW CMi	min	57798.4401	0.0015	AG	EW	1603	-Ir	45
FM CMi	min	57811.3414	0.0024	AG	EB	1603	-Ir	37
TV Cas	min	57968.5047	0.0006	AG	EA	1603	-Ir	40
XX Cas	min	57982.5458	0.0024	AG	EA	1603	-Ir	37
ZZ Cas	min	57980.3842	0.0046	AG	EB	1603	-Ir	34
AB Cas	min	57989.4152	0.0008	AG	EA+DSCTC	1603	-Ir	38
AH Cas	min	57780.6227	0.0003	SCI	EA	ST7		71
BS Cas	min	57799.3145	0.0002	SCI	EW	ST7	o	123
BS Cas	min	57800.4156	0.0001	SCI	EW	ST7	o	145
BS Cas	min	57800.6372	0.0001	SCI	EW	ST7	o	145
BU Cas	min	57982.4309	0.0023	AG	EA	1603	-Ir	35
EG Cas	min	57982.5590	0.0012	AG	EB	1603	-Ir	36
GG Cas	min	57995.3663	0.0025	AG	EA	1603	-Ir	41
GU Cas	min	58018.3748	0.0020	AG	EA	1603	-Ir	56
IR Cas	min	57995.3267	0.0010	AG	EB	1603	-Ir	42
IT Cas	min	58018.4616	0.0005	AG	EA+DSCTC:	1603	-Ir	57
MN Cas	min	57995.4479	0.0020	AG	EA	1603	-Ir	40
OX Cas	min	58005.5571	0.0029	AG	EA	1603	-Ir	50
PS Cas	max	57995.4510	0.0020	AG	RRAB	1603	-Ir	42
PV Cas	min	57939.5323	0.0012	AG	EA	1603	-Ir	26

Table 1: cont.

Variable	Ext	HJD 24.....	±	Obs	Type	Cam	Fil	n
PV Cas	min	57968.3821	0.0019	AG	EA	1603	-Ir	40
V0364 Cas	min	58019.3677	0.0006	AG	EA	1603	-Ir	34
V0375 Cas	min	57800.4204	0.0030	BRW	EB	383L+	V	208
V0375 Cas	min	57982.3908	0.0306	AG	EB	1603	-Ir	35
V0380 Cas	min	58001.4595	0.0009	AG	EA	1603	-Ir	44
V0380 Cas	min	58005.5349	0.0018	AG	EA	1603	-Ir	50
V0381 Cas	min	57980.4319	0.0007	AG	EA	1603	-Ir	33
V0389 Cas	min	58018.3254	0.0015	AG	EA	1603	-Ir	55
V0396 Cas	min	58005.4942	0.0012	AG	EA	1603	-Ir	50
V0459 Cas	min	57987.4172	0.0006	AG	EA	1603	-Ir	44
V0523 Cas	min	57995.4404	0.0011	AG	EW	1603	-Ir	41
V0523 Cas	min	57995.5562	0.0005	AG	EW	1603	-Ir	41
V0608 Cas	min	57989.4971	0.0010	AG	EW	1603	-Ir	38
V0646 Cas	min	57989.4811	0.0161	AG	EB	1603	-Ir	37
V1014 Cas	min	58018.4356	0.0020	AG	EB	1603	-Ir	48
V1107 Cas	min	57982.3807	0.0018	AG	EW	1603	-Ir	31
V1107 Cas	min	57982.5177	0.0027	AG	EW	1603	-Ir	31
V1139 Cas	min	57995.4774	0.0024	AG	EW	1603	-Ir	42
U Cep	min	57919.5056	0.0013	AG	EA/SD	1603	-Ir	24
RZ Cep	max	58001.3770	0.0010	AG	RRC	1603	-Ir	44
SU Cep	min	57939.4114	0.0015	AG	EB/KE	1603	-Ir	26
VW Cep	min	57841.3398	0.0016	AG	EW/KW	1603	-Ir	50
VW Cep	min	57841.4762	0.0021	AG	EW/KW	1603	-Ir	50
VW Cep	min	57841.6199	0.0012	AG	EW/KW	1603	-Ir	50
VZ Cep	min	58005.3961	0.0020	AG	EA	1603	-Ir	48
WY Cep	min	57901.4589	0.0008	AG	EB/KE:	1603	-Ir	31
XX Cep	min	57926.5129	0.0021	AG	EA/SD	1603	-Ir	22
XY Cep	min	57988.5233	0.0006	AG	EA/SD	1603	-Ir	43
XZ Cep	min	57901.4479	0.0025	AG	EB/DM:	1603	-Ir	31
ZZ Cep	min	57895.4360	0.0043	AG	EA/DM	1603	-Ir	27
AH Cep	min	57923.5087	0.0075	AG	EB/DM	1603	-Ir	25
BE Cep	min	57608.4134	0.0001	RATRCR	EW/KW	1600	V	167
BE Cep	min	57909.5214	0.0030	AG	EW/KW	1603	-Ir	24
BE Cep	min	57966.3895	0.0008	AG	EW/KW	1603	-Ir	27
DL Cep	min	57655.4957	0.0002	RATRCR	EB/DM	1600	V	164
EG Cep	min	57841.3551	0.0014	AG	EB	1603	-Ir	47
EG Cep	min	57841.6263	0.0008	AG	EB	1603	-Ir	47
EG Cep	min	57843.5329	0.0016	AG	EB	1603	-Ir	45
EG Cep	min	57973.4243	0.0006	AG	EB	1603	-Ir	38
EK Cep	min	57909.4107	0.0013	AG	EA/DM	1603	-Ir	26
GK Cep	min	57901.5121	0.0008	AG	EB/KE	1603	-Ir	32
GK Cep	min	58005.4287	0.0013	AG	EB/KE	1603	-Ir	46
GS Cep	min	57928.4608	0.0014	AG	EB/KE	1603	-Ir	25
KV Cep	min	57988.3420	0.0013	AG	EB	1603	-Ir	42
NN Cep	min	57923.4423	0.0031	AG	EA/DM	1603	-Ir	25
NW Cep	min	57988.4768	0.0009	AG	EA/SD:	1603	-Ir	43
V0338 Cep	min	57917.4804	0.0006	AG	EA	1603	-Ir	24
V0383 Cep	min	57940.5065	0.0045	AG	EB	1603	-Ir	27
V0397 Cep	min	57901.4068	0.0033	AG	EA	1603	-Ir	30
V0397 Cep	min	57926.4502	0.0027	AG	EA	1603	-Ir	22
V0736 Cep	min	57923.4190	0.0042	AG	EW	1603	-Ir	25
V0743 Cep	min	57988.2286	0.0036	AG	EA	1603	-Ir	91
V0746 Cep	min	57923.4906	0.0016	AG	EA	1603	-Ir	25
V0797 Cep	min	57727.3903	0.0020	RATRCR	EW	1600	V	25
V0806 Cep	min	57752.4983	0.0003	RATRCR	EA	1600	V	262
V0833 Cep	min	57899.4470	0.0035	AG	EB	1603	-Ir	24
V0849 Cep	min	58005.3999	0.0013	AG	EA	1603	-Ir	46
V0870 Cep	min	57909.4281	0.0015	AG	EW	1603	-Ir	26
V0886 Cep	min	58001.3307	0.0022	AG	EA	1603	-Ir	63
V0890 Cep	min	57909.4172	0.0018	AG	EA	1603	-Ir	28
V0900 Cep	min	57928.5113	0.0037	AG	EA	1603	-Ir	25
V0902 Cep	min	57579.4673	0.0005	RATRCR	EW	1600	V	86
V0902 Cep	min	57706.3471	0.0007	RATRCR	EW	1600	V	98
V0919 Cep	min	57642.5242	0.0004	RATRCR	EA	1600	V	207
V0919 Cep	min	57980.5125	0.0009	AG	EA	1603	-Ir	33
V0919 Cep	min	58005.5159	0.0017	AG	EA	1603	-Ir	50
V0927 Cep	min	57987.3661	0.0025	AG	EA	1603	-Ir	44
V0930 Cep	min	57987.4165	0.0019	AG	EW	1603	-Ir	44
V0934 Cep	min	57987.5234	0.0022	AG	EW	1603	-Ir	39
V0944 Cep	min	57989.5029	0.0008	AG	EA	1603	-Ir	36
V0954 Cep	min	57988.5292	0.0022	AG	EB	1603	-Ir	43

Table 1: cont.

Variable	Ext	HJD 24.....	±	Obs	Type	Cam	Fil	n
V0959 Cep	min	57988.5226	0.0017	AG	EW	1603	-Ir	43
V0960 Cep	min	57988.3629	0.0030	AG	EW	1603	-Ir	41
V0960 Cep	min	57988.5294	0.0017	AG	EW	1603	-Ir	41
V0961 Cep	min	57988.5119	0.0007	AG	EA	1603	-Ir	43
V1013 Cep	min	57966.5622	0.0011	AG	EW	1603	-Ir	27
U Com	max	57838.5980	0.0020	AG	RRC	1603	-Ir	45
RW Com	min	57838.4379	0.0013	AG	EW/KW	1603	-Ir	47
RW Com	min	57838.5566	0.0010	AG	EW/KW	1603	-Ir	47
RZ Com	min	57836.4206	0.0012	AG	EW/KW	1603	-Ir	36
RZ Com	min	57842.3444	0.0009	AG	EW/KW	1603	-Ir	47
RZ Com	min	57842.5132	0.0008	AG	EW/KW	1603	-Ir	47
SS Com	min	57775.5845	0.0002	RATRCR	EW/KW	1600	V	158
SU Com	max	57815.3850	0.0020	AG	RRAB	1603	-Ir	42
TU Com	max	57836.4620	0.0010	AG	RRAB	1603	-Ir	30
UX Com	min	57842.4477	0.0100	AG	EA/AR/RS	1603	-Ir	43
VY Com	min	57811.6077	0.0029	AG	EB/KE	1603	-Ir	58
AG Com	max	57852.4490	0.0020	AG	RRC	1603	-Ir	41
BL Com	max	57839.6390	0.0010	AG	RRAB	1603	-Ir	40
BO Com	max	57839.4320	0.0010	AG	RRAB	1603	-Ir	41
BU Com	max	57839.5440	0.0010	AG	RRC	1603	-Ir	41
BV Com	max	57811.5750	0.0010	AG	RRAB	1603	-Ir	58
BW Com	max	57815.3690	0.0050	AG	RRAB	1603	-Ir	53
CC Com	min2	57839.3723	0.0005	RATRCR	EW/KW	1600	V	44
CE Com	max	57815.4730	0.0020	AG	RRC	1603	-Ir	33
CK Com	max	57810.3680	0.0010	AG	RRAB	1603	-Ir	44
CK Com	max	57800.6480	0.0010	AG	RRAB	1603	-Ir	85
CK Com	max	57853.4380	0.0010	AG	RRAB	1603	-Ir	56
CM Com	min	57852.5754	0.0017	AG	E	1603	-Ir	41
CN Com	min	57839.4949	0.0020	AG	EB	1603	-Ir	54
CU Com	max	57852.4220	0.0020	AG	RRAB	1603	-Ir	41
CW Com	max	57852.3350	0.0050	AG	RRC	1603	-Ir	40
CY Com	max	57852.5180	0.0020	AG	RRAB	1603	-Ir	39
CZ Com	max	57852.4600	0.0030	AG	RRC	1603	-Ir	40
DD Com	min	57852.3319	0.0022	AG	EW/KW	1603	-Ir	40
DD Com	min	57852.4673	0.0029	AG	EW/KW	1603	-Ir	40
DD Com	min	57852.5979	0.0026	AG	EW/KW	1603	-Ir	40
DG Com	min	57852.3363	0.0006	AG	EB/SD	1603	-Ir	40
DK Com	max	57852.5200	0.0010	AG	RRAB	1603	-Ir	40
HY Com	max	57839.4330	0.0010	AG	RRC	1603	-Ir	54
LQ Com	min	57852.3162	0.0004	AG	EW	1603	-Ir	41
LQ Com	min	57852.4966	0.0015	AG	EW	1603	-Ir	41
LR Com	min	57836.4298	0.0020	AG	EA	1603	-Ir	37
LT Com	min	57844.4846	0.0014	AG	EB	1603	-Ir	39
LT Com	min	57867.5260	0.0022	AG	EB	1603	-Ir	44
MZ Com	min	57842.4489	0.0000	AG	EA/RS	1603	-Ir	47
U CrB	min	57846.5686	0.0018	AG	EA/SD	1603	-Ir	44
RT CrB	min	57855.5058	0.0027	AG	EA/AR:/RS	1603	-Ir	40
RW CrB	min	57852.5470	0.0031	AG	EA/SD:	1603	-Ir	50
TV CrB	max	57855.4990	0.0020	AG	RRAB	1603	-Ir	37
TW CrB	min	57853.5726	0.0012	AG	EB/KE	1603	-Ir	35
TW CrB	min	57874.4784	0.0006	AG	EB/KE	1603	-Ir	39
YY CrB	min	57846.5164	0.0008	AG	EW	1603	-Ir	41
YY CrB	min	57852.3524	0.0008	AG	EW	1603	-Ir	51
YY CrB	min	57852.5418	0.0003	AG	EW	1603	-Ir	51
AR CrB	min	57853.5266	0.0009	AG	EW	1603	-Ir	35
AR CrB	min	57874.3857	0.0008	AG	EW	1603	-Ir	39
AR CrB	min	57874.5849	0.0010	AG	EW	1603	-Ir	39
BR CrB	min	57846.5649	0.0080	AG	EW	1603	-Ir	41
WW Cyg	min	57902.4866	0.0008	AG	EA/SD	1603	-Ir	23
WZ Cyg	min	57902.4672	0.0016	AG	EB/K:	1603	-Ir	22
XX Cyg	min	57966.4173	0.0009	ALH	SXPHE	3200M	V	550
XX Cyg	max	57966.4485	0.0004	ALH	SXPHE	3200M	V	550
XX Cyg	min	57966.5520	0.0010	ALH	SXPHE	3200M	V	550
XX Cyg	max	57966.5836	0.0005	ALH	SXPHE	3200M	V	550
ZZ Cyg	min	57899.4943	0.0010	AG	EA/SD	1603	-Ir	23
BO Cyg	min	57644.4812	0.0003	RATRCR	EA/DM	1600	V	198
BR Cyg	min	57891.3617	0.0010	AG	EA/SD	1603	-Ir	34
CG Cyg	min	57909.4262	0.0013	AG	EA/SD/RS	1603	-Ir	25
CV Cyg	min	57902.5249	0.0010	AG	EW/DW	1603	-Ir	25
DK Cyg	min	57968.5129	0.0004	AG	EW/D	1603	-Ir	40
DL Cyg	min	57989.4886	0.0014	AG	EA/DM	1603	-Ir	37

Table 1: cont.

Variable	Ext	HJD 24.....	±	Obs	Type	Cam	Fil	n
GO Cyg	min	57909.5230	0.0010	AG	EB/KE	1603	-Ir	26
KR Cyg	min	57924.4177	0.0002	AG	EB	1603	-Ir	33
KR Cyg	min	57926.5294	0.0058	AG	EB	1603	-Ir	22
KR Cyg	min2	57260.5559	0.0010	FR	EB	1603	-Ir	349
MR Cyg	min	57988.4256	0.0005	AG	EA/SD	1603	-Ir	43
V0345 Cyg	min	57240.5923	0.0010	FR	EA/DM	1603	-Ir	295
V0345 Cyg	min	57952.5180	0.0005	FR	EA/DM	1603	-Ir	144
V0382 Cyg	min	57968.4790	0.0007	AG	EB	1603	-Ir	40
V0388 Cyg	min	57966.5260	0.0007	AG	EB/KE:	1603	-Ir	32
V0388 Cyg	min	57988.4333	0.0022	AG	EB/KE:	1603	-Ir	36
V0401 Cyg	min	57891.4771	0.0019	AG	EW/KE	1603	-Ir	28
V0401 Cyg	min	57912.4588	0.0019	AG	EW/KE	1603	-Ir	26
V0442 Cyg	min	57988.5716	0.0020	AG	EA	1603	-Ir	42
V0443 Cyg	min	57900.5393	0.0057	AG	EA	1603	-Ir	26
V0445 Cyg	min	57562.4491	0.0002	RATRCR	EA/SD	1600	V	132
V0445 Cyg	min	57638.4121	0.0002	RATRCR	EA/SD	1600	V	222
V0448 Cyg	min	57989.5281	0.0100	AG	EB/SD	1603	-Ir	55
V0453 Cyg	min	57966.4797	0.0026	AG	EA/D	1603	-Ir	32
V0456 Cyg	min	57900.5306	0.0011	AG	EA/SD:	1603	-Ir	27
V0456 Cyg	min	57982.5203	0.0006	AG	EA/SD:	1603	-Ir	37
V0463 Cyg	min	57913.4979	0.0022	AG	EA/DM	1603	-Ir	27
V0466 Cyg	min	57891.5290	0.0008	AG	EA	1603	-Ir	28
V0466 Cyg	min	57912.4029	0.0014	AG	EA	1603	-Ir	26
V0477 Cyg	min	57917.4794	0.0034	AG	EA/DM	1603	-Ir	30
V0477 Cyg	min	57924.5168	0.0019	AG	EA/DM	1603	-Ir	35
V0477 Cyg	min	57928.5091	0.0010	AG	EA/DM	1603	-Ir	25
V0477 Cyg	min	57964.4145	0.0014	AG	EA/DM	1603	-Ir	40
V0477 Cyg	min	57982.4904	0.0013	AG	EA/DM	1603	-Ir	35
V0478 Cyg	min	57924.4632	0.0013	AG	EA/DM	1603	-Ir	34
V0478 Cyg	min	57973.4339	0.0026	AG	EA/DM	1603	-Ir	38
V0483 Cyg	min	57982.4920	0.0061	AG	EB/DM	1603	-Ir	35
V0488 Cyg	min	57224.4557	0.0005	FR	EB/DW	red	-Ir	115
V0488 Cyg	min2	57952.5622	0.0009	FR	EB/DW	1603	-Ir	235
V0490 Cyg	min	57982.4061	0.0036	AG	EB	1603	-Ir	34
V0493 Cyg	min	57980.3974	0.0002	SCI	EA/KE:	ST7	o	51
V0498 Cyg	min	57902.4700	0.0036	AG	EA/DM	1603	-Ir	23
V0541 Cyg	min	57919.4069	0.0048	AG	EA/DM	1603	-Ir	25
V0541 Cyg	min	57926.4415	0.0007	AG	EA/DM	1603	-Ir	22
V0548 Cyg	min	57887.4487	0.0014	AG	EA/SD:	1603	-Ir	25
V0680 Cyg	min	57917.4864	0.0023	AG	EB/KE	1603	-Ir	29
V0687 Cyg	min	57992.3638	0.0018	AG	EA/SD:	1603	-Ir	36
V0700 Cyg	min	57982.5920	0.0028	AG	EW/KW	1603	-Ir	33
V0725 Cyg	min2	57260.4352	0.0004	FR	EA/KE:	1603	-Ir	343
V0725 Cyg	min2	57939.3866	0.0015	FR	EA/KE:	1603	-Ir	206
V0725 Cyg	min2	57952.5491	0.0015	FR	EA/KE:	1603	-Ir	242
V0728 Cyg	min	57923.4141	0.0017	AG	EA/SD:	1603	-Ir	24
V0753 Cyg	min	57913.4194	0.0007	AG	EA	1603	-Ir	27
V0787 Cyg	min	57895.4737	0.0006	AG	EA	1603	-Ir	27
V0796 Cyg	min	57884.4103	0.0021	AG	EA	1603	-Ir	44
V0796 Cyg	min	57901.5024	0.0007	AG	EA	1603	-Ir	31
V0796 Cyg	min	57912.5432	0.0044	AG	EA	1603	-Ir	27
V0796 Cyg	min	57918.4662	0.0013	AG	EA	1603	-Ir	30
V0796 Cyg	min	57924.3905	0.0021	AG	EA	1603	-Ir	35
V0796 Cyg	min	57952.5274	0.0016	AG	EA	1603	-Ir	34
V0828 Cyg	min	57928.4247	0.0059	AG	EB/DM	1603	-Ir	25
V0836 Cyg	min	57918.4894	0.0017	AG	EB/KE	1603	-Ir	25
V0885 Cyg	min	57891.4920	0.0033	AG	EB/DM	1603	-Ir	28
V0909 Cyg	min	57979.4777	0.0011	NWR	EA/DM	16IC	o	455
V1011 Cyg	min2	57924.4929	0.0028	FR	EA/D	1603	-Ir	48
V1034 Cyg	min	57926.5446	0.0001	AG	EB/SD:	1603	-Ir	22
V1034 Cyg	min2	57952.4455	0.0010	FR	EB/SD:	1603	-Ir	243
V1061 Cyg	min	57902.4870	0.0027	AG	EA/D	1603	-Ir	25
V1073 Cyg	min	57924.4154	0.0013	AG	EW/KE	1603	-Ir	34
V1083 Cyg	min	57926.4775	0.0019	AG	EB/DM	1603	-Ir	22
V1143 Cyg	min	57912.5159	0.0074	AG	EA/DM	1603	-Ir	27
V1171 Cyg	min	57924.5098	0.0019	AG	EA/KE:	1603	-Ir	35
V1171 Cyg	min	57924.5092	0.0005	FR	EA/KE:	1603	-Ir	134
V1305 Cyg	min	57940.5449	0.0001	SCI	EB/KE:	ST7	o	132
V1356 Cyg	min	57912.4009	0.0015	AG	EB/DM	1603	-Ir	26
V1413 Cyg	min	57989.5240	0.0087	AG	E	1603	-Ir	36
V1823 Cyg	min	57989.4055	0.0014	AG	RRAB	1603	-Ir	35

Table 1: cont.

Variable	Ext	HJD 24.....	±	Obs	Type	Cam	Fil	n
V1823 Cyg	min	58011.4071	0.0009	AG	RRAB	1603	-Ir	25
V1877 Cyg	min	57988.4312	0.0037	AG	E:	1603	-Ir	40
V1918 Cyg	min2	57657.3341	0.0002	RATRCR	EW/KW	1600	V	92
V1962 Cyg	max	57980.3838	0.0010	MZ	RRAB	ST7	-Ir	76
V1962 Cyg	max	58014.4442	0.0013	MZ	RRAB	ST7	-Ir	118
V1962 Cyg	max	58039.3413	0.0010	MZ	RRAB	ST7	-Ir	101
V1962 Cyg	max	58041.3756	0.0008	MZ	RRAB	ST7	-Ir	147
V1962 Cyg	max	58044.4241	0.0008	MZ	RRAB	ST7	-Ir	104
V2021 Cyg	min	57988.3368	0.0008	AG	EA	1603	-Ir	44
V2080 Cyg	min	57901.5134	0.0031	AG	EA	1603	-Ir	32
V2083 Cyg	min	57924.4965	0.0013	AG	EA	1603	-Ir	35
V2083 Cyg	min	57952.5070	0.0011	AG	EA	1603	-Ir	34
V2181 Cyg	min2	57240.4399	0.0003	FR	E	1603	-Ir	288
V2181 Cyg	min2	57260.5031	0.0004	FR	E	1603	-Ir	339
V2181 Cyg	min2	57939.5082	0.0008	FR	E	1603	-Ir	141
V2181 Cyg	min	57952.4127	0.0002	FR	E	1603	-Ir	236
V2197 Cyg	min	57922.4492	0.0013	AG	E	1603	-Ir	20
V2240 Cyg	min	58018.4136	0.0030	SCI	EW	ST7	o	108
V2278 Cyg	min	57928.4473	0.0003	SCI	EW	ST7	o	66
V2364 Cyg	min	57913.4375	0.0011	AG	EW	1603	-Ir	27
V2367 Cyg	max	57952.4117	0.0007	ALH	DSCT	3200M	V	510
V2367 Cyg	min	57952.5322	0.0012	ALH	DSCT	3200M	V	510
V2367 Cyg	max	57952.5882	0.0008	ALH	DSCT	3200M	V	510
V2422 Cyg	min	57973.4856	0.0081	AG	EB	1603	-Ir	39
V2455 Cyg	max	58041.3926	0.0035	AGT	DSCT	600D	TG	92
V2455 Cyg	min	58041.3584	0.0035	AGT	DSCT	600D	TG	92
V2456 Cyg	min	57924.5161	0.0015	AG	EB	1603	-Ir	32
V2477 Cyg	min	57891.5168	0.0002	AG	EW	1603	-Ir	33
V2486 Cyg	min	57939.4553	0.0006	AG	EA	1603	-Ir	26
V2497 Cyg	min	57992.5007	0.0029	AG	EW	1603	-Ir	32
V2517 Cyg	min	57913.4227	0.0016	AG	EA	1603	-Ir	27
V2519 Cyg	min	57891.5144	0.0048	AG	EA:	1603	-Ir	34
V2519 Cyg	min	57641.4990	0.0005	RATRCR	EA:	1600	V	196
V2520 Cyg	min	57905.4197	0.0007	AG	EA	1603	-Ir	21
V2520 Cyg	min	57909.4678	0.0016	AG	EA	1603	-Ir	28
V2541 Cyg	min	57940.3957	0.0032	AG	EA	1603	-Ir	25
V2545 Cyg	min	57905.4597	0.0053	AG	EW	1603	-Ir	20
V2545 Cyg	min	57966.5604	0.0027	AG	EW	1603	-Ir	32
V2545 Cyg	min	57988.3477	0.0015	AG	EW	1603	-Ir	36
V2545 Cyg	min	57988.5291	0.0026	AG	EW	1603	-Ir	36
V2546 Cyg	min	57905.5121	0.0001	AG	EW	1603	-Ir	19
V2546 Cyg	min	57966.5434	0.0017	AG	EW	1603	-Ir	32
V2546 Cyg	min	57988.3403	0.0006	AG	EW	1603	-Ir	42
V2549 Cyg	min	57966.5655	0.0020	AG	EA	1603	-Ir	32
V2549 Cyg	min	57988.3709	0.0008	AG	EA	1603	-Ir	36
V2551 Cyg	min	57895.4274	0.0028	AG	EW	1603	-Ir	29
V2551 Cyg	min	57895.5511	0.0053	AG	EW	1603	-Ir	29
V2552 Cyg	min	57901.4001	0.0011	AG	EW	1603	-Ir	31
V2552 Cyg	min	57901.5377	0.0012	AG	EW	1603	-Ir	31
V2558 Cyg	min	57988.3727	0.0014	AG	EA	1603	-Ir	27
V2643 Cyg	min	57919.4572	0.0018	AG	EB	1603	-Ir	23
V2657 Cyg	min	57988.4784	0.0016	AG	EW	1603	-Ir	44
V2702 Cyg	max	57240.4176	0.0008	FR	DSCT	1603	-Ir	304
V2702 Cyg	max	57240.5280	0.0010	FR	DSCT	1603	-Ir	304
V2702 Cyg	max	57260.3322	0.0013	FR	DSCT	1603	-Ir	357
V2702 Cyg	max	57260.4358	0.0010	FR	DSCT	1603	-Ir	357
V2702 Cyg	max	57260.5252	0.0010	FR	DSCT	1603	-Ir	357
V2702 Cyg	max	57260.6229	0.0012	FR	DSCT	1603	-Ir	357
V2702 Cyg	max	57939.4846	0.0010	FR	DSCT	1603	-Ir	154
V2702 Cyg	max	57952.4590	0.0003	FR	DSCT	1603	-Ir	237
V2702 Cyg	max	57952.5561	0.0003	FR	DSCT	1603	-Ir	237
V2703 Cyg	max	57224.4289	0.0010	FR	DSCTC	1603	-Ir	110
V2703 Cyg	max	57240.4524	0.0010	FR	DSCTC	1603	-Ir	291
V2703 Cyg	max	57260.3873	0.0010	FR	DSCTC	1603	-Ir	352
V2703 Cyg	max	57260.4952	0.0008	FR	DSCTC	1603	-Ir	352
V2703 Cyg	max	57939.4060	0.0012	FR	DSCTC	1603	-Ir	164
V2703 Cyg	max	57939.5258	0.0010	FR	DSCTC	1603	-Ir	164
V2703 Cyg	max	57952.5014	0.0010	FR	DSCTC	1603	-Ir	242
W Del	min	58001.6020	0.0009	AG	EA/SD	1603	-Ir	71
TY Del	min	57966.5215	0.0002	AG	EA/SD	1603	-Ir	32
AV Del	min	57966.4865	0.0011	AG	EA/SD	1603	-Ir	32

Table 1: cont.

Variable	Ext	HJD 24.....	±	Obs	Type	Cam	Fil	n
BV Del	max	57980.5880	0.0010	AG	RRAB	1603	-Ir	27
DM Del	min	57995.3839	0.0060	AG	EB/KE	1603	-Ir	39
EG Del	max	57980.5080	0.0020	AG	RRC	1603	-Ir	33
FZ Del	min	57966.4610	0.0015	AG	EA/SD	1603	-Ir	31
FZ Del	min	57968.4140	0.0003	AG	EA/SD	1603	-Ir	40
KO Del	min	57980.4596	0.0009	AG	EA	1603	-Ir	33
LY Del	min	57968.4791	0.0015	AG	EA	1603	-Ir	39
MR Del	min2	57585.4792	0.0002	RATRCR	EA	1600	R	95
MR Del	min	57952.4862	0.0014	AG	EA	1603	-Ir	34
OW Del	min	57968.5590	0.0014	AG	EA	1603	-Ir	38
OZ Del	min	57939.5155	0.0018	AG	EW	1603	-Ir	26
PP Del	min	58001.4952	0.0046	AG	E+RS	1603	-Ir	41
Z Dra	min	57846.4841	0.0000	AG	EA/SD	1603	-Ir	45
RR Dra	min	57926.5035	0.0006	AG	EA/SD	1603	-Ir	22
RW Dra	min	57923.4141	0.0011	ALH	RRAB	3200M	V	467
RW Dra	max	57923.4785	0.0006	ALH	RRAB	3200M	V	467
RX Dra	min	57899.4511	0.0011	AG	EA/DM	1603	-Ir	27
RZ Dra	min	57867.3876	0.0002	AG	EB/SD:	1603	-Ir	43
SW Dra	max	57825.3850	0.0010	AG	RRAB	1603	-Ir	57
TW Dra	min	57843.5019	0.0037	AG	EA/SD	1603	-Ir	45
TZ Dra	min	57873.4945	0.0005	AG	EA/SD	1603	-Ir	28
UZ Dra	min	57909.4109	0.0008	AG	EA/DM	1603	-Ir	28
AI Dra	min	57852.4655	0.0005	AG	EA/SD	1603	-Ir	51
AX Dra	min	57810.4075	0.0006	AG	EB	1603	-Ir	34
BE Dra	min	57852.5319	0.0002	RATRCR	EB/KE	1600	V	205
BF Dra	min	57887.4192	0.0030	AG	EA	1603	-Ir	54
BH Dra	min	57891.4238	0.0022	AG	EA/SD:	1603	-Ir	35
BK Dra	min	57964.3843	0.0021	ALH	RRAB	3200M	V	775
BK Dra	max	57964.4650	0.0009	ALH	RRAB	3200M	V	775
BS Dra	min	57879.4868	0.0006	AG	EA/DM	1603	-Ir	35
BU Dra	min	57836.3153	0.0029	AG	EA/SD:	1603	-Ir	38
CV Dra	min	57873.4931	0.0016	AG	IS	1603	-Ir	30
CV Dra	min	57879.3612	0.0018	AG	IS	1603	-Ir	36
FU Dra	min	57829.3795	0.0011	AG	EW	1603	-Ir	53
FU Dra	min	57829.5316	0.0008	AG	EW	1603	-Ir	53
FX Dra	min	57840.5773	0.0010	AG	EB	1603	-Ir	43
FX Dra	min	57852.4167	0.0012	AG	EB	1603	-Ir	54
GK Dra	min	57840.4139	0.0034	AG	EA	1603	-Ir	46
GM Dra	min	57841.4925	0.0023	AG	EW	1603	-Ir	39
GQ Dra	min	57867.5560	0.0007	AG	EB	1603	-Ir	44
HI Dra	min	57867.5546	0.0012	AG	RRC	1603	-Ir	43
HP Dra	min	57891.3860	0.0006	AG	EA	1603	-Ir	35
LN Dra	min	57867.4876	0.0021	AG	EB	1603	-Ir	44
MW Dra	min	57810.3451	0.0029	AG	EA	1603	-Ir	33
MY Dra	min	57781.5727	0.0002	RATRCR	EA	1600	V	148
OO Dra	min	57776.5471	0.0001	RATRCR	EA+DSCTC	1600	Clear	242
OW Dra	max	57839.5360	0.0010	AG	RRC	1603	-Ir	55
OX Dra	min	57466.3899	0.0015	RATRCR	EA	1600	V	38
V0341 Dra	min	57836.4680	0.0016	AG	EA	1603	-Ir	40
V0341 Dra	min	57425.5176	0.0002	RATRCR	EA	1600	V	182
V0341 Dra	min	57798.5138	0.0001	RATRCR	EA	1600	V	231
V0348 Dra	min	57846.5452	0.0026	AG	EW	1603	-Ir	45
V0349 Dra	min	57846.4561	0.0024	AG	EW	1603	-Ir	45
V0357 Dra	min	57840.5702	0.0016	AG	EW	1603	-Ir	46
V0372 Dra	min	57841.4291	0.0008	AG	EB/RS	1603	-Ir	46
V0374 Dra	min	57873.4503	0.0016	AG	EW	1603	-Ir	30
V0374 Dra	min	57879.5025	0.0020	AG	EW	1603	-Ir	36
V0381 Dra	min	57867.5280	0.0032	AG	EA+DSCTC	1603	-Ir	44
V0388 Dra	min2	57499.4343	0.0004	RATRCR	EB	1600	V	246
V0391 Dra	min	57879.3765	0.0027	AG	EA/RS	1603	-Ir	36
V0404 Dra	min	57874.5277	0.0004	RATRCR	EW	1600	V	119
V0421 Dra	min2	57507.5867	0.0008	RATRCR	EW	1600	V	213
V0423 Dra	min	57884.3848	0.0071	AG	EA	1603	-Ir	48
V0449 Dra	min	57514.4836	0.0004	RATRCR	EW	1600	V	217
S Equ	min	57966.4798	0.0003	AG	EA/SD	1603	-Ir	31
UZ Equ	min	57964.4235	0.0018	AG	EB	1603	-Ir	39
U Gem	min	54826.5025	0.0007	NWR	UGSS+E	16IC		64
U Gem	min	54830.5714	0.0012	NWR	UGSS+E	16IC		1779
U Gem	min	57752.3588	0.0010	NWR	UGSS+E	16IC		148
U Gem	min	57775.3482	0.0002	NWR	UGSS+E	16IC		1713
U Gem	min	57775.5297	0.0009	NWR	UGSS+E	16IC		1713

Table 1: cont.

Variable	Ext	HJD 24.....	±	Obs	Type	Cam	Fil	n
RR Gem	max	57798.5289	0.0040	BRW	RRAB	383L+	V	265
RW Gem	min	57425.2907	0.0001	RATRCR	EA/SD:	1600	V	108
SZ Gem	max	57800.3520	0.0010	AG	RRAB	1603	-Ir	52
SZ Gem	max	57831.4244	0.0040	BRW	RRAB	383L+	V	82
YY Gem	min	57775.3816	0.0001	RATRCR	EA/DM+UV	1600	V	48
AC Gem	min	57760.4006	0.0004	RATRCR	EB/DM:	1600	V	130
AY Gem	min	57811.3790	0.0005	AG	EA/SD:	1603	-Ir	38
V0339 Gem	min	57840.4140	0.0030	BRW	E:	383L+	V	374
V0397 Gem	max	57771.4318	0.0015	MZ	RRC	ST7	-Ir	142
V0397 Gem	max	57798.3815	0.0010	MZ	RRC	ST7	-Ir	120
V0435 Gem	min	54830.5592	0.0015	NWR	EW	16IC		1681
V0435 Gem	min	57752.3848	0.0008	NWR	EW	16IC		147
V0435 Gem	min	57775.4349	0.0008	NWR	EW	16IC		1604
V0437 Gem	min	57799.2903	0.0014	AG	EW	1603	-Ir	42
V0437 Gem	min	57799.4721	0.0008	AG	EW	1603	-Ir	42
RX Her	min	57909.4509	0.0016	AG	EA/DM	1603	-Ir	25
SZ Her	min	57874.4591	0.0005	AG	EA/SD	1603	-Ir	36
TT Her	min	57890.4207	0.0026	AG	EB/KE	1603	-Ir	39
TX Her	min	57855.5812	0.0014	AG	EA/DM	1603	-Ir	37
UX Her	min	57902.4503	0.0004	AG	EA/SD	1603	-Ir	26
UX Her	min	57919.4888	0.0007	JU	EA/SD	ST7	o	68
UX Her	min	57919.4833	0.0004	NWR	EA/SD	16IC	o	596
UX Her	min	57919.4833	0.0004	NWR	EA/SD	16IC	o	0
VZ Her	min	57926.4234	0.0010	ALH	RRAB	3200M	V	460
VZ Her	max	57926.4791	0.0007	ALH	RRAB	3200M	V	460
AK Her	min	57887.5406	0.0028	AG	EW/KW	1603	-Ir	26
AK Her	min	57917.4661	0.0002	SCI	EW/KW	ST7	o	131
CC Her	min	57890.4457	0.0036	AG	EA/SD	1603	-Ir	40
CN Her	max	57867.6565	0.0010	MS	RRAB	16803	V	89
DH Her	min	57912.4250	0.0049	AG	EA/SD	1603	-Ir	24
DY Her	max	57902.3920	0.0020	AG	DSCT	1603	-Ir	24
DY Her	max	57902.5400	0.0020	AG	DSCT	1603	-Ir	24
DY Her	min	57925.3824	0.0014	ALH	DSCT	3200M	V	594
DY Her	max	57925.4243	0.0006	ALH	DSCT	3200M	V	594
DY Her	min	57925.5333	0.0013	ALH	DSCT	3200M	V	594
DY Her	max	57925.5732	0.0007	ALH	DSCT	3200M	V	594
FN Her	min	57902.4650	0.0017	AG	EA/SD:	1603	-Ir	26
FW Her	min	57890.5342	0.0002	SCI	EB/KE	ST7	o	98
HN Her	max	57237.4199	0.0010	MS	RRAB	16803	LUM	88
HS Her	min	57900.4879	0.0033	AG	EA/DM	1603	-Ir	28
IK Her	min	57823.7057	0.0003	MS	EA	16803	V	94
IK Her	min	57524.6563	0.0007	MS	EA	16803	LUM	122
IK Her	min	57855.5892	0.0003	MS	EA	16803	V	134
LS Her	max	57874.4490	0.0010	AG	RRC	1603	-Ir	37
LT Her	min	57902.4898	0.0032	AG	EA/D	1603	-Ir	26
V0338 Her	min	57879.4294	0.0006	AG	EA/SD	1603	-Ir	35
V0342 Her	min	57884.4466	0.0017	AG	EB/SD:	1603	-Ir	40
V0359 Her	min	57879.3532	0.0018	AG	EA/SD	1603	-Ir	36
V0370 Her	max	57493.6161	0.0010	MS	RRAB	16803	V	97
V0370 Her	max	57931.5294	0.0010	MS	RRAB	16803	V	189
V0383 Her	max	57493.6306	0.0010	MS	RRC	16803	V	97
V0383 Her	max	57509.5362	0.0010	MS	RRC	16803	LUM	78
V0450 Her	min	57855.4086	0.0006	AG	EA/D	1603	-Ir	42
V0465 Her	min	57493.6654	0.0008	MS	EA/SD:	16803	V	97
V0465 Her	min	57509.5866	0.0010	MS	EA/SD:	16803	LUM	77
V0465 Her	min	57931.4030	0.0009	MS	EA/SD:	16803	V	190
V0468 Her	max	57509.5771	0.0010	MS	RRAB	16803	LUM	77
V0718 Her	max	57928.5692	0.0010	MS	EW/KW	16803	V	137
V0728 Her	min	57855.5411	0.0025	AG	EW/KW	1603	-Ir	35
V0728 Her	min	57873.4418	0.0011	AG	EW/KW	1603	-Ir	30
V0732 Her	min	57899.4514	0.0004	SCI	EW/KE	ST7	o	48
V0732 Her	min	57919.4333	0.0007	SCI	EW/KE	ST7	o	34
V0842 Her	min	57846.4655	0.0009	AG	EW	1603	-Ir	44
V0842 Her	min	57873.4940	0.0008	AG	EW	1603	-Ir	30
V0878 Her	min	57855.5559	0.0021	AG	EB	1603	-Ir	40
V0920 Her	min	57890.4745	0.0028	AG	E:	1603	-Ir	38
V0994 Her	min	57917.4997	0.0016	AG	EA	1603	-Ir	24
V1017 Her	min	57905.4285	0.0021	AG	EA	1603	-Ir	22
V1045 Her	min	57928.5553	0.0001	MS	EB	16803	V	184
V1049 Her	min	57895.4307	0.0050	AG	EB	1603	-Ir	28
V1049 Her	min	57931.4190	0.0008	MS	EB	16803	V	200

Table 1: cont.

Variable	Ext	HJD 24.....	±	Obs	Type	Cam	Fil	n
V1053 Her	min	57856.6368	0.0001	MS	EW	16803	V	144
V1053 Her	min	57852.6078	0.0001	MS	EW	16803	V	122
V1055 Her	min	57855.4778	0.0019	AG	EW	1603	-Ir	34
V1055 Her	min	57873.4572	0.0011	AG	EW	1603	-Ir	30
V1063 Her	min	57923.4529	0.0044	AG	EA	1603	-Ir	24
V1073 Her	min	57884.4901	0.0007	AG	EW	1603	-Ir	48
V1088 Her	min	57823.6598	0.0006	MS	EW	16803	V	115
V1088 Her	min	57524.4231	0.0003	MS	EW	16803	LUM	123
V1088 Her	min	57524.6018	0.0002	MS	EW	16803	LUM	123
V1088 Her	min	57237.3971	0.0003	MS	EW	16803	LUM	82
V1088 Her	min	57855.6313	0.0007	MS	EW	16803	V	150
V1097 Her	min	57884.4324	0.0006	AG	EW	1603	-Ir	41
V1119 Her	min	57895.4021	0.0036	AG	EB	1603	-Ir	29
V1139 Her	max	57912.3616	0.0006	ALH	SXPHE	3200M	V	352
V1139 Her	min	57912.4007	0.0013	ALH	SXPHE	3200M	V	352
V1139 Her	max	57912.4323	0.0008	ALH	SXPHE	3200M	V	352
V1139 Her	min	57912.4748	0.0015	ALH	SXPHE	3200M	V	352
V1139 Her	max	57912.5031	0.0006	ALH	SXPHE	3200M	V	352
V1139 Her	min	57912.5438	0.0011	ALH	SXPHE	3200M	V	352
V1139 Her	max	57912.5701	0.0006	ALH	SXPHE	3200M	V	352
V1153 Her	min	57873.4830	0.0025	AG	EW	1603	-Ir	30
V1158 Her	min	57879.4099	0.0015	AG	EW:	1603	-Ir	35
V1167 Her	min	57895.4989	0.0011	AG	EW	1603	-Ir	29
V1173 Her	min	57846.4892	0.0015	AG	EW	1603	-Ir	40
V1173 Her	min	57846.6220	0.0013	AG	EW	1603	-Ir	40
V1179 Her	min	57902.4166	0.0019	AG	EW	1603	-Ir	24
V1185 Her	min	57846.5470	0.0021	AG	EW	1603	-Ir	40
V1185 Her	min	57852.4830	0.0006	AG	EW	1603	-Ir	51
V1185 Her	min	57853.3829	0.0021	AG	EW	1603	-Ir	40
V1185 Her	min	57853.5603	0.0036	AG	EW	1603	-Ir	40
V1198 Her	min	57853.5594	0.0012	AG	EW	1603	-Ir	37
V1216 Her	min	57516.4482	0.0002	RATRCR	EW	1600	V	98
V1223 Her	min	57853.5702	0.0036	AG	EW	1603	-Ir	38
V1238 Her	min	57873.5305	0.0004	AG	EW	1603	-Ir	30
V1277 Her	min	57919.5028	0.0021	AG	EB	1603	-Ir	24
V1283 Her	max	57855.5060	0.0020	AG	RRC	1603	-Ir	28
V1289 Her	min	57873.4181	0.0031	AG	EW	1603	-Ir	28
V1289 Her	min	57873.5871	0.0000	AG	EW	1603	-Ir	28
V1298 Her	min	57890.4347	0.0015	AG	EA	1603	-Ir	39
V1321 Her	min	57855.4264	0.0028	AG	EW	1603	-Ir	32
V1321 Her	min	57855.5805	0.0020	AG	EW	1603	-Ir	32
V1321 Her	min	57656.4300	0.0002	RATRCR	EW	1600	V	149
V1331 Her	min	57891.3896	0.0017	AG	EA	1603	-Ir	35
V1351 Her	min	57900.4441	0.0047	AG	EA	1603	-Ir	27
V1355 Her	min	57873.5280	0.0004	RATRCR	EW	1600	V	122
V1355 Her	min	57867.5940	0.0005	MS	EW	16803	V	86
V1379 Her	min	57902.5316	0.0060	AG	EW	1603	-Ir	24
u. Her *)	min	57899.4396	0.0017	AG	EA/SD:	1603	-Ir	25
u. Her *)	min	57900.4716	0.0024	AG	EA/SD:	1603	-Ir	27
UU Hya	max	57837.4049	0.0021	WLH	RRAB	ST10	-IR	63
WY Hya	min	57811.3758	0.0009	AG	EW/KE	1603	-Ir	39
AV Hya	min	57812.3783	0.0016	AG	EB/KE	1603	-Ir	20
DE Hya	min	57800.4136	0.0012	AG	EA/SD	1603	-Ir	48
DF Hya	min	57811.3091	0.0001	AG	EW/KW	1603	-Ir	57
DF Hya	min	57811.4751	0.0010	AG	EW/KW	1603	-Ir	57
DF Hya	min	57841.3942	0.0001	WLH	EW/KW	ST10	-IR	81
DF Hya	min2	57780.3979	0.0002	RATRCR	EW/KW	1600	V	67
FG Hya	min	57811.3823	0.0008	AG	EW/KW	1603	-Ir	41
FG Hya	min	57811.5482	0.0013	AG	EW/KW	1603	-Ir	41
V0409 Hya	min	57812.3215	0.0012	AG	EW	1603	-Ir	22
V0474 Hya	min	57811.3064	0.0013	AG	EB	1603	-Ir	39
SW Lac	min	57968.4409	0.0006	AG	EW/KW	1603	-Ir	40
SW Lac	min	58001.3152	0.0030	AG	EW/KW	1603	-Ir	44
SW Lac	min	58001.4756	0.0003	AG	EW/KW	1603	-Ir	44
SW Lac	min	58019.4369	0.0002	AG	EW/KW	1603	-Ir	35
TW Lac	min	58018.4599	0.0005	AG	EA/SD	1603	-Ir	49
VX Lac	min	57964.4447	0.0003	AG	EA/SD	1603	-Ir	40
VX Lac	min	57980.5624	0.0008	AG	EA/SD	1603	-Ir	33
VX Lac	min	57987.5417	0.0015	AG	EA/SD	1603	-Ir	46
VY Lac	min	57987.3593	0.0011	AG	EB/KE	1603	-Ir	44
AR Lac	min	58018.4598	0.0011	AG	EA/AR/RS	1603	-Ir	46

Table 1: cont.

Variable	Ext	HJD 24.....	±	Obs	Type	Cam	Fil	n
AW Lac	min	57926.5191	0.0016	AG	EB/KE	1603	-Ir	22
CM Lac	min	58019.3260	0.0004	AG	EA/DM	1603	-Ir	32
CM Lac	min	58023.3382	0.0010	AG	EA/DM	1603	-Ir	50
CO Lac	min	57966.4618	0.0007	AG	EA/DM	1603	-Ir	32
CS Lac	min	57952.4773	0.0024	AG	EB/DM	1603	-Ir	34
CZ Lac	max	58018.3480	0.0010	AG	RRAB	1603	-Ir	45
DG Lac	min	57973.4292	0.0009	AG	EA/SD	1603	-Ir	38
DG Lac	min	57995.4934	0.0006	AG	EA/SD	1603	-Ir	41
EM Lac	min	57964.4144	0.0016	AG	EW/KW	1603	-Ir	40
EM Lac	min	57973.3629	0.0040	AG	EW/KW	1603	-Ir	31
EM Lac	min	57973.5569	0.0015	AG	EW/KW	1603	-Ir	31
EM Lac	min	57980.5629	0.0007	AG	EW/KW	1603	-Ir	34
EM Lac	min	57989.5136	0.0031	AG	EW/KW	1603	-Ir	38
EM Lac	min	57995.3512	0.0014	AG	EW/KW	1603	-Ir	42
EM Lac	min	57995.5449	0.0035	AG	EW/KW	1603	-Ir	42
EM Lac	min	58018.3101	0.0015	AG	EW/KW	1603	-Ir	46
EM Lac	min	58018.5056	0.0033	AG	EW/KW	1603	-Ir	46
EP Lac	min	57980.4274	0.0016	AG	EA/SD	1603	-Ir	33
ES Lac	min	57980.4498	0.0059	AG	EA/DM	1603	-Ir	32
ES Lac	min	57989.3616	0.0004	AG	EA/DM	1603	-Ir	38
ES Lac	min	57995.5455	0.0011	AG	EA/DM	1603	-Ir	41
IL Lac	min	57989.4324	0.0020	AG	E	1603	-Ir	37
IM Lac	min	57989.4419	0.0013	AG	EB/KE	1603	-Ir	37
IN Lac	min	57989.3772	0.0352	AG	LB:	1603	-Ir	34
IV Lac	max	57989.4030	0.0020	AG	RRAB	1603	-Ir	33
IZ Lac	min	58018.4312	0.0013	AG	EB/KE	1603	-Ir	48
KZ Lac	max	58017.3873	0.0008	ALH	DSCT	3200M	V	416
KZ Lac	min	58017.4589	0.0018	ALH	DSCT	3200M	V	416
KZ Lac	max	58017.4922	0.0008	ALH	DSCT	3200M	V	416
KZ Lac	min	58017.5630	0.0021	ALH	DSCT	3200M	V	416
KZ Lac	max	58017.5956	0.0009	ALH	DSCT	3200M	V	416
LY Lac	min	57988.3476	0.0003	AG	EA/KE	1603	-Ir	44
MZ Lac	min	57964.3684	0.0041	AG	EA	1603	-Ir	40
NW Lac	min	58018.4054	0.0026	AG	EA/KE	1603	-Ir	43
OZ Lac	min	57966.4327	0.0007	AG	E:	1603	-Ir	32
V0336 Lac	min	58018.3606	0.0041	AG	EA	1603	-Ir	40
V0338 Lac	min	57995.5863	0.0072	AG	EA:	1603	-Ir	42
V0342 Lac	min	57989.3658	0.0021	AG	EW	1603	-Ir	37
V0342 Lac	min	58018.4410	0.0011	AG	EW	1603	-Ir	48
V0344 Lac	min	58018.4050	0.0020	AG	EW/KW	1603	-Ir	48
V0364 Lac	min	58019.4180	0.0010	AG	EA/DM	1603	-Ir	33
V0401 Lac	min	57973.5226	0.0011	AG	EA	1603	-Ir	39
V0401 Lac	min	58005.5812	0.0039	AG	EA	1603	-Ir	48
V0441 Lac	min	57995.4150	0.0010	AG	EW	1603	-Ir	42
V0441 Lac	min	57995.5711	0.0014	AG	EW	1603	-Ir	42
V0457 Lac	min	57987.4712	0.0011	AG	EA	1603	-Ir	46
V0474 Lac	min	57966.5818	0.0006	AG	EB	1603	-Ir	32
V0482 Lac	min	58019.3694	0.0023	AG	EW	1603	-Ir	31
V0482 Lac	min	58023.4635	0.0018	AG	EW	1603	-Ir	50
V0488 Lac	min	58018.3407	0.0036	AG	EW	1603	-Ir	48
V0505 Lac	min	57928.4888	0.0018	AG	EW	1603	-Ir	23
V0505 Lac	min	57987.3473	0.0034	AG	EW	1603	-Ir	44
V0505 Lac	min	57987.5052	0.0014	AG	EW	1603	-Ir	44
V0519 Lac	min	57964.5440	0.0023	AG	E!	1603	-Ir	36
V0519 Lac	min	57980.4218	0.0046	AG	EW	1603	-Ir	32
Y Leo	min	57800.5694	0.0002	AG	EA/SD	1603	-Ir	111
Y Leo	min	57812.3723	0.0007	AG	EA/SD	1603	-Ir	22
RR Leo	max	57811.5060	0.0010	AG	RRAB	1603	-Ir	64
RR Leo	min	57840.4010	0.0014	ALH	RRAB	ST8XM	V	528
RR Leo	max	57840.4609	0.0008	ALH	RRAB	ST8XM	V	528
SS Leo	max	57839.5143	0.0010	BRW	RRAB	383L+	V	133
ST Leo	max	57841.5830	0.0050	AG	RRAB	1603	-Ir	48
ST Leo	max	57831.5326	0.0010	BRW	RRAB	383L+	V	107
UV Leo	min	57829.5093	0.0005	AG	EA/DW	1603	-Ir	49
UX Leo	min	57798.4981	0.0001	SCI	EA/SD:	ST7	o	91
UZ Leo	min	57829.5836	0.0011	AG	EW/KE	1603	-Ir	49
WY Leo	min	57829.3734	0.0002	SCI	EA/D	ST7	o	74
XX Leo	min	57844.5239	0.0013	AG	EB	1603	-Ir	34
XY Leo	min	57812.2807	0.0052	AG	EW/KW	1603	-Ir	28
XY Leo	min	57815.4045	0.0017	AG	EW/KW	1603	-Ir	40
XY Leo	min	57815.5443	0.0030	AG	EW/KW	1603	-Ir	40

Table 1: cont.

Variable	Ext	HJD 24.....	±	Obs	Type	Cam	Fil	n
XY Leo	min	57825.3486	0.0014	AG	EW/KW	1603	-Ir	53
XY Leo	min	57825.4916	0.0013	AG	EW/KW	1603	-Ir	53
XY Leo	min	57799.3529	0.0002	RATRCR	EW/KW	1600	V	93
XZ Leo	min	57815.3072	0.0019	AG	EW/KE	1603	-Ir	35
AG Leo	min	57825.4853	0.0038	AG	EA/D	1603	-Ir	50
AL Leo	min	57825.3801	0.0011	AG	EA/D	1603	-Ir	53
AM Leo	min	57829.4571	0.0022	AG	EW/KW	1603	-Ir	52
AM Leo	min	57829.6410	0.0010	AG	EW/KW	1603	-Ir	52
AP Leo	min	57829.3231	0.0016	AG	EW/KW	1603	-Ir	53
AP Leo	min	57829.5397	0.0012	AG	EW/KW	1603	-Ir	53
BS Leo	max	57811.3820	0.0010	AG	RRAB	1603	-Ir	57
BX Leo	max	57839.3600	0.0010	AG	RRC	1603	-Ir	62
CH Leo	max	57799.4293	0.0015	MZ	RRAB	ST7	-Ir	89
CM Leo	max	57815.4710	0.0010	AG	RRAB	1603	-Ir	50
ET Leo	min2	57829.4094	0.0002	RATRCR	EW:	1600	V	111
EX Leo	min	57843.3549	0.0021	AG	EW	1603	-Ir	42
EX Leo	min	57843.5688	0.0042	AG	EW	1603	-Ir	42
EX Leo	min	57844.3772	0.0022	AG	EW	1603	-Ir	39
EX Leo	min	57844.5769	0.0050	AG	EW	1603	-Ir	39
V LMi	max	57844.5460	0.0010	AG	RRAB	1603	-Ir	39
VW LMi	min	57810.2966	0.0017	AG	EW:	1603	-Ir	33
XX LMi	min	57811.3850	0.0033	AG	EW	1603	-Ir	63
XY LMi	min	57800.4405	0.0025	AG	EW	1603	-Ir	72
XY LMi	min	57800.6626	0.0008	AG	EW	1603	-Ir	72
XY LMi	min	57811.3675	0.0010	AG	EW	1603	-Ir	63
XY LMi	min	57811.5842	0.0009	AG	EW	1603	-Ir	63
AG LMi	min	57799.4106	0.0007	AG	EA	1603	-Ir	65
SZ Lyn	min	57799.3094	0.0012	ALH	DSCT	ST8XM	V	1075
SZ Lyn	max	57799.3477	0.0005	ALH	DSCT	ST8XM	V	1075
SZ Lyn	min	57799.4308	0.0010	ALH	DSCT	ST8XM	V	1075
SZ Lyn	max	57799.4680	0.0006	ALH	DSCT	ST8XM	V	1075
SZ Lyn	min	57799.5505	0.0011	ALH	DSCT	ST8XM	V	1075
UV Lyn	min	57799.5665	0.0010	BRW	EW/KW	383L+	V	253
AN Lyn	min	57811.4145	0.0008	ALH	DSCT	ST8XM	V	419
AN Lyn	max	57811.4682	0.0009	ALH	DSCT	ST8XM	V	419
AN Lyn	min	57811.5144	0.0007	ALH	DSCT	ST8XM	V	419
AN Lyn	max	57811.5664	0.0009	ALH	DSCT	ST8XM	V	419
AN Lyn	min	57811.6135	0.0010	ALH	DSCT	ST8XM	V	419
AN Lyn	max	57811.6648	0.0011	ALH	DSCT	ST8XM	V	419
AN Lyn	max	57825.3278	0.0017	ALH	DSCT	ST8XM	V	440
AN Lyn	min	57825.3709	0.0013	ALH	DSCT	ST8XM	V	440
AN Lyn	max	57825.4258	0.0017	ALH	DSCT	ST8XM	V	440
AN Lyn	min	57825.4703	0.0012	ALH	DSCT	ST8XM	V	440
AN Lyn	max	57825.5223	0.0016	ALH	DSCT	ST8XM	V	440
AN Lyn	min	57825.5698	0.0015	ALH	DSCT	ST8XM	V	440
AN Lyn	max	57825.6195	0.0020	ALH	DSCT	ST8XM	V	440
BG Lyn	min	57465.3838	0.0002	RATRCR	EB	1600	V	103
BK Lyn	max	57861.3547	0.0010	MS	NL	16803	V	133
BK Lyn	max	57861.4339	0.0010	MS	NL	16803	V	133
CN Lyn	min	57815.3246	0.0014	AG	EA	1603	-Ir	41
EK Lyn	min	57815.4634	0.0013	AG	EA	1603	-Ir	41
EM Lyn	max	57759.7035	0.0010	MS	RRAB	16803	V	166
FN Lyn	min	57799.3333	0.0010	AG	EA	1603	-Ir	53
FS Lyn	min	57396.5150	0.0003	RATRCR	EB	1600	V	137
FS Lyn	min	57840.4034	0.0003	RATRCR	EB	1600	V	98
FU Lyn	min	57500.4258	0.0005	RATRCR	EW	1600	V	158
FW Lyn	max	57838.4913	0.0010	MS	RRAB	16803	V	65
FW Lyn	max	57847.3682	0.0010	MS	RRAB	16803	V	124
FW Lyn	max	57861.4586	0.0010	MS	RRAB	16803	V	123
KP Lyn	min	57800.3013	0.0008	ALH	DSCT	ST8XM	V	683
KP Lyn	max	57800.3262	0.0004	ALH	DSCT	ST8XM	V	683
KP Lyn	min	57800.3774	0.0008	ALH	DSCT	ST8XM	V	683
KP Lyn	max	57800.4021	0.0004	ALH	DSCT	ST8XM	V	683
KP Lyn	min	57800.4530	0.0008	ALH	DSCT	ST8XM	V	683
KP Lyn	max	57800.4781	0.0004	ALH	DSCT	ST8XM	V	683
KP Lyn	min	57800.5300	0.0008	ALH	DSCT	ST8XM	V	683
KP Lyn	max	57800.5542	0.0004	ALH	DSCT	ST8XM	V	683
KP Lyn	min	57800.6050	0.0011	ALH	DSCT	ST8XM	V	683
RZ Lyr	max	57900.4827	0.0005	NWR	RRAB	16IC	o	321
TT Lyr	min	57928.4153	0.0005	AG	EA/SD	1603	-Ir	42
TZ Lyr	min	57873.4053	0.0030	AG	EB/D	1603	-Ir	30

Table 1: cont.

Variable	Ext	HJD 24.....	±	Obs	Type	Cam	Fil	n
TZ Lyr	min	57879.4887	0.0024	AG	EB/D	1603	-Ir	32
UZ Lyr	min	57891.4647	0.0006	AG	EA/SD	1603	-Ir	32
ZZ Lyr	max	58048.3111	0.0010	MZ	RRAB	ST7	-Ir	72
AA Lyr	min	57921.5336	0.0002	MS	EB/SD	16803	V	168
AA Lyr	min	57935.5017	0.0001	MS	EB/SD	16803	V	183
AA Lyr	min	57949.4685	0.0002	MS	EB/SD	16803	V	158
AA Lyr	min	57950.5030	0.0002	MS	EB/SD	16803	V	147
AA Lyr	min	57907.5667	0.0002	MS	EB/SD	16803	V	66
AA Lyr	min	57899.5494	0.0004	MS	EB/SD	16803	V	122
AA Lyr	min	57893.5987	0.0001	MS	EB/SD	16803	V	109
AA Lyr	min	57978.4380	0.0002	MS	EB/SD	16803	V	129
BN Lyr	min	57950.4180	0.0005	MS	EA/SD	16803	V	148
BN Lyr	min	57935.5683	0.0001	MS	EA/SD	16803	V	172
CN Lyr	max	57899.4767	0.0025	NWR	RRAB	16IC	o	205
DT Lyr	min	57899.5835	0.0014	MS	EA/SD:	16803	V	103
DT Lyr	min	57950.4053	0.0006	MS	EA/SD:	16803	V	142
DT Lyr	min	57949.6152	0.0005	MS	EA/SD:	16803	V	154
DT Lyr	min	57935.4347	0.0003	MS	EA/SD:	16803	V	150
DT Lyr	min	57978.3850	0.0015	MS	EA/SD:	16803	V	131
FL Lyr	min	57891.3725	0.0012	AG	EA/DM	1603	-Ir	35
HT Lyr	min	57527.5854	0.0001	MS	EB	16803	V	120
NV Lyr	min	57511.6319	0.0001	MS	EA/SD	16803	LUM	61
NV Lyr	min	57528.5872	0.0001	MS	EA/SD	16803	LUM	89
PU Lyr	max	57511.6280	0.0010	MS	RRAB	16803	LUM	61
PU Lyr	max	57528.4906	0.0010	MS	RRAB	16803	LUM	88
QV Lyr	max	57965.4255	0.0008	MZ	RRAB	ST7	-Ir	96
QV Lyr	max	57972.4076	0.0010	MZ	RRAB	ST7	-Ir	96
V0404 Lyr	min	57891.5553	0.0002	AG	EB/SD:	1603	-Ir	32
V0412 Lyr	min	57949.5797	0.0008	MS	EA/KE	16803	V	150
V0412 Lyr	min	57950.5031	0.0009	MS	EA/KE	16803	V	142
V0412 Lyr	min	57935.6058	0.0008	MS	EA/KE	16803	V	180
V0412 Lyr	min	57978.4537	0.0008	MS	EA/KE	16803	V	128
V0428 Lyr	min	57528.6328	0.0006	MS	EA/DM	16803	LUM	89
V0431 Lyr	min	57528.6263	0.0004	MS	EW/KW	16803	LUM	90
V0563 Lyr	min	57879.5713	0.0019	AG	EW	1603	-Ir	30
V0563 Lyr	min2	57923.4725	0.0019	JU	EW	ST7	o	70
V0563 Lyr	min	57966.5071	0.0003	MS	EW	16803	V	120
V0563 Lyr	min	57951.4885	0.0002	MS	EW	16803	V	207
V0563 Lyr	min	57974.5961	0.0020	MS	EW	16803	V	162
V0563 Lyr	min	57936.4691	0.0003	MS	EW	16803	V	98
V0563 Lyr	min	57944.5565	0.0003	MS	EW	16803	V	182
V0563 Lyr	min	57910.4759	0.0002	MS	EW	16803	V	172
V0569 Lyr	min	57515.5167	0.0002	RATRCR	EA	1600	V	149
V0582 Lyr	min	57560.5221	0.0000	MS	EW	16803	LUM	85
V0582 Lyr	min	57560.6505	0.0001	MS	EW	16803	LUM	85
V0582 Lyr	min	57566.4079	0.0002	MS	EW	16803	LUM	88
V0582 Lyr	min	57566.5369	0.0001	MS	EW	16803	LUM	88
V0594 Lyr	min	57343.3529	0.0005	MS	EW:	16803	V	25
V0594 Lyr	min	57597.4310	0.0004	MS	EW:	16803	V	54
V0594 Lyr	min	57558.3919	0.0008	MS	EW:	16803	LUM	164
V0594 Lyr	min	57558.5178	0.0002	MS	EW:	16803	LUM	164
V0594 Lyr	min	57558.6458	0.0003	MS	EW:	16803	LUM	164
V0594 Lyr	min	57536.6293	0.0005	MS	EW:	16803	LUM	38
V0594 Lyr	min	57476.6031	0.0002	MS	EW:	16803	LUM	61
V0596 Lyr	min	57558.6099	0.0004	MS	E!	16803	LUM	152
V0596 Lyr	min	57558.4106	0.0005	MS	E!	16803	LUM	152
V0596 Lyr	min	57536.5682	0.0010	MS	EW	16803	LUM	74
V0596 Lyr	min	57558.4401	0.0002	MS	EW	16803	LUM	164
V0596 Lyr	min	57558.5887	0.0001	MS	EW	16803	LUM	164
V0653 Lyr	min	57913.4192	0.0013	AG	EW	1603	-Ir	27
V0658 Lyr	min	57913.4288	0.0007	AG	EW	1603	-Ir	27
TU Mon	min	57798.4863	0.0022	AG	EA/SD	1603	-Ir	40
AO Mon	min	57810.3579	0.0011	AG	EA/DM	1603	-Ir	30
DD Mon	min	57742.4210	0.0002	RATRCR	EB/KE	1600	V	78
DU Mon	max	57799.3460	0.0010	AG	RRAB	1603	-Ir	184
DV Mon	max	57799.2630	0.0010	AG	RRAB	1603	-Ir	183
EP Mon	min	57810.3924	0.0019	AG	EA/KE:	1603	-Ir	29
HI Mon	min	57810.4438	0.0004	AG	EB/KE	1603	-Ir	30
V0386 Mon	max	57798.3970	0.0010	AG	RRAB	1603	-Ir	209
V0442 Mon	min	57799.2945	0.0021	AG	EA/DM	1603	-Ir	37
V0521 Mon	min	57810.3966	0.0019	AG	EA/DM	1603	-Ir	31

Table 1: cont.

Variable	Ext	HJD 24.....	±	Obs	Type	Cam	Fil	n
V0753 Mon	min	57798.4044	0.0018	AG	EB:	1603	-Ir	35
V0864 Mon	min	57798.4425	0.0012	AG	EW	1603	-Ir	36
V0868 Mon	min	57798.4035	0.0023	AG	EB	1603	-Ir	40
V0910 Mon	min	57799.4128	0.0011	AG	EA	1603	-Ir	37
V0935 Mon	min	57799.3879	0.0019	AG	EA	1603	-Ir	38
RV Oph	min	57900.4610	0.0005	AG	EA/SD	1603	-Ir	28
V0456 Oph	min	57922.4052	0.0027	AG	EA/DM	1603	-Ir	24
V0501 Oph	min	57909.4594	0.0015	AG	EA/SD:	1603	-Ir	28
V0502 Oph	min	57895.4315	0.0014	AG	EW/KW	1603	-Ir	26
V0508 Oph	min	57899.4714	0.0016	AG	EW/KW	1603	-Ir	23
V0508 Oph	min	57900.5085	0.0008	AG	EW/KW	1603	-Ir	28
V0566 Oph	min	57905.4796	0.0007	AG	EW/KW	1603	-Ir	19
V0839 Oph	min	57905.4634	0.0006	AG	EW/KW	1603	-Ir	14
V2563 Oph	min	57923.3822	0.0006	AG	E	1603	-Ir	25
V2610 Oph	min	57919.4917	0.0032	AG	EW	1603	-Ir	24
V2612 Oph	min	57919.5387	0.0015	AG	EW	1603	-Ir	24
V2713 Oph	min	57890.4535	0.0005	AG	EB	1603	-Ir	33
V2799 Oph	min	57919.4124	0.0022	AG	EA	1603	-Ir	24
V0343 Ori	min	57776.3485	0.0002	RATRCR	EW/DW	1600	V	116
V1851 Ori	min2	57722.4470	0.0002	RATRCR	EW	1600	V	96
V1851 Ori	min	57743.3567	0.0002	RATRCR	EW	1600	V	66
V1853 Ori	min	57720.3999	0.0010	RATRCR	EW	1600	V	54
V2787 Ori	min	57799.3770	0.0035	AG	EB	1603	-Ir	41
UX Peg	min	57992.4022	0.0005	AG	EA/SD	1603	-Ir	47
VV Peg	min	58018.4583	0.0011	ALH	RRAB	3200M	V	517
VV Peg	max	58018.5177	0.0014	ALH	RRAB	3200M	V	517
AT Peg	min	57989.4631	0.0004	AG	EA/SD	1603	-Ir	36
BN Peg	min	57988.3605	0.0025	AG	EA	1603	-Ir	42
BP Peg	max	55062.4217	0.0010	NWR	DSCT(B)	16IC		867
BP Peg	min	58043.2747	0.0014	ALH	DSCT(B)	3200M	V	446
BP Peg	max	58043.3163	0.0007	ALH	DSCT(B)	3200M	V	446
BP Peg	min	58043.3905	0.0009	ALH	DSCT(B)	3200M	V	446
BP Peg	max	58043.4206	0.0005	ALH	DSCT(B)	3200M	V	446
BP Peg	min	58043.4933	0.0012	ALH	DSCT(B)	3200M	V	446
BP Peg	max	58043.5289	0.0009	ALH	DSCT(B)	3200M	V	446
DI Peg	min	58011.3340	0.0045	AG	EA/SD	1603	-Ir	29
DY Peg	max	55062.5188	0.0010	NWR	SXPHE(B)	16IC		1753
DY Peg	max	55062.5916	0.0010	NWR	SXPHE(B)	16IC		1753
DY Peg	max	57995.4560	0.0035	AGT	SXPHE(B)	600D	TG	62
DY Peg	min	57995.4349	0.0035	AGT	SXPHE(B)	600D	TG	62
DY Peg	max	57995.3836	0.0035	AGT	SXPHE(B)	600D	TG	59
DY Peg	min	58042.3155	0.0009	ALH	SXPHE(B)	3200M	V	866
DY Peg	max	58042.3416	0.0004	ALH	SXPHE(B)	3200M	V	866
DY Peg	min	58042.3893	0.0009	ALH	SXPHE(B)	3200M	V	866
DY Peg	max	58042.4142	0.0004	ALH	SXPHE(B)	3200M	V	866
DY Peg	min	58042.4621	0.0010	ALH	SXPHE(B)	3200M	V	866
DY Peg	max	58042.4870	0.0005	ALH	SXPHE(B)	3200M	V	866
DY Peg	min	58042.5339	0.0011	ALH	SXPHE(B)	3200M	V	866
DY Peg	max	58042.5603	0.0006	ALH	SXPHE(B)	3200M	V	866
ER Peg	min	57980.5165	0.0017	AG	EA/SD	1603	-Ir	32
GP Peg	min	57952.5600	0.0025	AG	EA	1603	-Ir	33
KW Peg	min	58022.3333	0.0003	SCI	EA	ST7	o	76
V0357 Peg	min	58005.4222	0.0018	AG	EW	1603	-Ir	48
V0365 Peg	min	57973.4434	0.0011	AG	EB	1603	-Ir	38
V0404 Peg	min	57952.4399	0.0011	AG	EW	1603	-Ir	33
V0407 Peg	min	58011.4875	0.0003	AG	EW	1603	-Ir	28
V0461 Peg	min2	57640.3393	0.0006	RATRCR	EA:	1600	V	92
V0463 Peg	min2	57640.3727	0.0002	RATRCR	EW	1600	V	97
V0467 Peg	min	58023.3935	0.0020	AG	EW	1603	-Ir	53
V0473 Peg	min	57988.5128	0.0025	AG	EW	1603	-Ir	39
V0473 Peg	min	58023.3561	0.0028	AG	EW	1603	-Ir	53
V0478 Peg	min	57988.5341	0.0005	AG	EA	1603	-Ir	43
V0480 Peg	min	57964.4134	0.0022	AG	EW	1603	-Ir	29
V0481 Peg	min	57964.5532	0.0007	AG	EW	1603	-Ir	40
V0484 Peg	min	57964.4949	0.0039	AG	EW	1603	-Ir	37
V0505 Peg	max	58011.4220	0.0010	AG	RRAB	1603	-Ir	21
V0535 Peg	min	57952.4602	0.0015	AG	EW	1603	-Ir	34
V0544 Peg	max	57989.4860	0.0010	AG	RRAB	1603	-Ir	38
V0560 Peg	min	57952.4095	0.0043	AG	EA:	1603	-Ir	32
V0568 Peg	min	57980.4104	0.0010	AG	EW	1603	-Ir	33
V0568 Peg	min	57980.5349	0.0034	AG	EW	1603	-Ir	33

Table 1: cont.

Variable	Ext	HJD 24.....	±	Obs	Type	Cam	Fil	n
V0576 Peg	min	58011.3057	0.0001	AG	EW	1603	-Ir	30
V0576 Peg	min	58011.4385	0.0025	AG	EW	1603	-Ir	30
V0638 Peg	min	57992.4773	0.0017	AG	EW	1603	-Ir	46
V0638 Peg	min	57992.6168	0.0016	AG	EW	1603	-Ir	46
V0640 Peg	min	58023.4385	0.0019	AG	EW	1603	-Ir	46
V0669 Peg	min	57980.4360	0.0021	AG	EW	1603	-Ir	33
XZ Per	min	57726.6302	0.0001	RATRCR	EA/SD	1600	V	162
AN Per	max	57726.4680	0.0010	FR	RRAB	1603	-Ir	75
ET Per	max	58018.4070	0.0010	AG	RRAB	1603	-Ir	55
KQ Per	min	57840.3149	0.0018	FR	EA/SD:	1603	-Ir	68
KV Per	max	57771.2443	0.0015	MZ	RRC	ST7	-Ir	114
LX Per	min	57811.3669	0.0001	FR	EA/AR/RS	1603	-Ir	681
LX Per	min2	57823.3945	0.0020	FR	EA/AR/RS	1603	-Ir	82
V0570 Per	min2	57823.3153	0.0020	FR	EB:	1603	-Ir	288
V0751 Per	min	58018.4128	0.0013	AG	EA	1603	-Ir	57
V0930 Per	min	57752.4620	0.0019	FR	EA	1603	-Ir	94
EW Psc	min	57616.5244	0.0004	RATRCR	EW	1600	V	136
HN Psc	min	58019.3974	0.0029	AG	EW	1603	-Ir	29
HN Psc	min	58023.3531	0.0016	AG	EW	1603	-Ir	57
HN Psc	min	58023.5121	0.0020	AG	EW	1603	-Ir	57
V Sge	min	57924.4001	0.0035	AG	E+NL	1603	-Ir	33
V Sge	min	57964.4965	0.0006	AG	E+NL	1603	-Ir	40
CU Sge	min	57923.5027	0.0010	AG	EB/DW	1603	-Ir	25
CU Sge	min	57973.3799	0.0018	AG	EB/DW	1603	-Ir	38
CW Sge	min	57919.5139	0.0043	AG	EW/DW	1603	-Ir	24
DM Sge	min	57923.4378	0.0011	AG	EB/DM	1603	-Ir	24
FI Sge	max	57994.4796	0.0020	MZ	RRAB	ST7	-Ir	89
V0366 Sge	min	57923.4417	0.0020	AG	EB	1603	-Ir	24
V0375 Sge	min	57912.3977	0.0013	AG	EA	1603	-Ir	26
AO Ser	min	57879.3508	0.0007	AG	EA/SD	1603	-Ir	35
AU Ser	min	57874.3901	0.0016	AG	EW/KW:	1603	-Ir	38
AU Ser	min	57874.5808	0.0005	AG	EW/KW:	1603	-Ir	38
CX Ser	min2	57895.4535	0.0003	FR	EA/SD:	1603	-Ir	160
OU Ser	min	57867.4171	0.0016	AG	EW:	1603	-Ir	44
OU Ser	min	57867.5635	0.0022	AG	EW:	1603	-Ir	44
OU Ser	min	57887.4424	0.0025	AG	EW:	1603	-Ir	25
V0384 Ser	min	57515.3738	0.0002	RATRCR	EW	1600	V	86
V0384 Ser	min	57867.4178	0.0005	FR	EW	1603	-Ir	132
V0384 Ser	min2	57873.4597	0.0003	FR	EW	1603	-Ir	305
V0384 Ser	min	57873.5977	0.0002	FR	EW	1603	-Ir	305
V0384 Ser	min	57874.4044	0.0002	FR	EW	1603	-Ir	275
V0384 Ser	min2	57874.5349	0.0003	FR	EW	1603	-Ir	275
V0384 Ser	min	57879.5097	0.0002	FR	EW	1603	-Ir	215
V0384 Ser	min2	57890.3905	0.0004	FR	EW	1603	-Ir	269
V0384 Ser	min	57890.5276	0.0002	FR	EW	1603	-Ir	269
V0384 Ser	min2	57891.4657	0.0004	FR	EW	1603	-Ir	267
V0384 Ser	min	57900.4706	0.0003	FR	EW	1603	-Ir	206
V0384 Ser	min2	57901.4081	0.0002	FR	EW	1603	-Ir	229
V0384 Ser	min	57901.5451	0.0002	FR	EW	1603	-Ir	229
V0384 Ser	min	57918.6070	0.0006	MS	EW	16803	B	137
V0384 Ser	min	57918.4732	0.0004	MS	EW	16803	B	137
V0384 Ser	min	57892.5402	0.0009	MS	EW	16803	B	144
V0384 Ser	min	57892.4083	0.0007	MS	EW	16803	B	144
V0384 Ser	min	57876.5534	0.0005	MS	EW	16803	B	154
V0384 Ser	min	57918.4729	0.0003	MS	EW	16803	R	149
V0384 Ser	min	57918.6070	0.0004	MS	EW	16803	R	149
V0384 Ser	min	57892.4080	0.0003	MS	EW	16803	R	158
V0384 Ser	min	57892.5396	0.0004	MS	EW	16803	R	158
V0384 Ser	min	57876.5537	0.0002	MS	EW	16803	R	157
V0384 Ser	min	57918.4731	0.0004	MS	EW	16803	I	149
V0384 Ser	min	57918.6068	0.0004	MS	EW	16803	I	149
V0384 Ser	min	57892.5396	0.0004	MS	EW	16803	I	164
V0384 Ser	min	57892.4074	0.0007	MS	EW	16803	I	164
V0384 Ser	min	57876.5538	0.0003	MS	EW	16803	I	161
V0384 Ser	min	57876.5538	0.0003	MS	EW	16803	V	157
V0384 Ser	min	57876.4164	0.0002	MS	EW	16803	V	157
V0384 Ser	min	57892.5404	0.0005	MS	EW	16803	V	155
V0384 Ser	min	57892.4079	0.0004	MS	EW	16803	V	155
V0384 Ser	min	57918.4740	0.0003	MS	EW	16803	V	158
V0384 Ser	min	57918.6064	0.0003	MS	EW	16803	V	158
V0435 Ser	max	57895.5155	0.0010	FR	RRAB	1603	-Ir	162

Table 1: cont.

Variable	Ext	HJD 24.....	±	Obs	Type	Cam	Fil	n
V0505 Ser	min	57879.4853	0.0030	AG	EA+RS	1603	-Ir	35
V0505 Ser	min2	57867.3417	0.0020	FR	EA+RS	1603	-Ir	137
V0505 Ser	min2	57873.3362	0.0010	FR	EA+RS	1603	-Ir	297
V0505 Ser	min	57873.5404	0.0004	FR	EA+RS	1603	-Ir	297
V0505 Ser	min	57874.5324	0.0002	FR	EA+RS	1603	-Ir	256
V0505 Ser	min	57879.4861	0.0002	FR	EA+RS	1603	-Ir	219
V0505 Ser	min	57890.3855	0.0002	FR	EA+RS	1603	-Ir	248
V0505 Ser	min	57891.3759	0.0004	FR	EA+RS	1603	-Ir	243
V0505 Ser	min2	57900.5377	0.0008	FR	EA+RS	1603	-Ir	225
V0505 Ser	min2	57901.5228	0.0005	FR	EA+RS	1603	-Ir	242
V0505 Ser	min	57940.4224	0.0003	FR	EA+RS	1603	-Ir	322
V0505 Ser	min	57876.5125	0.0007	MSFR	EA+RS	16803	B	119
V0505 Ser	min	57876.5139	0.0003	MSFR	EA+RS	16803	I	156
V0505 Ser	min	57876.5142	0.0005	MSFR	EA+RS	16803	R	160
V0505 Ser	min	57876.5148	0.0005	MSFR	EA+RS	16803	V	151
V0505 Ser	min	57892.6095	0.0005	MSFR	EA+RS	16803	I	151
V0505 Ser	min	57892.6095	0.0015	MSFR	EA+RS	16803	R	160
V0505 Ser	min	57892.6161	0.0019	MSFR	EA+RS	16803	V	148
V0505 Ser	min	57918.6246	0.0018	MSFR	EA+RS	16803	B	146
V0505 Ser	min	57918.6233	0.0008	MSFR	EA+RS	16803	I	151
V0505 Ser	min	57918.6228	0.0003	MSFR	EA+RS	16803	R	140
V0505 Ser	min	57918.6234	0.0006	MSFR	EA+RS	16803	V	141
T Sex	max	57829.4660	0.0010	AG	RRC	1603	-Ir	39
U Sex	max	57840.3820	0.0010	AG	RRAB	1603	-Ir	44
V Sex	max	57840.3650	0.0010	AG	RR	1603	-Ir	46
Y Sex	min	57829.3243	0.0020	AG	EW/KW	1603	-Ir	41
Y Sex	min	57829.5296	0.0015	AG	EW/KW	1603	-Ir	41
Y Sex	min	57839.3970	0.0011	AG	EW/KW	1603	-Ir	40
RV Sex	max	57838.3470	0.0010	AG	RRAB	1603	-Ir	93
WW Sex	min	57836.3084	0.0047	AG	EA	1603	-Ir	33
WW Sex	min	57841.3359	0.0003	AG	EA	1603	V	31
WX Sex	min	57839.4913	0.0033	AG	EW	1603	-Ir	40
WX Sex	min	57840.3561	0.0007	AG	EW	1603	-Ir	46
WX Sex	min	57841.4290	0.0006	AG	EW	1603	-Ir	32
WY Sex	min	57829.4567	0.0009	AG	EW	1603	-Ir	50
WZ Sex	min	57836.4365	0.0045	AG	EB	1603	-Ir	33
AA Sex	max	57841.4470	0.0010	AG	RRAB	1603	-Ir	28
AC Sex	max	57829.4460	0.0010	AG	RRAB	1603	-Ir	50
AF Sex	max	57840.3480	0.0010	AG	RRAB	1603	-Ir	42
AI Sex	min	57840.4029	0.0024	AG	EB	1603	V	46
AM Sex	max	57829.4540	0.0020	AG	RRC	1603	-Ir	51
AR Sex	max	57841.4320	0.0010	AG	RRAB	1603	-Ir	35
AU Sex	max	57840.4100	0.0010	AG	RRAB	1603	-Ir	45
AX Sex	max	57840.3220	0.0010	AG	RRAB	1603	-Ir	46
BQ Sex	max	57867.4400	0.0010	AG	RRAB	1603	-Ir	238
BS Sex	max	57838.4990	0.0010	AG	RRAB	1603	-Ir	93
SV Tau	min	57800.2854	0.0001	SCI	EA/SD	ST7	o	66
WY Tau	min2	57725.4280	0.0002	RATRCR	EW/KE	1600	V	87
EN Tau	min	58038.5209	0.0001	MH	EA/SD:	314+	GT	288
CL Tri	min	57722.3036	0.0002	RATRCR	EA	1600	V	119
RV UMa	max	57842.4470	0.0010	AG	RRAB	1603	-Ir	47
RW UMa	min	57841.5349	0.0020	AG	EA/D/RS	1603	-Ir	50
SX UMa	max	57825.6060	0.0010	AG	RRC	1603	-Ir	59
SX UMa	max	57839.4250	0.0010	AG	RRC	1603	-Ir	55
SX UMa	min	57923.5553	0.0001	SCI	RRC	ST7	o	128
TU UMa	max	57841.3730	0.0010	AG	RRAB	1603	-Ir	35
TU UMa	min	57842.4057	0.0017	ALH	RRAB	ST8XM	V	527
TU UMa	max	57842.4880	0.0010	ALH	RRAB	ST8XM	V	527
TU UMa	max	57837.4670	0.0003	NWR	RRAB	16IC	o	2441
TX UMa	min	57833.3450	0.0004	AG	EA/SD	1603	-Ir	82
TX UMa	min	57836.4095	0.0005	AG	EA/SD	1603	-Ir	39
TY UMa	min	57838.4263	0.0001	SCI	EW/KW	ST7	o	282
TY UMa	min	57838.6029	0.0001	SCI	EW/KW	ST7	o	282
TY UMa	min2	57852.4316	0.0006	JU	EW/KW	ST7	o	70
VV UMa	min	57924.4969	0.0001	SCI	EA/SD	ST7	o	113
XZ UMa	min2	57838.3868	0.0023	JU	EA/SD	ST7	o	80
AA UMa	min	57864.3542	0.0005	JU	EW/KW	ST7	o	71
AA UMa	min2	57867.3951	0.0017	JU	EW/KW	ST7	o	54
AA UMa	min2	57873.4809	0.0010	JU	EW/KW	ST7	o	85
AB UMa	max	57842.5330	0.0010	AG	RRAB	1603	-Ir	47
AE UMa	min	57803.3198	0.0011	ALH	SXPHE:	ST8XM	V	630

Table 1: cont.

Variable	Ext	HJD 24.....	±	Obs	Type	Cam	Fil	n
AE UMa	max	57803.3519	0.0005	ALH	SXPHE:	ST8XM	V	630
AE UMa	min	57803.4124	0.0011	ALH	SXPHE:	ST8XM	V	630
AE UMa	max	57803.4427	0.0006	ALH	SXPHE:	ST8XM	V	630
AE UMa	min	57803.4994	0.0009	ALH	SXPHE:	ST8XM	V	630
AE UMa	max	57803.5231	0.0004	ALH	SXPHE:	ST8XM	V	630
AE UMa	min	57803.5801	0.0013	ALH	SXPHE:	ST8XM	V	630
AE UMa	max	57803.6077	0.0005	ALH	SXPHE:	ST8XM	V	630
AF UMa	min	57811.3368	0.0017	AG	EA/SD:	1603	-Ir	58
AW UMa	min	57825.4861	0.0019	AG	EW/KW	1603	-Ir	63
AW UMa	min	57833.3818	0.0011	AG	EW/KW	1603	-Ir	82
AW UMa	min	57837.5453	0.0015	NWR	EW/KW	16IC	o	2549
BH UMa	min	57925.4734	0.0002	SCI	EW/KE	ST7	o	83
BH UMa	min	57926.4997	0.0003	SCI	EW/KE	ST7	o	91
BS UMa	min	57456.4093	0.0002	RATRCR	EA	1600	Clear	121
GT UMa	min	57811.4870	0.0012	AG	EB	1603	-Ir	58
GW UMa	max	57833.4170	0.0010	AG	DSCT:	1603	-Ir	82
GW UMa	max	57836.4710	0.0010	AG	DSCT:	1603	-Ir	38
GW UMa	min	57829.4998	0.0011	ALH	DSCT:	ST8XM	V	899
GW UMa	max	57829.5578	0.0008	ALH	DSCT:	ST8XM	V	899
LP UMa	min	57839.3942	0.0001	SCI	EW	ST7	o	85
LP UMa	min	57839.5547	0.0002	SCI	EW	ST7	o	85
MS UMa	min2	57753.6231	0.0002	RATRCR	EW	1600	V	154
NU UMa	min	57812.3119	0.0019	AG	EA	1603	-Ir	20
PZ UMa	min	57446.5854	0.0003	RATRCR	EW	1600	V	200
V0342 UMa	min	57840.3938	0.0012	JU	EW	ST7	o	65
V0354 UMa	min	57825.4067	0.0024	AG	EW	1603	-Ir	54
V0354 UMa	min	57825.5452	0.0015	AG	EW	1603	-Ir	54
W UMi	min	57844.5117	0.0039	AG	EA/SD	1603	-Ir	42
W UMi	min	57457.5079	0.0001	RATRCR	EA/SD	1600	V	194
RS UMi	min	57840.4677	0.0029	AG	EA/D/RS	1603	-Ir	45
RT UMi	min	57843.5794	0.0013	AG	EA/SD	1603	-Ir	45
RT UMi	min	57844.5023	0.0061	AG	EA/SD	1603	-Ir	42
RU UMi	min	57812.3413	0.0005	AG	EB/DW	1603	-Ir	21
RZ UMi	min	57815.3557	0.0017	AG	EW/KW	1603	-Ir	40
RZ UMi	min	57815.5198	0.0023	AG	EW/KW	1603	-Ir	40
RZ UMi	min	57844.3688	0.0017	AG	EW/KW	1603	-Ir	42
RZ UMi	min	57844.5369	0.0011	AG	EW/KW	1603	-Ir	42
VV UMi	min	57901.4820	0.0032	AG	EA	1603	-Ir	32
VW UMi	min	57815.3535	0.0018	AG	EW	1603	-Ir	39
VW UMi	min	57844.4410	0.0015	AG	EW	1603	-Ir	42
VY UMi	min	57844.4573	0.0005	AG	EW	1603	-Ir	42
VY UMi	min	57844.6202	0.0011	AG	EW	1603	-Ir	42
VY UMi	min	57489.4391	0.0001	RATRCR	EW	1600	V	264
VY UMi	min2	57489.6014	0.0002	RATRCR	EW	1600	V	264
YZ UMi	max	57815.2960	0.0010	AG	DSCT	1603	-Ir	40
YZ UMi	max	57844.3800	0.0010	AG	DSCT	1603	-Ir	42
YZ UMi	max	57844.4720	0.0010	AG	DSCT	1603	-Ir	42
YZ UMi	max	57844.5720	0.0010	AG	DSCT	1603	-Ir	42
AL UMi	min	57511.4920	0.0007	RATRCR	EW	1600	V	206
AW Vir	min	57874.3561	0.0034	AG	EW/KW	1603	-Ir	37
AW Vir	min	57874.5313	0.0009	AG	EW/KW	1603	-Ir	37
AW Vir	min	57890.4625	0.0008	AG	EW/KW	1603	-Ir	35
AX Vir	min	57890.4466	0.0023	AG	EB/KE	1603	-Ir	35
AZ Vir	min	57867.4896	0.0020	AG	EW/KW	1603	-Ir	44
AZ Vir	min	57874.4810	0.0006	AG	EW/KW	1603	-Ir	37
BF Vir	min	57902.4566	0.0024	AG	EB/KE:	1603	-Ir	20
BH Vir	min	57902.4264	0.0009	AG	EA/DW/RS:	1603	-Ir	18
CG Vir	min	57887.3993	0.0008	AG	EB/D	1603	-Ir	19
FO Vir	min	57874.3999	0.0040	AG	EB/KE	1603	-Ir	34
HT Vir	min	57867.4654	0.0004	AG	EW/KW	1603	-Ir	44
HT Vir	min	57874.3970	0.0016	AG	EW/KW	1603	-Ir	37
LU Vir	min	57890.4180	0.0012	AG	EB:	1603	-Ir	34
PY Vir	min	57890.3953	0.0007	AG	EW	1603	-Ir	33
V0342 Vir	min	57890.3982	0.0008	AG	EA	1603	-Ir	35
V0415 Vir	min	57843.4527	0.0023	AG	EW	1603	-Ir	43
V0467 Vir	min	57890.4265	0.0015	AG	EW	1603	-Ir	34
V0639 Vir	min	57874.3981	0.0011	AG	EW	1603	-Ir	37
RS Vul	min	57923.4892	0.0019	AG	EA/SD:	1603	-Ir	25
AT Vul	min	57988.5491	0.0027	AG	EA/SD:	1603	-Ir	40
AW Vul	min	57939.4664	0.0005	AG	EA/SD:	1603	-Ir	26
AW Vul	min	57980.5955	0.0012	AG	EA/SD:	1603	-Ir	33

Table 1: cont.

Variable	Ext	HJD 24.....	±	Obs	Type	Cam	Fil	n
AX Vul	min	57980.3809	0.0005	AG	EA/SD:	1603	-Ir	34
AX Vul	min	57982.4071	0.0005	AG	EA/SD:	1603	-Ir	25
AZ Vul	min	57980.5069	0.0009	AG	EA/KE:	1603	-Ir	33
BE Vul	min	57913.4308	0.0020	AG	EA/SD	1603	-Ir	24
BO Vul	min	57913.5224	0.0010	AG	EA/SD	1603	-Ir	25
BP Vul	min	57964.4732	0.0008	AG	EA/SD	1603	-Ir	39
BP Vul	min	57966.4139	0.0013	AG	EA/SD	1603	-Ir	32
BS Vul	min	57905.5258	0.0012	AG	EB/KW	1603	-Ir	21
BU Vul	min	57926.4265	0.0005	AG	EA/SD	1603	-Ir	21
DR Vul	min	57901.4838	0.0013	AG	EA/DM	1603	-Ir	24
DR Vul	min	57919.4910	0.0009	AG	EA/DM	1603	-Ir	25
DR Vul	min	57928.4936	0.0010	AG	EA/DM	1603	-Ir	23
DR Vul	min	57964.5053	0.0010	AG	EA/DM	1603	-Ir	39
DR Vul	min	57992.5278	0.0011	AG	EA/DM	1603	-Ir	42
DR Vul	min	58001.5300	0.0021	AG	EA/DM	1603	-Ir	41
ER Vul	min	57919.4580	0.0027	AG	EW/DW/RS	1603	-Ir	22
FQ Vul	min	57952.4850	0.0012	AG	EA/D	1603	-Ir	33
FR Vul	min	57918.4732	0.0015	AG	EA	1603	-Ir	28
FR Vul	min	57952.3807	0.0003	AG	EA	1603	-Ir	34
GP Vul	min	57918.4043	0.0016	AG	EB/KE	1603	-Ir	32
V0491 Vul	min	57992.4718	0.0020	AG	EA	1603	-Ir	40
V0495 Vul	min	57918.4653	0.0011	AG	EA	1603	-Ir	27
V0496 Vul	min	57988.4044	0.0006	AG	EW	1603	-Ir	39
V0496 Vul	min	57988.5574	0.0028	AG	EW	1603	-Ir	39
V0502 Vul	min	57982.5482	0.0033	AG	EA	1603	-Ir	39
2MASS J08034298 Cnc	max	57833.4612	0.0010	MS		16803	V	72
2MASS J19131461+3329277 Lyr	max	57511.5609	0.0010	MS		16803	LUM	55
2MASS J20290715+5115180 Cyg	min	57263.4390	0.0005	FR		1603	-Ir	300
2MASS J20290715+5115180 CrB	min2	57264.5224	0.0022	FR		1603	-Ir	344
3UC 242-227216 Cyg	min2	57260.4890	0.0015	FR		1603	-Ir	166
3UC 242-227216 Cyg	min	57939.4376	0.0005	FR		1603	-Ir	202
3UC 242-227216 Cyg	min	57952.4284	0.0003	FR		1603	-Ir	148
3UC 242-230799 Cyg	min	57240.3736	0.0010	FR		1603	-Ir	291
3UC 242-230799 Cyg	min2	57260.3930	0.0008	FR		1603	-Ir	168
3UC 242-229922 Cyg	min2	57939.4824	0.0015	FR		1603	-Ir	161
3UC 243-228342 Cyg	min2	57240.4294	0.0006	FR		1603	-Ir	279
3UC 243-228342 Cyg	min	57260.3935	0.0003	FR		1603	-Ir	342
3UC 243-228342 Cyg	min2	57260.5618	0.0004	FR		1603	-Ir	342
3UC 243-228342 Cyg	min2	57939.3850	0.0006	FR		1603	-Ir	111
3UC 243-228342 Cyg	min2	57952.4699:	0.0015	FR		1603	-Ir	118
3UC 243-226799 Cyg	min2	57240.4667	0.0008	FR		1603	-Ir	284
3UC 243-226799 Cyg	min2	57260.3633	0.0008	FR		1603	-Ir	335
3UC 243-226799 Cyg	min	57260.5015	0.0008	FR		1603	-Ir	335
3UC 243-226799 Cyg	min2	57939.4532	0.0004	FR		1603	-Ir	197
3UC 243-226799 Cyg	min2	57952.4462	0.0003	FR		1603	-Ir	218
3UC 249-199508 Cyg	min	57924.5438	0.0005	FR		1603	-Ir	138
3UC 259-102457 Lyn	min	57754.5492	0.0005	MS	E!	16803	V	195
3UC 259-102457 Lyn	min	57754.7441	0.0006	MS	E!	16803	V	195
3UC 259-102457 Lyn	min	57759.6436	0.0004	MS	E!	16803	V	166
3UC 259-102457 Lyn	min	57828.3578	0.0009	MS	E!	16803	V	134
3UC 270-150925 Lyr	min	57558.5288	0.0006	MS	E!	16803	LUM	153
3UC 270 150854 Lyr	min	57558.5913	0.0006	MS	E!	16803	LUM	153
3UC 270-150925 Lyr	min	57536.6477	0.0012	MS	E!	16803	LUM	73
3UC 270-150925 Lyr	min	57476.6602	0.0006	MS	E!	16803	LUM	63
3UC 271-146132 Lyr	min	57558.6239	0.0007	MS	E!	16803	LUM	153
3UC 271-145965 Lyr	min	57536.6517	0.0011	MS	E!	16803	LUM	73
3UC 272-141916 Lyr	min	57558.4791	0.0002	MS	E!	16803	LUM	153
3UC 272-141934 Lyr	min	57558.5839	0.0007	MS	E!	16803	LUM	153
3UC 272-141916 Lyr	min	57343.2824	0.0007	MS	E!	16803	V	25
3UC 273-125122 Boo	min	57831.6507	0.0008	MS	E!	16803	V	100
3UC 273-125122 Boo	min	57848.5680	0.0009	MS	E!	16803	V	142
3UC 273-125122 Boo	min	57862.4376	0.0006	MS		16803	V	121
3UC 282-172128 Cyg	min	57257.4323	0.0005	FR		1603	-Ir	336
3UC 282-172128 Cyg	min2	57257.5812	0.0007	FR		1603	-Ir	336
3UC 282-172128 Cyg	min	57261.3695	0.0005	FR		1603	-Ir	324
3UC 282-172128 Cyg	min2	57261.5192	0.0005	FR		1603	-Ir	324
3UC 282-172128 Cyg	min2	57263.3414	0.0008	FR		1603	-Ir	149
3UC 282-172128 Cyg	min	57263.4923	0.0005	FR		1603	-Ir	149
3UC 282-172128 Cyg	min	57264.4012	0.0008	FR		1603	-Ir	177
3UC 285-064742 Per	min2	57657.4182	0.0010	FR		1603	-Ir	97
3UC 285-064742 Per	min2	57752.3468	0.0006	FR		1603	-Ir	95

Table 1: cont.

Variable	Ext	HJD 24.....	±	Obs	Type	Cam	Fil	n
3UC 285-064742 Per	min	57829.3295	0.0003	FR		1603	-Ir	111
3UC 285-064742 Per	min2	57840.3291	0.0009	FR		1603	-Ir	90
3UC 285-064742 Per	min	57844.3790	0.0004	FR		1603	-Ir	54
3UC 285-065032 Per	max	57657.4882	0.0017	FR		1603	-Ir	146
3UC 285-065032 Per	max	57752.3078	0.0012	FR		1603	-Ir	98
3UC 285-065032 Per	max	57753.3315	0.0009	FR		1603	-Ir	185
3UC 285-065032 Per	max	57829.3867	0.0019	FR		1603	-Ir	65
3UC 285-065032 Per	max	57838.3622	0.0017	FR		1603	-Ir	92
3UC 285-065032 Per	max	57839.3896	0.0024	FR		1603	-Ir	97
3UC 285-065032 Per	max	57840.4022	0.0012	FR		1603	-Ir	92
3UC 285-065032 Per	max	57842.4417	0.0020	FR		1603	-Ir	149
3UC 285-065032 Per	max	57843.4685	0.0015	FR		1603	-Ir	88
3UC 285-065321 Per	min	57829.3090	0.0010	FR		1603	-Ir	197
3UC 285-065321 Per	min	57838.4451	0.0008	FR		1603	-Ir	166
3UC 285-065321 Per	min	57839.3644	0.0007	FR		1603	-Ir	173
3UC 285-065321 Per	min	57840.2880	0.0010	FR		1603	-Ir	211
3UC 285-065474 Per	min2	57752.2415	0.0012	FR		1603	-Ir	92
3UC 285-065474 Per	min	57753.4104	0.0013	FR		1603	-Ir	91
3UC 285-065474 Per	min2	57842.3968	0.0029	FR		1603	-Ir	58
3UC 286-062756 Per	max	57657.5197	0.0010	FR		1603	-Ir	149
3UC 286-062756 Per	max	57839.4095	0.0010	FR		1603	-Ir	169
3UC 286-062756 Per	max	57840.4891	0.0020	FR		1603	-Ir	209
3UC 286-062756 Per	max	57843.3678	0.0011	FR		1603	-Ir	163
3UC 286-063889 Per	min	57657.5410	0.0032	FR		1603	-Ir	83
3UC 286-064360 Per	min2	57657.5420	0.0016	FR		1603	-Ir	90
3UC 286-064360 Per	min2	57753.3309	0.0008	FR		1603	-Ir	186
3UC 286-064360 Per	min	57840.3145	0.0010	FR		1603	-Ir	204
3UC 286-064360 Per	min	57844.3235	0.0020	FR		1603	-Ir	160
3UC230-244363 Vul	max	57980.4270	0.0010	AG		1603	-Ir	30
3UC 322-012905 Cas	min	57780.4947	0.0007	SCI		ST7		71
3UC 323-013086 Cas	min	57780.4543	0.0004	SCI		ST7	o	71
ASAS J062940+2031.3 Xxx	max	57760.0000	6.0000	BHE		DSI	-Ir	14
ASAS J063546+1928.6 Gem	min	57811.3388	0.0005	AG	EB’	1603	-Ir	38
ASAS J073131+0309.1 CMi	min	57800.5120	0.0020	AG		1603	-Ir	41
ASAS J083251+1333.7 Cnc	min	57798.4493	0.0019	AG		1603	-Ir	60
ASAS J084144+2530.6 Cnc	max	57815.4210	0.0010	AG	WU’	1603	-Ir	40
ASAS J093223+1555.7 Leo	min	57845.4966	0.0003	MS		16803	V	147
ASAS J093223+1555.7 Leo	min	57846.3873	0.0003	MS		16803	V	117
ASAS J095047+0126.4 Sex	min	57829.3793	0.0026	AG		1603	-Ir	39
ASAS J100622+2435.2 Leo	min	57811.3351	0.0054	AG		1603	-Ir	64
ASAS J100622+2435.2 Leo	min	57811.4624	0.0060	AG		1603	-Ir	64
ASAS J100622+2435.2 Leo	min	57811.5950	0.0015	AG		1603	-Ir	64
ASAS J144659+1316.7 Boo	min	57867.5010	0.0018	AG		1603	-Ir	44
ASAS J145716+2348.8 Boo	min	57852.5277	0.0027	AG		1603	-Ir	48
ASAS J181025+0047.7 Oph	min	57923.4733	0.0024	AG		1603	-Ir	24
ASAS J185725+4042.9 Lyr	min	57560.5465:	0.0005	MS	Al’	16803	LUM	81
ASAS J185340+4038.0 Lyr	min	57566.5197	0.0006	MS	WU’	16803	LUM	80
ASAS J185722+4150.3 Lyr	min	57566.4406	0.0003	MS	WU’	16803	LUM	79
ASAS J185324+2012.3 Her	max	57987.4100	0.0010	AG		1603	-Ir	37
ASAS J191547+1812.7 Sge	min	57923.5019	0.0006	AG	Al’	1603	-Ir	24
ASAS J191610+1918.3 Sge	min	57923.4981	0.0038	AG		1603	-Ir	24
ASAS J191745+0846.9 Aql	min	57940.5030	0.0039	AG		1603	-Ir	26
ASAS J191745+0846.9 Aql	min	57952.4742	0.0013	AG		1603	-Ir	34
ASAS J193522+2230.3 Vul	min	57905.4776	0.0013	AG		1603	-Ir	21
ASAS J193726+2225.6 Vul	min	57905.5049	0.0016	AG		1603	-Ir	20
ASAS J193235+5433.1 Cyg	min	57912.4978	0.0035	AG		1603	-Ir	27
ASAS J193947-0926.1 Aql	min	57995.4163	0.0016	AG		1603	-Ir	26
ASAS J194817+2615.1 Vul	min	57913.5007	0.0021	AG	EW!	1603	-Ir	25
ASAS J194817+2615.1 Vul	min	57918.4117	0.0046	AG	EW!	1603	-Ir	29
ASAS J194630+0234.0 Aql	min	57995.3574	0.0042	AG		1603	-Ir	30
ASAS J195821+0711.6 Aql	max	57952.4430	0.0020	AG		1603	-Ir	34
ASAS J195342+0205.4 Aql	min	57995.3865	0.0031	AG		1603	-Ir	31
ASAS J195821+0711.6 Aql	min	57987.4278	0.0020	AG		1603	-Ir	37
ASAS J195924+2257.0 Vul	min	57988.4571	0.0005	AG		1603	-Ir	33
ASAS J200126+0737.7 Aql	min	57952.5257	0.0017	AG		1603	-Ir	34
ASAS J201225+0959.4 Aql	min	57988.3858	0.0010	AG	EB:’	1603	-Ir	41
ASAS J202741+2145.0 Vul	min	57964.3974	0.0022	AG		1603	-Ir	39
ASAS J202741+2145.0 Vul	min	57966.4315	0.0018	AG		1603	-Ir	31
ASAS J203921+1746.2 Del	min	57982.5233	0.0014	AG		1603	-Ir	35
ASAS J203256+2414.0 Vul	min	57980.4407	0.0012	AG		1603	-Ir	34
ASAS J203256+2414.0 Vul	min	57982.3889	0.0046	AG		1603	-Ir	35

Table 1: cont.

Variable	Ext	HJD 24.....	±	Obs	Type	Cam	Fil	n
ASAS J203256+2414.0 Vul	min	57982.5642	0.0013	AG		1603	-Ir	35
ASAS J203508+2430.9 Vul	min	57980.4309	0.0058	AG		1603	-Ir	31
ASAS J203508+2430.9 Vul	min	57982.4553	0.0045	AG		1603	-Ir	36
ASAS J205847+2731.9 Vul	min	57919.4631	0.0013	AG		1603	-Ir	22
ASAS J210121+0447.9 Equ	min	57966.5418	0.0031	AG	EB:'	1603	-Ir	30
ASAS J220226+4831.3 Cyg	min	57973.4657	0.0008	AG	WU'	1603	-Ir	39
ASAS J220226+4831.3 Cyg	min	57988.4376	0.0006	AG	WU'	1603	-Ir	44
ASAS J220226+4831.3 Cyg	min	57988.5719	0.0013	AG	WU'	1603	-Ir	44
ASAS J220925+0808.0 Peg	min	57989.4569	0.0021	AG		1603	-Ir	36
CSS J080021.8+194353 Cnc	min	57733.5510	0.0007	MS	WU'	16803	V	164
CSS J080021.8+194353 Cnc	min	57733.7069	0.0010	MS	WU'	16803	V	164
CSS J080053.5+200959 Cnc	min	57733.5668	0.0008	MS	WU'	16803	V	164
CSS J080053.5+200959 Cnc	min	57733.7548	0.0005	MS	WU'	16803	V	164
CSS J080241.4+192609 Cnc	min	57733.6662	0.0007	MS	WU'	16803	V	167
CSS J080247.0+194641 Cnc	min	57733.6039	0.0005	MS	Al'	16803	V	159
CSS J080501.9+194716 Cnc	min	57833.4808	0.0028	MS	El'	16803	V	72
CSS J080501.9+194716 Cnc	max	57733.5203	0.0010	MS	El'	16803	V	162
CSS J080501.9+194716 Cnc	max	57733.6414	0.0010	MS	El'	16803	V	162
CSS J080501.9+194716 Cnc	max	57733.7593	0.0010	MS	El'	16803	V	162
CSS J080010.0+201937 Cnc	min	57733.5875	0.0011	MS	WU'	16803	V	165
CSS J080010.0+201937 Cnc	min	57733.7536	0.0005	MS	WU'	16803	V	165
CSS J080010.0+201937 Cnc	min	57855.3818	0.0007	MS	WU'	16803	V	102
CSS J080021.8+194353 Cnc	min	57855.3961	0.0007	MS	WU'	16803	V	97
CSS J080324.8+195206 Cnc	min	57855.0000	0.0000	MS	Al'	16803	V	106
CSS J080053.5+200959 Cnc	min	57855.3577	0.0008	MS	WU'	16803	V	108
CSS J080241.4+192609 Cnc	min	57855.3894	0.0015	MS	WU'	16803	V	161
CSS J082605.2+040738 Hya	min	57811.3621	0.0012	AG	WU'	1603	-Ir	41
CSS J082746.5+392213 Lyn	min	57754.5701	0.0006	MS	WU'	16803	V	193
CSS J082746.5+392213 Lyn	min	57754.7146	0.0005	MS	WU'	16803	V	193
CSS J082746.5+392213 Lyn	min	57759.6253	0.0006	MS	WU'	16803	V	166
CSS J082746.5+392213 Lyn	min	57724.6779	0.0009	MS	WU'	16803	V	57
CSS J082746.5+392213 Lyn	min	57735.6558	0.0018	MS	WU'	16803	V	117
CSS J082746.5+392213 Lyn	min	57828.3624	0.0011	MS	WU'	16803	V	134
CSS J082746.5+392213 Lyn	min	57828.5048	0.0007	MS	WU'	16803	V	134
CSS J082908.8+391600 Lyn	min	57735.7401	0.0004	MS	WU'	16803	V	88
CSS J082908.8+391600 Lyn	min	57759.5914	0.0007	MS	WU'	16803	V	166
CSS J082908.8+391600 Lyn	min	57759.7414	0.0010	MS	WU'	16803	V	166
CSS J082908.8+391600 Lyn	min	57828.4262	0.0005	MS	WU'	16803	V	134
CSS J082519.8+311916 Cnc	min	57856.4101	0.0006	MS	WU'	16803	V	116
CSS J082357.4+314158 Cnc	max	57856.3591	0.0010	MS	dS'	16803	V	116
CSS J082357.4+314158 Cnc	max	57856.4308	0.0010	MS	dS'	16803	V	116
CSS J082519.8+311916 Cnc	min	57854.4395	0.0004	MS	WU'	16803	V	116
CSS J082242.7+310918 Cnc	min	57854.4667	0.0006	MS	WU'	16803	V	114
CSS J082357.4+314158 Cnc	max	57854.3837	0.0010	MS	dS'	16803	V	113
CSS J082357.4+314158 Cnc	max	57854.4490	0.0010	MS	dS'	16803	V	113
CSS J083954.1+232016 Cnc	min	57843.4841	0.0024	AG	WU'	1603	-Ir	43
CSS J092924.7+162427 Leo	min	57845.4900	0.0009	MS	WU'	16803	V	143
CSS J092924.7+162427 Leo	min	57846.3874	0.0013	MS	WU'	16803	V	116
CSS J093655.3+042123 Hya	min	57837.3892	0.0009	WLH	WU'	ST10	-IR	63
CSS J093057.0+155713 Leo	max	57875.3770	0.0010	MS		16803	V	89
CSS J145944.9+470409 Boo	max	57846.5454	0.0010	MS		16803	V	74
CSS J145843.6+472829 Boo	min	57846.5807	0.0006	MS	WU'	16803	V	71
CSS J145900.9+165455 Boo	min	57845.6558	0.0010	MS	El'	16803	V	110
CSS J150145.5+473351 Boo	min	57846.5574	0.0005	MS	WU'	16803	V	76
CSS J152527.5+015600 Ser	max	57895.4210	0.0010	FR		1603	-Ir	164
CSS J160111.8+251634 Ser	min2	57867.4147	0.0007	FR	WU'	1603	-Ir	63
CSS J160111.8+251634 Ser	min2	57874.3665	0.0010	FR	WU'	1603	-Ir	245
CSS J160111.8+251634 Ser	min	57874.5310	0.0003	FR	WU'	1603	-Ir	245
CSS J160111.8+251634 Ser	min	57879.4923	0.0003	FR	WU'	1603	-Ir	193
CSS J160111.8+251634 Ser	min	57890.4173	0.0007	FR	WU'	1603	-Ir	246
CSS J160111.8+251634 Ser	min	57891.4085	0.0013	FR	WU'	1603	-Ir	245
CSS J160111.8+251634 Ser	min2	57900.5152	0.0008	FR	WU'	1603	-Ir	208
CSS J160111.8+251634 Ser	min2	57901.5096	0.0006	FR	WU'	1603	-Ir	230
CSS J160507.1+254500 CrB	max	57874.4743	0.0005	FR	RR'	1603	-Ir	247
CSS J160507.1+254500 CrB	max	57891.4318	0.0010	FR	RR'	1603	-Ir	257
CSS J160507.1+254500 CrB	max	57901.5217	0.0005	FR	RR'	1603	-Ir	234
CSS J160645.3+245557 Ser	max	57890.4074	0.0010	FR		1603	-Ir	254
CSS J160645.3+245557 Ser	max	57891.5108	0.0015	FR		1603	-Ir	246
CSS J160645.3+245557 Ser	max	57901.4040	0.0010	FR		1603	-Ir	223
CSS J165846.7+321954 Her	min	57524.4482	0.0006	MS	WU'	16803	LUM	122
CSS J165846.7+321954 Her	min	57524.5843	0.0007	MS	WU'	16803	LUM	122

Table 1: cont.

Variable	Ext	HJD 24.....	±	Obs	Type	Cam	Fil	n
CSS J165846.7+321954 Her	min	57823.6302	0.0036	MS	WU'	16803	V	107
CSS J165645.8+314802 Her	min	57823.6794	0.0006	MS	WU'	16803	V	113
CSS J165843.3+314517 Her	min	57855.5155	0.0006	MS	Al'	16803	V	142
CSS J165843.3+314517 Her	min	57524.6018	0.0007	MS	Al'	16803	LUM	119
CSS J165831.2+321307 Her	min	57823.6699	0.0005	MS	WU'	16803	V	114
CSS J165414.7+325945 Her	min	57823.6302	0.0036	MS	Al'	16803	V	107
CSS J165645.8+314802 Her	min	57855.5395	0.0001	MS	WU'	16803	V	144
CSS J165831.2+321307 Her	min	57855.6578	0.0007	MS	WU'	16803	V	145
CSS J165846.7+321954 Her	min	57855.5751	0.0022	MS	WU'	16803	V	144
CSS J165846.7+321954 Her	min	57237.4379	0.0020	MS	WU'	16803	LUM	86
CSS J165831.2+321307 Her	min	57524.5012	0.0009	MS	WU'	16803	LUM	126
CSS J165831.2+321307 Her	min	57237.4528	0.0009	MS	WU'	16803	LUM	85
CSS J165645.8+314802 Her	min	57524.5544	0.0005	MS	WU'	16803	LUM	122
CSS J165645.8+314802 Her	min	57237.4772	0.0008	MS	WU'	16803	LUM	89
CSS J170916.3+451523 Her	min	57928.4268	0.0010	MS	WU'	16803	V	178
CSS J170916.3+451523 Her	min	57928.6066	0.0008	MS	WU'	16803	V	178
CSS J171522.4+212438 Her	min	57493.6539	0.0005	MS	WU'	16803	V	94
CSS J171442.6+204032 Her	min	57493.6730	0.0007	MS	WU'	16803	V	99
CSS J171522.4+212438 Her	min	57509.5390	0.0004	MS	WU'	16803	LUM	77
CSS J171522.4+212438 Her	min	57509.6627	0.0006	MS	WU'	16803	LUM	77
CSS J171442.6+204032 Her	min	57509.5944	0.0003	MS	WU'	16803	LUM	77
CSS J171246.1+203807 Her	min	57509.5832	0.0003	MS	Al'	16803	LUM	77
CSS J171724.5+205011 Her	min	57509.5682	0.0010	MS	RR'	16803	LUM	77
CSS J171724.5+205011 Her	min	57931.5006	0.0006	MS	RR'	16803	V	190
CSS J171522.4+212438 Her	min	57931.4782	0.0006	MS	WU'	16803	V	198
CSS J171522.4+212438 Her	min	57931.6009	0.0004	MS	WU'	16803	V	198
CSS J171319.0+453025 Her	min	57928.4865	0.0013	MS	WU'	16803	V	188
CSS J171319.0+453025 Her	min	57928.6174	0.0009	MS	WU'	16803	V	188
CSS J171414.2+452253 Her	min	57928.4178	0.0005	MS	Al'	16803	V	188
CSS J171012.3+462314 Her	min	57928.4704	0.0007	MS	WU'	16803	V	182
CSS J171012.3+462314 Her	min	57928.6176	0.0006	MS	WU'	16803	V	182
CSS J171253.8+451249 Her	max	57928.4598	0.0010	MS	RR'	16803	V	188
CSS J180936.0+381423 Lyr	max	57527.5115	0.0010	MS	RR'	16803	V	112
CSS J181533.0+320105 Lyr	min	57518.5273	0.0011	MS	WU'	16803	LUM	62
CSS J181533.0+320105 Lyr	min	57522.6147	0.0003	MS	WU'	16803	LUM	40
CSS J181925.4+314212 Lyr	min	57518.5282	0.0010	MS	WU'	16803	LUM	61
CSS J181430.8+380754 Lyr	min	57527.5675	0.0006	MS	WU'	16803	V	117
CSS J181409.2+385306 Lyr	min	57527.5689	0.0008	MS	WU'	16803	V	120
CSS J181349.1+384235 Lyr	min	57527.5926	0.0002	MS	WU'	16803	V	112
CSS J181409.2+390502 Lyr	min	57527.5905	0.0009	MS	WU'	16803	V	112
CSS J184544.8+401721 Lyr	min	57564.4298	0.0001	MS	WU'	16803	V	95
CSS J184901.0+401609 Lyr	min	57564.3953	0.0008	MS	WU'	16803	V	110
CSS J184544.8+401721 Lyr	min	57910.5114	0.0005	MS	WU'	16803	V	168
CSS J184544.8+401721 Lyr	min	57944.4746	0.0005	MS	WU'	16803	V	205
CSS J184544.8+401721 Lyr	min	57944.6235	0.0003	MS	WU'	16803	V	205
CSS J184544.8+401721 Lyr	min	57951.3865	0.0004	MS	WU'	16803	V	205
CSS J184544.8+401721 Lyr	min	57951.5367	0.0003	MS	WU'	16803	V	205
CSS J184544.8+401721 Lyr	min	57966.4136	0.0029	MS	WU'	16803	V	130
CSS J184544.8+401721 Lyr	min	57966.5650	0.0003	MS	WU'	16803	V	130
CSS J184544.8+401721 Lyr	min	57974.3786	0.0003	MS	WU'	16803	V	158
CSS J184544.8+401721 Lyr	min	57974.5306	0.0011	MS	WU'	16803	V	158
CSS J184901.0+401609 Lyr	min	57951.5242	0.0010	MS	WU'	16803	V	199
CSS J184901.0+401609 Lyr	min	57951.3775	0.0004	MS	WU'	16803	V	199
CSS J184901.0+401609 Lyr	min	57944.6054	0.0018	MS	WU'	16803	V	178
CSS J184901.0+401609 Lyr	min	57944.4423	0.0007	MS	WU'	16803	V	178
CSS J184901.0+401609 Lyr	min	57936.4286	0.0017	MS	WU'	16803	V	97
CSS J184901.0+401609 Lyr	min	57910.4717	0.0006	MS	WU'	16803	V	161
CSS J184901.0+401609 Lyr	min	57910.6289	0.0007	MS	WU'	16803	V	161
CSS J184748.0+393430 Lyr	max	57910.4873	0.0010	MS	RR'	16803	V	166
CSS J184748.0+393430 Lyr	max	57974.5372	0.0010	MS	RR'	16803	V	163
CSS J184748.0+393430 Lyr	max	57966.4860	0.0010	MS	RR'	16803	V	131
CSS J184748.0+393430 Lyr	max	57951.4159	0.0010	MS	RR'	16803	V	201
CSS J205334.6+052523 Del	min	57966.5008	0.0020	AG		1603	-Ir	27
CSS J210101.4+131318 Del	min	57966.5724	0.0018	AG	WU'	1603	-Ir	31
GSC 01485-00645 Boo	min	57845.6451	0.0009	MS		16803	V	103
GSC 01485-00645 Boo	min	57847.5889	0.0010	MS		16803	V	129
GSC 02670-02219 Cyg	min	58007.4450	0.0008	MS		16803	V	167
GSC 02678-02360 Cyg	min	58037.4305	0.0030	MSFR		16803	V	127
GSC 02678-02360 Cyg	min	57977.5252	0.0006	MSFR		16803	V	211
GSC 02678-02360 Cyg	min	57897.6221	0.0006	MSFR		16803	V	108
GSC 02678-02360 Cyg	min	57943.4575	0.0005	MSFR		16803	V	197

Table 1: cont.

Variable	Ext	HJD 24.....	±	Obs	Type	Cam	Fil	n
GSC 02678-02360 Cyg	max	58013.3432	0.0008	MSFR		16803	V	160
GSC 02678-02360 Cyg	max	58036.4273	0.0006	MSFR		16803	V	125
GSC 02677-00092 Cyg	min	57977.4280	0.0005	MSFR		16803	V	187
GSC 03715-00043 Cam	min2	57727.5415	0.0002	RATRCR		1600	V	225
GSC 1134-0368 Peg	min	57964.4522	0.0006	AG	E!	1603	-Ir	26
GSC 1158-0921 Peg	max	58053.2620	0.0004	ALH	dS'	3200M	V	332
GSC 1158-0921 Peg	min	58053.3052	0.0019	ALH	dS'	3200M	V	332
GSC 1158-0921 Peg	max	58053.3263	0.0004	ALH	dS'	3200M	V	332
GSC 1158-0921 Peg	min	58053.3719	0.0015	ALH	dS'	3200M	V	332
GSC 1220-1131 Ari	min	58072.2974	0.0009	ALH		3200M	V	594
GSC 1220-1131 Ari	max	58072.3291	0.0007	ALH		3200M	V	594
GSC 1220-1131 Ari	min	58072.3793	0.0007	ALH		3200M	V	594
GSC 1220-1131 Ari	max	58072.4110	0.0005	ALH		3200M	V	594
GSC 1220-1131 Ari	min	58072.4600	0.0007	ALH		3200M	V	594
GSC 1220-1131 Ari	max	58072.4921	0.0006	ALH		3200M	V	594
GSC 1220-1131 Ari	min	58072.5418	0.0008	ALH		3200M	V	594
GSC 1463-0483 Boo	min	57839.4363	0.0007	AG		1603	-Ir	41
GSC 1463-0483 Boo	min	57839.5921	0.0019	AG		1603	-Ir	41
GSC 1687-0207 Peg	min	57988.3890	0.0019	AG	E!	1603	-Ir	36
GSC 1687-0207 Peg	min	57988.5710	0.0051	AG	E!	1603	-Ir	36
GSC 1750-1237 Psc	min	58054.3829	0.0010	ALH	V:'	3200M	V	453
GSC 1750-1237 Psc	max	58054.4131	0.0007	ALH	V:'	3200M	V	453
GSC 1750-1237 Psc	min	58054.4690	0.0011	ALH	V:'	3200M	V	453
GSC 1750-1237 Psc	max	58054.5001	0.0008	ALH	V:'	3200M	V	453
GSC 1750-1237 Psc	min	58054.5569	0.0013	ALH	V:'	3200M	V	453
GSC 1750-1237 Psc	max	58054.5870	0.0006	ALH	V:'	3200M	V	453
GSC 2038-00041 CrB	min	57867.4449	0.0020	FR		1603	-Ir	121
GSC 2038-00041 CrB	min	57873.3581	0.0002	FR		1603	-Ir	150
GSC 2043-1201 Her	max	57915.3803	0.0008	ALH		3200M	V	330
GSC 2043-1201 Her	min	57915.4240	0.0010	ALH		3200M	V	330
GSC 2043-1201 Her	max	57915.4582	0.0009	ALH		3200M	V	330
GSC 2043-1201 Her	min	57915.5021	0.0008	ALH		3200M	V	330
GSC 2043-1201 Her	max	57915.5364	0.0010	ALH		3200M	V	330
GSC 2043-1201 Her	min	57915.5795	0.0012	ALH		3200M	V	330
GSC 2080-0986 Her	min	57924.4296	0.0012	ALH		3200M	V	330
GSC 2080-0986 Her	max	57924.4607	0.0005	ALH		3200M	V	330
GSC 2080-0986 Her	min	57924.5303	0.0013	ALH		3200M	V	330
GSC 2080-0986 Her	max	57924.5606	0.0007	ALH		3200M	V	330
GSC 2108-1564 Her	min	57939.3853	0.0009	ALH		3200M	V	390
GSC 2108-1564 Her	max	57939.4196	0.0011	ALH		3200M	V	390
GSC 2108-1564 Her	min	57939.4834	0.0008	ALH		3200M	V	390
GSC 2108-1564 Her	max	57939.5178	0.0010	ALH		3200M	V	390
GSC 2108-1564 Her	min	57939.5811	0.0010	ALH		3200M	V	390
GSC 2134 0028 Lyr	min	57935.5188	0.0005	MS		16803	V	166
GSC 2134 0028 Lyr	min	57950.4827	0.0011	MS		16803	V	141
GSC 2134 0028 Lyr	min	57899.6148	0.0004	MS		16803	V	114
GSC 2134-01608 Lyr	min	57893.5568	0.0009	MS		16803	V	106
GSC 2134-01608 Lyr	min	57899.5962	0.0005	MS		16803	V	118
GSC 2134-01608 Lyr	min	57935.5869	0.0002	MS		16803	V	172
GSC 2134-01608 Lyr	min	57949.5088	0.0009	MS		16803	V	146
GSC 2134-01608 Lyr	min	57950.5639	0.0011	MS		16803	V	146
GSC 2134-01608 Lyr	min	57921.4041	0.0005	MS		16803	V	166
GSC 2134-00590 Lyr	min	57899.4960	0.0017	MS		16803	V	120
GSC 2134-00590 Lyr	min	57893.5282	0.0003	MS		16803	V	110
GSC 2134-00590 Lyr	min	57907.5978	0.0004	MS		16803	V	64
GSC 2134-00590 Lyr	min	57921.4534	0.0004	MS		16803	V	167
GSC 2134-00590 Lyr	min	57935.5246	0.0003	MS		16803	V	181
GSC 2134-00590 Lyr	min	57949.5935	0.0005	MS		16803	V	154
GSC 2134-00590 Lyr	min	57950.4462	0.0004	MS		16803	V	145
GSC 2134-01608 Lyr	min	57978.4069	0.0008	MS		16803	V	132
GSC 2134 0028 Lyr	min	57978.4974	0.0008	MS		16803	V	132
GSC 2134-00590 Lyr	min	57978.3744	0.0008	MS		16803	V	131
GSC 2134-00590 Lyr	min	57978.5865	0.0005	MS		16803	V	131
GSC 2290-1195 And	min	58041.3398	0.0016	ALH		3200M	V	464
GSC 2290-1195 And	max	58041.3645	0.0010	ALH		3200M	V	464
GSC 2290-1195 And	min	58041.4173	0.0017	ALH		3200M	V	464
GSC 2290-1195 And	max	58041.4437	0.0007	ALH		3200M	V	464
GSC 2290-1195 And	min	58041.4962	0.0016	ALH		3200M	V	464
GSC 2290-1195 And	max	58041.5236	0.0008	ALH		3200M	V	464
GSC 2290-1195 And	min	58041.5699	0.0020	ALH		3200M	V	464
GSC 2290-1195 And	max	58041.6027	0.0013	ALH		3200M	V	464

Table 1: cont.

Variable	Ext	HJD 24.....	±	Obs	Type	Cam	Fil	n
GSC 2527-2115 Com	max	57800.6520	0.0020	AG		1603	-Ir	84
GSC 2566-1398 Boo	min	57890.3516	0.0013	ALH	dS'	3200M	V	706
GSC 2566-1398 Boo	max	57890.3795	0.0004	ALH	dS'	3200M	V	706
GSC 2566-1398 Boo	min	57890.4427	0.0009	ALH	dS'	3200M	V	706
GSC 2566-1398 Boo	max	57890.4701	0.0003	ALH	dS'	3200M	V	706
GSC 2566-1398 Boo	min	57890.5332	0.0010	ALH	dS'	3200M	V	706
GSC 2566-1398 Boo	max	57890.5612	0.0004	ALH	dS'	3200M	V	706
GSC 2589-0536 Her	max	57928.3945	0.0010	ALH	dS'	3200M	V	284
GSC 2589-0536 Her	min	57928.4707	0.0021	ALH	dS'	3200M	V	284
GSC 2589-0536 Her	max	57928.5230	0.0014	ALH	dS'	3200M	V	284
GSC 2671-2330 Cyg	min	57905.4365	0.0015	AG		1603	-Ir	15
GSC 2671-02330 Cyg	min	57240.3563	0.0002	FR		1603	-Ir	292
GSC 2671-02330 Cyg	min2	57260.4107	0.0002	FR		1603	-Ir	355
GSC 2671-02330 Cyg	min	57939.3695	0.0020	FR		1603	-Ir	176
GSC 2670-02219 Cyg	min	57240.4479	0.0004	FR		1603	-Ir	286
GSC 2670-02219 Cyg	min2	57260.5818	0.0013	FR		1603	-Ir	347
GSC 2670-02219 Cyg	min	57939.4137	0.0010	FR		1603	-Ir	165
GSC 2670-02219 Cyg	min2	57952.4415	0.0010	FR		1603	-Ir	227
GSC 2670-04264 Cyg	min2	57260.4300	0.0003	FR		1603	-Ir	346
GSC 2670-00731 Cyg	max	57240.4144	0.0010	FR		1603	-Ir	289
GSC 2670-00731 Cyg	max	57240.5647	0.0012	FR		1603	-Ir	289
GSC 2670-00731 Cyg	max	57260.4381	0.0010	FR		1603	-Ir	344
GSC 2670-00731 Cyg	max	57260.5817	0.0013	FR		1603	-Ir	344
GSC 2670-00731 Cyg	max	57939.4812	0.0003	FR		1603	-Ir	163
GSC 2670-00731 Cyg	max	57952.5359	0.0003	FR		1603	-Ir	238
GSC 2671-00834 Cyg	min	57240.3900	0.0005	FR		1603	-Ir	288
GSC 2671-00834 Cyg	min	57260.4089	0.0004	FR		1603	-Ir	333
GSC 2671-00834 Cyg	min	57952.4839	0.0003	FR		1603	-Ir	250
GSC 2678-02360 Cyg	min2	57924.3825	0.0010	FR		1603	-Ir	149
GSC 2670-02219 Cyg	min	57939.4145	0.0012	MSFR		16803	V	151
GSC 2670-02219 Cyg	min	57938.5269	0.0005	MSFR		16803	V	157
GSC 2670-02219 Cyg	min	57932.5975	0.0012	MSFR		16803	V	74
GSC 2670-02219 Cyg	min	57954.5155	0.0005	MSFR		16803	V	128
GSC 2670-02219 Cyg	min	57961.6205	0.0009	MSFR		16803	V	165
GSC 2670 731 Cyg	max	57912.6076	0.0007	MSFR		16803	V	96
GSC 2670 731 Cyg	max	57932.5419	0.0010	MSFR		16803	V	58
GSC 2670 731 Cyg	max	57932.6384	0.0023	MSFR		16803	V	58
GSC 2670 731 Cyg	max	57938.4025	0.0015	MSFR		16803	V	148
GSC 2670 731 Cyg	max	57938.5555	0.0008	MSFR		16803	V	148
GSC 2670 731 Cyg	max	57939.4826	0.0010	MSFR		16803	V	155
GSC 2670 731 Cyg	max	57939.6318	0.0013	MSFR		16803	V	155
GSC 2670 731 Cyg	max	57942.5961	0.0008	MSFR		16803	V	93
GSC 2670 731 Cyg	max	57954.4011	0.0010	MSFR		16803	V	141
GSC 2670 731 Cyg	max	57954.5532	0.0011	MSFR		16803	V	141
GSC 2670 731 Cyg	max	57961.3973	0.0020	MSFR		16803	V	159
GSC 2685-1754 Cyg	min	57988.4793	0.0020	AG	E!	1603	-Ir	41
GSC 2695-03684 Cyg	min	57946.4898	0.0006	MSFR		16803	V	153
GSC 2695-03684 Cyg	min	57962.5695	0.0005	MSFR		16803	V	151
GSC 2695-03684 Cyg	min	57965.3624:	0.0015	MSFR		16803	V	152
GSC 2696-02758 Cyg	min	57976.5873	0.0010	MSFR		16803	V	120
GSC 2696-02758 Cyg	min	57962.6504	0.0008	MSFR		16803	V	99
GSC 2695-03684 Cyg	min	57976.5491	0.0008	MSFR		16803	V	218
GSC 2696-02758 Cyg	min	57946.3864	0.0006	MSFR		16803	V	158
GSC 2815-0790 And	max	58051.3049	0.0004	ALH	SX'	3200M	V	471
GSC 2815-0790 And	min	58051.3831	0.0016	ALH	SX'	3200M	V	471
GSC 2815-0790 And	max	58051.4123	0.0005	ALH	SX'	3200M	V	471
GSC 2815-0790 And	min	58051.4911	0.0016	ALH	SX'	3200M	V	471
GSC 2815-0790 And	max	58051.5190	0.0004	ALH	SX'	3200M	V	471
GSC 2815-0790 And	min	58051.5982	0.0011	ALH	SX'	3200M	V	471
GSC 2815-0790 And	max	58051.6260	0.0006	ALH	SX'	3200M	V	471
GSC 2843-1999 And	min	58080.3537	0.0012	ALH		3200M	V	521
GSC 2843-1999 And	max	58080.3761	0.0005	ALH		3200M	V	521
GSC 2843-1999 And	min	58080.4154	0.0012	ALH		3200M	V	521
GSC 2843-1999 And	max	58080.4381	0.0008	ALH		3200M	V	521
GSC 2843-1999 And	min	58080.4790	0.0017	ALH		3200M	V	521
GSC 2843-1999 And	max	58080.5000	0.0007	ALH		3200M	V	521
GSC 2843-1999 And	min	58080.5411	0.0009	ALH		3200M	V	521
GSC 2843-1999 And	max	58080.5623	0.0005	ALH		3200M	V	521
GSC 3004-0870 UMa	max	57843.3177	0.0005	ALH		ST8XM	V	511
GSC 3004-0870 UMa	min	57843.3742	0.0014	ALH		ST8XM	V	511
GSC 3004-0870 UMa	max	57843.4004	0.0006	ALH		ST8XM	V	511

Table 1: cont.

Variable	Ext	HJD 24.....	±	Obs	Type	Cam	Fil	n
GSC 3004-0870 UMa	min	57843.4576	0.0015	ALH		ST8XM	V	511
GSC 3004-0870 UMa	max	57843.4825	0.0006	ALH		ST8XM	V	511
GSC 3004-0870 UMa	min	57843.5397	0.0014	ALH		ST8XM	V	511
GSC 3004-0870 UMa	max	57843.5640	0.0005	ALH		ST8XM	V	511
GSC 3004-0870 UMa	min	57843.6215	0.0017	ALH		ST8XM	V	511
GSC 3021-0460 CVn	min	57842.4713	0.0045	AG	E!	1603	-Ir	40
GSC 3315-00071 Per	min	54845.4980	0.0030	FR		1603	-Ir	117
GSC 3315-00071 Per	min	55827.4601	0.0051	FR		1603	-Ir	30
GSC 3315-00071 Per	min	55978.4713	0.0010	FR		1603	-Ir	73
GSC 3315-00071 Per	min2	57811.4812	0.0012	FR		1603	-Ir	111
GSC 3315-00071 Per	min	57823.3079	0.0030	FR		1603	-Ir	40
GSC 3315-00386 Per	min	57811.4443	0.0047	FR		1603	-Ir	110
GSC 3339-00898 Per	max	57657.3555	0.0015	FR		1603	-Ir	144
GSC 3339-00898 Per	max	57657.4570	0.0015	FR		1603	-Ir	144
GSC 3339-00898 Per	max	57752.2679	0.0009	FR		1603	-Ir	198
GSC 3339-00898 Per	max	57752.3722	0.0007	FR		1603	-Ir	99
GSC 3339-00898 Per	max	57753.2577	0.0015	FR		1603	-Ir	93
GSC 3339-00898 Per	max	57829.3165	0.0015	FR		1603	-Ir	224
GSC 3339-00898 Per	max	57829.4175	0.0020	FR		1603	-Ir	112
GSC 3339-00898 Per	max	57838.4680	0.0010	FR		1603	-Ir	170
GSC 3339-00898 Per	max	57839.3417	0.0005	FR		1603	-Ir	178
GSC 3339-00898 Per	max	57839.4411	0.0007	FR		1603	-Ir	178
GSC 3339-00898 Per	max	57840.3428	0.0012	FR		1603	-Ir	206
GSC 3339-00898 Per	max	57842.4220	0.0008	FR		1603	-Ir	141
GSC 3339-00898 Per	max	57843.3131	0.0007	FR		1603	-Ir	117
GSC 3339-00898 Per	max	57844.3035	0.0010	FR		1603	-Ir	141
GSC 3339-00898 Per	max	57844.4064	0.0008	FR		1603	-Ir	141
GSC 3339-00242 Per	min	57842.4688	0.0020	FR		1603	-Ir	79
GSC 3339-00242 Per	min2	57844.3747	0.0028	FR		1603	-Ir	63
GSC 3585-02696 Cyg	min	57257.3389	0.0011	FR		1603	-Ir	362
GSC 3585-02696 Cyg	min2	57257.5650	0.0005	FR		1603	-Ir	362
GSC 3585-02696 Cyg	min2	57261.5289	0.0008	FR		1603	-Ir	338
GSC 3585-02696 Cyg	min	57263.5171	0.0007	FR		1603	-Ir	298
GSC 3585-02696 Cyg	min	57264.4016	0.0005	FR		1603	-Ir	362
GSC 3717-00153 Per	min2	57657.3934	0.0005	FR		1603	-Ir	97
GSC 3717-00153 Per	min	57657.6429	0.0036	FR		1603	-Ir	97
GSC 3717-00153 Per	min2	57752.3133	0.0004	FR		1603	-Ir	68
GSC 3717-00153 Per	min2	57829.4376	0.0005	FR		1603	-Ir	77
GSC 3717-00153 Per	min2	57838.3348	0.0009	FR		1603	-Ir	63
GSC 3717-00153 Per	min2	57839.3232	0.0003	FR		1603	-Ir	96
GSC 3717-00153 Per	min2	57840.3124	0.0003	FR		1603	-Ir	94
GSC 3717-00153 Per	min2	57843.2860	0.0010	FR		1603	-Ir	190
GSC 3717-00153 Per	min	57844.5091	0.0010	FR		1603	-Ir	181
GSC 3717-00293 Per	max	57657.3542	0.0016	FR		1603	-Ir	141
GSC 3717-00293 Per	max	57657.4848	0.0007	FR		1603	-Ir	141
GSC 3717-00293 Per	max	57657.6173	0.0017	FR		1603	-Ir	141
GSC 3717-00293 Per	max	57838.4363	0.0007	FR		1603	-Ir	92
GSC 3717-00293 Per	max	57839.4240	0.0008	FR		1603	-Ir	179
GSC 3717-00293 Per	max	57840.3570	0.0010	FR		1603	-Ir	100
GSC 3717-00293 Per	max	57842.4090	0.0010	FR		1603	-Ir	68
GSC 3717-00293 Per	max	57843.4083	0.0010	FR		1603	-Ir	75
GSC 3717-00293 Per	max	57844.3340	0.0010	FR		1603	-Ir	85
GSC 3832-0152 UMa	min	57838.3345	0.0012	ALH	dS'	ST8XM	V	504
GSC 3832-0152 UMa	max	57838.3617	0.0003	ALH	dS'	ST8XM	V	504
GSC 3832-0152 UMa	min	57838.4264	0.0010	ALH	dS'	ST8XM	V	504
GSC 3832-0152 UMa	max	57838.4531	0.0004	ALH	dS'	ST8XM	V	504
GSC 3832-0152 UMa	min	57838.5174	0.0011	ALH	dS'	ST8XM	V	504
GSC 3832-0152 UMa	max	57838.5442	0.0003	ALH	dS'	ST8XM	V	504
GSC 3832-0152 UMa	min	57838.6087	0.0010	ALH	dS'	ST8XM	V	504
GSC 3832-0152 UMa	max	57838.6356	0.0005	ALH	dS'	ST8XM	V	504
GSC 3983-0544 Lac	min	57964.4032	0.0033	AG	E!	1603	-Ir	40
GSC 3985-1258 Cas	min	57980.5063	0.0011	AG		1603	-Ir	31
GSC 3985-1258 Cas	min	57995.5123	0.0013	AG		1603	-Ir	42
GSC 4030-1992 Cas	min	57982.4697	0.0035	AG	E!	1603	-Ir	31
GSC 4417-0394 UMi	min	57913.3962	0.0011	ALH		3200M	V	351
GSC 4417-0394 UMi	max	57913.4321	0.0037	ALH		3200M	V	351
GSC 4417-0394 UMi	min	57913.5280	0.0013	ALH		3200M	V	351
GSC 4417-0394 UMi	max	57913.5643	0.0007	ALH		3200M	V	351
GSC 4500-0083 Cep	min	58045.2976	0.0009	ALH	dS'	3200M	V	468
GSC 4500-0083 Cep	max	58045.3271	0.0005	ALH	dS'	3200M	V	468
GSC 4500-0083 Cep	min	58045.3811	0.0010	ALH	dS'	3200M	V	468

Table 1: cont.

Variable	Ext	HJD 24.....	±	Obs	Type	Cam	Fil	n
GSC 4500-0083 Cep	max	58045.4128	0.0006	ALH	dS'	3200M	V	468
GSC 4500-0083 Cep	min	58045.4641	0.0013	ALH	dS'	3200M	V	468
GSC 4500-0083 Cep	max	58045.4987	0.0007	ALH	dS'	3200M	V	468
GSC 4500-0083 Cep	min	58045.5531	0.0011	ALH	dS'	3200M	V	468
GSC 4500-0083 Cep	max	58045.5835	0.0005	ALH	dS'	3200M	V	468
GSC 4552-1498 Dra	min	57841.4243	0.0010	ALH	dS'	ST8XM	V	506
GSC 4552-1498 Dra	max	57841.4444	0.0004	ALH	dS'	ST8XM	V	506
GSC 4552-1498 Dra	min	57841.4799	0.0011	ALH	dS'	ST8XM	V	506
GSC 4552-1498 Dra	max	57841.5001	0.0042	ALH	dS'	ST8XM	V	506
GSC 4552-1498 Dra	min	57841.5364	0.0008	ALH	dS'	ST8XM	V	506
GSC 4552-1498 Dra	max	57841.5556	0.0004	ALH	dS'	ST8XM	V	506
GSC 4552-1498 Dra	min	57841.5920	0.0011	ALH	dS'	ST8XM	V	506
GSC 4619-0450 Cep	min	58057.4026	0.0018	ALH	dS'	3200M	V	473
GSC 4619-0450 Cep	max	58057.4387	0.0006	ALH	dS'	3200M	V	473
GSC 4619-0450 Cep	min	58057.5334	0.0018	ALH	dS'	3200M	V	473
GSC 4619-0450 Cep	max	58057.5723	0.0007	ALH	dS'	3200M	V	473
GSC 4619-0450 Cep	min	58057.6670	0.0019	ALH	dS'	3200M	V	473
GSC 4920-0522 Leo	max	57838.3690	0.0010	AG		1603	-Ir	80
LINEAR 10250985 Boo	min	57850.6013	0.0005	MS	WU'	16803	V	203
LINEAR 10250985 Boo	min	57815.6232	0.0007	MS	WU'	16803	V	145
LINEAR 13095415 Boo	min	57845.6591	0.0013	MS	WU'	16803	V	110
LINEAR 13095415 Boo	min	57847.6707	0.0007	MS	WU'	16803	V	132
LINEAR 14083195 Ser	max	57895.4174	0.0015	FR	RR'	1603	-Ir	156
LINEAR 14089317 Ser	min	57895.5794:	0.0070	FR	Al'	1603	-Ir	166
LINEAR 14714767 Boo	min	57831.6326	0.0008	MS	WU'	16803	V	103
LINEAR 14714767 Boo	min	57848.5788	0.0003	MS	WU'	16803	V	140
LINEAR 14713979 Boo	min	57858.5667	0.0013	MS	RR'	16803	V	108
LINEAR 14714767 Boo	min	57858.5290	0.0004	MS	WU'	16803	V	112
LINEAR 14714767 Boo	min	57858.6675	0.0016	MS	WU'	16803	V	112
LINEAR 14713979 Boo	min	57862.5017	0.0014	MS	RR'	16803	V	188
LINEAR 14714767 Boo	min	57862.4324	0.0012	MS	WU'	16803	V	186
LINEAR 14714767 Boo	min	57862.5641	0.0009	MS	WU'	16803	V	186
LINEAR 19785439 Her	min	57855.5848	0.0012	MS	WU'	16803	V	124
LINEAR 19785439 Her	min	57823.6414	0.0006	MS	WU'	16803	V	113
LINEAR 19785439 Her	min	57524.5301	0.0006	MS	WU'	16803	LUM	124
LINEAR 19775800 Her	max	57524.4844	0.0010	MS	RR'	16803	LUM	124
LINEAR 19775800 Her	max	57855.5458	0.0010	MS	RR'	16803	V	142
LINEAR 20371308 Her	min	57856.6305	0.0005	MS	WU'	16803	V	130
LINEAR 20372537 Her	min	57856.5974	0.0007	MS	WU'	16803	V	135
LINEAR 20371308 Her	min	57852.6421	0.0004	MS	WU'	16803	V	130
LINEAR 20372537 Her	min	57852.5558	0.0006	MS	WU'	16803	V	130
LINEAR 20372537 Her	min	57852.7012	0.0004	MS	WU'	16803	V	130
LINEAR 440750 Cnc	min	57856.3322	0.0001	MS	WU'	16803	V	113
LINEAR 444083 Cnc	min	57856.3360	0.0004	MS	WU'	16803	V	119
LINEAR 444083 Cnc	min	57856.4583	0.0004	MS	WU'	16803	V	119
LINEAR 444083 Cnc	min	57854.3517	0.0004	MS	WU'	16803	V	105
LINEAR 444083 Cnc	min	57854.4750	0.0005	MS	WU'	16803	V	105
LINEAR 6499162 Lyn	min	57861.4943	0.0005	MS	Al'	16803	V	132
LINEAR 6500817 Lyn	min	57847.4488	0.0011	MS	WU'	16803	V	120
LINEAR 6500817 Lyn	min	57851.4208	0.0005	MS	WU'	16803	V	143
LINEAR 6500817 Lyn	min	57861.3421	0.0016	MS	WU'	16803	V	128
LINEAR 6500817 Lyn	min	57861.4814	0.0004	MS	WU'	16803	V	128
LINEAR 701058 Cnc	min	57854.3716	0.0019	MS	WU'	16803	V	125
LINEAR 703406 Cnc	min	57856.3918	0.0005	MS	WU'	16803	V	115
LINEAR 703406 Cnc	min	57854.4639	0.0012	MS	WU'	16803	V	118
LINEAR 9902637 Boo	min	57815.6622	0.0006	MS	WU'	16803	V	149
LINEAR 9902637 Boo	min	57820.5122	0.0007	MS	WU'	16803	V	165
LINEAR 9902637 Boo	min	57820.6680	0.0004	MS	WU'	16803	V	165
LINEAR 9906732 Boo	min	57844.5782	0.0007	MS	WU'	16803	V	117
LINEAR 9906732 Boo	min	57850.5384	0.0007	MS	WU'	16803	V	205
LINEAR 9906732 Boo	min	57850.6802	0.0012	MS	WU'	16803	V	205
LINEAR 9906732 Boo	min	57815.6334	0.0009	MS	WU'	16803	V	155
LINEAR 9906732 Boo	min	57820.6051	0.0006	MS	WU'	16803	V	178
LINEAR 9902637 Boo	min	57844.5974	0.0012	MS	WU'	16803	V	55
LINEAR 9902637 Boo	min	57850.6941	0.0006	MS	WU'	16803	V	205
LINEAR 9902637 Boo	min	57850.5362	0.0007	MS	WU'	16803	V	205
LINEAR 9901761 Boo	min	57850.4868	0.0017	MS	WU'	16803	V	204
LINEAR 9901761 Boo	min	57850.6571	0.0009	MS	WU'	16803	V	204
LINEAR 9901761 Boo	min	57844.5706	0.0008	MS	WU'	16803	V	110
LINEAR 9901761 Boo	min	57820.5784	0.0006	MS	WU'	16803	V	172
LINEAR 9901761 Boo	min	57815.6678	0.0008	MS	WU'	16803	V	145

Table 1: cont.

Variable	Ext	HJD 24.....	±	Obs	Type	Cam	Fil	n
NSVS 02622222 UMa	min	57722.5458	0.0003	RATRCR	EB:'	1600	V	227
NSVS 10142768 Cnc	min	57798.3649	0.0023	AG		1603	-Ir	60
NSVS 10142768 Cnc	min	57798.5560	0.0027	AG		1603	-Ir	60
NSVS 10123419 Cnc	min	57843.4258	0.0007	AG	WU'	1603	-Ir	43
NSVS 10123419 Cnc	min	57844.3427	0.0010	AG	WU'	1603	-Ir	39
NSVS 109935 Cam	min	57815.3057	0.0011	AG	PM'	1603	-Ir	43
NSVS 11480607 Del	min	57980.5047	0.0020	AG	EB:'	1603	-Ir	33
NSVS 11723163 Peg	min	57989.5342	0.0024	AG	WU'	1603	-Ir	36
NSVS 1203826 Dra	min	57887.4704	0.0010	AG	EB:'	1603	-Ir	25
NSVS 1206916 Dra	min	57887.4068	0.0031	AG	EB:'	1603	-Ir	24
NSVS 12667099 CMi	min	57800.4216	0.0016	AG		1603	-Ir	41
NSVS 12741654 CMi	min	57800.2964	0.0008	AG		1603	-Ir	50
NSVS 1305379 Cep	min	57973.4090	0.0037	AG		1603	-Ir	38
NSVS 13120542 Leo	min	57829.3884	0.0026	AG		1603	-Ir	53
NSVS 13120542 Leo	min	57829.5637	0.0008	AG		1603	-Ir	53
NSVS 1394144 Cep	min	57901.5097	0.0021	AG	EB:'	1603	-Ir	31
NSVS 1431216 Del	min	57968.4677	0.0022	AG		1603	-Ir	38
NSVS 1507733 Cas	min	57968.4609	0.0030	AG	EB:'	1603	-Ir	39
NSVS 1541003 Cas	min	57982.5475	0.0019	AG		1603	-Ir	41
NSVS 1543348 Cas	min	57992.3936	0.0018	AG	EB:'	1603	-Ir	31
NSVS 1625889 Cas	min	57980.4942	0.0018	AG		1603	-Ir	34
NSVS 173024 Cep	max	57987.3490	0.0010	AG		1603	-Ir	44
NSVS 173024 Cep	max	57987.4590	0.0010	AG		1603	-Ir	44
NSVS 1750812 Per	min	57995.4155	0.0013	AG		1603	-Ir	42
NSVS 1750812 Per	min	57995.6017	0.0010	AG		1603	-Ir	42
NSVS 207277 Cep	min	57926.4431	0.0005	AG		1603	-Ir	22
NSVS 222186 Cas	min	57968.5046	0.0020	AG		1603	-Ir	39
NSVS 2281526 Aur	min	57763.3830	0.0010	MS		16803	V	222
NSVS 2281526 Aur	min	57763.6112	0.0010	MS		16803	V	222
NSVS 2281526 Aur	max	57763.4819	0.0010	MS		16803	V	222
NSVS 2281526 Aur	max	57756.6320	0.0010	MS		16803	V	179
NSVS 2281526 Aur	min	57756.5396	0.0010	MS		16803	V	179
NSVS 2281526 Aur	max	57690.6696	0.0010	MS		16803	V	179
NSVS 2281526 Aur	min	57814.5002	0.0010	MS		16803	V	160
NSVS 2281526 Aur	max	57814.3626	0.0010	MS		16803	V	160
NSVS 2554499 UMa	min	57811.4018	0.0029	AG	EB:'	1603	-Ir	58
NSVS 2554499 UMa	min	57811.6027	0.0013	AG	EB:'	1603	-Ir	58
NSVS 2556336 UMa	min	57811.5708	0.0032	AG		1603	-Ir	58
NSVS 3068865 Dra	min	57884.5267	0.0007	AG	EB'	1603	-Ir	48
NSVS 3245311 Cyg	min	57973.5247	0.0024	AG	EB:'	1603	-Ir	39
NSVS 3536850 Cep	min	57989.4022	0.0014	AG		1603	-Ir	39
NSVS 3724203 Cas	min	57995.4463	0.0008	AG	EB:'	1603	-Ir	41
NSVS 3745507 Cas	min	57995.4531	0.0012	AG		1603	-Ir	41
NSVS 375645 Cas	min	57989.3678	0.0021	AG	EB:'	1603	-Ir	38
NSVS 375645 Cas	min	57989.5226	0.0023	AG	EB:'	1603	-Ir	38
NSVS 380858 Cas	min	57989.3992	0.0012	AG	EB:'	1603	-Ir	38
NSVS 380858 Cas	min	57989.5407	0.0075	AG	EB:'	1603	-Ir	38
NSVS 4813681 Lyn	min	57828.4964	0.0004	MS		16803	V	92
NSVS 4812501 Lyn	min	57828.3921	0.0002	MS	WU'	16803	V	125
NSVS 4812501 Lyn	min	57759.7383	0.0002	MS	WU'	16803	V	166
NSVS 4812501 Lyn	min	57759.5704	0.0002	MS	WU'	16803	V	166
NSVS 4812501 Lyn	min	57729.7393	0.0003	MS	WU'	16803	V	95
NSVS 4812501 Lyn	min	57724.7436	0.0003	MS	WU'	16803	V	56
NSVS 4810449 Lyn	min	57828.4407	0.0003	MS	WU'	16803	V	134
NSVS 4810449 Lyn	min	57759.5803	0.0002	MS	WU'	16803	V	166
NSVS 4810449 Lyn	min	57729.6098	0.0005	MS	WU'	16803	V	56
NSVS 4813681 Lyn	min	57853.4915	0.0007	MS		16803	V	100
NSVS 4812501 Lyn	min	57853.3949	0.0012	MS	WU'	16803	V	116
NSVS 4810449 Lyn	min	57853.4823	0.0003	MS	WU'	16803	V	119
NSVS 4810449 Lyn	min	57848.3610	0.0007	MS	WU'	16803	V	107
NSVS 4989337 UMa	min	57841.3582	0.0021	AG		1603	-Ir	35
NSVS 4992380 UMa	min	57841.3934	0.0017	AG		1603	-Ir	35
NSVS 5084132 CVn	min	57842.3885	0.0012	AG		1603	-Ir	49
NSVS 5084132 CVn	min	57842.5504	0.0022	AG		1603	-Ir	49
NSVS 5084132 CVn	min	57844.3337	0.0012	AG		1603	-Ir	42
NSVS 5084132 CVn	min	57844.4907	0.0039	AG		1603	-Ir	42
NSVS 5084132 CVn	min	57844.6478	0.0006	AG		1603	-Ir	42
NSVS 5084132 CVn	min	57846.4334	0.0017	AG		1603	-Ir	44
NSVS 5084132 CVn	min	57846.5967	0.0021	AG		1603	-Ir	44
NSVS 5149208 Boo	min	57879.3814	0.0009	AG		1603	-Ir	41
NSVS 5168364 Boo	min	57831.7140	0.0003	MS	WU'	16803	V	104

Table 1: cont.

Variable	Ext	HJD 24.....	±	Obs	Type	Cam	Fil	n
NSVS 5168364 Boo	min	57848.6667	0.0003	MS	WU’	16803	V	145
NSVS 5168364 Boo	min	57858.6008	0.0004	MS	WU’	16803	V	110
NSVS 5168364 Boo	min	57862.5400	0.0002	MS	WU’	16803	V	198
NSVS 5449927 Lyr	min	57913.4380	0.0031	AG	EB:’	1603	-Ir	26
NSVS 6041126 Lac	min	57989.4518	0.0017	AG		1603	-Ir	37
NSVS 6041126 Lac	min	57995.5559	0.0046	AG		1603	-Ir	42
NSVS 6109324 Lac	min	57964.4937	0.0037	AG		1603	-Ir	40
NSVS 6109324 Lac	min	57980.4913	0.0021	AG		1603	-Ir	33
NSVS 6109324 Lac	min	57987.3987	0.0023	AG		1603	-Ir	46
NSVS 6109324 Lac	min	57987.5235	0.0030	AG		1603	-Ir	46
NSVS 6110086 Lac	min	57964.4200	0.0013	AG	EB:’	1603	-Ir	36
NSVS 6110086 Lac	min	57980.5029	0.0018	AG	EB:’	1603	-Ir	32
NSVS 6110086 Lac	min	57987.3945	0.0010	AG	EB:’	1603	-Ir	46
NSVS 6110086 Lac	min	57987.6029	0.0031	AG	EB:’	1603	-Ir	46
NSVS 6127971 Lac	min	57968.4990	0.0012	AG	Al’	1603	-Ir	40
NSVS 6143186 And	min	57987.3599	0.0023	AG	EB:’	1603	-Ir	44
NSVS 6143186 And	min	57987.5948	0.0017	AG	EB:’	1603	-Ir	44
NSVS 6195117 And	min	57964.4728	0.0017	AG	EB:’	1603	-Ir	40
NSVS 7369453 Cnc	min	57856.4418	0.0006	MS	WU’	16803	V	119
NSVS 7369453 Cnc	min	57854.3937	0.0006	MS	WU’	16803	V	117
NSVS 7366900 Cnc	min	57854.4199	0.0020	MS		16803	V	103
NSVS 7442379 Cnc	min	57798.2914	0.0022	AG		1603	-Ir	137
NSVS 7442379 Cnc	min	57798.4571	0.0035	AG		1603	-Ir	137
NSVS 7446012 Lyn	max	57765.4767	0.0010	MS		16803	V	203
NSVS 7446012 Lyn	max	57765.5435	0.0010	MS		16803	V	203
NSVS 7446012 Lyn	max	57765.6131	0.0010	MS		16803	V	203
NSVS 7446012 Lyn	max	57765.6789	0.0010	MS		16803	V	203
NSVS 7446012 Lyn	max	57765.7463	0.0010	MS		16803	V	203
NSVS 7446012 Lyn	max	57838.5116	0.0010	MS		16803	V	65
NSVS 7446012 Lyn	max	57847.3866	0.0010	MS		16803	V	124
NSVS 7446012 Lyn	max	57847.4548	0.0010	MS		16803	V	124
NSVS 7446012 Lyn	max	57851.3843	0.0010	MS		16803	V	134
NSVS 7446012 Lyn	max	57851.4525	0.0010	MS		16803	V	134
NSVS 7446012 Lyn	max	57851.5201	0.0010	MS		16803	V	134
NSVS 7446012 Lyn	max	57861.3430	0.0000	MS		16803	V	121
NSVS 7446012 Lyn	max	57861.4105	0.0001	MS		16803	V	121
NSVS 7446012 Lyn	max	57861.4788	0.0001	MS		16803	V	121
NSVS 7619496 Com	min	57844.4470	0.0023	AG	EB:’	1603	-Ir	43
NSVS 8209613 Lyr	min	57921.4341	0.0003	MS	EB:’	16803	V	153
NSVS 8209613 Lyr	min	57893.5384	0.0003	MS	EB:’	16803	V	103
NSVS 8209613 Lyr	min	57978.5474	0.0005	MS	EB:’	16803	V	126
NSVS 8500709 Cyg	min	57905.4529	0.0058	AG	EB:’	1603	-Ir	17
NSVS 8554141 Cyg	min	57988.4484	0.0015	AG		1603	-Ir	32
NSVS 8559318 Vul	min	57982.3891	0.0024	AG	EB:’	1603	-Ir	35
NSVS 8559318 Vul	min	57982.5563	0.0015	AG	EB:’	1603	-Ir	35
NSVS 8638856 Cyg	min	57988.3590	0.0013	AG		1603	-Ir	41
NSVS 8638856 Cyg	min	57988.5745	0.0006	AG		1603	-Ir	41
NSVS 8713121 Cyg	min	57968.5091	0.0006	AG	EB:’	1603	-Ir	40
NSVS 889633 Dra	min	57825.3185	0.0024	AG	EB:’	1603	-Ir	56
NSVS 889633 Dra	min	57825.4954	0.0031	AG	EB:’	1603	-Ir	56
NSVS 890397 Dra	min	57812.2974	0.0014	AG	EB:’	1603	-Ir	22
NSVS 890397 Dra	min	57825.4512	0.0009	AG	EB:’	1603	-Ir	50
NSVS 890397 Dra	min	57825.5884	0.0004	AG	EB:’	1603	-Ir	50
NSVS 9000641 Peg	min	57952.4569	0.0015	AG	WU’	1603	-Ir	33
NSVS 9010274 Peg	min	57980.4665	0.0004	AG	WU’	1603	-Ir	33
NSVS 9010274 Peg	min	57980.6027	0.0003	AG	WU’	1603	-Ir	33
NSVS 9020413 And	min	57987.4243	0.0016	AG		1603	-Ir	44
NSVS 958941 Dra	min	57839.4046	0.0015	AG		1603	-Ir	55
NSVS 958941 Dra	min	57839.5989	0.0027	AG		1603	-Ir	55
NSVS 9784102 Gem	min	57811.3241	0.0020	AG		1603	-Ir	38
NSVS 994114 UMi	min	57840.4593	0.0019	AG	EB:’	1603	-Ir	45
ROTSE1 J125947.50+365843.6 CVn	min	57829.4946	0.0008	AG	RR’	1603	-Ir	53
ROTSE1 J144443.28+255752.4 Boo	min	57873.4374	0.0028	AG	EB’	1603	-Ir	28
ROTSE1 J164534.43+300749.3 Her	min	57887.4448	0.0018	AG	EB’	1603	-Ir	18
ROTSE1 J164534.43+300749.3 Her	min	57900.4968	0.0023	AG	EB’	1603	-Ir	28
ROTSE1 J171925.07+351602.7 Her	min	57856.6386	0.0007	MS	WU’	16803	V	138
ROTSE1 J171925.07+351602.7 Her	min	57852.5336	0.0003	MS	WU’	16803	V	134
ROTSE1 J171925.07+351602.7 Her	min	57852.6745	0.0002	MS	WU’	16803	V	134
ROTSE3 J172014.15+352919.1 Her	min	57856.6792	0.0006	MS		16803	V	137
ROTSE3 J172014.15+352919.1 Her	min	57852.5998	0.0004	MS		16803	V	117
ROTSE1 J173121.59+295658.4 Her	min	57887.5169	0.0024	AG	WU’	1603	-Ir	25

Table 1: cont.

Variable	Ext	HJD 24.....	±	Obs	Type	Cam	Fil	n
ROTSE1 J173121.59+295658.4 Her	min	57923.5391	0.0006	AG	WU'	1603	-Ir	24
ROTSE1 J175527.44+440654.3 Her	min	57879.4576	0.0029	AG	EB'	1603	-Ir	35
ROTSE1 J180323.71+335931.1 Her	min	57884.5219	0.0017	AG	EB'	1603	-Ir	47
ROTSE1 J184813.35+401846.0 Lyr	min	57910.4388	0.0017	MS	EB'	16803	V	169
ROTSE1 J184813.35+401846.0 Lyr	min	57910.6325	0.0004	MS	EB'	16803	V	169
ROTSE1 J184813.35+401846.0 Lyr	min	57944.4852	0.0005	MS	EB'	16803	V	180
ROTSE1 J184813.35+401846.0 Lyr	min	57951.4817	0.0004	MS	EB'	16803	V	200
ROTSE1 J184813.35+401846.0 Lyr	min	57966.4682	0.0011	MS	EB'	16803	V	126
ROTSE1 J184813.35+401846.0 Lyr	min	57974.4379	0.0005	MS	EB'	16803	V	156
ROTSE1 J185226.53+445527.8 Lyr	min	57597.3817	0.0007	MS	EB'	16803	V	54
ROTSE1 J185226.53+445527.8 Lyr	min	57558.4911	0.0004	MS	EB'	16803	LUM	153
ROTSE1 J185226.53+445527.8 Lyr	min	57536.5906	0.0002	MS	EB'	16803	LUM	73
ROTSE1 J231704.72+371849.0 And	min	57987.3937	0.0022	AG		1603	-Ir	44
ROTSE1 J231704.72+371849.0 And	min	57987.5550	0.0026	AG		1603	-Ir	44
1SWASP J201144.64+570512.7 Cyg	min	57891.4050	0.0030	AG	EB'	1603	-Ir	33
1SWASP J211659.16+400936.3 Cyg	min	57939.4481	0.0038	AG		1603	-Ir	26
1SWASP J230252.60+342300.8 Peg	min	57980.4716	0.0010	AG		1603	-Ir	32
TYC 2675-0663 Cyg	min	57924.4731	0.0027	AG		1603	-Ir	35
TYC 2675-0663 Cyg	min	57982.5532	0.0026	AG		1603	-Ir	35
TYC 2695-3163 Cyg	min	57988.4929	0.0014	AG		1603	-Ir	43
TYC 3151-2485-1 Cyg	min	57900.4428	0.0010	AG		1603	-Ir	27
TYC 3151-2485 Cyg	min	57924.5378	0.0025	AG		1603	-Ir	34
TYC 3151-2485 Cyg	min	57973.5675	0.0045	AG		1603	-Ir	38
TYC 3481-1550 Boo	min	57838.5301	0.0020	AG		1603	-Ir	49
TYC 3617-1828 Lac	min	57989.4763	0.0027	AG	E!	1603	-Ir	36
TYC 3985-0198 Cas	max	57964.4200	0.0030	AG		1603	-Ir	40
TYC 3985-0198 Cas	max	57964.5610	0.0030	AG		1603	-Ir	40
TYC 3985-0198 Cas	max	57980.4400	0.0010	AG		1603	-Ir	30
TYC 3985-0198 Cas	max	57980.5790	0.0010	AG		1603	-Ir	30
TYC 3985-0198 Cas	max	57995.4030	0.0010	AG		1603	-Ir	42
TYC 3985-0198 Cas	max	57995.5280	0.0010	AG		1603	-Ir	42
TYC 4034-1405 Cas	min	57989.3792	0.0015	AG		1603	-Ir	37
TYC 4285-0602 Cas	min	57982.4688	0.0003	AG	E!	1603	-Ir	33
TYC 5097-0641 Ser	min	57923.4975	0.0010	AG	E!	1603	-Ir	25
UCAC3 213-102451 Leo	min	57845.3744	0.0007	MS		16803	V	146
UCAC3 213-102451 Leo	min	57845.5202	0.0008	MS		16803	V	146
UCAC3 213-102451 Leo	min	57846.3925	0.0010	MS		16803	V	146
UCAC3 213-102451 Leo	min	57866.4526	0.0005	MS		16803	V	98
UCAC3 213-102451 Leo	min	57875.4024	0.0006	MS		16803	V	85
UCAC3 238-155503 Lyr	min	57921.4459	0.0003	MS		16803	V	153
UCAC3 238-155503 Lyr	min	57935.6361	0.0009	MS		16803	V	178
UCAC3 238-155503 Lyr	min	57893.5231	0.0004	MS		16803	V	110
UCAC3 238-155503 Lyr	min	57893.5231	0.0004	MS		16803	V	110
UCAC3 238-155503 Lyr	min	57921.4459	0.0003	MS		16803	V	153
UCAC3 238-155503 Lyr	min	57935.6361	0.0009	MS		16803	V	178
UCAC3 238-155503 Lyr	min	57949.0000	0.0000	MS		16803	V	154
UCAC3 238-156039 Lyr	min	57893.5738	0.0002	MS		16803	V	111
UCAC3 238-156039 Lyr	min	57907.6307	0.0003	MS		16803	V	67
UCAC3 242-230799 Cyg	min	57932.5504	0.0003	MSFR		16803	V	71
UCAC3 242-227216 Cyg	min	57932.5624	0.0005	MSFR		16803	V	75
UCAC3 242-227216 Cyg	min	57942.4929:	0.0030	MSFR		16803	V	87
UCAC3 242-227216 Cyg	min	57939.4395	0.0005	MSFR		16803	V	157
UCAC3 242-230799 Cyg	min	57954.5741	0.0010	MSFR		16803	V	130
UCAC3 242-227216 Cyg	min	57961.5985	0.0003	MSFR		16803	V	158
UCAC3 242-227216 Cyg	min	58007.5234	0.0010	MS		16803	V	167
UCAC3 248-200869 Cyg	min	57977.4894	0.0005	MSFR		16803	V	200
UCAC3 248-205306 Cyg	min	58012.3413	0.0007	MSFR		16803	V	60
UCAC3 250-235517 Cyg	min	57965.5454	0.0019	MSFR		16803	V	159
UCAC3 250-235517 Cyg	min	57962.3996	0.0011	MSFR		16803	V	161
UCAC3 250-235517 Cyg	min	57917.5497	0.0008	MSFR		16803	V	97
UCAC3 250-235517 Cyg	min	57894.6013	0.0014	MSFR		16803	V	37
UCAC3 250-234427 Cyg	min	57962.6161	0.0012	MSFR		16803	V	171
UCAC3 250-197400 Cyg	min	57897.5666	0.0004	MSFR		16803	V	110
UCAC3 250-197400 Cyg	min	57943.5003	0.0009	MSFR		16803	V	180
UCAC3 250-197400 Cyg	min	57977.5508	0.0010	MSFR		16803	V	212
UCAC3 250-197400 Cyg	min	58013.4311	0.0007	MSFR		16803	V	141
UCAC3 250-197400 Cyg	min	58037.4227	0.0006	MSFR		16803	V	131
UCAC3 250-197400 Cyg	min	58049.3100	0.0008	MSFR		16803	V	77
UCAC3 261-141499 Lyr	max	57564.4617	0.0010	MS		16803	V	104
UCAC3 261-141499 Lyr	max	57910.5109	0.0010	MS		16803	V	169
UCAC3 261-141499 Lyr	max	57910.6237	0.0010	MS		16803	V	169

Table 1: cont.

Variable	Ext	HJD 24.....	±	Obs	Type	Cam	Fil	n
UCAC3 261-141499 Lyr	max	57944.4282	0.0010	MS		16803	V	179
UCAC3 261-141499 Lyr	max	57944.5545	0.0010	MS		16803	V	179
UCAC3 261-141499 Lyr	max	57951.3849	0.0010	MS		16803	V	195
UCAC3 261-141499 Lyr	max	57951.5005	0.0010	MS		16803	V	195
UCAC3 261-141499 Lyr	max	57951.6259	0.0010	MS		16803	V	195
UCAC3 261-141499 Lyr	max	57974.4611	0.0010	MS		16803	V	144
UCAC3 261-141499 Lyr	max	57974.5659	0.0010	MS		16803	V	144
UCAC3 272-123185 Boo	min	57858.5284	0.0005	MS		16803	V	107
UCAC3 282-171491 Cyg	min	58033.4067	0.0012	MS		16803	V	142
UCAC3 282-171491 Cyg	min	58039.3890	0.0011	MS		16803	V	112
UCAC3 282-171491 Cyg	min	58040.3187	0.0010	MS		16803	V	137
UCAC3 282-171491 Cyg	min	58040.4503	0.0008	MS		16803	V	137
UCAC3 282-171491 Cyg	min	58051.3519	0.0003	MS		16803	V	86
UCAC3 282-171491 Cyg	min	58054.4083	0.0015	MS		16803	V	71
UCAC3 284-090047 Aur	min	57814.4125	0.0004	MS		16803	V	148
UCAC3 284-090447 Aur	min	57763.4532	0.0013	MS		16803	V	187
UCAC3 284-090447 Aur	min	57763.5764	0.0010	MS		16803	V	187
UCAC3 284-090447 Aur	min	57756.5807	0.0004	MS		16803	V	180
UCAC3 284-090447 Aur	min	57704.7066	0.0001	MS		16803	V	60
UCAC3 284-090447 Aur	min	57690.6960	0.0010	MS		16803	V	90
UCAC3 284-090447 Aur	min	57691.0000	0.0000	MS		16803	V	81
UCAC3 284-090934 Aur	min	57690.6672	0.0009	MS		16803	V	91
UCAC3 284-090934 Aur	min	57691.7230	0.0006	MS		16803	V	82
UCAC3 284-090934 Aur	min	57704.6796	0.0005	MS		16803	V	81
UCAC3 284-090934 Aur	min	57756.4943	0.0004	MS		16803	V	180
UCAC3 284-090934 Aur	min	57756.6261	0.0004	MS		16803	V	180
UCAC3 284-090934 Aur	min	57763.3685	0.0012	MS		16803	V	190
UCAC3 284-090934 Aur	min	57763.5022	0.0005	MS		16803	V	190
UCAC3 284-090447 Aur	min	57814.3829	0.0007	MS		16803	V	163
UCAC3 284-090934 Aur	min	57814.3915	0.0003	MS		16803	V	172
UCAC3 284-090934 Aur	min	57814.5251	0.0004	MS		16803	V	172
UCAC3 284-159698 Cyg	min	57605.5286	0.0004	MS		16803	V	185
UCAC3 284-159698 Cyg	min	57623.4910	0.0005	MS		16803	V	173
UCAC3 284-159698 Cyg	min	57691.2962	0.0004	MS		16803	V	145
UCAC3 284-159698 Cyg	min	57691.4618	0.0009	MS		16803	V	145
UCAC3 284-159698 Cyg	min	57916.5535	0.0004	MS		16803	V	95
UCAC3 284-159698 Cyg	min	57955.3918	0.0001	MS		16803	V	147
UCAC3 284-159698 Cyg	min	57955.5535	0.0006	MS		16803	V	147
UCAC3 284-159698 Cyg	min	57963.4822	0.0005	MS		16803	V	207
UCAC3 284-159698 Cyg	min	57963.6442	0.0005	MS		16803	V	207
UCAC3 284-159698 Cyg	min	57979.5043	0.0008	MS		16803	V	190
UCAC3 284-159698 Cyg	min	58010.4092	0.0007	MS		16803	V	186
UCAC3 284-159698 Cyg	min	58010.5779	0.0003	MS		16803	V	186
UCAC3 284-159698 Cyg	min	58015.4282	0.0020	MS		16803	V	154
UCAC3 285-090698 Aur	min	57763.4250	0.0008	MS		16803	V	197
UCAC3 285-157675 Cyg	min	57605.3787	0.0007	MS		16803	V	189
UCAC3 285-157675 Cyg	min	57605.5518	0.0010	MS		16803	V	189
UCAC3 285-157675 Cyg	min	57623.3637	0.0005	MS		16803	V	176
UCAC3 285-157675 Cyg	min	57623.5402	0.0005	MS		16803	V	176
UCAC3 285-157675 Cyg	min	57691.4224	0.0004	MS		16803	V	149
UCAC3 285-157675 Cyg	min	57916.5846	0.0005	MS		16803	V	102
UCAC3 285-157675 Cyg	min	57955.5481	0.0007	MS		16803	V	149
UCAC3 285-157675 Cyg	min	57963.4863	0.0017	MS		16803	V	209
UCAC3 285-157675 Cyg	min	57963.6553	0.0003	MS		16803	V	209
UCAC3 285-157675 Cyg	min	57979.5252	0.0004	MS		16803	V	235
UCAC3 285-157675 Cyg	min	58010.3880	0.0009	MS		16803	V	199
UCAC3 285-157675 Cyg	min	58010.5625	0.0008	MS		16803	V	199
UCAC3 285-157675 Cyg	min	58015.3194	0.0003	MS		16803	V	163
UCAC3 285-157675 Cyg	min	58015.5006	0.0006	MS		16803	V	163
UCAC3 285-155734 Cyg	min	57605.4102	0.0006	MS		16803	V	187
UCAC3 285-155734 Cyg	min	57605.5481	0.0005	MS		16803	V	187
UCAC3 285-155734 Cyg	min	57623.3462	0.0008	MS		16803	V	171
UCAC3 285-155734 Cyg	min	57623.4862	0.0012	MS		16803	V	171
UCAC3 285-155734 Cyg	min	57691.4125	0.0010	MS		16803	V	127
UCAC3 285-155734 Cyg	min	57955.4996	0.0008	MS		16803	V	134
UCAC3 285-155734 Cyg	min	57963.4074	0.0006	MS		16803	V	204
UCAC3 285-155734 Cyg	min	57963.5443	0.0006	MS		16803	V	204
UCAC3 285-155734 Cyg	min	57979.3635	0.0012	MS		16803	V	213
UCAC3 285-155734 Cyg	min	57979.5054	0.0009	MS		16803	V	213
UCAC3 285-155734 Cyg	min	57979.6369	0.0015	MS		16803	V	213
UCAC3 285-155734 Cyg	min	58010.4272	0.0008	MS		16803	V	181

Table 1: cont.

Variable	Ext	HJD 24.....	±	Obs	Type	Cam	Fil	n
UCAC3 285-155734 Cyg	min	58015.3681	0.0005	MS		16803	V	159
UCAC3 285-155734 Cyg	min	58015.5130	0.0008	MS		16803	V	159
UCAC3 285-155236 Cyg	min	58010.4079	0.0007	MS		16803	V	169
UCAC3 285-155236 Cyg	min	57979.5449	0.0018	MS		16803	V	206
UCAC3 285-155236 Cyg	min	57963.5051	0.0009	MS		16803	V	204
UCAC3 285-155236 Cyg	min	57916.6052	0.0006	MS		16803	V	102
UCAC3 285-155236 Cyg	min	57605.5379	0.0006	MS		16803	V	177
UCAC3 285-155236 Cyg	min	58015.4877	0.0002	MS		16803	V	154
UCAC3 285-064533 Per	min	57703.5076	0.0008	MS		16803	V	174
UCAC3 285-064533 Per	min	57703.6270	0.0008	MS		16803	V	174
UCAC3 285-064533 Per	min	57753.4032	0.0015	MS		16803	V	165
UCAC3 285-064533 Per	min	57753.2836	0.0009	MS		16803	V	165
UCAC3 285-064533 Per	min	57734.3881	0.0006	MS		16803	V	159
UCAC3 285-064533 Per	min	57734.5085	0.0007	MS		16803	V	159
UCAC3 285-064533 Per	min	57709.6807	0.0005	MS		16803	V	131
UCAC3 285-064533 Per	min	57709.5641	0.0006	MS		16803	V	131
UCAC3 285-064219 Per	min	57703.6864	0.0011	MSFR		16803	V	175
UCAC3 285-064219 Per	min	57709.7012	0.0015	MSFR		16803	V	139
UCAC3 285-064219 Per	min	57753.3733	0.0014	MSFR		16803	V	151
UCAC3 285-064219 Per	min	58015.6293	0.0012	MSFR		16803	V	95
UCAC3 285-064219 Per	min	58026.6725	0.0013	MSFR		16803	V	134
UCAC3 285-064219 Per	min	58054.5340	0.0019	MSFR		16803	V	158
UCAC3 286-155282 Cyg	min	57605.5380	0.0010	MS		16803	V	179
UCAC3 286-155282 Cyg	min	57979.4056	0.0008	MS		16803	V	229
UCAC3 286-155282 Cyg	min	57623.4137	0.0009	MS		16803	V	174
UCAC3 286-155282 Cyg	min	57963.3913	0.0010	MS		16803	V	204
UCAC3 286-155282 Cyg	min	57955.3869	0.0008	MS		16803	V	153
UCAC3 286-155282 Cyg	min	58015.4354	0.0009	MS		16803	V	160
UCAC3 286-155282 Cyg	min	58010.3614	0.0009	MS		16803	V	195
VSX J003310.0+621944 Cas	min	57980.4156	0.0021	AG		1603	-Ir	34
VSX J003310.0+621944 Cas	min	57980.5745	0.0039	AG		1603	-Ir	34
VSX J012609.1+605226 Cas	min	57982.3978	0.0084	AG		1603	-Ir	35
VSX J012609.1+605226 Cas	min	57982.5717	0.0009	AG		1603	-Ir	35
VSX J014547.6+550757 Cas	min	57995.4297	0.0022	AG		1603	-Ir	42
VSX J080433.6+204007 Cnc	min	57733.6506	0.0006	MS		16803	V	168
VSX J080433.6+204007 Cnc	min	57833.4964	0.0006	MS		16803	V	71
VSX J121407.1+762538 Cam	min	57840.3538	0.0028	AG		1603	-Ir	47
VSX J121407.1+762538 Cam	min	57840.4968	0.0027	AG		1603	-Ir	47
VSX J130338.2+882407 UMi	min	57901.3876	0.0010	AG		1603	-Ir	32
VSX J154654.0+883715 UMi	min	57901.4330	0.0034	AG		1603	-Ir	32
VSX J222216.8+56120 Cep	min	57988.3617	0.0006	AG		1603	-Ir	44
VSX J222216.8+56120 Cep	min	57988.5165	0.0018	AG		1603	-Ir	44
VSX J222216.8+56120 Cep	min	57988.5165	0.0018	AG		1603	-Ir	44
VSX J222216.8+56120 Cep	min	57988.5165	0.0018	AG		1603	-Ir	44
VSX J222216.8+56120 Cep	min	57988.5165	0.0018	AG		1603	-Ir	44
VSX J222216.8+56120 Cep	min	57988.5165	0.0018	AG		1603	-Ir	44
VSX J222216.8+56120 Cep	min	57988.5165	0.0018	AG		1603	-Ir	44
VSX J222216.8+56120 Cep	min	57988.5165	0.0018	AG		1603	-Ir	44
VSX J222216.8+56120 Cep	min	57988.5165	0.0018	AG		1603	-Ir	44
VSX J222216.8+56120 Cep	min	57988.5165	0.0018	AG		1603	-Ir	44
VSX J222216.8+56120 Cep	min	57988.5165	0.0018	AG		1603	-Ir	44
VSX J222216.8+56120 Cep	min	57988.5165	0.0018	AG		1603	-Ir	44
VSX J222216.8+56120 Cep	min	57988.5165	0.0018	AG		1603	-Ir	44
VSX J222216.8+56120 Cep	min	57988.5165	0.0018	AG		1603	-Ir	44
VSX J222216.8+56120 Cep	min	57988.5165	0.0018	AG		1603	-Ir	44
VSX J222216.8+56120 Cep	min	57988.5165	0.0018	AG		1603	-Ir	44
VSX J222216.8+56120 Cep	min	57988.5165	0.0018	AG		1603	-Ir	44
VSX J222216.8+56120 Cep	min	57988.5165	0.0018	AG		1603	-Ir	44
VSX J222216.8+56120 Cep	min	57988.5165	0.0018	AG		1603	-Ir	44
VSX J222216.8+56120 Cep	min	57988.5165	0.0018	AG		1603	-Ir	44
VSX J222216.8+56120 Cep	min	57988.5165	0.0018	AG		1603	-Ir	44
VSX J222216.8+56120 Cep	min	57988.5165	0.0018	AG		1603	-Ir	44

Observers:

MSFR	MS+FR
RATRCR	RAT+RCR
AG	Agerer, Franz; Zweikirchen
AGT	Augart, Dietmar; Weisenheim am Berg
ALH	Alich, Karsten; Schaffhausen CH
BHE	Boehme, Dietmar; Nessa
BRW	Braunwarth, Horst; Hamburg
DIE	Dietrich, Martin; Radebeul
FR	Frank, Peter; Velden
JU	Jungbluth, Hans; Karlsruhe
MH	Muehle, Wolfgang; Stuttgart
MS	Moschner, Wolfgang; Lennestadt
MZ	Maintz, Gisela; Bonn
NWR	Nawrath, Georg; Unna
SCI	Schmidt, Ulrich; Karlsruhe
WLH	Wollenhaupt, Guido; Oberwiesenthal

Remarks:

n	number of measurements
:	uncertain
min2	secondary minimum
Type	taken from GCVS-Catalog[1], observer (!) or CDS (`http://cdsportal.u-strasbg.fr/`) (')
*)	u. Her is 68 Her, not to be confused with U Her

Photometers:

314+	CCD-Camera-Atik-314+
314LC	CCD-camera-Atik-314LC
383L+	CCD-camera-Atik-383L+
3200M	CCD-camera-STT3200ME
1603	CCD-camera-Sigma-1603
ST7	CCD-camera-ST-7
ST10	CCD-camera-ST-10
ST8XM	CCD-camera-ST-8XMEI
ST10	CCD-camera-ST-10
16IC	CCD-Camera-16IC
16803	CCD-Camera-FLI-16803
1600	CCD-Camera-MI-G2-1600
600D	DSLR-Canon-EOS600D
DSI	Meade-DSI-ProIII
SWASP	Survey-SuperWASP

Filters:

o	without filter
V	V-filter
B	B-filter
R	R-filter
U	U-filter
I	I-filter
L	-U-I cut-off filter
Rc	R-filter Cousins
-I	IR cut-off filter
-U	U cut-off filter
L	-U-I cut-off filter

Reference:

Samus N.N., Kazarovets E.V., Durlevich O.V., Kireeva N.N., Pastukhova E.N., 2017, *Astronomy Reports,* **61**, 80

COMMISSIONS G1 AND G4 OF THE IAU
INFORMATION BULLETIN ON VARIABLE STARS

Volume 63 Number 6245 DOI: 10.22444/IBVS.6245

Konkoly Observatory
Budapest
20 July 2018

HU ISSN 0374 – 0676

THE PERIOD EVOLUTION OF V473 Tau

OZUYAR, D.[1]; STEVENS, I. R.[2]

[1] Ankara University, Faculty of Science, Dept. of Astronomy and Space Sciences, 06100, Tandogan, Ankara / Turkey, e-mail: dozuyar@ankara.edu.tr

[2] The University of Birmingham, School of Physics and Astronomy, Birmingham, B15 2TT, UK

Abstract

In this paper, the period evolution of the rotating chemically peculiar star V473 Tau is investigated. Even though the star has been observed for more than fifty years, for the first time four consecutive years of space-based data covering between 2007 and 2010 are presented. The data are from the *STEREO* satellite, and are combined with the archival results. The analysis shows that the rotation period of V473 Tau is 1.406829(10) days, and has slightly decreased with the variation rate of 0.11(3) s yr^{-1} over time. Also, the acceleration timescale of the star is found to be shorter than its main sequence lifetime. This indicates that the process of decrease in period might be reversible. On this basis, it can be suggested that V473 Tau has a possible magnetic acceleration and a differential rotation, which cause a variation in the movement of inertia, and hence the observed period change. Additionally, the evolution path of V473 Tau on the H-R diagram is evaluated. Accordingly, the position of the star on the diagram suggests that its magnetic properties develop before it reaches the main sequence or in the beginning of its main sequence lifetime.

1 Introduction

Chemically peculiar (CP) variables are spread between late-B and early-F spectral types, and thus contain various stars with effective temperatures greater than 6,500 K (Hubrig et al. 2005). These variables are comprised mostly of Ap and Bp stars, which differ from other types having the same temperature by their abnormal chemical compositions and slow rotations. The reason for the peculiarity is an under-abundance of solar-like elements, as well as an overabundance of both metal and rare-earth elements across their surfaces (Mikulasek et al. 2009). Magnetic fields, radiative acceleration, and atomic diffusion determine the surface distribution of elements (Kochukhov 2011), and lead them to be present in the form of spots and rings on the surface. Along with rotation, these non-uniformly distributed regions cause periodic variations in magnetic fields, line profile, and energy distribution, as well as in photometric brightness (oblique-rotator model). The periods of these variations are generally between a day and a week. Depending on the slow rotation, surface spot regions can remain stable for decades. Such a situation enables remarkably accurate calculations of surface distribution, rotation period, and rotational breaking mechanisms. However, only very few of the CP stars discovered in our galaxy and others exhibit periodic variations, and less than one-tenth of these have been observed for scientific investigation. In order to study this type of stars, accurate observations are needed (accuracy > 0.005 mag; Mikulasek et al. 2009). The high-precision instruments of the *STEREO* satellite are a quite suitable, space-based source, since seasonal and four-year *STEREO* observations provide a precision of 2.0×10^{-4} and 7.0×10^{-5} mmag, respectively.

2 Literature Review

The photometric variability of V473 Tau (A0Si, $V = 7.26$ mag) was first detected by Burke et al. (1970). They calculated the period of this variation as around 1.39(2) days, but this period value produced a light curve (LC) with a scattered maximum. Hence, Rakosch and Fiedler (1978) noted that their observations were more adaptable with a double period. Subsequently, Maitzen (1977) derived a rotation period of 2.7795(1) days, which was indeed twice that of previous values. As a result of the double period, two minima and maxima having different levels were formed in the LC; this situation was explained in terms of the different chemical regions on the surface. Most importantly, this was a significant case since a double wave structure was not a common condition among Si stars. In a recent study, Jerzykiewicz (2009) investigated rotation periods and found a value of 1.4068541(29) days in U, B, and V bands. However, he could not completely determine the origin of the variabilities as he was unable to conclude whether the star was an oblique rotator or a g-mode pulsator.

3 Analysis of the STEREO Data

The data were provided from the HI-1A instrument on-board the *STEREO-A* satellite. The HI-1A is capable of observing background stars with the magnitude of 12^m or brighter for a maximum of 20 days and a useful stellar photometer which covers the region around the ecliptic (20% of the sky) with the field of view of $20° \times 20°$. The nominal exposure time of the camera is 40 seconds, and putting 30 exposures together on board, a 40-minute integrated cadence has been obtained to transmit for each HI-1 image (Eyles et al. 2009). Therefore, the Nyquist frequency of the data is around 18 c d^{-1}. LCs mostly affected by solar activities were cleaned with a 3^{rd} order polynomial fit. Observation points greater than 3σ were clipped with a pipeline written in the Interactive Data Language (IDL) (For a more detailed description of the data preparation, refer to Sangaralingam and Stevens (2011) and Whittaker et al. (2012)). The LC of V473 Tau presented a sinusoidal characteristic due to spot modulation on the stellar surface. Therefore, all analyses were performed using the Lomb-Scargle (LS) algorithm since it is more sensitive to such variations. To determine a model of the sinusoidal LCs, the Levenberg-Marquardt Optimization method was applied, and the best fit was obtained after 5000 iterations. After the derivation of the model LC, random Gaussian noise with the mean of zero and the sigma value, which was determined from the cleaned curve, was produced and added to the model. This process was repeated 500 times. The most accurate frequencies and their uncertainties were assessed using the Monte-Carlo simulation algorithm. The results were compared to those derived from the Phase Dispersion Minimization (PDM, Stellingwerf, 1978) method and Period04 (Lenz & Breger, 2005). To perform O–C calculations and to investigate period variabilities over years, the best extremum times were obtained from the seasonal LCs, and were put together with data from the literature.

Table 1. Frequency analysis results of V473 Tau.

V473 Tau	LS ($c\ d^{-1}$)	Period04 ($c\ d^{-1}$)	PDM ($c\ d^{-1}$)	Amp. (mmag)
2007	0.7104(8)	0.7101(8)	0.7120(16)	8.63(25)
2008	0.7101(6)	0.7101(6)	0.7118(15)	10.93(24)
2009	0.7116(7)	0.7116(8)	0.7157(15)	8.62(24)
2010	0.7128(7)	0.7128(8)	0.7123(20)	9.20(25)
Comb.	0.710818(5)	0.710818(7)	0.711164(5)	9.33(13)

4 Results

In this research, we obtained four consecutive years of data between 2007 and 2010. As reported by other researchers, all the LCs had explicit periodicity. Individual LS, PDM and Period04 analyses of annual curves showed a frequency at around 0.71 $c\ d^{-1}$ (Table 1), but this result was slightly longer than the literature periods. Furthermore, we detected the existence of another strong peak at approximately 1.40 $c\ d^{-1}$ (0.71 days) on the LS periodogram (Figure 1).

Table 2. Available period values and extremum times for V473 Tau.

Time (year)	Period (day)	Freq. ($c\ d^{-1}$)	Ref.	Extremum Times (HJD)	Ref.
1963-1993	1.4068541(29)	0.710806(1)	1	2438451.1380(100)	1
1967-1968	1.39(2)	0.72(1)	2	2438451.1540(220)	1
1963-1964	1.39	0.72	3	2438750.7800(190)	1
1974	1.38975(5)	0.71955(3)	4	2439860.8060(230)	1
1990-1993	1.4066952	0.710886	5	2448480.6010(190)	1
1990-1993	1.407020(39)	0.7107(2)	6	2439870.6300(500)	2
2007	1.4069(6)	0.7108(3)	7	2438466.7297	3
2007-2010	1.406829(10)	0.710818(5)	8	2438466.3665(1300)	4
				2454241.5599(125)	8
				2454583.4049(129)	8
				2454922.4465(133)	8
				2455274.1565(135)	8

1: Jerzykiewicz (2009), 2: Burke et al. (1970), 3: Rakosch & Fiedler (1978)
4: Maitzen (1977) (P/2), 5: Dubath et al. (2011), 6: Rimoldini et al. (2012)
7: Wraight et al. (2012), 8: This study

Combining the four-year data, the precise rotation period of the star was determined with the help of the PDM and LS methods. Since the LS technique gave a better period, the main LC was plotted based on this value. Accordingly, the folded LC was clearly formed by a maximum and a broad minimum (Figure 2, upper left). The maximum was quite strong and had a flat top, indicating a cooler chemical structure on the surface. Moreover, there was a barely detectable bump in the middle of the minimum. From the Figure 2, it was clear that the light curve did not have a purely sinusoidal shape. As a result of this, it produced a Fourier spectrum comprised of an nf ($n = 1, 2, 3, \ldots$) harmonic series with decreasing amplitudes with increasing n. Therefore, the peak at 1.40 $c\ d^{-1}$ on the LS periodogram was the first harmonic of the main frequency.

Also, we produced a folded LC using the double *STEREO* period since Maitzen (1977) noted that his observations were compatible with the period value of 2.7795 days. As shown in Figure 2 (upper right), we derived a relatively clean LC with two minima and maxima. Even though the minimum at $\phi \approx 0.3$ was slightly more scattered than the other one, the consecutive structures appeared similar to each other. Therefore, we assumed that the period value of 1.41 days was the full rotation period.

To investigate a possible period variation, we collected all literature values given in Table 2, and present them in Figure 2 (bottom left) using black diamond symbols. Since some of them were the results of multi-observations, we used the combined *STEREO* period instead of seasonal periods (a red diamond symbol). As seen in the figure, we found two different period paths (≈1.390 and ≈1.408 days) since the quality and number of observation data differed from one study to another. Therefore, it was not possible to calculate any period variation using these values. However, when only the values given in Jerzykiewicz (2009) (10-year observations), Wraight et al. (2012), and this study (*STEREO* observations) were considered based on their reliabilities, the change in period suggested a possible period increase with a rate of 0.03 s y^{-1} in the star over 45 years.

In order to confirm such a variation, we analysed variabilities in the O–C diagram. For the calculation, the maximum times of the individual LCs were derived, and these values were combined with the epochs from the literature, given in Table 2. The epochs provided by Rakosch and Fiedler (1978), and Maitzen (1977) were converted from JD to HJD. Based on Figure 2 (right bottom), we found out that the O–C diagram of the star exhibited a period decrease with the variation rate of around $-1.27(30) \times 10^{-6}$ d y^{-1} or $-0.11(3)$ s y^{-1} (blue straight line). With the help of the LS period and using the best *STEREO* maximum time, we determined the light elements as:

$$HJD_{max} = 2454583.4049(129) + 1.406829(10)E - 2.44(58) \times 10^{-9}E^2 \ . \qquad (1)$$

Since this star was a single rotating variable, such a period decrease might most likely be explained by an acceleration in rotation after a magnetic braking, and might affect the dynamic structure of the star. Using the physical parameters $T = 11{,}081(280)$ K, $M = 2.59(14)$ $M_{\odot}$, $\log(L/L_{\odot}) = 1.64(15)$, and $R = 1.80(32)$ $R_{\odot}$, which was calculated from temperature and luminosity values provided, as given by Wraight et al. (2012), we roughly calculated the kinetic energy of the star and the rate at which energy increased as $E = 4.31(1.57) \times 10^{46}$ erg and $dE/dt = 2.46(1.07) \times 10^{33}$ erg s^{-1}. We also found the corresponding angular momentum and its variation rate to be around $J = 1.67(61) \times 10^{51}$ erg s and $dJ/dt = 4.77(2.07) \times 10^{37}$ erg. According to period and angular momentum variations, the acceleration time-scale of the star was approximately $\tau_{AC} = 1.11(63) \times 10^6$ yr, which was slightly higher than the duration derived from the variation rate of the kinetic energy ($\Delta\tau = E/(dE/dt) = 5.55(3.15) \times 10^5$ yr). We also found the main sequence lifetime of the star as $\tau_{MS} = 9.26(1.25) \times 10^8$ yr from the equation of $\tau_{\rm MS} = 10^{10}$ yr $\times$ $(M/M_{\odot})^{(1-\alpha)}$, where $\alpha = 3.5$ for main sequence stars and 10^{10} yr is the approximate lifetime of the Sun in the main sequence (Ghosh 2007; Koupelis and Kuhn 2007; Hansen and Kawaler 1994).

In addition to these, such a period decrease might be a result of a change in stellar mass with a rate of around $dM/dt = -1.92(88) \times 10^{-12}$ $M_{\odot}$ yr^{-1}, or a consequent of a change in radius with a rate of around $dR = -8.10(2.42) \times 10^{-7}$ $R_{\odot}$ yr^{-1}. Finally, we found the rotational velocity of the star to be $V_{eq} = 65(12)$ km s^{-1} with the help of our combined LS period and radius value ($R = 1.80(32)$ $R_{\odot}$), estimated from the parameters given above.

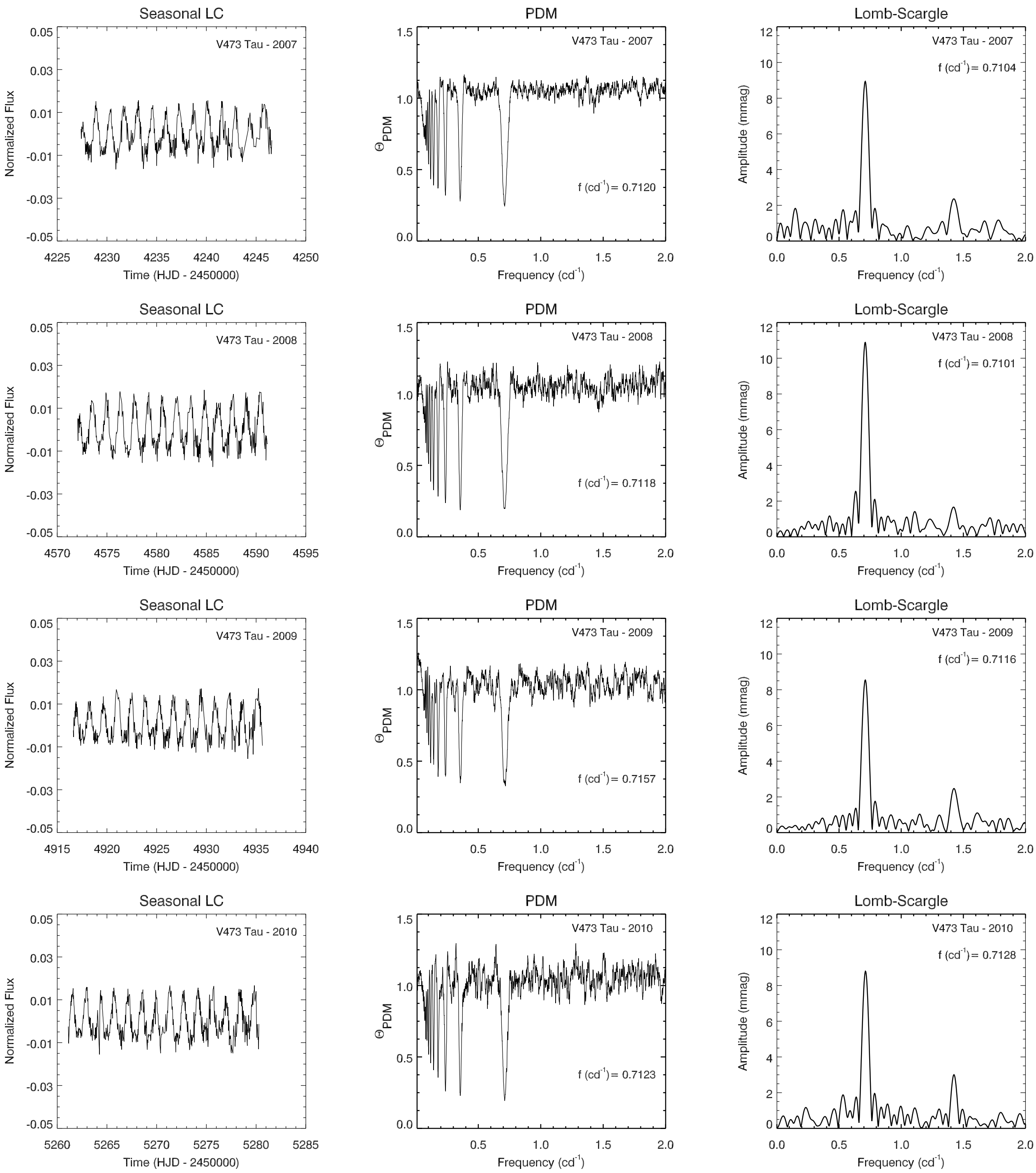

Figure 1. Annual light curves and related frequency periodograms of V473 Tau.

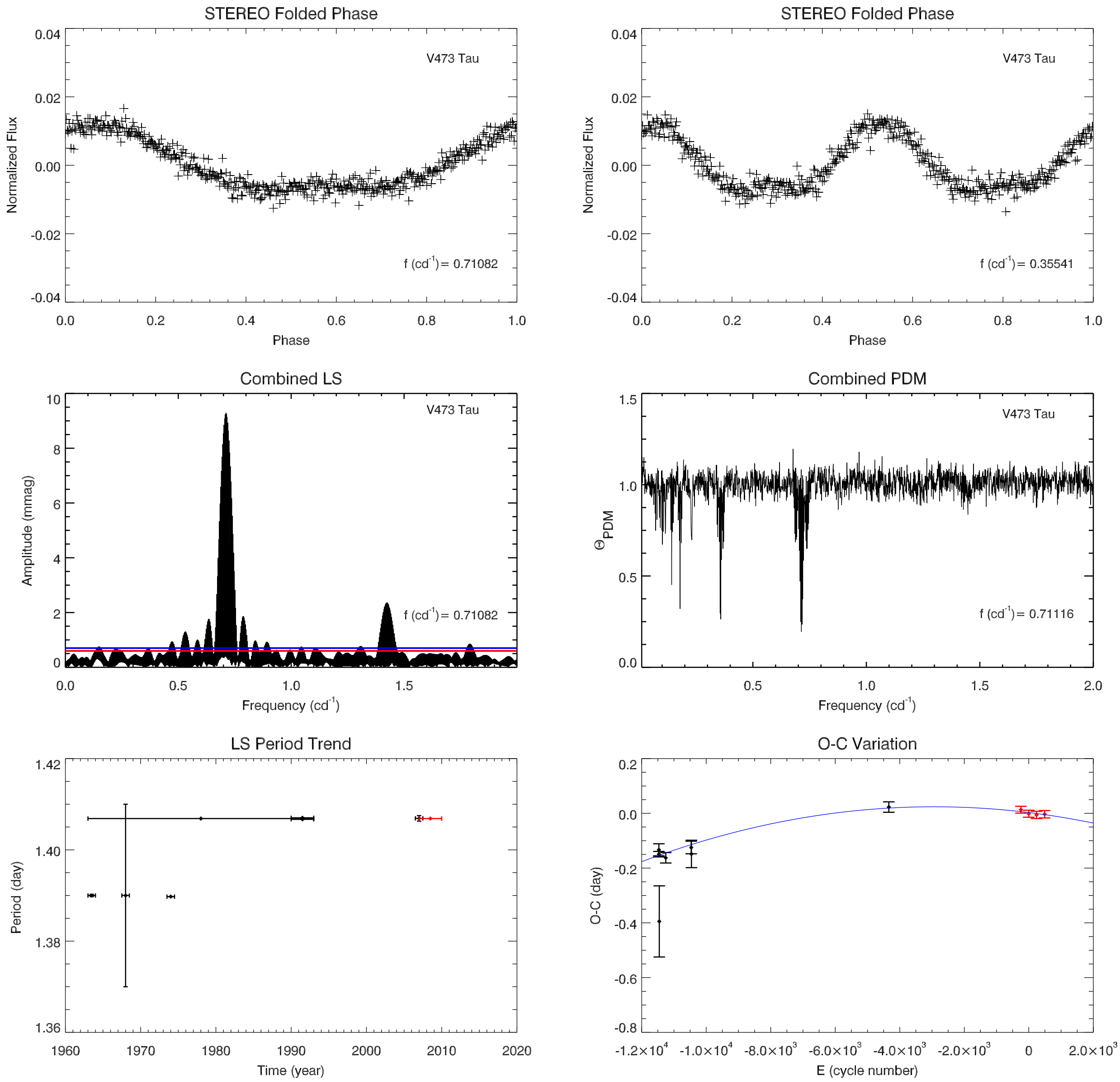

Figure 2. Folded light curves produced by the *STEREO* periods, frequency analyses of combined light curves as well as period and O–C variation graphics V473 Tau.

Table 3. The period, period variation rate, acceleration and main sequence lifetime as well as physical parameters of V473 Tau.

P (day)	dP/dt (s yr^{-1})	$\dot{P}/P$ (s^{-1})	τ_{ACC} (yr)	τ_{MS} (yr)
1.406830(10)	−0.11(3)	$-2.86(68)\times10^{-14}$	$-1.11(63)\times10^{6}$	$9.26(1.25)\times10^{8}$
$\log(L/L_\odot)$	$\log(T)$	M ($M_\odot$)	R ($R_\odot$)	V_{eq} (km s^{-1})
1.64(15)	4.045(11)	2.59(14)	1.80(32)	65(12)

5 Discussion

V473 Tau shows explicit period variation in the O–C diagram. Based on the diagram, it has been rotating 0.11(3) seconds faster per year. The variation rate in the period ($\dot{P}/P = 10^{-14}$ s^{-1}) is 10 times greater than that of the most massive mCP stars (Mikulášek et al. 2014). In addition, its acceleration time-scale is around $\tau_{MS} \sim 10^6$ yr, which is nearly three orders of magnitude ($\sim 0.8 \times 10^3$ yr) shorter than the main sequence lifetime of the star ($\tau_{MS} = 10^8$ yr). This, in turn, suggests that process of decrease in the period may be reversible. If so, the length of the cycle is roughly calculated as 92(11) yr (estimated by $T_{cyc} \sim P\,\sqrt{2/\dot{P}}$, Mikulášek et al. (2010)). Considering the fact that period variation processes may be reversible due to shorter acceleration time-scale than that of the main sequence lifetime, the rigid rotation hypothesis should be discarded and the differential rotation model should alternatively be discussed as expressed by Stępień (1998). In this model, the outer layers of stars differentially rotate with respect to denser interiors, and they are affected by global magnetic fields; an interaction between meridional circulations and magnetic fields takes place in a region within a star.

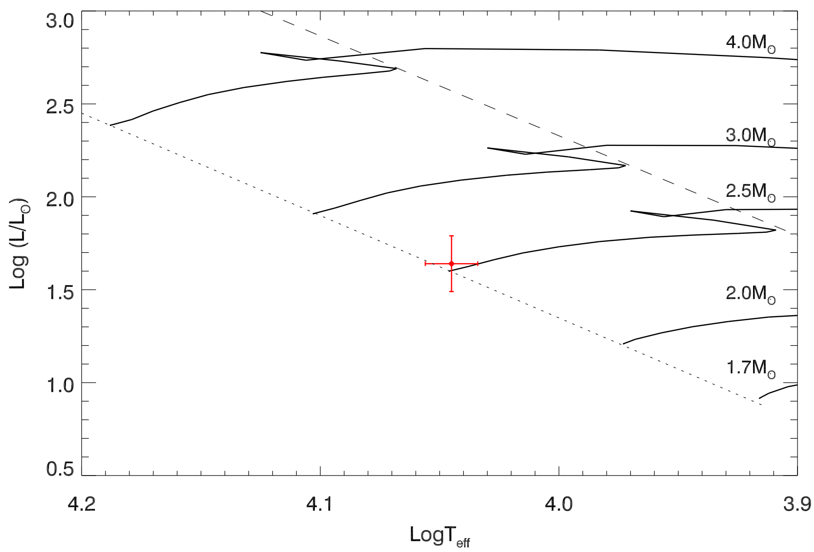

Figure 3. Positions of V473 Tau on the H-R diagram. Evolution paths for intermediate mass stars (continuous lines), zero age main sequence (dotted line), and terminal age main sequence lines (dashed line) are from Schaller et al. (1992).

This region is an interface between inner layers where circulation is dominant and the outer envelope is influenced by magnetism. As a result of differential rotation, a toroidal component of the internal magnetic field is produced, and it increases until the outer magnetically-confined envelope is forced to co-rotate with the interior. Hence, a cyclic increase and decrease in the moment of inertia occurs Stępień (1998). This means that an unexpected alternating variability of rotation periods can be observed. In this case, rotation acceleration in V473 Tau may be interpreted as a consequence of torsional oscillations produced by meridional circulations being in interaction with a magnetic field, and of rotational braking in outer layers caused by angular momentum loss via magnetically-confined stellar wind.

Additionally, the evolutionary track of the star on the H-R diagram is evaluated in this study (Figure 3). The temperature and luminosity values of the star are taken from Wraight et al. (2012). In Figure 3, evolution path for intermediate mass stars (continuous lines), zero age main sequence (dotted line), and terminal age main sequence lines (dashed line) are derived from Schaller et al. (1992). Based on the figure, the star is located close to the zero age main sequence, where its mass value is compatible with the theoretical evolution path.

Oetken (1985), Hubrig and Mathys (1994) state that the magnetism of CP stars develops in the final stages of main sequence evolution. Also, Hubrig et al. (2000) indicate that magnetic fields show up only in stars that complete at least 30% of their main sequence lifetimes. In the case of V473 Tau, since the magnetic structure of the star has already known, its position on the H-R diagram represents that it produces magnetic fields before reaching or in the beginning of the main sequence.

Acknowledgments: We acknowledge assistance from Vino Sangaralingam and Gemma Whittaker in the production of the data used in this study. The *STEREO* Heliospheric imager was developed by a collaboration that included the Rutherford Appleton Laboratory and the University of Birmingham, both in the United Kingdom, and the Centre Spatial de Liége (CSL), Belgium, and the US Naval Research Laboratory (NRL), Washington DC, USA. The *STEREO*/SECCHI project is an international consortium of the Naval Research Laboratory (USA), Lockheed Martin Solar and Astrophysics Lab (USA), NASA Goddard Space Flight Center (USA), Rutherford Appleton Laboratory (UK), University of Birmingham (UK), Max-Planck-Institut für Sonnensystemforschung (Germany), Centre Spatial de Liége (Belgium), Institut d'Optique Théorique et Applique (France) and Institut d'Astrophysique Spatiale (France).

References:

Burke, E.W., Jr., Rolland, W.W., and Boy, W.R., 1970, *Journal of the Royal Astronomical Society of Canada*, **64**, 353

Dubath, P., Rimoldini, L., Süveges, et al., 2011, *MNRAS*, **414**, 2602 DOI

Eyles, C.J., Harrison, R.A., Davis, C.J., et al., 2009, *Solar Phys.*, **254**, 387 DOI

Ghosh, P., 2007, Rotation And Accretion Powered Pulsars. Series: World Scientific Series in Astronomy and Astrophysics, ISBN: 978-981-02-4744-7. WORLD SCIENTIFIC, Edited by Pranab Ghosh, **10** DOI

Hansen, C.J. and Kawaler, S.D., 1994, *Science*, **265**, 1902

Hubrig, S. and Mathys, G., 1994, *AN*, **315**, 343 DOI

Hubrig, S., North, P., and Mathys, G., 2000, *ApJ*, **539**, 352 DOI

Hubrig, S., Nesvacil, N., Schöller, M., et al., 2005, *A&A*, **440**, L37 DOI
Jerzykiewicz, M., 2009, *Acta Astronomica*, **59**, 307
Kochukhov, O., 2011, *IAU Symp.*, **273**, 249 DOI
Koupelis, T. and Kuhn, K. F., 2007, In Quest of the Universe. ISBN. 978-0763708108, Jones & Bartlett Publishers, Sudbury
Lenz, P., Breger, M., 2005, *CoAst*, **146**, 53 DOI
Maitzen, H.M., 1977, *A&A*, **60**, L29
Mikulasek, Z., Szasz, G., Krticka, J., Zverko, J., Ziznovsky, J., Zejda, M., and Graf, T., 2009, arXiv:0905.2565
Mikulášek, Z., Krtička, J., Henry, G.W., de Villiers, S.N., Paunzen, E., and Zejda, M., 2010, *A&A*, **511**, L7 DOI
Mikulášek, Z., Krtička, J., Janík, J., Zejda, M., Henry, G.W., Paunzen, E., Žižňovský, J., and Zverko, J., 2014, Putting A Stars into Context: Evolution, Environment, and Related Stars, 270
Oetken, L., 1985, *AN*, **306**, 187 DOI
Rakosch, K.D. and Fiedler, W., 1978, *A&AS*, **31**, 83
Rimoldini, L., Dubath, P., Süveges, M., et al., 2012, *MNRAS*, **427**, 2917 DOI
Sangaralingam, V. and Stevens, I.R., 2011, *MNRAS*, **418**, 1325 DOI
Schaller, G., Schaerer, D., Meynet, G., and Maeder, A., 1992, *A&AS*, **96**, 269
Stellingwerf, R.F., 1978, *ApJ*, **224**, 953 DOI
Stępień, K., 1998, *A&A*, **337**, 754
Whittaker, G., Sangaralingam, V., and Stevens, I., 2012, *IAUS*, **282**, 143 DOI
Wraight, K.T., Fossati, L., Netopil, M., Paunzen, E., Rode-Paunzen, M., Bewsher, D., Norton, A.J., and White, G.J., 2012, *MNRAS*, **420**, 757 DOI

COMMISSIONS G1 AND G4 OF THE IAU
INFORMATION BULLETIN ON VARIABLE STARS
Volume 63 Number 6246 DOI: 10.22444/IBVS.6246

Konkoly Observatory
Budapest
20 July 2018

HU ISSN 0374 – 0676

PHOTOMETRY OF GS UMa: A SUSPECTED δ SCUTI VARIABLE

KAHRAMAN ALIÇAVUŞ, F.; RAHEEM, A.; ÇOBAN G. Ç.; TAMBULUT, E. M.; GÖGÜLTER, Ü.;BAŞ, L.; ÇEVIRICI, B.

Faculty of Sciences and Arts, Physics Department, Çanakkale Onsekiz Mart University, 17100, Çanakkale, Turkey
e-mail: filizkahraman01@gmail.com

Abstract

We present the time series analysis of GS UMa. GS UMa is a suspected δ Scuti variable with a primary frequency of 6.0987 d^{-1}.

δ Scuti stars are one of the most known pulsating variables which oscillate in radial and non-radial pressure, gravity and mixed modes mostly in a frequency ranges of 5−50 d^{-1} (Breger, 2000). Thanks to the space missions (*Kepler*, CoRoT, MOST), many new δ Scuti variables have been discovered. These discoveries have uncovered new problems about δ Scuti stars. One of the problems concerns the borders of the δ Scuti instability strip. Uytterhoeven et al. (2011) showed that there are many δ Scuti variables located outside their own instability strip. According to the theory, it is not expected to detect such variables beyond the borders.

GS UMa (V=$8\overset{m}{.}66$, HIP 51361, RA = $10^h29^m26\overset{s}{.}8$, DEC = $+39°46'08\overset{''}{.}5$) is a poorly classified δ Scuti variable. Its variability was first found by Duerbeck (1997) using the Hipparcos data. The star was defined as a suspect δ Scuti star by Kahraman Aliçavuş et al. (2017). They carried out a detailed spectroscopic analysis of the star and derived the atmospheric parameters (effective temperature $T_{\rm eff}$, surface gravity $\log g$, microturbulent velocity ξ), projected rotational velocity, and the chemical abundances of the variable. As a result of their analysis, they showed that the star is located outside the instability strip of δ Scuti stars. Therefore, in this study, we focus on the photometric observations of GS UMa to reveal its variability type.

Table 1: Information of the comparison (C1) and the check (C2) stars.

ID	Name	RA (J2000)	DEC (J2000)	V (mag)
C1	GSC 3002−00989	$10^h29^m15\overset{s}{.}5$	$+39^o\ 45'00\overset{''}{.}4$	9.89
C2	GSC 3002−00097	$10^h28^m58\overset{s}{.}1$	$+39^o\ 40'01\overset{''}{.}0$	9.30

Photometric observations of GS UMa were carried out at the Çanakkale Onsekiz Mart University Observatory with the Apogee ALTA U47 CCD mounted on the 30 cm Cassegrain-Schmidt telescope. The photometric data was obtained with Johnson B and

V filters on 4, 12, 19, 26, and 28 April 2018. About 25 hours of data was taken during the observation period. From the observations, the stars which do not exhibit any significant light variation, were selected to be comparison and check stars. Information of the comparison and check stars used are given in Table 1. The basic image reduction steps (bias, dark, and flat correction) were performed by using the C-Munipack[1] software.

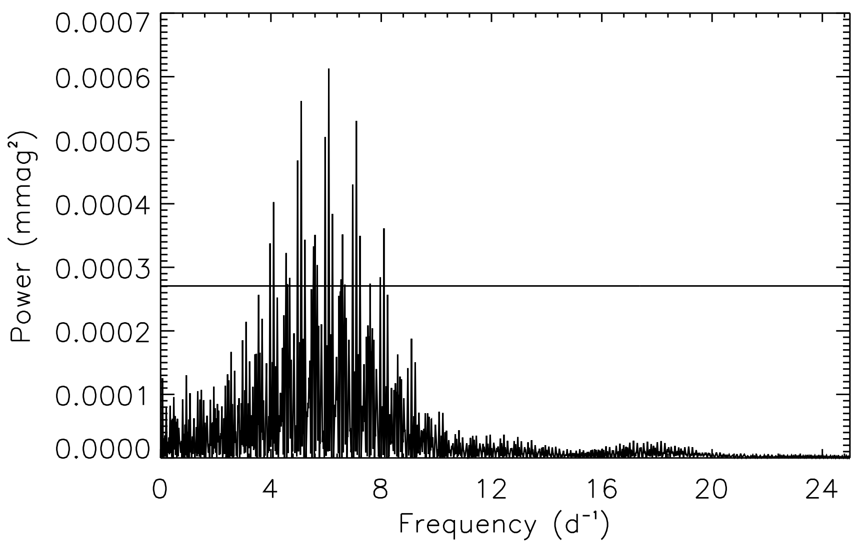

Figure 1. Power spectrum of GS UMa. Solid horizontal line represents the significance limit.

The observed light curves were analysed by using the Period04 program (Lenz & Breger 2005) to derive the pulsation period and amplitude of the star. As a result of this analysis, a significant pulsation frequency of 6.0987 d^{-1} with signal-to-noise (S/N) level higher than the significance limit ($S/N \geq 4$, Breger et al. 1993) and with 46.35 mmag pulsation amplitude in V filter was obtained. Furthermore, we detected a frequency value lower than 5 d^{-1}. However, its S/N level is lower than the significance limit. The existence of this frequency should be checked with new long-term observations. Additionally, we used the SuperWASP data[2] for the frequency analysis. In this analysis, we determined three significant frequencies. The obtained frequencies can be found in Table 2. The power spectrum and the comparison of the observed light curves with the calculated ones are shown in Fig. 1 and Fig. 2, respectively.

We calculated the pulsation constant (Q) value of the star by utilizing the below equation given by Petersen & Jørgensen (1972).

$$\log Q = -6.456 + 0.5 \log g + 0.1 M_{\rm Bol} + \log T_{\rm eff} + \log P$$

The $T_{\rm eff}$ and $\log g$ values were taken from Kahraman Aliçavuş et al. (2017). $M_{\rm Bol}$ was calculated using the bolometric correction value which was taken from Cox et al. (2000) and the *Gaia* parallax (Gaia Collaboration et al. 2016). As a result of this calculation, we determined the Q value to be $0\overset{\rm d}{.}069 \pm 0.012$. This value is out of range of Q for δ

[1] http://c-munipack.sourceforge.net/
[2] https://wasp.cerit-sc.cz/form

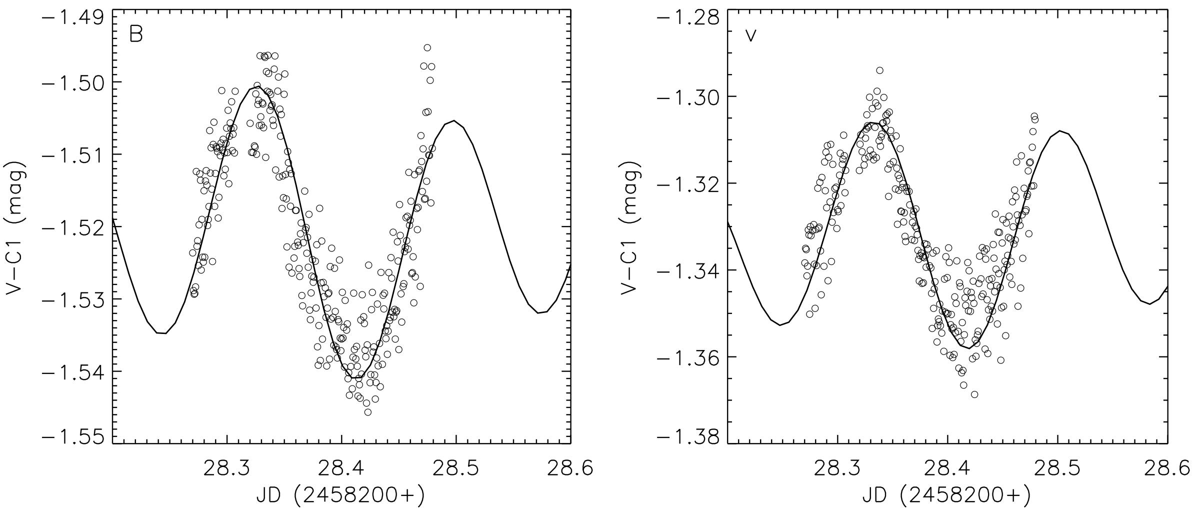

Figure 2. Comparison of the observed B (left panel) and V (right panel) light curves of GS UMa with the calculated light curves (solid lines).

Table 2: Frequencies detected in GS UMa.

Filter	Parameter	Frequency (d^{-1})	Amplitude (mmag)	S/N
B	f_1	6.0987±0.0014	38.76±1.62	24
V	f_1	6.0987±0.0013	46.35±0.99	18
SuperWASP	f_1	6.0972±0.0000	41.99±0.34	34
SuperWASP	$f_2 = 2f_1$	12.1944±0.0000	11.29±0.37	11
SuperWASP	f_3	5.0120±0.0056	6.68±0.61	5

Scuti stars according to the study of Antonello & Pastori (1981). However, it should be noticed that a limited number of stars were used in this study.

GS UMa is located beyond to the red border of δ Scuti and γ Doradus instability strip (Kahraman Aliçavuş et al., 2017). According to our frequency analysis results, the star shows δ Scuti-type pulsation. However, we also detected a frequency lower than 5 d^{-1}. This frequency is in the range of γ Doradus stars' pulsation frequency interval. In addition, it is shown that a large majority of δ Scuti stars ($\sim$98%) in the *Kepler* field show low frequencies (Balona, 2018). A most recent explanation of these low frequencies was explained by interaction between oscillation and convection (Xiong et al., 2016). Therefore, GS UMa simply might be a δ Scuti star exhibiting low frequency pulsation. However, to reveal this feature the star needs more high quality observations.

Acknowledgements: The authors would like to thank the reviewer for useful comments and suggestions. This research was carried out as a part of the Practical Astronomy course (14FZK416 / FZK466) of Physics Department of Çanakkale Onsekiz Mart University (Turkey). The lecturer FKA thanks her students for their enthusiasm in the study. This paper makes use of data from the first public release of the WASP data (Butters et al. 2010) as provided by the WASP consortium and services at the NASA Exoplanet Archive, which is operated by the California Institute of Technology, under contract with the National Aeronautics and Space Administration under the Exoplanet Exploration Program. This work has made use of data from the European Space Agency (ESA) mission Gaia (`http://www.cosmos.esa.int/gaia`), processed by the Gaia Data Processing and Analysis Consortium (DPAC, `http://www.cosmos.esa.int/web/gaia/dpac/consortium`). Funding for the DPAC has been provided by national institutions, in particular the institutions participating in the Gaia Multilateral Agreement. This research has made use of the SIMBAD data base, operated at CDS, Strasbourg, France.

References:

Antonello E. & Pastori L., 1981, *PASP*, **93**, 237 DOI

Balona L. A., 2018, *MNRAS*, **479**, 183 DOI

Breger, M., Stich, J., Garrido, R., et al. 1993, *A&A*, **271**, 482

Breger M., 2000, *ASPC*, **210**, 3

Butters, O. W., West, R. G., Anderson, D. R., et al. 2010, *A&A*, **520**, L10 DOI

Cox, A. N., Becker, S. A., & Pesnell, W. D. 2000, Allen's Astrophysical Quantities, **499**

Duerbeck, H. W., 1997, IBVS, **4513**, 1

Gaia Collaboration, Brown, A. G. A., Vallenari, A., et al. 2016, *A&A*, **595**, A2 DOI

Kahraman Aliçavuş, F., Niemczura, E., Polińska, M., et al. 2017, *MNRAS*, **470**, 4408 DOI

Lenz, P. & Breger, M. 2005, *CoAst*, **146**, 53 DOI

Petersen, J. O., & Jørgensen, H. E. 1972, *A&A*, **17**, 367

Uytterhoeven K., Moya, A., Grigahcène A., Guzik, J. A., Gutiérrez-Soto, J., et al., 2011, *A&A*, **534**, A125 DOI

Xiong D. R., Deng L., Zhang C., Wang K., 2016, *MNRAS*, **457**, 3163 DOI

COMMISSIONS G1 AND G4 OF THE IAU
INFORMATION BULLETIN ON VARIABLE STARS
Volume 63 Number 6247 DOI: 10.22444/IBVS.6247

Konkoly Observatory
Budapest
20 July 2018

HU ISSN 0374 – 0676

THE STATUS OF GSC 3870-01172 AS A MEMBER OF A TRIPLE OR QUADRUPLE SYSTEM

TERRELL, D.[1]; NELSON, ROBERT H.[2,3]

[1] Dept. of Space Studies, Southwest Research Institute, 1050 Walnut St., Suite 300, Boulder, CO 80302, USA, e-mail: terrell@boulder.swri.edu

[2] 1393 Garvin Street, Prince George, BC, Canada, V2M 3Z1 email: bob.nelson@shaw.ca

[3] Guest investigator, Dominion Astrophysical Observatory, Herzberg Institute of Astrophysics, National Research Council of Canada

Abstract

New photometry and radial velocities of the eclipsing binary GSC 3870–01172 are reported. Simultaneous analysis of the data using the Direct Distance Estimation method yields the absolute parameters, as well as the distance to the binary. A comparison of the distances and proper motions indicates that the nearby star GSC 3870-01361 may be a third component of the system.

GSC 3890-01172 was identified as a candidate W Ursae Majoris (W UMa) eclipsing binary star by the Northern Sky Variability Survey (Hoffman et al., 2009). The observations reported herein confirm that the system is indeed a W UMa binary. Standardized photometric observations in 2013 and 2016 show that the system has partial eclipses and exhibits small night-to-night variations. Radial velocities measured for both components allow us to perform a simultaneous solution that includes the distance to the system as an adjustable parameter.

The photometric observations were made at the Sonoita Research Observatory near Sonoita, AZ using a 0.5 m folded Newtonian telescope and a Santa Barbara Instrument Group STL-6303 CCD camera with Johnson-Cousins BV filters. The images were calibrated in the usual way by bias/dark subtraction and then flatfielding using IRAF (Tody, 1993). Instrumental magnitudes were then measured using PSF fitting with SExtractor (Bertin & Arnouts, 1996) and PSFEx (Bertin, 2011). Using the method described in Terrell et al. (2016), the instrumental magnitudes were transformed onto the standard system using APASS standards (Henden et al., 2012) from Data Release 9 (APASS DR9). The standard BV magnitudes are available from the IBVS web site as file 6247-t2.txt.

From 2016 to 2018, spectroscopic observations were made with the 1.85 m Plaskett telescope at the Dominion Astrophysical Observatory in Victoria, British Columbia. The 21181 configuration of the spectrograph was employed with a grating of 1800 lines/mm, blazed at 5000 Å, giving a reciprocal linear dispersion of 10 Å/mm in the first order. The wavelengths ranged from 5000 to 5260 Å, approximately. Frame reduction was performed by the software RaVeRe (Nelson 2013). See Nelson (2010) and Nelson et al. (2014) for further details. Radial velocities were determined using the Rucinski broadening functions (Rucinski, 2004; Nelson, 2010) as implemented in the software Broad (Nelson, 2013; Nelson et al., 2014). Table 1 gives the details of the radial velocity observations.

Table 1: Radial Velocity Observations of GSC 3870-01172.

DAO Image #	Mid Time (HJD−2400000)	Exposure (sec)	Phase at mid-exp.†	V_1 (km sec^{-1})	V_2 (km sec^{-1})
16-01283	57493.86414	1800	0.229	−260.3 ± 3.9	79.4 ± 5.2
16-01334	57496.00532	3600	0.783	268.7 ± 2.2	−79.2 ± 1.2
16-01362	57497.00402	1000	0.841	229.8 ± 2.2	−62.1 ± 2.3
16-01364	57497.01913	1120	0.888	175.8 ± 4.3	−34.1 ± 3.6
16-01444	57498.90975	1200	0.675	228.3 ± 3.9	−64.6 ± 3.8
16-01446	57498.93979	3600	0.767	264.5 ± 3.4	−76.5 ± 3.7
16-01511	57504.96601	1000	0.216	−250.3 ± 2.3	68.3 ± 3.5
16-01513	57504.97996	1200	0.258	−254.5 ± 1.8	70.4 ± 5.2
17-03943	57854.80597	940	0.198	−245.7 ± 1.2	80.2 ± 0.6
18-05325	58233.78010	900	0.368	−175.1 ± 3.9	69.3 ± 4.1
18-05375	58234.84434	900	0.626	175.3 ± 2.9	−64.7 ± 7.1
18-05393	58235.01831	312	0.159	−211.0 ± 5.5	80.4 ± 4.3
18-05423	58235.99037	900	0.135	−202.1 ± 3.7	63.2 ± 4.8
18-05518	58242.89512	900	0.273	−253.5 ± 3.6	73.7 ± 4.0

† Phases computed using the ephemeris parameters in Table 2 for the third body solution.

The BV light curves and the new radial velocities were analysed simultaneously with the 2013 version of the Wilson–Devinney program (WD; Wilson & Devinney, 1971; Wilson, 1979; Wilson, 2008). We assumed a value of 0.32 for the gravity darkening exponents of both stars and a value of 0.5 for the bolometric albedos, consistent with convective envelopes as expected from the surface temperatures of both components. Limb darkening coefficients were automatically computed at each iteration from the Van Hamme (1993) tables and the square-root limb darkening law gave substantially better results in the fits as compared to the logarithmic law. Weights for the various light and velocity curves were determined automatically by WD at each iteration.

WD mode 3, appropriate for overcontact binaries, was used in the solution process. The system exhibits partial eclipses so we cannot determine a photometric mass ratio with any reasonable degree of certainty (Terrell & Wilson, 2005), but the system is double-lined and thus a spectroscopic mass ratio can be determined. The radial velocities allow us to determine the absolute scale of the system and thus the luminosity of the system. Our standard magnitudes of the system can be converted into physical flux units via the calibrations of Wilson et al. (2010), enabling the distance to be a free parameter in the simultaneous light/velocity curve solution. See Wilson (2008) for details on this direct distance estimation (DDE) procedure. The lower mass star is eclipsed at primary minimum, making this a W-type system.

The system shows mild asymmetries in the light curves and we used a cool spot on star 2 to model them. The determinacy of spot parameters from light curve solutions is known to be fraught with difficulties, so we performed extensive tests using a combination of grid searches through the spot parameter space, as well as a genetic algorithm optimizer coupled with WD. In all, approximately 10^6 light curves were computed. Once various minima were discovered in the search, traditional differential corrections (DC) solutions were performed with WD to zero in on the local minima.

The initial solution assumed no third light and determined a distance to the binary of 107.4 ± 0.2 pc. The adjusted (a, V_γ, i, T_1,T_2, q, Ω, HJD$_0$, P, $\dot{P}$, and $\log(d)$) and derived

Table 2: Parameters from the light/velocity curve solution. Errors on the adjusted parameters are the internal errors from the least squares solution.

Parameter	No 3^{rd} Body	With 3^{rd} Body
a ($R_\odot$)	2.308 ± 0.006	2.281 ± 0.006
V_γ (km sec^{-1})	3.1 ± 0.3	3.2 ± 0.3
i (deg)	76.1 ± 0.1	76.6 ± 0.1
T_1 (K)	5459 ± 6	5492 ± 6
T_2 (K)	5315 ± 4	5333 ± 4
Ω_1	6.83 ± 0.03	6.98 ± 0.04
q	3.23 ± 0.02	3.35 ± 0.03
HJD_0	2456415.51108 ± 0.00008	2456415.51107 ± 0.00008
P (d)	0.326651 ± 0.0000001	0.326651 ± 0.0000001
$\dot{P}$	$1.7 \pm 0.2 \times 10^{-9}$	$1.8 \pm 0.2 \times 10^{-9}$
$log(d)^\dagger$	2.031 ± 0.001	2.034 ± 0.001
M_1 ($M_\odot$)	0.366 ± 0.003	0.343 ± 0.004
M_2 ($M_\odot$)	1.18 ± 0.01	1.15 ± 0.01
R_1 ($R_\odot$)	0.672 ± 0.002	0.636 ± 0.002
R_2 ($R_\odot$)	1.137 ± 0.008	1.132 ± 0.009
$L_{B,1}$ ($L_\odot$)	0.290 ± 0.003	0.290 ± 0.003
$L_{B,2}$ ($L_\odot$)	0.69 ± 0.01	0.70 ± 0.01
$L_{V,1}$ ($L_\odot$)	0.336 ± 0.003	0.333 ± 0.003
$L_{V,2}$ ($L_\odot$)	0.84 ± 0.01	0.85 ± 0.01
Spot longitude (rad)	0.6 ±0.1	0.6 ±0.1
Spot co-latitude (rad)	2.71 ±0.03	2.69 ±0.03
Spot radius (rad)	0.26 ±0.04	0.26 ±0.03
Spot temperature (rad)	0.8 ±0.1	0.8 ±0.1

† Distance d to the binary in parsecs.

parameters (masses, radii and bandpass luminosities) are shown in Table 2.

The *Gaia* DR2 distance is 108.3 ± 0.3 pc (Gaia Collaboration et al., 2018). We note that since binarity can affect the parallax determined by *Gaia* and DR2 does not include processing for binarity (Lindegren et al., 2018), this value may be revised in future *Gaia* data releases. For now we assume that since the binary components are very close, the parallax, and thus distance, is reasonably accurate for comparison to the distance derived from our analysis. Attempts to resolve the discrepancy between the two distance measurements by adjusting the interstellar extinction were not successful without unreasonably large extinction values, given the close distance and high galactic latitude of the system. Third light was also investigated and gave more reasonable results. Because of strong parameter correlations and the fact that the system only has partial eclipses and light curve asymmetries, we decided to fix third light at values appropriate for a grid of main sequence stars of various effective temperatures and solve for the full parameter set, including the distance, rather than allowing third light to adjust. The radii of the third bodies were computed via the $T_{\rm eff}$-R relation in Boyajian et al. (2012) and then the LC program from WD was used to compute the flux from the third body, which was then added to the DC input file. Because of the strong correlations between some of the spot parameters, we adjusted only one at a time (along with all of the other non-spot parameters), doing three DC iterations and then switching to another spot parameter for another three iterations, rotating through all four spot parameters. This approach to dealing with parameter correlations is similar to that described by Wilson and Biermann (1976).

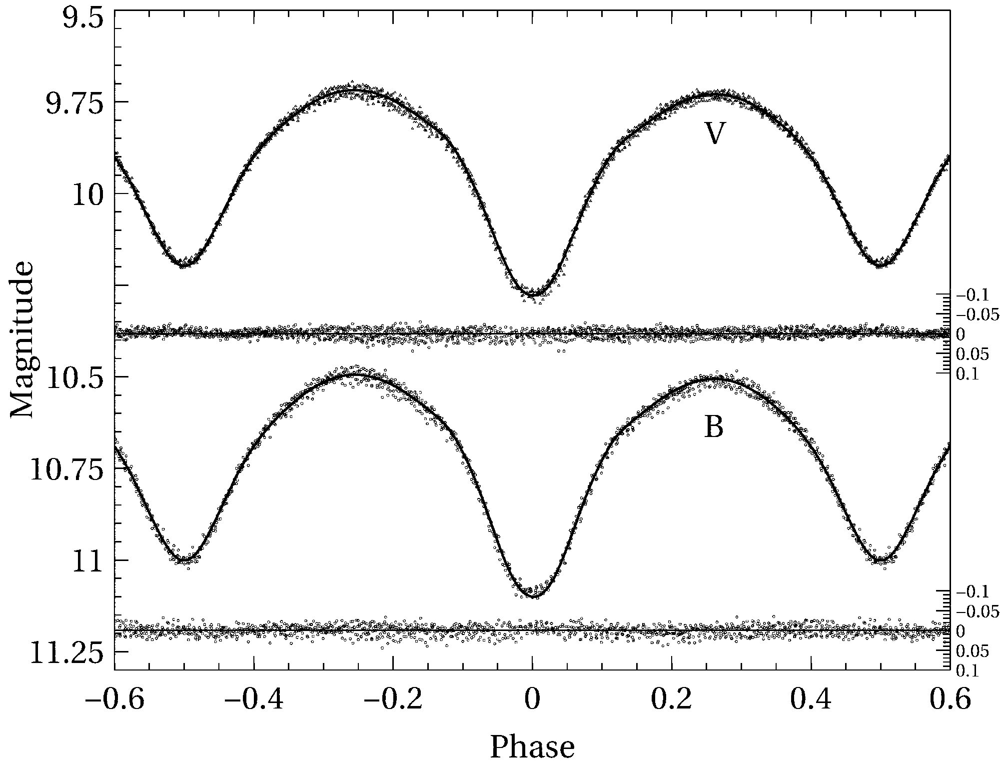

Figure 1. The fits to the B and V light curves of GSC 3870-01172. The residuals are plotted below each light curve.

The third body that resulted in a distance to the binary equal to the *Gaia* value was one with $T_{\rm eff}$=3750 K and $R = 0.514R_{\odot}$, making it a late K-type star. The adjusted and derived parameters for this solution are also shown in Table 2. Figure 1 shows the fits to the light curves and Figure 2 shows the fits to the radial velocity curves for the third body solution. Of the two solutions in Table 2, we favour the one that includes the third body for two reasons, while again noting the previously discussed caution about binarity affecting the *Gaia* DR2 parallax. Overcontact binaries are known to have a high frequency of third bodies (Pribulla & Rucinski, 2006) and the statistics are consistent with the hypothesis that all overcontact systems originated in multiple systems. Secondly, although the time baseline of our observations is small, we do find a statistically significant period change and this could be due to the influence of a third body.

GSC 3870-01361 (hereafter, "the companion") is about 46″ away from GSC 3870-01172 and the *Gaia* DR2 parallax puts it at 107.6±0.3 pc, *i.e.* at essentially the same distance as the binary, with a projected separation of about 4900 AU. The *Gaia* proper motions of the binary (15.98±0.05 mas yr^{-1} in right ascension and 30.83±0.06 mas year^{-1} in declination) and the companion (15.99 ± 0.05 mas year^{-1} and 30.61 ± 0.05 mas year^{-1}) are also very nearly equal. We measured the radial velocity of the companion on HJD 57854.85551 and found it to be 1.6 ± 1.5 km sec^{-1}, very close to our measured systemic velocity of the binary. Given that the companion's distance, proper motion and radial velocity are

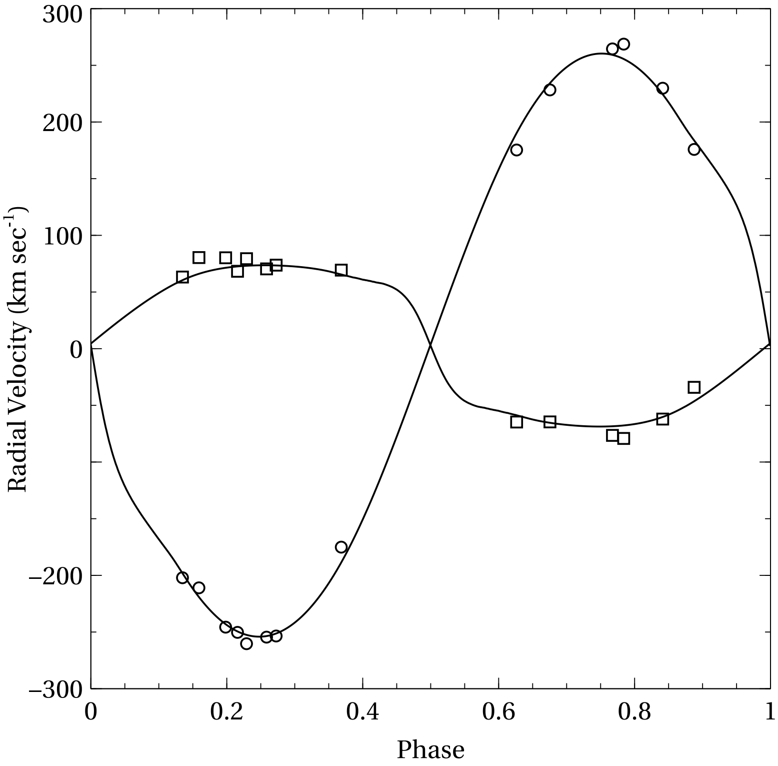

Figure 2. The fits to the radial velocity curves curves of GSC 3870-01172. The sizes of the error bars on the radial velocities are approximately the same size as the points.

nearly the same as GSC 3870-01172, we conclude that it is physically associated with the binary, making this at least a triple system, and potentially a quadruple system if our analysis of the eclipsing binary data indicating the presence of an unresolved body orbiting the binary is correct.

Acknowledgements: This research was made possible through the use of the AAVSO Photometric All-Sky Survey (APASS), funded by the Robert Martin Ayers Sciences Fund and U.S. National Science Foundation grant 1412587. It is a pleasure to thank the staff members at the DAO (David Bohlender, Dmitry Monin, and the late Les Saddlemyer) for their usual splendid help and assistance. We thank the referee for constructive comments that improved the paper.

References:

Bertin, E., 2011, *ASP Conf. Ser.*, **442**, 435
Bertin, E., Arnouts, S., 1996, *A&A Suppl. Ser.*, **117**, 393 DOI
Boyajian, T., et al., 2012, *ApJ*, **757**, 112 DOI
Gaia Collaboration, et al., 2018, *A&A*, **616**, 1 DOI
Henden, A. A., Levine, S. E., Terrell, D., Smith, T. C., Welch, D., 2012, *JAAVSO*, **40**, 430
Hoffman, D.I., Harrison, T.E.,, McNamara, B.J., 2009, *AJ*, **138**, 466 DOI
Lindegren, L., et al., 2018, *A&A*, **616**, 2 DOI

Nelson, R.H., 2010, "Spectroscopy for Eclipsing Binary Analysis" in The Alt-Az Initiative, Telescope Mirror & Instrument Developments (Collins Foundation Press, Santa Margarita, CA), R.M. Genet, J.M. Johnson and V. Wallen (eds.)
Nelson, R.H., 2013, Software by Bob Nelson, `https://www.variablestarssouth.org/bob-nelson/`
Nelson, R. H., Şenavcı, H.V. Baştürk, Ö., Bahar, E., 2014, *New Astronomy*, **29**, 57 DOI
Pribulla, T., Rucinski, S., 2006, *AJ*, **131**, 2986 DOI
Rucinski, S. M., 2004, *IAUS*, **215**, 17
Terrell, D., Gross, J., Cooney, W.R., 2016, *IBVS*, **6166**
Terrell, D., Wilson, R.E., 2005, *Ap&SS*, **296**, 221 DOI
Tody, D., 1993, *ASP Conf. Ser.*, **52**, 173
Van Hamme, W., 1993, *AJ*, **106**, 2096 DOI
Wilson, R.E., 1979, *ApJ*, **234**, 1054 DOI
Wilson, R.E., 2008, *ApJ*, **672**, 575 DOI
Wilson, R.E., Biermann, P., 1976, *A&A*, **48**, 349 DOI
Wilson, R.E., Devinney, E.J., 1971, *ApJ*, **166**, 605 DOI
Wilson, R.E., Van Hamme, W., Terrell, D., 2010, *ApJ*, **723**, 1469 DOI

COMMISSIONS G1 AND G4 OF THE IAU
INFORMATION BULLETIN ON VARIABLE STARS
Volume 63 Number 6248 DOI: 10.22444/IBVS.6248

Konkoly Observatory
Budapest
27 July 2018

HU ISSN 0374 – 0676

TYC 5353-1137-1: AN ENIGMATIC DOUBLY PERIODIC VARIABLE OF SEMIREGULAR AMPLITUDE

ROSALES, J. A., MENNICKENT, R. E.

Astronomy Department, University of Concepción, Concepción, Chile

e-mail: jrosales@astro-udec.cl; rmennick@astro-udec.cl

To date the Doubly Periodic Variables (DPVs) discovered by Mennickent et al. (2003) in the Large Magellanic Cloud (LMC) and the Small Magellanic Cloud (SMC) have been interpreted as semi-detached interacting binary stars with a B-type component surrounded by an optically thick disk. These stars seem to experience regular cycles of mass loss (Mennickent et al. 2008) and are characterized by orbital photometric variability on time scales of 2 to 100 days. These systems show a long period which is on average 33 times longer than the orbital period (Mennickent et al., 2016; Mennickent, 2017; Poleski et al., 2010). Currently, the DPVs found are Algol-type eclipsing (DPV/E) and ellipsoidal (DPV/ELL) system.

Therefore, we have performed a new search for DPVs of short period in the ASAS[1] catalog (Pojmanski, 1997), focusing on those stars with orbital periods between 2 to 3 days which also show variations in their brightness. From a total of 244 objects, we have found another candidate DPV, one whose mean brightness is gradually decreasing. By fitting a 3rd order polynomial to the mean magnitude (red line in Fig. 1.) and then moving it to zero for a second analysis, a gradual decrease over 2500 days was revealed. During the last 1000 days of this decrease, a 42% increase in the variation between the minimum and maximum values of the magnitude was observed (Fig. 1). We determined the orbital period by using the PDM (phase dispersion minimization) IRAF[2] software (Stellingwerf, 1978) and estimated the errors for the orbital period and the long cycle by visual inspection of the light curves phased with trial periods near the minimum of the periodogram given by the PDM. The two main frequencies of the system were disentangled using the code written by Zbigniew Kołaczkowski and described by Mennickent et al. (2012). This code was specially designed to adjust the orbital signal with a Fourier series and disentangle both frequencies using the fundamental frequencies and harmonics we supplied. The code removed this signal from the original time series thus allowing long periodicity to appear in a residual light curve, and we obtained both isolated light curves without additional frequencies, as shown in Figs. 2 and 3. We presented the search results and ephemeris in Table 1 and Fig. 1 (left) both of which illustrate the gradual brightness decrease in the ASAS photometry. In the right panel of this figure we show the photometric variation, ΔV shifted to average zero and, finally, the disentangled light curves in Figs. 2 and 3.

---

[1] `http://www.astrouw.edu.pl/asas/`

[2] IRAF is distributed by the National Optical Astronomy Observatories, which are operated by the Association of Universities for Research in Astronomy, Inc., under cooperative agreement with the National Science Foundation.

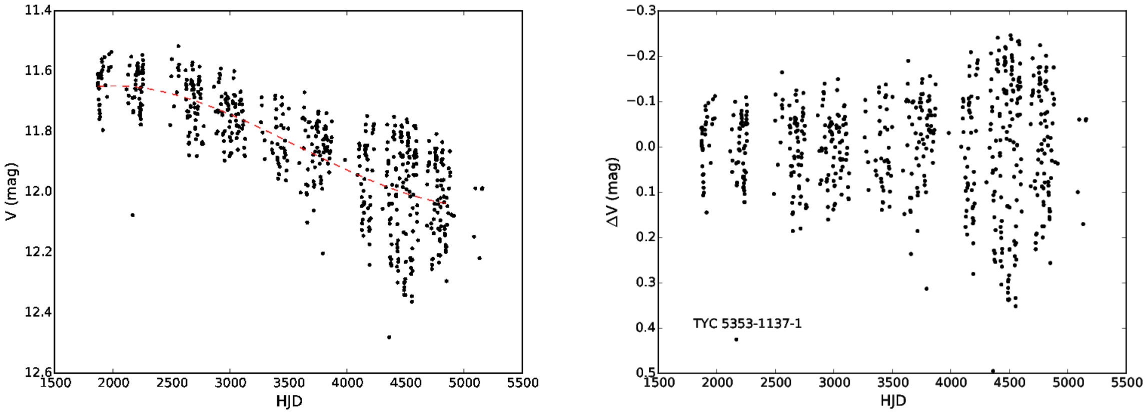

Figure 1. (Left) The ASAS photometry reveals a gradual decrease in the brightness of DPV TYC 5353-1137-1 over 2500 days, followed by an increase of 42% in the amplitude of the photometric variation over the last 1000 days (right). The red line corresponds to a 3rd-order polynomial representing the mean magnitude.

ASAS-ID	Other ID	RA (2000)	DEC (2000)	P_o (days)	P_l (days)	$T_0(min_o)$ -2450000	$T_0(max_l)$ -2450000	V (ASAS) (mag)
060418-1009.4	TYC 5353-1137-1	06:04:18.0	-10:09:24.0	2.028(1)	60.455(6)	4491.602390	4404.77653	11.56

Table 1: Parameters of the newly confirmed DPV TYC 5353-1137-1 and its orbital (P_o) and long periods (P_l). Epochs for both the minimum brightness of the orbital light curve and the maximum brightness of the long-cycle light curve are given.

This enigmatic DPV presents a variable amplitude in the light curve when it is phased using the orbital period at three different photometric datasets (Fig. 2.). The changes in the orbital light curve could be related to changes in disc size/temperature and spot temperature/position as proposed by Garcés et al. (2018) for the DPV OGLE-LMC-DPV-097. Afterwards we disentangled the light curve using the long period and phased it. For that, we used the same time intervals as those used for the orbital period as a way to analyze possible variations in the amplitude of this enigmatic phenomenon in the DPVs, and we apparently observed an effect of switch off-on of the long-cycle in the dataset of HJD between 2500 and 4000 (Fig. 3), this is observed for the first time in these kind of systems. Therefore, we consider TYC 5353-1137-1 to be an optimal target for further photometric monitoring and spectroscopic studies, due to that it will help us to test the mechanism based on cycles of the magnetic dynamo in the donor proposed by Schleicher & Mennickent (2017), the cause of mass loss in some Algol stars and the evolutionary process of the DPVs.

Acknowledgements: We acknowledge the anonymous referee whose comments helped to improve a first version of this report. R.E.M. gratefully acknowledges support by VRID-Enlace 218.016.004-1.0 and the Chilean Centro de Excelencia en Astrofísica y Tecnologías Afines (CATA) BASAL grant AFB-170002.

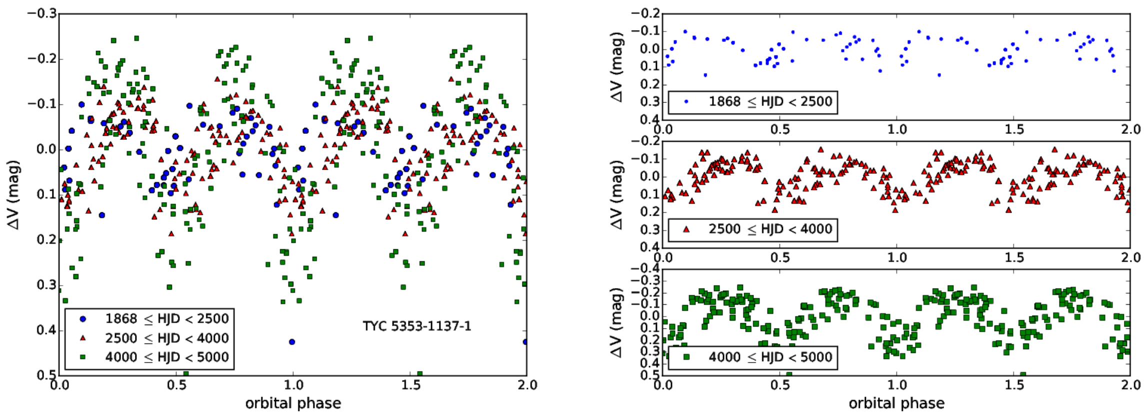

Figure 2. Disentangled ASAS V-band light curve of the new confirmed Doubly Periodic Variable. The orbital phase has been separated in the three datasets (HJD–2450000.0), representing the variation of the amplitude.

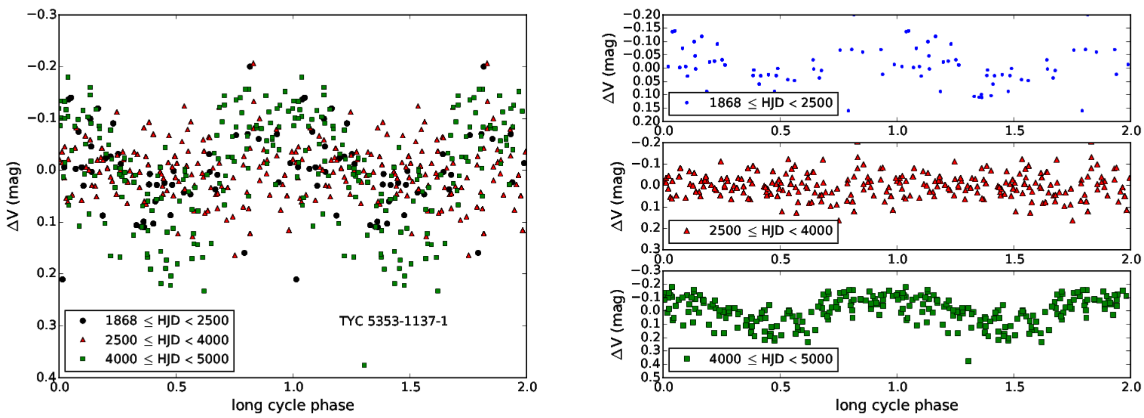

Figure 3. The long cycle phase has been disentangled and separated into three datasets (HJD–2450000.0). The first dataset shows less amplitude in the light curve of the long cycle (blue), during the second epoch an effect of switch off occurs (red), and the third dataset shows a remarkable increase in the amplitude of variability (green). Note the different y-axis scales in the panels.

References:

Garcés L, J., Mennickent, R. E., Djurasević, G.,Poleski, R., Soszyński, I., 2018, *MNRAS*, **477**, L11 DOI

Mennickent, R. E., Pietrzyński G., Diaz M., Gieren W., 2003, *A&A*, **399**, L47 DOI

Mennickent, R. E., Kołaczkowski, Z., Michalska, G., et al., 2008, *MNRAS*, **389**, 1605 DOI

Mennickent, R. E., Djurašević, G., Kołaczkowski, Z., Michalska, G., 2012, *MNRAS*, **421**, 862 DOI

Mennickent, R. E., Zharikov, S., Cabezas, M., et al., 2016, *MNRAS*, **461**, 1674 DOI

Mennickent, R. E. 2017, *Serbian Astronomical Journal*, **194**, 1 DOI

Pojmanski, G. 1997, *AcA*, **47**, 467

Poleski R., Soszyński I., Udalski A., et al., 2010, *AcA*, **60**, 179

Schleicher, D. R. G., Mennickent, R. E., 2017, *A&A*, **602**, A109 DOI

Stellingwerf, R. F., 1978, *ApJ*, **224**, 953 DOI

COMMISSIONS G1 AND G4 OF THE IAU
INFORMATION BULLETIN ON VARIABLE STARS
Volume 63 Number 6249 DOI: 10.22444/IBVS.6249

Konkoly Observatory
Budapest
27 July 2018

HU ISSN 0374 – 0676

PERIODIC Hα EMISSION IN THE ECLIPSING BINARY VV CEPHEI

POLLMANN, E.[1]; BENNETT, P. D.[2]; VOLLMANN, W.[3]; SOMOGYI, P.[4]

[1] Emil-Nolde-Straße 12, 51375 Leverkusen, Germany
[2] Dept. of Physics and Atmospheric Science, Dalhousie University, Halifax, NS, Canada
[3] Dammäckergasse 28/D1/20, A-1210, Wien, Austria
[4] Zrínyi u. 23, 2890 Tata, Hungary

Abstract

We present a high-cadence time series of spectroscopic observations of the Hα emission line profile obtained during the egress and total eclipse phases of the M supergiant binary VV Cephei (M2 Iab + B0-2 V) for the 2017-2018 eclipse. Medium-resolution spectroscopy, obtained at an almost nightly cadence by the ARAS Spectroscopy Group from April 2017 through June 2018, has been used to construct a time-series of equivalent widths (EWs) of the Hα emission line flux. The peak fluxes of the blue (V) component and the red (R) component relative to the continuum, as well as their ratio, V/R, have also been found. We report on a new 43.5-day periodic variation in the Hα emission that is present throughout the entire time series and, in particular, persists through mid-eclipse.

1 Introduction

VV Cephei (= HR 8383 = HD 208816; M2 Iab + B0-2? V) is the brightest, M supergiant eclipsing variable binary in the sky. At 5th magnitude, it is an easily accessible spectroscopic target for amateur astronomers. As is typical for red supergiants, the M star's apparent brightness is somewhat variable, $V = 4.9 - 5.4$ mag, with a dominant period of about 150 days. The VV Cep binary system consists of a red supergiant with mass about 20 solar masses and a hot, presumably main sequence, early B-type companion of comparable mass (Wright 1977). The red supergiant primary eclipses the much smaller (in radius) B-type secondary star every 20.34 years. The system is now (July 2018) midway through its 1.5-year long total eclipse that began in late October 2017. Total eclipse (2nd contact) began on JD 2458054 (2017 Oct 28) and mid-eclipse occurred on JD 2458288 (2018 June 19), based on the eclipse times of Leedjärv et al. (1999) for the 1997/98 eclipse and the 7430.5 d (20.34 yr) period of Wright (1977). The relative orbit of VV Cep is shown to scale in Fig. 1.

The optical spectrum of VV Cephei in the red spectral region is that of an M supergiant, but with strong Hα line emission from an accretion region around the hot companion (Wright 1977). This emission is probably due to accretion from the massive wind of the M supergiant, and not from mass transfer via Roche-lobe overflow. The large orbital eccentricity ($e = 0.346$; Wright 1977) and large mean orbital separation of $a/R_1 \approx 5.1$ (Bennett, private communication), where R_1 is the radius of the M supergiant, argue against the close binary nature required for Roche-lobe overflow to occur.

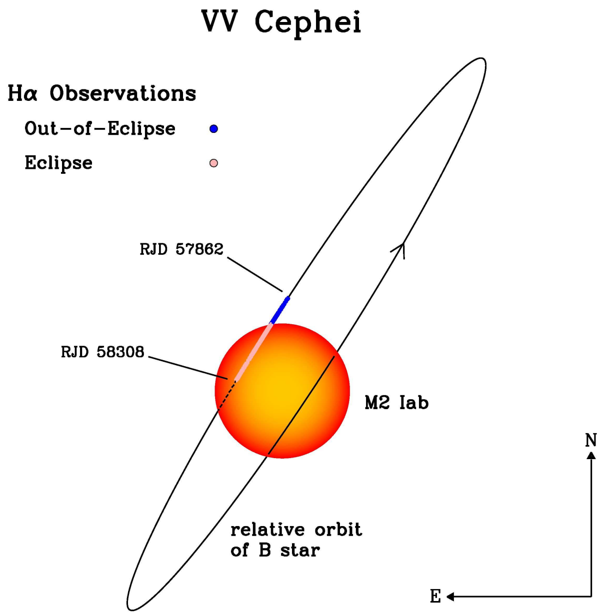

Figure 1. The relative orbit of VV Cephei to scale, as projected on the sky. The relative position of the hot B-type companion is shown by small blue circles out-of eclipse, and pink circles in total eclipse for the duration of the current data set.

The Hα emission line (Fig. 2) is prominent, with typical peak fluxes several times that of the M star continuum, and broad with a full width of $\pm$300 km s^{-1} out of eclipse. The only place in the system with velocities this large is deep in the gravitational potential of the B star and so the broad wings of Hα must be formed by rapidly infalling gas in the immediate vicinity of the B star. But, rather surprisingly for an emission region associated with the hot star, the Hα emission weakens and narrows in width, but does not completely vanish during total eclipse. This implies the existence of a spatially-extended region of Hα emission that remains uneclipsed must contribute significantly to the overall emission. Because of these difficulties, it remains unclear exactly where the Hα emission line is formed in VV Cep relative to the B star and the associated accretion region.

In structure, the Hα emission line appears doubled with two prominent peaks separated by self-absorption near line center (Fig. 2). Wright (1977) assumed that this profile was due to a single, intrinsic symmetric emission profile with superimposed absorption from low-velocity neutral hydrogen along the line of sight through the wind of the M supergiant. He found that the emission centroid followed the velocity of the B star around its orbit, moving back and forth in velocity with respect to the nearly fixed central absorption. By estimating the position of the (missing) intrinsic emission peak, and assuming it shared the radial velocity of the B star, Wright (1977) was able to derive an orbit solution for the companion. Therefore, with the orbit of the M supergiant primary already established, he was able to derive masses of about 20 solar masses for both stars of this eclipsing binary system.

However, Wright also noted that a difference of 1.7 km s^{-1} was found between the systemic velocities of the M star and B star orbital solutions, possibly an indication that the velocity of the Hα emission centroid is somewhat displaced from that of the hot star. One of the goals of the present observational campaign is to clarify the geometry of the Hα emission region by obtaining and analysing high-cadence spectroscopic observations

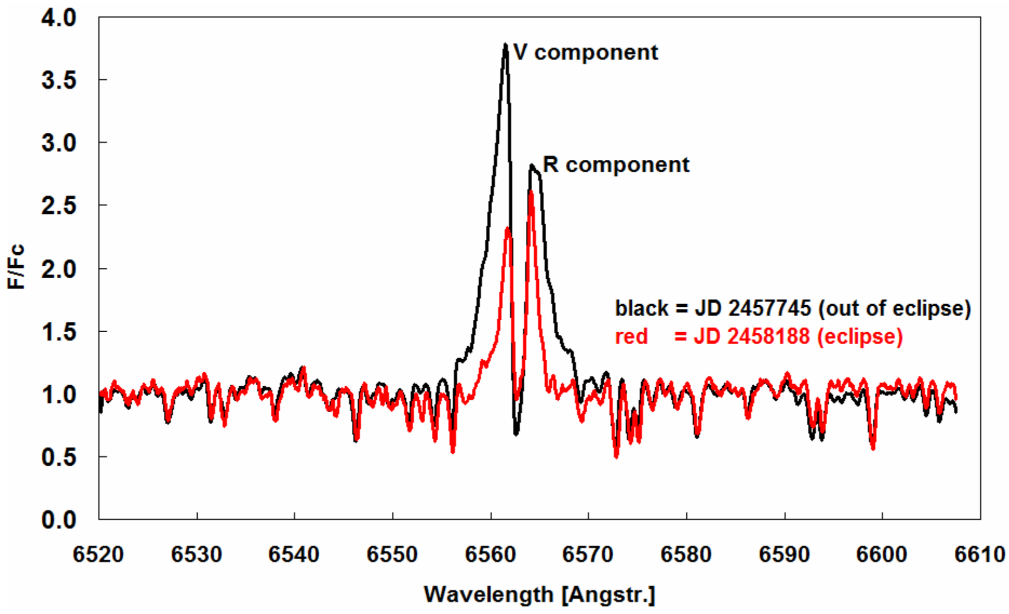

Figure 2. Medium-resolution spectrum of the Hα emission line in VV Cep; black: out-of-eclipse = 2016-12-23; red: total eclipse = 2018-03-10.

of VV Cep during the 2017-2018 eclipse period. It is hoped that this effort will lead to an improved orbit and masses for VV Cep, which is one of the most massive and luminous evolved binaries in the sky.

2 Observations

The work of the ARAS group (Pollmann, 2018) reported here consists of a long-term spectroscopic monitoring program of the Hα emission line of VV Cephei. Spectroscopic observations have been obtained on a regular basis of the red spectral region around Hα, on a regular basis with high-cadence (approximately nightly) monitoring from April 2017 (JD 2457850) through to July 2018 (JD 2458310). These medium-resolution Hα spectra ($R = \lambda/\Delta\lambda \sim 15000$) offer the opportunity to study the dynamics of the hot stars and its associated H II region, responsible for the Balmer lines (and continuum) recombination spectrum, with unprecedented time resolution.

For this observing campaign, for each spectrum, equivalent widths (EWs) of the entire Hα emission profile have been calculated, and peak fluxes of the blue (V) and red (R) emission components have been measured relative to the continuum. The V and R components are defined with reference to the central absorption that splits the Hα emission line profile into two (Fig. 2). The precise definition of continuum value used for the calculation of the EW is shown in Fig. 3, and details of the definition of the V and R components are given in Fig. 4.

One issue to be aware of when measuring Hα emission fluxes in VV Cep is that this emission originates from a source (near the B star companion) that is spatially distinct from that of the M supergiant's continuum. EWs are normally calculated with respect to the stellar continuum, but for VV Cep that continuum is itself somewhat variable and so

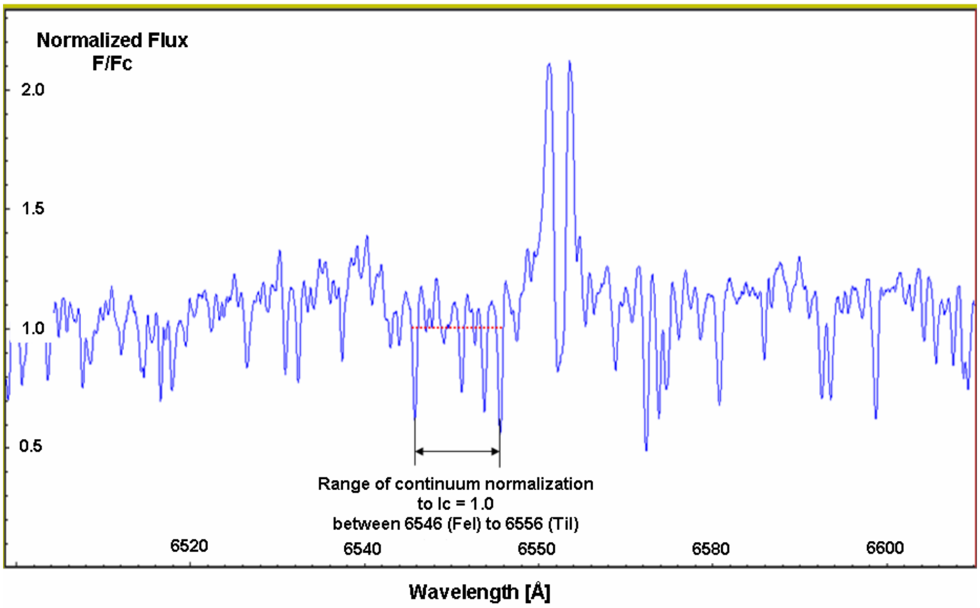

Figure 3. The continuum value used for the Hα EW calculation was the mean flux level between the Fe I 6546 Å and Ti I 6556 Å spectral lines indicated. The spectrum shown is of VV Cep on 2017 May 27 (JD 57900.45).

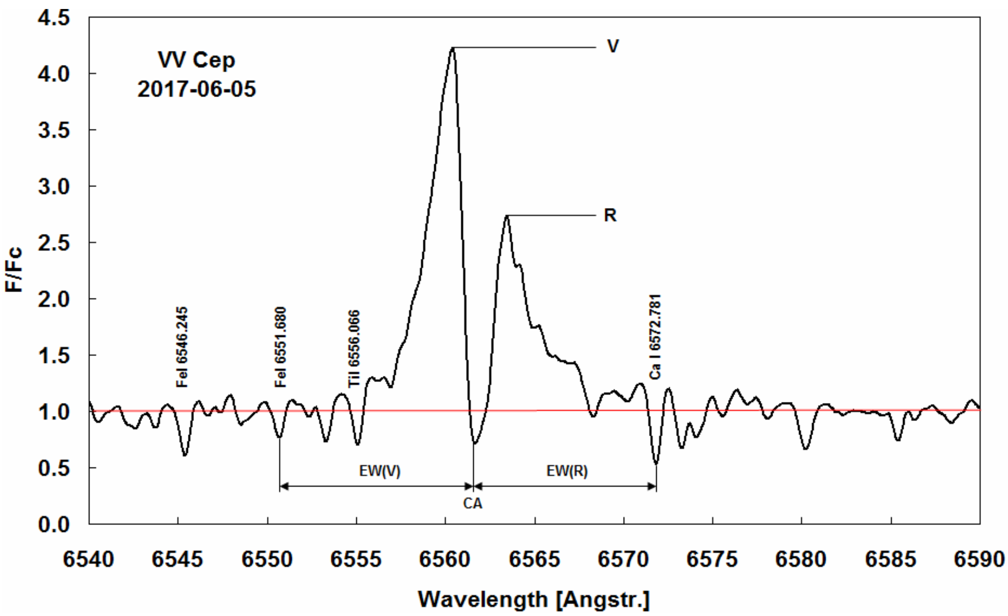

Figure 4. Definition of the V and R components.

the variability of the M supergiant introduces an apparent variation in the Hα emission flux inferred from the EW.

To obtain the intrinsic variation of the Hα component, the effect of the continuum variability should be removed. This can be done for EW observations by multiplying the raw EWs by a factor of $10^{-0.4\Delta V_0}$, where $\Delta V_0 = V - V_0$, and V is the V-band magnitude at the time of the observation, and $_V0$ is the long-term mean V magnitude. However, the data presented here have not been corrected in this manner.

Furthermore, neither of the V and R peak fluxes (which were measured relative to the M star continuum) have been corrected for M star variability, and so these values should be interpreted with caution. In places, the slow 150-day variability of the M supergiant can be seen in these fluxes. However, the effect of the variable continuum cancels out in the calculation of the blue-to-red ratio, V/R, and so that is the key diagnostic used in the present analysis.

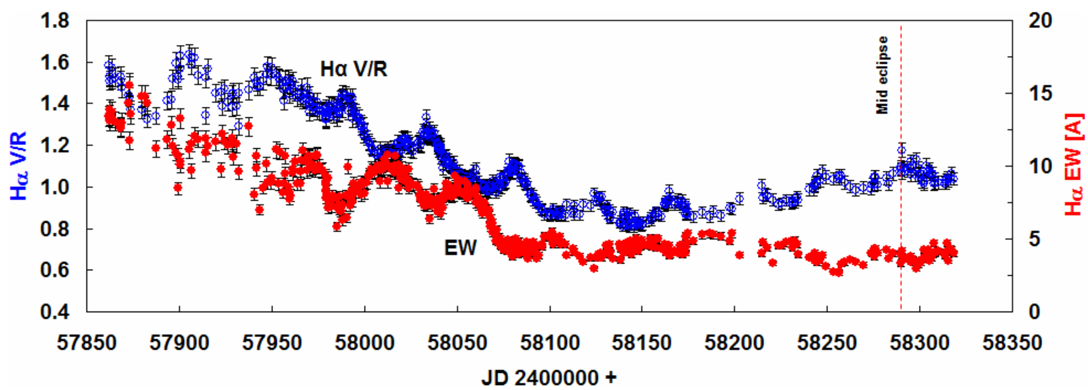

Figure 5. The total Hα emission flux (EW) behaviour [red points, refer to right axis] over the past year showing a 43.5-day periodic variation. The ratio of the Hα blue component peak flux (V) to the red component peak flux (R) is also shown [blue circles, refer to left axis]. Both components have the same 43.5-day period, but the V/R ratio varies antisynchronously with the EW variation. The predicted time of mid-eclipse (JD 2458289) is shown, from the 1997/1998 eclipse of ephemeris of Leedjärv et al. (1999) and the orbital period of Wright (1977).

The cyclic variability of the Hα EWs and the V/R ratio shown in Fig. 5 have been analysed in terms of a periodic behaviour and has led to the discovery of a persistent periodic variation of 43.5 days (Figs. 8 & 9) in the Hα EWs. This periodicity is present in the total EW, in the individual V and R peak fluxes, and most prominently in the V/R ratio. All of these components vary synchronously with the 43.5 day period, but the R flux varies with a consistently larger amplitude than the V flux. Hence the ratio V/R varies antisynchronously with that of the total EW.

What is surprising is that this 43.5 day periodicity persists into total eclipse when the hot companion and its associated accretion region have been occulted, and the total Hα flux has decreased substantially. However, the limited, out-of-eclipse U-band photometry available (Fig. 7 bottom) shows no obvious 43.5 day periodicity, suggesting that the B-star itself is not the source of the Hα variability; but, the size of the binary system is so large (the M star radius being $R_1 \sim 1000$ solar radii) that the wind crossing time to travel a stellar radius ($t_1 \sim 1$ year) is much greater than the 43.5 day period. This rules out some type of regular structure propagating in the M supergiant wind as a source of the

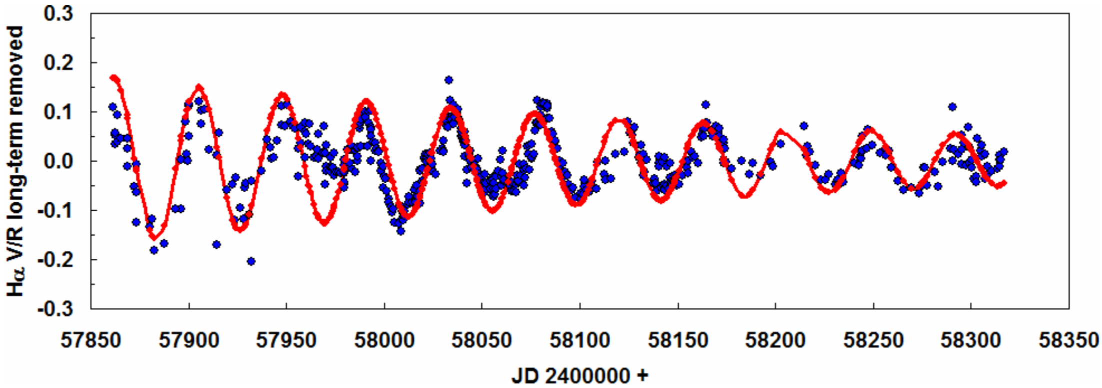

Figure 6. Hα V/R flux residuals (blue dots) after subtraction of the long-term trend in Fig. 5 due to eclipse ingress. An exponentially decaying periodic variation (red dots) has been fit to these residuals with the following function:
Fit to V/R residuals $= Ae^{-\varphi/T}\cos(2\pi\varphi)$; $A = 0.15$; $T = 15.0$; $\varphi = (JD - JD_0)/P$; $P = 43.5$ d; Epoch $\mathrm{JD}_0 = 2457905$.

variability because it would be virtually impossible to retain a coherent variation over the spatial scales required to explain the persistence of the variation through total eclipse. The inevitable conclusion is that the variability must be driven by variable excitation from the hot component, even when that component is totally eclipsed and hidden from our line of sight.

We will leave any further discussion of the nature of this 43.5 day variability to a future paper; in this current work we will merely present the observational material.

3 Summary and Results

The 43.5-day period is seen in both the total Hα EW (Fig. 5) and the blue-to-red flux peak ratio V/R (Fig. 5). The latter variation implies a periodic variation in net radial velocity also. This periodic variability has persisted well into totality through the present time just past mid-eclipse (July 2018). Going into eclipse, the overall Hα emission flux declines in peak intensity and in full width, indicating that the broad-line emission region originates in the immediate vicinity of the hot star, as expected. The decline of the EW into eclipse is much slower than expected for a point source, implying most of the emission comes from a substantially extended region.

The persistence of Hα emission through mid-eclipse implies about 1/3 of the emission comes from a very extended region with an area larger than the projected stellar disc of the M supergiant (with a stellar of radius $R_1 \sim 1000$ solar radii). The V/R flux ratio declined steadily during eclipse ingress, but started increasing at a slow rate well before mid-eclipse. This behaviour of the V/R curve implies the spatial configuration of the extended Hα emission is not symmetric about mid-eclipse. The secondary B star's out-of-eclipse continuum flux does not appear to be variable, and this would seem to eliminate the hot star as the source of the variability. The M supergiant, which dominates the V-band flux and is somewhat variable, has a much longer ∼150 day period (Fig. 7 top) and is not the source of the 43.5-day periodicity. Finally, the M supergiant's wind velocity (∼20 km s^{-1}) is low, implying long wind crossing times (of ∼ 1 year or more) for distances of the size of the Hα emitting region ($\geq R_1$). This wind timescale is too long to explain the 43.5-day variability. We conclude that the source of the excitation must be radiative in nature and originate from the hot component, but probably not from the B-type star itself.

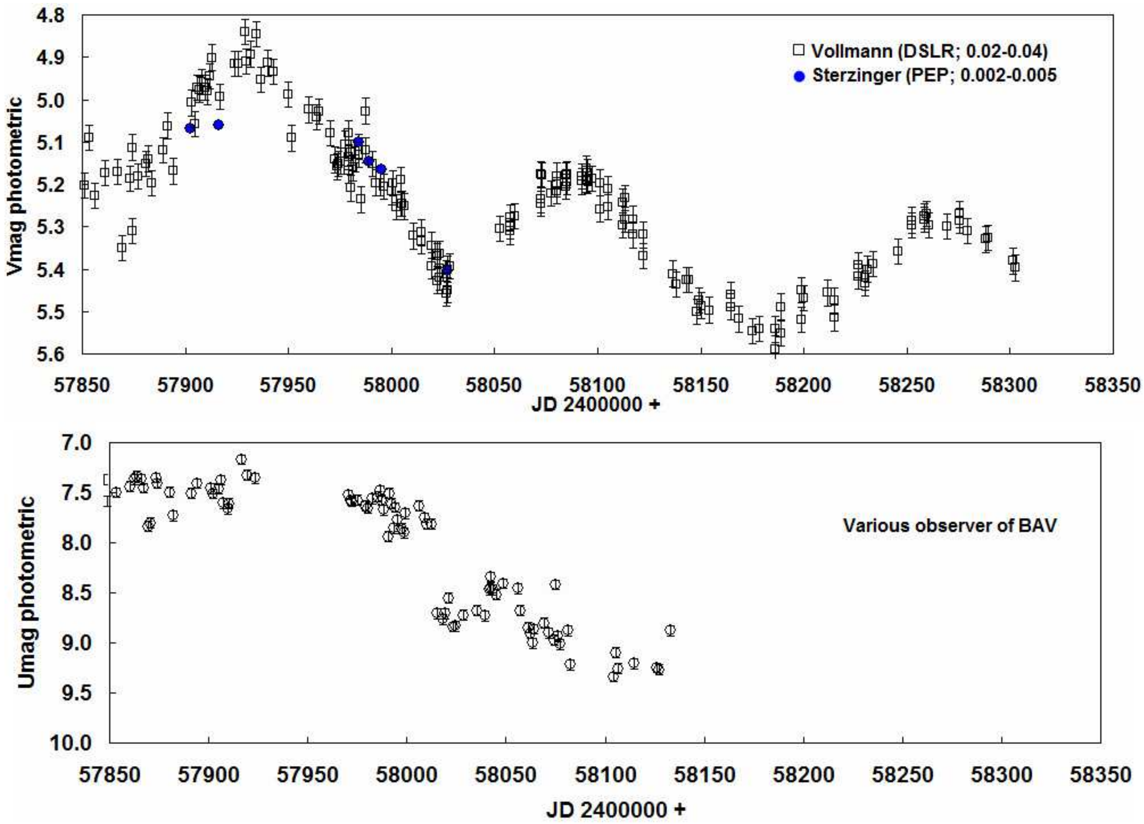

Figure 7. (top): V photometry of VV Cephei obtained over the same time period. There is no evidence of the 43.5-day period in this light curve (dominated by the M supergiant). (bottom): The U-band photometry available during the monitoring period, courtesy of the BAV, shows the onset of the eclipse around JD 2458000. The out-of-eclipse U-band photometry shows no obvious 43.5 day periodicity, although the time sampling is poor.

At present, just past the time of mid-eclipse, it seems prudent to publish the observational material in hand, and wait for the completion of totality and egress from eclipse. It is hoped that having the complete times series of Hα emission flux data over the entire eclipse period will help elucidate the source of this puzzling periodic variation. It would be most useful the amateur community could obtain high-cadence observations of the ultraviolet continuum of the B star, especially once the star emerges from eclipse. For this purpose, Strömgren u photometry would be ideal, although Johnson U photometry would still be useful. We will defer a discussion of the nature of the variability to a future paper that will incorporate a more complete dataset.

Acknowledgements: The results presented here were only possible with the many VV Cep Hα spectra contributed by the ARAS observers. We are grateful for their continuing support. We are also grateful to the various members of the BAV (BAV = Bundesdeutsche Arbeitsgemeinschaft Veränderliche Sterne) for providing the V and U brightnesses.

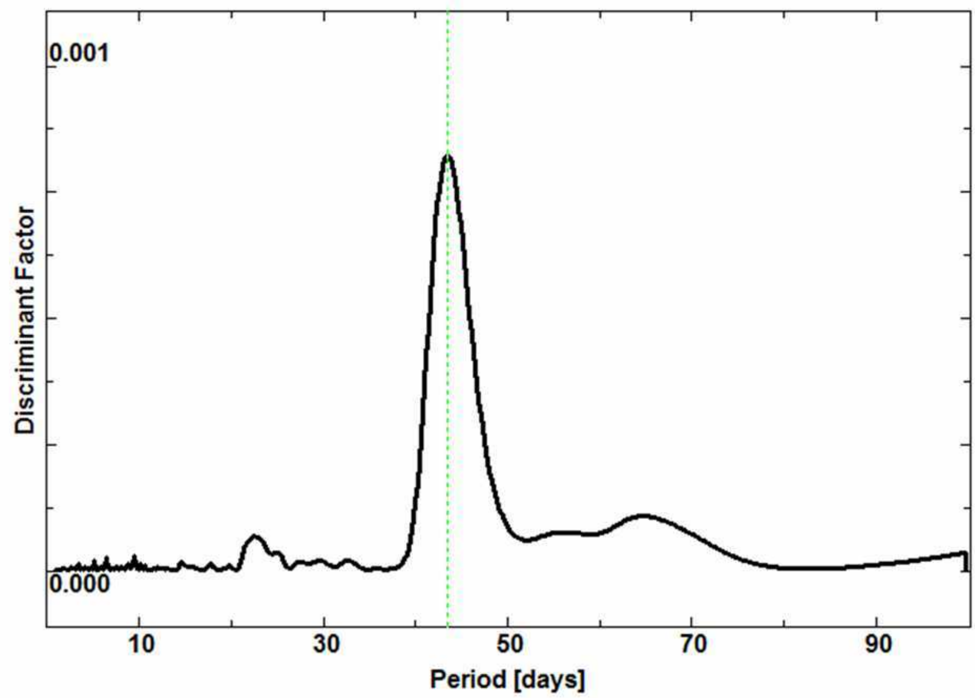

Figure 8. Scargle periodogram of the V/R flux residuals in Fig. 6, produced by the program AVE (Barbera 1998), showing the dominant 43.5 ± 0.12 day period.

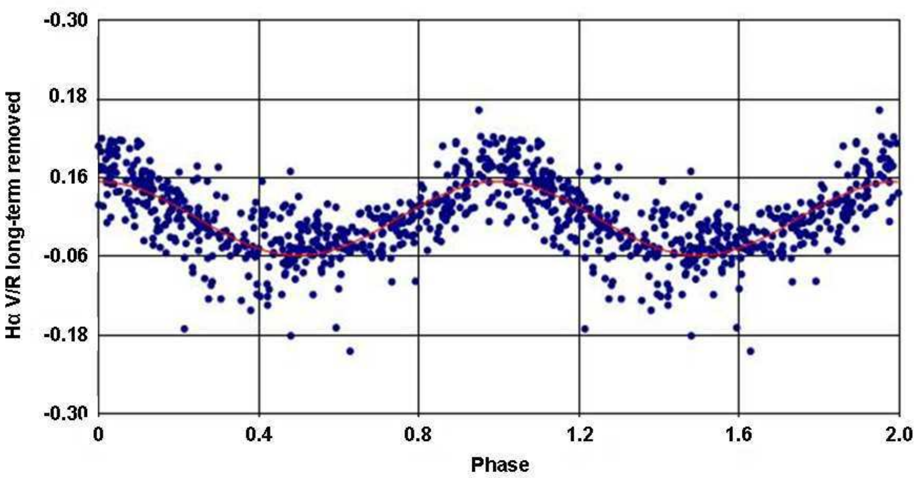

Figure 9. Phase plot of the found period of 43.5 days in Fig. 8; Epoch T_0 = JD 2457905.

Observers of the ARAS Spectroscopy Group
ARAS website - http://www.astrosurf.com/aras/ O. Garde, J. Foster, E. Bertrand, O. Thizy, M. Keiser, J. Guarro, E. Pollmann, C. Sawicki, P. Fosanelli, Dong Li, J. Martin, Ch. Kreider, U. Zurmühl, M. Trypsteen, P. Somogyi, V. Desnoux, J. Broussat, Th. Lemoult, Th. Griga, B. Koch, F. Neußer, K. Pixberg, M. Schwarz, T. Lester, J. Schirmer, E. Bryssinck.

ARAS Forum 28.11.17
http://www.spectro-aras.com/forum/viewtopic.php?f=19&t=1798&p=9863#p9863

References:

Barbera, R. 1999, AVE code, version 2.51, http://astrogea.org/soft/ave/aveint.htm
Bennett, P. D., Hagen-Bauer, W. 2015, "Giants of Eclipse: The zeta Aur Stars and other Binary Systems", Springer DOI
Leedjärv, L., Graczyk, D., Mikolajewsi, M. et al., 1999, *A&A*, **349**, 511
Pollmann, E. 2018, Moderator, VV Cep Campaign, ARAS Spectroscopy Forum, http://www.spectro-aras.com/forum/viewforum.php?f=19
Wright, K.O., 1977, *JRASC*, **71**, 152

COMMISSIONS G1 AND G4 OF THE IAU
INFORMATION BULLETIN ON VARIABLE STARS

Volume 63 Number 6250 DOI: 10.22444/IBVS.6250

Konkoly Observatory
Budapest
12 August 2018

HU ISSN 0374 – 0676

TIMES OF MINIMA OF SOME ECLIPSING BINARY STARS WITH ECCENTRIC MINIMA IN THE KEPLER FIELD II.

BULUT, İ.

Department of Space Sciences and Technologies, Faculty of Arts and Sciences, Çanakkale Onsekiz Mart University, Terzioğlu Kampüsü, TR-17020, Çanakkale, Turkey; e-mail: ibulut@comu.edu.tr

Abstract

We present several CCD minima observations of eclipsing binaries.

Observatory and telescope:

The *Kepler* photometer is a Schmidt telescope design with a 0.95-meter aperture and a 105 square deg (about 12 degree diameter) FOV.

Detector:	The photometer camera contains 42 CCDs with 2200x1024 pixels, where each pixel covers 4 arcsec.

Method of data reduction:

Photometry flux values were taken from the Kepler Eclipsing Binary Database (http://keplerebs.villanova.edu)

Method of minimum determination:

The times of minima and their errors were computed with the Kwee-van Woerden method (Kwee & van Woerden, 1956).

Remarks:

This paper is a continuation of the work published in IBVS 6219 (Bulut, 2017). In this study, we present 1086 minima times of 6 eclipsing binaries with eccentric orbit. The eclipse-timing variation O–C curves of the binary systems are shown in Fig. 1. The light elements for the systems were taken from Kepler Eclipsing Binary Catalog. Kepler light curves of KIC 9119405, KIC 10490960, KIC 12306808, KIC 9119405, KIC 10490960 from the selected systems were analyzed by Kjurkchieva et al. (2016) using the PHOEBE code.

Acknowledgements:

This paper includes data collected by the Kepler mission. Funding for the Kepler mission is provided by the NASA Science Mission directorate.

References:

Bulut, İ., 2017, *IBVS*, **6219** DOI
Kjurkchieva, D., Vasileva, D., Dimitrov, D., 2016, AJ, **152**, 189 DOI
Kwee, K. K., van Woerden, H., 1956, Bull. Astron. Inst. Netherlands **12**, 327

Times of minima:					
Star name	Time of min. HJD 2400000+	Error	Type	Filter	Rem.
KIC 9025914	55742.91570	0.00178	II	*Kepler*	
	55745.90252	0.00049	I	*Kepler*	
	55754.23282	0.00288	II	*Kepler*	
	55757.22378	0.00036	I	*Kepler*	
	55765.55403	0.00203	II	*Kepler*	
	55768.54436	0.0006	I	*Kepler*	
	55776.87526	0.00208	II	*Kepler*	
	55779.86392	0.00031	I	*Kepler*	
	55788.19814	0.00187	II	*Kepler*	
	55791.18441	0.00065	I	*Kepler*	
	55799.51493	0.00132	II	*Kepler*	
	55799.5151	0.001230	I	*Kepler*	
	55810.83542	0.00263	II	*Kepler*	
	55813.82412	0.00059	I	*Kepler*	
	55822.15608	0.00162	II	*Kepler*	
	55825.14500	0.00061	I	*Kepler*	
	55836.46502	0.00043	I	*Kepler*	
	55844.79488	0.00184	II	*Kepler*	
	55847.78486	0.00068	I	*Kepler*	
	55856.11602	0.00262	II	*Kepler*	
	55859.10672	0.00075	I	*Kepler*	
	55867.43542	0.00146	II	*Kepler*	
	55870.42628	0.00032	I	*Kepler*	
	55878.75661	0.00149	II	*Kepler*	
	55881.74679	0.00065	I	*Kepler*	
	55890.07832	0.00143	II	*Kepler*	
	55893.06699	0.00062	I	*Kepler*	
	55901.39876	0.00122	I	*Kepler*	
	55901.39883	0.00115	II	*Kepler*	
	55912.71821	0.00191	II	*Kepler*	
	55915.70667	0.00035	I	*Kepler*	
	55924.03973	0.00177	II	*Kepler*	
	55927.02756	0.00067	I	*Kepler*	
	55935.35856	0.00151	II	*Kepler*	
	55938.34844	0.00051	I	*Kepler*	
	55946.68025	0.00124	II	*Kepler*	
	55958.00112	0.00183	II	*Kepler*	
	55960.98833	0.00039	I	*Kepler*	
	55969.31944	0.00223	II	*Kepler*	
	55972.30882	0.0005	I	*Kepler*	
	55980.64115	0.00287	II	*Kepler*	
	55983.62945	0.00048	I	*Kepler*	
	55991.96039	0.00112	II	*Kepler*	

Times of minima:

Star name	Time of min. HJD 2400000+	Error	Type	Filter	Rem.
	55991.96066	0.00132	I	*Kepler*	
	56003.28155	0.00153	II	*Kepler*	
	56006.26906	0.00034	I	*Kepler*	
	56014.59762	0.00226	II	*Kepler*	
	56017.58991	0.00025	I	*Kepler*	
	56025.91845	0.00259	II	*Kepler*	
	56028.91063	0.00072	I	*Kepler*	
	56037.24605	0.00338	II	*Kepler*	
	56040.23074	0.00118	I	*Kepler*	
	56051.55020	0.00025	I	*Kepler*	
	56059.88035	0.00381	II	*Kepler*	
	56062.87113	0.00071	I	*Kepler*	
	56071.20326	0.00244	II	*Kepler*	
	56074.19134	0.00031	I	*Kepler*	
	56082.52190	0.00207	II	*Kepler*	
	56085.51096	0.00035	I	*Kepler*	
	56093.84382	0.00341	II	*Kepler*	
	56096.83145	0.00073	I	*Kepler*	
	56105.16127	0.00169	II	*Kepler*	
	56108.15242	0.00028	I	*Kepler*	
	56116.48259	0.00154	II	*Kepler*	
	56119.47190	0.00023	I	*Kepler*	
	56130.79247	0.00035	I	*Kepler*	
	56142.11328	0.00065	I	*Kepler*	
	56150.44433	0.00107	II	*Kepler*	
	56153.43332	0.00071	I	*Kepler*	
	56161.76605	0.00154	II	*Kepler*	
	56164.75375	0.00027	I	*Kepler*	
	56173.08397	0.00187	II	*Kepler*	
	56176.07346	0.00050	I	*Kepler*	
	56184.40438	0.00248	II	*Kepler*	
	56187.39409	0.00022	I	*Kepler*	
	56195.72497	0.00140	II	*Kepler*	
	56198.71356	0.00087	I	*Kepler*	
	56207.04527	0.00297	II	*Kepler*	
	56210.03533	0.00063	I	*Kepler*	
	56218.36557	0.00256	II	*Kepler*	
	56221.35500	0.00031	I	*Kepler*	
	56229.68498	0.00158	II	*Kepler*	
	56232.67477	0.00033	I	*Kepler*	
	56241.00644	0.00138	II	*Kepler*	
	56243.99563	0.00017	I	*Kepler*	
	56252.32937	0.00148	II	*Kepler*	

Times of minima:					
Star name	Time of min. HJD 2400000+	Error	Type	Filter	Rem.
	56255.31564	0.00038	I	*Kepler*	
	56263.64720	0.00137	II	*Kepler*	
	56266.63589	0.00041	I	*Kepler*	
	56274.96372	0.00341	II	*Kepler*	
	56277.95638	0.00046	I	*Kepler*	
	56286.28720	0.00371	II	*Kepler*	
	56289.27712	0.00076	I	*Kepler*	
	56297.60851	0.00454	II	*Kepler*	
	56300.59703	0.00057	I	*Kepler*	
	56308.92883	0.00090	II	*Kepler*	
	56308.92912	0.00096	I	*Kepler*	
	56323.23725	0.00021	I	*Kepler*	
	56331.57349	0.00224	II	*Kepler*	
	56334.55751	0.00052	I	*Kepler*	
	56342.88895	0.00195	II	*Kepler*	
	56345.87824	0.00062	I	*Kepler*	
	56354.21070	0.00242	II	*Kepler*	
	56357.19917	0.00054	I	*Kepler*	
	56365.52862	0.00330	II	*Kepler*	
	56368.51810	0.00077	I	*Kepler*	
	56376.84843	0.00189	II	*Kepler*	
	56379.83864	0.00049	I	*Kepler*	
	56388.16998	0.00209	II	*Kepler*	
	56399.49078	0.00124	II	*Kepler*	
	56402.48005	0.00034	I	*Kepler*	
	56410.80889	0.00132	II	*Kepler*	
	56413.80014	0.00018	I	*Kepler*	
	56422.13172	0.00153	II	*Kepler*	
KIC 9344623	54972.78272	0.00015	I	*Kepler*	
	54978.78395	0.00032	II	*Kepler*	
	54987.54228	0.00028	I	*Kepler*	
	54993.54376	0.00024	II	*Kepler*	
	55008.30305	0.00035	II	*Kepler*	
	55017.06133	0.00053	I	*Kepler*	
	55023.06270	0.00023	II	*Kepler*	
	55031.82054	0.00027	I	*Kepler*	
	55037.82191	0.00009	II	*Kepler*	
	55046.58028	0.00018	I	*Kepler*	
	55052.58156	0.00007	II	*Kepler*	
	55061.33982	0.00036	I	*Kepler*	
	55067.34077	0.00029	II	*Kepler*	
	55076.09920	0.00010	I	*Kepler*	
	55082.10038	0.00008	II	*Kepler*	

Times of minima:					
Star name	Time of min. HJD 2400000+	Error	Type	Filter	Rem.
	55090.85838	0.00022	I	*Kepler*	
	55096.85975	0.00029	II	*Kepler*	
	55105.61810	0.00028	I	*Kepler*	
	55111.61975	0.00036	II	*Kepler*	
	55120.37774	0.00023	I	*Kepler*	
	55126.37914	0.00038	II	*Kepler*	
	55135.13688	0.00014	I	*Kepler*	
	55141.13828	0.00034	II	*Kepler*	
	55149.89648	0.00012	I	*Kepler*	
	55164.65592	0.00024	I	*Kepler*	
	55170.65725	0.00012	II	*Kepler*	
	55179.41539	0.00031	I	*Kepler*	
	55282.73182	0.00007	I	*Kepler*	
	55288.73306	0.00012	II	*Kepler*	
	55297.49146	0.00017	I	*Kepler*	
	55303.49257	0.00032	II	*Kepler*	
	55312.25094	0.00023	I	*Kepler*	
	55318.25205	0.00018	II	*Kepler*	
	55327.01036	0.00014	I	*Kepler*	
	55333.01167	0.00013	II	*Kepler*	
	55341.76984	0.00024	I	*Kepler*	
	55347.77100	0.00023	II	*Kepler*	
	55356.52929	0.00009	I	*Kepler*	
	55362.53075	0.00031	II	*Kepler*	
	55377.29020	0.00011	II	*Kepler*	
	55386.04825	0.00007	I	*Kepler*	
	55392.04998	0.00025	II	*Kepler*	
	55400.80739	0.00024	I	*Kepler*	
	55406.80903	0.00034	II	*Kepler*	
	55415.56705	0.00006	I	*Kepler*	
	55421.56771	0.00029	II	*Kepler*	
	55430.32639	0.00030	I	*Kepler*	
	55436.32789	0.00009	II	*Kepler*	
	55445.08590	0.00014	I	*Kepler*	
	55451.08737	0.00031	II	*Kepler*	
	55459.84553	0.00039	I	*Kepler*	
	55465.84682	0.00026	II	*Kepler*	
	55474.60505	0.00011	I	*Kepler*	
	55480.60663	0.00031	II	*Kepler*	
	55489.36459	0.00018	I	*Kepler*	
	55495.36621	0.00018	II	*Kepler*	
	55504.12404	0.00027	I	*Kepler*	
	55510.12559	0.00019	II	*Kepler*	

Times of minima:					
Star name	Time of min. HJD 2400000+	Error	Type	Filter	Rem.
	55518.88353	0.00014	I	*Kepler*	
	55524.88521	0.00047	II	*Kepler*	
	55533.64308	0.00016	I	*Kepler*	
	55539.64428	0.00034	II	*Kepler*	
	55548.40237	0.00006	I	*Kepler*	
	55569.16349	0.00014	II	*Kepler*	
	55577.92150	0.00017	I	*Kepler*	
	55583.92278	0.00034	II	*Kepler*	
	55592.68100	0.00028	I	*Kepler*	
	55598.68212	0.00029	II	*Kepler*	
	55607.44021	0.00025	I	*Kepler*	
	55613.44191	0.00031	II	*Kepler*	
	55622.19986	0.0002	I	*Kepler*	
	55628.20133	0.00012	II	*Kepler*	
	55642.96075	0.00016	II	*Kepler*	
	55651.71863	0.00020	I	*Kepler*	
	55657.72017	0.00035	II	*Kepler*	
	55666.47816	0.0001	I	*Kepler*	
	55672.47951	0.00024	II	*Kepler*	
	55681.23760	0.00032	I	*Kepler*	
	55687.23906	0.00007	II	*Kepler*	
	55695.99719	0.00022	I	*Kepler*	
	55701.99853	0.00029	II	*Kepler*	
	55710.75652	0.00039	I	*Kepler*	
	55716.75831	0.00033	II	*Kepler*	
	55725.51606	0.00017	I	*Kepler*	
	55731.51756	0.00033	II	*Kepler*	
	55740.27565	0.00041	I	*Kepler*	
	55746.27729	0.00022	II	*Kepler*	
	55755.03517	0.00012	I	*Kepler*	
	55761.03666	0.00035	II	*Kepler*	
	55775.79607	0.00026	II	*Kepler*	
	55784.55397	0.00026	I	*Kepler*	
	55790.55573	0.00027	II	*Kepler*	
	55799.31356	0.00006	I	*Kepler*	
	55805.31510	0.00007	II	*Kepler*	
	55814.07303	0.00026	I	*Kepler*	
	55820.07462	0.00018	II	*Kepler*	
	55828.83200	0.00022	I	*Kepler*	
	55834.83436	0.00036	II	*Kepler*	
	55843.59189	0.00016	I	*Kepler*	
	55849.59351	0.00006	II	*Kepler*	
	55858.35156	0.00026	I	*Kepler*	

Times of minima:					
Star name	Time of min. HJD 2400000+	Error	Type	Filter	Rem.
	55864.35332	0.00033	II	*Kepler*	
	55873.11104	0.00008	I	*Kepler*	
	55879.11259	0.00028	II	*Kepler*	
	55887.87053	0.00016	I	*Kepler*	
	55893.87196	0.00009	II	*Kepler*	
	55902.63020	0.00052	I	*Kepler*	
	55908.63146	0.00006	II	*Kepler*	
	55917.38939	0.00006	I	*Kepler*	
	55923.39109	0.00026	II	*Kepler*	
	55938.15042	0.00004	II	*Kepler*	
	55946.90826	0.00013	I	*Kepler*	
	55952.90969	0.00014	II	*Kepler*	
	55961.66781	0.00019	I	*Kepler*	
	55967.66923	0.00013	II	*Kepler*	
	55976.42741	0.00017	I	*Kepler*	
	55982.42874	0.00033	II	*Kepler*	
	55991.18675	0.00028	I	*Kepler*	
	56005.94618	0.00023	I	*Kepler*	
	56011.94748	0.00031	II	*Kepler*	
	56020.70581	0.00022	I	*Kepler*	
	56026.70707	0.00028	II	*Kepler*	
	56035.46514	0.00007	I	*Kepler*	
	56041.46694	0.00028	II	*Kepler*	
	56050.22453	0.00025	I	*Kepler*	
	56056.22610	0.00033	II	*Kepler*	
	56064.98414	0.00007	I	*Kepler*	
	56070.98586	0.00023	II	*Kepler*	
	56079.74382	0.00029	I	*Kepler*	
	56085.74521	0.00035	II	*Kepler*	
	56094.50304	0.00010	I	*Kepler*	
	56100.50442	0.00027	II	*Kepler*	
	56109.26255	0.00011	I	*Kepler*	
	56115.26443	0.00031	II	*Kepler*	
	56130.02383	0.00025	II	*Kepler*	
	56144.78298	0.00016	II	*Kepler*	
	56153.54092	0.00019	I	*Kepler*	
	56159.54260	0.00002	II	*Kepler*	
	56168.30042	0.00017	I	*Kepler*	
	56174.30185	0.00024	II	*Kepler*	
	56183.05988	0.00025	I	*Kepler*	
	56189.06138	0.00011	II	*Kepler*	
	56197.81958	0.00017	I	*Kepler*	
	56203.82151	0.00062	II	*Kepler*	

Times of minima:					
Star name	Time of min. HJD 2400000+	Error	Type	Filter	Rem.
	56212.57889	0.00006	I	*Kepler*	
	56218.58036	0.00023	II	*Kepler*	
	56227.33844	0.00007	I	*Kepler*	
	56233.34013	0.00027	II	*Kepler*	
	56242.09784	0.00017	I	*Kepler*	
	56256.85730	0.00014	I	*Kepler*	
	56262.85913	0.00014	II	*Kepler*	
	56271.61671	0.00035	I	*Kepler*	
	56277.61829	0.00014	II	*Kepler*	
	56286.37643	0.00014	I	*Kepler*	
	56292.37793	0.00004	II	*Kepler*	
	56301.13570	0.00029	I	*Kepler*	
	56307.13720	0.00051	II	*Kepler*	
	56321.89695	0.00015	II	*Kepler*	
	56330.65489	0.00019	I	*Kepler*	
	56336.65634	0.00036	II	*Kepler*	
	56345.41418	0.00008	I	*Kepler*	
	56351.41597	0.00016	II	*Kepler*	
	56360.17366	0.00061	I	*Kepler*	
	56366.17545	0.00028	II	*Kepler*	
	56374.93320	0.00017	I	*Kepler*	
	56380.93459	0.00032	II	*Kepler*	
	56389.69265	0.00042	I	*Kepler*	
	56395.69421	0.00028	II	*Kepler*	
	56404.45205	0.00021	I	*Kepler*	
	56410.45378	0.00008	II	*Kepler*	
KIC 10296163	54959.38755	0.00035	I	*Kepler*	
	54962.54225	0.00194	II	*Kepler*	
	54968.68424	0.00027	I	*Kepler*	
	54971.83881	0.00144	II	*Kepler*	
	54977.98105	0.00022	I	*Kepler*	
	54981.13541	0.00102	II	*Kepler*	
	54987.27792	0.00017	I	*Kepler*	
	54990.43205	0.00104	II	*Kepler*	
	54996.57468	0.00051	I	*Kepler*	
	55005.87165	0.00008	I	*Kepler*	
	55009.02474	0.00087	II	*Kepler*	
	55018.32294	0.00058	II	*Kepler*	
	55024.46526	0.00007	I	*Kepler*	
	55027.61957	0.00064	II	*Kepler*	
	55033.76213	0.00015	I	*Kepler*	
	55036.91536	0.00100	II	*Kepler*	
	55043.05893	0.00014	I	*Kepler*	

Times of minima:					
Star name	Time of min. HJD 2400000+	Error	Type	Filter	Rem.
	55046.21225	0.00117	II	*Kepler*	
	55052.35577	0.00019	I	*Kepler*	
	55055.50892	0.00133	II	*Kepler*	
	55061.65221	0.00013	I	*Kepler*	
	55064.80791	0.00156	II	*Kepler*	
	55070.94941	0.00020	I	*Kepler*	
	55074.10422	0.00077	II	*Kepler*	
	55080.24623	0.00024	I	*Kepler*	
	55083.39923	0.00056	II	*Kepler*	
	55089.54318	0.00099	I	*Kepler*	
	55098.83939	0.00034	I	*Kepler*	
	55101.99324	0.00066	II	*Kepler*	
	55108.13618	0.00029	I	*Kepler*	
	55111.29042	0.00053	II	*Kepler*	
	55117.43328	0.00029	I	*Kepler*	
	55120.58713	0.00039	II	*Kepler*	
	55126.72975	0.00030	I	*Kepler*	
	55129.88365	0.00091	II	*Kepler*	
	55136.02654	0.00027	I	*Kepler*	
	55139.18061	0.00108	II	*Kepler*	
	55145.32359	0.00032	I	*Kepler*	
	55148.47739	0.00080	II	*Kepler*	
	55157.77412	0.00105	II	*Kepler*	
	55163.91730	0.00033	I	*Kepler*	
	55167.07187	0.00132	II	*Kepler*	
	55173.21412	0.00032	I	*Kepler*	
	55176.36931	0.00118	II	*Kepler*	
	55185.66613	0.00106	II	*Kepler*	
	55191.80769	0.00038	I	*Kepler*	
	55194.96164	0.00122	II	*Kepler*	
	55201.10403	0.00025	I	*Kepler*	
	55204.25799	0.00101	II	*Kepler*	
	55210.40121	0.00042	I	*Kepler*	
	55213.55551	0.00155	II	*Kepler*	
	55219.69772	0.00022	I	*Kepler*	
	55222.85222	0.00044	II	*Kepler*	
	55228.99462	0.00014	I	*Kepler*	
	55238.29125	0.00045	I	*Kepler*	
	55241.44582	0.00132	II	*Kepler*	
	55247.58833	0.00045	I	*Kepler*	
	55250.74255	0.00132	II	*Kepler*	
	55256.88479	0.00012	I	*Kepler*	
	55260.03849	0.00144	II	*Kepler*	

Times of minima:					
Star name	Time of min. HJD 2400000+	Error	Type	Filter	Rem.
	55266.18153	0.00015	I	*Kepler*	
	55269.33783	0.00095	II	*Kepler*	
	55278.63270	0.00104	II	*Kepler*	
	55284.77523	0.00013	I	*Kepler*	
	55287.93034	0.00096	II	*Kepler*	
	55294.07174	0.00048	I	*Kepler*	
	55297.22580	0.00110	II	*Kepler*	
	55303.36885	0.00018	I	*Kepler*	
	55306.52356	0.00103	II	*Kepler*	
	55312.66564	0.00026	I	*Kepler*	
	55315.82098	0.00120	II	*Kepler*	
	55321.96230	0.00036	I	*Kepler*	
	55325.11782	0.00105	II	*Kepler*	
	55331.25921	0.00029	I	*Kepler*	
	55334.41335	0.00069	II	*Kepler*	
	55340.55558	0.00028	I	*Kepler*	
	55343.71095	0.00125	II	*Kepler*	
	55349.85279	0.00038	I	*Kepler*	
	55353.00754	0.00139	II	*Kepler*	
	55359.14915	0.00018	I	*Kepler*	
	55362.30416	0.00143	II	*Kepler*	
	55368.44594	0.00010	I	*Kepler*	
	55377.74288	0.00048	I	*Kepler*	
	55380.89804	0.00095	II	*Kepler*	
	55387.03948	0.00010	I	*Kepler*	
	55390.19360	0.00115	II	*Kepler*	
	55396.33634	0.00005	I	*Kepler*	
	55405.63290	0.00046	I	*Kepler*	
	55408.78831	0.00116	II	*Kepler*	
	55414.92959	0.00043	I	*Kepler*	
	55418.08389	0.00122	II	*Kepler*	
	55424.22635	0.00041	I	*Kepler*	
	55427.38085	0.00093	II	*Kepler*	
	55433.52279	0.00054	I	*Kepler*	
	55436.67913	0.00096	II	*Kepler*	
	55442.82021	0.00024	I	*Kepler*	
	55445.97581	0.00116	II	*Kepler*	
	55452.11658	0.00034	I	*Kepler*	
	55455.27236	0.00119	II	*Kepler*	
	55461.41338	0.00043	I	*Kepler*	
	55572.97471	0.00041	I	*Kepler*	
	55576.12947	0.00134	II	*Kepler*	
	55582.27174	0.00042	I	*Kepler*	

Times of minima:					
Star name	Time of min. HJD 2400000+	Error	Type	Filter	Rem.
	55585.42668	0.00132	II	*Kepler*	
	55591.56825	0.00040	I	*Kepler*	
	55600.86469	0.00016	I	*Kepler*	
	55604.01964	0.00065	II	*Kepler*	
	55610.16162	0.00045	I	*Kepler*	
	55613.31622	0.00142	II	*Kepler*	
	55619.45855	0.00019	I	*Kepler*	
	55622.61325	0.00113	II	*Kepler*	
	55628.75518	0.00052	I	*Kepler*	
	55631.90990	0.00065	II	*Kepler*	
	55647.34864	0.00014	I	*Kepler*	
	55650.50252	0.00116	II	*Kepler*	
	55656.64543	0.00015	I	*Kepler*	
	55659.80051	0.00106	II	*Kepler*	
	55665.94221	0.00019	I	*Kepler*	
	55669.09723	0.00102	II	*Kepler*	
	55675.23862	0.00037	I	*Kepler*	
	55684.53538	0.00035	I	*Kepler*	
	55687.69066	0.00117	II	*Kepler*	
	55693.83217	0.00030	I	*Kepler*	
	55696.98723	0.00115	II	*Kepler*	
	55703.12894	0.00025	I	*Kepler*	
	55706.28441	0.00128	II	*Kepler*	
	55712.42607	0.00039	I	*Kepler*	
	55715.58012	0.00148	II	*Kepler*	
	55721.72256	0.00019	I	*Kepler*	
	55724.87537	0.00114	II	*Kepler*	
	55731.01938	0.00044	I	*Kepler*	
	55734.17287	0.00120	II	*Kepler*	
	55740.31593	0.00081	I	*Kepler*	
	55743.46941	0.00122	II	*Kepler*	
	55749.61301	0.00009	I	*Kepler*	
	55752.76711	0.00106	II	*Kepler*	
	55758.90963	0.00049	I	*Kepler*	
	55762.06403	0.00120	II	*Kepler*	
	55768.20636	0.00040	I	*Kepler*	
	55771.36016	0.00175	II	*Kepler*	
	55777.50313	0.00043	I	*Kepler*	
	55780.65599	0.00109	II	*Kepler*	
	55786.80027	0.00020	I	*Kepler*	
	55789.95265	0.00109	II	*Kepler*	
	55796.09709	0.00023	I	*Kepler*	
	55799.25005	0.00113	II	*Kepler*	

Times of minima:					
Star name	Time of min. HJD 2400000+	Error	Type	Filter	Rem.
	55805.39384	0.00025	I	*Kepler*	
	55808.54708	0.00123	II	*Kepler*	
	55814.69020	0.00032	I	*Kepler*	
	55817.84383	0.00127	II	*Kepler*	
	55823.98743	0.00029	I	*Kepler*	
	55827.13973	0.00135	II	*Kepler*	
	55935.54860	0.00040	I	*Kepler*	
	55938.69866	0.00078	II	*Kepler*	
	55944.84504	0.00019	I	*Kepler*	
	55947.99543	0.00057	II	*Kepler*	
	55954.14255	0.00109	I	*Kepler*	
	55957.29318	0.00089	II	*Kepler*	
	55963.43848	0.00013	I	*Kepler*	
	55966.58997	0.00077	II	*Kepler*	
	55972.73542	0.00047	I	*Kepler*	
	55975.88670	0.00090	II	*Kepler*	
	55982.03215	0.00047	I	*Kepler*	
	55985.18197	0.00075	II	*Kepler*	
	55991.32876	0.00051	I	*Kepler*	
	56000.62538	0.00051	I	*Kepler*	
	56003.77545	0.00058	II	*Kepler*	
	56009.92207	0.00049	I	*Kepler*	
	56013.07253	0.00063	II	*Kepler*	
	56019.21867	0.00047	I	*Kepler*	
	56022.36958	0.00128	II	*Kepler*	
	56028.51532	0.00043	I	*Kepler*	
	56031.66569	0.00099	II	*Kepler*	
	56037.81237	0.00022	I	*Kepler*	
	56040.96301	0.00138	II	*Kepler*	
	56047.10933	0.00055	I	*Kepler*	
	56050.26090	0.00068	II	*Kepler*	
	56056.40576	0.00031	I	*Kepler*	
	56059.55719	0.00134	II	*Kepler*	
	56065.70187	0.00031	I	*Kepler*	
	56068.85291	0.00093	II	*Kepler*	
	56074.99917	0.00039	I	*Kepler*	
	56077.99527	0.01242	II	*Kepler*	
	56084.29546	0.00017	I	*Kepler*	
	56087.44617	0.00094	II	*Kepler*	
	56093.59216	0.00011	I	*Kepler*	
	56096.74163	0.00085	II	*Kepler*	
	56102.88890	0.00003	I	*Kepler*	
	56112.18562	0.00019	I	*Kepler*	

Times of minima:					
Star name	Time of min. HJD 2400000+	Error	Type	Filter	Rem.
	56115.33399	0.00065	II	*Kepler*	
	56121.48197	0.00029	I	*Kepler*	
	56130.77886	0.00055	I	*Kepler*	
	56133.92924	0.0009	II	*Kepler*	
	56140.07582	0.00037	I	*Kepler*	
	56143.22610	0.00075	II	*Kepler*	
	56149.37194	0.00032	I	*Kepler*	
	56152.52259	0.00134	II	*Kepler*	
	56158.66859	0.00029	I	*Kepler*	
	56161.82011	0.00133	II	*Kepler*	
	56167.96560	0.00046	I	*Kepler*	
	56171.11621	0.00088	II	*Kepler*	
	56177.26231	0.00036	I	*Kepler*	
	56180.41178	0.00121	II	*Kepler*	
	56186.55897	0.00040	I	*Kepler*	
	56189.70993	0.00112	II	*Kepler*	
	56195.85529	0.00018	I	*Kepler*	
	56199.00521	0.00109	II	*Kepler*	
	56307.41555	0.00011	I	*Kepler*	
	56309.60183	0.00313	II	*Kepler*	
	56326.00903	0.00013	I	*Kepler*	
	56329.15975	0.00071	II	*Kepler*	
	56335.30538	0.00045	I	*Kepler*	
	56338.45775	0.00129	II	*Kepler*	
	56344.60247	0.00022	I	*Kepler*	
	56347.75343	0.00127	II	*Kepler*	
	56353.89878	0.0004	I	*Kepler*	
	56357.04923	0.00163	II	*Kepler*	
	56363.19551	0.00036	I	*Kepler*	
	56366.34755	0.00132	II	*Kepler*	
	56372.49265	0.00025	I	*Kepler*	
	56375.64369	0.00145	II	*Kepler*	
	56381.78907	0.00033	I	*Kepler*	
	56384.94040	0.00175	II	*Kepler*	
	56391.36153	0.03051	I	*Kepler*	
	56394.23762	0.00113	II	*Kepler*	
	56400.38238	0.00024	I	*Kepler*	
	56403.53351	0.00112	II	*Kepler*	
	56409.67918	0.00018	I	*Kepler*	
	56412.83101	0.00074	II	*Kepler*	
	56422.12689	0.00055	II	*Kepler*	

Times of minima:					
Star name	Time of min. HJD 2400000+	Error	Type	Filter	Rem.
KIC 9119405	54990.73824	0.00035	I	*Kepler*	
	54995.07313	0.00070	II	*Kepler*	
	55009.38458	0.00031	I	*Kepler*	
	55013.71958	0.00070	II	*Kepler*	
	55028.03089	0.00032	I	*Kepler*	
	55032.36581	0.00050	II	*Kepler*	
	55046.67722	0.00032	I	*Kepler*	
	55051.01209	0.00060	II	*Kepler*	
	55065.32354	0.00031	I	*Kepler*	
	55069.65851	0.00050	II	*Kepler*	
	55083.96994	0.00032	I	*Kepler*	
	55088.30476	0.00050	II	*Kepler*	
	55102.61621	0.00032	I	*Kepler*	
	55106.95111	0.00020	II	*Kepler*	
	55121.26244	0.00032	I	*Kepler*	
	55125.59740	0.00010	II	*Kepler*	
	55139.90884	0.00032	I	*Kepler*	
	55144.24373	0.00040	II	*Kepler*	
	55158.55514	0.00036	I	*Kepler*	
	55162.89010	0.00040	II	*Kepler*	
	55177.20142	0.00042	I	*Kepler*	
	55181.53633	0.00050	II	*Kepler*	
	55289.07932	0.00041	I	*Kepler*	
	55307.72577	0.00036	I	*Kepler*	
	55312.06051	0.00020	II	*Kepler*	
	55326.37204	0.00032	I	*Kepler*	
	55330.70690	0.00020	II	*Kepler*	
	55345.01834	0.00032	I	*Kepler*	
	55349.35322	0.00020	II	*Kepler*	
	55363.66470	0.00031	I	*Kepler*	
	55367.99954	0.00020	II	*Kepler*	
	55382.31106	0.00031	I	*Kepler*	
	55386.64585	0.00020	II	*Kepler*	
	55400.95733	0.00031	I	*Kepler*	
	55405.29221	0.00020	II	*Kepler*	
	55419.60369	0.00031	I	*Kepler*	
	55423.93842	0.00030	II	*Kepler*	
	55438.25006	0.00031	I	*Kepler*	
	55442.58475	0.00050	II	*Kepler*	
	55456.89634	0.00031	I	*Kepler*	
	55461.23118	0.00030	II	*Kepler*	
	55475.54269	0.00032	I	*Kepler*	
	55479.87750	0.00030	II	*Kepler*	

Times of minima:					
Star name	Time of min. HJD 2400000+	Error	Type	Filter	Rem.
	55494.18902	0.00031	I	*Kepler*	
	55498.52381	0.00030	II	*Kepler*	
	55512.83525	0.00033	I	*Kepler*	
	55517.17015	0.00010	II	*Kepler*	
	55531.48166	0.00034	I	*Kepler*	
	55535.81645	0.00030	II	*Kepler*	
	55550.12799	0.00034	I	*Kepler*	
	55568.77429	0.00034	I	*Kepler*	
	55573.10925	0.00020	II	*Kepler*	
	55587.42064	0.00034	I	*Kepler*	
	55606.06698	0.00034	I	*Kepler*	
	55624.71322	0.00032	I	*Kepler*	
	55643.35959	0.00032	I	*Kepler*	
	55662.00594	0.00032	I	*Kepler*	
	55680.65227	0.00033	I	*Kepler*	
	55684.98698	0.00050	II	*Kepler*	
	55699.29858	0.00032	I	*Kepler*	
	55703.63331	0.00050	II	*Kepler*	
	55717.94487	0.00032	I	*Kepler*	
	55722.27962	0.00050	II	*Kepler*	
	55736.59118	0.00032	I	*Kepler*	
	55740.92596	0.00050	II	*Kepler*	
	55755.23749	0.00032	I	*Kepler*	
	55759.57226	0.00050	II	*Kepler*	
	55773.88385	0.00032	I	*Kepler*	
	55778.21856	0.00020	II	*Kepler*	
	55792.53016	0.00032	I	*Kepler*	
	55796.86489	0.00020	II	*Kepler*	
	55811.17651	0.00032	I	*Kepler*	
	55815.51112	0.00040	II	*Kepler*	
	55829.82285	0.00032	I	*Kepler*	
	55834.15745	0.00040	II	*Kepler*	
	55848.46915	0.00032	I	*Kepler*	
	55852.80377	0.00050	II	*Kepler*	
	55867.11548	0.00032	I	*Kepler*	
	55871.45014	0.00050	II	*Kepler*	
	55885.76182	0.00032	I	*Kepler*	
	55890.09648	0.00040	II	*Kepler*	
	55904.40812	0.00032	I	*Kepler*	
	55908.74280	0.00030	II	*Kepler*	
	55923.05432	0.00032	I	*Kepler*	
	55927.38913	0.00030	II	*Kepler*	
	55941.70069	0.00032	I	*Kepler*	

Times of minima:					
Star name	Time of min. HJD 2400000+	Error	Type	Filter	Rem.
	55946.03542	0.00020	II	*Kepler*	
	55960.34703	0.00032	I	*Kepler*	
	55964.68176	0.00021	II	*Kepler*	
	55978.99326	0.00032	I	*Kepler*	
	55983.32806	0.00022	II	*Kepler*	
	55997.63955	0.00032	I	*Kepler*	
	56001.97438	0.00020	II	*Kepler*	
	56016.28606	0.00032	I	*Kepler*	
	56020.62071	0.00020	II	*Kepler*	
	56034.93235	0.00032	I	*Kepler*	
	56039.26717	0.00020	II	*Kepler*	
	56053.57861	0.00030	I	*Kepler*	
	56072.22499	0.00032	I	*Kepler*	
	56076.55971	0.00023	II	*Kepler*	
	56090.87135	0.00032	I	*Kepler*	
	56095.20605	0.00021	II	*Kepler*	
	56109.51764	0.00032	I	*Kepler*	
	56113.85237	0.00020	II	*Kepler*	
	56128.16403	0.00032	I	*Kepler*	
	56132.49869	0.00021	II	*Kepler*	
	56146.81034	0.00032	I	*Kepler*	
	56151.14501	0.00021	II	*Kepler*	
	56165.45679	0.00033	I	*Kepler*	
	56169.79142	0.00040	II	*Kepler*	
	56184.10305	0.000320	I	*Kepler*	
	56188.43770	0.00030	II	*Kepler*	
	56202.74916	0.00033	I	*Kepler*	
	56221.39550	0.00032	I	*Kepler*	
	56225.73032	0.00081	II	*Kepler*	
	56240.04184	0.00033	I	*Kepler*	
	56244.37655	0.00050	II	*Kepler*	
	56258.68816	0.00031	I	*Kepler*	
	56263.02291	0.00070	II	*Kepler*	
	56277.33446	0.00033	I	*Kepler*	
	56281.66918	0.00071	II	*Kepler*	
	56295.98095	0.00033	I	*Kepler*	
	56300.31547	0.00010	II	*Kepler*	
	56314.62719	0.00033	I	*Kepler*	
	56318.96179	0.00021	II	*Kepler*	
	56333.27345	0.00033	I	*Kepler*	
	56337.60810	0.00031	II	*Kepler*	
	56351.91981	0.00034	I	*Kepler*	
	56356.25447	0.00050	II	*Kepler*	
	56370.56620	0.00032	I	*Kepler*	
	56374.90079	0.00050	II	*Kepler*	

Times of minima:					
Star name	Time of min. HJD 2400000+	Error	Type	Filter	Rem.
KIC 10490960	54966.63793	0.00108	I	*Kepler*	
	54969.75971	0.00069	II	*Kepler*	
	54972.32046	0.00075	I	*Kepler*	
	54975.44229	0.00066	II	*Kepler*	
	54978.00294	0.00057	I	*Kepler*	
	54981.12505	0.00006	II	*Kepler*	
	54983.68444	0.00052	I	*Kepler*	
	54986.80770	0.00069	II	*Kepler*	
	54989.36661	0.00071	I	*Kepler*	
	54992.49036	0.00081	II	*Kepler*	
	54995.04957	0.00040	I	*Kepler*	
	55003.85511	0.00069	II	*Kepler*	
	55006.41445	0.00042	I	*Kepler*	
	55009.53736	0.00085	II	*Kepler*	
	55012.09732	0.00063	I	*Kepler*	
	55017.77917	0.00095	I	*Kepler*	
	55020.90199	0.00076	II	*Kepler*	
	55023.46135	0.00083	I	*Kepler*	
	55026.58425	0.00041	II	*Kepler*	
	55029.14371	0.00092	I	*Kepler*	
	55032.26733	0.00054	II	*Kepler*	
	55034.82637	0.00096	I	*Kepler*	
	55037.94916	0.00058	II	*Kepler*	
	55040.50906	0.00080	I	*Kepler*	
	55043.63138	0.00071	II	*Kepler*	
	55046.19156	0.00068	I	*Kepler*	
	55049.31370	0.00075	II	*Kepler*	
	55051.87400	0.00052	I	*Kepler*	
	55054.99628	0.00063	II	*Kepler*	
	55057.55691	0.00064	I	*Kepler*	
	55060.67868	0.00036	II	*Kepler*	
	55066.36160	0.00038	II	*Kepler*	
	55068.92097	0.00020	I	*Kepler*	
	55072.04343	0.00062	II	*Kepler*	
	55074.60304	0.00032	I	*Kepler*	
	55077.72639	0.00078	II	*Kepler*	
	55080.28614	0.00049	I	*Kepler*	
	55083.40846	0.00027	II	*Kepler*	
	55085.96774	0.00061	I	*Kepler*	
	55094.77298	0.00048	II	*Kepler*	
	55097.33334	0.00048	I	*Kepler*	
	55103.01610	0.00074	I	*Kepler*	
	55106.13798	0.00073	II	*Kepler*	

Times of minima:					
Star name	Time of min. HJD 2400000+	Error	Type	Filter	Rem.
	55108.69828	0.00047	I	*Kepler*	
	55111.82059	0.00069	II	*Kepler*	
	55117.50269	0.00031	II	*Kepler*	
	55120.06282	0.00021	I	*Kepler*	
	55123.18558	0.00184	II	*Kepler*	
	55125.74497	0.00048	I	*Kepler*	
	55128.86733	0.00069	II	*Kepler*	
	55131.42724	0.00063	I	*Kepler*	
	55134.54991	0.00098	II	*Kepler*	
	55137.10966	0.00074	I	*Kepler*	
	55140.2325	0.000640	II	*Kepler*	
	55142.79264	0.00070	I	*Kepler*	
	55145.91528	0.00084	II	*Kepler*	
	55148.47429	0.00105	I	*Kepler*	
	55151.59719	0.00067	II	*Kepler*	
	55157.27945	0.00042	II	*Kepler*	
	55159.83956	0.00076	I	*Kepler*	
	55162.96212	0.00020	II	*Kepler*	
	55165.52208	0.00060	I	*Kepler*	
	55168.64425	0.00024	II	*Kepler*	
	55171.20448	0.00053	I	*Kepler*	
	55174.32716	0.00056	II	*Kepler*	
	55176.88686	0.00026	I	*Kepler*	
	55180.00904	0.00062	II	*Kepler*	
	55185.69178	0.00039	II	*Kepler*	
	55188.25134	0.00035	I	*Kepler*	
	55191.37371	0.00043	II	*Kepler*	
	55193.93426	0.00046	I	*Kepler*	
	55197.05622	0.00039	II	*Kepler*	
	55199.61609	0.0008	I	*Kepler*	
	55202.73901	0.00083	II	*Kepler*	
	55205.29911	0.00110	I	*Kepler*	
	55208.42078	0.00104	II	*Kepler*	
	55210.98192	0.00107	I	*Kepler*	
	55214.10363	0.00091	II	*Kepler*	
	55219.78580	0.00124	II	*Kepler*	
	55222.34683	0.00095	I	*Kepler*	
	55225.46827	0.00105	II	*Kepler*	
	55228.02881	0.00066	I	*Kepler*	
	55236.83351	0.00089	II	*Kepler*	
	55239.39305	0.00035	I	*Kepler*	
	55242.51578	0.00074	II	*Kepler*	
	55245.07556	0.00033	I	*Kepler*	

Times of minima:					
Star name	Time of min. HJD 2400000+	Error	Type	Filter	Rem.
	55248.19790	0.00068	II	*Kepler*	
	55250.75792	0.00048	I	*Kepler*	
	55253.88025	0.00072	II	*Kepler*	
	55256.44049	0.00059	I	*Kepler*	
	55259.56273	0.00044	II	*Kepler*	
	55262.12292	0.00072	I	*Kepler*	
	55265.24530	0.00038	II	*Kepler*	
	55267.80550	0.00083	I	*Kepler*	
	55270.92781	0.00067	II	*Kepler*	
	55273.48758	0.00019	I	*Kepler*	
	55279.17030	0.00062	I	*Kepler*	
	55282.29305	0.00058	II	*Kepler*	
	55284.85270	0.00053	I	*Kepler*	
	55287.97554	0.00091	II	*Kepler*	
	55290.53522	0.00035	I	*Kepler*	
	55293.65787	0.00078	II	*Kepler*	
	55296.21731	0.00078	I	*Kepler*	
	55299.33949	0.00051	II	*Kepler*	
	55301.89946	0.00090	I	*Kepler*	
	55305.02239	0.00043	II	*Kepler*	
	55307.58245	0.00044	I	*Kepler*	
	55310.70444	0.00060	II	*Kepler*	
	55313.26459	0.00033	I	*Kepler*	
	55316.38725	0.00014	II	*Kepler*	
	55318.94782	0.00060	I	*Kepler*	
	55322.06948	0.00079	II	*Kepler*	
	55324.62933	0.00065	I	*Kepler*	
	55327.75216	0.00060	II	*Kepler*	
	55330.31218	0.00039	I	*Kepler*	
	55333.43394	0.00058	II	*Kepler*	
	55335.99400	0.00047	I	*Kepler*	
	55339.11625	0.00082	II	*Kepler*	
	55341.67703	0.00081	I	*Kepler*	
	55344.79894	0.00072	II	*Kepler*	
	55347.35892	0.00039	I	*Kepler*	
	55350.48167	0.00053	II	*Kepler*	
	55353.04199	0.00063	I	*Kepler*	
	55356.16397	0.00051	II	*Kepler*	
	55358.72442	0.00043	I	*Kepler*	
	55361.84663	0.00063	II	*Kepler*	
	55364.40639	0.00078	I	*Kepler*	
	55367.52917	0.00049	II	*Kepler*	
	55370.08895	0.00075	I	*Kepler*	

Times of minima:					
Star name	Time of min. HJD 2400000+	Error	Type	Filter	Rem.
	55373.21154	0.00012	II	*Kepler*	
	55375.77148	0.00049	I	*Kepler*	
	55378.89339	0.00065	II	*Kepler*	
	55381.45418	0.00072	I	*Kepler*	
	55384.57594	0.00073	II	*Kepler*	
	55387.13587	0.00050	I	*Kepler*	
	55390.25844	0.00009	II	*Kepler*	
	55392.81810	0.00056	I	*Kepler*	
	55395.94066	0.00019	II	*Kepler*	
	55398.50037	0.00059	I	*Kepler*	
	55401.62300	0.00043	II	*Kepler*	
	55404.18314	0.00082	I	*Kepler*	
	55407.30537	0.00045	II	*Kepler*	
	55409.86557	0.00025	I	*Kepler*	
	55412.98829	0.00022	II	*Kepler*	
	55415.54846	0.00062	I	*Kepler*	
	55418.67052	0.00073	II	*Kepler*	
	55421.23097	0.00050	I	*Kepler*	
	55424.35279	0.00020	II	*Kepler*	
	55426.91312	0.00032	I	*Kepler*	
	55430.03543	0.00033	II	*Kepler*	
	55435.71761	0.00046	II	*Kepler*	
	55438.27749	0.00019	I	*Kepler*	
	55441.39999	0.00062	II	*Kepler*	
	55443.95969	0.00035	I	*Kepler*	
	55447.08267	0.00018	II	*Kepler*	
	55449.64193	0.00046	I	*Kepler*	
	55452.76465	0.00045	II	*Kepler*	
	55455.32420	0.00059	I	*Kepler*	
	55458.44702	0.00043	II	*Kepler*	
	55461.00781	0.00031	I	*Kepler*	
	55568.97303	0.00104	I	*Kepler*	
	55572.09587	0.00092	II	*Kepler*	
	55574.65551	0.00040	I	*Kepler*	
	55577.77839	0.00090	II	*Kepler*	
	55580.33801	0.00093	I	*Kepler*	
	55583.46067	0.00068	II	*Kepler*	
	55586.02111	0.00040	I	*Kepler*	
	55589.14259	0.00083	II	*Kepler*	
	55591.70320	0.00053	I	*Kepler*	
	55597.38460	0.00075	I	*Kepler*	
	55600.50739	0.00033	II	*Kepler*	
	55603.06706	0.00083	I	*Kepler*	

Times of minima:					
Star name	Time of min. HJD 2400000+	Error	Type	Filter	Rem.
	55606.18994	0.00052	II	*Kepler*	
	55608.74993	0.00049	I	*Kepler*	
	55611.87273	0.00045	II	*Kepler*	
	55614.43214	0.00062	I	*Kepler*	
	55617.55499	0.00027	II	*Kepler*	
	55620.11444	0.00061	I	*Kepler*	
	55623.23716	0.00082	II	*Kepler*	
	55625.79771	0.00054	I	*Kepler*	
	55628.91952	0.00033	II	*Kepler*	
	55631.47970	0.00051	I	*Kepler*	
	55634.60219	0.00014	II	*Kepler*	
	55642.84465	0.00083	I	*Kepler*	
	55645.96695	0.00031	II	*Kepler*	
	55648.52682	0.00029	I	*Kepler*	
	55651.64901	0.00070	II	*Kepler*	
	55654.20927	0.00068	I	*Kepler*	
	55657.33154	0.00055	II	*Kepler*	
	55659.89254	0.00095	I	*Kepler*	
	55663.01384	0.00109	II	*Kepler*	
	55665.57423	0.00120	I	*Kepler*	
	55668.69630	0.00115	II	*Kepler*	
	55671.25692	0.00073	I	*Kepler*	
	55674.37867	0.00107	II	*Kepler*	
	55676.93923	0.00034	I	*Kepler*	
	55680.06113	0.00062	II	*Kepler*	
	55682.62175	0.00069	I	*Kepler*	
	55685.74359	0.00031	II	*Kepler*	
	55688.30402	0.00064	I	*Kepler*	
	55691.42590	0.00074	II	*Kepler*	
	55693.98562	0.00064	I	*Kepler*	
	55697.10842	0.00016	II	*Kepler*	
	55699.66790	0.00077	I	*Kepler*	
	55702.79132	0.00055	II	*Kepler*	
	55705.35051	0.00033	I	*Kepler*	
	55708.47399	0.00066	II	*Kepler*	
	55711.03327	0.00016	I	*Kepler*	
	55714.15594	0.00035	II	*Kepler*	
	55716.71643	0.00071	I	*Kepler*	
	55719.83768	0.00070	II	*Kepler*	
	55722.39813	0.00041	I	*Kepler*	
	55725.52037	0.00093	II	*Kepler*	
	55728.08108	0.00050	I	*Kepler*	
	55731.20306	0.00092	II	*Kepler*	

Times of minima:					
Star name	Time of min. HJD 2400000+	Error	Type	Filter	Rem.
	55733.76303	0.00073	I	*Kepler*	
	55736.88575	0.00083	II	*Kepler*	
	55742.56814	0.00070	II	*Kepler*	
	55745.12796	0.00028	I	*Kepler*	
	55748.24980	0.00062	II	*Kepler*	
	55750.81099	0.00090	I	*Kepler*	
	55753.93286	0.00037	II	*Kepler*	
	55756.49374	0.00085	I	*Kepler*	
	55759.61506	0.00029	II	*Kepler*	
	55762.17607	0.00082	I	*Kepler*	
	55765.29722	0.00025	II	*Kepler*	
	55767.85760	0.00095	I	*Kepler*	
	55770.97932	0.00050	II	*Kepler*	
	55773.53995	0.00083	I	*Kepler*	
	55776.66170	0.00059	II	*Kepler*	
	55779.22237	0.00022	I	*Kepler*	
	55782.34393	0.00078	II	*Kepler*	
	55784.90524	0.00071	I	*Kepler*	
	55788.02628	0.00086	II	*Kepler*	
	55790.58741	0.00062	I	*Kepler*	
	55793.70940	0.00026	II	*Kepler*	
	55796.26977	0.00045	I	*Kepler*	
	55799.39199	0.00070	II	*Kepler*	
	55801.95260	0.00168	I	*Kepler*	
	55805.07436	0.00055	II	*Kepler*	
	55807.63435	0.00023	I	*Kepler*	
	55810.75696	0.00056	II	*Kepler*	
	55813.31679	0.00025	I	*Kepler*	
	55816.43880	0.00074	II	*Kepler*	
	55818.99928	0.00045	I	*Kepler*	
	55822.12160	0.00067	II	*Kepler*	
	55824.68164	0.00052	I	*Kepler*	
	55827.80414	0.00089	II	*Kepler*	
	55830.36461	0.00040	I	*Kepler*	
	55932.64733	0.00083	I	*Kepler*	
	55935.76968	0.00024	II	*Kepler*	
	55938.33004	0.00053	I	*Kepler*	
	55941.45192	0.00014	II	*Kepler*	
	55944.01174	0.00072	I	*Kepler*	
	55947.13471	0.00057	II	*Kepler*	
	55952.81664	0.00061	II	*Kepler*	
	55955.37666	0.00027	I	*Kepler*	
	55958.49862	0.00093	II	*Kepler*	

Times of minima:					
Star name	Time of min. HJD 2400000+	Error	Type	Filter	Rem.
	55961.05985	0.00063	I	*Kepler*	
	55964.18167	0.00040	II	*Kepler*	
	55966.74188	0.00092	I	*Kepler*	
	55969.86414	0.00098	II	*Kepler*	
	55972.42448	0.00123	I	*Kepler*	
	55975.54660	0.00104	II	*Kepler*	
	55978.10737	0.00099	I	*Kepler*	
	55981.22855	0.00089	II	*Kepler*	
	55983.78935	0.00068	I	*Kepler*	
	55989.47144	0.00026	I	*Kepler*	
	55992.59368	0.00040	II	*Kepler*	
	55998.27600	0.00027	II	*Kepler*	
	56000.83624	0.00060	I	*Kepler*	
	56003.95891	0.00078	II	*Kepler*	
	56006.51896	0.00026	I	*Kepler*	
	56009.64157	0.00077	II	*Kepler*	
	56012.20122	0.00020	I	*Kepler*	
	56017.88365	0.00083	I	*Kepler*	
	56021.00541	0.00064	II	*Kepler*	
	56023.56621	0.00070	I	*Kepler*	
	56026.68853	0.00076	II	*Kepler*	
	56029.24774	0.00062	I	*Kepler*	
	56032.37053	0.00017	II	*Kepler*	
	56034.93055	0.00083	I	*Kepler*	
	56038.05233	0.00036	II	*Kepler*	
	56040.61239	0.00102	I	*Kepler*	
	56043.73512	0.00059	II	*Kepler*	
	56046.29536	0.00057	I	*Kepler*	
	56049.41697	0.00062	II	*Kepler*	
	56051.97809	0.00082	I	*Kepler*	
	56055.09970	0.00061	II	*Kepler*	
	56057.66012	0.00036	I	*Kepler*	
	56060.78258	0.00074	II	*Kepler*	
	56063.34304	0.00052	I	*Kepler*	
	56066.46530	0.00010	II	*Kepler*	
	56069.02475	0.00057	I	*Kepler*	
	56072.14770	0.00024	II	*Kepler*	
	56074.70732	0.00071	I	*Kepler*	
	56080.38998	0.00019	I	*Kepler*	
	56083.51213	0.00054	II	*Kepler*	
	56086.07227	0.00018	I	*Kepler*	
	56089.19427	0.00066	II	*Kepler*	
	56091.75445	0.00027	I	*Kepler*	

Times of minima:					
Star name	Time of min. HJD 2400000+	Error	Type	Filter	Rem.
	56094.87666	0.00083	II	*Kepler*	
	56097.43730	0.00056	I	*Kepler*	
	56100.55906	0.00067	II	*Kepler*	
	56103.12021	0.00110	I	*Kepler*	
	56108.80169	0.00068	I	*Kepler*	
	56111.92429	0.00068	II	*Kepler*	
	56114.48466	0.00014	I	*Kepler*	
	56117.60643	0.00046	II	*Kepler*	
	56120.16689	0.00012	I	*Kepler*	
	56131.53164	0.00041	I	*Kepler*	
	56134.65375	0.00010	II	*Kepler*	
	56137.21372	0.00030	I	*Kepler*	
	56140.33611	0.00025	II	*Kepler*	
	56142.89648	0.00073	I	*Kepler*	
	56146.01879	0.00042	II	*Kepler*	
	56148.57920	0.00010	I	*Kepler*	
	56151.70128	0.00059	II	*Kepler*	
	56154.26141	0.00081	I	*Kepler*	
	56157.38340	0.00056	II	*Kepler*	
	56159.94443	0.00075	I	*Kepler*	
	56163.06574	0.00074	II	*Kepler*	
	56165.62705	0.00072	I	*Kepler*	
	56168.74781	0.00062	II	*Kepler*	
	56171.30877	0.00104	I	*Kepler*	
	56174.43057	0.00099	II	*Kepler*	
	56176.99093	0.00080	I	*Kepler*	
	56180.11262	0.00090	II	*Kepler*	
	56182.67350	0.00091	I	*Kepler*	
	56185.79585	0.00066	II	*Kepler*	
	56188.35540	0.00028	I	*Kepler*	
	56191.47806	0.00027	II	*Kepler*	
	56194.03750	0.00053	I	*Kepler*	
	56197.16062	0.00009	II	*Kepler*	
	56199.71978	0.00074	I	*Kepler*	
	56202.84287	0.00070	II	*Kepler*	
	56307.68614	0.00038	I	*Kepler*	
	56322.17331	0.00093	II	*Kepler*	
	56324.73372	0.00084	I	*Kepler*	
	56327.85563	0.00049	II	*Kepler*	
	56330.41641	0.00091	I	*Kepler*	
	56333.53829	0.00065	II	*Kepler*	
	56336.09836	0.00042	I	*Kepler*	
	56339.22095	0.00077	II	*Kepler*	

Times of minima:					
Star name	Time of min. HJD 2400000+	Error	Type	Filter	Rem.
	56341.78074	0.00058	I	*Kepler*	
	56344.90362	0.00072	II	*Kepler*	
	56347.46380	0.00027	I	*Kepler*	
	56350.58575	0.00057	II	*Kepler*	
	56353.14583	0.00023	I	*Kepler*	
	56356.26873	0.00095	II	*Kepler*	
	56361.95098	0.00070	II	*Kepler*	
	56364.51091	0.00062	I	*Kepler*	
	56367.63293	0.00050	II	*Kepler*	
	56370.19260	0.00047	I	*Kepler*	
	56373.31506	0.00055	II	*Kepler*	
	56375.87601	0.00043	I	*Kepler*	
	56378.99698	0.00041	II	*Kepler*	
	56381.55766	0.00082	I	*Kepler*	
	56384.67997	0.00044	II	*Kepler*	
	56387.24051	0.00018	I	*Kepler*	
	56390.36243	0.00032	II	*Kepler*	
	56392.92262	0.00046	I	*Kepler*	
	56396.04474	0.00078	II	*Kepler*	
	56398.60572	0.00060	I	*Kepler*	
	56401.72756	0.00112	II	*Kepler*	
	56404.28812	0.00040	I	*Kepler*	
	56407.41022	0.00094	II	*Kepler*	
	56409.97031	0.00032	I	*Kepler*	
	56413.09211	0.00034	I	*Kepler*	
	56413.09213	0.00068	II	*Kepler*	
	56421.33469	0.00036	I	*Kepler*	
KIC 12306808	54954.29547	0.00020	II	*Kepler*	
	54971.12858	0.00011	I	*Kepler*	
	54992.17388	0.00012	II	*Kepler*	
	55009.00700	0.00009	I	*Kepler*	
	55030.05259	0.00006	II	*Kepler*	
	55046.88544	0.00008	I	*Kepler*	
	55067.93088	0.00008	II	*Kepler*	
	55084.76408	0.00006	I	*Kepler*	
	55105.80946	0.00008	II	*Kepler*	
	55122.64265	0.00013	I	*Kepler*	
	55143.68807	0.00014	II	*Kepler*	
	55160.52115	0.00008	I	*Kepler*	
	55181.56642	0.00013	II	*Kepler*	
	55198.39979	0.00026	I	*Kepler*	
	55219.44492	0.00017	II	*Kepler*	
	55236.27821	0.00028	I	*Kepler*	

Times of minima:					
Star name	Time of min. HJD 2400000+	Error	Type	Filter	Rem.
	55257.32331	0.00013	II	*Kepler*	
	55274.15641	0.00015	I	*Kepler*	
	55295.20184	0.00010	II	*Kepler*	
	55312.03483	0.00020	I	*Kepler*	
	55333.08021	0.00015	II	*Kepler*	
	55349.91348	0.00015	I	*Kepler*	
	55370.95900	0.00020	II	*Kepler*	
	55387.79182	0.00012	I	*Kepler*	
	55408.83721	0.00010	II	*Kepler*	
	55425.67051	0.00017	I	*Kepler*	
	55446.71582	0.00005	II	*Kepler*	
	55463.54873	0.00017	I	*Kepler*	
	55484.59417	0.00010	II	*Kepler*	
	55501.42735	0.00008	I	*Kepler*	
	55522.47270	0.00018	II	*Kepler*	
	55539.30576	0.00013	I	*Kepler*	
	55577.18423	0.00014	I	*Kepler*	
	55598.22968	0.00021	II	*Kepler*	
	55615.06310	0.00020	I	*Kepler*	
	55652.94130	0.00008	I	*Kepler*	
	55673.98684	0.00018	II	*Kepler*	
	55690.81966	0.00013	I	*Kepler*	
	55711.86523	0.00014	II	*Kepler*	
	55728.69830	0.00017	I	*Kepler*	
	55749.74362	0.00006	II	*Kepler*	
	55766.57686	0.00015	I	*Kepler*	
	55787.62221	0.00013	II	*Kepler*	
	55804.45526	0.00019	I	*Kepler*	
	55825.50061	0.00018	II	*Kepler*	
	55842.33374	0.00012	I	*Kepler*	
	55863.37880	0.00022	II	*Kepler*	
	55880.21230	0.00010	I	*Kepler*	
	55901.25762	0.00021	II	*Kepler*	
	55918.09082	0.00010	I	*Kepler*	
	55939.13592	0.00017	II	*Kepler*	
	55955.96881	0.00033	I	*Kepler*	
	55977.01458	0.00007	II	*Kepler*	
	56031.72606	0.00017	I	*Kepler*	
	56052.77162	0.00020	II	*Kepler*	
	56069.60477	0.00019	I	*Kepler*	
	56090.64979	0.00010	II	*Kepler*	
	56107.48300	0.00016	I	*Kepler*	
	56145.36158	0.00007	I	*Kepler*	

Times of minima:

Star name	Time of min. HJD 2400000+	Error	Type	Filter	Rem.
	56166.40681	0.00023	II	*Kepler*	
	56183.24002	0.00010	I	*Kepler*	
	56221.11855	0.00008	I	*Kepler*	
	56242.16363	0.00033	II	*Kepler*	
	56258.99697	0.00007	I	*Kepler*	
	56280.04191	0.00019	II	*Kepler*	
	56296.87567	0.00015	I	*Kepler*	
	56334.75400	0.00016	I	*Kepler*	
	56355.79909	0.00014	II	*Kepler*	
	56372.63262	0.00017	I	*Kepler*	
	56410.51117	0.00013	I	*Kepler*	

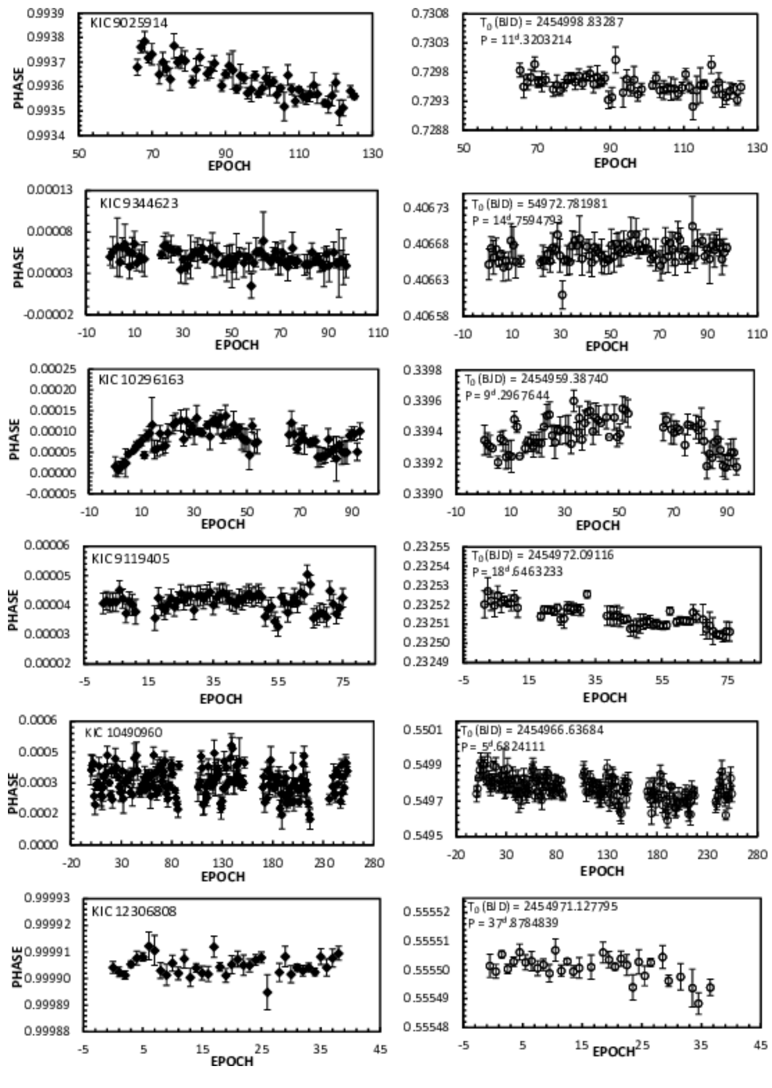

Figure 1. The eclipse-timing variation O–C curves for KIC 9025914, KIC 9344623, KIC 10296163, KIC 9119405, KIC 10490960, and KIC 12306808, determined for primary and secondary minima separately. The left-hand panels are for the primary and the right-panels are for the secondary.

COMMISSIONS G1 AND G4 OF THE IAU
INFORMATION BULLETIN ON VARIABLE STARS
Volume 63 Number 6251 DOI: 10.22444/IBVS.6251

Konkoly Observatory
Budapest
16 August 2018

HU ISSN 0374 – 0676

PHOTOMETRY OF OV BOOTIS AT THE 2017 OUTBURST

TANABE, KENJI[1]; AKAZAWA, HIDEHIKO[1]; FUKUDA, NAOYA[1]

[1] Department of Biosphere-Geosphere Science, Okayama University of Science, Ridaicho 1-1,Okayama 700-0005, Japan, e-mail: tanabe@big.ous.ac.jp

Abstract

We present our photometric results of OV Boo obtained during the 2017 outburst.

On March 14.63 UT, 2017, a Japanese observer, Masaru Mukai detected, a bright outburst of the dwarf nova OV Bootis which showed the system increasing from quiescent magnitude of $\sim$ 18.5 to a magnitude of 11.4. Mukai's detection was performed under the collaboration with Seiichi Yoshida (the leader of the MISAO Project, see `http://www.aerith.net/misao/`, an image-data analysis group). Soon after the discovery, at 14.76 UT, Hidehiko Akazawa, one of the co-authors of the present paper, started time-series photometry at his personal observatory. Observational journal is given in Table 1. During this early stage, photometric observations were performed using both Rc and clear filter. Here we present only the data with R_C filter which will highlight the behaviour due to Hα emission.

OV Boo was originally discovered as one of 32 new cataclysmic variable stars (CVs) by the Sloan Digital Sky Survey (SDSS) in 2003. During its quiescence stage, OV Boo (previous designation was SDSS J1507+52, or simply J1507) was first investigated by Szkody et al.(2005) together with other CVs. They obtained its orbital period to be 67 min, an exceptionally short period (below the so-called period minimum: ($\approx$ 75 min; see for example, Paczynski (1981)), from its light curve that showed deep eclipses. They also obtained its spectrum, with double-peaked Hα emission line possibly from its accretion disk. However, the star was too faint to obtain its radial velocity curve. This object seems to have experienced a long-lasting (33 years) quiescence (Bengtsson 2017). From this point of view, the behaviour of this variable star was similar to a WZ Sge-type dwarf nova (DN), a subclass of SU UMa-type DN with larger outburst amplitude, having very short orbital period($\approx$ 80 min) and very long (some 10 years) quiescence interval (so-called supercycle) between successive outbursts. However, its orbital period is much shorter than the period minimum and seems to be against the standard theory of dwarf nova evolution (see, for example, Hellier (2001), chapter 4). In fact Littlefair et al. (2007) investigated the binary structure of this star by high speed photometry and obtained each mass of the binary system, suggesting that this DN is an exotic one because of their low mass (below the hydrogen-burning limit) secondary star. Uthas et al. (2011; see also the chapter 5 in her PhD Thesis) proposed that this binary system has a possibility of being a member of Galactic halo.

Table 1: Journal of CCD Observation by H. Akazawa

Date (UT)	Start (JD-2457800.0)	End (JD-2457800.0)	Exposure (sec)	Number	D (cm)	period (day)
14/March	27.22999	27.36664	90	127	20cm	0.0462
15/March	28.07363	28.36378	120	203	20cm	0.0459
17/March	30.03679	30.35659	120	224	20cm	0.0462
18/March	31.03488	31.35771	120	228	20cm	0.0464
19/March	32.13840	32.35218	180	102	20cm	0.0464
21/March	34.13840	34.35495	180	153	20cm	0.0462
25/March	38.18257	38.35186	180	75	20cm	0.0464
27/March	40.19713	40.24581	180	24	20cm	–
28/March	41.08435	41.27145	180	41	20cm	–

The 2017 outburst of OV Boo is a good (probably the best and lucky) chance to investigate the nature of this peculiar cataclysmic variable star. One of the most important problems is to determine whether this outburst of OV Boo is the superoutburst of SU UMa-type (or WZ Sge-type) or not.

Photometric precision is up to 0.015 magnitude but depends on daily sky condition. Time-series photometric data are processed by the software AIP4Win ver.2. The basic properties of variable star (OV Boo) and comparison stars for calibration are shown in Table 2.

Overall light curve at the early stage (the first 2 weeks) is given in Figure 1. Representative light curves are given in the upper panel of Figures 2 and 3. Tentative period analysis for the daily humps are performed by the Phase Dispersion Minimization (PDM) method (Stellingwerf 1978). The values of the period (day) of hump for each night are in the last column of Table 1. The complete period analysis by PDM for the entire data during the early stage of the outburst is given below. Also we calculate the error of the obtained period by applying the linear regression to the O–C diagram.

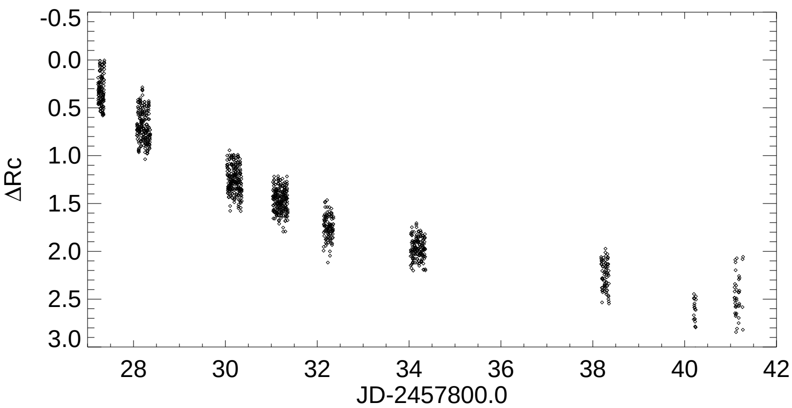

Figure 1. Overall light curve of the R_C data during the early stage of outburst. ΔR_C denotes the R_C magnitude difference from the peak outburst brightness.

Temporal change of the outburst during the early stage is shown in Figure 4. From this, we can see the double-peaked profile in the light curve. This may be due to multiple sources of bright regions on its accretion disk. Such a profile suggests us a connection

Table 2: The Basic Properties on Variable Star and Comparison Stars used: Positions and magnitudes

Star	GSC	RA 15^h	Dec $+52^\circ$	V	R
V	OV Boo	$07^m22.35^s$	$30'07.7''$	*var*	*var*
C1	03868-01067	$07^m16.48^s$	$33'14.82''$	11.5	11.2
C2	03868-00859	$06^m20.81^s$	$28'32.41''$	12.2	11.9

with the spectroscopic feature of Hα emission obtained by Szkody et al. (2005).

Overall period by PDM for the entire data of the early stage of the 2017 outburst is given in Figure 5. The obtained period is 0.0461538 day = 66.46 min. Taking into account the time-resolution (from 1.5 min to 3 min), this value of the period is close to the orbital one obtained by Littlefair et al. (2007) (66.61 min).

The error of the above period obtained can be estimated by making use of the O–C diagram. If we take the tentative period derived from the PDM and the earliest recorded maximum as an epoch, we can present an O–C diagram of this stage (Figure 6). A tentative ephemeris used here is as follows:

$$T_{\rm max} = 2457827.26654 + 0.04615E \quad ; \quad E = 1, 2, 3, \cdots$$

Applying a linear regression to our O–C diagram,we obtain as follows:

$$P = 66.613 \pm 0.009 \quad \text{min.}$$

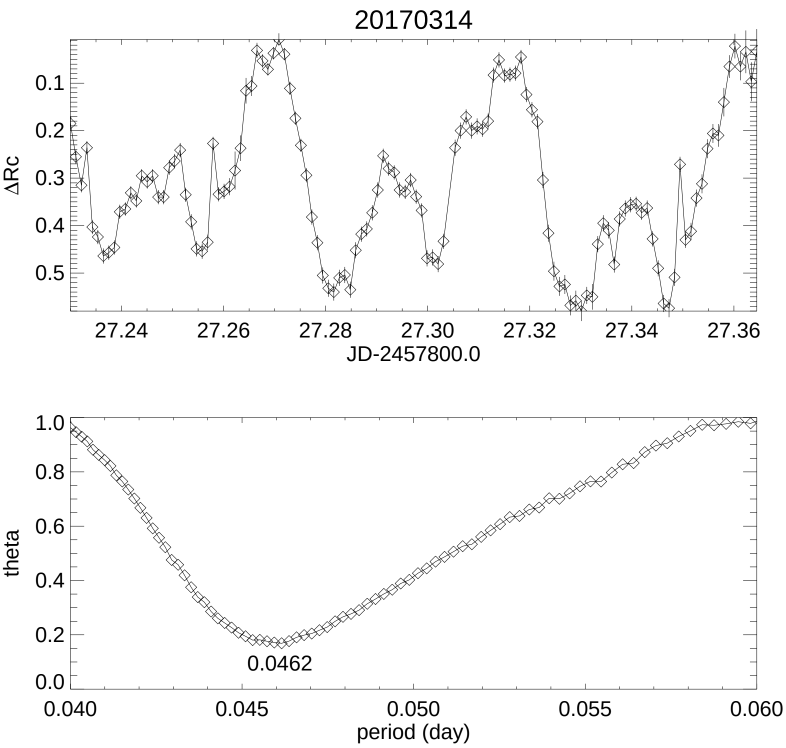

Figure 2. Representative light curve (upper panel) and corresponding θ diagram: March 14th.

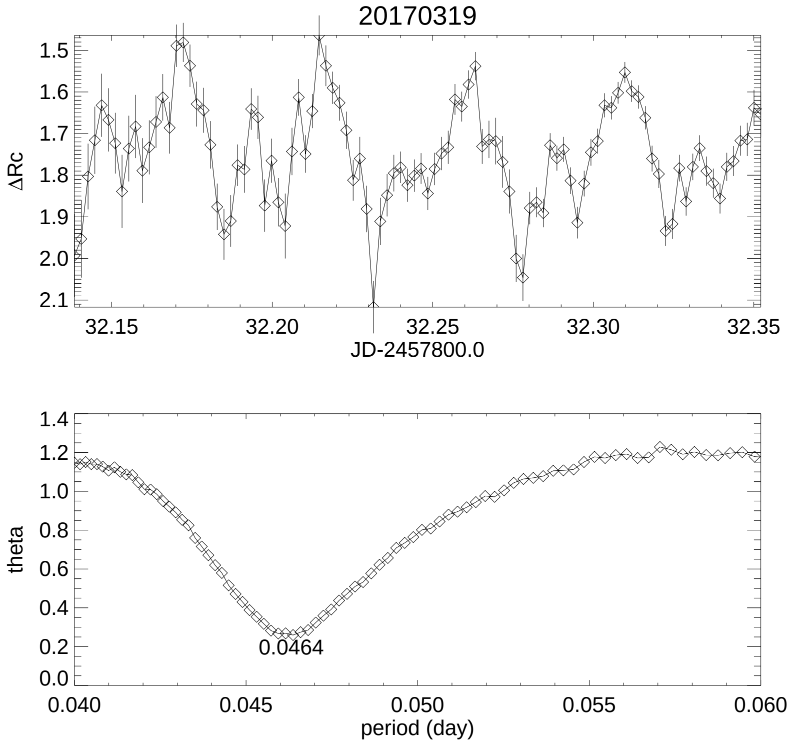

Figure 3. Representative light curve (upper panel) and corresponding θ diagram: March 19th.

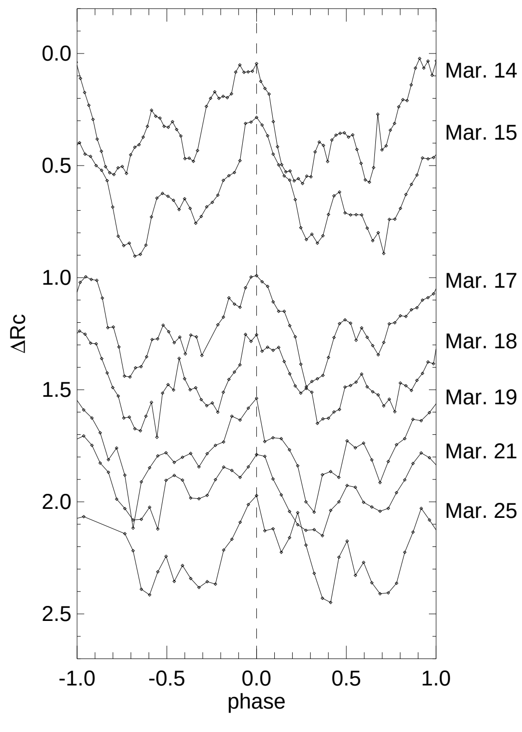

Figure 4. Daily change of R_C light curve during the early stage of 2017 outburst. Abscissa is the phase corresponding 0.04615 day. Ordinate is the same as Fig. 1

This value of the period together with the error is thought to be almost identical to the orbital period P_{orb} obtained by Littlefair et al. (2007).

In addition, we could not detect the so-called common superhump. We are now preparing a report on the later stage of OV Boo's 2017 outburst.

We conclude that from the behaviour of the early stage of 2017 outburst, in spite of high ($\approx$ 7 mag) amplitude, this ultra-short period cataclysmic binary star seems to be different from either WZ Sge-type or SU UMa-type DNe. Moreover OV Boo is a different type of DN from other ultra-short orbital period DNe including EI Psc (64.87 min) and CSS130418 (64.84 min). This may be due to too small mass of the secondary star of OV Boo (Littlefair et al., 2007) to give rise to elliptical disk around the primary (white dwarf) star.

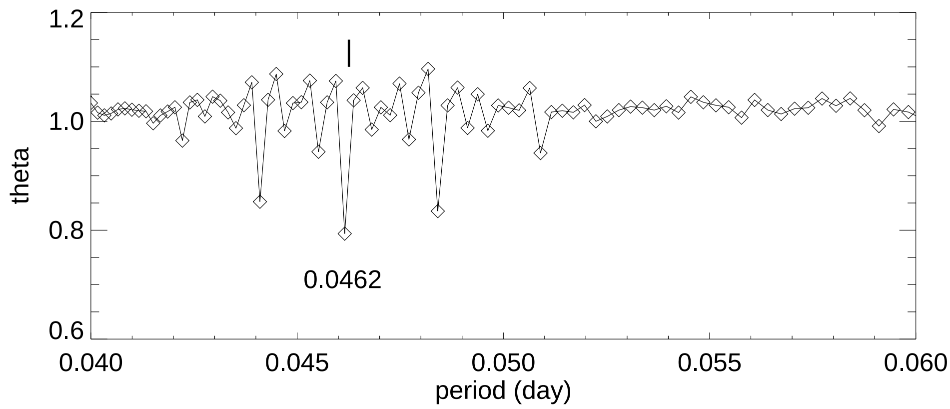

Figure 5. θ diagram for the entire data of the early stage (March of 2017) outburst. Abscissa is the period (day). Vertical line denotes the orbital period obtained by Littlefair et al. (2007).

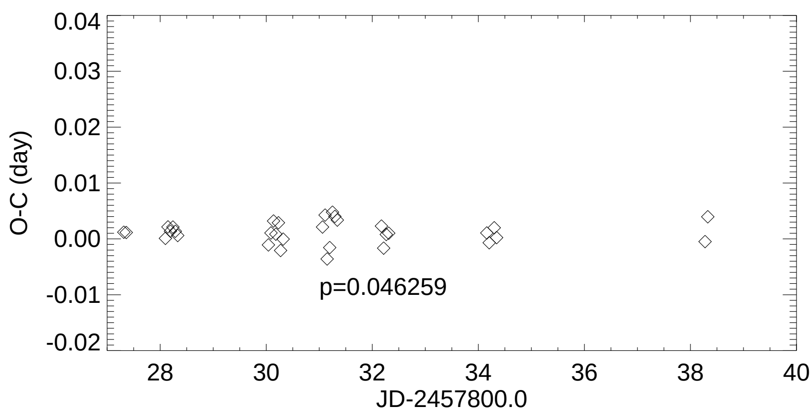

Figure 6. A tentative O–C diagram during the early stage of 2017 outburst.

The authors are grateful to the observers who detected and confirmed the outburst of OV Boo. One of the authors (K. Tanabe) expresses gratitude to Rosa Poggiani (University of Pisa) for her advice.

References:

Bengtsson, H.; Kato, T., 2017, vsnet-alert, ♯ **20792**
Hellier, C., 2001, *Cataclysmic Variable Stars*, Cambridge
Littlefair, S.P. et al., 2007, *MNRAS*, **381**, 827
Paczynski, B., 1981, *AcA*, **31**, 1
Szkody, P. et al., 2005, *AJ*, **129**, 2386
Stellingwerf, R. F., 1978, *ApJ*, **224**, 953
Uthas, H. et al., 2011, *MNRAS*, **414**, L85
Uthas, H., 2011, PhD Thesis

COMMISSIONS G1 AND G4 OF THE IAU
INFORMATION BULLETIN ON VARIABLE STARS
Volume 63 Number 6252 DOI: 10.22444/IBVS.6252

Konkoly Observatory
Budapest
24 August 2018

HU ISSN 0374 – 0676

THE PERIOD ANALYSIS OF THE HIERARCHICAL SYSTEM DI Peg

OZUYAR, D.; ELMASLI, A.; CALISKAN, S.

[1] Ankara University, Faculty of Science, Dept. of Astronomy and Space Sciences, 06100, Tandogan, Ankara / Turkey, e-mail: dozuyar@ankara.edu.tr

Abstract

The existence of an additional body around a binary system can be detected by the help of the light-travel time effect. Due to the motions of the binary and the companion stars around the common mass center of the ternary system, the light-time effect produces an irregularity on the eclipse timings. Monitoring the variations in these timings, sub-stellar or planet companions orbiting around the binary system can be identified. In this paper, additional bodies orbiting the Algol-type binary DI Peg are examined by using the archival eclipse timings including our CCD data observed at the Ankara University Kreiken Observatory. More than five hundred minimum times equivalent to about nine decades are employed to identify the orbital behaviour of the binary system. The best fit to the timings shows that the orbital period of DI Peg has variations due to an integration of two sinusoids with the periods of $P_3 = 49.50 \pm 0.36$ yr and $P_4 = 27.40 \pm 0.24$ yr. The orbital change is thought to be most likely due to the existence of two M-type red dwarf companions with the masses of $M_3 = 0.213 \pm 0.021$ M$_\odot$ and $M_4 = 0.151 \pm 0.008$ M$_\odot$, assuming that the orbits of additional bodies are co-planar with the orbit of the binary system. Also, the residuals of two sinusoidal fits still seem to show another modulation with the period of roughly $P = 19.5$ yr. The origin of this modulation is not clear and more observational data are required to reveal if the periodicity is caused by another object gravitationally bounded to the system.

1 Introduction

Hierarchical multi-body star systems (Evans 1968) form in different ways, such as from interaction/capture in a globular star cluster (van den Berk et al. 2007), from a massive primordial disk involving accretion processes and/or local disk instabilities (Lim and Takakuwa 2006; Marzari et al. 2009) or from a non-hierarchical star system by angular momentum and energy exchange via mutual gravitational interactions (Reipurth 2000). These systems can be basically classified into two groups; circumbinary and circumstellar systems. In circumbinary systems, one or more additional bodies move around a binary star and they are known as companions on P-type orbits (Dvorak 1986). A transiting circumbinary planet, PH1b, around KIC 4862625 which consists of two binary pairs; the quadruple systems HD 98800 (Furlan et al. 2007) and SZ Her (Lee et al. 2012) can be given as examples of such a hierarchy. On the other hand, the systems with companions orbiting one component of a binary pair are the other type of hierarchical systems (circumstellar or S-type configuration; Schwarz et al. 2011). The example of such a system can be found in Neuhäuser et al. (2007) and Chauvin et al. (2007).

A hierarchical circumbinary system can be detected by observing the timings of the mid-eclipse times of the binary companion. The presence of an additional body causes a change in the relative distance of the eclipsing pair to the observer depending on the motion of the third body around the barycenter of the triple system. This binary wobble leads a periodic variation in conjunction times. As a result, the eclipses present lags or advances in the timings of minimum light (Irwin 1952). As known, the light-time effect is a geometrical feature and the third object produces a sinusoidal-like variation in the binary orbital. If the archival database is large and sufficient enough, this variation in eclipse timings provides an opportunity to understand the nature of the multi-body system (Pribulla et al. 2012).

In this sense, space-based missions offer a unique opportunity for the discovery of companions orbiting eclipsing binaries. For example, Kepler provides continuous and highly homogeneous light curves over the time interval of four years. Thus, its photometric observations enable new discoveries of multiple star systems, such as triple, quadruple or even quintuple ones. Indeed, there are a large number of multiple star systems identified from the Kepler observations. Conroy et al. (2014) present a catalog, which includes precise minimum times and third body signals for 1279 close binaries in the latest Kepler Eclipsing Binary Catalog. They find 236 binaries having third body signals. Borkovits et al. (2015) report O–C analysis of 26 compact hierarchical triple stars in the Kepler field. Borkovits et al. (2016) identify the existence of a third body in 222 of 2600 Kepler binaries. The quadruple system KIC 7177553 (Lehmann et al. 2016) consists of two eccentric binaries with a separation of 0.4 arcsec (167 au). The outer orbit's period is in the range of 1000-3000 yr. Another quadruple star system, EPIC 220204960, contains two slightly eccentric binaries with orbital periods of 13.27 and 14.41 days (Rappaport et al. 2017). These binaries are in a quadruple system with an outer period of 1 yr and a physical separation of 30 au. An example for a quintuple star system is EPIC 212651213 and EPIC 212651234 (Rappaport et al. 2016). In this system, EPIC 212651213 hosts two eclipsing binaries with orbital periods of 5.1 and 13.1 days. EPIC 212651234 is a single star with a projected physical separation of about 0.013 pc to EPIC 212651213. It is also stated that EPIC 212651213 and EPIC 212651234 are gravitationally bound to each other.

DI Peg (HIP 116167, GSC 01175-00013, BD+14 5006) was discovered by Morgenroth (1934) and identified to be an Algol type eclipsing binary (F4IV+ K4) by Rucinski (1967) and Lu (1992). From the photographic observations, Jensch (1934) determined the period of the system to be $\sim 0^{\rm d}\!.711811$. Rucinski (1967) analysed the photoelectric observations of Kruszewski (1964) and derived the first orbital solutions. Based on the results, he suggested the existence of a third light which provided 24% contribution to the total light of the system. More photometric studies were performed by Chou and Kitamura (1968), Binnendijk (1973), Chaubey (1982), Lu (1992), and Yang et al. (2014).

Gaposchkin (1953) detected a variation in the orbital period of the star. Ahnert (1974) and Vinkó (1992) proposed a possible light-time effect in the system and they gave periods of ~ 62.4 and ~ 22.1 yr. By using the spectroscopic solutions, Lu (1992) determined the system parameters as $a = 4.14(0.05)$ R$_\odot$, $V_0 = +43.8(2.0)$ km s^{-1}, $K_1 = 185.2(2.4)$ km s^{-1}, $K_2 = 109.0(2.1)$ km s^{-1}, $T_0 =$ HJD 48213.8851(0.0022) and $q_{\rm sp} = 0.59(0.01)$.

Rafert (1982) derived a downward quadratic ephemeris with a cyclic variation in the O–C diagram. Unlike this, Hanna and Amin (2013) obtained a cyclic modulation with the period of 55 years, superimposed on an upward parabolic variation. The long-term orbital period increase was found to be $dP/dt = 0.17$ s/century and interpreted as a mass transfer from the evolved secondary component to the primary one with the rate of 1.52×10^{-8} M$_\odot$/yr. The cyclic variation was attributed to a low-mass third body with the mass of $M_3 \sim 0.2200 \pm 0.0006$ M$_\odot$. The parameters of the third body were given as

$e_3 = 0.77(7)$ and $w_3 = 300° \pm 10°$.

Recently, Yang et al. (2014) reproduced the photometric models with the help of new multi-color observations and previously published ones in literature. They determined the system parameters as $i = 89.^{\circ}02 \pm 0.^{\circ}11$, $M_1 = 1.19(2)$ $M_{\odot}$, $M_2 = 0.70(2)$ $M_{\odot}$, $L_1 = 3.70(4)$ $L_{\odot}$, and $L_2 = 0.53(2)$ $L_{\odot}$. According to the results, they stated that the system had a low third light whose fill-out factor for the more massive component was $f_{\rm p} = 78.2(4)$. Their O–C curve also indicated that the orbital period of DI Peg has changed in a complicated mode, such that the period of the star possibly showed two light-time orbits with the modulation periods of $P_3 \sim 54.6(5)$ yr and $P_4 \sim 23.0(6)$ yr, respectively. The masses of the inner and outer sub-stellar objects were given to be $M_{in} \sim 0.095$ $M_{\odot}$ and $M_{out} \sim 0.170$ $M_{\odot}$. On the basis of these results, Yang et al. (2014) suggested that the system has consists of four objects.

The aim of this study is to perform a detailed period analysis of DI Peg for the parameter determination of the additional bodies in the system by using the new and all available archival minimum times. For this purpose, the paper is organized as follows; the observations are presented in Section 2, the analysis is described in Section 3, the results related to the analysis are discussed in Section 4.

2 Observations

We observed DI Peg in V and R filters on the nights of 1 and 2 November 2017 at the Ankara University Kreiken Observatory. Observations were carried out by using an Apogee ALTA U47 + CCD camera (1024 × 1024 pixels) with Johnson $UBVRI$ filters mounted on a 35 cm telescope. In the observing process, BD+14 5004 was chosen as the comparison star (Table 1). Bias, dark, and flat corrections were performed and all images were reduced by using the MaxIm DL software[1]. The individual differential magnitudes were computed by subtracting the variable star from the comparison (V-C). The data covered two minima, the timings of which were determined as Min I $= 2458060.4456 \pm 0.0001$ and Min II $= 2458059.3779 \pm 0.0002$ with the method of Kwee and van Woerden (1956). The values were an average of the minimum times obtained in V and R colors during the same point.

Table 1. Spectral types, brightness, filters and exposure times are given for DI Peg and its comparison star BD+14 5004.

Star		Spectral Type	V (mag)	Filters	Exposure Times (s)
DI Peg	Variable	F4-IV	9.52	R, V	35, 35
BD+14 5004	Comparison	K4	9.83	R, V	35, 35

3 Analysis

The O–C diagram of DI Peg covering a time span of 88 years (Figure 1) was constructed from 85 primary, 14 secondary CCD; 45 primary, 9 secondary photoelectric; 17 primary photographic and 340 visual minimum times. These minima were collected from various observers listed in Table 1. The uncertainties of these values are not given in the table and can be accessed directly from their sources. The light elements of DI Peg were derived from the linear least-square fit applied to the CCD and photoelectric minimum times.

[1] https://diffractionlimited.com/help/maximdl/MaxIm-DL.htm

Table 1: All available minimum times of DI Peg in archives

Min. Time (HJD-2400000)	Typ.	Meth.	Ref.	Min. Time (HJD-2400000)	Typ.	Meth.	Ref.
25644.3150	1	pg	Guthnick & Prager ; AN 258	37193.5400	1	vi	B.Czerlunczakiewic ; AA 17.62
25918.3510	1	vi	A.Jensch ; AN 252.395	37196.3810	1	vis	B.Czerlunczakiewic ; EBC 1-32
26000.2330	1	vi	A.Jensch ; AN 252.395	37196.3830	1	vi	J.Rodzinski ; AA 18.332
26249.3640	1	pg	A.Jensch ; AN 252.395	37196.3910	1	vis	A.Slowik ; EBC 1-32
26266.4440	1	pg	A.Jensch ; AN 252.395	37270.4040	1	vi	F.Gerhart ; AN 288.72
26624.4580	1	pg	A.Jensch ; AN 252.395	37517.4080	1	vi	A.Slowikowna ; AA 17.62
26960.4600	1	vi	A.Jensch ; AN 252.395	37522.3946	1	pe	A.Kruszewski ; AA 17.275
26980.3840	1	vi	A.Jensch ; AN 252.395	37523.4620	2	pe	A.Kruszewski ; AA 17.275
27738.4740	1	vi	R.Szafraniec ; AAC 4.81	37527.3776	1	pe	A.Kruszewski ; AA 17.275
28432.4910	1	vi	W.Opalski ; BBG 1.47	37544.4610	1	pe	A.Kruszewski ; AA 17.275
28434.6270	1	vi	W.Opalski ; BBG 1.47	37556.5410	1	vis	H.Brancewicz ; AA 17.62
28452.4170	1	vi	W.Opalski ; BBG 1.47	37559.4096	1	pe	A.Kruszewski ; AA 17.275
28454.5570	1	vi	W.Opalski ; BBG 1.47	37626.3190	1	vi	R.Gizinski ; BAVM 15
28457.4050	1	vi	W.Opalski ; BBG 1.47	37668.3160	1	pg	H.Huth ; MVS 3.170
28459.5410	1	vi	W.Opalski ; BBG 1.47	37870.4760	1	vi	H.Huth ; MVS 3.170
28460.2510	1	vi	W.Opalski ; BBG 1.47	37907.4920	1	pg	H.Huth ; MVS 3.170
31273.3460	1	vi	W.Zessewitsch ; IODE 4.2.290	37932.3960	1	vi	E.Pohl ; AN 288.72
32441.4410	1	vi	R.Szafraniec ; AAC 4.81	37932.3970	1	vi	F.Gerhart ; AN 288.72
32794.4970	1	vi	R.Szafraniec ; AAC 4.113	37932.4060	1	pg	H.Huth ; MVS 3.170
32809.4430	1	vi	R.Szafraniec ; AAC 4.113	37934.5370	1	vi	K.Klocke ; BAVM 15
33170.3340	1	vi	R.Szafraniec ; AAC 5.5	37944.5060	1	vi	J.Duball ; BAVM 15
33187.4120	1	vi	R.Szafraniec ; AAC 5.5	37947.3540	1	vi	W.Braune ; BAVM 15
33538.3440	1	vi	R.Szafraniec ; AAC 5.7	37956.6032	1	pe	Chou & Kitamura ; JKAS 1
33570.3780	1	vi	R.Szafraniec ; AAC 5.11	37983.6528	1	pe	Chou & Kitamura ; JKAS 1
33871.4780	1	vi	R.Szafraniec ; AAC 5.11	38253.4300	1	vi	P.Flin ; AA 17.62
33913.4740	1	vi	A.Kruszewski ; AA 6.140	38255.5610	1	vi	H.Huth ; MVS 3.170
33916.3240	1	vi	A.Kruszewski ; AA 6.140	38290.4530	1	pg	H.Huth ; MVS 3.170
33918.4510	1	vi	A.Kruszewski ; AA 6.140	38322.4780	1	vi	V.Orlovius ; AN 288.72
33928.4240	1	vi	R.Szafraniec ; AAC 5.11	38399.3620	1	vi	P.Hoffmann ; BAVM 18
34239.4900	1	vi	R.Szafraniec ; AAC 5.53	38591.5270	1	pg	H.Huth ; MVS 3.170
34254.4410	1	vi	R.Szafraniec ; AAC 5.191	39006.5324	1	pe	S.M.Rucinski ; AA 17.275
34580.4550	1	vi	R.Szafraniec ; AAC 5.191	39026.4630	1	vi	W.Braune ; BAVM 18
34664.4400	1	vi	R.Szafraniec ; AAC 5.191	39046.3940	1	vi	W.Braune ; BAVM 18
35010.3850	1	vi	R.Szafraniec ; AAC 5.194	39056.3620	1	vi	W.Braune ; BAVM 18
35341.3830	1	vi	R.Szafraniec ; AA 6.143	39061.3430	1	vi	K.Locher ; ORI 95
35366.3020	1	vi	R.Szafraniec ; AA 6.143	39352.4790	1	vi	W.Braune ; BAVM 23
35699.4320	1	vi	R.Szafraniec ; AA 7.190	39374.5440	1	vi	K.Locher ; ORI 100
35719.3550	1	vi	R.Szafraniec ; AA 7.190	39387.3600	1	vi	W.Braune ; BAVM 23
35731.4490	1	vi	R.Szafraniec ; AA 7.190	39389.4960	1	vi	W.Braune ; BAVM 23
35746.4090	1	vi	R.Szafraniec ; AA 7.190	39407.2890	1	vi	M.Seidl ; BAVM 23
35838.2310	1	pg	H.Huth ; MVS 3.170	39407.2930	1	vi	K.Locher ; ORI 100
36079.5490	1	pg	H.Huth ; MVS 3.170	39419.4010	1	vi	S.Hazer ; AN 291.113
36450.3900	1	vi	R.Szafraniec ; AA 9.49	39683.4680	1	vi	K.Locher ; ORI 103
36455.3779	1	vi	J.Kordylewski ; SAC 30.108	39827.2630	1	vi	K.Locher ; ORI 105
36462.4880	1	pg	H.Huth ; MVS 3.170	40088.4990	1	vi	F.Hromada ; BRNO 9
36818.3880	1	pg	H.Huth ; MVS 3.170	40114.8356	1	pe	L.Binnendijk ; AJ 78.97
40127.6488	1	pe	L.Binnendijk ; AJ 78.97	41928.5370	1	vi	W.Quester ; BAVM 28
40128.3600	1	vi	P.Flin ; IBVS 328	41931.3750	1	vi	R.Germann ; BBS 11
40159.6796	1	pe	L.Binnendijk ; AJ 78.97	41931.3930	1	vi	I.Kohoutek ; BRNO 17
40175.3430	1	vi	W.Braune ; BAVM 23	41941.3530	1	vi	H.Peter ; BBS 11
40424.4746	1	pe	N.Gudur ; IBVS 456	41983.3490	1	pg	P.Ahnert ; MVS 7.38
40471.4540	1	vi	J.Silhan ; BRNO 9	41983.3560	1	vi	J.Hudec ; BRNO 17
40476.4370	1	vi	J.Silhan ; BRNO 9	41988.3210	1	vi	R.Germann ; BBS 12
40483.5590	1	vi	M.Fernandes ; BAVM 26	42008.2630	1	vi	H.Peter ; BBS 12
40500.6394	1	pe	L.Binnendijk ; AJ 78.97	42274.4860	1	vi	J.Hudec ; BRNO 20
40506.3380	1	vi	K.Rausal ; BRNO 12	42289.4270	1	vi	H.Peter ; BBS 17
40512.7402	1	pe	L.Binnendijk ; AJ 78.97	42289.4290	1	pe	O.Demircan ; IBVS 1053
40526.2640	1	vi	K.Locher ; ORI 116	42301.5400	1	vi	J.Hudec ; BRNO 20
40725.5750	1	vi	K.Locher ; ORI 119	42304.3760	1	vi	R.Germann ; BBS 17
40772.5510	1	vi	K.Locher ; ORI 120	42304.3960	1	vi	M.Vlcek ; BRNO 20
40812.4130	1	vi	W.Braune ; BAVM 25	42403.3170	1	vi	K.Locher ; BBS 19
40837.3269	1	pe	O.Demircan ; IBVS 530	42403.3220	1	vi	H.Peter ; BBS 19
40837.3290	1	vi	W.Braune ; BAVM 25	42403.3240	1	vi	R.Diethelm ; BBS 19
40837.3300	1	vi	J.Hubscher ; BAVM 25	42739.2950	1	vi	W.Braune ; BAVM 29
40839.4630	1	vi	R.Diethelm ; ORI 121	42739.3000	1	vi	H.Peter ; BBS 24
40854.4130	1	vi	M.Geseova ; BRNO 12	42754.2470	1	vi	H.Peter ; BBS 25
40856.5400	1	vi	M.Geseova ; BRNO 12	42776.2960	1	vi	R.Germann ; BBS 25
40859.3930	1	pe	C.Endres ; IBVS 530	42786.2710	1	vi	R.Germann ; BBS 26
40859.3960	1	pg	P.Ahnert ; MVS 6.9	42786.2750	1	vi	H.Peter ; BBS 26
40886.4480	1	vi	H.Gese ; BRNO 12	42796.2400	1	vi	H.Peter ; BBS 26
40911.3530	1	vi	K.Locher ; ORI 122	42990.5700	1	vi	K.Locher ; BBS 29
40921.3240	1	vi	K.Locher ; ORI 122	42993.4120	1	vi	K.Locher ; BBS 29
41155.5040	1	vi	L.Frasinski ; IBVS 584	43013.3510	1	vi	R.Germann ; BBS 29
41177.5740	1	vi	K.Locher ; ORI 126	43015.4802	1	pe	J.Ebersberger ; IBVS 1358
41210.3240	1	vi	H.Peter ; ORI 127	43015.4840	1	vi	P.Simecek ; BRNO 21
41232.3940	1	vi	K.Locher ; ORI 127	43034.7010	1	vi	G.Samolyk ; AOEB 2
41247.3320	1	vi	K.Locher ; ORI 129	43040.3980	1	vi	K.Locher ; BBS 30
41267.2632	1	vi	W.Braune ; BAVM 25	43069.5700	1	vi	E.Halbach ; AOEB 2
41513.5560	1	vi	K.Locher ; BBS 4	43069.5830	1	vi	G.Samolyk ; AOEB 2
41550.5620	1	vi	K.Locher ; BBS 5	43071.0029	1	pe	H.D.Kennedy ; IBVS 2118
41563.3810	1	vi	H.Peter ; BBS 5	43112.2910	1	vi	R.Germann ; BBS 31
41565.5120	1	vi	K.Locher ; BBS 5	43134.3600	1	vi	R.Germann ; BBS 31
41580.4600	1	vi	K.Locher ; BBS 5	43154.2880	1	vi	R.Germann ; BBS 32
41595.4070	1	vi	R.Diethelm ; BBS 6	43311.5940	1	vi	K.Locher ; BBS 33
41597.5432	1	vi	W.Quester ; BAVM 26	43341.4850	1	vi	K.Vojtek ; BRNO 21
41605.3720	1	vi	W.Quester ; BAVM 26	43371.3870	1	vi	R.Germann ; BBS 34
41605.3730	1	vi	K.Locher ; BBS 6	43391.3190	1	vi	R.Germann ; BBS 35
41605.3780	1	vi	H.Peter ; BBS 6	43393.4570	1	vi	K.Locher ; BBS 35
41657.3370	1	vi	R.Diethelm ; BBS 7	43393.4730	1	vi	P.Ivan ; BRNO 21
41682.2470	1	vi	J.Hubscher ; BAVM 26	43403.4350	1	vi	P.Ivan ; BRNO 21
41682.2500	1	vi	W.Braune ; BAVM 26	43425.4940	1	vi	K.Vojtek ; BRNO 21
41921.4270	1	vi	Z.Pokorny ; BRNO 17	43433.3230	1	vi	D.Lichtenknecker ; BAVM 31
43434.0295	1	pe	H.D.Kennedy ; IBVS 2118	44517.4160	1	vi	G.Mavrofridis ; BBS 51
43435.4610	1	vi	D.Lichtenknecker ; BAVM 31	44517.4190	1	vi	G.Stefanopoulos ; BBS 52
43455.3900	1	vi	J.Soukopova ; BRNO 21	44524.5340	1	vi	G.Mavrofridis ; BBS 51
43460.3740	1	vi	D.Sasselov ; BRNO 21	44532.3640	1	vi	W.Braune ; BAVM 32
43490.2640	1	vi	J.Mrazek ; BRNO 21	44543.0401	1	pe	H.D.Kennedy ; IBVS 2118
43495.2440	1	vi	R.Germann ; BBS 36	44557.9879	1	pe	H.D.Kennedy ; IBVS 2118
43517.3180	1	vi	R.Germann ; BBS 36	44567.2420	1	vi	H.Peter ; BBS 51
43689.5710	1	vi	K.Locher ; BBS 37	44567.2450	1	vi	R.Germann ; BBS 51
43724.4540	1	vi	P.Simecek ; BRNO 23	44593.5840	1	vi	G.Hanson ; AOEB 2
43725.5179	2	pe	Z.Tufekcioglu ; IBVS 1495	44636.2870	1	vi	R.Germann ; BBS 52
43729.4333	1	pe	Z.Tufekcioglu ; IBVS 1495	44823.4940	1	vi	T.Kaczkowski ; MVS 9.90
43729.4380	1	vi	P.Ivan ; BRNO 23	44823.5000	1	vi	T.Graf ; BRNO 26
43756.4831	1	pe	Z.Tufekcioglu ; IBVS 1495	44843.4272	1	pe	E.Derman et al. ; IBVS 2159
43776.4140	1	vi	D.Lichtenknecker ; BAVM 31	44848.4102	1	pe	E.Derman et al. ; IBVS 2159
43780.3277	2	pe	Z.Tufekcioglu ; IBVS 1495	44853.3920	1	vi	H.Peter ; BBS 57
43791.3540	1	vi	R.Germann ; BBS 39	44853.3950	1	vi	K.Carbol ; BRNO 26
43791.3700	1	vi	H.Peter ; BBS 39	44883.2830	1	vi	N.Stoikidis ; BBS 57
43802.7600	1	vi	G.Samolyk ; AOEB 2	44890.4100	1	vi	H.Peter ; BBS 57
43803.4650	1	vi	H.Peter ; BBS 39	44893.2550	1	vi	N.Stoikidis ; BBS 57
43806.3090	1	vi	R.Germann ; BBS 39	44900.3870	1	vi	G.Mavrofridis ; BBS 57

Table 1 – continued from previous page

Min. Time (HJD-2400000)	Typ.	Meth.	Ref.	Min. Time (HJD-2400000)	Typ.	Meth.	Ref.
43863.2560	1	vi	R.Germann ; BBS 41	44910.3300	1	vi	N.Stoikidis ; BBS 57
43878.2020	1	vi	K.Locher ; BBS 41	44925.2840	1	vi	H.Peter ; BBS 57
44077.5070	1	vi	D.Svelohva ; BRNO 23	45170.8580	1	vi	E.Halbach ; AOEB 2
44092.4600	1	vi	K.Locher ; BBS 44	45196.4870	1	pe	A.Buchtler ; IBVS 2385
44102.4260	1	vi	V.Wagner ; BRNO 23	45201.4690	1	pe	M.Prikryl ; BRNO 26
44117.3690	1	vi	R.Germann ; BBS 44	45201.4720	1	vi	H.Peter ; BBS 62
44117.3770	1	vi	H.Peter ; BBS 44	45228.5220	1	vi	N.Machkova ; BRNO 26
44134.4580	1	vi	H.Peter ; BBS 45	45231.3690	1	vi	G.Mavrofridis ; BBS 63
44143.3560	2	pe	Z.Aslan et al. ; IBVS 1908	45235.6450	1	vi	G.Samolyk ; AOEB 2
44144.4227	1	pe	Z.Aslan et al. ; IBVS 1908	45258.4170	1	vi	H.Bohutinska ; BRNO 26
44164.3545	1	pe	U.S.Chaubey ; ASS 81.283	45554.5250	1	vi	P.Svoboda ; BRNO 26
44166.4920	1	vi	T.Brelstaff ; VSSC 59.19	45579.4470	1	vi	P.Svoboda ; BRNO 26
44189.2670	1	vi	H.Peter ; BBS 45	45609.3400	1	pg	M.Dietrich ; MVS 10.104
44219.1650	1	pe	U.S.Chaubey ; ASS 81.283	45609.3440	1	vi	M.Zejda ; BRNO 26
44435.5650	1	vi	K.Locher ; BBS 49	45624.2920	1	vi	N.Stoikidis ; BBS 69
44440.5400	1	vi	R.Germann ; BBS 49	45671.2750	1	vi	P.Svoboda ; BRNO 26
44445.5250	1	vi	K.Locher ; BBS 49	45915.4230	1	vi	H.Peter ; BBS 73
44455.4900	1	vi	K.Chyzny ; MVS 9.18	45976.6430	1	vi	D.Williams ; AOEB 2
44470.4380	1	vi	P.Kucera ; BRNO 23	45976.6500	1	vi	S.Cook ; AOEB 2
44474.7030	1	vi	G.Samolyk ; AOEB 2	45981.6290	1	vi	S.Cook ; AOEB 2
44490.3640	1	vi	R.Diethelm ; BBS 50	45992.3030	1	vi	A.Paschke ; BBS 74
44490.3660	1	vi	H.Peter ; BBS 50	46002.2610	1	vi	A.Paschke ; BBS 74
44497.4860	1	vi	G.Mavrofridis ; BBS 51	46019.3490	1	vi	S.Krampol ; BRNO 27
44502.4654	1	pe	D.Elias ; BBS 54	46028.6090	1	vi	D.Williams ; AOEB 2
44502.4690	1	vi	D.Mourikis ; BBS 50	46028.6110	1	vi	G.Samolyk ; AOEB 2
44512.4340	1	vi	H.Peter ; BBS 50	46029.3160	1	vi	A.Paschke ; BBS 74
46033.5850	1	vi	S.Cook ; AOEB 2	48148.3950	1	vi	J.Pietz ; BAVM 59
46038.5670	1	vi	D.Williams ; AOEB 2	48205.3360	1	vi	J.Pietz ; BAVM 59
46038.5680	1	vi	G.Samolyk ; AOEB 2	48219.5690	1	vi	G.Samolyk ; AOEB 2
46043.5530	1	vi	D.Williams ; AOEB 2	48266.5520	1	vi	G.Samolyk ; AOEB 2
46290.5420	1	vi	S.Stefanisko ; BRNO 27	48480.8140	1	vi	G.Samolyk ; AOEB 2
46294.1170	1	vi	T.Kato ; VSB 47	48481.5240	1	vi	J.Sojka ; BRNO 31
46305.5010	1	vi	A.Paschke ; BBS 81	48500.0280	1	vis	Hipparcos ; ESA, 2001
46320.4500	1	vi	A.Paschke ; BBS 81	48506.4230	1	vi	L.Honzik ; BRNO 31
46344.6500	1	vi	S.Cook ; AOEB 2	48543.8039	2	CCD	Hipparcos ; ESA, 2001
46350.3450	1	vi	A.Paschke ; BBS 81	48545.5870	1	vi	G.Samolyk ; AOEB 2
46355.3240	1	vi	O.Grugel ; BAVM 43	48554.8375	1	CCD	Hipparcos ; ESA, 2001
46360.3040	1	vi	M.Dietrich ; MVS 11.19	48859.5040	1	vi	J.Chlachula ; BRNO 31
46360.3100	1	vi	O.Grugel ; BAVM 43	48863.7660	1	vi	D.Williams ; AOEB 2
46382.3710	1	vi	M.Dietrich ; MVS 11.19	48873.7330	1	vi	R.Hill ; AOEB 2
46413.6980	1	vi	G.Samolyk ; AOEB 2	48894.3760	1	vi	R.Baule ; BAVM 62
46422.2380	1	vi	A.Paschke ; BBS 81	48935.3002	2	pe	S.ozdemir ; IBVS 4380
46656.4230	1	vi	M.Muller ; BAVM 46	48939.2161	1	pe	S.Selam ; IBVS 4380
46678.4870	1	vi	P.Hajek ; BRNO 28	49215.4130	1	vi	P.Stuchlik ; BRNO 31
46678.4900	1	vi	A.Paschke ; BBS 81	49224.6500	1	vi	S.Cook ; AOEB 2
46738.2760	1	vi	D.Hanzl ; BRNO 28	49241.7350	1	vi	D.Williams ; AOEB 2
46743.2730	1	vi	A.Stuhl ; BRNO 31	49246.3631	2	pe	H.Ak ; IBVS 4380
46759.6390	1	vi	G.Samolyk ; AOEB 2	49248.4963	2	pe	A.Akalin ; IBVS 4380
46769.6070	1	vi	G.Samolyk ; AOEB 2	49276.2546	2	pe	H.Dundar ; IBVS 4380
46774.5910	1	vi	G.Samolyk ; AOEB 2	49277.3259	1	pe	A.Akalin ; IBVS 4380
46779.5640	1	vi	G.Samolyk ; AOEB 2	49333.5600	1	vi	G.Samolyk ; AOEB 2
46999.5200	1	vi	G.Mavrofridis ; BBS 86	49543.5440	1	vi	C.Barani ; BBS 108
47014.4630	1	vi	F.Hroch ; BRNO 30	49543.5500	1	vis	F.Acerbi ; BBS 107
47014.4664	1	vi	E.Wunder ; BAVM 50	49553.5085	1	pe	B.Gurol ; IBVS 4380
47029.4110	1	vi	L.Prokesova ; BRNO 30	49602.6300	1	vi	G.Samolyk ; AOEB 2
47031.5490	1	vi	J.Kolar ; BRNO 30	49743.5640	1	vi	G.Samolyk ; AOEB 8
47034.4000	1	vi	M.Jechumtal ; BRNO 30	49948.5775	1	vi	M.Zibar ; BRNO 32
47039.3790	1	vi	O.Beck ; BRNO 30	49950.7020	1	CCD	S.Cook ; AOEB 8
47054.3330	1	vi	G.Mavrofridis ; BBS 86	50008.3599	1	CCD	W.Kleikamp ; BAVM 90
47066.4290	1	vi	A.Paschke ; BBS 86	50008.3603	1	CCD	M.Wolf ; BBS 110
47091.3460	1	vi	G.Mavrofridis ; BBS 86	50013.3417	1	vi	J.Cechal ; BRNO 32
47107.7180	1	vi	R.Hill ; AOEB 2	50044.6700	1	vi	G.Samolyk ; AOEB 8
47387.4590	1	vi	P.Adamek ; BRNO 30	50050.3564	1	pe	B.Gurol ; IBVS 4380
47387.4610	1	vi	A.Epple ; BAVM 52	50313.7370	1	vi	G.Samolyk ; AOEB 8
47392.4390	1	vi	P.Adamek ; BRNO 30	50318.7140	1	CCD	S.Cook ; AOEB 8
47464.3440	1	vi	G.Samolyk ; AOEB 2	50368.5414	1	vi	A.Dedoch ; BRNO 32
47469.3150	1	vi	G.Samolyk ; AOEB 2	50376.3686	1	CCD	W.Kleikamp ; BAVM 102
47474.3180	1	vi	H.Peter ; BBS 90	50396.3000	1	vi	M.Dietrich ; BAVM 101
47794.6200	1	vi	G.Samolyk ; AOEB 2	50423.3560	1	vi	D.Girrbach ; BAVM 101
47851.5610	1	vi	G.Samolyk ; AOEB 2	50667.4989	1	vi	J.Polak ; BRNO 32
47853.6930	1	vi	M.Smith ; AOEB 2	50672.4793	1	pe	D.Husar ; BAVM 111
48123.4760	1	vi	M.Copikova ; BRNO 31	50672.4805	1	pe	W.Ogloza ; IBVS 4534
50672.4909	1	vi	J.Minar ; BRNO 32	53251.3810	1	vi	R.Obertrifter ; BAVM 202
50712.3428	1	pe	D.Husar ; BAVM 111	53251.3840	1	vi	G.-U.Flechsig ; BAVM 174
50716.6150	1	vi	G.Samolyk ; AOEB 8	53251.3860	1	vi	K.Rutz ; BAVM 174
50717.3278	1	vi	L.Brat ; BRNO 32	53251.3910	1	vi	W.Braune ; BAVM 174
50717.3305	1	vi	P.Sobotka ; BRNO 32	53262.4225	2	CCD	F.Agerer ; BAVM 173
50717.3370	1	pg	M.Dietrich ; BAVM 113	53265.6239	1	vi	W.Ogloza et al. ; IBVS 5843
50719.4618	1	pe	D.Husar ; BAVM 111	53267.7510	1	CCD	W.Ogloza et al. ; IBVS 5843
50754.3480	1	vi	R.Meyer ; BAVM 113	53267.7592	1	CCD	G.Samolyk ; AOEB 11
51035.4000	1	pe	B.Gurol ; IBVS 5069	53272.7416	1	CCD	W.Ogloza et al. ; IBVS 5843
51045.4699	1	vi	M.Vetrovcova ; BRNO 32	53282.7068	1	CCD	W.Ogloza et al. ; IBVS 5843
51076.7940	1	vi	D.Williams ; AOEB 8	53285.5570	1	vi	G.Chaple ; AOEB 11
51079.6400	1	vi	D.Williams ; AOEB 8	53290.5400	1	vi	G.Chaple ; AOEB 11
51084.6290	1	vi	G.Samolyk ; AOEB 8	53292.6790	1	vi	C.Stephan ; AOEB 11
51141.5690	1	vi	G.Samolyk ; AOEB 8	53317.5870	1	pe	G.Lubcke ; JAAVSO 41;328
51422.0120	1	CCD	A.Paschke ; Amateur	53325.4174	1	CCD	W.Quester ; BAVM 173
51432.7010	1	vi	D.Williams ; AOEB 8	53614.4169	1	CCD	V.Bakis et al. ; IBVS 5662
51433.4096	1	CCD	L.Kral ; BRNO 32	53619.3969	1	vi	P.Hejduk ; OEJV 0074
51452.6310	1	vi	G.Samolyk ; AOEB 8	53634.3450	1	CCD	M.Dietrich ; BAVM 178
51467.5790	1	vi	D.Williams ; AOEB 8	53645.0238	1	CCD	Kubotera ; VSB 44
51807.4721	2	CCD	W.Kleikamp ; BAVM 152	53645.7354	1	CCD	G.Samolyk ; AOEB 11
51818.5020	1	CCD	H.Achterberg ; BAVM 152	53671.3609	1	CCD	R.Ehrenberger ; OEJV 0074
51842.7060	1	vi	R.Hill ; AOEB 8	53674.9210	1	vi	Hirosawa ; VSB 44
51868.3321	1	CCD	M.Dietrich ; BAVM 152	53728.3061	1	CCD	J.Coloma ; AOEB 11
52168.7180	1	vi	D.Williams ; AOEB 8	53945.4760	1	CCD	K.Rutz ; BAVM 187
52203.5970	1	vi	D.Williams ; AOEB 8	53967.4772	2	CCD	S.Parimucha et al. ; IBVS 5777
52278.3363	1	CCD	G.Maintz ; BAVM 152	53991.3226	1	vi	S.Dogru et al. ; IBVS 5746
52530.3191	1	CCD	M.Dietrich ; BAVM 158	53992.3940	1	vi	W.Braune ; BAVM 187
52542.7862	2	CCD	Karska & Maciejewski ; IBVS 5380	53993.1031	1	CCD	K.Nagai et al. ; VSB 45
52567.3312	1	CCD	U.Schmidt ; BAVM 158	54016.5920	1	vi	G.Chaple ; AOEB 12
52572.6843	2	CCD	Karska & Maciejewski ; IBVS 5380	54023.7150	1	vi	D.Williams ; AOEB 12
52573.0329	1	CCD	Karska & Maciejewski ; IBVS 5380	54024.4239	1	CCD	F.Agerer ; BAVM 183
52594.3820	1	pe	T.Tanriverdi et al. ; IBVS 5407	54027.2706	1	CCD	R.Ehrenberger ; OEJV 0074
52843.5166	1	CCD	B.Gurol et al. ; IBVS 5791	54032.9670	1	vi	K.Nagai et al. ; VSB 45
52848.5024	1	vi	L.Marcin ; OEJV 0074	54058.5920	1	vi	C.Stephan ; AOEB 12
52848.5081	1	vi	J.Pcola ; OEJV 0074	54059.3020	1	pe	H.V. Senavci et al. ; IBVS 5754
52888.3606	1	CCD	T.Krajci ; IBVS 5592	54063.5720	1	vi	C.Stephan ; AOEB 12
52903.3083	1	CCD	M.Dietrich ; BAVM 172	54070.3254	2	pe	H.V. Senavci et al. ; IBVS 5754
52908.2924	1	CCD	M.Dietrich ; BAVM 172	54096.3177	1	CCD	R.Ehrenberger ; OEJV 0074
52911.1395	1	CCD	Nakajima ; VSB 42	54298.4676	1	vi	M.Mruz ; OEJV 0094
52950.2871	1	CCD	B.Schlereth ; BAVM 172	54309.5089	2	CCD	S.Parimucha et al. ; IBVS 5898
52986.5913	1	CCD	S.Dvorak ; AOEB 11	54335.4878	1	pe	T.Kilicoglu et al. ; IBVS 5801

Table 1 – continued from previous page

Min. Time (HJD-2400000)	Typ.	Meth.	Ref.	Min. Time (HJD-2400000)	Typ.	Meth.	Ref.
52993.7110	1	vi	G.Samolyk ; AOEB 11	54335.4887	1	CCD	L.melcer ; OEJV 0074
53001.5420	1	vi	D.Williams ; AOEB 11	54345.4486	1	CCD	S.Caliskan ; Nat. Ast. Cong., 2008
53236.4399	1	vis	J.Cernu ; OEJV 0074	54351.5003	2	CCD	S.Caliskan ; Nat. Ast. Cong., 2008
53236.4400	1	pe	B.Albayrak et al. ; IBVS 5649	54394.5693	1	CCD	G.Samolyk ; JAAVSO 36(2);171
53236.4476	1	vi	M.Zdvoruk ; OEJV 0074	54416.6361	1	CCD	J.Bialozynski ; JAAVSO 36(2);171
54436.5670	1	CCD	S.Dvorak ; IBVS 5814	56501.5600	1	CCD	K.Rutz ; BAVM 234
54710.6180	1	CCD	G.Samolyk ; JAAVSO 36(2);186	56537.8635	1	CCD	G.Samolyk ; JAAVSO 41;328
54738.3787	1	CCD	S.Parimucha et al. ; IBVS 5898	56557.7934	1	CCD	B.Manske ; JAAVSO 41;328
54774.6840	1	CCD	R.Diethelm ; IBVS 5871	56557.7946	1	CCD	G.Frey ; JAAVSO 42;426
54799.5955	1	CCD	K.Menzies ; JAAVSO 37(1);44	56565.6246	1	CCD	B.Manske ; JAAVSO 41;328
55044.4620	1	CCD	N.Erkan et al. ; IBVS 5924	56567.7599	1	CCD	G.Frey ; JAAVSO 42;426
55064.3929	1	CCD	G.-U.Flechsig ; BAVM 212	56572.7430	1	CCD	G.Frey ; JAAVSO 42;426
55085.7474	1	CCD	G.Samolyk ; JAAVSO 38;120	56577.7255	1	CCD	G.Frey ; JAAVSO 42;426
55116.3557	1	CCD	N.Erkan et al. ; IBVS 5924	56587.6911	1	CCD	G.Frey ; JAAVSO 42;426
55429.5569	1	CCD	S.Dogru et al. ; IBVS 5988	56588.4035	1	CCD	F.Agerer ; BAVM 234
55498.2485	2	CCD	S.Parimucha et al. ; IBVS 5980	56597.6568	1	CCD	G.Frey ; JAAVSO 42;426
55524.9404	1	CCD	K.Hirosawa ; VSB 51	56602.6394	1	CCD	G.Frey ; JAAVSO 42;426
55561.2440	1	CCD	L.melcer ; OEJV 0137	56905.5192	2	CCD	M. Masek ; BRNO 40
55820.3460	1	CCD	A.Paschke ; OEJV 0142	56929.3667	1	CCD	F.Agerer ; BAVM 239
55820.3461	1	CCD	M.Dietrich ; BAVM 225	56930.4362	1	CCD	F.Agerer ; BAVM 239
55867.3270	1	CCD	L.melcer ; OEJV 0160	56953.5685	1	CCD	N.Simmons ; JAAVSO 43-1
55887.2592	1	CCD	D.Buhme ; BAVM 225	56955.7049	1	CCD	G.Frey ; JAAVSO 44-1
56163.4447	1	CCD	S.Parimucha et al. ; IBVS 6044	57251.8222	1	CCD	K.Menzies ; JAAVSO 43-2
56210.0691	2	CCD	Y. Yang ; AJ 147	57267.4823	1	CCD	E. Bahar ; IBVS 6209
56211.1365	1	CCD	Y. Yang ; AJ 147	57278.5163	1	CCD	F.Agerer ; IBVS 6196
56212.2052	2	CCD	Y. Yang ; AJ 147	57308.7680	1	CCD	G.Frey ; JAAVSO 44-1
56219.6785	1	CCD	G.Frey ; JAAVSO 42;426	57327.2750	2	CCD	S.Parimucha ; IBVS 6167
56229.6439	1	CCD	G.Frey ; JAAVSO 42;426	57390.6267	1	CCD	R.Sabo ; JAAVSO 44-1
56231.7796	1	CCD	G.Frey ; JAAVSO 42;426	58059.3779	2	CCD	our study ; –
56256.6934	1	CCD	G.Frey ; JAAVSO 42;426	58060.4456	1	CCD	our study ; –

Thus, the new ephemeris was calculated as;

$$\mathrm{HJD_{MinI}} = 2455867.327300(81) + 0\overset{\mathrm{d}}{.}711816455(19) \times E. \qquad (1)$$

The O–C diagram shown in Figure 1 (top panel) displayed two sinusoidal curves superimposed on each other. Of which, the primary curve had an eccentric cyclic change which had almost three maximum and two minima. Also, the residuals from the sinusoidal fit showed another low-amplitude, short-period and eccentric cyclic modulation having three minima and four maxima. Our observational CCD minima were the last two points plotted on the O–C diagram. These points allowed us to determine the turn point of the last maximum of the O–C curve.

We first used the Period04 program (Lenz and Breger 2005) to analyse the weighted data. Then, we extracted the individual frequencies causing the fluctuations. Two frequencies of f_1 = 0.000041375 c/E (A_1=0.0082, S/N = 7.84) and f_2 = 0.000072382 c/E (A_1=0.0059, S/N = 18.04), shown in Figure 2, were detected. These frequencies corresponded to two periods of 47.10 ± 0.63 and 26.92 ± 0.44 years, respectively. When these two theoretical frequencies were adjusted to the O–C diagram in Figure 1, they were in good agreement with observational data. For the eccentricities seen in the curves, the light-time effect caused by the third and fourth bodies in the system was considered. In order to derive light-time orbits and the parameters of the third and fourth additional bodies, we used the equations given by Irwin (1952). Furthermore, the computer code called OC2LTE30 (Ak et al. 2004) was used to determine the orbital parameters. All of these results are presented in Table 2.

In Figure 1, the orbital parameters of the third and fourth body are presented in the second and the third panels. The sum of these lines, which corresponds to the total theoretical O–C curve, are shown as the continuous line in the first panel. The sum of the least squares of the total residuals is 1.6×10^{-2} day^2. The estimated errors of these parameters arise from the non-linear least-squares method, on which the inverse problem solving method is based. This method does not take into account the error of each observation point and the possible correlations of fitted parameters with each other. Therefore, the standard error values given for the parameters may be smaller than they should be. So, the standard error values given in the table should be considered as the lowest limits.

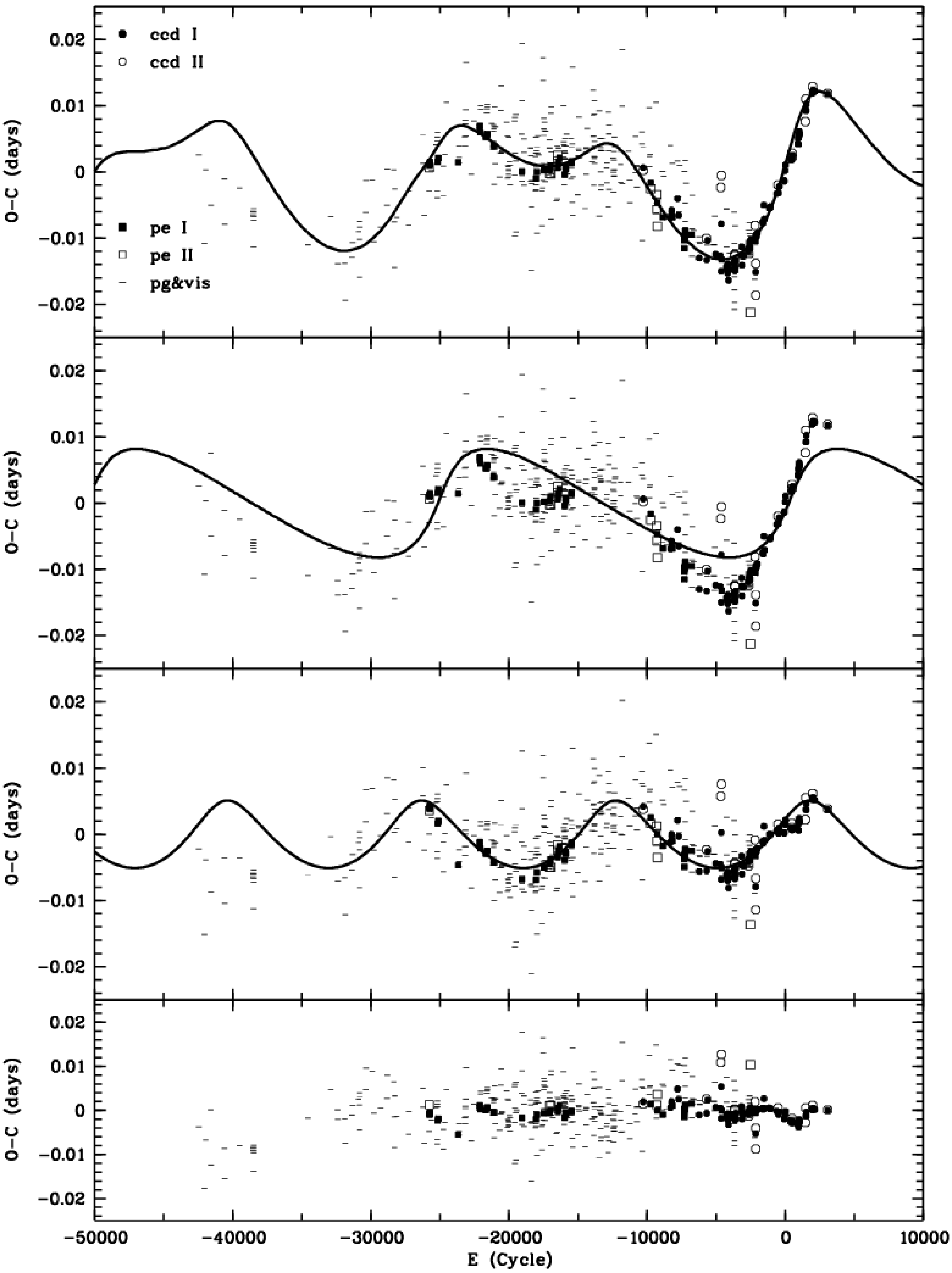

Figure 1. The O–C diagram of DI Peg. The first panel shows the overall data and the total theoretical O–C variation (continuous line). While the second panel presents the primary and highly eccentric sinosoidal variation, the residual data which have another sinusoidal modulation are displayed in the third panel. The final residuals are given in the last panel.

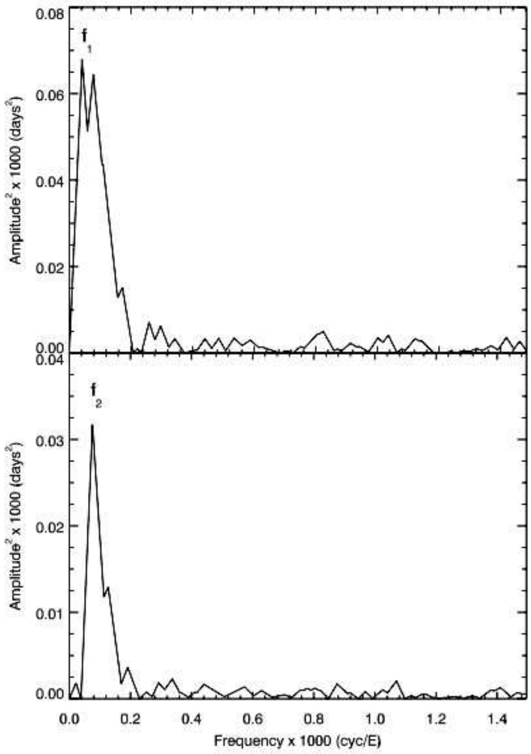

Figure 2. The two frequencies of $f_1 = 0.000041375$ and $f_2 = 0.000072382$ c/E detected by PERIOD04.

Table 2. Parameters and standard errors derived from O–C analysis of each additional body.

Parameters	Third Body	Fourth Body
$P_{3,4}$ [years]	49.50 ± 0.36	27.40 ± 0.24
A [days]	0.0082 ± 0.0002	0.0051 ± 0.0002
e'	0.61 ± 0.06	0.30 ± 0.08
ω' [°]	7.00 ± 1.74	75.00 ± 3.63
T' [HJD]	2456220 ± 261	2456860 ± 150
$f\ (m_{3,4})$ [$M_\odot$]	0.0023 ± 0.0007	0.0009 ± 0.0001
$m[M\odot]$	0.2135 ± 0.0213	0.1505 ± 0.0075
$L_{\rm Bol}$ [$L_\odot$]	0.0061 ± 0.0017	0.0025 ± 0.0003
$M_{\rm Bol}$ [mag]	10.23 ± 0.27	11.22 ± 0.14
$m_{\rm Bol}$ [mag]	18.22 ± 1.38	19.21 ± 1.24
θ [arcsec]	0.0915 ± 0.0277	0.0625 ± 0.0184
$\sum(O-C)^2$ [day^2]	260×10^{-4}	138×10^{-4}

4 Results and Discussion

An O–C diagram is a special plot generally used to determine period changes that are difficult to detect by direct measurements. If there is not any measurable change in period, then the O–C difference generates a straight line. If any variation in period is detected, however, the O–C data generate a structure that displays the characteristic of the mechanism causing this variation. These mechanisms can be arranged as: mass transfer between components or mass loss from the system, spin-orbital interactions, angular momentum loss through stellar winds, gravitational waves, oscillations in rotation, differential rotation, apsidal motion, presence of a third light, and magnetic activity (Mikulasek et al. 2012).

In terms of binarity, orbital period change is quite an important subject since it is related to the formation, structure, and evolution of binary stars. These variables gain and lose mass and angular momentum as specified by Roche geometry. These events are the first proposed mechanisms to explain observed period changes. Both of these mechanisms can increase or decrease the period of the system and generate parabolic structures in the O–C diagram. The mass transfer between components is more effective in changing the orbital period than the mass loss from the system. The most basic case to be considered for exchanging material between components is conservative mass transfer. In this case, the mass lost by one component is gained by the companion star, so the total mass of the system and thus the total orbital angular momentum is preserved.

Among the common mechanisms given above, apsidal motion involves a change in the orientation of the system's major axis, since the potential energy between the components does not exactly obey Newton's gravitational law. In the O–C diagram, the times for secondary and primary minima shift in opposite directions. However, as this mechanism requires large eccentricities, it is rarely observed (Zavala et al. 2002). Alternatively, it is assumed that the cyclic pattern is caused by the presence of a third body in the system. Based on this assumption, the primary and secondary eclipse times are produced by the motion of the binary around the common centre of mass of a triple system. In this case, the periodic pattern arises from the light-time effect (Borkovits and Hegedüs 1996).

Apart from these, another mechanism to cause period variation in binary stars is magnetic activity cycles. In the systems having late-type components, if the shape of the companion star is distorted by tidal and centrifugal forces, changes in the internal rotation associated with a magnetic activity cycle vary the gravitational quadrupole moment. As the quadrupole moment increases, the gravitational field increases leading to a decrease in the period. Otherwise, if the quadrupole moment decreases, the orbital period increases (Applegate 1992). Magnetic activity produces cyclic modulations in the O–C diagram, and their periods are from years to decades.

In Algols, alternate orbital period changes are well known in systems with a late-type secondary star (Zavala et al. 2002). For a binary system, cyclic period variability are generally thought to be caused by either magnetic activity in one or both components (Applegate 1992) or light-time effect due to a third body (Irwin 1952). In terms of magnetic activity, observed oscillations are arisen from the variations of the gravitational quadrupole moment (ΔQ), which is typically around $10^{51} - 10^{52}$ g cm^2 for close binaries and can be calculated from the equation of

$$\frac{\Delta P}{P} = \frac{-9\Delta Q}{Ma^2} \approx \frac{2\pi A_{\rm sin}}{P_{\rm sin}} \tag{2}$$

where M is the mass of the active component (Lanza 2002).

In the case of DI Peg, the O–C diagram shows neither a parabolic change which is an indication of a mass transfer between the components or a mass loss from the system, nor anti-correlation between the primary and secondary minimum timings that is a sign for a change in the orientation of the binary's major axis. On the other hand, it is known that the star has a late-type companion (K4). For this reason, there is a potential that this component may show magnetic activity. In order to search this possibility, we calculate the gravitational quadrupole moment (ΔQ) of the secondary star by using

$\Delta P/P = 3.20 \times 10^{-6}$ which is calculated in this study and by adopting $M_1 = 1.18(3)$ M$_\odot$, $M_2 = 0.70(2)$ M$_\odot$, and $a = 4.14(5)$ R$_\odot$ from Lu (1992). As a result, we find the variation of the quadrupole moment of the star to be $\Delta Q_2 = 4.11 \times 10^{49}$ g cm^2. Since this result is clearly smaller than the typical value and the sinusoidal variations are eccentric, it is unlikely that magnetic activity is responsible for the periodic modulations in DI Peg.

Therefore, two sinusoidal changes can be more likely attributed to the light-time effects due to the presence of two additional bodies. Since the third body is confirmed from the spectroscopic study by Lu (1992), we calculate the specific parameters of the third body under the assumption of the presence of an object gravitationally bound to the system. From the O–C diagram, the period and amplitude of the primary modulation are found to be 49.50±0.36 yr and 0.0082 days. The projected distance of the mass center of the eclipsing pair to the center of mass of the triple system is around 1.78±0.16 au. By using these values the mass function of the third-body is found to be 0.0023(7). If the third-body orbit is co-planar with the orbit of the system (i.e., $i \sim 90°$), its mass would be 0.21(2) M$_\odot$. Also, from the Kepler's third law, the semi-major axis of the orbit is computed as 15.75(7) au. By adopting the parallax of the star from van Leeuwen (2007), we derive the distance of d $\sim$ 191(43) parsecs and hence the maximum angular separation of the third body from the eclipsing pair to be 0.091(28) arcsec. Using the mass-luminosity relation for main-sequence stars given by Demircan and Kahraman (1991), we can estimate the bolometric absolute magnitude of the third body for the given distance to be about $M_{\rm bol} = 10.23(27)$ mag. According to Allen's table (Cox 2000), the spectral type for the third body can be estimated to be M3, which points a red dwarf.

Additionally, as mentioned in the previous section, the residuals from the sine fit show another low-amplitude, short-period and eccentric cyclic modulation. This variation is also interpreted as the existence of a fourth body physically connected to the system by Yang et al. (2014). From the O–C diagram, we calculated the period and amplitude of the secondary modulation as 27.40(24) yr and 0.0051(2) days. The mass function and the mass of the fourth body are $f(m_4) = 0.0009(1)$ and $M_4 = 0.151(75)$ M$_\odot$. Assuming that the object orbits in the same plane as the system and taking the aforementioned distance value into account, we find the angular separation of the fourth body from the eclipsing pair to be 0.0615(183) arcsec. By using the mass-luminosity relation for main-sequence stars given by Demircan and Kahraman (1991), we estimate the bolometric absolute magnitude of the fourth body to be about $M_{bol} = 11.22(14)$ mag. According to Allen's table (Cox 2000), the additional fourth body may be a M4 spectral type red dwarf.

Additionally, from Figure 1, the residuals of two sinusoidal fits still seem to show another modulation. The period and amplitude of this modulation are roughly $P =$ 19.5 years and $A = 0.004$ days. However, it is not possible to attribute this change as another object that is in orbit around the binary system. Therefore, we recommend future photometric and spectroscopic observations to reveal the true nature of DI Peg.

Acknowledgements We thank Ankara University Kreiken Observatory for the support of project number T35_2017_IV_06. This research has made use of the SIMBAD database, operated at CDS, Strasbourg, France, and of NASA's Astrophysics Data System Bibliographic Services.

References:

Ahnert P., 1974, *MitVS*, **6**, 158
Ak, T., Albayrak, B., Selam, S.O., Tanriverdi, T.: 2004, *NewA*, **9**, 265 DOI

Applegate, J.H., 1992, *ApJ* **385**, 621 DOI
Binnendijk, L. 1973, *AJ*, **78**, 97 DOI
Borkovits, T. and Hegedűs, T., 1996, *A&AS* **120**, 63
Borkovits, T., Rappaport, S., Hajdu, T., Sztakovics, J., 2015, *MNRAS* **448**, 946 DOI
Borkovits, T., Hajdu, T., Sztakovics, J., Rappaport, S., Levine, A., Bíró, I.B., Klagyivik, P., 2016, *MNRAS* **455**, 4136 DOI
Chaubey, U. S., 1982, *Ap&SS*, **81**, 283 DOI
Chauvin G., Lagrange A.-M., Udry S., Mayor M., 2007, *A&A*, **475**, 723 DOI
Chou, K. C., and Kitamura, M., 1968, *JKAS*, **1**, 1
Conroy, K.E., Prša, A., Stassun, K.G., Orosz, J.A., Fabrycky, D.C., Welsh, W.F., 2014, *AJ* **147**, 45 DOI
Cox A. N., 2000, *Allan's astrophysical quantities*, New York, AIP Press, Springer
Demircan O., Kahraman G., 1991, *Ap&SS*, **181**, 313 DOI
Dvorak R., 1986, *A&A*, **167**, 379
Evans D. S., 1968, *QJRAS*, **9**, 388
Furlan E., et al., 2007, *ApJ*, **664**, 1176 DOI
Hanna M. A., Amin S. M., 2013, *JKAS*, **46**, 151 DOI
Gaposchkin, S., 1953, *AnHar*, **113**, 67C
Irwin J. B., 1952, *ApJ*, **116**, 211 DOI
Jensch, A., 1934, *AN*, **252**, 393 DOI
Kruszewski, A.: 1964, *AcA*, **14**, 241
Kwee K. K., van Woerden H., 1956, *BAN*, **12**, 327
Lanza, A.F. and Rodonò, M.: 2002, *AN* **323**, 424 DOI
Lee J. W., Lee C.-U., Kim S.-L., Kim H.-I., Park J.-H., 2012, *AJ*, **143**, 34 DOI
Lehmann, H., Borkovits, T., Rappaport, S.A., Ngo, H., Mawet, D., Csizmadia, S., Forgács-Dajka, E., 2016, *ApJ* **819**, 33 DOI
Lim J., Takakuwa S., 2006, *ApJ*, 653, 425 DOI
Lenz, P., and Breger, M.: 2005, *CoAst*, **146**, 53 DOI
Lu, W., 1992, *AcA*, **42**, 73
Marzari F., Scholl H., Thébault P., Baruteau C., 2009, *A&A*, **508**, 1493 DOI
Mikulášek, Z., Zejda, M., Janík, J., 2012, *IAUS*, **282**, 391 DOI
Morgenroth, O., 1934, *AN*, **252**, 389 DOI
Neuhäuser R., Mugrauer M., Fukagawa M., Torres G., Schmidt T., 2007, *A&A*, **462**, 777 DOI
Pribulla T., et al., 2012, *AN*, **333**, 754 DOI
Qian, S., 2001, *MNRAS*, **328**, 914 DOI
Rafert J. B., 1982, *PASP*, **94**, 485 DOI
Rappaport, S., Lehmann, H., Kalomeni, B., Borkovits, et al., 2016, *MNRAS* **462**, 1812 DOI
Rappaport, S., Vanderburg, A., Borkovits, T., et al., 2017, *MNRAS* **467**, 2160 DOI
Reipurth B., 2000, *AJ*, **120**, 3177 DOI
Rucinski, R., 1967, *AcA*, **17**, 271
Schwarz R., Haghighipour N., Eggl S., Pilat-Lohinger E., Funk B., 2011, *MNRAS*, **414**, 2763 DOI
van den Berk J., Portegies Zwart S. F., McMillan S. L. W., 2007, *MNRAS*, **379**, 111 DOI
van Leeuwen F., 2007, *A&A*, **474**, 653 DOI
Vinkó, J., 1992, *IBVS*, **3757**, 1
Yang Y.-G., Yang Y., Li S.-Z., 2014, *AJ*, **147**, 145 DOI
Zavala, R.T., McNamara, B.J., Harrison, T.E., et al., 2002, *AJ* **123**, 450. DOI

COMMISSIONS G1 AND G4 OF THE IAU
INFORMATION BULLETIN ON VARIABLE STARS
Volume 63 Number 6253 DOI: 10.22444/IBVS.6253

Konkoly Observatory
Budapest
12 September 2018

HU ISSN 0374 – 0676

SU Aur:
A DEEP FADING EVENT IN VISIBLE AND NEAR-INFRARED BANDS

GRANKIN, K.N.[1]; SHENAVRIN, V.I.[2]; IRSMAMBETOVA, T.R.[2]; PETROV, P.P.[1]

[1] Crimean Astrophysical Observatory, 298409 Nauchny, Republic of Crimea

[2] Lomonosov Moscow State Univ., Sternberg Astron. Inst., Universitetsky pr. 13, 119234 Moscow, Russia

email: konstantin.grankin@craocrimea.ru, vshen@inbox.ru, veratri@yandex.ru, petrogen@rambler.ru

SU Aur is one of the brightest classical T Tauri stars (cTTS). It is located in the Taurus-Aurigae star-forming region at the distance of about 140 pc. The star is of spectral type G2 III-IV. Its mass $M = 1.9 \pm 0.1 M_\odot$ and luminosity $L = 9.2 \pm 2.8 L_\odot$ (Grankin 2016) place it among the intermediate-mass TTS. More massive young stars belong to the class of HAeBe stars. As a cTTS, SU Aur possesses an active accretion disk. The rate of mass accretion is estimated as $0.5 - 0.6 \times 10^{-8} M_\odot$ yr^{-1} (Calvet et al. 2004), which is near the mean value for cTTS. The inner radius of accretion disk, determined from long-baseline interferometry, is about 0.18 AU (Akeson et al. 2005). The images of the circumstellar environment of SU Aur directly show that the disk extends out to 500 AU (Jeffers et al. 2014).

SU Aur is a rapid rotator with $v \sin i \approx 66$ km s^{-1} (Petrov et al. 1996), which implies a high inclination of rotational axis to the line of sight. SU Aur has been a subject of several spectroscopic monitoring programs (Giampapa et al. 1993; Johns and Basri 1995; Petrov et al. 1996; Unruh et al. 2004). The emission line profiles indicated both accretion and outflows. Periodic modulations of the blue- and red-shifted absorption components in the Balmer line profiles showed a period of 2.7–3.0 days. It was interpreted as a rotational modulation due to inclination of the magnetic dipole axis with respect to rotation axis of the star (Johns and Basri 1995). Multi-site spectroscopy campaign of SU Aur found a period of 2.7 days in variation of the HeI 5876Å emission line and revealed that the wind and infall signatures are out of phase in this star (Unruh et al. 2004), which supports the model of oblique rotator. SU Aur is an X-ray emitter with luminosity of $\sim 8 \times 10^{30}$ erg s^{-1} in the 0.5 – 10 keV band (Skinner and Walter 1998). This indicates a high level of magnetic activity of the star.

SU Aur is an irregular variable. It has a long photometric history (Timoshenko 1981; Herbst and Shevchenko 1999; DeWarf et al. 2003). Analysis of long-term observations of several tens of cTTS, performed during 1983 – 2003, showed that SU Aur belongs to a small group of four stars that exhibits the largest seasonal variations in their photometric amplitude (Grankin et al. 2007). The long term light curve of these objects is characterized by a nearly constant maximum brightness level with a usually small amplitude of variability, but interrupted at times by deep fading episodes. In particular, during these 20 years, the average level of brightness of SU Aur varied smoothly from $9^{\rm m}\!.08$ to $9^{\rm m}\!.51$ with a characteristic time of 5–6 years (Grankin et al. 2007, Fig. 2). At the same time, several deep fadings were recorded with the amplitude up to $0^{\rm m}_{.}8$–$0^{\rm m}_{.}9$, and the minimal values of brightness were close to $10^{\rm m}_{.}0$ in the V band. More intensive photometric monitoring, lasting several months, allowed to detect three such deep fading episodes within 190 days (DeWarf et al. 2003). Several similar deep dimmings can be found in the ASAS-SN and AAVSO databases. Typically, the duration of such events is from a few days to weeks.

Two sources of irregular light variability are usually considered in cTTS: 1) hot spots at the base of accretion channels, whose continuous radiation veils the photospheric spectrum of the star, and 2) circumstellar dust. In the case of SU Aur the veiling in visible spectrum is small or absent. This may be due to a small contrast of a hot accretion spot in front of the hot photosphere of the G2 star. It means that accretion has a minor effect on the visible brightness of the star, and the observed light variability is solely due to the variable circumstellar extinction.

The high inclination of SU Aur implies that the line of sight to the star intersects the disk wind, and the dust in the disk wind may be the main cause of the circumstellar extinction (Babina et al. 2016). Therefore, SU Aur is a suitable object for studying the distribution of dust in the disk wind.

In three seasons of 2015-2018 we carried out a series of optical and near infrared (NIR) photometry of SU Aur. In course of this photometric monitoring we detected an event of a deep fading of the star in spring of 2018. In this paper we present preliminary analysis of our photometry.

Simultaneous optical ($BVRI$) and infrared ($JHKLM$) photometry was carried out from September 2015 till April 2018. In the NIR region the star was observed at the 125-cm telescope of the Crimean Astronomical Station (CAS) of the Moscow University. InSb-photometer with a standard $JHKLM$ system was used. Technical characteristics of the photometer, methods of observations and calculations of magnitudes were described in details by Shenavrin et al. (2011). The standard error of the measured magnitudes of SU Aur is about $0^{\rm m}_{.}02$ in $JHKL$ bands, and about $0^{\rm m}_{.}05$ in M band.

The optical $BVRI$ photometry of the star was carried out at the Crimean Astrophysical Observatory (CrAO) at 1.25m telescope, using alternatively a five-channel photometer and the PL23042 CCD camera. Some additional $BVRI$ photometry was obtained with two CCD cameras (PL4022 and Apogee Aspen) at the Zeiss-600 telescope of CAS. The typical rms error in the $BVRI$ bands were 0.04, 0.02, 0.03, $0^{\rm m}_{.}03$, correspondingly.

The light-curves of SU Aur in the two seasons of our observation are shown in Fig. 1, with the minimum of brightness at $JD = 2458144$. During this eclipse-like event the star's brightness dropped to $10^{\rm m}_{.}8$ in the V band. In such a weak state ($10^{\rm m}_{.}70$-$10^{\rm m}_{.}82$), the star stayed for three days. Unfortunately, we have no observations at the moments of the beginning and the endings of the minimum. If we use $9^{\rm m}_{.}8$ as the bright state, then the maximum duration of this event is 17 days. The minimum was also traced in the JHK light curves, but not in the LM bands. The pattern of light variability may be illustrated with the spectral energy distribution (SED). Fig. 2 shows the SEDs of SU Aur, corrected for *interstellar* extinction $A_V = 0^{\rm m}_{.}9$ (Grankin 2016), in three dates of observations: at high brightness, at minimum and after egress off the minimum. The observed SED at maximal brightness is approximated as a sum of two black bodies at $T_{\rm eff} = 5945$ K (the stellar photosphere) and $T_{\rm eff} = 1650$ K (a hot dust). At lower brightness the SEDs of stellar photosphere are distorted by the variable circumstellar extinction. One can also note the increased NIR flux at the moments of low visual flux. The relative depth of the eclipse-like minimum in the light-curves in different bands roughly corresponds to the interstellar reddening law with the ratio $A_V/E(B-V) \sim 4$. This confirms that the eclipse was caused by a cloud of small dust particles.

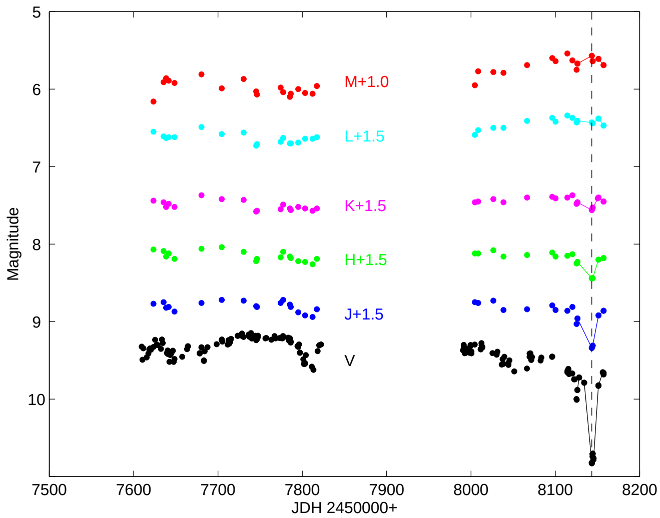

Figure 1. Light curves of SU Aur in $VJHKLM$ bands in 2016–2018. The moment of the dimming event is marked with a dashed line.

Figure 1 also shows that during the second season (2017-2018), before the eclipse-like event, there was a gradual decrease of brightness in the V band with simultaneous increase of brightness in the L and M bands. This may be interpreted as appearance of a hot dust which radiates the additional IR flux. The hot dust may be lifted up by the disk wind from the inner region of the disk near the star (Safier 1993). The same dust causes the observed decrease of brightness of SU Aur in the V band, and probably is responsible for the eclipse-like event. Similar effect was even more clearly seen in another cTTS, namely RW Aur A (Shenavrin et al. 2015). The decrease of visual brightness of RW Aur A in 2014 was accompanied by a considerable increase in the IR flux.

In the case of SU Aur the orbital period at the inner radius of the accretion disk is $P_{\rm orb} \approx 20$ days, and the orbital velocity $V_{\rm orb} \approx 100$ kms^{-1}, which is comparable to the disk wind velocity (e.g. Kurosawa et al. 2006). During one orbital period a hypothetical dust cloud is lifted up from the disk plane and never returns to the line of sight, therefore there is no periodicity in the light minima. Taking into account the duration of the minimum (about 12 days), the obscuring matter was not a distinct cloud but rather a smoothed non-uniformly distributed dust in the disk wind. A more detailed analysis using spectral data will be published elsewhere.

This work was supported by the Russian Foundation for Basic Research (RFBR grant 16-02-00140).

References:

Akeson, R.L., Walker, C.H., Wood, K., et al., 2005, *ApJ*, **622**, 440 DOI
Babina, E.V., Artemenko, S.A., Petrov, P.P., 2016 *Astron. Rep.*, **42**, 193 DOI
Calvet,N., Muzerolle, J., Briceno, C., et al., 2004, *AJ*, **128**, 1294 DOI
DeWarf, L.E., Sepinsky, J.F., Guinan, E.F., et al., 2003, *ApJ*, **590**, 357 DOI

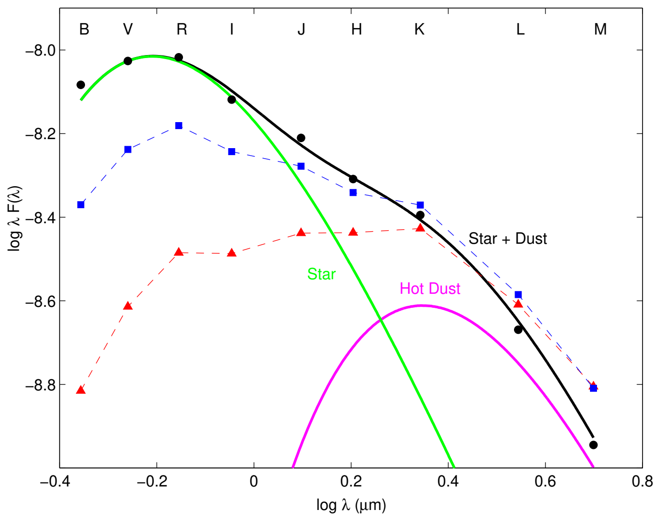

Figure 2. Spectral energy distributions of SU Aur from our visual/NIR photometry. The flux F is expressed in units of erg cm^{-2}s^{-1}. Filled circles - bright state (07.09.2017), triangles - deep minimum (25.01.2018), and squares - after egress (01.02.2018). The upper solid envelope curve is a sum of stellar radiation at high brightness and the radiation of a hot dust with $T = 1650$ K.

Giampapa, M.S., Basri, G.S., Johns, C.M., et al., 1993, *ApJS*, **89**, 321 DOI
Grankin, K.N., 2016, *AstL*, **42**, 314 DOI
Grankin, K.N., Melnikov, S.Yu., Bouvier, J., et al., 2007, *A&A*, **461**, 183 DOI
Jeffers, S.V., Min, M., Canovas, H., et al., 2014, *A&A*, **561**, A23 DOI
Herbst, W., Shevchenko, V.S., 1999, *AJ*, **118**, 1043 DOI
Johns, C.M., Basri, G., 1995, *ApJ*, **449**, 341 DOI
Kurosawa, R., Harries, T.J., Symington, N.H., 2006, *MNRAS*, **370**, 580 DOI
Petrov, P.P, Gullbring, E., Ilyin, L., et al., 1996, *A&A*, **314**, 821
Safier, P.N., 1993, *ApJ*, **408**, 115 DOI
Shenavrin, V.I., Taranova, O.G., and Nadzhip, A.E., 2011, *Astron. Rep.*, **55**, 31 DOI
Shenavrin, V.I., Petrov, P.P., Grankin, K.N., 2015, *IBVS*, **6143**
Skinner, S.L., Walter, F.M., 1998, *ApJ*, **509**, 761 DOI
Timoshenko, L.V., 1981, *Astrophysics*, **17**, 394
Unruh, Y.C., Donati, J.-F., Oliveira, J. M., et al., 2004, *MNRAS*, **348**, 1301 DOI

COMMISSIONS G1 AND G4 OF THE IAU
INFORMATION BULLETIN ON VARIABLE STARS
Volume 63 Number 6254 DOI: 10.22444/IBVS.6254

Konkoly Observatory
Budapest
14 September 2018

HU ISSN 0374 – 0676

THE VARIABLE CARBON STAR CGCS 6107

NESCI, R.[1]; CALABRESI, M.[2]; ROSSI, C.[3]; OCHNER, P.[4]

[1] INAF/IAPS, via Fosso del Cavaliere 100, 00133 Roma, Italy, e-mail: roberto.nesci@iaps.inaf.it

[2] Frasso Sabino Observatory, MPC 157, Italy

[3] INAF/OAR, Monteporzio, Italy

[4] INAF/OAPD Asiago, and Universitá di Padova, Italy

Abstract

The spectroscopic and photometric variability of CGCS 6107 has been studied with four telescopes from 2015 to 2018. The star varied between R=11.4 and 14.2 mag with a time scale of ∼500 days. An appreciable color variation was observed, the star being bluer when brighter. Hα emission was present around maxima. The spectrum is that of an N type giant veiled by a variable dusty envelope.

1 Introduction

Carbon stars on the Asymptotic Giant Branch (AGB) are supposed to be in the last phase of stellar evolution after the Third Dredge-Up and before the ejection of the planetary nebula. Given their evolutionary status they are expected to be variable.

Out of the 6891 stars listed in the Catalog of Galactic Carbon Stars (CGCS, Alksnis et al. 2001), 851 are reported as variables in the General Catalog of Variable stars (GCVS, Samus et al. 2017, CDS B/gcvs): 385 of them have also a period or variability time-scale reported, but only 150 are classified as Miras. The VSX catalog (Watson et al. 2016), updated more frequently, reports much more (1985) variables among the CGCS stars, 957 of them with a quoted period, but only 270 are classified as Miras or likely Miras: it appears therefore that only a minority of the AGB carbon stars are Mira variables.

Automatic surveys with robotic telescopes, dedicated to the detection of transient sources (Supernovae, Gamma Ray Bursts, Near Earth Asteroids, etc.) in large sky areas, contain large amounts of data which can significantly improve our knowledge in this topic: given that this is not the main goal of the science teams operating these telescopes, these large databases are still partially unexplored from this aspect.

We report here the results of our recent study on the variability of the carbon star CGCS 6107, to stimulate the curiosity for strongly variable sources and prompt similar researches in the available databases.

2 CGCS 6107

The star (05:49:32.31 +46:35:57.9, J2000) is a very bright infrared source detected by IRAS, at low galactic latitude in the Auriga constellation ($b = 9.68°$). Its IRAS-LRS spectrum is classified F (Kwok et al. 1997) suggestive of a late spectral type M or C with small amount of circumstellar dust.

It was spectroscopically observed in the optical by Cohen et al. (1996) and classified as C-,4, with a significant Hα emission. It is listed in the CGCS but without any indication of variability. It is not covered by the Sloan DR14[1].

The star is present in the main infrared catalogs: 2MASS (Cutri et al., 2003), WISE, (Cutri et al. 2013), and AKARI (Ishihara et al. 2010). The 2MASS $J - H$;$H - K$ colors of the star are $J - H = 2.10$, $H - K = 1.67$ mag, so it is located well inside the region of the moderately obscured carbon stars, even when small color changes are taken into account, but is not included in the catalog of Infrared Carbon Stars by Chen and Yang (2012).

Only in 2015 the star was pointed out as variable by the Japanese amateur astronomer Shigehisa Fujikawa (2015): spectra taken 3 days after discovery by Munari (2015) with the 122 cm telescope of the Asiago (Pennar) Observatory showed a carbon star spectrum and confirmed the presence of Hα emission.

At the time of writing, the star is listed as variable in the VSX catalog but the variability amplitude is simply given by an upper limit.

3 Photometric observations and calibrations

Soon after Fujikawa's announcement, we started a photometric monitoring of CGCS 6107 with 3 telescopes: the 152 cm of Loiano (Bologna Observatory), the 37 cm of Frasso Sabino (IAU 157) and the 30 cm of Foligno Observatory (IAU K56). The Loiano and Frasso Sabino telescopes were equipped with CCD cameras and Bessell *BVRI* filters; the Foligno telescope was equipped with a commercial digital camera (DSLR, Nikon D90 up to 2018 and red extended Canon 550D camera afterwards). Loiano and Frasso Sabino provided good quality photometry in a few nights, Foligno allowed a denser monitoring with lower accuracy.

Twenty stars included in the field of view of all the involved telescopes were selected from the UCAC4 catalog to define a comparison sequence, and are listed in Table 1. Aperture photometry was performed using IRAF/apphot[2] with radius equal to the average FWHM of each image.

The UCAC4 catalog gives magnitudes in the $r_{\rm Sloan}$ and $i_{\rm Sloan}$ bands, which are somewhat different from the Bessell's ones, and our star is quite red ($R - I \sim 2$), therefore a systematic color term is expected: however there were no stars of comparable colors in the field of view so that we could not compute reliable corrections. We feel this is not critical for the aim of this paper, devoted just to the study of the light curve and of possible color changes of the star, and not to a comparison with theoretical stellar atmosphere models. A linear fit between instrumental and catalog magnitudes provided the calibration curve to evaluate the magnitude of the variable. The slope of the line was always very close to 1.0, as expected for an ideal linear detector. The rms deviation of the comparison stars magnitudes with respect to the fitting line was adopted as true photometric uncertainty of the variable star magnitude. Given the non-standard color separation provided by the

[1] http://www.sdss.org/dr14/

[2] IRAF is distributed by the NOAO, which is operated by AURA, under contract with NSF.

Table 1: Comparison sequence for CGCS 6107.

RAJ2000	DJ2000	V	r_{Sloan}	i_{Sloan}
87.2972	+46.6587	15.011	14.675	14.325
87.3021	+46.5742	16.480	16.065	15.824
87.3159	+46.6300	14.974	14.666	14.386
87.3199	+46.6041	15.571	15.251	14.995
87.3203	+46.5450	14.776	14.306	13.855
87.3346	+46.6278	16.649	16.092	15.913
87.3428	+46.6124	16.144	16.008	15.855
87.3438	+46.6657	14.768	14.239	13.719
87.3502	+46.5741	14.503	14.205	13.931
87.3587	+46.6625	14.290	14.061	13.807
87.3587	+46.5612	15.088	14.811	14.559
87.3836	+46.5586	14.607	14.347	14.060
87.3851	+46.6097	15.209	14.835	14.455
87.3912	+46.6528	14.204	13.992	13.804
87.3993	+46.6128	14.210	13.943	13.652
87.4040	+46.6005	15.809	15.401	15.077
87.4108	+46.6139	15.749	15.439	15.092
87.4122	+46.6229	15.739	15.459	15.180
87.4423	+46.5407	15.542	15.031	14.431
87.4811	+46.6385	15.392	14.713	14.036

DSLR cameras of Foligno, we performed a few nearly simultaneous observations with the Frasso Sabino telescope to establish proper systematic corrections for the V and R bands.

The V and r_{Sloan} magnitudes of our star were always inside, or shortly outside, the range of the comparison stars, while the i_{Sloan} magnitudes were always well outside the range, so these values are extrapolated and less reliable.

4 Light curve

Our photometric data in the V and r_{Sloan} bands are reported in Table 2: column 1 is JD−2,400,000, columns 2, 3, 4 and 5 are magnitudes with their errors, column 6 is the instrument used, coded as follows (FR= Frasso Sabino; EK= Cima Ekar; LO= Loiano; NI= Foligno with Nikon D90; CA= Foligno with Canon 550D). Magnitudes fainter than $V \sim 16$ could not be measured with the 30cm telescope.

A light curve of our star starting from 2014-01-19 can be recovered from the ASAS-SN database (Shappee et al. (2014); Kochanek et al. (2017)[3], which became public only in 2018. These data are taken with an unfiltered FLI CCD camera and tied to Johnson's V-band using the APASS 9 catalog. Below $V \sim 16$, these V magnitudes have uncertainties of several tenths, due to the short exposure times used by the survey.

Fig. 1 reports the ASAS-SN light curve (stars) and our r_{Sloan} light curve (squares) on a common magnitude scale, showing a very good agreement of the overall shape in the common time interval. The source is characterised by very large variations (> 2.5 mag), with a time scale (peak to peak distance) of about 500 days: the variation amplitude is not

[3]`https://asas-sn.osu.edu`

Table 2: Observed magnitudes of CGCS 6107 (all telescopes).

JD	V	err_V	r	err_r	tel
57332	13.54	0.02	11.30	0.02	FR
57367	13.98	0.06	11.70	0.10	NI
57402	14.12	0.06	11.60	0.04	LO
57439	14.56	0.05	12.40	0.20	NI
57449	14.69	0.08	12.50	0.10	NI
57473	15.04	0.06	12.67	0.10	NI
57482	15.12	0.08	12.98	0.10	NI
57492	15.18	0.08	12.80	0.10	NI
57498	15.40	0.10	13.20	0.10	NI
57503	15.40	0.05	13.10	0.10	NI
57507	15.51	0.12	13.20	0.10	NI
57694	15.44	0.04	13.24	0.10	NI
57708	15.35	0.08	13.15	0.10	NI
57735	15.04	0.07	12.85	0.10	NI
57741	15.00	0.07	12.80	0.10	NI
57768	14.89	0.06	12.70	0.05	NI
57774	14.79	0.04	12.67	0.06	NI
57796	14.73	0.04	12.62	0.10	NI
57799	14.73	0.03	12.81	0.09	NI
57799	14.78	0.04	12.40	0.06	LO
57814	14.75	0.04	12.68	0.05	NI
57829	14.70	0.04	12.59	0.08	NI
57840	14.75	0.02	12.47	0.02	FO
57857	14.63	0.06	12.51	0.10	NI
57879	14.70	0.10	12.71	0.07	NI
58085	——	——	14.21	0.07	NI
58093	——	——	14.22	0.10	NI
58106	——	——	14.03	0.10	NI
58109	17.05	0.15	14.03	0.04	FR
58120	——	——	13.90	0.10	NI
58139	——	——	13.70	0.10	NI
58141	16.57	0.03	13.70	0.03	FR
58153	——	——	13.48	0.08	NI
58159	16.32	0.02	13.50	0.03	FR
58164	——	——	13.41	0.09	CA
58186	——	——	13.38	0.09	CA
58200	——	——	13.26	0.08	CA
58202	——	——	13.17	0.07	CA
58212	15.90	0.10	13.19	0.06	CA
58215	15.89	0.04	13.18	0.02	FR
58224	15.70	0.10	13.01	0.06	CA
58229	15.75	0.03	12.86	0.04	LO
58232	15.70	0.10	12.86	0.07	CA

constant, suggesting a classification of Semi Regular rather than of Mira type variability. As mentioned in the Introduction, only a small fraction of the AGB carbon stars shows a regular Mira type light curve, so our finding is not unusual. Similar large amplitude variations, superimposed on longer term trends in the light curve, have been reported also for other carbon stars with strong infrared excess recently studied by our group (see e.g. Gaudenzi et al. 2017; Nesci et al. 2018).

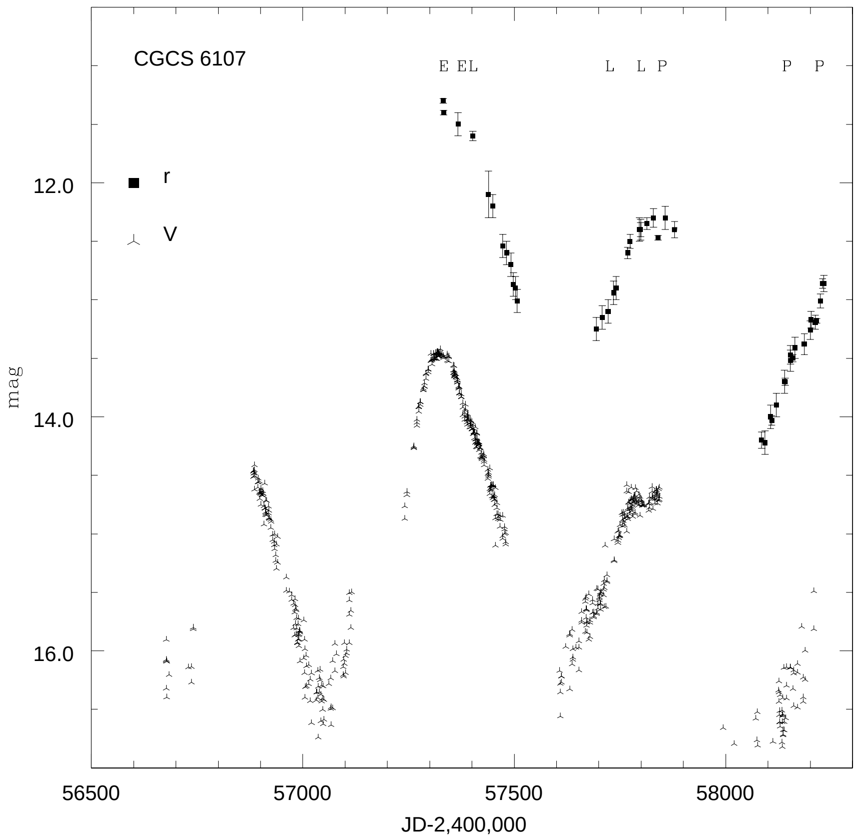

Figure 1. The light curve of CGCS 6107 from our observations in the r band, (squares with error bars) and the ASAS-SN light curve in the V band (stars). Vertical scale in magnitudes. The letters in the upper side mark the dates of the spectroscopic observations listed in Table 5: E=Ekar, L=Loiano, P=Pennar.

An FFT analysis with Period04 (Lenz and Breger 2005) of the ASAS-SN light curve shows a main peak at 543 days, blended with its (fainter) alias at 1083 days; a further peak at 201 days has a low power and is of limited importance in the light curve fit. The period of 543 days is fully compatible with our dataset.

Despite that the star is a semiregular rather than a Mira, we show in Fig. 2 the optical light curve folded with the formal 543 days period. The substantial scatter around phase 0 is mainly due to the variable amplitude of the light curve, as apparent from Fig. 1.

Color indices $(V - r)$ and $(r - i)$ of the star were measured at different flux levels and are collected in Table 3: the star appears markedly redder when fainter.

We have also measured the star magnitudes on historic plates of the DSS, recoverable

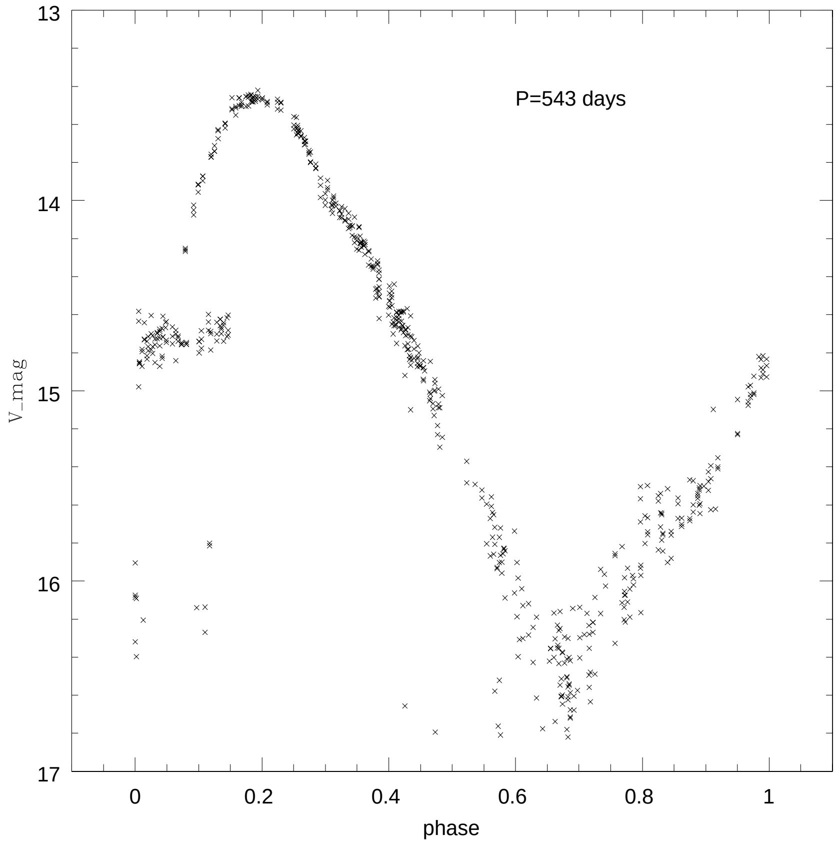

Figure 2. Phased optical light curve of CGCS 6107 from ASAS-SN data folded with the 543 day period.

Table 3: Color indices of CGCS 6107.

Telescope	date	$r_{\rm Sloan}$	$V - r_{\rm Sloan}$	$r - i_{\rm Sloan}$
Frasso Sabino	2015-11-06	11.30	2.24	1.89
Loiano	2016-01-15	11.61	2.50	1.95
Loiano	2016-11-29	12.89	2.60	2.01
Loiano	2017-02-14	12.40	2.38	—-
Frasso Sabino	2017-03-27	12.47	2.28	2.10
Frasso Sabino	2017-12-22	14.04	3.14	2.44
Frasso Sabino	2018-01-23	13.70	2.86	2.37
Frasso Sabino	2018-02-10	13.50	2.82	2.31
Frasso Sabino	2018-04-06	13.18	2.71	2.24
Loiano	2018-04-20	12.86	2.89	2.05

Table 4: Observed magnitudes of CGCS 6107 (all telescopes).

Emulsion	band	date	mag
103a-E	r	1952-12-21	12.6
QuickV	V	1983-01-14	16.4
IIIaF	r	1989-10-05	16.4
IIIaF	r	1989-10-29	16.2
IV-N	i	1996-11-03	12.2
IV-N	i	1999-10-13	12.3

from the Space Telescope Science Institute, using our comparison sequence. The calibration curve was markedly non linear, so we could not measure the B magnitude with our UCAC4 sequence because well outside the range. The results for the V, $r_{\rm Sloan}$, $i_{\rm Sloan}$ filters are collected in Table 4 and confirm the variability of the star in the past.

In the infrared the star was observed for 3 years (from 1990-02-09 to 1993-04-15) with weekly sampling by the DIRBE instrument (Smith et al. 2004; Price et al. 2010) on board the COBE satellite, in the 3.6 μm and 4.9 μm bands. The star was not classified as variable in the DIRBE catalog (Price et al. 2010) according to the strict criteria adopted, but an eye inspection of the data suggested a possible variability. B.J. Smith kindly confirmed to us that no contamination by nearby sources was present for this star, so we made an independent analysis of the published data and we built the light curves at 3.5 and 4.9 μm applying a running mean of 5 consecutive measures: the result is shown in Fig. 3.

A peak-to-peak amplitude of about 1.3 mag is evident, with a time scale of about 500 days, similar to the optical one. The amplitude is similar to that measured for the 'bona fide' variables of similar periods in the Price et al. (2010) catalog.

A deeper analysis of the IR light curves in each band and of the averaged (3.5 and 4.9 μm) fluxes with the FFT technique shows several peaks in the power spectrum with comparable intensities and significantly different phases: for the averaged curve the peaks are around 558, 254, 133, 105, and 76 days (see Fig.4). The presence of so many peaks with similar power suggests a rather noisy pattern in the light curve: actually a single period is quite inadequate to reproduce its overall shape. The actual variability range and time scale are therefore ill-defined from these data. We recall that CGCS 6107 is near the detection limit of the DIRBE instrument, and some details of the light curve might be of instrumental origin. In the spectral energy distribution, the average DIRBE fluxes fit well between the 2MASS (1.25, 1.65, and 2.2 μm) and the AKARI (9 and 18 μm) values.

5 Spectroscopic observations

Spectra of the star were taken at different dates with the Asiago (Cima Ekar 182 cm and Pennar 122 cm) and the Loiano 152 cm Observatories, with luminosity levels ranging from r = 11.4 to 13.7 mag; data reduction was performed with the standard IRAF procedures. The observations log is given in Table 5: column 1 is the telescope, column 2 the date, column 3 the spectral resolution in Å, column 4 the r magnitude at the time of observation, column 5 the Hα equivalent width in Å. These last values are strongly affected by the

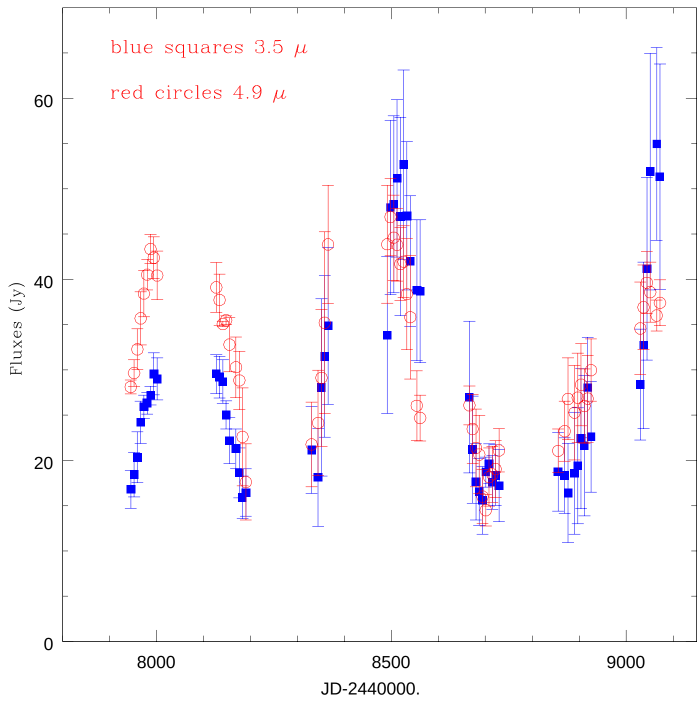

Figure 3. The light curve of CGCS 6107 at 3.5 and 4.9 μm from the DIRBE data after a 5-point running mean. Error bars are the rms deviation form the mean of the averaged points. We remark that these errors are quite large and of very different size in different years. The 4.9 μm data seem of better quality.

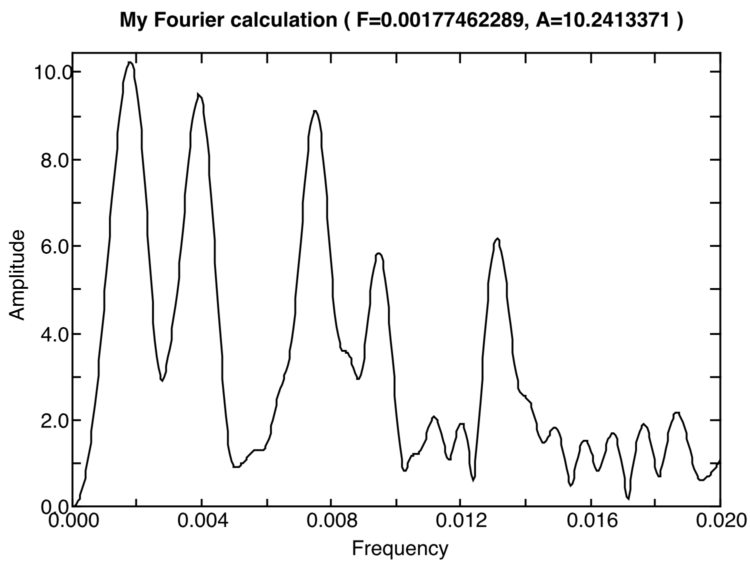

Figure 4. The power spectrum of CGCS 6107 from the DIRBE data: it is evident that several frequencies of similar power are present, indicating a complex structure.

variability of the continuum and typical errors are about 0.3 Å. In the last row we report the data relative to the observation by Cohen et al. (1996) taken with the 100 cm Lick reflector. This spectrum was taken in December 1987 and showed Hα in emission: from the published plot we derived an approximate equivalent width of 7 Å, comparable to our measures.

The dates of our spectroscopic observations are also marked in the bottom of Fig. 1 to better put them in the context of the stellar light-curve.

Characteristic spectra at different epochs are reported in Fig. 5. All the spectra are typical of an N type giant, moderately obscured by dust in the circumstellar envelope, with the blue region strongly underexposed.

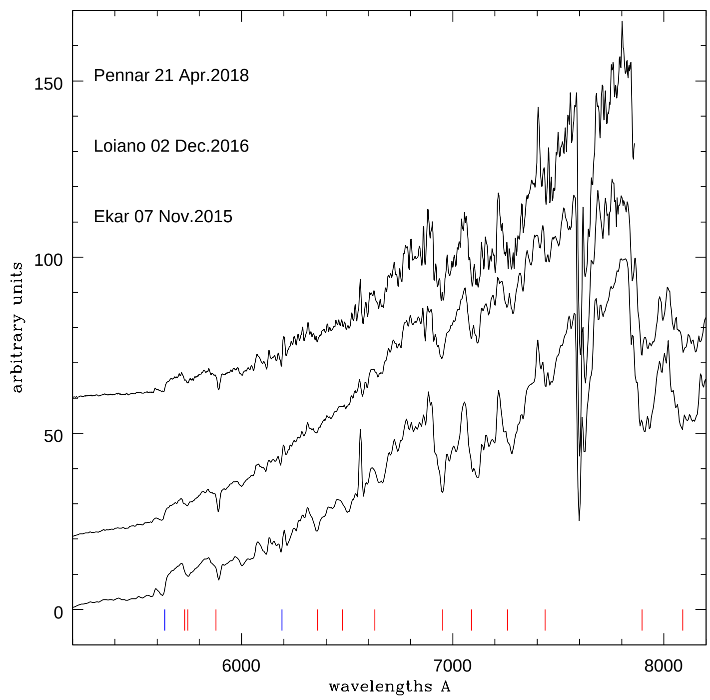

Figure 5. Optical spectra of CGCS 6107 at different dates and luminosities. The y axis represents relative intensities corrected for the atmospheric extinction. The spectra are normalised at 7800 Å. The main molecular bandheads are color-coded: blue = C_2; red = CN. The telluric bands of O_2 and H_2O molecules, overlapped to the CN red system, have not been removed. The spectra are vertically shifted to each other for ease of comparison. From bottom to top: 2015-11-07 (r∼11.4), 2016-12-02 (r∼12.8), 2018-04-21 (r∼13.0).

Red-ward of 5000 Å the molecular absorption bands of C_2 (Swan) and the red system of CN can be easily identified[4]. The 6260 Å of the $C_{13}N_{14}$ is clearly visible in the bright states; the two absorptions of atomic lines of K at 7665, 7699 Å are always visible. The 5889-5895 Å NaD absorption is possibly produced in the circumstellar envelope. The Balmer Hα emission line is also recorded with different intensities in different epochs.

Spectral changes are correlated with the optical flux: the continuum and the strength of Hα and of the absorption bands are always affected by the veiling effect, mainly during

[4]most notably $\lambda\lambda$ 5636, 6122 and 6192 Å of C_2; 5730, 5746, 5878, 6013, 6206, 6360, 6478, 6631, 6925, 7088, 7259, 7437, 7876-7945 and 8150 Å of CN.

Table 5: Spectroscopic observations logbook.

Telescope	date	res. (Å)	r	Hα (Å)
Cima Ekar	2015-11-07	8.0	11.4	−8.3
Cima Ekar	2015-11-15	8.0	11.7	−7.9
Cima Ekar	2015-12-20	8.0	11.7	−7.8
Loiano	2016-01-15	10.0	11.6	−7.2
Loiano	2016-12-02	10.0	12.8	—
Loiano	2017-02-14	10.0	12.4	−4.8
Pennar	2017-04-06	6.9	12.5	−5.6
Pennar	2018-01-27	6.9	13.7	—
Pennar	2018-04-13	6.9	13.0	−5.7
Pennar	2018-04-21	6.9	13.0	−5.9
Lick	1987-12-XX	11	V=17.3:	−7

faint photometric phases. Hα emission was present at the end of 2015, the beginning of our monitoring, when the star was in bright state; it was not present one year later, during a faint state; again the emission was present near the next maximum, disappeared again when faint and rose again during the more recent brightening. In the fainter states (December 2016 and January 2018) the depth of the molecular absorption bands was also reduced, while the equivalent width of the NaD lines in absorption did not vary significantly.

6 Conclusions

We have found that the variability of the carbon star CGCS 6107 is compatible with a quasi regular periodicity on a time scale of about 543 days; the star may be classified as a SR variable because its average magnitude in each cycle is not constant. Historic observations from DSS plates also show large variability.

A definite change of the color indices $(V-r)$ and $(r-i)$ was detected, with the source being bluer when brighter. The Hα line was in emission during maxima while disappeared in the fainter parts of the light curve: this is not unusual among AGB carbon stars. Overall the photometric and spectroscopic properties are similar to those of other variable carbon stars also studied by our group, like BIS 036 (HP Cam) or BIS 184 (Gaudenzi et al. 2017).

The absolute K magnitude of CGCS 6107 may be estimated from the relation (Whitelock et al. 2012):

$$M(K) = -3.69 \times (\log P - 2.38) - 7.18(\pm 0.37)$$

which yields $M(K) = -8.35$: this gives an estimated distance of 4.9 kpc, with a probable range 5.8-4.2 kpc. The total galactic absorption in the K band in the direction of the star is 0.13, much less than the uncertainty on the actual average K magnitude of the star, given its variability.

The Gaia DR2 catalog (Gaia collaboration 2018), just published when we were finishing this paper, gives a parallax of 0.270 (±0.104) mas, corresponding to a distance of 3.7 (−1.0; +2.1) kpc, in fair agreement with our estimate.

Acknowledgements: We thank the Padova and Bologna Observatories for the time allocations. This work has made use of the VIZIER, SIMBAD, IRSA, VSX, ASAS-SN, STScI and Gaia DR2 databases.

References:

Alksnis, A., Balklavs, A., Dzervitis, U., et al., 2001, *Baltic Astronomy*, **10**, 1
Bessell, M.S., Brett, J.M. 1988, *PASP*, **100**, 1134 DOI
Chen, P.S. and Yang, X.H., 2012, *AJ*, **143**, 36 DOI
Cohen, M, Wainscoat, R.J., Walker, H.J., Volk, K., 1996, *AJ*, **111**, 1333 DOI
Cutri, R.M., Skrutskie, M.F., vanDyk, S., et al., 2003, *CDS on-line catalog*, II/246
Cutri R.M., et al. 2013, *WISE* All-Sky Data Release, IPAC/Caltech; VizieR On-line Data Catalog: II/328
Fujikawa, S., 2015, *IAU CBAT*, TCP J05493243+4636023
Gaia collaboration, 2018, *A&A*, 616, A1 DOI
Gaudenzi, S., Nesci, R., Rossi, C., et al., 2017, *Rev. Mex. A&A*, 53, 507
Ishihara, D., Onaka, T., Kataza, H., et al. 2010, *A&A*, **514**, A1 DOI; AKARI/IRC Mid-Infrared All-Sky Survey; Vizier On-line Data Catalog II/297
Kochanek, C.S., Shappee, J.L., Stanek, K.Z., et al., 2017, *PASP*, **129**, 4502 DOI
Kwok, S., Volk, K., Bidelman, W.P., 1997, *ApJS*, **112**, 557 DOI
Lenz P. and Breger M., 2005, *CoAst*, **146**, 53
Munari, U., 2015, *IAU CBAT*, TCP J05493243+4636023
Nesci, R., Rossi, C., Tuvikene, T., et al. 2018, *Rev. Mex. A&A*, **54**, 341
Price, S.D., Smith, B.J., Kuchar, T.A., et al. 2010, *ApJS*, **190**, 203 DOI
Samus, N.N., Kazarovets, E.V., Durlevich, O.V., et al., 2017, GCVS v5.1, *CDS Vizier catalog*, B/gcvs
Shappee, B.J., Prieto, J.L., Grupe, D., et al., 2014, *ApJ*, **788**, 48 DOI
Smith, B.J., Price, S.D., Baker, R.I., 2004, *ApJS*, **154**, 673 DOI
Watson, C., Henden, A. A., Price, A. 2016, *AAVSO International Variable Star Index VSX*, yCat, 102027
Whitelock, P.A., 2012, *Ap&SS*, **341**, 123 DOI
Zacharias, N., Finch, C.T., Girard, T.M., et al., 2013, *AJ*, **145**, 44 DOI

COMMISSIONS G1 AND G4 OF THE IAU
INFORMATION BULLETIN ON VARIABLE STARS
Volume 63 Number 6255 DOI: 10.22444/IBVS.6255

Konkoly Observatory
Budapest
15 September 2018

HU ISSN 0374 – 0676

REVISED COORDINATES OF VARIABLES IN THE FIELD OF M16-M17

NESCI, R.

INAF/IAPS, via Fosso del Cavaliere 100, 00133 Roma, Italy, e-mail: roberto.nesci@iaps.inaf.it

Abstract

The identifications of the variable stars published on IBVS #985 have been checked on the basis of the original finding charts and digitized Asiago plates. Cross check with the 2MASS catalog allowed to get more accurate coordinates. For 19 stars (out of 207) a significant coordinates difference is found and new identifications are given. The interpretation of NSV 10848 as a Nova is briefly discussed.

1 Introduction

A list of 207 red variables was published by Maffei (1975) on the basis of 7 years of observations using infrared (I-N + RG5) and blue (103aO) plates taken with the Asiago Observatory Schmidt (65/90/215 cm) telescope. The plates cover a field of 2.5 degrees radius centered at galactic coordinates $l = 16°$, $b = 0°$(midway between M16 and M17). This variable stars sample is statistically well defined, being magnitude limited. A catalog including the finding charts for all the stars, and the phased light curves for 176 Mira and SR stars, is available at CDS (Maffei and Tosti 2013), based on a printed publication of the Perugia University: unfortunately, in a few cases the finding charts are of poor quality.

In the course of a larger on-going research on the Mira stars of the galactic plane, I found for some of these stars strong inconsistencies between the optical and the near infrared (JHK) magnitudes, derived from the cross correlation of the General Catalog of Variable Stars (Vizier B/gcvs, Samus et al. 2017) with the 2MASS (Cutri et al. 2003) catalog, suggesting that some misidentifications have occurred. This may have happened given that in the original paper (Maffei 1975) the coordinates were given with an accuracy of $6''(0\overset{'}{.}1)$ and the galactic plane is very crowded of stars.

In the family archive of the late Prof. Paolo Maffei[1] I was able to recover the original paper enlargements of the Asiago plates, with pencil annotations by Maffei of the detected variables. Also all the original Asiago plates were available as fits files, from scans made at Perugia University (Nesci et al. 2014).

[1]http://www.archiviomaffei.org

Table 1: Revised 2MASS identifications of variable stars in the field of M16-M17.

Maffei id	Name	2MASS counterpart	comment
M005	NSV 10849	2MASS J18110190-1422595	small offset
M024	NSV 10899	2MASS J18295552-1518384	45″ offset
M027	NSV 10671	2MASS J18212641-1311525	small offset
M028	NSV 10677	2MASS J18213621-1242312	1′ offset
M035	NSV 10522	2MASS J18182855-1725289	small offset
M051	NSV 10408	2MASS J18144139-1503536	small offset
M053	NSV 10741	2MASS J18242539-1703515	2 bright NIR stars very near
M086	V3918 Sgr	2MASS J18290441-1353350	coordinates misprint
M087	NSV 10832	2MASS J18274962-1343087	small offset
M089	V3904 Sgr	2MASS J18110608-1613039	small offset
M091	NSV 10249	2MASS J18082415-1535166	coordinates misprint
M127	V3950 Sgr	2MASS J18283838-1603253	small offset
M150	NSV 10848	J2000 18:28:11.7 -13:44:37	probable Nova
M151	V409 Sct	2MASS J18294001-1400178	30″ offset
M161	NSV 10490	2MASS J18171849-1734104	small offset
M166	NSV 10299	2MASS J18102428-1532157	30″ offset
M174	NSV 10271	2MASS J18091451-1429483	small offset
M183	NSV 10772	2MASS J18254743-1611475	small offset
M184	NSV 10757	2MASS J18250968-1610350	small offset

2 Identification

Comparison of the original finding charts with the digitized Asiago plates, the Digitized Sky Survey (IV-N emulsion), the SIMBAD archive, and its interactive AladinLite tool, allowed to check the identification of all the variables and to find the 2MASS counterpart. In a few cases the published finding chart was not accurate enough to identify the star, and I had to look at the original plates blinking some of them to pick up the real variable. Overall, only in 19 cases, out of 207, was the position given by SIMBAD found to be significantly incorrect (more than 2″), leading to misidentification or lack of a NIR counterpart in SIMBAD.

For these stars I report in Table 1 the original Maffei provisional number, the variable star name as given in GCVS or NSV, the actual 2MASS counterpart, and a comment. In the case of NSV 10848, classified by Maffei as a probable Nova, no 2MASS counterpart was found.

Out of these stars, only 3 are Miras, V3918 Sgr, V3904 Sgr, and V409 Sct, while V3950 Sgr is an SRa. All the others are classified by Maffei as irregular or eclipsing variables.

3 Remarks on individual stars

Having defined accurate coordinates, I checked if these variables had been rediscovered by other surveys. This sky area is not covered by the VVV survey (Minniti et al. 2010) but is covered by the Galactic Disk Survey (GDS, Hackstein et al. 2015): remarkably, only four of our stars were rediscovered by the survey. As a further check, I also looked for these stars in the VSX on-line database[2]: only two stars have coordinates consistent

[2]https://www.aavso.org/vsx/

with the 2MASS counterpart, namely M087 and V409 Sct. Below are further comments on some remarkable stars.

M024: identified by finding chart. Independently rediscovered by the GDS survey as GDS_J1829555-151838.

M028: mismatch between coordinates and finding chart; the actual variable was found blinking some Asiago plates.

M053: two very near bright stars in 2MASS, the right one is the eastern (and brighter) one.

M086: the published finding chart is wrong, star identified with the original chart and plates. Independently rediscovered by the GDS survey as GDS_J1829044-135334.

M087: independently rediscovered by the GDS survey as GDS_J1827496-134308.

M091: offset of several arcmin, identified with the original finding chart.

M127: independently rediscovered by the GDS survey as GDS_J1828384-160325.

M151 (V409 Sct): SIMBAD identifies this star with another very bright NIR star 30″N, which is the variable GDS_J1829396-135936. However, Maffei's coordinates and finding chart consistently point to 2MASSJ18294001-1400178. Checked also blinking the original plates.

M166: coordinates misprint, found with the finding chart.

4 The possible Nova

M150 (NSV 10848) was indicated by Maffei as a possible Nova; I have checked that the star was visible on 2 IR plates only: #860 (1967-09-25) and #913 (1967-10-03) while it was invisible on the simultaneous B ones. It was still not visible on 1967-09-05, and it was not possible to define when the star went below the threshold because no other plates were taken until June of the following year. The star never reappeared in the following years.

Maffei (1975) does not report magnitudes for this star. From the digitized plates, using the UCAC4 (Zacharias et al. 2012) catalog as reference and aperture photometry with IRAF/apphot, I derived a brightness of $I \sim 13.3$ mag for both plates, and an upper limit of $B = 17.5$ mag. The star was therefore very red ($B - I > 4.0$). If the observed color is due just to absorption, the $E(B-V)$ is at least 1.7 mag and the absorption in the I band is at least 3.2 mag. The distance of the Nova (assuming an absolute magnitude $M = -8$) would be less than 40 kpc, compatible with being inside our Galaxy.

Besides the classification as a Nova, an alternative identification could be with a cataclysmic variable of the WZ Sge type. These stars undergo large (6 mag or more) brightenings at several years interval, so it is not strange that only one such brightening was detected during this monitoring sampled to look for long period variables (120 plates from 1967 to 1975). In this case the star might be visible still now, likely in quiescence around the 20th magnitude, surely reddened by interstellar absorption. The PanSTARRS/DR1 image (Chambers et al. 2016) shows a possible candidate at RA 18:28:11.7, DEC −13:44:37 (J2000), with magnitudes $g = 21.65$, $r = 20.05$, $i = 19.07$, $z = 18.52$. The star is present also in Gaia DR2 (Gaia collaboration, 2018) as source id 4104434785790095104, with magnitudes $G = 19.70$ mag, $G_{\rm Bp} = 19.84$ mag, $G_{\rm Rp} = 18.21$ mag. The $G_{\rm Bp} - G_{\rm Rp}$ color (1.63) is much redder than the expected one ($G_{\rm Bp} - G_{\rm Rp} \sim 0$) for a quiescent WZ Sge star. Assuming an intrinsic PanSTARRS color $g - z = -0.4$ as WZ Sge in quiescence, the color excess would be $E(B - V) = 1.5$, corresponding to an absorption of $A_i = 3.15$ and $A_g = 5.74$. The differential absorption between the B and I Asiago bands would be therefore only $\sim$2.6 mag and the star in outburst should have been visible also on the blue plates: the Nova interpretation is therefore more likely.

Acknowledgements: The Digitized Sky Survey is available on-line from the Space Telescope Science Institute at `http://archive.stsci.edu/cgi-bin/dss_plate_finder`. The SIMBAD AladinLite tool is on-line at `http://simbad.u-strasbg.fr/simbad/`. This work has made use of the VIZIER, SIMBAD, STScI, GDK, VSX, and Gaia DR2 databases.

References:

Chambers, K. C., Magnier, E. A., Metcalfe, N., et al. 2016, *arXiv:1612.05560*
Cutri, R.M., Skrutskie, M.F., vanDyk, S., et al., 2003, *CDS Vizier catalog*, II/246
Gaia collaboration, 2018, *A&A*, **616**, A1 DOI
Hackstein, M., Fein, Ch., Haas, M., et al., 2015, *AN*, **336**, 590 DOI
Maffei, P., 1975, *IBVS*, **985**, 1
Maffei, P. and Tosti, G. 2013 *CDS Vizier catalog*, II/320
Minniti, D., Lucas, P.W., Emerson, J.P., et al., 2010, *New Astronomy*, **15**, 433 DOI
Nesci, R., Bagaglia, M., Nucciarelli, G. 2014, *Astroplate 2014, Prague*, 75
Samus, N.N., Kazarovets, E.V., Durlevich, O.V., et al., 2017, GCVS v5.1, *CDS Vizier catalog*, B/gcvs
Zacharias N., Finch C.T., Girard T.M., 2012, *CDS Vizier catalog*, I/322A

COMMISSIONS G1 AND G4 OF THE IAU
INFORMATION BULLETIN ON VARIABLE STARS
Volume 63 Number 6256 DOI: 10.22444/IBVS.6256

Konkoly Observatory
Budapest
10 December 2018

HU ISSN 0374 – 0676

PERIOD ANALYSIS, ROCHE MODELING AND ABSOLUTE PARAMETERS FOR AU Ser, AN OVERCONTACT BINARY SYSTEM

ALTON, K.B.[1]; NELSON, R.H[2]; TERRELL, D.[3]

[1] Desert Bloom and UnderOak Observatories, 70 Summit Ave, Cedar Knolls, NJ, USA, email: kbalton@optonline.net

[2] Mountain Ash Observatory, 1393 Garvin Street, Prince George, BC, V2M 3Z1, Canada

[3] Department of Space Studies, Southwest Research Institute, 1050 Walnut St., Suite 400, Boulder, CO 80302, USA

Abstract

CCD photometric data collected at UnderOak Observatory (UO) and Desert Bloom Observatory (DBO) in three bandpasses (B, V and I_C) produced 10 new times of minimum for AU Ser which were used to revise the linear ephemeris. These results captured in 2011 and 2018 reinforced a longstanding observation that the shape of the light curve from this W UMa binary system (P=0.386497 d) is highly variable. Significantly skewed peaks and differences at maximum light were detected during quadrature which could only be simulated during Roche modeling by positioning a hot spot on the secondary star close to the neck between both constituents. Historically this system has been variously classified as an F8, G5 and K0 system; however, this study supports more recent reports that AU Ser is best described as spectral type K1V-K2V. A fresh assessment of eclipse time residuals over the past 80 years has provided additional insight regarding cyclical changes in orbital period experienced by this interesting variable star.

1 Introduction

The W UMa variable AU Ser was first discovered by Hoffmeister (1935), visually observed by Soloviev (1951) and photographically recorded by Huth (1964). Since 1972, at least four different studies have produced photoelectrically-derived light curves (Binnendijk 1972; Kennedy 1985; Li et al. 1992; Li et al. 1998). CCD photometric (V-mag) data for this system were also captured by the All Sky Automated Survey (ASAS) between 2003 and 2009 (Pojmański 2005). Two spectroscopic investigations of this system (Hrivnak 1993; Pribulla et al. 2009) produced radial velocity (RV) results critical to determining a mass ratio ($q = 0.71 \pm 0.02$) and total mass.

From the earliest studies it was obvious that AU Ser is subject to photospheric disturbances most likely resulting from either large cool spot(s) akin to sunspots or hot spot(s) potentially produced during mass transfer. Kałużny (1986) was the first to propose that the prominent light curve (LC) asymmetry observed during quadrature may be related to a hot spot located at the neck between both stars. Djurašević (1993) argued otherwise that based on a good fit to an RS CVn-based model (Djurašević 1992) for a detached system, there was no reasonable expectation for a hot spot to exist beyond the equatorial zone of a star. Light curves generated by Li et al. (1998) further highlight the challenge in modeling this overcontact binary and even proposed the existence of short period oscillations at 0.0003 and 0.008 Hz. Period studies (Qian et al. 1999; Gürol 2005, Amin 2015 and Nelson et al. 2016) from eclipse timings that extend as far back as 1936 have revealed secular changes over the past 80 years. An underlying sinusoidal relationship in the eclipse timing differences (ETD) led the most recent three investigators to propose a third body orbiting the binary pair. Various opinions abound, but there is a general consensus that the secular decrease in eclipse timings most likely results from mass transfer and that the cyclic light-time-effect (LiTE) originates from the gravitational influence of an unseen third star. Herein we report on the analysis of new multicolor (BVI_C) LC data acquired in 2011 and 2018 along with a retrospective analysis of all evaluable LCs from AU Ser that are available from the literature. Furthermore, fresh LiTE analyses supported by the addition of 10 new eclipse timings has resulted in the refinement of a period solution for a putative gravitationally-bound third body.

2 Data

The imaging apparatus used during 2011 at UnderOak Observatory (UO; NJ, USA) included a 0.28-m Schmidt-Cassegrain telescope with an SBIG ST-8XME CCD camera mounted at the Cassegrain focus. Additional time-series photometric observations were acquired in 2018 at Desert Bloom Observatory (DBO: Benson, AZ, USA) with an SBIG STT-1603ME CCD camera mounted at the Cassegrain focus of a 0.4-m catadioptric telescope. In both cases photometric B, V and I_C filters manufactured to match the Bessell prescription were used during each guided exposure (UO:75 s and DBO:60 s). Specifics regarding image acquisition, calibration, registration and reduction to catalog-based magnitudes (MPO Canopus) have been reported elsewhere for UO (Alton 2016) and DBO (Alton 2018). Roche type modeling was performed with the assistance of Binary Maker 3 (BM3; Bradstreet and Steelman 2002), WDwint56a (Nelson 2009), and PHOEBE 0.31a (Prša and Zwitter 2005), the latter two of which employ the Wilson-Devinney (W-D) code (Wilson and Devinney 1971; Wilson 1979; Wilson 1990). Spatial renderings of AU Ser were also produced by BM3 once model fits were finalized. Times-of-minimum were calculated using the method of Kwee and van Woerden (1956).

3 Results

3.1 Photometry and Ephemerides

An ensemble of five stars in the same field-of-view with AU Ser (Fig. 1) was used to ultimately derive catalog-based magnitudes (Table 1). These stars exhibited no evidence of inherent variability (V and $I_C < 0.03$ mag and $B < 0.05$ mag) beyond experimental error over each imaging session. Photometric data in B (n=270), V (n=276), and I_C (n=284) were processed to generate bandpass specific LCs collected between 11 July 2011 and 22 July 2011 (Figs. 2 & 3). Additional photometric data acquired during a recent photometric campaign (29 May - 11 June 2018) in B (n=372), V (n=372) and I_C (n=374), were similarly folded by Fourier analysis (Figs. 2 & 3).

In total, six new secondary (s) and four primary (p) minima were captured during this investigation which also included a single isolated session on 25 June 2015 at UO. All times-of-minima were averaged (Table 2) from each session since the chronological order of eclipse timings (ET) showed no color dependency. The Fourier routine (FALC;

Table 1. FOV identity, name, astrometric coordinates and color index $(B-V)$ for the target (AU Ser=T) and comparison stars (1-5) used for ensemble aperture photometry

FOV Identity	Name	$\alpha_{2000.0}$ hh mm ss	$\delta_{2000.0}$ $^{\circ}\ '\ ''$	MPOSC3[a] $(B-V)$
1	TYC 01502-1573-1	15 56 43.12	+22 16 01.6	0.685
2	GSC 01502-1653	15 56 35.24	+22 15 35.3	0.577
3	GSC 01502-1352	15 56 23.66	+22 16 06.6	1.070
4	TYC 01502-1613-1	15 56 23.12	+22 17 25.9	1.153
5	GSC 01502-1418	15 56 16.13	+22 14 27.6	0.621
T	AU Ser	15 56 49.47	+22 16 01.6	0.834

a: MPOSC3 is a hybrid catalog which includes a large subset of the Carlsberg Meridian Catalog (CMC-14) as well as from the Sloan Digital Sky Survey (Warner 2007).

Harris 1989) in MPO Canopus (2015) provided an identical period solution (0.386497 $\pm$ 0.000001d) for the multicolor data captured in 2011 and 2018. An updated linear ephemeris equation (1) based on the linear elements defined by Kreiner (2004) was calculated using the last 7 years (Table 2) of published ET data:

$$\text{Min I(Hel.)} = 2458280.7899(14) + 0.3864965(1)\ E. \tag{1}$$

Given the complex changes in orbital period observed for this system (see Section 3.6), new eclipse timings for AU Ser should be determined on a regular basis to maintain an accurate record about the behavior of this variable system.

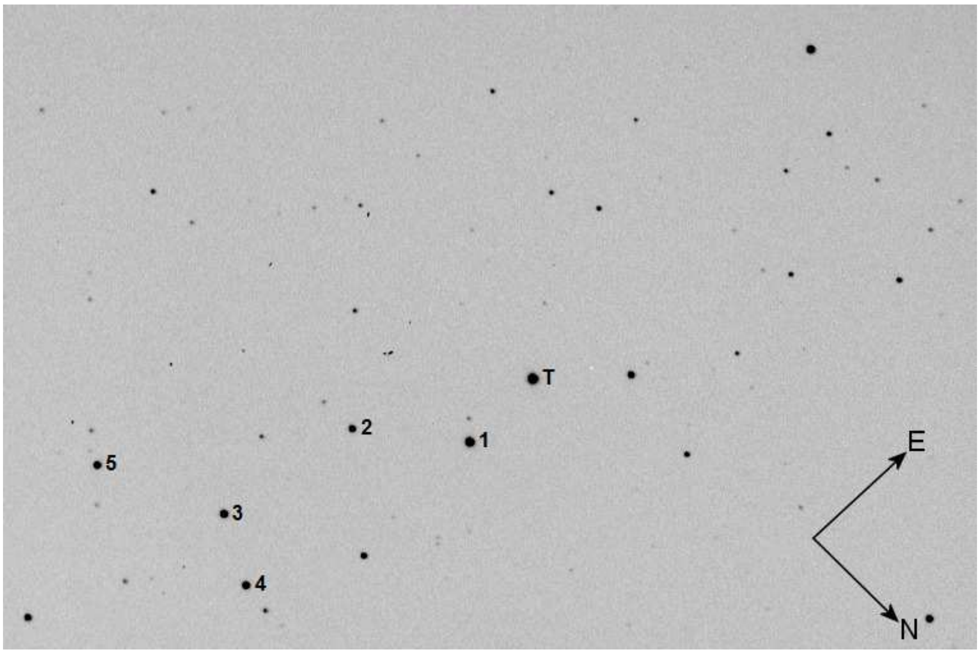

Figure 1. Observed field-of-view (FOV) for AU Ser (T=target) obtained at DBO. The comparison stars are marked according to the numbers (1-5) assigned in Table 1.

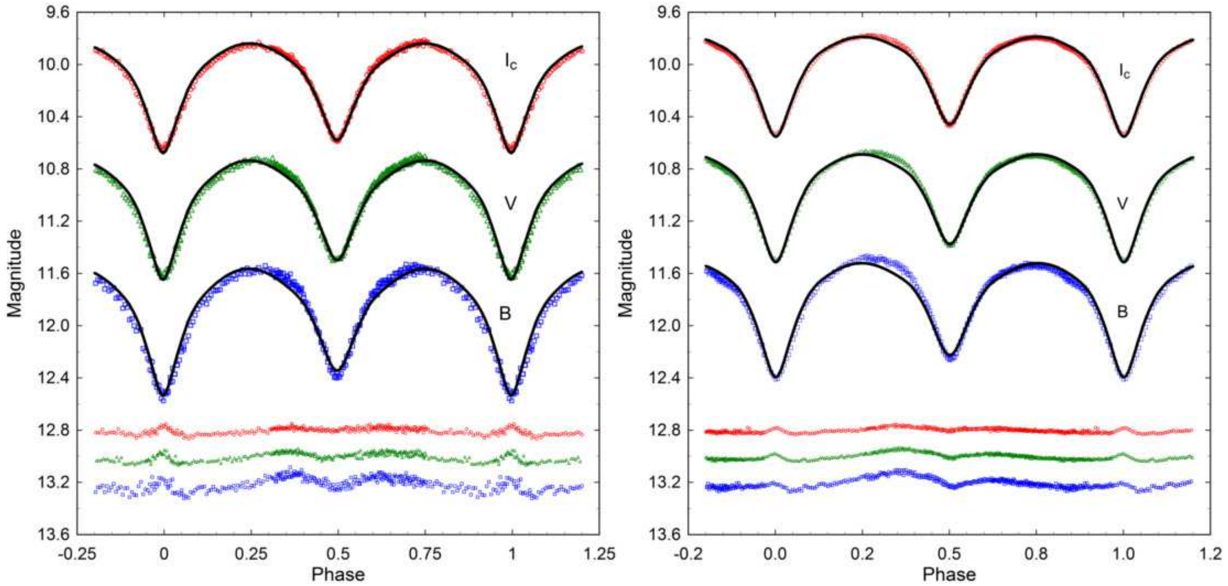

Figure 2. Folded ($P = 0.386497 \pm 0.000001$ d) light curves (BVI_C-mag) for AU Ser produced from data collected in 2011 at UO (left) and during 2018 at DBO (right). Roche model fits using the W-D code were determined without the addition of a spot. For presentation convenience, the corresponding residuals shown at the bottom are offset from zero.

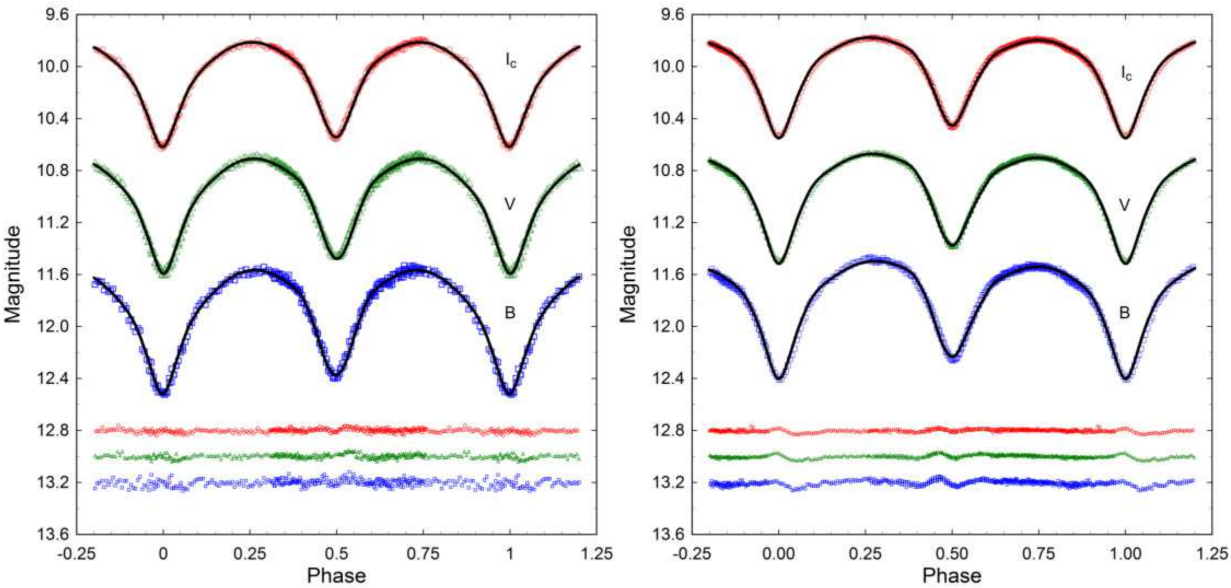

Figure 3. Folded ($P = 0.386497 \pm 0.000001$ d) light curves (BVI_C mag) for AU Ser produced from data collected in 2011 at UO (left) and during 2018 at DBO (right). Roche model fits using the W-D code were determined with the addition of a single hot spot in the neck region of the secondary star. For presentation convenience, the corresponding residuals shown at the bottom are offset from zero.

Table 2. Eclipse time differences (ETD) between 2011 and 2018 calculated from published times of minima (ToM) for AU Ser along with ten new values reported for the first time in this study

HJD (ToM) -2400000	Cycle Number	ETD	Minimum Type	Reference
55753.6815 (1)[a]	8417.5	−0.00055	s	This study
55756.5814 (14)	8425	0.00059	p	This study
55760.6388 (1)	8435.5	−0.00021	s	This study
55764.6971 (3)	8446	−0.00010	p	This study
56034.8573 (1)	9145	−0.00175	p	1
56065.3904 (4)	9224	−0.00196	p	2
56511.4074 (2)	10378	−0.00318	p	3
56782.5374 (9)	11079.5	−0.00126	s	4
56783.5018 (7)	11082	−0.00310	p	4
56787.3675 (1)	11092	−0.00238	p	5
56787.3678 (1)	11092	−0.00207	p	6
56812.4894 (9)	11157	−0.00282	p	4
57084.9700 (1)	11862	−0.00303	p	7
57108.1609 ([b])	11922	−0.00199	p	8
57135.7953 (3)	11993.5	−0.00217	s	7
57136.5691 (20)	11995.5	−0.00136	s	9
57198.6010 (2)	12156	−0.00237	p	This study
57246.3338 (1)	12279.5	−0.00198	s	5
57414.6499 (3)	12715	−0.00555	p	10
57480.5515 (7)	12885.5	−0.00182	s	5
57514.3682 (16)	12973	−0.00366	p	9
57514.5613 (8)	12973.5	−0.00381	s	9
57515.5275 (8)	12976	−0.00386	p	9
58257.7919 (2)	14896.5	−0.00810	s	This study
58267.8408 (1)	14922.5	−0.00817	s	This study
58274.7979 (1)	14940.5	−0.00804	s	This study
58276.7312 (1)	14945.5	−0.00720	s	This study
58280.7886 (1)	14956	−0.00802	p	This study

a: Throughout this paper tabulated uncertainty in least significant figure(s) provided within adjacent parentheses.
b: not reported;
1. Diethelm 2012; 2. Hübscher & Lehmann 2013 3. Hoňková et al. 2014; 4. Hübscher & Lehmann 2015; 5. Parimucha et al. 2016; 6. Hoňková et al. 2015; 7. Nelson 2016; 8. Nagai 2016; 9. Hübscher 2017; 10. Juryšek et al. 2017

3.2 Light Curve Behavior from 2011 and 2018

As is typical for overcontact binary systems, light curves from AU Ser (Figs. 2 & 3) exhibit minima which are separated by 0.5 phase (ϕ) and consistent with synchronous rotation in a circular orbit. Maximum light during the 2011 campaign was nearly equal (Max I $\sim$ Max II) within each bandpass; however, there is significant displacement whereby the brightest values occur after $\phi = 0.25$ (+0.03) and before $\phi = 0.75$ (-0.03). This effect is most obvious in B band and results in skewed peaks during quadrature. Similar behavior is observed with the 2018 light curves (Figs. 2 & 3), except that during this epoch Max I is notably brighter than Max II. It would appear that some kind of surface phenomenon distorts maximum light. Data from folded 2011 LCs B, V and I_C mag) were binned into equal phase intervals (0.002) to produce plots in which color index changes in $B-V$ (Fig. 4: left) and $V-I_C$ (Fig. 4: right) were examined during each orbital phase. Deviation is quite remarkable suggesting that the localized effective temperature increased considerably during quadrature when the neck is maximally exposed.

Surface inhomogeneities have been associated with the presence of cool starspot(s), hot region(s), gas stream impact on either stellar partner, and/or other unknown mechanisms (Yakut and Eggleton 2005). As will be described in more detail in Section 3.4, positioning a hot spot on or near the neck region of the secondary star provided much improved Roche model solutions for the light curve asymmetry observed from 1969-2018. As mentioned earlier, Kałużny (1986) first proposed that a hot spot was responsible for the pronounced asymmetry observed in light curves captured in 1969 and 1970 by Binnendjik (1972). This is in contrast to Roche modeling (W-D) performed by Gürol (2005) who concluded these LCs along with those collected in 1995 (Li et al. 1998) and 2003 (Gürol 2005) were best fit with cool spots on the secondary. Gürol (2005) did, however, show that simulated light curves collected in 1991 (Li et al. 1998) and 1992 (Li et al. 1998) benefited from hot spots on the secondary albeit not in the neck region. It should also be mentioned that Gürol (2005) took an unorthodox approach by allowing A_2, the reflection-coefficient of the secondary, to freely vary during model optimization by differential corrections (DC). As a result the derived values were much larger (3.25–4.44) than the bolometric albedo value (0.5) usually assigned to systems with a convective envelope.

3.3 Effective Temperature

Color index $(B-V)$ data from UO and five other surveys (Table 3) were corrected using the interstellar extinction ($A_V = 0.065$; E(B-V) = 0.021 assuming R = 3.1) estimated for targets within the Milky Way Galaxy according to Amôres and Lépine (2005). The interstellar extinction model GALExtin[1] requires the Galactic coordinates (l, b) and the estimated distance in kpc. In this case the value for A_V (0.065) corresponds to a target located within 164 pc (see Section 3.5). By contrast the dust maps constructed by Schlegel et al. (1998) and updated by Schlafly and Finkbeiner (2011) determine extinction ($A_V =$ 0.172) based on total dust infrared emission in any given direction and not the extinction within a certain distance. In many cases the net effect for relatively close (<1 kpc) stellar objects within the Milky Way Galaxy is an overestimation of reddening. The mean result for intrinsic color, $(B-V)_0 = 0.859 \pm 0.021$, which was adopted for subsequent Roche modeling corresponds to an effective temperature of 5140 K (Pecaut and Mamajek 2013) and ranges in spectral class between K1V and K2V. The $(V-I_C)_0$ color index estimate (0.91 ± 0.02) for the primary star taken at Min II when the secondary nearly reaches total

[1] http://www.galextin.org/v1p0/

Table 3. Effective temperature of AU Ser based upon dereddened $(B-V)^{a}$ data from various surveys and the present study

Stellar Attribute	Terrell et al. (2012)	2MASS	SDSS-DR8	UCAC4	ASCC[d]	This Study
$(B-V)_0$	0.867	0.820	0.878	0.882	0.806	0.851
$T^{b}_{\rm eff}$ (K)	5113	5267	5082	5071	5295	5158
Spectral Class[b]	K1-K2V	K0-K1V	K1-K2V	K1V-K2V	G9V-K0V	K1-K2V

a: E(B-V)= 0.021
b: Interpolated Teff and spectral class range estimated from Pecaut and Mamajek (2013)
c: Median value for $(B-V)_0 = 0.859 \pm 0.021$; $T_{\rm eff1} = 5140 \pm 125$ K corresponds to spectral class K1V-K2V
d: All-sky Combined Catalog of 2.5 million stars 3rd version (Kharchenko 2001)

eclipse is also consistent with a K1V-K2V spectral class (Pecaut and Mamajek 2013). Further support for our adopted $T_{\rm eff1}$ value comes from the Gaia DR2 database in which the nominal $T_{\rm eff}$ (5006 K) for this system is estimated to lie between 4761 and 5197 K (Andrae et al. 2018).

3.4 Roche Modeling

3.4.1 Simultaneous LC and RV solutions

The program PHOEBE 0.31a (Prša and Zwitter 2005) which features a user friendly interface to the WD2003 code (Wilson and Devinney 1971; Wilson 1979; Wilson 1990) was primarily used for initial Roche modeling of LC and RV data. Uncertainty estimates for each of the fitted parameters were ultimately derived using WDwint56a (Nelson 2009), a Windows front-end to the WD2003 source code. In both cases "Mode 3" (Wilson and Leung 1977) designated for overcontact binary systems was selected for fitting while each curve was weighted based upon observational scatter. Bolometric albedo ($A_{1,2}$=0.5) and gravity darkening coefficients ($g_{1,2}$ = 0.32) for stars with convective envelopes were respectively assigned according to Ruciński (1969) and Lucy (1967). New logarithmic limb darkening coefficients (x_1, x_2, y_1, y_2) were interpolated (Van Hamme 1993) following any change in the effective temperature for the secondary ($T_{\rm eff2}$) star. The effective temperature of the more massive and brighter primary constituent was fixed ($T_{\rm eff1}$ = 5140 K). RV data published by Pribulla et al. (2009) were also used to further refine a LC solution for AU Ser. These data, collected in 2008, were obtained using the broadening functions extracted from the Mg I triplet region (5184 Å) located within the V bandpass. As appropriate, RV data were modeled (WDwint56a) with LC data to produce the best simultaneous fits using multiple parameter subsets during DC iterations. The corresponding parameters which were varied included the center-of-mass velocity ($V\gamma$), semi-major axis (SMA), mass ratio (q), surface potential ($\Omega_1 = \Omega_2$), inclination (i) and $T_{\rm eff2}$.

Preliminary Roche modeling attempts had revealed that the addition of a hot spot in the neck region of the secondary star was critical to successfully obtaining a good fit of the LC data. It should also be pointed out that the RV solution for the secondary (RV_2) was sensitive to the absence/presence of a hot spot in the neck region (Fig. 5). This was potentially troubling since the RV data were collected in 2008 and the other multi-color LCs to be evaluated were acquired in 2011 and 2018. Fortuitously, as will be revealed in Section 3.4.3, all evaluable LCs dating from 1969 exhibit skewness about maximum light which can be simulated by the addition of a hot spot near the neck region of the secondary star. Unlike the 2011 LC in which Max I ∼ Max II, sparse LC data (ASAS) collected in 2008 clearly exhibit a negative OConnell effect (O'Connell 1951) where Max II is much brighter (Δ Max I - Max II = -0.059) than Max I (Table 4). In this regard, the well-sampled LC (V mag) collected in 1991 (Li et al. 1992) is the closest match ((Max I - Max II) = -0.026) to that captured during the 2008 survey. Both LCs (1991 and 2008) produced similar results ($q = 0.684 \pm 0.006$ vs. 0.699 ± 0.006) when simultaneously modeled with the 2008 RV data. The mean mass ratio value (0.692 ± 0.006) calculated from the 1991 and 2008 LCs was utilized for subsequent Roche modeling and fixed during DC iterations.

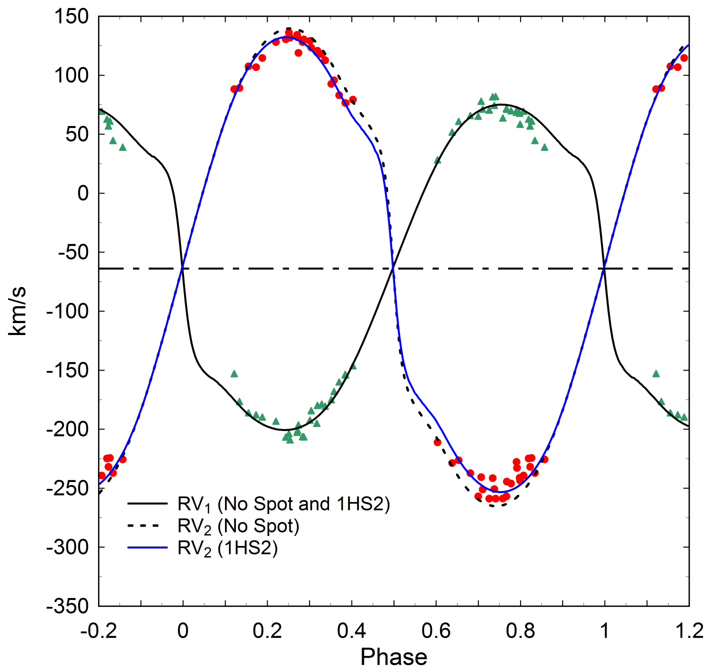

Figure 4. Simultaneous radial velocity (RV) solution for AU Ser without and with a single hot spot in the neck region of the secondary star (1HS2).

3.4.2 Light Curves from 2011 and 2018

As mentioned previously, Roche modeling was constrained using the mass ratio ($q = 0.692 \pm 0.006$) determined after simultaneously modeling RV and LC data (Section 3.4.1). This value is slightly lower than that ($q_{\rm sp} = 0.71$) determined using RV data alone by Hrivnak (1993) and Pribulla et al. (2009). All other parameters except for $T_{\rm eff1}$, $A_{1,2}$ and $g_{1,2}$ were allowed to vary during DC iterations. Multi-color parameter values and results from modeling the 2011 and 2018 LCs are found in Table 5. Corresponding unspotted (Fig. 2) simulations reveal the poor model fit during quadrature which could be significantly improved by the addition of a hot spot near the neck region shared by both stars (Fig. 3).

It is important to point out that the errors listed in Tables 5 and 6 are minimum values from the covariance matrix of the fit which assumed exact values for all fixed parameters. The incorporation of a spot to address LC asymmetry adds another layer of uncertainty due to potential degeneracy of the parameter space during Roche modeling. The shape and location of spot(s) can be highly correlated with many other parameters (e.g. inclination and surface temperature) such that the solution may not be unique.

The fill-out parameter (f) which corresponds to the degree of overcontact between each star was calculated (Eq. 2) according to Kallrath and Milone (1997):

$$f = (\Omega_{\rm inner} - \Omega_{1,2})/(\Omega_{\rm inner} - \Omega_{\rm outer}) \,, \qquad (2)$$

where $\Omega_{\rm outer}$ is the outer critical Roche equipotential, $\Omega_{\rm inner}$ is the value for the inner critical Roche equipotential and $\Omega_{1,2}$ denotes the common envelope surface potential for the binary system. An interesting finding (Table 6) is that the fill-out factor varies substantially (1.5 - 27.3%). One possibility considered was an association between the fill-out factor and the O'Connell effect, however, this proved not to be the case. Attempts to model the LC data from 2018 (f = 4%) as a detached (Mode 2) and semi-detached (Mode 5) system never approached the best Roche lobe fits achieved when AU Ser was considered an overcontact system (Mode 3).

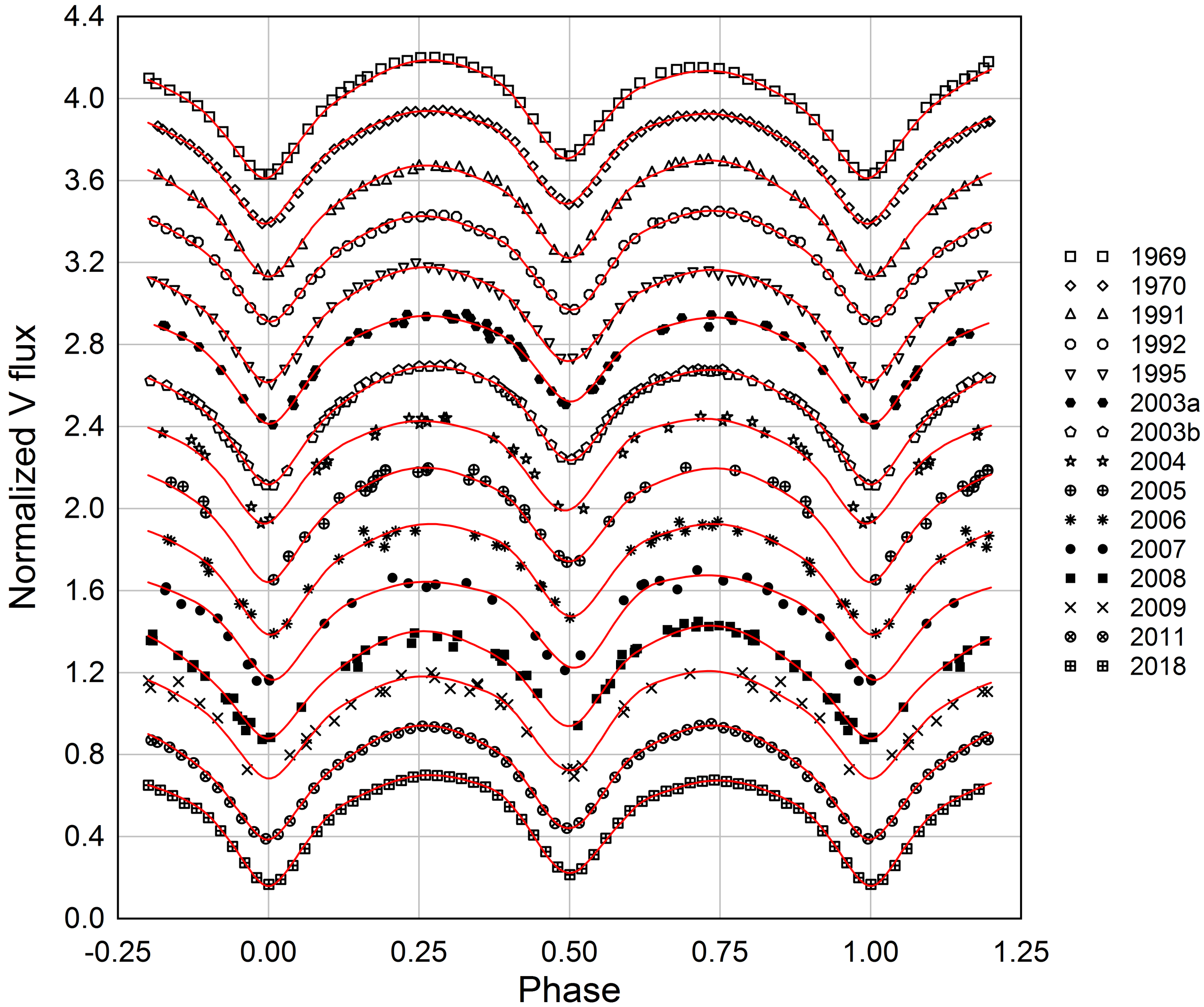

Figure 5. Folded ($P = 0.386497 \pm 0.000001$ d) light curves for AU Ser produced from published V mag data collected between 1969 to 2009 as well as new results reported herein from 2011 and 2018. In each case, Roche modeling with the W-D code required the addition of a single hot spot in the neck region of the secondary star in order to achieve the best fits.

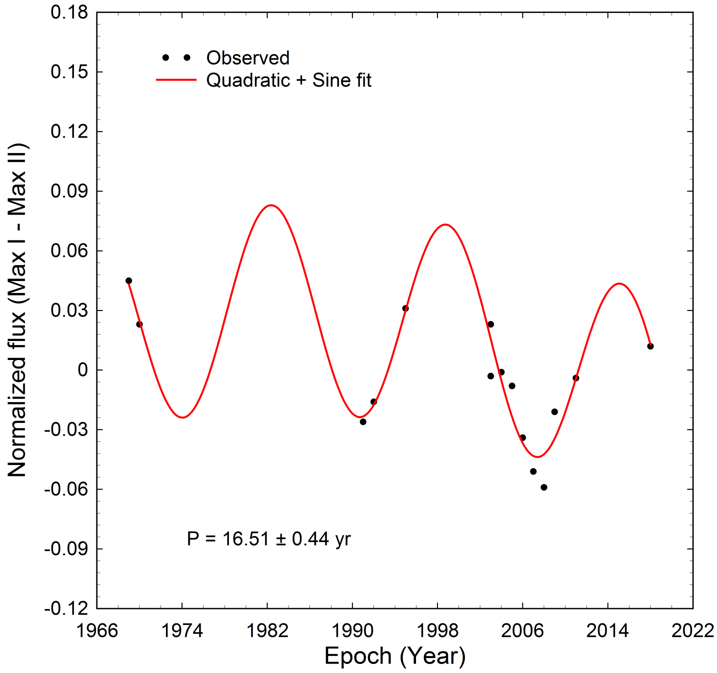

Figure 6. LC variations in Max I-Max II between 1969 and 2018. Differences were fit to a quadratic + sinusoidal expression. The results suggested that there is a ∼ 16.5 yr cycle that may be associated with the O'Connell effect.

Table 4. Differences (± SD) in normalized V-flux relative to Max I

Year	Max I-Min I	Max I-Min II	Max I-Max II
1969[1]	0.572 (6)	0.479 (7)	0.045 (6)
1970[1]	0.561 (6)	0.465 (8)	0.023 (6)
1991[2]	0.562 (8)	0.478 (6)	−0.026 (8)
1992[2]	0.540 (9)	0.484 (6)	−0.016 (7)
1995[3]	0.544 (7)	0.423 (9)	0.031 (4)
2003a[4]	0.586 (6)	0.458 (4)	0.023 (4)
2003b[5]	0.527 (9)	0.436 (6)	−0.003 (7)
2004[5]	0.502 (13)	0.463 (12)	−0.001 (8)
2005[5]	0.564 (26)	0.455 (11)	−0.008 (7)
2006[5]	0.492 (11)	0.404 (11)	−0.034 (8)
2007[5]	0.480 (10)	0.422 (16)	−0.051 (5)
2008[5]	0.500 (8)	0.425 (9)	−0.059 (5)
2009[5]	0.447 (13)	0.453 (15)	−0.021 (6)
2011[6]	0.554 (7)	0.502 (6)	−0.004 (8)
2018[6]	0.496 (6)	0.462 (6)	0.012 (6)

(1) Binnendjik 1972; (2) Li et al. 1992; (3) Li et al. 1998; (4) Gürol 2005;
(5) ASAS survey (Pojmański et al. 2005); (6) Present study

Table 5. Light curve parameters employed for Roche modeling and derived geometric elements for the AU Ser light curves captured in 2011 and 2018

Parameter[a]	2011 No Spot	2011 Spotted	2018 No Spot	2018 Spotted
$T_{\rm eff1}$ (K)[b]	5140	5140	5140	5140
$T_{\rm eff2}$ (K)	5005 (3)	5006 (2)	4973 (2)	4986 (1)
$q(m_2/m_1)$	0.692 (6)	0.692 (6)	0.692 (6)	0.692 (6)
A[b]	0.5	0.5	0.5	0.5
g[b]	0.32	0.32	0.32	0.32
$\Omega_1 = \Omega_2$	3.106 (5)	3.124 (3)	3.225 (3)	3.213 (1)
i°	84.62 (24)	83.03 (10)	83.81 (24)	82.43 (10)
$A_S = T_S/T$	—	1.15 (1)	—	1.12 (1)
Θ_S (spot co-latitude)[c]	—	72.6 (5)	—	90 (9)
ϕ_S (spot longitude)[c]	—	359.8 (2)	—	11.0 (3)
r_S (angular radius)[c]	—	35 (1)	—	30 (2)
$L_1/(L_1+L_2)_B$[d]	0.6244 (8)	0.6247 (4)	0.6387 (12)	0.6339 (6)
$L_1/(L_1+L_2)_V$	0.6150 (5)	0.6153 (2)	0.6272 (3)	0.6233 (1)
$L_1/(L_1+L_2)_{I_C}$	0.6048 (5)	0.6053 (2)	0.6146 (3)	0.6117 (1)
r_1 (pole)	0.3990 (2)	0.4055 (8)	0.3990 (2)	0.3877 (4)
r_1 (side)	0.4242 (6)	0.4321 (10)	0.4242 (6)	0.4094 (5)
r_1 (back)	0.4615 (9)	0.4709 (14)	0.4615 (9)	0.4392 (7)
r_2 (pole)	0.3447 (5)	0.3444 (8)	0.3447 (5)	0.3264 (4)
r_2 (side)	0.3634 (6)	0.3636 (10)	0.3634 (6)	0.3416 (5)
r_2 (back)	0.4053 (10)	0.4083 (16)	0.4053 (10)	0.3739 (7)
Fill-out factor (%)	30.5	25.9	1.1	4.0
rms (B)[e]	0.04611	0.02499	0.03430	0.01821
rms (V)[e]	0.02646	0.01478	0.02281	0.01228
rms (I_C)[e]	0.02034	0.01314	0.01530	0.00976

a: All error estimates for $T_{\rm eff2}$, q, $\Omega_{1,2}$, A_S, Θ_S, ϕ_S, r_S, $r_{1,2}$, L_1 from WDwint56a (Nelson 2009)
b: Fixed during DC
c: Secondary spot temperature, location and size parameters in degrees
d: Bandpass dependent fractional luminosity; L_1 and L_2 refer to scaled luminosities of the primary (more massive) and secondary stars, respectively
e: Root mean square error of model fit

3.4.3 Retrospective analysis of LCs from 1969-2009

W-D modeling (V mag) of the six previously published LCs (Binnendjik 1972; Li et al. 1992; Li et al. 1998; Gürol 2005) was performed with and without a hot spot located near the neck region in a manner similar to that previously described for the 2011 and 2018 data. In addition, sparsely sampled ASAS survey data (V mag) collected between 2003 and 2009 (Pojmański et al. 2005) were phased to produce yearly LCs (Fig. 6) using the ANOVA routine (Schwarzenberg-Czerny 1996) in Peranso 2.5 (Paunzen and Vanmunster 2016). Only the spotted solutions from this retrospective analysis are included herein. Roche modeling of the LCs generated during this period of time provided additional information to chronicle the behavior of AU Ser over a longer period of time than was available to Gürol (2005). Relative V-flux levels at Min I, Min II, Max I and Max II were estimated using polynomial fits near each LC region of interest. A positive OConnell effect (Max I > Max II) was observed in 1969, 1970, 1995, 2003a and 2018, whereas Max II > Max I in 1991, 1992, and between 2005-2009. LCs from 2003b, 2004 and 2011 did not exhibit any meaningful ($\leq$0.004) differences in maximum light (Table 4). It should be noted that photometric data captured by Gürol (2005) in 2003 occurred between 22 July and 26 Aug 2003, whereas the majority (80%) of the data during the ASAS survey were acquired before 22 July 2003. This may explain differences in the modeling results (2003a vs. 2003b).

A quadratic + sinusoidal fit (Fig. 7) of flux normalized Max I - Max II values over time (1969-2011) uncovered a periodic change (16.51 ± 0.44 yr) in the LCs. Gürol (2005) performed a similar analysis but over a shorter time frame (1969-2003) and arrived at a different conclusion which suggested the most probable period for flux variation relative to Max I ranged between 32 and 35 yr. Upon further examination, one finds that Gürol (2005) proposed two other possible solutions at 8.9 and 17.3 yr. It is not hard to imagine period harmonics which are simple multiples in the ratio 8.5:17:34. The middle value closely approximates the more robust period estimate from this study and indicates that flux change relative to that observed at Max I occurred nearly every 17 yr and corresponds to the transition from a positive to negative O'Connell effect. Furthermore, assessment of the LCs and each corresponding Roche model fit (Table 6) offer compelling evidence for persistent feature(s) on AU Ser that skew maximum light to occur after $\phi = 0.25$ and then before $\phi = 0.75$; the best fits were consistently achieved by positioning a hot spot on or near the neck region of the secondary star.

As depicted in Figure 8, spatial models of AU Ser showing the sequence of hot spot locations were rendered with BM3 using the physical and geometric elements determined from all LCs investigated herein. As might be expected, the longitudinal position of the hot spot relative to the neck center (0°) is highly correlated (r=0.913) with the difference between Max I and Max II (Fig. 9). A working hypothesis posits the transfer of mass from the primary to the secondary; the net effect is a tightening of the orbital radius and as is observed (Section 3.6), a decrease in orbital period. The transfer of matter and energy onto the secondary is mediated through the neck region and may result in the formation of a hot spot (Maceroni and van't Veer 1993). Not surprisingly when comparing the multi-color LCs from 2011 and 2018, increased brightness and skewed timings during maximum light were observed in the more energetic region (B bandpass) of the visual spectrum. Although not uncommon for overcontact binaries, X-ray emission coincident with the position for AU Ser was detected by Szczygieł et al. (2008) using a combined database generated from the ASAS and ROSAT All Sky Survey. In this case, it is not known whether X-ray emission corresponds to changes in orbital phase when a putative hot spot would be maximally exposed.

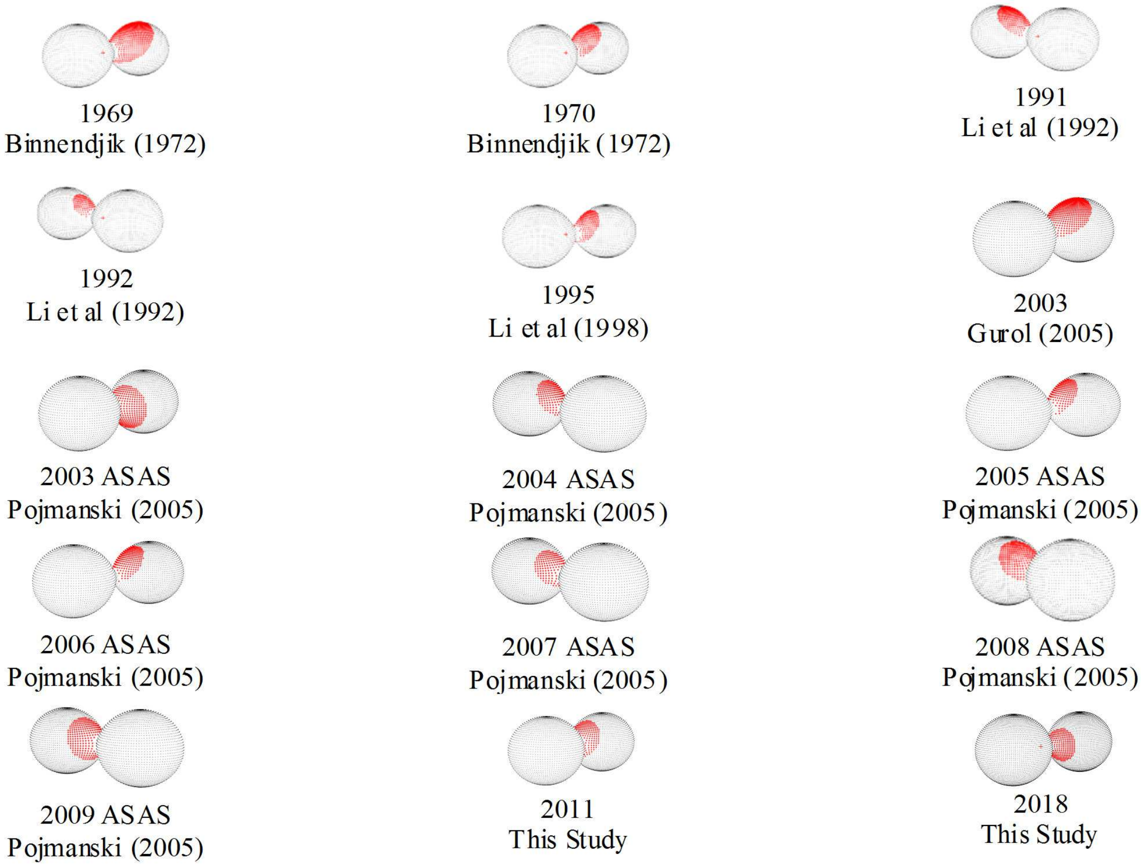

Figure 7. AU Ser spatial models rendered with BM3 showing movement of the hot spot on or near the neck region of the secondary star between 1969-2018

Table 6. Light curve (V mag) parameters employed for Roche modeling (spotted) and derived geometric elements from AU Ser light curves captured between 1969 and 2018.

Parameter	1969[1]	1970[1]	1991[2]	1992[2]	1995[3]	2003a[4]	2003b[5]	2004[5]	2005[5]	2006[5]	2007[5]	2008[5]	2009[5]	2011[6]	2018[6]
$T_{\rm eff1}$ (K)[b]	5140	5140	5140	5140	5140	5140	5140	5140	5140	5140	5140	5140	5140	5140	5140
$T_{\rm eff1}$ (K)	4907(3)	4896(2)	4942(4)	4991(5)	4875(6)	4863(4)	4896(7)	4969(9)	4882(11)	4916(12)	4954(12)	4998(24)	5054(13)	5014(1)	4986(1)
$q(m_2/m_1)$	0.692(6)	0.692(6)	0.684(6)	0.692(6)	0.692(6)	0.692(6)	0.692(6)	0.692(6)	0.692(6)	0.692(6)	0.692(6)	0.699(6)	0.692(6)	0.692(6)	0.692(6)
A[b]	0.5	0.5	0.5	0.5	0.5	0.5	0.5	0.5	0.5	0.5	0.5	0.5	0.5	0.5	0.5
g[b]	0.32	0.32	0.32	0.32	0.32	0.32	0.32	0.32	0.32	0.32	0.32	0.32	0.32	0.32	0.32
$\Omega_{1,2}$	3.18(1)	3.19(1)	3.12(1)	3.16(1)	3.16(1)	3.18(1)	3.23(1)	3.22(1)	3.17(2)	3.19(2)	3.21(2)	3.19(2)	3.19(3)	3.13(3)	3.21(1)
i°	82.1(2)	82.0(1)	82.2(1)	81.5(3)	83.0(4)	83.2(2)	82.0(4)	81.0(1)	82.3(7)	81.2(8)	81.3(7)	82.7(1.8)	80.2(1.1)	82.8(1)	82.4(1)
$A_S = T_{\rm S}/T$	1.11(1)	1.16(1)	1.17(1)	1.19(1)	1.11(1)	1.13(1)	1.14(1)	1.11(1)	1.11(1)	1.14(1)	1.15(2)	1.12(1)	1.12(1)	1.14(1)	1.12(1)
$\Theta_{\rm S}$ (co-lat.)[c]	49.6 (1.3)	59.6 (1.3)	50 (12)	65 (3)	70 (7)	46.2 (2)	19.6 (1)	70 (4)	65 (15)	62 (5)	56 (18)	59 (12)	79.5 (7.3)	71.1 (1)	90 (1)
$\phi_{\rm S}$ (long.)[c]	18.5 (1.1)	4.2 (4)	352 (3)	350 (1)	5 (2)	6 (1)	6 (2)	355 (4)	2(5)	0 (3)	345 (5)	350 (6)	350 (6)	0(1)	11 (1)
r_S (radius)[c]	60.1 (6)	37.3 (2)	40 (1)	25 (1)	35 (1)	48 (1)	48 (1)	33.8 (1.6)	34 (3)	35 (8)	28 (3)	36 (2)	36 (2)	35 (1)	30 (1)
Fill-out (%)	12.9	10.4	24.4	15	17	13	5.3	1.5	13.7	10.4	10.0	27.3	5.8	25.7	4

1. Binnendijk 1970; 2. Li et al. 1992; 3. Li et al. 1998; 4. Gürol 2005; 5. Pojmański et al. 2005; 6. This study
a: All error estimates for T_{eff2}, q, $\Omega_{1,2}$, A_S, Θ_S, ϕ_S, r_S from WDwint56a (Nelson 2009)
b: Values fixed during DC
c: Positional (Θ and ϕ) and size ($r_{\rm S}$) spot parameters in degrees

Table 7. Mean absolute parameters (±SD) for AU Ser using results from the simultaneous (LC and RV) Roche model fit of V mag data from 1991 and 2008.

Parameter	Primary	Secondary
Mass ($M_\odot$)	0.85 (3)	0.59 (2)
Radius ($R_\odot$)	1.04 (1)	0.88 (1)
a ($R_\odot$)	2.52 (3)	—
Luminosity ($L_\odot$)	0.675 (13)	0.427 (9)
$M_{\rm bol}$	5.177 (22)	5.675 (22)
log(g)	4.336 (16)	4.323 (16)

3.5 Absolute Parameters

Absolute parameters (Table 7) were derived for each star in this A-type W UMa binary system using results from the best fit spotted model simulations from 1991 and 2008. Aside from a spectroscopic mass ratio ($q_{\rm sp}$), another critical piece of information supplied by an RV experiment is the determination of the orbital speeds ($v_{\rm 1r}$ $+v_{\rm 2r}$) whereby the total mass can be readily calculated according to Eq. 3 when the orbital inclination is also known:

$$(m_1 + m_2)\sin^3 i = (P/2\pi G)(v_{\rm 1r} + v_{\rm 2r})^3. \tag{3}$$

In this case from the mean simultaneous fit of LC and RV data (1991 and 2008), $K_1 = 135.2{\pm}1.1$ km/s , $K_2 = 195.5{\pm}1.8$ km/s, $V_\gamma = -63.8{\pm}0.68$ km/s and $i = 82.5{\pm}1.8°$. The total mass of the system was determined to be 1.44 ± 0.05 $M_\odot$ so it follows that since $q = 0.692 \pm 0.006$ then the primary mass = 0.85 ± 0.03 $M_\odot$ and secondary mass = 0.59 ± 0.02 $M_\odot$.

The semi-major axis, $a(R_\odot) = 2.52{\pm}0.03$, was calculated according to Newton's version (Eq. 4) of Keplers third law where:

$$a^3 = G \times P^2(M_1 + M_2)/4\pi^2. \tag{4}$$

The effective radii of each Roche lobe (R_L) can be calculated to within an error of 1% over the entire range of mass ratios ($0 < q < \infty$) according to the expression (5) derived by Eggleton (1983):

$$r_L = (0.49q^{(2/3)})/(0.6q^{(2/3)} + \ln(1 + q^{(1/3)})) \tag{5}$$

from which values for r_1 (0.4112 ± 0.0005) and r_2 (0.3475 ± 0.0005) were respectively determined for the primary and secondary stars. Since the semi-major axis and the volume radii are known, one can calculate the solar radii for both binary constituents where $R_1 = a \times r_1 = 1.04 \pm 0.01$ $R_\odot$ and $R_2 = a \times r_2 = 0.88 \pm 0.01$ $R_\odot$.

The bolometric magnitudes ($Mbol_{1,2}$) and luminosity in solar units ($L_\odot$) for the primary (L_1) and secondary stars (L_2) were calculated from well known relationships for bolometric magnitude (Eq. 6) and luminosity (Eq. 7) where:

$$M_{bol1,2} = 4.75 - 5\log(R_{1,2}/R_\odot) - 10\log(T_{1,2}/T_\odot) \tag{6}$$

and

$$L_{1,2} = (R_{1,2}/R_\odot)^2(T_{1,2}/T_\odot)^4. \tag{7}$$

Pooling the results for T_{eff2} across all LCs (1991-2018) leads to a mean value of 4943 ± 58 K (Table 6). Assuming that $T_{\rm eff1} = 5140$ K and $T_\odot = 5778$ K, then $L_\odot$ for the primary and secondary are 0.675 ± 0.013 and 0.427 ± 0.020, respectively. Bolometric magnitudes were calculated to be $M_{\rm bol1} = 5.127 \pm 0.009$ and $M_{\rm bol2} = 5.691 \pm 0.052$. Combining the bolometric magnitudes resulted in an absolute value ($M_V = 4.663 \pm 0.009$) when adjusted with the bolometric correction (BC$= -0.272$) interpolated from Pecaut and Mamajek (2013). Substituting into the Eq. 8, the distance modulus:

$$d(\mathrm{pc}) = 10^{((m-M_V)-A_V+5)/5)}, \tag{8}$$

where $m = V_{\rm avg}(10.71 \pm 0.01)$ and $A_V = 0.065$ leads to an estimated distance of 171 ± 2 pc to AU Ser which is 5% higher than that (164 ± 1 pc) calculated directly from parallax data recently included in the Gaia DR2 release (Brown et al. 2018). Although not unreasonable, this discrepancy may result from the use of MPOSC3-catalog based magnitudes rather than determining values from absolute photometry with reference star field standards.

3.6 Period analyses from eclipse time differences

Over the years there have been many period studies of this system. Kennedy (1985) was the first to suggest that changes had occurred in the eclipse timing differences (ETDs) for AU Ser. Qian et al. (1999) performed the first systematic examination of period and light time variations for this system and noted that the orbital period suddenly decreased between 1987 and 1988. They suggested there might be a connection between the light curve asymmetries and sudden changes in the orbital period. The next detailed analysis of the ETDs was conducted by Gürol (2005) in which he modeled the residuals over time with a quadratic plus sinusoidal equation and subsequently dismissed the notion of a sudden period change. Furthermore Gürol (2005) proposed that the predominant cyclic behavior with a period of about 94 yr was most likely associated with the light-time-effect (LiTE) caused by an invisible but gravitationally bound third star.

A case, albeit somewhat less convincing, can be made which argues against the presence of a gravitationally-bound third body. It should be noted that during our Roche modeling, l_3, the third light parameter, was not significantly different from zero when allowed to freely vary during iterative DC. This implies that a putative gravitational partner in this system is either too small to detect during simulations of the observed light curve data or that some other phenomena are responsible for the $\sim$94 yr periodicity in the eclipse timing residuals. Assuming that the putative third body is still on the main sequence its absolute luminosity can be estimated according to the mass-luminosity relationship where $L \sim M^{3.5}$. The fractional luminosity of the third constituent (L_3) can be calculated from the expression (Eq. 9):

$$L_3(\%) = (100 \times M^{3.5}_{3,\rm min})/(L_1 + L_2 + M^{3.5}_{3,\rm min}) \tag{9}$$

where M_3 is the minimum mass determined when $i = 90°$ and L_1 and L_2 are the luminosities in solar units ($L_\odot$) determined for the primary and secondary stars (Table 7).

Comparisons among third body solutions proposed by Gürol (2005), Amin (2015), Nelson et al. (2016) and this study are summarized in Table 8. According to our LiTE modeling, the luminosity contributed by a third body ($L_3 \sim 1.2\%$) where $M_3 = 0.293\ M_\odot$ would be challenging to detect photometrically. However, the minimum mass estimates for a third body reported (Table 8) by Amin (2015) and Gürol (2005) would have resulted in even greater contributions ($L_3 > 6\%$) to the total luminosity of the system. According to their LiTE modeling results, this extra light (l) should have been detected during W-D modeling of LC data. Finally, another confounding result arguing against LiTE comes from an RV study in which Pribulla et al. (2009) did not see spectroscopic evidence for a third body in the broadening functions. It is clear that additional high-precision photometric and spectroscopic data will be necessary to fully tease out the effect(s) which lead to episodic changes in the eclipse timings for AU Ser.

Amin (2015) and Nelson et al. (2016) re-examined the period behavior of AU Ser using ETD data gathered between 1936 and 2015. Modeling efforts by Amin (2015) which included 39 new minima times led to values for a putative third body which contrast sharply with the period (P_3) and semi-amplitude (A) reported by Gürol (2005) and Nelson et al. (2016). There was, however, general concurrence between Amin (2015) and Gürol (2005) that the mechanism for a light-time effect was probably not due to cycles in magnetic activity attributed to Applegate (1992). This is further supported using an empirical relationship (Eq. 10) between the length of orbital period modulation and angular velocity ($\omega = 2\pi/P_{\rm orb}$) that was developed by Lanza and Rodonò (1999):

$$\log P_{\rm mod}[y] = 0.018 - 0.36 \times \log\left(2\pi(P_{\rm orb}[s])\right). \tag{10}$$

In this case any period modulation resulting from a change in the gravitational quadrupole moment would probably be closer to 23 yr for AU Ser, not the longer periods ($P_3 >$ 42 yr) proposed by Gürol (2005) and Amin (2015). Significant differences in the quadratic coefficient were reported depending upon whether or not visual (vis) and photographic (pg) data were included in the analyses. This disparity points out the vagaries associated with period change and mass transfer analysis from eclipse timing residuals; other factors contributing to error are discussed in depth in a series of papers by Nelson et al. (2014; 2015; 2016). Ironically in Nelson et al. (2016), several widely different LiTE solutions emerged: A_1 (an update to the analysis of Gürol (2005) but using LiTE analysis in which $P_3 = 29.9$ yr), B_1 (another update to Gürol 2005 where $P_3 = 96.4$ yr), and finally a new fit, solution C ($P_3 = 38.6$ yr). Nelson et al. (2016) concluded that it was "problematic which solution to choose"; however they favored solution A_1. Here again it was evident with our fresh analysis which includes ETs reported by Gürol (2005) and Amin (2015) and 10 new ETs from this study, that many early pg and vis eclipse timings identified as outliers in Fig. 10 seemingly describe a completely different pattern than all the others derived from ccd and photoelectric (pe) analyses. Removal of these data from consideration was not taken lightly, however, as it became very clear after multiple model iterations, their inclusion made it impossible to properly simulate the orbital period variability of AU Ser after 1969. This would severely limit the ability to predict future behavior of AU Ser and thus derive a robust hypothesis for the underlying sinusoidal-like variations in the orbital period. Data included in all subsequent (1969-2018) curve fitting were weighted in the ratio 0.04:1:1 (vis:pe:ccd).

Stepping back for a moment to first principles, shifts in the times of minimum light under the influence of a third body orbiting a binary system can be evaluated according to the generalized expression (Eq. 11):

$$(\mathrm{ETD})_{fitted} = c_0 + c_1 E + c_2 E^2 + \tau, \tag{11}$$

where c_0, c_1 and c_2 are constants, E = cycle or epoch number, and τ = time difference due to orbital motion, an expression derived by Irwin (1952; 1959). Ignoring the last term (τ=0) for the moment, initial curve fitting (scaled Levenberg-Marquardt algorithm) revealed a quadratic coefficient ($c_2 \approx -5.0 \times 10^{-11}$) that is less than zero (downwardly turned parabola) suggesting that the orbital period is decreasing at a constant rate. A secular change defined by a parabola is often attributed to mass transfer or by angular momentum loss (AML) due to magnetic stellar wind. Ideally when AML dominates the net effect is a decreasing orbital period whereas the opposite is observed with conservative mass transfer from the secondary to the primary star. Notably, residuals from the quadratic model fit also describe an underlying sinusoidal-like variation in the orbital period. As long as this sinusoidal curve appears symmetrical as suggested in the middle panel of Fig. 10, this behavior can be fit in its simplest form using a quadratic formula (Eq. 12) modulated with a sine term (τ) such that:

$$(\mathrm{ETD})_{\mathrm{fitted}} = c_0 + c_1 E + c_2 E^2 + c_3 \sin(c_4 E + c_5) \quad (12)$$

where c_0, c_1 and c_2 are constants, E = cycle number, and τ = time difference due to orbital motion. This simplified light-time effect (LiTE) analysis using a scaled Levenberg-Marquardt (L-M) algorithm assumes that the putative third body revolves about a common gravitational center in a circular orbit (e=0). The amplitude of the oscillation, as defined by the coefficient of the sine term (c_3), was determined to be 0.0116 ± 0.0003 d while the period of the sinusoidal oscillations was calculated ($P_3 = 31.2 \pm 0.3$ yr) according to the expression (Eq. 13):

$$P_3 = 2\pi P/\omega\,, \quad (13)$$

where ω, the angular frequency, is defined by the coefficient c_4 (0.000213 ± 0.000004) and P is the orbital period of the binary pair in days. Cyclic changes of eclipse timings may result from the gravitational influence of unseen companion(s) and/or periodic changes in the magnetic activity of either binary constituent. It has been well documented that a significant percentage ($> 50\%$) of overcontact binaries exist as multiple systems (Pribulla et al. 2006; D'Angelo et al. 2006). Additional analyses including the associated parameters in the LiTE equation (Irwin 1952; 1959) were derived using the Solver routine in an Excel spreadsheet described by Nelson et al. (2016). These parameters include: P_3 (orbital period of star 3 and the 1-2 pair about their common center of mass), e (orbital eccentricity), ω (argument of periastron), t_3 (time of periastron passage) and the semi-amplitude (A) of the light-time effect. The semi-amplitude is further defined as $A = a_{12}\sin(i_3) \times c^{-1}$ where a_{12} = semi-major axis of the 1-2 pair's orbit about the center of mass of the 3-star system, i_3 = orbital inclination of the 3-star system, and c = speed of light. These five parameters, as well as the coefficients c_0, c_1, and c_2 from Eq. 12 add up to a total of eight variables which are factored into LiTE modeling. It was apparent from our simplified L-M solution ($P_3 = 31.2 \pm 0.3$ yr) which included 10 new times-of-minima (Table 8) that period (P_3) solutions A_1 (29.8 yr) and A_2 (29.4 yr) from Nelson et al. (2016) were very close. We repeated this simplest solution which fixes the third body with a circular orbit (e=0) and another where e is allowed to vary using the aforementioned eight parameter Excel Solver routine to optimize the LiTE fit. These two analyses produced similar results when comparing the root mean square errors (Table 8). The latter solution in which a putative third body revolves in a somewhat eccentric orbit ($e = 0.168$) appears to offer a slightly improved fit but at the expense of an increased error estimate for P_3 (31.36 ± 1.18 vs. 31.49 ± 0.40 yr). Nonetheless, considering an improbably stable circular orbit for a circumbinary star, we arrive at a preferred solution in which the orbit is slightly elliptical ($e = 0.168 \pm 0.023$). Thereafter it was possible to subtract out the LiTE component of the ETD values leaving, in this case, a parabolic relationship with quadratic constant $c_2 = -6.19(20) \times 10^{-11}$ d (Fig. 10). Assuming that the secular decrease in orbital period is associated with mass loss from the primary to the secondary, then a period rate loss ($dP/dt = -1.17(4) \times 10^{-7}$ d/yr) can be estimated from Eq. 14:

$$dP/dt = 2 \times (365.24) \times c_2/P. \quad (14)$$

Table 8. Putative period change, mass loss and third-body solution to the light-time effect observed from changes in AU Ser eclipse timings

Parameter	Units	Gürol (2005)	Amin (2015)	Nelson et al. (2016)	This study	This study
t_0	HJD[a]	44722.4515	44722.4683 (14)	44722.4472	44722.4725	44722.4725
t_3 (init, epoch)	[d]	10023.9468		10857 (533)	—	10176 (2666)
P_3 (period)	[yr]	94.15	43 (3)	29.8 (5)	31.49 (40)	31.36 (1.18)
A (Amplitude)	[d]	0.0355	0.0197 (16)	0.0110 (3)	0.0109 (2)	0.0116 (4)
e (eccentricity)		0.48	0.52 (12)	0	0	0.168 (23)
ω, arg. periast.	°	147.7	—	—	—	163.7 (20.5)
$a_{12}\sin(i)$	[AU]	—	3.66 (30)	1.90 (5)	1.89 (3)	2.01 (8)
$f(m_3)$	$M_\odot$	0.034199	0.02662 (13)	0.0077 (5)	0.0068 (4)	0.0082 (14)
M_3 (i=90°)	$M_\odot$	0.53	0.475 (1)	—	0.271	0.293
M_3 (i=60°)	$M_\odot$	—	0.564 (1)	—	0.319	0.342
M_3 (i=30°)	$M_\odot$	—	1.153 (3)	—	0.612	0.661
c_2 (Quad. coeff.)	$\times 10^{-11}$	−7.29	−4.69	−6.8 (3)	−6.28 (8)	−6.19 (20)
dP/dt	10^{-7} d/yr	−1.378	−0.887	—	−1.19 (1)	−1.17 (4)
dM_1/dt	$10^{-7} M_\odot$/yr	−2.598	—	—	−1.95 (8)	−1.93 (10)
rss[b]					0.000643433	0.000612608

a: HJD-24000000
b: Residual Sum of Squares (rss)

Finally, the rate of conservative mass transfer was calculated using Eq. 15:

$$dM/dt = M_1 M_2/(3P(M_1 - M_2))dP/dt, \qquad (15)$$

where M_1 is the mass of the primary star in solar units, M_2 is the mass of the secondary star in solar units, and P is the orbital period of binary pair. Accordingly, the mass-transfer rate (dM_1/dt) for AU Ser was estimated to be $-1.93(10) \times 10^{-7} M_\odot$/yr.

4 Conclusions

Reported herein are the first BVI_C CCD-based light curves for AU Ser which have also produced 10 new times of minimum for this A-type W UMa binary system. Evidence from this study and other surveys suggested that the effective temperature of the primary star was $\sim$ 5140 K which corresponds to a spectral class range between K1V and K2V. During Roche modeling with the W-D code, a spotted solution was necessary since all evaluable LCs from 1969 to 2018 exhibited asymmetry with regard to intensity and/or peak skewness during quadrature (maximum light was displaced after $\phi = 0.25$ and before $\phi = 0.75$). Positioning a single hot spot on the secondary near the neck between both stars produced the best Roche model fits. The relative location of the secondary hot spot corresponded to cyclical changes ($\sim$ 16.5 yr) which appeared to be associated with the so-called "O'Connell effect". Regression analyses performed using ETDs indicate that the orbital period for AU Ser has been decreasing at a rate of $\sim 1.18 \times 10^{-7}$ d yr^{-1}. This secular change in orbital period may be related to mass transfer from the primary onto the secondary and is consistent with the appearance of a persistent hot spot in the neck region of the secondary star. LiTE analysis on a subset of time-of-minimum observations spanning the last 49 years uncovered a sinusoidal-like variation ($P_3 \sim 31.36$ yr) in the orbital period of the binary pair. This was most likely associated with the gravitational influence of a third body, however, the possibility of other forces at play (eg. cycles in

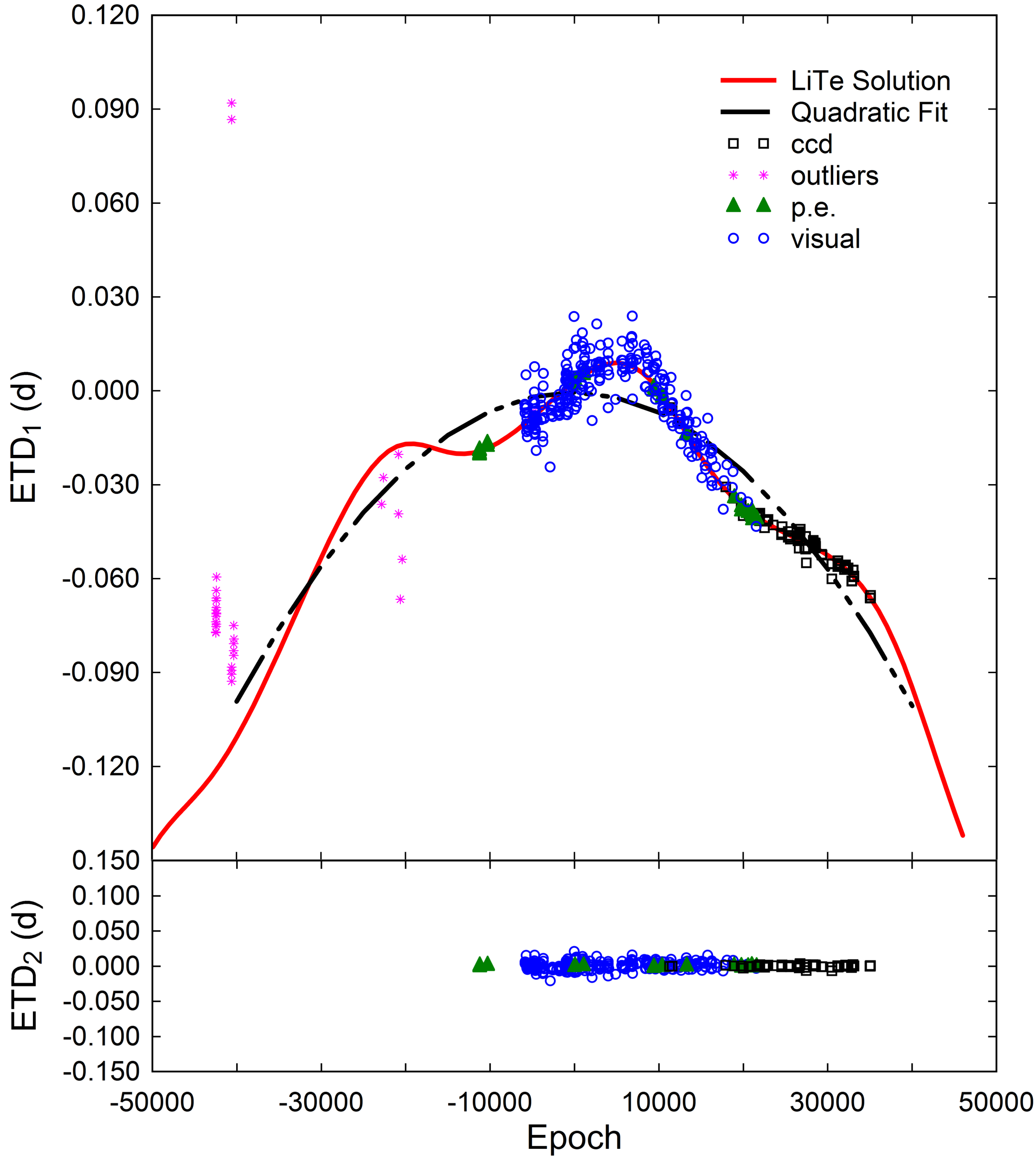

Figure 8. Preferred LiTE solution ($P_3 = 31.36 \pm 1.2$ yr) incorporating 10 new eclipse timings for AU Ser. The top panel includes all eclipse time differences (ETD_1) however the model fit does not include those labeled as "Outliers = *". The bottom panel shows the residuals (ETD_2) remaining from the final LiTE fit.

magnetic activity) cannot be completely discounted. As is often the case with complex behaviors uncovered by analyzing secular changes in overcontact binary systems, many more years of data will likely be required to confirm the true nature of periodic variation observed in the eclipse timings.

Acknowledgements: This research has made use of the SIMBAD database, operated at Centre de Donnes astronomiques de Strasbourg, France, the Northern Sky Variability Survey hosted by the Los Alamos National Laboratory and the International Variable Star Index maintained by the AAVSO. The diligence and dedication shown by all associated with these organizations is very much appreciated. We are indebted to the many observers who have published a wealth of eclipse timing data for AU Ser over the past 80+ years. This work has also made use of data from the European Space Agency (ESA) mission Gaia. This research did not receive any grant from funding agencies in the public, commercial, or not-for-profit sectors. In addition, we gratefully acknowledge the insightful comments from Prof. Robert Wilson and the careful review and commentary from an anonymous referee.

References:

Alton, K.B. 2016, *JAAVSO*, **44**, 87
Alton, K.B. 2018, *IBVS*, **63**, 6241 DOI
Amin, S.M. 2015, *J. Korean Astron. Soc.*, **48**, 1
Amôres, E.B. and Lépine, J.R.D. 2005, *AJ*, **130**, 659 DOI
Andrae, R., Fouesneau, M., Creevey, O., et al. 2018, *A&A*, **616**, A8 DOI
Applegate, J. 1992, *ApJ*, **385**, 621 DOI
Binnendijk, L. 1972, *AJ*, **77**, 603 DOI
Bradstreet, D.H. and Steelman D.P. 2002, *Bull. A.A.S.*, **34**, 1224
Brown, A.G.A., Vallenari, A., Prusti, T., et al. 2018, *A&A*, **616**, A1 DOI
D'Angelo, C., van Kerkwijk, M.H., Ruciński, S.M. 2006, *AJ*, **132**, 650
Diethelm, R. 2012, *IBVS*, **61**, 6029
Djurašević, G. 1992, *Ap&SS*, **196**, 241 DOI
Djurašević, G. 1993, *Ap&SS*, **206**, 207 DOI
Eggleton, P.P. 1983, *ApJ*, **268**, 368 DOI
Gürol, B. 2005, *New Astron.*, **10**, 653 DOI
Harris, A.W., Young, J.W., Bowell, E., et al. 1989, *Icarus*, **77**, 171 DOI
Hoffmeister, C. 1935, *AN*, **255**, 401.
Hoňková K., Juryšek J., Lehký M., et al. 2014, *OEJV*, **0165**.
Hoňková K., Juryšek J., Lehký M., et al. 2015, *OEJV*, **0168**.
Hrivnak, B. 1993, *ASP Conference Series*, **38**, 269
Hübscher, J. 2017, *IBVS*, **62**, 6196 DOI
Hübscher, J. and Lehmann, P.B. 2013, *IBVS*, **61**, 6070
Hübscher, J. and Lehmann, P.B. 2015, *IBVS*, **62**, 6149
Huth, H. 1964, *Mitt. Sonneberg*, **2**, 126
Irwin, J.B., 1952, *ApJ*, **116**, 211 DOI
Irwin, J.B., 1959, *ApJ*, **64**, 149 DOI
Juryšek, J., Hoňková K., Šmelcer, L. et al. 2017 *OEJV*, **0179**
Kallrath, J. and Milone, E. F. 1999, *Eclipsing Binary Stars: Modeling and Analysis*, Springer, New York
Kałużny, J. 1986, *AcA*, **36**, 113

Kennedy, H.D. 1985, *IBVS*, **28**, 2742
Kharchenko, N.V. 2001, *Kinematika i Fizika Nebesnykh Tel*, **17**, 409
Kreiner, J.M. 2004, *AcA*, **54**, 207
Kwee, K.K. and Woerden, H. van 1956, *B.A.N.*, **12**, 327
Lanza, A.F. and Rodonò, M. 1999, *A&A*, **349**, 887
Li, Z-Y., Zhan, Z-S., and Li, Y-L. 1992, *IBVS*, **39**, 3802
Li, Z-Y., Ding, Y-R., Zhang, Z-S., and Li, Y-L. 1998, *A&AS*, **131**, 115 DOI
Lucy, L.B. 1967, *Z. Astrophys.*, **65**, 89
Maceroni, C. and van't Veer, F. 1993, *A&A*, **277**, 515.
Minor Planet Observer 2015, MPO Software Suite, BDW Publishing, Colorado Springs, CO (`http://www.minorplanetobserver.com`)
Nagai, K. 2016, *Variable Star Bulletin of Japan*, **61**
Nelson, R.H. 2009, *WDwint56a: Astronomy Software by Bob Nelson* (`https://www.variablestarssouth.org/bob-nelson/`).
Nelson, R.H. 2016, *IBVS*, **62**, 6164
Nelson, R.H., Terrell, D., and Milone, E.F. 2014, *New Astron. Rev.*, **59**, 1 (Paper 1) DOI
Nelson, R.H., Terrell, D., and Milone, E.F. 2015, *New Astron. Rev.*, **69**, 1 (Paper 2) DOI
Nelson, R.H., Terrell, D., and Milone, E.F. 2016, *New Astron. Rev.*, **70**, 1 (Paper 3) DOI
O'Connell, D.J.K. 1951, *Pub. Riverview College Obs.*, **2**, 85
Parimucha, Š., Dubovský, P., Kudak, V. and Perig, V. 2016, *IBVS*, **62**, 6167
Paunzen, E. and Vanmunster, T. 2016, *AN*, **337**, 239
Pecaut, M.J. and Mamajek, E.E. 2013, *ApJS*, **208**, 9 DOI
Pojmański, G., Pilecki, B., and Szczygieł, D. 2005, *AcA*, **55**, 275
Pribulla, T. and Ruciński, S.M. 2006, *AJ*, **131**, 2986
Pribulla, T., Ruciński, S.M., Debon, H., et al. 2009, *AJ*, **137**, 3646 DOI
Prša, A., and Zwitter, T. 2005, *ApJ*, **628**, 426 DOI
Qian, S., Qingyao, L. and Yang, Y. 1999, *A&A*, **341**, 799
Ruciński, S. M. 1969, *AcA*, **19**, 245
Schlafly, E. F. and Finkbeiner, D. P. 2011, *ApJ*, **737**, 103 DOI
Schlegel, D. J., Finkbeiner, D. P., and Davis, M. 1998, *ApJ*, **500**, 525. DOI
Schwarzenberg-Czerny, A. 1996, *ApJ*, **460**, L107 DOI
Soloviev, A.V. 1951, *Tadjik Obs. Circ.* **No. 21**.
Szczygieł, D.M., Socrates, A., Paczyński, B., et al. 2008, *AcA*, **58**, 405.
Terrell, D., Gross, J. and Cooney, W.R. 2012, *AJ*, **143**, 99
Van Hamme, W. 1993, *ApJ*, **106**, 2096 DOI
Warner, B. 2007, *Minor Planet Bulletin*, **34**, 113
Wilson, R.E. 1979, *ApJ*, **234**, 1054 DOI
Wilson, R.E. 1990, *ApJ*, **356**, 613 DOI
Wilson, R.E. and Devinney, E.J. 1971, *ApJ*, **166**, 605 DOI
Wilson, R.E. and Leung, K-M. 1977, *ApJ*, **211**, 853 DOI
Yakut, K. and Eggleton, P.P. 2005, *ApJ*, **629**, 1055 DOI

COMMISSIONS G1 AND G4 OF THE IAU
INFORMATION BULLETIN ON VARIABLE STARS
Volume 63 Number 6257 DOI: 10.22444/IBVS.6257

Konkoly Observatory
Budapest
19 January 2019

HU ISSN 0374 – 0676

UU Aqr – NO SUPERHUMPS BUT VARIATIONS ON THE TIME SCALE OF DAYS

BRUCH, ALBERT

[1] Laboratório Nacional de Astrofísica, Rua Estados Unidos, 154, CEP 37504-364, Itajubá – MG, Brazil

Abstract

Recently, brightness variations occurring on *twice* the accretion disk precession period in the old nova and permanent superhump system V603 Aql have been observed by Bruch & Cook (2018). In an attempt to detect a similar effect in other cataclysmic variables reported to contain permanent superhumps the novalike variable UU Aqr was observed during 11 nights in September 2018. While no traces of superhumps were seen in the data, rendering the quest for variations related to the disk precession period obsolete, the system exhibits regular variations with a period of ∼4 days.

The light curves of some cataclysmic variables exhibit photometric variations, termed superhumps, with periods slightly longer than their orbital periods. They are thought to be caused by stresses induced by the periodic passage of the secondary star close to the extended part of the accretion disk which in these cases is not circular but elliptically deformed (Whitehurst, 1988). The period is longer than the orbital period because the major axis of the accretion disk precesses. An alternative model is promoted by Smak (2009): the irradiation of the secondary star by the primary component varies because of rotating non-axisymmetric vertical structures in the accretion disk, leading to a modulation of the mass transfer rate and in consequence to variable dissipation of kinetic energy. The superhump phenomenon occurs always during supermaxima of the short-period dwarf novae of SU UMa subtype. However, some novalike variables and old nova also exhibit superhumps (see, e.g., Patterson, 1999). (Although these are normally termed "permanent superhumpers", superhumps in these systems may not always be that permanent!)

One of them is the old nova V603 Aql which has an orbital period of $P_{\rm orb} = 3.32$ h and a well established (albeit slightly variable) superhump period of $P_{\rm SH} \approx 3.5$ h. Recently, Bruch & Cook (2018) found an additional period in the light curve of V603 Aql which is related to the beat between $P_{\rm orb}$ and $P_{\rm SH}$, confirming marginal evidence for this phenomenon presented earlier by Suleimanov et al. (2004). Some other permanent superhump systems with limited evidence for a similar behaviour are listed by Yang et al. (2017). On the other hand, in SU UMa type dwarf novae with high orbital inclination variations of the system brightness on the beat period are common (Smak, 2009; 2013) and can readily be explained in Smak's model by the non-axisymmetric structures in the outer disk. As confirmed observationally by Smak (2009) such modulation should therefore not be seen in low inclination systems. Consequently, the beat period related variations seen in V603 Aql can not be explained within Smak's model because the orbital inclination of $13^{\rm o} \pm 2^{\rm o}$ (Arenas et al. 2000) is far to low. Moreover, quite intriguingly and in contrast to the finding of Suleimanov et al. (2004) the period observed very clearly by Bruch & Cook (2018) is not equal to the beat between $P_{\rm orb}$ and $P_{\rm SH}$ and thus the precession period, $P_{\rm prec}$, of the accretion disk, but exactly twice this value. While there is no obvious reason why the system brightness should change with the precession period in this low inclination system a modulation with $2 \times P_{\rm prec}$ is even more mysterious.

In an attempt to verify if similar variations related to $P_{\rm prec}$ occur in other systems exhibiting permanent superhumps as a first step towards an understanding, I observed a series of light curves of the novalike cataclysmic variable UU Aqr. This is an eclipsing system with an orbital period of 0.16580429 days ($\approx 3^{\rm h}56^{\rm m}$) (Baptista et al. 1994). Patterson et al. (2005) observed a strong superhump in 2000 with a period of $4^{\rm h}12^{\rm m}$. But note that in 1998 their observations yielded only marginal evidence for superhump-like variations. The orbital and superhump periods imply a precession period for the accretion disk of 3.12 days.

I used the 60 cm Boller & Chivens telescope of the Observatório do Pico dos Dias, Brazil, to observe UU Aqr in 11 nights between 2018, September 6 and 17. Light curves in unfiltered light spanning more than 8 hours in most of the nights were obtained at a time resolution of 5 sec. Synthetic aperture photometry of UU Aqr was performed on the original images (using a blue-sensitive IKon-L936-BEX2-DD CCD) after bias subtraction and flat-fielding, employing the MIRA software system (Bruch 1993). Magnitudes were measured relative to the primary comparison star #05 (Henden & Honeycutt, 1995; $V = 13.804$). For cataclysmic variables the throughput of the instrumentation corresponds roughly to V (Bruch, 2018). The light curves are shown in Fig. 1 where the time and magnitude scales are the same for all frames. Apart from eclipses they are characterized by rather strong flickering and modest variations on the time scale of hours which, however, exhibit no obvious regularity.

As an aside I draw attention to the strong variability of the eclipse depth which occurs even during subsequent cycles. This is particularly striking on September 6/7, where the eclipse close to UT 23 h hardly stands out in the light curve. Apparently, the secondary star in UU Aqr only partially covers the brighter parts of the primary and variations in the brightness of the central region of the accretion disk can strongly modulate the eclipse depth.

Turning now to the main purpose of the observations of UU Aqr, i.e., the investigation of a possible relationship between orbital, superhump and accretion disk precession period, I first masked the eclipses because they would dominate any period search algorithm. In order to remove any light travel time effects in the solar system, time was then transformed into barycentric Julian Dates on the Barycentric Dynamical Time scale, using the online tool of Eastman et al. (2010). Thereafter, all light curves were combined into a single data set. The result is shown in the upper frame of Fig. 2.

A power spectrum of the combined light curve was calculated using the Lomb-Scargle algorithm (Lomb 1976; Scargle 1982). The lower frame of Fig. 2 contains the resulting periodogram. Several peaks are visible, but none of them stands out among the others. Moreover, the power spectra of subsets of all data do not contain significant signals at the same frequencies. Therefore, none of the peaks in the power spectra of the combined data indicates a stable period in UU Aqr. In particular, neither the orbital period nor the previously observed superhump period manifest themselves in the power spectrum. The respective frequencies are marked by the blue and red vertical lines in the figure, respectively. The right hand inset contains a blown-up version of a small frequency range around $1/P_{\rm orb}$ and $1/P_{\rm SH}$. It must therefore be concluded that the superhumps seen in

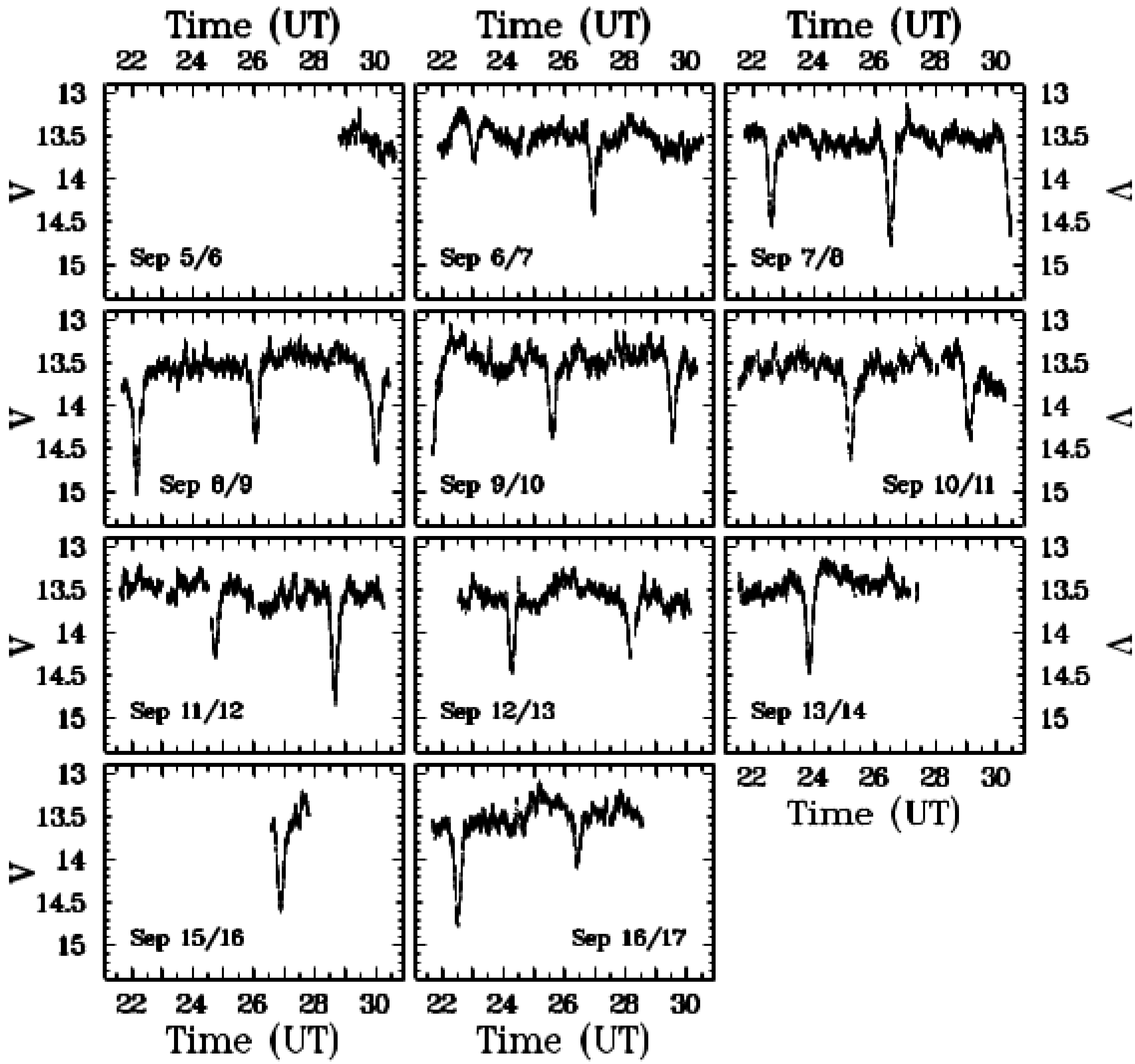

Figure 1. Light curves of UU Aqr observed in 11 nights in 2018 September, all drawn on the same time and magnitude scale.

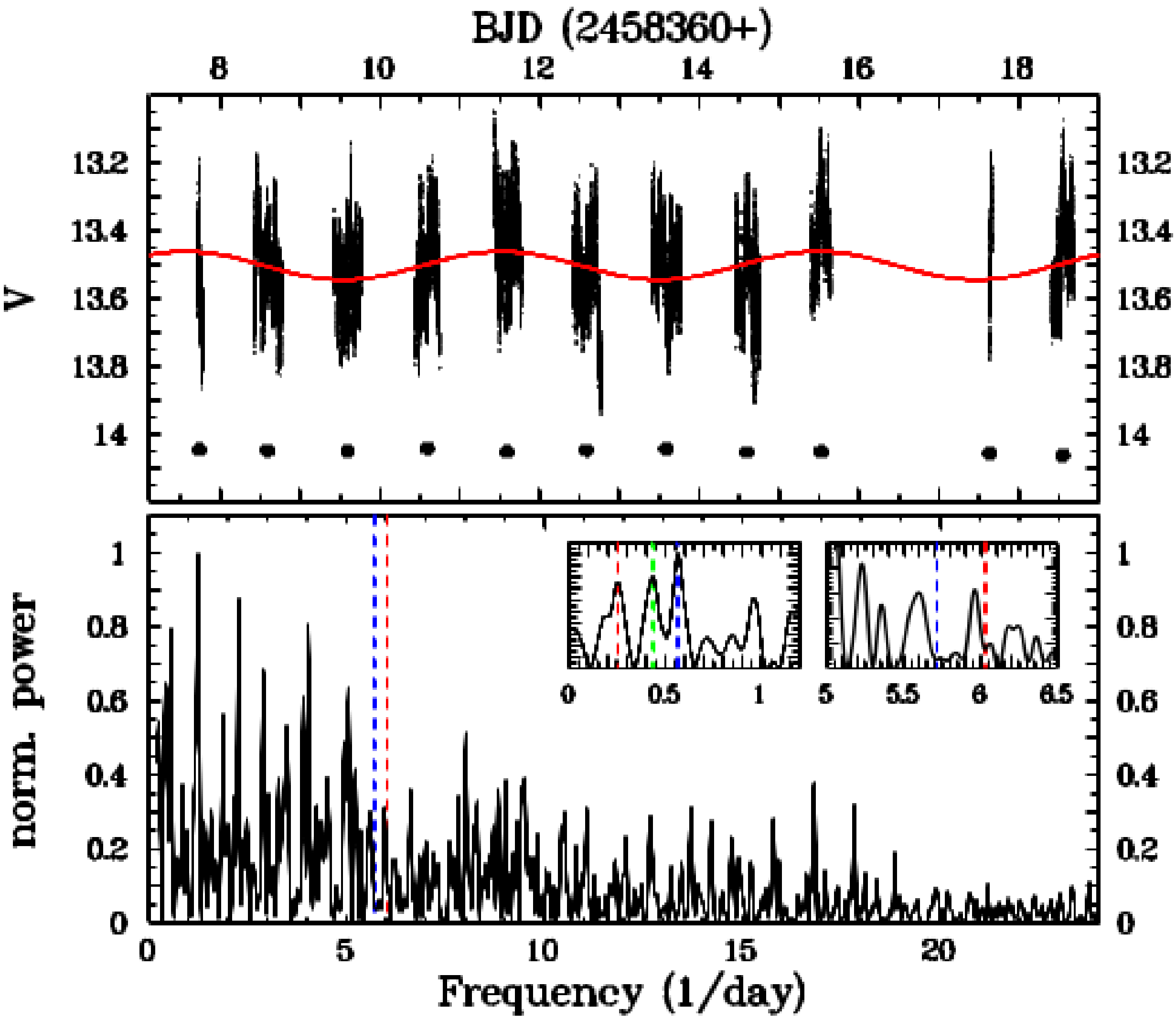

Figure 2. *Top:* The combined light curves of UU Aqr of 2018, September, after removal of eclipses. The dots below the light curves represent the nightly averages of the magnitude difference between the primary comparison star and a check star. *Bottom:* Lomb-Scargle periodogram of the light curves shown in the upper frame. The broken vertical lines indicate the orbital (red) and previously observed superhump frequency (blue). In inserts show blown up versions of a small part of the periodogram around the orbital and superhump frequencies (right) and of the low frequency part of the spectrum (left), with some prominent peaks marked by vertical lines.

2000 by Patterson et al. (2005) have vanished. The absence of any signal at $1/P_{\rm orb}$ also indicates that apart from the eclipses UU Aqr does not exhibit orbital variations such as a an orbital hump – often seen in cataclysmic variables – caused by a hot spot at the location where the matter transferred from the secondary star hits the accretion disk.

The absence of superhumps turns the quest for variations related to the beat between orbit and superhump obsolete. Even so, the combined light curve (upper frame of Fig. 2) contains systematic night-to-night variations which apparently are not random. Their significance can be assessed through the behaviour of the comparison and check stars. Since the nightly averages of the magnitude differences between the primary comparison star and 4 check stars revealed a slight (amplitude ≤ 0.02 mag) systematic variation of the former, well approximated by a third order polynomial, a corresponding correction has been applied to all light curves. The comparison – check star light curves then becomes virtually flat. One of them is plotted (shifted in magnitude by an arbitrary constant) below the UU Aqr light curve in Fig. 2.

The long-term variations should reveal themselves also at the low frequency end of the power spectrum which is plotted at an enlarged scale in the left-hand inset of the figure. The strongest peaks are marked by coloured vertical lines and correspond to periods of 3.966, 2.304 and 1.773 days. There is no obvious mutual relationship between these values or with the orbital or superhump period. Moreover, it is not straightforward to assess their statistical significance. Least squares sine fits with these periods yield half amplitudes of 0.042, 0.045, and 0.051 mag, respectively. The shorter periods do not reveal themselves intuitively to the eye. They are also not seen clearly in the power spectra of subsets of the data. However, trusting in the high capability of the human brain for pattern recognition, the reality of the $\sim$4 day period (red curve in the figure) is more convincing. While the data may not be sufficient to claim that this variation is really periodic and stable over time, it occurs on the same order of magnitude of the expected disk precession period if the superhumps were present. However, this may be a mere coincidence.

Concluding, I remark that in September 2018 UU Aqr did not exhibit superhumps and that these are thus not a permanent feature in the light curve of the system. This renders impossible the original purpose of this work, i.e., the investigation of brightness variations related to the precession period between the orbit and superhump periods. Nevertheless, UU Aqr exhibits systematic brightness variations on similar time scales, although the data do not permit a definite claim for their stability and repeatability.

Acknowledgements: This work is exclusively based on observations obtained at the Observatório do Pico dos Dias, maintained by the Laboratório Nacional de Astrofísica, a branch of the Ministério da Ciência, Tecnologia, Inovação e Comunicações da República Federativa do Brasil.

References:

Arenas, J., Catalán, M.S., Augusteijn, T., Retter, A., 2000, *MNRAS*, **311**, 135 DOI
Baptista, R., Steiner, J.E., Cieslinski, D., 1994, *ApJ*, **433**, 332 DOI
Bruch, A. 1993, "MIRA: A Reference Guide", Astron. Inst. Univ. Münster
Bruch, A., 2018, *New Astr.*, **58**, 53 DOI
Bruch, A., Cook, L.M., 2018, *New Astr.*, **63**, 1 DOI
Eastman, J., Siverd, R., Gaudi, B.S., 2010, *PASP*, **122**, 935 DOI
Henden, A.A., Honeycutt, R.K., 1995, *PASP*, **107**, 324 DOI

Lomb, N.R., 1976, *Ap&SS*, **39**, 447 DOI

Patterson, J., 1999, in S. Mineshige & C. Wheeler (eds.) "Disk Instabilities in Close Binary Systems", Universal Academy Press, Tokyo, p. 61

Patterson, J., Kemp, J., Harvey, D.A., et al., 2005, *PASP*, **117**, 1204 DOI

Scargle, J.D., 1982, *ApJ*, **263**, 853 DOI

Smak, J., 2009, *Acta Astr.*, **59**, 121

Smak, J., 2013, *Acta Astr.*, **63**, 369

Suleimanov, V., Bikmaev, I., Belyakov, K., et al., 2004, *Astron. Lett.*, **30**, 615 DOI

Whitehurst, R., 1988, *MNRAS*, **232**, 35 DOI

Yang, M.T.-C., Chou, Y., Ngeow, C.-C., et al., 2017, *PASP*, **129**, 4202 /DOI10.1088/1538-3873/aa7a99

COMMISSIONS G1 AND G4 OF THE IAU
INFORMATION BULLETIN ON VARIABLE STARS
Volume 63 Number 6257 DOI: 10.22444/IBVS.6257

Konkoly Observatory
Budapest
08 January 2019

HU ISSN 0374 – 0676

DISTANCE, LUMINOSITY AND EVOLUTIONARY STATUS OF ϵ AURIGAE (F0IAEP) FROM GAIA DR2 PARALLAX

M. PARTHASARATHY; S. MUNEER

Indian Institute of Astrophysics, Bangalore – 560034, India

e-mail: m-partha@hotmail.com; muneers@iiap.res.in

Abstract

From Gaia DR2 parallax of ϵ Aurigae the distance, M_v, M_{bol}, and $\log(L_*/L_\odot sun)$ are found to be 445 parsecs, −6.5 mag, −6.5 mag, and 4.5 respectively. These results clearly indicate that ϵ Aurigae (F0Iae) is post-AGB star. The progenitor of ϵ Aurigae is most likely an intermediate mass star of 4 to 5 solar masses or the progenitor may be a star which is lower limit of a super-AGB star.

1 Introduction

ϵ Aurigae (HD 31964) is an eclipsing binary system with an orbital period of 27.1 years. The primary minimum in the light curve is caused by a large, disk-shaped invisible companion. There is no secondary minimum in the light curve. The primary eclipse is total with a depth of 0.8 magnitudes and duration of the totality phase is 330 days. The primary eclipse depth is independent of the wavelength over a wide wavelength range. It is a single-lined spectroscopic binary (Stefanik et al. 2010). ϵ Aurigae has been studied for the past 100 years or more; even then the masses of the components, the nature and origin of the disk-shaped secondary and the evolutionary stage of the components are still under debate. There are two models now for ϵ Aurigae, a F0Iaep star. A high-mass star with a mass in the range of 15 or 20 solar masses to 50 solar masses and $M_v = -9$ to -10 mag, or a post-AGB star whose progenitor was a low or intermediate mass star.

The proposed models of the disk-shaped secondary range from a swarm of meteorites to a black hole (Ludendorff 1924, Cameron 1971). Huang (1965) proposed that the secondary is an opaque disk of cool material seen edge on. The results of the 1955 eclipse, earlier literature and models of ϵ Aurigae were reviewed by Wright (1970), Kopal (1971), Wilson (1971), Gyldenkerne (1970), Sahade and Wood (1978).

Many new results and facts have emerged from detailed spectroscopic, photometric and interferometric observations carried out from far UV to far IR during the 1982–1984 and 2009–2011 eclipses of ϵ Aurigae (see Stencel, 2012, and references therein, and Gibson & Stencel, 2018). Eggleton & Pringle (1985) were the first ones to propose that ϵ Aurigae is in post-ABG stage of evolution.

One of the major problems that prevented the understanding of the evolutionary stage of ϵ Aurigae was its distance remained unknown until the recent Gaia mission. Several researchers in the past have used distance of 1 Kpc to 1.5 kpc resulting in high luminosity and high mass for ϵ Aurigae. Recently from the Gaia DR2 we have relatively accurate parallax of ϵ Aurigae. In this paper we report the results based on the Gaia DR2 parallax of ϵ Aurigae and derive its luminosity and discuss its evolutionary status.

2 Distance, Luminosity and Evolutionary Status

Gaia DR2 parallax of ϵ Aurigae is found to be 2.4144 ± 0.5119 mas (Gaia Collaboration, 2018). The distance of ϵ Aurigae from its parallax is 414 parsecs, but according to Bailer-Jones et al. (2018), going from a Gaia parallax to distance is a non-trivial issue and cannot be obtained by simply inverting the parallax. In the following we adopt the distance given by the inference procedure developed by Bailer-Jones et al. (2018): 444.893 ± 94.326 parsecs. Using this distance and observed V magnitude ($V = 2.99$ mag) and observed $B-V$ color ($B-V = 0.54$ mag), the intrinsic color of a F0Ia star is $(B-V)_0 = 0.17$ mag, and hence the observed $E(B-V)$ is 0.38 mag (which we adopted here). More details of derived $E(B-V)$ values can be found in the papers of Hack & Selvelli (1979), Castelli (1978), Ake & Simon (1984), Stencel (2012), all these values agree with our adopted $E(B-V)$ value. Using the above mentioned data we find $\mathrm{M}_v = -6.467 \pm 0.350$ mag.

For F0Ia stars the bolometric corrections are almost zero. Therefore we adopt $\mathrm{M}_v = \mathrm{M}_{\mathrm{bol}} = -6.467 \pm 0.350$ mag. Hence the luminosity of ϵ Aurigae is $\log(\mathrm{L}_*/\mathrm{L}_\odot) = 4.5 \pm 0.35$.

To understand the evolutionary status of ϵ Aurigae we have used the post-AGB evolutionary models from the paper of Miller-Bertolami (2016) for initial masses 0.8 solar masses to 4 solar masses with solar metallicity. The location of ϵ Aurigae in the HR diagram of Miller-Bertolami indicates that it is a post-AGB star and the progenitor initial mass is about 4 solar masses to 5 solar masses. ϵ Aurigae seems to have evolved from a intermediate mass star or from a super-AGB star.

3 Discussion and Conclusions

Mass-transfer stream with rare-earth elements from ϵ Aurigae (Griffin & Stencel 2013) and low $^{12}\mathrm{C}/^{13}\mathrm{C}$ ratio = 5 (Stencel et al. 2015) observed during the third contact of the eclipse also confirms that ϵ Aurigae is a post-AGB star. Using the MESA code, Gibson & Stencel (2018) conclude that ϵ Aurigae is a post-RGB/ pre-AGB star. Based on the Gaia DR2 data we conclude that the distance to ϵ Aurigae is 445 parsecs. Its absolute brightness is $\mathrm{M}_v = -6.5$ mag and it is a post-AGB star. It seems to have evolved from a intermediate mass star of 4 to 5 solar masses or the progenitor star may be on the lower limit of super-AGB stars (Hidalgo et al. 2018).

References:

Ake, T. B., Simon, T., 1984, *NASCP*, **2349**, 361

Bailer-Jones, C. A. L., Rybizki, J., Fouesneau, M., Mantelet, G., Andre, R., 2018, *AJ*, **156**, 58 DOI

Cameron, A. G. W., 1971, *Nature*, **229**, 178 DOI

Castelli, F., 1978, *A&A*, **69**, 23

Eggleton, P. P., Pringle, J. E., 1985, *ApJ*, **288**, 275 DOI

Gaia Collaboration, 2018, *A&A*, **616**, 1 DOI

Gibson, J. L., Stencel, R. E., 2018, *MNRAS*, **476**, 5026 DOI
Griffin, R. E., Stencel, R. E., 2013, *PASP*, **125**, 775 DOI
Gyldenkerne, K., 1970, *Vistas Astr.*, **12**, 199 DOI
Hack, M., Selvelli, P. L., 1979, *A&A*, **75**, 316
Hidalgo, S. L., et al., 2018, *ApJ*, **856**, 125 DOI
Huang, S.-S., 1965, *ApJ*, **141**, 976 DOI
Kopal, Z., 1971, *Ap&SS*, **10**, 332 DOI
Ludendorff, H., 1924, *Sitzber. Berlin. Preuss. Akad. Wiss*, **9**, 49
Miller-Bertolami, M. M., 2016, *A&A* **588**, A25 DOI
Sahade, J., Wood, F. B., 1978, in *Interacting Binary Stars, Pergamon Press, New York*, p 152
Stefanik, R., Lovegrove, J., Pera, V., Latham, D., Zajac, J., Mazeh, T., 2010, *AJ*, **139**, 1254 DOI
Stencel, R. E., 2012, *JAAVSO*, **40**, 618 DOI
Stencel, R. E., Blatherwick, R., Geballe, T., 2015, *AJ*, **149**, 109 DOI
Wilson, R. E., 1971, *ApJ*, **170**, 529 DOI
Wright, K. O., 1970, *Vistas Astro.*, **12**, 147 DOI

COMMISSIONS G1 AND G4 OF THE IAU
INFORMATION BULLETIN ON VARIABLE STARS
Volume 63 Number 6259 DOI: 10.22444/IBVS.6259

Konkoly Observatory
Budapest
29 January 2019

HU ISSN 0374 – 0676

DETECTION OF A δ SCUTI–TYPE PULSATING COMPONENT IN THE DETACHED ECLIPSING BINARY SYSTEM TU CMa

MKRTICHIAN, D.E.

National Astronomical Research Institute of Thailand, 260 Moo 4, T. Donkaew, A. Maerim, Chiangmai, 50180 Thailand. e-mail: davidmkrt@gmail.com

Abstract

We report the detection of 30.5 min low-amplitude (A=0.003 mag) δ Scuti-type pulsations in an A5V-A7V type component of the detached eclipsing binary system TU CMa.

TU CMa is a 1.127803854-day (Haans et al. 2015) detached eclipsing binary system with A5V-A7V primary and F8V-G0V secondary components (Garces et al. 2017). It was included in our program to search for pulsating components that have the primary component lying inside the instability strip and hence can be potentially pulsating.

Visual inspection of the SWASP data of TU CMa taken from their archive[1] revealed about 0.02-day short-period, low-amplitude light variations. For the safe detection of possible pulsations, we selected the best quality nights for TU CMa from the SWASP data, namely HJD 2454105, 2454131, 2454132, 2454133, 2454134, 2454135, 2454433, 2454434, 2454436, 2454456, 2454462 and 2454485. The pulsation variations were searched for in the out-of-eclipse parts of the light curves after removal of slow orbital variations using low order polynomial fits. For the period search, we used the Period04 software (Lenz & Breger, 2005) based on a Discrete Fourier Transform (DFT) analysis.

The DFT amplitude-frequency spectrum of the TU CMa residual data is shown in Figure 1. We detected a clear signal at 47.3197±0.0002 c/d (P = 30.5 min) with an amplitude of 0.0038 mag. The phased light curve binned into 20-phase intervals is shown in Figure 2.

Using the mass M=1.761±0.012 $M_\odot$ and the radius R= 1.553±0.002 $R_\odot$ for the primary component from Garces et al. (2017) we calculated the mean density of the pulsating component as $\rho/\rho\odot$=0.4702. The calculated pulsation constant for the discovered 30.5 min ($P = 0.021$ day) pulsation mode, $Q = P\sqrt{\rho_*/\rho_\odot} = 0.014$, corresponds to a fourth or fifth overtone low degree ($\ell = 0 - 3$) mode.

Conclusion: We report the detection of a 30.5 min low amplitude (A=0.003 mag) δ Scuti-type pulsation in an A5V-A7V type component of the detached eclipsing binary system TU CMa. The calculated pulsation constant corresponds to pulsations in the 4-5th overtone low-degree mode (Fitch, 1981). The parameters of the binary system and

[1] https://wasp.cerit-sc.cz

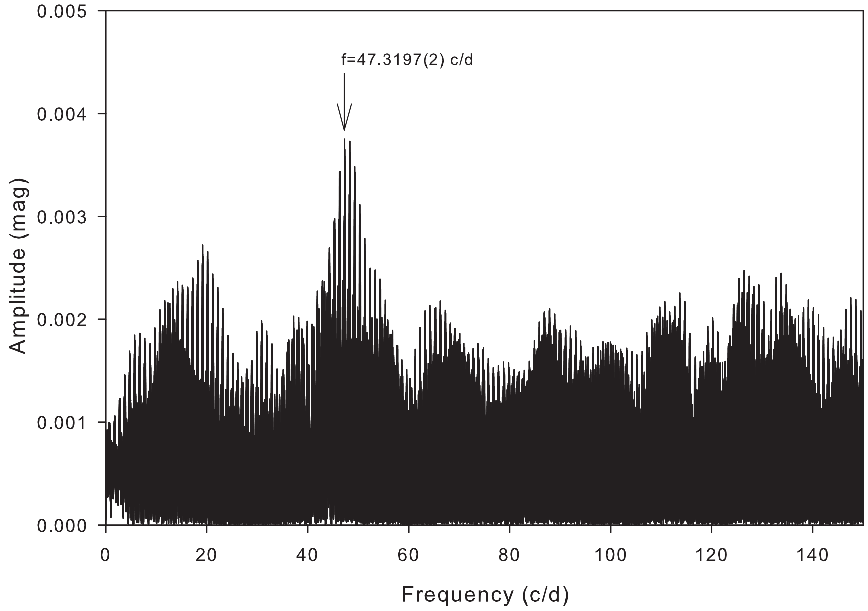

Figure 1. The DFT amplitude spectrum of the primary A5V-A7V component. The dominant peak is at 47.3197 ±0.0002 c/d.

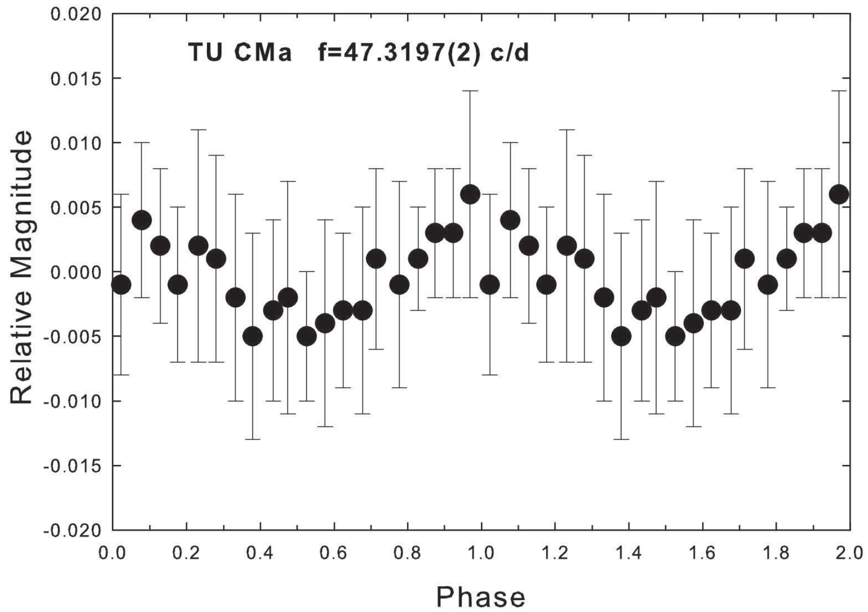

Figure 2. The phase-binned pulsation light variations of TU CMa. The phase of the maximum light corresponds to HJD 2454107.9776.

components of TU CMa are accurately determined and are good input parameters for theoretical pulsational modelling. This binary system can be a good target for further more accurate and detailed photometric observations of pulsations in order to detect a low-amplitude pulsation spectrum, for the eclipse mode identification of the dominant mode and for comparison with theoretical pulsation models.

Acknowledgements: I acknowledge this work as part of the research activity supported by the National Astronomical Research Institute of Thailand (NARIT), Ministry of Science and Technology of Thailand.

This paper makes use of data from the DR1 of the WASP data (Butters et al. 2010) as provided by the WASP consortium, and the computing and storage facilities at the CERIT Scientific Cloud, reg. no. CZ.1.05/3.2.00/08.0144 which is operated by Masaryk University, Czech Republic (Paunzen et al., 2014).

References:

Butters, O. W., et al., 2010, *A&A*,**520**, L10 DOI
Fitch, W. S., 1981, *ApJ*, **249**, 218 DOI
Garcés, J. L., Mennickent, R. E., & Zharikov, S, 2017, *PASP* **129**, 044203 DOI
Haans, G. K., et al., 2015, *PKAS*, 30, 205 DOI
Lenz, P., Breger M., 2005, *Communications in Asteroseismology*,**146**, 53 DOI
Paunzen, E., Kuba, M., West, R.G., Zejda, M., 2014, *IBVS*, **6090**

COMMISSIONS G1 AND G4 OF THE IAU
INFORMATION BULLETIN ON VARIABLE STARS
Volume 63 Number 6260 DOI: 10.22444/IBVS.6260

Konkoly Observatory
Budapest
30 January 2019
HU ISSN 0374 – 0676

HD220735 AND HD30110, NEW SHORT PERIOD VARIABLE STARS

PEÑA, J. H.[1,2,3], SONI, A.[1,3], RENTERÍA, A.[1,3] & PIÑA, D. S.[1,3]

[1] Instituto de Astronomía, Universidad Nacional Autónoma de México, Cd. México
e-mail: jhpena@astro.unam.mx

[2] Observatorio Astronómico Nacional, Tonantzintla

[3] Facultad de Ciencias, Universidad Nacional Autónoma de México

Abstract

We have obtained $uvby-\beta$ photoelectric photometry with the 0.84 m telescope of the San Pedro Martir Observatory, México, for the stars HD220735 and HD30110 which were found to be new variable stars. For these stars we determined some of their physical characteristics, such as effective temperature and surface gravity.

1 Introduction

Confirming the variability and establishing the nature of suspected variables is an important matter. As a continuation of our search for high-amplitude δ Scuti (HADS) stars, several from a list of suspected variables from the study of Nichols et al. (2010) were tested for variability. Based on this, we carried out a systematic analysis of four of them: HD30110, HD217587, HD221012, and HD220735 and determined variability in the first and last one.

2 Observations

These were all done at the Observatorio Astronómico Nacional de San Pedro Mártir México. The 0.84 m telescope, to which a spectrophotometer was attached, was utilized at all times. The observing season was carried out over several nights in October and November, 2016. Table 1 lists the log of the observations.

2.1 Data acquisition and reduction

The procedure to determine the physical parameters has been reported elsewhere (Peña et al., 2016). If the photometric system is well-defined and calibrated, it provides an efficient way to investigate physical conditions such as effective temperature and surface gravity via a direct comparison of the unreddened indexes with those obtained from the theoretical models. These calibrations have already been described and used in previous analyses (Peña & Peniche; 1994; Peña & Sareyan, 2006).

Table 1: Log of observing seasons.

Date yr/mo/day	Target 1	Target 2	Target 3	HJD 245+(day)
16/10/2526	HD217587	HD30110	Cephs	7687
16/10/2627	HD221012	HD30110	Cephs	7688
16/10/2728	cloudy			7689
16/10/2829	HD30110	HD221012	Cephs	7690
16/10/2930	HD220735			7691
16/10/3031	cloudy			7692
16/11/3101	HD220735	HD30110	Cephs	7693
16/11/0102	HD30110	HD221012		7694
16/11/0203	CC And	V0367 CAM	Cephs	7695

Table 2: Transformation coefficients obtained for the observed season

season	B	D	F	J	H	I	L
Oct 2016	0.031	1.008	1.031	−0.004	1.015	0.159	−1.362
σ	0.028	0.003	0.015	0.017	0.005	0.004	0.060

The reduction was done considering the accuracy of the standard stars. As was stated in Peña et al. (2016) reporting on BO Lyn, the observational pattern, as well as the reduction procedure, have been employed at the SPM Observatory since 1986 and hence, have been described many times. A detailed description of the methodology can be found in Peña et al. (2007). Over the seven nights of observation, the following procedure was used: for each measurement at least five ten-second integrations of each star and one ten-second integration of the sky for the *uvby* filters and the narrow and wide filters that define Hβ were taken. What must be emphasized here are the transformation coefficients for the observed season (Table 2) and the season errors which were evaluated using the ninety-one observed standard stars. These uncertainties were calculated through the differences in magnitude and colors for (V, $b-y$, m_1, c_1 and Hβ) which are (0.054, 0.012, 0.019, 0.025, 0.012), for a total of 94 points in *uvby* and 68 points in Hβ, respectively, which provide a numerical evaluation of our uncertainties. Emphasis must be made on the large range of the standard stars in the magnitude and color indexes values: V:(5.62, 8.00); $(b-y)$:(−0.09, 0.88); m_1:(−0.09, 0.67); c_1:(−0.02, 1.32) and Hβ:(2.50, 2.90).

To verify the consistency of the data from our derived standard stars values, mean values for each one were calculated as well as their standard deviations. These are presented in Table 3 in decreasing brightness. The last column of this Table is N, the number of entries. In all but HD190849 the standard deviations are on the order of hundredths of magnitude. The large dispersion of this star could be due to variability, as in the case of HD 115520 (Peña et al., 2007)

The file `6260-t7.txt` lists the photometric values of HD 220735. In this Table column 1 reports the time of the observation in HJD, columns 2 to 5 list the Strömgren values V, $(b-y)$, m_1 and c_1, respectively; column 6, Hβ; the remaining columns list the unreddened indexes [m1], [c1] & [u-b]. The data of HD 30110 is also available online as `6260-t8.txt`. The photometry of the light

Table 3: Mean photometric values and standard deviations of standard stars

ID	V	$(b-y)$	m_1	c_1	β	σV	$\sigma(b-y)$	σm_1	σc_1	$\sigma\beta$	N
BS8085	5.196	0.670	0.657	0.159		0.016	0.003	0.026	0.015		6
HD013871	5.782	0.285	0.158	0.526		0.033	0.001	0.014	0.003		8
HD015335	5.893	0.373	0.157	0.386		0.013	0.002	0.019	0.005		6
HD057006	5.905	0.336	0.151	0.490		0.015	0.003	0.021	0.002		4
HD035520	5.911	0.142	0.062	1.328		0.024	0.003	0.014	0.002		8
HD224165	5.933	0.715	0.543	0.250		0.101	0.002	0.001	0.001		2
HD033203	6.013	0.615	−0.181	0.006		0.012	0.004	0.012	0.006		8
BS8086	6.044	0.814	0.635	0.103		0.025	0.004	0.027	0.014		6
HD202314	6.184	0.691	0.449	0.299		0.031	0.004	0.022	0.010		7
HD056386	6.187	−0.006	0.114	0.990		0.010	0.001	0.021	0.004		4
HD221661	6.202	0.599	0.410	0.374		0.086	0.002	0.004	0.001		2
HD015596	6.225	0.562	0.270	0.386		0.012	0.002	0.020	0.005		6
HD217754	6.426	0.205	0.188	0.783		0.179	0.001	0.001	0.001		2
HD033632	6.477	0.340	0.145	0.351		0.005	0.002	0.014	0.005		8
HD028354	6.536	0.005	0.116	0.785		0.007	0.002	0.015	0.005		8
HD013936	6.573	0.023	0.129	1.123		0.009	0.002	0.018	0.007		6
BS8389	6.582	0.029	0.115	1.104		0.015	0.003	0.016	0.008		7
HD043461	6.621	0.013	0.061	0.580		0.025	0.002	0.015	0.007		6
HD042089	6.644	0.585	0.328	0.532		0.022	0.003	0.021	0.008		6
HD012884	6.754	0.087	0.208	0.898		0.028	0.001	0.017	0.004		7
HD018066	6.967	0.760	0.549	0.337		0.015	0.002	0.025	0.010		6
HD055036	6.996	0.257	0.020	1.358		0.016	0.002	0.016	0.011		3
HD044812	7.002	0.668	0.451	0.302		0.006	0.003	0.024	0.010		6
HD224055	7.141	0.599	−0.144	0.213							1
HD208344	7.226	0.071	0.177	1.094		0.075	0.003	0.017	0.004		7
HD049564	7.391	0.843	0.694	0.362		0.019	0.001	0.028	0.008		4
HD204132	7.541	0.369	0.061	1.328		0.037	0.003	0.019	0.009		7
HD028304	7.721	0.147	0.029	0.612		0.006	0.003	0.015	0.004		7
HD048691	7.820	0.143	−0.039	−0.015		0.007	0.002	0.016	0.011		5
HD013801	7.939	0.213	0.161	0.688		0.012	0.001	0.016	0.006		7
HD031125	7.921	0.027	0.173	0.994		0.010	0.002	0.015	0.005		8
HD047777	7.927	−0.055	0.064	0.116		0.010	0.002	0.024	0.017		5
HD219364	7.952	0.686	0.530	0.382		0.021	0.002	0.004	0.011		2
HD013997	7.990	0.479	0.314	0.360		0.010	0.003	0.020	0.004		7
HD207608	8.054	0.312	0.145	0.528		0.055	0.004	0.017	0.003		7
HD052955	8.329	0.414	0.201	0.359							1

curves of the variables is presented in Figures 1 and 2.

3 Newly found delta Scuti stars

Since there were two newly found variables, HD 30110 and HD 220735, among the several observed stars, the analysis of each one of them is presented separately. These stars, according to Simbad have no previous reports on their variability.

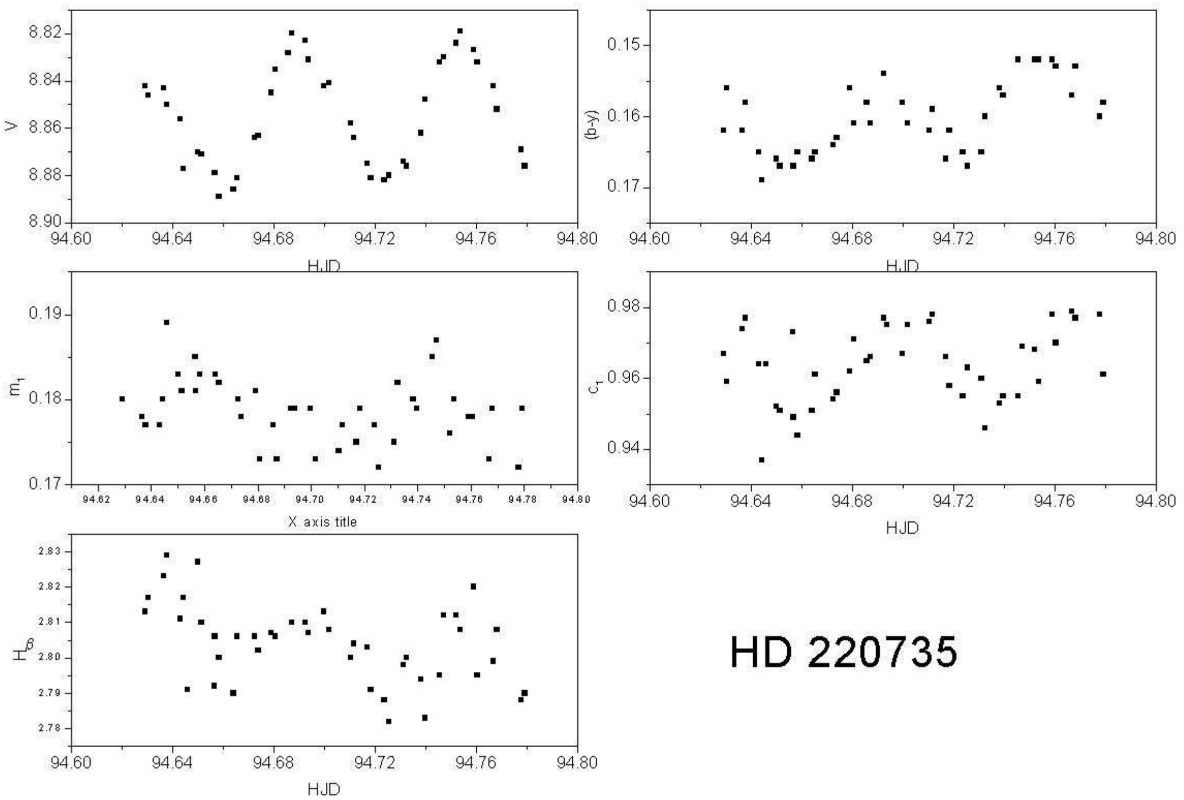

Figure 1. Light curve of HD 220735 in $uvby-\beta$ photoelectric photometry. Top, left, V magnitude, top right, $(b-y)$; middle left, m_1, middle right, c_1 and bottom left, Hβ.

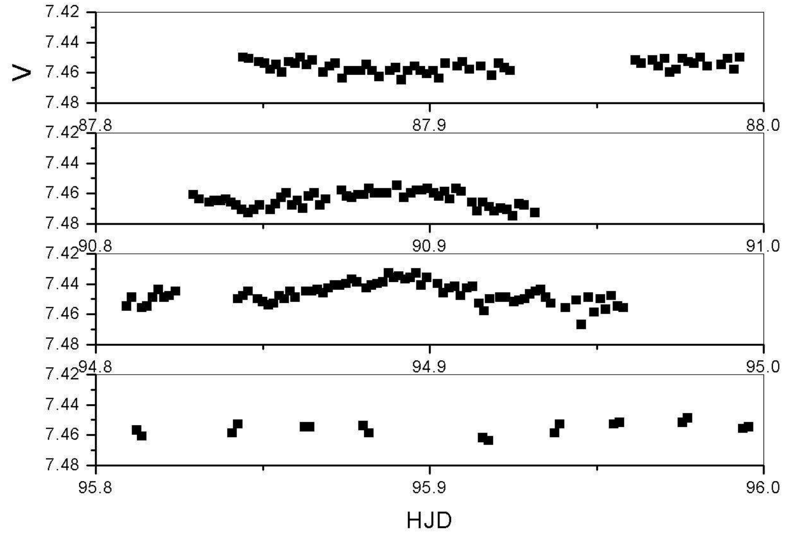

Figure 2. Light curve of HD 30110 in the V filter. We present the light curve for the four nights the star was observed.

3.1 HD 220735

This star was observed on only one night for a sufficient time span to cover two cycles. To determine the periodic behavior of HD220735 the following methods were employed. In the first method differences of the two consecutive times of maximum light were evaluated to determine a coarse period since it was observed for a time span long enough to reach two times of maximum light. The times of maximum light were found at HJD94.68757 and HJD94.7534. The difference of these maxima gave 0.0658 d, which gives a coarse period of pulsation of this star.

As a second method, we used a time series method amply utilized by the δ Scuti star community: PERIOD04 (Lenz & Breger, 2005). The V magnitude of the $uvby-\beta$ set was analyzed with this code.

The analysis of these data gave the results listed in Table 4 with a zero point of 8.854 mag, residuals of 0.0078 mag and 13 iterations. This frequency coarsely agrees with that determined by the difference of the two maximae: 0.0638 d. The analysis of PERIOD04 is presented in Figure 3. Beginning at the top is the periodogram of the original data; next are the consecutive sets of residuals. The scale of the Y axis shows the relative importance of the residuals. However, it is obvious that the data of only one night cannot provide an accurate period determination. To complicate things more, this preliminary analysis suggests the presence of a second frequency, a common phenomena with δ Scuti stars.

3.2 HD 30110

This star was observed on the nights of JD2457687, JD2457690, JD2457694 and a few points on JD2457695. Although it is clearly variable, especially on nights

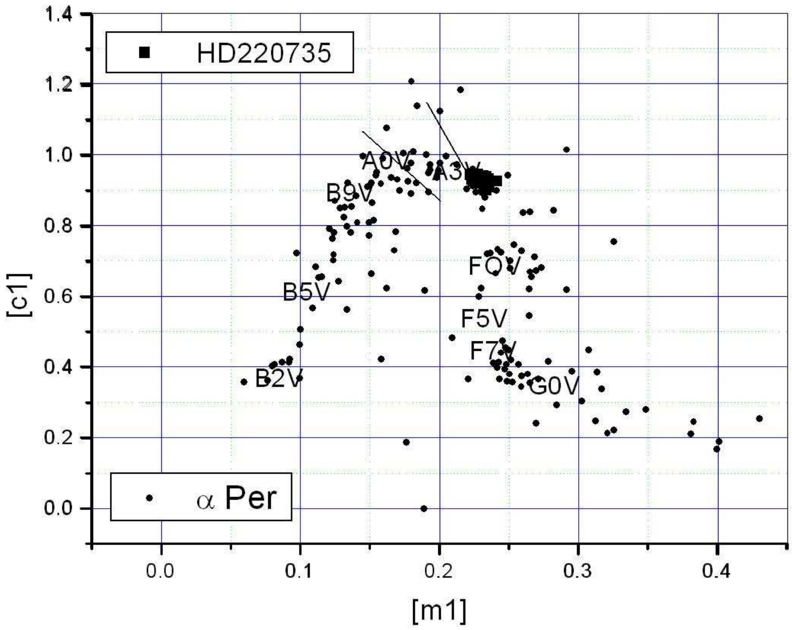

Figure 3. Position of the HD220735 star in the $[m_1] - [c_1]$ diagram of alpha Per (Peña & Sareyan, 2006)

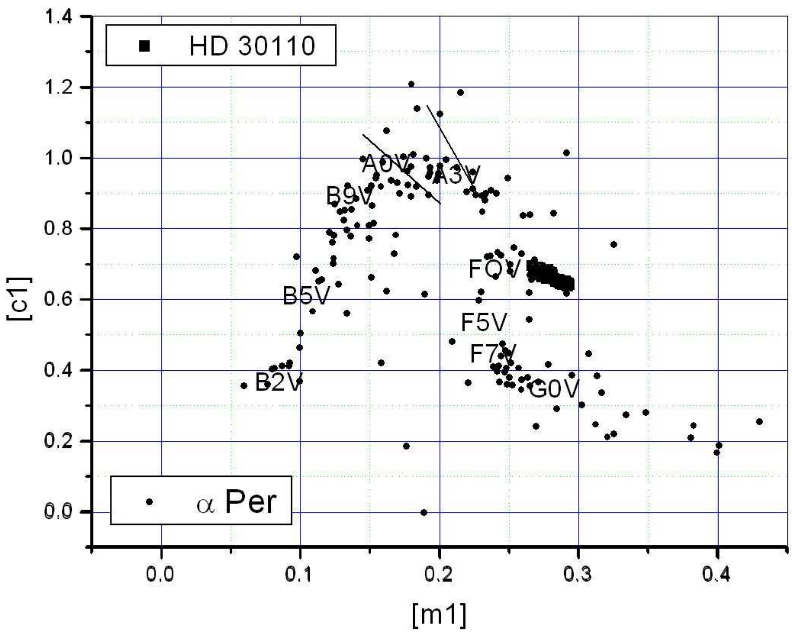

Figure 4. Position of the HD30110 star in the $[m_1] - [c_1]$ diagram of alpha Per (Peña & Sareyan, 2006)

Table 4: Output of PERIOD04 with the V magnitude of HD 220735 of the present paper's $uvby-\beta$ data

Nr.	Frequency	Amplitude	Phase
F1	15.666	0.026	0.8586
F2	29.6147	0.0056	0.6816

Table 5: Output of PERIOD04 with the V magnitude of HD 30110 of the present paper's $uvby-\beta$ data

Nr.	Frequency	Amplitude	Phase
F1	0.6223	0.0105	0.7757
F2	9.2300	0.0049	0.9286

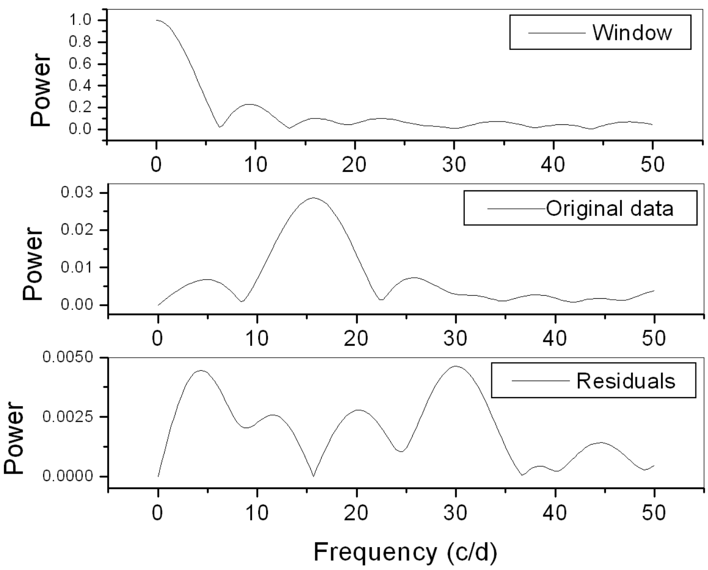

Figure 5. Frequency spectrum of HD 220735 with the SPM V data. Top to bottom: first is the frequency spectrum of the window, and middle, that of the original data and bottom, the set of residuals. We call attention to the scale of the Y axis to show the relative importance of each frequency.

Table 6: Reddening and parameters of HD 30110 and HD220735

HD	$E(b-y)$	Distance PP	Tycho	Gaia DR2	Gaia DR2*
HD30110	0.016 ± 0.015	82 ± 18	96.3	98.9	98.7
HD220735	0.035 ± 0.011	322 ± 33	—	427	422

JD2457690, JD2457694, due to the fact that it shows a broad maximum, no determination of the peak could be done. A time series analysis was done with PERIOD04. The analysis gave the results listed in Table 5 with a zero point of 7.455 mag, residuals of 0.0040 mag and 10 iterations. We do not need to emphasize that more data are needed before the true behaviour of this star can be determined.

4 Physical Parameters

To determine physical parameters, unreddened photometric values have to be determined through appropriate calibrations. These calibrations were proposed by Nissen (1988) for A and F type stars. Therefore, it is necessary to first determine the range of variation in spectral class of HD 30110 and HD220735. The spectral types can be determined very accurately with the $uvby-\beta$ photometric data. We determined their unreddened photometric indexes $[m_1]$ and $[c_1]$ and positioned them in the plot determined for alpha Per, whose stars have well-determined spectral types. This has been done and is presented in Figures 4 and 5 where we can see that the spectral type is A3-A4 for HD 220735 (Figure 4) and F type for HD 30110 (Figure 5). Hence, in both cases the prescription of Nissen (1988) is applicable.

The application of the above mentioned numerical unreddening package of Nissen's (1988) provided the results for HD30110 and HD220735.

Since a period was determined for HD220735, mean values were calculated for $E(b-y)$ for two cases: i) the whole data sample and ii) in phase limits between 0.3 and 0.8, which is customary for pulsating stars to avoid the maximum. Unfortunately no metal content [Fe/H] was determined for either star. The uncertainty is merely the standard deviation.

The results are summarized in Table 6 which lists the reddening $E(b-y)$, and distance (in pc). Furthermore, our distance values were compared with the available data of Tycho and Gaia DR2. In the case of Gaia, we are using the distance obtained directly inverting the parallax and the distances obtained by the correction perform by Bailer-Jones et al. (2018). Here we can see, as expected, that the discrepancies between Gaia DR2 and the Bailer-Jones corrections are larger at greater distances.

Table 6 presents also the summary of the distances values for both stars: HD 30110 (= Tycho 3745-489-1 = Gaia DR2 278914871261809920) and HD 220735 (= Tycho 2237-986-1 = Gaia DR2 2839969578847249280). The first two columns show the ID and reddening $E(b-y)$; the third, fourth, fifth and sixth present the distance values from present paper, Tycho, Gaia DR2 and Distance corrected Gaia DR2, respectively.

To determine the range of the effective temperature and surface gravity in which the stars vary we must locate the determined unrreddened points in some theoretical grids such as those of Lester, Gray and Kurucz (1986, hereinafter LGK86) developed for $uvby$–β photometric data for several metallicities. Hence, in order to locate our unreddened points in the theoretical grids of LGK86, a metallicity has to be assumed. Due to their proximity to the Sun, the model we considered was, therefore, that of solar composition [Fe/H]= 0.0.

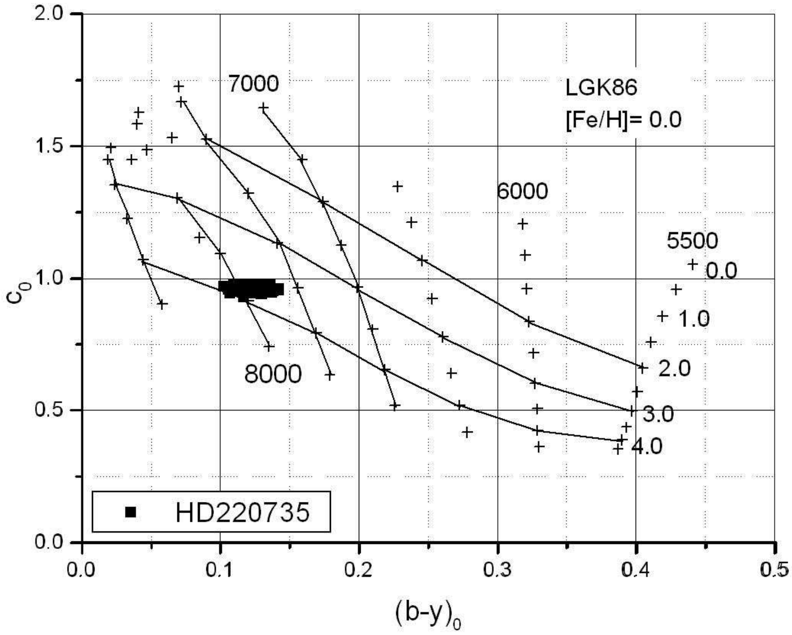

Figure 6. Position of the HD220735 star in the grids of LGK86.

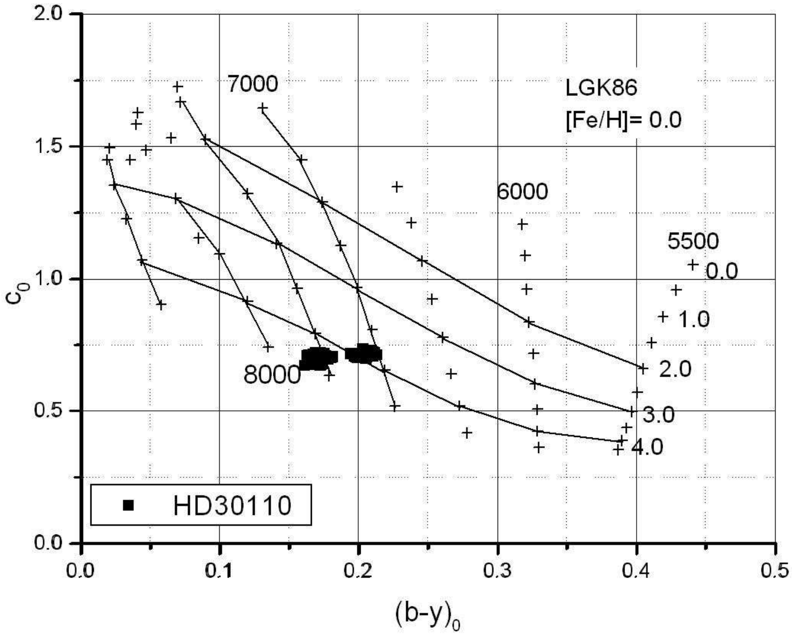

Figure 7. Position of the HD30110 star in the grids of LGK86.

As can be seen in Figures 6 and 7, in the case of [Fe/H] = 0.0 the HD 220735 star varies between an effective temperature of 7600 K and 8100 K; the surface gravity $\log g$ varies between 3.5 and 4.0. The other star, HD30110 has a temperature range that varies between 7000 and 7700 K and its surface gravity range is between 4 and 4.5

Table 7 lists these values. Column 1 shows the phase, column 2 lists the temperature obtained from the plot for each [Fe/H] value; column 3, the effective temperature obtained from the theoretical relation reported by Rodriguez (1989) based on a relation of Petersen & Jorgensen (1972, hereinafter P&J72) $T_e = 6850 + 1250 \times (\beta - 2.684)/0.144$ for each value and averaged in the corresponding phase bin and column 4, the mean value. Column 5 shows the surface gravity $\log g$ from the plot.

5 Conclusions

In the present study we have determined HD30110 and HD220375 to be not previously reported variable stars. Physical characteristics determined are consistent with the determined spectral type.

Acknowledgements. We would like to thank the staff of the OAN at SPM for their assistance in securing the observations and to the GAOOT group for fruitful discussions. This work was partially supported by PAPIIT IN104917 and PAPIME PE113016. Proofreading and typing were done by J. Miller and J. Orta, respectively. C. Villarreal, C. Guzmán, F. Ruiz, A. Díaz B. Juárez and G. Pérez assisted us at different stages. AAS thanks the IA for allotting the telescope time. The comments and suggestions of an anonymous referee improved this paper. We have made use of the SIMBAD databases operated at CDS, Strasbourg, France and NASA ADS Astronomy Query Form.

References:

Arellano-Ferro, A. & Parrao, L., 1988, *Reporte Técnico*, **57**, IA-UNAM.
Bailer-Jones, C. A. L.; Rybizki, J. et al., 2018, *AJ*, **156**, 58 DOI
Lenz, P. & Breger, M., 2005, *CoAst*, **146**, 53 DOI
Lester, J.B., Gray, R.O. & Kurucz, R.I. 1986, *ApJS*, **61**, 509 DOI
Nichols, J. S., Henden, A. A., Huenemoerder, D. P. et al. 2010, *ApJS*, **188**, 473 DOI
Nissen, P. 1988, *A&A*, **199**, 146
Peña, J. H. & Peniche, R., 1994, *RMxAA*, **28**, 139
Peña, J. H. & Sareyan, J. P., 2006, *RMxAA*, **42**, 179
Peña, J. H., Sareyan, P., Cervantes-Sodi, B. et al., 2007, *RMxAA*, **43**, 217
Peña, J. H., Rentería, et al., 2016, *RMxAA*, **52**, 385
Petersen, J. O. & Jorgensen, H. E., 1972, *A&A*, **17**, 367
Rodriguez, E., 1989, PhD Thesis, Universidad de Granada, Spain

COMMISSIONS G1 AND G4 OF THE IAU
INFORMATION BULLETIN ON VARIABLE STARS
Volume 63 Number 6261 DOI: 10.22444/IBVS.6261

Konkoly Observatory
Budapest
21 February 2019

HU ISSN 0374 – 0676

THE 82ND NAME-LIST OF VARIABLE STARS. PART I – RA 0^h TO 18^h, NOVAE AND GLOBULAR-CLUSTER VARIABLES

KAZAROVETS, E.V.[1]; SAMUS, N.N.[1,2]; DURLEVICH, O.V.[2]; KHRUSLOV, A.V.[2,1]; KIREEVA, N.N.[1]; PASTUKHOVA, E.N.[1]

[1] Institute of Astronomy, Russian Academy of Sciences, 48, Pyatnitskaya Str., Moscow 119017, Russia
[helene@inasan.ru, samus@sai.msu.ru, kireeva@sai.msu.ru, pastukhova@sai.msu.ru]

[2] Sternberg Astronomical Institute, M.V. Lomonosov University of Moscow, 13, University Ave., Moscow 119992, Russia
[gcvs@sai.msu.ru, khruslov@bk.ru]

Abstract

We present the first part of a new Name-List of variable stars containing information on 1291 variable stars recently designated in the system of the General Catalogue of Variable Stars. With the exception of Novae and other unusual variables named upon request from the IAU CBAT or by our initiative, these stars are in the range of J2000.0 right ascensions from 0 hours to 18 hours 00 minutes. The paper also announces GCVS designations for 324 known variables in 10 globular clusters.

This publication, Part I of the 82nd Name-List of Variable Stars, contains information on 1291 stars newly named in the system of the General Catalogue of Variable Stars (GCVS; Samus et al., 2017), 34 of them being extraordinary namings for Novae.

Like in the recent Name-Lists, NL 80 and NL 81, we separate the catalogue of newly designated variables (to be presented at the GCVS web site) from the Name-List proper. Table 1 of the current Name-List contains the new GCVS name, equatorial coordinates (rounded to an accuracy sufficient for identification), and variability type for each star. The order of stars in Table 1 corresponds to the order of stars in the GCVS. The electronic version of the Name-List at http://www.sai.msu.su/gcvs/gcvs/nl82, to be presented in the nearest future, will additionally contain variability ranges, light elements, spectral types, identifications with astronomical catalogues, detailed remarks, bibliographic references for the newly named variable stars, accurate coordinates and proper motions (with references to corresponding positional catalogs or sources in the literature). The majority of variable stars in NL 82 are included into the Name-List with coordinates from Gaia DR2 (Gaia Collaboration, 2018).

We continued naming Novae and variables of special interest upon requests from the IAU Bureau of Astronomical Telegrams and in other extraordinary cases requiring quick naming. Part I of the 82th Name-List contains 34 Novae with names announced in Kazarovets and Samus (2017, 2018). They are included in Table 1 and, besides, listed in Table 2 that contains, along with GCVS names, preliminary designations of these stars. During the preparations of the Name-list, we also identified 18 unnamed Novae and a probable FU Ori star in overlooked publications. We give them their GCVS names in the normal order. A list of these stars is presented in Table 3; besides, they are included in Table 1.

The Name-list also contains (Table 4) the first part of the list of variable stars in globular clusters we select for adding to the GCVS. For reasons of tradition, globular-cluster members were usually left outside the General Catalogue, despite the fact that many globular clusters are, beyond doubt, members of our Galaxy and that variable stars in open clusters are being regularly named in the system of the GCVS. During the long history, quite a number of variable stars, members of globular clusters, found their way to the GCVS, but the vast majority of them were listed only in special catalogues. Including globular-cluster variable stars into the GCVS was made difficult, among other reasons, by the fact that most lists of such stars contained only their rectangular coordinates with respect to the (sometimes not clearly defined) center of each globular cluster. Samus et al. (2009) compiled a catalogue of accurate equatorial coordinates for 3398 variable stars in 103 globular clusters. After that, equatorial coordinates were introduced into the electronic version of the Catalogue of variable stars in globular clusters (Clement et al., 2001).

The existing catalogues of variable stars in globular clusters contain, besides well-studied variables, also stars that, in the GCVS tradition, would be considered "suspected variable stars". They also seriously differ from the GCVS in their format.

For the present Name-list, we selected 10 globular clusters in four constellations (Apus, Ara, Aquila, Aquarius). The electronic catalogue of variable stars in globular clusters (http://www.astro.utoronto.ca/∼cclement/cat/listngc.html) contains 406 stars in these clusters. We now add 324 of them to the GCVS. For these stars, we revised, once again, their equatorial coordinates: in a number of cases, Gaia-DR2 identifications were possible. Then, we studied available publications and provided classification in the GCVS style. For some periodic stars, it was possible to improve their light elements using the available electronic databases of photometric observations. The work aimed at incorporating globular-cluster variable stars satisfying our criteria into the GCVS will be continued.

The total number of named variable stars, not counting designated non-existing stars or stars subsequently identified with earlier-named variables, is now 53 468.

Acknowledgements. This study was supported in part by the Programme P-28 of the Presidium of Russian Academy of Sciences.

References:

Clement, C.M., Muzzin, A., Dufton, Q., et al. 2001, *AJ*, **122**, 2587 DOI

Gaia Collaboration: Brown, A.G.A., Vallenari, A., Prusti, T., et al. 2018, *A&A*, **616**, A1 DOI

Kazarovets, E.V., Samus, N.N., 2017, *Perem. Zvezdy/Variable Stars*, **37**, No. 4

Kazarovets, E.V., Samus, N.N., 2018, *Perem. Zvezdy/Variable Stars*, **38**, No. 5

Samus, N.N., Kazarovets, E.V., Durlevich, O.V., Kireeva, N.N., Pastukhova, E.N. 2017, *Astronomy Reports*, **61**, 80 DOI

Samus, N.N., Kazarovets, E.V., Pastukhova, E.N., Tsvetkova, T.M., Durlevich, O.V. 2009, *PASP*, **121**, 1378 DOI

Table 1

Name		R.A., Decl., 2000.0 h m s ° ' "	Type	Name		R.A., Decl., 2000.0 h m s ° ' "	Type
V0782	And	00 01 28.3 +39 15 53	EA	V0831	Aur	05 05 07.9 +42 42 28	EA
V0783	And	00 02 05.3 +38 13 23	EW	V0832	Aur	05 06 17.4 +35 47 38	UGSU
V0784	And	00 20 37.9 +31 29 06	RR(B)	V0833	Aur	05 08 33.0 +34 04 43	EB
V0785	And	00 26 30.0 +42 12 32	EW	V0834	Aur	05 10 36.8 +33 30 33	EW:
V0786	And	00 26 41.2 +41 59 22	EA	V0835	Aur	05 10 49.5 +33 50 46	EB
V0787	And	00 33 17.0 +26 31 24	RR(B)	V0836	Aur	05 13 39.2 +42 37 15	LB
V0788	And	00 39 38.4 +30 09 41	RR(B)	V0837	Aur	05 18 07.5 +36 49 50	EW
V0789	And	00 40 18.0 +27 26 04	EA	V0838	Aur	05 24 22.1 +42 05 58	EA
V0790	And	00 56 10.9 +41 17 01	EW	V0839	Aur	05 26 11.8 +41 45 08	EA
V0791	And	01 09 22.3 +36 02 18	DSCT	V0840	Aur	05 29 26.9 +46 11 47	EW
V0792	And	01 17 03.5 +49 33 09	EA	V0841	Aur	05 31 51.0 +36 03 59	EW
V0793	And	01 18 53.2 +36 21 55	EW	V0842	Aur	05 32 55.0 +54 19 26	EB
V0794	And	01 20 12.8 +48 36 41	EA	V0843	Aur	05 34 22.3 +31 22 08	EB
V0795	And	01 21 46.6 +44 46 44	EB	V0844	Aur	05 43 05.6 +53 02 35	EW
V0796	And	01 29 26.9 +38 33 38	RR(B)	V0845	Aur	05 43 52.4 +33 44 39	EB
V0797	And	01 36 23.2 +48 00 28	RRC	V0846	Aur	05 46 19.1 +32 01 11	EW
V0798	And	01 43 01.8 +37 50 58	EA	V0847	Aur	05 46 46.9 +44 33 49	EB
V0799	And	01 52 21.6 +41 25 06	EA	V0848	Aur	05 48 08.0 +32 48 59	M
V0800	And	01 54 19.4 +37 08 15	SRB	V0849	Aur	05 48 24.0 +30 57 04	EA+EA
V0801	And	02 00 09.1 +43 02 43	EW	V0850	Aur	05 49 06.5 +41 56 40	EA
V0802	And	02 05 15.8 +41 28 14	EB	V0851	Aur	05 49 16.1 +41 18 19	EA
V0803	And	02 09 47.6 +47 04 33	EW	V0852	Aur	05 49 33.9 +51 29 06	EA
V0804	And	02 10 19.1 +46 40 44	EB	V0853	Aur	05 54 17.0 +44 25 34	EW
V0805	And	02 10 25.4 +46 45 21	EW	V0854	Aur	05 58 05.5 +51 36 40	EA
V0806	And	02 23 30.8 +40 04 50	EB	V0855	Aur	06 05 51.8 +31 56 48	EW
V0807	And	02 26 51.1 +37 33 02	EP+DSCT	V0856	Aur	06 12 34.8 +49 37 40	EA
V0808	And	02 27 38.7 +43 14 43	SXPHE	V0857	Aur	06 13 34.4 +49 14 05	E
CO	Ant	09 27 55.0 -39 10 53	EW	V0858	Aur	06 30 58.2 +38 31 22	RRAB
CP	Ant	10 05 50.3 -28 25 25	EB	V0859	Aur	06 36 52.2 +30 44 05	EB
CQ	Ant	10 09 05.1 -36 50 03	M	V0860	Aur	07 09 55.5 +36 43 56	EW
CR	Ant	10 19 16.8 -28 19 25	EB	V0861	Aur	07 25 07.6 +39 03 41	RR(B)
CS	Ant	10 54 55.1 -35 20 53	EW	V0381	Boo	13 47 01.8 +20 56 59	RR(B)
V1046	Ara	17 00 46.8 -53 19 51	M	V0382	Boo	13 51 18.2 +08 12 09	EA
V1047	Ara	17 25 09.3 -49 52 04	SRB	V0383	Boo	13 55 12.5 +09 46 10	RR(B)
V1048	Ara	17 26 38.2 -63 48 54	ELL:	V0384	Boo	13 56 45.3 +26 06 41	RR(B)
V1049	Ara	17 29 14.8 -59 39 55	DSCT	V0385	Boo	13 56 46.1 +22 45 11	EB
V1050	Ara	17 35 02.5 -49 26 26	BE	V0386	Boo	13 58 22.8 +09 13 29	RR(B)
V1051	Ara	17 35 50.9 -53 04 48	DSCT	V0387	Boo	14 05 33.3 +11 46 39	EW
DM	Ari	01 48 50.2 +22 46 37	EB	V0388	Boo	14 07 02.4 +10 26 24	RR(B)
DN	Ari	01 52 16.8 +24 48 31	RR(B)	V0389	Boo	14 08 03.9 +23 03 42	EB
DO	Ari	01 53 42.6 +15 52 16	RR(B)	V0390	Boo	14 14 39.0 +31 01 46	BY
DP	Ari	02 09 50.4 +12 26 36	RR(B)	V0391	Boo	14 15 47.0 +08 08 11	EW
DQ	Ari	02 15 54.8 +25 34 40	RR(B)	V0392	Boo	14 16 04.8 +29 59 08	RRC
DR	Ari	02 16 30.3 +21 17 50	DSCT	V0393	Boo	14 20 12.4 +49 52 06	RRAB
DS	Ari	02 27 26.4 +11 56 50	EW	V0394	Boo	14 21 58.7 +34 27 24	RR(B)
DT	Ari	02 48 18.0 +11 12 40	RR(B)	V0395	Boo	14 24 54.2 +11 47 45	RR(B)
DU	Ari	03 10 04.3 +27 51 53	EW	V0396	Boo	14 25 47.2 +22 10 09	RR(B)
DV	Ari	03 13 25.6 +15 21 47	RR(B)	V0397	Boo	14 31 50.4 +17 57 22	RR(B)
DW	Ari	03 17 00.7 +19 08 39	EW	V0398	Boo	14 34 29.8 +26 57 28	RRC
V0826	Aur	04 55 19.6 +45 14 21	EW	V0399	Boo	14 34 54.0 +27 09 36	RR(B)
V0827	Aur	04 55 26.2 +44 20 40	LB	V0400	Boo	14 36 02.9 +37 05 29	EW
V0828	Aur	04 57 18.3 +40 56 43	EW	V0401	Boo	14 36 49.6 +32 39 50	RR(B)
V0829	Aur	05 02 30.0 +45 10 43	UV+BY:	V0402	Boo	14 39 35.6 +15 44 22	EB
V0830	Aur	05 02 56.8 +50 32 15	EW	V0403	Boo	14 40 18.1 +20 01 32	RR(B)

Table 1 (Continued)

Name		R.A., Decl., 2000.0 (h m s ° ' ")	Type	Name		R.A., Decl., 2000.0 (h m s ° ' ")	Type
V0404	Boo	14 43 51.7 +44 44 44	EA	V0612	Cam	07 14 55.9 +73 15 40	EA
V0405	Boo	14 44 01.0 +34 02 44	RR(B)	V0613	Cam	07 36 20.4 +75 59 18	EW
V0406	Boo	14 44 43.4 +25 57 53	EW	V0614	Cam	08 25 17.7 +84 25 23	EW
V0407	Boo	14 45 18.6 +35 28 05	EW	V0615	Cam	09 02 02.4 +76 57 08	EW
V0408	Boo	14 47 29.9 +11 58 39	DSCT	V0616	Cam	09 05 52.6 +82 03 44	EB
V0409	Boo	14 49 54.8 +17 16 17	EW:	V0617	Cam	09 06 10.8 +80 39 57	SR
V0410	Boo	14 50 07.6 +38 14 56	DSCT	NN	Cnc	08 01 22.2 +21 21 11	RR(B)
V0411	Boo	14 53 55.2 +39 32 21	RR(B)	NO	Cnc	08 04 41.3 +21 24 20	EB
V0412	Boo	14 58 11.8 +25 26 32	RR(B)	NP	Cnc	08 09 35.3 +12 09 00	RR(B)
V0413	Boo	15 03 58.2 +34 46 48	RR(B)	NQ	Cnc	08 11 38.0 +28 02 16	EW
V0414	Boo	15 07 36.0 +10 05 02	RRC	NR	Cnc	08 11 51.7 +08 23 00	EW
V0415	Boo	15 07 40.6 +12 41 43	RR(B)	NS	Cnc	08 12 56.8 +19 11 58	E+NL
V0416	Boo	15 36 17.0 +46 29 32	EB	NT	Cnc	08 13 18.0 +28 42 14	EB
V0417	Boo	15 41 37.0 +51 59 25	DSCT	NU	Cnc	08 14 29.8 +31 11 15	RR(B)
TY	Cae	04 22 00.6 −45 03 13	EW	NV	Cnc	08 16 12.9 +26 41 14	EB
V0573	Cam	03 16 49.4 +58 24 41	EW	NW	Cnc	08 16 52.4 +09 27 57	RR(B)
V0574	Cam	03 17 05.3 +63 23 02	EA	NX	Cnc	08 20 13.3 +32 21 26	EW
V0575	Cam	03 17 07.8 +57 29 26	E/RS	NY	Cnc	08 21 22.8 +08 50 02	EW
V0576	Cam	03 17 11.3 +60 28 27	EA	NZ	Cnc	08 22 09.3 +24 02 29	EW
V0577	Cam	03 18 35.1 +62 21 49	EW	OO	Cnc	08 24 26.3 +18 42 29	RR(B)
V0578	Cam	03 20 01.0 +59 38 37	EW	OP	Cnc	08 26 30.9 +17 02 53	EW
V0579	Cam	03 21 08.1 +58 51 24	EA	OQ	Cnc	08 26 40.6 +31 14 59	EB
V0580	Cam	03 21 54.0 +60 25 39	EW	OR	Cnc	08 27 13.5 +17 40 36	EA:
V0581	Cam	03 22 19.5 +62 20 51	RRC:	OS	Cnc	08 28 04.2 +17 59 31	EW
V0582	Cam	03 23 30.4 +59 00 14	EA	OT	Cnc	08 31 27.9 +19 53 04	EW
V0583	Cam	03 25 12.9 +61 47 17	EA	OU	Cnc	08 31 55.5 +09 42 54	EW
V0584	Cam	03 25 42.3 +59 33 33	EW	OV	Cnc	08 31 56.7 +17 43 15	EB
V0585	Cam	03 27 04.2 +62 02 12	EB	OW	Cnc	08 32 51.1 +13 33 42	EW
V0586	Cam	03 27 28.0 +55 41 51	EB	OX	Cnc	08 34 16.8 +13 58 56	EW
V0587	Cam	03 30 24.4 +59 58 47	EW	OY	Cnc	08 39 27.1 +23 35 36	EW
V0588	Cam	03 31 13.9 +63 58 44	CEP	OZ	Cnc	08 39 54.2 +23 20 17	EW
V0589	Cam	03 32 52.5 +59 36 52	EW	PP	Cnc	08 41 44.2 +25 30 31	DSCT
V0590	Cam	03 33 13.8 +60 27 00	EW	PQ	Cnc	08 42 06.0 +21 26 12	EW
V0591	Cam	03 33 21.1 +60 20 34	EB	PR	Cnc	08 45 29.4 +24 16 31	RR(B)
V0592	Cam	03 34 59.0 +62 36 53	EA	PS	Cnc	08 48 38.2 +09 51 15	RR(B)
V0593	Cam	03 35 18.8 +60 37 28	EB	PT	Cnc	08 51 27.9 +25 27 54	EA
V0594	Cam	03 36 39.1 +57 56 54	BY:	PU	Cnc	08 52 13.3 +09 32 17	RR(B)
V0595	Cam	03 37 14.8 +60 02 41	DSCT	PV	Cnc	08 58 21.1 +09 17 38	EW
V0596	Cam	03 37 33.6 +60 09 26	EB	PW	Cnc	08 58 42.7 +17 39 38	RRC
V0597	Cam	03 37 41.8 +61 24 41	EB	PX	Cnc	08 58 42.8 +17 39 25	EA
V0598	Cam	03 38 34.9 +57 41 44	EB	PY	Cnc	08 58 43.0 +14 53 10	EW
V0599	Cam	03 38 54.2 +60 35 50	EB	PZ	Cnc	09 00 19.7 +14 21 28	EW
V0600	Cam	03 41 17.7 +62 27 43	EA	QQ	Cnc	09 02 22.3 +18 33 40	RR(B)
V0601	Cam	03 42 35.1 +76 45 17	EW	QR	Cnc	09 03 13.9 +11 11 40	EB
V0602	Cam	03 45 55.7 +60 11 47	LB:	QS	Cnc	09 06 37.8 +24 12 14	EW
V0603	Cam	03 58 49.2 +57 15 18	EB	QT	Cnc	09 07 03.0 +31 13 25	EW
V0604	Cam	05 17 37.1 +69 51 47	EW	QU	Cnc	09 16 37.7 +07 11 25	RR(B)
V0605	Cam	05 18 35.8 +69 48 59	EW	QV	Cnc	09 17 43.8 +09 57 23	EW
V0606	Cam	05 21 39.1 +62 20 19	RR	HK	CVn	12 13 57.2 +45 28 57	RR(B)
V0607	Cam	05 46 03.6 +66 55 25	EB	HL	CVn	12 17 00.5 +36 33 16	RR(B)
V0608	Cam	06 26 01.8 +82 21 28	EA	HM	CVn	12 17 13.2 +45 47 04	RR(B)
V0609	Cam	06 29 57.7 +76 43 00	EW	HN	CVn	12 28 09.6 +35 33 39	DSCT
V0610	Cam	07 01 44.5 +63 53 03	RR(B)	HO	CVn	12 44 09.8 +36 03 23	EW
V0611	Cam	07 14 14.4 +73 27 30	DSCT	HP	CVn	12 50 17.8 +42 57 30	RR(B)

Table 1 (Continued)

Name		R.A., Decl., 2000.0 h m s ° ' "	Type	Name		R.A., Decl., 2000.0 h m s ° ' "	Type
HQ	CVn	12 59 47.5 +36 58 44	EB	V1296	Cas	00 00 24.5 +55 27 48	EW
HR	CVn	13 01 11.2 +42 02 14	EW	V1297	Cas	00 06 37.4 +55 27 22	EW
HS	CVn	13 01 37.1 +39 41 37	RR(B)	V1298	Cas	00 14 13.8 +60 27 03	EB
HT	CVn	13 06 58.4 +36 27 21	EA	V1299	Cas	00 23 30.0 +61 17 40	EA
HU	CVn	13 07 05.5 +36 57 58	EW	V1300	Cas	00 24 15.1 +60 35 01	EB
HV	CVn	13 12 59.9 +37 07 02	RR(B)	V1301	Cas	00 30 33.1 +57 43 47	EW
HW	CVn	13 23 08.7 +42 46 13	EW	V1302	Cas	00 35 26.0 +61 14 48	LB
HX	CVn	13 29 00.4 +34 12 42	RR(B)	V1303	Cas	00 36 08.4 +74 30 10	EW
HY	CVn	13 34 17.8 +39 43 14	EW	V1304	Cas	00 36 25.9 +60 45 36	LB
HZ	CVn	14 05 51.5 +37 46 52	EW	V1305	Cas	00 40 46.4 +46 56 57	EB
II	CVn	14 06 46.6 +37 47 14	EW	V1306	Cas	00 46 25.2 +61 39 11	GCAS
V0436	CMa	06 12 36.0 −28 16 27	EW	V1307	Cas	00 46 51.0 +60 17 46	LB
V0437	CMa	06 15 29.5 −18 37 31	SRB	V1308	Cas	00 52 13.0 +65 12 26	SR
V0438	CMa	06 16 02.4 −14 26 04	EB	V1309	Cas	01 04 04.8 +63 17 11	LB
V0439	CMa	06 18 14.9 −14 41 09	EW	V1310	Cas	01 08 03.3 +49 05 55	EB
V0440	CMa	06 19 21.4 −15 50 37	EW	V1311	Cas	01 09 53.7 +60 10 44	EA
V0441	CMa	06 28 21.2 −12 51 33	GDOR	V1312	Cas	01 11 14.9 +60 10 57	EA/RS
V0442	CMa	06 54 34.0 −11 23 30	GDOR	V1313	Cas	01 11 54.5 +63 05 00	LB
V0443	CMa	06 54 49.5 −31 34 45	SRB	V1314	Cas	01 15 10.0 +65 28 47	EA
V0444	CMa	07 11 48.4 −13 08 52	EW	V1315	Cas	01 16 59.7 +63 32 06	BY:
V0435	CMa	07 13 45.8 −21 12 31	NA	V1316	Cas	01 17 32.7 +52 51 44	EA
V0445	CMa	07 17 29.5 −15 36 12	EA	V1317	Cas	01 20 01.9 +62 17 08	EA
V0446	CMa	07 19 14.8 −19 54 24	ACV:	V1318	Cas	01 22 06.2 +62 32 40	EW
V0447	CMa	07 20 18.3 −19 42 47	EW	V1319	Cas	01 24 40.4 +63 08 30	EB
V0448	CMa	07 21 28.2 −14 37 19	EW	V1320	Cas	01 26 09.1 +60 52 26	EW
V0449	CMa	07 23 33.1 −15 54 13	EB	V1321	Cas	01 32 32.8 +55 15 26	EW
V0450	CMa	07 25 15.0 −11 35 50	EA	V1322	Cas	01 33 26.5 +56 25 17	EW
V0451	CMa	07 26 41.4 −22 08 54	SRD+EB	V1323	Cas	01 33 28.7 +59 30 02	EA:
FN	CMi	07 07 01.0 +06 34 59	EB	V1324	Cas	01 33 38.5 +71 02 37	EA
FO	CMi	07 09 56.3 +12 06 08	EB	V1325	Cas	01 34 05.0 +68 34 23	EB
FP	CMi	07 18 23.0 +09 02 24	EB	V1326	Cas	01 35 15.5 +59 58 11	EA
FQ	CMi	07 25 44.5 −00 07 41	EA	V1327	Cas	01 38 03.2 +65 38 09	EB
FR	CMi	07 27 08.1 +09 16 39	EW	V1328	Cas	01 43 18.0 +65 09 26	EB
FS	CMi	07 37 58.5 +05 52 28	DSCT	V1329	Cas	02 01 28.6 +63 54 26	EA
FT	CMi	07 41 42.3 +07 29 26	EW	V1330	Cas	02 05 14.2 +69 32 30	EB
FU	CMi	07 42 05.0 +00 44 09	EW	V1331	Cas	02 08 25.5 +65 58 18	EW
FV	CMi	07 53 10.3 +04 25 37	EW	V1332	Cas	02 09 51.4 +66 59 38	EA
FW	CMi	07 59 31.9 +05 08 07	EB	V1333	Cas	02 11 27.8 +64 49 39	EB
FX	CMi	08 03 52.1 +06 19 25	EA	V1334	Cas	02 13 50.8 +65 46 26	EA
FY	CMi	08 05 45.5 +02 03 02	EB	V1335	Cas	02 22 51.5 +60 30 26	EW
V0907	Car	06 57 11.3 −51 21 10	SRB	V1336	Cas	02 24 35.1 +61 05 35	SR
V0908	Car	07 31 03.3 −52 54 44	SR	V1337	Cas	02 27 48.6 +61 27 56	EW
V0909	Car	08 56 31.5 −57 00 41	BY:	V1338	Cas	02 34 18.8 +63 12 43	EW
V0910	Car	09 53 54.9 −58 49 42	SXARI:	V1339	Cas	02 36 47.0 +63 21 53	EA
V0911	Car	10 05 23.6 −70 41 31	SR	V1340	Cas	02 38 54.4 +63 37 40	EA
V0912	Car	10 06 25.5 −59 12 54	ACV:	V1341	Cas	02 39 14.7 +58 08 19	EW
V0906	Car	10 36 15.4 −59 35 54	NA	V1342	Cas	02 40 02.5 +61 07 44	EA
V0913	Car	10 50 22.1 −58 53 26	ACV	V1343	Cas	02 43 50.9 +58 26 00	EW
V0914	Car	10 51 34.4 −60 47 57	ELL	V1344	Cas	02 44 53.5 +61 55 14	EA
V0915	Car	10 56 42.3 −62 17 41	RS:	V1345	Cas	02 45 04.1 +57 43 09	RRC:
V0916	Car	11 09 11.9 −60 46 48	DCEP	V1346	Cas	02 45 41.2 +58 06 40	EW
V0917	Car	11 09 18.3 −64 29 41	SRA	V1347	Cas	02 46 25.5 +59 37 02	EB
V0918	Car	11 10 28.9 −61 18 15	CWA	V1348	Cas	02 46 46.1 +57 59 23	EW
V0919	Car	11 17 07.1 −64 36 57	NA	V1349	Cas	02 47 31.1 +62 41 03	EW

Table 1 (Continued)

Name	R.A., Decl., 2000.0	Type	Name	R.A., Decl., 2000.0	Type
	h m s o ' "			h m s o ' "	
V1350 Cas	02 47 55.6 +61 53 19	EW	V1418 Cen	13 29 24.7 -47 01 44	SR
V1351 Cas	02 47 56.3 +63 09 02	EW	V1419 Cen	13 30 47.4 -48 01 08	SRB
V1352 Cas	02 48 05.6 +57 56 04	DCEP	V1420 Cen	13 30 56.9 -48 19 25	SR
V1353 Cas	02 48 29.5 +63 16 27	EW	V1421 Cen	13 32 13.2 -32 02 04	DSCT
V1354 Cas	02 49 58.3 +63 31 10	EW	V1422 Cen	13 43 56.2 -30 20 40	SRB
V1355 Cas	02 50 53.6 +63 01 39	RRAB	V1423 Cen	13 54 03.8 -46 29 49	EW
V1356 Cas	02 51 12.3 +62 19 56	EA	V1424 Cen	14 06 02.8 -58 32 45	INT:
V1357 Cas	02 51 41.8 +61 23 50	EB	V1404 Cen	14 07 31.3 -63 13 12	NA
V1358 Cas	02 52 05.0 +63 11 13	EW	V1425 Cen	14 09 47.8 -61 44 58	SRS
V1359 Cas	02 52 26.2 +66 29 26	EW	V1426 Cen	14 15 34.0 -34 13 40	UG
V1360 Cas	02 52 44.5 +62 00 14	EA	V1427 Cen	14 21 36.7 -63 19 36	NA
V1361 Cas	02 53 00.5 +57 32 34	EA	V1428 Cen	14 25 04.4 -58 45 34	NA
V1362 Cas	02 53 11.2 +58 00 19	EA	V1429 Cen	14 28 21.6 -38 12 14	DSCT
V1363 Cas	02 54 31.0 +63 22 06	E/RS	V1430 Cen	14 41 03.2 -62 45 58	SR
V1364 Cas	02 56 06.3 +63 45 16	EB	V1019 Cep	00 28 28.0 +78 57 43	EW
V1365 Cas	02 57 04.5 +58 42 37	EW	V1020 Cep	02 09 37.7 +79 03 33	EW
V1366 Cas	02 57 22.4 +61 38 21	EA	V1021 Cep	03 06 44.8 +77 30 13	EA
V1367 Cas	02 57 24.0 +60 16 54	EW	V1022 Cep	03 38 33.1 +78 00 41	RRAB
V1368 Cas	02 57 32.2 +60 17 38	EW	V1023 Cep	03 39 26.7 +77 26 56	LB
V1369 Cas	02 58 07.1 +60 42 24	EB:	V1024 Cep	05 06 48.3 +83 19 23	NL+E
V1370 Cas	02 58 28.6 +58 15 34	EB	KS Cet	00 04 00.6 -09 03 52	RR(B)
V1371 Cas	02 59 37.0 +59 51 45	EW	KT Cet	00 12 34.2 -22 55 17	M
V1372 Cas	03 00 07.7 +58 56 26	EB	KU Cet	00 45 45.3 -24 45 16	EW
V1373 Cas	03 03 13.6 +58 41 35	EW	KV Cet	00 46 23.8 -03 15 08	EB
V1374 Cas	03 03 21.9 +63 16 13	EW	KW Cet	00 53 21.2 -11 58 34	SR:
V1375 Cas	03 04 26.4 +62 39 08	EW	KX Cet	01 03 40.4 -17 21 39	EW
V1376 Cas	03 05 04.5 +58 27 54	EB	KY Cet	01 06 36.6 +02 31 02	RRC
V1377 Cas	03 06 17.4 +58 44 09	EW	KZ Cet	01 22 12.6 +02 13 21	RRAB
V1378 Cas	03 06 39.6 +58 55 10	EW:	LL Cet	01 24 17.0 +01 12 19	SR
V1379 Cas	03 06 59.2 +62 19 37	EB	LM Cet	01 27 55.3 -23 01 41	EB
V1380 Cas	03 07 07.6 +63 01 38	EW	LN Cet	01 44 54.2 -14 36 43	RR(B)
V1381 Cas	03 09 26.4 +62 22 09	EA	LO Cet	01 51 00.2 -10 05 24	EW
V1382 Cas	03 10 50.1 +58 30 04	EB	LP Cet	01 54 50.2 +00 15 01	RRAB
V1383 Cas	03 12 18.0 +76 51 20	LB	LQ Cet	01 59 03.1 -04 25 28	RR(B)
V1384 Cas	03 13 47.0 +63 20 58	DCEP	LR Cet	02 24 27.9 -10 40 35	EA
V1385 Cas	03 13 52.2 +62 07 33	EA	LS Cet	02 24 29.7 +08 12 31	DSCT
V1386 Cas	03 14 03.4 +61 44 43	EA	LT Cet	02 34 39.4 +04 55 28	RRC
V1387 Cas	03 14 55.3 +62 38 56	EA	LU Cet	02 53 45.0 +05 06 34	GDOR
V1388 Cas	03 15 07.4 +63 19 53	L	LV Cet	02 59 19.8 +06 43 43	EA
V1389 Cas	03 15 48.1 +60 31 02	EA	LW Cet	03 17 59.1 +02 30 12	EW
V1390 Cas	03 23 00.2 +72 35 49	EW	FM Cir	13 53 27.6 -67 25 01	NA
V1406 Cen	11 14 59.4 -36 12 51	EW	FN Cir	14 37 10.1 -64 48 05	BE
V1407 Cen	11 19 31.5 -39 50 48	EW	FO Cir	14 55 07.3 -60 26 40	NA
V1408 Cen	11 24 37.2 -59 59 37	ACV:	FP Cir	15 23 15.4 -56 03 43	DSCT
V1409 Cen	11 40 33.5 -56 41 46	SR	BR Col	05 05 20.9 -37 43 39	EW
V1410 Cen	11 49 29.2 -42 30 49	EW	BS Col	06 02 34.4 -33 32 11	EA/RS
V1411 Cen	12 14 03.1 -41 47 40	EW	BT Col	06 03 34.5 -28 34 27	EW
V1412 Cen	12 46 06.5 -42 38 06	CWB	BU Col	06 26 34.8 -38 56 50	EW
V1413 Cen	12 53 50.8 -37 03 24	EB	QU Com	11 59 42.6 +15 15 30	RR(B)
V1414 Cen	13 09 20.5 -34 09 20	EW	QV Com	12 00 24.1 +13 51 04	EW
V1405 Cen	13 20 55.4 -63 42 19	NB	QW Com	12 08 12.2 +23 21 43	RR(B)
V1415 Cen	13 22 31.5 -48 08 29	SRB	QX Com	12 18 03.4 +28 38 32	RR(B)
V1416 Cen	13 23 33.0 -48 34 08	SRB	QY Com	12 24 48.8 +22 11 37	RR(B)
V1417 Cen	13 27 26.1 -46 27 17	RRC	QZ Com	12 32 04.8 +18 20 10	RRC

Table 1 (Continued)

Name		R.A., Decl., 2000.0 h m s ° ' "	Type	Name		R.A., Decl., 2000.0 h m s ° ' "	Type
V0335	Com	12 47 46.3 +20 15 48	RR(B)	V0556	Dra	16 57 33.9 +59 31 52	EA
V0336	Com	12 48 42.7 +15 41 35	RR(B)	V0557	Dra	17 03 58.6 +52 01 37	RR(B)
V0337	Com	13 02 12.8 +17 50 21	RR(B)	V0558	Dra	17 10 02.9 +52 23 39	RR(B)
V0338	Com	13 03 44.7 +17 58 07	RR(B)	V0559	Dra	17 12 46.9 +57 03 10	EW
V0339	Com	13 15 18.7 +25 10 06	EW	V0560	Dra	17 15 22.5 +55 33 28	RR(B)
V0340	Com	13 19 46.8 +14 40 22	RR(B)	V0561	Dra	17 19 26.6 +53 49 43	RR(B)
V0341	Com	13 23 22.1 +26 13 44	RR(B)	V0562	Dra	17 23 10.7 +58 25 47	EB
V0342	Com	13 23 23.8 +17 55 58	RR(B)	V0563	Dra	17 25 13.9 +51 26 26	EW
V0343	Com	13 26 12.0 +18 44 45	RR(B)	V0564	Dra	17 35 32.3 +57 48 09	EB
DD	CrB	15 33 49.4 +37 59 28	EA	V0565	Dra	17 38 49.8 +57 12 23	EW
DE	CrB	15 46 19.2 +36 34 05	RR(B)	OW	Eri	02 34 59.1 -39 37 05	EW
DF	CrB	15 48 18.1 +32 21 46	EW	OX	Eri	02 55 33.3 -47 50 42	UG
DG	CrB	15 49 51.1 +29 31 28	RR(B)	OY	Eri	02 59 59.2 -39 58 12	EW
DH	CrB	16 01 28.5 +28 15 54	RR(B)	OZ	Eri	04 34 05.8 -07 06 54	EW
DI	CrB	16 05 31.2 +29 56 42	RR(B)	PP	Eri	05 00 31.5 -09 14 14	EB
DK	CrB	16 11 18.0 +33 07 13	EA	PQ	Eri	05 01 35.2 -08 38 36	EB
DL	CrB	16 11 32.5 +33 06 05	EA	BL	For	03 07 49.9 -36 52 02	EW
DM	CrB	16 15 59.4 +38 52 10	BY	BM	For	03 32 18.8 -35 39 15	DSCT
AB	Crv	12 01 11.0 -22 02 11	EW	V0477	Gem	06 07 26.6 +22 05 48	BE+X
AC	Crv	12 02 30.5 -21 13 14	EW	V0478	Gem	06 11 56.3 +23 30 29	EW
AD	Crv	12 11 43.6 -16 45 01	RRC	V0479	Gem	06 15 38.2 +21 50 08	M
AE	Crv	12 19 06.3 -24 00 57	EW	V0480	Gem	06 18 50.4 +22 05 12	EW
AF	Crv	12 21 18.7 -13 59 53	EW	V0481	Gem	06 22 29.5 +27 34 42	EW
AG	Crv	12 22 07.9 -12 03 16	RR(B)	V0482	Gem	06 24 00.8 +20 28 13	EW
AH	Crv	12 27 26.3 -13 00 28	RR(B)	V0483	Gem	06 25 41.6 +22 06 20	DSCT
AS	Crt	10 59 53.3 -09 31 41	EW	V0484	Gem	06 26 57.7 +24 29 07	UG
AT	Crt	11 03 04.4 -22 29 18	RRAB	V0485	Gem	06 31 03.8 +20 11 38	RRC:
AU	Crt	11 09 10.5 -16 23 48	EA	V0486	Gem	06 35 46.2 +19 28 28	EW
AV	Crt	11 10 14.2 -20 07 07	E	V0487	Gem	06 40 03.0 +28 25 34	BY+UV
AW	Crt	11 11 34.8 -13 26 10	EW	V0488	Gem	07 04 52.4 +10 27 24	DSCT
AX	Crt	11 14 36.6 -16 10 46	RR(B)	V0489	Gem	07 10 48.9 +24 36 54	EW
AY	Crt	11 25 21.2 -11 16 10	RR(B)	V0490	Gem	07 11 00.1 +24 49 17	EA
AZ	Crt	11 26 56.4 -09 25 48	EA	V0491	Gem	07 11 35.2 +24 24 56	RRAB
BB	Crt	11 27 21.8 -09 17 36	EB	V0492	Gem	07 11 43.1 +24 29 55	EB
BC	Crt	11 30 22.3 -15 21 53	EA	V0493	Gem	07 13 27.3 +20 55 53	UGSU
BD	Crt	11 33 18.3 -09 34 00	EB	V0494	Gem	07 19 59.5 +25 43 40	EW
BE	Crt	11 38 15.7 -13 18 53	EW	V0495	Gem	07 20 29.5 +23 40 07	EA
FU	Cru	12 11 00.6 -60 29 04	EW	V0496	Gem	07 21 24.6 +25 59 07	EW
FV	Cru	12 11 05.6 -60 29 25	EW	V0497	Gem	07 25 13.3 +30 49 41	EB
FW	Cru	12 11 10.7 -60 29 54	EW	V0498	Gem	07 26 27.0 +18 41 23	EA
FX	Cru	12 14 44.8 -62 45 29	DSCTC	V0499	Gem	07 27 09.8 +29 17 16	EB
BL	Dor	04 16 55.2 -49 27 10	EW	V0500	Gem	07 27 40.1 +26 23 04	ELL/RS
BM	Dor	04 19 35.9 -50 26 15	EA	V0501	Gem	07 30 45.1 +15 05 25	EB
BN	Dor	04 49 26.8 -68 45 06	SR	V0502	Gem	07 30 58.2 +25 34 12	EB
V0546	Dra	11 41 14.4 +75 42 22	RR(B)	V0503	Gem	07 32 04.9 +15 04 25	EB
V0547	Dra	12 28 20.9 +68 36 59	EW	V0504	Gem	07 34 30.9 +33 59 00	EW
V0548	Dra	14 49 27.7 +57 17 55	EW	V0505	Gem	07 41 02.5 +30 47 25	EW
V0549	Dra	15 33 45.8 +63 37 12	EW	V0506	Gem	07 41 09.3 +19 19 30	RR(B)
V0550	Dra	15 47 10.6 +53 02 11	EW	V0507	Gem	07 43 15.4 +30 38 40	EW
V0551	Dra	16 27 44.2 +56 45 59	EW	V0508	Gem	07 45 02.2 +31 43 34	EW
V0552	Dra	16 29 40.3 +57 20 33	DSCT	V0509	Gem	07 45 33.5 +27 42 42	EW
V0553	Dra	16 35 50.5 +66 19 33	DSCT	V0510	Gem	07 46 58.6 +22 44 48	EW
V0554	Dra	16 41 05.8 +60 36 22	EW	V0511	Gem	07 47 06.2 +19 31 23	EW
V0555	Dra	16 44 25.4 +52 51 46	RR(B)	V0512	Gem	07 47 22.5 +22 04 14	EA+DSCT

Table 1 (Continued)

Name	R.A., Decl., 2000.0	Type	Name	R.A., Decl., 2000.0	Type
	h m s ° ' "			h m s ° ' "	
V0513 Gem	07 47 26.6 +26 23 46	UV	V1497 Her	17 28 57.9 +15 10 46	EW
V0514 Gem	07 49 00.8 +28 34 26	EA	V1498 Her	17 30 03.2 +34 45 09	EW
V0515 Gem	07 51 02.2 +34 24 06	EW	V1499 Her	17 30 10.8 +45 22 05	RR(B)
V0516 Gem	07 55 40.6 +26 46 20	UG	V1500 Her	17 31 37.5 +19 23 59	EW
V0517 Gem	07 57 01.5 +30 36 33	RR(B)	V1501 Her	17 35 20.9 +30 30 11	EW
V0518 Gem	07 57 34.4 +26 51 52	EW	V1502 Her	17 37 00.8 +25 32 11	DSCT
V0519 Gem	08 00 15.5 +28 20 58	DSCTC:	V1503 Her	17 40 16.2 +31 59 50	RRC
V0520 Gem	08 04 46.1 +32 01 42	RR(B)	V1504 Her	17 44 00.1 +34 21 06	EB
V0521 Gem	08 06 06.5 +30 08 54	EW	V1505 Her	17 47 27.4 +40 35 07	DSCT
V1452 Her	15 49 16.8 +42 24 24	RR(B)	V1506 Her	17 50 44.3 +49 54 34	EW
V1453 Her	16 01 56.0 +20 28 22	EW	V1507 Her	17 51 38.6 +39 03 00	RR(B)
V1454 Her	16 08 47.2 +25 11 44	EW	V1508 Her	17 53 02.5 +37 13 13	DSCTC
V1455 Her	16 12 40.4 +08 27 00	EB	V1509 Her	17 54 57.4 +24 46 14	EW
V1456 Her	16 15 18.8 +23 44 12	EW	V1510 Her	17 54 58.2 +37 29 02	EW
V1457 Her	16 17 34.1 +41 03 42	RR(B)	V1511 Her	17 55 27.5 +44 06 55	EW
V1458 Her	16 18 57.8 +26 13 38	EW	V1512 Her	17 55 29.2 +21 31 28	EW
V1459 Her	16 20 22.1 +12 05 33	EW	V1513 Her	17 56 09.3 +43 00 54	DSCT
V1460 Her	16 21 17.4 +44 12 54	UG+E	V1514 Her	17 56 32.3 +32 48 04	EW
V1461 Her	16 24 27.5 +18 24 50	RR(B)	V1515 Her	17 57 25.7 +46 15 47	EW
V1462 Her	16 26 43.1 +23 29 42	DSCT	AO Hor	03 02 48.2 -61 25 45	EW
V1463 Her	16 26 53.8 +14 10 16	EB	AP Hor	03 10 11.4 -58 30 04	SR
V1464 Her	16 28 44.6 +06 49 45	EW	AQ Hor	04 06 15.8 -42 50 02	EW
V1465 Her	16 29 22.2 +16 59 38	EA	V0607 Hya	08 11 17.1 -08 24 10	EW
V1466 Her	16 30 18.5 +06 26 26	RR(B)	V0608 Hya	08 12 03.0 +05 09 27	EW
V1467 Her	16 32 00.0 +33 51 35	RRC	V0609 Hya	08 14 08.1 +00 29 11	EW
V1468 Her	16 32 45.6 +32 40 51	RR(B)	V0610 Hya	08 18 04.7 -06 27 49	EA
V1469 Her	16 35 01.1 +35 47 02	RRAB	V0611 Hya	08 19 03.4 -08 56 04	EW
V1470 Her	16 35 10.7 +05 50 47	EW	V0612 Hya	08 21 44.4 -01 45 53	EB
V1471 Her	16 38 04.8 +34 33 36	RRAB	V0613 Hya	08 25 49.4 -02 01 25	EA
V1472 Her	16 39 13.4 +48 11 03	RR(B)	V0614 Hya	08 25 59.6 -06 13 44	EW
V1473 Her	16 43 18.7 +26 48 26	RRAB	V0615 Hya	08 27 22.0 +02 51 27	EW
V1474 Her	16 43 45.0 +33 06 51	RR(B)	V0616 Hya	08 31 16.2 -08 59 32	EW
V1475 Her	16 43 49.6 +32 56 38	EW	V0617 Hya	08 32 08.9 -16 42 09	EA
V1476 Her	16 43 57.8 +26 17 44	EA	V0618 Hya	08 33 21.2 -08 28 12	EW
V1477 Her	16 44 45.4 +23 21 32	RR(B)	V0619 Hya	08 33 23.9 -04 57 37	EB
V1478 Her	16 46 47.7 +40 51 17	RR(B)	V0620 Hya	08 35 22.3 -13 50 22	EB
V1479 Her	16 48 14.2 +43 30 25	LB	V0621 Hya	08 36 57.8 -04 52 53	RR(B)
V1480 Her	16 48 22.8 +04 47 17	RR(B)	V0622 Hya	08 38 12.9 +02 59 34	EW
V1481 Her	16 48 27.0 +14 54 08	RR(B)	V0623 Hya	08 39 39.3 -05 05 00	RR(B)
V1482 Her	16 48 44.1 +07 32 05	RR(B)	V0624 Hya	08 40 25.7 +05 01 06	RR(B)
V1483 Her	16 48 59.1 +24 43 55	RR(B)	V0625 Hya	08 43 04.0 -03 42 52	EW
V1484 Her	16 50 09.5 +14 28 20	RR(B)	V0626 Hya	08 43 39.5 -13 54 24	EW
V1485 Her	16 56 32.0 +30 22 22	EW	V0627 Hya	08 44 08.7 -04 06 40	EW
V1486 Her	16 57 09.7 +21 40 02	RR(B)	V0628 Hya	08 47 32.9 +05 32 58	EW
V1487 Her	16 57 34.6 +27 48 10	EW	V0629 Hya	08 49 25.2 -15 15 17	EW
V1488 Her	16 57 40.3 +20 53 34	RR(B)	V0630 Hya	08 52 55.6 +05 36 53	EW
V1489 Her	16 57 57.1 +20 26 16	RR(B)	V0631 Hya	08 54 32.0 +00 00 06	EB
V1490 Her	16 59 39.8 +15 09 59	EW	V0632 Hya	08 55 24.6 -16 27 21	EW
V1491 Her	17 03 41.3 +49 33 24	RR(B)	V0633 Hya	08 57 11.8 -16 38 45	EW
V1492 Her	17 19 14.3 +44 06 50	RR(B)	V0634 Hya	09 00 46.5 -00 13 10	EA
V1493 Her	17 23 03.6 +23 12 42	EB	V0635 Hya	09 00 52.2 +04 56 08	RR(B)
V1494 Her	17 27 18.0 +43 16 24	EW	V0636 Hya	09 01 13.9 -02 23 22	EA
V1495 Her	17 28 02.5 +23 16 46	EW	V0637 Hya	09 06 19.0 -15 48 11	EB
V1496 Her	17 28 31.5 +22 34 19	DSCT	V0638 Hya	09 07 56.8 -15 38 36	EW

Table 1 (Continued)

Name		R.A., Decl., 2000.0 h m s	o ' "	Type	Name		R.A., Decl., 2000.0 h m s	o ' "	Type
V0639	Hya	09 08 08.4	-01 45 38	EA:	PV	Leo	09 53 38.8	+08 55 10	EB
V0640	Hya	09 10 24.6	-10 47 56	EB	PW	Leo	09 55 44.9	+18 23 08	RR(B)
V0641	Hya	09 18 48.7	-03 25 02	EB	PX	Leo	09 57 25.9	+32 01 18	RR(B)
V0642	Hya	09 23 01.2	-06 58 09	EB	PY	Leo	10 06 44.1	+21 56 59	RR(B)
V0643	Hya	09 29 15.3	-14 05 55	EW	PZ	Leo	10 14 00.3	+09 39 24	RR(B)
V0644	Hya	09 31 46.2	-04 24 45	EW	QQ	Leo	10 23 47.6	+15 59 12	RR(B)
V0645	Hya	09 32 01.9	-13 34 09	EW	QR	Leo	10 26 43.7	+09 49 23	RR(B)
V0646	Hya	09 33 04.3	+04 41 51	EW	QS	Leo	10 34 06.6	+07 12 08	RR(B)
V0647	Hya	09 33 51.7	-02 35 14	EB	QT	Leo	10 34 39.5	+24 52 06	LB
V0648	Hya	09 38 13.5	-01 04 28	EA	QU	Leo	10 35 59.3	+19 38 35	RR(B)
V0649	Hya	09 38 22.0	+02 57 09	EW	QV	Leo	10 43 06.2	+09 03 40	RR(B)
V0650	Hya	09 53 50.8	-14 27 26	EB	QW	Leo	10 49 42.4	+14 10 22	EW
V0651	Hya	09 54 21.0	-13 26 38	EW	QX	Leo	10 57 30.2	-05 51 38	EW
V0652	Hya	09 57 06.8	-20 14 08	EW	QY	Leo	10 57 31.4	+04 57 04	RR(B)
V0653	Hya	09 57 33.0	-13 08 04	EA	QZ	Leo	11 00 04.5	+05 44 05	EW
V0654	Hya	10 05 03.4	-14 16 22	EW	V0335	Leo	11 03 51.8	+17 36 10	RR(B)
V0655	Hya	10 05 23.7	-14 16 18	EW	V0336	Leo	11 05 04.9	-01 29 43	EB
V0656	Hya	10 07 49.9	-16 14 06	EW	V0337	Leo	11 13 07.2	-00 05 33	EA
V0657	Hya	10 11 13.9	-14 12 53	EW	V0338	Leo	11 16 45.0	+23 59 28	RR(B)
V0658	Hya	10 23 28.6	-15 39 52	EW	V0339	Leo	11 16 52.8	+14 04 25	EW
V0659	Hya	10 29 16.6	-12 36 52	RR(B)	V0340	Leo	11 19 22.5	+17 13 24	RR(B)
V0660	Hya	10 30 37.2	-29 02 43	EA	V0341	Leo	11 25 18.4	-00 47 15	DSCT
V0661	Hya	10 31 27.5	-12 53 59	EW	V0342	Leo	11 27 59.3	-01 55 17	EA
V0662	Hya	10 31 30.8	-23 00 54	EW	V0343	Leo	11 28 45.5	-02 16 01	RR(B)
V0663	Hya	10 31 54.3	-25 15 42	RRAB	V0344	Leo	11 30 22.6	+08 54 43	RR(B)
V0664	Hya	10 32 22.9	-12 19 45	RR(B)	V0345	Leo	11 33 28.0	+22 59 21	RR(B)
V0665	Hya	10 36 05.4	-23 37 10	EW	V0346	Leo	11 35 49.4	-06 25 45	EW
V0666	Hya	10 38 30.8	-25 45 01	RRAB	V0347	Leo	11 37 22.8	+13 12 14	EB
V0667	Hya	10 41 25.6	-14 58 42	EW	V0348	Leo	11 40 30.9	+16 47 36	RRC:
V0668	Hya	10 41 55.7	-11 54 20	EW	V0349	Leo	11 45 14.8	+11 39 30	EW
V0669	Hya	10 44 10.6	-22 54 03	RRC	V0350	Leo	11 45 17.7	+17 31 16	RR(B)
V0670	Hya	10 46 03.5	-20 00 59	RRAB	V0351	Leo	11 46 31.4	+13 51 59	RR(B)
V0671	Hya	10 46 26.6	-27 22 35	EB	AQ	LMi	09 49 57.5	+40 56 26	LB
V0672	Hya	10 52 43.0	-28 31 56	EA	AR	LMi	09 50 42.0	+33 08 17	RR(B)
V0673	Hya	11 05 54.0	-25 57 11	DSCT	AS	LMi	09 53 10.0	+33 53 53	EA
V0674	Hya	11 53 36.1	-29 05 53	DSCT	AT	LMi	09 53 11.9	+40 08 19	EW
V0675	Hya	13 44 30.5	-27 03 03	EW	AU	LMi	09 56 00.7	+40 41 29	BY:
V0676	Hya	14 15 36.7	-28 43 11	SRB	AV	LMi	10 05 25.3	+31 49 17	RR(B)
V0677	Hya	14 40 50.7	-26 54 50	RRAB	AW	LMi	10 20 00.0	+30 17 54	RRC
V0678	Hya	14 52 46.8	-28 40 20	RRAB	AX	LMi	10 20 40.3	+28 37 02	RR(B)
DP	Hyi	00 06 20.8	-76 21 48	EW	AY	LMi	10 24 22.4	+36 55 24	RRC
DQ	Hyi	00 13 26.9	-81 47 43	EA	AZ	LMi	10 25 06.2	+30 36 09	RR(B)
DR	Hyi	02 07 34.5	-61 16 16	NL	BB	LMi	10 47 11.4	+25 33 02	RR(B)
DS	Hyi	02 13 01.4	-69 38 44	RRAB	BR	Lep	05 31 21.6	-15 40 06	EW
DT	Hyi	02 26 43.2	-76 34 38	NA:	BS	Lep	05 39 55.2	-12 40 13	EB
DU	Hyi	03 55 06.2	-69 23 41	NA	V0369	Lib	14 40 34.2	-13 03 56	EW
OY	Leo	09 25 39.2	+06 31 56	EW	V0370	Lib	14 46 04.0	-09 25 10	EA
OZ	Leo	09 27 02.8	+16 18 53	EW	V0371	Lib	14 49 57.8	-15 38 29	EB
PP	Leo	09 30 57.0	+15 57 14	RRAB	V0372	Lib	14 53 40.0	-01 07 49	EB
PQ	Leo	09 32 23.4	+15 55 46	EW	V0373	Lib	15 09 57.5	-11 53 08	EW
PR	Leo	09 32 27.7	+13 11 48	EA	V0374	Lib	15 23 31.1	-16 19 26	EB
PS	Leo	09 43 11.0	+16 09 54	RR(B)	V0375	Lib	15 37 07.9	-06 06 18	EB
PT	Leo	09 44 40.4	+26 32 07	EW	V0376	Lib	15 38 49.8	-10 09 31	EB
PU	Leo	09 52 47.2	+10 08 38	EB	V0377	Lib	15 42 01.7	-04 21 51	RR(B)

Table 1 (Continued)

Name	R.A., Decl., 2000.0	Type	Name	R.A., Decl., 2000.0	Type
	h m s ° ' "			h m s ° ' "	
V0378 Lib	15 46 20.0 -11 40 32	EW	V1022 Mon	07 38 35.6 -01 47 27	EW
V0379 Lib	15 51 56.6 -18 03 19	RR(B)	V1023 Mon	07 39 17.6 -07 38 47	EB
V0409 Lup	15 11 46.2 -35 47 22	EW	V1024 Mon	07 40 53.6 -01 46 01	EW
V0410 Lup	15 20 22.8 -34 05 13	EW	V1025 Mon	07 48 02.7 -02 45 32	EA
V0407 Lup	15 29 01.8 -44 49 40	NA	V1026 Mon	07 54 18.9 -07 10 43	EB
V0408 Lup	15 38 43.9 -47 44 42	NA	V1027 Mon	07 57 02.4 -03 59 33	EW
LU Lyn	07 20 40.0 +58 22 52	EW	V1028 Mon	08 00 23.4 -04 28 31	EW
LV Lyn	07 44 54.8 +44 29 09	RR(B)	V1029 Mon	08 01 07.4 -06 10 40	EW
LW Lyn	07 54 12.9 +37 34 42	RR(B)	V0357 Mus	11 26 15.0 -65 31 24	NA
LX Lyn	08 01 50.0 +47 14 33	EW	V0358 Mus	11 36 07.9 -74 04 24	DSCT
LY Lyn	08 01 51.5 +41 32 36	EW	V0555 Nor	15 41 45.4 -53 08 07	NA
LZ Lyn	08 05 37.8 +52 21 11	EB	V0557 Nor	15 49 51.7 -54 16 30	UG
MM Lyn	08 08 46.9 +33 54 03	RR(B)	V0558 Nor	16 01 36.2 -54 08 36	LB
MN Lyn	08 09 34.0 +44 34 18	EW	V0556 Nor	16 14 32.9 -53 30 15	NA
MO Lyn	08 10 53.4 +52 56 58	EB	V0559 Nor	16 21 59.1 -51 08 41	NA
MP Lyn	08 11 54.1 +57 31 00	EA	V0560 Nor	16 29 24.7 -59 51 46	IT:
MQ Lyn	08 25 19.8 +37 48 25	RRC	V3667 Oph	16 02 57.7 -07 55 46	EA
MR Lyn	08 48 26.2 +36 20 08	RR(B)	V3668 Oph	16 03 00.0 -06 34 48	EB
MS Lyn	08 51 13.4 +34 44 49	UGSU	V3669 Oph	16 26 40.0 -19 50 17	SR:
MT Lyn	08 56 43.1 +43 20 21	RR(B)	V3670 Oph	16 27 34.6 -16 41 20	SR
MU Lyn	08 57 05.0 +41 46 18	EA	V3671 Oph	16 29 18.7 -21 11 55	SR
MV Lyn	08 58 09.5 +36 31 21	RR(B)	V3672 Oph	16 30 58.2 -17 53 54	LB:
MW Lyn	09 04 04.5 +43 12 57	RRC	V3673 Oph	16 30 59.3 -13 06 33	RRAB
MX Lyn	09 04 21.0 +41 55 13	BY	V3674 Oph	16 31 59.1 -19 32 10	LB:
MY Lyn	09 07 29.3 +42 28 06	RS	V3675 Oph	16 35 01.0 -18 37 44	CWB:
MZ Lyn	09 08 47.1 +42 29 15	RS	V3676 Oph	16 37 27.7 -20 21 10	SR
NN Lyn	09 10 39.9 +45 57 02	EW	V3677 Oph	16 38 01.8 -18 40 09	SR
NO Lyn	09 12 22.6 +40 25 31	BY	V3678 Oph	16 38 20.4 -13 25 01	EB
NP Lyn	09 14 52.4 +34 18 35	DSCT	V3679 Oph	16 39 03.0 -21 06 39	SR
V0997 Mon	06 26 04.6 +01 18 47	EB	V3680 Oph	16 39 37.2 -17 52 59	SR
V0998 Mon	06 27 40.5 -00 35 23	EA	V3681 Oph	16 41 44.4 -12 58 57	SR
V0999 Mon	06 27 56.1 -07 30 59	EW	V3682 Oph	16 42 59.9 -12 30 54	EW
V1000 Mon	06 31 48.6 +07 03 15	EB	V3683 Oph	16 45 45.7 -03 40 30	EA
V1001 Mon	06 35 59.6 +07 45 28	DSCTC	V3684 Oph	16 46 30.8 -08 38 29	EW
V1002 Mon	06 38 45.8 -06 44 10	EA	V3685 Oph	16 47 54.9 -08 44 26	EA
V1003 Mon	06 44 40.7 +00 19 02	EB	V3686 Oph	16 51 00.8 -16 02 18	EA
V1004 Mon	06 48 35.2 -05 34 15	EB	V3687 Oph	16 55 27.7 -04 14 38	EW
V1005 Mon	06 51 14.4 +07 53 58	EA/RS	V3688 Oph	17 00 40.0 +01 10 08	SR
V1006 Mon	06 51 44.7 -00 34 35	EB	V3689 Oph	17 01 21.0 -05 57 57	EB
V1007 Mon	06 54 54.1 +09 07 32	EA	V3690 Oph	17 01 40.1 +04 05 32	SRB
V1008 Mon	06 58 18.5 +10 28 28	EW	V3691 Oph	17 08 19.8 -25 58 33	M
V1009 Mon	07 01 16.8 +07 17 11	EW	V3692 Oph	17 08 21.8 -01 09 22	EW
V1010 Mon	07 02 41.5 -02 35 02	M:	V3693 Oph	17 09 03.8 +00 43 35	RRAB
V1011 Mon	07 06 15.3 -05 45 04	EB	V3665 Oph	17 14 02.5 -28 49 23	NA
V1012 Mon	07 11 42.4 -06 43 29	EW	V3694 Oph	17 18 24.7 -28 49 52	RRC:
V1013 Mon	07 12 10.2 -09 53 54	EW	V3663 Oph	17 18 45.1 -24 54 23	NA
V1014 Mon	07 12 20.8 -05 25 54	EA	V3695 Oph	17 20 05.0 +07 47 30	EW
V1015 Mon	07 12 50.9 -00 22 05	EA	V3664 Oph	17 24 40.0 -24 21 47	N:
V1016 Mon	07 13 15.0 +00 59 39	EW	V3696 Oph	17 28 46.7 +06 07 10	EA
V1017 Mon	07 13 50.4 -06 43 49	EW	V3697 Oph	17 32 19.7 -01 34 12	EA
V1018 Mon	07 14 12.6 -03 41 30	LPB	V3698 Oph	17 32 23.1 -29 48 38	NA
V1019 Mon	07 16 37.5 -07 00 00	EB	V3699 Oph	17 33 50.8 +04 03 11	LB
V1020 Mon	07 35 33.4 -01 54 23	EW	V3661 Oph	17 35 50.4 -29 34 24	NA
V1021 Mon	07 36 13.8 -03 01 23	EB	V3700 Oph	17 36 59.6 -29 51 56	NA

Table 1 (Continued)

Name	R.A., Decl., 2000.0	Type	Name	R.A., Decl., 2000.0	Type
	h m s o ' "			h m s o ' "	
V3701 Oph	17 36 59.7 -29 08 15	NB	V1069 Per	01 59 35.6 +53 02 49	ELL
V3702 Oph	17 38 17.4 -18 35 27	FU:	V1070 Per	02 26 44.7 +56 50 32	EA
V3662 Oph	17 39 46.1 -24 57 56	NA	V1071 Per	02 32 14.6 +55 56 25	EW
V3703 Oph	17 40 23.6 -01 55 47	EA	V1072 Per	02 41 48.6 +37 28 48	EW
V3666 Oph	17 42 24.1 -20 53 09	NA	V1073 Per	02 44 48.8 +36 34 46	EW
V3704 Oph	17 43 20.3 -04 29 57	XM:	V1074 Per	02 45 47.1 +55 56 56	EB
V3705 Oph	17 52 45.1 +07 00 42	DSCT	V1075 Per	02 58 28.6 +37 09 07	EW
V2829 Ori	04 48 02.7 +09 54 58	EA	V1076 Per	02 58 47.0 +57 12 12	RRC
V2830 Ori	04 59 55.0 +10 17 18	DCEP	V1077 Per	03 00 51.9 +56 42 21	LB
V2831 Ori	05 01 10.6 -02 54 25	EA	V1078 Per	03 04 08.2 +38 30 54	DSCT
V2832 Ori	05 02 00.5 +10 37 23	EW	V1079 Per	03 05 52.4 +56 58 23	BY:
V2833 Ori	05 02 03.7 -02 48 08	EW	V1080 Per	03 06 23.8 +42 51 04	EW
V2834 Ori	05 05 36.2 -02 03 18	RR(B)	V1081 Per	03 06 41.1 +42 47 01	EA
V2835 Ori	05 15 01.1 -02 19 50	EW	V1082 Per	03 07 34.8 +42 33 36	EW
V2836 Ori	05 16 41.0 +05 32 11	EW	V1083 Per	03 08 45.1 +42 37 20	EW
V2837 Ori	05 16 54.1 +03 32 52	EA+NL	V1084 Per	03 08 48.9 +42 33 18	EW
V2838 Ori	05 17 30.8 +13 52 29	EW	V1085 Per	03 09 48.7 +42 49 29	EA
V2839 Ori	05 17 44.8 +01 56 00	EW	V1086 Per	03 09 58.7 +56 59 42	EW
V2840 Ori	05 18 42.3 +14 25 05	EW	V1087 Per	03 10 04.3 +56 36 30	EW
V2841 Ori	05 20 36.8 +03 04 02	EW	V1088 Per	03 10 05.8 +42 25 58	EW
V2842 Ori	05 21 08.2 +03 02 52	EA	V1089 Per	03 11 37.2 +43 22 32	EW
V2843 Ori	05 28 25.9 +09 39 44	EW	V1090 Per	03 22 42.5 +39 06 35	DSCT
V2844 Ori	05 29 25.2 -04 30 45	UVN	V1091 Per	03 25 00.9 +46 04 10	EW
V2845 Ori	05 32 03.1 -06 42 03	UVN	V1092 Per	03 26 38.9 +42 43 25	EW
V2846 Ori	05 32 48.4 -04 41 44	BY+UV	V1093 Per	03 38 30.7 +36 54 46	EW
V2847 Ori	05 33 57.9 -04 35 44	UVN	V1094 Per	03 45 12.3 +39 37 19	EW
V2848 Ori	05 34 22.5 -09 52 56	EA	V1095 Per	03 57 05.3 +32 22 36	EW
V2849 Ori	05 34 49.2 -05 04 38	UVN	V1096 Per	03 57 17.9 +32 06 20	EW
V2850 Ori	05 35 36.7 -03 13 01	UVN	V1097 Per	04 02 52.8 +49 57 53	EB
V2851 Ori	05 35 38.8 -06 08 38	UVN	V1098 Per	04 21 57.8 +47 10 04	EA
V2852 Ori	06 05 26.8 +20 10 23	UV	V1099 Per	04 22 11.3 +31 02 12	UV:
V2853 Ori	06 06 23.1 +08 03 49	RR(B)	V1100 Per	04 35 25.6 +45 01 05	EW
V2854 Ori	06 12 45.2 +11 34 01	EB	V1101 Per	04 35 36.4 +44 52 50	EB
V2855 Ori	06 15 17.7 +06 04 13	DSCT	V1102 Per	04 36 00.1 +44 50 40	EA
V2856 Ori	06 18 55.0 +20 35 55	EA	V1103 Per	04 36 09.6 +44 54 04	EA
V2857 Ori	06 19 43.6 +18 15 19	SR	V1104 Per	04 36 20.2 +44 46 21	DSCTC
V2858 Ori	06 20 48.7 -00 11 09	EW	V1105 Per	04 36 36.0 +44 44 51	EB
V2859 Ori	06 23 34.8 +12 04 47	EA	V1106 Per	04 36 37.0 +45 09 48	EW
V0454 Pav	17 57 03.2 -64 11 02	M	V1107 Per	04 37 02.0 +42 05 52	EA
V0687 Peg	00 07 09.6 +26 21 28	EW	V1108 Per	04 37 22.0 +44 57 48	RRAB
V1055 Per	01 32 18.2 +53 17 49	EA	V1109 Per	04 37 52.9 +44 52 32	EB
V1056 Per	01 34 58.5 +54 16 38	EW	V1110 Per	04 41 33.0 +44 06 14	EW
V1057 Per	01 35 36.8 +54 28 34	DSCTC:	V1111 Per	04 49 57.2 +47 19 44	EB
V1058 Per	01 35 40.6 +54 16 24	EW	BD Pic	05 42 20.0 -59 29 03	EW
V1059 Per	01 35 45.6 +54 23 57	EA	BE Pic	06 45 08.8 -59 06 00	M
V1060 Per	01 35 56.0 +54 11 42	EB	LM Psc	00 34 12.6 +20 52 26	EW
V1061 Per	01 36 09.0 +54 19 57	DSCTC	LN Psc	00 40 50.7 +07 16 14	EW
V1062 Per	01 36 26.0 +54 04 15	DSCTC	LO Psc	00 53 28.2 +25 36 23	EW
V1063 Per	01 37 25.2 +54 18 48	EB	LP Psc	01 02 26.7 +25 23 58	EA
V1064 Per	01 37 42.4 +54 15 05	DSCTC	LQ Psc	01 05 12.4 +12 49 56	EA
V1065 Per	01 37 52.9 +54 22 50	EW	LR Psc	01 06 18.4 +08 46 14	DSCT
V1066 Per	01 37 57.6 +54 09 21	EB	LS Psc	01 45 28.6 +12 54 25	DSCT
V1067 Per	01 38 03.2 +54 05 58	EW	V0736 Pup	07 31 49.9 -50 50 12	SRA
V1068 Per	01 49 56.8 +53 35 02	UG	V0737 Pup	07 32 14.2 -18 43 54	ACV:

Table 1 (Continued)

Name	R.A., 2000.0 (h m s)	Decl., 2000.0 (o ' ")	Type	Name	R.A., 2000.0 (h m s)	Decl., 2000.0 (o ' ")	Type
V0738 Pup	07 39 59.9	-13 53 40	EA	V1669 Sco	16 05 23.2	-28 46 34	SR
V0739 Pup	07 51 27.4	-41 36 15	RRAB	V1670 Sco	16 07 12.6	-28 12 55	SR:
V0740 Pup	07 51 31.2	-14 43 53	EW	V1671 Sco	16 07 59.3	-21 01 12	SR
V0741 Pup	07 55 03.3	-32 46 11	ELL:	V1672 Sco	16 10 25.0	-27 54 18	LB
V0742 Pup	07 55 14.1	-13 30 53	EB	V1673 Sco	16 11 37.6	-26 45 29	SRB
V0743 Pup	07 58 42.2	-25 36 01	RR(B)	V1674 Sco	16 11 59.8	-17 03 14	M
V0744 Pup	08 01 01.2	-45 43 39	ACV:	V1675 Sco	16 12 20.8	-19 49 57	M
V0745 Pup	08 09 45.8	-12 13 25	EW	V1676 Sco	16 13 26.3	-28 07 28	SR:
V0746 Pup	08 16 04.7	-23 07 27	LB:	V1677 Sco	16 13 35.8	-28 47 23	EW
V0747 Pup	08 23 42.2	-13 40 44	EW	V1678 Sco	16 14 51.9	-28 14 38	LB
V0748 Pup	08 23 51.3	-37 03 49	SRB	V1679 Sco	16 15 17.2	-28 35 53	SR
V0749 Pup	08 24 52.4	-11 30 29	EA	V1680 Sco	16 15 22.5	-27 18 21	LB:
V0750 Pup	08 25 41.1	-15 38 15	EW	V1681 Sco	16 15 49.1	-26 43 54	LB:
V0751 Pup	08 25 51.6	-16 22 47	EA	V1682 Sco	16 16 46.5	-20 11 55	M
EH Pyx	09 18 02.4	-30 22 32	RRC	V1683 Sco	16 18 59.6	-11 43 55	LB
V5854 Sgr	17 49 57.3	-29 14 38	N	V1684 Sco	16 19 00.0	-28 36 55	SR
V5858 Sgr	17 50 36.1	-30 01 47	NA	V1685 Sco	16 19 17.5	-18 50 36	SRA
V5859 Sgr	17 52 17.9	-28 27 10	LB	V1686 Sco	16 20 08.4	-20 00 23	LB
V5860 Sgr	17 52 58.2	-27 36 00	CEP(B)	V1687 Sco	16 21 37.7	-20 00 37	SR
V5861 Sgr	17 54 34.8	-23 32 22	NA	V1688 Sco	16 24 50.3	-18 39 22	LB
V5862 Sgr	17 55 20.4	-23 23 55	NA:	V1689 Sco	16 25 15.1	-19 31 21	SR:
V5863 Sgr	17 56 49.4	-27 13 28	NA	V1690 Sco	16 25 45.5	-28 33 31	LB
V5864 Sgr	17 57 11.9	-28 51 48	CEP(B)	V1691 Sco	16 25 56.8	-28 31 41	SRB
V5865 Sgr	17 58 04.8	-29 47 49	M	V1692 Sco	16 26 59.0	-18 53 57	SRB
V5866 Sgr	17 58 18.0	-26 31 52	NA:	V1693 Sco	16 28 41.4	-33 44 20	EW
V5867 Sgr	17 58 28.5	-30 07 29	SRB	V1694 Sco	16 29 18.4	-25 52 12	M
V5868 Sgr	17 58 28.8	-30 01 18	M	V1695 Sco	16 29 53.5	-28 33 50	SR
V5869 Sgr	17 58 39.3	-29 45 06	M	V1696 Sco	16 31 54.9	-28 42 44	SR
V5870 Sgr	17 58 42.6	-30 01 46	M	V1697 Sco	16 34 31.2	-28 32 36	LB:
V5871 Sgr	17 58 57.3	-30 00 30	M	V1698 Sco	16 37 23.7	-28 51 19	LB
V5872 Sgr	17 59 11.6	-29 57 05	M	V1699 Sco	16 41 00.0	-28 27 18	SR:
V5873 Sgr	17 59 17.1	-29 49 29	M	V1662 Sco	16 48 49.7	-44 57 03	NA
V5874 Sgr	17 59 33.8	-29 50 27	SRB	V1657 Sco	16 52 18.6	-37 54 16	N
V5875 Sgr	17 59 38.4	-29 33 22	EA+ZAND:	V1663 Sco	17 03 47.6	-38 16 58	NA
V5876 Sgr	17 59 40.3	-28 41 46	M	V1661 Sco	17 18 06.4	-32 04 28	NA
V5877 Sgr	17 59 43.1	-27 44 19	M	V1656 Sco	17 22 51.5	-31 58 37	NA
V5878 Sgr	17 59 43.2	-28 32 57	M	V1660 Sco	17 30 34.1	-31 06 07	N
V5879 Sgr	17 59 44.2	-30 03 11	M	V1700 Sco	17 33 52.4	-36 37 38	ACV:
V5880 Sgr	17 59 44.6	-28 07 02	M	V1655 Sco	17 38 19.3	-37 25 09	NA
V5881 Sgr	17 59 48.5	-28 12 44	M	V1659 Sco	17 42 57.7	-33 25 43	N
V5882 Sgr	17 59 49.0	-29 55 56	M	V1701 Sco	17 43 33.5	-30 30 29	N:
V5883 Sgr	17 59 49.4	-27 49 29	M	V1702 Sco	17 43 37.4	-40 43 17	M
V5884 Sgr	17 59 51.0	-29 49 45	M	V1658 Sco	17 48 12.8	-32 35 13	NA
V5885 Sgr	17 59 55.4	-29 26 46	M	V1703 Sco	17 50 19.2	-33 39 07	NB:
V5886 Sgr	17 59 59.9	-29 31 05	M	V1704 Sco	17 53 02.4	-38 34 18	M
V5853 Sgr	18 01 07.8	-26 31 43	NA	V1705 Sco	17 56 10.4	-30 04 36	NA
V5857 Sgr	18 04 09.4	-18 03 56	NA	DQ Scl	00 04 50.9	-30 29 56	EW
V5855 Sgr	18 10 28.3	-27 29 59	NA	DR Scl	01 04 57.6	-25 42 06	RRAB
V5856 Sgr	18 20 52.2	-28 22 12	NA	DS Scl	01 06 42.2	-33 08 58	EW
V1664 Sco	15 59 29.1	-27 17 59	SRB	DT Scl	01 09 50.7	-28 32 18	RRAB
V1665 Sco	16 00 15.4	-20 38 44	SRB	V0611 Sct	18 25 29.9	-09 47 33	NA
V1666 Sco	16 02 47.2	-26 25 24	SRB	V0613 Sct	18 29 22.9	-14 30 44	NA
V1667 Sco	16 03 51.4	-14 58 06	EA	V0612 Sct	18 31 45.9	-14 18 56	NB
V1668 Sco	16 05 19.2	-26 02 08	SRB	V0636 Ser	15 11 44.6	+16 54 26	EW

Table 1 (Continued)

Name		R.A., Decl., 2000.0 h m s ° ' "	Type	Name		R.A., Decl., 2000.0 h m s ° ' "	Type
V0637	Ser	15 13 07.6 +12 08 04	RR(B)	DH	Tri	01 44 57.5 +33 41 18	EW
V0638	Ser	15 13 22.0 +18 15 58	DSCT	DI	Tri	02 10 24.1 +30 13 36	RR(B)
V0639	Ser	15 15 16.3 -00 51 24	RRAB	DK	Tri	02 17 24.7 +28 44 30	BY
V0640	Ser	15 16 54.5 +00 48 26	EW	DL	Tri	02 17 25.3 +28 44 42	BY
V0641	Ser	15 16 59.7 -00 52 54	RRC:	V0362	TrA	15 24 15.3 -65 48 37	M
V0642	Ser	15 30 14.3 +06 50 52	EA	V0363	TrA	16 23 30.6 -67 20 40	DSCT
V0643	Ser	15 36 02.0 +11 06 59	DSCT	EY	Tuc	01 00 53.4 -75 11 54	EW
V0644	Ser	15 39 51.1 +10 54 20	EW	V0431	UMa	08 56 13.8 +69 34 21	EW
V0645	Ser	15 46 13.5 -00 26 06	DSCT	V0432	UMa	08 57 07.4 +49 09 03	RRAB
V0646	Ser	15 49 41.4 +13 59 36	RR(B)	V0433	UMa	09 06 29.0 +49 34 22	EW
V0647	Ser	15 52 51.4 +06 06 06	DSCT	V0434	UMa	09 13 22.8 +51 35 04	EB
V0648	Ser	15 53 23.7 +08 47 22	EA	V0435	UMa	09 18 21.3 +51 07 46	LB
V0649	Ser	15 54 04.4 +18 51 20	RR(B)	V0436	UMa	09 21 02.5 +49 05 54	DSCT
V0650	Ser	15 59 27.7 +05 28 04	EA	V0437	UMa	09 21 40.8 +43 47 48	EB
V0651	Ser	16 00 13.0 +09 23 06	EW	V0438	UMa	09 25 13.0 +45 30 42	EW
V0652	Ser	16 00 33.8 +25 02 13	EW	V0439	UMa	09 28 39.8 +50 44 02	EA
V0653	Ser	16 01 11.9 +25 16 35	EW	V0440	UMa	09 30 02.5 +42 49 31	EW
V0654	Ser	16 08 25.2 +12 19 08	RR(B)	V0441	UMa	09 30 10.7 +53 39 00	EA
V0655	Ser	16 08 39.8 +07 47 23	EA	V0442	UMa	09 30 10.9 +53 38 58	EW
V0656	Ser	16 12 14.4 +03 01 07	EA	V0443	UMa	09 34 43.6 +42 08 32	EW
V0657	Ser	16 17 28.2 -00 53 51	SR	V0444	UMa	09 35 16.0 +49 08 23	EB
V0658	Ser	16 19 53.2 -00 39 34	EA	V0445	UMa	09 35 25.2 +49 38 29	EA/RS
CH	Sex	09 42 20.9 -01 06 51	EB	V0446	UMa	09 35 58.8 +49 22 34	EW
CI	Sex	09 42 25.0 -10 40 33	EW	V0447	UMa	09 37 23.5 +55 08 48	DSCT
CK	Sex	09 47 08.9 -09 39 01	EW	V0448	UMa	09 38 04.0 +41 33 45	RR(B)
CL	Sex	09 49 29.1 +05 46 08	EW	V0449	UMa	09 38 42.5 +46 54 17	EW
CM	Sex	09 55 01.2 -01 47 46	EW	V0450	UMa	09 42 05.2 +47 22 04	RS
CN	Sex	09 56 28.3 +06 03 33	EW	V0451	UMa	09 45 58.2 +45 48 14	EA
CO	Sex	09 58 54.2 -02 09 16	EB	V0452	UMa	09 47 50.5 +44 02 38	EW
CP	Sex	10 03 29.4 -03 00 47	EW	V0453	UMa	09 47 54.9 +70 01 28	EB
CQ	Sex	10 05 39.0 -06 07 07	EW	V0454	UMa	09 49 37.1 +42 34 00	BY
CR	Sex	10 08 18.7 -09 22 31	EB	V0455	UMa	09 53 30.3 +44 17 01	BY
CS	Sex	10 11 09.1 -08 09 24	EW	V0456	UMa	09 54 02.4 +42 57 18	EW
CT	Sex	10 16 06.0 -02 35 24	EB	V0457	UMa	09 54 22.2 +50 56 50	EW
CU	Sex	10 16 18.1 -08 55 31	EW	V0458	UMa	09 54 43.3 +43 19 17	EW
CV	Sex	10 18 04.2 -04 18 36	EW	V0459	UMa	09 54 59.7 +43 36 27	EA/RS:
CW	Sex	10 23 08.5 +00 23 30	RR(B)	V0460	UMa	09 55 39.4 +43 19 18	EA/RS
CX	Sex	10 42 07.9 -02 29 57	RR(B)	V0461	UMa	09 56 44.2 +43 00 46	EA
CY	Sex	10 44 18.7 -03 18 51	RR(B)	V0462	UMa	09 59 38.1 +43 52 46	RR(B)
CZ	Sex	10 45 45.2 -08 35 33	EW	V0463	UMa	10 02 03.7 +46 05 04	ELL
DD	Sex	10 47 09.6 -02 06 18	EW	V0464	UMa	10 02 59.6 +45 28 15	RR(B)
DE	Sex	10 48 34.0 -03 37 28	EW	V0465	UMa	10 14 06.2 +46 27 01	EB
V1417	Tau	03 36 26.8 +17 26 55	EB	V0466	UMa	10 18 09.5 +64 37 03	EW
V1418	Tau	03 40 39.4 +16 06 20	EA	V0467	UMa	10 19 09.7 +41 46 11	EW
V1419	Tau	03 44 40.0 +03 04 25	EW	V0468	UMa	10 21 35.3 +40 31 41	DSCT
V1420	Tau	03 45 20.7 +16 35 03	EA	V0469	UMa	10 21 40.9 +50 17 33	DSCTC
V1421	Tau	04 21 22.4 +26 05 21	UV	V0470	UMa	10 22 11.4 +45 20 04	RR(B)
V1422	Tau	04 40 42.9 +22 38 12	SR	V0471	UMa	10 24 57.5 +42 40 22	RR(B)
V1423	Tau	05 16 16.8 +18 56 31	EB	V0472	UMa	10 36 13.3 +62 23 39	EW
V1424	Tau	05 17 05.8 +19 05 56	SR	V0473	UMa	10 54 18.8 +43 40 38	RR(B)
V1425	Tau	05 39 52.2 +20 01 10	DSCT	V0474	UMa	10 55 02.5 +61 42 17	DSCT
V1426	Tau	05 47 38.8 +14 37 34	EB	V0475	UMa	11 11 09.1 +32 15 59	RR(B)
V1427	Tau	05 59 20.3 +28 01 39	EB	V0476	UMa	11 21 09.7 +44 08 12	EW
DG	Tri	01 32 54.1 +32 29 35	EW	V0477	UMa	11 33 51.9 +44 57 40	RR(B)

Table 1 (Continued)

Name	R.A., Decl., 2000.0	Type	Name	R.A., Decl., 2000.0	Type
	h m s ° ’ "			h m s ° ’ "	
V0478 UMa	11 36 00.0 +51 39 09	EW	V0693 Vir	13 07 10.3 +08 42 09	EW
V0479 UMa	11 38 35.5 +31 57 36	RR(B)	V0694 Vir	13 08 47.9 +14 10 12	RR(B)
V0480 UMa	11 45 36.5 +51 30 41	EW	V0695 Vir	13 10 00.7 +10 45 32	EW
V0481 UMa	11 52 11.0 +55 48 08	RRC	V0696 Vir	13 13 42.5 -10 13 56	RR(B)
V0482 UMa	11 52 24.4 +57 03 04	RRAB	V0697 Vir	13 15 31.0 -14 26 55	EW
V0483 UMa	11 53 04.4 +56 11 40	EA	V0698 Vir	13 16 31.5 +03 01 04	RR(B)
V0484 UMa	11 54 14.0 +52 19 22	BY	V0699 Vir	13 16 41.3 -03 36 15	RR(B)
V0485 UMa	11 54 26.6 +52 41 37	EA	V0700 Vir	13 17 42.9 -00 33 45	EW
V0486 UMa	11 57 53.8 +53 02 48	RRC:	V0701 Vir	13 19 26.3 +08 43 37	EA
V0487 UMa	11 59 23.0 +53 00 21	EA	V0702 Vir	13 20 37.0 +01 09 45	RRAB
V0488 UMa	11 59 27.1 +52 12 24	RRC	V0703 Vir	13 21 53.3 +09 01 31	RR(B)
V0489 UMa	12 00 01.6 +56 13 54	BY	V0704 Vir	13 24 55.1 -16 30 26	RR(B)
V0490 UMa	12 02 38.5 +52 30 08	EA	V0705 Vir	13 26 52.6 +03 54 46	RR(B)
V0491 UMa	12 03 29.7 +53 34 09	RRAB	V0706 Vir	13 27 45.5 +00 19 26	RRAB
V0492 UMa	12 03 32.5 +39 53 38	EW	V0707 Vir	13 28 54.9 +02 26 14	RR(B)
V0493 UMa	12 04 33.0 +55 36 04	RRAB	V0708 Vir	13 31 06.0 +05 23 08	RR(B)
V0494 UMa	12 06 37.4 +55 06 22	EW	V0709 Vir	13 31 15.7 -03 41 08	EB
V0495 UMa	13 03 01.6 +60 01 16	DSCT	V0710 Vir	13 32 31.5 -12 17 42	EA
V0496 UMa	13 21 04.1 +56 09 58	AM	V0711 Vir	13 36 50.2 -11 43 42	RR(B)
V0497 UMa	13 45 21.7 +54 11 52	DSCT	V0712 Vir	13 41 57.4 +05 31 26	EB
V0498 UMa	13 54 35.9 +50 27 15	RRAB	V0713 Vir	13 45 29.6 +00 21 56	RRAB
BC UMi	15 22 39.8 +74 15 17	SXPHE	V0714 Vir	13 48 55.0 +00 46 22	RRC
BD UMi	15 32 57.5 +70 42 16	EA	V0715 Vir	13 51 50.8 -02 12 30	EW
BE UMi	15 43 36.7 +75 15 41	EA+NL	V0716 Vir	13 52 33.4 -00 33 37	RRAB
V0550 Vel	08 21 23.5 -44 23 23	SRA	V0717 Vir	13 55 24.6 -09 13 00	EW
V0549 Vel	08 50 29.6 -47 45 28	NA:	V0718 Vir	13 57 38.2 +00 20 56	RRAB
V0551 Vel	09 23 39.3 -41 26 49	DSCTC	V0719 Vir	13 58 48.6 -15 30 02	EW
V0552 Vel	09 27 10.7 -40 22 05	ACV	V0720 Vir	14 03 12.5 +00 48 03	RRAB
V0553 Vel	10 33 18.4 -52 55 10	ACV:	V0721 Vir	14 06 41.3 +01 08 18	RRAB
V0554 Vel	11 02 39.4 -44 23 57	DSCT	V0722 Vir	14 10 41.7 +01 02 27	EA
V0671 Vir	11 53 26.5 +06 07 56	EW	V0723 Vir	14 11 13.4 +06 40 14	RRC
V0672 Vir	11 53 27.6 +05 51 34	EW	V0724 Vir	14 17 24.6 -00 00 56	RRAB
V0673 Vir	11 55 57.9 +07 20 11	EW	V0725 Vir	14 21 12.3 +00 39 36	RRAB
V0674 Vir	12 12 50.6 -11 39 09	RR(B)	V0726 Vir	14 21 43.4 -00 12 26	EW
V0675 Vir	12 13 08.2 +11 16 59	RR(B)	V0727 Vir	14 23 21.7 -00 07 05	CWB:
V0676 Vir	12 19 34.4 -10 21 44	EW	V0728 Vir	14 23 37.1 +00 25 03	RRAB
V0677 Vir	12 19 44.8 +08 40 56	EA	V0729 Vir	14 24 43.4 +04 38 50	DSCT
V0678 Vir	12 31 48.1 -02 06 02	EW	V0730 Vir	14 25 02.5 -00 53 32	RRC:
V0679 Vir	12 32 11.1 +12 55 57	RR(B)	V0731 Vir	14 25 30.3 -00 51 54	RRAB
V0680 Vir	12 38 15.6 +10 35 31	RR(B)	V0732 Vir	14 29 18.4 -03 26 40	EP
V0681 Vir	12 38 18.7 +09 04 40	RR(B)	V0733 Vir	14 29 42.4 -04 17 08	EW
V0682 Vir	12 38 29.8 +00 20 02	RRC	V0734 Vir	14 29 54.7 +00 18 23	RR(B)
V0683 Vir	12 48 19.4 +07 20 49	UG	V0735 Vir	14 33 52.9 +02 08 00	RR(B)
V0684 Vir	12 51 12.4 +01 28 09	RR(B)	V0736 Vir	14 34 32.6 +01 02 17	RRAB
V0685 Vir	12 53 47.4 +09 43 09	RR(B)	V0737 Vir	14 34 33.4 +01 02 08	RR(B)
V0686 Vir	12 57 52.7 -11 55 12	RR(B)	V0738 Vir	14 40 10.7 +06 17 12	EA
V0687 Vir	12 58 16.0 +10 41 14	EA	V0739 Vir	14 42 44.4 -00 39 55	EA
V0688 Vir	12 59 17.3 +01 02 40	RRAB	V0740 Vir	14 54 14.6 +00 23 10	RRAB
V0689 Vir	12 59 57.8 -06 27 59	EW	V0741 Vir	15 02 57.7 +00 15 36	RRAB
V0690 Vir	13 03 23.5 -14 25 07	EW	V0742 Vir	15 08 17.6 +06 32 14	RR(B)
V0691 Vir	13 05 12.7 +10 28 40	RR(B)	AO Vol	07 05 12.5 -71 48 13	RRAB
V0692 Vir	13 05 29.6 -12 21 49	EA			

Table 2. Novae (Kazarovets and Samus 2017, 2018)

GCVS	Nova name	GCVS	Nova name
V0435 CMa	Nova CMa 2018	V5854 Sgr	OGLE-2016-NOVA-02
V0906 Car	Nova Car 2018	V5855 Sgr	Nova Sgr 2016 No. 3
V1404 Cen	OGLE-2015-NOVA-03	V5856 Sgr	Nova Sgr 2016 No. 4
V1405 Cen	Nova Cen 2017	V5857 Sgr	Nova Sgr 2018
FM Cir	Nova Cir 2018	V1655 Sco	Nova Sco 2016 No. 1
V0407 Lup	Nova Lup 2016	V1656 Sco	Nova Sco 2016 No. 2
V0408 Lup	Nova Lup 2018	V1657 Sco	Nova Sco 2017
V0357 Mus	Nova Mus 2018	V1658 Sco	OGLE-2015-NOVA-01
V0555 Nor	Nova Nor 2016	V1659 Sco	Nova Sco 2016 No. 3
V0556 Nor	Nova Nor 2018	V1660 Sco	Nova Sco 2017
V3661 Oph	Nova Oph 2016	V1661 Sco	Nova Sco 2018 No. 1
V3662 Oph	Nova Oph 2017 No. 1	V1662 Sco	Nova Sco 2018 No. 2
V3663 Oph	Nova Oph 2017 No. 2	V1663 Sco	Nova Sco 2018 No. 3
V3664 Oph	Nova Oph 2018 No. 1	V0611 Sct	Nova Sct 2016
V3665 Oph	Nova Oph 2018 No. 2	V0612 Sct	Nova Sct 2017
V3666 Oph	Nova Oph 2018 No. 3	V0613 Sct	Nova Sct 2018
V5853 Sgr	Nova Sgr 2016 No. 2	V0549 Vel	Nova Vel 2017

Table 3. Novae and rare-type variables in Table 1

GCVS	Nova name	GCVS	Nova name
V0919 Car	OGLE-2014-NOVA-07	V3702 Oph	IRAS 17353–1833 (FU:)
V1427 Cen	OGLE-2014-NOVA-08	V5858 Sgr	OGLE-1997-NOVA-01
V1428 Cen	Nova Cen 2012 No. 2	V5861 Sgr	OGLE-2010-NOVA-01
FO Cir	OGLE-2014-NOVA-09	V5862 Sgr	OGLE-2014-NOVA-01
DT Hyi	OGLE-2013-NOVA-03	V5863 Sgr	OGLE-2012-NOVA-01
DU Hyi	OGLE-2013-NOVA-01	V5866 Sgr	OGLE-2014-NOVA-05
V0559 Nor	VVV-NOV-005 (2010)	V1701 Sco	VVV-NOV-04 (2010)
V3698 Oph	OGLE-2011-NOVA-01	V1703 Sco	OGLE-2011-BLG-1444
V3700 Oph	OGLE-2011-NOVA-02	V1705 Sco	OGLE-2008-NOVA-01
V3701 Oph	OGLE-2010-NOVA-02		

Table 4. New GCVS names for globular-cluster variables

Name (GCVS)	Name in globular cluster	R.A., Decl., 2000.0 h m s ° ' "	Type
V0395 Aps	IC 4499 V078	14 58 36.8 -82 11 18	RR(B)
V0396 Aps	IC 4499 V026	14 58 44.9 -82 10 19	RRAB
V0397 Aps	IC 4499 V019	14 58 53.4 -82 13 20	RRAB
V0398 Aps	IC 4499 V153	14 59 10.4 -82 15 47	RRC
V0399 Aps	IC 4499 V046	14 59 12.0 -82 16 57	RRAB
V0400 Aps	IC 4499 V025	14 59 13.6 -82 13 03	RRAB
V0401 Aps	IC 4499 V069	14 59 15.2 -82 12 40	RRC
V0402 Aps	IC 4499 V085	14 59 17.8 -82 07 47	RRAB
V0403 Aps	IC 4499 V109	14 59 20.8 -82 11 20	RR(B)
V0404 Aps	IC 4499 V063	14 59 24.4 -82 14 06	RR(B)
V0405 Aps	IC 4499 V038	14 59 28.3 -82 12 01	RRAB
V0406 Aps	IC 4499 V003	14 59 28.8 -82 14 40	RRAB
V0407 Aps	IC 4499 V089	14 59 37.8 -82 12 57	RRC
V0408 Aps	IC 4499 V016	14 59 37.8 -82 12 01	RRAB
V0409 Aps	IC 4499 V044	14 59 38.8 -82 11 54	RRAB
V0410 Aps	IC 4499 V018	14 59 41.6 -82 13 16	RR(B)
V0411 Aps	IC 4499 V058	14 59 44.5 -82 14 03	RRAB
V0412 Aps	IC 4499 V055	14 59 49.4 -82 13 26	RRC
V0413 Aps	IC 4499 V097	14 59 51.3 -82 14 24	RRC
V0414 Aps	IC 4499 V095	14 59 52.0 -82 12 15	RRC
V0415 Aps	IC 4499 V005	14 59 54.4 -82 13 40	RRAB
V0416 Aps	IC 4499 V024	14 59 54.8 -82 13 24	RRAB
V0417 Aps	IC 4499 V004	14 59 54.8 -82 12 38	RRAB
V0418 Aps	IC 4499 V112	14 59 55.4 -82 11 50	RRAB
V0419 Aps	IC 4499 V056	14 59 55.8 -82 12 45	RRC
V0420 Aps	IC 4499 V020	14 59 56.6 -82 10 14	RRAB
V0421 Aps	IC 4499 V071	14 59 57.2 -82 13 19	RR(B)
V0422 Aps	IC 4499 V084	14 59 58.2 -82 12 11	RRAB
V0423 Aps	IC 4499 V017	15 00 00.1 -82 12 32	RRAB
V0424 Aps	IC 4499 V096	15 00 06.2 -82 12 22	RRC
V0425 Aps	IC 4499 V028	15 00 06.8 -82 13 36	RRAB
V0426 Aps	IC 4499 V057	15 00 07.1 -82 11 57	RRAB
V0427 Aps	IC 4499 V015	15 00 08.4 -82 13 00	RRAB
V0428 Aps	IC 4499 V072	15 00 09.4 -82 14 02	RRAB
V0429 Aps	IC 4499 V006	15 00 09.5 -82 12 17	RRAB
V0430 Aps	IC 4499 V061	15 00 10.4 -82 11 54	RRAB
V0431 Aps	IC 4499 V090	15 00 13.7 -82 13 12	RR(B)
V0432 Aps	IC 4499 V010	15 00 14.9 -82 11 41	RR(B)
V0433 Aps	IC 4499 V172	15 00 17.1 -82 11 34	SXPHE
V0434 Aps	IC 4499 V027	15 00 18.3 -82 10 59	RRAB
V0435 Aps	IC 4499 V007	15 00 18.5 -82 09 22	RRAB
V0436 Aps	IC 4499 V049	15 00 19.4 -82 14 09	RRAB
V0437 Aps	IC 4499 V074	15 00 20.2 -82 11 44	RRAB
V0438 Aps	IC 4499 V037	15 00 20.7 -82 13 48	RRAB
V0439 Aps	IC 4499 V083	15 00 21.4 -82 12 20	RRAB
V0440 Aps	IC 4499 V082	15 00 22.4 -82 12 42	RRAB
V0441 Aps	IC 4499 V106	15 00 22.5 -82 10 26	RRAB
V0442 Aps	IC 4499 V014	15 00 23.8 -82 13 08	RRAB
V0443 Aps	IC 4499 V041	15 00 25.9 -82 09 50	RRAB
V0444 Aps	IC 4499 V167	15 00 26.1 -82 12 35	RRAB
V0445 Aps	IC 4499 V087	15 00 26.2 -82 11 33	RR(B)
V0446 Aps	IC 4499 V031	15 00 26.5 -82 11 14	RR(B)
V0447 Aps	IC 4499 V103	15 00 26.8 -82 11 57	RRC
V0448 Aps	IC 4499 V065	15 00 29.4 -82 14 29	RR(B)

Table 4 (Continued)

Name (GCVS)	Name in globular cluster	R.A., Decl., 2000.0 h m s o ’ "	Type
V0449 Aps	IC 4499 V093	15 00 29.5 -82 13 22	RR(B)
V0450 Aps	IC 4499 V029	15 00 32.5 -82 13 02	RRC
V0451 Aps	IC 4499 V047	15 00 32.5 -82 14 23	RRAB
V0452 Aps	IC 4499 V013	15 00 33.8 -82 13 06	RRAB
V0453 Aps	IC 4499 V002	15 00 34.3 -82 14 24	RRAB
V0454 Aps	IC 4499 V081	15 00 34.8 -82 13 00	RRC
V0455 Aps	IC 4499 V080	15 00 35.9 -82 17 33	RRAB
V0456 Aps	IC 4499 V052	15 00 37.8 -82 09 54	RRAB
V0457 Aps	IC 4499 V111	15 00 40.6 -82 15 28	RRC
V0458 Aps	IC 4499 V171	15 00 42.3 -82 13 45	RRC
V0459 Aps	IC 4499 V048	15 00 43.3 -82 12 51	RRAB
V0460 Aps	IC 4499 V009	15 00 44.3 -82 11 01	RRAB
V0461 Aps	IC 4499 V051	15 00 44.4 -82 12 38	RR(B)
V0462 Aps	IC 4499 V070	15 00 44.6 -82 13 06	RRAB
V0463 Aps	IC 4499 V059	15 00 47.6 -82 13 30	RR(B)
V0464 Aps	IC 4499 V033	15 00 48.2 -82 17 21	RRAB
V0465 Aps	IC 4499 V077	15 00 49.0 -82 11 56	RRC
V0466 Aps	IC 4499 V021	15 00 49.7 -82 10 21	RR(B)
V0467 Aps	IC 4499 V043	15 00 50.0 -82 16 41	RRAB
V0468 Aps	IC 4499 V032	15 00 50.1 -82 12 58	RRC
V0469 Aps	IC 4499 V088	15 00 51.8 -82 11 55	RRAB
V0470 Aps	IC 4499 V008	15 00 52.3 -82 11 09	RR(B)
V0471 Aps	IC 4499 V001	15 00 53.0 -82 12 50	RRAB
V0472 Aps	IC 4499 V030	15 00 54.2 -82 13 19	RRAB
V0473 Aps	IC 4499 V045	15 00 55.7 -82 08 34	RRAB
V0474 Aps	IC 4499 V064	15 00 56.1 -82 11 50	RRAB
V0475 Aps	IC 4499 V034	15 00 57.7 -82 14 49	RRAB
V0476 Aps	IC 4499 V023	15 00 58.3 -82 13 23	RRAB
V0477 Aps	IC 4499 V011	15 00 59.0 -82 13 15	RRAB
V0478 Aps	IC 4499 V050	15 01 03.1 -82 13 33	RRAB
V0479 Aps	IC 4499 V054	15 01 04.8 -82 16 44	RRAB
V0480 Aps	IC 4499 V012	15 01 05.1 -82 11 43	RRAB
V0481 Aps	IC 4499 V040	15 01 06.3 -82 08 03	RRAB
V0482 Aps	IC 4499 V092	15 01 07.8 -82 10 27	RRC
V0483 Aps	IC 4499 V042	15 01 08.4 -82 13 09	RR(B)
V0484 Aps	IC 4499 V108	15 01 10.9 -82 12 38	RRAB
V0485 Aps	IC 4499 V066	15 01 14.1 -82 11 25	RRAB
V0486 Aps	IC 4499 V053	15 01 14.6 -82 14 36	RRAB
V0487 Aps	IC 4499 V036	15 01 30.0 -82 12 36	RRAB
V0488 Aps	IC 4499 V073	15 02 16.1 -82 17 18	RR(B)
V0489 Aps	IC 4499 V098	15 02 17.0 -82 13 21	RRC
V0490 Aps	IC 4499 V062	15 02 20.5 -82 14 02	RRAB
V0491 Aps	IC 4499 V022	15 02 23.0 -82 11 31	RRAB
V0492 Aps	IC 4499 V076	15 02 45.4 -82 07 37	RRAB
V0493 Aps	NGC 6101 V016	16 24 45.7 -72 15 03	RRC
V0494 Aps	NGC 6101 V017	16 25 04.9 -72 07 11	RRC:
V0495 Aps	NGC 6101 V022	16 25 17.1 -72 11 41	RRC
V0496 Aps	NGC 6101 V007	16 25 19.7 -72 10 51	RRC
V0497 Aps	NGC 6101 V018	16 25 27.6 -72 16 14	RRC
V0498 Aps	NGC 6101 V010	16 25 30.3 -72 12 48	RRC
V0499 Aps	NGC 6101 V019	16 25 34.0 -72 08 59	RRC
V0500 Aps	NGC 6101 V009	16 25 48.4 -72 11 26	RRC
V0501 Aps	NGC 6101 V006	16 25 50.4 -72 11 10	RRC

Table 4 (Continued)

Name (GCVS)	Name in globular cluster	R.A., Decl., 2000.0 h m s o ’ "	Type
V0502 Aps	NGC 6101 V002	16 26 01.7 -72 13 30	RRC
V0503 Aps	NGC 6101 V001	16 26 02.7 -72 11 14	RRC
V0504 Aps	NGC 6101 V020	16 26 05.8 -72 12 13	RRAB
V0505 Aps	NGC 6101 V003	16 26 12.3 -72 13 00	RRAB
V0506 Aps	NGC 6101 V004	16 26 15.8 -72 11 53	RRC
V0507 Aps	NGC 6101 V008	16 26 22.7 -72 11 28	RRC
V0508 Aps	NGC 6101 V005	16 26 29.2 -72 09 51	RRC
V0509 Aps	NGC 6101 V021	16 26 57.3 -72 08 50	RRC
V0510 Aps	NGC 6101 V011	16 28 11.2 -71 57 43	RRAB:
V1052 Ara	NGC 6352 V004	17 25 24.7 -48 26 58	SRB
V1053 Ara	NGC 6352 V005	17 25 37.5 -48 22 10	SR
V1054 Ara	NGC 6362 V077	17 30 51.2 -66 55 29	EA
V1055 Ara	NGC 6362 V045	17 30 52.7 -66 58 59	EW
V1056 Ara	NGC 6362 V025	17 30 54.4 -67 06 19	RRAB
V1057 Ara	NGC 6362 V076	17 31 04.3 -67 03 24	EA
V1058 Ara	NGC 6362 V042	17 31 09.0 -66 51 39	EA
V1059 Ara	NGC 6362 V008	17 31 10.1 -67 01 01	RRC
V1060 Ara	NGC 6362 V012	17 31 13.1 -67 04 31	RRAB
V1061 Ara	NGC 6362 V075	17 31 14.3 -66 55 28	BY
V1062 Ara	NGC 6362 V013	17 31 15.1 -67 04 48	RRAB
V1063 Ara	NGC 6362 V073	17 31 16.9 -67 03 36	EA
V1064 Ara	NGC 6362 V074	17 31 17.6 -66 59 58	EW
V1065 Ara	NGC 6362 V027	17 31 21.6 -66 56 28	RRC
V1066 Ara	NGC 6362 V072	17 31 29.0 -67 02 34	SXPHE
V1067 Ara	NGC 6362 V037	17 31 32.2 -67 02 04	RR:
V1068 Ara	NGC 6362 V041	17 31 35.4 -67 04 03	EA
V1069 Ara	NGC 6362 V071	17 31 36.6 -67 02 14	EA
V1070 Ara	NGC 6362 V070	17 31 38.9 -67 02 54	EW
V1071 Ara	NGC 6362 V030	17 31 39.6 -67 01 34	RRAB
V1072 Ara	NGC 6362 V003	17 31 40.9 -67 04 16	RR(B)
V1073 Ara	NGC 6362 V036	17 31 43.6 -67 02 17	RRC
V1074 Ara	NGC 6362 V038	17 31 43.6 -67 02 58	SXPHE
V1075 Ara	NGC 6362 V069	17 31 43.7 -67 01 47	BY
V1076 Ara	NGC 6362 V068	17 31 44.9 -67 03 21	BY:
V1077 Ara	NGC 6362 V067	17 31 45.5 -67 04 26	EW
V1078 Ara	NGC 6362 V065	17 31 47.7 -67 03 53	EA
V1079 Ara	NGC 6362 V066	17 31 48.0 -67 01 58	EA
V1080 Ara	NGC 6362 V031	17 31 49.2 -67 01 21	RRAB
V1081 Ara	NGC 6362 V011	17 31 49.9 -67 01 58	RRC
V1082 Ara	NGC 6362 V002	17 31 50.2 -67 04 25	RRAB
V1083 Ara	NGC 6362 V029	17 31 52.5 -67 03 20	RRAB
V1084 Ara	NGC 6362 V034	17 31 52.8 -67 03 35	RRB01:
V1085 Ara	NGC 6362 V001	17 31 54.8 -67 02 46	RRAB
V1086 Ara	NGC 6362 V016	17 31 58.1 -67 07 12	RRAB
V1087 Ara	NGC 6362 V064	17 31 58.2 -67 03 46	SXPHE
V1088 Ara	NGC 6362 V007	17 31 58.5 -67 01 01	RRAB
V1089 Ara	NGC 6362 V026	17 31 58.9 -67 03 22	RRAB
V1090 Ara	NGC 6362 V028	17 31 59.2 -67 02 08	RRC
V1091 Ara	NGC 6362 V048	17 31 59.8 -67 03 50	SXPHE
V1092 Ara	NGC 6362 V023	17 32 00.1 -67 03 08	RRC
V1093 Ara	NGC 6362 V032	17 32 01.8 -67 02 13	RRAB
V1094 Ara	NGC 6362 V020	17 32 02.6 -67 02 59	RRAB

Table 4 (Continued)

Name (GCVS)	Name in globular cluster	R.A., Decl., 2000.0 h m s ° ' "	Type
V1095 Ara	NGC 6362 V015	17 32 03.5 -67 02 44	RRC
V1096 Ara	NGC 6362 V063	17 32 03.5 -67 08 22	EB
V1097 Ara	NGC 6362 V006	17 32 03.8 -66 59 52	RRC
V1098 Ara	NGC 6362 V040	17 32 04.1 -67 03 46	EA
V1099 Ara	NGC 6362 V062	17 32 05.8 -67 03 08	EA
V1100 Ara	NGC 6362 V024	17 32 07.2 -67 03 21	RRC
V1101 Ara	NGC 6362 V035	17 32 08.2 -67 03 03	RRC
V1102 Ara	NGC 6362 V039	17 32 08.5 -67 03 15	EW
V1103 Ara	NGC 6362 V005	17 32 08.8 -67 02 59	RRAB
V1104 Ara	NGC 6362 V047	17 32 13.0 -67 02 38	SXPHE
V1105 Ara	NGC 6362 V018	17 32 13.6 -67 01 34	RRAB
V1106 Ara	NGC 6362 V019	17 32 16.0 -67 03 10	RRAB
V1107 Ara	NGC 6362 V061	17 32 18.1 -67 03 39	BY:
V1108 Ara	NGC 6362 V021	17 32 22.6 -67 04 31	RRC
V1109 Ara	NGC 6362 V060	17 32 23.3 -66 55 27	BY
V1110 Ara	NGC 6362 V049	17 32 24.1 -67 04 00	EB
V1111 Ara	NGC 6362 V059	17 32 24.7 -67 06 41	ELL
V1112 Ara	NGC 6362 V046	17 32 25.0 -67 00 31	SXPHE
V1113 Ara	NGC 6362 V010	17 32 26.1 -66 56 53	RRC
V1114 Ara	NGC 6362 V022	17 32 26.7 -67 07 55	RRC
V1115 Ara	NGC 6362 V058	17 32 28.1 -67 08 44	BY
V1116 Ara	NGC 6362 V017	17 32 29.5 -67 03 51	RRC
V1117 Ara	NGC 6362 V057	17 32 46.1 -66 55 33	BY:
V1118 Ara	NGC 6362 V033	17 32 47.9 -66 56 36	RRC
V1119 Ara	NGC 6362 V056	17 32 52.8 -66 58 28	EW
V1120 Ara	NGC 6362 V054	17 32 54.0 -67 05 56	EA
V1121 Ara	NGC 6362 V055	17 32 54.1 -66 55 36	ELL
V1122 Ara	NGC 6362 V014	17 32 58.0 -67 02 13	RRC
V1123 Ara	NGC 6362 V053	17 33 09.8 -66 51 22	EW
V1124 Ara	NGC 6362 V052	17 33 10.7 -67 13 17	EW
V1125 Ara	NGC 6362 V044	17 33 26.0 -66 53 44	RRAB
V1126 Ara	NGC 6362 V043	17 34 03.3 -66 52 54	EW
V1127 Ara	NGC 6397 V009	17 40 02.2 -53 35 45	EW
V1128 Ara	NGC 6397 V010	17 40 37.6 -53 40 36	SXPHE
V1129 Ara	NGC 6397 V024	17 40 39.0 -53 40 23	GDOR:
V1130 Ara	NGC 6397 V023	17 40 39.2 -53 40 47	SXPHE
V1131 Ara	NGC 6397 V008	17 40 39.3 -53 38 47	EW
V1132 Ara	NGC 6397 V032	17 40 40.3 -53 41 25	EA:
V1133 Ara	NGC 6397 V022	17 40 41.2 -53 40 42	RR(B):
V1134 Ara	NGC 6397 V021	17 40 41.4 -53 40 24	SXPHE
V1135 Ara	NGC 6397 V012	17 40 41.4 -53 40 20	EW:
V1136 Ara	NGC 6397 V020	17 40 41.5 -53 40 34	GDOR:
V1137 Ara	NGC 6397 V034	17 40 42.3 -53 40 29	UG
V1138 Ara	NGC 6397 V031	17 40 42.6 -53 40 27	ELL:
V1139 Ara	NGC 6397 V033	17 40 42.6 -53 40 19	NL
V1140 Ara	NGC 6397 V019	17 40 42.8 -53 40 23	EW
V1141 Ara	NGC 6397 V035	17 40 43.3 -53 41 55	ELL:
V1142 Ara	NGC 6397 V018	17 40 43.6 -53 40 28	EA
V1143 Ara	NGC 6397 V007	17 40 43.8 -53 40 35	EW
V1144 Ara	NGC 6397 V017	17 40 43.8 -53 41 16	ELL:
V1145 Ara	NGC 6397 V011	17 40 44.1 -53 40 40	SXPHE
V1146 Ara	NGC 6397 V016	17 40 44.6 -53 40 42	ELL
V1147 Ara	NGC 6397 V015	17 40 45.4 -53 40 25	SXPHE

Table 4 (Continued)

Name (GCVS)	Name in globular cluster	R.A., Decl., 2000.0 h m s o ’ "	Type
V1148 Ara	NGC 6397 V014	17 40 46.3 -53 41 16	E
V1149 Ara	NGC 6397 V013	17 40 48.8 -53 39 49	EW
V1150 Ara	NGC 6397 V006	17 40 53.4 -53 43 40	EW:
V1151 Ara	NGC 6397 V030	17 40 54.6 -53 40 45	EA:
V1152 Ara	NGC 6397 V029	17 40 59.6 -53 40 39	ELL:
V1153 Ara	NGC 6397 V028	17 41 02.7 -53 39 47	SR:
V1154 Ara	NGC 6397 V005	17 41 05.5 -53 33 36	EA:
V1155 Ara	NGC 6397 V004	17 41 08.8 -53 42 34	EW
V1156 Ara	NGC 6397 V027	17 41 13.8 -53 41 14	ELL:
V1902 Aql	NGC 6749 V001	19 05 20.0 +01 55 57	CWB
V1903 Aql	NGC 6760 V002	19 11 11.9 +01 00 16	SRB:
V1904 Aql	NGC 6760 V003	19 11 14.3 +01 01 47	M
V1905 Aql	NGC 6760 V004	19 11 15.0 +01 02 37	M
V1906 Aql	NGC 6760 V001	19 11 16.0 +01 00 59	LB:
V0384 Aqr	NGC 6981 V032	20 53 18.8 -12 33 02	RRAB
V0385 Aqr	NGC 6981 V025	20 53 18.9 -12 31 14	RRC
V0386 Aqr	NGC 6981 V004	20 53 20.8 -12 31 43	RRAB
V0387 Aqr	NGC 6981 V023	20 53 21.1 -12 30 22	RRAB
V0388 Aqr	NGC 6981 V021	20 53 22.4 -12 32 06	RRAB
V0389 Aqr	NGC 6981 V015	20 53 23.8 -12 32 39	RRAB
V0390 Aqr	NGC 6981 V020	20 53 24.2 -12 32 04	RRAB
V0391 Aqr	NGC 6981 V055	20 53 24.4 -12 31 27	SXPHE
V0392 Aqr	NGC 6981 V003	20 53 24.6 -12 33 17	RRAB
V0393 Aqr	NGC 6981 V010	20 53 24.8 -12 33 31	RRAB
V0394 Aqr	NGC 6981 V005	20 53 25.6 -12 32 42	RRAB
V0395 Aqr	NGC 6981 V029	20 53 25.8 -12 33 12	RRAB
V0396 Aqr	NGC 6981 V018	20 53 26.2 -12 32 55	RRAB
V0397 Aqr	NGC 6981 V048	20 53 26.4 -12 32 27	RRAB
V0398 Aqr	NGC 6981 V036	20 53 27.0 -12 32 17	RRAB
V0399 Aqr	NGC 6981 V053	20 53 27.0 -12 32 17	RRAB
V0400 Aqr	NGC 6981 V014	20 53 27.2 -12 31 43	RRAB
V0401 Aqr	NGC 6981 V024	20 53 27.2 -12 32 42	RRC
V0402 Aqr	NGC 6981 V057	20 53 27.3 -12 32 13	RRC
V0403 Aqr	NGC 6981 V043	20 53 27.4 -12 32 22	RRC
V0404 Aqr	NGC 6981 V008	20 53 27.6 -12 30 48	RRAB
V0405 Aqr	NGC 6981 V007	20 53 27.8 -12 31 19	RRAB
V0406 Aqr	NGC 6981 V016	20 53 27.9 -12 32 37	RRAB
V0407 Aqr	NGC 6981 V052	20 53 27.9 -12 32 02	RRAB
V0408 Aqr	NGC 6981 V044	20 53 28.0 -12 32 30	RRAB
V0409 Aqr	NGC 6981 V031	20 53 28.2 -12 31 43	RRAB
V0410 Aqr	NGC 6981 V017	20 53 28.2 -12 33 00	RRAB
V0411 Aqr	NGC 6981 V050	20 53 28.2 -12 31 58	RRAB
V0412 Aqr	NGC 6981 V049	20 53 28.3 -12 32 11	RRAB
V0413 Aqr	NGC 6981 V051	20 53 28.4 -12 32 32	RRAB
V0414 Aqr	NGC 6981 V012	20 53 28.6 -12 32 39	RRC
V0415 Aqr	NGC 6981 V009	20 53 28.6 -12 31 28	RRAB
V0416 Aqr	NGC 6981 V054	20 53 28.6 -12 32 02	SXPHE
V0417 Aqr	NGC 6981 V045	20 53 28.7 -12 32 20	RRC
V0418 Aqr	NGC 6981 V042	20 53 28.8 -12 32 17	LB:
V0419 Aqr	NGC 6981 V013	20 53 28.9 -12 32 02	RRAB
V0420 Aqr	NGC 6981 V056	20 53 28.9 -12 33 06	SXPHE

Table 4 (Continued)

Name (GCVS)	Name in globular cluster	R.A., Decl., 2000.0 h m s o ' "	Type
V0421 Aqr	NGC 6981 V046	20 53 29.0 -12 32 26	RRC
V0422 Aqr	NGC 6981 V047	20 53 29.7 -12 32 26	RRAB:
V0423 Aqr	NGC 6981 V001	20 53 31.1 -12 33 12	RRAB
V0424 Aqr	NGC 6981 V011	20 53 32.0 -12 32 52	RRAB
V0425 Aqr	NGC 6981 V028	20 53 32.2 -12 30 56	RRAB
V0426 Aqr	NGC 6981 V002	20 53 34.6 -12 29 02	RRAB
V0427 Aqr	NGC 6981 V039	20 53 41.0 -12 28 16	RRAB
V0428 Aqr	NGC 6981 V027	20 53 42.6 -12 36 07	RRAB
V0429 Aqr	NGC 6981 V035	20 53 43.6 -12 31 52	RRAB
V0430 Aqr	NGC 6981 V060	20 53 46.6 -12 27 32	RRAB
V0431 Aqr	NGC 6981 V059	20 53 48.9 -12 36 45	RRAB
V0432 Aqr	NGC 7089 V018	21 33 14.0 -01 01 05	RRC
V0433 Aqr	NGC 7089 V009	21 33 15.2 -00 51 24	RRAB
V0434 Aqr	NGC 7089 V013	21 33 21.5 -00 48 03	RRAB
V0435 Aqr	NGC 7089 V008	21 33 22.3 -00 50 12	RRAB
V0436 Aqr	NGC 7089 V029	21 33 22.5 -00 50 52	RRC
V0437 Aqr	NGC 7089 V012	21 33 22.6 -00 48 33	RRAB
V0438 Aqr	NGC 7089 V027	21 33 23.2 -00 47 14	RRC
V0439 Aqr	NGC 7089 V033	21 33 23.4 -00 49 35	RRC
V0440 Aqr	NGC 7089 V002	21 33 23.7 -00 48 05	RRAB
V0441 Aqr	NGC 7089 V005	21 33 23.8 -00 49 13	CWA
V0442 Aqr	NGC 7089 V016	21 33 24.6 -00 49 39	RRAB
V0443 Aqr	NGC 7089 V004	21 33 24.7 -00 48 45	RRAB
V0444 Aqr	NGC 7089 V040	21 33 25.6 -00 49 16	RRAB:
V0445 Aqr	NGC 7089 V037	21 33 26.0 -00 49 18	RRAB
V0446 Aqr	NGC 7089 V025	21 33 26.9 -00 49 56	RRAB
V0447 Aqr	NGC 7089 V022	21 33 26.9 -00 48 33	RRAB
V0448 Aqr	NGC 7089 V017	21 33 27.0 -00 50 18	RRAB
V0449 Aqr	NGC 7089 V028	21 33 27.4 -00 47 36	RRAB
V0450 Aqr	NGC 7089 V039	21 33 27.4 -00 50 07	RRAB
V0451 Aqr	NGC 7089 V006	21 33 27.5 -00 50 00	CWA
V0452 Aqr	NGC 7089 V024	21 33 27.7 -00 51 05	RRC
V0453 Aqr	NGC 7089 V035	21 33 27.9 -00 47 32	RRC
V0454 Aqr	NGC 7089 V041	21 33 28.0 -00 49 24	RRAB
V0455 Aqr	NGC 7089 V042	21 33 28.4 -00 49 55	RRC
V0456 Aqr	NGC 7089 V001	21 33 28.5 -00 47 55	CWA
V0457 Aqr	NGC 7089 V032	21 33 30.1 -00 49 58	RRC
V0458 Aqr	NGC 7089 V031	21 33 30.2 -00 49 19	RRAB
V0459 Aqr	NGC 7089 V036	21 33 30.7 -00 49 13	RRC
V0460 Aqr	NGC 7089 V038	21 33 31.2 -00 49 24	RRAB
V0461 Aqr	NGC 7089 V034	21 33 31.3 -00 49 57	RRC
V0462 Aqr	NGC 7089 V026	21 33 31.6 -00 49 23	RRC
V0463 Aqr	NGC 7089 V056	21 33 31.6 -00 50 13	SXPHE
V0464 Aqr	NGC 7089 V015	21 33 32.2 -00 50 30	RRC
V0465 Aqr	NGC 7089 V014	21 33 32.4 -00 50 21	RRAB
V0466 Aqr	NGC 7089 V011	21 33 32.4 -00 49 06	RV
V0467 Aqr	NGC 7089 V023	21 33 32.5 -00 50 03	RRAB
V0468 Aqr	NGC 7089 V010	21 33 32.7 -00 48 35	RRAB
V0469 Aqr	NGC 7089 V030	21 33 32.9 -00 48 31	RRC
V0470 Aqr	NGC 7089 V007	21 33 37.0 -00 52 23	RRAB
V0471 Aqr	NGC 7089 V003	21 33 41.6 -00 49 53	RRAB
V0472 Aqr	NGC 7089 V019	21 33 42.8 -00 57 44	RRC
V0473 Aqr	NGC 7089 V021	21 33 49.0 -00 45 45	RRAB

Table 4 (Continued)

Name (GCVS)	Name in globular cluster	R.A., Decl., 2000.0 h m s o ' "	Type
V0474 Aqr	NGC 7089 V020	21 33 53.1 -00 47 57	RRC
V0475 Aqr	NGC 7492 V007	23 08 19.8 -15 37 34	SXPHE
V0476 Aqr	NGC 7492 V004	23 08 23.2 -15 39 06	SR:
V0477 Aqr	NGC 7492 V002	23 08 25.0 -15 35 53	RRC
V0478 Aqr	NGC 7492 V001	23 08 26.7 -15 34 59	RRAB
V0479 Aqr	NGC 7492 V006	23 08 29.1 -15 36 51	SXPHE
V0480 Aqr	NGC 7492 V003	23 08 29.3 -15 41 46	RRC
V0481 Aqr	NGC 7492 V005	23 08 39.0 -15 34 36	L:

COMMISSIONS G1 AND G4 OF THE IAU
INFORMATION BULLETIN ON VARIABLE STARS
Volume 63 Number 6262 DOI: 10.22444/IBVS.6262

Konkoly Observatory
Budapest
12 August 2019

HU ISSN 0374 – 0676

CCD MINIMA FOR SELECTED ECLIPSING BINARIES IN 2018

NELSON, ROBERT H.

1393 Garvin Street, Prince George, BC, Canada, V2M 3Z1 ; e-mail: bob.nelson@shaw.ca

Observatory and telescope:
Mountain Ash Observatory (MAO): 33 cm f/4.5 Newtonian on a Paramount ME Desert Blooms Observatory (DBO): 40 cm f/6.8 SCT on a Paramount Taurus 400

Detector:	MAO: SBIG ST–10XME, 6.8 μm pixels, FOV: $34.4' \times 23.2'$, $-10° > T > -30$°C; DBO: SBIB STT–1603, 9.0 μ pixels, FOV: $18.3' \times 11.5'$, $-10° > T > -30$°C

Method of data reduction:
Bias and dark subtraction, flat-fielding using light-box flats; aperture photometry–all using MIRA, by Mirametrics. Check stars were used throughout.

Method of minimum determination:
Digital tracing paper method, bisection of chords, curve fitting, and (occasionally) Kwee and van Woerden (1956).

Times of minima:							
Star name	GCVS type	Time of Min HJD-2400000	Error (days)	Ecl. Type	Obs.	Filter	O–C (days)
BX And	EW/DW	58384.8386	0.0001	I	mao	c	-0.0004
LO And	EW/KW	58397.6610	0.0003	II	mao	c	-0.0346
QX And	EW	58377.8063	0.0005	II	DBO	*BVRI*	0.0013
QX And	EW	58466.6305	0.0005	I	DBO	c	0.0024
V0404 And	EA/RS	58394.6588	0.0003	I	mao	c	-0.0007
V0530 And	EB	58396.6929	0.0002	I	mao	*VRI*	0.0005
G2837–1343	na	58391.7108	0.0002	II	mao	*R*	0.0399
V1814 Aql	EA	58250.9462	0.0006	I	DBO	c	0.0002
CX Aqr	EA/SD	58377.7753	0.0002	I	DBO	c	0
SS Ari	EW/KW	58350.8589	0.0002	I	mao	c	0.0004
BM Ari	EW	58454.7159	0.0003	II	DBO	c	0.0025
BN Ari	EW/KW	58343.8804	0.0003	I	mao	c	0.0029
AH Aur	EW/DW	58396.0016	0.0003	I	mao	*VRI*	-0.0004
EP Aur	EB	58389.9048	0.0002	I	mao	c	-0.0013
V0410 Aur	EW	58394.907	0.015	II	mao	*VRI*	-0.0087
V0599 Aur	EW	58374.9446	0.0002	I	DBO	c	0.0015
TY Boo	EW/KW	58205.8350	0.0004	II	mao	c	-0.0006
TZ Boo	EW/KW	58173.8809	0.0002	I	mao	c	-0.0052
TZ Boo	EW/KW	58260.8003	0.0004	II	DBO	*VRI*	-0.006
TZ Boo	EW/KW	58261.6918	0.0004	II	DBO	c	-0.006
TZ Boo	EW/KW	58261.8426	0.0005	I	DBO	c	-0.0038
VW Boo	EW/KW	58207.9287	0.0005	I	DBO	*VRI*	0
GM Boo	EW	58208.8832	0.0003	II	mao	*VRI*	0.0003
GN Boo	EW	58175.9543	0.0004	I	mao	c	0.0009
GN Boo	EW	58213.8040	0.0007	II	mao	*VRI*	-0.0008
GN Boo	EW	58237.7821	0.0002	I	DBO	c	-0.0002
GN Boo	EW	58237.9337	0.0003	II	DBO	*VRI*	0.0006
GN Boo	EW	58251.8080	0.0003	II	mao	c	0.0011
GN Boo	EW	58291.7671	0.0003	I	DBO	c	-0.0023
GT Boo	EB	58247.7722	0.0004	I	mao	*I*	0.0004
IK Boo	EW	58171.8683	0.0002	I	mao	c	-0.0002
PU Boo	EW	58167.8911	0.0002	I	mao	*R*	-0.0037
V0339 Boo	EW	58174.0024	0.0002	II	mao	c	0.0014
V0339 Boo	EW	58210.829	0.001	I	mao	c	0.0029
CP Cam	EB	58483.6092	0.0003	I	mao	c	-0.0011
CV Cam	EB	58375.8630	0.0003	I	mao	c	0.0014
OQ Cam	EW	58396.811	0.002	I	mao	*V*	0.002
V0337 Cam	EB	58442.6576	0.0001	I	mao	c	0.0009
V0447 Cam	EB	58397.9361	0.0005	I	mao	*BVR*	0.0059
V0473 Cam	EW	58390.9625	0.0004	I	mao	*R*	-0.001
V0474 Cam	EW	58392.9503	0.0002	I	mao	*V*	0.0002
G3715–0043	E	58374.8695	0.0004	II	mao	c	-0.0027

Times of minima:							
Star name	GCVS type	Time of Min HJD-2400000	Error (days)	Ecl. Type	Obs.	Filter	O-C (days)
ZZ Cas	EB/KE	58370.860	0.001	II	DBO	c	0.0018
GT Cas	EA/SD	58369.8164	0.0003	I	DBO	*BVI*	-0.0017
IR Cas	EB	58390.8032	0.0002	I	DBO	*BVRI*	-0.0024
IR Cas	EB	58391.8266	0.0002	II	DBO	*R*	0
MN Cas	EA/DM	58378.8299	0.0005	I	DBO	*R*	-0.0014
V0608 Cas	E:	58390.8227	0.0003	I	mao	*R*	0
XY Cep	EA/SD	58379.7395	0.0002	I	DBO	c	0.0135
V0957 Cep	EA	58367.7675	0.0003	I	mao	c	0.0041
UZ CMi	EW/DW	58464.8710	0.0003	I	mao	c	0.0049
XZ CMi	EA	58170.6598	0.0002	I	mao	c	0.0008
TX Cnc	EW/KW	58438.9332	0.0004	I	mao	*BVR*	-0.002
EH Cnc	EW	58216.6716	0.0002	II	DBO	*VRI*	0
HN Cnc	EW	58164.6977	0.0002	I	mao	*R*	0.0024
G1936–0040	ESD-EC	58450.8507	0.0007	II	DBO	c	0.0006
RW Com	EW/KW	58159.8050	0.0005	II	mao	c	0
RZ Com	EW/KW	58169.8508	0.0002	II	mao	c	0.001
RZ Com	EW/KW	58246.8611	0.0004	I	DBO	*B*	0.0008
RZ Com	EW/KW	58250.7519	0.0003	II	DBO	c	-0.0013
RZ Com	EW/KW	58253.7986	0.0002	II	DBO	c	-0.0011
CC Com	EW/KW	58196.7724	0.0001	I	mao	c	0.0003
RW CrB	EA/SD:	58189.9658	0.0003	I	mao	*R*	0.0017
AR CrB	EW	58246.7039	0.0002	I	DBO	*BVI*	-0.0007
AS CrB	EW	58206.9171	0.0006	I	DBO	c	0.0031
BX CrB	EW	58254.8370	0.0004	I	DBO	c	-0.0005
DF CVn	EW	58195.7101	0.0003	I	mao	c	-0.0009
DL CVn	EB	58190.7488	0.0005	II	DBO	*BVI*	0.0039
DR CVn	EW?	58176.0200	0.0004	II	DBO	c	0
DR CVn	EW?	58179.9638	0.0007	II	DBO	c	-0.0049
DR CVn	EW?	58180.961	0.001	II	DBO	*VRI*	-1041.5
DR CVn	EW?	58189.8349	0.0005	II	DBO	*R*	0.0051
DR CVn	EW?	58193.953	0.002	I	DBO	*BVI*	-0.0008
DX CVn	EW?	58208.7058	0.0006	II	mao	*VRI*	-0.0007
EG CVn	EW?	58195.7931	0.0002	II	DBO	*R*	-0.0021
GM CVn	EW	58271.8634	0.0004	I	DBO	*I*	-0.0015
WZ Cyg	EB	58259.8702	0.0004	II	mao	*R*	0.0002
GO Cyg	EB/KE	58256.9240	0.0002	I	mao	c	-0.0016
GO Cyg	EB/KE	58275.945	0.001	II	DBO	*VI*	-0.0014
GO Cyg	EB/KE	58279.8928	0.0005	I	DBO	*BVI*	-0.0013
GO Cyg	EB/KE	58289.9414	0.0004	I	DBO	*BVI*	-0.0014
GO Cyg	EB/KE	58293.888	0.001	II	DBO	c	-0.0025
V0401 Cyg	EW/KE	58244.9033	0.0008	I	mao	*BVI*	0.0025
V0456 Cyg	EA/SD:	58224.9254	0.0001	I	mao	c	-0.0005
V1918 Cyg	EW/KW	58251.8950	0.0003	II	mao	*R*	-0.0005

Times of minima:

Star name	GCVS type	Time of Min HJD-2400000	Error (days)	Ecl. Type	Obs.	Filter	O-C (days)
V2197 Cyg	E	58297.8412	0.0002	I	DBO	c	0
V2282 Cyg	EW	58242.8628	0.0002	II	DBO	*R*	-0.0002
V2282 Cyg	EW	58260.8366	0.0004	II	mao	*VRI*	0.0006
V2364 Cyg	EW	58242.9638	0.0003	II	DBO	c	0.0019
V2477 Cyg	EW	58223.9324	0.0002	I	mao	c	-0.0002
V2643 Cyg	EB	58357.755	0.001	II	mao	*BVI*	0.0086
AX Dra	EB	58169.771	0.001	II	mao	c	-0.0012
BE Dra	EB/KE	58255.8986	0.0007	I	mao	c	-0.0007
V0357 Dra	EW	58197.8948	0.0005	I	DBO	c	0.0022
V0373 Dra	EW	58255.7708	0.0004	I	mao	c	0.0019
V0374 Dra	EW	58210.9524	0.0004	II	mao	*VRI*	0.0022
V0380 Dra	EA	58272.7057	0.0002	I	DBO	*B*	-0.0041
V0402 Dra	EW	58267.8907	0.0003	II	mao	c	0.011
V0450 Dra	EW	58210.715	0.001	I	mao	c	-0.0002
V0509 Dra	EW	58270.8751	0.0003	I	DBO	*V*	0.0001
G3864–1315	E?	58210.7704	0.0003	I	DBO	c	0.0001
G3870–1172	EW	58223.8601	0.0002	I	mao	c	0.0006
G3929–1500	EW	58267.7953	0.0002	I	mao	*VRI*	0
G4449–0995	EW	58188.9538	0.0004	I	mao	c	0
WW Gem	EB/KE	58158.7042	0.0003	I	mao	c	-0.0034
GW Gem	EB/SD	58389.9731	0.0004	II	mao	c	-0.0006
V0373 Gem	EB	58460.783	0.002	II	mao	*BVRI*	0
V0404 Gem	EW	58450.7982	0.0003	I	DBO	c	-0.0006
G1886–1869	EC	58396.9663	0.0003	I	mao	c	-0.0002
SZ Her	EA/SD	58168.9725	0.0001	I	mao	c	-0.0009
V0842 Her	EW	58189.8680	0.0002	I	mao	*R*	0.0013
V0878 Her	EB	58246.8374	0.0002	II	mao	*V*	0.001
V1033 Her	EW?	58224.8852	0.0001	I	DBO	c	0.0025
V1035 Her	EA	58224.8367	0.0007	II	mao	c	-0.0015
V1047 Her	EW	58261.8062	0.0004	II	mao	c	-0.0015
V1097 Her	EW	58212.9825	0.0002	II	DBO	*VRI*	-0.0047
V1097 Her	EW	58220.9263	0.0002	II	DBO	*VRI*	0.0003
V1097 Her	EW	58253.9439	0.0001	I	DBO	*R*	0.0001
V1103 Her	EW	58195.9446	0.0002	II	DBO	c	0.0005
V1160 Her	EW	58224.7783	0.0004	II	mao	c	-0.0027
V1167 Her	EW?	58210.9671	0.0002	I	DBO	*VRI*	-0.0004
V1198 Her	EW	58289.7359	0.0003	II	DBO	*VRI*	0.0054
V1233 Her	EW	58256.7670	0.0002	II	mao	*R*	0
G2058–0753	E	58249.8858	0.0003	II	DBO	c	0.0001
G2093–1834	EB	58256.8930	0.0001	I	DBO	*V*	0
AV Hya	EB/KE	58159.889	0.005	II	DBO	c	0.0021
AV Hya	EB/KE	58172.865	0.003	II	DBO	c	-0.0065
AV Hya	EB/KE	58179.709	0.001	II	DBO	*VRI*	0.0035

Times of minima:

Star name	GCVS type	Time of Min HJD-2400000	Error (days)	Ecl. Type	Obs.	Filter	O-C (days)
AV Hya	EB/KE	58180.7346	0.0007	I	DBO	*BVI*	0.004
AV Hya	EB/KE	58183.8052	0.0005	II	DBO	c	-0.0007
AV Hya	EB/KE	58193.7163	0.0002	I	DBO	c	0.0011
DF Hya	EW/KW	58462.9370	0.0002	II	DBO	*R*	0.0024
EU Hya	EA/DW	58187.7328	0.0005	I	DBO	c	0.0011
V0488 Lac	EW	58350.7507	0.0004	II	mao	*BVI*	0
Y Leo	EA/SD	58159.7092	0.0002	I	mao	c	0.0065
DU Leo	EA/SD	58218.7406	0.0003	II	DBO	*VRI*	0.0004
ET Leo	EW?	58171.756	0.002	II	mao	c	0.0004
MW Leo	EA?	58472.9151	0.0003	I	DBO	c	-0.0001
WZ LMi	EW	58189.7497	0.0004	II	mao	*R*	0.0036
AG LMi	EA	58162.9487	0.0002	I	DBO	c	0.0004
AG LMi	EA	58220.7063	0.0002	I	DBO	c	-0.0002
AG LMi	EA	58222.7451	0.0002	II	DBO	c	0.0001
AG LMi	EA	58254.6819	0.0002	I	DBO	c	0
SW Lyn	EA/DW	58224.7179	0.0003	I	DBO	*R*	-0.0097
V0591 Lyr	EW	58268.8121	0.0003	II	DBO	*R*	-0.0001
V0591 Lyr	EW	58269.8632	0.0002	I	mao	*B*	-0.0004
V0592 Lyr	EW	58253.8375	0.0002	II	mao	c	0.0008
V0653 Lyr	EW	58264.7957	0.0005	II	mao	*R*	0.0005
V0658 Lyr	EW	58369.68	0.01	I	DBO	*BVI*	-0.0045
V0664 Lyr	EW	58210.8802	0.0004	II	DBO	c	0
V0740 Lyr	EW	58205.939	0.002	II	mao	c	0.0017
G3104–1085	EW?	58258.8184	0.0004	I	DBO	c	0.0008
G3104–1085	EW?	58268.7924	0.0003	I	DBO	c	0.0006
G3104–1085	EW?	58269.8795	0.0004	II	mao	*BVI*	0.0036
V0927 Mon	EW	58168.6524	0.0002	I	mao	c	-0.0004
ES Ori	EA/DM	58465.8017	0.0005	I	DBO	c	-0.0003
V1363 Ori	EW	58483.7341	0.0003	II	mao	c	0.0023
V1848 Ori	EW	58437.9035	0.0003	II	DBO	c	-0.0001
V1848 Ori	EW	58462.8071	0.0005	I	DBO	*R*	-0.0002
V0481 Peg	EW	58370.752	0.001	I	mao	c	0.0017
V0619 Peg	EW	58394.7546	0.0003	II	mao	*BVI*	-0.0008
IT Per	EA/SD	58397.9225	0.0006	I	DBO	c	-0.0034
IT Per	EA/SD	58440.8692	0.0003	I	DBO	*BVR*	-0.0007
IT Per	EA/SD	58444.714	0.003	II	DBO	*V*	0.0099
KW Per	EB/SD	58397.7904	0.0002	I	mao	c	0.0003
V0873 Per	EW	58441.6127	0.0003	II	mao	*BVR*	-0.0006
V0881 Per	EW/KW	58380.8957	0.0007	I	mao	*BVRI*	-0.0045
V0881 Per	EW/KW	58474.6429	0.0003	I	mao	c	-0.0024
V0959 Per	EA	58441.7096	0.0002	I	mao	*BVR*	0.0004
CP Psc	EB:	58450.7422	0.0003	I	DBO	c	-0.001
DV Psc	E/RS	58466.5896	0.0002	I	DBO	c	0.0025

Times of minima:							
Star name	GCVS type	Time of Min HJD-2400000	Error (days)	Ecl. Type	Obs.	Filter	O-C (days)
HL Psc	EB/RS	58464.5964	0.0003	II	mao	c	-0.0022
AU Ser	EW/KW:	58257.7919	0.0002	II	mao	c	-0.0012
V0384 Ser	EW?	58236.9110	0.0003	I	DBO	c	0.0001
RZ Tau	EW/DW	58369.9830	0.0002	II	DBO	*R*	0.0011
RZ Tau	EW/DW	58372.8933	0.0004	II	DBO	c	0.0016
RZ Tau	EW/DW	58373.9321	0.0003	I	DBO	c	0.0012
RZ Tau	EW/DW	58378.9199	0.0002	I	DBO	*R*	0.0009
RZ Tau	EW/DW	58379.9587	0.0004	II	DBO	c	0.0005
AN Tau	EB/DM	58367.9374	0.0004	II	mao	*BVI*	0.0029
EQ Tau	EW/DW	58395.8948	0.0003	I	mao	*VRI*	-0.0016
V1238 Tau	EW	58384.9544	0.0001	II	mao	*BVRI*	-0.0056
V1369 Tau	EA	58450.9152	0.0005	I	DBO	*R*	0.0023
G1804–0539	E	58391.8365	0.0004	I	mao	c	0.0002
V Tri	EB/SD	58456.6086	0.0001	I	DBO	c	0.0023
RS Tri	EA/DM	58476.6315	0.0003	I	DBO	c	0.0072
RV Tri	EA/SD	58471.7778	0.0002	I	DBO	c	0.0009
TY UMa	EW/KW	58199.7167	0.0003	I	DBO	c	-0.0037
XY UMa	EB/DW/RS	58250.6710	0.0004	II	DBO	c	-0.0023
ES UMa	EW	58158.8296	0.0004	II	mao	*V*	-0.0002
HV UMa	EW	58161.862	0.001	II	mao	c	-0.0021
HV UMa	EW	58180.701	0.002	I	mao	*VRI*	0.0017
HV UMa	EW	58182.831	0.002	I	mao	*R*	-0.0006
HV UMa	EW	58185.6709	0.0005	I	mao	c	-0.0037
MQ UMa	EW	58461.9538	0.0004	I	mao	c	0.0039
V0354 UMa	EW	58463.0124	0.0008	II	DBO	*R*	0.005
VY UMi	EW	58188.8980	0.0002	II	mao	c	0.0057
AH Vir	EW/KW	58168.884	0.001	II	mao	*R*	-0.0025
AZ Vir	EW/KW	58196.8748	0.0003	II	mao	c	0.0081
BO Vul	EA/SD	58370.8030	0.0001	i	DBO	c	0.0003
BO Vul	EA/SD	58373.721	0.002	II	DBO	c	-0.0005

Remarks:

To save space, GSC star names have been shortened to a leading "G" only; times of minimum are heliocentric Julian dates with the leading 24 removed.
O–C values were computed using elements computed from the O–C database listed in the references (Nelson, 2016).
The observatory, Desert Blooms in Benson AZ, is described in Nelson (2017).

Acknowledgements:

Thanks are due to Environment Canada for the website satellite views (see reference below) that were essential in predicting clear times for observing runs in this cloudy locale. Thanks are also due to Attilla Danko for his "Clear Sky Charts", (see below). This research has made use of the SIMBAD database, operated at CDS, Strasbourg, France.

References:

Danko, A., Clear Sky Charts, http://cleardarksky.com/
Kwee, K. K., van Woerden, H., 1956, *Bull. Astron. Inst. Netherlands*, **12**, 327
Nelson, R.H. 2016, Bob Nelson's O-C Files, http://www.aavso.org/bob-nelsons-o-c-files
Nelson, R.H., 2017, *IBVS*, No. 5224
Satellite Images for North America, http://gfx.weatheroffice.ec.gc.ca/

COMMISSIONS G1 AND G4 OF THE IAU
INFORMATION BULLETIN ON VARIABLE STARS
Volume 63 Number 6263 DOI: 10.22444/IBVS.6263

Konkoly Observatory
Budapest
27 March 2019

HU ISSN 0374 – 0676

ON THE PERIOD AND LIGHT CURVE OF THE A-TYPE W UMa BINARY GSC 3208 1986

EATON, JOEL A.[1]; ODELL, ANDREW P.[2]; POLAKIS, THOMAS A.[3]

[1] 7050 Bakerville Road, Waverly, TN 37185 USA; e-mail: eatonjoel@yahoo.com

[2] Dept of Physics and Astronomy, NAU Box 6010, Flagstaff AZ 86011 USA; e-mail: WCorvi@yahoo.com

[3] Command Module Observatory, 121 W. Alameda Dr., Tempe, AZ 85282 USA; e-mail: tpolakis@cox.net

Abstract

We present a new period study and light-curve solutions for the A-Type W UMa binary GSC 3208 1986. Contrary to a previous claim by R. G. Samec et al. of a rapidly decreasing period, the system's period is *increasing* moderately on a timescale of 2×10^6 years. The light curve is variable on the time scale of years, which can be understood by changes in how much it overfills its Roche lobe.

Contact binaries are binaries close enough that their components are enclosed in a common, probably convective envelope (Lucy 1968). The best known members of this class are the W Ursae Majoris systems (Binnendijk 1970), although there are other rarer binaries that may be in marginal contact (e.g., Kałużny 1983, 1986a–d; Siwak et al. 2010). Binnendijk (pp. 218-221) defined two varieties of these W UMa systems, A-types, with transit primary eclipses, and W-types, with occultation primaries. Given the direct dependence of the ratio of radii on mass ratio in contact binaries, these A- and W-type classes correspond to q=M_2/M_1 less than and greater than 1.0, respectively.

GSC 3308 1986 (α(2000)=$22^{\rm h}25^{\rm m}16\overset{\rm s}{.}0$, δ(2000)=$+41^\circ27'51\overset{''}{.}9$) is a faint A-type W UMa binary observed and analyzed by Samec et al. (2015a; hereafter SAMEC). SAMEC obtained four nights of photometry ($\sigma_{\rm B}$≈0.006) and found an F3 V spectral type from a spectrum taken at the Dominion Astrophysical Observatory, a mass ratio of q=0.24, and that the star overfills its Roche lobe by 39%. These properties are not surprising for such a system, but SAMEC also derived a very rapid period *decrease*, corresponding to a timescale of $3{\times}10^5$ years. This seems unlikely for what they claim is an "ancient" contact system, especially if caused by magnetic braking, their favored period-change mechanism.

1 Ephemeris

Suspecting that the radical period decrease might result from R. G. Samec's previously documented (Odell et al. 2011) error of confusing Modified Julian Date (Heliocentric Julian Date – 2,400,000.5) with Reduced Julian Date (HJD – 2,400,000.0) in data from the Northern Sky Variability Survey (NSVS, see Wozniak et al. 2004), we obtained the archival data from the NSVS and SuperWASP (SWASP, see Butters et al. 2010) web sites. We have subsequently obtained new light curves for 2017 and 2018 (Polakis; *BVRI* on the

UBV/Cousins system; Table 1, provided as online table `6263-t1.txt` at the IBVS web site) and added the published photometry of Liakos & Niarchos (2011) and SAMEC to give nine seasonal light curves. Using these, we find a very different result than SAMEC. We have derived new effective times of minimum for these nine epochs by fitting those seasonal light curves with the Wilson-Devinney code to measure phase shifts with respect to the ephemeris of Eq. 1. These are listed in Table 2; the errors given are the σ's calculated by the W–D code multiplied by a factor of three per Popper (1984).

Table 2. O–C Residuals for linear and quadratic elements (days).

Epoch (Obs) RJD	Cycle (N)	(Obs–Calc) linear (Eq. 1)	(Obs–Calc) quadratic (Eq. 2)	Source of data
51464.1096 ± 0.0010	-11693	0.0022	-0.0017	NSVS
53247.4351 ± 0.0003	-7285	-0.0005	0.0003	SWASP 2004
53989.8134 ± 0.0006	-5450	-0.0014	0.0003	SWASP 2006
54324.7939 ± 0.00011	-4622	-0.0018	0.0000	SWASP 2007 Epoch1
54374.1509 ± 0.00013	-4500	-0.0019	-0.0001	SWASP 2007 Epoch2
55410.2457 ± 0.0005	-1939	-0.0013	-0.0001	Liakos&Niarchos
56194.7011 ± 0.0003	0	0.0000	-0.0001	Samec
57925.8458 ± 0.0003	4279	0.0055	-0.0003	Polakis 2017
58415.7787 ± 0.0002	5490	0.0081	0.0001	Polakis 2018

In analyzing the period, we first used a preliminary linear ephemeris derived by Odell from the NSVS plus Polakis' 2017 data, namely

$$\text{HJD } \text{T}_{\text{min}} \text{ I} = 2,456,194.7011 + 0.4045663 \times \text{N}, \tag{1}$$

to phase all the data into annual/seasonal light curves. Then we derived the deviations of the phases from this linear ephemeris with the W-D code as noted above, and then fit those deviations with a second-order polynomial to determine the following quadratic ephemeris:

$$\text{HJD } \text{T}_{\text{min}} \text{ I} = 2,456,194.7012(1) + 0.40456718(1) \times \text{N} + 1.03(5) \times 10^{-10} \times \text{N}^2. \tag{2}$$

In this equation the numbers in parentheses are errors in the last decimal place, and N is the cycle number. Fig. 1 shows the deviations from Eq. 1 and the quadratic fit.

2 Spectra

Odell obtained two spectra of GSC 3208 1986 with the Boller&Chivens Spectrograph on the Steward Observatory 90-inch telescope around 1 June 2015, specifically at HJD 2,457,173.9734 (phase 0.55) and HJD 2,457,174.8694 (phase 0.76). These spectra covered the wavelength range 3900–4750 Å and are consistent with the F3 V spectral type of SAMEC. They give radial velocities for the components of $\text{RV}_1 = 22.1 \pm 7.2$ km s^{-1} for the phase near conjunction and $\text{RV}_1 = 86.9 \pm 8.2$ km s^{-1} and $\text{RV}_2 = -298 \pm 25$ km s^{-1} for the quadrature. These values give a crude indication of the velocity amplitudes of the components, $K_1 = 91 \pm 16$ km s^{-1} and $K_2 = 294 \pm 25$ km s^{-1} with $\gamma = -4$ km s^{-1}. The resulting spectroscopic mass ratio $q = 0.30 \pm 0.03$ is $\sim$ consistent with the photometric mass ratio.

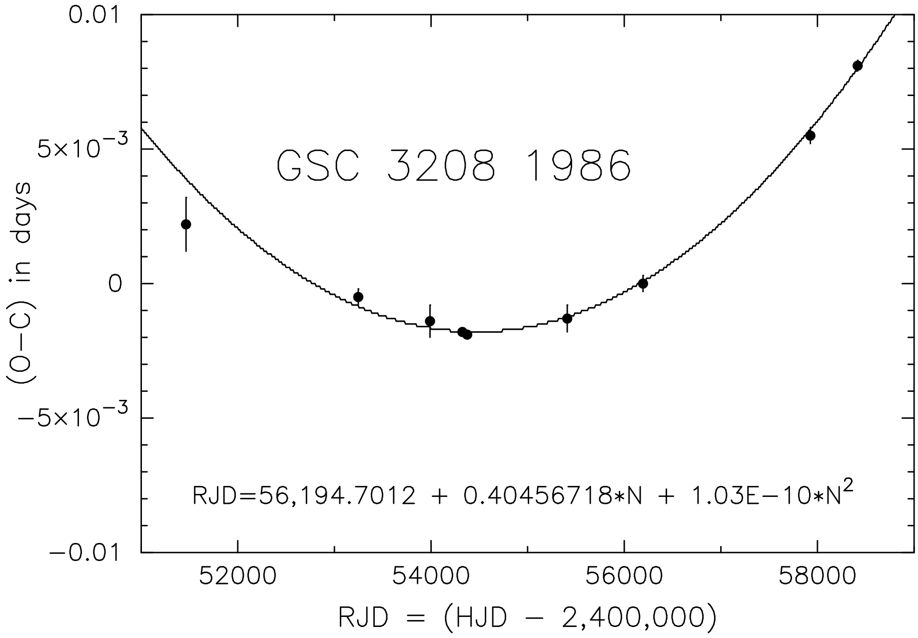

Figure 1. O–C Diagram for GSC 3208 1986.

3 Light curve

The extensive observations from SWASP give us the opportunity to solve well-defined light curves for the three years, 2007, 2006, and 2004. The data for 2007 are by far the best and most numerous, so we will concentrate on them. Consequently, we have formed 200 normal points derived from the roughly 11,300 SWASP observations for 2007, giving them in online Table 3 (available through the IBVS website as `6263-t3.txt`) as orbital phase (based on Eq. 1), magnitude, and a standard deviation of the mean for each magnitude. The typical normal point has an uncertainty of $\sigma = 0.0019$ mag (S.D.), nominally giving about the same total weight as the photometry published by SAMEC, but the SWASP data cover enough time to average out the typical wavelength-independent observational errors of data taken on a mere four nights. These data represent a broad band in the optical, corresponding roughly to V of the UBV system. Fig. 2 shows the SWASP light curves for 2007 (Table 3) with a representation of the solution of Table 4 plotted as a solid line.

We have solved this light curve with the Wilson-Devinney code [2003 version; see Wilson & Devinney (1971); Wilson (1990,94)], finding the elements in the second column of Table 4. These are roughly consistent with SAMEC's solution (Table 4, Col. 4). In calculating this solution we adopted SAMEC's temperature of the primary, convective gravity darkening (Lucy 1967), convective reflection effect (Rucinski 1969), the Kurucz-atmospheres option in the W-D code, and a linear limb-darkening coefficient from Van Hamme (1993). We accounted for a slight O'Connell effect in the normal points with a small dark spot on the leading hemisphere of the primary component. The small χ^2 indicates the model fits the data as well as can be expected. For completeness, we calculated a solution for 2007 with radiative gravity darkening and reflection effect, because in the past there was some inkling that these hotter A-type systems might be radiative, but the fit was much worse, by a factor of two in χ^2. This radiative solution had a significantly lower fillout, 13%, as expected from the well-known correlation between fillout and gravity

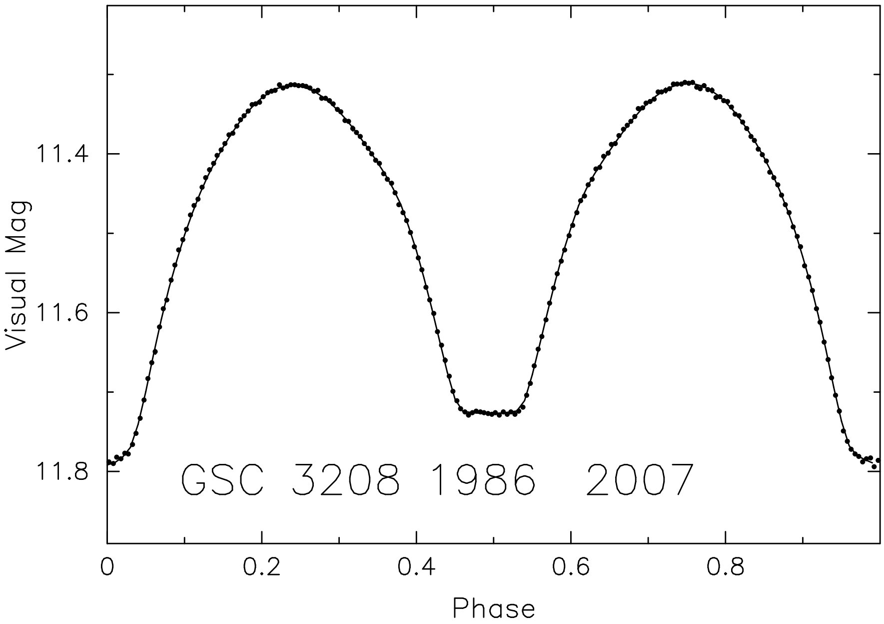

Figure 2. Light curve solution for SWASP, normal points for 2007.

darkening.

The other two years of SWASP data had somewhat different light curves which we have solved by varying those elements of the 2007 solution that might conceivably change on the timescale of a few years. Some elements, such as q and i, cannot change materially on such a short timescale, so we are left with temperatures and fillout that might change. Keeping q, i, T_1 fixed, we get the solution in Col. 3 of Table 4 for 2004. A greater depth of both eclipses in 2004 led to a larger overfilling of the Roche lobe. The solution for 2006 had a marginally larger fillout, 39%, for the worst data of the three years ($\sigma = 0.014$ mag). The differences between 2007 and 2004 might conceivably result from a change in the photometric band of the observations, but it would require a shift at least as great as from V to B between the two years. A shift of this magnitude is rather unlikely (see Butters et al. 2010, Fig. 1).

All of these solutions imply that the standard overcontact model fits GSC 3208 1986 well. Values of T_{mult}, which measures the ratio of T_2 as measured in W-D, Mode 3, to its value for W-D, Mode 1, (no break in temperature at the neck between the components), are 1.0 for all practical purposes, so the temperature varies smoothly over the surface as determined by the gravity-darkening law. The solution for a radiative envelope, however, does not have this property and gives a significantly worse fit, so the envelope is not likely to be radiative.

You may have noticed that the quoted errors of our solution for 2007 and SAMEC's solution for 2012 are inconsistent, although the two data sets have roughly the same weight (#points/σ^2). This probably results from the way such uncertainties are calculated. If we calculate the uncertainty of each element independently of all the others, we get values for the 2007 SWASP solution similar to those quoted by SAMEC. However, if we let elements q, i, Ω, T_2, and the x's vary simultaneously, we get the uncertainties listed. Adding g and A_{bol} to the mix gives even bigger uncertainties, doubling the reported uncertainty of Ω. This result confirms Popper's (1984) insinuation that the uncertainties derived by the

Table 4. GSC 3208 1986: Light curve solutions

Parameter (1)	2007-SWASP (2)	2004-SWASP (3)	2012-SAMEC (4)	2017-Polakis (5)	2018-Polakis (6)
x_1=x_2 (fixed)	0.51	0.51	Non-linear	0.63,0.51,0.41,0.33	0.63,0.51,0.41,0.33
g (fixed)	0.32	0.32	0.32	0.32	0.32
$A_{\rm bol}$(fixed)	0.50	0.50	0.50	0.50	0.50
i (deg)	85.60 ± 0.27	85.60 (fixed)	85.8 ± 0.1	85.60 (fixed)	85.60 (fixed)
q (M_2/M_1)	0.2424 ± 0.0011	0.2424 (fixed)	0.2374 ± 0.0002	0.2424 (fixed)	0.2424 (fixed)
Ω	2.2811 ± 0.0020	2.269 ± 0.0020	2.261 ± 0.001	2.273 ± 0.0018	2.279 ± 0.0016
fillout	35.3 ± 1.3%	49.1 ± 1.3%	39 ± 0.7%	40.3 ± 1.2%	36.8 ± 1.0%
T_1 (K, fixed)	6875	6875	6875	6875	6875
T_2 (K)	6757 ± 22	6789 ± 10	6760 ± ?	6745 ± 11	6725 ± 8
$T_{\rm mult}$	0.9950 ± 0.0032	1.0009 ± 0.0014	0.9968	0.9948	0.9909
σ (mag)	0.0019/point	0.0066/point	∼ 0.006/point	∼ 0.013/point	∼ 0.013/point
χ^2/DOF	1.2	1.1	∼1.44	∼ 2.2	∼ 1.0
			Spot on the Primary Component		
lat,long (deg)	0,270	0,270	none	none	none
$r_{\rm spot}$(deg)	1.7	1.7			
$T_{\rm spot}$	(black)	(black)			

W-D code are misleading. It also points to the intuitive truth that our assumptions about limb darkening, gravity darkening, and reflection effect will inevitably bias the results for all these contact and near-contact binaries.

Acknowledgements: We thank Steward Observatory for allocating the telescope time to obtain the spectra we used. This paper makes use of data from the Data Release 1 of the WASP data (Butters et al. 2010) as provided by the WASP consortium, and the computing and storage facilities at the CERIT Scientific Cloud, reg. no. CZ.1.05/3.2.00/08.0144, which is operated by Masaryk University, Czech Republic. It also uses data from the Northern Sky Variability Survey created jointly by the Los Alamos National Laboratory and University of Michigan.

References:

Binnendijk, L., 1970, *ARA&Ap*, **12**, 217 DOI
Butters, O. W. et al., 2010, *A&A* **520**, L10 (SuperWASP)
Kałużny, J., 1983, *AcA*, **33**, 345
Kałużny, J., 1986a, *AcA*, **36**, 105
Kałużny, J., 1986b, *AcA*, **36**, 113
Kałużny, J., 1986c, *AcA*, **36**, 121
Kałużny, J., 1986d, *PASP*, **98**, 662
Liakos, A., Niarchos, P., 2011, *IBVS*, 5999, 2
Lucy, L. B., 1967, *ZsfAp*, **65**, 89
Lucy, L. B., 1968, *ApJ*, **151**, 1123 DOI
Odell, A.P., Wils, P., Dirks, C., Guvenen, B., O'Malley, C.J., Villarreal, A.S., Weinzettle, R.M., 2011, *IBVS*, 6001
Popper, D. M., 1984, *AJ*, **89**, 132 DOI
Rucinski, S.M., 1969, *AcA*, **19**, 245

Samec, R. G., Kring, J. D., Robb, R., Van Hamme, W., Faulkner, D. R., 2015a, *AJ*, **149**, 90 (SAMEC) DOI
Samec, R. G., Benkendorf, B., Dignan, J. B., Robb, R., Kring, J., Faulkner, D. R., 2015b, *AJ*, **149**, 146 DOI
Siwak, M., Zola, S., Koziel-Wierzbowska, D., 2010, *AcA*, **60**, 305
Van Hamme, W., 1993, *AJ*, **106**, 2096 DOI
Wilson, R.E., Devinney, E.J., 1971, *ApJ*, **166**, 605 DOI
Wilson, R. E., 1990, *ApJ*, **356**, 613 DOI
Wilson, R. E., 1994, *PASP*, **106**, 921 DOI
Wozniak, P. R. et al., 2004, *AJ*, **127**, 2436 (NSVS) DOI

COMMISSIONS G1 AND G4 OF THE IAU
INFORMATION BULLETIN ON VARIABLE STARS
Volume 63 Number 6264 DOI: 10.22444/IBVS.6264

Konkoly Observatory
Budapest
25 April 2019

HU ISSN 0374 – 0676

A NEW VARIABLE IN THE FIELD OF WD1145+017

SEREBRYANSKIY, A.

Fesenkov Astrophysical Institute, Observatory 23, 050020 Almaty, Kazakhstan

e-mail: alex@aphi.kz

Abstract

Revisit of the CCD archive obtained during long-time monitoring of the white dwarf WD1145+015 at Tien-Shan Observatory revealed a new variable star, identified as Gaia DR2 3796400796427214848. It was inferred that this star is of spectral type G7V-G8V. The amount of photometric data allows performing detailed analysis of this target, revealing its rotational-modulation variability. The period of variation is 6.33 h which makes this star an ultra-fast rotator. The stability of variability might be due to "magnetic saturation" of the angular momentum loss. Yet another possible interpretation of the brightness variation is an elliptical variable binary system.

1 Introduction

The field around WD1145+017 has been continuously monitored at Tien-Shan Observatory (TSO, Kazakhstan) since 2016. Recently, we developed a new code for automatic processing and PSF-photometry of all targets on the CCD frames (Serebryanskiy et al., 2018). This code is based on the IRAF[1] realization in `python` (`pyraf`), `astropy`[2] library, `scamp` (Bertin, 2006), `astroquery`, to name just a few. Using this code a new variable was found while processing CCD-images of the field of WD1145+017 obtained in 2016-2018.

2 Observations

The field around WD1145+017 was observed during 2016-2018 at TSO using the "Zeiss-1000" telescope equipped with an Apogee Alta U9000 CCD camera using a Kodak KAF-09000 chip with 3056×3056 pixels and 12 μm pixel size. Equivalent focus length of the "Zeiss-1000" is 6665.0 mm using a specially designed focus reducer and field corrector which provide $19' \times 19'$ FOV with a scale of $0\farcs37$/px. To improve the SNR, observations were performed in 2×2 binning which reduce resolution to $0\farcs75$/px. The cadence of the observations was 40, 60 and 90 sec depending on the filter. More information about observation is provided in Table 1. The new variable, identified as Gaia DR2 3796400796427214848, and WD1145+017 are indicated in the finding chart given in Figure 1.

[1]Image Reduction and Analysis Facility, http://iraf.noao.edu
[2]This research made use of Astropy, a community-developed core Python package for Astronomy (Astropy Collaboration, 2018)

Table 1: Log of observations.

Date	BJD interval 2457451+	Duration [hours]	Number of frames	Filter	Exposure [sec]
03.03.2016	0.170767 − 0.478716	7.39	351	Johnson R	60
04.03.2016	1.178087 − 1.485414	7.38	350	Johnson R	60
05.03.2016	2.208392 − 2.482231	6.57	312	Johnson R	60
06.03.2016	3.164791 − 3.480801	7.58	338	Johnson R	60
08.03.2016	5.241870 − 5.463236	5.31	253	clear	60
09.03.2016	6.198473 − 6.452463	6.10	288	clear	60
14.04.2016	42.115488 − 42.329463	5.14	233	clear	60
23.04.2016	51.240633 − 51.355715	2.76	130	Johnson R	60
26.02.2017	360.208351 − 360.519519	7.47	382	clear	60
03.07.2017	369.304570 − 369.395335	2.18	70	Johnson V	90
14.04.2017	407.108791 − 407.312858	4.90	151	Johnson V	90
07.05.2018	795.139439 − 795.306060	4.00	233	clear	40

Light curves for all stars on the field were computed using the systematics removal algorithm by Tamuz et al. (2005). The light curve for the new variable star is shown in Figure 2 and reveal the presence of variability with a period of several hours. This new variable is not listed either in the Simbad Database or in the General Catalogue of Variable Stars.

Querying Gaia Data Release 2 (Gaia Collaboration, 2018) reveals the following parameters for this object: RA(J2000)=11:48:47.79, DEC(J2000)=+01:23:39.4, $G = 16.2725 \pm 0.0020$ mag, $G_{\rm BP} = 16.7102 \pm 0.0104$ mag, $G_{\rm RP} = 15.6506 \pm 0.0068$ mag, parallax $\pi = 0.6594 \pm 0.1032$ mas, $\mathrm{T_{eff}} = 5149.17^{+94}_{-102}$ K.

3 Light curve analysis

Using the light curves from individual nights two merged light curves were compiled: 1) the "long" one using all light curves and 2) "short" one using light curves for 2016 only. Then, the period search was performed using the Generalized Lomb-Scargle algorithm realized in `gatspy` (VanderPlas et al., 2015) and Phase Dispersion Minimization (`PyAstronomy`). The necessity to use a "short" merged light curve is dictated by several reasons: 1) to avoid the long duration gap in the data, 2) to avoid possible period variations. The corresponding frequency spectra are shown in Figures 3 and 4. The periods found are presented in Tables 2 and 3.

Table 2: Periods estimated using the "long" merged light curve.

Mode	f c/d	σ_f c/d
f1	3.788^a, 3.789^b	0.01
f2	7.576^a, 7.576^b	0.01

^{a} - GLS, ^{b} - PDM

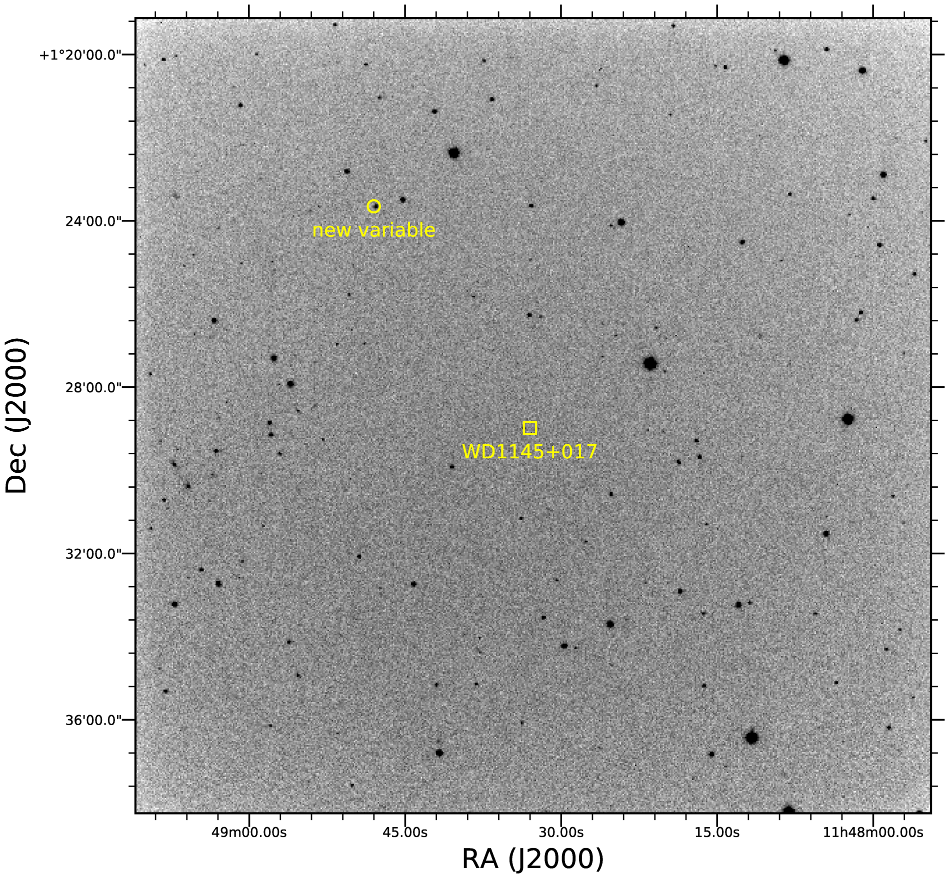

Figure 1. Finding chart of the field around WD1145+017,with the new variable, Gaia DR2 3796400796427214848, indicated.

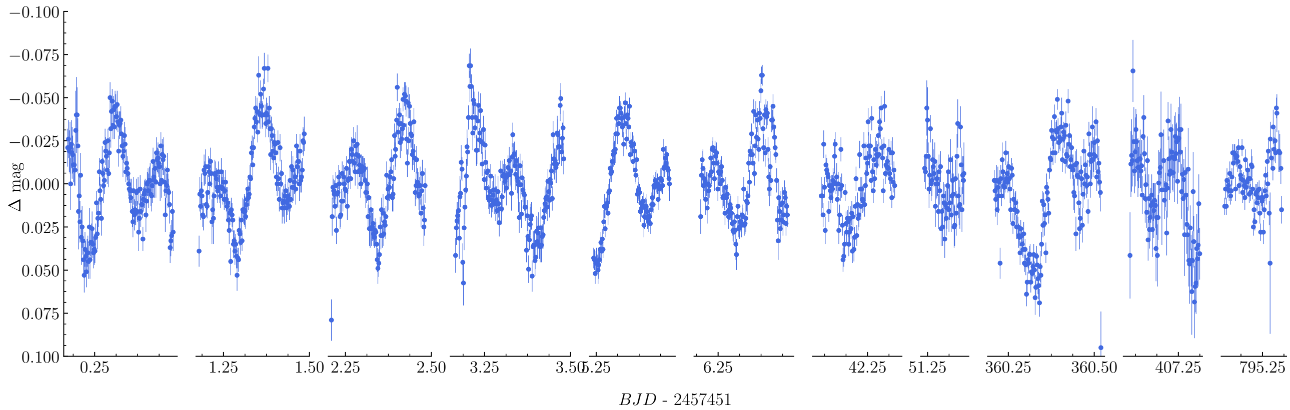

Figure 2. Light curves of the new variable in the field of WD1145+017.

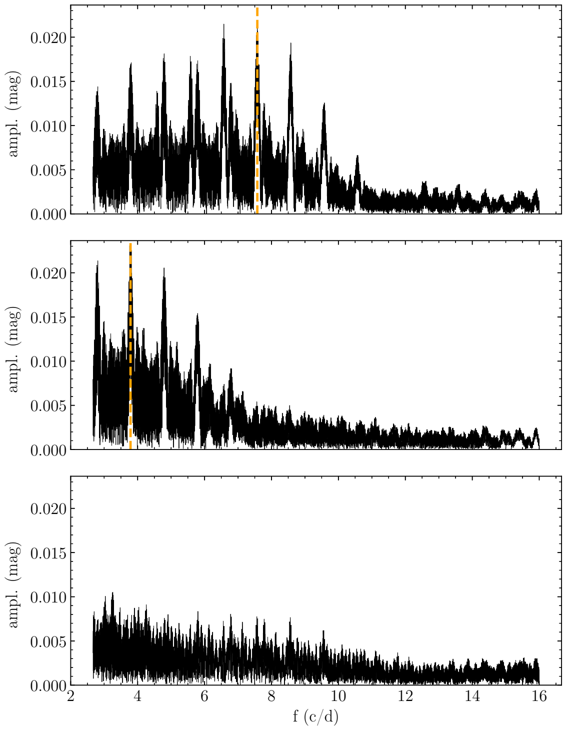

Figure 3. GLS frequency spectrum using the "long" merged light curve with the found periodicity indicated.

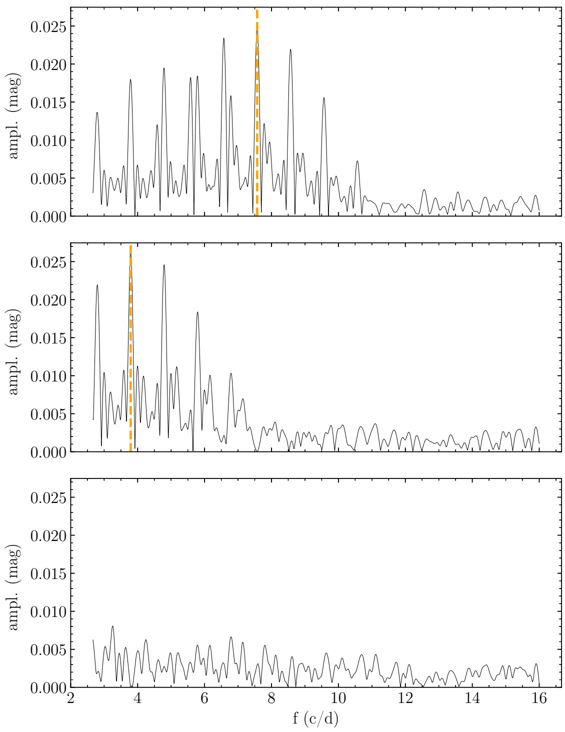

Figure 4. GLS frequency spectrum using the "short" merged light curve with the found periodicity indicated.

Table 3: Periods estimated using the "short" merged light curve.

Mode	f c/d	σ_f c/d
f1	3.793^a, 3.789^b	0.01
f2	7.572^a, 7.577^b	0.01

^{a} - GLS, ^{b} - PDM

The main period is ≈6.33 h, and the second period is almost exactly half of the main one which might be an indication that this is rotation modulated variability. To check this assumption and to determine other parameters of the modes the light curves for individual nights were fitted using Equation (1) with fixed Π_1 parameter and five free parameters: $A_0, A_1, A_2, \phi_1, \phi_2$.

$$y_{fit} = A_0 + A_1 \sin(2\pi(t - \phi_1)/\Pi_1/2) + A_2 \cos(2\pi(t - \phi_2)/(\Pi_1)) \quad (1)$$

Examples of the fitting results are shown in Figure 5 and Figure 6 for two different epochs of observations.

The figures show that the second period is indeed half of the first one and the period of the first variation is stable. The amplitudes of the two modes are shown in Figure 7. This indicates that we are dealing with rotational modulation variability.

The two phases, ϕ_1 and ϕ_2, and the constant period Π_1 were used to compute the O–C diagram shown in Figure 8. The O–C diagram was fitted using Equation (2). The observed O–C diagram for two phases and corresponding fitting results are shown in Figure 8.

$$(O - C) = \Delta E_0 + P \cdot E + \frac{1}{2} P \cdot \frac{dP}{dt} \cdot E^2 \quad (2)$$

From O–C fitting it was found that for the first harmonic (phase ϕ_1) $\dot{P}_1$ = (-4.3 ± 0.4) × 10 $^{-6}$ d y^{-1}, for the second harmonic (phase ϕ_2) $\dot{P}_2$ = (76.0 ± 3.0) × 10 $^{-6}$ dy^{-1}.

3.1 Interpretation

To interpret the variability and evolutionary status of this new variable I first estimated the color index $(B-V)$ of this star from our multicolor photometry obtained on May 13, 2017. The results are: $(B-V) = 0.713 \pm 0.04$ mag, $(V-R) = 0.365 \pm 0.02$ mag. The color excess from Edge et al. (2013) is E$(B-V)$ = 0.0220 mag.

Moreover, using the value for $T_{\rm eff}$ and results of Eker et al. (2015) one can find that $\log(M/M_\odot) \approx -0.1$, $\log(L/L_\odot) \approx -0.5$, and $\log(R/R_\odot) \approx -0.1$. From Table 3 by Miller (2015), we get [Fe/H] ≈ -0.580, with $\rho = 0.0756$.

The location of this star in the color-magnitude diagram is shown in Figure 9. I used a 4×4 degree area around the target to build this diagram. Based on this information I conclude that this star is of spectral type G7V-G8V. Considering its proper motion ($\mu_\alpha = -3.9$ mas/y, $\mu_\delta = -9.4$ mas/y) and distance ($\pi \sim 0.7$ mas) I estimated the components of space velocity of this target: (U,V,W) = 7 km s^{-1}, –75 km s^{-1}, –20 km s^{-1}. Since there is no information on radial velocity for this star in these catalogs I used

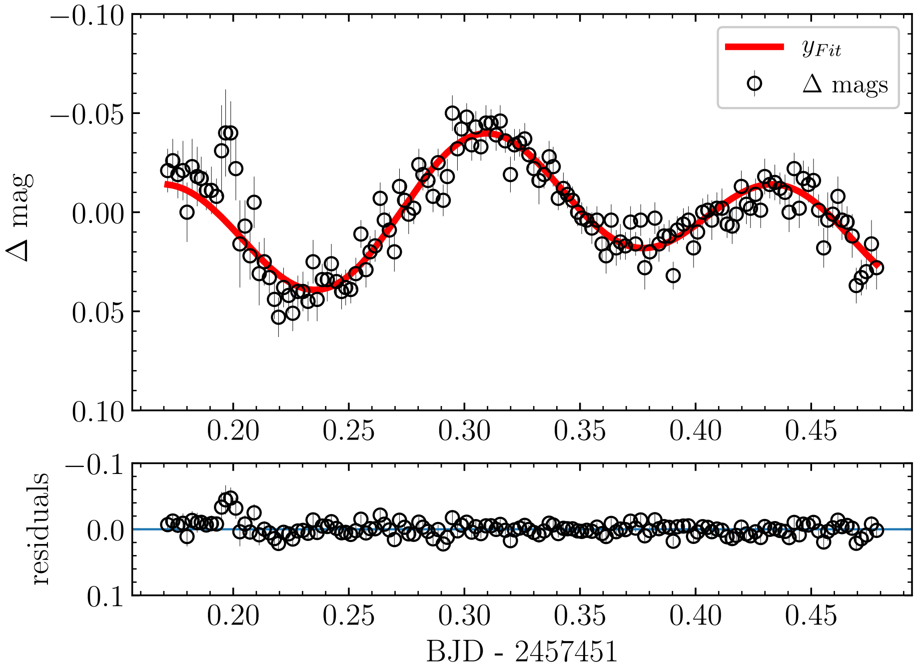

Figure 5. Top: the light curve of the new variable observed on 03.03.2016 (open circles) and fit results using Equation (1) (solid red line). Bottom: residual.

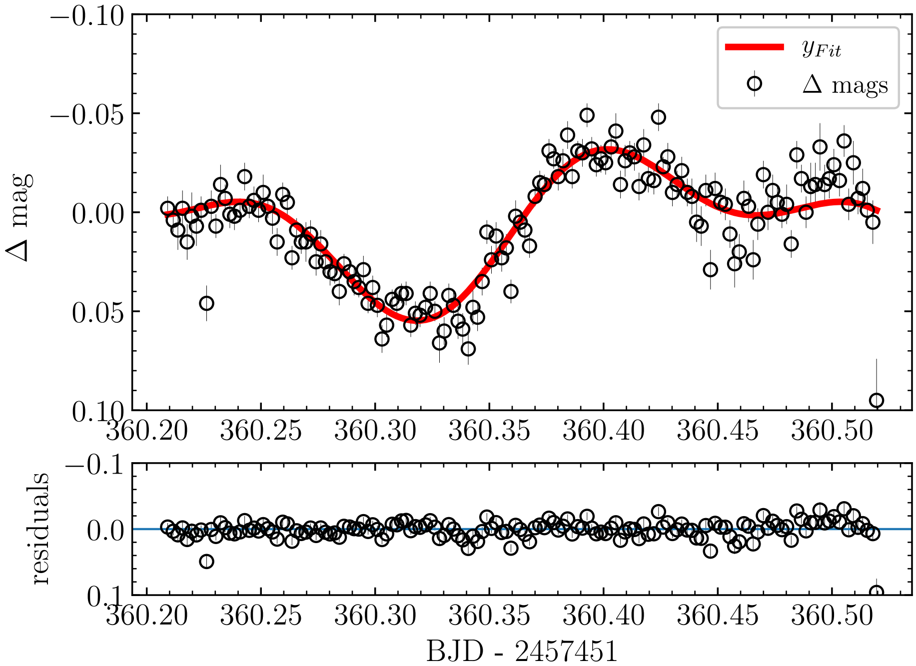

Figure 6. Top: the light curve of the new variable observed on 26.02.2017 (open circles) and fit results using Equation (1) (solid red line). Bottom: residual.

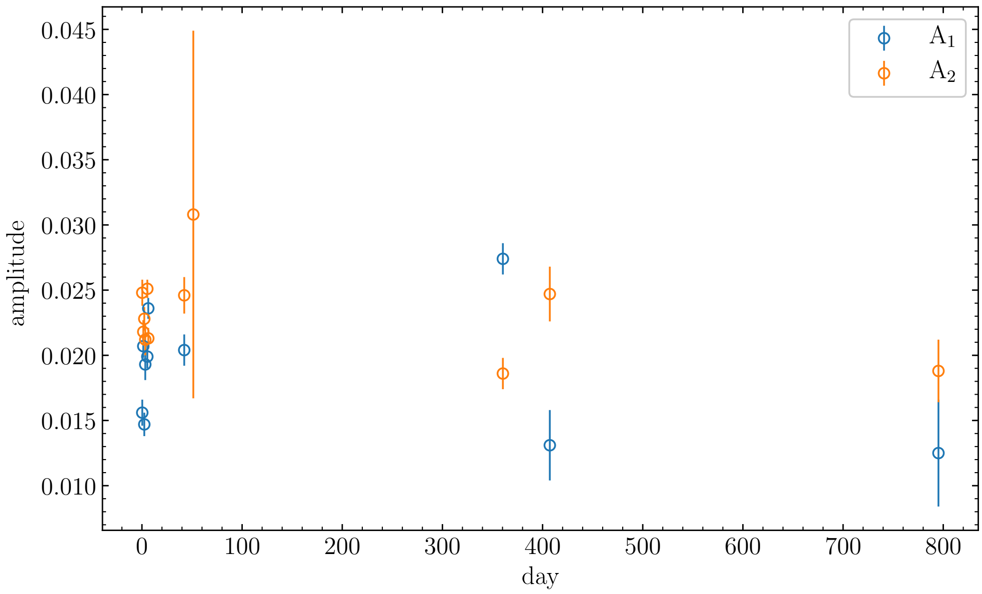

Figure 7. Amplitudes A_1 and A_2 determined from fitting Equation (1) to individual light curve as a function of epoch of observation

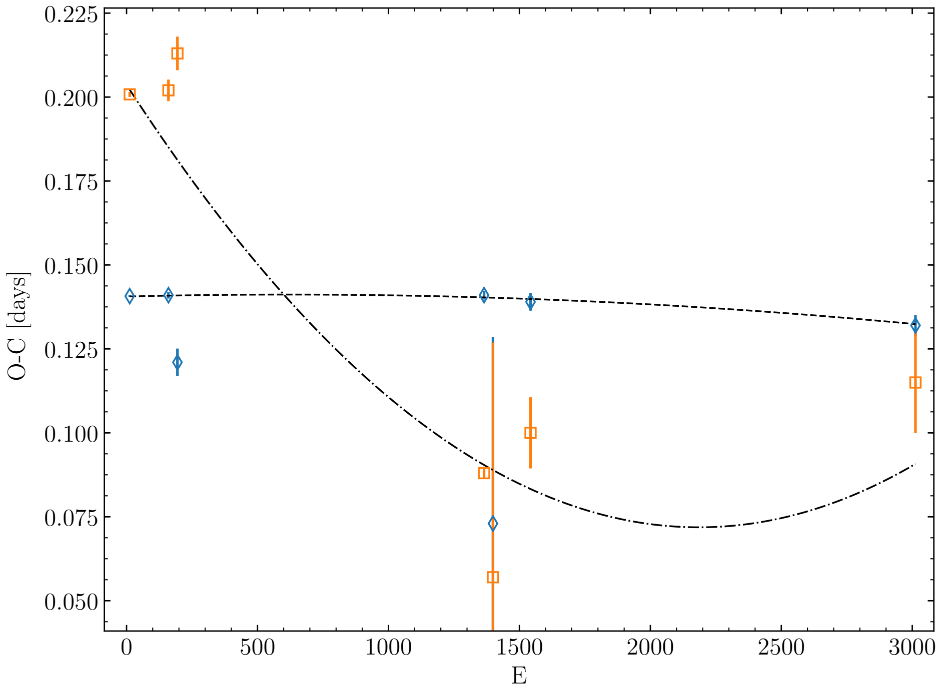

Figure 8. O–C computed from ϕ_1 (blue symbols) and ϕ_2 (red symbols) as a function of epoch E. Dashed lines are results of fitting using Equation (2).

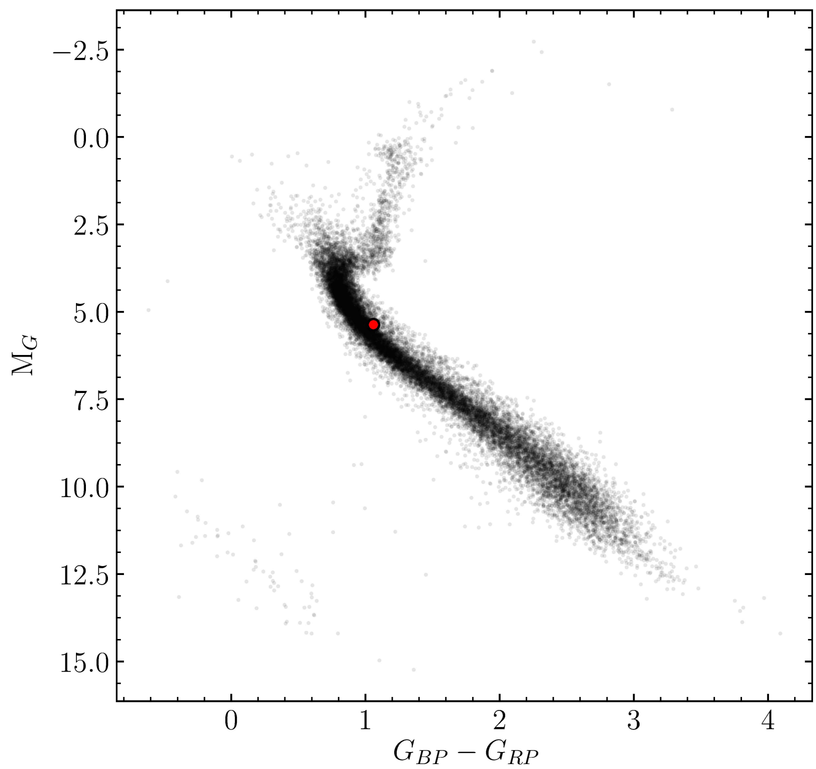

Figure 9. Color-magnitude diagram from Gaia Data Release 2 (Gaia Collaboration, 2018) for the stars in the field 4×4 degrees around the new variable star indicated by red symbol.

results from Sperauskas et al. (2016). The kinematics and metallicity indicate that this star belongs to Galactic disk.

If we assume that variability is caused by rotational modulation by a stellar spot then the period of 6.33 h and the radius of the star imply that this star is ultra-fast rotator ($\sim$ 190 km s^{-1}) which is usually an indication of young age. The possible explanation of existence of such fast rotators may be given by "magnetic saturation" of the angular momentum loss during evolution of the star and dependence of the saturation process on stellar mass.

To explain the amplitude and coherence of the variability the star spot area should be quite large and stable. It is known that bigger sports for cooler stars survive longer. But, as one can deduce using Equation (8) of (Giles et al., 2017) for r.m.s. = 0.016 and $T_{\rm eff}$=5100 K for our target gives us $\tau_{AR} \approx 200$ days which is confirmed by Figure 8 from the same work for G stars. This is as twice as shorter than observed stability (amplitude and phase) in our case.

This leads us to another (less possible) interpretation - semidetached binary system of ellipsoidal variation. To model this system I used "nightfall"[3] with a fixed period of rotation being 0.2640 days and fixed $T_{\rm eff}$ = 5100 K of the primary. I also fixed the mass of the primary to $M_{\rm prim} = 0.796$ M$\odot$. I assume that the primary is filled its Roche lobe and has synchronous rotation while secondary one is below the Roche lob and rotates asynchronous with factor $\sim$ 10.

The folded light curves for two filters and the modeled light curves are shown in Figure 10. The physical parameters of the system from the best fit "nightfall" modeling are

[3]https://www.hs.uni-hamburg.de/DE/Ins/Per/Wichmann/Nightfall.html

Table 4: Estimated system parameters from “nightfall” modeling.

$T_{\rm eff}^{\rm prim}$	$T_{\rm eff}^{\rm sec}$	$M_{\rm prim}$ $(M/M\odot)$	$M_{\rm sec}$ $(M/M\odot)$	i	Ω	e
5100 K	12170 K	0.796	0.524	49.64	64.20	0.047

shown in Table 4. I should note that this system is not an eclipsing but elliptical variable (see Figure 11 for a vizualization of the system configuration at different phases).

The period of rotation 0.2640 d is below the short limit for contact and semidetached binaries of 0.22 d.

We plan to observe this system in February-March of 2019 both photometrically and spec

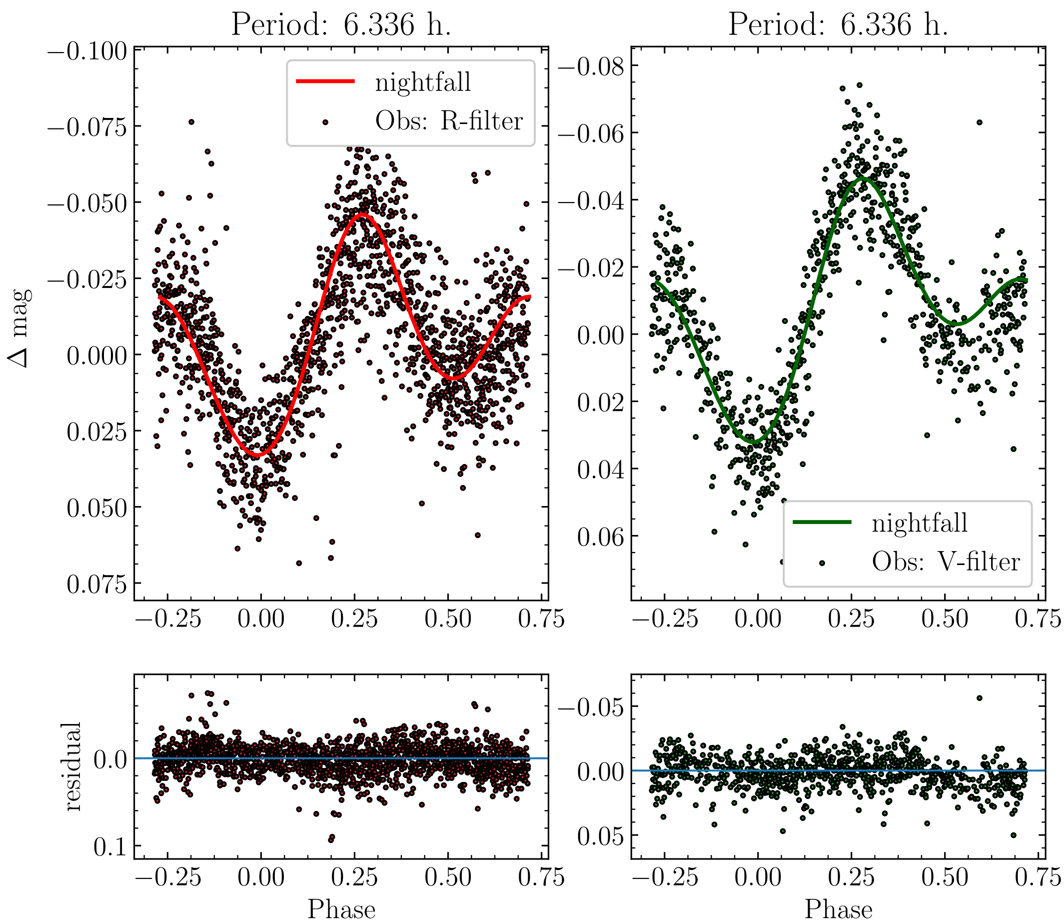

Figure 10. Top panels: folded observed light curves for filter R (on the left) and filter V and corresponding modeled light curves using “nightfall”. Bottom panels: corresponding residuals.

Acknowledgements: The work was carried out within the framework of Project No. BR05236322 “Studies of physical processes in extragalactic and galactic objects and their subsystems”, financed by the Ministry of Education and Science of the Republic of Kazakhstan.

This work has made use of data from the European Space Agency (ESA) mission *Gaia*

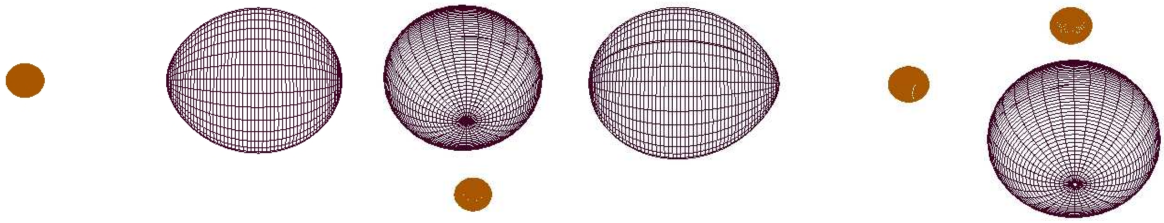

Figure 11. The space configuration of the binary system at phases = (0°, 90°, 180°, 270°) from left to right. This is elliptical variable system without the eclipse.

(`https://www.cosmos.esa.int/gaia`), processed by the *Gaia* Data Processing and Analysis Consortium (DPAC, `https://www.cosmos.esa.int/web/gaia/dpac/consortium`). Funding for the DPAC has been provided by national institutions, in particular the institutions participating in the *Gaia* Multilateral Agreement.

The author thanks the anonymous referee for his/her thorough review of the manuscript and highly appreciates suggestions and comments, which significantly contributed to improving the quality of this paper.

References:

Bertin, E., 2006, *ASP Conference Series*, **351**, 112
Edge, A. et al., 2013, *The Messenger*, **154**, 32 (VizieR: II/343/viking2)
Eker, Z. et al., 2015, *ApJ*, **149**, 131 DOI
Gaia Collaboration, 2018 *A&A*, **616**, id.A1, 22 DOI
Hartman, J. D., Bakos, G.Á., 2016, *Astronomy and Computing*, **17**, 1 DOI
Giles, H. A. C., Collier Cameron, A., Haywood, R. D., 2017 *MNRAS*, **472**, 1618 DOI
Serebryanskiy, A., Serebryakov, S., Ergeshev, A., 2018, *NEWS of the National Academy of Sciences of the Republic of Kazakhstan, Physico-Mathematical Series*, **3**, No. 319, pp. 122–133
Kim, D.-W., Bailer-Jones, C. A. L., 2016, *A&A*, **587**, A18 DOI
Miller, A. 2015, *ApJ*, **811**, 30 DOI
Sperauskas, J. et al., 2016 *A&A*, **596**, A116 DOI
Tamuz, O., Mazeh, T., North, P., 2005, *MNRAS*, **367**, 1521 DOI
VanderPlas, J. T., Ivezić, Ž, 2015, *ApJ*, **812**, 18 DOI

COMMISSIONS G1 AND G4 OF THE IAU
INFORMATION BULLETIN ON VARIABLE STARS
Volume 63 Number 6265 DOI: 10.22444/IBVS.6265

Konkoly Observatory
Budapest
8 May 2019

HU ISSN 0374 – 0676

THE RS CVn CANDIDATE DG Ari: ORBITAL AND LONG CYCLES REVEALED

ROJAS, G.; ROSALES, J. A.; CELEDÓN, I.; GARCÉS, J.; MENNICKENT, R. E.; VILLEGAS, F.

Astronomy Department, University of Concepción, Concepción, Chile. e-mail: gonzrojas@udec.cl

Abstract

DG Ari (ASAS J025521+1539.4) is a variable star that was found in the search of binary stars with periods longer than 30 days in ASAS catalogue . The source shows two periodic component in its light curve. We estimate both, the orbital period, and the long-term cycle using PDM. Additionally, we present a match with the soft X-ray source 1RXSJ025521.3+153951 located at similar position. According with these results, we discuss about its nature as a RS CVn candidate.

DG Ari is a periodic variable star located in the Aries constellation. There is a discrepancy in the determined period of the source, one being half of the other, which suggests two different explanations for its properties. Here we present some evidence that support the election of one of the possible periods. We present a general overview of the RS CVn class, following by observational data analysis that support the selected period, and finally, a brief discussion on the nature of the source.

RS Canum Venaticorum is an eclipsing binary star, the first time that the variability of this source was noticed was by Ceraski (1914). Later, the variability was well studied, and the object gave the name to a subcategory of binary systems with the same behaviour. The principal characteristics are presented in the following paragraph.

Hall (1976) have defined some binaries with orbital periods between 1 and 14 days, which present strong H and K emission in the spectrum outside the eclipse and have been defined as RS CVn stars, wherein the systems with periods longer than 14 days were classified as part of the long period group. Some of these objects are eclipsing variable systems, and show additional photometric variations, probably caused by chromospheric activity cycles lasting some years (Buccini & Mauas, 2009). These systems are composed of F-K type dwarf/giant stars. The systems with smaller orbital periods exhibit strong magnetic activity, which is thought to be related to rapid rotation of one of the components. A remarkable characteristic of these objects is the presence of soft X-ray emissions from the source, first studied by Walter et al. (1978, 1980). The X-ray emissions from those sources are considered as a tracer of coronal activity in stars. They offer laboratories to study stellar activity in post-main-sequence stars influenced by tidal effects (Strassmeier, 2009). The presence of cool spots on eclipsing RS CVn-type systems is responsible for significant variability in their light curves outside eclipses (Berdyugina, 2005).

The ROSAT space telescope was German-British-American astrophysics mission dedicated to survey the sky in X-rays. The faint X-ray source, called 1RXSJ025521.3+153951 in the ROSAT All-Sky Survey Faint Source Catalog[1] (Voges et al., 2000), was matched later to an ASAS object (ASAS J025521+1539.4) by Szczygiel et al. (2008), as a part of a larger project to search stars displaying coronal activity in the ASAS catalogue. This object shows X-ray and bolometric luminosities of $\log(L_{\rm x})= 29.207$ (log(ergs s^{-1})) and $\log(L_{\rm bol})$=32.769 (log(ergs s^{-1})) respectively, which we consider as evidence that could indicate that it is a RS CVn system.

From the ASAS catalogue[2] we get for the system $\alpha_{2000} = 02^{\rm h}{:}55^{\rm m}{:}21^{\rm s}$, $\delta_{2000} = 15^\circ{:}39'{:}24''$, $V = 11.2$ mag and $B - V = 0.53$ mag. We determined a orbital period of 34.0241856 d using the PDM IRAF[3] software (Stellingwerf, 1978). We determined the errors for the orbital period and long cycle by visual inspection of the phased light curves with trial periods near the minimum of the periodogram given by PDM. The parameters obtained from the light curve of DG Ari were summarised in Table 1. Two main frequencies of the system were disentangled using the code written by Zbigniew Kolaczkowski, described by Mennickent et al. (2012), wich is a multi-harmonic Fourier decomposition, and obtained both isolated light curves (Figures 1 and 2). We suspect that the long variability is related with the movement of a starspot over the surface of a magnetically active star present in the system. This variability is shown in Fig. 2.

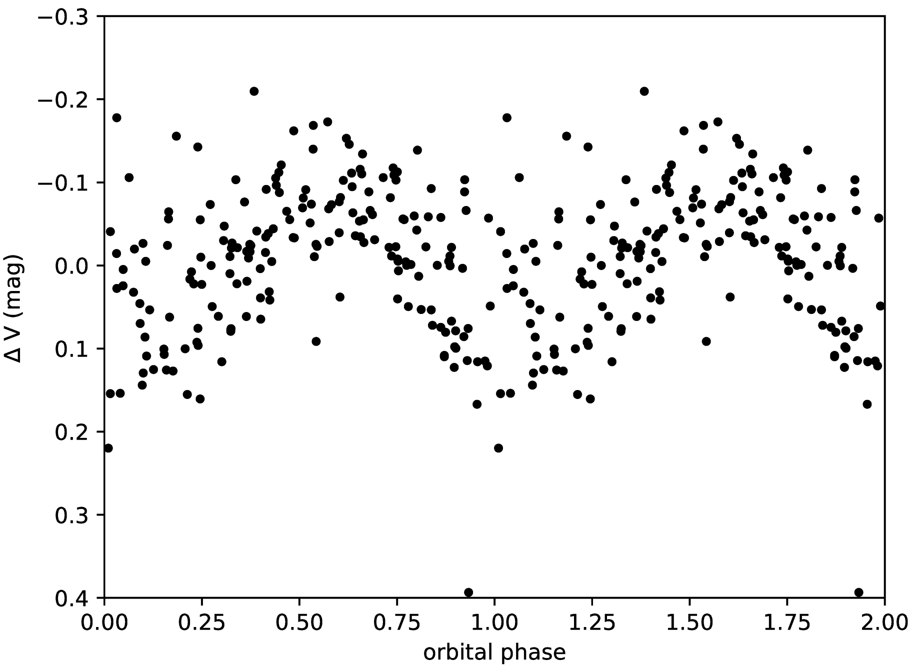

Figure 1. Disentangled light curve of DG Ari showing the short-term orbital variation.

Additional to the ASAS data, we present here observations from the Northern Sky Variability Survey (NSVS). Those data were obtained from the first generation Robotic Optical Transient Search Experiment (ROTSE-I). For the source, we found a total of 126

[1]http://www.xray.mpe.mpg.de/rosat/survey/rass-fsc/

[2]http://www.astrouw.edu.pl/asas/

[3]IRAF is distributed by the National Optical Astronomy Observatories, which are operated by the Association of Universities for Research in Astronomy, Inc., under cooperative agreement with the National Science Foundation.

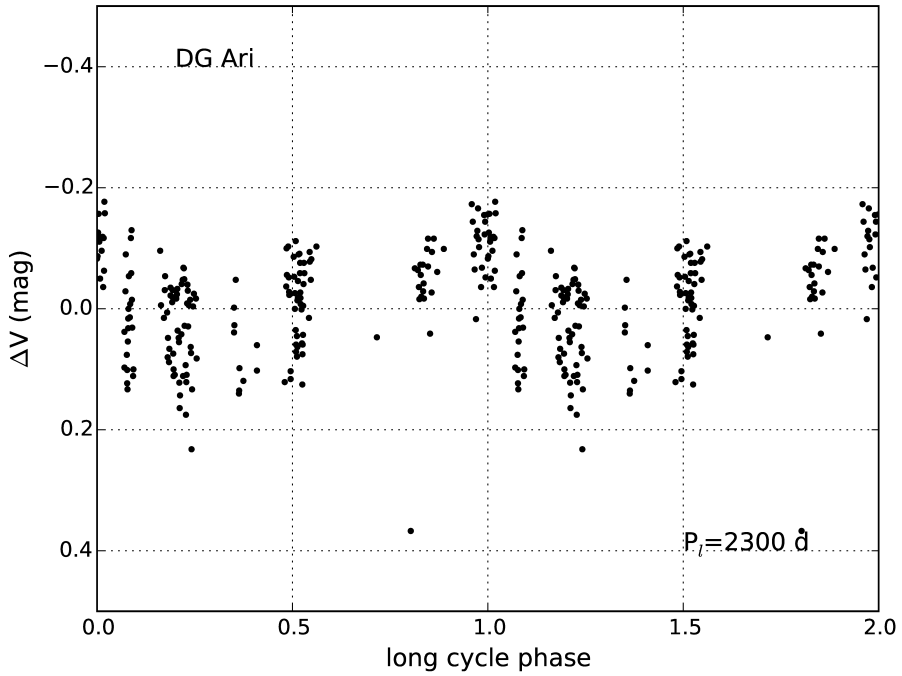

Figure 2. Disentangled light curve of DG Ari showing the long-cycle variation.

points that are qualified as good points by SKYDOT. The median ROTSE magnitude presented for the object is 11.166 ± 0.012 mag. The light curve is shown in Fig. 3. The reason we are not showing the long period phase light curve is that the time series covers only 157 days, too short compared to the long cycle, therefore, is impossible to cover the total phase of the long variation.

These results are consistent with Lloyd et al. (2011), who identified this object as a chromospherically active star in the ROTSE-1 database. They identified the object as GSC 01224–00894, with a period of 33.998 days, roughly similar to the period reported here. They also identified the object as a possible RS CVn variable.

In Figure 4 we show, the position of the faint X-ray source 1RXSJ025521.3+153951 (marked with a cross) and the ASAS object J025521+1539.4 (the brightest nearest star) separated a distance of 27.356″ (Szczygiel et al., 2008). Image taken from Aladin Lite[4].

The possibility to fit two different periods, one being half of the other, is related to the nature of the source. For the first case, when the period is 34.024 days, the possible source could be a magnetically active star, and the periodicity would be related to the presence of a spot on its surface, which means that the associated period is the rotational period of the object.

The other possibility is when the period is twice the mentioned period, as ASAS catalogue suggest. It is possible to see both eclipses on the light curve, and the nature of the source could correspond to a binary system were one of the stellar component shows

[4] `https://aladin.u-strasbg.fr/AladinLite/`

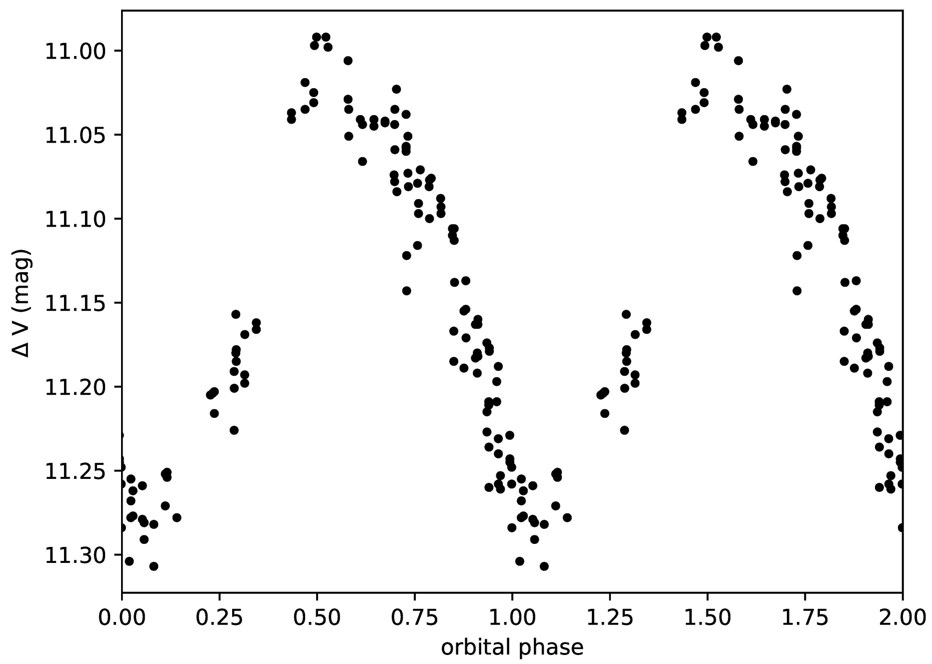

Figure 3. Phased light curve of DG Ari, the period we used was 34.024 d. Data from the NSVS database.

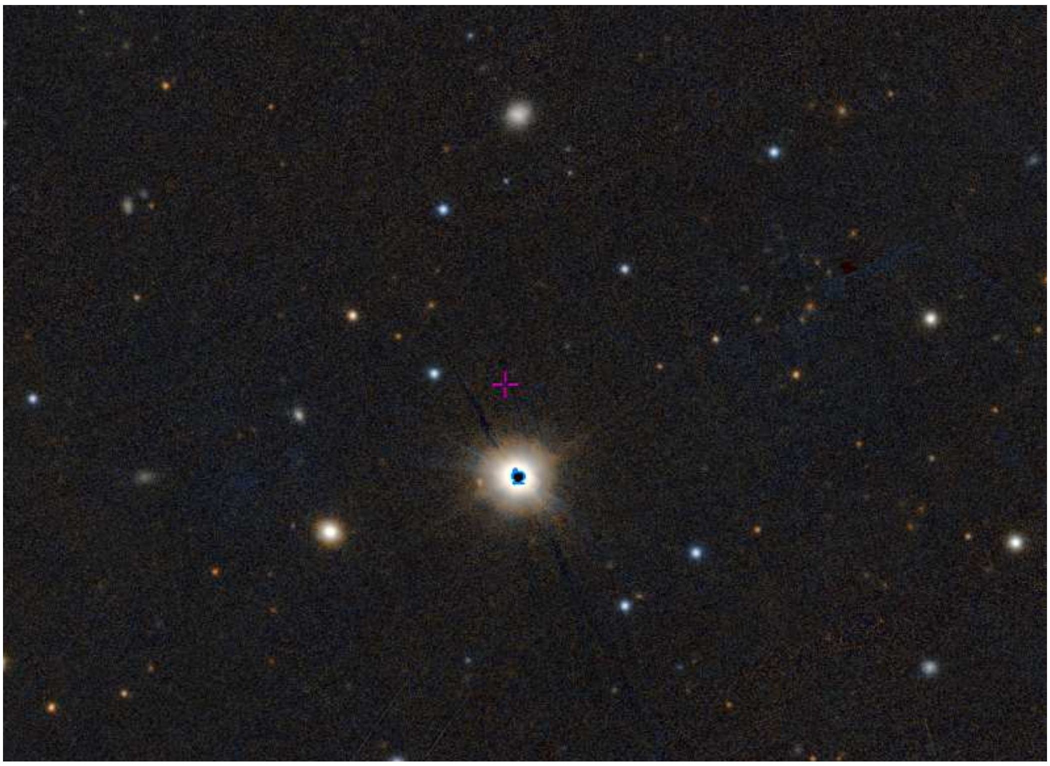

Figure 4. Position in the sky of 1RXSJ025521.3+153951 marked with the central cross. The brightest nearest star correspond to the position of DG Ari. The FoV of the image is 7.2′.

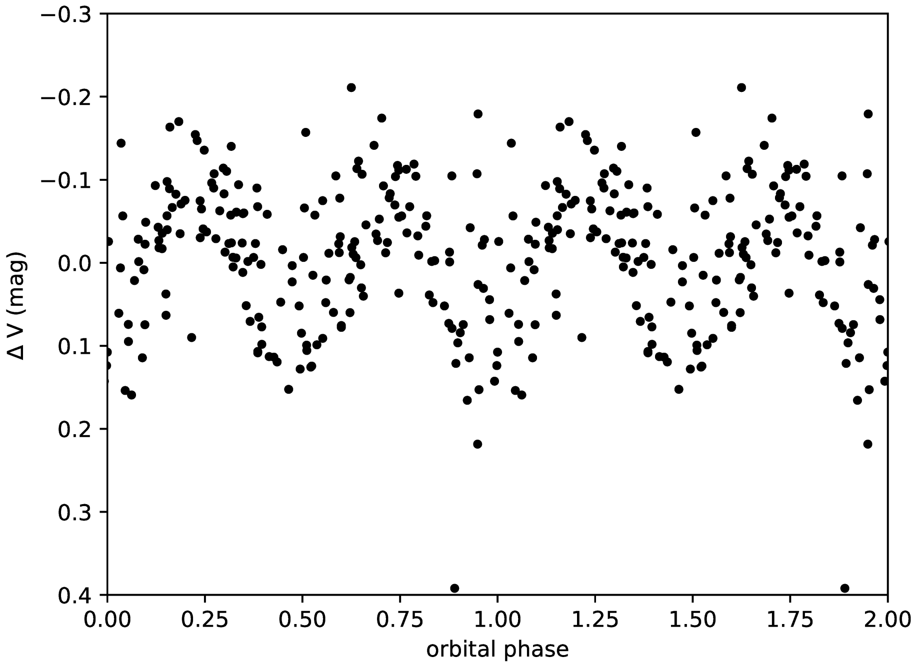

Figure 5. Phased light curve for DG Ari with period of 68.205 days, from the NSVS database.

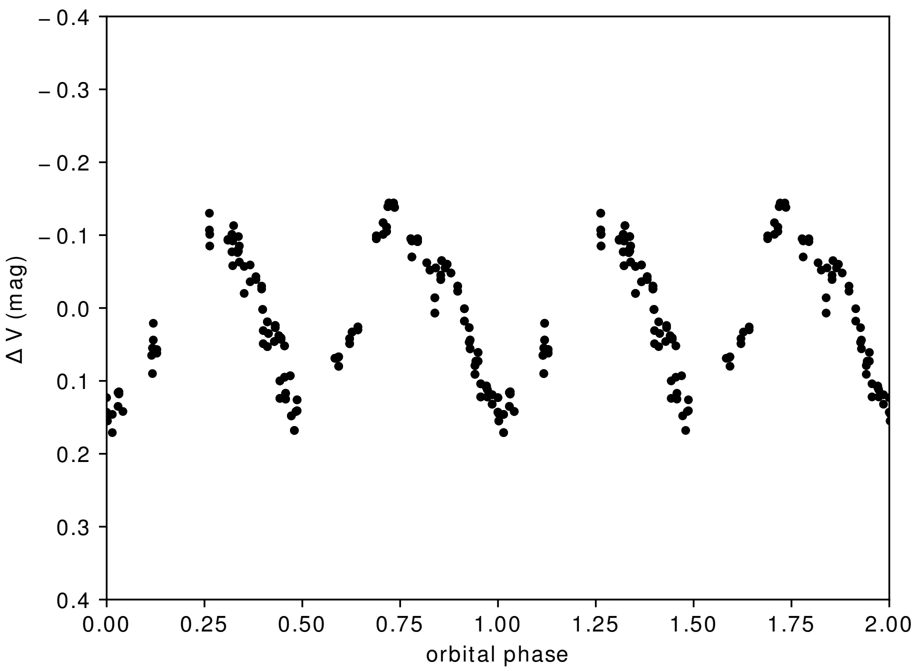

Figure 6. Phased light curve for DG Ari with period of 68.205 days, ASAS observations.

Table 1: Parameters of DG Ari including its orbital (P_o) and long period (P_l). Epoch for both the minimum brightness of the orbital light curve and the maximum brightness of the long-cycle light curve are given.

ASAS-ID	025521+1539.4
Other ID	DG Ari
RA (2000)	02:55:21
DEC (2000)	15:39:24.0
P_o (d)	34.0241856
P_l (d)	2300.291
$T_0(\min_o)$ (HJD–2450000)	3016.60213
$T_0(\max_l)$ (HJD–2450000)	4760.72312
V (ASAS) (mag)	11.2

magnetic activity. In Figures 5 and 6 we show the possibility of a different period of 68.8 days. From the shape of the light curve in this case, we assume that the system should have very close components, but the period is too long, so the stellar components must be very massive, which is a doubtful scenario. The explanation we assume for the long term variability, is the presence of a cyclic activity on the source, related to the number of star spots on the star with period similar to 6.5 years. We expect to study the spectral characteristics of this object in the future, in order to understand the possible nature of DG Ari.

References:

Berdyugina, S. V., 2005, *Living Reviews in Solar Physics*, **2**, 8 DOI
Buccino, A. P., Mauas, P. J. D., 2009, *A&A*, **495**, 287 DOI
Ceraski, W., 1914, *AN*, **197**, 256
Hall, D. S., 1976, *IAU Colloq. 29: Multiple Periodic Variable Stars*, **60**, 287 DOI
Lloyd, C.; Schirmer, J.; Bernhard, K.; Frank, P., 2011, *OEJV*, **136**, 1
Mennickent, R. E., Djurašević, G., Kołaczkowski, Z., & Michalska, G. 2012, *MNRAS*, **421**, 862 DOI
Percy, J. R., Soondarsingh, D., Velocci, V. 2001, *JAAVSO*, **29**, 82 DOI
Pojmanski, G. 1997, *AcA*, **47**, 467
Stellingwerf, R. F. 1978, *ApJ*, **224**, 953 DOI
Strassmeier, K. G. 2009, *Astr. Astron. Reviews*, **17**, 251 DOI
Szczygiel, D. M., Socrates, A., Paczynski, B., Pojmanski, G., Pilecki, B., 2008, *AcA*, **58**, 405
Voges, W., Aschenbach, B., Boller, T. et al., 2000, *IAU Circular*, 7432, 1
Walter, F., Charles, P., Bowyer, S., 1978, *ApJ*, **225**, L119 DOI
Walter, F. M., Cash, W., Charles, P. A., Bowyer, C. S., 1980, *ApJ*, **236**, 212 DOI

COMMISSIONS G1 AND G4 OF THE IAU
INFORMATION BULLETIN ON VARIABLE STARS
Volume 63 Number 6266 DOI: 10.22444/IBVS.6266

Konkoly Observatory
Budapest
8 May 2019

HU ISSN 0374 – 0676

RZ COMAE – A W-TYPE OVERCONTACT ECLIPSING BINARY

NELSON, R.H.[1,2,3]; ALTON, K.B.[3,4]

[1] Mountain Ash Observatory, 1393 Garvin Street, Prince George, BC, Canada, V2M 3Z1 email: bob.nelson@shaw.ca

[2] Guest investigator, Dominion Astrophysical Observatory, Herzberg Institute of Astrophysics, National Research Council of Canada

[3] Desert Bloom Observatory, Benson AZ, 31°56.′454 N, 110°15.′450 W

[4] UnderOak Observatory, 70 Summit Ave, Cedar Knolls, NJ, USA, email: kbalton@optonline.net

Abstract

RZ Com (GSC 1990-2841) is a short period (P = 0.3385 d) W UMa–type binary system, type–W, which has had, over the years, two spectroscopic and numerous light curve studies. The various mass determinations show a large scatter. Here we present the results of new light curve and radial velocity observations, and a fresh analysis by the Wilson-Devinney 2003 code. We have been able to obtain a unified model for photometric five datasets, each used one or more filters. The main model parameters such as mass ratio, temperature, potential, and inclination were in close agreement, as were derived quantities such as mass, stellar radius, etc. Only the spot parameters differed, as one might expect. Further, we determined a distance estimate, r = 204 ± 5 pc, in good agreement with the *Gaia* value of r = 203.1 ± 3.7 pc. We also presented four new eclipse timings, performed a renewed period analysis attaining a LiTE fit. With that we determined a rate of intrinsic period change $dP/dt = 3.86(2) \times 10^{-8}$ days/year, and–assuming conservative processes–a rate of mass exchange $dm_1/dt = -4.1(3) \times 10^{-8}\ M_\odot$/year which means that the less massive star is losing mass to its companion.

The identity of the discoverer of the variability of RZ Com (AN 5.1929; TYC 1990-2841-1) is not clear. However, we do know that S. Gaposchkin (1932, 1938) obtained early photometric light curves and times of minima, and deduced an inclination of 81°. Likely it was he who first identified the system as a W Ursae Majoris type.

Thereafter, Struve & Gratton (1948) performed spectrographic observations at the McDonald Observatory using the 2.08-m reflector, the f/2 Schmidt camera, the Cassegrain spectrograph with its glass prisms, and 103a-O film. As the reciprocal dispersion was 76 Å/mm, there was considerable scatter in their radial velocity (RV) plots (rms deviation from curves of best fit 36 km/s). However, they did deduce a spectral type of 'approximately' K0, a system velocity of -12 km/s, amplitudes K_1 and K_2 of 270 and 130 km/s respectively, and therefore a mass ratio of $q = m_2/m_1 = 2.1$. Further, they also observed that the more massive component was eclipsed at secondary minimum. (This type of system, later described as W-Type by Binnendijk (1970), features the hotter, less massive star eclipsed at primary minimum. That event, the deeper eclipse, is then an occultation, resulting in a short interval of constant light. We will follow the convention of designating that star as m_1, hence mass ratios of $q = m_2/m_1 > 1$ will ensue.)

Kopal (1955) in his classification of some 63 close binary systems listed RZ Com with solar masses of 0.8 and 1.6, spectral types of G9 and K0, and $\log T$ (temperature) values of 3.72 and 3.71 respectively [corresponding to $T_1 = 5250$ K and $T_2 = 5230$ K]. The next photometric observations were by Broglia (1960) using a yellow ($\lambda = 5300$ Å) filter. Although the paper is unavailable, Binnendijk (1964) described the normal (binned) results and kindly reproduced the data. Thus, in 1958 Broglia obtained two sets of these light curves within an interval of about four months, and noted changes to the light curve during that interval. The primary minima, with short periods of constant light (during the total eclipses), were the same, but the second light curve was about 0.02 magnitudes brighter everywhere else. Binnendijk (1964) analyzed the light curves of Broglia using the rectification method, and determined (amongst other things) an inclination of 81.1°. He then combined the RV elements from Struve & Gratton (1948) to obtain masses of $m_1 = 0.77\,M_\odot$ and $m_2 = 1.59\,M_\odot$. Broglia had assumed that the differences in the light curves could be explained by a change in the outer surface of the smaller component during secondary eclipse. However, because of the asymmetry in the light curves, Binnendijk suggested that the effect could be better explained by an asymmetrically positioned subluminous region (viz., a dark spot) on the facing (back) side of the larger star.

Pointing out that the Russell-Merrill (1952) rectification method breaks down for contact binaries, (Wilson & Devinney, 1973) discussed progress in physical models to that date (see references therein). Promoting the advantages of their newly published physical light curve analysis package Wilson & Devinney (1971), they then re-analyzed the photometric data of Broglia (1960) along with the radial velocity data of Struve & Gratton (1948). However, in an apparent effort to illustrate systems that could be analyzed by mode 1 (overcontact, $T_1 = T_2$), they made some unorthodox assumptions. Admitting that using radiative atmospheres was unusual for G9+K0 systems, they went ahead anyway and allowed the gravity exponent g to vary, obtaining the very different values of $g = 1.13$ and 1.51 for data taken for the same binary system separated by only two or three months. An anonymous referee pointed out that the 1973 W–D code did not include the capability of adding spots; hence that might explain the "strange gravity darkening exponents".

They also concluded that the system was in marginal contact, with the first data set indicating slightly overcontact and the second, undercontact. [Using their values for the mass ratio and potential, we found the fillout parameters to be 0.0418 and −0.0589, respectively.] It does not seem possible to us on physical grounds that the system could change so significantly on such a short time span. In their paper there is no discussion of the possibility of a star spot or of third light. In view of their unphysical assumptions, one might be tempted to reject their results entirely; however the closeness of their curve fits causes one to pause. At the very least, the situation raises unsettling questions about uniqueness of WD solutions.

The next spectroscopic observations were by McLean & Hilditch (1983) at the Dominion Astrophysical Observatory (DAO) at Victoria, B.C., Canada using the 1.83-m Plaskett telescope, the Cassegrain spectrograph, and IIa-O plates. Reciprocal dispersion was 30 Å/mm. Although there was moderate scatter in their data [rms deviation from curves of best fit ~ 25 km/s], they did deduce a system velocity of −1.8(5) km/s, and amplitudes K_1 and K_2 of 248.0(9) and 107.0(6) km/s respectively.

Thereafter photometric observations were taken by Rovithis & Rovithis-Livaniou (1984) at the Kryonerion Astrophysical Station in Greece, using the 1.2 m Cassegrain reflector with a two-beam multi-mode photometer. Their published data, in B and V light, display an unusual shape and although nine new times of minima were reported, they made no attempt to model the data. Numerous attempts by the lead author at modelling their light curves (which more represent those of a detached system) all failed. Therefore the validity of their data must remain questionable.

Table 1: Various determinations of the RZ Com spectral type.

Reference	Sp. Type
Struve & Gratton (1948)	K0
Wood et al. (1980)	F7+K0
Batten et al. (1989)	G2Vn
Perryman et al. (1997) - Hipparcos Cat.	G0Vn

Rovithis-Livaniou et al. (2002) also published a paper attempting to analyze the period variations; however the listed data—while numerous—did not allow for any meaningful conclusions about the period behaviour due to the limited time interval spanned by the data. In addition, they did point to the lack of agreement as to the spectral type, referencing four disparate classifications. These are given in Table 1.

Xiang & Zhou (2004) obtained a B band light curve at the Yunan Observatory in China using the 1.00-m reflector telescope and a CCD camera. They extracted five new times of minima from their published data and proceeded to perform a photometric analysis using the 1992 version of the Wilson-Devinney code. Using the 'q-search' method they obtained two solution sets with mass ratio values of 0.8 and 2.2 and "[could not] say which of the two results is accurate". This is in spite of the fact that there were two radial velocity datasets available Struve & Gratton (1948); McLean & Hilditch, (1983) which would have resolved the issue. Unfortunately, there also seemed to be some confusion between the different naming conventions (for m_1 and m_2) typically used by spectroscopists and photometrists.

Lastly, Qian (2001) and Qian & He (2005) presented period analyses. The latter paper presented four new times of minima and a light time effect (LiTE) analysis of the—by now—extensive data set. The analysis was updated in a review paper by Nelson et al. (2016), who obtained similar results. Both LiTE fitting results, along with those of this paper, are presented in Table 14.

Because more modern techniques promised to improve the radial velocity data, the lead author (R.H.N.) first secured, in the springs of 2016, 2017, and 2018, a total of 14 medium resolution (R$\sim$10000 on average) spectra of RZ Com at the DAO using the 1.83 m Plaskett Telescope. This system features a Cassegrain spectrograph fitted with (in this case) the 21181Yb grating (1800 lines/mm and blazed at 5000 Å) which produces a first order linear dispersion of 10 Å/mm. The wavelengths ranged from 5000 to 5260 Å, approximately. A log of observations is given in Table 2 and an eclipse timing diagram, in Figs. 11 and 12 later in the paper. The latter was used to derive the following elements (Eq 1), used for both this photometric data set and also RV phasing:

$$\text{JD (Hel) Min I} = 2458253.6296\ (152) + 0.3385075\ (4) \tag{1}$$

where the quantities in brackets are the standard errors of the preceding quantities in units of the last digit.

Frame reduction was performed by software RaVeRe (Nelson 2013). See Nelson (2010) and Nelson et al. (2014) for further details. The normalized spectra are reproduced in Fig. 1, sorted by phase (the vertical scale is arbitrary). Note towards the right the strong neutral iron lines (at 5167.487 and 5171.595 Å) and the strong neutral magnesium triplet (at 5167.33, 5172.68, and 5183.61 Å).

Radial velocities were determined using the Rucinski broadening functions (Rucinski 2004, Nelson 2010) as implemented in software Broad25 (Nelson 2013). See Nelson

Table 2: Log of DAO observations.

DAO Image #	Mid Time (HJD−2400000)	Exposure (sec)	Phase at Mid-exp	V_1 (km/s)	V_2 (km/s)
16-1275	57493.7798	2831	0.294	−228.7 (4.9)	133.0 (5.1)
16-1331	57495.9583	3600	0.729	254.1 (2.2)	−94.3 (6.1)
16-1431	57498.6938	3600	0.810	241.6 (2.6)	−89.2 (4.5)
16-1433	57498.7365	3600	0.937	—	−33.0 (2.6)
16-1439	57498.8335	3600	0.223	−232.8 (4.0)	123.4 (4.1)
16.1441	57498.8774	3600	0.353	−173.1 (2.5)	85.3 (2.3)
16-1455	57499.6844	2400	0.737	270.4 (3.0)	−103.5 (3.2)
16-1467	57500.8635	1605	0.220	−235.2 (3.7)	122.4 (4.9)
16-1484	57504.7129	2100	0.592	136.6 (7.1)	−81.4 (4.5)
16-1502	57504.9060	1800	0.162	−203.0 (4.6)	103.4 (3.5)
17-3989	57859.7304	900	0.365	−177.9 (4.9)	116.7 (3.1)
18-5239	58231.8677	1800	0.712	258.7 (3.2)	−102.1 (5.5)
18-5342	58233.9179	1800	0.769	268.7 (2.3)	−101.7 (6.7)
18-5486	58241.8496	1800	0.200	−222.4 (3.9)	114.5 (2.0)

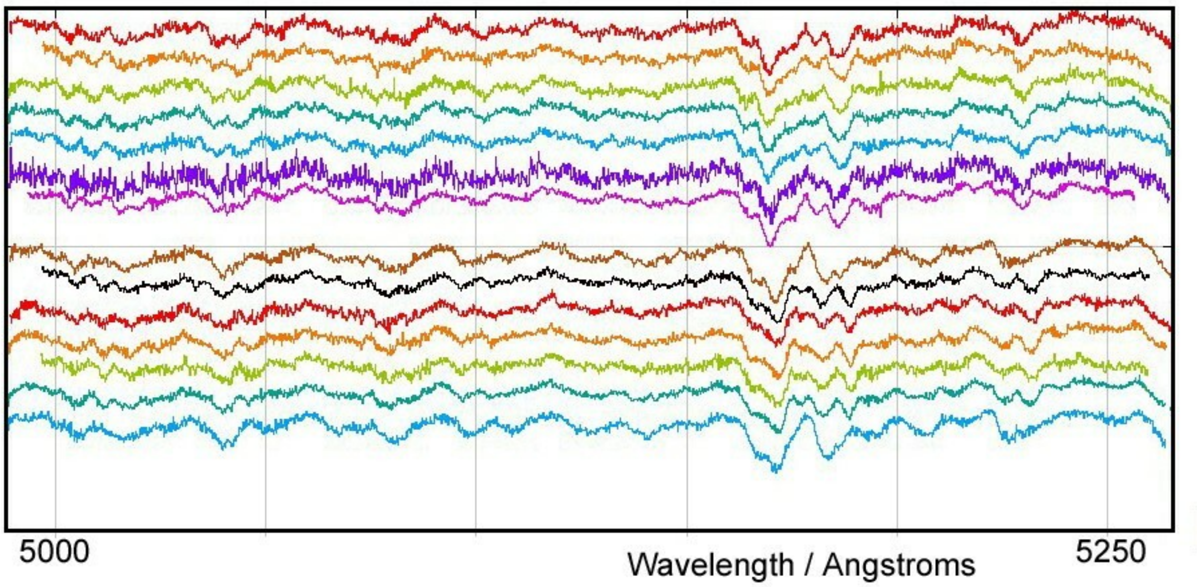

Figure 1. RZ Com spectra at phases 0.162, 0.200, 0.220, 0.223, 0.294, 0.353, 0.365, 0.592, 0.712, 0.729, 0.737, 0.769, 0.810, 0.937 (from top to bottom). Each has been shifted vertically for clarity. The vertical scale is arbitrary.

et al. (2014) for further details. An Excel worksheet (with built-in macros written by him) was used to do the necessary radial velocity conversions to geocentric and back to heliocentric values (Nelson 2014). The resulting RV determinations are also presented in Table 2 along with standard errors (in units of the last digits, enclosed in brackets). The mean rms errors for RV_1 and RV_2 are 6.9 and 11.7 km/s, respectively, and the overall rms deviation from the (sinusoidal) curves of best fit is 12.6 km/s. The best fit yielded the values $K_1 = 249.5(0.7)$ km/s, $K_2 = 114.9(0.9)$ km/s and $V_\gamma = 11.5(0.5)$ km/s, and thus a mass ratio $q_{\rm sp} = K_1/K_2 = m_2/m_1 = 2.17(2)$.

Representative broadening functions, at phases 0.223 and 0.737 are depicted in Figs. 2 and 3, respectively (the vertical scale is arbitrary). Smoothing by a Gaussian filter is routinely done in order to centroid the peak values for determining the radial velocities.

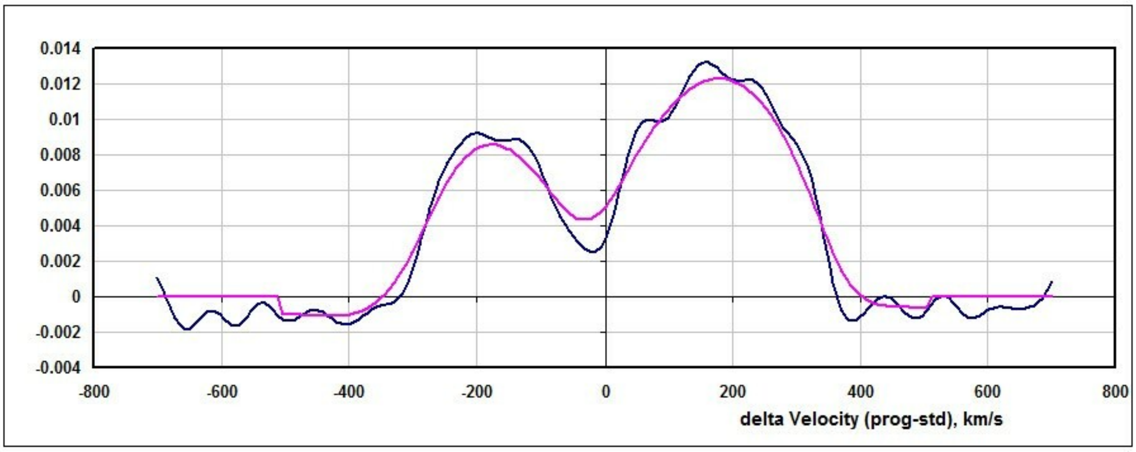

Figure 2. Broadening functions (arbitrary intensity) at phase 0.223—smoothed and unsmoothed.

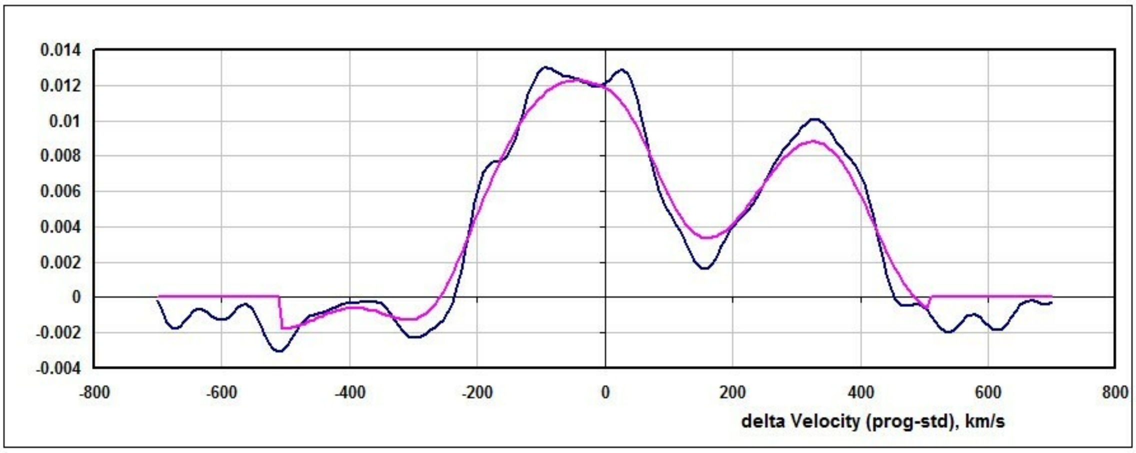

Figure 3. Broadening functions (arbitrary intensity) at phase 0.223—smoothed and unsmoothed.

During four nights in 2018, May 8-18, the lead author took a total of 164 frames in V, 168 in $R_{\rm C}$ (Cousins) and 165 in the $I_{\rm C}$ (Cousins) bands at Desert Blooms Observatory, jointly owned by the authors. Hosted at the San Pedro Observatory complex located

Table 3: Details of variable, comparison and check stars.

Object	TYC	RA (J2000)	Dec (J2000)	V (mag)	$B-V$ (mag)
Variable	1990-2841-1	$12^h35^m05.06^s$	$+23°20'14''.0$	10.440 (32)	+0.506 (49)
Comparison	1990-1707-1	$12^h34^m24.41^s$	$+23°27'14''.4$	10.571 (57)	0.415 (60)
Check	1990-3503-1	$12^h35^m18.50^s$	$+23°18'11''.4$	12.161 (48)	0.537 (56)

near Benson Arizona, the telescope is operated remotely. It consists of a Software Bisque Taurus 400 equatorial fork mount, a Meade LX-200 40 cm Schmidt-Cassegrain optical assembly operating at f/7, a SBIG STT-1603 XME CCD camera (with a field of view $11 \times 18'$), and a filter wheel with the usual B, V, R_C, and I_C filters. For unattended operation, automatic focusing is required owing to the large temperature changes throughout the night (typically +35°to +10°C in late spring).

Standard reductions were then applied (see Nelson et al. 2014 for more details). The variable, comparison, and check stars are listed in Table 3. The coordinates are from the Gaia Catalogue, DR2 and magnitudes are from the APASS catalogue DR9 (Henden, et al. 2009, 2010; Smith et al. 2010).

Radial velocity and light curve analysis was carried out using the 2003 version of the Wilson-Devinney (WD) analysis program with Kurucz atmospheres (Wilson & Devinney, 1971, Wilson et al. 1972, Kurucz 1979, Wilson 1990, Kallrath & Milone 1998, Wilson 1998) as implemented in the Windows front-end software WDwint Nelson (2013). In this process, the first task one faces is to determine the effective temperature of the more luminous component, either from the published spectral type or by some other means. However, as noted in Table 1, the correct classification is unclear. Following the initial classification of Struve & Gratton (1948), which was from actual spectra, and also that of earlier workers, the lead author initiated modelling assuming a spectral type of K0 and an effective temperature T_2 of 5247 ± 150 K based on the calibration of Flower (1996). The choice of this later spectral type was further justified because the computed total mass from the RV curves (assuming 90° inclination) was 1.70 solar masses which nicely corresponds to the tabular value of 1.60 solar masses for a main-sequence G9+K0 pair. Also, because the system was known to be of the W-type subclass (the secondary star in this convention) is the more massive, and can be expected to be more luminous, therefore dominating the classification spectra. Therefore temperature T_2 was held fixed, and temperature T_1 was varied to attain the best fit. (In view of the 'approximate' characterization of Struve & Gratton's classification, the error estimate for T_2 is based on $1\frac{1}{2}$ subclasses.) From the interpolated tables of Cox (2000), a $\log g$ value of 4.476 (cgs) was assumed.

An interpolation program by Terrell (1994), available from Nelson (2013) gave the Van Hamme (1993) limb darkening values; and finally, a logarithmic (LD=2) law for the limb darkening coefficients was selected, appropriate for temperatures < 8500 K (ibid.). The limb darkening coefficients are listed below in Table 4. The values for the second star are based on the later-determined temperature of $T_1 = 5420$ K, $\log g_1 = 4.475$ (and assumed spectral type of G8.) Convective envelopes for both stars were used, appropriate for cooler stars (hence values gravity exponent $g = 0.32$ and albedo $A = 0.5$ were used for each).

From the GCVS 4 designation (EW/KW) and from the shape of the light curve, mode 3 (overcontact) mode was used. Initial fitting was accomplished in LC mode by examining the computed and actual light curves in one passband (V), and adjusting the parameters. Thereafter, convergence using differential corrections (DC) and the method of multiple subsets was reached in a small number of iterations. (See Wilson & Devinney (1971) and

Table 4: Limb darkening values from Van Hamme (1993) for $T_{1,2}$ and $\log g_{1,2}$ as above. The Y band was used in Broglia (1960) and corresponds to a central wavelength of 5300 Angstroms.

Band	x_1	x_2	y_1	y_2
B	0.849	0.851	0.078	0.040
Y	0.795	0.802	0.166	0.150
V	0.782	0.790	0.187	0.156
R_C	0.713	0.725	0.220	0.198
I_C	0.628	0.638	0.223	0.207
Bol	0.648	0.647	0.188	0.175

Kallrath & Milone (1998) for an explanation of the method.) The subsets were: (a, V_γ, q, L_1), (T_1, Ω_1), and (i, L_1). Following the recommendation of Binnendijk (1964), a cool spot was added to star 2 near the neck (that is, with a longitude near 0°). At the time, it was believed necessary to add third light, l3.

Following the example of Alton (2010) in which a unified physical light curve model for AC Boo was achieved for no fewer than eight data sets (the light curve differences being due to a time-varying cool spot), the lead author (RHN) proceeded to attempt the same feat using the data sets of Broglia (1960), Xiang & Zhou (2004), Rovithis & Rovithis-Livaniou (1984), and He & Qian (2008). No solution for the third (R&R-L) data set was possible owing to the strange, non-standard shape of the light curves, and to the disparate eclipse depths between light curves. The eclipse depths were comparable in the blue bandpass while, in the visual bandpass, the secondary depth was much shallower. (No known mechanism could account for this disparity, so modelling attempts were abandoned.)

However, comparable fits were achieved for the present data set, and for those of the other three listed above. All spots were placed on star 2 (the more massive) with the exception of the data of Xiang & Zhou (2004), for which the best solution involved no spot. However, there was a snag. When the co-author (KBA) joined the study, he pointed out that, based on his compilation of contemporary colour magnitude differences ($B-V$), the system was likely hotter. Further, the Tycho catalogue Wright, et al., (2003) lists the system as G0Vn, temperature $T_2 = 6030$ K, $\log g_2 = 4.371$. (It was later determined that $T_1 = 6236$ K and $\log g_1 = 4.365$).

No definitive stellar classification supported by UV or-visible spectra is published for RZ Com. Instead, we relied upon an ensemble of $B - V$ colour indices from astrometric and photometric catalogues available through VizieR and those published by Terrell et al. (2012). (See Table 5.) Colour excess was estimated according to Amôres & Lépine (2005) using the companion program ALextin which requires the Galactic coordinates (l,b) and an estimated distance in kpc. The most recent parallax values reported in Gaia DR2 were used (Gaia Collaboration, 2018). Accordingly Alextin iterated a value for interstellar extinction AV, (which led to the corresponding dereddening $E(B-V) = A_V/3.1$ correction for objects within the Milky Way Galaxy and ultimately intrinsic colour $(B - V)_0$). Outliers within the different sources used for $B - V$ colour indices were statistically eliminated from consideration using Grubbs Test (Grubbs 1950) as implemented in the Real Statistics package for Excel. Thereafter the median $(B - V)_0$ result was used to define the effective temperature of the more luminous star and its corresponding spectral class Pecaut & Mamajek (2013). When we used this approach, the adopted effective temperature ($T_{\rm eff2} = 6070$ K) for RZ Com (Table 5) proved to be slightly higher (6070 vs. 5989 K) but within the confidence intervals reported in the Gaia DR2 release of stellar

Table 5: Spectral classification of RZ Com based upon dereddened[a] $(B-V)$ data from various catalogues and surveys.

Catalogue/Survey	$(B-V)_0$	$T^{\rm b}_{\rm eff2}$	Spectral Class[C]
Tycho	0.5100	6240	F7V-F8V
2MASS	0.5539	6034	F9V-G0V
SDSS-DR9	0.5154	6216	F7V-F8V
Terrell et al. (2012)	0.5456	6072	F8V-F9V
APASS	0.4996	6280	F6V-F7V
ASCC	0.5506	6047	F8V-F9V

a: $E(B-V) = 0.0074$;
b: $T_{\rm eff2}$ interpolated + spectral class assigned for most luminous star from Pecaut & Mamajek (2013);
c: Median value for $(B-V)_0 = 0.546 \pm 0.008$; $T_{\rm eff2} = 6070 \pm 93$ K; Spectral class = F8V-F9V

Table 6: New times of minima for V500 Cyg obtained in this study.

Band.	x_1	x_2	y_1	y_2
B	0.841	0.825	0.209	0.185
Y	0.781	0.786	0.230	0.200
V	0.721	0.740	0.267	0.258
$R_{\rm C}$	0.681	0.668	0.279	0.272
$I_{\rm C}$	0.568	0.584	0.271	0.264
Bol	0.640	0.644	0.233	0.225

parameters (Andrae et al. 2018).

It could be argued that the orbital phase at which each of the above $(B-V)_0$ observations was taken is unknown, and therefore taking the mean is questionable. However, in view of the fact that the temperatures of each component are shown below to be very close, it is unlikely that the colour indices could vary to any great extent over an orbital cycle, and certainly less than the variations between values displayed above.

Accordingly, revised values from the van Hamme tables for $T_{1,2} = 6276$, 6070 K, $\log g_{1,2} = 4.365$, 4.371 respectively were determined and listed in Table 6.

We will start with the 2018 data sets presented in this paper; the two solutions are presented in Table 7. Owing to the fact that the light curve plots are virtually indistinguishable, only one plot (B) is presented in Fig. 4.

From Mochnacki (1981), the fill-out factor is $f = (\Omega_{\rm I} - \Omega)/(\Omega_{\rm I} - \Omega_{\rm O})$, where Ω is the modified Kopal potential of the system, $\Omega_{\rm I}$ is that of the inner Lagrangian surface, and $\Omega_{\rm O}$, that of the outer Lagrangian surface, was also calculated.

For the most part, the error estimates (for this data set only) are those provided by the WD routines and are known to be underestimated; however, it is a common practice to quote these values and we do so here. Also, estimating the uncertainties in temperatures T_1 and T_2 is somewhat problematic. A common practice is to quote the temperature difference over–say–one spectral sub-class. assuming that the classification is good to one spectral sub-class, (the precision being unknown in this case). In addition, various different calibrations have been made Flower (1996) and Pecaut & Mamajek (2013), and classification is ± one sub-class, an uncertainty of ± 200 K to the absolute temperatures of each, would be reasonable. (The modelling error in temperature T_1, relative to T_2, is indicated by the WD output to be much smaller, around 9 K.)

Trials were also run with the spot on the neck side of star 1 (the hotter star); however, all trials resulted in residuals higher by about 5%. Also, starting with solution B ($T_2 =$

Table 7: Wilson-Devinney parameters for the present dataset.

WD Quantity	Sol'n A	Sol'n B	Error	Unit
Temperature, T_1	5420	6276	200	K
Temperature, T_2	5257	6070	[fixed]	K
$q = m_2/m_1$	2.174	2.179	0.009	—
Potential, $\Omega_1 = \Omega_2$	5.396	5.393	0.010	—
Inclination, i	86.3	86.8	0.6	degrees
Fill-out factor, f_1	0.100	0.11	0.01	—
Semi-major axis, a	2.49	2.49	0.02	$R_\odot$
System RV, V_γ	12.4	12.4	1.4	km/s
Phase shift	0.0021	0.0021	0.0001	—
L_3 (V)	0.021	—	0.003	—
L_3 (R_C)	0.015	—	0.003	—
L_3 (I_C)	0.009	—	0.004	—
$L_1/(L_1 + L_2)$ (V)	0.367	0.364	0.001	—
$L_1/(L_1 + L_2)$ (R_C)	0.361	0.359	0.001	—
$L_1/(L_1 + L_2)$ (I_C)	0.357	0.355	0.001	—
Spot co-latitude	48	47	5	deg
Spot longitude	10	9.1	2	deg
Spot radius	24.9	23.7	0.5	deg
Spot temp. factor	0.912	0.886	0.009	—
r_1 (pole)	0.3017	0.3024	0.0011	orb. rad.
r_1 (side)	0.3160	0.3168	0.0014	orb. rad.
r_1 (back)	0.3544	0.3560	0.0024	orb. rad.
r_2 (pole)	0.4293	0.4303	0.0009	orb. rad.
r_2 (side)	0.4586	0.4599	0.0012	orb. rad.
r_2 (back)	0.4894	0.4910	0.0016	orb. rad.
$\Sigma\omega^2_{res}$	0.0399	0.0393	—	—

6070 K) further trials were run with third light, however they did not improve the fit. An effort was made to go back to test the idea that solution A could be improved by deleting third light. A number of trials were run with no success. In view of the fact that solution B ($T_2 = 6070$ K) of is considered to be the optimum solution, there seemed to be no point in pursuing the matter further. The question then arises as to why we include Solution A at all. The answer is that it can serve as a cautionary tale to modellers in that different parameters can lead to nearly identical residuals and identical plots. In the case of AR CrB, this effect is illustrated more rigorously after adjusting the effective temperature of the more luminous star by as much as 3σ (Alton & Nelson 2018). It is the task of the modeller to sort out the best values based on external criteria.

The light curve data and the fitted curves from this paper are depicted in Fig. 4 (from top to bottom: V, R_C, and I_C), shifted by 0.1 flux units. The residuals in the sense (observed-calculated) are also plotted, shifted downward, and from each other by 0.05 units.

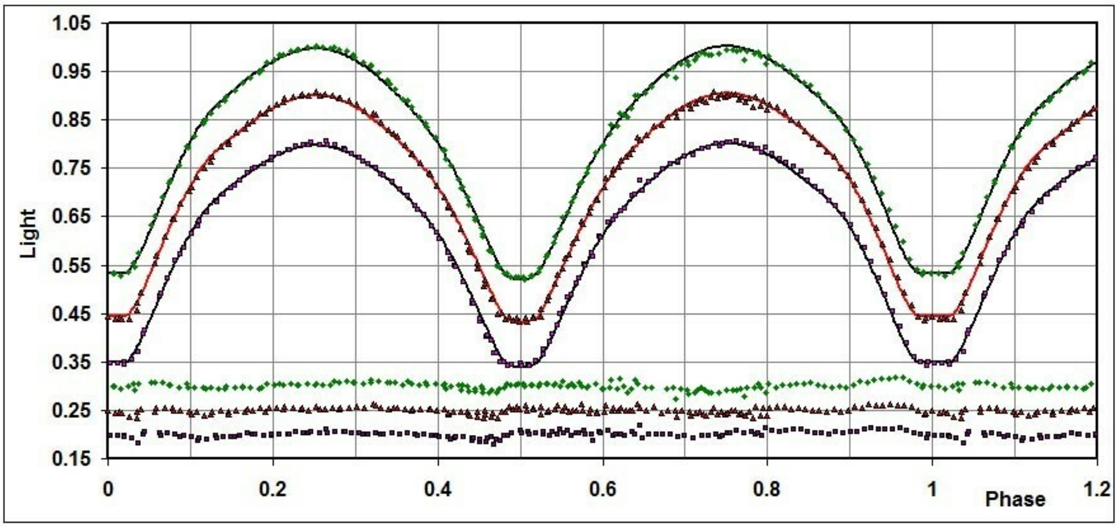

Figure 4. (top to bottom) V, R_C, and I_C light curves for RZ Com (this paper) – Data, WD fit, residuals. For clarity, the top three curves were offset by 0.10 divisions, while the bottom three, by 0.05 divisions.

Next, the data sets from Broglia (1960) were modelled, starting with data set 1. The solutions from this paper, along with those in Wilson & Devinney (1973), are presented in Table 8.

Next, the second dataset from Broglia (1960) was modelled. The solutions from this paper, along with those in Wilson & Devinney (1973), are presented in Table 9.

This time, the plots for both data sets are combined and presented in Fig. 5. Once again, plots for the two solutions are indistinguishable; hence only one figure is required.

Next, the data set from Xiang & Zhou (2004) was modelled. The problem here is that, visually, one can see there is significantly greater scatter in the data from phase 0.8 to 1.0. An analysis of the rms deviations for the curves of best fit using bins of 0.05 phase revealed that weights of 0.1 for phase 0.8 to 1.0, and 1 everywhere else were appropriate. With this modification, modelling proceeded.

Table 8: Wilson-Devinney parameters for the first dataset of Broglia (1960).

WD Quantity.	W&D 1973	Sol'n A	Sol'n B	Error	Unit
Temperature, T_1	5500	5420	6307	19	K
Temperature, T_2	5564	5257	6070	[fixed]	K
$q = m_2/m_1$	2.292 (30)	2.185	2.22	0.02	—
Potential, $\Omega_1 = \Omega_2$	5.618 (54)	5.396	5.44	0.03	—
Inclination, i	86.04 (51)	85.7	86.0	1.1	deg.
Fill-out factor, f_1	0.042	0.12	0.15	0.02	—
Semi-major axis, a	na	2.49	2.48	0.02	$R_\odot$
System RV, V_γ	na	12.4	12.2	1.2	km/s
Phase shift	—	0.0006	0.0006	0.0004	—
L_3 (Y)	—	0.015	—	—	—
$L_1/(L_1 + L_2)$ (Y)	na	0.366	0.366	—	—
Spot co-latitude	—	76	80	10	deg
Spot longitude	—	4	3.5	8	deg
Spot radius	—	27	26.6	4	deg
Spot temp. factor	—	0.9596	0.946	0.016	—
r_1 (pole)	0.2924 (44)	0.3026	0.3023	0.0026	orb. rad.
r_1 (side)	0.3056 (52)	0.3172	0.3169	0.0033	orb. rad.
r_1 (back)	0.3403 (82)	0.3567	0.3573	0.0058	orb. rad.
r_2 (pole)	0.4287 4(2)	0.4310	0.4333	0.0022	orb. rad.
r_2 (side)	0.4574 (55)	0.4608	0.4636	0.0029	orb. rad.
r_2 (back)	0.4859 (71)	0.4921	0.4952	0.0040	orb. rad.
$\Sigma\omega^2_{\rm res}$	—	0.0046	0.0046	—	—

Table 9: Wilson-Devinney parameters for the second dataset of Broglia (1960).

WD Quantity..	W&D 1973	Sol'n A	Sol'n B	Error	Unit
Temperature, T_1	5500	5470	6325	14	K
Temperature, T_2	5552	5257	6070	[fixed]	K
$q = m_2/m_1$	2.394 (20)	2.19	2.20	0.04	—
Potential, $\Omega_1 = \Omega_2$	5.869 (40)	5.40	5.40	0.09	—
Inclination, i	85.72 (31)	86.3	86.3	0.6	degrees
Fill-out factor, f_1	-0.059	0.12	0.13	0.03	—
Semi-major axis, a	na	2.49	2.49	0.02	$R_\odot$
System RV, V_γ	na	12.4	12.4	1.1	km/s
Phase shift	—	0.0001	0.0001	0.0003	—
L_3 (Y)	—	0.013	—	—	—
$L_1/(L_1 + L_2)$ (Y)	na	0.376	0.377	—	—
Spot co-latitude	—	115	115	10	deg
Spot longitude	—	0	0	8	deg
Spot radius	—	27.0	27	4	deg
Spot temp. factor	—	0.971	0.971	0.016	—
r_1 (pole)	0.2805 (30)	0.3030	0.3038	0.0083	orb. rad.
r_1 (side)	0.2918 (35)	0.3177	0.3186	0.0101	orb. rad.
r_1 (back)	0.3211 (52)	0.3577	0.3596	0.0176	orb. rad.
r_2 (pole)	0.4240 (29)	0.4317	0.4331	0.0074	orb. rad.
r_2 (side)	0.4509 (37)	0.4617	0.4635	0.0098	orb. rad.
r_2 (back)	0.4761 (47)	0.4933	0.4955	0.0132	orb. rad.
$\Sigma\omega^2_{\rm res}$	—	0.0077	0.0040	—	—

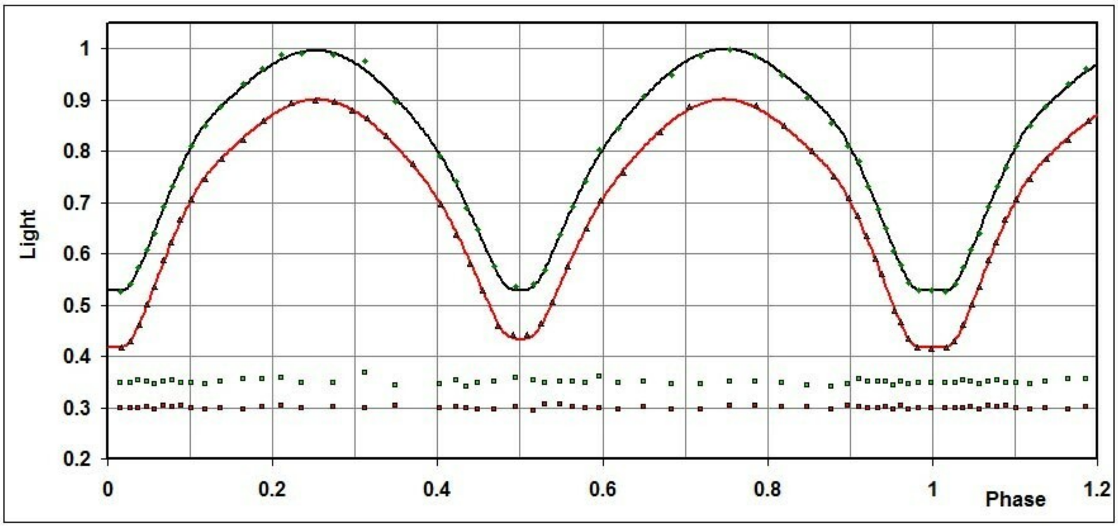

Figure 5. Y light curves (1 & 2) of Broglia (1960) – Data, our WD fits, residuals. For clarity, the curves have been offset as in Fig. 4.

The two solutions from this paper, along with those from Xiang & Zhou (2004), are presented in Table 10.

This time, there is a significant difference in the plots for solutions A & B; hence both are presented, in Figs. 6 and 7.

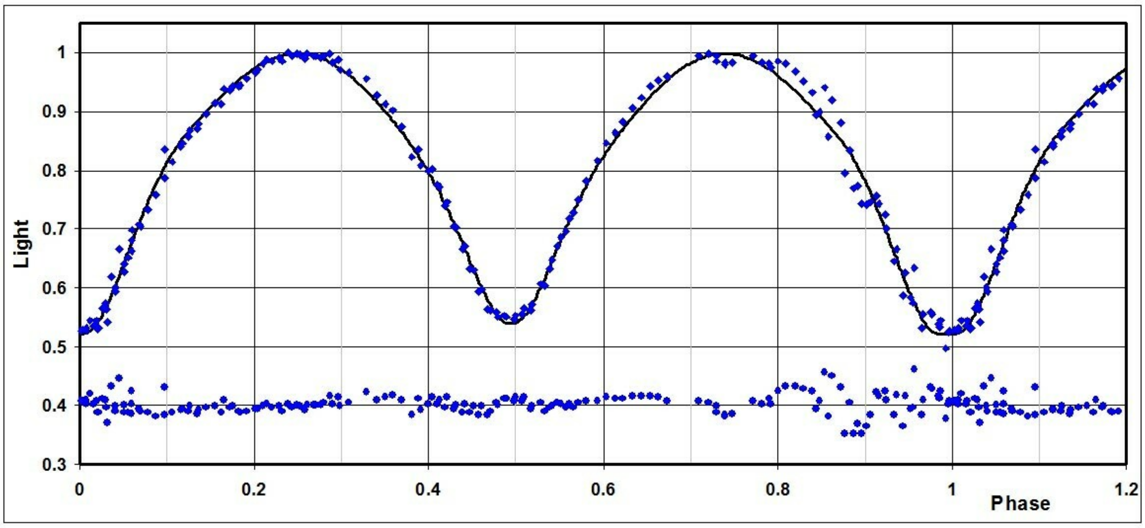

Figure 6. B light curve of Xiang & Zhou (2004): – Data, our WD fit A, (residuals offset)

And, lastly, we modelled the data of He & Qian (2008). As the analysis occurred late in the paper writing, we did not attempt a fit using the lower temperatures, but merely started with the parameters obtained from the other datasets. To our surprise, the spot had moved significantly in longitude. The results are listed in Table 11.

The light curve data from He & Qian (2008) and the fitted curves from this paper are depicted in Fig. 8 (from top to bottom: B and V), shifted by 0.1 flux units. The

Table 10: Wilson-Devinney parameters for the dataset of Xiang & Zhou (2004).

WD Quantity...	Xiang & Zhou Tbl 5	Xiang & Zhou Tbl 6	Sol'n A	Sol'n B	Error	Unit
Temperature, T_1	4900	4900	5425	6289	18	K
Temperature, T_2	4842	4802 (9)	5257	6070	[fixed]	K
$q = m_2/m_1$	2.226 (13)	0.772 (9)	2.19	2.20	0.02	—
Potential, $\Omega_1 = \Omega_2$	5.267 (15)	3.330 (14)	5.39	5.40	0.02	—
Inclination, i	79.67 (28)	78.40 (31)	83.2	81.6	0.5	degrees
Fill-out factor, f_1	na	na	0.13	0.12	0.01	—
Semi-major axis, a	na	na	2.49	2.51	0.02	$R_\odot$
System RV, V_γ	na	na	12.4	12.2	1.1	km/s
Phase shift	na	na	-0.0056	-0.0055	0.0005	—
L_3 (B)	—	—	0.053	—	—	—
$L_1/(L_1+L_2)$ (B)	0.3699 (31)	0.3833 (11)	0.378	0.376	0.002	—
r_1 (pole)	0.3090 (8)	0.4051 (14)	0.3039	0.3039	0.0027	orb. rad.
r_1 (side)	0.3246 (10)	0.4376 (17)	0.3187	0.3188	0.0034	orb. rad.
r_1 (back)	0.3676 (17)	0.4376 (17)	0.3595	0.3599	0.0062	orb. rad.
r_2 (pole)	0.4327 (17)	0.3403 (34)	0.4327	0.4334	0.0018	orb. rad.
r_2 (side)	0.4634 (23)	0.3573 (43)	0.4630	0.4639	0.0025	orb. rad.
r_2 (back)	0.4967 (33)	0.3921 (69)	0.4949	0.4960	0.0036	orb. rad.
$\Sigma\omega^2_{\rm res}$	0.003617	0.004221	0.0091	0.0088	—	—

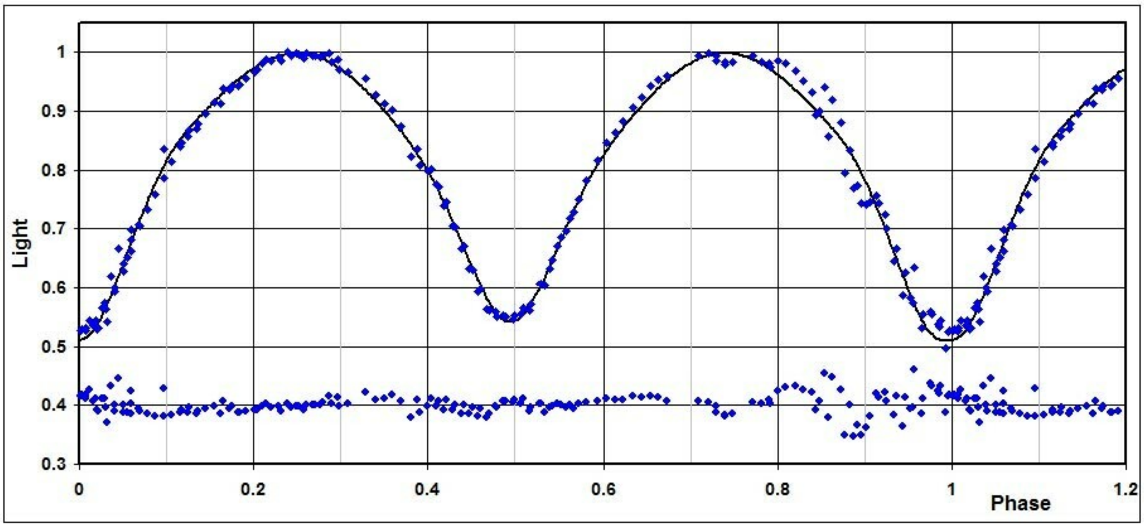

Figure 7. *B* light curve of Xiang & Zhou (2004): our solution B – Data, our WD fit B, (residuals offset)

Table 11: Wilson-Devinney parameters for the dataset of He & Qian (2008).

WD Quantity....	He & Qian 2008	Our sol'n	Error	Unit
Temperature, T_1	5000	6267	13	K
Temperature, T_2	4900 (8)	6070	—	K
$q = m_2/m_1$	2.351 (31)	2.174	0.062	—
Potential, $\Omega_1 = \Omega_2$	5.620 (45)	5.38	0.19	—
Inclination, i	81.4 (4)	84.9	0.4	degrees
Fill-out factor, f_1	0.201 (74)	0.11	0.01	—
Semi-major axis, a	—	2.49	0.03	$R_\odot$
System RV, V_γ	—	12.4	1.8	km/s
Phase shift	—	-0.0005	0.0003	—
$L_1/(L_1 + L_2)$ (B)	0.3471 (37)	—	—	—
$L_1/(L_1 + L_2)$ (V)	0.3545 (41)	0.364	0.001	—
r_1 (pole)	0.2971 (45)	0.3026	0.0177	orb. rad.
r_1 (side)	0.3113 (55)	0.3171	0.0215	orb. rad.
r_1 (back)	0.3512 (98)	0.3664	0.0362	orb. rad.
r_2 (pole)	0.4371 (37)	0.4302	0.0163	orb. rad.
r_2 (side)	0.4682 (49)	0.4598	0.0215	orb. rad.
r_2 (back)	0.4990 (67)	0.4910	0.0287	orb. rad.
$\Sigma\omega^2_{\rm res}$	0.00101	0.0235	—	—

residuals in the sense (observed-calculated) are also plotted, shifted downward, and from each other by 0.05 units.

The radial velocities are plotted in Fig. 9. Three-dimensional representations created using Binary Maker 3 (Bradstreet, 1993) for each of the studied epochs are shown in Fig. 10. (The crosses represent the centres of mass of the individual stars and of the system as a whole.)

From the WD output parameters we calculated the fundamental properties corresponding to each of the $T_2 = 6070$ K solutions; the results are listed in Table 12. Most of the errors are output or derived estimates from the WD routines. The values from Hilditch et al. (1988) as reported in Yildiz & Doğan (2013; hereafter Y&D) are included in column 2 for comparison.

Also included for comparison in Table 12 are the interpolated values from Pecaut & Mamajek (2013) for single main-sequence stars (as a function of temperature), in column 8. As noted in Y&D, the values for the more massive star m_2 (in our convention) are not far off the main sequence values. On the other hand, the less massive star is either underluminous for a star of its temperature (and therefore spectral class), or is over-luminous for a main sequence star of the same mass. From the interpolated tables of Pecaut & Mamajek (2013), the primary of mass 0.57 $M_\odot$ should have a luminosity of 0.093 $L_\odot$. See the concluding remarks for more discussion on this point.

To determine the distances r for the present data in the last row, we proceeded as follows: First the WD routine gave the absolute bolometric magnitudes of each component; these were then converted to the absolute visual (V) magnitudes of both, $M_{V,1}$ and $M_{V,2}$, using the bolometric corrections BC $= -0.06$ and -0.08 for stars 1 and 2 respectively. The latter were taken from tables constructed from Pecaut & Mamajek (2013). The absolute V magnitude was then computed in the usual way, getting $M_V = 3.84 \pm 0.03$ magnitudes.

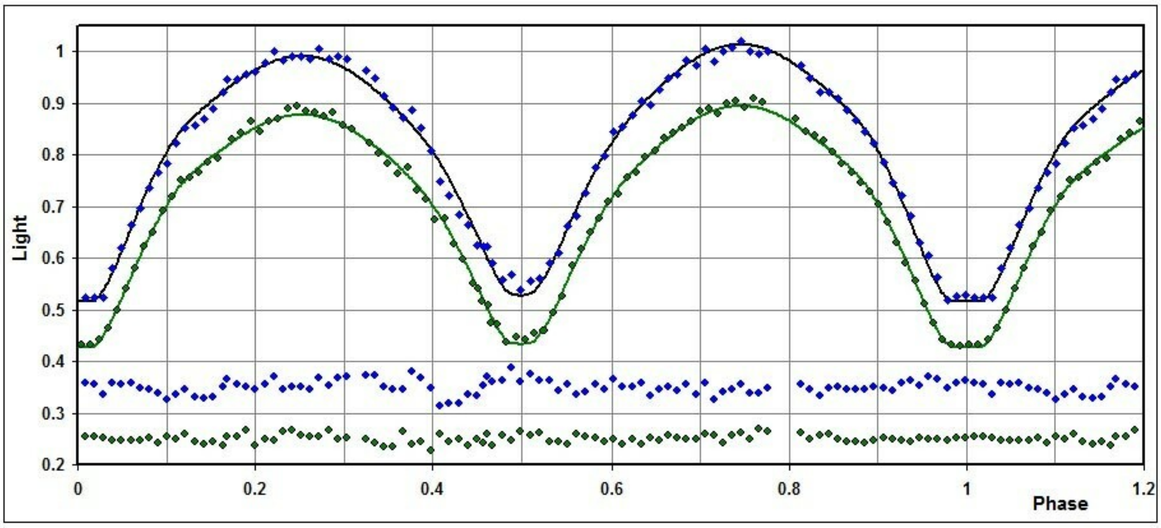

Figure 8. B and V light curves of He & Qian (2008) – Data, our WD fits, residuals. For clarity, the curves have been offset as in Fig. 4.

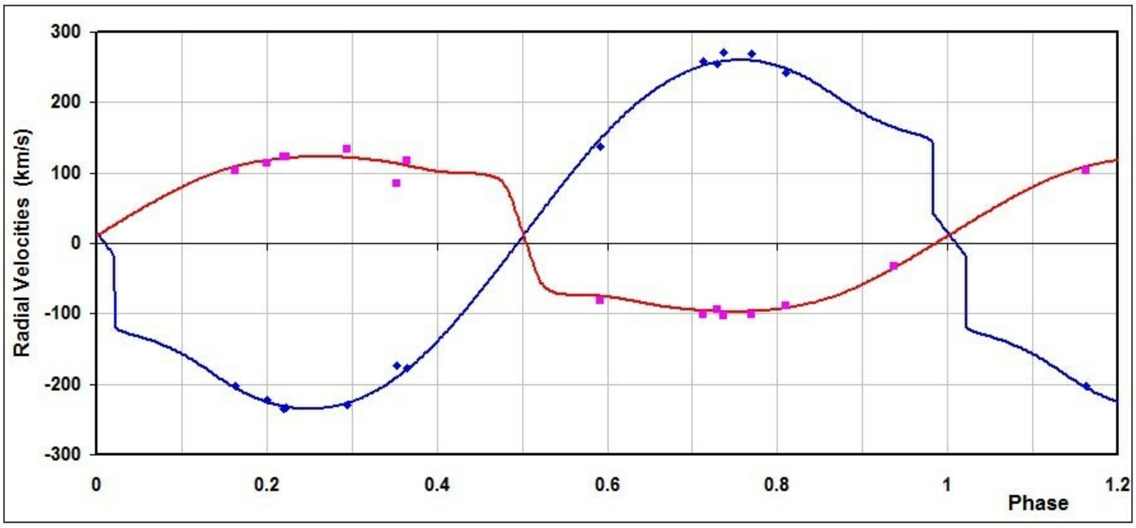

Figure 9. Radial velocity curves for RZ Com (this paper) – Data and WD Fit.

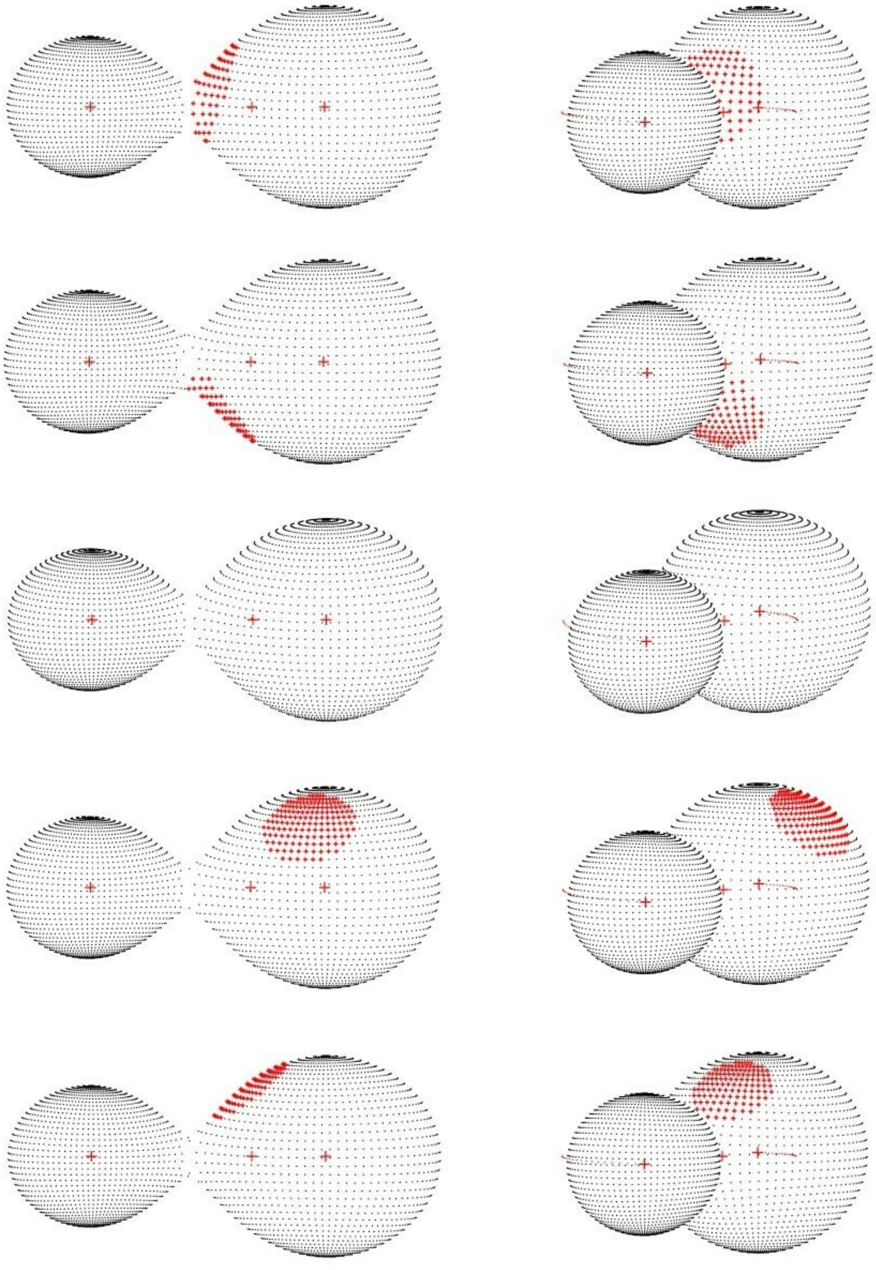

Figure 10. Binary Maker 3 representations of the system. Top to bottom: Broglia (1960) data set 1, Broglia (1960) data set 2, Xiang & Zhou (2004), He & Qian (2008), dataset from this paper (2018). Left to right: phase 0.25, phase 0.42.

Table 12: Fundamental parameters. Errors are for the data set of this paper only.

Quantity	Hilditch (1988)	Broglia 1	Broglia 2	Xiang-Zhou	He & Qian	This dataset	Error	Cox (2000)	unit unit
Temp., T_1	6457 (298)	6307	6325	6289	6267	6246	200	—	K
Temp., T_2	6166 (284)	6070	6070	6070	6070	6070	[fixed]	—	K
Mass, m_1	0.55 (4)	0.557	0.570	0.582	0.574	0.573	0.007	1.55	$M_\odot$
Mass, m_2	1.23 (9)	1.239	1.253	1.282	1.248	1.249	0.009	1.16	$M_\odot$
Radius, R_1	0.78 (2)	0.81	0.82	0.83	0.82	0.82	0.01	1.22	$R_\odot$
Radius, R_2	1.12 (3)	1.16	1.16	1.17	1.15	1.15	0.01	1.11	$R_\odot$
$M_{\rm bol,1}$	—	4.86	4.82	4.83	4.87	4.87	0.01	3.77	mag
$M_{\rm bol,2}$	—	4.26	4.25	4.41	4.26	4.26	0.01	4.12	mag
$\log g_1$	—	4.36	4.36	4.37	4.37	4.37	0.01	4.36	cgs
$\log g_2$	—	4.40	4.41	4.41	4.41	4.41	0.01	4.37	cgs
Luminosity, L_1	0.93 (15)	0.94	0.97	0.96	0.93	0.93	0.03	2.04	$L_\odot$
Luminosity, L_2	1.62 (26)	1.63	1.64	1.68	1.63	1.63	0.03	1.16	$L_\odot$
Distance, r	—	204	204	204	201	204	5	—	pc

The apparent magnitude in the V passband was $V = 10.44 \pm 0.03$, taken from the APASS catalogue (Henden et al., 2009, 2010; Smith et al. 2010). In order to check that the values were obtained at the correct phase (i.e., near phase 0.25 or 0.75—when the flux from both stars was maximum), photometry at these phases was analysed using the comparison star and its V magnitude of 10.571 (57), also taken from the APASS catalogue. The result: $V = 10.437$ (5) where the error stated is the standard error of the mean; including the error in the comparison magnitude, resulted in $V = 10.44$ (6).

Because of the system's high galactic latitude (+84.7°), and as we will see, its close proximity, interstellar absorption, A_V may be ignored initially. Therefore using the standard relation (Eq 2) with $A_V = 0$, we calculated a value for the distance as $r = 209$ pc:

$$r = 10^{0.2(V-Mv-A_V+5)} \text{ parcsec} \tag{2}$$

Galactic extinction was obtained from a model by Amôres & Lépine (2005). The code available in IDL (and converted by the author to a Visual Basic routine) assumes that the interstellar dust is well mixed with the dust, that the galaxy is axi-symmetric, that the gas density in the disk is a function of the Galactic radius and of the distance from the Galactic plane, and that extinction is proportional to the column density of the gas, Using Galactic coordinates of $l = 257.7516°$ and $b = +84.7047°$ (SIMBAD), and the initial distance estimate of $d = 0.208$ kpc, a value of $A_V = 0.070$ magnitude was determined. A further iteration revealed little change in A_V. Substitution into (2) gave $r = 202$ pc. Similar calculations were carried out for the other datasets.

However, there was a problem. The value derived from the Schlegel dust maps (Schlegel et al. 1998)[1], and including the factor sin(galactic latitude) is $A_V = 0.045$ mag. As this value pertains to the absorption all the way through the Galactic arm (a distance of approximately 0.3 kpc), the value from Amôres & Lépine appears to overestimate interstellar extinction in this region of the sky. If we take 2/3 of the Schlegel value ($2/3 \times 0.045$) we get $A_V = 0.03$ mag. Substitution into (2) gave $r = 206$ pc, close to the above value. Therefore we adopt the mean of the two computed values, 204 pc. The same procedure was used with the other datasets in Table 12.

The errors were assigned as follows: $\delta M_{\rm bol,1} = \delta M_{\rm bol,2} = 0.02$, $\delta BC_1 = \delta BC_2 = 0.005$ (the variation of 1/2 spectral sub-class), $\delta V = 0.04$, all in magnitudes. Combining the errors rigorously (i.e., by adding the variances) yielded an estimated error in r of 5 pc.

[1] available at: `http://www.astro.princeton.edu/~schlegel/dust/data/data.html`, by Schlegel, D. J., Finkbeiner, D. P., Krigel, A. (2013)

Table 13: New times of minima for RZ Com obtained in this study.

Min (Hel)−2400000	Type	Error (days)
58169.8508	II	0.0002
58246.8611	I	0.0004
58250.7519	II	0.0002
58253.7986	II	0.0002

Table 14: LiTE parameters from various sources.

LiTE Quantity	Qian &He 2005	He & Qian 2008	Nelson et al. 2016	This work	Unit
Period, P_3	44.8 (7)	45.1 (6)	41.4 (5)	41.4 (7)	years
Amplitude, A	0.0058 (5)	0.0065 (1)	0.0063 (3)	0.0063 (4)	days
Eccentricity, e_3	0	0	0.30 (11)	0.30 (12)	—
Arg. Periastr., ω_3	260 (7)	278 (7)-	472 (25)	472 (35)	degrees
Periastron time	—	—	42744 (1790)	42772 (2643)	HJD−2400000
$a_1 2 \sin i$	1.00 (9)	1.12 (2)	1.09 (6)	1.10 (6)	AU
$f\ (m_3)$	0.00051 (13)	—	0.00076 (12)	0.00077 (14)	$M_\odot$
dP/dt (1-2 pair)	4.12	3.97	3.86 (8)	3.84 (2)	10-8 d/yr

The Gaia DR2 catalogue lists, for RZ Com, a parallax of 4.898 ± 0.088 mas. This translates to a distance of 203.1 ± 3.7 pc, consistent with all our distance estimates.

Four new times of minima emerged from the observations; these are reported in Table 13. Each is the mean of three values (one for each filter). For each filter, five methods of minimum determination, as implemented in software Minima23 Nelson (2013) were used: the digital tracing paper method, bisection of chords, sliding integrations (Ghedini 1982), curve fitting using five Fourier terms, and Kwee and van Woerden (Kwee & Woerden 1956, Ghedini 1982). There was no significant difference between corresponding values for the different filters. Because, in the literature, many (or perhaps most) error estimates can be shown to be low (sometimes unrealistically so), the estimated errors were taken as double the standard deviations of the various determinations. Also, a minimum error value of 0.0002 days was adopted for the same reason.

The period behaviour of this system is very interesting, and was earlier examined in Nelson et al. (2016). An eclipse timing difference (O–C) plot using the same timings dating from 1927 but updated with more recent points was used. Earlier fits are due to Qian & He (2005) and He & Qian (2008). As with Nelson et al. (2016), derivations of the light time effect (LiTE) using relations from Irwin (1952, 1959), resulted in a good fit. Standard weighting was used: pg = 0.2, vis = 0.1, and PE, CCD = 1.0.

As the reader will see in Table 14, parameters in the updated fit differ only slightly (if at all) from Nelson et al. (2016).

The eclipse timing difference (O–C) plot with all available timings together with the latest LiTE fit is depicted in Fig. 11.

From the definition of the mass function given in equation 3:

$$f(m_3) = (m_3 \sin i')^3/(m_1 + m_2 + m_3)^2 \tag{3}$$

and the value from this work, we were able to estimate a value for m_3. Assuming that the inclination i' of the putative third star orbit is the same as that of the eclipsing pair (viz. 85°), we calculated mass m_3 by iteration, obtaining the value $m_3 = 0.144$ (8) $M_\odot$. From the tables of Cox (2000) for main sequence stars, we read that the luminosity would be 0.0009 $L_\odot$, which is far too faint to be of any consequence to the modelling process here.

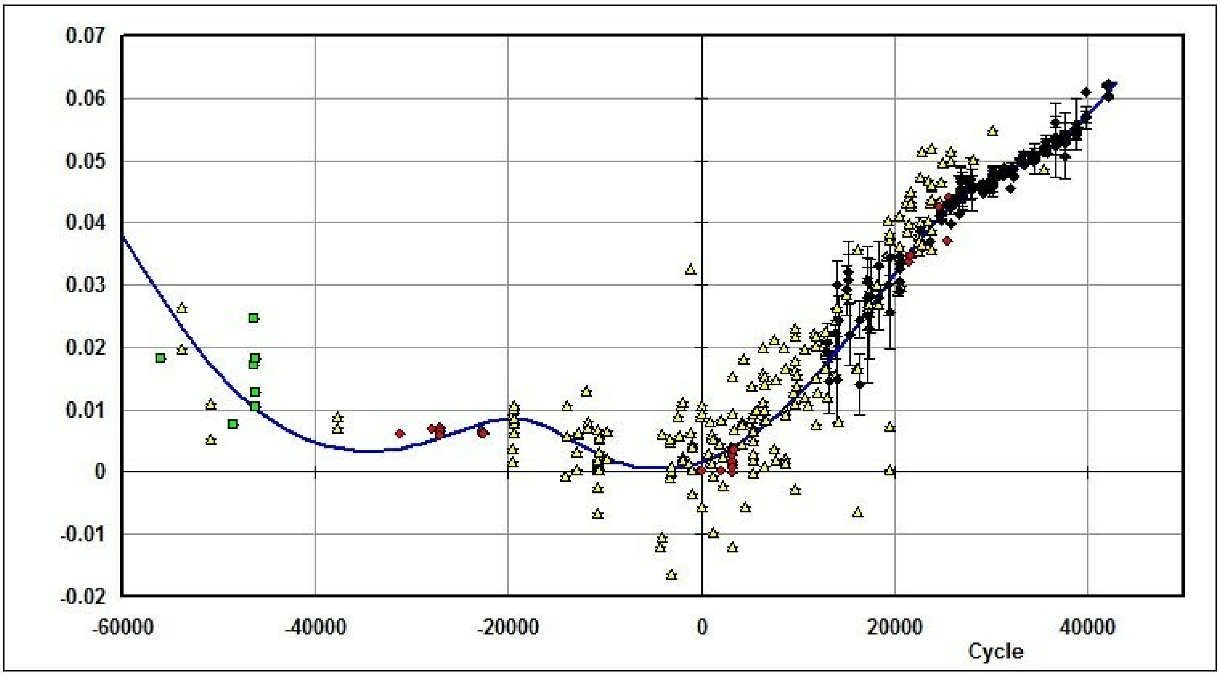

Figure 11. RZ Com – eclipse timing (O–C) diagram with LiTE fit (see text). [Note: (green) squares = photographic; (yellow) pyramids = visual; (red) circles = photoelectric; and (black) diamonds = CCD.] Elements used to generate this plot are given in Equation 4.

$$\text{JD (Hel) Min I} = 2443967.9371\ (29) + 0.33850604\ (5)\ \text{E} \tag{4}$$

In order to phase the photometric and radial velocity curves correctly, a different set of elements, applying to the interval over which the data were taken, was required. For the present data set, timings from 2014-2018 were used with the exclusion of all else; the results of the fit are shown in Fig. 12.

This resulted in the elements of Equation 5 given below. These elements were used for all phasing of the RV and present photometric data.

$$\text{JD (Hel) Min I} = 2458253.6296\ (29) + 0.3385075\ (5)\ \text{E} \tag{5}$$

Similar fits were used for the other data sets. Elements for the Broglia (1960) photometric data were:

$$\text{JD (Hel) Min I} = 2458253.5711\ (12) + 0.33850598\ (5)\ \text{E} \tag{6}$$

and those for the Xiang & Zhou (2004) photometric data:

$$\text{JD (Hel) Min I} = 2458253.6628\ (29) + 0.3385088\ (5)\ \text{E} \tag{7}$$

Elements were not required for the data of He & Qian (2008) as their reported data were already phased.

The Excel file for the eclipse timing data and analysis for this system (and for many others) is available at Nelson (2016).

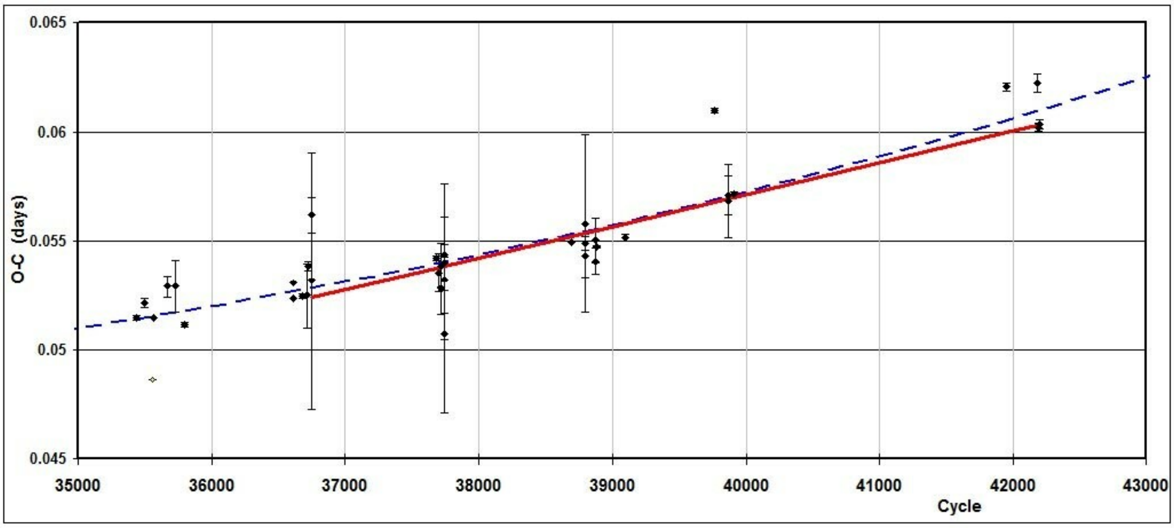

Figure 12. RZ Com – eclipse timing (O–C) diagram with LiTE fit (dashed line) and linear fit for the range

Further, once the LiTE fit was achieved, it was now possible to plot the residuals (see Fig. 13); that is the O–C values minus the LiTE component (see Nelson et al. 2016 for details).

The equation of the line of best fit is:

$$O - C = 0.0078\ (8) + 6.6\ (1) \times 10^{-7}\ \mathrm{E} + 1.79(0.12) \times 10^{-11}\ \mathrm{E}^2 \tag{8}$$

From the quadratic coefficient, c2 one calculates the intrinsic rate of period change, dP/dt by:

$$dP/dt = 2c_2 365.24/P = 3.86\ (21) \times 10^{-8}\ \text{days/year} \tag{9}$$

where P = the orbital period of the eclipsing pair.

If this (constant) rate of period change is due to conservative mass exchange, we may calculate this rate by (see Nelson et al. 2016 for references):

$$dm_1/dt = [3P(1/m_2 - 1/m_1)]^{-1}\, dP/dt \tag{10}$$

Substituting the mean stellar masses for m_1 and m_2 from Table 12, we obtained the value $dm1/dt = -4.1\ (3) \times 10^{-8}\ \mathrm{M}_\odot$/year which means that (as is often the case) the less massive star is losing mass to its companion.

However, it is not clear that the condition of conservative mass transfer is valid. Y&D concluded that, for overcontact binaries, only 34 per cent of the mass from the lesser massive star is transferred to the more massive one. Hence, the value for dm_1/dt should be treated with caution. See also Yildiz (2014).

In conclusion, we have shown that–contrary to the conclusion of Wilson & Devinney (1973), but in agreement with the results of Hilditch et al. (1988), and He & Qian (2008)– this binary system is a W-type overcontact binary with a low fillout factor. Our finding is buttressed by the fact that all our attempts to model the light curve data of this paper as a detached or semi-detached system have failed. Changes recommended in differential corrections always drove the model into mode 3 (overcontact binary).

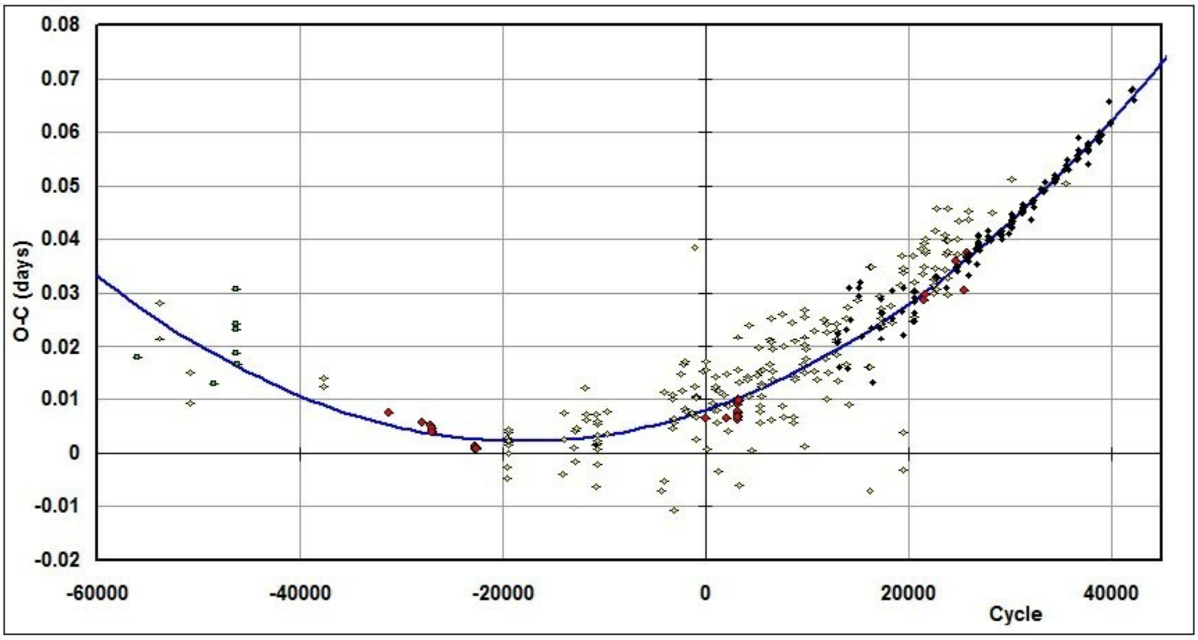

Figure 13. The O–C values for RZ Com minus the LiTE component with the quadratic of best fit.

With our values for the fill-out factor ranging from 0.10 to 0.13, that makes the system a slightly-overcontact binary, typical of the W-types (Rucinski 1974, Kallrath & Milone 1998). Further, our reciprocal mass ratio q$' = m_1/m_2 = 1/q = 0.45$ lies in the middle of the 'moderate' range ($0.4 < q' < 0.6$), typical of the W-type (Kallrath & Milone 1998).

We also found unified solutions for all the datasets (except as noted) spanning some 60 years. A cool spot on the more massive star accounted for the changes in the light curves over time, giving plausible spot configurations. There appears to be an easy progression between the two data sets of Broglia, and also between the datasets of He & Qian, and with ours. There seemed to be no spot at the epoch of the Xiang & Zhou dataset, however, the higher scatter in their dataset does not allow one to be sure. RZ Com is probably a good candidate for extensive coverage in order to map in detail the progression of the spot.

From Table 12, it is evident that star 1 is underluminous compared to a main sequence star of the same temperature or spectral type, or that it is undermassive for its spectral type the two conditions are equivalent (because a less massive star would have a smaller radius, a smaller emitting area, and hence a lower luminosity). This discrepancy was also noted in Wilson & Devinney (1973) who found 'masses which seem incompatible with their position on the H-R diagram'. However, there is an explanation. According to the calculations of Y&D, the initial mass of the hotter star of RZ Com (designated the primary here, the secondary in Y&D), was much higher, starting at 1.58 $M_\odot$ followed by a period of mass exchange, ending up with a mass of 0.55 $M_\odot$, not far from our value of 0.573(7) $M_\odot$. Again, according to Y&D, the luminosity of our primary (m_1) would depend as much on its initial mass as it does on its present mass, hence the excess luminosity [for its mass]. Y&D also determined the main-sequence age to be 2.09 Gyr.

Acknowledgements: It is a pleasure to thank the staff members at the DAO (Dmitry Monin, David Bohlender, and the late Les Saddlmyer) for their usual splendid help and assistance. Many thanks are also due to the San Pedro Observatory resident astronomer/technician, Dean Salman for his tireless help. Much use was made of the VizieR search tool along with the SIMBAD and O–C Gateway (B.R.N.O.)[2] databases. This research has made use of the APASS database, located at the AAVSO web site. Funding for APASS has been provided by the Robert Martin Ayers Sciences Fund.

References:

Alton, K. B., 2010, *JAVSO*, **38**, 57
Alton, K. B., Nelson, R. H., 2018, *MNRAS*, **479**, 3197 DOI
Amôres, E. B., Lépine, J. R. D., 2005, *AJ*, **130**, 659 DOI
Andrae,R., Fouesneau, M., Creevey, O., et al., 2018, *A&A* (arXiv: 1804.09374)
Batten A. H., Fletcher J. M., MCarthy D. G., 1989, *Publ. DAO*, **17**
Binnendijk, L., 1964, *AJ*, **69**, 154 DOI
Binnendijk, L., 1970, *Vistas in Astronomy*, **12**, 217 DOI
Bradstreet, D. H., 1993, "Binary Maker 2.0 – An Interactive Graphical Tool for Preliminary Light Curve Analysis", in Milone, E.F. (ed.) Light Curve Modelling of Eclipsing Binary Stars, pp 151-166 (Springer, New York, N.Y.) DOI
Broglia, P., 1960, *Contributi Milano-Merate*, **165**
Gaia Collaboration, 2018, *A&A*, **616**, 1 DOI
Cox, A. N., ed., 2000, *Allen's Astrophysical Quantities*, 4th ed., (Springer, New York, NY) DOI
Flower, P. J., 1996, *ApJ*, **469**, 355 DOI
Gaposchkin, S., 1932, *VeBB*, **9**, 1
Gaposchkin, S., 1938, *Variable Stars* (Harvard Monograph No. 5, Harvard U. Press)
Ghedini, S., 1982, Software for Photometric Astronomy, (Willmann-Bell Inc.)
Grubbs, F. E. 1950, *Annals of Mathematical Statistics*, **21**, 27 DOI
He, J.-J., Qian, S.-B., 2008, *ChJAA*, **8**, 465 DOI
Henden, A. A., Welch, D. L., Terrell, D., Levine, S. E. 2009, The AAVSO Photometric All-Sky Survey, *AAS*, **214**, 407.02
Henden, A. A., Terrell, D., Welch, D., Smith, T. C. 2010, New Results from the AAVSO Photometric All Sky Survey, *AAS*, **215**, 470.11
Hilditch R. W., King D. J., McFarlane T. M., 1988, *MNRAS*, **231**, 341 DOI
Irwin, J. B., 1952, *ApJ*, **116**, 211 DOI
Irwin, J. B., 1959, *AJ*, **64**, 149 DOI
Kallrath, J. & Milone, E.F., 1998, *Eclipsing Binary Stars–Modeling and Analysis* (Springer-Verlag) DOI
Kopal, Z., 1955, *AnAp*, **18**, 379
Kurucz, R. L., 1979, *ApJS*, **40**, 1 DOI
Kwee, K. K., van Woerden, H., 1956, *BAN*, **12**, 327
McLean, B. J., Hilditch, R. W., 1983, *MNRAS*, **203**, 1 DOI
Mochnacki, S. W., 1981, *ApJ*, **245**, 650 DOI
Nelson, R. H., 2010, "Spectroscopy for Eclipsing Binary Analysis" in The Alt-Az Initiative, Telescope Mirror & Instrument Developments (Collins Foundation Press, Santa Margarita, CA), R.M. Genet, J.M. Johnson and V. Wallen (eds)
Nelson, R. H., 2013, Software by Bob Nelson, `https://www.variablestarssouth.org/bob-nelson/`

[2] O–C Gateway, Paschke, A. `http://var2.astro.cz/ocgate/`

Nelson, R. H., 2014, Spreadsheets, by Bob Nelson,
https://www.variablestarssouth.org/bob-nelson/
Nelson, R. H., Şenavci, H. V., Baştürk, Ö, Bahar, E., 2014, *NewA*, **29**, 57 DOI
Nelson, R. H., Terrell, D., Milone, E. F., 2016, *NewAR*, **70**, 1 DOI
Nelson, R. H., 2016, Bob Nelson's O–C Files,
http://www.aavso.org/bob-nelsons-o-c-files
Pecaut, M. J., Mamajek, E. E. 2013, *ApJS*, **208**, 9 DOI
Perryman, M. A. C. et al. 1997, *A&A*, **500**, 501,
Qian, S.-B., 2001, *MNRAS*, **328**, 635 DOI
Qian, S.-B., He, J.-J., 2005, *PASJ*, **57**, 977 DOI
Rovithis, P., Rovithis-Livaniou, E., 1984, *A&AS*, **58**, 679
Rovithis-Livaniou, E., Rovithis, P., Djurašević, G., 2002, *IBVS*, **5235**, 1
Rucinski, S. M., 1974, *AcA*, **24**, 119
Rucinski, S M., 2004, *IAUS*, **215**, 17
Russell, H. N., Merrill, J. E., 1952, "The Determination of the Elements of Eclipsing Binary Stars", *Contributions from the Princeton University Observatory*, **26**, 1
Schlegel, D. J., Finkbeiner, D. P., Davis, M., 1998, *ApJ*, **500**, 525 DOI
Smith, T. C., Henden, A., Terrell, D., 2010, AAVSO Photometric All-Sky Survey Implementation at the Dark Ridge Observatory, SAS.
Struve, O., Gratton, L., 1948, *ApJ*, **108**, 497 DOI
Terrell, D., Gross, J., Cooney, W. P. Jr., 2012, *AJ*, **143**, 99 DOI
Terrell, D., 1994, *Van Hamme Limb Darkening Tables, vers. 1.1.*
Van Hamme, W., 1993, *AJ*, **106**, 2096 DOI
Wilson, R. E., Devinney, E. J., 1971, *ApJ*, **166**, 605 DOI
Wilson, R. E., Devinney, E. J., 1973, *ApJ*, **182**, 539 DOI
Wilson, R. E., DeLuccia, M. R., Johnston, K., Mango, S. A., 1972, *ApJ*, **177**, 191 DOI
Wilson, R. E., 1990, *ApJ*, **356**, 613 DOI
Wilson, R. E., 1998, Documentation of Eclipsing Binary Computer Model (available from the author)
Wood F. B., Oliver J. P., Florkowski D. R., Ko h R. H., 1980, *A Finding List for Observers of Interacting Binary Stars*, Univ. of Pennsylvania Press
Wright, C. O., et al., 2003, *AJ*, **125**, 359 DOI
Xiang, F. Y. and Zhou, Y. C., 2004, *NewA*, **9**, 273 DOI
Yildiz, M., Doğan, T., 2013, *MNRAS*, **430**, 2029 DOI
Yildiz, M., 2014, *MNRAS*, **437**, 185 DOI

COMMISSIONS G1 AND G4 OF THE IAU
INFORMATION BULLETIN ON VARIABLE STARS
Volume 63 Number 6267 DOI: 10.22444/IBVS.6267

Konkoly Observatory
Budapest
8 May 2019

HU ISSN 0374 – 0676

NEW LIGHT ON R ARAE

BLANE, D.; BLACKFORD, M.G.; BUDDING, E.; REED, P.A.

Variable Star Section, Royal Astronomical Society of New Zealand, New Zealand

Abstract

In mid-2018, efforts were renewed to check on the highly active mass-transfer process shown by the classical Algol system R Arae. We present new light curves and times of light minimum from this project.We also extend R Arae's period O–C diagram to include the new results. The new data are consistent with the strong mass transfer scenario of Reed (2011). Recent and ongoing studies of this interesting system are referred to.

1 Introduction

In the early 1980s investigators using satellite observational techniques were drawing attention to the relatively bright southern binary system R Arae, which superficially resembles a 'classical' Algol, but with mass transfer on a more enhanced scale than typical, and with additional photometric peculiarities that may be related to relatively dense and uneven accretion structures (Kondo et al., 1985; Nield et al., 1986; Reed, 2011). Kondo et al. (1985), perhaps with the symmetric, smoothly rounded light curve of Gaposchkin (1953) in mind, compared the system to the well-known massive and strongly interactive binary β Lyrae, despite the 3-times greater period of the latter.

The period steadily increased from about 4.42495 d in the year of its discovery by Roberts (1894) to the 4.425132 d given by Nield (1986; for HJD 2446585.161) and continues to do so according to Reed (2011), who obtained a mean rate of increase of 5.15×10^{-9} d d^{-1} over 116 y. Reed deduced, from this period extension, that the Roche-Lobe filling component in the binary was shedding matter to its companion at a rate of about 3.06×10^{-7} M$_\odot$ y^{-1}.

Reliable parametrization of R Arae has been compromised by the significant ($\sim$ 10%) level of short term variability that adds into the light curve (Banks, 1990). Such variations can occur even in one night's observations, as noted by Forbes et al. (1988), Budding (1989), and confirmed in Bakiş et al's (2016) study that included a short term photometric sequence from the HIPPARCOS satellite.

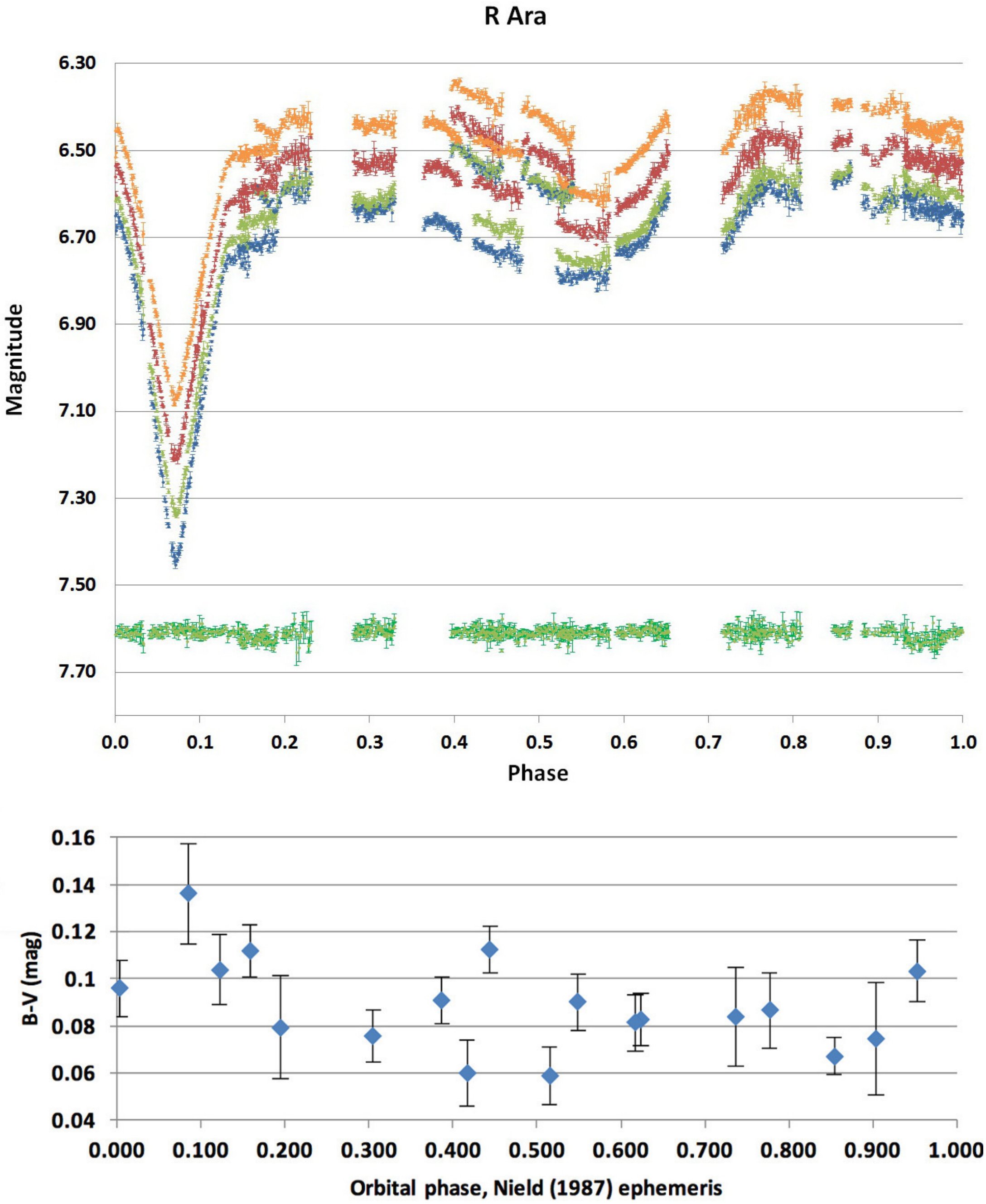

Figure 1. *BVRI* light curves and $B - V$ colour curve of R Arae in mid-2018. The epoch and period from Nield (1987) were used for the phase calculation, see also Reed (2011).

2 New data

Light curves of R Arae were produced in Jun 2018 (DB) and Jul-Aug 2018 (MGB) as contributions to the Southern Binaries Programme of the VSS, stimulated by a new data request (PAR). For the June data, images were obtained with a 150 mm f5 refractor and a Canon 1300D DSLR camera mounted on a GEM goto mounting. Aperture photometry was facilitated using the IRIS software package. The camera's G magnitudes were linearly transformed to the Johnson V band using MS-Excel. Differential extinction was not applied. Each adopted measurement was the average obtained from 10 separate field images.

The Jul 7–Aug 19 data were gathered over 19 nights using an 80 mm f6 refractor and SBIG STT 3200ME CCD camera with Astrodon filters. These observations were extinction corrected and linearly transformed to standard Johnson-Cousins BVR_CI_C system. In Fig. 1 we present these latter data (upper panel: blue points B, green V, red R_C, orange I_C). The lower green points show the check star, HD149519, shifted to an average value of 7.6 for easy display. Its actual measured average V value was 8.547 mag. The (binned) $B - V$ colour curve is shown in the lower panel. The 19 separate runs consist of typically $\sim$ 50 points. The light-curves show the same kind of previously reported behaviour, with some features having a degree of persistence, for example the rise and decline into the primary eclipse, while other transient occurrences have a stochastic quality (Forbes, 1988).

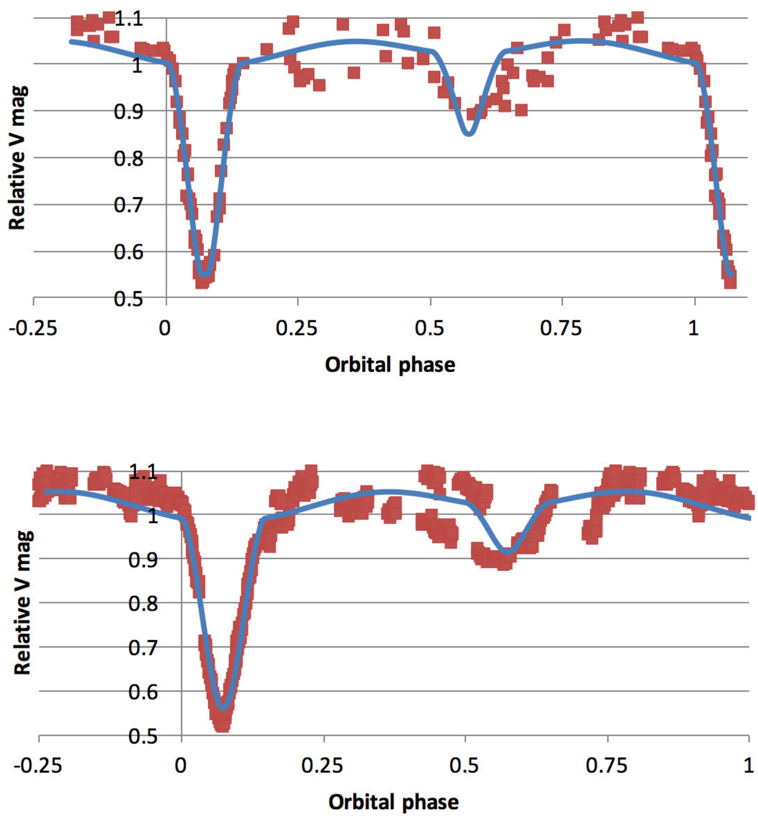

Figure 2. The V light curves of 2018 Jun (DB, upper panel) and Jul-Aug (MB, lower panel), fitted with a classical Algol model. The phase shifts noted below are clearly visible in the light curves.

In the $B-V$ colour curve (lower panel) we have binned each of the 18 sets of data into single average points, together with their s.d. dispersions. It is clear that the vagaries of colour are significantly greater than the standard deviation within the groups. The system is redder at mid-occultation, however – by about 0.06 mag. There is a suggestion of some blueing around the transit, but that is not uniform. The average $B-V$ in the out-of-eclipse regions is 0.081 mag. These irregularities mean that parameters associated with fitting the light curves with standard models are not well-defined. Even so, a classical Algol model will approximately fit, as shown in Fig. 2, though other possibilities cannot be ruled out from photometric evidence alone. The significant secondary minimum and relatively low depth of the primary might be associated with a detached pair; though, when the light from the close companion (included in aperture photometry) is taken into account, the depth of the primary eclipse implies a secondary size comparable to its surrounding Roche lobe (Nield, 1987).

Bakiş et al. (2016), posited a model of cyclic phenomena in their account, though the question of why certain Algols show variable light curves (Piotrowski et al., 1974) and not all was more squarely addressed in the review of Reed (2012), who noted that certain period and mass-ratio combinations are propitious in allowing the development of relatively large and unsteady accretion structures. This model is in keeping with the relatively large rate of period increase demonstrated by Reed (2011) and confirmed in the latest (2018) times of minima illustrated in Fig. 3.

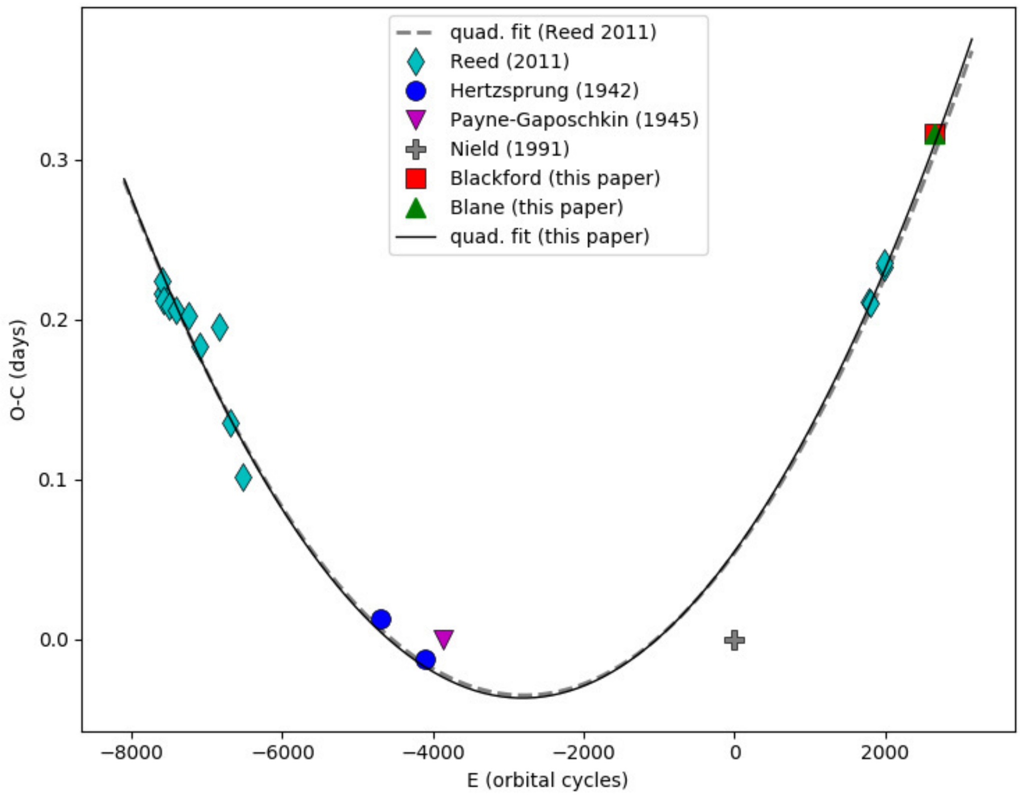

Figure 3. O–C variation as predicted by Reed (2011) and confirmed by our latest times of minima.

Times of primary minimum have been calculated as HJD 2458307.6501 (DB) and HJD 2458312.0758 (MGB), which give O–C values of 0.3157 d at cycle number 2649, and 0.3163 d at cycle 2650 from Nield's epoch.

It is of interest to note that relevant precise photometric data from NASA's Transiting Exoplanet Survey Satellite (TESS) should become available fromSector 12, that is expected to run between May 21 and June 19 this year. The foregoing BVR_CI_C information, not available from TESS, should then have a useful complementary role. Other complementary data on R Arae is available from KELT (Collins et al., 2018), together with spectroscopic data planned from MINERVA (Wittenmyer et al., 2018) or contained in the University of Canterbury Mt John Observatory HERCULES archive. This present report will thus hopefully contribute to ongoing observational work on this intriguing active close binary system.

Acknowledgements We appreciate the helpful suggestions of Dr L. Molnár, editor of the IBVS, regarding this contribution, and keenly appreciate the support that the IBVS has given to this kind of research over the years.

References:

Banks, T., 1990, *IBVS*, 3455
Bakiş, H., Bakiş, V., Eker, Z., Demircan, O., 2016, *MNRAS*, **458**, 508 DOI
Budding, E., 1989, *Space Science Reviews*, **50**, 205 DOI
Collins, K. A., Collins, K. I., Pepper, J., et al., 2018, *ApJ*, **156**, 234 DOI
Forbes, M., Budding, E., Priestley, J., 1988, *IBVS*, 3278
Gaposchkin, S., 1953, *Annals of Harvard Coll. Obs.*, **113**, 67
Kondo, Y., McCluskey, G.E. Jr., Parsons, S. B., 1985, *ApJ*, **295**, 580 DOI
Nield, K. M., Priestley, J., Budding, E., 1986, *IBVS*, 2491
Piotrowski, S. L., Rucińksi, S. M., Semeniuk, I., 1974, *AcA*, **24**, 389
Reed, P. A., 2011, *IBVS*, 5975
Reed, P. A., 2012, *IAUS*, **282**, 325 DOI
Roberts, A. W., 1894, *AJ*, **14**, 113 DOI
Wittenmyer, R., Horner, J., Carter, B. D., et al, 2018, arXiv:1806.09282

COMMISSIONS G1 AND G4 OF THE IAU
INFORMATION BULLETIN ON VARIABLE STARS
Volume 63 Number 6268 DOI: 10.22444/IBVS.6268

Konkoly Observatory
Budapest
8 May 2019

HU ISSN 0374 – 0676

NEW DOUBLE PERIODIC VARIABLE STARS IN THE ASAS-SN CATALOG

ROSALES, J. A.; MENNICKENT, R. E.

Astronomy Department, University of Concepción, Concepción, Chile. e-mail: jrosales@astro-udec.cl

Abstract

We report the discovery of 3 new Double Periodic Variables based on the analysis of ASAS-SN light curves: GSD J11630570-510306, V593 Sco and TYC 6939-678-1. These systems have orbital periods between 10 and 20 days and long cycles between 300 and 600 days.

1 Introduction

The Double Periodic Variable stars constitute enigmatic stellar systems discovered just in recent years. These systems are close binary stars of intermediate mass, the majority of the studied DPV are in a semi-detached stage undergoing mass transfer, and show a second photometric variability. This variation was observed for the first time in the Magellanic Clouds by Mennickent et al. (2003), and these long periods are on average 33 times longer than the orbital period (Poleski et al., 2010; Mennickent, 2017; Rosales Guzmán et al., 2018). To date, it has been observed that the more evolved star is generally of the A/F/G spectral type, while the companion is always of B spectral type surrounded by an optically and geometrically thick accretion disk ()Barría et al., 2013; Mennickent et al., 2015; Rosales Guzmán et al., 2018). In addition, the second period was associated to cycles of magnetic dynamo in the more evolved star (donor), based on the Applegate mechanism (Applegate & Patterson, 1987) as proposed by Schleicher & Mennickent (2017). However, recently some changes have been observed in some light curves of DPVs and these could be related to variations in the disc size/temperature and the spot temperature/position (Garcés L et al., 2018). Some one of the DPVs were recently discovered using online catalogs such as ASAS–3 and most of the DPVs which have been discovered are Algol type eclipsing (DPV/E), Ellipsoidal (DPV/ELL) binaries and even a DPV of semi-regular amplitude has been found (Rosales, 2018). Therefore, we believe these catalogs are a big repository to search for new DPVs and must be reviewed periodically.

2 Photometric analysis and ephemeris

We have carried out a visual inspection to find new DPVs using the ASAS-SN Variable Stars Database [1] considering orbital periods between 10 to 40 days. We checked a total of 894 eclipsing binaries, such as the Detached Algol (EA), Beta Lyrae (EB) and Ellipsoidal (ELL) type binaries, and we found 3 new DPVs characterized by a deep primary eclipse. The orbital periods were determined using the Period Dispersion Minimization (PDM) task of IRAF[2] software (Stellingwerf, 1978). The errors were estimated through visual inspection of the light curves phased with trial periods close to the minimum of the periodogram until the light curves began to increase their dispersion. Through a code written by Zbigniew Kołaczkowski specially developed for the Double Periodic Variables stars, we have disentangled the two main photometric frequencies of every system. Specifically, the code adjusts the orbital signal to Fourier series consisting of the fundamental frequency plus their harmonics. This removes the signal from the original time series letting the long periodicity in a residual light curve. As a result, we obtained the light curves without the additional frequencies in isolated light curves.

We summarized the results in Table 1 and the disentangled light curves are shown in Figure 1. They show deep primary eclipses and relatively long orbital periods. The Double Periodic Variable ASAS-SN-V J163056.92-510307.1 appears cataloged as an eclipsing Algol (EA) type in the ASAS-SN Catalog with a 0.71 mag deep primary eclipse. Apparently it is a system of low inclination, which would allow to perform a detailed study of the more evolved star and to obtain relevant information about the stellar dynamo. In addition, the full amplitude of the long cycle in the V-band is 27% with respect to the total brightness of the light curve, and the long period is $P_l = 29.5P_o$. The DPV V593 Sco is other eclipsing Algol with a 1.1 mag mag deep primary eclipse, wherein the second variability is observed at the photometric data as function of the Heliocentric Julian Days (HJD, see Fig. 2) and reveals an orbital modulation typical of a DPV of circular orbit with a full amplitude of the long cycle of 43% of the total brightness. Its long period is 33 times the orbital period, i.e. $P_l = 33P_o$. The DPV TYC 6939-678-1 is cataloged as an eclipsing β Lyrae type (EB) with a 0.55 mag deep primary eclipse, within which the second photometric variability in the photometric data as a function of the HJD is easily observed, and its full amplitude is 21% of the total brightness of the light curve as shown. In addition it shows an increase of the data dispersion around ϕ_l =-0.5 and 0.5. Its respective long period is 31 times the orbital period. A peculiarity of the long cycles in these DPVs that have been discovered is that they are characterized by a quasi-sinusoidal variability.

Owing to the relevance of the mass loss/transfer process in close binary systems it was necessary to analyze every system using WISE Image Service[3] (Wright et al., 2010) with an image cutout of 300 arcsec and we confirmed the absence of nebulosity around these systems. In addition, these systems were not detected as X-ray sources by ROSAT survey[4] nor as Gamma-ray sources by Fermi SSC survey[5]. We consider that these Double Periodic Variable stars are optimal targets for further spectropolarimetry studies because these could help to constrain the mechanism based on magnetic dynamo in the donor star proposed by Schleicher & Mennickent (2017) and these could help us to understand

[1] `https://asas-sn.osu.edu/variables`

[2] IRAF is distributed by the National Optical Astronomy Observatories, which are operated by the Association of Universities for Research in Astronomy, Inc., under cooperative agreement with the National Science Foundation.

[3] `https://irsa.ipac.caltech.edu/applications/wise/`

[4] `http://www.xray.mpe.mpg.de/rosat/survey/rass-fsc/`

[5] `https://fermi.gsfc.nasa.gov/cgi-bin/ssc/LAT/LATDataQuery.cgi`

even more about the evolutionary process of DPV stars using models similar to those developed for the interacting binary V495 Centauri by Rosales et al. (2019).

Table 1: New confirmed Double Periodic Variables stars in the southern hemisphere and their respective orbital (P_o) and long (P_l) periods. Epochs for the minimum brightness of the orbital light curve and maximum brightness of the long cycle light curve are given and the value $T^{\star} = T - 2450000$. The brightness values are from ASAS-SN Catalog of Variable stars: II. The Apparent magnitudes were obtained from SIMBAD and APASS-DR9.

ASAS-SN ID	J163056.92-510307.1	J165917.75-350652.9	J212958.78-230007.2
Other ID	GDS J1630570-510306	V593 Sco	TYC 6939-678-1
RA (hh mm ss)	16 30 56.918	16 59 17.753	21 29 58.778
DEC (dd mm ss)	-51 03 07.056	-35 06 52.884	-23 00 07.164
P_o (days)	10.200(1)	17.502(8)	20.140(4)
P_l (days)	301.824:	582.610:	615.733:
$T_0^{\star}(\min_o)$	7457.85259	7670.49845	7191.75781
$T_0^{\star}(\max_l)$	7607.56973	7561.72467	7675.76706
V (SIMBAD)	12.919(38)*	13.523(36)*	11.640(140)
B (SIMBAD)	13.788(38)*	14.404(90)*	12.240(180)

Note: The apparent magnitudes marked with the asterisk symbol (*) were obtained from APASS-DR9[6].

Acknowledgements: We acknowledge support by Fondecyt 1190621.

References:

Applegate, J. H., & Patterson, J. 1987, *ApJL* , **322**, L99 DOI

Barría, D., Mennickent, R. E., Schmidtobreick, L., et al. 2013, *A&A*, **552**, A63 DOI

Garcés L, J., Mennickent, R. E., Djurašević, G., Poleski, R., & Soszyński, I. 2018, *MNRAS*, **477**, L11 DOI

Mennickent, R. E. 2017, *Serbian Astronomical Journal*, **194**, 1 DOI

Mennickent, R. E., Djurašević, G., Cabezas, M., et al. 2015, *MNRAS*, **448**, 1137 DOI

Mennickent, R. E., Pietrzyński, G., Diaz, M., & Gieren, W. 2003, *A&A*, **399**, L47 DOI

Poleski, R., Soszyński, I., Udalski, A., et al. 2010, *AcA*, **60**, 179

Rosales, J. A., Mennickent, R. E., Schleicher, D. R. G., & Senhadji, A. A. 2019, *MNRAS*, **483**, 862 DOI

Rosales Guzmán, J. A., Mennickent, R. E., Djurašević, G., Araya, I., & Curé, M. 2018, *MNRAS*, **476**, 3039 DOI

Rosales, J. A., Mennickent, R. E. 2018, *IBVS*, **6248**, 1 DOI

Schleicher, D. R. G., & Mennickent, R. E. 2017,*A&A*, **602**, A109 DOI

Stellingwerf, R. F. 1978, *ApJ*, **224**, 953 DOI

Wright, E. L., Eisenhardt, P. R. M., Mainzer, A. K., et al. 2010, *AJ*, **140**, 1868 DOI

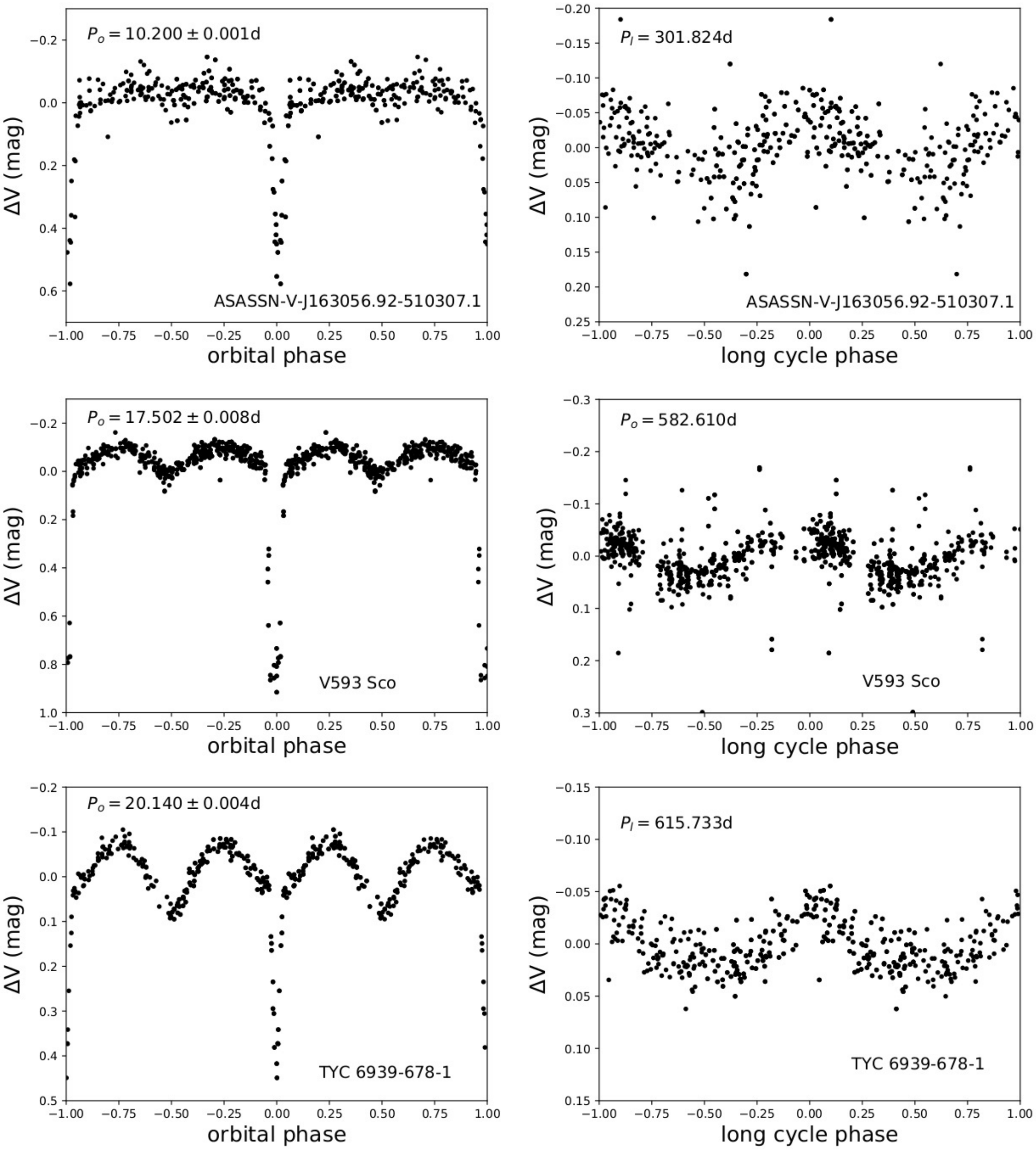

Figure 1. Disentangled ASAS-SN V-band light curves of three new Double Periodic Variables stars. The left hand side corresponds to light curves phased using the orbital periods, while on the right hand side is observed the long cycle of every system.

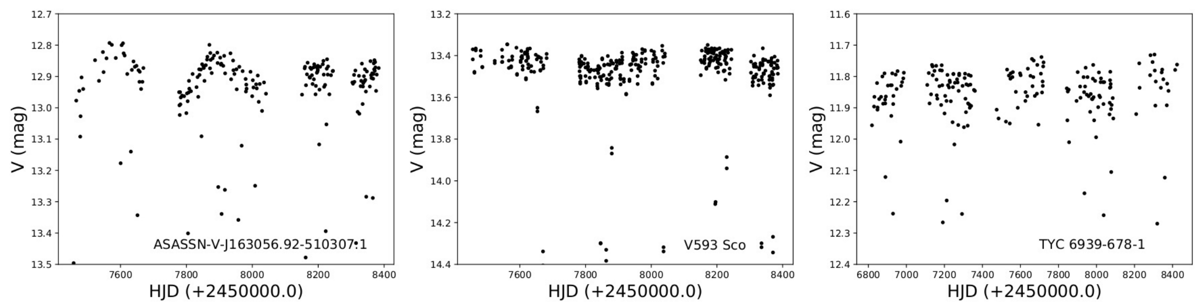

Figure 2. Photometric data as function of the Heliocentric Julian Days wherein is easily observed the second photometric variability of the new discovered DPVs.

COMMISSIONS G1 AND G4 OF THE IAU
INFORMATION BULLETIN ON VARIABLE STARS

Volume 63 Number 6269 DOI: 10.22444/IBVS.6269

Konkoly Observatory
Budapest
3 June 2019

HU ISSN 0374 – 0676

A NEW EPHEMERIS AND FUNDAMENTAL PARAMETERS FOR THE ECLIPSING BINARY STAR GSC 03612-1565 = V2647 CYG

KOZYREVA, V. S.[1]; KUSAKIN, A. V.[2]; BOGOMAZOV, A. I.[1], KRAJCI, T.[3]

[1] M. V. Lomonosov Moscow State University, P. K. Sternberg Astronomical Institute, 13, Universitetskij prospect, Moscow, 119991, Russia

[2] National Space Agency, Fesenkov Astrophysical Institute, 23 Observatory, Almaty, 050020, Kazakhstan

[3] Astrokolkhoz Observatory, Center for Backyard Astrophysics, New Mexico, PO Box 1351 Cloudcroft, NM 83117, USA

Abstract

High precision light curves were obtained for the GSC 03612-1565 = V2647 Cyg eclipsing binary system in 2009 and in 2018. The solution for these curves allowed to estimate the limb darkening coefficients and spectral classes of components (F5V–F8V). Also a new ephemeris was computed, it is very different in comparison to a previous study by Otero et al. (2006). The circular orbit instead the elliptical was found.

The investigated star (V2647 Cyg, its $\mathrm{RA_{J2000}}$ is 21:47:03, its $\mathrm{Dec_{J2000}}$ is +50:03:17, its orbital period is $P_{orb} = 3.9035242$ days) was discovered in ASAS survey (Pojmanski, 2002). It was included in the list of fifty new eclipsing binaries with elliptical orbits found in ASAS, Hipparcos and NSVS databases by Otero et al. (2006), who also noted that primary eclipses of this star can be secondary eclipses and gave following ephemeris for V2647 Cyg:

$$\mathrm{Min\ I} = \mathrm{HJD}\,2453671.255 + 5.85527 \times E, \qquad (1)$$

where E is the number of orbital cycles since the initial epoch. The secondary minimum phase was equal to 0.334, this high shift relative to the phase 0.5 indicated that the star's orbit could be an ellipse with a high eccentricity. Such stars are very interesting objects, because they possess the apsidal motion that helps to study the concentration of the matter of the star to its center and to compare the star's matter distribution with theoretical models.

Our photometric observations of V2647 Cyg were conducted using three telescopes: (1) at Tien Shan Observatory of Fesenkov Astrophysical Institute using the V filter in August 2009 (with the Ritchey–Chritien-350 telescope and the ST-402 CCD sensor), (2) at Astrokolkhoz observatory (New Mexico) in December 2009 with the ACP AAVSOnet Wright 30 telescope using V filter, and an SBIG ST-9 CCD sensor, (3) during 2018 at Tien Shan Observatory with Zeiss-1000 telescope and the Apogee U900 CCD sensor, in V and R filters.

Observations inside minima were obtained in August 2009 (Min II) and in December 2009 (Min I). These minima occurred practically according to Equation 1. Reference stars

TYC 3612-718-1 (V=10.71^m) and TYC 3612-1006-1 (V=11.24^m) were almost constant during observations (they showed a variability less than 0.005^m). The depth of Min II in V filter in 2009 was 0.725^m, and the depth of Min I was 0.475^m. So, it seemed that the primary star was the secondary and and vice versa as was noted by Otero et al. (2006).

Subsequent observations of V2647 Cyg were conducted in 2018. On 8 and 10 January both kind of minima were obtained, and the depths of these minima corresponded their names (i.e., Min I was deeper than Min II). In August 2018 we obtained Min I that was of the same value as Min I in January 2018, and it is the same as the value of Min II in 2009. The difference between minima in 2009 and 2018 can be related to the change of the orbit's inclination or to the variability of the components of the system. For the first explanation the change should be catastrophic (too rapid). Practically precise coincidence of the primary minimum's value in 2018 and the secondary minimum's value in 2009 also excludes the variability as an explanation.

V2647 Cyg also was observed by Super-WASP project (Butters et al., 2010, Paunzen et al., 2014), data were downloaded[1,2], and compiled light curves were analysed using Equation 1. These data gave three minima for this system, all minima followed each other strictly after 1/3 of the orbital period. The explanation of such effect could be the only one: Ephemeris 1 was wrong. Using a set of five minima we found an exact ephemeris. We also found that the orbit was almost a circle. So, the primary minima (according to Equation 1) in 2009 were the secondary minima and vice versa, whereas in 2018 positions of minima coincided with predictions of Equation 1. Our new ephemeris is:

$$\text{Min I} = \text{HJD}\,2458127.1346 + 3.9035242 \times E. \tag{2}$$

To find times of minima for the system the photometric elements were computed. For Super-WASP observations it was impossible to calculate times of minima, because they did not contain minima with both branches.

For estimations of the system's parameters we used a computer code by Kozyreva & Zakharov (2001). The components assumed to be spherical and the limb darkening was linear. These assumptions can be good approximations, because the system should be well detached. A minimization algorithm was quasi-newtonian with analytically calculated derivatives of the functional (Gill & Murray, 1978). The minimizing functional includes the sum of the squares of observed minus calculated values of the stars' magnitudes in all points and simple linear limitations on the parameters. The influence of limb darkening coefficients u_1 and u_2 on the brightness of the system appears on such parts of light curves that correspond to intersections of disks of components. A reliable determination of u_1 and u_2 from light curves can be made only with very high precision observations ($\sigma_{o-c} \leq 0.005^m$), and light curves obtained during the intersection of disks should be continuous.

Two minima obtained in 2018 (Min II in January and Min I in August, see Figure 1) satisfied the described requirements. Limb darkening coefficients in V filter were: $u_1 = 0.59$, $u_2 = 0.61$. Usually such quantities correspond to stars with spectral types F5-F8 (van Hamme, 1993). Earlier it was not possible to obtain limb darkening coefficients from calculations of photometric elements, because the mean square error σ_{o-c} was higher than 0.005^m, and only in latest observations σ_{o-c} became equal to 0.004^m. It would be interesting to compare such simple estimations of the spectral type with determinations made using independent methods (until now there are no spectral observations of V2647

[1]https://exoplanetarchive.ipac.caltech.edu/docs/SuperWASPMission.html
[2]http://wasp.cerit-sc.cz/

Cyg). Obtained photometric elements can be found in Table 1. Eccentricity of the orbit was found to be close to zero in contradiction with Otero et al. (2006). The notations in Table 1 are following: r_1 and r_2 are radii of stars in units of the semi-major axis, i is the inclination angle of their orbit to the plane of the sky, e is its eccentricity, ω is the periastron longitude, L_1 and L_2 are the luminosities of the components in units of the total system's luminosity, L_3 is the third light in the same units, u_1 and u_2 are limb darkening coefficient of components, L_1/L_2 is the ratio of luminosities of both stars, I_1/I_2 is the ratio of their surface brightnesses, σ_{o-c} is the standard deviation of the light curve.

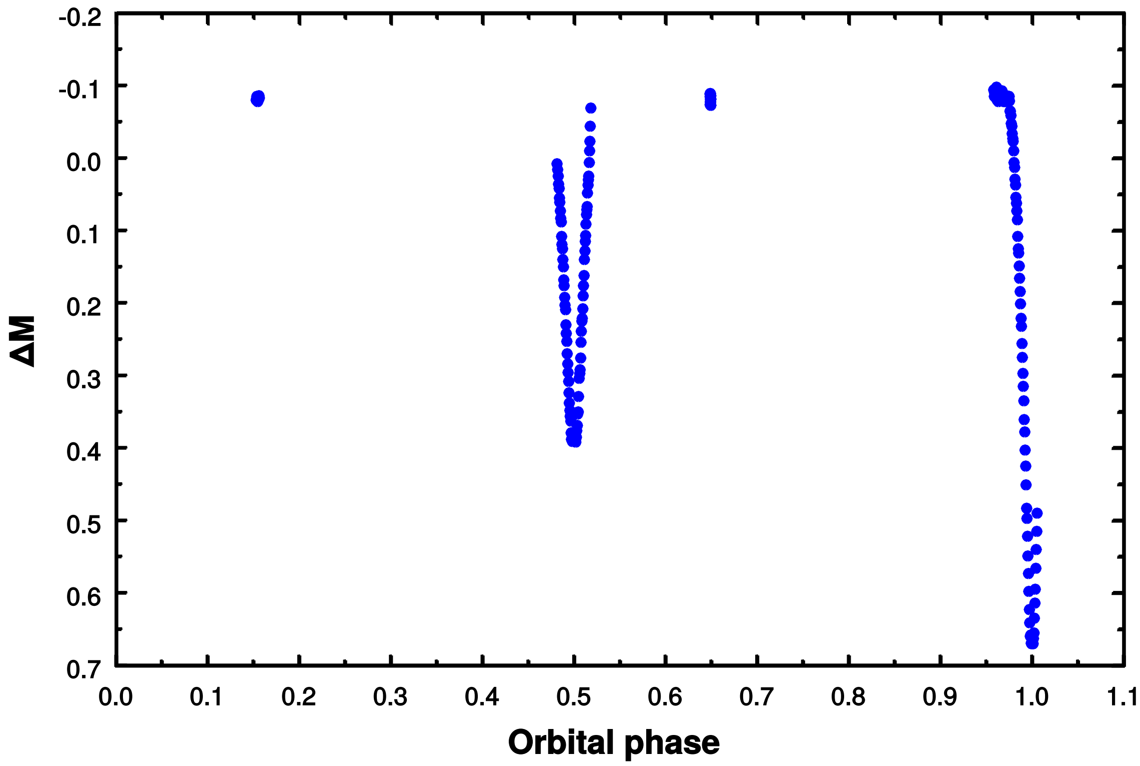

Figure 1. A sample light curve of V2647 Cyg in V filter. Horizontal axis presents the orbital phase in Ephemeris 2, vertical axis presents the difference of the stellar magnitude between V2647 Cyg and TYC 3612 1006-1.

It is possible to make some constraints on spectral classes of the components. The star's parallax is $0.00276'' \pm 0.00006''$ (Lindegren et al., 2018), it corresponds to the distance to the object $358.4^{+8.0}_{-7.7}$ parsecs (Bailer-Jones et al., 2018). It is possible to estimate absorption in V band, A_v is less than 0.1^m according to the mean absorption in V filter in the galactic plane. The visual stellar magnitude and $B-V$ colour index for V2647 are $m_V = 11.05^m$ and $B-V = 0.48^m \pm 0.07^m$ (Høg et al., 2000). Taking into account estimations of spectral types made above, the difference between apparent and absolute stellar magnitudes, and the estimation of absorption one can obtain the distance to the star to be equal to 370 ± 30 parsecs. This value is in adequate agreement with the estimation of the distance from the parallax value (and $B-V = 0.48^m$ does not contradict it). So we can claim that spectral types of both components are in the range F5V-F8V.

Non-symmetry of minima of light curves of systems with elliptical orbits, physical fluctuations of brightness, and errors of measurements lead to differences in results obtained using different methods. In our method we take a conjunction as the time of minimum, i.e., such configurations when the distance between centers of stars projected to the plane of the sky are minimal. To find times of conjunctions we used all set of minima and took additional information from other light curves (for example, a possible existence of systematic errors from light curves of reference stars) assuming several geometric parameters to be constant. Such a method allows to find times of conjunctions with higher precision than estimations of times of minima using only light curve points from an individual minimum of brightness.

To calculate times of minima for V2647 Cyg in Table 2 obtained from our observations in 2009 and 2018 we used fixed parameters from the column 3 (2018 V) in Table 1. Minima were found for observations in V and R filters for 2018 observations and their average values were calculated for Table 2. Also we showed times of minima published by Brat et al. (2008). In the table, (O–C) is the difference between the observed time of minima (in the first column) and the value calculated using Ephemeris 2. "Min" is the type of a minimum (primary or secondary). To find variations of the orbital period due to the influence of additional companions or physical processes the observations of the system should be continued.

The value of the V2647 Cyg orbital period in General Catalogue of Variable stars (Samus et al., 2017) should be updated: a new period is $P_{orb} = 3.9035242$ days.

Light curves obtained at Tien Shan Observatory can be found as additional tables.

Acknowledgements: This research has made use of the SIMBAD database, operated at CDS, Strasbourg, France (Wenger et al., 2000). Also it has made use of NASA's Astrophysics Data System. The authors thanks the anonymous referee for valuable comments.

The work of A. V. Kusakin was carried out within the framework of Project No. BR05236322 "Studies of physical processes in extragalactic and galactic objects and their subsystems", financed by the Ministry of Education and Science of the Republic of Kazakhstan.

References:

Bailer-Jones C. A. L., Rybizki J., Fouesneau M., Mantelet G., Andrae R., 2018, *AJ*, **156**, 58 DOI

Brat L., Šmelcer, L., Kuèáková, H., et al., 2008, *OEJV*, **94**, 1

Butters O. W., West R. G., Anderson D. R., et al., 2010, *A&A*, **520**, L10 DOI

Gill P. E., Murray W., 1978, *Mathematical Programming*, **14**, 349 DOI

Høg E., Fabricius C., Makarov V. V., Urban S., Corbin T., Wycoff G., Bastian U., Schwekendiek P., Wicenec A., 2000, *A&A*, **355**, L27

Kozyreva V. S., Zakharov A. I., 2001, *Astronomy Letters*, **27**, 712 DOI

Lindegren L. et al., 2018, *A&A*, **616**, A2 DOI

Otero S. A., Wils R., Hoogeveen G., Dubovsky P. A., 2006, *IBVS*, **5681**

Samus N. N., Kazarovets E. V., Durlevich O. V., Kireeva N. N., Pastukhova E. N., 2017, *Astronomy Reports*, **61**, 80 DOI

Paunzen E., Kuba M., West R. G., Zejda M., 2014, *IBVS*, **6090**

Pojmanski G., 2002, *AcA*, **52**, 397

van Hamme W., 1993, *AJ*, **106**, 2096 DOI

Wenger M., Ochsenbein F., Egret D., et al., 2000, *A&A Supplement*, **143**, 9 DOI

Table 1. Photometric elements of V2647 Cyg computed using observations in 2009 in V filter, and in 2018 in V and R filters. See text for notations.

Element	2009 (V)	2018 (V)	2018 (R)
r_1	0.088 ± 0.001	0.089 ± 0.01	0.089 ± 0.01
r_2	0.075 ± 0.001	0.077 ± 001	0.076 ± 0.01
i	$89.6° \pm 0.2°$	$89.9° \pm 0.1°$	$89.9° \pm 0.1°$
e	0.002 ± 0.001	0.003 ± 0.001	0.007 ± 0.003
ω	$280.3° \pm 0.5°$	$264.1° \pm 0.3°$	$268.0° \pm 0.4°$
L_1	0.644 ± 0.020	0.628 ± 0.01	0.618 ± 0.030
L_2	0.351 ± 0.020	0.353 ± 0.01	0.360 ± 0.030
L_3	0.010 ± 0.020	0.02 ± 0.020	0.02 ± 0.020
u_1	0.59 (fixed)	0.59 ± 0.4	0.49 (fixed)
u_2	0.61 (fixed)	0.61 ± 0.4	0.48 (fixed)
L_1/L_2	1.835 ± 0.015	1.837 ± 0.005	1.720 ± 0.015
I_1/I_2	1.320 ± 0.04	1.325 ± 0.10	1.260 ± 0.04
σ_{o-c}	0.0086^m	0.0040^m	0.0040^m

Table 2. Times of minima of V2647 Cyg from our observations and from the literature. See text for notations.

HJD-2400000	(O–C)	Min	Reference
53817.6437	–0.0002	II	Brat et al. (2008)
53905.4734	0.0002	I	Brat et al. (2008)
55043.3510	0.0005	I	this study
55193.6373	0.0011	II	this study
58127.1346	0.0000	I	this study
58129.0864	0.0000	II	this study
58357.4432	0.0007	I	this study

COMMISSIONS G1 AND G4 OF THE IAU
INFORMATION BULLETIN ON VARIABLE STARS
Volume 63 Number 6270 DOI: 10.22444/IBVS.6270

Konkoly Observatory
Budapest
3 June 2019

HU ISSN 0374 – 0676

V1097 Her – A W-TYPE OVERCONTACT ECLIPSING BINARY

NELSON, ROBERT H.[1,2]; RUSSELL, ROBB[3]

[1] Mountain Ash Observatory, 1393 Garvin Street, Prince George, BC, Canada, V2M 3Z1
email: bob.nelson@shaw.ca

[2] Guest investigator, Dominion Astrophysical Observatory, Herzberg Institute of Astrophysics, National Research Council of Canada

[3] Department of Physics and Astronomy, University of Victoria, Victoria, BC, Canada
email: robb@uvic.ca

Abstract

V1097 Her, an overcontact (W-type) eclipsing binary, has a short period, a relatively low degree of contact (or fill-out parameter), and an increasing period. It has now been classified: for the more luminous star a spectral type of F8.5V±1 has been determined. B,V,Ic light curves and, for the first time, radial velocity curves for the overcontact binary V1097 Her have been obtained; these have been subjected to a Wilson-Devinney analysis, yielding fundamental parameters; in particular masses of 0.41 ± 0.01 and 1.11 ± 0.02 $M_\odot$ and luminosities of 0.77 ± 0.01 and 1.75 ± 0.03 $L_\odot$ respectively. The distance estimate of $r = 237 \pm 11$ pc is consistent with the Gaia value of $r = 250.3 \pm 1.4$ pc (Bailer-Jones et al., 2018; Gaia Collaboration, 2018). A period analysis, again believed to be the first ever, has been undertaken, revealing a constant rate of period increase of $\mathrm{d}P/\mathrm{d}t = (1.85 \pm 0.11) \times 10^{-7}$ d/yr.

As a by-product of the ROTSE all-sky survey (Akerlof et al., 2000), well over 1000 new periodic variables were discovered. One of these, V1097 Her (ROTSE1 J173327.94+265547.5, NSVS 8002361, TYC 2083-1870-1) was identified as a EW-type eclipsing binary with a period of 0.360819 d and an amplitude of 0.458 mag (clear filter). Follow-up CCD observations for this system and three others were performed by Bälttler and Diethelm (2002) who obtained new light curves and many new times of minima, one result of which was to refine the period for V1097 Her, obtaining $P = 0.360847$ d (no error estimate). Subsequently, there have been many new published eclipse timings.

An eclipse timing difference (O–C) plot using all the timings from 1999 (earliest) to 2018 is depicted in Fig. 1. Although there is considerable scatter, a quadratic relation over the data collection interval (cycle 28800 to 30770 for the RVs and cycle –3205 to 16047 for the light curve data) was obtained; equation (1) below defines the weighted quadratic fit. (Note: in it, and throughout the paper, figures in brackets denote the error estimates in units of the last digit.)

$$\mathrm{JD\,(Hel)_{MinI}} = 2452463.4068(3) + 0.36084705(1)\mathrm{E} + 8.4(5) \times 10^{-11}\mathrm{E}^2 \qquad (1)$$

A weighted linear least-squares fit for the data from cycle 6881 (2009) to cycle 15129 (2017) yielded the fit of equation (2), used in all phasing.

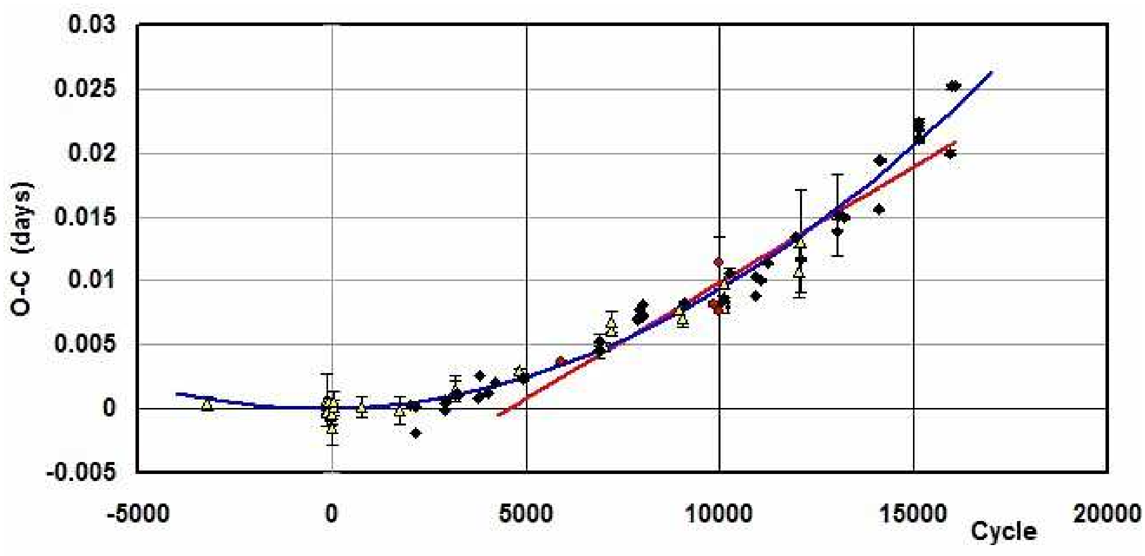

Figure 1. V1097 Her – eclipse timing (O-C) plot with the quadratic fit. Legend: (yellow-filled) triangles - visual, (red) circles - photoelectric, and (black) diamonds - CCD.

$$\mathrm{JD\,(Hel)}_{\mathrm{MinI}} = 2458253.9395(10) + 0.3608488(1)\mathrm{E} \quad (2)$$

The Excel file (and many others) are available at Nelson (2017). The 5000+ files are updated annually. Further eclipse timings are recommended in order to detect, or alternatively rule out a light time effect (LiTE).

There has been no light curve analysis for this system. In order to rectify this lack, the lead author first secured, in April of 2009, 2011, 2015, and 2016 and in September of 2017, a total of 14 medium resolution (R∼10000 on average) spectra of V1097 Her at the Dominion Astrophysical Observatory (DAO) in Victoria, British Columbia, Canada using the Cassegrain spectrograph attached to the 1.85 m Plaskett Telescope. He used the 21181 configuration with the 1800Yb grating (1800 lines/mm, blazed at 5000 Å), which gave a reciprocal linear dispersion of 10 Å/mm in the first order. The wavelengths ranged from 5000 to 5260 Å, approximately. A log of observations is given in Table 1.

Frame reduction was performed by software *RaVeRe* (Nelson 2013). See Nelson (2010a) and Nelson et al. (2014) for further details. The normalized spectra are reproduced in Fig. 2, sorted by phase. Note towards the right the strong neutral iron lines (at 5167.487 and 5171.595 Å) and the strong neutral magnesium triplet (at 5167.33, 5172.68, and 5183.61 Å).

Radial velocities were determined using the Rucinski broadening functions (Rucinski 2004, Nelson 2010a) as implemented in software *Broad25* (Nelson 2013). See Nelson et al. (2014) for further details. An Excel worksheet with built-in macros (written by him) was used to do the necessary radial velocity conversions to geocentric and back to heliocentric values (Nelson 2014). The resulting RV determinations are also presented in Table 1. The mean rms errors for RV1 and RV2 are 8.5 and 7.8 km/s, respectively, and the overall rms deviation from the (sinusoidal) curves of best fit is 8.3 km/s. The best fit yielded the values $K_1 = 250.0(1.5)$ km/s, $K_2 = 87.1(1.5)$ km/s and $V_\gamma = 14.9(1.0)$ km/s, and thus a mass ratio $q_{sp} = K_1/K_2 = M_2/M_1 = 2.87(5)$.

Representative broadening functions, at phases 0.24 and 0.78 are depicted in Figs. 3

Table 1: Log of DAO observations

DAO Image #	Mid Time (HJD-2400000)	Exposure (sec)	Phase at mid-exp	V_1 (km/s)	V_2 (km/s)
09-5354	54927.0236	3378	0.302	–215.1 (8.2)	103.9 (8.6)
09-5396	54928.8629	3600	0.400	—	73.1 (8.1)
09-5425	54929.8849	3600	0.232	–228.1 (7.1)	97.0 (3.2)
11-2578	55670.8957	3600	0.756	258.0 (1.9)	–56.6 (3.0)
11-2675	55674.8901	3600	0.826	225.9 (4.3)	–76.2 (3.9)
15-3150	57121.8629	3600	0.746	270.7 (3.1)	–74.9 (4.2)
16-1288	57493.9341	3600	0.847	245.1 (2.9)	–65.1 (2.6)
16-1328	57495.9094	3600	0.321	–208.2 (3.3)	92.3 (2.0)
16-1358	57496.9657	3000	0.248	–237.5 (3.3)	91.3 (3.0)
17-4017	57859.9463	2500	0.158	–189.7 (1.0)	81.7 (0.2)
17-13704	57997.8196	2500	0.239	–233.8 (1.5)	99.1 (9.3)
17-15737	57998.6748	2500	0.609	—	–32.9 (6.5)
17-15793	57999.8174	2500	0.775	274.5 (10.2)	–71.6 (4.9)
17-15950	58008.8000	2500	0.668	217.8 (2.7)	–67.9 (5.6)

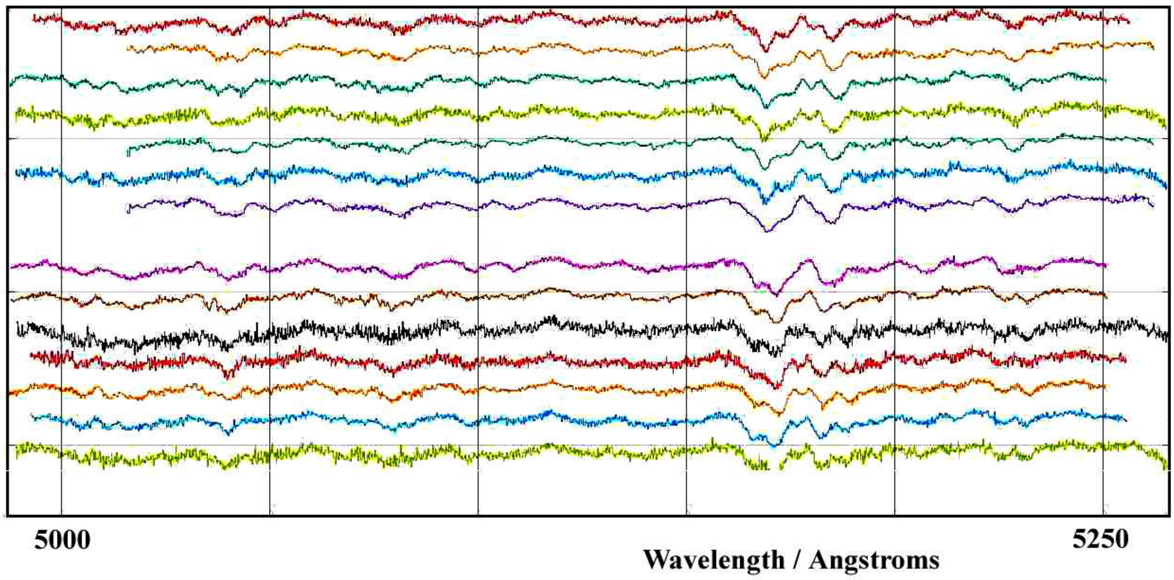

Figure 2. V1097 Her spectra at phases 0.16, 0.23, 0.24, 0.25, 0.30, 0, 32, 0.40, 0.61, 0.67, 0.75, 0.76, 0.78, 0.83, 0.85 (from top to bottom)

and 4, respectively. Smoothing by a Gaussian filter is routinely done in order to centroid the peak values for determining the radial velocities.

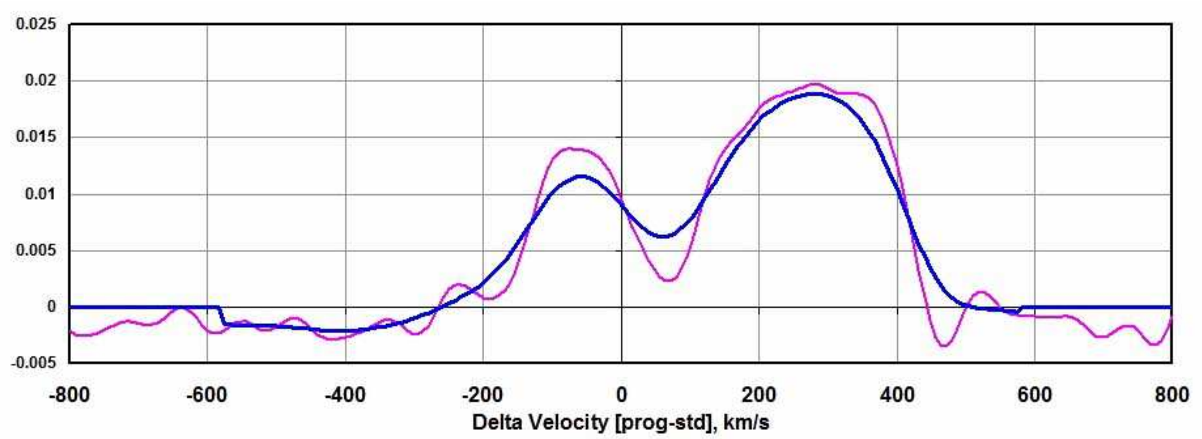

Figure 3. Broadening functions at phase 0.24–smoothed and unsmoothed.

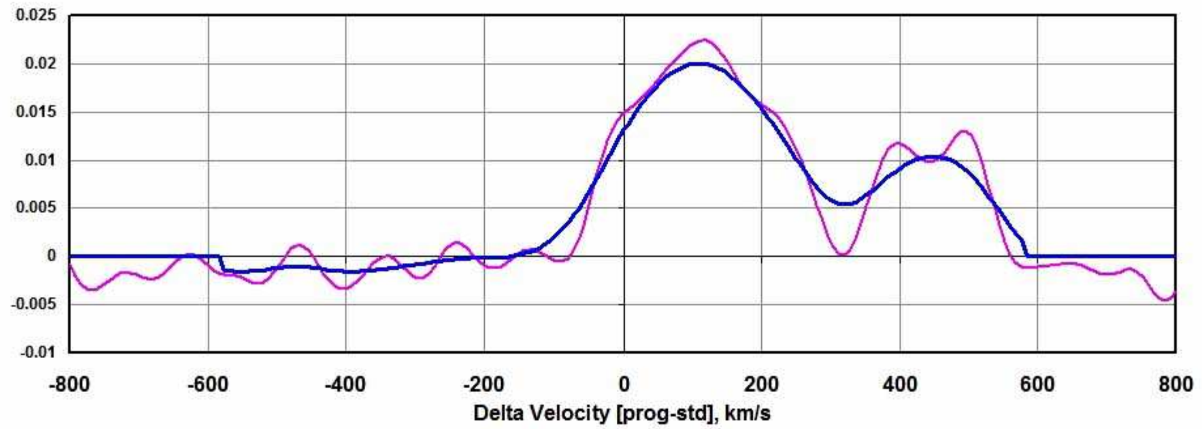

Figure 4. Broadening functions at phase 0.78–smoothed and unsmoothed.

In June of 2011, and again in 2012, the lead author took a total of 87 frames in V, 88 in R_C (Cousins) and 118 in the I_C (Cousins) band at his private observatory in Prince George, BC, Canada. The telescope was a 33 cm f/4.5 Newtonian on a Paramount ME mount; the cameras used were the SBIG ST-7XME and ST-10XME.

Standard reductions were then applied (see Nelson et al., 2014 for more details). The variable, comparison and check stars are listed in Table 2. The coordinates for V1097 Her, the comparison, and check stars (rounded to integral seconds) are from the Tycho Catalogue (Høg et al., 2000), the magnitudes are taken from the AAVSO Photometric All-Sky Survey (APASS, DR9)[1] catalogue (Henden et al., 2012)

The 2003 version of the Wilson-Devinney (WD) light curve and radial velocity analysis program with Kurucz atmospheres (Wilson and Devinney, 1971; Wilson, 1990; Kallrath

[1] https://www.aavso.org/download-apass-data

Table 2: Details of variable, comparison and check stars.

Object	GSC	RA (J2000)	Dec (J2000)	V (mag)	$B-V$ (mag)
Variable	2083-1870	17:33:28	+26:55:47	10.91 (6)	0.58 (10)
Comparison	2083-1693	17:33:37	+26:58:38	10.33 (4)	0.05 (4)
Check	2083-2141	17:33:43	+26:47:56	10.07 (4)	1.49 (7)

and Milone; 1998, Wilson, 1998) as implemented in the Windows front-end software WDwint (Nelson 2013) was used to analyze the data.

For classification purposes, one of the authors (R.M.R.) took two low resolution spectra, on 2013 June 22 (HJD = 2456465.7981; mid exposure, UTC). He used the 1.85 m Plaskett telescope at the Dominion Astrophysical Observatory (DAO) in Victoria, British Columbia, Canada with the Cassegrain spectrograph in the 2131 configuration, resulting in a reciprocal dispersion of 60 Å/mm. The two spectra were very similar (see Fig. 5). The strength of the Calcium H&K lines, G-band, Hγ, Fe I 4384, Ca I 4227, and Hδ lines all indicated a F8.5V±1 spectral classification for V1097 Her.

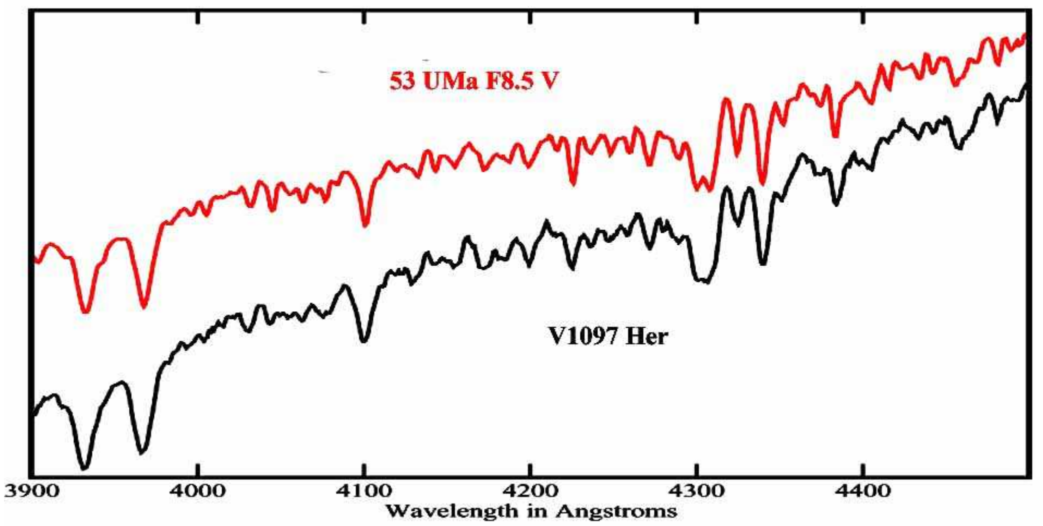

Figure 5. Classification spectra for V1097 Her.

Interpolated tables from Flower (1996) gave a temperature $T_2 = 6191 \pm 162$ K and $\log g = 4.369 \pm 0.006$ (cgs). (The quoted errors refer to one and one half spectral subclass.) An interpolation program by Terrell (1994, available from Nelson 2013) gave the Van Hamme (1993) limb darkening values; and finally, a logarithmic (LD=2) law for the limb darkening coefficients was selected, appropriate for temperatures < 8500 K (ibid.). The limb darkening coefficients are listed below in Table 3. (The values for the second star are based on the later-determined temperature of 6191 K and assumed spectral type of F8.) Convective envelopes for both stars were used, appropriate for cooler stars hence values gravity exponent $g = 0.32$ and albedo $A = 0.5$ were used for each (Lucy, 1967; Rucinski, 1969, respectively).

From the GCVS 4 designation (EW) and from the shape of the light curve, mode 3 (overcontact binary) was used. Later on, mode 2 (detached) was tried. but DC adjust-

Table 3: Limb darkening values from Van Hamme (1993)

Band	x_1	x_2	y_1	y_2
V	0.735	0.739	0.263	0.259
R_C	0.663	0.667	0.274	0.272
I_C	0.579	0.583	0.265	0.264
Bol	0.645	0.644	0.227	0.226

ments required decreases in potential 2 below the critical value, so mode 2 was abandoned.

It was noted immediately that the curve heights at Max I (phase 0.25) and Max II (phase 0.75) were significantly different. This is the O'Connell effect (Davidge & Milone, 1984, and references therein) and is usually explained by the presence of one or more star spots. Accordingly, one was added first to star 2, and this gave good results. (Moving the spot to star 1 gave poorer results and was abandoned.)

Convergence by the method of multiple subsets was reached in a small number of iterations. (The subsets were: (i, q, L_1, R), (T_2, Ω_1), (i, R, Tf), and (i, Lng, R) where i = inclination, q = mass ratio, L_1 = luminosity (scale factor), Ω_1 = potential, Lng = spot longitude, R = spot radius, and Tf = temperature factor). Quantities a (semi-major axis), φ (phase correction), and V_γ (system centre of mass radial velocity) were uncorrelated and therefore could be added to any subset for adjustment.

Detailed reflections were tried, with nref = 3, but there was little–if any–difference in the fit from the simple treatment. There are certain uncertainties in the process (see Csizmadia et al., 2013, Kurucz, 2002). On the other hand, the solution is very weakly dependent on the exact values used.

The model is presented in Table 4. For the most part, the error estimates are those provided by the WD routines and are known to be low; however, it is a common practice to quote these values and we do so here. Also, estimating the uncertainties in temperatures T_1 and T_2 is somewhat problematic. A common practice is to quote the temperature difference over–say–one spectral sub-class. (the case here). In addition, various different calibrations have been made (Cox, 2000, page 388–390 and references therein, and Flower, 1996), and the variations between the various calibrations can be significant. If the classification is ± one sub-class, an uncertainty of ± 150 K to the absolute temperatures of each, would be typical. The modelling error in temperature T_2, relative to T_1, is indicated by the WD output to be much smaller, around 3 K (and is clearly much too low).

The light curve data and the fitted curves are depicted in Figures 6–8. The residuals (in the sense observed-calculated) are also plotted, shifted upwards by 0.55 units.

The Radial Velocities are shown in Fig. 9. A three-dimensional representation from *Binary Maker 3* (Bradstreet, 1993) is shown in Fig. 10 and one for the potentials, in Fig. 11.

The WD output fundamental parameters and errors are listed in Table 5. To save space, those for a similar system, AC Boo (Nelson 2010b), are listed here in column 5-6 and discussed later. Most of the errors are output or derived estimates from the WD routines. From Kallrath & Milone (1998, see also Mochnacki 1981), the fill-out factor is $f = (\Omega_I - \Omega)/(\Omega_I - \Omega_O)$, where Ω is the modified Kopal potential of the system, Ω_I is

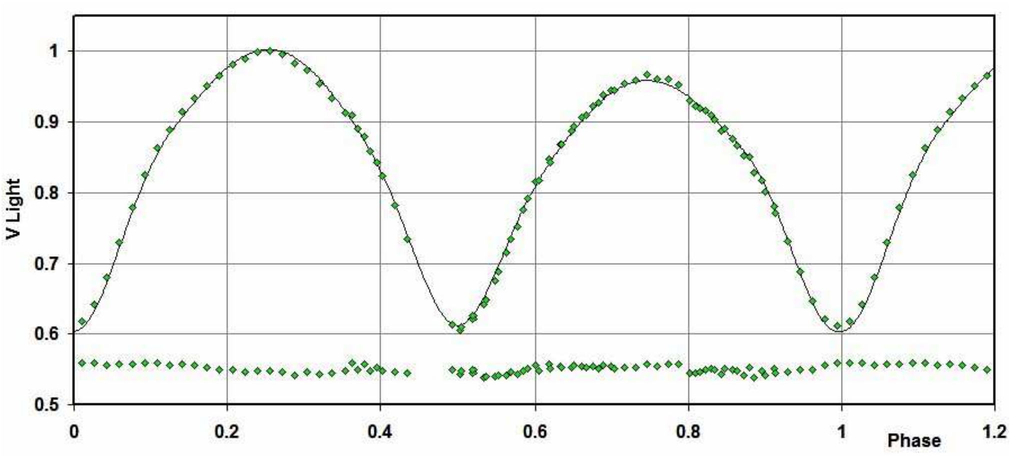

Figure 6. *V* Light Curves for V1097 Her – Data, WD fit, and residuals.

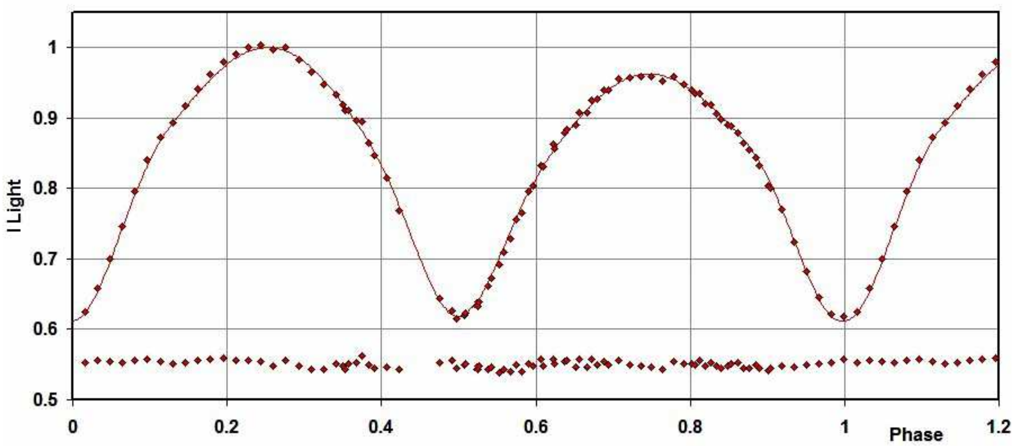

Figure 7. *R* Light Curves for V1097 Her – Data, WD fit, and residuals.

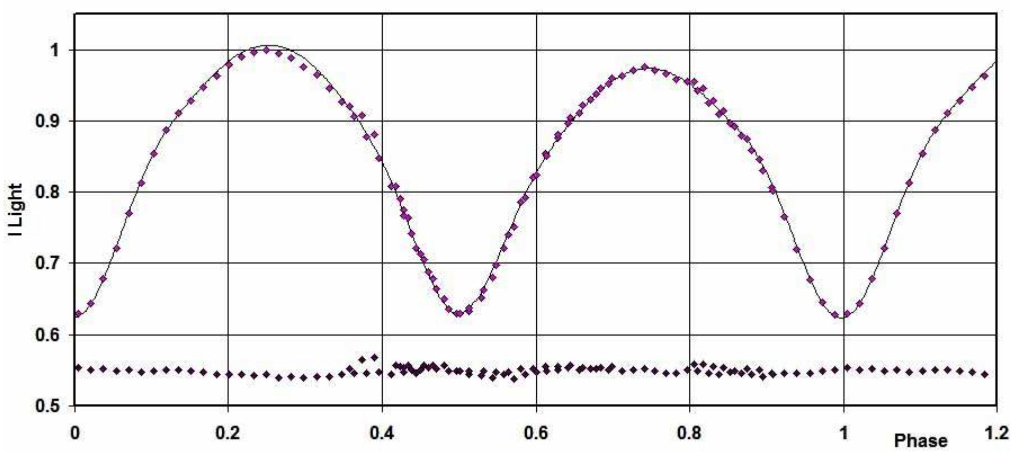

Figure 8. *I* Light Curves for V1097 Her – Data, WD fit, and residuals.

Table 4: Wilson-Devinney parameters

WD Quantity	Value	error	Unit
Temperature, T_1	6250	3	K
Temperature, T_2	6095	[fixed]	K
$q = m_2/m_1$	2.74	0.05	—
Potential, $\Omega_1 = \Omega_2$	6.115	0.007	—
Inclination, i	76.9	0.1	degrees
Semi-maj. axis, a	2.50	0.04	solar radii
V_γ	13.4	1.7	km/s
Phase shift	-0.0030	0.0002	—
Fill-out, f_1	0.13	0.05	
$L_1/(L_1 + L_2)$ (V)	0.312	0.001	—
$L_1/(L_1 + L_2)$ (R_C)	0.309	0.001	—
$L_1/(L_1 + L_2)$ (I_C)	0.305	0.001	—
r_1 (pole)	0.2870	0.0009	orbital radii
r_1 (side)	0.3008	0.0011	orbital radii
r_1 (back)	0.3425	0.0020	orbital radii
r_2 (pole)	0.4507	0.0006	orbital radii
r_2 (side)	0.4849	0.0008	orbital radii
r_2 (back)	0.5152	0.0011	orbital radii
Spot co-latitude	59	10	degrees
Spot longitude	280	3	degrees
Spot radius	21.3	0.5	degrees
Spot temp. factor	0.873	0.002	—
$\Sigma\omega^2_{res}$	0.0285	—	—

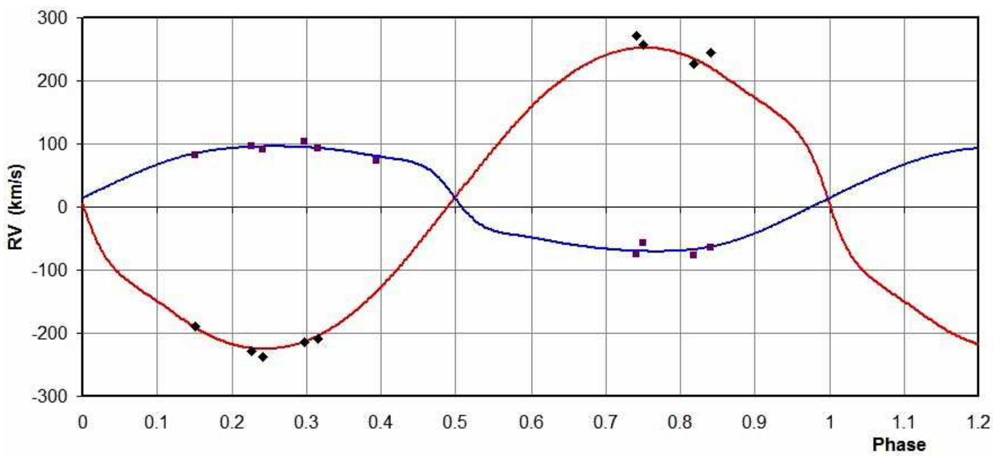

Figure 9. Radial velocity curves for V1097 Her – Data and WD Fit. The primary is represented by (black) diamonds; the secondary, by (purple) squares.

that of the inner Lagrangian surface, and Ω_O, that of the outer Lagrangian surface, was also calculated. In the case of the masses (and mass ratio elsewhere), errors were assigned on the basis of a detailed analysis of errors in the radial velocities (and derived quantities thereof). See Nelson (2015a) for an explanation of the method.

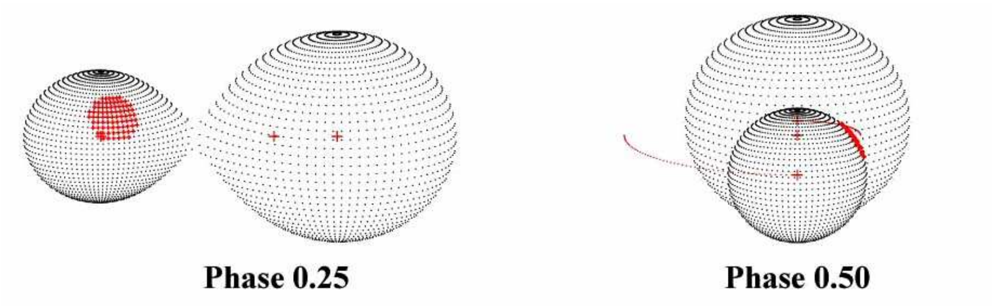

Figure 10. Binary Maker 3 representation of the system – at phases 0.25 and 0.50.

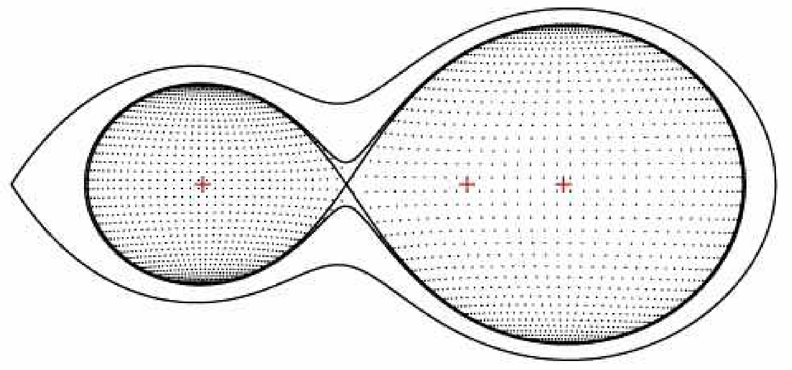

Figure 11. Binary Maker 3 representation of the potentials showing the relatively low degree of contact.

To determine the distance r in column 2, the analysis proceeded as follows: First the WD routine gave the absolute bolometric magnitudes of each component; these were then converted to the absolute visual (V) magnitudes of both, $M_V, 1$ and $M_{V,2}$, by adding the bolometric corrections BC = –0.060 (15) and –0.075 (15) for stars 1 and 2 respectively. The latter were taken from interpolated tables constructed from Cox (2000). The absolute magnitude was then computed in the usual way for adding magnitudes getting $M_V = 3.79 \pm 0.04$ mag. The apparent magnitude in the V passband was $V = 10.91 \pm 0.055$, taken from the APASS Catalogue (Henden et al. 2009, 2010, 2012; Smith et al., 2010).

Ignoring interstellar absorption (i.e., setting $A_V = 0$), we calculated a preliminary value for the distance $r = 265$ pc from the standard relation:

$$r = 10^{0.2(V - M_V - A_V + 5)} \quad \text{pc} \tag{3}$$

Galactic extinction was obtained from a model by Amôres & Lépine (2005). The simple code *extin* (in IDL) assumes that the interstellar dust is well mixed with the dust, that the galaxy is axisymmetric, that the gas density in the disk is a function of the Galactic radius

Table 5: Fundamental parameters of V1097 Her and AC Boo.

Quantity	V1097 Her	Error	unit	AC Boo	Error
Temperature, T_1	6250	150	K	6250	250
Temperature, T_2	6095	150	K	6241	250
Mass, m_1	0.43	0.01	$M_\odot$	0.36	0.03
Mass, m_2	1.19	0.02	$M_\odot$	1.20	0.05
Radius, R_1	0.78	0.02	$R_\odot$	0.69	0.01
Radius, R_2	1.21	0.01	$R_\odot$	1.19	0.01
$M_{bol,1}$	4.98	0.02	mag	5.26	0.02
$M_{bol,2}$	4.13	0.02	mag	4.07	0.02
$\log g_1$	4.29	0.01	cgs	4.32	0.01
$\log g_2$	4.34	0.01	cgs	4.36	0.01
Luminosity, L_1	0.84	0.01	$L_\odot$	0.65	0.09
Luminosity, L_2	1.84	0.03	$L_\odot$	1.94	0.28
Fill-out factor, f	0.13	0.05	—	0.02	
Distance, r	258	8	pc	182	13
Gaia DR2 distance, r	250.3	1.4	pc	156.8	0.6

and of the distance from the Galactic plane, and that extinction is proportional to the column density of the gas, Using Galactic coordinates of $l = 50.5821°$ and $b = 28.11817°$ (SIMBAD), and the initial distance estimate of $d = 0.265$ kpc, a value of $A_V = 0.127$ mag was determined. Further iterations left the value of A_V essentially unchanged. Then, substitution into Eq. (2) yielded a distance of 250 pc.

The same authors provided a more detailed model, *extinspiral* which attempts to take into account the spiral arms of the Galaxy. Starting with an initial distance value $r = 0.265$ kpc as before, we get a somewhat different initial value of $A_V = 0.0609$. Further iterations resulted in no perceptible change in A_V. Then, substitution into Eq. (2) yields a distance of 258 pc.

The errors were assigned as follows: $\delta M_{bol,1} = \delta M_{bol,2} = 0.015$, $\delta BC1 = \delta BC2 = 0.015$ (the variation of 1 and one half spectral sub-classes), $\delta V = 0.055$, all in magnitudes. At this point, it is not clear how to determine the uncertainties in the extinction values A_V from the Amôres & Lépine model. However, if we take half the difference between the two values we get $\delta A_V = 0.03$. Combining the errors rigorously (i.e., by adding the variances) yielded an estimated uncertainty in r of $\pm\, 8$ pc.

By contrast, reference to the dust tables of Schlegel et al. (1998) revealed a value of $E[B-V] = 0.0474$ for those galactic coordinates, virtually identical with the above values. However, because their $E[B-V]$ values have been derived from full-sky far-infrared measurements, they therefore apply to objects outside of the Galaxy, not the case here. As half the thickness of the Galactic disk is approximately 150 pc (Abell et al., 1991), and the galactic latitude is 28.1° (SIMBAD), that makes the path length $150/\sin(28.1) = 320$ pc. Assuming that the absorption is constant along the path length, we can take $A_V = (237/302) \times 0.145 = 0.113$. Again substituting the value into equation 2 we get $r = 251$ pc, reassuringly not very different from the pervious estimates. Taking δA_V as half of A_V results in an error estimate for r of $\pm\, 10$ pc.

Another approach, the classical one, is to determine galactic extinction from the tabulated value for the intrinsic $B-V$ colour index and take the difference (observed–tabulated) to get the colour excess $E[B-V]$. So, for a spectral type F8.5, we have (Cox,

Table 6: Estimating the interstellar absorption

Extinction determination	$E[B-V]$ mag	A_V mag	r pc	err pc
Amôres & Lépine (2005) simple model	0.0416	0.1270	250	8
Amôres & Lépine (2005) spiral model	0.0609	0.1857	258	8
Schlegel et al. (1998)	0.0474	0.113	251	10
Classical	0.04	0.122	251	38

2000), $(B-V)_{\rm tables} = 0.54(4)$. From the APASS catalogue we have $(B-V)_{\rm obs} = 0.58(6)$ yielding $E[B-V] = 0.04(7)$ mag. Using the relation $A_V = R\,E[B-V]$ for $R = 3.0$ or 3.1 (we use 3.05 here), we get $A_V = 0.12(34)$ mag and distance $r = 251$ pc, almost identical with the above, but with the higher uncertainty of $\pm\,38$ pc. Especially in view of the large uncertainties in determining $E[B-V]$, it is not surprising that this method results in much larger uncertainties in the final result. It is clear that determining $E[B-V]$ by one of the external methods described above is superior.

We have listed the results in Table 6.

We adopt the weighted mean $r = 253 \pm 5$ pc. However, any of the above distance determinations is consistent with the Gaia distance of 250.3 ± 1.4 pc, which is clearly more reliable.

Conclusion

As mentioned in the abstract, this system has been classified for the first time: the more luminous component has a spectral type of F8.5 V ($\pm\,1$ spectral subclass). Wilson-Devinney light- and radial velocity–curve analysis has determined masses of 0.41(1) and 1.11(2) $M_\odot$ and luminosities of 0.77(1) and 1.75(3) $L_\odot$ respectively. The mass of the secondary (cooler, more massive) star is consistent with the main sequence (interpolated) value of 1.15 $M_\odot$ while the luminosity is higher than the interpolated value of 1.35 $L_\odot$ suggesting a slightly evolved state. On the other hand, the secondary is undermassive for its presumed spectral type (F9, assigned for its temperature) and over-luminous. This is consistent with the model of the evolution of an overcontact system in which the present primary (hotter, less massive) started out as the more massive, losing much of its mass to the present secondary (Yildiz and Doğan, 2013).

This system is surprisingly similar to AC Boo (Nelson 2010b; Alton 2010). In addition to the very similar parameters listed in Table 5, each is type W, each has a spot, in each the more massive star is slightly evolved, and each has a varying orbital period. In the case of AC Boo however, it was shown by Nelson (2015b) that the eclipsing system likely has a companion, and that the more complex period variation may be explained by a light time effect (Irwin 1952, 1959). For AC Boo, the data span some 87 years whereas for V1097 Her, the data span only some 19 years, so one would not expect LiTE behaviour (if it exists) to become evident yet. Further eclipse timings spanning several decades are required to settle the matter. At this stage it is impossible to conclude anything with regard to a possible mass transfer rate because other causes of period change (such as LiTE) have not been ruled out or otherwise accounted for.

Acknowledgements It is a pleasure to thank the staff members at the DAO (Dmitry Monin, David Bohlender, and the late Les Saddlmyer) for their usual splendid help and assistance. Much use was made of the SIMBAD database during this research.

This work has made use of data from the European Space Agency (ESA) mission Gaia (https://www.cosmos.esa.int/gaia), processed by the Gaia Data Processing and Analysis Consortium (DPAC, https://www.cosmos.esa.int/web/gaia/dpac/consortium). Funding for the DPAC has been provided by national institutions, in particular the institutions participating in the Gaia Multilateral Agreement.

References:

Abell, G.O, Morrison, D., and Wolff, S.C., 1991, Exploration of the Universe, (Saunders), p. 539

Akerlof, C., et al., 2000, *AJ*, **119**, 1901

Alton, K. B., 2010, *JAVSO*, **38**, 57

Amôres, E.B., Lépine, J.R.D., 2005, *AJ*, **130**, 659 DOI

Bailer-Jones, C.A.L., et al., 2018, *AJ*, **156**, 58 DOI

Blättler, E. and Diethelm, R., 2002, *IBVS*, 5306

Bradstreet, D. H., 1993, "Binary Maker 2.0 – An Interactive Graphical Tool for Preliminary Light Curve Analysis", in Milone, E.F. (ed.) Light Curve Modelling of Eclipsing Binary Stars, pp 151-166 (Springer, New York, N.Y.) DOI

Cox, A. N., ed., 2000, *Allen's Astrophysical Quantities*, 4th ed., (Springer, New York, NY) DOI

Csizmadia, S., Pasternacki, T., Dreyer, C., Cabrera, A., Erikson, A., Rauer, H., 2013, *A&A*, **549**, A9 DOI

Davidge, T.J., Milone, E.F., 1984, *ApJS*, **55**, 571 DOI

Flower, P. J., 1996, *ApJ*, **469**, 355 DOI

Gaia Collaboration, 2018, *A&A*, **616**, 1 DOI

Henden, A. A., Welch, D. L., Terrell, D., Levine, S. E. 2009, The AAVSO Photometric All-Sky Survey, *AAS*, **214**, 407.02

Henden, A. A., Terrell, D., Welch, D., Smith, T. C. 2010, New Results from the AAVSO Photometric All Sky Survey, *AAS*, **215**, 470.11

Henden, A. A., Levine, S. E., Terrell, D., Smith, T. C., Welch, D., 2012, *JAAVSO*, **40**, 430

Høg, E., et al., 2000 *A&A*, **355**, L27

Irwin, J. B., 1952, *ApJ*, **116**, 211 DOI

Irwin, J. B., 1959, *AJ*, **64**, 149 DOI

Kallrath, J. & Milone, E.F., 1998, *Eclipsing Binary Stars–Modeling and Analysis* (Springer-Verlag) DOI

Kurucz, R.L., 2002, *BaltA*, **11**, 101

Lucy, L.B., 1967, *Zeit. für Astroph.*, **65**, 89

Mochnacki, S. W. 1981, *ApJ*, **245**, 650 DOI

Nelson, R. H., 2010, "Spectroscopy for Eclipsing Binary Analysis" in The Alt-Az Initiative, Telescope Mirror & Instrument Developments (Collins Foundation Press, Santa Margarita, CA), R.M. Genet, J.M. Johnson and V. Wallen (eds) [available on ResearchGate]

Nelson, R.H., 2010b, *IBVS*, 5951

Nelson, R. H., 2013, Software by Bob Nelson, `https://www.variablestarssouth.org/bob-nelson/`

Nelson, R. H., 2014, Spreadsheets, by Bob Nelson, `https://www.variablestarssouth.org/bob-nelson/`

Nelson, R.H., 2015a, *NewA*, **34**, 159 DOI
Nelson, R.H., 2015b, *IBVS*, 6142
Nelson, R.H., 2017, Bob Nelson's O–C Files, http://www.aavso.org/ [enter "O-C" in the search box]
Nelson, R. H., Şenavci, H. V., Baştürk, Ö, Bahar, E., 2014, *NewA*, **29**, 57 DOI
Rucinski, S. M., 1969, *AcA*, **19**, 245
Rucinski, S M., 2004, "Advantages of the Broadening Function (BF) over the Cross-Correlation Function (CCF)", in Stellar Rotation, *IAUS*, **215**, 17
Schlegel, D. J., Finkbeiner, D. P., Davis, M., 1998, *ApJ*, **500**, 525 DOI
Smith, T. C., Henden, A., Terrell, D., 2010, AAVSO Photometric All-Sky Survey Implementation at the Dark Ridge Observatory, SAS.
Terrell, D., 1994, Van Hamme Limb Darkening Tables, vers. 1.1.
Van Hamme, W., 1993, *AJ*, **106**, 2096 DOI
Wilson, R. E., Devinney, E. J., 1971, *ApJ*, **166**, 605 DOI
Wilson, R. E., 1990, *ApJ*, **356**, 613 DOI
Wilson, R. E., 1998, Documentation of Eclipsing Binary Computer Model (available from the author)
Yildiz, M., Doğan, T., 2013, *MNRAS*, **430**, 2029 DOI

COMMISSIONS G1 AND G4 OF THE IAU
INFORMATION BULLETIN ON VARIABLE STARS
Volume 63 Number 6271 DOI: 10.22444/IBVS.6271

Konkoly Observatory
Budapest
3 June 2019

HU ISSN 0374 – 0676

18 NEW VARIABLES IN THE PUPPIS FIELD

TITZ-WEIDER, R.[1]; CSIZMADIA, SZ.[1]; DREYER, C.[1]; EIGMÜLLER, P.[1]; FRUTH, T.[2]; CABRERA, J.[1]; ERIKSON, A.[1]; RAUER, H.[1,3,4]

[1] DLR, Institut fr Planetenforschung, Rutherfordstr 2, 12489 Berlin, Germany, e-mail: ruth.titz@dlr.de

[2] DLR, German Space Operation Center, Mnchner Str. 20, 82234 Wessling, Germany

[3] FU Berlin, Institut fr Geologische Wissenschaften, Malteserstr. 74-100, 12249 Berlin, Germany

[4] TU Berlin, Zentrum fr Astronomie und Astrophysik, 10623 Berlin, Germany

The Puppis field was observed between 2011 and 2014 in the search for transiting extrasolar planets. To characterize the field, an automatic variable search was applied as described by Fruth et al. (2012). With the automatic procedure 1829 new variables were discovered and 26 previously known variables were confirmed (Dreyer et al. 2018).

Beyond this work, the data was also analysed for potential transit events by the Box-Fitting Least Square (BLS) method (Kovac et al. 2002, Fruth et al. 2013). This yielded a list of objects with tentative period, duration and depth, not included in the list of Dreyer et al (2018). The light curves of these potential candidates were visually inspected and further modelled by TLCM, a transit light curve model to get the basic parameters, developed by Csizmadia (2020). Thereby the period was confirmed or improved and the type of binary was determined. Identification and variability data for the stars are summarized in Tables 1–2; phase curves for each variable are presented in Figures 1–18. Photometry data files are also available online.

References:

Csizmadia Sz., 2020, *MNRAS*, under review
Dreyer, C. et al., 2018, *AJ*, **156**, 204 DOI
Fruth, T., et al., 2012, *AJ*, **143**, 140 DOI

Table 1: Cross-identification and coordinates.

Object Internal ID	2MASS ID	Coordinates RA$_{2000}$	Dec$_{2000}$	Data file
F20a.005815	07333745-3259436	$07^{h}33^{m}37^{s}.4$	$-32°59'43''.7$	6271-t3.txt
F20a.018824	07303116-3222418	$07^{h}30^{m}31^{s}.2$	$-32°22'41''.8$	6271-t4.txt
F20a.026583	07310564–3159570	$07^{h}31^{m}05^{s}.7$	$-31°59\ 58''.0$	6271-t5.txt
F20b.010782	07262660–3106585	$07^{h}26^{m}26^{s}.61$	$-31°06'58''.57$	6271-t6.txt
F20b.017823	07291727–3049085	$07^{h}29^{m}17^{s}.3$	$-30°49'08''.5$	6271-t7.txt
F20b.032711	07275882–3007572	$07^{h}27^{m}58^{s}.81$	$-30°07'57''.62$	6271-t8.txt
F20c.005922	07300259–2940196	$07^{h}30^{m}02^{s}.59$	$-29°40'19''.58$	6271-t9.txt
F20c.014909	07293525–2917331	$07^{h}29^{m}35^{s}.25$	$-29°17'33''.05$	6271-t10.txt
F20c.015941	07331914–2914089	$07^{h}33^{m}19^{s}.16$	$-29°14'09''.01$	6271-t11.txt
F20d.004702	07290369–2802282	$07^{h}29^{m}03^{s}.69$	$-28°02'28''.25$	6271-t12.txt
F20d.006126	07310929–2758334	$07^{h}31^{m}09^{s}.29$	$-27°58'33''.41$	6271-t13.txt
F20d.011593	07300456–2745258	$07^{h}30^{m}04^{s}.57$	$-27°45'25''.80$	6271-t14.txt
F20d.013162	07274514–2741386	$07^{h}27^{m}45^{s}.1$	$-27°41'38''.5$	6271-t15.txt
F20d.013467	07304375–2740426	$07^{h}30^{m}43^{s}.75$	$-27°40'42''.49$	6271-t16.txt
F20d.013718	07292644–2740120	$07^{h}29^{m}26^{s}.44$	$-27°40'11''.86$	6271-t17.txt
F20d.014956	07293465–2737019	$07^{h}29^{m}34^{s}.65$	$-27°37'01''.79$	6271-t18.txt
F20d.020854	07284737–2720366	$07^{h}28^{m}47^{s}.39$	$-27°20'36''.60$	6271-t19.txt
F20d.029101	07273592–2647430	$07^{h}27^{m}35^{s}.9$	$-26°47'43''.0$	6271-t20.txt

Table 2: Variability parameters.

Object internal ID	Type	Period (d)	Epoch HJD-2455875	Brightness (mag)	Band
F20a.005815	EB	2.08	77.64	15.45	white
F20a.018824	EB	3.66	71.76	14.26	white
F20a.026583	EB	1.17	76.60	13.93	white
F20b.010782	EB	2.72	8.72	13.99	white
F20b.017823	EB	3.05	84.75	14.50	white
F20b.032711	EB	1.565	83.111	14.40	white
F20c.005922	EB	6.379	65.8	14.44	white
F20c.014909	EB	9.34	5.67	13.37	white
F20c.015941	EB	9.76	99.67	14.82	white
F20d.004702	EB	0.778	10.75	15.29	white
F20d.006126	EB	1.874	33.66	12.72	white
F20d.011593	EB	1.48	64.74	14.43	white
F20d.013162	EB	2.115	0.816	15.41	white
F20d.013467	EB	1.695	65.58	14.47	white
F20d.013718	EB	1.397	70.622	14.26	white
F20d.014956	EB	1.402	5.28864	15.58	white
F20d.020854	EB	8.794	75.75	15.45	white
F20d.029101	EB	5.927	0.738	13.78	white

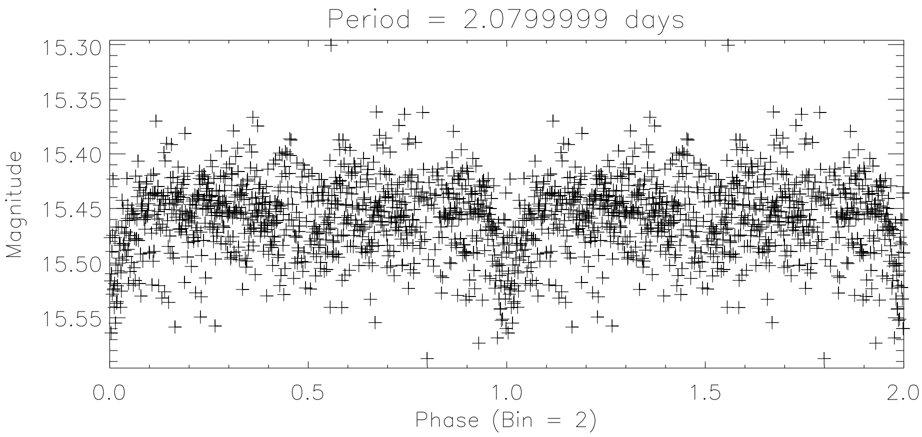

Figure 1. Phase curve of F20a.005815

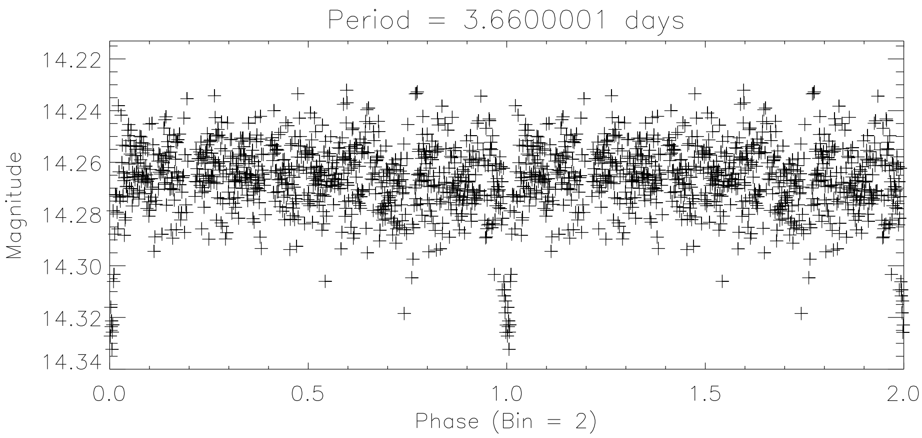

Figure 2. Phase curve of F20a.018824

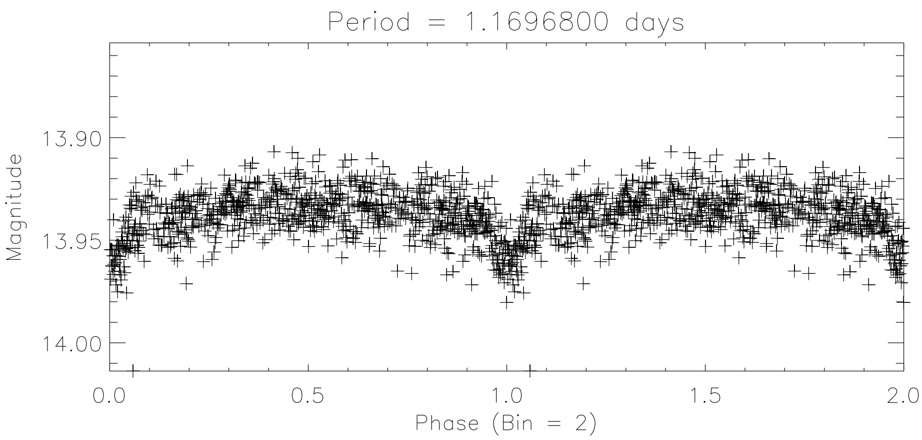

Figure 3. Phase curve of F20a.026583

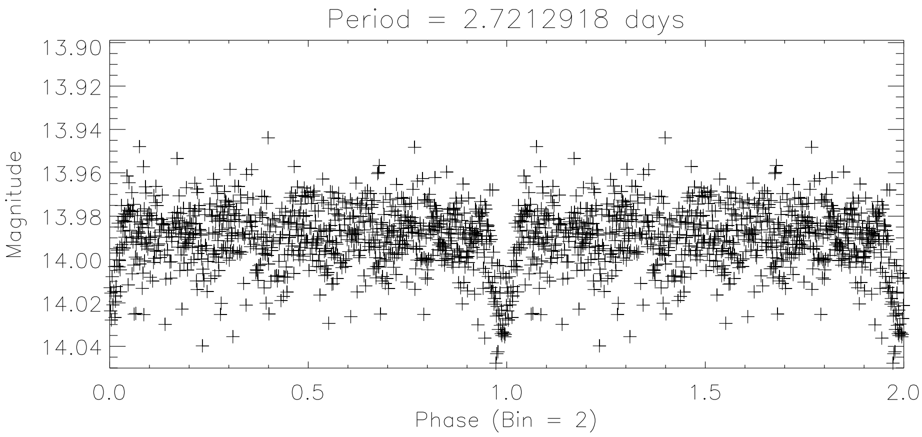

Figure 4. Phase curve of F20b.010782

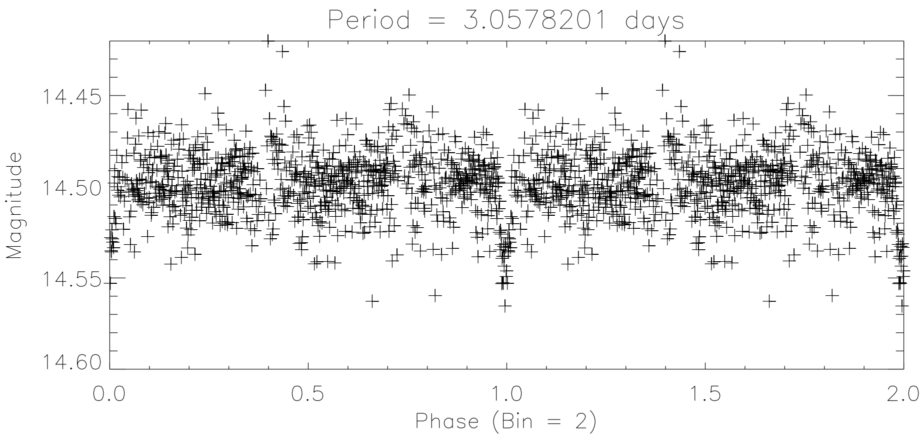

Figure 5. Phase curve of F20b.017823

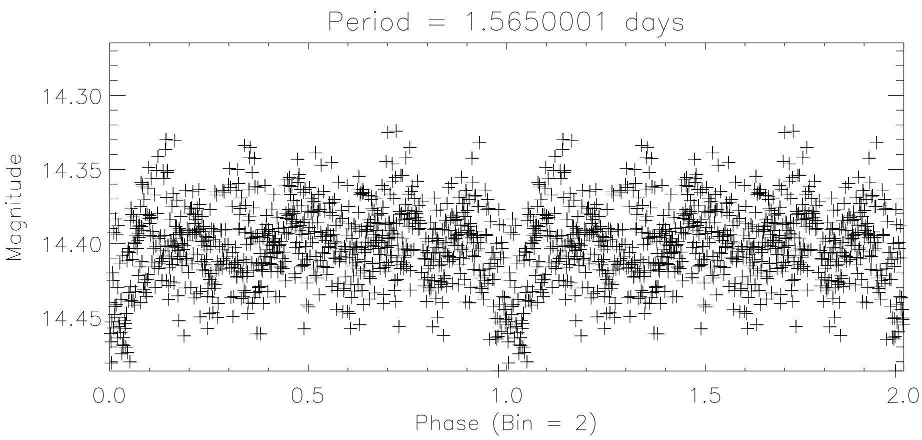

Figure 6. Phase curve of F20b.032711

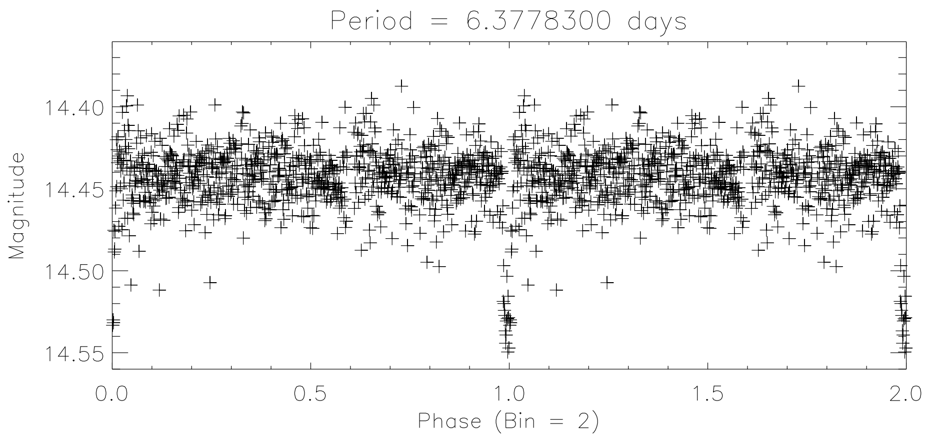

Figure 7. Phase curve of F20c.005922

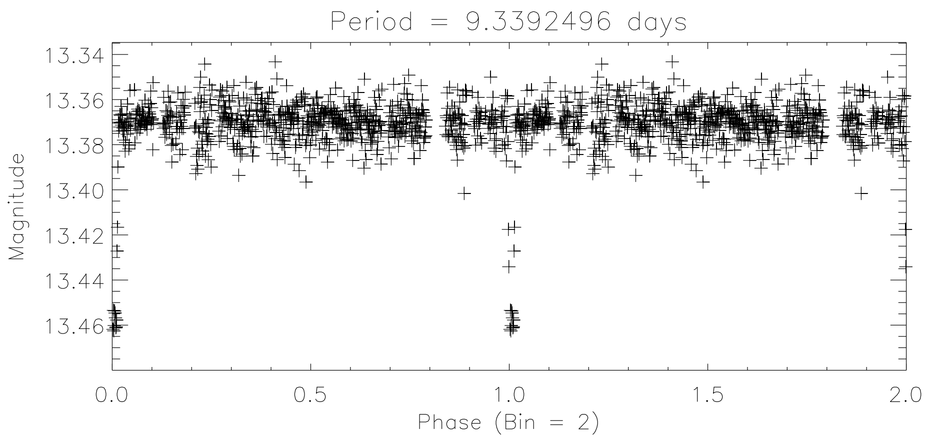

Figure 8. Phase curve of F20c.014909

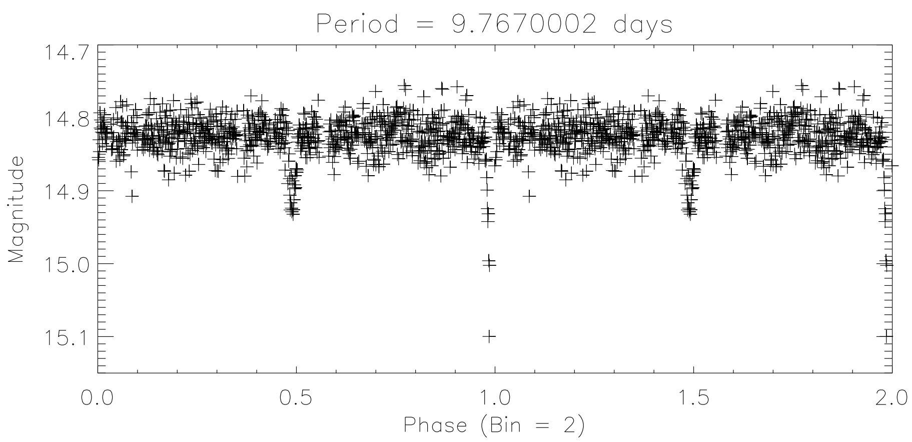

Figure 9. Phase curve of F20c.015941

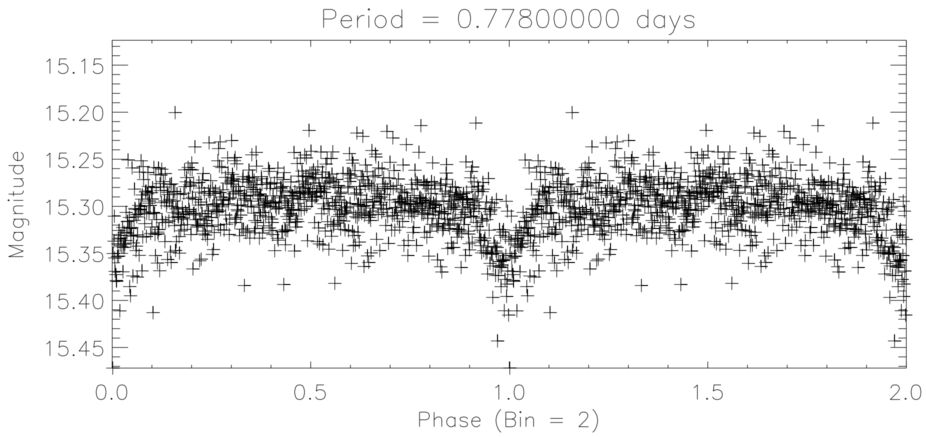

Figure 10. Phase curve of F20d.004702

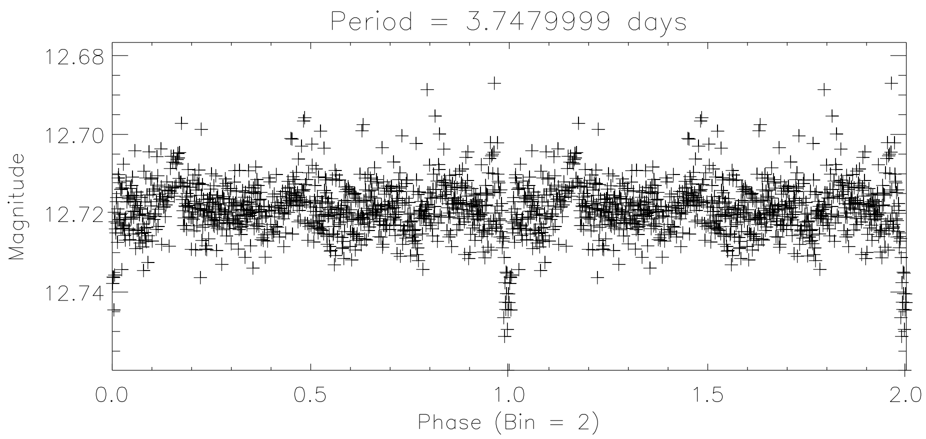

Figure 11. Phase curve of F20d.006126

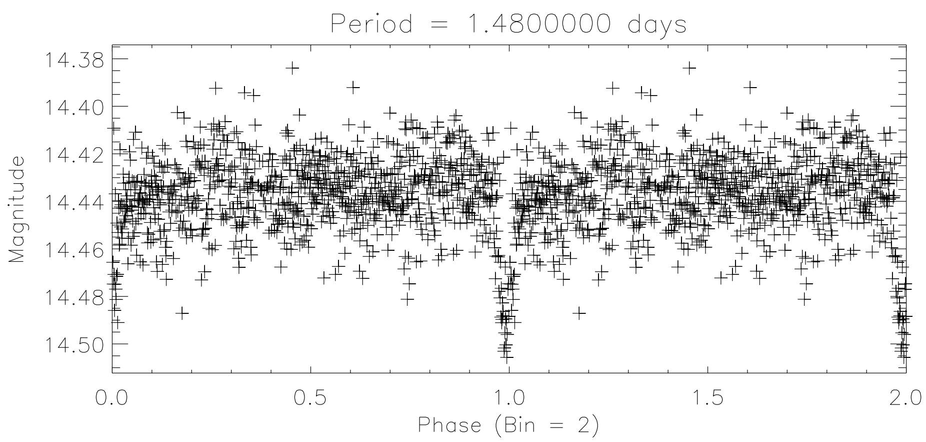

Figure 12. Phase curve of F20d.011593

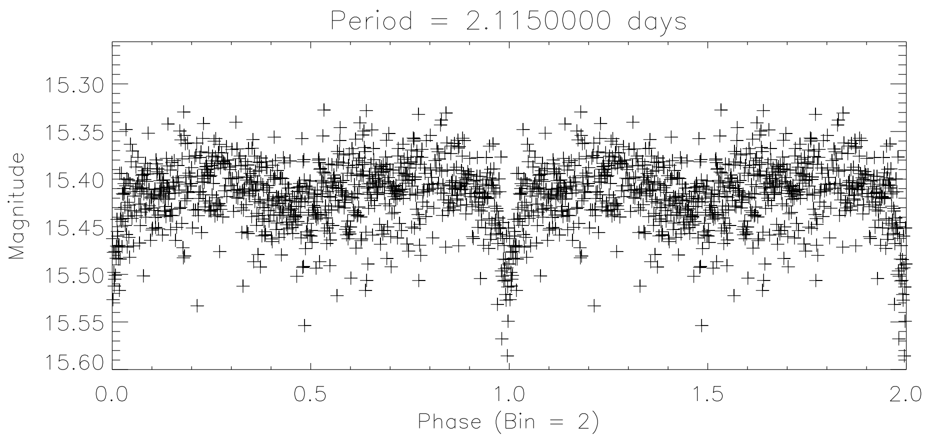

Figure 13. Phase curve of F20d.013162

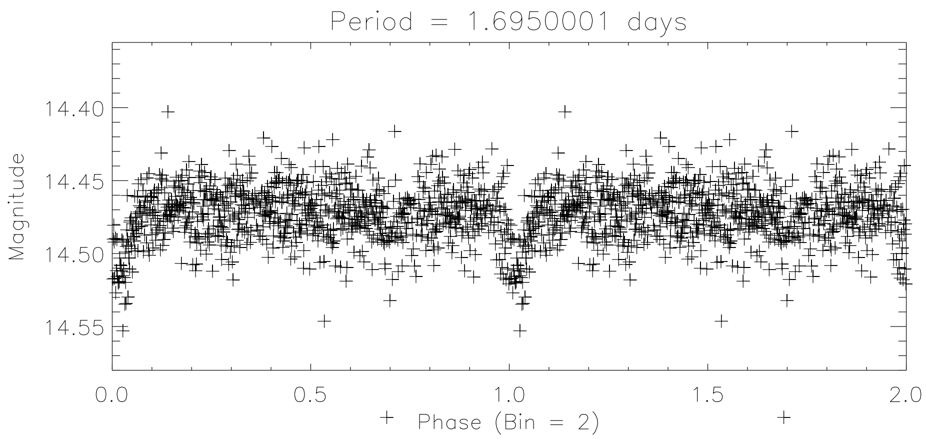

Figure 14. Phase curve of F20d.013467

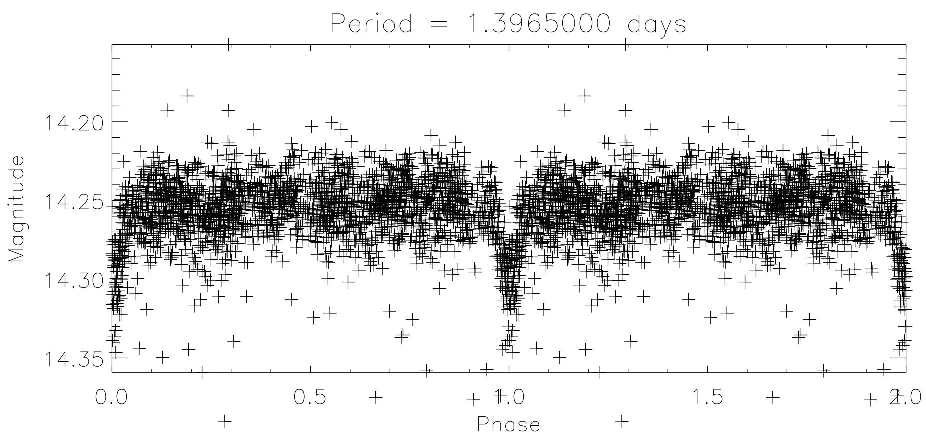

Figure 15. Phase curve of F20d.013718

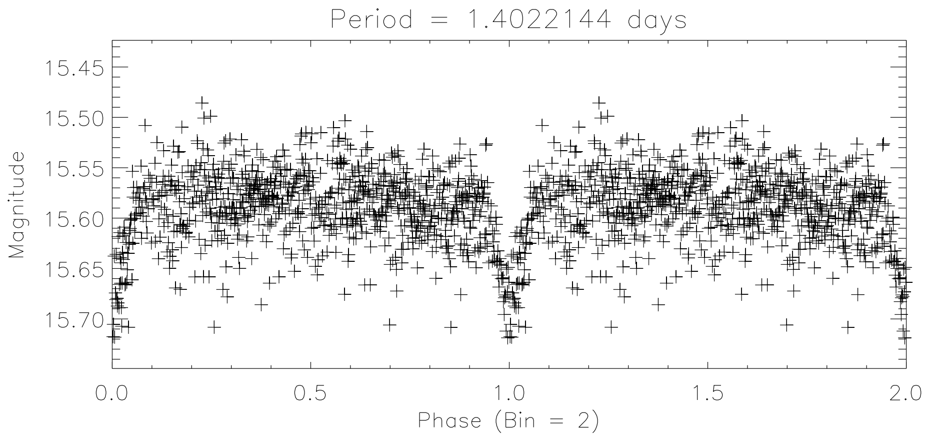

Figure 16. Phase curve of F20d.014956

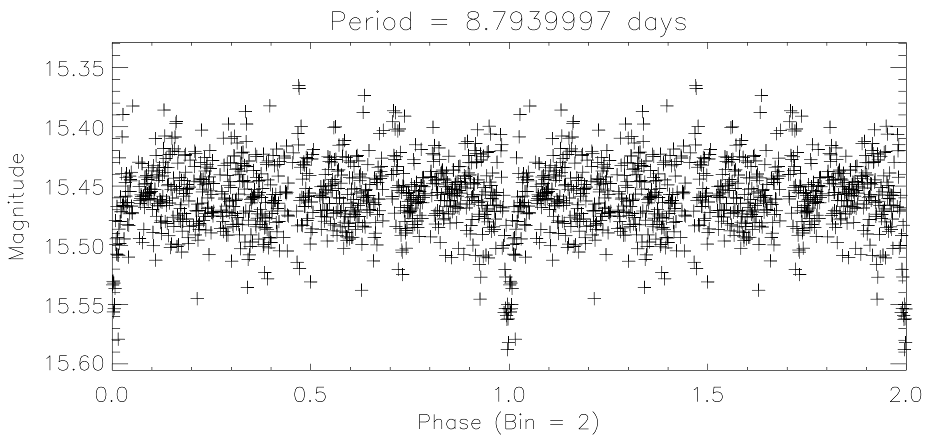

Figure 17. Phase curve of F20d.020854

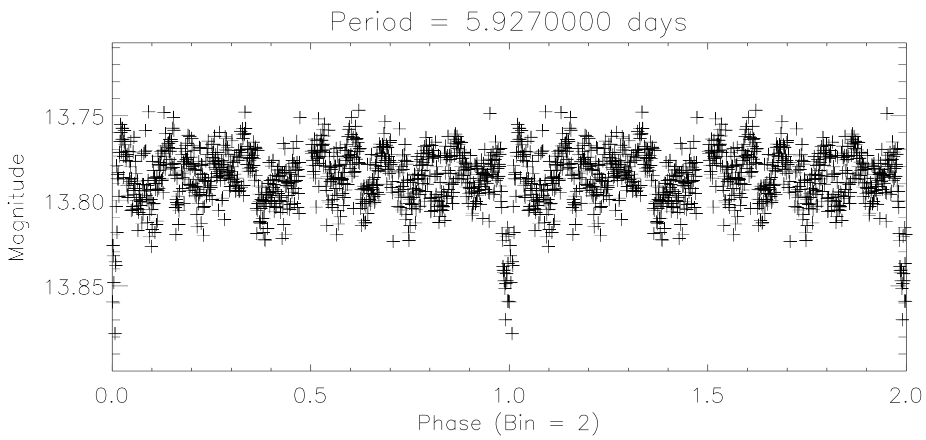

Figure 18. Phase curve of F20d.029101

COMMISSIONS 27 AND 42 OF THE IAU
INFORMATION BULLETIN ON VARIABLE STARS

Number 6299

Konkoly Observatory
Budapest
9 October 2017

HU ISSN 0374 – 0676

OBSERVATIONS OF VARIABLES

Date: 18 April 2017

Reported by:
Gazeas, K. - Department of Astrophysics, Astronomy and Mechanics, National and Kapodistrian University of Athens, GR 15784, Zografos, Athens, Greece, kgaze@phys.uoa.gr

Name of the object:
USNO-A2.0 1200-15055584

Remarks:
Detected on 15 June 2015 in the FoV of V404 Cyg. The corresponding FoV was observed in a long (120 sec) and short (10 sec) cadence, therefore two light curves and data tables are provided.

RA(J2000)	Dec(J2000)	type	Mag.	Period (day)	Epoch
20 24 25.404	+33 57 11.83	EW	15.4(Rmag -USNO A2.0)	0.260914(7)	2457190.4942(6)

Cross-identification(s):
USNO-A2.0 1200-15055584 = GSC 2.3 N33E061689 = UCAC4 620-101941

Date: 4 October 2017

Reported by:
Vasilii Moskvin - Cremian Astrophysical Observatory, mvv@craocrimea.ru

Name of the object:
GSC 03553-00845

Remarks:
Remarks: During the transit observation the exoplanets HAT-P-37b recorded a minimum of the W UMa-type binary system GSC 03553-00845. Then several more observations of this object were made. Observations were made in the filter R. Figure 1 shows these observations folded with the elements:

$$\mathrm{Min\,I} = \mathrm{HJD}\,2457892.487112 + 0.43547E$$

The standard deviation for the check star is 0.01 mag. Different symbols represent different days. Reduction of the CCD frames was made with Maxim DL software.
Acknowledgements: This research made use of the Simbad data base, operated at CDS, Strasbourg, France.

References:

Guo, Di-Fu et al., 2014, *Publ. Astron. Soc. Japan*, **66**, 100 DOI

COMMISSIONS G1 AND G4 OF THE IAU
INFORMATION BULLETIN ON VARIABLE STARS

Volume 63 Number 6300 DOI: 10.22444/IBVS.6300

Konkoly Observatory
Budapest
9 October 2017

HU ISSN 0374 – 0676

REPORTS ON NEW DISCOVERIES

Date: 18 April 2017

Observer(s) and affiliation(s):
Gazeas, K. - Department of Astrophysics, Astronomy and Mechanics, National and Kapodistrian University of Athens, GR 15784, Zografos, Athens, Greece, kgaze@phys.uoa.gr
Karmi, S. - Department of Astrophysics, Astronomy and Mechanics, National and Kapodistrian University of Athens, GR 15784, Zografos, Athens, Greece, phohal@hotmail.com

RA(J2000)	Dec(J2000)	type	Mag.
21 14 49.143	+44 34 16.13	EW	15.9(Rmag -USNO A2.0)

Period	Epoch
0.50069(9)	2456815.424(2)

Cross-identification(s):
USNO-A2.0 1275-15108427 = GSC 2.3 N31H089347 = UCAC4 673-095718

Remark: Detected on 31 May 2014 in the FoV of GSC 3181:2419.

RA(J2000)	Dec(J2000)	type	Mag.
21 16 34.235	+44 37 27.22	DSCT	13.9(Rmag -USNO A2.0)

Period	Epoch
0.1689(2)	2456833.518(14)

Cross-identification(s):
USNO-A2.0 1275-15192807 = GSC 3181:2781 = UCAC4 674-095557

Remark: Detected on 31 May 2014 in the FoV of GSC 3181:2419. Epoch refers to maximum light.

RA(J2000)	Dec(J2000)	type	Mag.
02 39 44.562	+48 57 37.18	EW	16.2(Rmag -USNO A2.0)

Period	Epoch
0.350221(19)	2457339.5375(14)

Cross-identification(s):
USNO-A2.0 1350-02565514 = GSC 2.3 NCHW044927

Remark: Detected on 10 November 2015 in the FoV of KL Per.

RA(J2000)	Dec(J2000)	type	Mag.
02 41 13.043	+48 58 46.79	DSCT	15.1(Rmag -USNO A2.0)

Period	Epoch
0.0766(2)	2457337.355(2)

Cross-identification(s):
USNO-A2.0 1350-02593309 = GSC 2.3 NCHZ031290 = UCAC4 695-018090

Remark: Detected on 10 November 2015 in the FoV of KL Per. Epoch refers to maximum light.

RA(J2000)	**Dec(J2000)**	**type**	**Mag.**
02 41 48.085	+48 47 22.39	EW	16.1(Rmag -USNO A2.0)

Period	**Epoch**
0.33652(2)	2457339.3488(18)

Cross-identification(s):
USNO-A2.0 1350-02604882 = GSC 2.3 NCHW043104 = UCAC4 694-017475

Remark: Detected on 10 November 2015 in the FoV of KL Per. Epoch refers to maximum light.

Date: 18 April 2017

Observer(s) and affiliation(s):
Gazeas, K. - Department of Astrophysics, Astronomy and Mechanics, National and Kapodistrian University of Athens, GR 15784, Zografos, Athens, Greece, kgaze@phys.uoa.gr

RA(J2000)	**Dec(J2000)**	**type**	**Mag.**
20 00 57.378	+19 06 55.55	EW	13.8(Rmag -USNO A2.0)

Period	**Epoch**
0.20633(10)	2457235.399(4)

Cross-identification(s):
USNO-A2.0 1050-16046558 = GSC 2.3 N1U0066500 = UCAC4 546-115254

Remark: Detected on 24 July 2015 in the FoV of CW Sge.

Date: 18 April 2017

Observer(s) and affiliation(s):
Paschalis I. Nikolaos - Nunki Private Observatory, GR 37002 Xanemos, Skiathos, Greece nikolaospaschalis@gmail.com
Gazeas, K. - Department of Astrophysics, Astronomy and Mechanics, National and Kapodistrian University of Athens, GR 15784, Zografos, Athens, Greece, kgaze@phys.uoa.gr

RA(J2000)	**Dec(J2000)**	**type**	**Mag.**
06 29 37.41	+29 12 34.54	EW	12.82(VTmag -TYC2)

Period	**Epoch**
0.41852(1)	2457515.2961(3)

Cross-identification(s):
GSC 1891-0714 = TYC 1891-0714-1 = 2MASS J06293740+2912347

Remark: Detected on 21 December 2015 in the FoV of the exoplanet WASP-12b.

RA(J2000)	**Dec(J2000)**	**type**	**Mag.**
06 30 10.25	+30 03 29.9	EA	12.80(R mag USNO-A2)

Period	**Epoch**
1.42536(5)	2457519.2922(3)

Cross-identification(s):
GSC 2422-1063 = USNO-A2.0 1200-04854379 = 2MASS 06301026+3003296

Remark: Detected on 21 December 2015 in the FoV of the exoplanet WASP-12b.

Date: 21 April 2017

Observer(s) and affiliation(s):
Serebryanskiy, A. - Fesenkov Astrophysical Institute, Observatory 23, 050020 Almaty, Kazakhstan aserebryanskiy@yahoo.com Reva, I. - Fesenkov Astrophysical Institute, Observatory 23, 050020 Almaty, Kazakhstan

RA(J2000)	**Dec(J2000)**	**type**	**Mag.**
07 59 49.22	-10 39 30.77	DSCT	14.71 (R mag)

Period	**Epoch**
-	-

Cross-identification(s):
UCAC4 397-036372

Remark: The preliminary image reduction which includes dark subtraction, flat fielding and registration was made in IRAF. The combined CCD image in filter V is show on Figure `6300-f17.jpg`. The world coordinate system was assigned to the images using `wcstools` package (D.Mink 1997, 1999, 2002). The sources on the frames were identified by `sextractor` software (Bertin & Arnouts 1996). Totally about 2700 sources were identified. The coordinates of the stars in ICRS system were determined by `wcstools/imcat` utilizing UCAC4 catalog. The photometric information was extracted with IRAF `noao.daophot` package using the method of PSF photometry. Before we compute differential photometric light curves for each star we identify the known variables on the filed (see, for example Arentoft et al., 2007 and references therein) and visually inspect each initial light curve for selection of possible reference stars and check stars. The differential light curves for each star were calculated using method of improved reference light curve (Fernández et al., 2012). 12 stars were selected as reference stars and 77 stars as the auxiliary stars. The light curve of the UCAC4 397-036372 is shown in Figure `6300-f18.jpg`. The star's location is indicated by red square in finding chart (`6300-f19.jpg`).

Date: 16 May 2017

Observer(s) and affiliation(s):
Gazeas, K. - Department of Astrophysics, Astronomy and Mechanics, National and Kapodistrian University of Athens, GR 15784, Zografos, Athens, Greece, kgaze@phys.uoa.gr Karampotsiou, E. - Department of Astrophysics, Astronomy and Mechanics, National and Kapodistrian University of Athens, GR 15784, Zografos, Athens, Greece, sevi.kar@gmail.com

RA(J2000)	**Dec(J2000)**	**type**	**Mag.**
22 07 16.884	+26 55 23.64	EB	15.8(Rmag - USNO A2.0)

Period	**Epoch**
0.6078(1)	2457266.3921(4)

Cross-identification(s):
USNO 1125-19083473 = 2MASS J22071685+2655235 = GSC2.2 N033000118553

Remark: Detected on 27 August 2015 in the FoV of 1SWASP J220734.47+265528.6.

RA(J2000)	**Dec(J2000)**	**type**	**Mag.**
22 07 48.657	+26 49 19.01	EW	14.6(Rmag -USNO-A2.0)

Period	**Epoch**
0.44247(4)	2457262.3547(4)

Cross-identification(s):
USNO 1125-19090391 = 2MASS J22074863+2649185 = GSC2.2 N0330001721

Remark: Detected on 27 August 2015 in the FoV of 1SWASP J220734.47+265528.6.

Date: 18 September 2017

Observer(s) and affiliation(s):
Liakos, A. - National Observatory of Athens, Institute for Astronomy, Astrophysics, Space Applications, and Remote Sensing, I. Metaxa & Vas. Pavlou St., GR-152 36, Palaia Penteli, Athens, Hellas (Greece) alliakos@noa.gr

RA(J2000)	**Dec(J2000)**	**type**	**Mag.**
22 26 20.47	+54 48 25.2	EW	15.9 (r)

Period	**Epoch**
-	-

Cross-identification(s):
UCAC4 725-090762 = 2MASS J22262047+5448251 = XPM 289-0675303 = IPHAS J222620.47+544825.2

Remark: Detected in the FoV of the planetary nebula A66 79 (PNG 102.9-02.3).

Date: 11 December 2017

Observer(s) and affiliation(s):
Liakos, A. - National Observatory of Athens, Institute for Astronomy, Astrophysics, Space Applications, and Remote Sensing, I. Metaxa & Vas. Pavlou St., GR-152 36, Palaia Penteli, Athens, Hellas (Greece) alliakos@noa.gr

RA(J2000)	**Dec(J2000)**	**type**	**Mag.**
22 16 56.85	+57 21 25.8	EW	18.9 (J) (UGPS catalogue)

Period	**Epoch**
0.42572	2458031.45394

Cross-identification(s):
UGPS J221656.43+572125.5

Remark: Detected in the FoV of the planetary nebula M2-51 (PNG 103.2+00.6).

RA(J2000)	**Dec(J2000)**	**type**	**Mag.**
22 16 19.6	+57 23 58.3	DSCT	15.2 (R) (USNO A2.0)

Period	**Epoch**
0.091110(3)	-

Cross-identification(s):
USNO A2.0 1425-13112208 = NOMAD1 1473-0485131 = 2MASS J22161965+5723582

Remark: Detected in the FoV of the planetary nebula M2-51 (PNG 103.2+00.6).

RA(J2000)	**Dec(J2000)**	**type**	**Mag.**
22 16 03.84	+57 26 13.8	EB	16.8 (R) (USNO A2.0)

Period	**Epoch**
0.41338	2458039.24476

Cross-identification(s):
USNO-A2.0 1425-13104193 = NOMAD1 1474-0478834

Remark: Detected in the FoV of the planetary nebula M2-51 (PNG 103.2+00.6).

Date: 29 January 2018

Observer(s) and affiliation(s):
Kendurkar, Malhar Raghunath - College of New Caledonia, Prince George Astronomical Observatory, Prince George, BC, Canada malhar.kendurkar@gmail.com Nelson, Robert H. - Mountain Ash Observatory, Prince George, BC, Canada bob.nelson@shaw.ca

RA(J2000)	Dec(J2000)	type	Mag.
07 11 54.54	+07 40 01	DSCT	

Period	Epoch
0.092 ± 0.001	24058095.935

Cross-identification(s):
GSC 0762-2924

Remark: GSC 0762-2924 was discovered to be variable by the lead author during a routine 'data mining' search of many past images taken by the co-author during eclipsing binary studies. We classify the star, in the field of BX CMi, as a pulsating variable star because of the asymmetric shape of the light curve. The period of 0.092±0.001 days is typical for a Delta Scuti star (Hoffmeister et al., 1985), but the amplitude in the R (Cousins) filter of about 0.06 magnitudes puts it at the low amplitude end (ibid). The light curve changed noticeably between the two runs. Times of maximum light were JDhel(max) = 24 58095.935±0.001 and 58078.004 ±0.001(spanning 195 cycles). The comparison star was GSC 0762-2154. The search and follow-up images were taken at observatories described in Nelson (2017a, 2017b), respectively.

References:

Arentoft, T., De Ridder, J., Grundahl, F., Glowienka, L., Waelkens, C., Dupret, M.-A., Grigahcène, A., Lefever, K., Jensen, H. R., Reyniers, M., Frandsen, S., Kjeldsen, H., 2007, *A&A*, **465**, 965 DOI

Bertin, E., Arnouts, S., 1996, *A&AS*, **117**, 393 DOI

Fernández Fernández, J., Chou, D.-Y., Pan, Y.-C., Wang, L.-H., 2012, *PASP*, **124**, 507 DOI

Hoffmeister, C., Richter, G, and Wenzel, W. 1985, Variable Stars (Springer Verlag)

Mink, D., 1997, *ASP Conf. Ser.*, **125**, 249

Mink, D., 1999, *ASP Conf. Ser.*, **172**, 498

Mink, D., 2002, *ASP Conf. Ser.*, **281**, 169

Nelson, Robert H. 2017a, *IBVS*, **6192** DOI

Nelson, Robert H. 2017b, *IBVS*, **6224** DOI